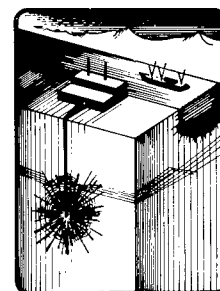


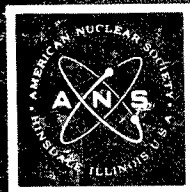
Symposium on

ENGINEERING WITH NUCLEAR EXPLOSIVES

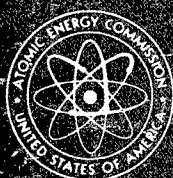
JANUARY 14-16, 1970
LAS VEGAS, NEVADA



SPONSORED BY
THE AMERICAN
NUCLEAR SOCIETY



IN COOPERATION
WITH
THE UNITED STATES
ATOMIC ENERGY
COMMISSION



ORGANIZING COMMITTEE:

P. Kruger, General Chairman
Stanford University

J. Knox, Program Chairman
Lawrence Radiation Laboratory

H. Goffe, Local Chairman
CER Geonuclear

W. Talley, Finance Chairman
University of California, Davis

J. Philip, Publication Chairman
USAEC, San Francisco

F. Chilton, Publicity Chairman
Stanford Research Institute

**Reproduced From
Best Available Copy**

PROCEEDINGS

DISTRIBUTION STATEMENT A
Approved for Public Release
Distribution Unlimited

LOVELACE FOUNDATION
DOCUMENT LIBRARY

20000920 206

"Let Us Beat Swords into Plowshares"

Evgeniy Vuchetich
Gift to United Nations.
December 1959

LEGAL NOTICE

This report was prepared as an account of Government sponsored work. Neither the United States, nor the Commission, nor any person acting on behalf of the Commission:

A. Makes any warranty or representation, expressed or implied, with respect to the accuracy, completeness, or usefulness of the information contained in this report, or that the use of any information, apparatus, method, or process disclosed in this report may not infringe privately owned rights; or

B. Assumes any liabilities with respect to the use of, or for damages resulting from the use of any information, apparatus, method, or process disclosed in this report.

As used in the above, "person acting on behalf of the Commission" includes any employee or contractor of the Commission, or employee of such contractor, to the extent that such employee or contractor of the Commission, or employee of such contractor prepares, disseminates, or provides access to, any information pursuant to his employment or contract with the Commission, or his employment with such contractor.

This report has been reproduced directly from the best available copy.

Printed in USA. This report consists of 2 volumes. ~~Price \$6.00 for the 2 volume set.~~ Available from the Clearinghouse for Federal Scientific and Technical Information, National Bureau of Standards, U. S. Department of Commerce, Springfield, Virginia 22151.

Symposium On
ENGINEERING WITH NUCLEAR EXPLOSIVES

**January 14-16, 1970
Las Vegas, Nevada**

PROCEEDINGS

Issuance Date: May 1970

Sponsored By
The American Nuclear Society
In Cooperation with
United States Atomic Energy Commission

DISTRIBUTION STATEMENT A
Approved for Public Release
Distribution Unlimited

CONTENTS

VOLUME 1

Foreword	iii
Preface	v
Technical Group for Nuclear Explosion Engineering	vi
PLENARY SESSION	
Improving the Quality of Life—Can Plowshare Help?	1
<i>T. J. Thompson</i>	
The Future of Plowshare	5
<i>J. S. Kelley</i>	
An Industrial View of the Plowshare Program	13
<i>S. Smith</i>	
Nuclear Explosive Development	24
<i>B. C. Groseclose</i>	
Underground Nuclear Explosions	29
<i>G. H. Higgins</i>	
Engineering Effects of Underground Nuclear Explosions	43
<i>C. R. Boardman</i>	
Emplacement Engineering	68
<i>E. E. Hill</i>	
UNDERGROUND NUCLEAR EFFECTS I	
Summary of Geonuclear Effects	75
<i>D. E. Rawson</i>	
Loading-Unloading Pressure-Volume Curves for Rocks	89
<i>D. R. Stephens and E. M. Lilley</i>	
Dynamic Elastic Moduli of Rocks Under Pressure	110
<i>R. N. Schock</i>	
The Influence of Environment on the Inelastic Behavior of Rocks	127
<i>H. C. Heard</i>	
Numerical Simulation of Stress Wave Propagation from Underground Nuclear Explosions	142
<i>J. T. Cherry and F. L. Petersen</i>	
Theoretical Model of the Early Phases of an Underground Explosion	221
<i>I. G. Cameron and G. C. Scorgie</i>	
Computation of Fluid Flow in Distending Tunnels with Mass, Momentum and Energy Exchange with the Walls	230
<i>J. R. Maw</i>	

The French Experimentation at the Underground Nuclear Testing Site in the Sahara Desert	240
<i>A. Gauvenet</i>	

EXCAVATION I

Summary of Nuclear-Excavation Applications	245
<i>J. Toman</i>	
Status of the Interoceanic Canal Study	280
<i>R. H. Groves</i>	
The Nonproliferation Treaty and Peaceful Uses of Nuclear Explosives	294
<i>T. Ehrlich</i>	
Results of the Schooner Excavation Experiment	306
<i>H. A. Tewes</i>	
Nuclear Cratering on a Digital Computer	334
<i>R. W. Terhune and T. F. Stubbs</i>	
Excavation Research with Chemical Explosives	360
<i>W. E. Vandenberg and W. C. Day</i>	

RADIOACTIVITY I

Radioactivity from Plowshare Applications—Safety Considerations	375
<i>H. A. Tewes</i>	
Diffusion and Deposition of the Schooner Clouds	381
<i>T. V. Crawford</i>	
Postshot Distribution and Movement of Radionuclides in Nuclear Crater Ejecta	400
<i>J. J. Koranda, J. R. Martin, R. W. Wikkerink, and M. L. Stuart</i>	
Radioecological Studies of Tritium Movement in a Tropical Rain Forest	422
<i>J. R. Martin, C. F. Jordan, J. J. Koranda, and J. R. Kline</i>	
Summary of USSR Reports on Mechanical and Radioactivity Effects of Underground Nuclear Explosions	439
<i>P. Kruger</i>	

UNDERGROUND NUCLEAR EFFECTS II

Cavity Pressure History of Contained Nuclear Explosions	463
<i>C. E. Chapin</i>	

Thermodynamics of the Silica-Steam System	481
<i>O. H. Krikorian</i>	
Comments on Some of the Physical Chemical Questions Associated with the Analysis of Water in Earth Materials	493
<i>E. Catalano</i>	
Underground Nuclear Explosion Effects in Granite Rock Fracturing	505
<i>S. Derlich</i>	
Estimating the Size of the Cavity and Surrounding Failed Region for Underground Nuclear Explosions from Scaling Rules	519
<i>L. A. Rogers</i>	
Scaling Criteria for Rock Dynamic Experiments	545
<i>B. K. Crowley</i>	
Nuclear Ecology or Can a Liberal Be a Conservationist?	560
<i>Professor Edward Teller</i>	
OIL AND GAS	
Hydrocarbon Production with Nuclear Explosives	567
<i>J. W. Watkins</i>	
Economics of Nuclear Gas Stimulation	577
<i>G. W. Frank, H. F. Coffey, and G. R. Luetkehans</i>	
Project Rulison: A Preliminary Report	597
<i>M. Reynolds, Jr., B. G. Bray, and R. L. Mann</i>	
Engineering with Nuclear Explosives near Populated Areas—A Survey from the Technological and Economic Viewpoint	629
<i>K. Parker</i>	
Nuclear Stimulation of Oil—Reservoirs	649
<i>F. Delort and F. Supiot</i>	
Gasbuggy in Perspective	662
<i>A. Holzer</i>	
Determining the Explosion Effects on the Gasbuggy Reservoir from Computer Simulation of the Postshot Gas Production History	698
<i>L. A. Rogers</i>	
Gasbuggy Reservoir Evaluation—1969 Report	722
<i>C. H. Atkinson and D. C. Ward</i>	
An Evaluation of Water Production from the Gasbuggy Reentry Well	732
<i>D. V. Power and C. R. Bowman</i>	
Project Rulison: Film Presentation	752
<i>R. H. Campbell</i>	

RADIOACTIVITY II	
Studies of Radioactivity from Nuclear Explosions for Peaceful Purposes	753
<i>R. A. Siddons</i>	
Gas Quality Analysis and Evaluation Program for Project Gasbuggy	775
<i>C. F. Smith</i>	
Interpreting the Chemical Results of the Gasbuggy Experiment	794
<i>R. W. Taylor, E. L. Lee, and J. H. Hill</i>	
Additional Comments on the Chemical Results of the Gasbuggy Experiment	815
<i>Russell E. Duff</i>	
Behavior of Radionuclides in Nuclear Gas Stimulation Applications	818
<i>C. F. Smith</i>	
A Preliminary Assessment of the Radiological Implications of Commercial Utilization of Natural Gas from a Nuclearily Stimulated Well	831
<i>D. G. Jacobs, E. G. Struxness, and C. R. Bowman</i>	
Study of Chemical Reactions in the Nuclear Underground Explosion—Incidence on Radioactivity	850
<i>J. Picq</i>	

VOLUME 2

MINERAL RECOVERY	
Summary Paper on Nuclear Mining	859
<i>S. D. Michaelson</i>	
Nuclear Technology and Mineral Recovery	864
<i>R. M. Stewart</i>	
In-situ Recovery of Copper from Sulfide Ore Bodies Following Nuclear Fracturing	877
<i>J. B. Rosenbaum and W. A. McKinney</i>	
Particle-Size Distribution Study: Piledriver Event	888
<i>D. D. Rabb</i>	
Chemical Mining of Primary Copper Ores by Use of Nuclear Technology	909
<i>A. E. Lewis</i>	
Overburden Stripping from Deeply Buried Orebodies by Controlled Nuclear Explosive Casting	918
<i>L. W. Saperstein and R. Mishra</i>	
NUCLEAR OPERATIONS	
Nuclear Operations Summary: Engineering Organization for Plowshare Nuclear Operations	931
<i>G. A. Broadman</i>	
Environmental Control for Nuclear Explosives	938
<i>A. W. Lundberg and W. H. Wells</i>	

Integrated Control System for Nuclear Explosives	964
<i>W. F. Ragsdale</i>	
Emplacement and Stemming of Nuclear Explosives for Plowshare Applications	974
<i>J. L. Cramer</i>	
Control of the Dynamic Environment Produced by Underground Nuclear Explosives	979
<i>D. L. Bernreuter, E. C. Jackson, and A. B. Miller</i>	
Interoceanic Canal Excavation Scheduling Via Computer Simulation	994
<i>O. C. Baldonado</i>	
Reliability Implications for Commercial Plowshare Applications	1014
<i>T. D. Brumleve</i>	
SEISMIC EFFECTS	
Explosion-Produced Ground Motion: Technical Summary with Respect to Seismic Hazards	1024
<i>H. C. Rodean</i>	
Prediction of Seismic Motion from Contained and Excavation Nuclear Detonations	1051
<i>R. A. Mueller</i>	
Seismic Motions from Project Rulison	1069
<i>P. C. Loux</i>	
The Effects of the Rulison Event on Buildings and Other Surface Structures	1083
<i>L. Lee and R. E. Skjei</i>	
Origins of Displacements Caused by Underground Nuclear Explosions	1095
<i>J. S. Rinehart</i>	
On the Prediction of Building Damage from Ground Motion	1103
<i>J. A. Blume</i>	
Magnitude Determination for Large Underground Nuclear Explosions	1118
<i>L. D. Porter</i>	
Compressional Seismic Waves Recorded During Underground Nuclear Explosion Tests in Hoggar	1136
<i>H. Ferrieux</i>	
Directivity of Seismic Radiation from a Series of Line Charges	1150
<i>T. J. Ahrens</i>	
WATER RESOURCES DEVELOPMENT	
Review: Water Resources Development	1160
<i>D. K. Todd</i>	
Nuclear Explosives in Water-Resource Management	1164
<i>A. M. Piper</i>	
Project Aquarius—Control of Radioisotopes and Safety	1169
<i>R. Post</i>	

Project Aquarius—Geohydrologic Investigation	1174
<i>W. J. Ganus</i>	
Aquarius Study—Engineering and Economic Considerations	1184
<i>R. F. Griffin</i>	
Mechanics of Slide Dams	1198
<i>G. A. Young</i>	
The Use of a Rubble Chimney for Denitrification of Irrigation Return Waters	1222
<i>R. B. Evans and P. Kruger</i>	
SCIENTIFIC APPLICATIONS	
The Present Status of Scientific Applications of Nuclear Explosions	1246
<i>G. A. Cowan and B. C. Diven</i>	
Use of Nuclear Explosives in Measurement of Nuclear Properties of Fissile Materials	1253
<i>B. C. Diven</i>	
Elastic Neutron Interaction Measurements with a Moderated Bomb Source Spectrum	1257
<i>M. M. Hoffman</i>	
Production of Heavy Nuclides in Nuclear Devices	1269
<i>S. F. Eccles</i>	
The Recovery and Study of Heavy Nuclides Produced in a Nuclear Explosion—The Hutch Event	1283
<i>R. W. Hoff and E. K. Hulet</i>	
Thermonuclear Neutron Sources—A New Isotope Production Technology	1295
<i>R. A. Heckman</i>	
Symmetry of Neutron-Induced ^{235}U Fission at Individual Resonances. III	1306
<i>G. A. Cowan, B. P. Bayhurst, R. J. Prestwood, J. S. Gilmore, and G. W. Knobeloch,</i>	
UNDERGROUND ENGINEERING APPLICATIONS	
Review of Possible Peaceful Applications of Nuclear Explosions in the National Economy of the Soviet Union	1315
<i>P. A. Witherspoon</i>	
Why Nuclear Geostorage Systems for Petroleum?	1322
<i>L. van der Harst and C. F. Knutson</i>	
Technical Considerations for Plowshare Applications to Oil Shale	1343
<i>D. B. Lombard, B. G. Bray, and H. W. Sohns</i>	
Oil Shale Research Related to Proposed Nuclear Projects	1364
<i>H. C. Carpenter, H. W. Sohns, and G. U. Dinneen</i>	
The Economics of Plowshare Geothermal Power	1376
<i>J. B. Burnham and D. H. Stewart</i>	

On the Use of Nuclear Explosives for Stimulation of Geothermal Heat	1384	Possible Techniques for Decontamination of Natural Gas from Gas Wells Stimulated by a Nuclear Explosion	1589
<i>M. D. Nordyke</i>		<i>J. A. Wethington, Jr.</i>	
UNDERGROUND NUCLEAR EFFECTS III		Radioactive Contamination of Oil Produced from Nuclear-Broken Shale	1597
Dimensional Analysis for the Mechanical Effects of Some Underground Explosions	1386	<i>W. D. Arnold and D. J. Crouse</i>	
<i>F. Delort</i>		NUCLEAR EXCAVATION II	
Study of the Mineralogical Transformations of Granite by Underground Nuclear Explosions	1406	Ejecta from Single-Charge Cratering Explosions	1613
<i>J. Faure</i>		<i>R. H. Carlson</i>	
Subsidence Caused by an Underground Nuclear Explosion	1428	An Interior Seaway for Northern Africa	1643
<i>W. W. Hakala</i>		<i>J. B. F. Champlin, J. W. Poston, and J. A. Lake</i>	
Simulation of the Chemical Environment of a Nuclear Explosion with Exploding Wires	1456	Stability of Nuclear Crater Slopes in Rock	1661
<i>W. Meyer and O. U. J. Block</i>		<i>R. W. Fleming, A. D. Frandsen, and R. L. LaFrenz</i>	
Possible Hazard Reduction by Using Distributed Phased Nuclear Explosions	1474	A Concept of Row Crater Enhancement	1679
<i>F. Chilton and J. Cheney</i>		<i>B. B. Redpath</i>	
NUCLEAR EXCAVATION EFFECTS		Torres Strait: A Channel Clearing Project	1692
Review: Airblast Effects	1485	<i>S. Bankert</i>	
<i>J. W. Reed</i>		A Study of Underground Explosion Cratering Phenomena in Desert Alluvium	1701
Close-in Airblast from Underground Explosions	1508	<i>H. C. Saxe and D. D. DelManzo, Jr.</i>	
<i>L. J. Vortman</i>		A Simple Technique to Determine the Size Distribution of Nuclear Crater Fallout and Ejecta	1726
Prediction of Gamma Exposure Rates in Large Nuclear Craters	1544	<i>B. D. Anderson, II</i>	
<i>T. M. Tami and W. C. Day</i>		Schooner Ejecta Studies	1746
RADIOACTIVITY III		<i>R. W. Henny</i>	
Reduction of Radioactivity Produced by Nuclear Explosives	1563	Closing Remarks	1771
<i>R. M. Lessler</i>		<i>G. C. Werth</i>	
Radioactive Contamination of Copper Produced Using Nuclear Explosives	1569	LIST OF ATTENDEES	1776
<i>D. J. Crouse, W. D. Arnold, and F. J. Hurst</i>		AUTHOR INDEX	1785

MINERAL RECOVERY

A SUMMARY PAPER ON NUCLEAR MINING

S. D. Michaelson 1/

Fifteen years ago a handful of men began to dream of the potentials of nuclear energy in peaceful applications. In 1957, AEC's Plowshare program was organized to promote and coordinate the work which might convert the dreams into realities. Then, some specific ideas for using nuclear energy in mining were set down in meaningful detail and with reasonable thought. In the 12 years of the Plowshare program nuclear energy concepts for mining have been developed in increasing detail and for a fairly broad range of possible applications. Although it may seem, at times, that progress is slow and month-to-month achievements almost nonexistent, a closer look throws a somewhat different light on the picture.

In the first 7 years of Plowshare, from 1957 through 1964, the most obvious mining applications were delineated. These included the use of nuclear explosives to break ore for block caving, for in-situ leaching, and for stripping overburden from large low-grade deposits. Although numerous variations of these applications have been proposed in recent years, these three basic concepts still appear to hold the greatest potential. During those same seven years a number of DOD and Plowshare tests, involving both conventional and nuclear explosives, were conducted so that the phenomena and parameters bearing on mining applications could be evaluated in addition to acquiring other data. The tests, such as Projects Gnome, Sedan, Hard Hat and Danny Boy, have been discussed and reported at these and other meetings, and it would be redundant to review them now. Suffice it to say that from these tests and related work in AEC laboratories, scaling laws for relating yield, crater size, chimney size, fracture extent, and rock types were largely confirmed. Chimney rubble size distribution was determined and contamination problems were evaluated. Aside from these findings, however, the most important development during that 7-year period was the policy that relevant engineering data would be released for industry itself to evaluate specific potential applications for nuclear explosives.

On May 6, 1964, the Atomic Energy Commission released a schedule of projected charges for peaceful nuclear explosive devices. Although certain costs such as safety related costs were not then described (and are still rather nebulous), the charge schedule, together with engineering design parameters from the tests, did permit industry to estimate costs of breaking rock with cratering, retarc or confined explosive techniques. With due recognition to such fine papers as "Nuclear Explosives in Mining", by Flangas

1/ Chief Engineer, Kennecott Copper Corporation, Metal Mining Division, Salt Lake City, Utah

and Rabb, and others working in the field, it was not until these projected charges were published in 1964 that industry could project nuclear explosive excavation costs to make meaningful evaluations of specific nuclear explosive applications with anywhere near acceptable degrees of confidence.

The past five years have not produced any fundamentally new concepts for the mining industry. Nevertheless, these years have been fruitful. Any undertaking is rendered more efficient as the unknown quantities are reduced. The recently published technical literature demonstrates that our predictive capabilities relating to nuclear explosives have come a long way in the recent period. In mining, as in any other nuclear explosive application, we must be concerned with weather, air blast effects, ground motion, and the response of nearby structures. It would be unnecessary and presumptuous to recount the technical advancement in each of these areas. It is important, however, to recognize the beneficial effect of these advances on costs of the safety and protection programs that must be borne by the user. Additionally it is important that we can benefit from our improved ability to predict the in-situ blast effects, i.e., cavity formation, size, and fracturing effects in the halo area. Findings regarding permeability such as resulted from the Pile Driver studies are obviously important in evaluating in-situ leaching applications.

I would be remiss even in this Mining Session if I did not recognize the Plowshare experiments of Rulison and Gas Buggy, for these are the first two profit-oriented tests which have been conducted to date by industry. With our long and extensive involvement in Project Sloop, I know from experience that these two projects have made major contributions for all potential users of nuclear explosives. Some of these contributions are obviously in the Research and Development category, but they have also greatly assisted us in providing costs and other pertinent data for fielding such a test. The participants are to be commended for releasing to industry so much of the pertinent information and planning requirements for these tests.

There is another important aspect to the achievements of recent years and this has to do with the several proposed nuclear explosive mining schemes which have been proposed. It is significant that these schemes now are coming from mining people, i.e., from people with particular applications for particular locations and unique orebodies. From these studies we are deriving both a diversity of ideas and a more practical insight into the technical and public-related problems inherent in nuclear applications for mining.

The Sentinel Mining Company of Australia studied the possibility, and subsequently shelved the concept, of using nuclear explosives to create a mine harbor at Cape Keraudren. Their apparently insurmountable problems in attempting to hurdle political and safety obstacles are most enlightening. I understand from news reports that similar problems are coming to light in the proposed plan of Hancock and Wright for mining an iron orebody at Wittenoom Gorge. It is interesting to note that this latter plan has apparently satisfied technical and economic criteria.

"Project Sloop", a scheme proposed over ten years ago by Kennecott for testing the application of nuclear explosives for in-situ leaching of copper has not, as yet, reached the contract stage. Nevertheless, tech-

nical progress has been made and because of my close association with this project I should like to report on the latest developments. To review, the project proposes to fracture a typical large deep-seated low-grade copper orebody near Safford, Arizona. The test would include injection of acid solutions through drill holes and collection of the copper-bearing solutions in underground galleries developed by rehabilitating an existing shaft and drift. The anticipated cost of the experiment was approximately \$13 million. As originally planned and conceived, Kennecott Copper and the Atomic Energy Commission each were to assume approximately one-half of the total cost. Kennecott approved the necessary funds three years ago but at approximately that same time, Federal budget restrictions precluded any significant cost participation by the Atomic Energy Commission. The project, therefore, was set back in time to allow Kennecott an opportunity to re-evaluate the plan and its potential in view of the increased cost they would have to shoulder. These evaluations are now complete and I expect that a decision regarding continuation of the work with AEC should be made soon.

I believe that Plowshare developments over the last several years have not significantly changed the economics of nuclear explosives for mining. William Hardwick in a Bureau of Mines Report of Investigations (No. 6696) published in 1967, presented two tables of estimated costs for breaking rock. He predicted costs varying from 9.2 to 1.8 cents per ton with 10 to 100-kiloton devices placed at optimum depth for breakage. He further indicated that at minimum confinement depths, the cost would increase by a factor of 6 and be 55.2 to 10.8 cents per ton for similar device yields. His costs refer to the ore broken in the retarc and chimney respectively. Our cost estimates for the Project Sloop concept indicated a somewhat higher cost due to the increased depth of burial required and the resulting smaller chimney. His cost basis is apparently the published projected charges for thermonuclear explosives plus a minimal allowance for related construction and safety. We believe his costs could be achieved, but only if the applications were carried out on a routine and sustained basis so that the high safety and support costs could be distributed over a number of detonations. By comparison, current drilling and blasting practice in open pit mines gives rock fragmentation costs of approximately 5 cents per ton and total mining costs including loading, haulage and general, in the range of 25 to 35 cents per ton of material handled.

As long ago as 1961 Flangas and Rabb estimated mining costs of two to three dollars per ton for an underground nuclear explosive stoping concept. This estimate was based on results of the Ranier experiment. Today's mining costs for larger deposits are in this same range with conventional methods. Therefore, it appears that, at these cost levels, a nuclear device does not represent a major breakthrough for underground mining but does, instead, offer an alternative technique for use when conventional methods, such as block caving in competent ground, are marginal, sub-marginal, or not applicable. In view of this cost picture, I believe it is safe to say that mining schemes using nuclear explosives fall generally in the same cost frame as conventional mining schemes. This would indicate that a purely technical decision to use either nuclear explosives or conventional techniques will, in most cases, be based on the specifics and subtleties of each deposit and location. Under this assumption we will be forced to examine not general concepts, but the particular mining economics of each situation in complete

detail before we can say that one alternate or the other holds greatest potential.

The Safford orebody which I mentioned before in regard to Project Sloop is very large, is overlain by several hundred feet of completely barren, hard cap rock and the portions of interest contain approximately one-half of one percent total copper. The nuclear explosive concept for development of this property includes placement of devices at the lower boundary of the easily leachable oxide ore zone. The conventional mining scheme would involve stripping and mining followed by heap leaching. Our analyses indicate that it would take approximately fifteen 20-kiloton contained nuclear devices to adequately fracture the portion of the orebody suitable for in-situ leaching. This scheme does not contemplate leaching only broken ore in the chimney but would also include leaching of the fractured halo zone.

A nuclear fracturing in-situ operation has a major economic advantage in that the ore does not have to be transported. There is, however, more certainty that less of the total mineralized zones in deposits like Safford can be in-situ leached after nuclear blasting than can be heap leached in conventional mining.

If you will recall the various schemes which you have seen proposed over the last years you will recognize that, like Sloop, many include the use of multiple devices of approximately the 20-kiloton size. Due to safety and shock problems associated with a nuclear detonation it is unlikely that devices much larger than 20 kilotons will find broad mining application in this country. It also appears unlikely that cratering and retarc applications will be acceptable to the AEC and public in the near future except in isolated instances. Based on current knowledge it can be assumed that a 20-kiloton device will achieve broken rock in a chimney for approximately 50 cents per ton and that the chimney will contain approximately one million tons. It follows that for a commercial operation, at least ten devices and probably several times ten devices, would be required for full development of a major orebody, regardless of whether the plan is for in-situ leaching or for some caving method. The tremendous power of even low-yield devices is sufficient to collapse mine openings located nearby. This creates a problem which I am sure has come up in all of the plans which have been proposed. The miner is faced with two alternatives: all or a substantial portion of the orebody can be fractured initially by detonating a series of devices over a period of months; or as a second alternative, a small portion of the orebody can be developed and completely mined out before an adjacent area is developed. The first alternative necessitates tying up large sums of money for long periods of time and carries the undesirable possibility that changing economic conditions would render the development inefficient or useless. The second alternative could involve destruction of costly underground development or preclude orderly progress through the orebody.

I have not brought up this problem to discourage the application of nuclear devices in mining. On the contrary, I have brought it up because I believe it is typical of the major hurdles being encountered by those attempting to develop applications and the sooner we focus attention on them, the sooner we can achieve economic utilization of this alternate explosive. There is a solution to the problem mentioned. It is in knowing precisely what inter-

action can be expected from one detonation to another and how best to protect previously developed underground openings.

The AEC, through its Plowshare organization, has in the past conducted numerous tests which have provided certain design parameters for mine applications. It is time now, I think, that the Plowshare organization consider a new series of tests, at N.T.S. if desired, to answer the particular problems of potential user groups.

The mining industry uses nearly one million tons of explosives per year in the United States alone. We have some considerable knowledge from this long and extensive use of design techniques which achieve efficient explosive utilization for routine and specialized applications. Certainly we recognize our needs and the specific problems that are encountered more fully than many non-industry personnel. I suggest, therefore, that designs for Plowshare tests be developed jointly by the Plowshare organization and industry to assure that reasonable and appropriate questions concerning industrial applications are answered.

On November 10, 1969, the AEC formally announced the establishment of the Office of Peaceful Nuclear Explosives. This was a long-awaited and vitally-needed organizational change and should greatly facilitate the development of mining applications. I trust that this office, in recognition of the heavy cost of nuclear mining experiments and the broad potential benefits for efficient mineral resource development, will develop an easy interchange with industry so that both parties can discuss, plan and decide where and how to use nuclear devices to decrease mining costs and thereby increase the nation's capability to supply its metal needs at competitive prices.

NUCLEAR TECHNOLOGY AND MINERAL RECOVERY

Richard M. Stewart, Director Mining Research
Karl E. Niermeyer, Senior Research Engineer
The Anaconda Company
Salt Lake City, Utah

You will notice as I proceed that the proposed title of my talk, "Nuclear Technology and Mineral Recovery," becomes rather limited in scope. The particular aspect of nuclear technology most applicable to the mineral field, as has been pointed out by various authors, is nuclear blasting. The prime target for this nuclear blasting has usually been a large disseminated deposit of copper mineralization which, because of large dimensions, employs the nuclear devices most effectively.

From the work of the AEC we know that the larger nuclear devices fragment rock for a lower energy cost per unit of ground broken than do smaller nuclear devices or chemical explosives.

A mineralized deposit near the surface is usually not amenable to nuclear fragmentation, nor are the more deeply buried thin deposits. Also, one would not anticipate fragmenting a zone of excessively erratic mineralization with nuclear devices.

Many of our mineralized areas would be eliminated using the above criteria, so at this point you are well aware that my self-imposed limitation is to nuclear blasting and large disseminated copper deposits.

As with most other industries, copper mining faces rising costs and greater demands for its products.

One of the rising cost features peculiar to extractive industries is the reliance placed on production from lower grade deposits as the higher grade deposits are depleted. As the grade or metal content of an orebody decreases more material must be handled to produce a given amount of metal. The increased volume of ore which must be handled as the grade declines requires expansion of facilities and higher capital expenditures. Expansion of facilities for mining, milling, and concentrating of the ore increases the per unit capital cost of the end product--copper. Increased copper consumption will aggravate this situation with demand for more metal, much of which will have to be obtained from lower grade deposits.

As the higher grade deposits are depleted, future production will come from those deposits which cannot be exploited economically today. Therefore, the small, high-grade deposit which presently cannot support the necessary capital expenditures, the lower

grade deposits, the deeply buried deposit, and those which have a high ratio of waste to ore will be the probable sources of copper in the future.

We have increased the size of equipment and improved our machine efficiencies to keep up with the demands made by the copper industry. As emphasis is placed on lower grade deposits to meet future demand, new methods offering opportunities for improved costs must be considered.

Most familiar of the proposed new methods is in situ leaching, often mentioned in conjunction with nuclear blasting. The union of the two technologies originated with the initial consideration of Kennecott's Project Sloop in 1958. Nuclear blasting would be used to fragment the orebody, after which the solution will be introduced at the top of the column of broken ore, leaching out copper values on its migration to the bottom of the broken zone, where the solution will be collected and processed through the recovery system.

Although the physical handling of ore and waste and their costs are eliminated, various investigators have raised many questions which affect the economics of an operating system. Questions of total copper recovery, rate of copper recovery, radioactive contamination, fracture healing, precipitation of iron compounds in the leaching zone, reagent consumption, solution collection, and others have to be answered before we know if this new technology is one of the viable solutions to the problems confronting the industry.

Many investigators--Heiss and Morgenstern, Hardwick, Smith and Young, Hansen, Thomas, and others--believe nuclear blasting and in situ leaching are compatible and will compete economically with conventional systems.

Because statistics have not been kept on dump leaching operations for any great length of time and because of the difficulty of sampling a dump during and after leaching, copper recovery figures are not too reliable. At one Western operation, over a five-year period a copper recovery rate of 4-1/2% per year was recorded. The operator assumes that the rate of recovery will fall, but is reluctant to estimate how much and when.

The British Columbia Research Council has run column leaching tests on samples from various locations. From one sulfide dump sample under their test conditions, 34.1% of the copper was extracted in 600 days. Of this percentage, 1.9% was extracted in the last one-half year. In a similar test performed on an oxide dump sample, 45.8% was extracted in 600 days with only 0.9% extracted in the last half year of the test.

Other tests by the B.C. Research Council checked the variation in leachability with depth in copper sulfide mineralization. The microbiological extraction of copper declined with increasing depth from 59.3% for the interval of 45 ft to 145 ft to 26.6% for the interval of 260 ft to 360 ft. Sampling showed that a biologically sterile solution extracted 26.5% of the copper in the uppermost 10 ft and only 12.6% in the lower 10 ft of a gross sample taken between the depths of 60 and 110 ft. (See Figure 1.)

Other investigators feel that a recovery factor of 30% is about the best that can be expected in a dump leaching operation. Many people in the industry also express views that the recovery associated with dump leaching will be this low.

In dump leaching operations because more copper is ordinarily added to the pile per day than is extracted, the recovery factor is of little importance. The leaching operation is usually a profitable auxiliary to a conventional open pit operation in which the ore is mined and then processed through a concentrator.

In a nuclear in situ application, however, the recovery factor becomes much more important, the copper output from the mineralized zone would have to pay for the cost of the entire operation. Fracture healing, blinding by clays and precipitates, and channeling are all factors which will govern how much of the copper mineralization is actually contacted and hence dissolved. Loss of dissolved copper through contact with clay will decrease the percentage recovered. J. K. Grunig pointed out that he had not arrived at an adequate explanation for copper lost through this mechanism. Compaction of dumps by wheeled vehicles, which adversely affects the distribution of the leaching solution in the normal dump leach operation, will be absent in a nuclear in situ operation. Another factor which affects the copper recovery is solution recovery. Any solution which is lost through the cavity walls or otherwise bypasses the solution collection circuit carries with it contained copper which decreases the overall recovery factor. Smith and Young in their paper, "Nuclear Explosives and Mining Costs," state that "The in situ leaching will recover 40% of the ore (probably the most difficult assumption to justify)."

The consensus is that the copper recovery of the conventional oxide plant is much higher than the recovery projected for a nuclear in situ operation.

In considering an hypothetical mining situation, the present method of production of copper would be used to the lowest economically feasible grade to both conserve resources and return the minimum acceptable profit. Below that lowest feasible grade we have the choice of leaving the mineral values in place in the ground, raising the price of copper, or of using the new technology. With the present production processes and copper prices, we would have a mineralized zone; whereas, with the nuclear in situ technology there would hopefully be an orebody. The difference between the mineralized zone and the orebody is expressed in one word--profitability.

At a recent meeting of the Atomic Industrial Forum (AIF), in the presentation by William L. Oakley on the "Hard Core Costs of Projects Gasbuggy and Rulison," the hard core costs were shown to be on the order of \$2.9 million each. A concluding statement in this paper was, "I am optimistic that we can meet the \$1 to \$1.5 million target which has sometimes been given as the economic test. Plowshare must face initially."

Using the \$1.5 million figure for all nuclear related costs and assuming that a 50 kiloton device in a fully contained condition will break roughly five million tons (see Figure 2), the nuclear related costs per pound of copper recovered from various grades of material at different copper recoveries will be as

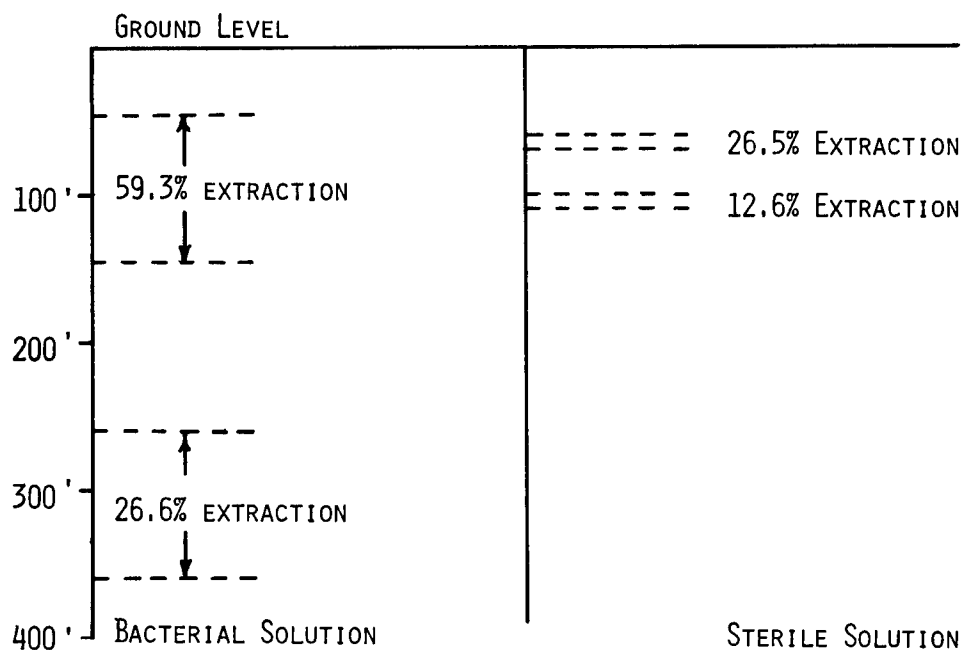


FIGURE 1
VARIATION OF LEACHABILITY WITH DEPTH

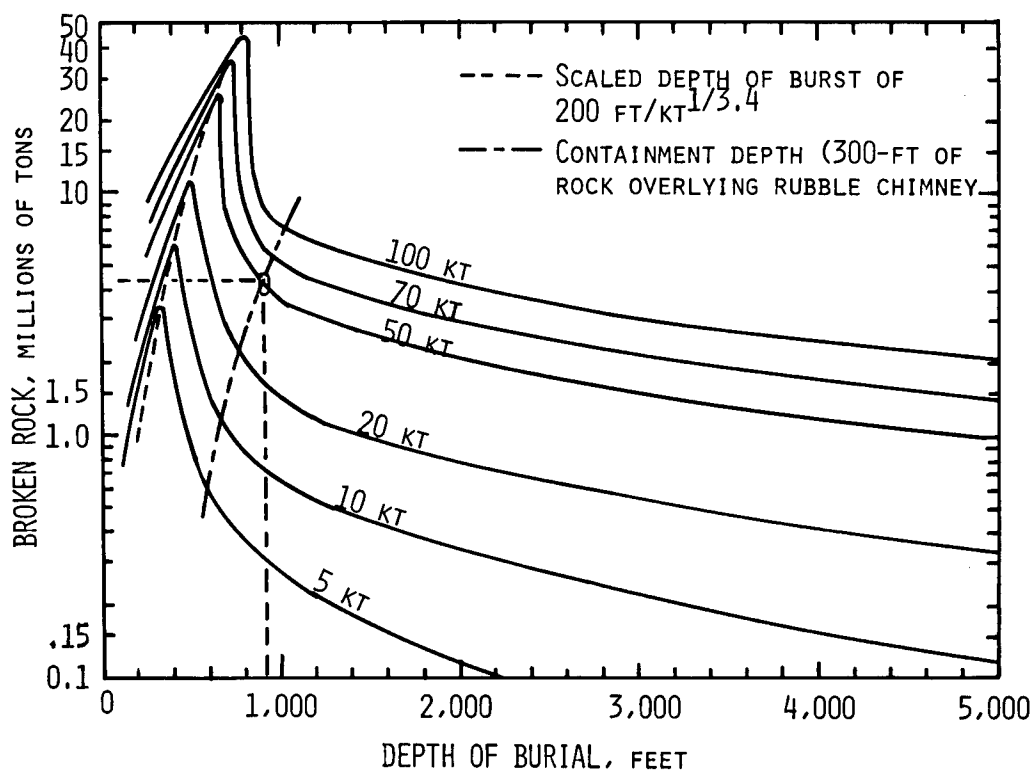
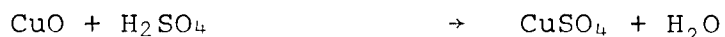


FIGURE 2
TONNAGE CURVES OF ROCK BROKEN BY INTERMEDIATE UNDERGROUND NUCLEAR EXPLOSIONS, (COURTESY, LAWRENCE RADIATION LABORATORY, UCRL 12180.)

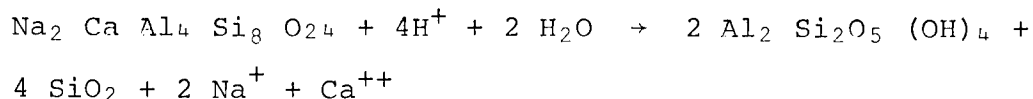
shown in Figure 3. If the containment condition is altered to a retard depth and if all other conditions remain equal, the fracturing cost per pound of copper recovered would be on the order of 1/6 the costs since the volume of rock broken would be six times as large. The retard depth is that depth of burial at which an explosive produces an inverted cone of fragmented material, the surface elevation of which is greater than the elevation of the original ground. Maximum tonnage is broken with an explosive in this configuration.

At this point, it should be noted that the copper mineralization in the fracture halo which surrounds the cavity is not considered in the following discussion, although if it were recovered the unit fracturing costs would be decreased.

A leachable ore of copper is commonly one which contains the oxide and simple sulfide minerals of copper. If the mineralized zone is deficient in iron pyrite which breaks down in the presence of water and oxygen to form sulfuric acid, then all of the acid for a leaching operation must be added. The acid is consumed by either the oxides or simple sulfides of copper in the ore to form copper sulfate as follows:



In the cementation portion of the circuit, free sulfuric acid reacts with iron to form ferrous sulfate. Other consumers of acid are the clay and carbonate constituents of the rock itself. A typical clay reaction would be



Since the acid consumption is primarily dependent upon factors other than the amount and kind of copper mineral present, it appears more realistic to assume a feed rate of acid per ton of material rather than on the basis of pounds of acid per pound of copper produced.

In Figure 4 the acid cost per pound of recovered copper is indicated at different recoveries for various grades of ore when the acid cost is \$20 per ton. The acid consumption of 50 lbs per ton of material presupposes an orebody which is low in acid-consuming constituents.

Iron consumption, as has been pointed out previously, is dependent upon the hydrogen ion and also the ferric ion concentration in the leaching solution. Table 1 shows some typical iron consumption figures for various operating cementation plants. At a cost of \$50 per ton for iron, the iron cost per lb of recovered copper ranges from 3-1/4¢ to 7-1/4¢.

The next consideration is the cost of a solution recovery system and a copper recovery system. The nuclear device previously mentioned had a 50-kton yield. For containment, this device

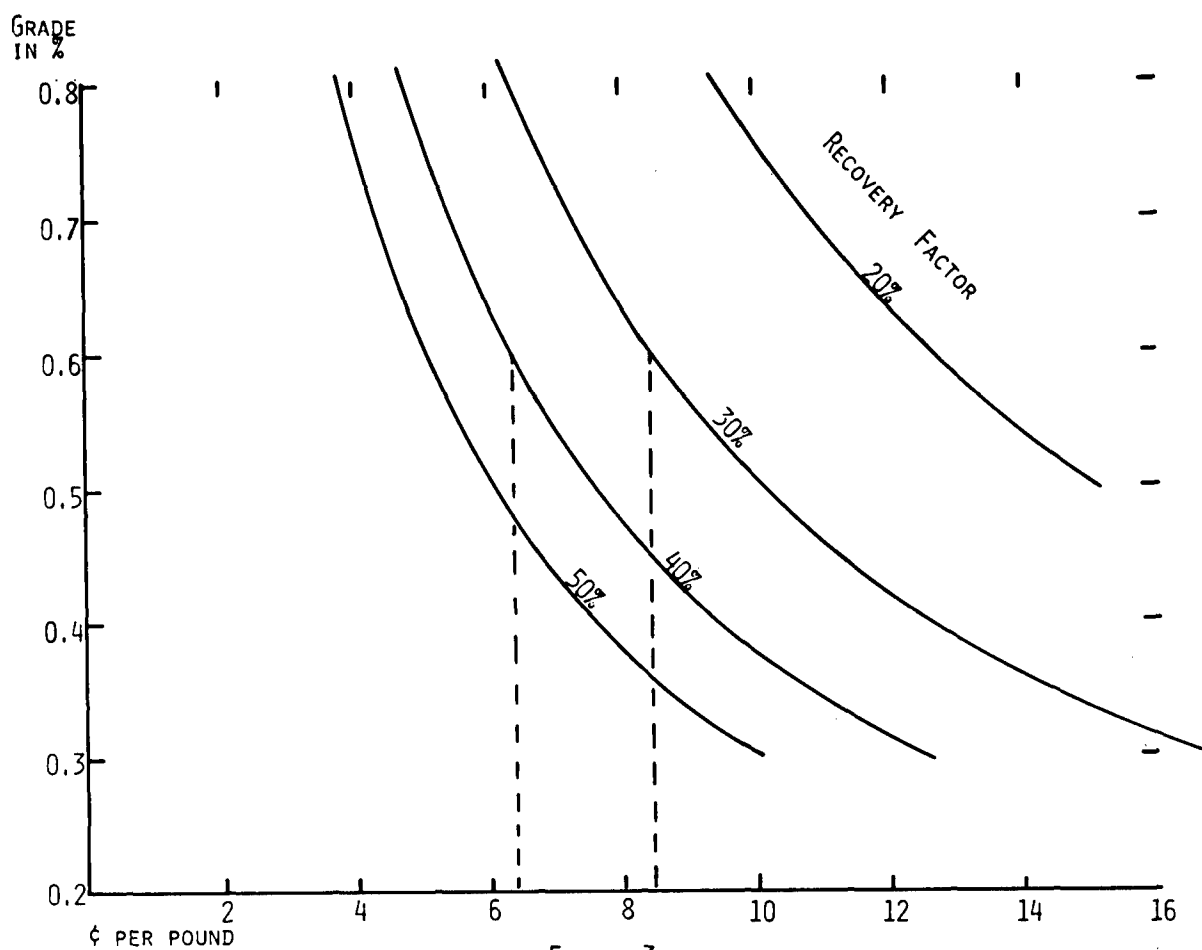
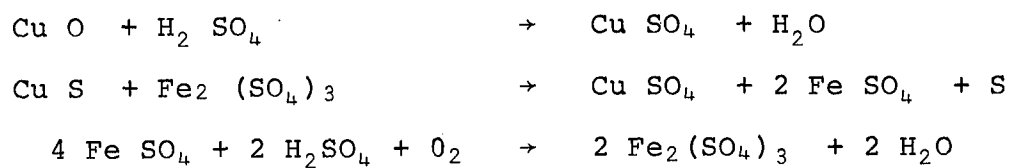


FIGURE 3
FRACTURING COST IN CENTS PER POUND OF RECOVERED COPPER



Typical Copper Mineral Reactions

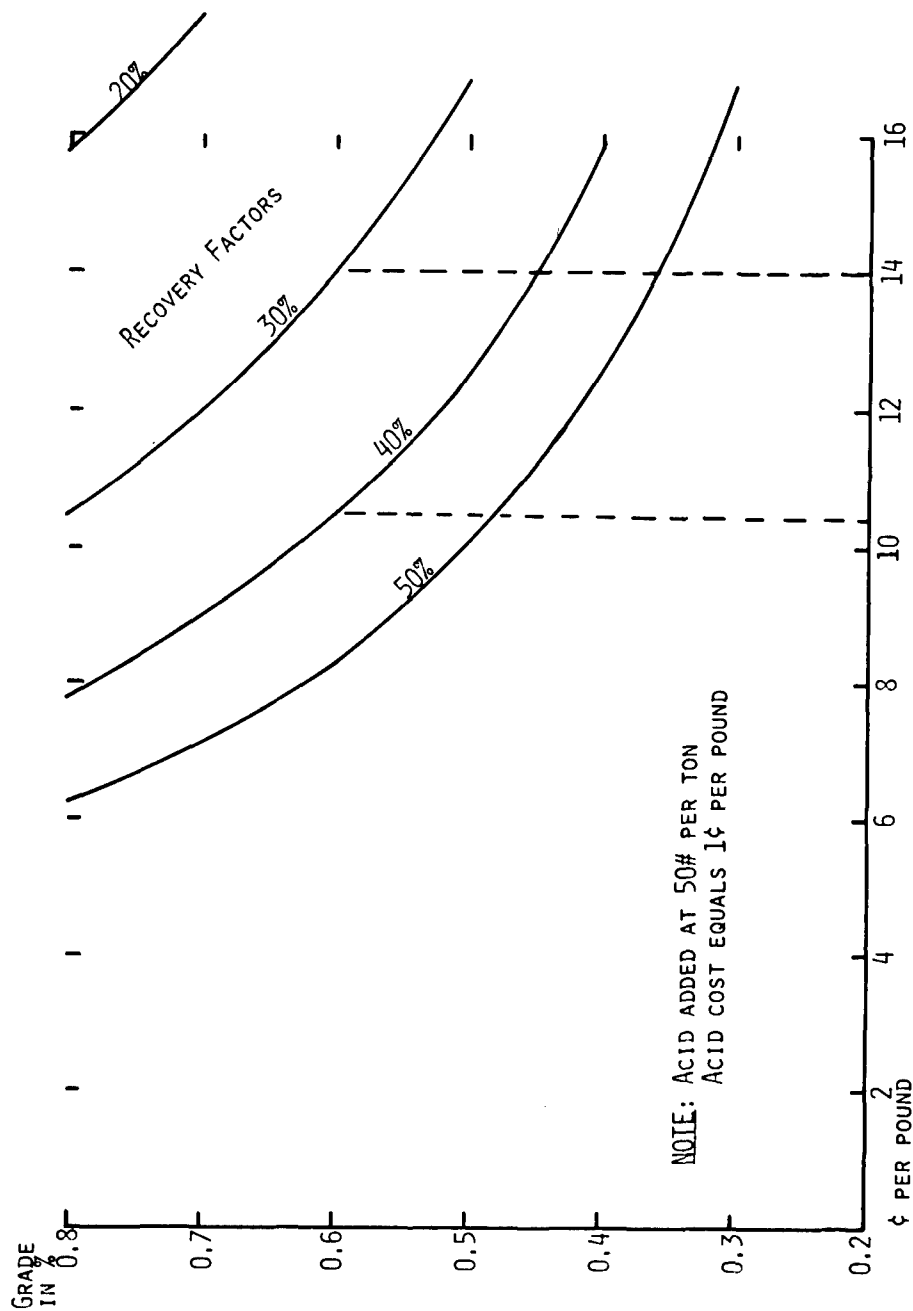
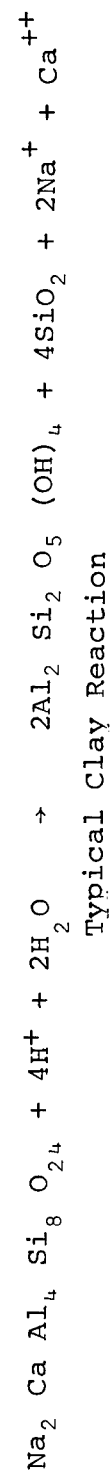


FIGURE 4
ACID COST IN CENTS PER POUND OF RECOVERED COPPER

Andesine

Kaolinite



would be buried at a depth of roughly 900 ft and would form a chimney 600 ft high which should approximate the thickness of the mineralized zone. Lawrence Radiation Laboratory (LRL) information shows that minor damage to mine workings is sustained at a distance of roughly 3800 ft. (See Figure 5.)

From a 0.6% Cu ore and using a 40% recovery factor, 24 million lbs of copper would be produced from the 5 million tons broken by a contained 50-kton device. This amount of copper could be produced in two years from a pregnant solution with a concentration of one gram per liter flowing at the rate of 2500 gpm.

Let us assume then that each 50-kiloton blast will fragment sufficient copper-bearing rock to sustain a recovery plant for two years. Let us also assume that the recovery plant is written off in a period of ten years.

An underground recovery system is based on sinking a shaft and driving access drifts from which solution collector holes would be drilled upward into the chimney. The shaft would be located outside the damage range (3800 ft) of subsequent nuclear shots. The \$2.5 million cost shown in Table 2 distributed over 120 million lbs of copper, ten years production, amounts to 2¢ per lb of copper produced.

The plant capital cost for a flow of 2500 gpm is \$1.25 million when the cost for each 1000 gpm of capacity is \$0.5 million. Therefore, over a ten-year plant life the capital cost is 1¢ per lb of copper produced.

Table 3 shows the pound cost figure for a 0.6% grade ore at different recoveries. The total cost of labor has been taken as 2¢ per lb, and the marketing cost, including smelting, refining, and transportation, is 8¢.

An alternate method of recovery of copper from a pregnant solution should also be considered, although the benefits derived are not limited to a nuclear in situ operation. In a solvent extraction-electrowinning system, the copper-laden solution is placed in contact with an organic compound which has an affinity for the copper ion. This copper-rich compound is then processed in an aqueous phase and the copper ions are stripped from it. The organic material is then recirculated to continue its function of concentration of the copper ion. The copper-rich aqueous solution is then introduced into electrolytic cells where the copper is electroplated on cathodes. The product is a high purity copper which requires no smelting or refining.

This technique eliminates the need for iron scrap, and also produces sulfuric acid in the electrolytic cell which can be put into the leaching circuit. Typical plant capital costs for this type of installation per daily ton of copper produced are \$200,000, which includes both the solvent extraction and the electrowinning sections.

Table 4 shows a comparison of estimated costs for a cementation circuit and a solvent extraction-electrowinning circuit. The possible savings of 5¢ per lb of copper recovered warrants serious consideration of this process.

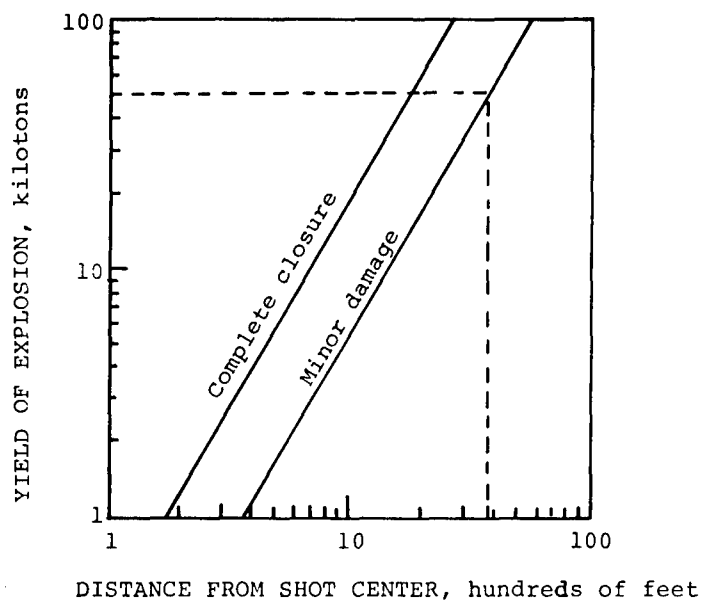


Figure 5
Damage to Mine Workings from Nuclear
Explosions in Granite Rock.
(Courtesy, Lawrence Radiation
Laboratory UCRL 14201.)

Table 1

Iron Consumption at Various Properties

<u>Plant</u>	<u>Pounds of Iron per lb of Copper*</u>	<u>Iron Cost per lb of Recovered Copper**</u>
Rio Tinto, Spain	1.4	
Silver Bell, Arizona	1.5	
Ray, Arizona	1.8	
Esperanza, Arizona	1.35	
Bagdad, Arizona	1.7	
Miami, Arizona	1.3	3.25¢
Cananea, Mexico	2.9	7.25¢

* Fracturing a Deposit with Nuclear Explosives and Recovering
Copper by the In-Situ Leaching Method by William R. Hardwick.

** Calculated by author, using iron cost of \$50 per ton.

Table 2

Capital Costs - Underground Recovery System

Shaft	1000 ft @ \$700/ft	=	\$ 700,000
Drifts	8000 ft @ \$ 75/ft	=	600,000
Drill Holes	40,000 ft @ \$20/ft	=	800,000
Miscellaneous and Contingency		=	<u>400,000</u>
Total			<u>\$2,500,000</u>

Table 3

Production Cost per Pound of Copper

	Recovery Grade	40% 0.6%	30% 0.6%
Capital		3¢	4¢ *
Labor		2¢	2¢
Fracturing **		6.3¢	8.3¢
Acid **		10.5¢	14¢
Iron ***		3.5¢	3.5¢
Smelting, Refining, etc.		<u>8¢</u>	<u>8¢</u>
Total		<u>33.3¢</u>	<u>39.8¢</u>

* Capital cost calculated as being inversely proportional to the % recovered.

** From Figures 3 and 6.

*** The iron consumption is minimal at 1.4 per lb of copper.

Table 4

Cementation vs. Solvent Extraction and Electrowinning
in Cents per Pound of Copper Produced

		Leach and Precipitation	SX EW
Capital	Recovery	1.0¢ 2.0¢	2.0¢ 2.0¢
Labor		2.0¢	4.0¢
Supplies	(included in iron, acid, etc.)		3.0¢
Fracturing		6.3¢	6.3¢
Acid		10.5¢	9.0¢ *
Iron		3.5¢	-
Smelting, Refining, etc.		8.0¢	Transportation 2.0¢
		<hr/>	<hr/>
	Total	<u>33.3¢</u>	<u>28.3¢</u>

* The acid generated valued at 1½¢ is fed back into the leaching circuit.

In situ leaching has been practiced for years in underground copper mines throughout the world. Ground which has been fragmented due to subsidence over old mined-out areas and low-grade mineralization, which has remained after block caving operations, has been leached successfully. In a nuclear in situ operation we intentionally fragment the rock and then leach it to extract the values. Most of the development work for a solution collection system in old mine areas and block caved areas had been done during the original mining operations, which paid for driving these openings. In virgin ground, the cost of this development work must be borne by the in situ leaching operation. We know that in situ leaching as a method for the extraction of copper values is physically feasible. We need to know if the nuclear in situ method is economically feasible. The answers to questions of total recovery, rate of recovery, contamination, etc., must be found so that we know if we are talking of mineralized zones or orebodies.

Bibliography

1. Smith-Young, 1960, Nuclear Explosives and Mining Cost; UCRL 5928.
2. Flanges-Shaffer, 1960, Application of Nuclear Explosives to Block Caving Mining; UCRL 5949.
3. Holmes and Narver, 1968 (?), Projects Utilizing Nuclear Explosives.
4. Rodean, 1967, Research for Understanding and Constructively using Underground Nuclear Explosives; UCRL 50276.
5. Rawson, 1966, Industrial Application of Contained Nuclear Explosives; UCRL 14756.
6. Hansen, Sept 1965, Nuclear Blasting: Space Age Mining Tool Ready for Use; *World Mining*.
7. A New Reagent for Liquid Ion Exchange Recovery of Copper; *Mining Engineering*, Dec 1965.
8. Bluebird Mine Boosts Output New Electrolytic Plant to be Built, *EMJ*, Oct 1967.
9. BC Research Council Review of Progress, Nov 1968.
10. R. S. Shoemaker and R. M. Darrah, The Economics of Heap Leaching; *Mining Engineering*, Dec 1968.
11. J. K. Grunig, 1966, Some Factors of Ore and Solution Chemistry in the Heap Leaching of Copper Ores. (Paper at Pacific Northwest Minerals and Metals Regional Conference)
12. W. L. Oakley, 1969, Hard Core Costs of Projects Gasbuggy and Rulison; Atomic Industrial Forum, Dec 1969.

IN SITU RECOVERY OF COPPER FROM SULFIDE ORE BODIES
FOLLOWING NUCLEAR FRACTURING

by

Joe B. Rosenbaum^{1/} and W. A. McKinney^{2/}

ABSTRACT

Leaching now yields about 12 percent of the Nation's annual new copper production. About 200,000 tons of copper a year is being won by heap and vat leaching of ore, dump leaching of waste, and in-place leaching of caved underground workings. Although in-place leaching was practiced as long ago as the 15th century, it is little used and contributes only a few percent of the total leach copper production. Current technology in this area is exemplified by practice at the Miami, Ariz., mine of the Miami Copper Co.

Despite its limited use, the concept of extracting copper by in-place leaching without physically mining and transporting the ore continues to present intriguing cost saving possibilities. Project SLOOP has been proposed as an experiment to test the feasibility of nuclear fracturing and acid leaching the oxidized portion of a deep ore body near Safford, Ariz. However, the bulk of the copper in deep ore deposits occurs as sulfide minerals that are not easily soluble in acid solutions.

This paper explores the concept of in-place leaching of nuclear fractured, deeply buried copper sulfide deposits. On the assumption that fracturing of rock and solution injection and collection would be feasible, an assessment is made of solution systems that might be employed for the different copper sulfide minerals in porphyry ore bodies. These include the conventional ferric sulfate-sulfuric acid systems and combinations of sulfide mineral oxidants and different acids.

^{1/} Research Director

^{2/} Supervisory metallurgist

The authors are with the Salt Lake City Metallurgy Research Center, Bureau of Mines, U. S. Department of the Interior, Salt Lake City, Utah.

INTRODUCTION

The feasibility of Project SLOOP, an experiment to investigate nuclear fracturing and in-place leaching of copper from a buried oxide ore body, is being considered as a joint undertaking of the Kennecott Copper Co., the Atomic Energy Commission, and the Interior Department's Bureau of Mines. The project is described in a report issued by the Atomic Energy Commission in June 1967 (1,4).^{3/} A 20-kiloton blast, to be followed by leaching of the oxidized copper minerals from the chimney and surrounding fractured zone by sulfuric acid solution, is contemplated.

The Safford, Ariz., copper ore body contains about 900 million tons of oxidized ore overlying an equal or greater tonnage of ore in mixed oxide-sulfide, and sulfide ore zones. Oxidized copper minerals, such as those in the Safford deposit, are soluble in dilute sulfuric acid solution. Vat leaching tests by Kennecott of oxide ore from underground development showed 70 to 80 percent of the copper was extracted in 7 days from ore crushed to pass a 3/8-inch screen. Although about half of the copper in the Safford deposit occurs as readily acid soluble, oxidized minerals, the copper in most deep U. S. deposits that might be fractured by a nuclear explosion is present as relatively acid insoluble sulfide minerals.

Dilute sulfuric acid solution alone is not an effective solvent for copper sulfide minerals; oxidation of the sulfides to copper oxide or sulfate must first take place. Air and ferric iron are the oxidants used in leaching sulfide copper from waste dumps and caved mine workings. Bacteria present in all dumps and mines accelerate the oxidation of sulfides by air. They are most effective at temperatures of 35° C and a solution pH of 2.0 to 2.5 (8, 13). When utilizing conventional dump and caved ore leaching practice, the sulfide minerals are dissolved at a rate 100- to 1,000-fold slower than the oxide minerals. The slowness with which sulfide minerals dissolve must be seriously considered in assessing the feasibility of underground fracturing and in-place leaching of copper deposits. In the absence of directly applicable field experience in leaching copper from broken and fractured in-place sulfide minerals, some useful guidance in projecting copper recovery from a nuclear experiment may be derived from waste dump and caved mine leaching technology.

This paper presents a capsule review of current copper leaching technology and knowledge with emphasis on those aspects that appear relevant to in-place leaching of sulfide copper minerals.

COPPER LEACHING PRACTICE

Leaching of copper, followed by cementation on iron, direct electrolysis, or solvent extraction in conjunction with electrolysis, now yields about 200,000 tons of copper a year in the Western United States. One or more leaching methods--vat, heap, dump, or in-place--are practiced at about 20 locations.

Vat leaching comprises the percolating of dilute sulfuric acid through crushed and sized oxidized ore that is bedded in rectangular tanks with a filter bottom. Slimes made in crushing may be agglomerated and leached with the coarse material or leached separately by agitation. The leach cycle is hours in the agitator and 1 to 2 weeks in the vats.

^{3/} Underlined numbers in parentheses refer to items in the list of references at the end of this report.

Heap leaching is used principally for dilute sulfuric acid leaching of copper from uncrushed porous, oxidized ore that has been piled on prepared drainage pads. The leach cycle duration is in months.

Dump leaching is used to extract copper from low tenor uncrushed strip waste material that must be moved during mining. Both oxide and sulfide minerals in the waste rock may dissolve during years of exposure to oxidizing solutions of dilute sulfuric acid.

In-place leaching is employed to extract copper from broken low grade rock in and overlying a now abandoned copper mine. As with dump leaching, the cycle duration is in years. There is thus time for the oxidation and dissolution of sulfide minerals.

Of the leaching methods currently employed, only dump and in-place leaching are used to dissolve copper sulfides. These methods rely on air for the requisite oxidation reactions.

Waste dumps are roughly analagous to the rubble chimney from a nuclear explosive in that both contain masses of broken rock ranging in size from dust to large boulders. An essential difference is that the dump has free access to air at all exposed surfaces, whereas the latter is enclosed in an underground tomb. Current in-place leaching sites also contain rubble like that in a chimney; furthermore, the broken rock is essentially buried. Such sites differ from the chimney in that large surface areas and extensive underground workings are exposed to air. Neither dumps nor present in-place mine sites bear significant resemblance to the fractured zone that surrounds the chimney and contains most of the ore to be leached in a nuclear experiment.

Individual dumps range in size from about 5 million tons in Duval's Mineral Park operation, to over a billion tons in the largest dump at Kennecott's Bingham Canyon mine. Sulfide mineralization in U. S. dumps ranges from predominantly chalcocite to predominantly chalcopyrite. The former is the easiest and the latter the most difficult copper mineral to dissolve.

In conventional dump leaching, the solution used is a dilute sulfuric acid containing iron sulfates. After passage through the dump, the copper is cemented on iron and the solution then reacidified, if necessary, and recycled to the dump. The solution is introduced on or into dumps by spraying, by flooding, or by using vertical perforated pipes. Solution flow rates vary with the dump height, permeability, and copper mineral content, but are ordinarily adjusted to yield a copper concentration of about 1 gram per liter or 8 pounds per 1,000 gallons in the dump effluent. After several weeks or months of continuous leaching and declining copper yield, leaching is recessed and the dump or section of dump rested for several months. The dump remains moist and oxidation of sulfide minerals continues during the rest period.

Dumps settle and compact on aging. Acid leaching has been likened to an accelerated weathering process and clays that are formed along with the hydrolysis products of ferric and aluminum sulfates tend to plug the dump. Permeability rates have been reported to range from 240 gallons per square foot per day in a new dump to 30 gallons per square foot per day after years of leaching (9).

Although solution composition data from operating dumps are widely variable, the analyses in table I generally characterizes precipitation plant barren, dump influent, and dump effluent solutions.

TABLE I. - Analysis of dump solutions

	Chalcocite mineralization				Chalcopyrite mineralization			
	pH	grams per liter			pH	grams per liter		
		Cu	Fe ⁺²	Fe ⁺³		Cu	Fe ⁺²	Fe ⁺³
Precipitation								
plant barren	3.4	0.01	2	0	3.0	0.05	7	0
Dump influent	3.0	.01	2	0	2.8	.05	7	0
Dump effluent	2.4	1.2	0.1	1	2.4	1.2	3	1.5

Of significance is the showing that ferrous iron is oxidized and acid generated concurrent with copper dissolution as the solution flows through the dump. This is indicative of widespread air penetration into the dump to effect the oxidation of sulfides and ferrous ion. Oxygen dissolved in the solution entering the dump is too low to be of importance in the oxidation reactions. Over a pound of iron goes into solution for each pound of copper cemented. Unless holding tanks or reservoirs are provided on the surface for oxidation, precipitation, and removal of the added iron, hydrolysis with precipitation of the added iron occurs in the dump.

In-place leaching was formerly practiced in caved stopes at the Ohio mine, Bingham Canyon, Utah, and in worked-out areas of the Ray mines in Arizona. The only current example of in-place leaching is the Miami mine in Arizona. At Miami, acid solution from the copper cementation plant is distributed by sprays on the subsided surface overlying the block caved area. Leach solution percolates through 600 feet of broken rock to a collection reservoir in the old mine. From there it is pumped to a surface plant for cementation of the copper on shredded iron cans.

Most of the copper, in the form of mixed oxides and sulfides, occurs in the lower 150 feet of the rubble column. More acid is added to the precipitation plant effluent than is customary in dump leaching. The resultant pH of liquor to the rubble is 1.4. Liquor from the rubble is at pH 2.4. and contains about 2 grams per liter copper and 1 gram per liter each of ferrous and ferric iron. As in dump leaching, oxidation by air plays a dominant role. Also, as in dump leaching, over a pound of iron is precipitated in the rubble column for each pound of copper removed.

Copper leaching practices in the Western United States are comprehensively described in a recent Bureau of Mines publication (11).

AIR AND FERRIC SULFATE OXIDATION OF SULFIDES

In addition to the principal copper sulfides, chalcocite, and chalcopyrite, copper sulfide deposits contain minor amounts of bornite and covellite. Also, the iron sulfide, pyrite, or the related form pyrrhotite, almost always occurs in copper sulfide mineral deposits. The chemical formulas for these minerals are shown in table II.

Inspection of the chemical formula for these minerals shows that chalcocite and bornite are deficient in sulfur for the formation of cupric sulfate. This means that pyrite or added sulfuric acid must be present for the complete dissolution of chalcocite and bornite. Both bornite and covellite are less soluble than chalcocite and more soluble than chalcopyrite in typical dump leach solution. This discussion of chemical reactions and rates

will be confined, therefore, to the principal copper sulfide minerals, chalcocite and chalcopyrite with brief mention of pyrite, which has an accessory role in copper sulfide mineral dissolution.

TABLE II. - Chemical composition of copper and iron sulfides

		Analysis, percent		
		Cu	Fe	S
Pyrite	FeS ₂	-	47	53
Pyrrhotite	Fe _{n-1} S _n	-	Variable	Variable
Chalcocite	Cu ₂ S	80	-	20
Bornite	Cu ₅ FeS ₄	63	11	26
Covellite	CuS	66	-	34
Chalcopyrite	CuFeS ₂	35	30	35

As mentioned previously, air is the oxidizing media in conventional dump and caved mine leaching. In addition to the direct oxidation of sulfides, oxygen from the air converts ferrous to ferric ion, and the ferric sulfate in turn oxidizes copper sulfide minerals. Oxidation by injection of liquid oxygen into dumps has been tried experimentally but has not been adopted in practice.

The classic early work on reactions involving copper sulfides was by Sullivan (12) in 1933. In recent years, numerous investigators, including Forward and Warren (5), Woodcock (16, 17), Thomas (14), and Dutrizac (2), have explored and explained the dissolution of sulfide minerals.

To minimize problems in duplicating test data that arise from the heterogeneity of mineral deposits and diversity of behavior of ostensibly identical mineral species, synthetic copper minerals were used in some of the laboratory studies. Tables III, IV, and V show the principal reactions that are believed to occur in dilute sulfuric acid leaching of pyrite, chalcocite, and chalcopyrite with air and ferric iron as oxidants. Actual mechanisms probably involve other intermediate and side reactions.

TABLE III. - Oxygen and ferric sulfate leaching of pyrite

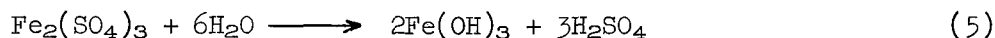
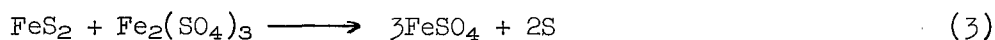
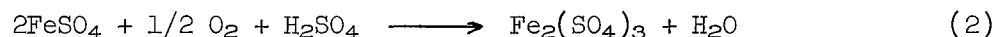
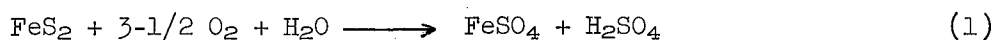
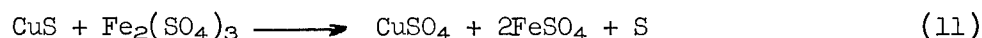
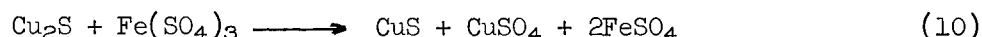
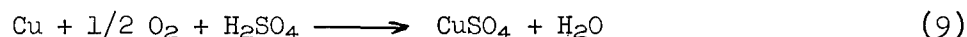
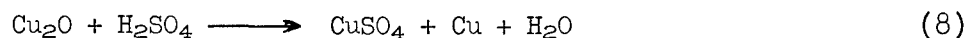
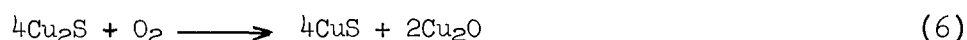
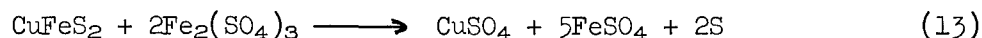


TABLE IV. - Acid and ferric sulfate leaching of chalcociteTABLE V. - Acid and ferric sulfate leaching of chalcopyrite

Equations 1 through 5, respectively, show (1) oxidation of pyrite by oxygen to form ferrous sulfate and sulfuric acid, (2) oxygenation of ferrous sulfate to ferric sulfate, (3) attack of pyrite by ferric sulfate to yield ferrous sulfate and elemental sulfur, (4) oxygenation of sulfur to make sulfuric acid, and (5) hydrolysis of ferric sulfate to precipitate iron hydroxide and liberate sulfuric acid. The net result of pyrite oxidation is to furnish acid and ferric sulfate for dissolution of copper minerals. All the reactions are speeded by increasing temperature. The precipitation of ferric hydroxide (reaction 5) occurs at pH of about 2.8 or higher. Once the ferric hydroxide dehydrates in a dump, it resists resolution even at a pH as low as 2.

The equations in table IV shows chalcocite reacts in stages with either oxygen or ferric sulfate. Equation 9 shows the oxygenation and dissolution of elemental copper formed in reactions 7 and 8. Ferric sulfate solution also oxidizes and dissolves elemental copper as shown by Wadsworth (15). Covellite if formed in the first stage reaction of chalcocite with ferric sulfate. The second stage reaction is slower as ferric ion must diffuse in and cupric and ferrous ions out through a thickening layer of sulfur on the covellite surface. The system is further complicated by slow oxidation of the sulfur film to sulfuric acid. Significantly, covellite freshly formed in the first stage oxidation of chalcocite is much easier to oxidize and dissolve than natural covellite.

Despite the apparent simplicity of equations 12 and 13 in table V, the attack of oxygen and ferric sulfate on chalcopyrite is much slower than on chalcocite. As with the covellite oxidation (reaction 11), the speed appears to be limited by diffusion through a thickening film of sulfur on the mineral surface.

Laboratory studies on the dissolution rates of copper sulfides have generally been conducted on finely ground minerals in vigorously agitated pulps. Although such laboratory studies do not simulate leaching dump and caved materials, the results do delineate some of the essential conditions for leaching copper sulfide mineral. In general, the leach solution should have a pH of about 2.5 or less, and contain about 2 grams ferric iron per liter. Maximum aeration is desirable and increasing temperature markedly speeds the oxidation and leach reaction. Unless precautions are taken to sterilize the

mineral samples, bacteria that catalyze the air oxidation of sulfides are always present. The bacteria are destroyed at a temperature over 45° C and are feeble workers in the cold.

Only speculative data is available on the rate of copper leaching from dumps and caved mines. This is because the copper content of mining waste in the dump or left in a caved area is imperfectly known, and sampling of a dump to determine its copper content is impractical. During the first year of leaching, dumps containing some oxides may yield an estimated 20 percent of the copper. Thereafter, chalcocite dumps may leach at a rate of about 5 to 10 percent a year, and chalcopyrite dumps at 1 to 2 percent a year.

The set-up we used in experimental leaching of waste dump samples is pictured in figure 1. Rock, in size from powder to 2 feet, was obtained from waste dumps representative of predominantly chalcocite, predominantly chalcopyrite, and all chalcopyrite mineralization. Each drum was loaded with 550 to 600 pounds of rock. A head analysis of 0.21 percent copper is being used in calculating extraction from the chalcocite-type waste, which is still being leached. Head assays of 0.38 percent copper were calculated for the chalcopyrite-type samples based on leach residue analysis and amount of copper dissolved.

Sulfuric acid solutions at pH 2 and containing 2 to 4 grams per liter ferric iron were percolated through the rock at a rate of 26 gallons per square foot per day. The tests were conducted at ambient temperature of about 25° C. Our microbiologist determined that suitable bacteria were present. When the copper content of the effluent solution reached 1 gram per liter, a fresh acid-ferric sulfate solution was substituted. The effluent also contained 4 to 9 grams Fe^{+3} per liter and 1 to 4 grams H_2SO_4 per liter.

Extraction curves are shown in figure 2. In 205 days of leaching, 53 percent of the copper was dissolved from the chalcocite-bearing rock and the extraction curve was still rising. Leaching for 340 days dissolved 16 percent of the copper from predominantly chalcopyrite-bearing rock and the extraction curve had nearly flattened. In 500 days, only 9 percent of the copper was dissolved from rock containing chalcopyrite as the sole copper mineral. Two-thirds of the extracted copper was dissolved in the first 250 days.

In a complementary test, sized fractions of the chalcocite-type waste have been leached for 205 days and similar fractions of the chalcopyrite-type wastes were leached for 340 days in the same manner as the dump run material. Rock to the respective leach drums was mine run less 1/4 inch fines, minus 3 inches with fines, and minus 3 inches without fines. Copper extraction from each size fraction was generally about the same as obtained from the unsized dump run material. About 1 percent higher extraction was obtained in leaching minus 3 inch material containing the fines.

Like the laboratory agitation leaching data, our findings too are only generally applicable to dump and caved mine leaching. Aeration was probably better and solution channeling less of a problem than in commercial dumps. But, temperatures 20° C or more higher than in our drums are often attained in commercial dumps, and this would materially accelerate oxidation and leaching.

Pressure oxidation leaching using air or oxygen at an oxygen partial pressure of about 100 pounds per square inch and temperatures of 200° C or more dissolves even chalcopyrite in a few hours. The mineral must be finely ground and vigorous agitation is needed to distribute the oxygen. This is much easier to do in laboratory than in commercial-sized equipment as



FIGURE 1. - Percolation Leaching of Copper Waste Dump Rock in Stainless Steel Drums.

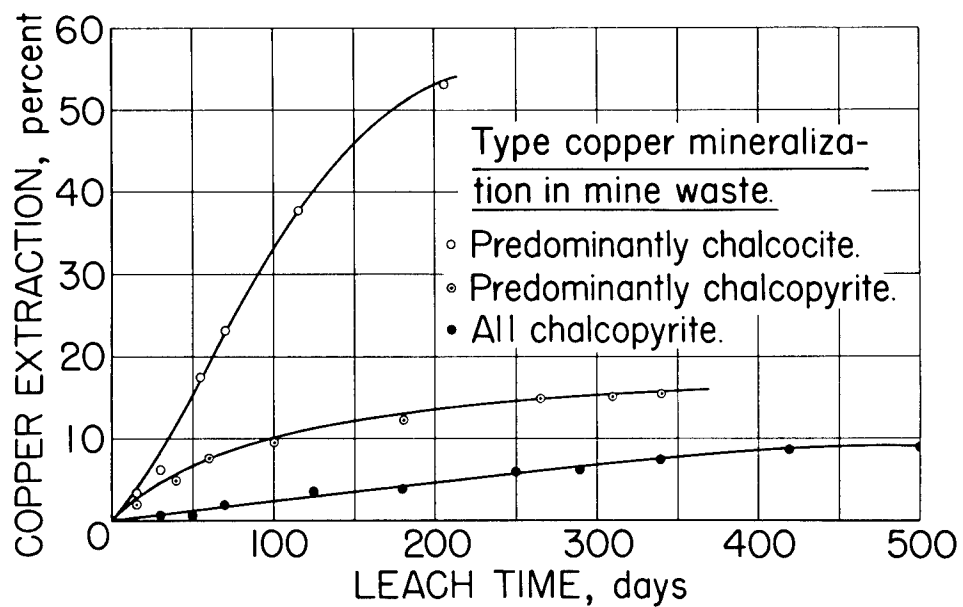


FIGURE 2 - Rate of Copper Extraction During Percolation Leaching of Three Dump Samples.

indicated by several abortive attempts at commercial acid pressure leaching of sulfides in this country. Most acid pressure leaching in the laboratory and plant has been done in autoclaves on high value concentrate containing 20 percent or more of sulfide sulfur. This much sulfur is needed to provide fuel for autogenous heating by the oxidation reaction. If a feasible way could be found to heat and oxygen pressurize the leach solution in a fractured ore body, the dissolution of sulfide minerals would be greatly accelerated. Agitation for distribution of oxygen and finely ground mineral would be lacking underground and, therefore, leach rates would still be much slower than in the laboratory experiments.

Cyanide, Nitric Acid and Chlorine Leach Systems

Chalcocite, but not chalcopyrite, is soluble in strong cyanide solution. Subsequently, Cu_2S can be precipitated by acidulating the solution. The HCN evolved is absorbed in lime water to form $\text{Ca}(\text{CN})_2$ for reuse (3, 10). A tight formation with absolute assurance that cyanide could not get into ground water supplies would be requisite for its use underground. This is true also about leaching with sulfuric acid as copper itself cannot be tolerated in ground water sources. However, retention of sulfates in the leached rock is of little economic importance, whereas foreseeable difficulty in adequate recovery of cyanide from a nuclear chimney or fracture zone precludes the use of so expensive a reagent.

Nitric acid is an active solvent for copper sulfides (7). However, its cost is high enough so that recovery of the acid and of nitrous oxide which forms in the reaction with sulfides is essential. Like cyanide, nitrates are toxic and must be rigorously excluded from ground water. These reasons appear to preclude the use of nitric acid for in-place leaching of low-grade copper ore.

Application of chlorides and chlorine in dissolution of sulfides has been discussed by Forward and Warren (5). Although hydrochloric acid does not dissolve copper sulfides, an acid ferric chloride solution appears superior to ferric sulfate for oxidation and dissolution of chalcocite. Such a solution can be conveniently made by addition of sodium chloride to a sulfuric acid-ferric sulfate solution. Although numerous patents have been issued for ferric chloride leaching processes, these are not employed in dump leaching because the slight advantage over ferric sulfate in leaching of chalcocite does not compensate for the major corrosion problems that use of chlorides engenders.

Chlorine was used in the 1880s in Spain for the oxidation of ferrous to ferric ion for leaching low-grade copper sulfide ore. Chlorine, even at ambient temperatures, also is a powerful oxidant for sulfide minerals (6). A test in our laboratory in which chalcopyrite ore was percolation leached, using acid-ferric sulfate solution with added chlorine, dissolved 14 percent of the copper in 14 days. Without chlorine, a year's leaching was required to dissolve this much copper. After 45 days leaching with added chlorine, 46 percent of the copper had been extracted. However, chlorine consumption was 10 pounds per pound of copper dissolved, a possibly prohibitive reagent cost. In commercial practice, chlorides formed by oxidation of the sulfides would magnify corrosion problems.

SUMMARY

For evaluating its leachability, a nuclear chimney of copper sulfide ore reduced to rubble may be considered as roughly analogous to a copper mine waste dump. No operating parallel is known for guiding copper extraction projections from the fractured zone that surrounds the chimney. Acid-ferric sulfate solution conventionally used in waste dump leaching may be employed for leaching a chimney. At temperatures of about 30° C, bacteria might serve to catalyze the air oxidation of ferrous to ferric iron either in the chimney with forced ventilation or on the surface. Oxidation with chlorine or other oxidants also may be used to convert ferrous ion to the ferric form for leaching. At temperatures of 20° to 40° C, the dissolution of chalcocite may take years and dissolution of chalcopyrite takes decades. Heating of the solution offers a possible means of markedly accelerating the leaching rate. Chlorine, if available at low cost, also might be used to speed copper dissolution by direct attack on the sulfide minerals.

REFERENCES

1. Atomic Energy Commission, SLOOP, PNE 1300, Nuclear Explosives-Peaceful Applications, June 1, 1967, 44 pp.
2. Dutrizac, J. E., R. J. C. McDonald, and T. R. Ingraham. The Kinetics of Dissolution of Bornite in Acidified Ferric Sulfate Solution. (To be published in Transactions, Metallurgical Society, AIME.)
3. Eng. and Min. J., Copper Leaching With Cyanide, A Review of Five Inventions, v. 168, No. 9, September 1967, pp. 123-127.
4. _____. Kennecott Sets Sites on Nuclear Test for In Situ Recovery of Copper, v. 168, No. 11, November 1967, pp. 116-122.
5. Forward, F. A. and I. H. Warren. Extraction of Metals From Sulfide Ores by Wet Methods. Metallurgical Reviews, v. 5, No. 18, 1960, pp. 137-164.
6. Jackson, K. J. and J. D. H. Strickland. The Dissolution of Sulfide Ores in Acid Chlorine Solutions: A Study of the More Common Sulfide Minerals. Trans. AIME, v. 212, 1958, pp. 373-379.
7. Liddell, Donald M. Handbook of Nonferrous Metallurgy. McGraw-Hill Publishing Co., 1945, 355 pp.
8. Malouf, E. E. and J. D. Prater. Role of Bacteria in the Oxidation of Sulfide Ores. J. Metals, v. 13, 1961, pp. 353-356.
9. _____. New Technology of Leaching Waste Dumps. Min. Cong. J., v. 48, No. 11, 1962, pp. 82-85.
10. Rose, D. H., V. Lessels, and D. J. Buckwalter. White Pine Experiments With Cyanide Leaching of Copper Tailings. Min. Engr., August 1967, pp. 60-63.
11. Sheffer, Herman W. and LaMar G. Evans. Copper Leaching Practices in the Western United States. BuMines Inf. Circ. 8341, 1968, 57 pp.

12. Sullivan, John D. Chemical and Physical Features of Copper Leaching. Trans. AIME, v. 106, 1933, pp. 515-546.
13. Sutton, J. A. and J. D. Corrick. Leaching Copper-Sulfide Minerals With Selected Autotrophic Bacteria. BuMines Rept. of Inv. 6423, 1964, 23 pp.
14. Thomas, G., T. R. Ingraham, and R. J. C. McDonald. Kinetics of Dissolution of Synthetic Digenite and Chalcocite in Aqueous Acidic Ferric Sulfate Solutions. Canadian Metallurgical Quarterly, v. 6, No. 3, pp. 281-292.
15. Wadsworth, M. E. and D. R. Wadia. Reaction Rate Study of the Dissolution of Cuprite in Sulfuric Acid. J. Metals, v. 7, 1955, pp. 755-759.
16. Woodcock, J. R. Some Aspects of the Oxidation of Sulfide Minerals in Aqueous Suspension. Proceedings of the Australian IMM, No. 198, 1961, pp. 47-84.
17. _____. Copper Waste Dump Leaching. Proceedings of the Australian IMM, No. 224, 1967, pp. 47-66.

PARTICLE-SIZE DISTRIBUTION STUDY: PILEDRIIVER EVENT

David D. Rabb

Lawrence Radiation Laboratory, University of California
Livermore, California 94550

PREFACE

Results of a recent underground drilling program at PILEDRIIVER allows revision of the previous estimates of cavity geometry reported in UCRL-50489, Size Distribution study of PILEDRIIVER Particles, October 1968. Also, additional data relative to fractures, leaching, and radioactivity have been incorporated into this report. These cursory investigations only serve to point out the fact that if nuclear explosives are ever used to break ore for commercial purposes, radioactivity in leaching OFF-solutions will be a critical factor.

ABSTRACT

Reentry was made by mining into the chimney of broken rock created by a nuclear detonation in granite at a depth of 1500 feet. The chimney was 160 ft in radius and 890 ft high. An injection of radioactive melt was encountered at 300 ft from shot point. Radiochemical analyses determined that the yield of PILEDRIIVER nuclear device was 61 ± 10 kt.

Two samples of chimney rubble totalling over 5,000 lb were obtained during the postshot exploration. These samples of broken granite underwent screen analysis, a radioactivity-distribution study, and cursory leaching tests.

The two samples were separated into 25 different size-fractions. An average of the particle-size data from the two samples showed that 17% of the material is between 20 mesh and 1 in.; 42% between 1 and 6 in.; and 34% between 6 in. and 3 ft.

The distribution of radioactivity varies markedly with the particle size. The minus 100-mesh material comprizes less than 1.5% of the weight but contains almost 20% of the radioactivity. Small-scale batch-leaching tests showed that 25% of the radioactivity could be removed in a few hours by a film-percolation leach with distilled water, and 40% with dilute acid. Brief studies were made of the microfractures in the broken rock and of the radioactivity created by the PILEDRIIVER explosion.

INTRODUCTION

Because underground nuclear explosions result in material (broken rock) which may be subsequently mined¹ either by conventional ore withdrawal or by

in-place solution mining (in-situ leaching), the size distribution of the broken particles is of particular interest. If solution mining is contemplated, some questions arise about size distribution: What is the maximum size? What sizes constitute the bulk of the material? What is the percentage of fines? And, are there significant variations in size distribution between different materials or in different areas of the same material? Furthermore, what are the amounts, species, and concentrations of radioactivity associated with each size-fraction at any one site, and how do they behave during solution mining and metal recovery?

The PILEDRIIVER Event of June 2, 1966 was an underground nuclear explosion test in granite rock* at the Nevada Test Site (NTS), sponsored by the Department of Defense, as part of a study of the shock-hardening of underground structures. Depth of burst was about 1500 ft, and yield was 61 ± 10 kt. The site is near the 5-kt HARDHAT chimney, which had been explored earlier by the Lawrence Radiation Laboratory.² Because PILEDRIIVER had a much larger yield than HARDHAT and was close by in the same medium, LRL proposed exploratory reentry work.

- (a) to define the chimney geometry and associated wall-rock conditions,
- (b) to determine the characteristics and distribution of rubble and radioactivity in the chimney,
- (c) to gain information pertinent to in-situ leaching, and
- (d) to secure a sample of melt for radiochemical analysis and determination of yield.

The LRL program involved five phases:

1. A drilling program from the surface to intercept the top of the chimney, to obtain gas samples, and to measure the volume of chimney voids.
2. A mining program to determine the chimney radius, to examine the wall rock near the chimney, and to secure samples of chimney rubble for size-distribution and radioactivity studies.
3. A leaching investigation to gain preliminary data on the leachability of material in or near the chimney and on the concentrations of the specific nuclides in this leach solution.
4. An underground drilling program to obtain samples of rock for shock-effects studies and for verification of the radius of the lower hemisphere of the cavity formed during the explosion.
5. If possible, acquisition of a sample of melt for a yield determination by radiochemistry.

DRILLING PROGRAM

Immediately after the PILEDRIIVER detonation, geophones recorded "noise" for only 14 sec; therefore, there was no certainty that there had been a collapse. However, reentry drilling (Fig. 1) from the surface in July 1967 lost circulation at a depth of 610 ft, where a 2-ft void was encountered.³

Pressurization tests in the hole above this point indicated relatively low permeability but at points below 610 ft, pressures could not be maintained

*The Climax granite stock in Area 15, NTS, North of Yucca Flat, is a well-defined and well-characterized medium, ideal for effects studies.

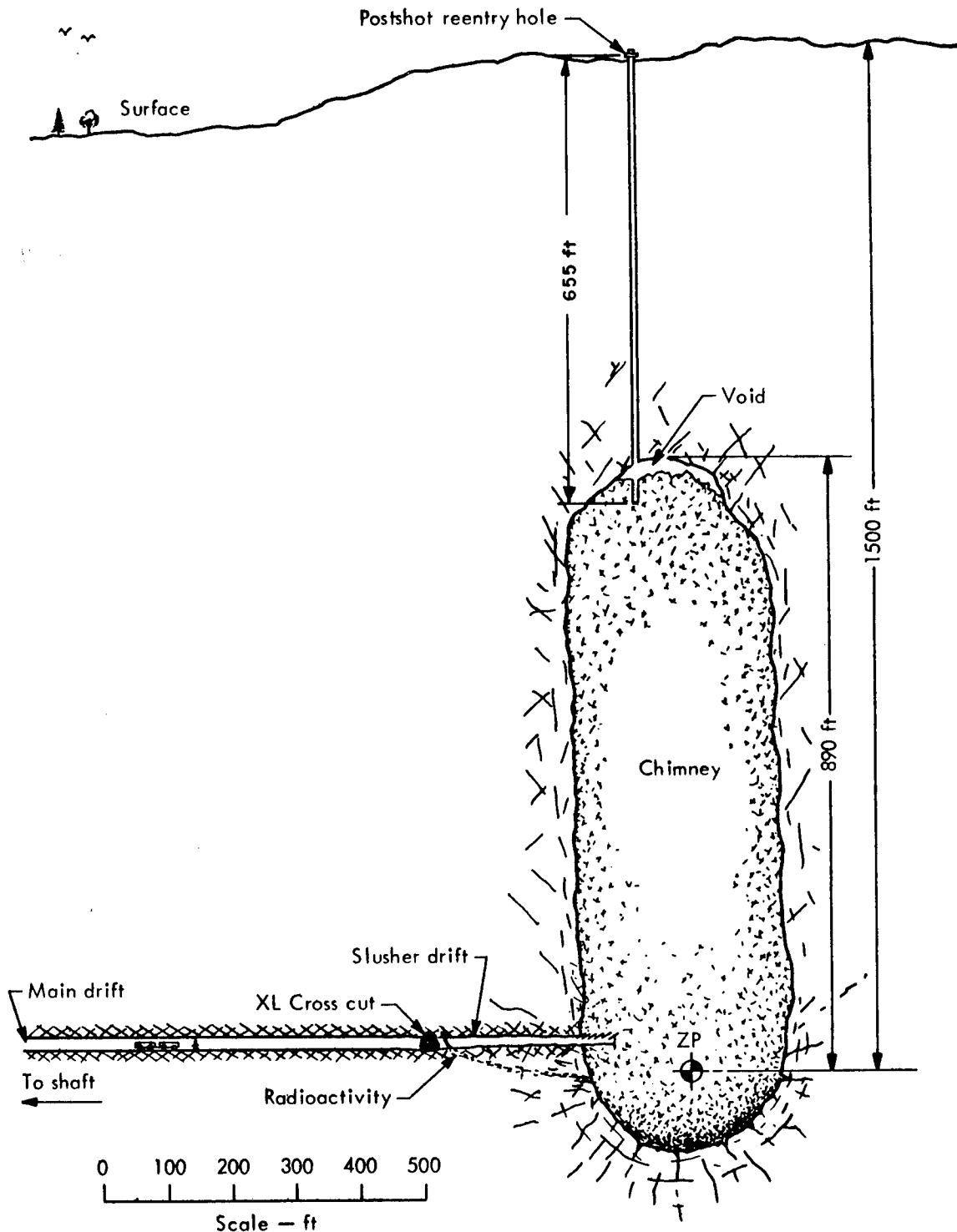


Fig. 1. Postshot configuration of PILEDRIVER.

greater than 0.1 psig, suggesting high permeability. Drilling rates below 610 ft were relatively high, averaging 1 ft/min, or greater, with frequent evident voids and a complete loss of drilling fluids. Subsequent TV camera runs and stereo pictures proved that this void marked the top of the chimney, indicating a chimney height of 890 ft. (See Fig. 2 for a view into the top of the chimney.)

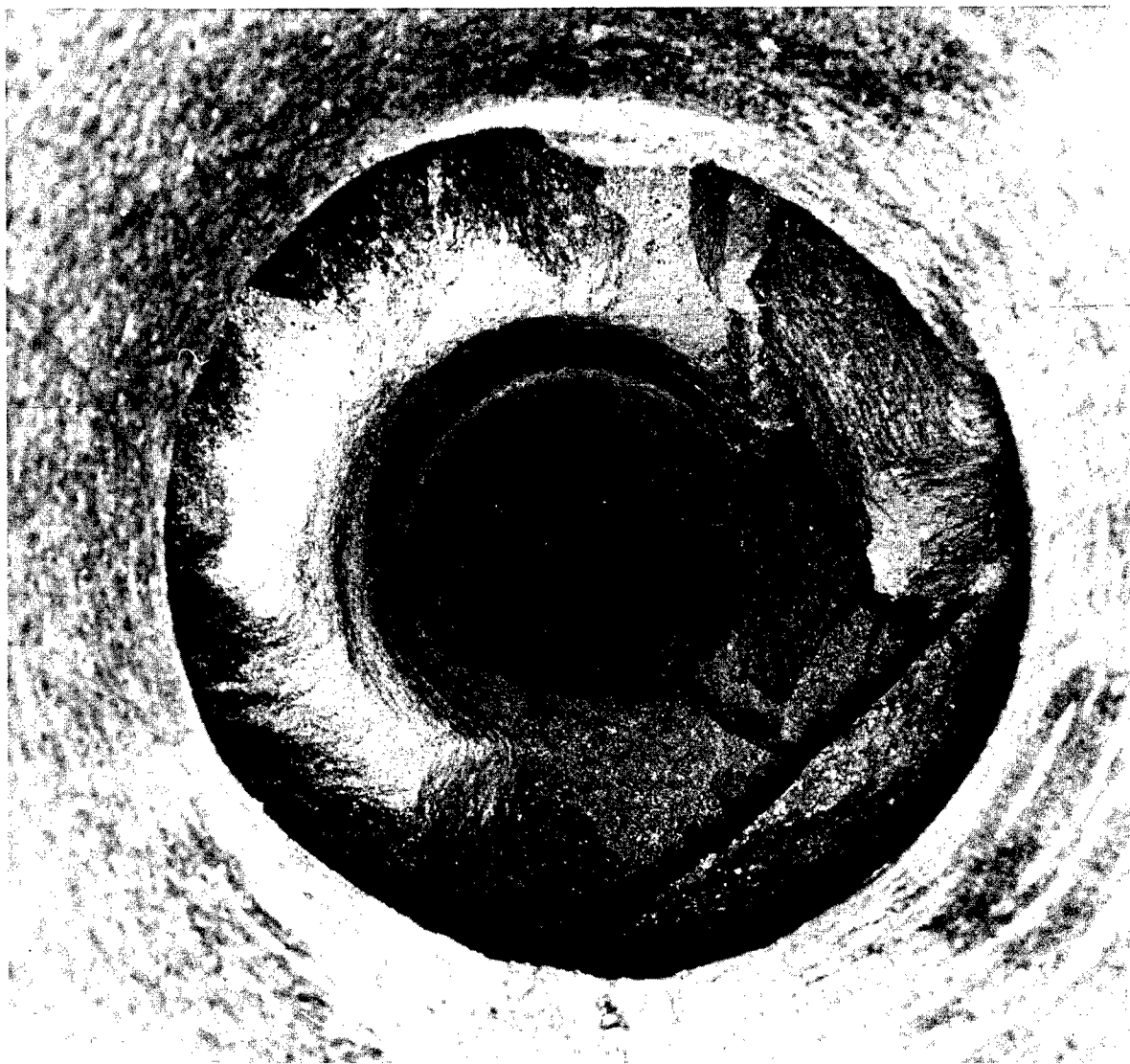


Fig. 2. Looking down into the top of the PILEDRIVER chimney from the 608-ft level.

At 655 ft (total depth), the drill string was pulled up 30 ft to make a connection. When an attempt was made to resume drilling, the hole had caved. Since this condition could result in loss of drill stem and loss of the hole, it was considered advisable to suspend further drilling until after density, gamma, TV, and other hole-logging surveys could be performed and a gas sample could be obtained. The maximum temperature recorded in the top of the chimney was 89° F in an area where preshot ground temperature was about 75° F. Gas samples indicated maximum beta and gamma radioactivity of 2 mR/hr. The measured volume of the voids in the chimney was about 1.3 million cubic ft.³ The chimney was estimated to contain about 4,000,000 tons of broken rock, depending upon the configuration of the upper portion of the chimney.

When the chimney was penetrated, there was a slight negative pressure due to high barometric pressure at the surface at that time. Later, during the exploratory underground mining operations, air in the mine frequently became high in carbon dioxide (> 10%) and low in oxygen (< 16%), with traces of carbon monoxide. This condition seemed dependent upon surface barometric pressure during long shutdowns (over weekends or because of NTS test

activity). A 100-ft³/min exhaust fan installed at the drill-hole collar kept the cavity gas from bleeding into underground workings and alleviated this condition.

MINING PROGRAM

On the basis of previous experience in granite at HARDHAT and SHOAL Events,^{4,5} the absence of a large apical void and the relatively high chimney (890 vs 500 ft) at PILEDRIIVER were unexpected. Because of these interesting anomalies, because data from PILEDRIIVER is applicable to SLOOP (the proposed copper-leach project in Arizona), and because a yield determination from a melt sample by means of radiochemistry was desired, the main drift used by the DOD for postshot exploration was extended toward the chimney. This effort by LRL started in September 1967 and terminated in October of that year.

The DOD postshot exploration from February through August 1967 reopened the main drift to the so-called XL cross-cut, 100 ft above and 312 ft from the center line over ZP* (see Figs. 1 and 4). When the drift was extended approximately 20 ft beyond the XL cross-cut to a point about 300 ft from the ZP, a thin vein of radioactive glass slag was encountered in a fissure between the top of the sand stemming and the granite back of the tunnel (Fig. 3). Maximum beta-plus-gamma radiation readings were about 600 mR on contact.

Chemical analyses by Los Alamos Scientific Laboratory (LASL) of a sample of this glass indicated that the yield was about as expected, 61 ± 10 kt. Because 14 months had intervened between the shot data and the analyses, the reported yield has a relatively wide range of uncertainty. Our LRL estimates based on seismic data at shot-time implied a yield of about 68 kt.⁶

To isolate this contaminated area, a slusher drift was started in the left rib to bypass the hot area (Figs. 4 and 5). This drift angled off the main drift near the XL cross-cut (Station 1140) for 50 ft, and then drove directly for the centerline over the ZP. Muck from slusher drift averaged about 3 mR on contact. This activity may have been partially gaseous krypton-85 and radon-222, because the activity decreased to about 1/2 mR within a few hours after removal to open air.⁷

When the slusher drift was in by 140 ft, the edge of the chimney (Fig. 6) was encountered at Station 1280; therefore, the apparent chimney radius at this point (about 105 ft above ZP) is 160 ft.

Subsequent core drilling from Station 1140 toward the ZP showed the cavity radius in the lower hemisphere to be 132 ft.⁸ If the yield is 70 kt, as is possible, this radius is consistent with the established formula, $R = 16 W^{1/3}$. Preshot computer calculations, however, predicted a cavity radius of 146 ft. Factors that may account for the relatively large chimney radius of 160 ft at the reentry tunnel level, about 110 ft above ZP, include a preshot 2-gallon-per-minute flow of water into the explosion area, a steeply dipping, wide shear zone within the cavity radius, and the previously untried depth of the explosion. Also, the PILEDRIIVER chimney could possibly be tilted slightly off the vertical, that is, some 15 ft off centerline at this point. If this is a fact, continuation of the reentry drift across the chimney would probably discover the opposite chimney edge at about Station 1570 (130 ft beyond center-line); the chimney diameter at this point, then, would be more like 145 ft. The value 145 would agree with past experience; usually, chimney radii of contained nuclear explosions have been found to average about 9% greater than the radii of the

*Zero point (ZP), or detonation point, is the center of emplacement of the explosive.

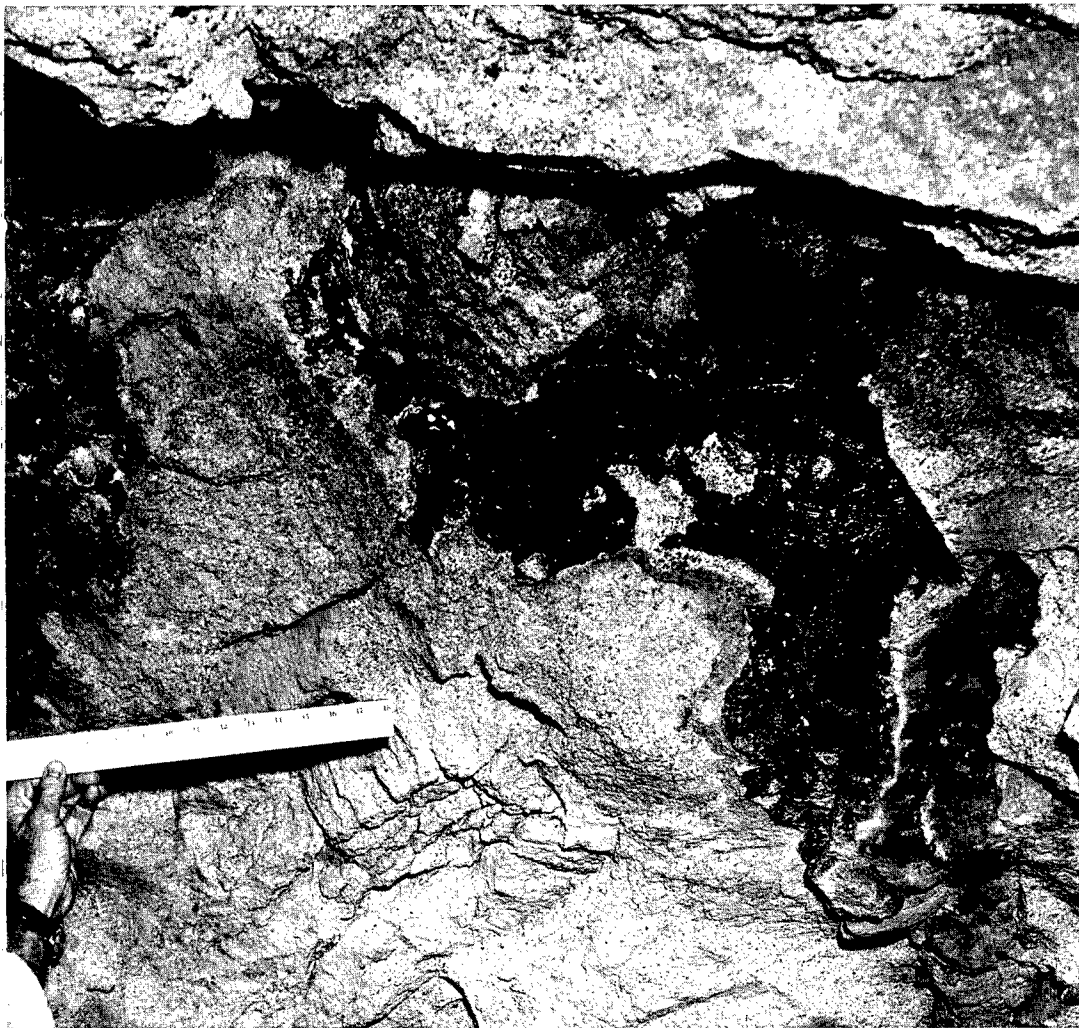


Fig. 3. A radioactive slag near the PILEDRIVER chimney.

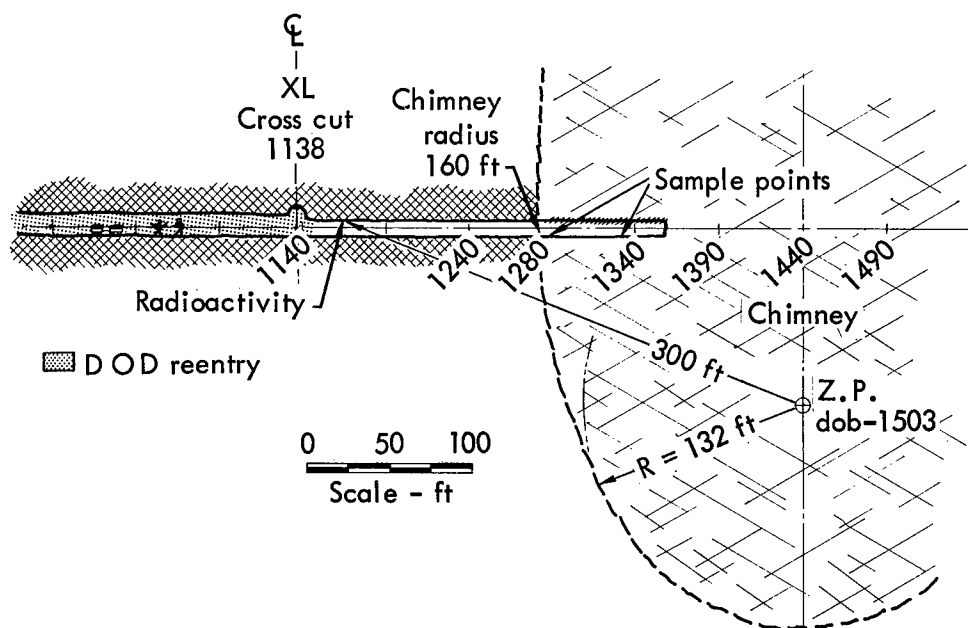


Fig. 4. Elevation: PILEDRIVER reentry.

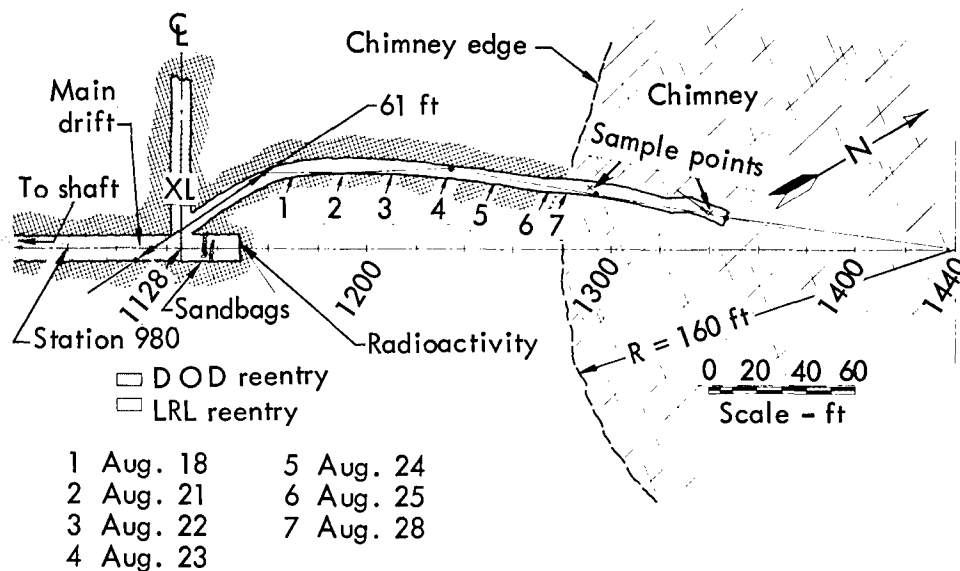


Fig. 5. Plan: PILEDRIIVER reentry.

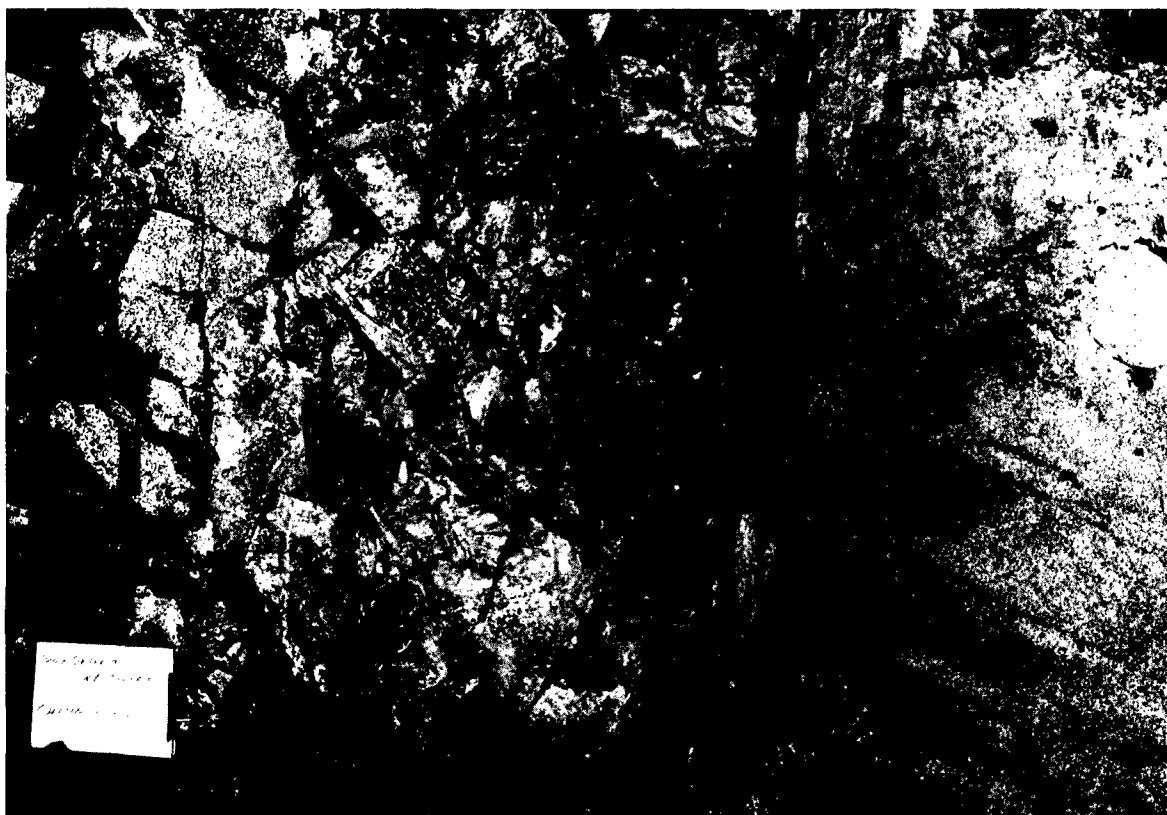


Fig. 6. Chimney edge, PILEDRIIVER reentry.

initial cavities.⁹ Incidentally the dominant fracture pattern and shear zone dip in this area is about 75 to 80 degrees. Figure 6 shows the relatively solid rock outside the chimney, the broken rubble inside it, and an obvious chimney wall or edge.

Further penetration into the chimney reached Station 1347, 67 ft inside the chimney, where work was discontinued because available funds were

expended. The total length of the slusher drift was 207 ft; the latter half of the drift was worked by double-slushing.

PARTICLE-SIZE-DISTRIBUTION STUDY

To determine the distribution of particle sizes in the rubble, two representative samples of the broken granite (or chimney rubble) were secured. Sample I (1387.5 lb) was taken from a point 10 ft into the chimney at Station 1290, which is shown in Fig. 7. Sample II (3350.75 lb) was taken from 60 ft in at Station 1340, which is shown in Fig. 8. Sample II was noticeably coarser than



Fig. 7. Material at the location from which Sample I was taken.



Fig. 8. Material at the location from which Sample II was taken.

Sample I. In addition, two 300- to 500-lb boulders were recovered at the site of Sample II. At the U.S. Bureau of Mines (BuMines) Station, Salt Lake City, Utah, the two samples were separated into the six particle-size fractions listed in Table I, and weighed. Note that Sample I had no material in the plus 3-ft fraction. Later, each sample was separated further into the size-fractions listed in Table II.

All the samples were screened dry with U.S. Standard screens, either with a conventional vibrating screen base or with a rotap,* depending on the

*An automatic shaking mechanism to aid in screen analysis.

Table I. Particle-size distribution of PILEDRIIVER chimney-rubble samples from screen analysis.

Particle size		Max particle size (in.)	Weight percent ^a								
			% of total			Cumulative %					
Minus	Plus		I	II	Av	I	II	Av	I	II	Av
--	3 ft	about 60	--	7	3	0	7	3	--	100	100
3 ft	6 in.	36	25	43	34	25	50	38	100	93	96
6 in.	1 in.	6	47	36	42	71	87	80	75	50	63
1 in.	1/4 in.	1	17	6	12	89	93	92	28	14	21
1/4 in.	20 mesh	0.25	7	4	5	96	96	96	11	8	9
20 mesh		0.0331	4	4	4	100	100	100	4	4	4
			100	100	100						

^aTo nearest significant figure.

sieve size. All screens or sieves were run for 15 min to insure clean, complete separation of the size-fractions.

From Tables I and II, it is evident that only about 25% of Sample I, or, 50% of Sample II is larger than 6 in., and only a few boulders are larger than 3 ft. On the average, about 17% of the material falls between 20 mesh and 1 in., 42% between 1 and 6 in., and 34% between 6 in. and 3 ft; that is, over 90% is in a size range which is amenable to "heap leaching." Another important point for a possible leaching operation is the relatively small amount of fines, less than 2% of minus 100-mesh material for either sample. It is the consensus of individuals experienced in dump leaching of copper ores¹⁰ that the particle-size distribution of this material makes it amenable to conventional leaching.

Figure 9 shows the results of plotting on a semi-log scale the amount of material for each size-fraction (weight percentage) against the maximum particle size (nominal sieve opening). For a log-normal distribution there should be a fairly straight line, but this is not the case. There is a distinct break in the curve for Sample II at a particle size of about 2 in. and again at 6 in. It is believed that the rock tends to break into pieces of these dimensions because of the spacing of natural fractures. However, only Sample II shows this phenomenon. Sample I, which was from a weak shear zone which possessed no dominant fracture spacing, had no such breakage pattern.

The influence of grain size of the mineral particles in the rock is shown by the breaks in the slope of the curve at about 4 mesh and about 16 mesh. This becomes more evident if the vertical scale is expanded as in Fig. 10. The slight break in the curve at about 80 mesh (Fig. 10) is believed to be the separation point of the natural slimes from the sand formed during the detonation.

In addition to the screen analyses of Samples I and II, a study was based on field observations and photographs of chimney rubble (as the slusher drift advanced); the result was the particle-size distribution in column 2 of Table III. These data are considered to be more representative of the average particle-size distribution in the PILEDRIIVER chimney than are those deduced from particle-size analyses of Samples I or II. Comparison of these data with those available from Table II, however, shows that the particle sizes of Sample II agree closely with the estimate considered typical for hard rock.

Table II. Detailed particle-size distribution and radioactivity distribution of PILEDRIVER chimney-rubble samples from the screen analyses.

Sample			Weight percent ^a						Radioactivity ^a											
Particle size ASTM-U. S. Std. sieve series			Nominal sieve opening (in.)			% of total			Cumulative %			1000's of counts/min/g			% of total			Cumulative %		
Minus	Plus		I	II	Av	I	II	Av	I	II	Av	I	II	Av	I	II	Av	I	II	Av
—	3 ft	boulder	—	7	3	—	7	3	—	100	100	—	0.3	—	—	3	1	—	100	100
3 ft	6 in.	36	25	43	34	25	50	38	100	93	96	0.3	0.2	3	12	8	100	97	99	
6 in.	3 in.	6.0000	21	20	20	46	70	58	75	50	63	0.5	0.3	3	8	5	97	85	91	
3 in.	2 in.	3.0000	13	9	11	57	79	69	54	31	42	1.0	0.5	4	6	5	94	78	86	
2 in.	1 in.	2.0000	13	8	11	71	87	80	42	22	32	2.0	0.8	9	8	8	90	72	81	
1 in.	1/2 in.	1.0000	13	4	9	84	91	89	28	14	21	4.0	1.1	18	6	12	81	64	73	
1/2 in.	1/4 in.	0.4950	5	2	3	89	93	92	15	11	13	6.0	1.3	9	3	6	63	58	60	
1/4 in.	4 mesh	0.2450	0.4	0.1	0.2	89	93	92	11	8	9	7.0	1.6	0.1	negligible	negligible	54	55	55	
4 mesh	6 mesh	0.1870	1.9	0.6	1.2	91	94	93	10	7	8	9.1	2.2	6	2	4	54	55	55	
6	8	0.1320	1.4	0.7	1.0	93	94	94	8	7	7	8.2	2.4	4	2	3	48	53	51	
8	12	0.0937	1.1	0.5	0.8	94	95	95	7	6	6	10.0	3.1	4	2	3	44	51	48	
12	16	0.0661	1.1	0.6	0.9	95	95	96	6	6	6	10.4	3.6	4	3	3	41	49	45	
16	20	0.0469	0.7	0.6	0.7	96	96	96	5	5	5	14.5	4.2	4	3	3	37	46	42	
20	30	0.0331	0.8	0.8	0.8	97	97	97	4	4	4	16.5	4.9	4	5	5	33	43	38	
30	40	0.0234	0.7	0.7	0.7	97	97	97	3	4	3	18.5	5.8	5	5	5	29	38	34	
40	50	0.0165	0.4	0.5	0.4	98	98	98	3	3	3	19.8	6.0	3	4	3	24	33	29	
50	60	0.117	0.4	0.3	0.4	98	98	98	2	3	2	21.3	7.1	3	3	3	21	30	26	
60	80	0.0098	0.4	0.5	0.5	99	98	98	2	3	2	22.8	7.1	3	5	4	19	27	23	
80	100	0.0070	0.2	0.2	0.2	99	99	99	1.4	1.8	1.6	23.3	6.8	1	2	2	16	22	19	
100	140	0.0059	0.3	0.4	0.3	99	99	99	1.2	1.5	1.4	25.9	7.5	3	4	3	14	21	17	
140	170	0.0041	0.1	0.2	0.2	99	99	99	0.9	1.1	1.0	29.4	8.2	1	2	2	12	17	14	
170	200	0.0035	0.2	0.3	0.2	99	100	99	0.8	1.0	0.9	30.4	9.5	2	3	2	10	15	12	
200	270	0.0029	0.2	0.4	0.3	100	100	100	0.6	0.8	0.7	36.2	10.9	3	5	4	9	11	10	
270	325	0.0021	0.1	0.1	0.1	100	100	100	0.4	0.4	0.4	38.5	11.8	1	2	2	6	6	6	
—	—	0.0017	0.3	0.3	0.3	100	100	100	0.3	0.3	0.3	50.1	12.8	5	4	5	5	4	5	

^aTo nearest significant figure.

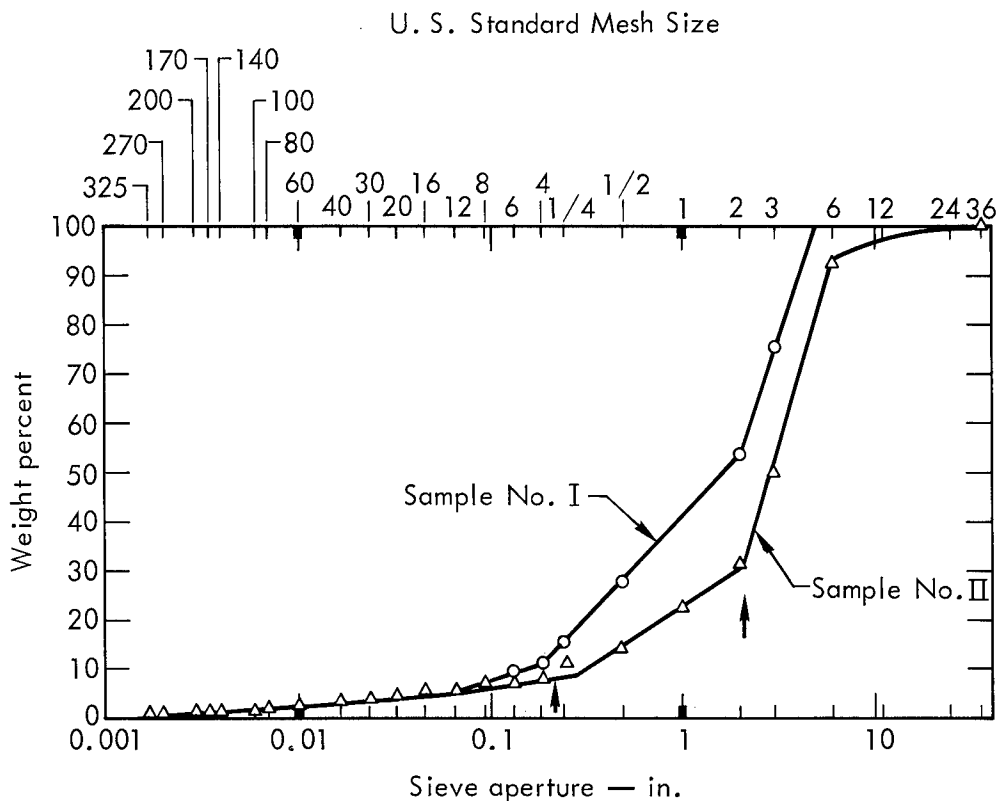


Fig. 9. Weight percent vs particle-size distribution for Samples I and II. The arrows mark the breaks in the curves. On the horizontal scale, all the large ticks refer to sieve aperture, and all the small ticks refer to mesh size.

Also in Table III, this average PILEDRIIVER particle-size distribution is compared with similar data from HARDHAT granite, DANNY BOY basalt, pre-SCHOONER rhyolite, and BuMines Anvil Point (Rifle) oil shale. The differences between the PILEDRIIVER data and those from the rock types listed in Table III emphasize that the petrology is not consistent and predictable from one location to another. Not only are there great differences among different rock types, but there are differences within a few feet in one rock type. Each specific location must be studied separately and evaluated on the basis of its own unique characteristics.

The final column in Table III is the author's estimate of a particle-size distribution that might be encountered from nuclear blasts in a rock typical of some ore deposits. Note that 80% of the material is smaller than 3 ft, about 50% is smaller than 1 ft, and about 5% is minus 20-mesh. The bulk of the material, about 70%, is between 1 in. and 3 ft. For the PILEDRIIVER rubble, this number is closer to 80%. As mentioned before, this combination of few very large boulders and almost no fines is favorable for in-place leaching.

DISTRIBUTION OF RADIOACTIVITY

The particle size-fractions of the two samples were studied further to determine the distribution of radioactivity by size. Representative samples of each fraction were placed in a scintillation well-counter to record the gross-gamma activity in counts/min per gram. The energy level of the counter was set at 0 to 0.71 MeV. From these data, the total counts per min and the percent of total activity in each size-fraction were calculated (see Table II), and the cumulative percentage of radioactivity in each size-fraction plotted (Fig. 11).

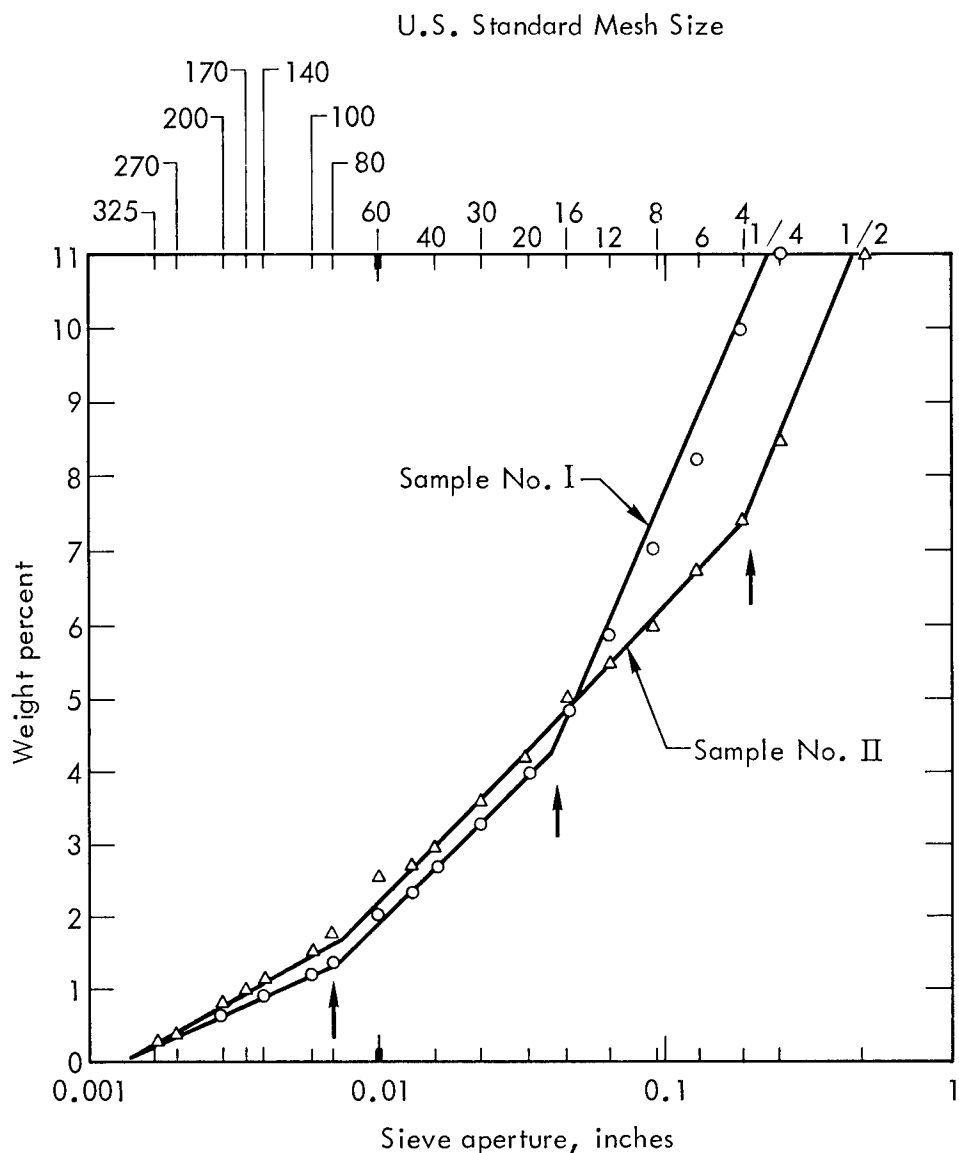


Fig. 10. Weight percent vs particle-size distribution on an expanded scale for Samples I and II. The arrows mark the breaks in the curves. On the horizontal scale, all the large ticks refer to sieve aperture, and all the small ticks refer to mesh size.

In order to save time and effort in sample preparation, a brief study was made to determine whether the total counts per minute was affected by particle size. In duplicate counting runs, 1/4-in., 10-, and 60-mesh material were compared with equal weights of the same material finely ground to about 100 mesh. The geometry of the two compared samples was the same except that the depths of material in the counting vials varied slightly. This small (less than 10% maximum) difference in depth of samples had no significant effect, and the results were essentially the same, provided that the samples were equal in weight. The gross-gamma counts varied directly with the weight of the sample. In other words, provided that portions of the same particle size-fraction were of equal weight, they gave the same counts, regardless of the degree of fineness of the material being counted.

Table III. Comparative particle size distributions.

1	Cumulative weight percent						
	2	3	4	5	6	7	8
Size (smaller than)	PILEDRIIVER (observed ^a)	PILEDRIIVER Sample II ^b	HARDHAT ^{c,d}	DANNY BOY ^{d,e}	Pre- SCHOONER delta ^{d,f}	Oil shale ^g	Estimated typical for hard rock ^h
6 ft	99.5	100	100	100	100	—	100
5 ft	—	—	95	88	100	—	94-96
4 ft	98	—	88	83	92	99	90-95
3 ft	95	93	75	75	74	—	80-85
2 ft	85	—	60	63	57	96	60-75
1 ft	60	—	40	43	38	90	40-60
6 in.	45	50	30	30	28	70	30-40
4 in.	30	—	25	24	25	—	25-30
3 in.	—	31	—	—	—	17	20-30
2 in.	20	—	20	15	20	—	15-20
1-1/2 in.	—	—	16	13	18	—	13-18
1 in.	15	14	14	11	16	—	15
3/4 in.	—	—	12	9	14	—	12
1/2 in.	11	11	10	8	12	—	10
3/8 in.	—	—	9	7	11	—	8
# 4	10	8	7	5	8	—	6
20 mesh ⁱ	5	4	5	—	—	—	5

^aField observation and measurements by S. Hansen and D. Rabb (1967), unpublished data.

^bBased on data from Table II.

^cEstimate based on visual estimates from field observations and measurements published by Boardman, Rabb and MacArthur (1963),¹¹ and size determinations by Rodean (1964) from photographs taken of HARDHAT rubble.¹²

^dData is in approximate agreement with Hansen and Toman (1965).¹³

^eU. S. Army Engineer Waterways Experiment Station, C. E., "Investigations of Manufacture of Rip-Rap and Aggregate by Nuclear Methods," PNE-5003.¹⁴

^fU. S. Army Engineer Waterways Experiment Station, C. E., "Project Pre-SCHOONER, Geologic Investigations and Engineering Properties of Craters," PNE-505.¹⁵

^gDerived from D. Lombard (1965).¹⁶

^hGrossly dependent upon fracture pattern and type of rock at specific site.

ⁱDependent upon grain size of host rock.

From the data in Table II and in Figs. 10 and 11, it is evident that the observed radioactivity per gram varies inversely with particle size, and is, roughly a function of surface area. This generalization does not hold true for the minus 100-mesh sizes, probably because of the less-than-spherical shapes of the fine shards of the mineral grains. Although Sample I contains more gross-gamma activity than Sample II by a factor of 3, the results of this study indicate that in both samples the minus 100-mesh material comprises only 1.5% of the total weight but traps 20% of the radioactivity. Conversely, the plus 1-in. portion comprises 80% of the weight but traps only 20% of the radioactivity. The higher concentrations of gross gamma in the fine material.

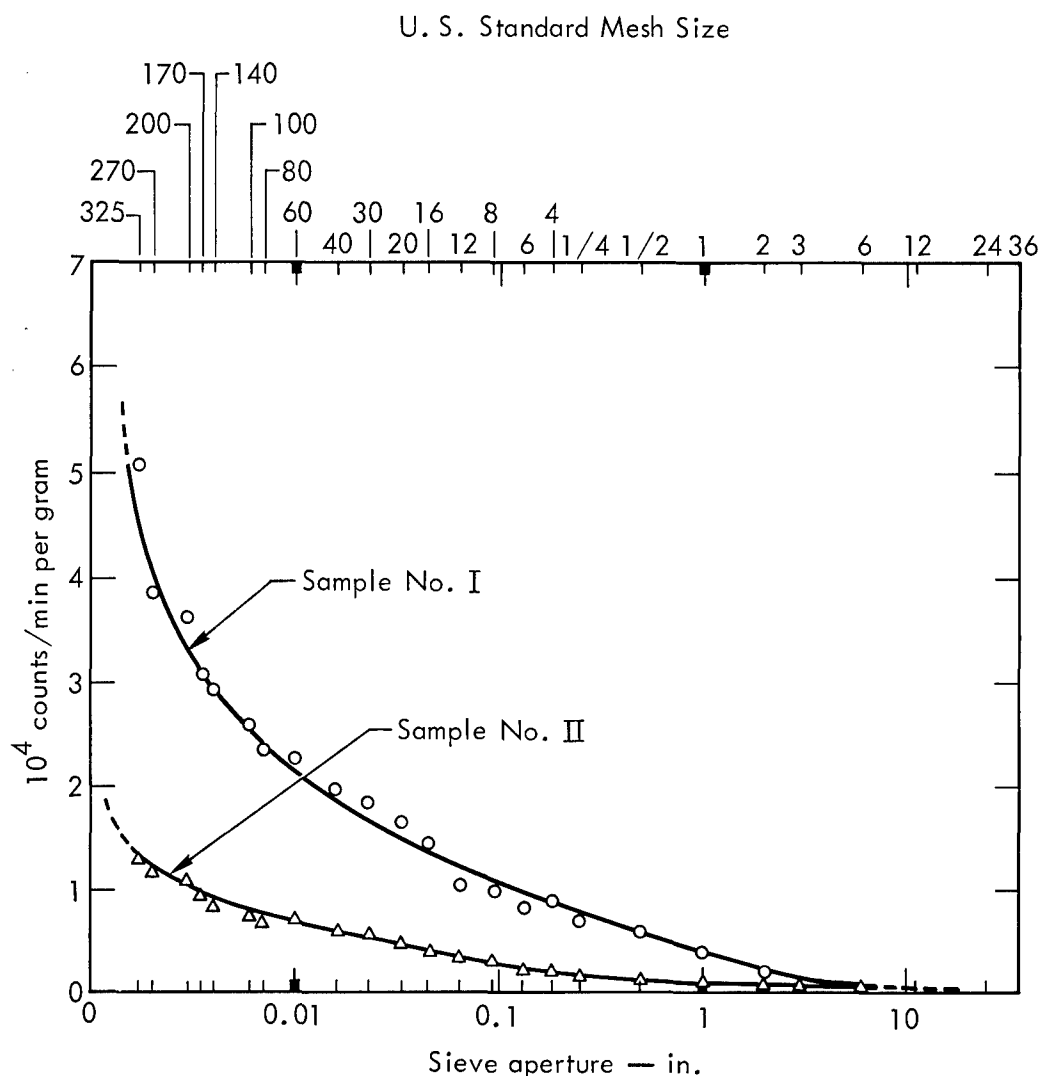


Fig. 11. Radioactivity vs particle-size distribution for Samples I and II. On the horizontal scale, all the large ticks refer to sieve aperture, and all the small ticks refer to mesh size.

may present a potential hazard if sand-slime filters are used to clarify leaching solutions. The slimes from leaching solutions off a chimney could contain a considerable concentration of radioactivity. The magnitude of this problem depends upon the conditions at the individual site and upon the particular nuclear explosive used. It must be evaluated separately for each site.

One theory as to why there is a higher concentration of radioactivity near the edge of the chimney is the following: In the early stages of the explosion, when the cavity is growing and overlying rock is being moved, there is tendency for plug-fault, or cork-type, movement. The rock directly over zero point moves up *en masse*, and most of the separation or shearing movement occurs in the cylindrical interface approximately representing the chimney wall. As the plug pops up, there are many stepfaults. This fault series or shear zone is

evident in the offsets of the horizontal "barber-pole" hole which was explored after the HARDHAT Event (see Fig. 12).^{1,2} This phenomenon allows gasses and radioactivity to penetrate in this area more readily than in the center of the chimney. Therefore, Sample I contained more radioactivity than Sample II.

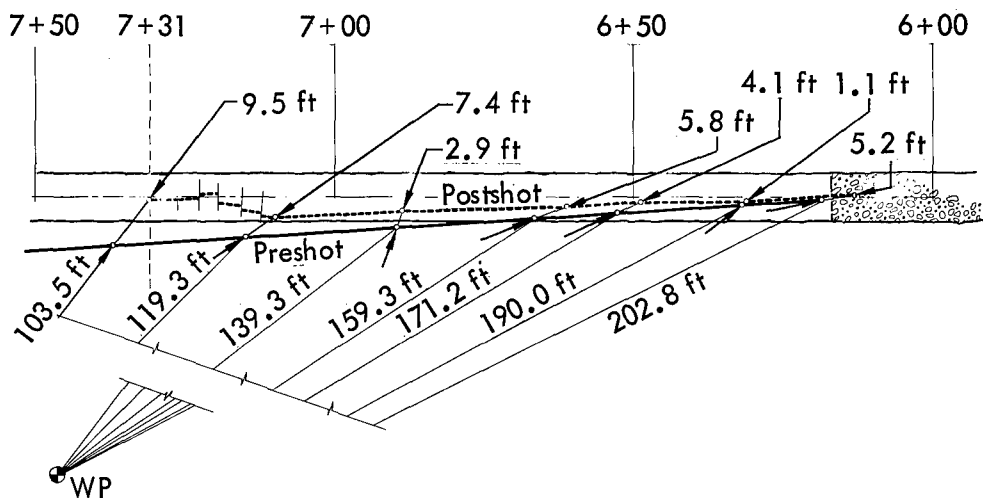


Fig. 12. Cross section of the postshot-reentry exploration drift showing the postshot movement of the "barber pole."

SMALL-SCALE BATCH-LEACHING TESTS

To obtain a preliminary approximation of the behavior of radioactivity during leaching in place, representative portions of particle size-fractions of Samples I and II were subjected to a simulated film-percolation leach test as follows.

A measured amount of liquid at room temperature (70 to 75° F) was dripped slowly over a weighed sample of the sized material, and the effluent OFF-solution (and slimes) were collected. Duplicate tests were made for each size-fraction sample, one with 0.1 N sulphuric acid solution ($\text{pH} \approx 1.5$) and the other with distilled water. Each sample was suspended in a stainless steel funnel over an enamel tub. Every attempt was made to slowly wet all the surfaces with no jetting, hydraulic washing, or mechanical scrubbing. The leaching cycle was continued for about 2 hr or until the radioactivity in the effluent was negligible. Then the sample was rinsed with water and dried, and a representative sample was prepared for gross-gamma analysis in the scintillation well-counter. In Table IV, the counts/min in the tails (residue) from water and acid leaching are compared with the counts/min in the untreated heads samples.

The results indicate that an average of about 25% of the radioactivity is removed by the short-time, water percolation leach, and about 40% by the dilute acid. It appears that about 33% of the radioactivity in the nuclear chimney would be removed in the first slug of leach liquor, and a large portion of this activity would be in the slimes. After that, additional dissolution and extration would proceed at a slower rate. It will probably take years for 60 or 75% extration from such a chimney.

Additional investigations were done to determine the rate and depth of penetration of leaching solutions into 6- to 8-in. granite boulders collected after the PILEDIVER event from near the explosion area; these postshot

Table IV. Percolation leach-test results.

Sample	Particle size		Radioactivity (counts/min/g)			% removed by leaching	
	Minus	Plus	Heads	Tails		Acid	Water
				Acid	Water		
I	—	6 in.	0.3	0.15	0.3	50	0
	6 in.	1 in.	2.9	1.5	1.8	48	38
	1 in.	1/4 in.	4.3	1.9	2.2	56	51
	1/4 in.	20 mesh	9.9	6.1	8.1	38	18
	20 mesh	—	22.1	12.6	12.7	43	43
Average						47	30
II	—	6 in.	0.2	0.5	0.15	75	25
	6 in.	1 in.	0.5	0.37	0.45	25	10
	1 in.	1/4 in.	1.3	0.8	1.1	38	15
	1/4 in.	20 mesh	3.8	2.8	3.0	26	21
	20 mesh	—	7.9	5.3	6.1	33	23
Average						40	19

samples were compared to similar pieces obtained during preshot mining activities. When fluorescent dye was added to the leaching solution, subsequent cutting and examination under black light showed that the postshot samples contained many more interior microfractures than did chunks of rock from the same area mined by conventional methods before the event. These very fine fractures allow leaching solutions to penetrate faster, deeper, and more completely into the interior of the rock.¹⁷ The postshot and preshot samples are depicted in Fig. 13.

Another study of the close-in effects of shock pressures on samples from the same granite stock showed that microfractures, plastic deformation, and physical properties all varied with specific distances from the shot point.¹⁸

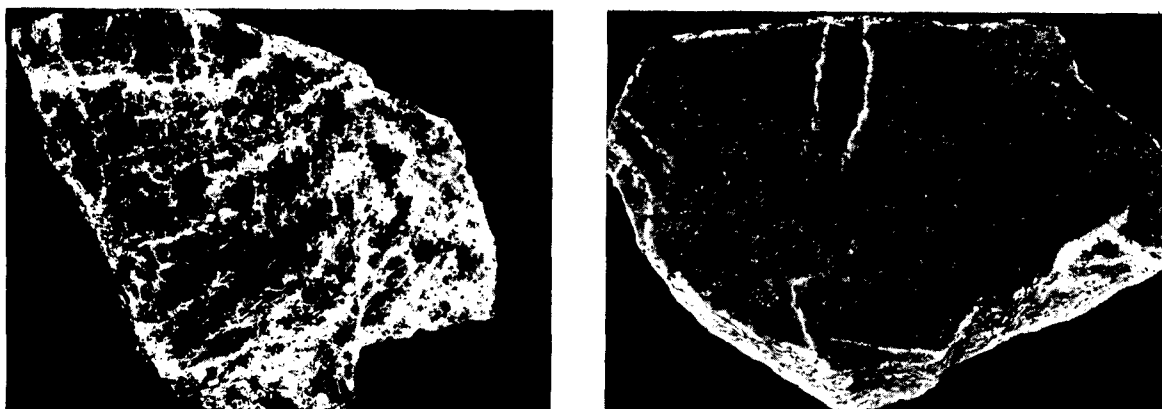


Fig. 13. Left: granite boulder, postshot, showing the fractures produced by the nearby PILEDRIVER nuclear explosion. Right: Granite boulder, preshot, mined by conventional mining methods.

Preliminary assays for Ru, Cs, Sr, Ce, and Eu on some of the size-fractions of the two samples of PILEDRIVER rubble indicate that each of these nuclides is distributed throughout the various particle sizes in the same proportion as the gross-gamma activity is distributed. Therefore, it appears that chemical analyses of the heads sample and of one selected size-fraction will permit a close approximation of the specific activities in the other size-fractions, thus saving analytical time and labor.

In an attempt to prove that radioactivity in PILEDRIVER rubble is concentrated on (and confined to) the surface of the particles, microradiographs were prepared of several size-fractions of Sample I. Because of the very low level of activity, no clear confirmation of this theory was attained.

Generally speaking, the bulk of the radioactivity produced in any contained nuclear explosion, either as fission products or induced activity, is trapped in the glassy melt as it solidifies. There are, however, some isotopes which escape entrapment and can be found in quantity in the chimney, notably $^{89,90}\text{Sr}$ and ^{137}Cs , which are decay products of gaseous precursors (Kr and Xe), and $^{103,106}\text{Ru}$ and $^{141,144}\text{Ce}$ which are transported as volatile compounds to considerable distances from the melt zone.

Estimates by LRL radiochemists based on extensive postshot analyses of the radioactivity distribution from PILEDRIVER indicated that about 25% of the $^{103,106}\text{Ru}$ produced was trapped in the melt and 75% was volatilized and deposited in the chimney and surrounding area.¹⁹ For ^{137}Cs the estimate was 12% in the melt and 88% not in the melt. No estimate was made for Sr and Ce. In addition, ^{125}Sb , $^{95}\text{Zr}/^{95}\text{Nb}$, ^{147}Pm , and ^{185}W were shown to be depleted to unspecified degrees in the slag and correspondingly enriched in the nonmelt area.¹⁹ Distribution of other isotopes was 95% or more in the glass with the remainder elsewhere. Because of the availability of these volatile compounds dispersed up in the chimney and deposited on rubble surface, they are relatively soluble; i.e., up to 60% in dilute sulphuric acid (0.1 N) as compared to only 2% or less of the radioactivity in the glassy slag. Twice as much radioactivity, however, was dissolved from the frothy portion of the slag as from the glassy slag. When specified radionuclides are considered, the extraction of Ru or Sr was five times that of Cs, in either froth or glass.

Other long-lived fission products which are soluble in the dilute acids commonly used in leaching and which frequently show up in acid leaching solutions off of chimney rubble are ^{91}Y , ^{185}W and $^{154,155}\text{Eu}$. Also, Sc and Fe may be significant at early (2 month) reentry, and Co and Se, at the estimated time for normal mining reentry (8 months). For PILEDRIVER chimney rubble, up to 60% of the Sr present was dissolved; Ru, 40%; Cs, 20; and Ce, 15.

Any Cs, and most of the Ag and Zr-Nb, in the leaching solution seem to be adsorbed by the clays and rock minerals and do not leave the leach bed. In one test in which a measured amount of ^{137}Cs was added to the circulating leach solution, essentially all was adsorbed; the effluent off-solution was barren of Cs even after 15 cycles. Similar tests with Ru, Sr, Co, Ce, and Y showed that negligible amounts were adsorbed; these nuclides tended to stay in the acidic leaching solutions. Strontium adsorption was weak but erratic (10 to 70%), depending upon pH.²⁰ All isotopes were adsorbed least in the more highly acid conditions; for example, Ru: less than 5% was retained in the ore at pH 2, but 40% was retained at pH 3 and 95% at pH 4.²⁰ If iron is precipitated (as basic sulphates) at any point in the circuit, the Ru tends to drop out quantitatively with the iron.

In the copper precipitation step, over 50% of the soluble Ru and 20% of the Zr-Nb followed the cement copper. No Cs or other soluble isotope was precipitated in appreciable quantity with the cement copper except Ru and

Zr-Nb. Possible Ru could be scavenged from solution by a resin (e.g. Dowex 1), activated charcoal, or copper beads, or a clean separation might be effected on a liquid ion exchange media such as LIX-64. Most of the Zr-Nb in the pregnant leach solution may also be picked up by the LIX-64, but in one test the concentration was so low that the results were inconclusive.²⁰

Direct smelting of the Ru-contaminated cement copper under reducing conditions showed that all the Ru reported in the blister copper.²⁰ Electrolytic refining, however, should give a relatively pure copper cathode. About 66% of the Ru remains in the electrolyte, 33% goes to the mud, and only 1% follows the copper. Additional studies are required to determine whether Ru builds up in the electrolyte, and if so, to find a means of control. It was also reported that of the total induced activity in the chimney, only 5% went into solution and only 6% of this soluble fraction (principally Zr and Se) went with the cement copper.²⁰ These isotopes were later tied up in the slag during smelting and thereby eliminated.

Tritium produced from lithium in the ore or from a fission device is likely to be the most abundant radionuclide in the chimney. In laboratory tests at LRL it was possible to flush out 95% of the tritium in small-volume, advancing displacement wash of solution which contained only 5% of the copper. Tritium cannot be reduced in concentration by ion exchange, but only by dilution. The tritium in the water in the wet cement copper evaporates during smelting and does not contaminate the electrolytic copper produce. Limited studies were made at LRL of the effect of low-level concentrations of specific radioactive isotopes on the efficiency of the autotrophic bacteria* so important in some leaching systems. Results indicated that exposure to a few mR from a ⁶⁰Co source or from small concentrations of ¹⁰⁶Ru or ¹³⁷Cs tended to stimulate the activity and growth of the bacteria.²¹ After four or five days, however, the bacterial population dropped essentially to zero because reproduction had been arrested. Further investigations of this phenomenon are required if nuclear explosives are to be used to break up ore bodies prior to leaching.

Acknowledgments

This work was performed under the auspices of the U.S. Atomic Energy Commission.

Special thanks are given to individuals contributing to this work: Gaylan Adair (REECO Mine Superintendent, NTS) for the design and economical accomplishment of the reentry, Hugh Wilson (USBuMines, Salt Lake City) for sample preparation, C. R. Boardman (LRL Geologist) for the drilling program, J. S. Kahn and the LRL Geo-Sciences Group for guidance, supervision, and radioactivity analyses, and M. D. Nordyke for a critical reading and aid in data interpretation.

Also, to the DOD Staff for PILEDRIVER Event: Lt. Col. Bernard Robinson, DOD, DASA, Test Director, Sandia Base, Albuquerque, New Mexico, and Prof. J. L. Merritt, Chief Scientist, Univ. of Illinois, for their invaluable cooperation.

*Thiobacillus thiooxidans and Thiobacillus ferro-oxidans.

References

1. D. D. Rabb, A Mining Experiment in Granite, Lawrence Radiation Laboratory, Livermore, California, Rept. UCRL-7608 (1963).
2. D. D. Rabb, Block Caving, Nuclear Style, Mining Engineering, 48-52 (1964).
3. C. R. Boardman, Results of an Exploration into the Top of the Piledriver Chimney, Lawrence Radiation Laboratory, Livermore, California, Rept. UCRL-50385 (1967).
4. C. R. Boardman, Some Characteristics of the Hardhat Chimney and Surrounding Wall Rock, Lawrence Radiation Laboratory, Livermore, California, Rept. UCRL-50177 (1966).
5. C. R. Boardman, A Measurement of the Volume of Void in the Shoal Chimney, Lawrence Radiation Laboratory, Livermore, California, Rept. UCRL-50150 (1966).
6. D. L. Springer, Lawrence Radiation Laboratory, Livermore, California, private communication (1967).
7. H. A. Tewes, Lawrence Radiation Laboratory, Livermore, California, private communication (1968).
8. T. S. Sterrett, Lawrence Radiation Laboratory, Livermore, California, Report in process on PILEDRIVER Underground Drilling Results.
9. C. R. Boardman, Lawrence Radiation Laboratory, Livermore, California, private communication (1968).
10. E. E. Malouf, Metallurgist, Kennecott Copper Corporation, Salt Lake City, Utah; William R. Hardwick, Engineer, U.S. Bureau of Mines, Tucson, Arizona; and Dr. George Griswold, New Mexico Institute of Mining and Technology, Socorro, New Mexico, private communications (1968).
11. C. R. Boardman, D. D. Rabb, and R. D. McArthur, Characteristic Effects of Contained Nuclear Explosives for Evaluation of Mining Applications, Lawrence Radiation Laboratory, Livermore, California, Rept. UCRL-7350 Rev. I (1963).
12. H. C. Rodean, The Particle Statistics of Rubble Produced by Underground Nuclear Explosions, Lawrence Radiation Laboratory, Livermore, California, Rept. UCRL-12129 (1964).
13. S. M. Hansen and J. Toman, Aggregate Production with Nuclear Explosives, Lawrence Radiation Laboratory, Livermore, California, Rept. UCRL-12180 Rev. I (1965).
14. U.S. Army Corps of Engineers, Waterways Experiment Station, Vicksburg, Miss., Investigations of Manufacture of Rip-Rap and Aggregate by Nuclear Methods, AEC Rept. PNE-5003 (1965).
15. U.S. Army Corps of Engineers, Waterways Experiment Station, Vicksburg, Miss., Project Pre-Schooner, Geologic Investigations and Engineering Properties of Craters, AEC Rept. PNE-505 (1967).

16. D. B. Lombard, The Particle Size Distribution and Bulk Permeability of Oil Shale Rubble, Lawrence Radiation Laboratory, Livermore, California, Rept. UCRL-14294 (1965).
17. D. D. Rabb, Penetration of Leach Solution into Rocks Fractured by a Nuclear Explosive, Lawrence Radiation Laboratory, Livermore, California, Rept. UCRL-71173 (1968).
18. Nicholas M. Short, Effects of Shock Pressures from a Nuclear Explosion on Mechanical and Optical Properties of Granodiorite, J. Geophys. Res. 71, 1195-1215 (1966).
19. Austin Prindle, Lawrence Radiation Laboratory, Livermore, California, private communication (1968).
20. D. J. Crouse, W. D. Arnold, and F. J. Hearst, Nuclear Explosives in Copper Ore Processing, Chemical Applications of Nuclear Explosions, Oak Ridge Nat'l. Lab., Tenn., Rept. ORNL-TM-1191 (1965).
21. D. D. Rabb, Leaching of Copper Ores and the Use of Bacteria, Lawrence Radiation Laboratory, Livermore, California, Rept. UCID-4958 (1965).

CHEMICAL MINING OF PRIMARY COPPER ORES BY USE OF NUCLEAR TECHNOLOGY*

A. E. Lewis

Lawrence Radiation Laboratory, University of California
Livermore, California 94550

ABSTRACT

Chemical mining of primary copper ores, with nuclear explosives to break the ore and in-situ hydrostatic pressure to accelerate dissolution of primary ore minerals, may be feasible. A contained nuclear explosion well below the water table would be used to provide a mass of broken ore in a flooded "chimney." The hydrostatic pressure in the chimney should increase the solubility of oxygen in a water-sulfuric acid system enough to allow primary copper minerals such as chalcopyrite and bornite to be dissolved in an acceptably short time. Circulation and collection would be accomplished through drill holes.

This method should be especially applicable to the deep portions of porphyry copper deposits that are not economical to mine by present techniques.

INTRODUCTION

Primary copper deposits consist of copper minerals unaltered by weathering or associated processes. Many such primary deposits have been upgraded by processes of oxidation and supergene enrichment to concentrations that make them economical ore deposits. The geologic process that acts on primary sulfides is one of oxidation and weathering, chiefly above the water table, and downward percolation and redeposition of the copper in the form of secondary sulfides, oxides, carbonates, and other copper-containing minerals. The enrichment process is therefore a near-surface process, although subsequent geological events may result in the burial or removal by erosion of the ore deposits.

Most ore deposits have been developed by mining the enriched and oxidized zone of such deposits. Only where the primary ore is rich enough has it been economical to mine at depth or, with large and efficient earth-moving equipment, to mine large deposits in open-pit mines. Leaching techniques have been applied economically to the oxidized parts of ore deposits or to those that can be oxidized by alternate solution and weathering or bacterial oxidation. Because of the low permeability of such ore deposits, this has not been done in-place, with the exception of some leaching operations conducted on caved material in mine workings. Primary sulfides such as chalcopyrite have not been economically leachable by present technology. These ores have been processed by sulfide concentration and smelting. Large deposits of primary sulfides remain undeveloped because they lie too deep to mine economically, their size is too small to allow the economics of large-scale mining operations, the grade is too low, or various combinations of these factors.

*Work performed under the auspices of the U. S. Atomic Energy Commission.

Reserves of copper would be considerably increased if an economical process of obtaining copper from deep primary copper sulfides were available.

In this paper, we describe a process that might make this possible.

PROCESS FOR CHEMICAL MINING OF PRIMARY COPPER ORES

In the process proposed, a nuclear chimney is created in a copper ore body (Fig. 1). The chimney is formed well below the water table and is filled with water either by natural inflow or by artificial addition. At least two holes

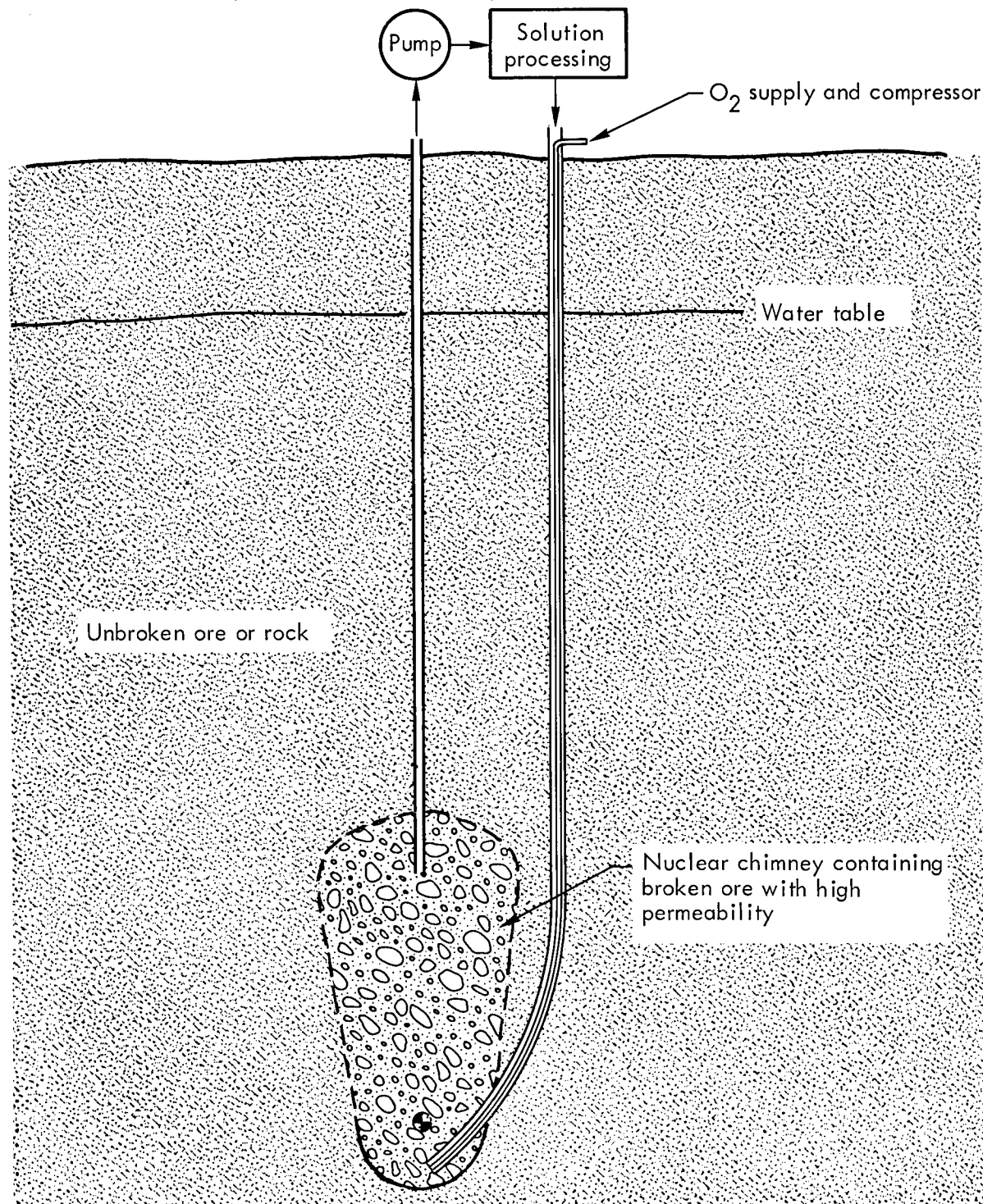


Fig. 1. Illustration of chemical mining by use of hydrostatic pressure in a nuclear chimney to increase the solubility of oxygen.

are drilled into the chimney, one near the bottom and one near the top. Oxygen gas is then pumped into the bottom of the chimney and allowed to rise upward. Any excess not reacting will rise to the surface through the well leading out of the top of the chimney. If insufficient sulfuric acid is produced in the oxidation of pyrite and copper-bearing sulfides, acid may be added.

Circulation and recovery of copper from the solution is begun when the concentration of copper is high enough to optimize profitability. The rate of circulation will depend upon various factors that remain to be determined, such as the liquid-to-rock ratio in the chimney, the size of the solution-processing plant, the chemistry of the solution process, and local hydrologic conditions. Losses of solution or addition of new water to the system from surrounding rocks can be effectively controlled by maintaining a pressure balance between the chimney and the surrounding country rocks. If the hydrostatic head in the chimney is equal to the hydrostatic head in the wall rock, no lateral migration is possible except by diffusion, which is expected to be negligibly slow. A small pressure gradient will induce circulation through the chimney as long as the permeability of the chimney is significantly greater than that of the wall rock. The permeability of a nuclear chimney in rock typical of most ore bodies is expected to be almost infinite, compared to the permeability of unbroken ore. If the permeability of the wall rock is low enough, the pressure in the chimney may be increased above that due to the hydrostatic head of the water table, by raising the water level in both holes above the water table. This would also reduce pumping costs in regions where the water table is deep.

We have shown thus far how a flooded chimney can act as a pressure vessel below the water table even if the wall rocks are permeable.

SOLUBILITY OF CHALCOPYRITE IN SULFURIC ACID SYSTEM

At low hydrostatic pressure, chalcopyrite (CuFeS_2) and most other primary sulfide minerals are not dissolved by sulfuric acid solutions, or the rate of solution is so slow that any such process is impractical. The rate-limiting step appears to be associated with the oxidation of the primary sulfides. Addition of oxidizing agents is known to increase the rate of solution by sulfuric acid solutions. In present heap leaching operations, air is introduced by downward-percolating leach solutions and is effective to a limited extent in oxidizing the sulfides. The maximum partial pressure of O_2 is 0.2 atm, resulting in a very slow oxidation. Bacteria have been used to some extent to accelerate the oxidation. Other oxidants, especially Fe^{3+} and Cl_2 , have been observed to accelerate the oxidation of sulfide minerals more effectively than O_2 .¹ Because the solubility of O_2 in water or acid solutions is a function of the partial pressure of O_2 , the amount of O_2 that can be put into solution is increased by increasing the pressure. Various experimenters have described processes in which oxygen is introduced into sulphuric acid solutions under pressure, using air or oxygen. The minerals oxidized and dissolved include pyrite,² chalcocite,³ and chalcopyrite.⁴ Because these processes were designed to be conducted in an autoclave, experiments were conducted at temperatures above 100°C and at pressures as high as 500 psi of oxygen. Significantly fast reaction times were obtained in a few hours under these conditions. It seems likely that under the temperatures and pressures obtainable in a nuclear chimney, significant rates of solution can be attained in weeks or months if not days. Hydrostatic pressures in a nuclear chimney depend on the head of water and are approximately 435 psi or 30 bars for each 1000 ft below the water table. We expect temperatures averaging near 50°C in most regions. A few experiments were conducted to determine whether the rate of solubility of chalcopyrite is in fact proportional to the partial pressure of oxygen under conditions of hydrostatic pressure and temperature typical for this application. A mixture of pure chalcopyrite and quartz (+14 and -8 mesh) was placed

in a pressure vessel, immersed in water, and pressurized by slowly bubbling oxygen gas through it. The vessel was maintained at a temperature of 50°C, and the copper content of the solution was measured as a function of time. The results are shown in Fig. 2. The slopes of the curves at two pressures

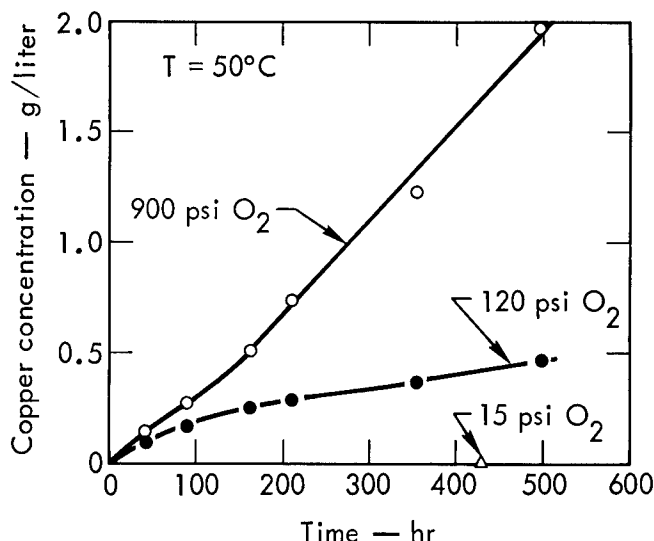


Fig. 2. Relative solubility rate of chalcopyrite in water for several oxygen pressures.

of O₂ are proportional to the pressures, showing that the rate of solution is proportional to the oxygen partial pressure under these conditions.

Most ore deposits contain pyrite (FeS₂) in addition to copper sulfides. The amount of sulfuric acid produced by the oxidation of pyrite, or consumed by other minerals such as carbonates, will determine how much, if any, acid must be supplied to the mining process at a particular site.

RADIOACTIVITY

Most fission products are trapped in the insoluble glass at the bottom of the chimney. The fission products of concern in chemical mining are the more volatile and soluble products that are deposited in the chimney. If a fusion or thermonuclear device is used, the fission products can be greatly reduced, although higher tritium concentrations are produced. The fission-fusion ratio of the explosive must therefore be fixed so as to minimize the problems of designing a safe processing plant. Experiments are needed in appropriate rocks in order to understand the solution chemistry in nuclear chimneys. With such information the proper device can be selected and a suitable processing plant can be designed.

NUCLEAR EXPLOSIVE EFFECTS AND EXPERIMENTAL OUTLINE

The cavity produced by a nuclear explosive in a typical porphyry copper is probably about the same size as that produced in a "granite." The cavity radius can be calculated⁵ from

$$R_c = \frac{CW^{1/3}}{(\rho H)^\alpha}$$

where C is a constant for each rock type ($C \approx 100$ for "granite"), ρ = density, α is a constant which may be determined from the water content ($\alpha = 0.32$ for $\sim 2.5\%$ H₂O), W is the yield of the explosive in kilotons, and H is the depth of burial (DOB) in meters. The radius (R_c) and volume of the cavity (V_c) as

functions of depth of burial, yield, and scale depth of burial are shown in Fig. 3. To contain the explosion underground, one must bury the explosive deeper than $90W^{1/3}$, and the yield is limited by the amount of seismic damage that can be tolerated at a specific site.

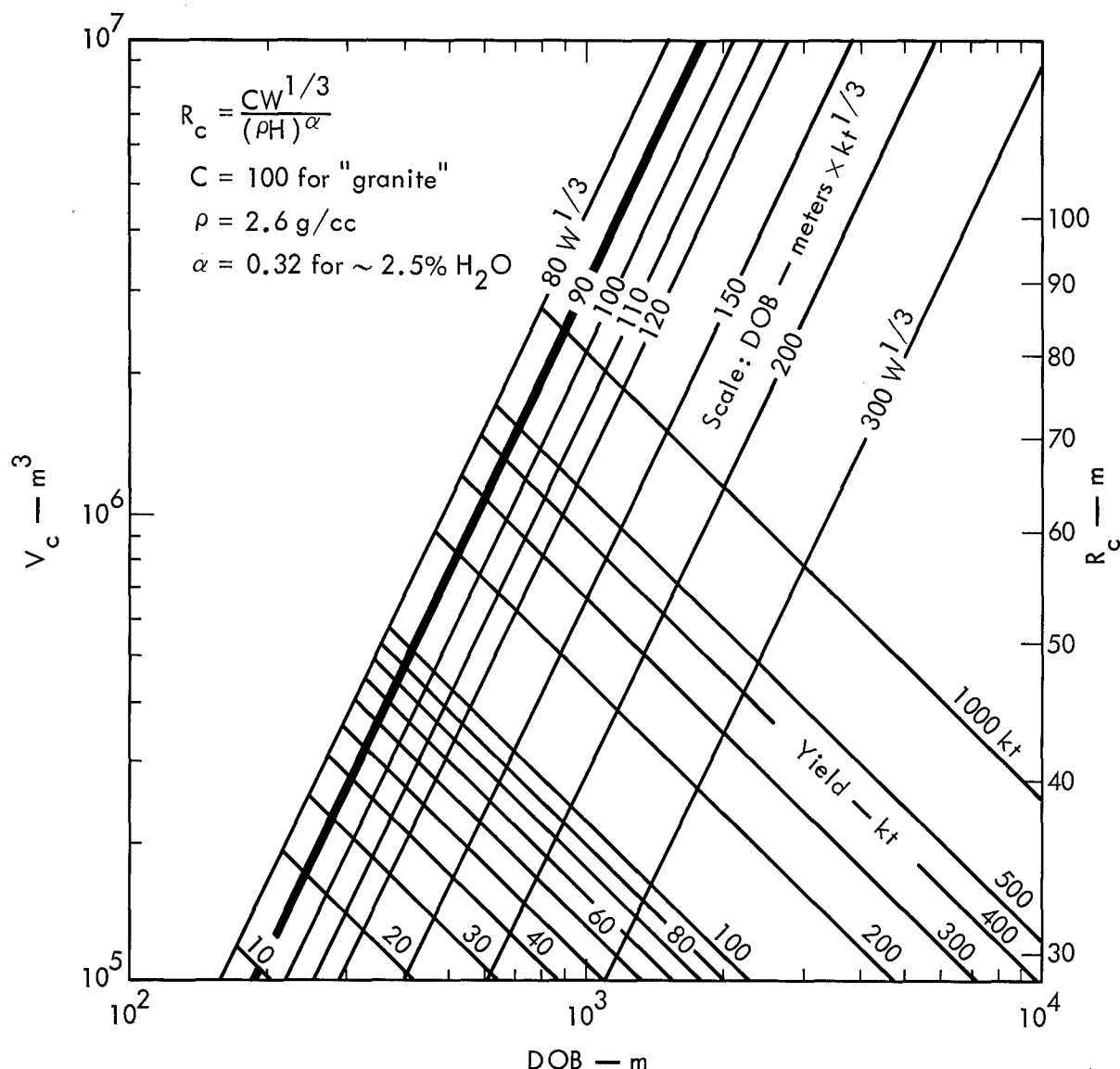


Fig. 3. Graph showing relationships among cavity radius (R_c), cavity volume (V_c), yield (W), depth of burial (DOB or H), and scale depth of burial (SDOB).

The volume of rock broken is dependent only on the bulking factor (B) (Fig. 4). B is a measure of the amount of open space introduced into the broken rock by distributing the cavity volume throughout the chimney [$B = V_c/(V_c + V_r)$]. Unfortunately, B is not well known in nuclear chimneys because it is calculated from a known cavity volume and an uncertain chimney geometry (Fig. 5). Given a measured height, it can be seen that B can be in error if the slope of the chimney wall is uncertain.

It is not conclusive from available data whether chimney walls are vertical or slope outward to some extent,⁶ and bulking factors are therefore

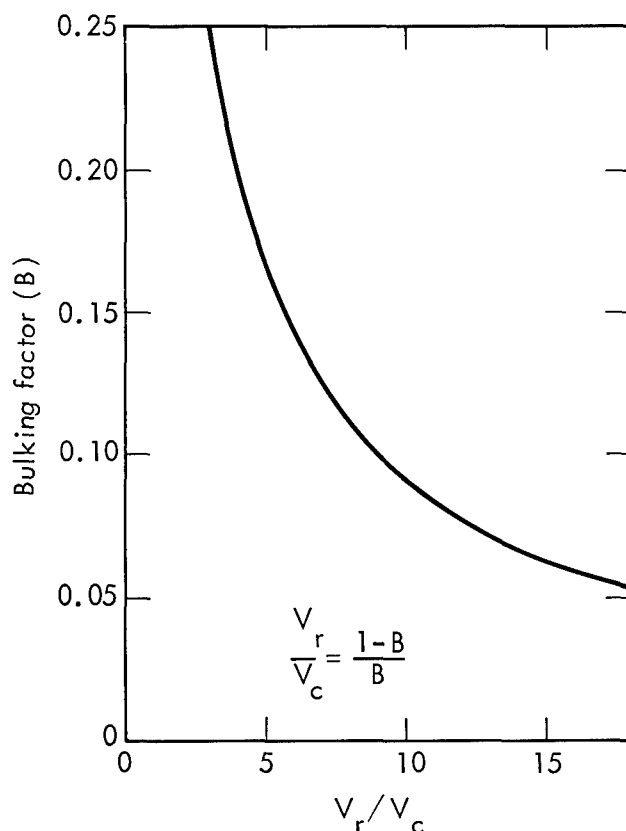


Fig. 4. Ratio of rock volume in chimney (V_r) to cavity volume (V_c) as a function of bulking factor (B).

unknown to the extent that the chimney volume is unknown. Figure 6 shows the maximum concentration of metal in solution for 100% recovery, as a function of ore grade and bulking factor.

Figures 3 through 6 can be used to estimate the dimensions of chimneys produced under various conditions and to evaluate the economics of mineral recovery, allowing the user to make his own assumptions of such variables as chimney geometry, bulking factor, cost of drilling, process and capital costs, and price of copper.

The following is an example of what we believe to be a reasonable, although perhaps conservative, evaluation of a possible experiment. The assumptions are as follows:

$W = 100 \text{ kt}$
 $DOB = 750 \text{ m (2440 ft)}$
 Water level at 50 m
 $B = 0.15$
 $\phi = 3 \text{ deg (slope of chimney wall)}$
 Copper price = 0.1¢/g ($\sim 45\text{¢/lb}$)
 50% recovery of copper from ore
 Ore grade = 0.5% copper
 $\rho \text{ of rock} = 2.7 \text{ g/cc}$

A cavity with a radius of $\sim 41 \text{ m}$ and a volume of $2.9 \times 10^5 \text{ m}^3$ would be produced. The chimney would have a height of $6.1 R_c$ or 250 m above the shot point and would contain $5.6 V_c$ or $1.6 \times 10^6 \text{ m}^3$ of rock. This would provide a hydrostatic pressure in the chimney varying from 1000 psi at the bottom of the chimney to 650 psi at the top. After 50% of the copper

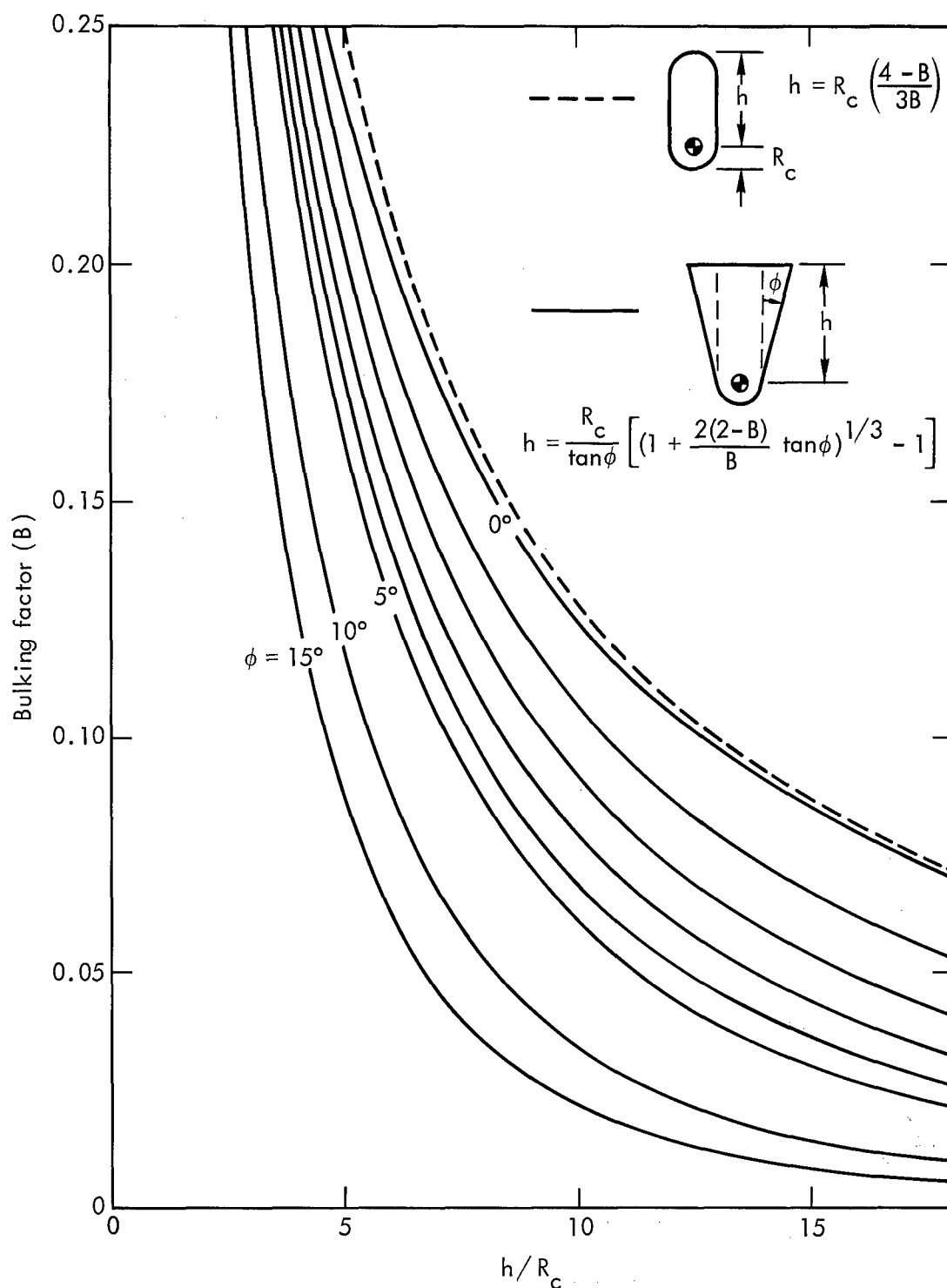


Fig. 5. Ratio of chimney height to cavity radius (h/R_c) for several chimney shapes as a function of bulking factor (B).

is in solution in the chimney, the solution will contain 38 g/liter. The total amount of copper in solution is $38 V_c \times 10^3 = 11 \times 10^9$ g, worth \$11 million.

The cost of detonating a nuclear device off the Nevada Test Site on an experimental basis is estimated to be about \$3 million. Other major expenses are the costs of drilling an emplacement hole and two mining holes and building an oxygen plant and a solution-processing plant. One million dollars should easily cover drilling costs. Oxygen delivered at a rate of

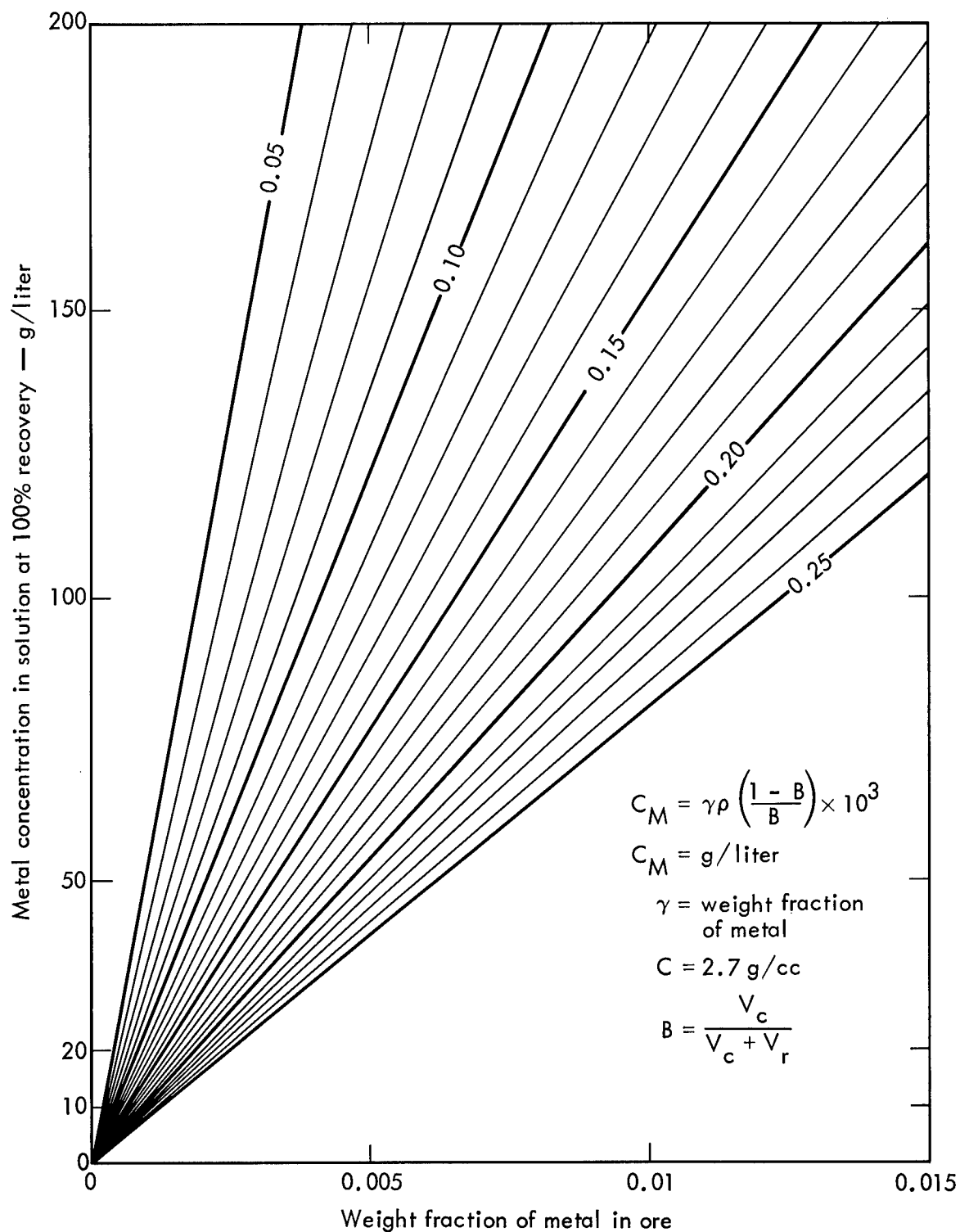


Fig. 6. Maximum possible concentration of metal in solution versus ore grade for various values of bulking factor (B).

5000 ft³/hr is estimated at \$7000/yr. The rate of circulation can be adjusted to permit a relatively inexpensive, small-capacity, solution-processing plant to be used. This experiment, therefore, not only can pay for itself, but there appears to be enough profit to pay for the data-acquisition essential to any new industrial technology.

In developing an ore body it would be necessary to use many shots to produce a multiple-chimney complex designed to fit the ore-body geometry.

A considerable saving could be expected, compared to an experiment consisting of a single shot.

CONCLUSION

We believe that the method of chemical mining proposed here is technically feasible and economically very promising. Among the questions to be answered are whether the proper distribution of oxygen and the required circulation of liquid in the chimney can be maintained. The actual rate of solution and the percent recovery possible must also be determined. Measurements of radioactivity in the chimney are essential for the design of the processing plant. These questions can best be answered by full-scale experiments, although some information can be obtained by laboratory experiments and by calculational analysis.

This method of mining offers many advantages. Large increases in reserves of low-cost copper would be obtained without the necessity of finding new ore deposits, because the type of deposit minable by this technique exists below many known deposits and can be developed easily. Production could be started rapidly, compared with underground or open-pit mining, and with a relatively small capital investment. Further advantages are that no dumps or open pits will be produced to disfigure the landscape; waste solutions are circulated back into the chimney, thereby avoiding any stream pollution; and there will be no atmospheric pollution common to smelting operations.

REFERENCES

1. E. Peters and H. Majima, The Physical Chemistry of Leaching of Sulphide Materials, Paper No. A68-32, presented at TMS-AIME Annual Meeting, February 1968, New York.
2. P. H. Johnson, "Acid-Ferric Sulfate Solutions for Chemical Mining," Mining Engr., 64-68 (August 1965).
3. H. Veltman, S. Pellegriai, and V. N. Mackin, "Direct Acid Pressure Leaching of Chalcocite Concentrate," J. Metals, 21-25 (February 1967).
4. A. Vizolyi, H. Veltman, I. H. Warren, and V. N. Mackin, "Copper and Elemental Sulphur from Chalcopyrite by Pressure Leaching," J. Metals, 52-59 (November 1967).
5. G. H. Higgins and T. R. Butkovich, Effect of Water Content Yield Medium and Depth of Burst on Cavity Radii, Lawrence Radiation Laboratory, Livermore, Rept. UCRL-50203 (February 1967).
6. T. Sterrett, Post-Piledriver Evaluation Program-Drilling, Lawrence Radiation Laboratory, Livermore, Rept. UCRL-50765 (September 1969).

Overburden Stripping From Deeply
Buried Orebodies by Controlled Nuclear
Explosive Casting
by L. W. Saperstein* and R. Mishra*

Abstract

Previous schemes to strip the overburden from a deeply-buried orebody by nuclear explosives have been hampered by various constraints. These are the notions that surface topography should slope in the desired direction to facilitate casting; that the orebody should be stripped all at once, meaning that an unsafe and unnaturally high yield will be detonated; or that the overburden be broken and cast, in a manner akin to conventional blasting, with a series of explosions linked by milli-second delays, such delays being an unproven and, perhaps non-permissible technology; and, finally, that the schemes leave an excessive amount of overburden to be removed by conventional means.

It is proposed that deep orebodies, idealized by a 250-ft. thick copper porphyry under 600 feet of cover, be stripped in successive rows, using available row-charge technology. A first row, of greater magnitude than those succeeding, is used to expose the orebody. The second row is placed so as to throw overburden into the void created by the first. All rows are placed so as not to damage the ore. Except for the first row, all rows utilize directed throwing. After a row is detonated, the ore beneath it would be removed by conventional means. The void thus created would provide space for the successive row to fire into. Further, the additional free-face provided by the void imparts a major direction to the ejecta. Because of the directed nature of the throw, ore removal does not have to proceed directly beneath the row slope. Advantages to this scheme are its adaptability to terrain; its reduction in overburden to be removed by conventional methods; its increased speed in uncovering ore; its reduction of unit costs; and its adaptability to production rates.

An example, utilizing the idealized orebody shows that production of ore can begin within a year of project approval versus four or five years for the same orebody developed conventionally; that no more than eight percent of the overburden has to be handled conventionally; and that unit cost for overburden removal is about four cents per ton, which is a two to ten-fold reduction in present-day costs.

* Department of Mining, The Pennsylvania State University,
University Park, Pennsylvania 16802

Introduction

The world is experiencing an inflationary demand for metals that has created an almost impossible to ease pressure on mineral producers. An increasing per capita demand for durable goods, inside a generally increasing population, has placed a spiralling demand on materials producers. A further pressure, quite unrelated to the technical problems of production, is caused by the political instability in the developing nations, many of which contain large natural resource deposits. A consequence of this pressure is that producers are actively seeking new ore deposits. Deposits that are, without a doubt, going to be lower grade, or more difficult to extract, than present ones.

As existing orebodies are depleted, the producers are willing to extract metal from orebodies of consistently lower tenor. Generally, in order to maintain earnings, a low-grade orebody must be sufficiently large to allow a proper amortization of investment. This means, however, that large sums of money must be committed to an orebody that may or may not turn a profit. Consequently, success or failure may hinge on the reduction of a few cents from operating costs. For example, by investing in large-scale materials handling equipment, some of the newest southwestern copper producers can open-pit a ton of ore for eight to twelve cents. This figure represents a two-to three-fold reduction on the average per ton cost (27¢) given by Pfleider^{15*} for fifteen open-pit copper mines in the American hemisphere. Thus, in face of rising demand, producers are turning to lower and lower grade orebodies. It is not implied that these orebodies have less total metal than the older, richer bodies, only that they have less metal per ton of rock. The lower grade results in lower unit profits and more difficult beneficiation.

Waste Removal from Open-pit Mines

In recent years, the extraction of large low-grade orebodies has been by open-pit methods. Briefly, this implies that the worthless, or waste, rock that covers the orebody is removed, or stripped, and dumped to one side and then the ore itself is removed. Open-pitting is different from underground operations, where selective mining takes only ore and leaves waste in place. The low unit cost of handling material in the open pit allows this handling of waste. The amount of waste, in tons, that must be handled for every ton of ore mined is called the stripping ratio; obviously, there are economic limits, dependent on the ore tenor, to stripping ratios.

Conventionally, there is little to distinguish waste mining from ore mining. Similar cycles of drilling, blasting, loading, and hauling are practised in both ore and waste.^{15*} Therefore the deeper the ore is to be found the more expensive it will be to mine because of the added stripping costs. Stripping ratios reported for the fifteen copper mines ranged from one to four with one outlier at 8.5. Given the low unit operating cost that has been reported, it becomes apparent that

*Superscript numbers indicate references listed at the end of the paper.

further cost reduction can be achieved only by complete change of mining method. One possible variation is the removal of waste overburden by casting with nuclear explosives.

In using conventional high explosives, the engineer is aware that the explosive will break and then throw the rock. Ordinarily, explosive emplacement is designed to minimize throw; however, in some instances, the round is overloaded so that throw becomes appreciable.¹⁶ This throw or casting may be necessary to get the rock into some better position, for example, for clean up by a shovel. The notion becomes apparent that if the round is overloaded, not with high explosives but with nuclear explosives, the throw may become of such a magnitude that the waste is spoiled directly into its storage areas without the intermediary help of shovels and trucks.

Nuclear Casting

Nuclear excavation schemes have been discussed for some time, 1,5,6,7,9,11,12,13,14 and it is not intended to review them here. In addition, several good reports have selectively covered nuclear stripping of ore bodies.^{2,16} It is intended to review these reports and then to propose an extension of their methods so as to make the nuclear method more efficient and flexible. The reference to "nuclear" is understood to be a shortening of nuclear explosive excavation.

Originally, it was concluded in a report by P. L. Russell that an orebody should be relatively small to be amenable to nuclear stripping.¹⁶ This was because it was conjectured that a crater from only one device could be used for stripping. Obviously, this report was written before the feasibility of nuclear row charges was generally known. The report stated that lack of control of throw was a disadvantage to nuclear stripping; and that sloping terrain, necessary to augment the throw, was desirable. With the conjecture of one crater for stripping the entire orebody, a further stipulation was made. In order to have sufficient crater diameter, without disturbing the ore, the minimum waste thickness had to be 200 feet. This report, like those subsequent, realized that a high-priority in its scheme was the need for no disturbance or dilution of the ore. The report had further use in that it catalogued some of the major copper orebodies in terms of their linear dimensions and depth of cover. Russell did propose an orebody of average dimensions, and it is this body that is used as a base for subsequent calculations.

It was also suggested in this report that it might be possible to bury the nuclear explosive such that the waste over the orebody would be ejected and the ore itself would be shattered or ruptured by the blast. This would mean careful placement of the explosive so that the ore would coincide with the plastic zone of the crater.¹⁷ A savings of the conventional drilling and blasting cost in the ore removal is assumed to be effected. Present opinion, however, holds that any such savings would be more than offset by the hazards involved in trying to work around rock that has been rendered incompetent and radioactive.

The Anaconda Company, in a report from its research laboratory, recognized that unit cost reductions are best achieved in large-scale operations.² They, therefore, proposed a large stripping operation with some thirty nuclear explosives. These explosives were to be placed in an approximately square array and were to be fired with milli-second delays. The timing sequence would set off the outer ring first, followed by those explosives remaining in the center of the firing area. It was decided that a certain amount of ground slope would be necessary to augment the throw. The report concluded that approximately 65 percent of the broken waste would be thrown and the remaining 35 percent would be removed conventionally. Approximately 14 percent of the waste would be unbroken, and would also be removed conventionally. Thus only 57 percent of the waste is removed nuclearly. The report indicated the then common costs for many of these mining operations.

Unfortunately, the Anaconda scheme has many drawbacks. The notion of delay blasting, while common in high-explosive work, is probably unacceptable in nuclear work. The first, or zero-delay, blast would disrupt the communication lines to the subsequent blasts, causing the non-permissible situation of an armed but uncontrolled device. An array of devices, as suggested, with a total yield of 20 megatons would lead to impossible situations in respect to ground shock, air blast, and residual radioactivity. Finally, the dependence on ground slope limits the general applicability of the scheme.

Representative Orebody

The feasibility of the proposed system will be demonstrated on a sample orebody that is representative of some of the more deeply-buried ore masses in the copper porphyry district of the southwestern United States. The dimensions of this sample are similar to those suggested by Russell.¹⁶ Horizontally, the ore zone is considered to be roughly square with an edge length of 5000 feet. Overburden thickness is taken at an average of 600 feet; the overburden, itself, is considered to consist of incompetent, fractured acid rock covered by a minor thickness of alluvium. The physical properties of the overburden are similar to those of granular material. To present the most difficult case for throwing, the surface is taken to be flat. The ore averages 250 feet of thickness, is relatively uniform, and has an average copper content of 0.45%. Considering a tonnage factor of 0.085 tons/ft.³, 532 million tons of ore are present.

This orebody is similar to many of those in the copper district. Figure 1 depicts this deposit. Since the purpose of this paper is to demonstrate that nuclear blasting can turn a marginal property into a profitable one, it is assumed that the ore zone is mineable and is therefore uniform throughout its measured extent. Thus an orebody is proposed that, if the per ton of ore charges for waste removal were small, would be quite profitable. Deposits of similar grade and depth are now being considered for mining. The lakeshore property in Arizona,⁸ although not flat, is one. Because of the depth of the lakeshore body and a zone of high-grade at depth, this deposit will be mined by both open-pit and underground methods. The Anaconda Company is currently bringing its Twin Buttes open pit into ore production. They stripped 200 million tons of overburden, with a thickness between 450 and 500 feet, in order to

begin production. Twin Buttes has an ore zone that averages between 0.5 and 0.7 percent copper and is much thicker than that in the proposed sample. A last example is the San Manuel Orebody in Pinal County, Arizona.¹⁸ Because of its depth and contorted shape, this deposit is currently being mined by block-caving methods. Nonetheless, it would be well-suited for nuclear stripping.

Proposed Method

Nuclear stripping has the desirable advantage that as overburden thickness increases, the per ton charge for waste removal decreases because the explosive cost does not increase proportionally with an increase in yield. There are, however, the undesirable elements of seismic shock, air blast, and radioactive pollution of the environment. It is for these reasons that the orebody is presumed to be relatively isolated and well above the ground water table. Some estimates of exclusion zones and re-entry times are given at the end of the paper.

The proposed method is an adaptation of the stripping methods used in surface coal mining. Essentially, a strip of overburden is removed and the coal beneath it is mined. A void then exists for the deposition of the next strip of overburden. Mining proceeds in this fashion until all the coal is removed. Since the waste has been spoiled almost in the same place that it came from, it is possible to level and reclaim the mined out property.

Row-charge nuclear blasting is utilized to strip and prepare for mining the hypothetical orebody. In this method, one row of charges is blasted at a time, thereby minimizing the concomitant hazards of the explosion. Carefully observing the depth of the orebody a first row of explosives is emplaced such that it creates a channel immediately adjacent to the orebody and sufficiently deep that it contains the overburden that is to be cast by the second row of explosives. Selecting a depth of cut for the first row enables the depth of burst, width of the cut, yield of explosives, and spacing to be read from Figure 2, which is plotted from the given data for explosives in alluvium.^{17,20} Knowledge of device spacing allows calculation of the number of required explosives for this row.

Choosing 775 feet as the depth of cut for the hypothetical deposit, the remaining parameters are depth of burst, 1330 feet, width of cut, 2560 feet, explosive spacing, 1280 feet, and yield of each explosive, 2000 kt. To provide sufficient room at the ends of the channel, five charges are used. They are placed 720 feet from the vertical extension of the orebody limits so that the resulting crater is just tangent to the edge of the deposit as shown in Figure 3. Approximately 263 million tons of waste, more than the entire project at Twin Buttes, would be removed by this first blast.

In addition to providing a void, the first row provides a change in the geometry of the free face of an adjacent second row. Blasted material tends to move normally to the free face that has the lowest burden. Consequently, if the second row is properly placed, upon detonation most of the throw will be

directed toward the first row. From row charge experiments, it is observed that the slopes of an ordinary row are stable;⁴ also that the face configuration resulting from a directed blast is stable.¹⁹ Therefore, it seems plausible to use a second row of explosives, buried just on the shallow side of optimum, to throw an amount of the overburden into the void of row one. If 80-kt explosives, buried at 525 feet, are used, then, from Figure 2, spacing is 470 feet and 13 devices are needed. The explosives are placed so that they are equidistant from the free surface measured vertically or horizontally. This position should give maximum throw to the overburden. Figure 4 is an idealized cross-sectional view of the effect of row 2; Figure 5 shows more detail of the cut and also of the method of ore extraction.

Although this report is solely of hypothesis, there appears to be good evidence for the supposition that row 2 will clean its cut as shown in Figure 5. Extension of high-explosive technology is one such reason; the evidence of land-slide dam experiments is another.⁴ Additionally, if the shape of a surface crater is oriented so that its free surface is parallel to the slope of row 1, it is easily seen that the cut of row 2 results. Finally, the geologic plane between ore and waste, in many instances, will give a good breaking surface. Planimetric examination of Figure 5 shows that approximately 92 percent of the waste is directly spoiled. The expected slope angle is parallel to the original slope of row 1, and is close to 45 degrees.

After a suitable "cooling" time, the mine is re-entered and work on three jobs begins. Two crews start material handling operations, and a third crew starts to drill emplacement holes for row 3. Of those crews on material handling, one is, of course, cleaning up the remaining eight percent of the overburden, and the other is beginning to load ore. Loading is done with Quarry-Mine style shovels, and haulage is with trucks in the 100-ton range.¹⁵ The shovels load directly, without drilling and blasting, as the nuclear blast has fractured much of this rock. As ore mining proceeds to depth, the possibility of insufficient fracturing for direct loading exists. If the signals of shovel tooth wear and bucket filling factors indicate this, then drilling for high-explosive blasting will commence. Benches are of 50-feet height and have working widths of not less than 100 feet. The final slope angle is maintained at 45 degrees. Although disastrous failure of the slope will not occur, it is quite possible that loose rock could work its way down the slope. Hence, one of the upper benches is maintained as a safety zone; that is, left purposely wide. A later section describes radiation shielding for the machine operators.

Once the ore beneath row 2 is removed, a void exists for blasting into by row 3. Therefore mining can proceed in an orderly fashion until the deposit is depleted. The hypothetical orebody requires eleven production rows to complete mining.

The only rehandling of material that is envisioned is for that from production rows which falls short and lands on the existing ore slopes. For the 250-foot thickness this is a minor problem that can be handled by clean up bulldozers. For greater thickness, however, the amount of rehandling could become

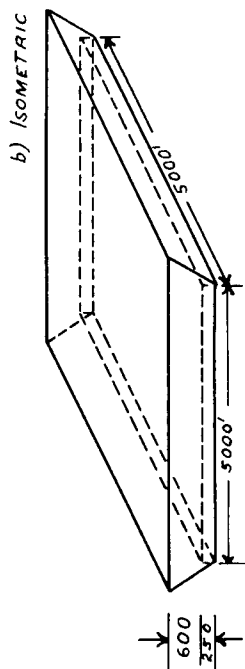
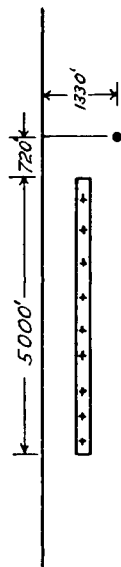
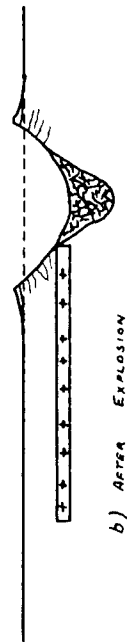


FIGURE 1: THE OREBODY AND ITS OVERBURDEN



a) BEFORE EXPLOSION



b) AFTER EXPLOSION

FIGURE 3: LOCATION OF SINGLE END CUT

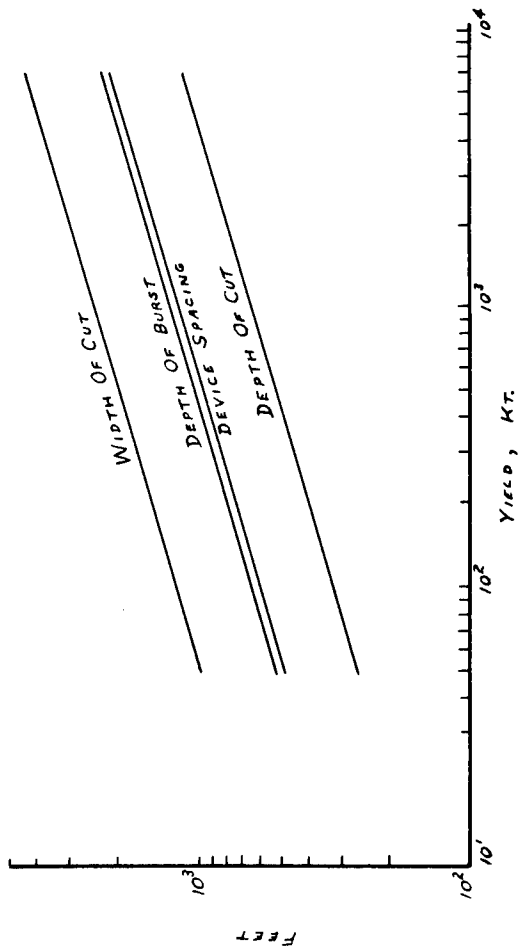
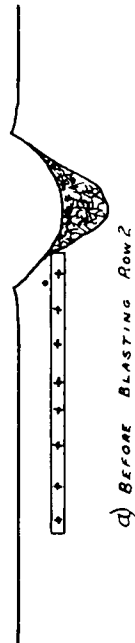
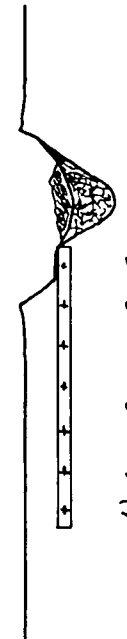


FIGURE 2: YIELD \sqrt{E} ROW PARAMETERS



a) BEFORE BLASTING ROW 2



b) AFTER BLASTING ROW 2

FIGURE 4: DIRECTED BLASTING

considerable enough to detract from the economy of the method. Individual project designs will have to consider this problem separately.

If greater production rates are desired, then the deposit can be attacked from two sides as shown in Figure 6. Working two faces has the advantage of maintaining more consistent production. Hence, when one face is "cooling" the other is feeding the mill. The double-face method casts approximately 94 percent of the overburden.

Comparative Costs and Completion Times

In order to begin this comparison, certain basic cost and profit information is presented. The recoverable value of copper, considering a price of 52 cents per pound,²¹ a grade of 0.45 percent, and 90 percent metal recovery, is 2241 million dollars. The price of conventionally mining and removing a ton of rock, although placed at nearly 25 cents in Pfleider,¹⁵ can be more realistically assumed to be 12 cents for this type of orebody. The given cost averages the lower cost of mining unconsolidated rock without blasting, and the higher cost of mining rock that needs blasting. Other standard costs, taken from the Anaconda report² include milling the ore at 60 cents per ton and smelting and refining at 80 cents per tons of ore. These costs do not include depreciation. Capital costs involved are 150 million dollars for a concentrator, 60 million for a smelter, and 60 million for one set of pit equipment.

Assuming a safe slope of 45 degrees, approximately 2 billion tons of overburden have to be removed at a cost of 240 million dollars, in order to conventionally mine this deposit. The pit equipment considered, approximately 150 trucks, fifteen shovels, 15 drills, and miscellaneous service equipment, has a daily production rate of 300,000 tons per day. With a 250-day work year, it will take 34 years to completely mine this deposit. For the first five years, no ore can be mined. Since the average life of this pit equipment is between 5 and 7 years, it will be replaced four times. The total cost of production is therefore 1560 million dollars, and the total profit -- not considering the time value of money -- is approximately 681 million dollars.

Using the Anaconda method² on the hypothetical orebody, which means that the need for a sloping land surface is ignored, a profit of 870 million dollars is created. It is doubtful that this system would work; but if it did, it would remove 57 percent of the overburden. Using the report's nuclear costs and 12 cents per ton for stripping the remaining 43 percent leads to an overburden removal cost of 171 million dollars. Pit equipment is only replaced twice; thus total cost is 1371 million dollars. Stripping can be completed in 15 years and ore production can begin within a year of project approval.

The proposed method, with one opening row, creates a profit of 1002 million dollars. Stripping costs are assessed with 8 percent removed conventionally and 92 percent by nuclear means. The nuclear operations involve drilling and explosive purchase as major items and safety and hazard evaluations as minor items. These items are detailed as five, 2000-kt ex-

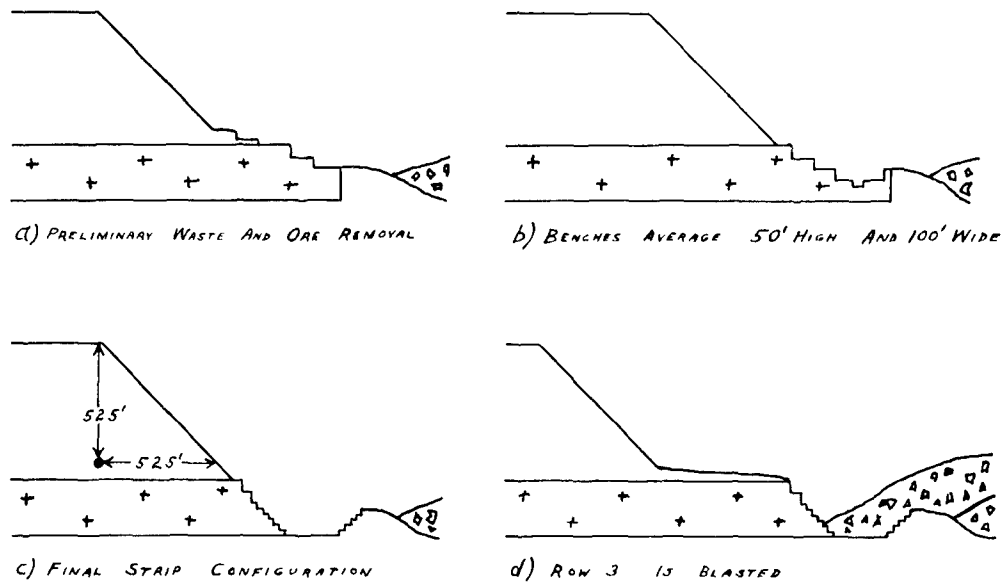


FIGURE 5: DETAILS OF THE STRIPPING SEQUENCE

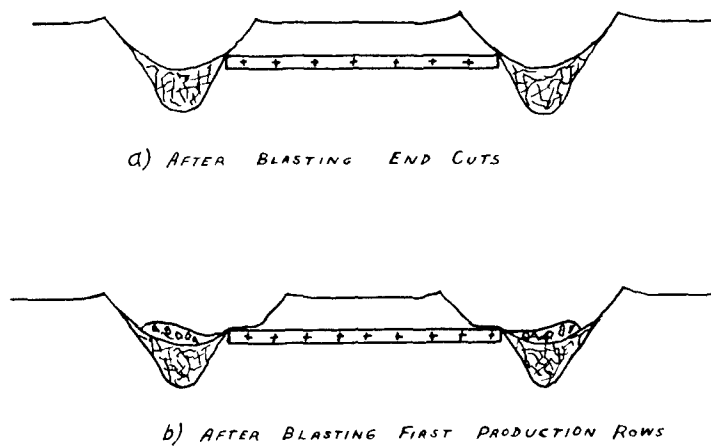


FIGURE 6: DOUBLE-CUT METHOD

plosives buried at 1328 feet, and 143, 80-kt explosives buried at 525 feet. The explosives cost 600,000 dollars apiece for the larger and 450,000 for the smaller.¹⁰ The larger size require a 72-inch hole which, uncased, costs 90 dollars per foot. The smaller size goes in a 48-inch hole which costs 34 dollars per foot. These costs are for moderately soft material.¹⁰ The total overburden removal cost becomes 97 million dollars, which includes 70 million for direct nuclear costs, seven million (10 percent) for contingencies, and 20 million for conventional stripping. In this scheme, the pit equipment is replaced only once and the total cost is 1237 million dollars. The beauty of this scheme is not only the high total value of the profit, but the fact that its present value is so much higher than in the other methods. This is because ore can be mined within four months of project approval. With an ore mining rate of 100,000 tons per day, the mine is depleted in 21 years of 250 work days.

The double-cut method gives much the same profit, the added nuclear costs being offset by the lowered conventional stripping costs, but halves the mining rate. Table 1 compares the four methods, giving per ton stripping costs and expected profits.

Table 1
Mining Methods Compared

Method	Total Nuclear Explosive, Mt.	Time to first ore production	Waste Strip- ping cost, ¢/ton	Percent Waste Conven. Removed	Pro- fit Mill- ion \$
Conventional	--	5 years	12	100	681
Anaconda ² Nuclear	25	1 year	8.6	43	870
Nuclear Row Stripping: Single Cut	22	4 mos.	4.9	8	1002
Double Cut	30	4 mos.	4.7	6	1007

To conclude this section on costs, a few comparisons are made. Figure 7 is a plot of total expected profit vs the conventional per ton mining cost. Three methods are plotted: conventional mining, Anaconda nuclear, and nuclear row stripping. Not only does row stripping present the highest profits; but because it leaves the least overburden for conventional removal, its profits decline the least with an increase in per ton removal costs. Figure 8 is a plot of expected profit vs change in overburden thickness. All the other parameters, as presented here, remain constant. Again the nuclear method gives the highest profits for any depth, shows the least decline in profits with increasing depth, and has the greatest depth before break-even. Returning to the constant depth of 600 feet, the break-even ore grade for the three methods can be calculated. In conventional mining, zero profits are expected at 0.34 percent copper; the Anaconda method breaks even at 0.30 percent; and the proposed row stripping breaks even at 0.27 percent. Of course, the conventional break-even grade varies the most with a change in per ton removal costs. These figures are an added

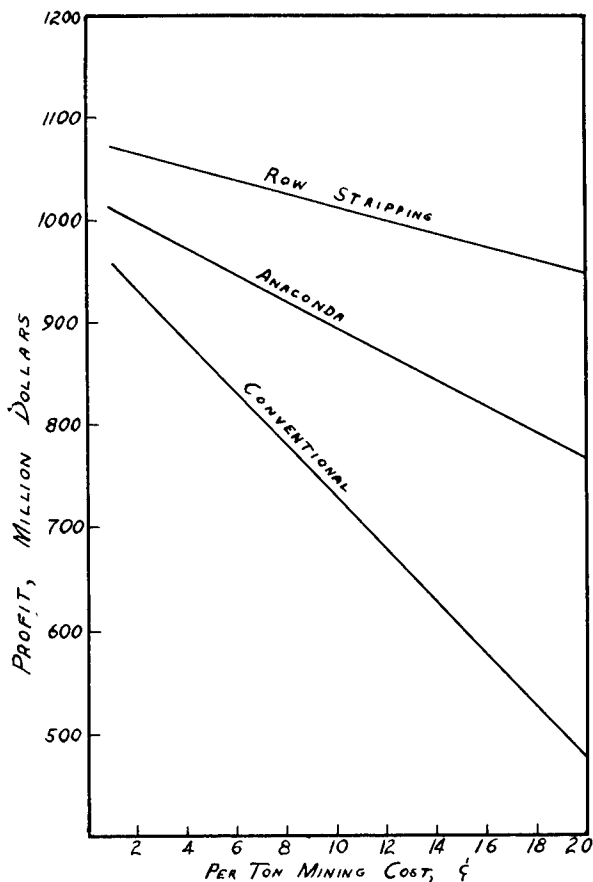


FIGURE 7: PROFIT VS CONVENTIONAL MINING COST

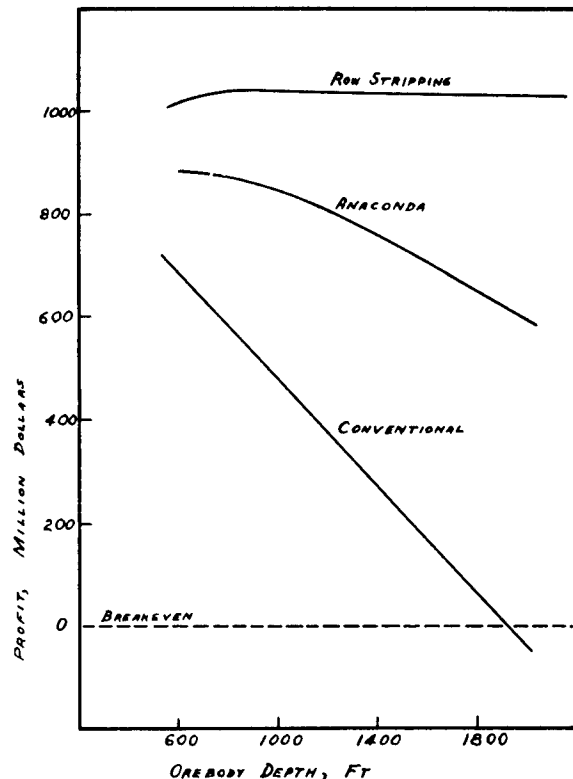


FIGURE 8: PROFIT VS OREBODY DEPTH

indication that, in addition to engineering feasibility, the nuclear row method gives greatest profits in a deeply-buried orebody.

Safety

It is clearly understood that the greatest drawbacks to any nuclear method are the safety hazards attendant to such an explosion. Although it is stated that nuclear craters and rows are reasonably safe from radiation because the explosion zone is buried under fallback,¹⁷ this assumption does not apply to nuclear stripping of orebodies. Precisely because this "hottest" material must be removed by machine does radiation become the greatest hazard in this scheme.

Fortunately, this problem is not insurmountable. Today, in the open-pit copper mines of the Southwest, operators are protected from the debilitating effects of heat, dust, and noise by placing them in air-conditioned and insulated cabs. In the modern open-pit mine all communications are done by radio and it is rare to see a man on foot. Thus, it seems relatively easy to protect the workers from the radiation hazards. Rather than depending upon "cooling" below maximum permissible dose rates, the workers would be actively protected by properly shielding their cabs, by insuring that the air they breathed was properly filtered, and by developing operating

schemes such that no worker could leave his cab unless he was wearing protective clothes. The only large inconvenience foreseeable is for the geologists and surveyors who must spend long periods of time exposed in the pit.

The mine should be separated into "hot" zones and safe zones and rigid control established for entry from one to another. For instance, no worker would be allowed to go from a safe zone to a "hot" zone unless he were shielded. A shielded cab would be a safe zone and a worker would not be allowed to enter it from a "hot" zone unless he were properly cleaned. Hence rules for returning into the safe zone would have also to be maintained. For example, a truck returning from the pit, "hot", to the shop, safe, would have to be thoroughly steam cleaned to remove radioactive debris.

It is assumed that the ore, shielded by 75 feet of waste at the shot point, is relatively "cool" or safe. Care must be taken to avoid contamination of the ore by the waste. The concentrator and smelter, assumed to be safe zones, should be built sufficiently upwind from the mine to avoid local fall-out. No shot would be permitted on a day when the wind was shifting from its prevailing direction.

There are methods for calculating exclusion zones^{10,17} for seismic damage, airblast, and local fall-out, but these require input information from the shot area for their exact calculation. Typically, however, for the five 2000-kt shots fired simultaneously, an exclusion zone of 40 to 50 miles will insure no building damage claims and will also insure that the populace is not exposed to dose rates that are as high as maximum permissible. Consequently, a mining scheme is proposed that has engineering feasibility, economic viability, and that can meet the safety demands presently promulgated for near-surface nuclear explosions.

References

- 1) Adelmann, C. R. Jr., "Mining with Nuclear Explosives," U.C.R.L. 5678, Lawrence Radiation Lab.
- 2) The Anaconda Company Research Lab., "Nuclear Mining Feasibility Study, Final Report," U.C.R.L. 13104, Lawrence Radiation Lab.
- 3) Anonymous, "A New Look at Mine Stripping," Engineering and Mining Journal, Vol. 168, April 1967, P. 91-95.
- 4) Anonymous, Plowshare Series Report No. 2, "Excavation," U.C.R.L. 5676, Lawrence Radiation Lab., May 14, 1959.
- 5) Bacigalupi, C. M., "Large-Scale Excavations with Nuclear Explosives," U.C.R.L. 5457, Lawrence Radiation Lab., Jan. 1959.
- 6) Circeo, L. J. Jr., "Engineering Properties and Applications of Nuclear Excavations," U.C.R.L. 7657, Lawrence Radiation Lab., Feb. 5, 1964.

- 7) Flangas, W. G., and Rabb, D. D., "Nuclear Explosives in Mining," U.C.R.L. 6636, Lawrence Radiation Laboratory, September 26, 1961.
- 8) Harper, H. E., and Reynolds, J. R., "The Lakeshore Copper Deposit," Mining Congress Journal, Vol. 55, No. 11, Nov. 1969, pp. 26 - 30.
- 9) Hoy, R. B., "Application of Nuclear Explosives in Mining," Mining Engineering, Vol. 14, September 1962, pp. 48 - 56.
- 10) Hughes, B. C., "Nuclear Construction Engineering Technology," NCG Technical Report 2, U. S. Army Engineer Nuclear Cratering Group, Sept. 1968.
- 11) Johnson, G. W., "Excavation with Nuclear Explosives," U.C.R.L. 5917, Lawrence Radiation Lab., Nov. 1, 1960.
- 12) Merritt, M. L., "Earth Moving by Nuclear Explosives," SCTM-78-59 (51), Sandia Corp., March 1959.
- 13) Nordyke, M. D., "On Cratering," U.C.R.L. 6578, Lawrence Radiation Lab., Aug. 22, 1961.
- 14) Nordyke, M. D., and Circeo, L. J. Jr., "Progress in Nuclear Excavation Technology," U.C.R.L. 12248, Lawrence Radiation Lab., Dec. 12, 1964.
- 15) Pfleider, E. P. (ed.), Surface Mining, AIME, New York, 1968, 1061 p.
- 16) Russell, P. L., "Stripping Overburden Using Nuclear Explosives," Society of Mining Engineers of AIME, Transactions, vol. 229, June 1964, pp. 192-200.
- 17) Teller, E., Talley, W. K., Higgins, G. H., and Johnson, G.W., The Constructive Uses of Nuclear Explosives, McGraw-Hill, New York, 1968, 320 p.
- 18) Titley, S. R., and Hicks, C. L. (eds.), Geology of the Porphyry Copper Deposits, University of Arizona Press, Tucson, 1966, 287 p.
- 19) Toman, J. and Hansen, S. M., "Aggregate Production with Nuclear Explosives," U.C.R.L. 12180, Rev. 2, Lawrence Radiation Lab., May 12, 1965.
- 20) Vortmann, L. J., "The Effect of Row Charge Spacing and Depth on Crater Dimensions," SC-4730 (RR), Sandia Corporation, Nov. 1963.
- 21) The Wall Street Journal, Dec. 20, 1969.

NUCLEAR OPERATIONS

NUCLEAR OPERATIONS SUMMARY ENGINEERING ORGANIZATION FOR PLOWSHARE NUCLEAR OPERATIONS*

Gene A. Broadman
Lawrence Radiation Laboratory, University of California
Livermore, California 94550

INTRODUCTION

The availability of nuclear explosives for peaceful projects has given the engineer a new dimension in his thinking. He can now seek methods of adapting Plowshare to a variety of industrial applications. The full potential of the Plowshare Program can only be attained when industry begins to use nuclear explosives on a regular basis, for economically sound projects. It is the purpose of this paper to help the engineer familiarize himself with Plowshare technology to hasten the day when "Plowshare goes commercial."

An engineering project utilizing nuclear explosives ordinarily involves three main phases:

Phase I (a) The theoretical and empirical analysis of effects.
(b) Projected economic and/or scientific evaluation.
(c) A safety analysis.

Phase II (a) Field construction.
(b) Safe detonation of the nuclear explosive.
(c) Data acquisition.

Phase III The evaluation and/or exploitation of the results.

This paper will be restricted to Phase II, referred to collectively as the "nuclear operation."

PLOWSHARE NUCLEAR OPERATION

The nuclear operation, or field program, of a Plowshare engineering project† has as its prime objective the safe and successful detonation of the nuclear explosive(s). To accomplish this objective means the nuclear explosive

*Work performed under the auspices of the U. S. Atomic Energy Commission.

†An engineering project will be defined as one that uses the nuclear explosive as a tool because it is the most economical way to do a job. In contrast, a scientific experiment or demonstration is not necessarily limited by strict economic bounds, but enhances the understanding of phenomenology for future use. In the latter case, the collection of data from diagnostic systems is usually the prime objective.

system has been emplaced underground to its proper working depth, detonated when required, and that all radioactive debris is contained underground. This must be carried out in a timely and economic manner without injury to personnel, damage to property, or violation of security requirements.

The basic elements of the nuclear operation are (see Fig. 1):

1. A site (new or existing) must be developed to accept the nuclear explosive system. This includes roads, power, communications, and emplacement holes.
2. The nuclear system. This includes the nuclear explosive, its environmental protection canister and a method to monitor, control, and detonate the explosive.
3. Instrumentation systems. This includes sensors and recording facilities for phenomenology measurements (optional).
4. An emplacement system. This includes equipment and hardware to place the nuclear and instrumentation systems with their associated electrical cables underground to working depth.
5. A stemming plan. This includes equipment and materials to back-fill the explosive and instrumentation holes.
6. Shock isolation systems to protect equipment and facilities from seismic effects experienced during the detonation.
7. A comprehensive industrial and nuclear explosive safety program that identifies potential hazards and delineates emergency actions.
8. A security plan that assures that all classified information and hardware is properly protected.
9. Engineering management that provides methods of projecting realistic schedules, budgetary control, and project coordination.

To assure ourselves that the work elements within the nuclear operation are executed on a timely and economic basis, we organize a nuclear operations engineering team (see Fig. 2). This team is headed by an engineering project manager and is composed of engineers from various disciplines and skilled technicians. Each engineering subgroup within the team is organized along functional lines, and is responsible for the following areas within the nuclear operation:

I. Engineering Project Manager (EPM)

The EPM is directly responsible for all engineering aspects of the nuclear operation. It is his job to continuously review and approve methods of operation, and designs of the various engineering groups on the nuclear operations team. He assures himself that all project objectives are clearly defined, and that interfaces and responsibilities between groups are identified. When provided with input from key members of the various engineering groups, he establishes an overall nuclear operation schedule and budget. He then continuously checks to see that these time and fiscal restrictions are being met.

The EPM will issue initial nuclear operation project scope letters, write periodic progress reports, and issue updated scheduling information in some form of a computerized "critical path" program. It is his responsibility to write the nuclear operation final summary report.

It cannot be emphasized too strongly that the EPM and key members of the nuclear operation team must clearly understand the objectives, time schedule, and fiscal limitations of the overall project. Simple misunderstandings often compound into major project crises in this phase of a project. It is important for the most economical and efficient operation that the EPM and his key engineers participate in the early planning and formulation phase of a project. Furthermore, they must know and understand other project participants, their organizations, objectives, limitations, and responsibilities.

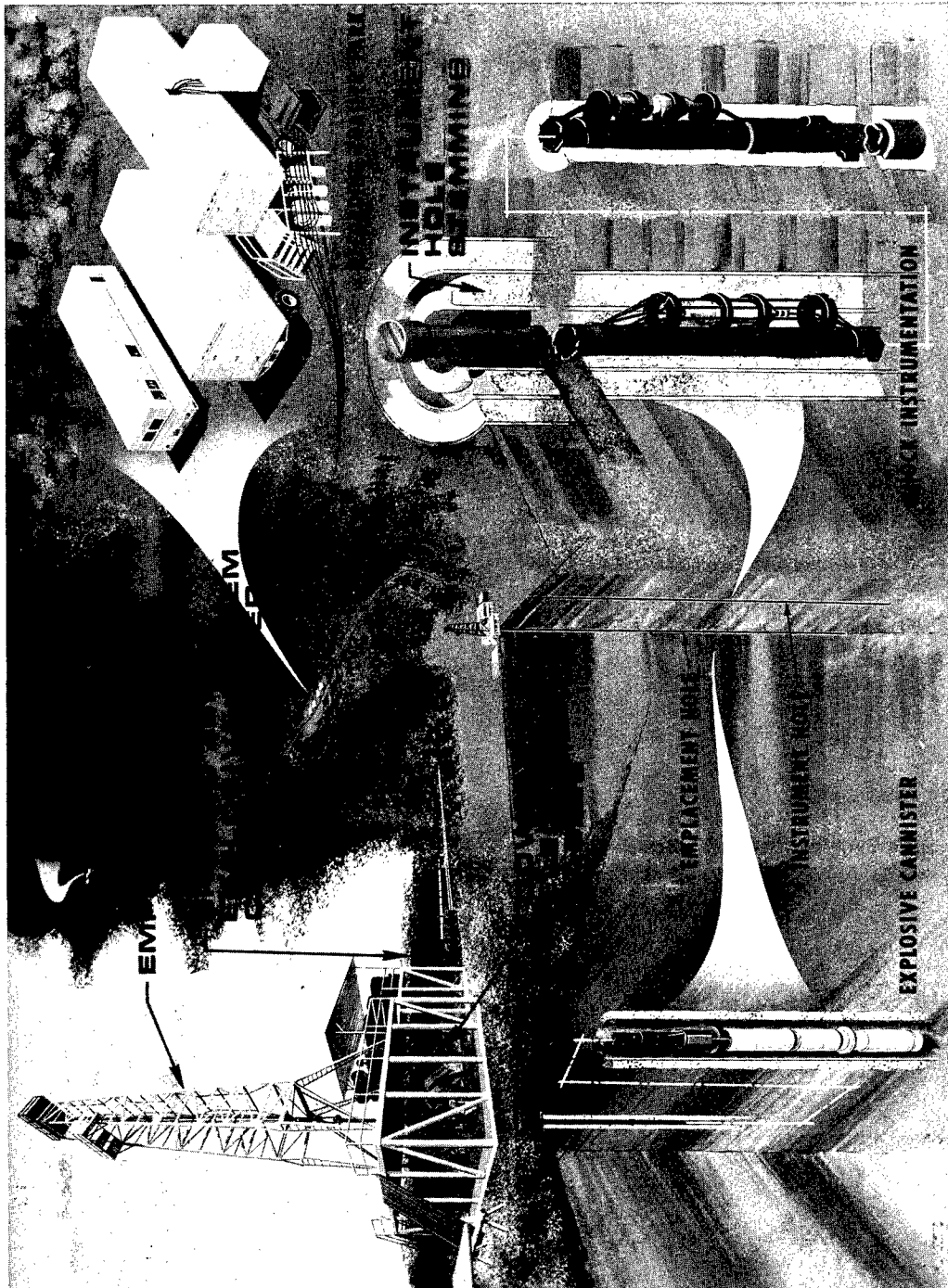


Fig. 1. Basic elements of the nuclear operation.

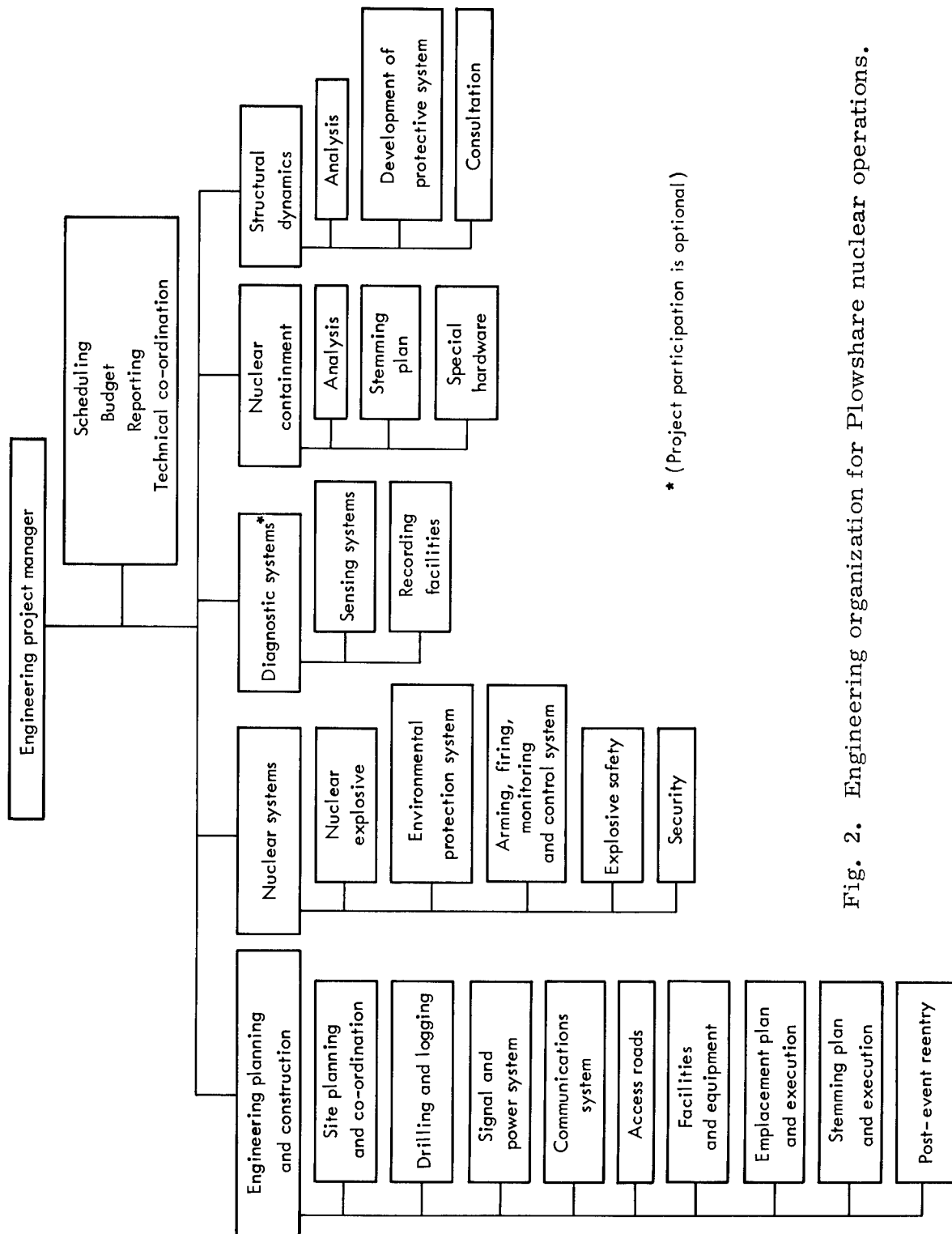


Fig. 2. Engineering organization for Plowshare nuclear operations.

II. Engineering Planning and Construction (EP&C) Group

Engineers working in this area are primarily responsible for construction designs and criteria requirements necessary to conduct the nuclear operation. Typical areas of interest are:

- A. Site layout, including building locations, electrical cabling, power requirements, communications, road, and special equipment locations.
- B. Hole drilling, cementing, coring, and logging. Engineers from this group coordinate requirements from user groups for emplacement and instrumentation holes. They specify the necessary coring and logging, and mandrel clearance requirements (simulates both explosive and instrumentation packages) for these holes.
- C. Emplacement. This group develops the emplacement plan. They see that acceptable emplacement equipment is selected and properly checked out. Of special interest is the handling of the explosive package (knowing its handling limitations, if any) and support and protection of downhole firing and instrumentation cabling.
- D. Stemming Plan. It is the EP&C engineer's job to see that the approved stemming plan is properly executed. To do this, he must "sign off" on a stemming plan check sheet, prepare material balance sheets, and keep an accurate log of this operation. Failure to properly execute the approved stemming plan can result in very costly remedial work to "make it right."
- E. Post-shot drilling usually involves special equipment and techniques. Engineers in this group must be familiar with radioactive sample requirements and techniques to recover them. They arrange for special personnel and handling equipment to get "hot" samples to appropriate groups expeditiously.

EP&C engineers deal extensively with numerous agencies, participants, and contractors to coordinate the nuclear operation team's construction criteria and see that it is being properly carried out.

Erroneous interpretation, overlooked details, and unsatisfactory execution of construction criteria can result in costly time delays and expensive reworks. Because the construction phase of a project involves large dollar expenditures and usually paces the execution schedule, engineers working in this area must play a large role in the planning, budgeting, and scheduling of the field program.

III. Nuclear Systems Engineering Group

The nuclear systems engineers are directly responsible for the nuclear explosive, its safety, security, and detonation. It is their job to see that the nuclear explosive is properly assembled, checked out, and transported to the project site ready for use. Strict safety and security procedures are written and approved before the nuclear explosive can be moved into the field. A small security force and special hazards control personnel will assist the nuclear systems engineer in implementing these procedures.

In conjunction with the nuclear explosive, there is always an environmental protection system. This system, often referred to as the explosive canister, can vary from a simple steel cylindrical sight barrier, to a complex

high-strength, internal-temperature-controlled, deep-submerging pressure vessel. Usually because of conflicting physical restraints of explosive size (always too large in diameter) and emplacement hole size (always too small), the engineer has a challenging design problem. To solve this problem, the engineer must have a complete understanding of the environmental restrictions within which the nuclear explosive can live and operate. He must know the downhole environment (temperature, pressure, mud, oil, etc.). With this background information, his design can evolve, and in turn, he will then be able to specify an emplacement hole diameter and straightness requirement.

To assure a safe and successful detonation of the nuclear explosive, the explosive systems engineer must design a compatible arming, firing, monitoring, and control system (AFMC). The AFMC system basically consists of two parts: (1) A downhole portion, which consists of electro-mechanical arming, monitoring, and firing components housed within the explosive canister and suitable electrical cables and connectors to link the system to surface ground zero; and (2) an uphole portion which typically consists of a small explosive system control center located at ground zero (GZ), a control link between GZ (either hardwire or RF) and a control point located at a safe distance from GZ. The GZ explosive system control center provides a junction point for the downhole and uphole portions of the AFMC system. It is always a "restricted area" after the nuclear explosive arrives on-site, and is subject to special safety and security precautions. The CP is "the top end" of the AFMC system. It is from here that electrical signals will be generated and sent to the downhole portion of the system to detonate the nuclear explosive.

During the course of the nuclear operation and prior to emplacement of the nuclear package, the explosive systems engineer will conduct a number of active systems checks. These checks, commonly referred to as "dry runs," will exercise the entire arming, firing, monitoring, and control system from the CP to the nuclear explosive canister. During, and immediately after, the explosive emplacement and back-stemming, passive cable and component checks will be made to assure that no damage to the downhole system has occurred.

After these system checks have been satisfactorily completed, the explosive systems engineer will inform the project manager that he is ready to proceed into the final explosive arming operation. When given the approval by the project manager, he will then proceed to arm and detonate the nuclear explosive.

IV. Containment Group

The principal task of engineers working in this area is to develop technology and systems for the complete containment of any radioactive gases or debris created by underground detonation of the nuclear explosive. The containment system or "stemming plan" usually consists of backfilling the emplacement and instrument holes with granular materials (sand, pea gravel, etc.) grouts, and special elastomeric compounds in various combinations.

Special attention must be paid to electrical cables or "other conduits" that extend from the shot horizon to the surface. Detonations in medias with natural pressure sources often require unique emplacement hole completion hardware.

Stemming and emplacement plans should be designed with careful consideration given to the post-shot reentry. Good planning in this area can result in substantial cost savings.

V. Structural Dynamics Group

Engineers in this group predict close-in ground motions resulting from the nuclear detonation. They design systems for the prevention of damage to sensitive data-recording structures and equipment exposed to this hostile environment. In addition, they have analytical tools to predict structural response and damage control methods for other "close-in" structures or equipment such as well heads, mechanical pumps, portable power plants, etc.

VI. Diagnostic Instrumentation Engineering Group*

Plowshare projects often have extensive subsurface and surface instrumentation systems to make phenomenology measurements. Engineers in this group develop and field instrumentation systems that provide seismic, surface motion, and underground shock measurement data. Information from this instrumentation is then used to correlate with theoretical analysis and develop empirical models.

FUTURE CONCEPTS

The nature of tasks associated with the nuclear operation phase of a project are such that it is here engineers can play a most vital role. With the exception of the nuclear system and some aspects of containment technology, all of the work areas within the nuclear operation are unclassified. Industrial people can and should participate heavily in this phase of a project. As more industrial groups participate in this area, new ideas, techniques and methods of standardization will develop that will result in significant economies for nuclear explosive applications.

As individual industries develop their own expertise in nuclear explosive engineering technology, the demand for nuclear explosives for commercial projects will greatly increase. Some time in the near future, one can envision a company being able to request and get a nuclear detonation as simply as they can now procure a well-logging service. A method to accomplish this would be by the formation of a special governmental agency, self-supporting, non-profit public corporation, or licensing of private companies to provide an explosive service function. This organization would supply the explosive environmental system, explosive safety, security, and detonation service for a pre-published schedule of fees. This service, combined with guide lines on emplacement hole requirements, environmental limitations, approved emplacement systems, and methods to accomplish proper stemming requirements should enable industry to plan, evaluate, and execute their own projects.

*Participation is optional, depending on project objectives.

ENVIRONMENTAL CONTROL FOR NUCLEAR EXPLOSIVES*

A. W. Lundberg and W. H. Wells
Lawrence Radiation Laboratory, University of California
Livermore, California 94550

INTRODUCTION

Peaceful applications introduce some new environmental considerations into the design of nuclear explosives. Much of the experience gained in weapon work can be applied, but the requirement of survival in a very deep hole is not found in any military system. We will briefly mention the overall environment and make a few comparisons with some general characteristics of the weapon environment. The major portion of this paper is devoted to the special problems of pressure and temperature found in the emplacement environment. Potential users should know where we stand with regard to survival in hostile environments in terms of feasibility and possible effects on field operations.

In all applications there are several things competing for the available diameter. Given that explosives can be made to work over a range of diameters and that necessary environmental control is feasible, all further discussions can be related to the cost of providing a hole big enough to accomplish the task. The items competing for diameter are:

- 1) bare nuclear assembly
- 2) insulation and cooling system if needed
- 3) pressure canister
- 4) shielding material
- 5) emplacement clearance

All of these must be considered with the cost of the hole in optimizing an overall design. Conditions in a particular location will affect the shielding requirements and the emplacement clearance. The nuclear assembly can vary in size, but the long development time requires that decisions be made quite early, perhaps in ignorance of the economic details of a particular application. The pressure canister is a relatively straightforward design problem that can be resolved by giving appropriate consideration to all of the design requirements. In particular for 20,000 psi pressure in the emplacement hole, a canister of heat-treated alloy steel having a yield strength of 200,000 psi and a wall thickness which is about .07 times the outside diameter is adequate and straightforward to fabricate.

The insulation and cooling requirements are not settled by compromise between competing elements of the design. There is a more basic question: Can adequate cooling be provided at reasonable cost? Some insulation is required, and some means of controlling thermal gradients in the assembly must be included. Even if these can be provided at small cost in diameter, how is the temperature difference between the world and the explosive to be maintained?

*Work performed under the auspices of the U. S. Atomic Energy Commission.

ENVIRONMENTS

The complete set of environmental problems in the design of nuclear explosives can be separated into two groups: (1) surface handling, and (2) emplacement.

A. Surface Handling

Surface handling includes everything from the beginning of fabrication through storage and shipping to delivery at the top of the hole. Most of the problems in this category can be treated with methods and materials that have been developed for weapons. There will be some differences between the environments of the explosives for excavation and for underground applications due to size, weight, or other unique features.

In many respects the different requirements of explosives for peaceful applications must be recognized. The storage life will be shorter—a few months instead of several years. In transportation and storage, the temperature range can be limited at modest cost and no loss of usefulness. Delivery time can be planned in advance and scheduled with the other work of the project, unlike the minimum response time allowed for a military system.

Details of the surface handling environment are not yet specified, but no serious difficulties are expected.

B. Emplacement

Discussions of emplacement environment generally are limited to the conditions at the bottom of the hole. It is true that the design is usually controlled by those conditions, but the trip from the surface cannot be overlooked. In addition to the increasing pressure and temperature, shock, vibration and abrasion must be considered.

The vibration and shock are not expected to be any more severe than in surface handling, except for one possible situation. Jarring an explosive that becomes stuck in the hole may require only that the assembly not become hazardous for further removal and return to the manufacturer. Maintaining high reliability under such extremely unusual conditions is not necessary.

The emplacement environment assumed in our studies is summarized as follows:

Excavation explosive:

1500 psi external pressure,
150°F ambient temperature.

Underground engineering explosive:

20,000 psi external pressure,
450°F ambient temperature.

In all cases, abrasion during emplacement must be considered. All emplacements are assumed to be in fluid-filled holes. Effects of these environments on the design of the overall explosive assembly are discussed in the following section.

EXCAVATION EXPLOSIVE

The thermal environment of the excavation explosive is not a serious problem. The maximum temperature expected is roughly 150°F, and with some development effort this can be tolerated by the assembly. If some applications do require thermal control, the larger diameter and relatively shallow burial depths permit many solutions to the problem.

General characteristics of the excavation explosives are given in Table I. Two sets of numbers are presented, the smaller diameter being possible if shielding can be placed into an under-reamed section of the hole. If under-reaming is not possible, all required shielding must be sent down as part of the "emplacement package," but not necessarily inside the pressure vessel.

Table I. Characteristics of excavation explosives.

Yield (Mt)	Emplacement Package Diameter	
	Under-reamed for shielding	No under-reaming
0.3	50 inches	65 inches
0.7	50	65
1.0	50	65
1.5	68	84
3.0	68	84
Length	15-35 ft	17-37 ft
Weight	15-22 tons	20-30 tons

Canister design for the excavation explosive is dominated by radioactivity considerations. Shielding is included in the overall assembly, and the vessel itself, in the region of the explosive, is fabricated of materials that do not contribute significantly to the total radioactivity problem. Fiberglass-reinforced plastic is the most likely material in this situation.

External pressure loading is the requirement leading to the selection of wall thickness and method of construction. In these sizes, as listed in Table I, buckling is the controlling mode of failure. Two designs are shown in Figs. 1 and 2, a single wall with enough thickness to resist buckling, and a double-wall design utilizing the shielding material to maintain the spacing of the walls. The double-wall design will permit greater control over the shielding material, but may also require a skin of abrasion-resistant plastic because not as much protection is given by the steel flanges.

The distribution of shielding material between internal and external locations is somewhat arbitrary. If the hole can be under-reamed and adequate shielding reliably placed, then the emplacement package should be of minimum diameter and thus have only a minimum of internal shielding. Obviously, shielding material contained in the emplacement package will be more reliably placed, but requires a larger hole.

UNDERGROUND ENGINEERING EXPLOSIVE

Pressure and temperature are serious problems for explosives in deep holes. Currently available designs and those expected in the foreseeable future will not tolerate the environment directly and must be protected. For a nuclear explosive, the preferable environment would be about 1 atmosphere of pressure and a maximum temperature of about 150°F for extended periods of time.

Recalling the environment statement made earlier, 20,000 psi and 450°F, it should be clear that we have assumed some very severe conditions for the explosive in deeply buried applications. The deepest emplacement, heaviest mud, and steepest geothermal gradient have been used in estimating the environment. If canisters and cooling systems can be developed for these extreme conditions, then providing explosives for intermediate depths will be considerably easier.

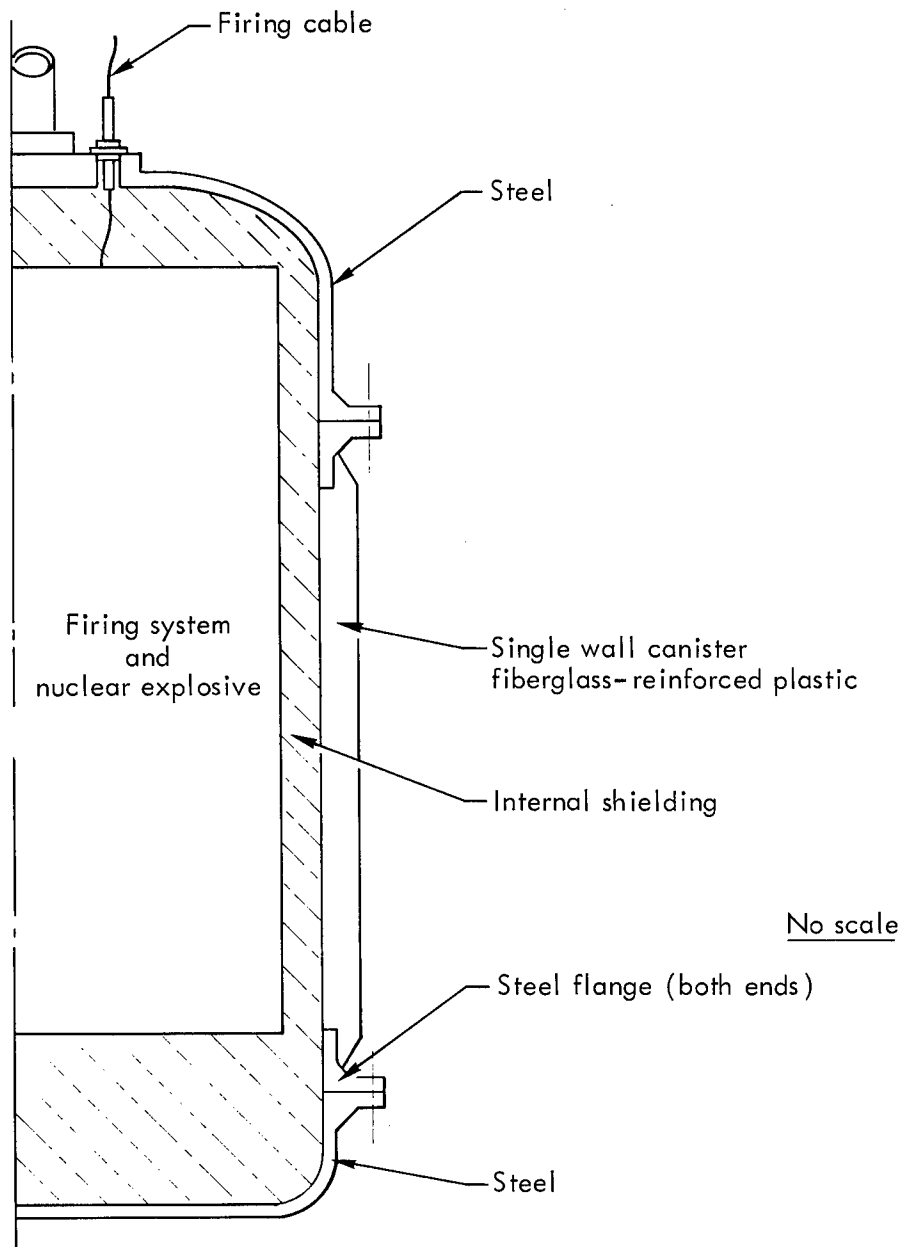


Fig. 1. Excavation explosive (schematic).

One question worth discussing here is whether or not the nuclear explosive itself can be designed to tolerate the environment. Surely some improvement is possible, but can we count on any real changes in the near future?

The problem of abrasion requires that some relatively substantial structure enclose the explosive. This probably will be at least half an inch in wall thickness and is not substantially different from a steel vessel strong enough to take the full external pressure.

A higher allowable temperature in the explosive will reduce the cooling load. It appears possible that the temperature capability can be raised from

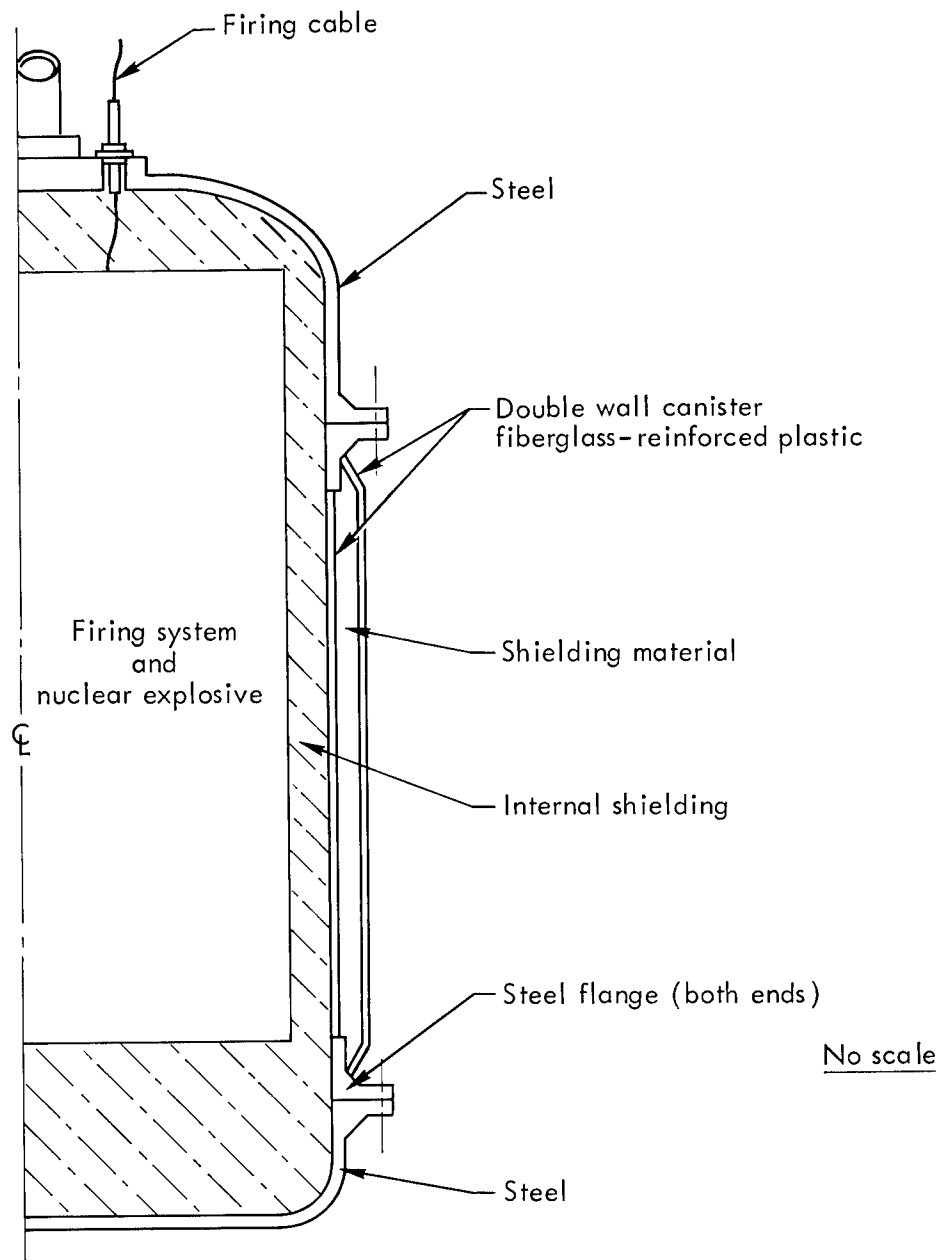


Fig. 2. Excavation explosive (schematic).

150°F to 200°F or 225°F without extensive material development. However, it is not likely that any major improvement will be made along this line in time for experimental use in the next few years.

The net result of the foregoing comments is that we have established the goal of providing adequate protection for explosives built of today's materials in an extremely hostile environment.

A schematic representation of a typical explosive for underground engineering applications is shown in Fig. 3.

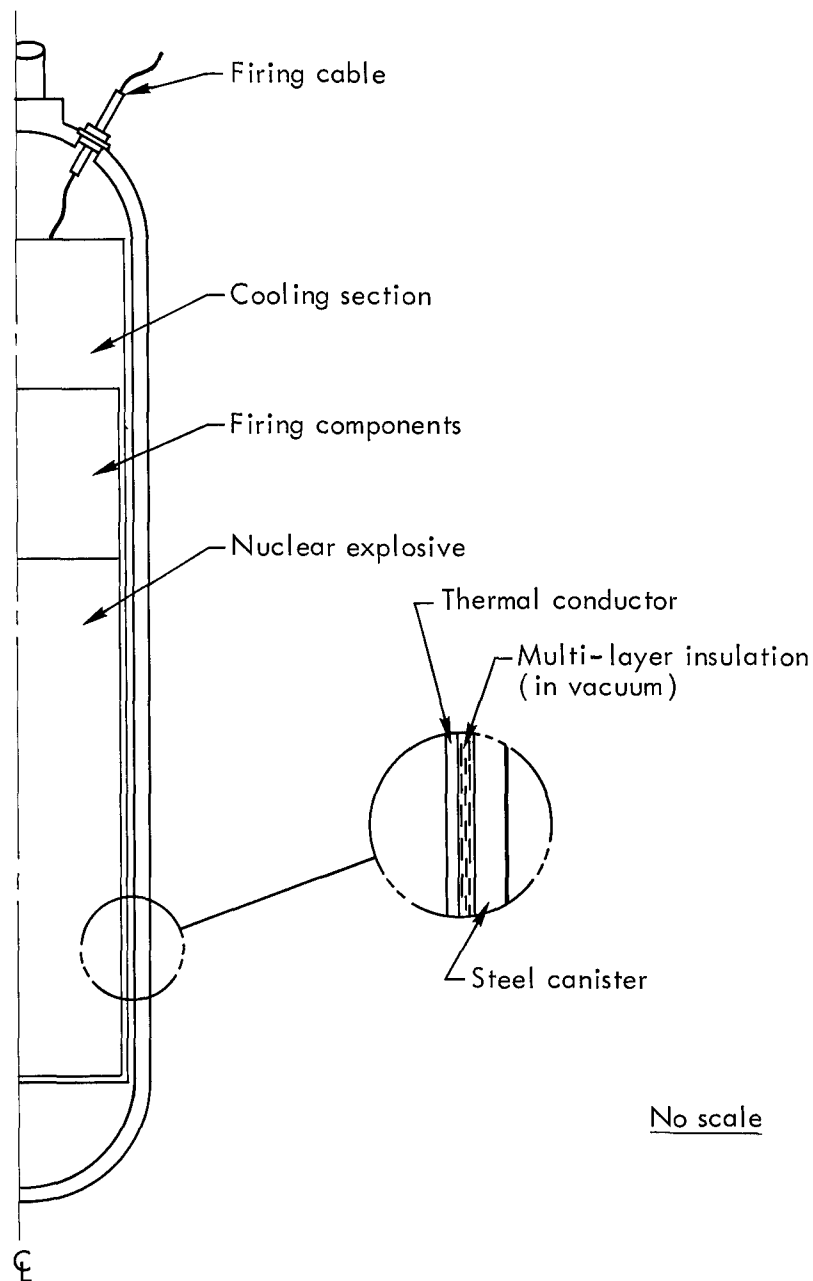


Fig. 3. Underground engineering explosive (schematic).

THERMAL INSULATION

Assuming the acceptance of the proposition that the deep hole refrigeration task is one of some difficulty, it follows that mitigation of this task through application of thermal insulation is desirable. A perusal of the state of the art of insulation techniques, such as reported by Glaser *et al.*¹ shows that vacuum multi-layer insulation is at least an order of magnitude better than any other approach. Its superiority rests in the fact that it works directly on the two main mechanisms of heat transfer in insulation. Radiation transfer is reduced by multiple reflective layers, and conduction is reduced by minimizing the amount of material in the conduction path.

The layered systems that appear most attractive for the application are: (1) Alternate layers of aluminum foil and fiberglass paper (or similar low-density spacer), and (2) layers of very thin aluminized, crinkled, plastic sheet.

The former system has shown the lowest apparent thermal conductivity, but the latter is nearly as good. The in-plane conductivity of the former is much higher because of the greater amount of aluminum present, and this results in easier placement and joining techniques for the plastic film system. Aluminum foils are typically 0.001 in. thick with spacing generally about 100 per inch. The aluminized plastic sheet material is typically 0.00025 in. thick with a layer of vacuum-deposited aluminum (or other metal) measured in angstroms. Polyester films have been the most common plastic substrate, but as indicated by Glaser¹ its temperature limit is about 300°F. Polyimide film is reported in the same reference to be useable to 750°F.

The dependence of the multi-layer insulation behavior on gas pressure level through it has been quite thoroughly investigated for cryogenic conditions as indicated by Glaser.¹ One readily concludes from this work that a pressure of at most 10^{-3} torr must be maintained. Since this application is at substantially higher temperature than the cryogenic application, it is qualitatively clear that the radiation mode of heat transfer is relatively more important. This will tend to make the system less sensitive to an increase in gas pressure, but the degree is presently unknown. We have never had any doubt that the vacuum must be pre-established and the system closed. One must then reach an acceptable equilibrium pressure. If the insulation is an integral part of the explosive device, it is likely that a high-temperature outgassing bake will not be permissible. While it appears feasible to establish adequate vacuum without baking, the point needs to be demonstrated.

We have identified two generic approaches to the placement of the insulation. As suggested by Elliott² one can pre-fabricate overlapping metal dewar-type vessels, or alternatively one can utilize the metal structure of the explosive device and the canister as the vacuum wall. The concept of the former approach is illustrated in Fig. 4.

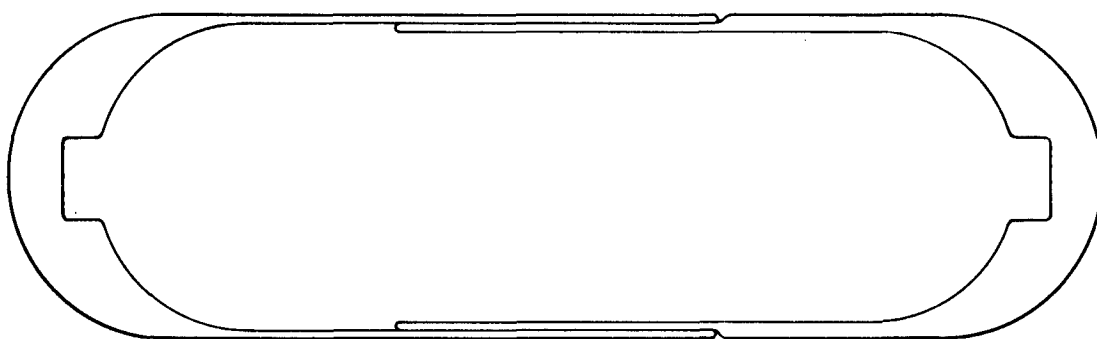


Fig. 4. Conceptual overlapping dewars.

One can readily find some pro and con arguments for the two approaches. These are given in Table II.

Table II. Some relative merits of two insulation placement approaches.

	Integral Vacuum Wall	Overlapping Dewars
Bakeable at high temperature	No (?)	Yes
Allows maximum insulation thickness	Yes	No
Utilizes minimum part of available diameter	Yes	No
Adaptable to fabricate at a specialized facility	No	Yes

The best choice from the two approaches is not presently clear.

Review of available literature and discussion with suppliers of the material indicate that as thickness decreases, no degradation of the apparent thermal conductivity occurs until about 0.1-in. thickness and ten reflective surfaces is reached. It is indicated that if the thickness is reduced to 0.05 in. and five reflective surfaces are used, the apparent thermal conductivity may be increased by about a factor of two. There is a good possibility that it will be desirable to use such a thickness in limited areas to maximize the space available for the nuclear explosive.

In order to establish an approximate refrigeration heat load, the following numbers are presented as typical:

Area of insulation having 1/2-in. thickness — 10 ft²
 Area of insulation having 1/16-in. thickness — 1 ft²

Figure 5 is extracted from Glaser's report¹ and is used as a basis for extrapolating apparent thermal conductivity to 400°F. The extrapolated value is: $k = 0.00026$ Btu/hr ft °F. This value is used for the 1/2-in. thickness, whereas a value twice this is used for the 1/16-in. thickness. Assuming these numbers as well as a temperature difference of 350°F, we estimate the heat load through the insulation as 78 Btu/hr (23 W).

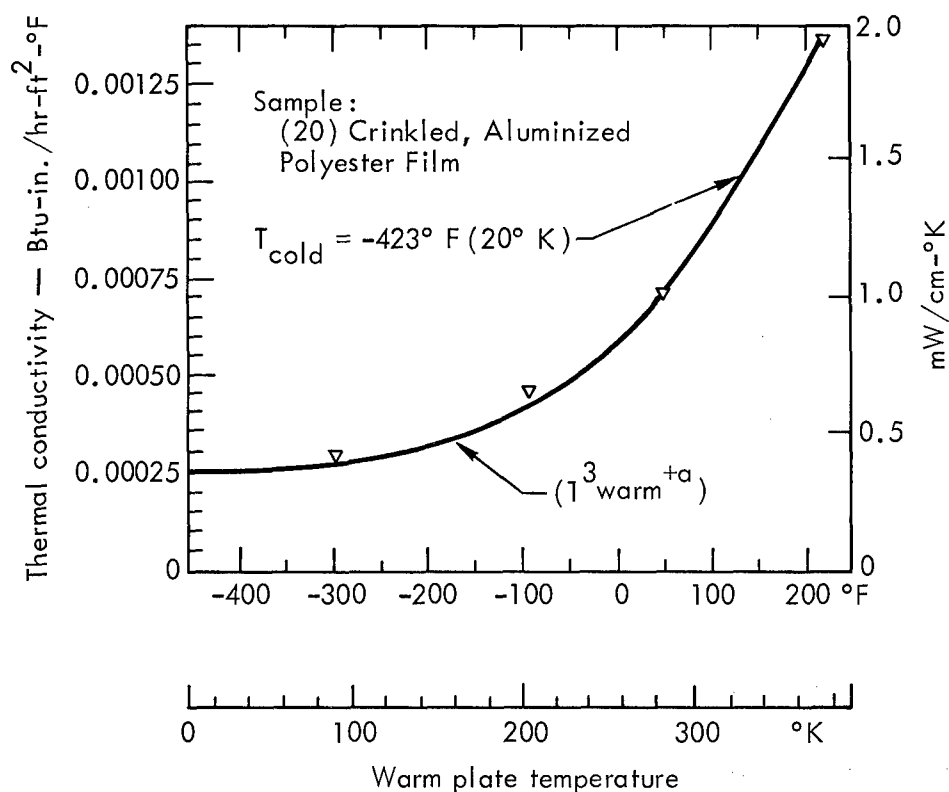


Fig. 5. Effect of boundary temperature on thermal conductivity of crinkled, aluminized polyester film.

One must allow for conduction through structural support. One of the most efficient means, in the thermal sense, of providing structural support is to utilize high-strength wires in bicycle-spoke fashion. The wires can be of a metal with low thermal conductivity such as stainless steel. The conduction heat load through 100 - 0.030-in. diameter by 1-in. long stainless steel wires with 350°F temperature difference is about 7 W. It appears reasonable to assume that such wire can also include any necessary electrical communication, so the 7 W can be said to include that effect.

A study of Glaser's¹ and other literature makes it clear that one is apt to encounter substantial degradation of the insulation performance wherever penetrations are made and at joints in the insulation between different shaped regions. Principally for these reasons, we have taken 100 W as a representative refrigeration heat load for feasibility studies.

CLOSED CYCLE CONSIDERATIONS

A. General

A literature search has revealed no precedent for the requirement of cooling to approximately 100°F while rejecting heat from a closed refrigeration cycle at 350° to 450°F. It is thus implicit that significant development effort would be required for these conditions, even though thermodynamic and other feasibility considerations are favorable. Practically all of the closed-cycle experience uncovered falls into two categories:

1. Commercial systems which refrigerate to temperatures not far above or below the freezing point of water, and which reject heat at temperatures not far from 100°F.
2. Cryogenic systems which reject heat at about room temperature and refrigerate to substantially below room temperature.

B. Heat Rejection to Surroundings

Some heat transfer aspects of rejecting heat to the surroundings can be investigated without any detailed knowledge of the refrigeration system beyond an assumed value of the coefficient of performance (COP). Anticipating that a small heat rejection surface area is apt to lead to excessive temperature rise at the sink, the steady-state conduction problem surrounding a line sink was investigated. Previous unpublished experience at LRL with unsteady heat rejection calculations for the Gasbuggy shot indicates that steady state is approached in about two months. Any state prior to steady state has a lower temperature around the sink than does steady state, and thus the steady state is a conservative design situation.

The refrigeration sink is a source insofar as conduction into the surrounding media is concerned. The only means available to increase the rejection surface is that of a length increase. Thus it is appropriate to treat conduction from a line source. Maxwell³ obtained the solution for the analogous problem in electrostatics. His solution, expressed in heat conduction terms and taking $T(\infty) = 0$, is

$$T = \frac{Q}{4\pi k} \frac{1}{\sqrt{A^2 - B^2}} \ln \frac{A + \sqrt{A^2 - B^2}}{B} \quad (1)$$

This gives the temperature at the (isothermal) slender ellipsoid having semi-axes A and B. For the problems of interest, $A \gg B$, and thus

$$T = \frac{Q}{2\pi kL} \ln \frac{L}{r} \quad (2)$$

where $L = 2A$ and the radius r is substituted for B . The actual shape of the sink would likely be cylindrical, but the areas of slender ellipsoids and their enclosing cylinders are sufficiently alike as to obviate a present distinction. Let n be the ratio of rejected heat to refrigeration heat load, and thus

$$n = 1 + \frac{1}{\phi} . \quad (3)$$

Using $r = 1/2$ ft, $k = 1$ (Btu/ft hr °F) as typifying rock, Table III is obtained when the refrigeration heat load is 100 W (341 Btu/hr):

Table III. Steady-state temperature rise (°F) of 1-ft-diam heat sink.

COP (ϕ)	n	L			
		5 ft	20 ft	100 ft	500 ft
∞	1	25	10	3	0.8
0.25	5	120	48	14	4
1/9	10	250	100	29	8
1/99	100	2500	1000	290	75

It is reasonable to conclude that any heat sink needs to be elongated and if the coefficient of performance is low, then the sink needs to be quite long.

The degree to which the region surrounding the refrigerated package is heated by rejected heat may be investigated by a simple steady-state approximation. Assume that the line rejection sink is located a distance D above the (point) refrigerated package. Replacing the line sink by a point sink the same distance away produces a conservative situation. This is shown in Fig. 6.

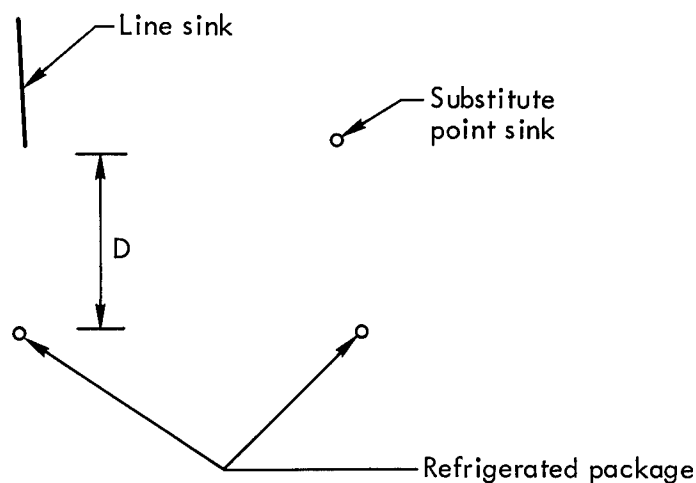


Fig. 6. Model for conduction calculation.

As may be found in any text on conduction heat transfer, the distribution of the temperature rise around a point source is

$$T = \frac{Q}{4\pi kD}$$

with Q and k as defined above the temperature rise (°F) in Table IV results.

Table IV. Temperature rise at refrigerated package (°F).

COP (ϕ)	n	D		
		10 ft	20 ft	100 ft
∞	1	0.1	0.1	0.01
1/9	10	1	0.7	1
1/99	100	14	7	1.4

The numbers are also conservative in that no account is taken of the depression in temperature due to the refrigeration effect. Clearly, no problem is indicated.

It is proposed to use a gravity-driven water reflux pipe as the long heat sink. This pipe would be located above the refrigerated package. Heat rejection from the refrigerator would cause boiling in a pool at the bottom of the reflux pipe. Immediately above the pool would be an insulated section which would largely prevent condensation in that region. Above that the pipe would have good thermal contact with the strata, and condensation with gravity reflux of the condensate would occur. Appendix 1 estimates two temperature differences associated with such a reflux pipe—namely that associated with condensation and the laminar film, and that associated with pool boiling. It is shown that the former is totally negligible, and the latter should be less than 10°F. Broadly speaking, the water gravity reflux pipe seems to be a straightforward method of getting any reasonably required heat sink area.

C. Specific Closed Cycles

In considering closed cycles the remoteness, severity of environment, and lack of precedent have been taken to favor simplicity, and as is usually the case this tends to exclude the more efficient approaches. In particular, the traditional mechanical vapor compression has not been seriously viewed as a contender for this reason. A number of approaches should appear attractive, given an electro-mechanical actuator developed for this stringent environment which could either cause compression of a gas or oscillatory motion in a fluid. Oscillatory motion could be useful in the simple pulse tube devices proposed by Gifford.⁴ It would be required that the device operate in an environment of about 450°F with allowance for its own temperature rise above this. The critical areas appear to be bearings and electrical insulation. It appears certain that existing technology provides the feasibility for these areas, but it appears equally certain that such devices are not commercial items and development would be required.

Choice of approaches to be considered is necessarily somewhat subjective, but the following seemed to fit the above guidelines to some degree.

1. Thermoelectric

The most advance work on thermoelectric refrigeration which we found reported was aimed at cryogenic applications. That reported by Shelpuk *et al.*⁵ is a good example of a sophisticated approach to this problem. As is typical, the work utilized room temperature as the sink. Following Goldschmid,⁶ the maximum temperature difference which can be attained (zero refrigeration load) with a single stage Peltier refrigerating device is:

$$\Delta T_{\max} = 2T_m \frac{\sqrt{1 + ZT_m} - 1}{\sqrt{1 + ZT_m} + 1}$$

T_m is the mean of the two temperatures and Z is the thermoelectric figure of merit. Z contains the appropriate thermoelectric performance as well as the electrical resistivity and the thermal conductivity for the material in the appropriate fashion to be useful for refrigeration considerations. It is defined in a manner such that a high value leads to good refrigeration performance. Data given by Wright,⁷ confirmed by data in Shelpuk *et al.*,⁵ indicates that a value of Z around $3 \times 10^{-3} \text{ } ^\circ\text{K}^{-1}$ is about the best currently achievable. Taking $T_h = 400^\circ\text{F} = 478^\circ\text{K}$, by trial and error one can deduce

$$\Delta T_m = 156^\circ\text{K} = 281^\circ\text{F}.$$

This is less than our most severe postulated condition, so it is clear that thermoelectric devices would have to be cascaded if our problem were solved with such a figure of merit. Shelpuk *et al.*⁵ deduce the infinite cascade COP which is closely analogous to the position that the Carnot COP occupies in other thermodynamic cycles. It is the limit on what can be done allowing for the fact that there is Joule heating and thermal conduction, tending to carry heat into the refrigerator. Shelpuk *et al.* leave the expression in integral form, and for their purposes solved it numerically. This was necessary because Z was not a constant in their range of temperatures. For our immediate purpose, it probably suffices to treat Z as being constant. This results in a closed form solution for the infinite stage COP. Following Shelpuk *et al.*, we solved for the inverse of the infinite cascade COP (ϕ_∞) and called it the specific Power P_s . The following expression resulted:

$$P_s = \frac{1}{\phi_\infty} = e^{f(T)} - 1$$

where

$$f(T) = 2 \ln \frac{\sqrt{1 + ZT_h} - 1}{\sqrt{1 + ZT_c} - 1} + \frac{2}{\sqrt{1 + ZT_c} - 1} - \frac{2}{\sqrt{1 + ZT_h} - 1}.$$

Good performance means reducing P_s and thus $f(T)$. Perusal of the above expression reveals that for constant Z , increasing the temperature level results in improved performance. Therefore we should expect to be able to do somewhat better than Shelpuk *et al.* did. If we take $T_c = 100^\circ\text{F} = 311^\circ\text{K}$ and $T_h = 400^\circ\text{F} = 478^\circ\text{K}$, $Z = 3 \times 10^{-3} \text{ }^\circ\text{K}^{-1}$ it turns out that

$$P_s = 12.2$$

Shelpuk *et al.* evaluated P_s for a similar temperature ratio, but rejecting heat at 300°K . They allowed for reduced values of Z at lower temperatures and calculated the infinite stage $P_s = 30$. They built a five-stage Peltier refrigerator and obtained an actual P_s about 2.4 times that for the infinite cascade. Because of the beneficial effect of increased temperature our ideal number of cycles should be less than for the cryogenic conditions. Thus one would expect fewer than five stages to be optimum. This should lead to less degradation from the infinite cascade behavior. If we take the degradation factor as 2 instead of 2.4, we end up with an estimated COP of about 0.04 which is interesting if rather low. The performance which Shelpuk *et al.* achieved was the result of a fairly large development effort, employing rather elaborate fabrication and assembly techniques. It appears that a substantial development effort would also be required to obtain good results toward our ends.

2. Absorption

Absorption cycles are potentially interesting for this application in that they have been operated in certain instances with no moving parts, implying good reliability.

The absorption cycles replace the mechanical vapor compressor with a chemical means of placing the refrigerant vapor in condensed form. A basic requirement is that of finding a refrigerant-absorber combination where the vapor pressure of refrigerant over the combination at the available rejection

temperature is less than the vapor pressure of the pure refrigerant at the evaporator temperature. Given that condition it is possible for the refrigerant to be evaporated at the desired low temperature and absorbed at the available high temperature where both processes are at the same pressure. In order to have a closed cycle with the common situation where all states of both materials are either liquid or vapor, it is necessary to raise the pressure of the combination so that refrigerant can be driven from the combination and recondensed essentially pure at the available rejection temperature. This latter requirement of condensing the refrigerant at the rejection temperature implies that one must reject heat at a temperature less than the critical temperature for condensation to be possible. This rules out the use of ammonia over its critical temperature of 271.4°F (133°C). Ammonia and water is one of the two most common refrigerant-absorber combinations used in commercial practice.

Raising the pressure of the refrigerant-absorber combination requires only pressurization of a liquid, and thus the mechanical work is small. Frequently in commercial practice, the pressure difference is also small so that thermosyphons or vapor-lift pumps can be used, thus eliminating all machinery from the system. The second prevalent combination is water and lithium bromide. Our conditions are well below the critical temperature for water 706.1°F (374.5°C), but it is apparent that the necessary states imply pressure differences of several hundred psi and clearly mechanical pumps would be required where water is the refrigerant.

Ellington *et al.*⁸ give data and extrapolations which indicate that water-lithium bromide or water-lithium iodide solutions have too high vapor pressures for our most severe conditions. The same reference gives no data on any specific combination which operates in the vapor-liquid states that is capable of meeting our potential requirement of rejecting heat at over 400°F.

If one deletes the requirement that the cycle be closed and requires only that the refrigerant be absorbed on a once through basis, some interesting possibilities result. These are discussed under heat capacity approaches.

3. Jet Compression

Figure 7 shows the elements of a jet-driven, closed-cycle refrigeration system containing no moving parts and operating with the only energy input as heat. This figure is intended to be a conceptual representation where a single condensible fluid is employed. The standpipe provides the necessary pressure differences to produce saturation at the three desired temperatures. The flow and pressure characteristics of the jet compressor must be compatible with these pressures.

Steam jet refrigeration is a common industrial tool, but generally the systems are not closed cycles and are found to be economic where heat or steam are available as by-products. When one examines the height of standpipe necessary for common refrigerating fluids such as water, and especially for our high-temperature conditions, it is apparent that the standpipe dimensions become excessive. One can in principle use fluids with high density and low vapor pressure to circumvent this problem. This was done in a system employing mercury as the driving fluid for the two-stage ejector and water as the refrigerant. Whitney⁹ describes this system which achieved semi-commercial status as a household refrigerator.

This system as reported comes the closest to meeting our temperature requirements than any other encountered. The mercury boiler operates at about 660°F. The water evaporator operates at about 20°F, utilizing anti-freeze (unspecified) to prevent freezing. The water condenser operates at

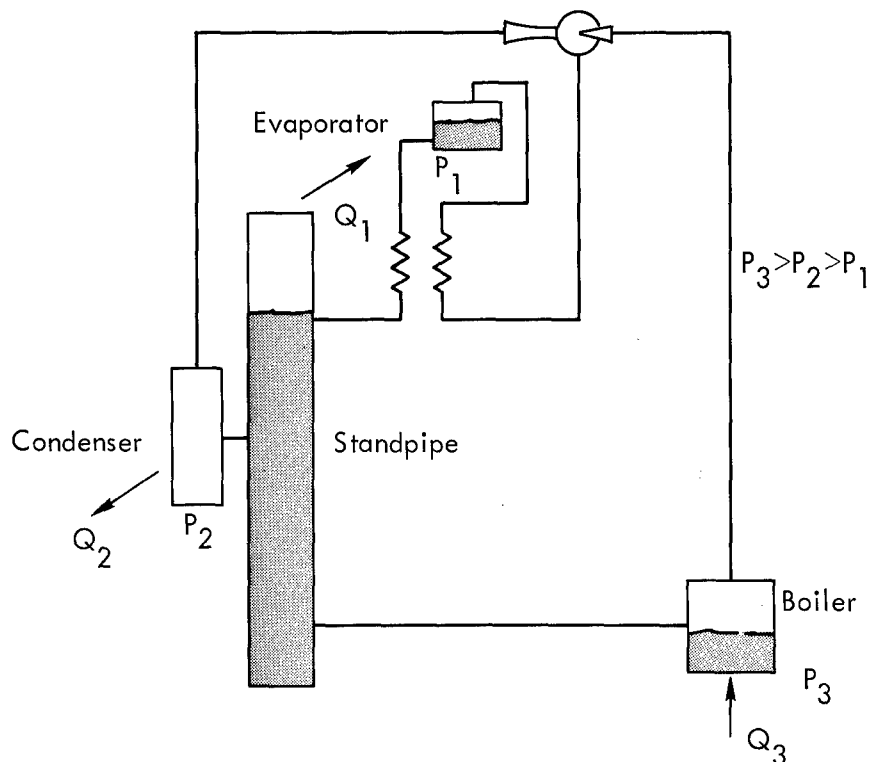


Fig. 7. Schematic jet compression refrigerator.

about 115°F. The latter temperature is not available to us for heat rejection. Condensing water at the available 350° to 450°F leads to excessively high pressure to be useful in the system as described by Whitney.⁹ Conceivably the use of a refrigerant with a low vapor pressure such as diphenyl could be made compatible with this type system. In any event it appears clear that considerable development would be necessary. The ability to perform a preliminary analysis of this approach is handicapped by the state of knowledge of jet compressors or ejectors. Analysis of these devices does not proceed readily from first principles and the most useful data is proprietary data generated by manufacturers. Work and Haedrich¹⁰ present considerable data on ejectors and generalization of desirable properties of fluids for ejector refrigeration, but little help in selection of specific fluids for particular cases.

SYSTEMS OPERATED THROUGH FLOW PASSAGES TO THE SURFACE

A. Flow Theory

Disregarding for the moment the problem of providing the flow passage per se, it is clear that being able to exchange fluid with the surface can result in considerable simplification of the elements located underground relative to a complete closed cycle. One can logically argue for substantial improvement in the ease of performing various functions on the surface relative to doing the same job underground. Most such approaches which we were able to conceptualize consisted of at least a vent line to the surface, and possibly a supply line if the system is to operate in steady flow. Since most refrigerative processes utilizing fluids involve expansion, it is likely that the vent pipe will be the largest one, and thus its required size is likely to be a controlling factor in the feasibility of a particular approach.

In consideration of the details of emplacement, one can argue convincingly that the flow conduit would have to be tubing small enough in diameter to be

handled essentially as cable, probably including spooling. In addition to handling considerations, a strong case can be made regarding the practical impossibility of obtaining a hermetic seal where large numbers of screwed joints are involved. The decisive pressure as regards strength is probably that of the fluid in the emplacement hole tending to collapse the tubing. For an external pressure of 20,000 psi, preliminary stress analysis indicates that the wall thickness of the tube needs to be about 1/8 to 1/10 of the outside diameter of the tubing.

The differential equation relating the pressure and vertical position (measured downward) for upward flow of compressible fluid in a constant area duct is:

$$\frac{dP}{dx} = \gamma + \frac{f}{D} \frac{\gamma v^2}{2g} - \frac{\gamma}{g} v \frac{dv}{dx} \quad (4)$$

where

- P = pressure (absolute)
- γ = fluid density
- v = fluid velocity
- D = duct inside diameter
- f = friction factor (as defined by Darcy-Weisbach relation)
- g = gravity
- x = vertical distance (measured downward)

The terms represent, respectively: first, change in hydrostatic pressure; second, the change in pressure due to wall friction; and third, the change in pressure due to momentum change as the fluid accelerates. Several simplifying assumptions have been made in the following analysis:

1. The fluid has been assumed to behave as a perfect gas.
2. The momentum change term has been assumed to be negligible.
3. The fluid temperature is assumed equal to the unmodified temperature of the strata.

The validity of the first of these assumptions will be examined shortly. Including the momentum change term results in a non-linear differential equation which can be solved numerically in relatively straightforward fashion. Its exclusion results in only a few percent error. An elementary treatment of the transient nature of the fluid temperature in the duct reveals that for the following example, a thermal entry length of about 1.5 ft exists, after which the fluid is within about 0.01°F of the strata. It is further assumed that the geothermal temperature is linear in x. In addition, one has available the continuity relation. Thus we have three more equations:

$$\frac{P}{\gamma} = RT \quad (5)$$

$$T = Bx \quad (6)$$

$$\frac{\pi}{4} D^2 \gamma v = \dot{w} \quad (7)$$

where

- T = absolute temperature
- R = gas constant
- B = constant of proportionality defining geothermal temperature
- \dot{w} = mass flow rate

The form of Eq. (6) implies that the origin for x is the point above the earth where the geothermal temperature extrapolates linearly to absolute zero. The friction factor is assumed constant. Neglecting the last term of Eq. (4) and combining Eqs. (4), (5), (6), and (7) yields

$$\frac{dP}{dx} = \frac{1}{RB} \frac{P}{x} + \frac{8RB\dot{w}^2 f}{\pi^2 D^5 g} \frac{x}{P} \quad (8)$$

Equation (8) is readily solved and may be written in the following form:

$$D = \left[\frac{8fRB\dot{w}^2}{\pi^2 g \left(1 - \frac{1}{RB}\right)} \left(\frac{x_2}{P_2}\right)^2 \frac{\left(\frac{x_1}{x_2}\right)^{2\left(1 - \frac{1}{RB}\right)} - 1}{\left(\frac{P_1}{P_2}\right)^2 \left(\frac{x_2}{x_1}\right)^{\frac{2}{RB} - 1}} \right]^{\frac{1}{5}} \quad (9)$$

The subscript 1 refers to pipe entry at the hole bottom, 2 refers to any station above that. Equation (9) is useful for sizing the flow passage given inlet and exit conditions. Qualitatively the pressure profile is as shown in Fig. 8.

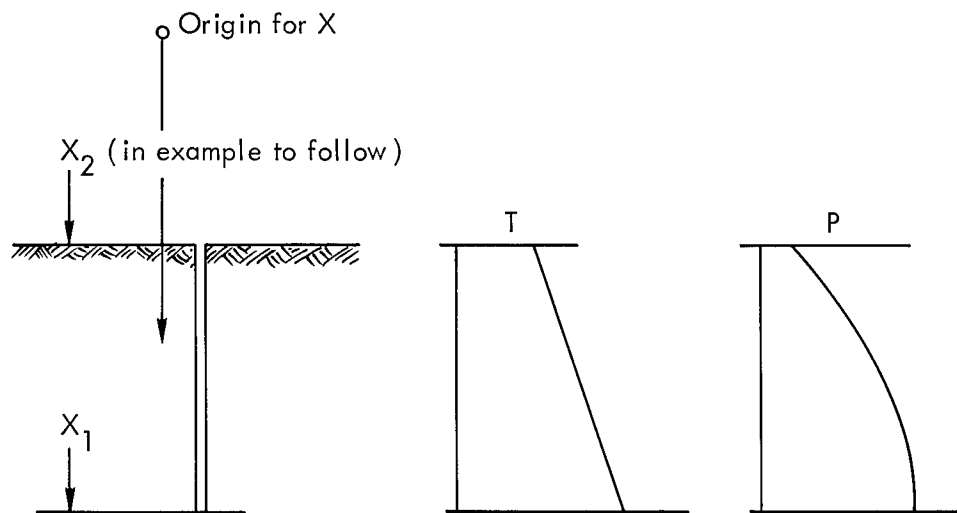


Fig. 8. Schematic of system using vent pipe to surface.

B. Example

The example is taken to be a case with an intermediate depth and temperature. The refrigeration load is assumed to be reduced to a low level by use of layered vacuum insulation. Thus,

$$x_2 - x_1 = 12,000 \text{ ft}$$

$$T_1 = 260^\circ\text{F} = 720 \text{ R}$$

$$T_2 = 70^\circ\text{F} = 530 \text{ R}$$

Refrigeration heat load = 100 W = 341.2 Btu/hr.

Refrigeration evaporator temperature = 100°F.

Fitting the two geothermal temperature points to the expression $T = Bx$ gives

$$B = 0.015833 \text{ }^{\circ}\text{R/ft}$$

$$x_1 = 45,470 \text{ ft}$$

$$x_2 = 33,470 \text{ ft}$$

Ammonia is taken to be the refrigerant on the basis of having a high latent heat of vaporization and a high vapor pressure. The latter is important in that it results in a reasonably high density and thus tends to reduce the size of the vent pipe. It follows that water is not satisfactory. The gas constant R is taken to be 90 ft/°R. The validity of this number will be examined later. In order to calculate the flow rate, it is necessary to evaluate the enthalpy change available for producing the refrigeration effect. Figure 11 is extracted from Canjor and Manning.¹¹ It is presumed that the ammonia enters the system as saturated liquid at the local ambient temperature. With evaporation at 100°F and the ambient temperature subsequently re-attained the initial and final states for ideal processes are represented by points A and B on Fig. 11. The two straight lines connecting the points represent a possible idealized process. Since the enthalpy change between points C and B can be available for pre-heating the liquid, it is reasonable to expect that an enthalpy change greater than that between points A and C will be available for cooling. The change between A and B is 270 Btu/lb and will be used to represent the cooling effect. The flow rate is

$$\dot{w} = \frac{341.2 \text{ Btu/hr}}{270 \text{ Btu/lb}} = 1.2637 \text{ lb/hr} = 3.51029 \times 10^{-4} \text{ lb/sec}.$$

The pressures are as follows:

$$P_1 = 215 \text{ psia} = 30,960 \text{ psfa (saturation pressure at 100°F)},$$

$$P_2 = 14.7 \text{ psia} = 2116.8 \text{ psfa (venting to atmosphere)}.$$

The friction factor is taken to be for smooth pipe. It is available from any standard fluid mechanics reference, e. g., Rouse.¹² The value of f is rather insensitive to changing the other quantities and so may be arrived at quickly by trial and error. The value so arrived at for this problem is $f = 0.036$. Using these values in Eq. (9) yields

$$D = 0.137 \text{ in.}$$

Using the entry and exit states of the ammonia vapor and NBS tables of data for ammonia¹³ one may deduce the apparent gas constant from $R = P/\gamma T$. The data are given in Table V.

Table V. Data for calculating apparent gas constant.

Pressure (psia)	Temperature (°F)	$\frac{1}{\gamma} \left(\frac{\text{ft}^3}{\text{lb}} \right)$ from NBS Tables	Apparent $R \left(\frac{\text{ft}}{^{\circ}\text{R}} \right)$
215	260	1.996	85.8
14.7	70	22.49	89.8

It is indicated that the perfect gas assumption is adequate for the immediate purpose.

Some manner of control will be necessary to maintain correct temperature and flow rate. The following is one way which looks simple and practical. Figure 9 shows the evaporator chamber, low side float valve to maintain proper liquid level in the evaporator, and an evaporator pressure regulator which keeps the vapor pressure (and thus the temperature) in the evaporator at a constant value.

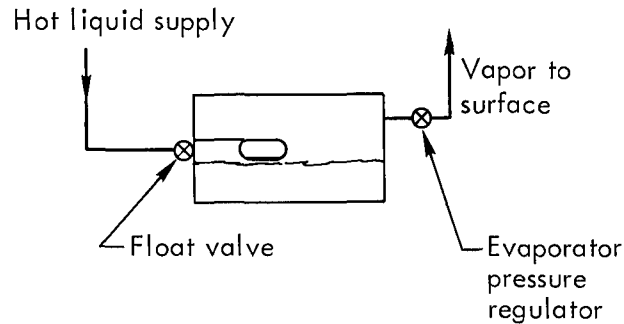


Fig. 9. Evaporator schematic.

Three means of supplying the hot liquid are immediately obvious:

1. Liquid stored in a tank at ambient strata temperature without means for recharge.
2. Same as (1) but with provision for recharge through the single tube to the surface.
3. A separate supply line from the surface.

The second scheme can be implemented as shown in Fig. 10.

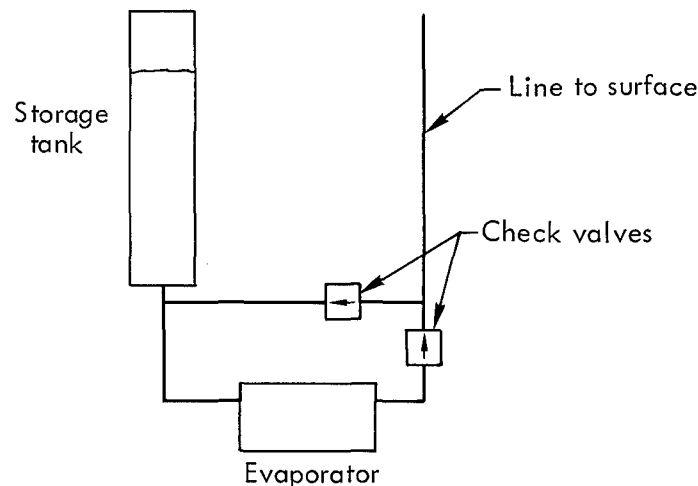


Fig. 10. Single-pipe refrigeration system.

Schemes 1 and 2 have the advantage of having only one line to the surface. The advantages of 2 over 1 are that a smaller reservoir can be used, and it can have indefinite life. For purposes of this paper, it should suffice to say that 3 requires a supply line which is smaller than the return line. The obvious questions for the first two schemes are, respectively:

1. Will a reasonable size tank permit a reasonable life?
2. Will the line sized for exhaust to the surface permit recharge in a short enough time that there is not an excessive temperature rise in the refrigerated package?

With regard to the former question, using numbers for the example case already given and the properties of liquid ammonia from NBS (1923) the weight, volume, and example storage volume shape for liquid ammonia are as follows for 30 days of operation:

Weight	909.9 lb
Volume	42.1 ft ³
Example shape of volume	10 in. diam × 77.2 ft

Using properties of liquid ammonia, one may deduce that a recharge time of 15 minutes is feasible for the system in Fig. 10.

In the event that the ambient temperature were above critical for the particular fluid, in general the approach can still be operable. By way of illustration, if one assumes the liquid were stored at 400°F, the fluid pressure in the emplacement hole were 10,000 psi, and it were desired to evaporate at 100°F; one must operate between points D and E, on Fig. 11, which are analogous to A and B. The 10,000 psi pressure is assumed transmitted into the storage tank.

HEAT CAPACITY APPROACHES

The intended context of this category is to cover those approaches which have no communication with the surface, but rather carry along their time-limited cooling ability in some stored form. Obviously, the elimination of a necessity for powering a device from the surface, whether it be electrically or through fluid flow, is a significant advantage. One readily conceives two versions of this.

A. Heat Capacity Stored in Insulated Volume

For this purpose one seeks a material which maximizes the heat absorbed for a given acceptable temperature change. It is typified in Elliott's proposal² for Plowshare deep underground explosives. His proposal is to utilize the enthalpy change of water in going from -65°F to +165°F. The approximate enthalpy changes are given in Table VI.

Table VI. Water enthalpy change available for cooling.

State Change	Approximate Enthalpy Change	
	Btu/lb	Btu/ft ³
-65°F to +32°F	46	3,900
ice to water	144	8,100
+32°F to +165°F	133	8,300
Total	323	20,300

The specified temperature range presumably arises from typical military requirements and a supposed capability of nuclear explosives to withstand that range. There is a clear advantage to utilizing a phase change in that one gets enthalpy change with no temperature change. Pursuit of materials exhibiting large enthalpy change per unit volume has been extensive in connection with heat absorption for domestic solar heating applications. Goldstein¹⁴ made such a search. The highest volumetric enthalpy change for a (non-evaporating) phase change, useable in our temperature range, was for Na₂HPO₄ · 12 H₂O. At 97°F this material becomes a lower hydrate by releasing water. The resultant liquid, which is a solution of the lower hydrate in the now free water can be said to have melted. Goldstein¹⁴ reports a volumetric enthalpy change of 11,600 Btu/ft³. In addition to having a significantly higher enthalpy change than that for ice, the transition temperature has the minor advantage of probably

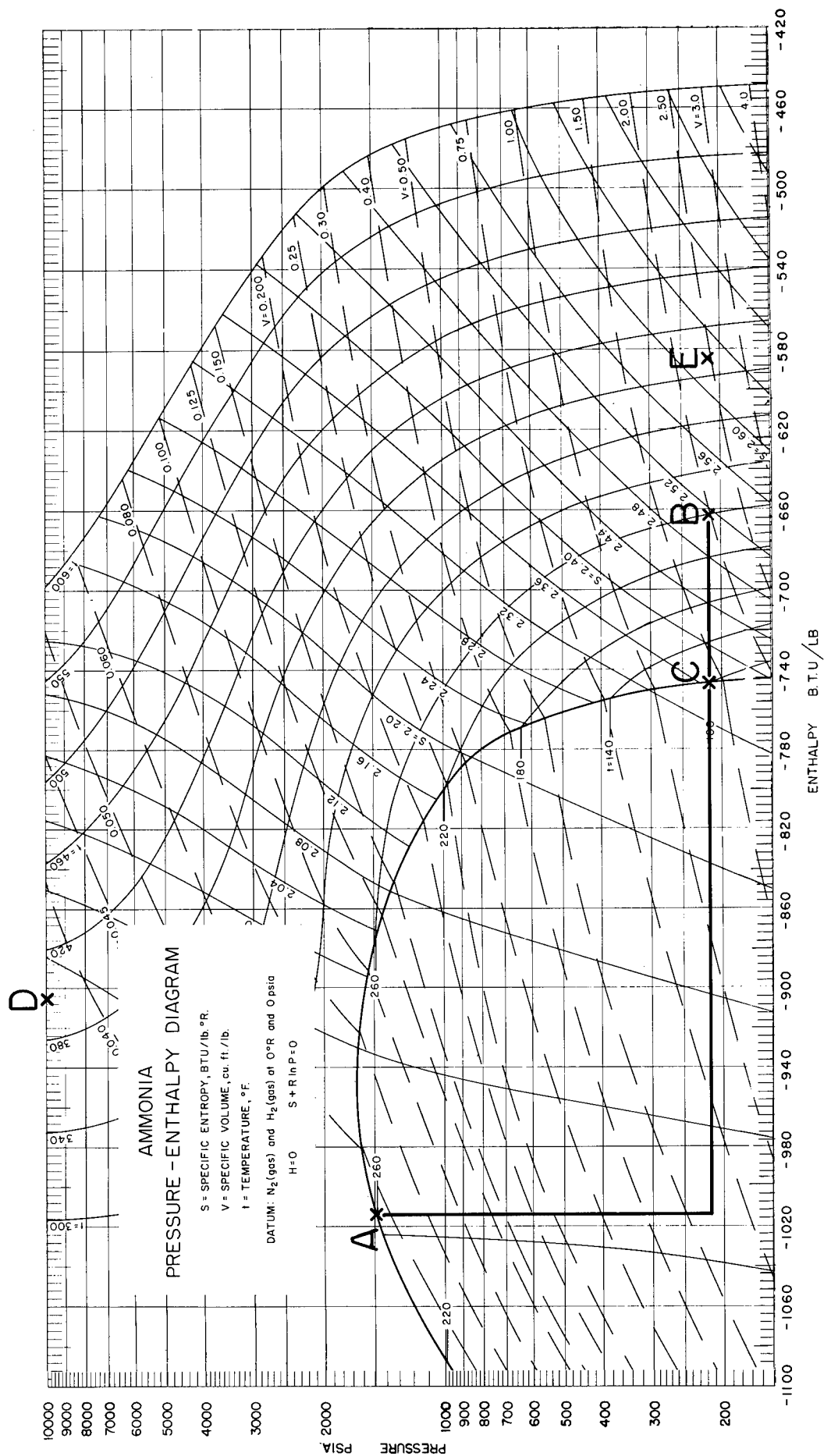


Fig. 11. Ammonia pressure-enthalpy diagram.

not requiring refrigeration prior to emplacement. One troublesome feature of this type of approach is that as one adds more heat capacity to gain greater life, one also increases the volume of the cool zone and the refrigeration heat load. As the length containing the heat sink material becomes sufficiently long, one approaches a life limit corresponding to radial heat flow into the heat sink material. The following numbers will indicate whether or not we are near that limit. Let us presume for the moment that the refrigeration load is fixed at 100 W (341 Btu/hr). Considering the numbers just discussed on heat sink materials, assume the material can absorb 15,000 Btu/ft³ (allowing some temperature change). Assume further that the package requiring refrigeration is 4 ft long by 8 in. in diameter. Let us take 30 days as a life objective. The volume of the refrigerated package is 1.26 ft³. The total heat absorbed must be 341 Btu/hr × 720 hr = 246,000 Btu. The required volume of heat sink material must be 246,000 ÷ 15,000 = 16.4 ft³. Assuming the heat sink material must occupy the same diameter, this implies that the ratio of the length of the heat sink to that of the refrigerated package is $\frac{16.4}{1.26} = 13$. Undoubtedly the initial assumption of a fixed 100 W heat load is therefore invalid. Considering the relative length of these values it is fair to conclude that we are near the limiting situation of a very long package of heat sink material.

Appendix 2 gives an expression for approximating the limiting time for a very long cylinder of heat sink material. This is:

$$t_{\max} = 0.014 \frac{D^2 Q}{k \Delta T}$$

letting

$$D = 8 \text{ in.} = \frac{2}{3}$$

$$Q = 15,000 \text{ Btu/ft}^3$$

$$k = 0.00026 \text{ Btu/hr ft } ^\circ\text{F}$$

$$\Delta T = 300^\circ\text{F}$$

$$\text{gives } t_{\max} = 1200 \text{ hr.}$$

The above argument indicates that this type of heat capacity approach is probably feasible. The available time is especially sensitive to the diameter which can be used for heat storage material. It appears that no other approach will have the simplicity of this one.

B. Heat Capacity Stored at Ambient Temperature

If one were able to utilize the latent heat of vaporization in a stored-capacity-type system, substantial gains in the heat capacity per unit volume of the substance are possible. In the case of water, which might well be the best practical fluid in this regard, the latent heat of vaporization is approximately six times that of its heat of fusion. A second advantage accrues in that if the substance is stored at our ambient temperature as saturated liquid, the enthalpy change available for cooling is not greatly reduced from the situation where the liquid is stored at our refrigerated temperature. Referring to Fig. 12, which is taken from Meyer *et al.*,¹⁵ in the former case one can operate ideally along the route of A B C D E where the enthalpy change between D and E is utilized to pre-cool water along A B. The enthalpy change available for cooling is the difference between C and D, or about 860 Btu/lb. This implies about one week cooling capability for each cubic foot of water when the cooling load is 100 W. In the latter case, the enthalpy change available for cooling is about 1030 Btu/lb. This means that the liquid can be stored outside the insulated volume, and one does not encounter the surface-to-volume limitations encountered for the earlier type heat capacity system.

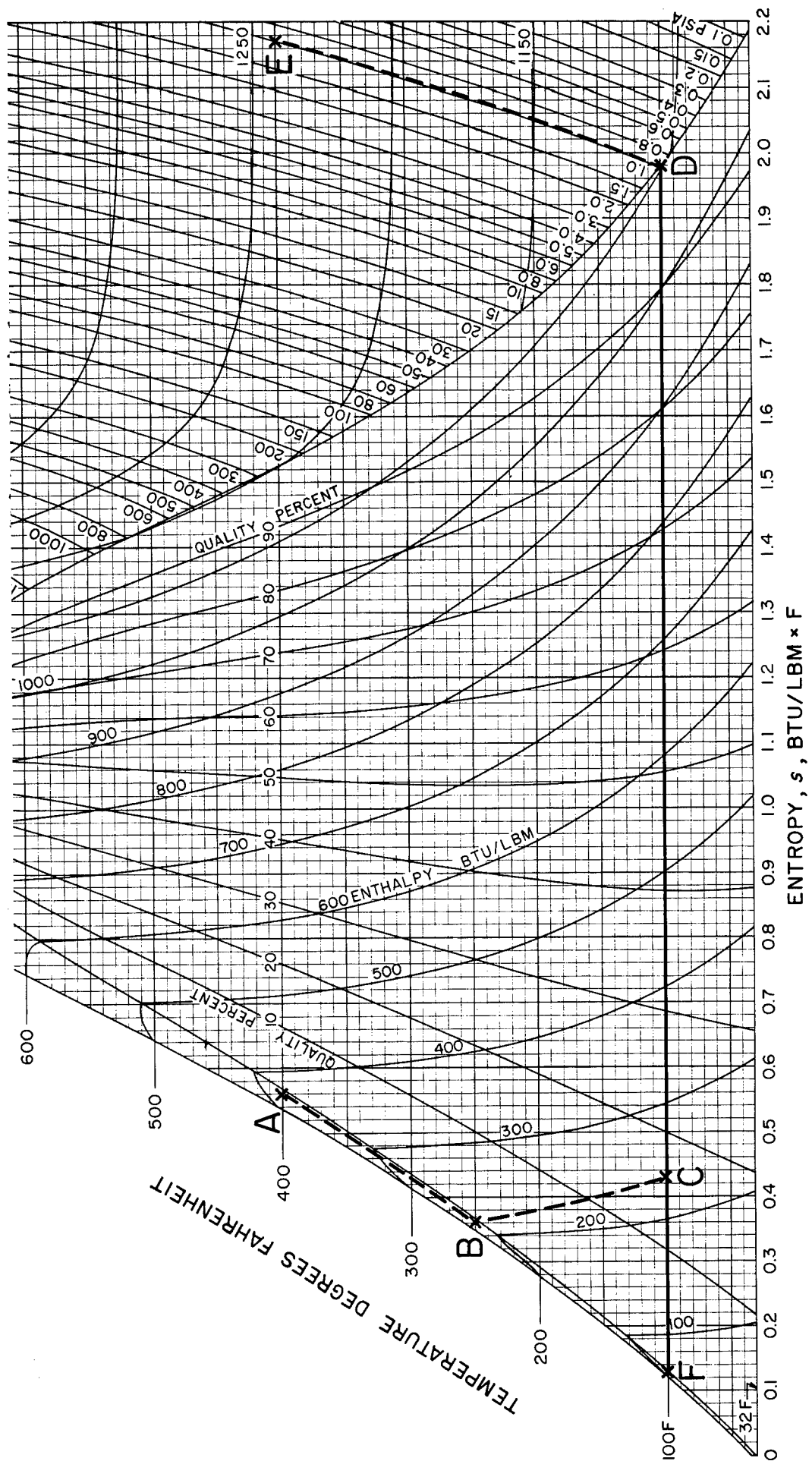


Fig. 12. Temperature versus entropy for water.

Having proceeded this far, it is now necessary to find a place to put the water vapor. If one attempts simply to provide volume for the vapor, the volume required for a reasonable time turns out to be greater than the volume of the emplacement hole.

Following what is done in a portion of the absorption cycles we can search for chemical means to absorb the water in a condensed state. Assuming we wish to evaporate water for refrigeration at 100°F, where the vapor pressure is about 1 psia (52 mm Hg), it will be necessary for the vapor pressure over the combination of water and absorber (assumed to be at ambient temperature) to be less than 1 psia in order to support a mass transfer mechanism. If we take the ambient temperature for this search as 450°F (232°C), the requirement is to find a substance with water in solution or chemically held that has an equilibrium vapor pressure of water less than 52 mm Hg at 232°C, a very low pressure of the absorbent, and that has an interestingly high water content. Table VII lists some of the encouraging data which has been found.

Table VII. Water vapor pressure over potential absorbers.

System	Partial Pressure of Water at Temp.		Ratio of Water Absorbed to Absorbent	Source of Data*
	mm Hg	°C		
Solution of NaOH and H ₂ O	52	232	About 15% interpolation in table is coarse	ICT vol. III p. 370
CaO + H ₂ O → Ca(OH) ₂	2.7	301	31%	ICT vol. VII p. 294
BaO + H ₂ O → Ba(OH) ₂	9.2	630	11.7%	ICT vol. VII p. 299
Li ₂ O + H ₂ O → 2LiOH	2.3	520	62%	ICT vol. VII p. 301

*Reference 16.

There appears to be little doubt that this approach is feasible. Factors affecting the absorption rates, such as grain size, bulk density in the container, and the necessity for separators probably can be determined empirically. The high ambient temperature appears favorable to obtaining adequate absorption rates. Also dissipation of heat of absorption into the strata must be dealt with. In addition, there are a number of ammoniates with adequately low partial pressure of ammonia, but the high heat of vaporization appears clearly to favor water as the refrigerant. In concept we visualize an arrangement similar to that of Fig. 10, except that the vent line terminates in a vessel containing the absorbent and no recharge provision is present.

The absorption task is considerably simplified over that in the normal closed absorption cycle in that there is no necessity to deal with separating the water from the absorber.

CONCLUSION

Nuclear explosives can be protected in very hostile environments with an additional diameter about 10% of the overall diameter. Canisters with the required characteristics can be built of conventional materials, and cooling systems can be developed having adequate performance.

Closed-cycle cooling systems are essentially unlimited in life, but will require extensive development efforts. Maintaining communication with such systems adds to the complexity of emplacement operations in that added electrical cable or tubing must be installed.

Open-cycle systems of limited life can be provided with only modest development effort. The disadvantage of limited life is not too great, in that with good insulation lifetimes up to 100 days can be provided.

The water-absorber system looks most interesting at this time. In the future, when time at temperature is reduced by streamlined emplacement and stemming procedures, the stored heat-capacity concepts will deserve to be re-examined.

APPENDIX 1 TEMPERATURE DROPS ASSOCIATED WITH GRAVITY REFLUX PIPES

The Nusselt theory for filmwise condensation on vertical surface treats the situation where the gravity-induced flow is laminar. As outlined by McAdams,¹⁷ the criterion for whether flow is laminar is

$$\frac{4\Gamma}{\mu} = 1800$$

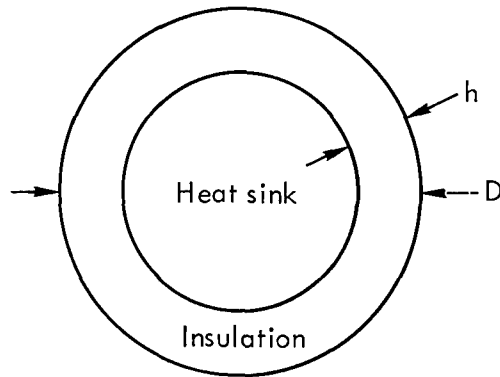
where Γ is the mass flow rate per unit width (not thickness) of flowing film and μ is the liquid viscosity. Assuming the situation to be condensation of steam at 450°F with a heat of condensation of 770 Btu/lb, the pipe inside diameter is 6 in., the liquid viscosity is 0.28 lb/hr-ft, and that the heat to be rejected is 1 kW, the quantity $4\Gamma/\mu$ is 40 indicating that the flow is well within the laminar range. It may be noted that this conclusion is independent of the length of the reflux pipes. Using the above numbers and the methods outlined by McAdams, one can deduce that the temperature drop across the film is about 0.005°F.

If the heated surface of the evaporator which feeds the gravity reflux pipe is a flat bottom to a pool, then the data of Jakob¹⁸ indicates that the temperature difference between the pool and its bottom will be about 10°F when the pressure is 1 atmosphere. Data from page 382 of Ref. 17 indicates that the temperature difference may be lower for higher pressures. It appears likely that some pool bottom configuration other than flat would lower this temperature difference.

APPENDIX 2 OPTIMUM INSULATION THICKNESS FOR A HEAT SINK WITH RADIAL INFLOW OF HEAT

The following quantities define the problem:

- D—Diameter of cylinder containing insulation
- h—Insulation thickness
- k—Thermal conductivity of insulation
- ΔT —Temperature difference across insulation
- Q—Heat capacity of heat sink material per unit volume.



The heat capacity per unit length is

$$\frac{\pi}{4} (D - 2h)^2 Q .$$

The heat flow rate per unit length is

$$\frac{2\pi k\Delta T}{\ln \frac{D}{D - 2h}}$$

The time t required to "use up" the heat capacity is

$$t = \frac{\frac{\pi}{4} (D - 2h)^2 Q}{\frac{2\pi k\Delta T}{\ln \frac{D}{D - 2h}}} = \frac{(D - 2h)^2 Q}{8k\Delta T} \ln \frac{D}{D - 2h} .$$

The maximum time as a function of h is obtained in the usual fashion by setting $\frac{dt}{dh} = 0$. This yields the optimum

$$\frac{h}{D} \Big|_{\text{opt}} = \frac{1}{2} \left(1 - \frac{1}{e^{1/2}} \right) = 0.197$$

$$\text{and } t_{\text{max}} = 0.014 \frac{D^2 Q}{k\Delta T} .$$

REFERENCES

1. P. E. Glaser, I. A. Black, R. S. Lindstrom, F. E. Reucia and A. E. Wechsler, "Thermal Insulation Systems," NASA-SP-5027, 1967, by A. D. Little, Inc., for NASA.
2. A. J. Elliott, "Study of a Self-Contained Temperature Control System for Plowshare," Report No. SCL-DR-69-111, Sandia Laboratories, Livermore, October 1969.
3. J. C. Maxwell, Electricity and Magnetism, (Dover Publ., New York, 1954).
4. W. E. Gifford and R. C. Longworth, Trans. ASME, Series B, Eng. Industry, 86, 264 (1964).
5. B. Shelpuk, M. S. Crouthamel, A. Amith and M. Yim, "Low-Temperature Solid-State Cooling Technology," Technical Report AFFDL-TR-68-128, by Radio Corporation of America for U. S. Air Force Flight Dynamics Laboratory, August 1968.

6. H. J. Goldsmid, Applications of Thermoelectricity, (Methuen & Co. Ltd., London, 1960).
7. D. A. Wright, Direct Generation of Electricity, (Academic Press, New York, 1965).
8. R. T. Ellington, G. Kunst, R. E. Peck and J. F. Reed, "The Absorption Cooling Process—A Critical Literature Review," Institute of Gas Technology Research Bulletin No. 14, The Institute of Gas Technology, Chicago, 1957.
9. L. F. Whitney, "The Mercury Ejector Refrigerator," Refrigeration Engineering, September 1932, p. 143.
10. L. T. Work and V. W. Haedrich, Ind. Engr. Chem. 31, 464 (1939).
11. L. N. Canjar and F. S. Manning, Thermodynamic Properties and Reduced Correlations for Gases, (Gulf Publ. Co., Houston, 1967).
12. H. Rouse, Elementary Mechanics of Fluids, (John Wiley & Sons, New York, 1947).
13. U.S. Dept. of Commerce, "Tables of Thermodynamic Properties of Ammonia," Circular of the Bureau of Standards No. 142, 1st Ed., April 1923.
14. M. Goldstein, "Some Physical Chemical Aspects of Heat Storage," Published in vol. 5, Proc. U.N. Conf. New Sources of Energy, Rome, August 1961.
15. C. A. Meyer, R. B. McClintock, G. J. Silvestri and R. C. Spencer, Thermodynamic and Transport Properties of Steam, (ASME, New York, 1967).
16. E. W. Washburn (ed.), International Critical Tables of Numerical Data; Physics, Chemistry, and Technology, National Research Council, (McGraw-Hill, New York, 1930).
17. W. H. McAdams, Heat Transmission, Chapt. 13, (McGraw-Hill, New York, 1954).
18. M. Jakob, Heat Transfer, Vol. 1, Chapter 29, (John Wiley & Sons, New York, 1949).

INTEGRATED CONTROL SYSTEM FOR NUCLEAR EXPLOSIVES*

William F. Ragsdale
Lawrence Radiation Laboratory, University of California
Livermore, California 94550

ABSTRACT

The Integrated Control System (ICS) has been developed to facilitate Plowshare nuclear detonations by following a unified system approach. This system consolidates the techniques for firing, safety program, scientific program, and communications. Maximum emphasis is placed upon control and data transmission by radio rather than hardwire or coaxial cable.

The ICS consists of a Command Point (CP) Trailer, a radio repeater station, a field station (the ICE Box), and several chassis located in the explosive canister. Commands originate in the CP and are transmitted via microwave radio to the ICE Box; monitors are returned to the CP from the canister, the ICE Box, and sensors near ground zero.

The system allows complete checkout and operation before shipment to the field. The explosive canister may be dry-run at the assembly area (at NTS) before shipment to the field.

The basic detonation functions for every event are:

1. Arming and firing commands in the explosive canister and at surface ground zero.
2. Environmental monitors and suitable arming monitors in the explosive canister.
3. Safety monitors at the zero site for weather, RAMS (Remote Area Monitoring System), and cavity collapse.

Secondary functions that may be required for a specific project are:

4. Scientific program of phenomenology measurements.
5. Explosive performance measurements.
6. Ground zero television.
7. Auxiliary communications such as local telephones, VHF radio.

By combining functions that have previously been performed by separate organizations and systems, the ICS attempts a minimum cost detonation service. Economy of operation results because:

1. Operating personnel work on more than one sub-system.
2. Interfaces and interface complexity are minimized.

*Work performed under the auspices of the U.S. Atomic Energy Commission.

3. A reduced dependence upon signal cables results from a microwave-based system.
4. Pre-fabrication allows test operation before shipment to the field and minimizes setup time in the field.

The ICS is in use on the Sturtevant event and is scheduled for the Yawl event at the Nevada Test Site.

INTRODUCTION

Industrial application of Plowshare technology requires efficient procedures and equipment for the safe and reliable detonation of nuclear explosives. The electronic functions involved in the detonation are examples of activities where coordination and planning can make significant improvements over past operations. Monitoring the condition of the explosive in a hostile environment, firing the explosive, collection and display of safety program data, and some local communication service are tasks that reach peak activity during the few days preceding the detonation. Integration of these tasks will lead to smoother field operations and better use of personnel.

The Integrated Control System (ICS) described here is a step toward the kind of control system suitable for industrial applications. The main objectives of the development were to facilitate the execution of Plowshare experiments in remote locations and to demonstrate the advantages of combining several functions into a single operational system. Two general criteria were stated to guide the design of the equipment: (1) Minimize the need for fixed facilities in the field, and (2) eliminate interfaces wherever possible. Although the ICS has more capability than would probably be required for industrial applications, the basic design concepts will still apply. Underground engineering applications have stimulated much of the development, but the system concepts and hardware can be applied to excavations projects as well.

FUNCTIONS

Many functions are handled by the ICS, but not all are required for every detonation. The list given below is quite complete in terms of system capability. Each item in the list is discussed in following paragraphs.

A. Essential for any detonation:

1. Transmit arming and firing commands to the explosive.
2. Display monitors from explosive during arming.
3. Display monitors of environmental condition of explosive during emplacement, stemming, and other pre-detonation activities.
4. Display monitors from safety program instruments in the field.

B. Usually found with experimental detonations:

1. Transmit commands to associated experimental apparatus.
2. Record explosive performance data.
3. Record phenomenology data.
4. Transmit site surveillance television.
5. Provide local communications.

Arming and firing commands must be sent to the explosive canister in the proper sequence and at the proper time. Safety provisions to prevent inadvertent or unauthorized detonation are discussed later.

Monitors are used to verify the progress of the arming sequence and to operate an interlock chain allowing completion of the firing process. In most cases, several steps are involved before any irreversible action takes place, permitting automatic or manual interruption of the procedure.

It is essential that the condition of the explosive be known at all times, especially when the environment is such that reliability depends on proper operation of a cooling system. Monitors observed during emplacement and stemming also verify the condition of the control cable.

Safety program data such as weather conditions, radioactivity levels, and ground motion are required in carrying out the safe reentry to the site of a fully-contained detonation. Excavation projects involve safety considerations beyond the range of the ICS.

Explosive performance, phenomenology, and other experimental data are recorded by cameras or tape recorders. Commands and monitors are required for this equipment as well as power control for experimental apparatus.

Television surveillance of the detonation site may be for personnel safety or for recording the surface effects of the detonation.

Communication is needed between the Control Point (CP) and the detonation site for checkout of all equipment before explosive emplacement begins, and also in final preparations for firing.

Several different arrangements of explosives must be considered in the design of a control system. Figure 1 shows a few of the possibilities. Details of a particular job will influence the selection of surface hardware; i. e., the

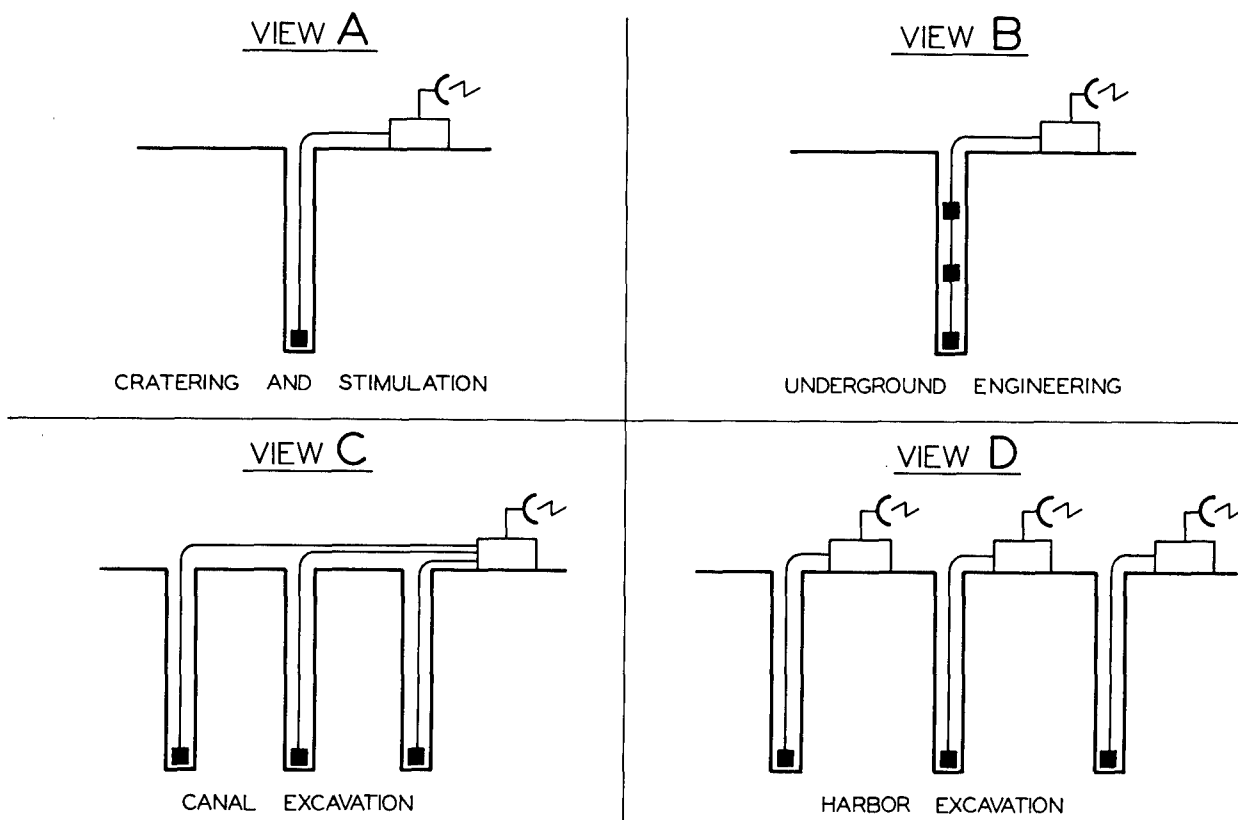


Fig. 1. Possible ICS applications.

choice between additional receiver-transmitter units or short runs of surface cable. The example labeled "Harbor Excavation" assumes that there is shallow rough water between the emplacement holes, and even for spacing of a few hundred feet, cable would be too vulnerable. In all cases, the equipment in the explosive canister is the same, and the control room requires no changes.

SYSTEM DESCRIPTION

Three major elements make up the Integrated Control System: Control Room, Integrated Control Element (ICE) Box, and the equipment packaged in the explosive canister. Communication between the control room and the ICE Box at ground zero is by microwave radio, and from ICE Box to the explosive canister is by coaxial cable. Ancillary equipment, such as a basic power supply at ground zero and a microwave repeater station, are also included in the complete system. Figure 2 is a pictorial view of the ICS.

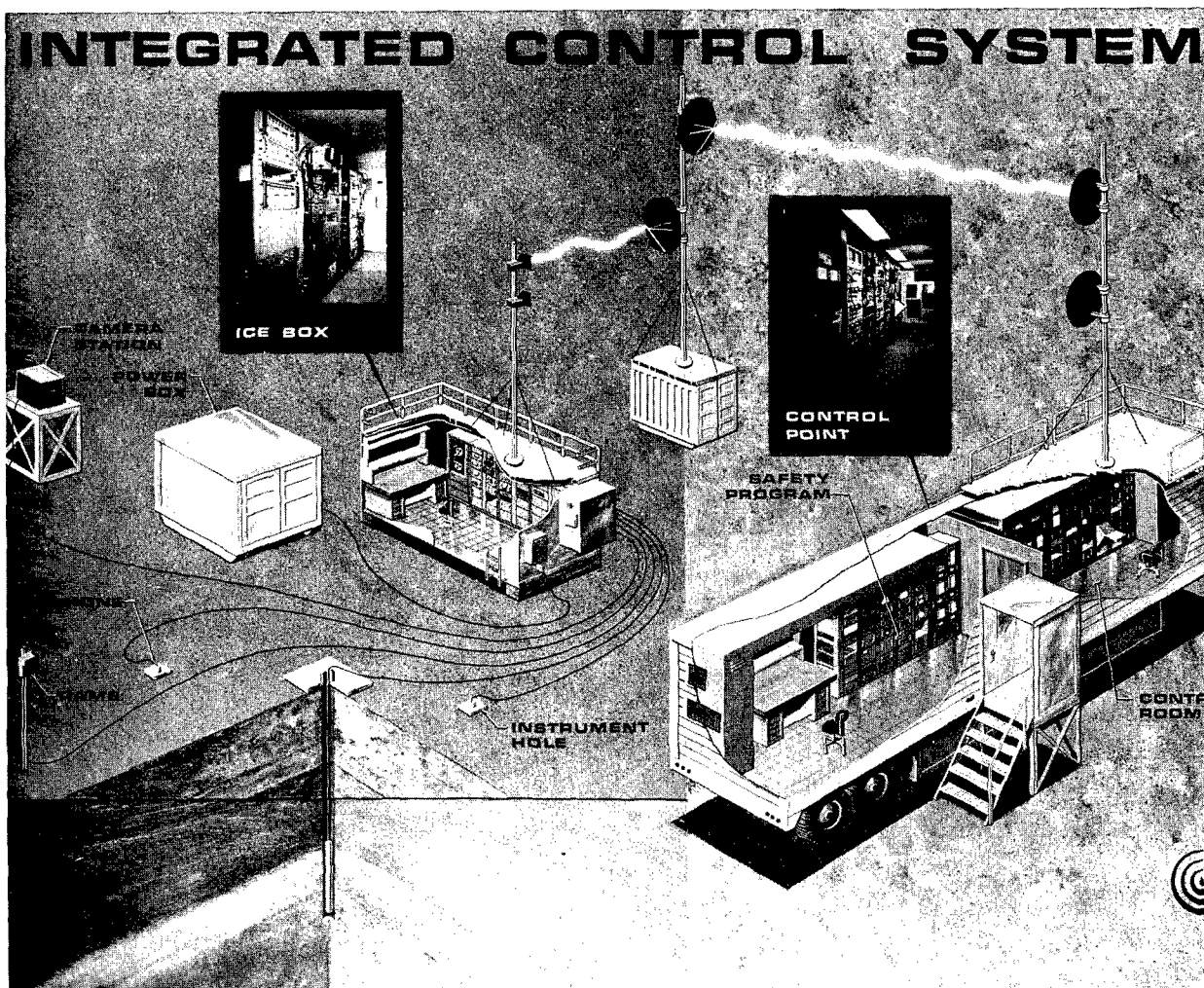


Fig. 2. Integrated control system.

The Control Room includes the following items:

1. Control console
2. Monitor displays (lights and strip charts)
3. Clocks showing world time and countdown time

4. Microwave equipment
5. Safety program data displays (weather, radiation, ground motion, etc.)
6. Communications to Test Manager, etc.
7. Standby power system

The control room is built into a trailer that includes air-conditioning equipment and provides mountings for the radio antenna (see Fig. 3). It is assumed that basic power for the trailer is available, either from commercial lines or from the local power system at the control point. Standby power is included to maintain communication with the ICE Box and the outside world in the event of local power failure. The detonation could be conducted and safety data monitored for several hours; sufficient time to restore power or establish other safety controls if needed.

The ICE Box (Fig. 4), an $8 \times 8 \times 20$ ft, air-conditioned, commercial cargo container, houses all the necessary electronic equipment for a particular event. It is powered from the Power Box, an $8 \times 8 \times 15$ -ft transportainer outfitted with two identical diesel generators. One generator supplies the power, and in case it fails, the other circuit can be switched in automatically.

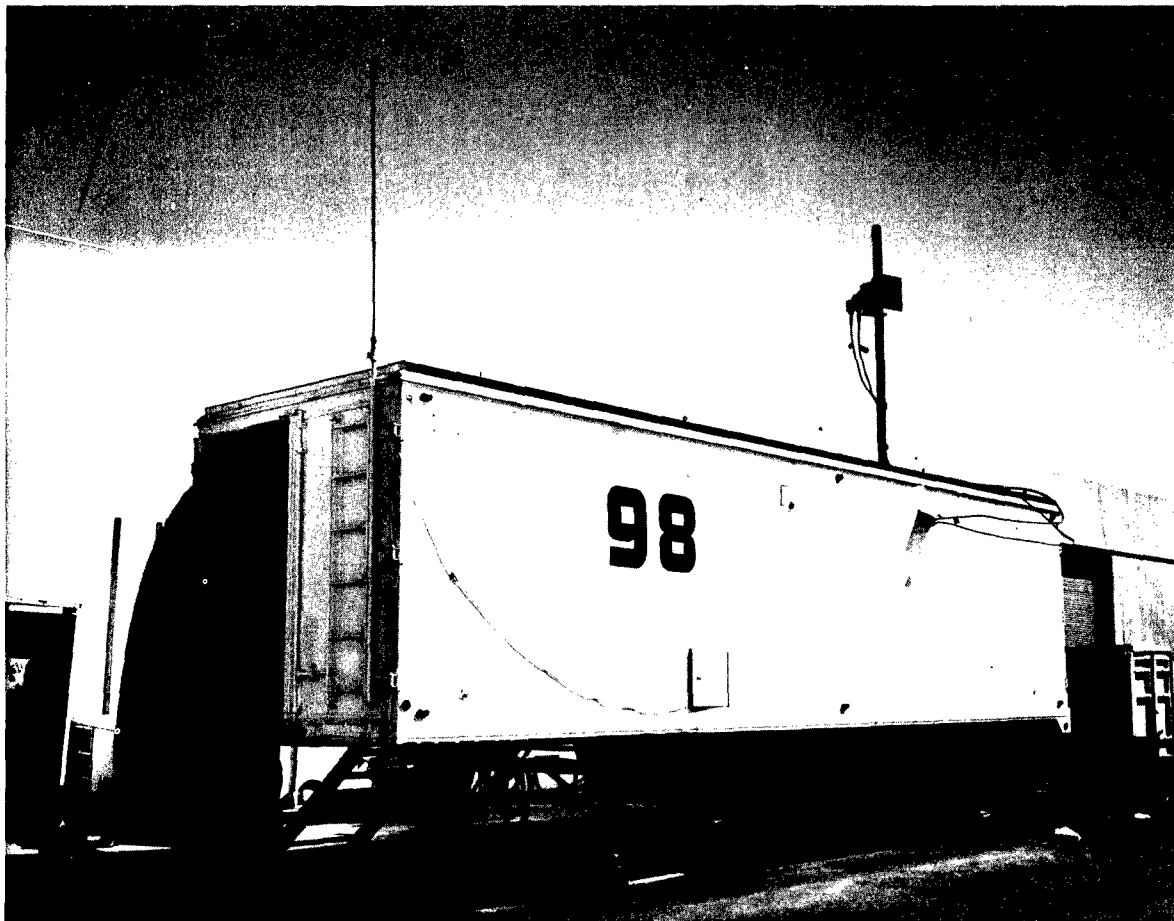


Fig. 3. Control room – Trailer 98.

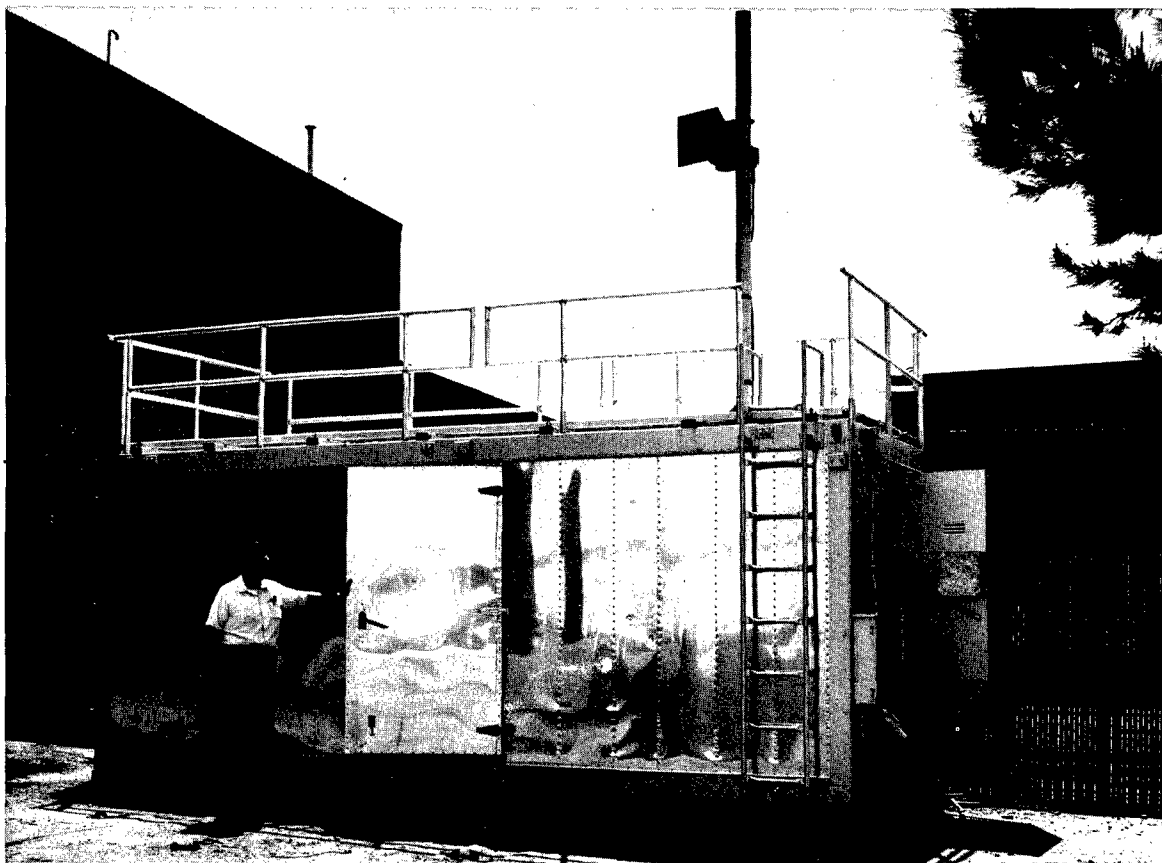


Fig. 4. ICE Box.

The ICE Box is the Ground Zero terminal of the microwave link. It distributes the commands downhole and to close-in surface installations, provides all downhole power, and transmits the downhole monitors as well as all necessary pre- and post-shot safety information such as weather, TV surveillance, radiation area monitoring, and geophone data to the CP. There is also room for a tape recorder and a few oscilloscopes to record explosive performance and phenomenology data.

In the case of a fully-contained detonation, the ICE Box will be located no more than a few hundred feet from the emplacement hole. Shock-loading of the box during the ground motion will be mitigated by crushable foam pads, reducing the accelerations to about 5 g's maximum, a safe limit for the equipment inside.

An expendable version of the ICE Box may be used for excavation events, or it should be located and protected suitably for recovery.

The explosive canister contains a command and monitor system, as well as power supplies for the various sub-systems involved in the firing of the explosive. A dummy explosive system is shown in Fig. 5. This assembly is placed into a pressure vessel before shipment to the field.

A coaxial cable carries power and all information between the ICE Box and the explosive canister. Power is controlled in the ICE Box by commands from the control room. Power is continuously available to the downhole power supply. This power is 200 V dc at 1 ampere or less. It is converted by the downhole power supply to +28, ± 15 , +5 V dc for command and monitor chassis use.

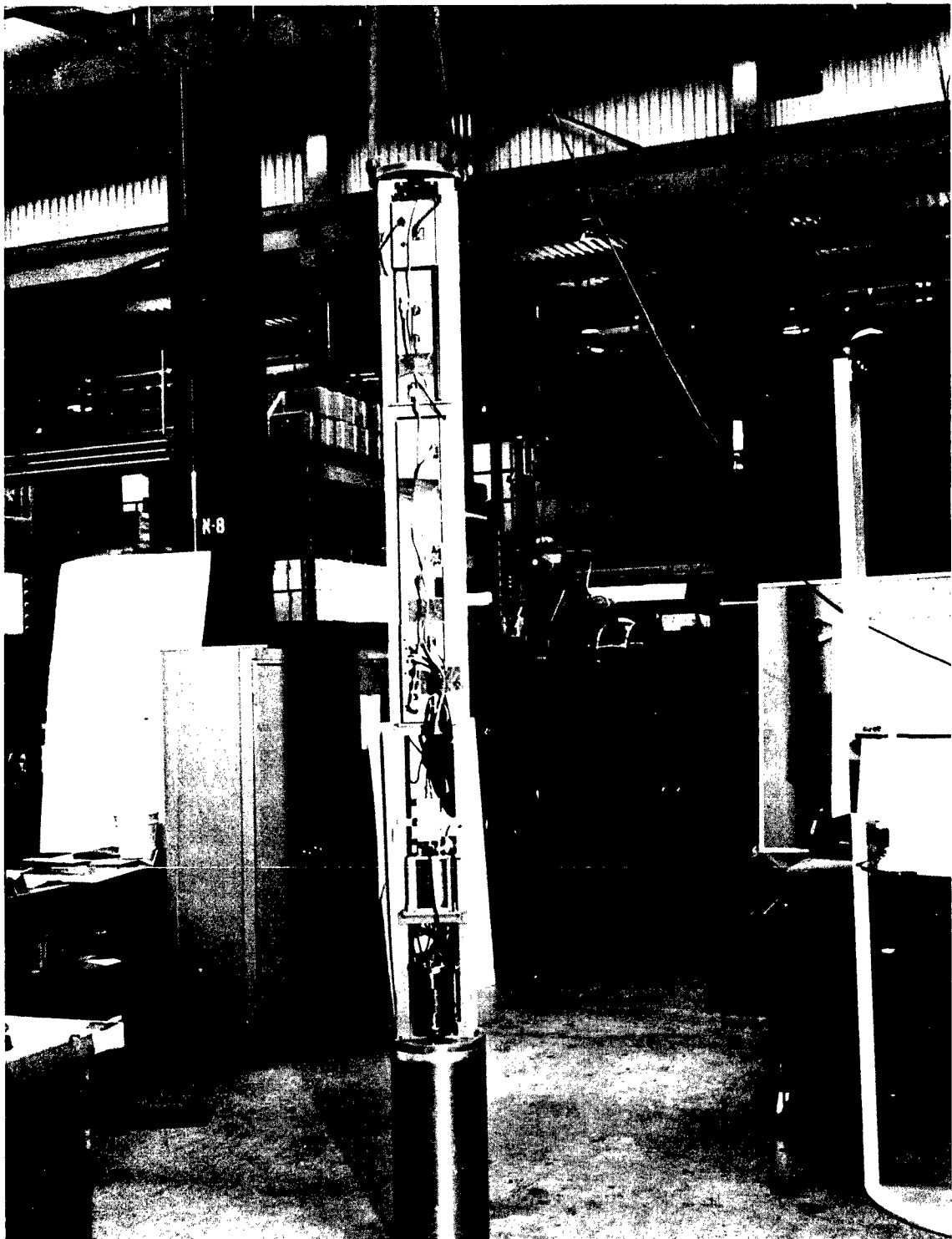


Fig. 5. Dummy assembly.

Power for arming of the explosive, the only function involving nuclear safety, is controlled in the ICE Box. On command from the control room, this 120-V ac, 400-Hz power is mixed with the dc monitor power on the coaxial cable. In the canister, the arming power is separated by a tuned filter and transformed to supply the arming system. Safety is assured by physical control of the 400-Hz power supply in the ICE Box.

Commands and monitors pass over the microwave and the cable with minimum change in data format. Commands are encoded on a multiplex format modulating a 93-kHz subcarrier. This subcarrier is superimposed on the cable to the canister. Monitors are multiplexed on a 165-kHz carrier on the coaxial cable and included in the microwave signal back to the control room.

Commands are decoded at the ICE Box, in the explosive canister, or at other locations as required. Monitors are collected from the explosive canister, the ICE Box, safety program instruments, or other experiments at the detonation site. Depending on the number of channels involved, commands and monitors may be handled in the ground zero area by coaxial cable to remote decoder or monitor units, or by multiconductor cable direct from the decoder or monitor unit in the ICE Box.

Appendix I gives additional information about the detailed design concepts that have been used. Reference 1 also goes into additional detail on the characteristics and capabilities of the system.

OPERATION OF THE INTEGRATED CONTROL SYSTEM

Field operations have been considered throughout the design and development of the ICS. The general criteria stated in the introduction are largely the result of observations of field operations in the past.

Three phases of activity can be identified in applications of the ICS:

1. Assembly and operation before shipment.
2. Field setup and checkout before explosive arrives.
3. Emplacement and detonation.

The ICS is designed to be fully mobile, and is to be completely set up and checked out at some well-equipped location such as LRL-Livermore before being shipped to the detonation site. Preparations for shipment do not require disassembly except for radio antennae.

Field operations begin with a week or two of setup and checkout before the explosive arrives. This phase is mainly to check for damage in shipment.

Before emplacement begins, a final check of the explosive canister system is made. With certain critical items, such as detonators or other one-shot devices disconnected and temporarily replaced by simulators, the complete system is operated as it will be for the actual detonation. Replacing the internal connections and closing the canister prepares the explosive for emplacement.

During emplacement and stemming the monitor system is operated at intervals, or perhaps continuously for checking on the cable and the performance of any environmental protection system.

Preparation for firing includes a final check of the safety instrumentation and all recording systems and completion of the ICE Box connections to permit arming power to be put onto the coaxial cable to the explosive. The countdown to the detonation is begun when approval is given by the Test Manager.

After a deeply buried detonation, the ICE Box continues to transmit safety program data back to the control room until no longer required.

FUTURE MODIFICATIONS

The present design is not considered to be the ultimate in many respects. A few comments are in order on the things that we now recognize as possible changes. Other changes will surely develop as the system is used and specific applications lead to consideration of unique requirements.

1. Radio Link — Microwave has bandwidth for carrying a great deal of information. Future systems will probably not require the bandwidth, and operations may be simplified with VHF radio. It may be possible to use a pre-existing radio net in the detonation area.
2. Simpler explosives will come with time and engineering development. The number of commands and monitors may be reduced considerably.
3. Experimental measurements will diminish, reducing the need for bandwidth and the recording capability.
4. Television surveillance of ground zero may be eliminated or at least replaced by a slow-scan process so that a picture sufficient for the purpose may be sent over the VHF radio or a telephone line.
5. Safety program activities will diminish, or at least become more efficient as experience is gained in particular areas. Confidence in containment requires experience.

CONCLUSION

The ICS approach for fielding Plowshare events presents the first major departure from the routine weapons test procedures. It allows for more efficient use of manpower by combining all functions under a single control, a minimum fielding time, and hopefully, elimination of technical delays in the field by shipping a completely checked-out system after all site preparations are completed and accepted.

Communication techniques, multiplexing, and data transmission formats provide flexibility needed for the variety of Plowshare experiments over the next few years.

Basic design concepts used in the ICS development will allow industrial systems to evolve as the needs become more clearly defined.

APPENDIX I. ICS DESIGN GUIDANCE

The following discussion gives the major concepts constituting the Integrated Firing System Concept. This is based upon earlier generations of the Simplified Firing System (SFS) of which this is SFS-IV. These items develop a consistent set of constraints, with trade-offs possible within these constraints. Ranking of these concepts indicates the approximate emphasis each has on the performance, but not necessarily the importance or cost of the detail areas.

1. Signals, both command and monitor, should traverse the system from CP to the device canister with a minimum of change. The intent is to reduce and simplify interface equipment and checkout required. This requirement infers that the signals should be compatible with cable and radio transmission and require the minimum of equipment at any transition of transmission mode.

2. The system should have available a large number of commands and monitors. Suitable magnitudes are in the hundreds if not thousands. Past experience demonstrates the trend for signal requirements to grow, even though only a limited number may be required at any given time. The system should have command and monitor frames expandable by simple assembly or mixing techniques rather than by re-design or duplication of systems. Two types of commands are used, manual and countdown time-based.
3. Separation of arming and operating power should exist. Positive lockout means for arming power should exist before and after arming party setup. Arming power should be of a type ordinarily unavailable and dissimilar from interference, transients, or types likely to be accidentally generated in the system environment.
4. Energy flow and isolation must be considered throughout the system. This includes power, command and monitor signal flow, as well as spurious signals. Shielding, isolation, and limiting should be used to enhance safety, reliability, and performance.
5. Field hardware and adjustments should be minimized. Equipment should require a minimum of setup and checkout in the field. System qualification should only require checks in the field to detect deviations from previous measurements. This field qualification is based upon the prepackaging and checkout before shipment to the field.
6. Reliability analysis should be utilized to balance overall reliability of the system. The design should use techniques to insure reasonable equipment lifetime, consistent with limitations such as device shelf-life, cable and connector lifetime, and the emplacement environment.
7. Formats of transmissions should reflect performance functional requirements. Commands should be binary (on-off). Monitors should be analog with binary capability (transducers, temperature, voltages). This requirement reduces the need for field threshold detectors consistent with No. 5; analog transmission eliminates the need for analog-digital converters in the field, again consistent with No. 1 and No. 5.

REFERENCE

1. M.D. Nordyke, A.W. Lundberg, and W.F. Ragsdale, "Plowshare Streamlined Operational System," Lawrence Radiation Laboratory, Livermore, UCRL-50658, June 1969.

ADDITIONAL REFERENCES

W.F. Ragsdale, "Integrated Control System," Lawrence Radiation Laboratory, Livermore, UCID-15391, October 1968.

"Operation Safeguard," Machine Design, October 26, 1969, p. 34.

EMPLACEMENT AND STEMMING OF NUCLEAR EXPLOSIVES FOR PLOWSHARE APPLICATIONS*

J. L. Cramer

Lawrence Radiation Laboratory, University of California
Livermore, California 94550

This paper will discuss the various methods used for emplacement and design considerations that must be taken into account when the emplacement and stemming method is selected. The step-by-step field procedure will not be discussed in this paper.

The task of emplacing and stemming the nuclear explosive is common to all Plowshare experiments today. All present-day applications of a nuclear explosive for Plowshare experiments require that the detonation take place some distance below the surface of the ground. This is normally done by lowering the explosive into an emplacement hole to a desired depth and then backfilling the hole with a suitable stemming material. At first glance it seems like a very straightforward, simple task to perform. It would appear to be a task that could become a standard procedure for all experiments; however, this is not the case. In actuality, the emplacement and stemming of a nuclear explosive must almost be a custom design. It varies with the application of the experiment, i.e., cratering or underground engineering. It also varies with the condition of the hole, the available equipment to do the job, the actual purpose of the stemming, possible postshot reentry, hydrology, geology, and future production. A very important item that must always be considered is the protection of the firing and signal cables during the downhole and stemming operation. Each of these things must be considered; ignoring any one of them could jeopardize one of the objectives of the experiment or perhaps even the experiment itself.

It should be emphasized that for a multiple-shot program such as would be used to develop a gas field where the geology, depths of burial etc. are the same, the emplacement and stemming operation would be standardized, as would all other parts of the program. However, for individual experiments in totally different areas, complete standardization of the emplacement and stemming is impossible.

First, the methods of lowering the explosive into the hole for cratering experiments will be discussed. One method uses flatwire rope pendants and a crane. These pendants can be made up in various lengths up to 80 ft as the situation demands. They are equipped with eyes and clevises which are connected with a pin. The emplacement is accomplished by adding pendants one at a time and lowering them into the hole with a crane. The downhole load is supported by a strongback while a new pendant is added. The downhole signal and instrument cables are fastened to the flatwire rope as it is lowered into the hole. This method of emplacement was used on Cabriolet and Buggy, two recent cratering shots at the Nevada Test Site.

*Work performed under the auspices of the U. S. Atomic Energy Commission.

Another method also using flatwire rope involves winding a continuous length on a special winch. The explosive is connected to the end and the flatwire rope is slowly spooled off the winch into the hole. This method is limited both in weight and depth, depending upon the capacity of the winch. Normally, explosives can be placed by this method to depths of 1600 ft, depending upon the weight of the downhole package. This method of emplacement is particularly adaptable to cratering shots in dry formations where there is not the problem of reentry to consider, or is stemming particularly difficult.

In the event that an explosive must be placed below the water table, both emplacement and stemming become more difficult. A cratering shot now under consideration has a configuration with the shot point approximately 500 ft below the water table. In order to stem a hole like this, there must be access to the bottom of the hole with grout tubing. The design of stemming for cratering shots covered later will make the reason for this apparent. To provide an access to the bottom of the hole with tubing without jeopardizing the cables, the flatwire rope has been replaced with small-diameter casing as the supporting member for the explosive canister. The casing is slotted in intervals, which will allow tubing to be run down the inside of the casing and permit the grout plugs to be pumped at any desired location. This method has a distinct advantage in giving full protection to the cables no matter how many times tubing is run in and out of the hole.

So far, underground engineering experiments have differed from cratering experiments in that they have been conducted in remote locations where the drill rig is the only large equipment readily available. Therefore, emplacement upon tubing, casing or drill pipe is generally the approach that has been considered. It is sometimes possible to effect considerable economic savings in the postshot reentry by emplacing the explosive on casing of sufficient size to allow reentry through the casing, rather than having to drill a new hole costing tens or hundreds of thousands of dollars. This is a case where the cost of a new hole, depth of the explosive, rapidity of reentry, and perhaps high-pressure gas problems must be considered when an economic decision is made. Salmon, Sterling and Gasbuggy were emplaced by this method. In all three projects, the emplacement casing was used for reentry or clean-out of the hole in the postshot activities.

Another method of emplacement was recently used by Los Alamos Scientific Laboratory in the emplacement of the Rulison explosive. In this case, a lightweight package was emplaced to about 8400 ft on its firing cable in a dry hole cased to total depth. The firing cable was encased in a wire rope very similar to the electric logging lines used in the drilling industry. The emplacement went very rapidly, and this appears to be a very desirable way of emplacing explosives to great depths when hole conditions, stemming requirements and reentry methods will permit.

Now a few words about stemming design. Stemming serves different purposes, depending upon the type of experiment. As with the method of emplacement, the design is also dependent upon hole conditions, cable protection, geologic environment and possible reentry. For cratering experiments where the hole is normally greater than 4 ft in diameter, the stemming must prevent premature release of high-pressure radioactive gases. It is also desirable that the stemming in the vicinity of the explosive approximate the characteristics of the surrounding media to prevent at early times abnormal cavity shapes. Code calculations assume that early cavity shapes are roughly spherical in shape. Matters would be unduly complicated by having a situation in which the stemming material was highly compressible compared to the surrounding media, which would cause an irregular cavity growth. Therefore,

an attempt is made to approximate the natural media directly above and below the explosive.

Stemming for cratering experiments usually consists of placing concrete or grout plugs with sand and gravel layers between them. Three plugs are normally used—one directly above the explosive, another about mid-point in the hole, and the third one at the top. The length of plugs varies depending upon depth of burial, washout or gage of the hole and other considerations. Placing the plugs in a dry hole is reasonably easy and can be done by several methods. Cratering experiments to date have not been very deep, and the task has been accomplished by placing concrete through a tremie pipe, or sand-cement grout through tubing. If the hole is large enough, the cables can be visibly observed as the pipe or tubing is run into the hole so that there is no contact between the cables and the pipe, which could damage the cables. However, when the explosive is placed below the water table, this method is no longer acceptable because of the risk of damaging cables. For that situation, the previously described method of using slotted casing for the emplacement string would be used, allowing grout tubing to be run inside the casing to the desired depth.

Stemming plans for deeply buried underground engineering applications are more complicated. The stemming must not only prevent the release of radioactive materials or radioactive contamination of the atmosphere, but must also prevent the resulting chimney from being flooded. Most applications for underground engineering require a dry, rubble-filled cavity as an end result whether it be for gas production, gas storage, oil retorting, copper leaching or most of the other foreseeable applications. It is not uncommon for the explosive depth to be below one or more aquifers; therefore, the emplacement hole must be sufficiently sealed to prevent postshot flooding through the emplacement hole itself. Because of the ease of emplacement at great depths, grout or cement plugs are normally used for this purpose. To clarify terminology at this point, cement plugs are normally some standard oil-well cementing mix; grout is the same mix with fine sand added. Dry sand or small gravel is often used where possible because of the ease of emplacement and economics. However, small-diameter wet holes make sand or other granular stemming unattractive because of the possibility of the material bridging. Stemming plans for deeply buried underground shots must be compatible with the method of emplacement and postshot reentry plans. We believe it prudent to stem an experiment in a gas-bearing formation with grout to a point outside the maximum expected fracture radius. The remainder of the stemming could be granular material or grout, depending on hole conditions, geology, and reentry plans.

A few of the other considerations affecting stemming design are: whether the hole is cased or uncased, whether the hole is dry or wet, the diameter of the hole, and location of subsurface instrument packages.

Schemes are presently under consideration which will permit rapid sampling or production from an underground cavity without resorting to a major drilling effort. In one method, shown in Fig. 1, the annulus between emplacement casing and the hole wall would be stemmed as usual. The bore of the emplacement casing, however, would be stemmed only from the explosive to a point just below the minimum predicted chimney height. A series of valves or rupture disks would be installed in the emplacement casing above the maximum predicted chimney height. The stemming would shield the valves or disks from the initial blast and after collapse of the chimney, they would only be subjected to the formation pressure. The valves could then be opened from the surface electrically, or the rupture disks could be broken by pressurizing the emplacement casing from the surface. Since the casing

would be expected to break or part in the chimney region, direct communication with the chimney would be established. Fluid stemming such as drilling mud, which could easily be removed, could optionally be used to stem the

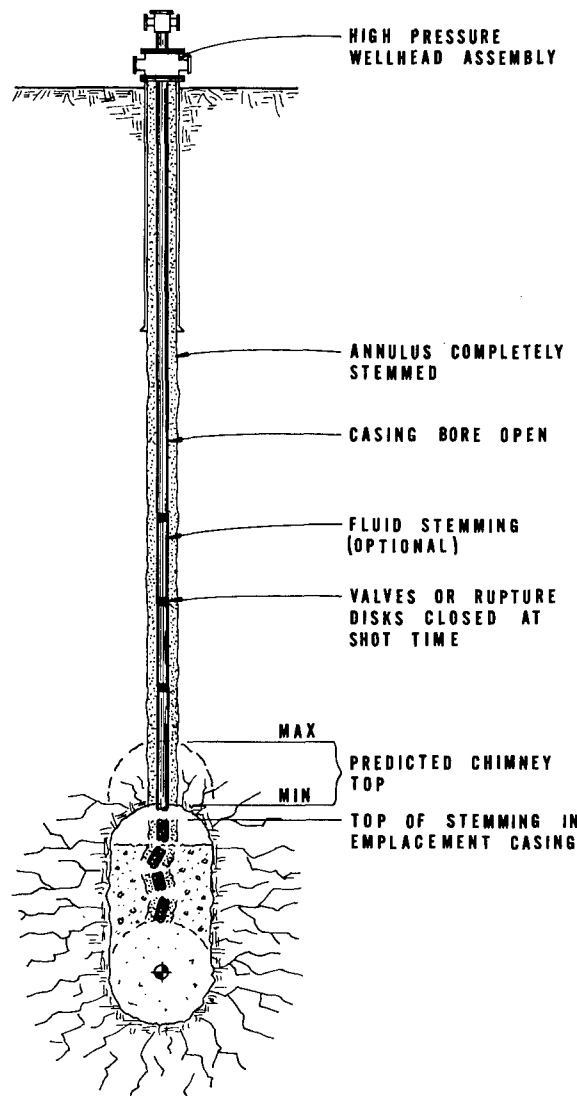


Fig. 1. Method of emplacement and stemming for rapid postshot reentry.

emplacement casing bore above or between the valves. Of course, a high-pressure well-head assembly would be installed preshot on the surface to guarantee containment.

Another method of simplifying the postshot drilling operation would be to put a highly drillable aluminum or aluminum alloy casing in the lower part of the emplacement string. In the past, when a nuclear chimney has been reentered, the casing has been found collapsed or bent or partially offset just before it reached the chimney, which complicated the drilling. This highly drillable aluminum portion of the string could very quickly be milled up, saving considerable time in the reentry operation. The cost of drilling a new hole to the chimney postshot must be balanced against the cost of installing the rapid reentry system, plus any additional cost that might be required for the safety program because of the system.

A few of the considerations which come to mind that tend to make each case unique are: Is the hole deviation sufficient to cause the cables to be abraded upon the walls of the hole, and if so, what steps must be taken to protect the cables? Will the heat of hydration from the grout or cement plugs exceed the temperature limitations of the signal cables? Are the fluid pressures in a wet hole, or the temperatures in a very deep hole sufficient to damage signal cables? In a winter operation, will the low temperatures require preheating of the cables to maintain their flexibility, and will the use of special steels and metallurgic practices be required to prevent temperature embrittlement?

One must also consider the stemming load of the granular material on the emplacement string as the granular stemming begins to consolidate. Firing and signal cables running down the emplacement hole are quite susceptible to damage from this loading. Cable abrasion when granular stemming is dropped down the hole must be considered. To what extent does the condition of the hole or the experiment warrant the establishment of alternate emergency procedures? For example, assume that a very lightweight aluminum casing at the bottom of the string is being used, and the explosive canister gets stuck. Should a screwed connection inside the aluminum casing at the top of the explosive canister be included to permit attachment of a strong steel drill pipe for recovery, if necessary?

These are but a few of the special considerations that must be taken into account along with the standard problems of loads, working stresses, safety factors, and safety codes. It should be emphasized in closing that there are no standard procedures available, and that each experiment must be designed after considering the many variables associated with it to give the maximum in safety, reliability, flexibility and economic savings.

CONTROL OF THE DYNAMIC ENVIRONMENT PRODUCED BY UNDERGROUND NUCLEAR EXPLOSIVES*

D. L. Bernreuter, E. C. Jackson, and A. B. Miller
Lawrence Radiation Laboratory, University of California
Livermore, California 94550

INTRODUCTION

One important aspect of any underground nuclear explosion is recording, retrieval and analysis of experiment and/or device performance. Most of the information is recorded or conditioned on sensitive electronic equipment and often transmitted via antennas that must remain in alignment. Sometimes diagnostic packages are located in towers near surface ground zero (SGZ). Also, some equipment is needed for timing and firing as well as safety requirements. Generally it is desirable to locate this equipment as close to SGZ as possible. This paper is a summary of LRL's method of controlling the dynamic environment in order to get good quality data and protect equipment while optimizing the cost.

The overall problem blends together: (1) definition of input, i.e. ground shock parameters; (2) shock sensitivity or fragility level of equipment to the input and purpose (i.e. does it record or transmit through shock arrival time?); and (3) design of a fail-safe shock mount (SM) system to modify the shock environment when required.

Before any SM system can be designed, items 1 and 2 must be answered as the ground shock can vary over a wide range and the sensitivity/fragility of the equipment can vary from less than $1/2$ g to more than 100 g's, particularly if recording is done through shock arrival time. Keeping antennas in alignment is a somewhat different problem. Whenever possible the design of the SM system is based only on peak input parameters of the ground motion since detailed time histories of the ground motions are very difficult to predict. For towers and other systems which require detailed time histories, computer codes have been developed which allow a parametric study of the input ground motion's effect on the response of the system. This paper deals mainly with the close-in region where the dynamic environment is quite severe. In this region, non-standard methods and analysis are required. Out of this region, more standard methods can be used.

PREDICTION OF THE DYNAMIC ENVIRONMENT

Prediction of the surface ground motion for our purposes relies heavily on empirical data and methods. A procedure for scaling and extrapolation from one event to another is required, since there is seldom available a previous event similar enough, i.e., yield, depth of burial (DOB), geology, and measurements of ground motion, for direct comparison.

*Work performed under the auspices of the U.S. Atomic Energy Commission.

Reference 1 gives a detailed discussion of scaling rules which have been worked out from a combination of theory and empirical data to relate the parameters from events of different yields. No corrections (in the scaling rules) are made for geology, DOB, etc. To scale for yield, all ranges (distance from center of detonation) are divided by the cube-root of the yield expressed in kilotons. Accelerations are scaled by multiplying by the cube-root of the yield, velocities are not changed, displacements and time are corrected by dividing by the cube-root of the yield. It is difficult to predict detailed time histories of the ground motion parameters other than for very closely related events; even then there are often important differences in the structure of the pulse. Peak values can be predicted somewhat better.

Most of the published data dealing with surface motion are for distances greater than 5 kilometers. To extrapolate this data in closer leads to gross errors, as the nature of the ground motions is different. Close-in the ground motion is governed by the spall phenomenon and "slap down" as the spall gap closes. Just out of the spall zone, the first arrival of the stress wave is the peak value. Somewhere in this region (out to about 5 km) the maximum disturbance shifts from the first arrival to later arrivals; hence reflected waves, shear waves, surface waves and geological anomalies play a much greater role far out. For estimating the ground motion in close, we use the curves given in this paper, which are based on unpublished data. For ground motion farther out, data from Murphy and Lahoud² and Mickey³ may be used.

There are three classes of events to consider:

1. Over-buried—gas stimulation
2. Fully contained
3. Cratering

Very little data exist for 1 and 3. However, since the lithostatic pressures are so much smaller than those created by the device, little difference should exist in the scaled ground motions between 1 and 2. There is also some correlation of surface ground zero (SGZ) data between 2 and 3, i.e., for cases in tuff and rock, indicating that data obtained for fully contained events are applicable to cratering events. Other than yield, DOB and range effects, the other important parameter which greatly influences the ground motion is geology. In general, velocity correlates best and acceleration and displacement correlate poorly as they are more strongly influenced by both geology and yield, as can be seen in part from the scaling. In fact, geology plays such an important role that it is very difficult to sort out the different effects, particularly for the surface motion because the layers near the surface are usually much more nonhomogenous and weathered than the deeper layers.

The most important geological parameter is the porosity along with the degree of saturation of the media. This can be seen from Fig. 1 which gives the peak (positive) particle velocities versus scaled range for various geologies for fully contained events. As can be seen, velocities for hard rock and saturated (to the surface) media are almost the same as velocities for saturated tuff around the center of detonation with a dry tuff overburden.

The effect of geology shows up even more strongly in the peak particle acceleration. In the spall zone—a typical time history is given in Fig. 2—the slap-down acceleration is often much higher than the initial acceleration; however, there appears to be no way to correlate the slap-down acceleration. At slap down, the radial and tangential components of acceleration also have large spikes and there may be more than one spike. The spall zone will normally extend out to about where the peak particle velocity has fallen to about 2 fps. Normally at the edge of the spall zone the slap down is soft, but not always. The initial peak particle acceleration correlates somewhat better. Figure 3 gives the initial scaled peak particle acceleration versus scaled

first 7 salvos on the first pass are diversion shots, made up of a total of 65 devices. The program for Route 25E is also a two-pass schedule made up of 12 and 9 salvos for the first and second passes, respectively, for a total of 146 devices. The first 4 salvos are diversion shots consisting of 24 devices total. In this program, salvos are grouped into sets. For example, salvos 6 and 7 make up the first set for the first pass on Route 17A. All the salvos in a set are readied for firing continuously. Then the set waits for good firing weather. When the proper weather occurs, the salvos are detonated one after the other. A cool-off period takes place after a set of salvos is detonated. Work may also proceed on the succeeding salvos while a salvo or set of salvos is waiting for the appropriate weather to fire. Five fallout weather categories were used for Route 17A and three fallout weather categories for Route 25E. Only Category I air blast data is used.

The simulated schedules for this revised detonation program were later compared to the published schedule. (5, 6)

The devices which make up a given salvo are successively emplaced and stemmed. The emplacement crew(s) sequentially emplaces the devices that make up the salvo; the stemming crew(s) stems a particular device after it is emplaced, assuming they have completed their previous stemming. In the simulations for the initial detonation program, evacuation takes place after the last device in a salvo has been stemmed and the salvo is fired when the weather permits. The emplacement crew(s) and stemming crew(s) remain idle until the previous salvo has been fired. However, as part of the plan for the revised program, they work continuously on all the salvos which make up a set.

Two conditions have to be satisfied with regard to meteorology. These conditions can best be described by a high altitude delay function and a low altitude delay function. These functions essentially specify the percentage of days in a particular month which satisfy both meteorological conditions and thus enable the salvo to be fired. The high altitude function specifies the percentage of days it is feasible to fire with respect to air blast, whereas the low altitude function specifies the percentage of days it is possible to fire with respect to radiation fallout. The probabilities of firing may vary according to the time of the year, the device yields, and the geographic location of the salvo. The weather data used in the simulation are given in Tables II and III. Note that weather data can be given as a percentage value or as the actual number of good days for any 1 month.

All these constraints are followed by the simulation. What it does most uniquely is display the schedule based on the basic operations needed for each device for each salvo and sample the fallout and air blast weather probability of firing.

MAIN COMPUTATIONAL BLOCKS OF THE SIMULATION PROGRAM

Block 1: Specify the case description, devices per salvo, salvo firing sequence, fallout weather, and air blast weather.

Category Month	FALLOUT					AIR BLAST		
	Route 17A		Route 25E		All Others	Routes 17A and 25E, All Salvos		
	Salvos 1 - 9	Salvos 10 - 19	Salvos 20 - 25	Salvo 7		I	I - VI	I - VII
June	71	58	9.7	10	35	0	19	100
February	71	64	10.7	21	47	33	21	100
March	29	29	3.2	59	71	0	23	100
April	40	40	10	26	36	15	37	100
May	39	32	6.5	10	16	43	58	100
June	4	0	6.7*	0	0	14	70	100
July	10	6.5	3.2	22	26	10	52	100
August	14	3.2	3.2	16	19	44	58	100
September	7	6.7	3.7*	3.3	3.2	44	50	100
October	19*	19*	22.8*	3.2	6.5	20	29	100
November	53	50	23.4	20	23	19	50	100
December	42	39	19.3	26	52	18	52	100

Note: Fallout pattern is to the south unless asterisked, in which case half of those periods have patterns to the north.

TABLE II
FREQUENCY OF ACCEPTABLE FALLOUT AND AIR BLAST WEATHER
(IN PERCENT) - INITIAL DETONATION PROGRAM

Category Month	ROUTE 17A					ROUTE 25E		
	B	C	D	E	E	A	B	C
January	22	19	18	3	0	16	10	3
February	20	22	18	3	1	18	12	7
March	9	12	9	1	0	17	21	17
April	12	19	12	3	2	13	10	7
May	12	10	10	2	2	7	6	5
June	1	0	0	0	0	1	1	1
July	3	3	2	1	1	8	7	6
August	4	2	1	1	0	7	7	7
September	1	1	1	1	1	2	2	2
October	5	5	5	3	2	2	2	1
November	17	17	16	7	5	7	7	6
December	13	14	12	7	5	16	14	9

For Route 17A:

Category B: Salvos 8-10, 18-20

Category C: Salvos 4-7

Category D: Salvos 1, 11-13,
21-24

Category E: Salvos 2, 3, 14-16

Category F: Salvo 25

For Route 25E:

Category A: Salvos 2, 4

Category D: Salvos 1, 3, 5, 6,
8-10, 12-14,
16-21

Category C: Salvos 7, 11, 15

Air blast data for initial and revised detonation programs are identical.

TABLE III
AVERAGE FALLOUT DATA (GOOD DAYS PER MONTH)
REVISED DETONATION PROGRAM

Block 2: Specify the starting time, reentry time, and salvos to be fired.

Block 3: Compute the number of devices per salvo and the number of salvos in a set.

Block 4: Stem, emplace, and ready the devices which make up a salvo or a set of salvos.

Block 5: Fire the salvo, or the salvos in a set, if weather permits.

Block 6: Repeat Blocks 3, 4, and 5 for other salvos or sets of salvos in the detonation plan.

Block 7: Output information.

Block 1 is used to specify several "functions" needed for the simulation. These are:

- a. The number of devices per salvo for each salvo.
- b. The salvo firing sequence for the case under consideration.
- c. Fallout delay weather.
- d. Air blast delay weather.

Because of the different device yields and the geographic location of the salvos, several fallout delay weather functions are defined. Air blast weather is defined in terms of severe restriction (Category I), modest restriction (Category I-VI), and no restriction (Category VII).

The starting time for the operation is specified in Block 2, together with the total number of devices to be fired. This starting time is a calendar time in hours. The salvos are then operated one by one, using the number of devices in each salvo and the salvo sequence. The number of devices to be emplaced and stemmed is determined in Block 3 for each salvo under consideration. Block 4 gives the emplacement and stemming sequence. The simulator advances the clock corresponding to the time it takes to perform every operation. It is noted at this point that when one performs an intermittent drill - case - emplace - stem - fire - drill operation, a program change is made between Blocks 3 and 4 to take into account the drilling operation.

Block 5 indicates the firing sequence. The salvo is fired only if the weather satisfies the radiation fallout and air blast effect criteria. One can thus investigate the effect of different weather restrictions on the schedule by changing the fallout and air blast weather delay functions in Block 1. In Block 5, the time of operation and the salvo type and number are utilized to specify the appropriate fallout and air blast weather delay functions.

Block 6 tests whether the last salvo fired was the last salvo in the pass; if not, the next salvo in the sequence is considered and the process repeated.

After the last salvo has been fired, the simulation permits a printout of the statistics on the simulation time, delay times, utilization of the crews, total number of devices, and total number of salvos. This is done in Block 7.

AVERAGING THE INFORMATION

To permit obtaining the schedule from the simulation, time is printed out immediately after firing the salvo. Ten simulation trials for each case were made and the results were averaged out. A plot of the results leads to a graph of the mean, maximum, and minimum time to accomplish a pass for a given set of constraints. Such a graph is shown in Figure 1. Note the large changes in the slope of the curves caused by drastic changes in the meteorological data which applies to the individual salvos. Note also the elongation of the time to accomplish the detonation of one salvo during the bad weather months.

For the rest of the results discussed in this paper, only the mean will be used.

SIMULATION BASED ON THE INITIAL DETONATION PROGRAM

For this set of simulations, the emplacement and stemming crews stop working after a salvo is ready and is waiting to be detonated. Work does not proceed on the next salvo until after the previous salvo has been fired and until after a specified reentry period has elapsed. Start time is October 1 for Route 17A and November 1 for Route 25E. This was done to take advantage of the good weather months for firing.

The first set of simulations was used to investigate the time it takes to accomplish the first pass out of a two-pass and out of a three-pass schedule. The results are shown in Figure 2. Note the almost linear behavior at the beginning. There is more variability during the bad weather months. Category (I-VI) air blast data was used in Figure 2.

Figure 3 shows the large changes in time to accomplish the first pass out of three-pass schedule for both routes using different degrees of weather restriction due to air blast. It is clear that changing air blast restriction from no restriction (Category I-VII), medium restriction (Category I-VI) and maximum restriction (Category I) varies the schedule tremendously. For example, for Route 17A the first pass is seen to take 4.6, 7.4, and 12 months, respectively, for the different air blast restriction categories.

Figure 4 shows the effect of doubling the emplacement and stemming crews. This does not induce a major change in the schedule; in fact, the savings correspond to no more than 1 month for each pass. However, the cost trade-off studies that were made⁽²⁾ show that double crews are advantageous; hence, double crews were used in the simulations for the revised detonation program.

Figure 5 shows the effect of varying from 1 day to 1 week the reentry time after detonating each salvo. Again, it is seen that reentry time does not have a very significant effect on the schedule.

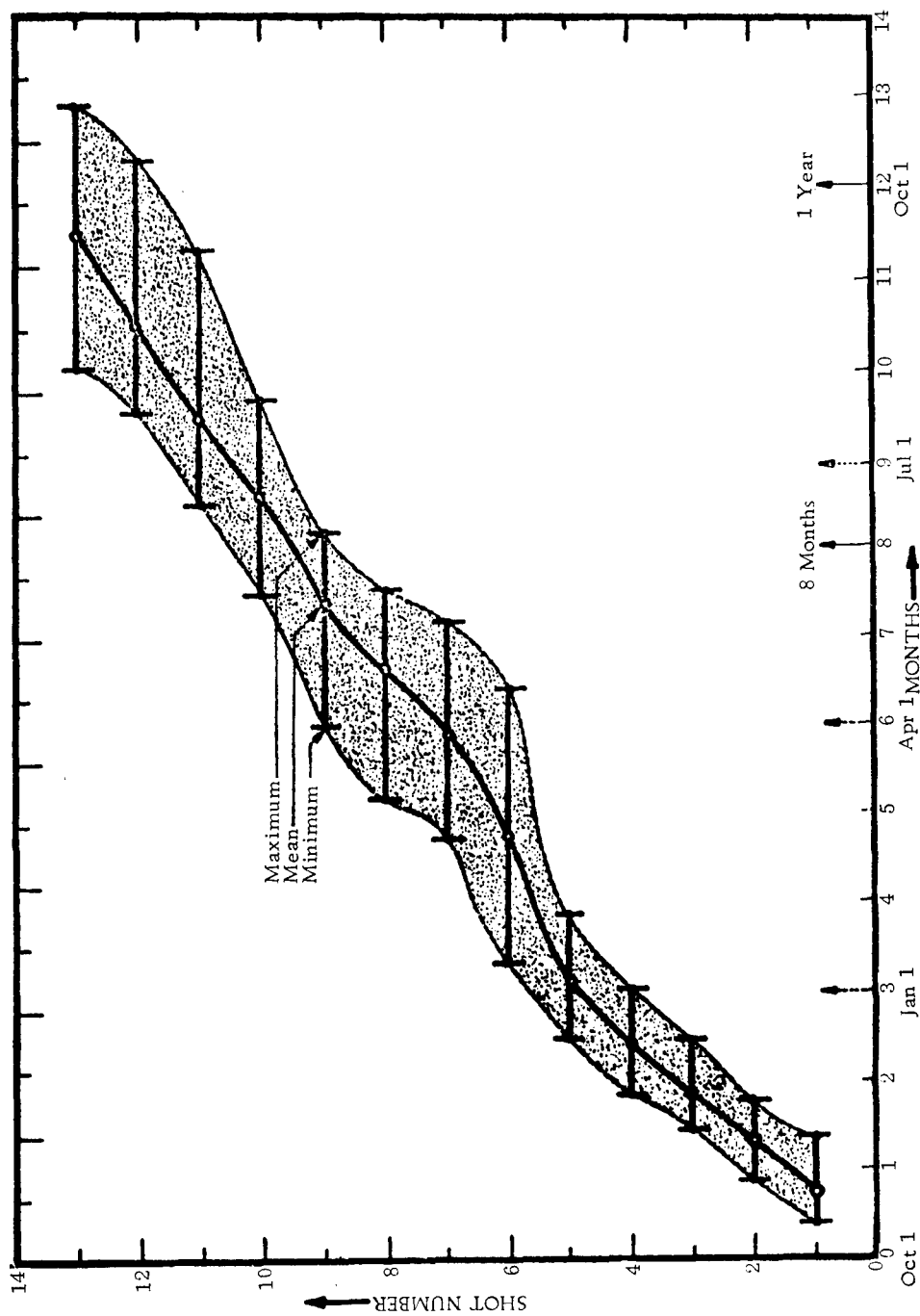


FIGURE 1
A TYPICAL SIMULATED SCHEDULE

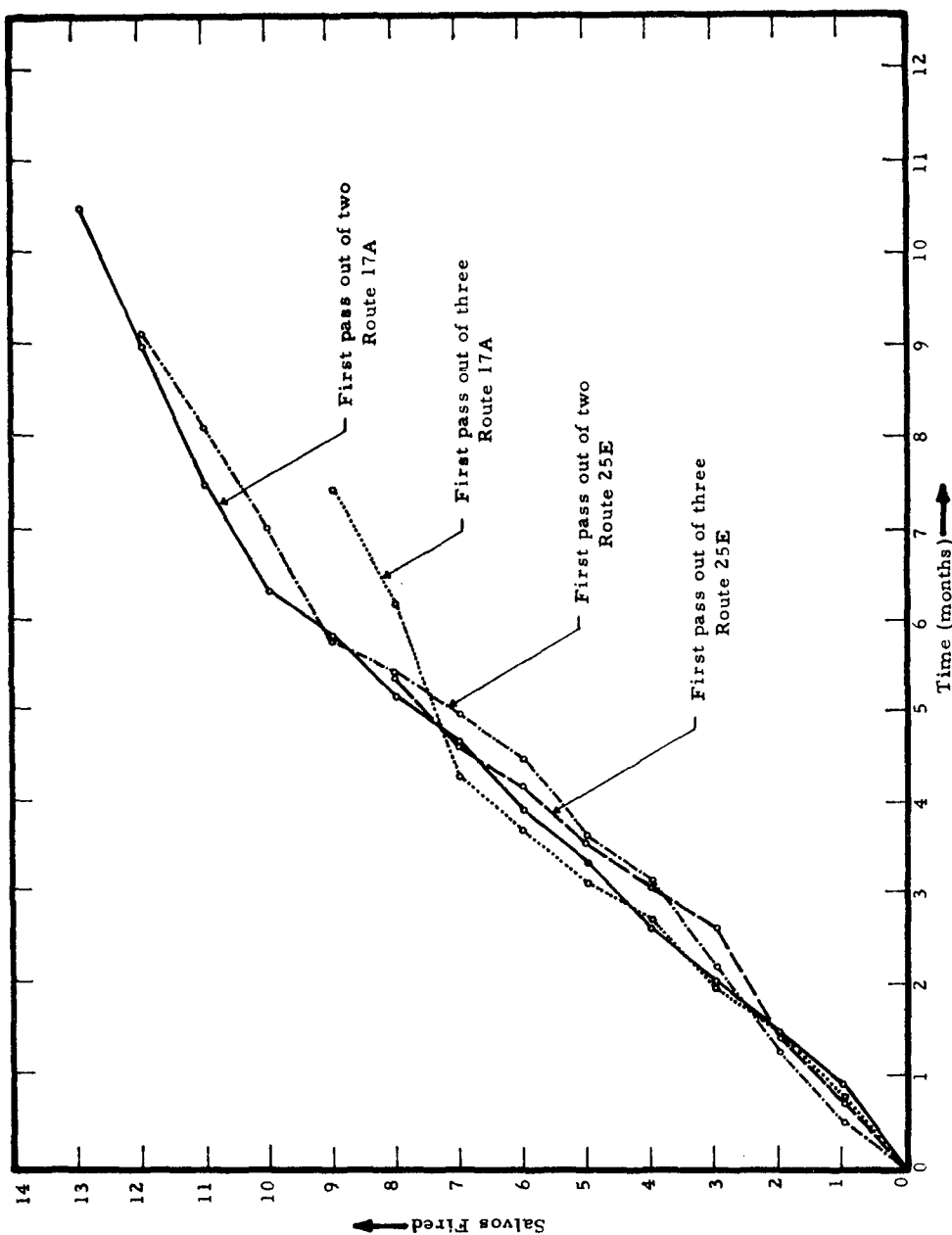


FIGURE 2
 AVERAGE SCHEDULES OF VARIOUS PASSES
 INITIAL DETONATION PROGRAM

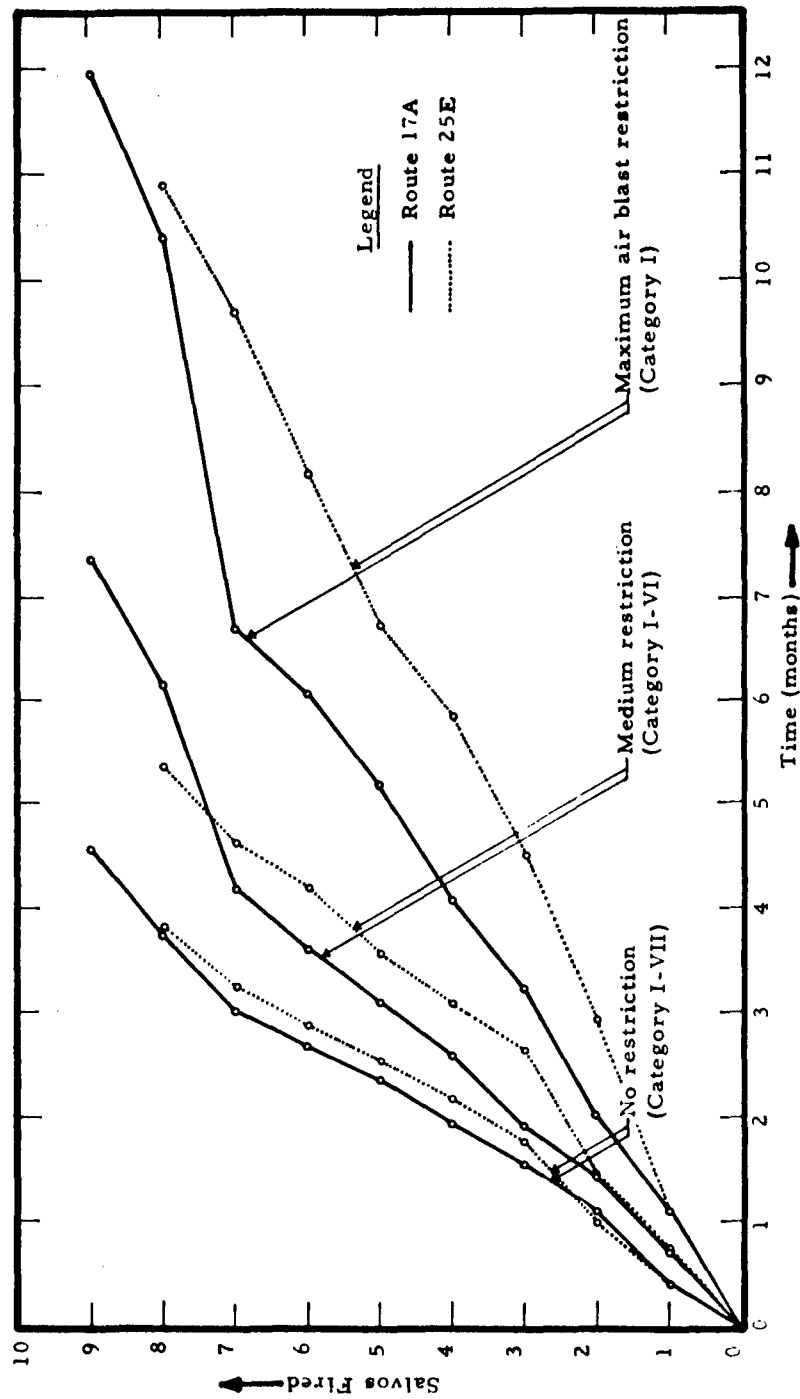


FIGURE 3

AVERAGE SCHEDULES SHOWING THE EFFECT OF AIR BLAST RESTRICTION
INITIAL DETONATION PROGRAM

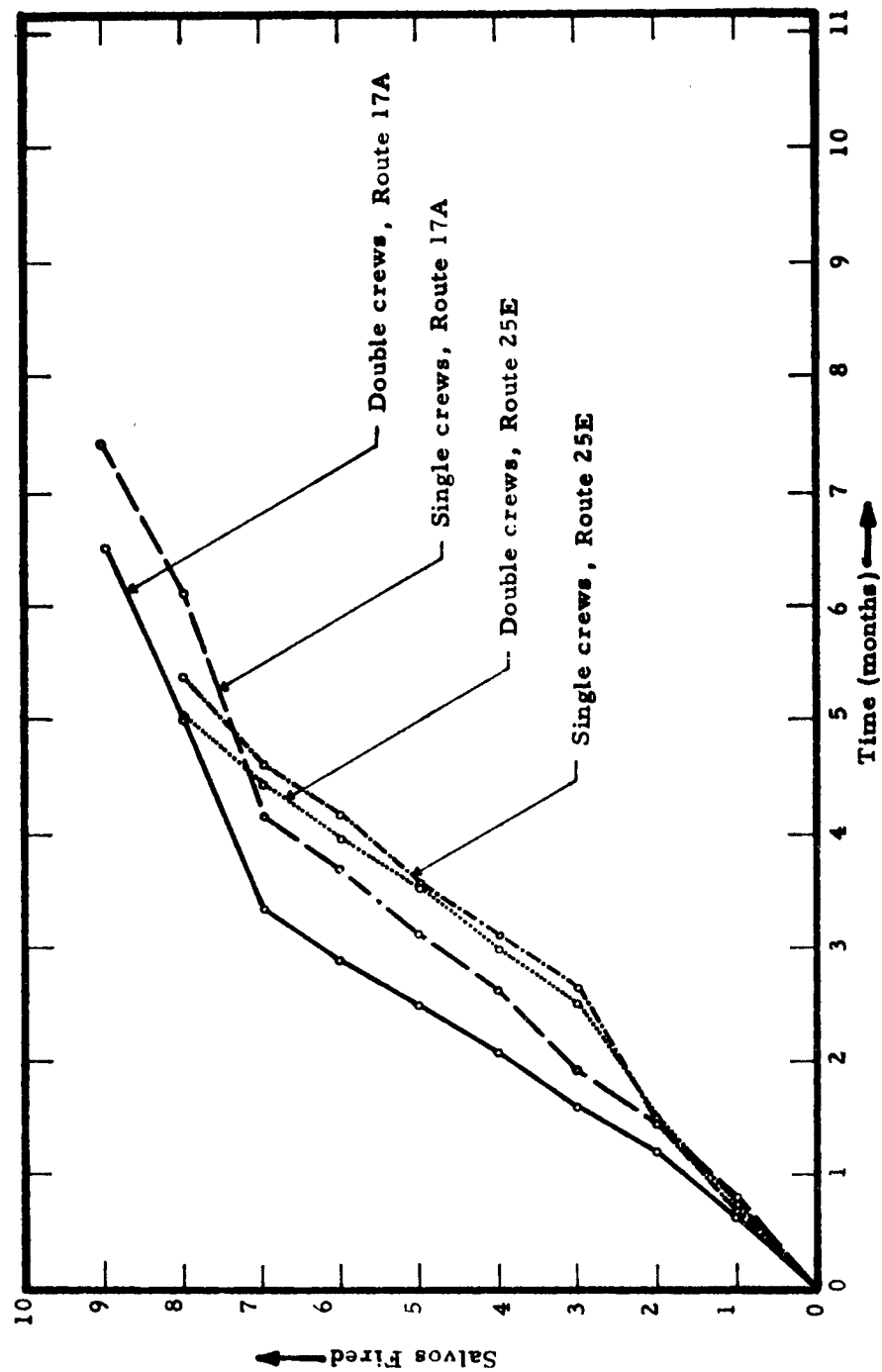


FIGURE 4

AVERAGE SCHEDULES SHOWING THE EFFECT OF DOUBLING CREWS
INITIAL DETONATION PROGRAM

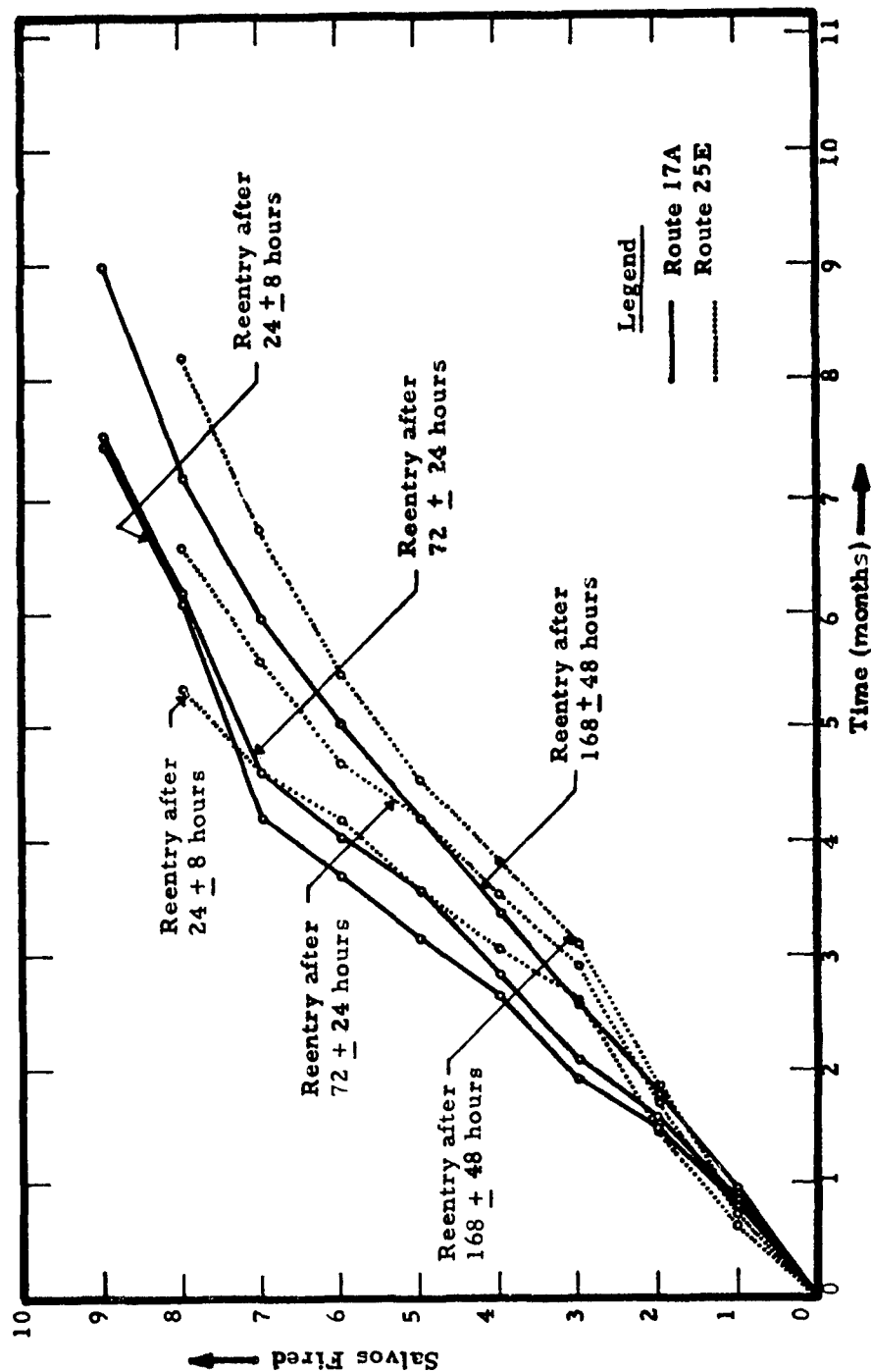


FIGURE 5

AVERAGE SCHEDULES SHOWING THE EFFECT OF REENTRY TIME
INITIAL DETONATION PROGRAM

Concern over the response of the holes was expressed while a salvo is detonated; therefore, a simulation was also made for the case of the intermittent drill - case - emplace - stem - fire - drill operations. The results are shown in Figure 6. It takes 49 and 44 months for Routes 17A and 25E, respectively. The general slope of the curve is almost constant. This is because the 1 month allocated to drilling and casing for each salvo tends to average out any variations in the weather delays.

Although the results are not shown here, simulations were carried out to determine the probability of being able to fire a salvo when the wind is blowing to the north on Route 17A. It was found that there is a 92 percent chance of firing one salvo and a 67 percent chance of firing a second salvo. Note that one or two salvos less to fire decreases to a large degree the time to accomplish a pass.

EVALUATION OF FINAL SCHEDULE BASED ON THE REVISED DETONATION PROGRAM USING SIMULATION TECHNIQUES

Data and Assumptions

Final schedules were published for both Route 17A⁽⁵⁾ and Route 25E,⁽⁶⁾ and these were evaluated using the simulation techniques discussed earlier. These schedules were based on the revised detonation program and with a different set of constraints. The two major constraints consist of:

- a. The use of Category I only for air blast restriction.
- b. The device emplacement activities for subsequent salvos were permitted while waiting for suitable firing weather for the earlier salvo or sets of salvos.

Basically, the revised program consists of a two-pass schedule for both routes. The salvos are arranged into sets. Table IV shows the grouping of salvos into sets, plus the data that goes with them. For example, Salvos 6 and 7 make up the first set of salvos for the first pass on Route 17A. A set of salvos is continuously readied for firing; and once ready, the set waits for favorable weather to fire as a whole. As soon as the weather is favorable, the salvos in the set are detonated one after the other with just 10 hours interval between salvos. On the first pass for both routes, work stops while a set of salvos is awaiting favorable detonation weather. However, on the second pass for both routes, work is allowed to continue on subsequent sets of salvos while other salvos are waiting for favorable detonation weather. The reentry delay periods were taken from the published schedules. Five fallout categories were used for Route 17A and three for Route 25E. Only Category I air blast data was used since this was indicated in References 5 and 6 to be essential.

Discussion of the Results

The simulated schedule for the revised detonation program for Route 17A is shown in Figure 7; for Route 25E it is shown in Figure 8.

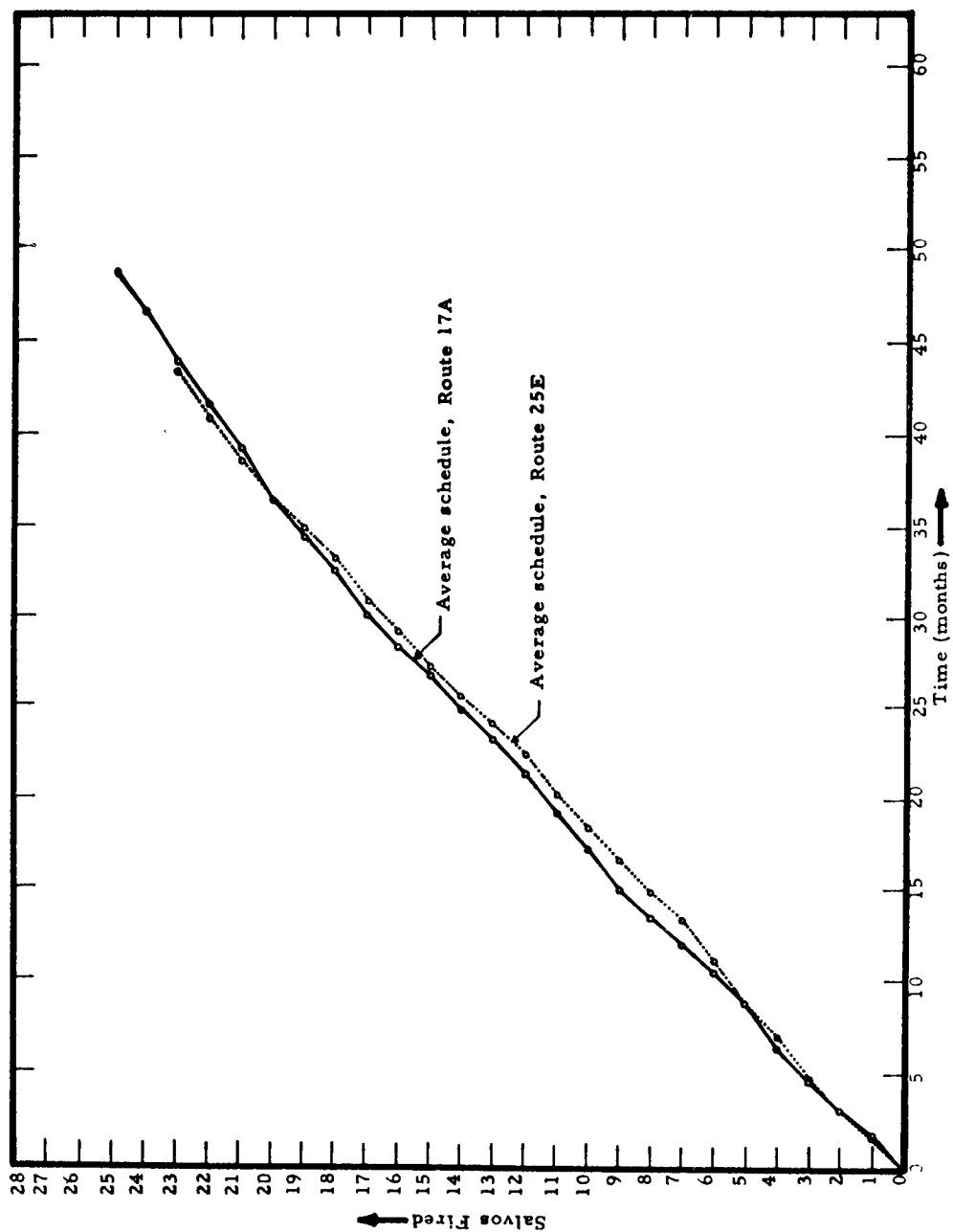


FIGURE 6

AVERAGE SCHEDULE FOR INTERMITTENT DRILL - READY - FIRE SEQUENCE
INITIAL DETONATION PROGRAM

Pass No.	Salvo Set	ROUTE 17A		ROUTE 25E	
		Salvos	Reentry Time	Salvos	Reentry Time
1	1	6, 7	4 days	2	(a)
	2	2, 3	5 weeks	1, 3	6 weeks
	3	1, 4, 5	4.5 weeks	5, 6, 7, 8, 14	5 weeks
	4	8, 9, 10	11 weeks	9, 12	
	5	11-16			
2	1	18, 19, 20	(b)	13-16	(c)
	2	21-27	(b)	17-21	(c)

(a) Salvos 2, 1, and 3 are continuously prepared so that Salvos 1 and 3 are readied while Salvo 2 waits for detonation.

(b) Salvos 18-27 are continuously prepared.

(c) Salvos 13-21 are continuously prepared.

TABLE IV
SETS OF SALVOS, REVISED DETONATION PROGRAM

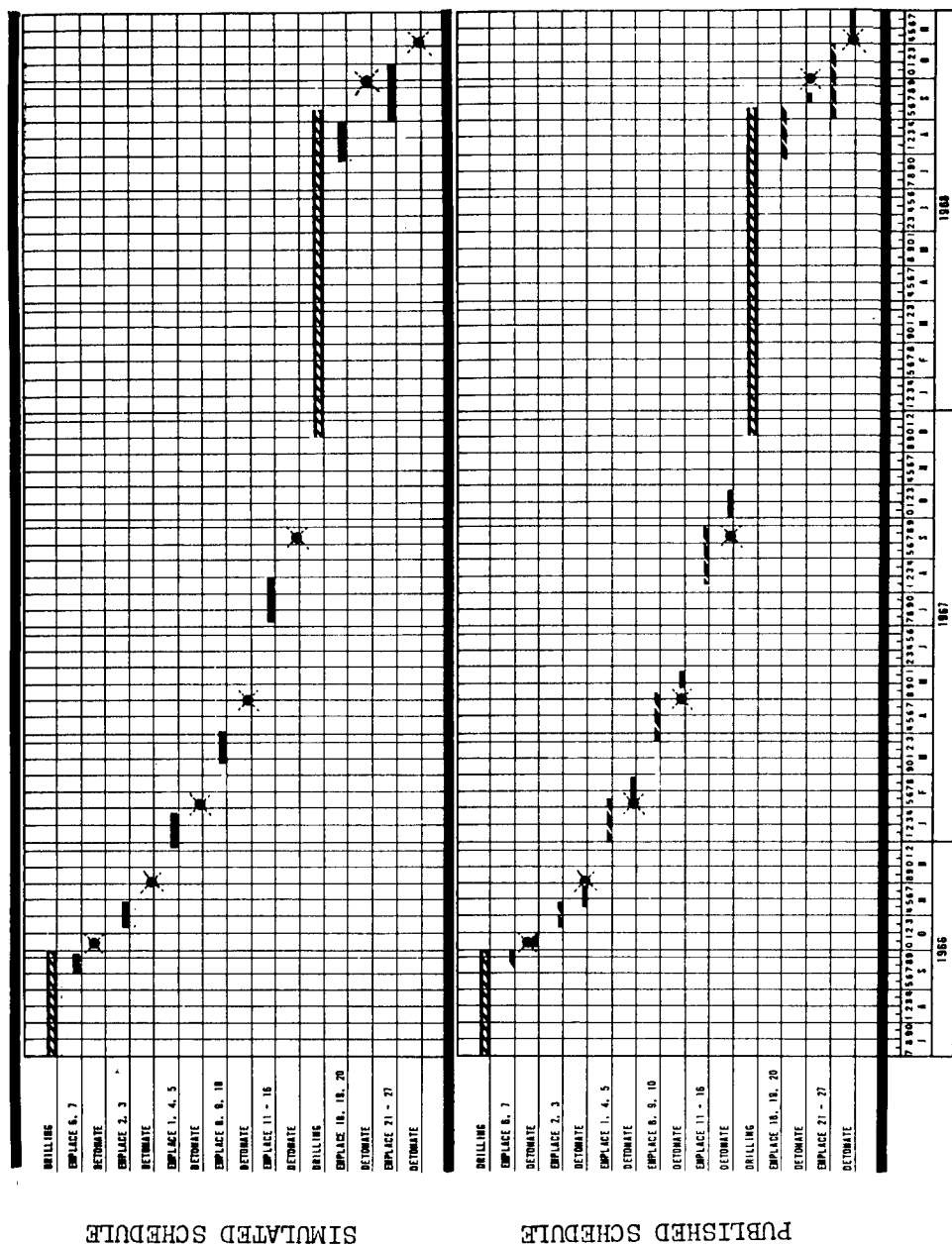


FIGURE 7

SIMULATED VERSUS PUBLISHED SCHEDULE, ROUTE 17A
REVISED DETONATION PROGRAM
✱ Denotes Simulated Detonation Time

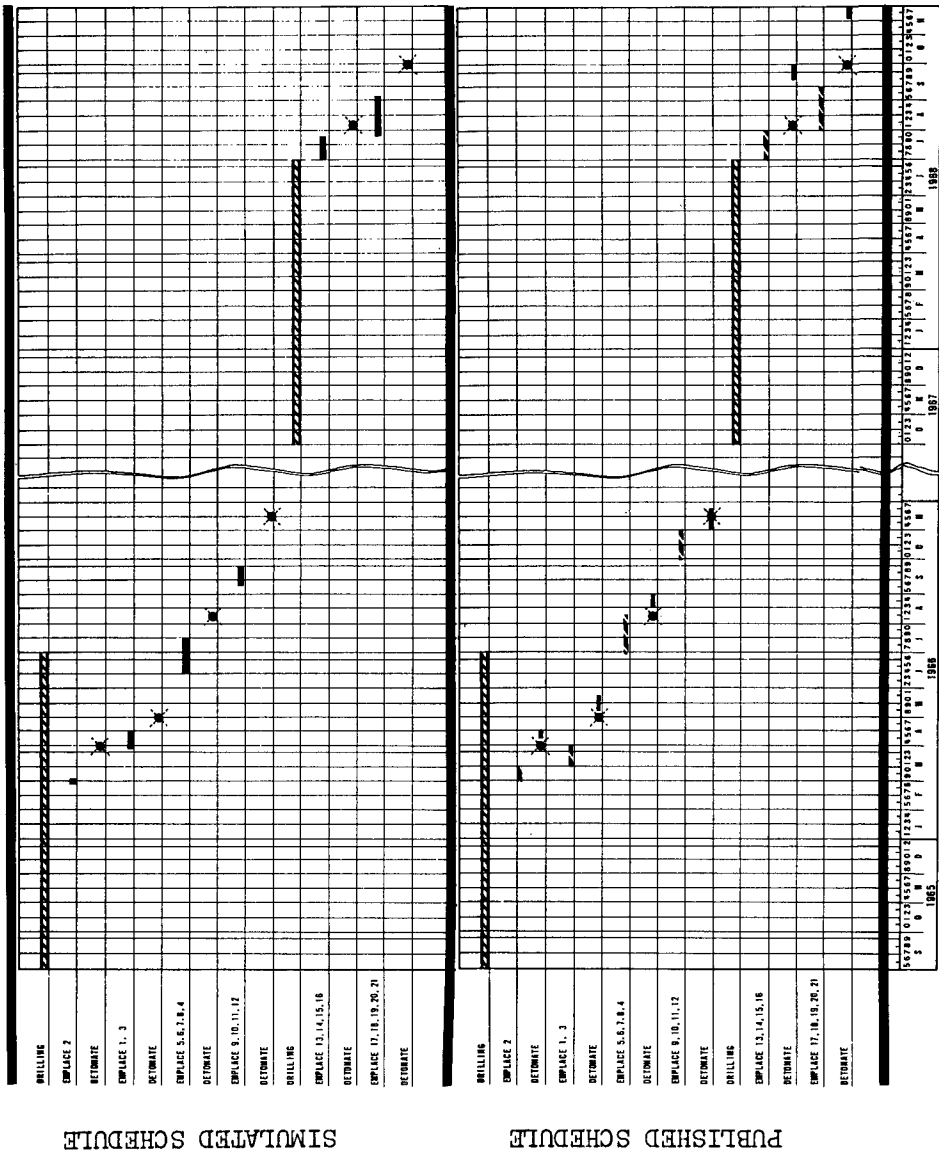


Figure 7 shows that the first pass for Route 17A takes 52 weeks to complete, exclusive of the time it takes to drill the holes. The second pass is seen to take 14.5 weeks, again exclusive of the drilling period.

Figure 8 shows that the first pass for Route 25E takes 37 weeks, and the second pass requires 13.7 weeks.

Comparison of Simulated Schedule Versus Published Schedule

It must be emphasized at this point that the only data used from the published detonation program were:

- a. The reentry period after each set of salvos.
- b. The detonation sequence and grouping of salvos into sets.

Everything else in the simulation comprises an independent assessment of the schedule. Therefore, it is interesting to compare the schedules as published with those from the simulation. These comparisons are also shown in Figures 7 and 8. The ends of the detonation times, as given by the simulation and the published schedule, have been superimposed. Note that there is a high degree of similarity in the results.

CONCLUSIONS AND RECOMMENDATIONS

Computer simulation techniques using the GPSS/360 language have been used to evaluate and assess several schedules for the interoceanic canal project. The assessment of the schedule for a huge project like the proposed sea level canal is very difficult due to the many factors involved in the operations. For example, the effect of the weather, which is random in nature, can be accounted for by simulation techniques using the frequency data of good days for firing. This assessment was made easily by using simulation techniques. A typical assessment for a schedule consists of ten simulation trials taking a total of 90 seconds of computer time on an IBM 360/50 machine.

Several schedules were simulated based on data for the different detonation programs for Routes 17A and 25E. Simulation games were played by varying specific parameters like the detonation sequence, the number of emplacement and stemming crews, air blast restriction, fallout data, and the reentry period after each row charge detonation. The results of the simulation were also used to evaluate several schemes from a cost point of view. For example, based on these trade-off studies, ⁽²⁾ it was found that double emplacement and stemming crews should be used; this conclusion led to the use of double crews in simulating the revised detonation program. A comparison of the schedules using simulation techniques with those which were made independently and published shows them to be similar.

It is clear that the simulation method is an effective, concise, and easy way to assess or establish a schedule for the interoceanic canal project, or other complex projects. The use of this technique is recommended.

REFERENCES

1. General Purpose Simulation System/360, User's Manual, IBM Application Program H20-0326-2, 1968.
2. Computer Simulation of Nuclear Operations for the Sea Level Canal, HN-20-213, prepared for the U. S. Atomic Energy Commission, Nevada Operations Office, by Holmes & Narver, Inc., November 1969.
3. Preliminary Detonation Program, LRL Interim Assessment, June 1969.
4. Letter from G. J. Ferber, Environmental Science Services Administration, to R. S. Holmes, Nuclear Cratering Group, dated August 28, 1969.
5. Letter from A. W. Klement, Jr., U. S. Atomic Energy Commission, Nevada Operations Office, to T. J. McCarvill, et al., dated September 4, 1969.
6. Letter (NCG-IC) from R. S. Holmes, Nuclear Cratering Group, to A. W. Klement, Jr., U. S. Atomic Energy Commission, Nevada Operations Office, dated September 11, 1969.

RELIABILITY IMPLICATIONS FOR COMMERCIAL PLOWSHARE APPLICATIONS

T. D. Brumleve
Plowshare Systems Research Division
Sandia Laboratories, Livermore

ABSTRACT

Based on the premise that there will always be a finite chance of a Plowshare project failure, the implications of such a failure are examined. It is suggested that the optimum reliability level will not necessarily be the highest attainable, but rather that which results in minimum average project cost. The type of performance guarantee that the U. S. should provide for nuclear explosive services, the determination of nuclear yield, courses of action to take in the event of failure, and methods to offset remedial costs are discussed.

Introduction

In the midst of optimistic efforts to apply the unique capabilities of Plowshare nuclear explosives for the betterment of human conditions, it is disturbing to contemplate the possibility of a failure. Yet, no matter how reliable Plowshare nuclear explosives are, there will always be a finite chance of failure. It is the purpose of this paper to discuss a number of implications arising from this possibility. These implications should be recognized by the AEC and by potential users because they may have an important bearing on the design of the nuclear explosives, on the formulation of operational plans, and on the structuring of agreements between the U. S. government and commercial users of nuclear explosion services.

Reliability/Cost Relationships

There are reasons to believe that the most desirable level of reliability will not be the highest attainable. Rather, the optimum reliability will probably be that which results in a minimum average project* cost.

*The term project, or Plowshare project, refers to the nuclear explosion service to be provided by the U. S.

Reliability will affect costs in two contrasting ways. On the one hand, the reliability goal for Plowshare projects will have a direct influence on the cost of producing the nuclear explosive. That is, as the reliability goal is upgraded, production costs will rise because of the need for tighter quality control measures such as special manufacturing processes, meticulous inspections, and extensive testing.* In the interest of reducing production costs, therefore, a lower reliability goal is desirable. On the other hand, the less reliable the explosive is, the more frequently failures will occur, and the higher will be the collective remedial costs incurred over an extended period. In the interest of reducing these long term remedial costs, therefore, a higher reliability is desirable.

The relationship of these two types of costs can be illustrated by introducing the concept of expected remedial cost. Expected remedial cost is defined as the product of the remedial cost incurred as a result of a Plowshare nuclear explosive failure and the probability that the failure will occur. It can also be considered as an average additional cost per project assuming that the remedial costs of occasional failures are amortized over all projects. For example, suppose that a failure occurs in one out of a hundred projects, and that it costs one million dollars to remedy the failure and successfully complete the project; the expected remedial cost (per project) would therefore be ten thousand dollars.

The basic project cost will consist of the production cost of the nuclear explosive along with all costs associated with its fielding.** The sum of the basic project cost and expected remedial cost represents an average Plowshare project cost. These cost relationships are illustrated in Figure 1 over a range of failure probability. Note that there is an optimum reliability for which average project cost will be a minimum.

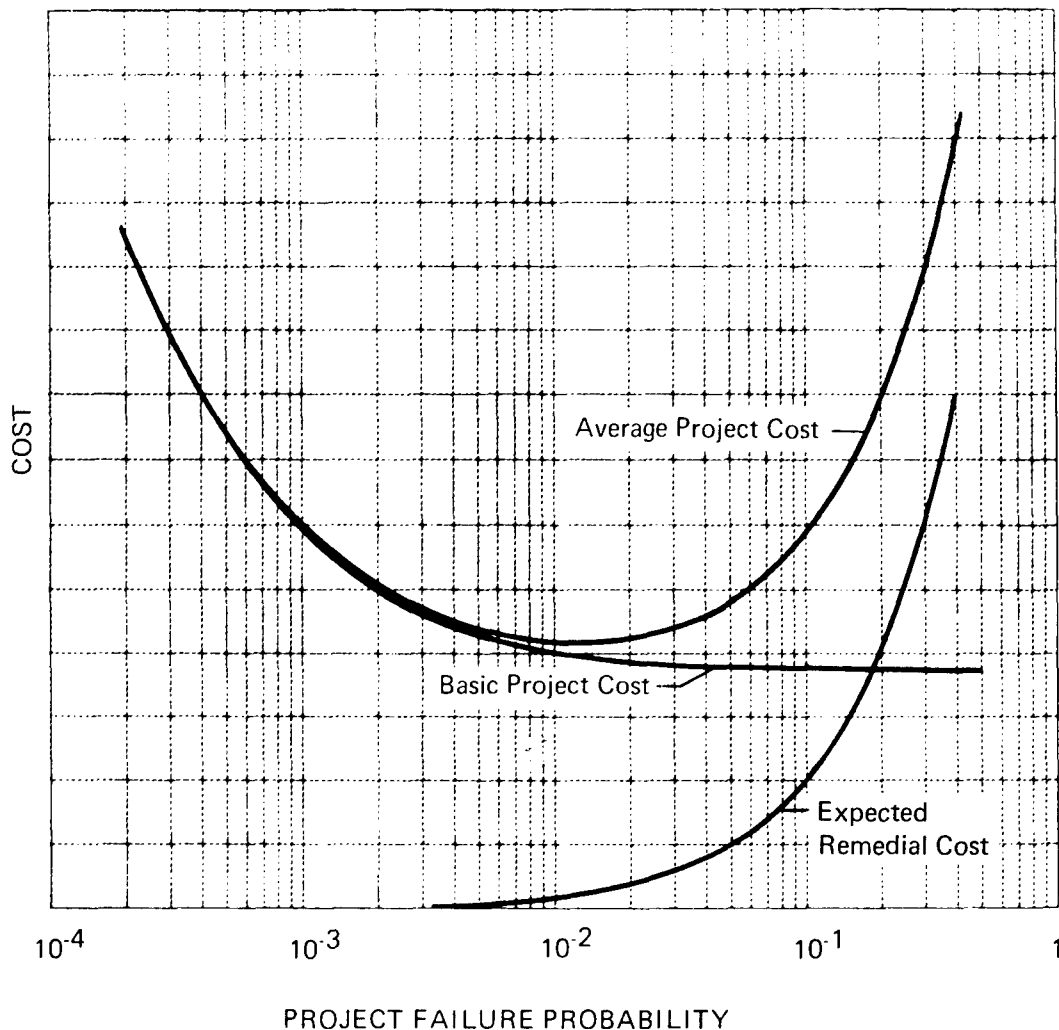
Because sufficient information is not yet available, it is not presently possible to draw these curves precisely, but preliminary evaluations indicate that the optimum reliability will be on the order of 0.99.

Performance Guarantee

If a foreign government or a domestic commercial user enters into a contract with the U. S. to secure a Plowshare nuclear explosion service, it will undoubtedly expect the U. S. to guarantee the service according to some pre-established criterion. This practice would be consistent with a long standing tradition for major purchases in which a manufacturer or a service

*To achieve high reliability, research and development costs will also be higher, but under present AEC policy such costs would not be included in the cost of the nuclear explosive service.

**Includes costs of transportation, security, control systems, A & F personnel, and other costs incurred in providing the nuclear explosion service.



Basic Project Cost:	Production Cost of nuclear explosive and fielding costs consisting of transportation, security, control systems, A & F personnel, and other costs incurred by the U.S.
Expected Remedial Cost:	Product of the remedial cost which would be incurred as a result of a nuclear explosive failure and the probability that the failure will occur.
Average Project Cost:	Sum of the Basic Project Cost and Expected Remedial Cost.

Figure 1. Cost-Reliability Relationships

company guarantees that its product will perform within specifications or that its service will conform to contract agreements. The guarantee that the U. S. provides for its nuclear explosion service must, however, be in accord with the policy statement in the Atomic Energy Act that "...the development, use, and control of atomic energy shall be directed so as to promote world peace, improve the general welfare, increase the standard of living, and strengthen free competition in private enterprise..." and with the U. S. commitment in the Non-Proliferation Treaty that nuclear explosion services will be provided on a nondiscriminatory basis.

The following options illustrate the range of performance guarantees which might be considered:

1. best effort only with no guarantee of results,
2. guarantee of nominal yield within a specified tolerance range in the selected location,
3. guarantee of the effect, such as crater or cavity size, tons of rock broken, or gas-flow enhancement.

The first option, guaranteeing best effort only with no guarantee of results, might be acceptable for certain experimental projects; but this approach is probably not acceptable for general commercial or civil engineering applications. Furthermore, such a guarantee might tend to impede the use of Plowshare explosives since commercial users might be reluctant to risk large amounts of capital on the basis of such a guarantee--particularly when so little detailed information on the nuclear explosives will be available because of classification constraints. Consequently, this type of guarantee for commercial applications does not seem to be compatible with the AEC's goal to promote peaceful uses of atomic energy.

The third option, guaranteeing the desired effect, would constitute a very extensive responsibility which would require a great deal of detailed investigation on the part of the U. S. for each application. This option might promote the use of Plowshare by virtually guaranteeing a profitable application, but it would require a great deal of control by the AEC over details of utilization extending far beyond matters directly related to the nuclear explosives. Because of this intrusion of government control into matters of commercial applications which could be handled by the commercial user, this option could prove adverse to free competition in private enterprise and difficult to administer without discrimination. At any rate, such a responsibility could rapidly become very unwieldy and probably represents far greater involvement than would be warranted or desired by the U. S. government.

The second option, guaranteeing nominal yield, seems to be the most suitable basis for determining satisfactory performance. Unlike effects, nuclear yield is predictable for a variety of applications and is a determinate parameter which lends itself to the establishment of unambiguous performance criteria. Therefore, this type of guarantee could more readily be administered on a nondiscriminatory basis. Although precise measurement is not necessarily easy, various practical means of yield determination have been developed. Tolerance limits above and below nominal yield can be

established to accommodate both expected yield variation and reasonable measurement accuracy. For commercial applications tolerances somewhat wider than those desirable for nuclear experiments will probably be acceptable. Furthermore, even if another criterion were used to guarantee performance, the AEC would probably still want to determine nuclear yield in order to maintain a record of the performance of its nuclear explosives.

Determination of Nuclear Yield

It will be assumed hereafter that nominal yield within a specified tolerance range in a selected location will be used to define project success. Given such a specification it will presumably be necessary to measure nuclear yield on each shot to determine whether or not the yield is within the specified range. Zero yield clearly constitutes a failure. Partial yield (below the lower tolerance limit) could be considered a partial success rather than a success or a failure. Too much yield (greater than the upper tolerance limit) may or may not be detrimental depending upon the application.

A variety of methods have been used to determine nuclear yield in past nuclear experiments. These methods are of three general types: (1) reaction history, (2) radiation chemistry, and (3) ground shock techniques. Each method has distinct advantages and disadvantages. Selecting the best method for commercial applications will require evaluation of the technical feasibility, accuracy, cost, and the value of the data to the AEC and to the user.

Reaction history techniques make use of real-time measurements of phenomena which occur during a nuclear reaction, and they can be used with both excavation and underground engineering applications. For the purpose of yield determination these phenomenological measurements are compared with corresponding ones already acquired by detonating similar devices of known yield. Consequently, the overall accuracy achievable is highly dependent on the amount of baseline data available from experiments in which yield has been determined by other means. Because most devices detonate at nominal yield, most of whatever data exists for a given device will be for the nominal condition; and the reaction history method is, therefore, a useful one to confirm nominality. However, in any case where yield is substantially above or below nominal, the shortage of comparative baseline data will reduce the accuracy of reaction history techniques. Because some of these reactions take place in the submicrosecond time realm, high-frequency and rather complex instrumentation is necessary and would thus add considerable complexity and cost to the nuclear explosive, down-hole cabling, surface instrumentation, and field operations.

In a typical underground detonation a large percentage of the detonation products are trapped within vaporized and melted rock which solidifies near the bottom of the chimney. Radiation chemistry analysis of this solid debris or "glass melt" is generally considered to be the most accurate method for determining fission yield (\pm five percent is often quoted). Fusion yield can also be determined, although somewhat less accurately. However, these techniques are costly since drill-back into the melt region, recovery of samples, and extensive analysis are required. Analysis of gaseous samples can also be used to determine fission yield within 10 to 15 percent.

The prospects for determining fusion yields through analysis of gas samples are not yet clear, but researchers at LRL are hopeful and studies are continuing. An advantage of the gas technique is that it should add relatively little to operational costs because it would be quite easy to emplace the necessary tracer gases along with the nuclear explosive, and the necessary chimney reentry is required anyway in all potential underground engineering applications identified to date. For excavation applications, samples of particulate debris can be readily collected and analyzed to determine yield.

A variety of ground shock techniques have been used on nuclear experiments to determine yield. All of these techniques measure some characteristic of the ground shock environment such as particle velocity, peak pressure, or time-of-arrival. Certain techniques use transducers located close to the nuclear device while others locate them at great distances. The accuracies which can be achieved are highly dependent upon how well the medium between the nuclear device and the transducer is known and upon its homogeneity. Close-in measurements of particle velocity, time of arrival, or peak pressure can be made in the emplacement hole. Accuracies of ± 15 percent or better can be achieved in well known media. While somewhat less complex than radiation chemistry or reaction history, employment of these methods nevertheless will complicate emplacement operations, particularly in deep holes.

Seismic measurements near the surface or at great distances are undoubtedly the simplest and least costly, but they are also the least accurate. While reasonably accurate results (± 10 to 25 percent) can be achieved in well-calibrated areas such as NTS, greater uncertainties can be anticipated in most Plowshare applications. A possible exception might be the development of a type of natural resources "field" in which a number of Plowshare explosives would be used in the same geologic media. It is also worth noting that although special seismic measurements are made in connection with NTS experiments, seismic stations throughout the world regularly report their determinations of the magnitude of seismic disturbances such as earthquakes and nuclear detonations. While these measurements are not very accurate indicators of nuclear yield, they do give the order of magnitude; and the information is essentially free.

Unlike ground shock techniques, many aspects of reaction history and radiation chemistry techniques are classified. This is a significant disadvantage in that the AEC would be unable to reveal details of yield determination by these methods. Thus the user would have to accept the AEC's determination of yield without the opportunity for checking either the data or the analysis. However, it might be acceptable to clear a few specialists in industry to provide a capability for independent analysis.

Weighing the foregoing considerations along with the importance of minimizing cost and streamlining field operations, it seems that an attractive prospect might be to determine success or failure in a gross manner with seismic techniques and to resolve any questions concerning partial yield with radiation chemistry analysis of gas samples (or, if necessary, solid samples) when the chimney is re-entered. However, all of the factors mentioned above need to be considered in greater depth, for the methods used may have considerable impact on operations, on fielding costs, and on

agreements between the AEC and domestic or foreign commercial users of nuclear explosion services.

Failure Contingencies

In the event of a failure, there are a number of alternative courses of action that might be taken--among them, the following:

1. recover the explosive and repair or replace it,
2. destroy the explosive and emplace a new one,
3. emplace a new explosive near the dud so that the dud will be destroyed when the new explosive is detonated,
4. disable or destroy the explosive and abandon the project.

Several factors will have to be considered in deciding upon a course of action. If the nuclear explosive were recovered, possible safety and security problems would be avoided, unnecessary contamination of the natural resource would be prevented, and the valuable explosive could be reclaimed. However, recovery may be technically difficult or in some cases completely impractical, and it would probably be very costly.

A command disable/destruct capability could be incorporated in the nuclear explosive for only slight additional cost and with a reliability largely independent of the rest of the system. There would, of course, be local contamination resulting from the destruction of a dud device, and it would be dispersed still further by detonating a replacement nuclear explosive. This dispersion could have detrimental effects on the exploitation of underground resources, and in excavation applications it could have substantial safety and security consequences.

In the event of a failure of one among several explosives in a cratering application, the problem appears to be particularly vexing. The HE of the dud explosive may or may not have been detonated by the shock effects from the adjacent nuclear explosive, and it might be difficult to determine which is the case. If the HE has been sympathetically detonated, most of the resulting contamination will probably be contained beneath the unexcavated mound. The mound can then be excavated either by conventional means or by emplacing and detonating one or more replacement nuclear explosives. If conventional techniques are used, heavy equipment operators and other personnel may be exposed to a contamination hazard as the excavation progresses. If nuclear explosives are used, the nuclear debris from the dud explosive may be thrown out of the crater and deposited on or within the crater lips. In either case, the contamination might be hazardous, and cleanup operations could be troublesome and expensive.

If the HE of the dud explosive has not sympathetically detonated, it may be possible to recover the explosive. This might be difficult, however, because of the fractured and disarranged state of the overburden and because the location of the explosive may have been shifted. If the remnant mound is excavated by conventional means, the dud explosive might be encountered unexpectedly, presenting some hazard to personnel. Effective measures

could be taken in the design and utilization of the nuclear explosive to virtually eliminate any hazard of an accidental nuclear detonation; but the possibility of an HE detonation, if the explosive is struck by excavation equipment, would still remain. A solution to this potential problem might be to develop an effective method for determining the precise location of a dud explosive and thus preclude accidental contact.

The foregoing considerations raise a number of questions which have yet to be investigated:

1. Under what conditions will it be technically feasible to recover a dud nuclear explosive?
2. What will be the magnitude of recovery costs?
3. Under what conditions might it be acceptable to abandon a dud explosive?
4. In the case of multiples, what is the probability that the HE of a dud nuclear explosive will be detonated (non-nuclearly) by the adjacent nuclear detonations?
5. What will be the nature and magnitude of the radiological contamination resulting from a sympathetic, one-point detonation in excavation or underground engineering applications?
6. How might the location of a dud explosive be shifted by adjacent nuclear detonations, and how might the explosive be located?
7. Will the resultant levels of additional contamination from a dud explosive be tolerable if replacement nuclear explosives are used to excavate a remnant mound in excavation applications?
8. Could conventional excavation techniques be used to excavate a remnant mound without subjecting equipment operators and other personnel to undue radiological or HE hazards?

These and other questions will need to be answered before failure contingency plans can be formulated. The appropriate course of action chosen will undoubtedly depend upon the applications, and remedial costs will be drastically affected by that choice.

It is expected that failure contingency provisions will have to be included in Plowshare project agreements with both foreign and domestic users. The potential costs of remedial actions will need to be estimated in order to establish adequate funding provisions. Thus, both the probable courses of action and the associated costs will need to be evaluated before the U. S. enters into agreements to provide commercial nuclear explosion services.

Success Insurance

When a failure occurs, the remedial costs may be very high. The cost of supplying a new nuclear explosive and drilling or redrilling an emplacement hole will add to whatever costs are incurred in recovering or

disposing of the dud explosive. These remedial costs could easily be two to four times the cost of a normal nuclear explosion service.

Present indications are that the U. S. will want to administer the commercial use of a Plowshare explosive service on a fully reimbursable basis, neither subsidizing domestic or foreign projects nor incurring losses on them. Thus an arrangement whereby the U. S. simply sustains the loss when a failure occurs is probably not acceptable. On the average, the frequency at which failures occur and remedial costs accrue will be a function of the failure probability of the nuclear explosive and its associated control system. By using the concept of expected remedial cost discussed previously, occasional failures could be amortized over all projects. By incrementing the amount charged for a nuclear explosion service by the expected remedial cost, the AEC could provide a form of self-insurance.

The following example will illustrate this approach. Suppose the basic explosion costs were \$300,000 (device cost plus fielding costs), and remedial costs in the event of a failure were estimated at \$1,000,000 (recovery, new device, and fielding costs). If the failure probability was estimated at 10^{-2} , the Expected Remedial Cost (ERC) would be:

$$\text{ERC} = (\$1,000,000) (10^{-2}) = \$10,000$$

Thus, the amount to be charged for the nuclear explosion service would be \$300,000 plus \$10,000, or \$310,000. This method could be employed by using an average ERC for all projects or by using an individual adjustment for each project. As remedial cost estimates or predicted reliabilities changed, adjustments could be made accordingly in the price of the nuclear explosion service.

Remuneration for Partial Project Success

It should be recognized that by the time Plowshare nuclear explosives are being used regularly for commercial purposes, most of these explosives will no longer be experimental devices but instead will be proven nuclear explosives, produced in quantity, and with a considerable history of use. Under such conditions the most likely yield by far should be nominal yield. There would, however, be some small likelihood of zero yield, a still smaller likelihood of partial yield, and there would remain a very small chance for excessive yield up to the theoretical maximum.

Therefore, between a clear success and a clear failure lies a spectrum of possible partial or excessive yield conditions which might be termed partial successes. In the event a Plowshare explosive were to yield 50 kt, for example, instead of an expected 200 kt, a foreign or domestic user might be justified in expecting some kind of remuneration. Similar problems, plus possibly excessive collateral damage, might result if an explosive were to produce a yield well above the nominal range. The nature and amount of remuneration which would be equitable would depend upon the application. In some cases, 25 percent of nominal yield might be equivalent to a complete failure; in others, it might simply mean a profit reduction or a diminished utility for the project. Such situations probably hold considerable

potential for disputes between the U. S. Government and the user. The possibilities should be discussed and basic agreement reached prior to contract finalization. If disputes develop on such matters with foreign users, arbitration by an international organization such as the International Atomic Energy Agency (IAEA) may be appropriate.

In conclusion, the likelihood of a failure of a Plowshare nuclear explosive will undoubtedly remain small, but there are a number of important implications which arise from the possibility. Reliability implications can be expected to influence the design of nuclear explosives, the formulation of operational plans and the structuring of AEC/industry agreements. Several of the questions which have yet to be resolved must await further development of the nuclear explosives and the techniques for their use; however, consideration of some questions could proceed now. Resolution of many of these questions will require the joint efforts of both the AEC and potential industrial users. In particular, industry could assist in (1) identifying and evaluating alternative methods for recovering a dud nuclear explosive, (2) estimating costs of remedial actions to be taken in the event a failure occurs, and (3) formulating mutually acceptable failure contingencies in AEC/industry agreements for commercial nuclear explosion services. Joint studies on such matters and a continuing awareness of reliability implications by both the AEC and industry will allow steps to be taken to minimize the consequences of a possible failure and thereby contribute to the orderly progress of the Plowshare program.

SEISMIC EFFECTS

EXPLOSION-PRODUCED GROUND MOTION: TECHNICAL SUMMARY WITH RESPECT TO SEISMIC HAZARDS*

Howard C. Rodean

Lawrence Radiation Laboratory, University of California
Livermore, California 94550

ABSTRACT

This paper summarizes the present technical knowledge, experimental and theoretical, of how underground nuclear explosions produce seismic motion that may be a hazard at distances measured in tens of kilometers. The effects of explosion yield and rock properties (at the explosion, along the signal propagation path, and at the site where a hazard may exist) on the ground motion are described in detail, and some consideration is given to the relation between ground motion and damage criteria.

The energy released in a nuclear explosion is sufficient to vaporize the explosive and to generate an intense shock wave that is propagated outward into the surrounding rock. Part of the energy transported by the shock wave is dissipated in the shocked material. The shock wave strength decreases with distance from the center of the explosion as a consequence of this energy loss and because of geometric (approximately spherical) divergence. The dissipated energy fraction ranges from over 95% (for competent rocks like granite) to over 99% (for crushable, porous rocks like alluvium) of the explosion yield. Therefore, the energy fraction that is radiated in the form of seismic waves ranges from a few percent down to a few tenths of a percent. This is consistent with the observation that explosions in granite produce more severe ground motion than corresponding explosions in alluvium.

The effects of explosion yield and rock properties on the frequency spectrum of the seismic source function are demonstrated by both experimental measurements and theoretical analysis. The characteristics of an ideal elastic medium are such that its frequency response is that of a low-pass filter, with its cutoff frequency being a function of the elastic properties of the material and the radius at which the explosion-produced stress wave becomes elastic. There is further frequency- and distance-dependent attenuation (especially of the higher frequencies) of the seismic waves, because rocks are not perfectly elastic but anelastic.

If an underground explosion is spherical and the surrounding medium is homogeneous and isotropic, only compressional or P waves are generated. This is an idealization; both P and shear or S waves are produced, with P waves being predominant. The interaction of these waves with the inhomogeneities within the earth and the free surface of the earth produce additional

*Work performed under the auspices of the U. S. Atomic Energy Commission.

reflected and refracted P and S waves, plus Rayleigh (or R) and Love (or L) waves that travel along the surface. As a consequence, the surface ground motion at a location where seismic damage is of concern is a complex mixture of several types of waves: some are generated in the vicinity of the explosion, and others at various points along different propagation paths. They arrive at different times because of different propagation velocities and transmission paths. In addition, the surface or receiver response to these waves is a function of local geology; e.g., the least severe motion occurs on hard rock.

The problem of seismic motion pertinent to property damage is therefore very complicated because the damage-producing part of the wave train does not appear to be the first arrival but some subsequent portion. There may be some valid correlations between damage (i.e., architectural like cracked plaster as well as structural) and measured values of frequency-dependent displacement, velocity, and acceleration; but it is not known which waves are associated with these measurements.

Therefore, the prediction of ground motion for seismic damage assessment is, at present, based on extrapolation of past experience and not upon calculations from the first principles of mechanics. This does not mean that these calculations are not of value in damage prediction. However, correlation between theoretical calculations and experimental measurements of ground motion will probably be on a statistical basis because it generally will be impractical to determine all pertinent details of the geology from the explosion to sites where seismic damage may be of concern.

INTRODUCTION

At the Third Plowshare Symposium, almost six years ago, three of the four papers on explosion seismology discussed safety-related items, and the fourth¹ was concerned with the use of nuclear explosives in studying the structure of the earth. Mickey² summarized ground motion measurements (for distances out to a few tens of kilometers and yields up to about 200 kt, and presented empirical predictive equations based on these measurements. Hankins³ discussed seismic measurements made at distances out to a few hundred kilometers. Cauthen⁴ reviewed the observed effects of explosion-produced ground motion on structures and equipment, and proposed a criterion for a property damage threshold that was based mostly on experience with chemical explosives.

Since then, over 150 nuclear explosions have been announced by the U. S. Atomic Energy Commission. Most of these took place at the Nevada Test Site. Other detonations occurred at the Supplementary Test Sites (in the central part of Nevada and on the island of Amchitka) and in New Mexico, Colorado and Mississippi. The maximum yield has increased during this time from about 200 kt to over a megaton. It is therefore timely to have a session on Seismic Effects at this, the Fourth Plowshare Symposium. Two of the papers in this session describe the seismic effects of the latest Plowshare event, Rulison. The others are more general in that they are based on experience to date and present information that may be used to assess the seismic hazards of future events. This is an important matter because it has been demonstrated that seismic hazards, not airblast or radioactivity, can impose the principal constraints on possible Plowshare operations—especially in the case of "underground engineering" applications of contained nuclear explosions.

This paper, as implied by the word "summary" in the title, includes a discussion of the experimental and theoretical knowledge gained since the last Symposium. In its function as a "review" paper, it also contains some fundamental information in order that it may provide a background for the other more specialized papers.

UNDERGROUND NUCLEAR EXPLOSIONS

The energy released in the detonation of a nuclear explosive is sufficient to transform the explosive from the solid to the gaseous state, with the gas being at a temperature of millions of degrees and a pressure of millions of atmospheres. As indicated in Fig. 1, an outward-propagating shock wave immediately begins to vaporize the adjacent rock (<1 msec), the shock wave subsequently melts and cracks the surrounding rock while the rock vapor-filled cavity begins to expand (3 msec), the cavity attains its maximum size at about the same time the outgoing shock decays to an elastic wave (50 msec), and shortly afterward (3 sec) the cavity usually begins to collapse to form a chimney (final configuration). This figure depicts the sequence of events for a contained explosion; the corresponding sequence for a cratering shot is given in Fig. 2.

There are three principal sources of seismic signals from underground nuclear explosions, which are illustrated in Fig. 3. The first, and most significant, is the explosion itself. The second is chimney or mound collapse which involves the fall of millions of tons of rock. The third appears to be a consequence of explosion-produced strain changes in the neighboring kilometers of rock which are released as a series of aftershocks. The aftershocks have been observed following explosions with body-wave magnitudes ≥ 5.0 .^{5,6} For the purposes of this paper, only the seismic motion that is directly produced by the explosion is considered. This is because experience to date is that the seismic motions from collapse and aftershocks are at least one order of magnitude smaller than those from the explosion itself.^{5,7}

The seismic signals that are emitted downward from the explosion itself (not from chimney collapse or aftershocks) are those which are recorded as the first arrivals at epicentral distances of several hundred to a few thousand kilometers.^{8,9} At these distances there appears to be no noticeable differences between the signals (used to determine magnitude) from contained and cratering events, all other conditions such as yield and geology being equal. However, as reported by Klepinger and Mueller¹⁰ and as discussed by Mueller in this Symposium, cratering explosions produce seismic signals at lesser distances that have less high-frequency content than the signals from deeper, contained explosions. On the other hand, it was found in a theoretical study of an explosive source in a layered medium¹¹ that the low-frequency portion of the spectrum decreased in amplitude as explosion depth was reduced. It appears that the effect of explosion depth on seismic frequency spectra is worthy of further investigation.

DISSIMILARITIES OF EARTHQUAKES AND EXPLOSIONS

There are many differences between earthquakes and explosions; those of concern in this paper are the differences in relative energy content of the various types of elastic waves generated by these two types of events.

Two types of elastic waves may be propagated within an isotropic, homogeneous elastic solid body: compressional or P waves and shear or S waves. If a finite, three-dimensional wave source (e.g., an explosion) is perfectly spherical, only P waves are generated; if not, both P and S waves are produced.^{12,13} Observations near underground nuclear explosions indicate that mostly P and relatively few S waves are generally produced, implying that such explosions tend to be spherical. One major exception is the Sterling event in the Salmon cavity (Fig. 4) which produced relatively large-amplitude vertically-polarized S waves because of the vertical asymmetry of the explosion environment.¹⁴ In contrast, earthquakes generally produce strong S waves as well as P waves, indicating the geometry of earthquake sources is

CAVITY-CHIMNEY FORMATION HISTORY

FIVE KILOTONS IN GRANITE

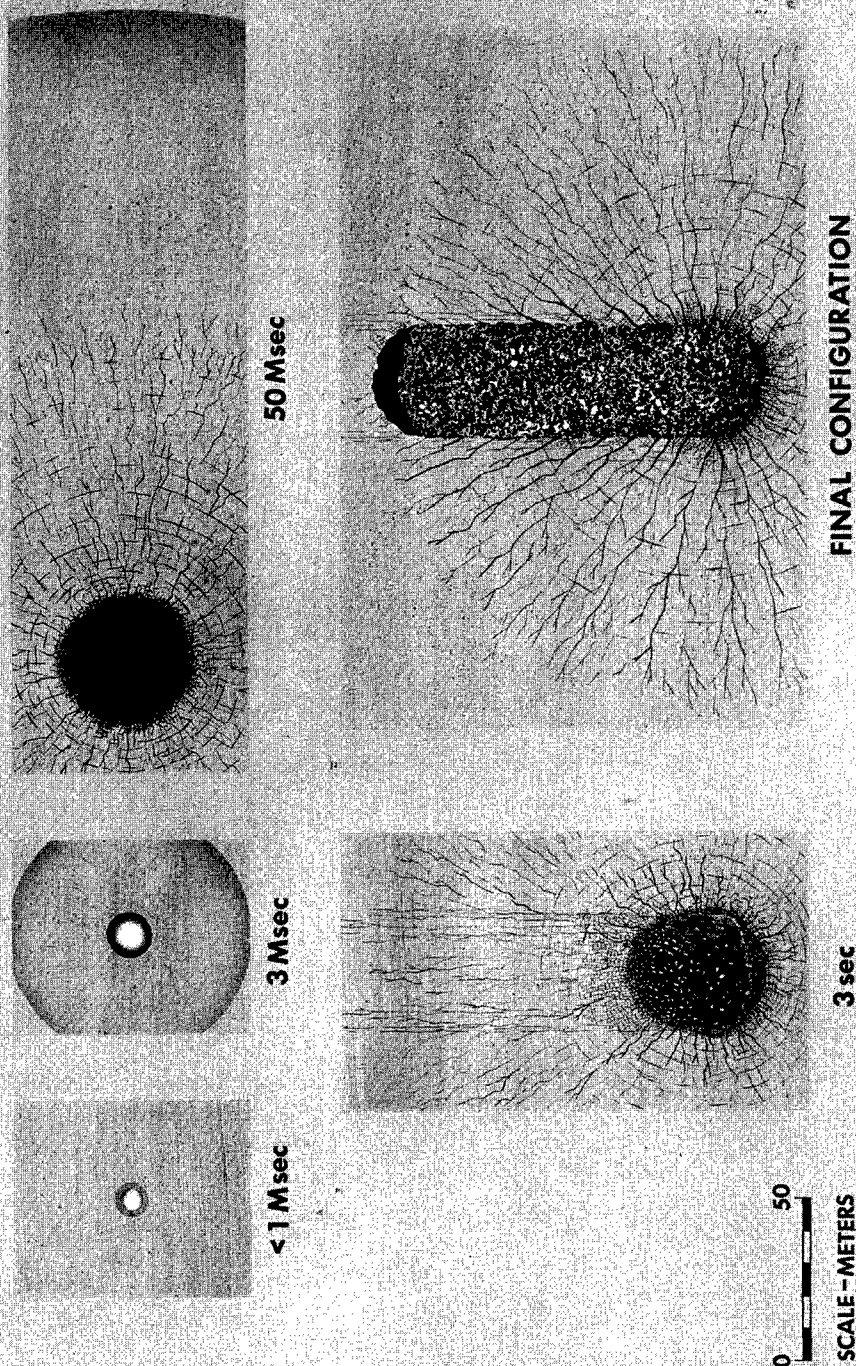


Fig. 1. Cavity-chimney formation history (5 kt in granite).

CRATER FORMATION HISTORY

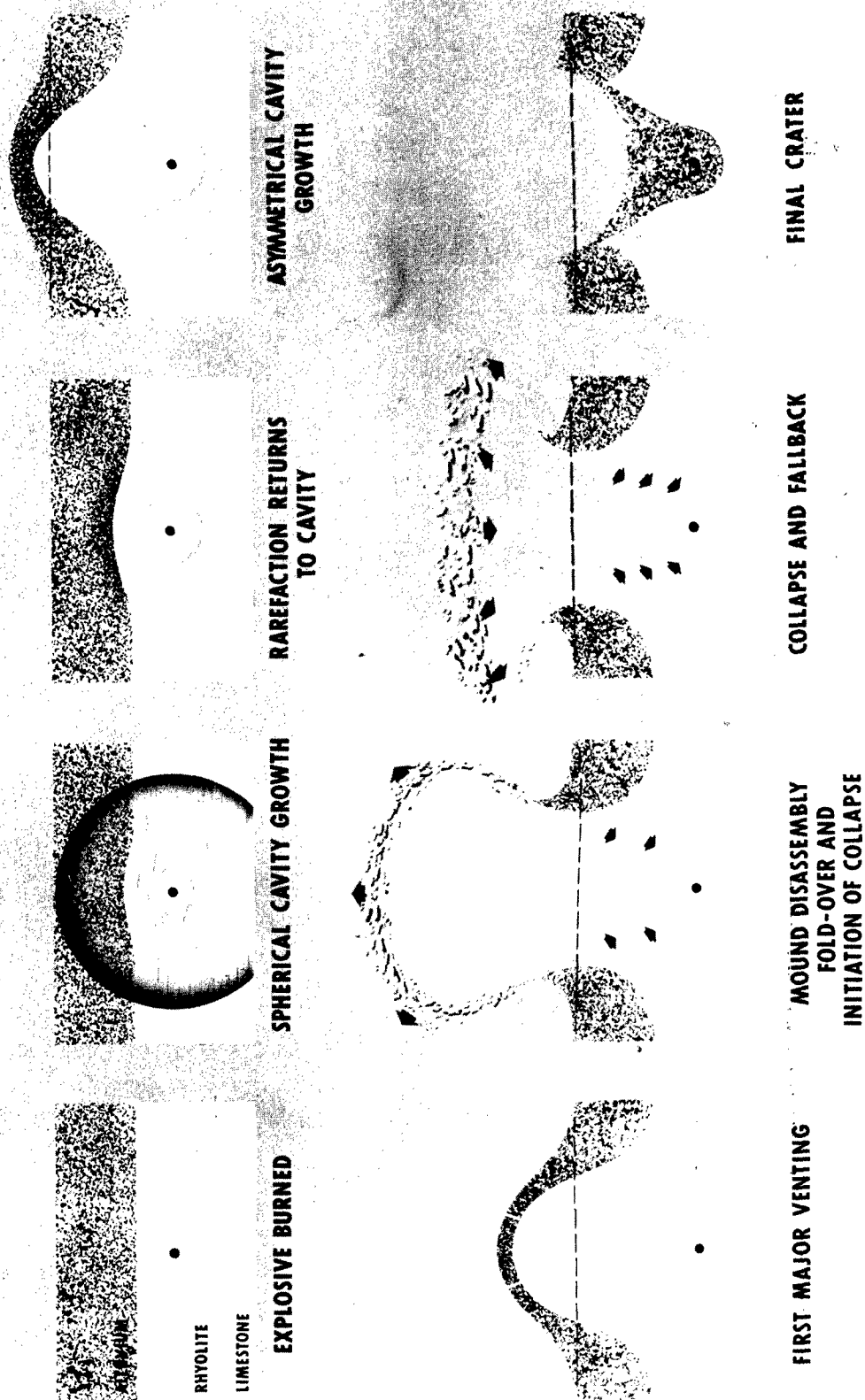


Fig. 2. Crater formation history.

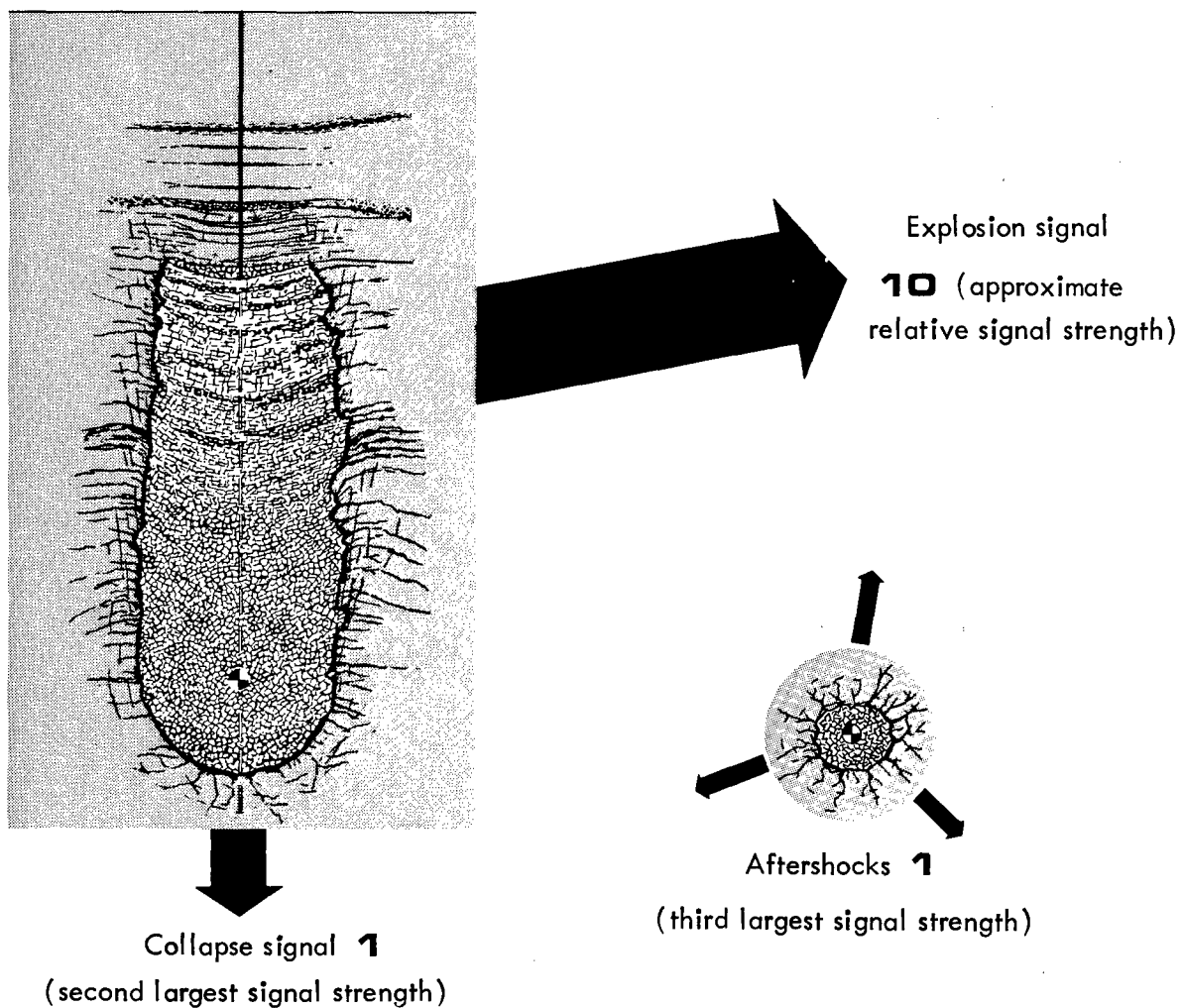


Fig. 3. Three sources of seismic signals.

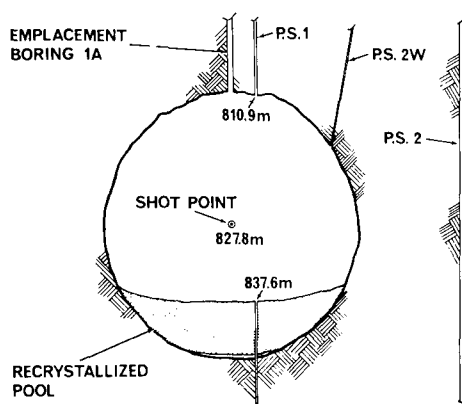


Fig. 4. The Sterling event in the Salmon cavity (Ref. 14).

types of waves, including the directions of particle motion relative to the directions of wave propagation, are illustrated in Fig. 5.

The principal seismic method of distinguishing earthquakes from explosions at distances of thousands of kilometers is that of comparing the surface

not spherical. Of course, it must be remembered that the earth is not homogeneous, and that partial conversion of P waves to S waves and vice versa is associated with reflections and refractions of elastic waves by various inhomogeneities. In the case of one important inhomogeneity, the free surface of the earth, the impinging P and S waves also interact with the surface in such a manner that Rayleigh or R waves^{15,16} and (under special conditions of layering), Love or L waves^{15,17} are generated. Unlike P and S waves which travel within an elastic body (hence the term "body waves"), R and L wave motions are concentrated at and near the surface so are called surface waves. These four

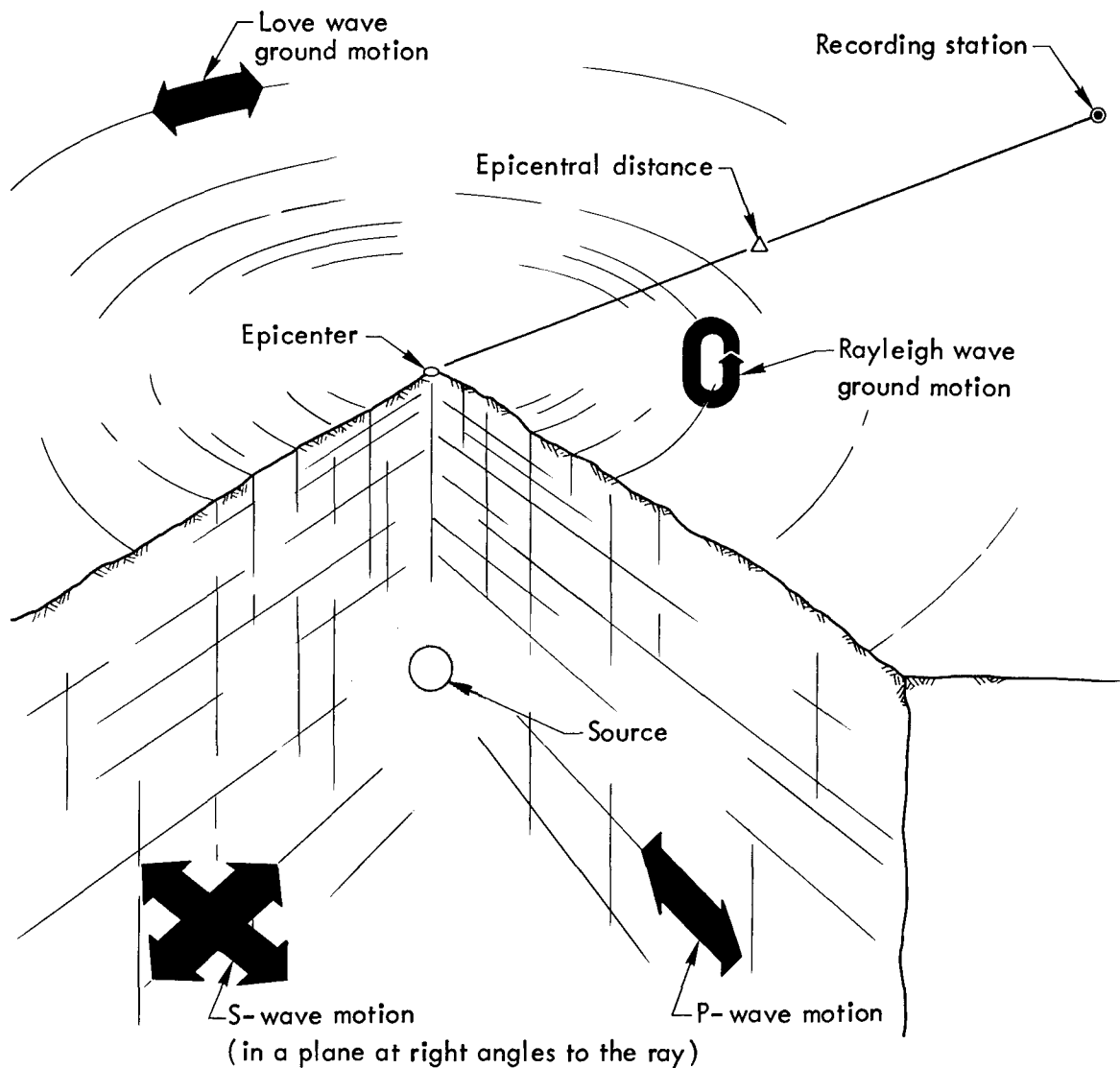


Fig. 5. Four types of elastic waves.

(R)-wave magnitude with the body (P)-wave magnitude.^{*18-21} This method of distinguishing the two types of events is illustrated in Fig. 6. It is apparent that earthquakes tend to produce significantly stronger R-wave signals than do explosions with the same body-wave magnitude. This may be a consequence of explosions producing relatively weak S waves and hence weak R waves, as indicated by the theoretical study with two different source functions by Alterman and Abramovici.²²

The news media often report that either an earthquake or an explosion (especially a high-yield explosion) had a certain body-wave magnitude (say 5),

*The magnitude scale was originally introduced in order "to take some of the nonsense out of earthquake statistics."²³ However, "magnitude has varied definitions with non universally accepted"²⁴ because it is an empirical quantity that is a function of the signal amplitude and period as recorded by a seismograph and a correction factor for epicentral distance (great circle distance from the seismograph to the point on the surface of the earth directly over the event).

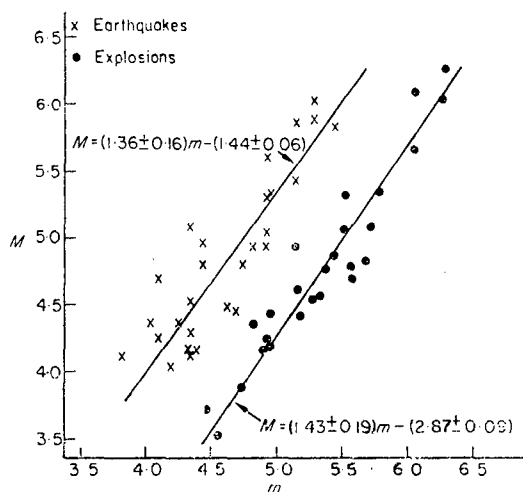


Fig. 6. Canadian mean surface-wave magnitude (M) versus body-wave magnitude (m) for 28 earthquakes and 26 nuclear explosions in Southwestern North America. (Ref. 20).

thereby tending to create the erroneous impression that a magnitude 5 explosion generates just as much seismic wave energy as a magnitude 5 earthquake. This is not true. Such magnitude data only indicate that the P-wave signals from both kinds of magnitude 5 events are of comparable strength. As indicated in the preceding paragraph, nuclear explosions tend to produce much weaker S and R waves than do earthquakes of comparable body-wave magnitude. As a consequence, the seismic wave energy associated with an earthquake of a given body-wave magnitude is at least ten times that of an explosion of equal magnitude.²⁵ Therefore, a magnitude 5 explosion does not have the same potential for causing, through ground motion, damage and injury as does a magnitude 5 earthquake.

GEOLOGY AND SEISMIC WAVE MAGNITUDE

Geology affects the generation, propagation and reception of seismic waves. That is, certain physical and chemical properties of different kinds of rock have influences on seismic waves. It has been noted for decades that damage from a given earthquake tends to be more severe for property on fill or alluvium deposits than on hard rock. Alcock²⁶ presents the results of recent studies of the effects of "receiver" geology. It soon became apparent during the past decade of underground nuclear testing that the seismic motion is also a strong function of the geology surrounding the explosive (or "transmitter"). This is demonstrated at all distances from the explosion: in the inelastic region by the peak radial stress measurements plotted as a function of scaled radius in Fig. 7,²⁷ the reduced displacement potentials (or seismic source functions) measured in the elastic region²⁸ which are presented in Fig. 12, and the body-wave magnitudes based on seismic measurements at hundreds and thousands of kilometers^{20,24,29} (also LRSM* reports) which are plotted in Fig. 8. This latter figure also illustrates the variation of magnitude with yield, and some of the better-known nuclear explosions (including cratering experiments) are identified.

The effect of geology on seismic motion may also be considered in terms of the fraction of the explosion energy that is converted into seismic wave energy. Explosions are very inefficient in this respect. Analysis of postshot rock temperatures for eight nuclear detonations in tuff, granite and salt indicates that 90 to 95% of the energy released remains as residual thermal energy in the vicinity of the explosion if complete containment is achieved.³⁰ More detailed studies of the Salmon event in salt indicate that about 90% of the

* LRSM (long range seismic measurements) reports are published by The Geotechnical Corporation and the UED Earth Sciences Division, Teledyne, Inc., under contract to the U.S. Air Force Technical Applications Center (AFTAC). The LRSM program began in 1961 and is supported by the Advanced Research Projects Agency (ARPA).

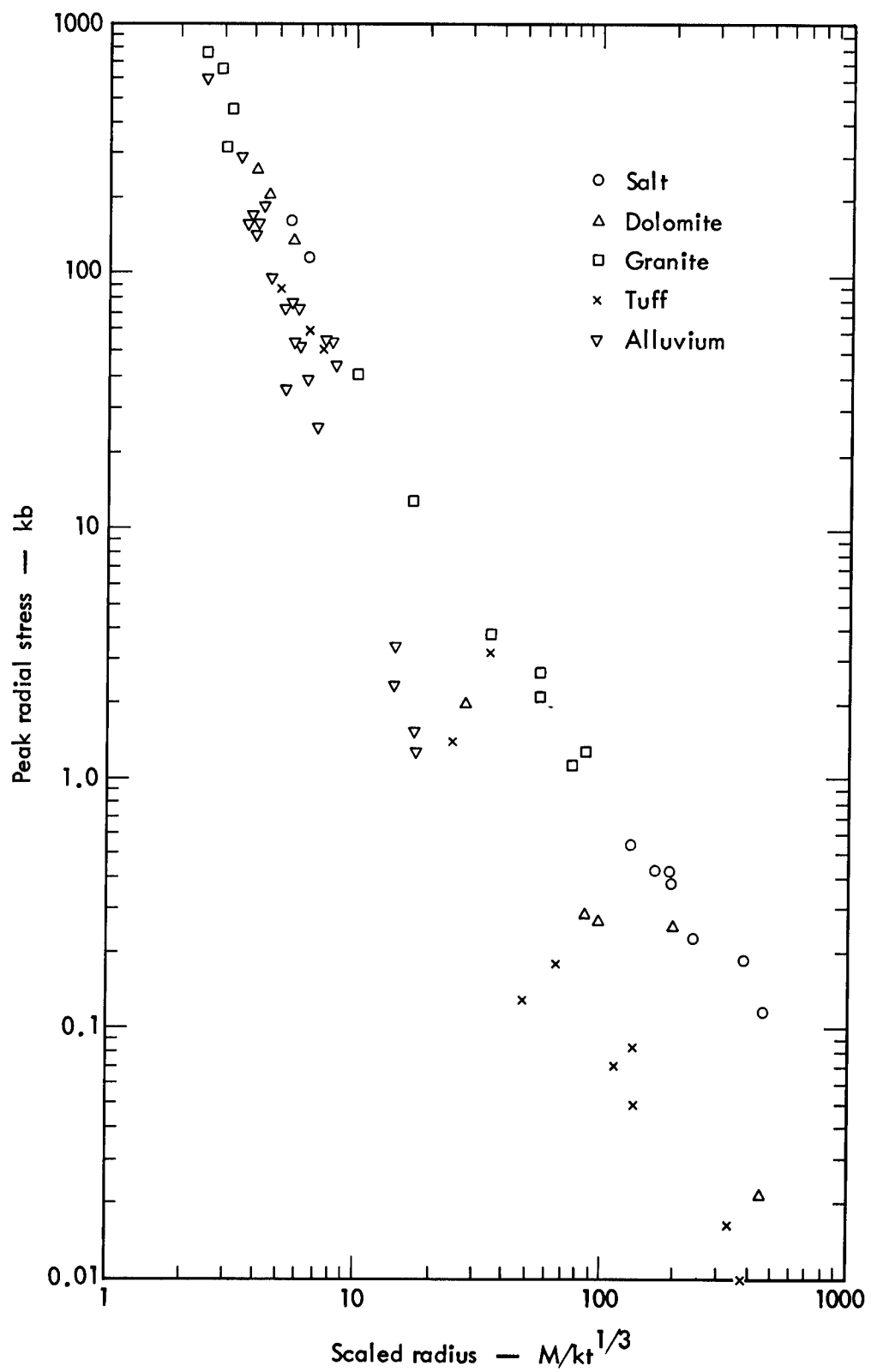


Fig. 7. Peak radial stress versus scaled radius and rock type for nuclear explosions.

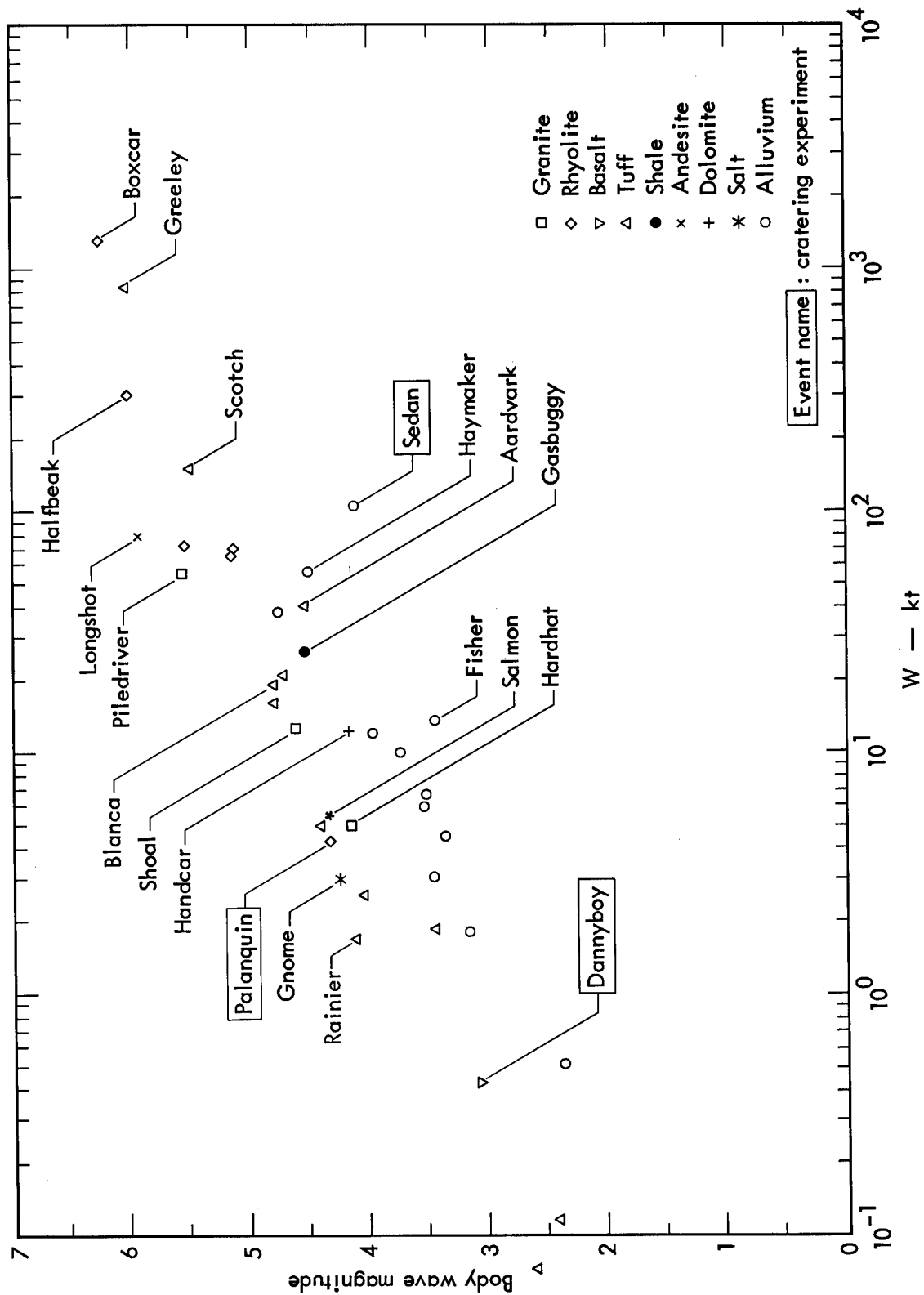


Fig. 8. Body-wave magnitude versus explosion yield and rock type.

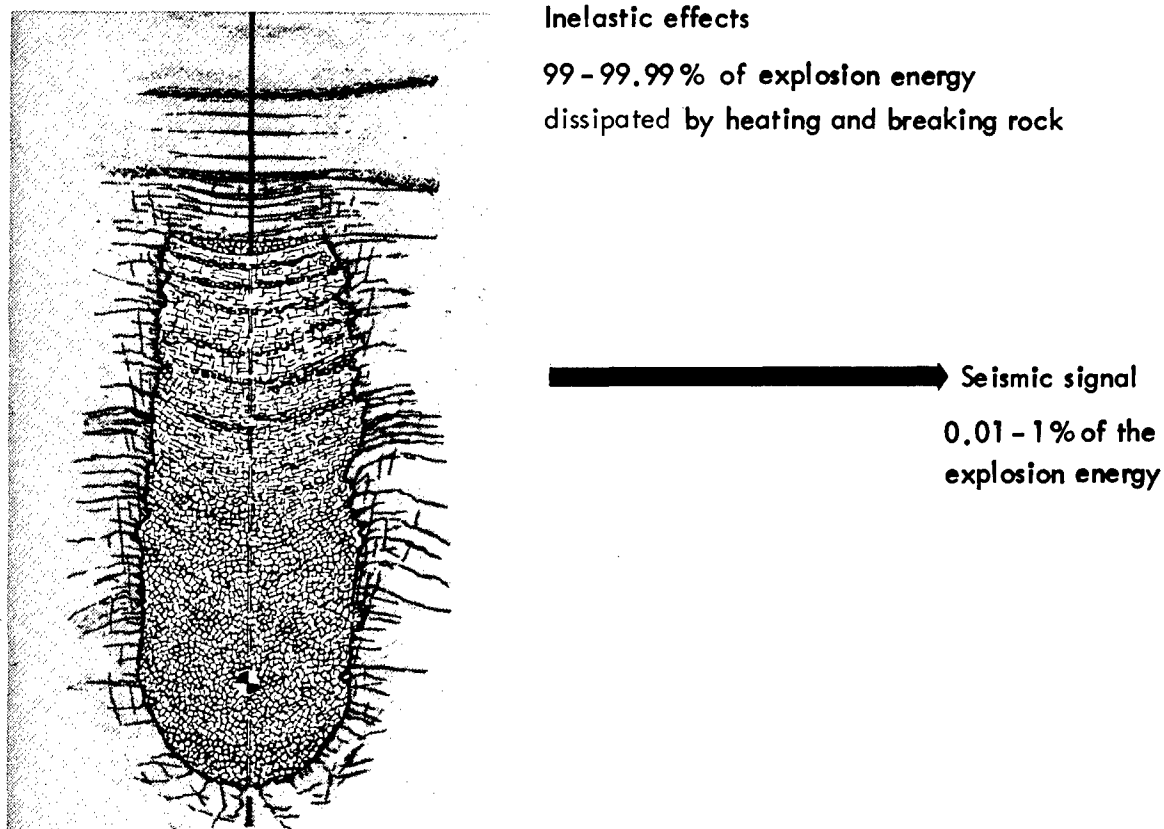


Fig. 9. Distribution of explosion energy.

total energy released was deposited within 50 meters of the explosion, not including the energy dissipated in crushing and fracturing the salt out to 90 meters from the edge of the 17-m-radius cavity.³¹ It is apparent that the energy radiated from an explosion in the form of seismic waves is a relatively small quantity which is the difference between two much larger quantities: the explosion energy and the energy dissipated in the inelastic region. Therefore, it is not surprising that various estimates of the radiated seismic energy fraction differ considerably relative to each other.^{2,32,33} In general, as illustrated in Fig. 9, these fractions range from about 1% for competent rocks like granite or salt to hundredths of 1% for dry alluvium.

SEISMIC WAVE GENERATION, PROPAGATION AND MEASUREMENT

A spherical P-wave source (approximating an explosion) in an isotropic, homogeneous elastic medium may be defined in terms of a pressure p applied to the walls of a spherical cavity with radius R . The equation for the reduced displacement potential X (a solution of the elastic wave equation)²⁸ may be written in terms of a natural undamped frequency $\omega_0 = 2b/R$ and a damping ratio $\zeta = b/a$, where a is the P-wave velocity and b is the S-wave velocity.³⁴ The Laplace transform of this equation is

$$\frac{\hat{X}(s)}{\hat{p}(s)} = \frac{R/\rho}{s^2 + 2\zeta\omega_0 s + \omega_0^2} \quad (1)^*$$

*This equation is mathematically identical to that used to describe linear electrical (resistance-inductance-capacitance) circuits and mechanical (dashpot-spring-mass) systems.³⁵

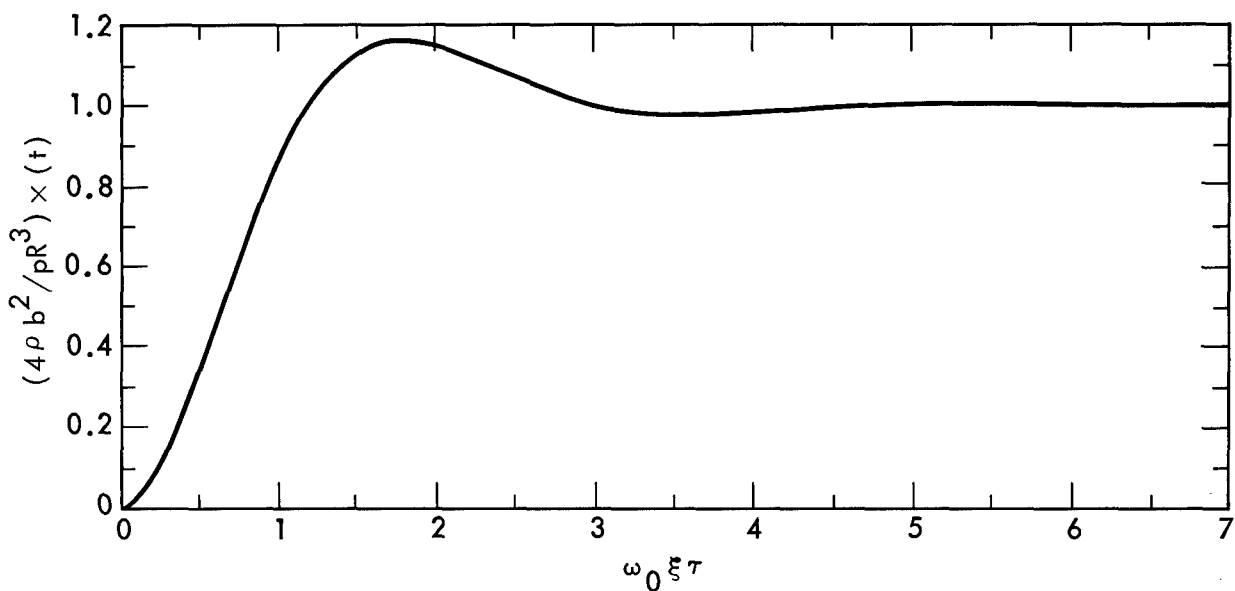


Fig. 10. Time domain solution of a P-wave equation.

where s is a complex variable with the dimension of reciprocal time and ρ is the medium density. The elastic body system is underdamped because $a > b$. This is illustrated in Fig. 10 which presents the time domain solution of Eq. (1), assuming a step function for the cavity pressure $p(t)$. The response of the system is a damped sinusoidal oscillation with a decay time constant $(\zeta\omega_0)^{-1}$ and a damped oscillation frequency $\omega_0(1 - \zeta^2)^{1/2}$. Therefore, the solution for any time-dependent input function of p consists of superimposed, damped, sinusoidal oscillations. If Eq. (1) is converted from a Laplace to a Fourier transform by letting $s \rightarrow i\omega$, the result is

$$\frac{\hat{\underline{\underline{X}}}(i\omega)}{\hat{\underline{\underline{p}}}(i\omega)} = \frac{R^3/4\rho b^2}{1 - \Omega^2 + 2i\zeta\Omega} \quad (2)^*$$

where $\Omega = \omega/\omega_0$. The solution for the Fourier amplitude[†] of this equation, assuming a step function for $p(t)$ is plotted in Fig. 11. ($|i\omega\hat{\underline{\underline{X}}}(i\omega)|$ is plotted instead of $\hat{\underline{\underline{X}}}(i\omega)$ because the solution for $|\hat{\underline{\underline{X}}}(i\omega)| \rightarrow \infty$ as $\omega \rightarrow 0$.) It is apparent that the principal content of this spectrum is for the frequencies $\omega < \omega_0$ where ω_0 may be defined as the cutoff frequency of the low-pass filter. The low-pass filter characteristics of an ideal elastic medium are accentuated, as illustrated by the dashed line in Fig. 11, by anelastic attenuation which preferentially attenuates the higher frequencies as an exponential function of distance times frequency.³⁷

The Fourier amplitudes of the reduced displacement potentials measured on four nuclear events and scaled to a yield of 5 kt are plotted in Fig. 12.²⁸ It is shown that the different properties of alluvium, tuff, granite and salt have a significant effect on the seismic source function. A comparison of Fig. 11 with

* This equation is mathematically identical to that which describes a low-pass filter.³⁶

† The Fourier amplitude is defined as the absolute value of the magnitude of the Fourier transform in the complex plane.

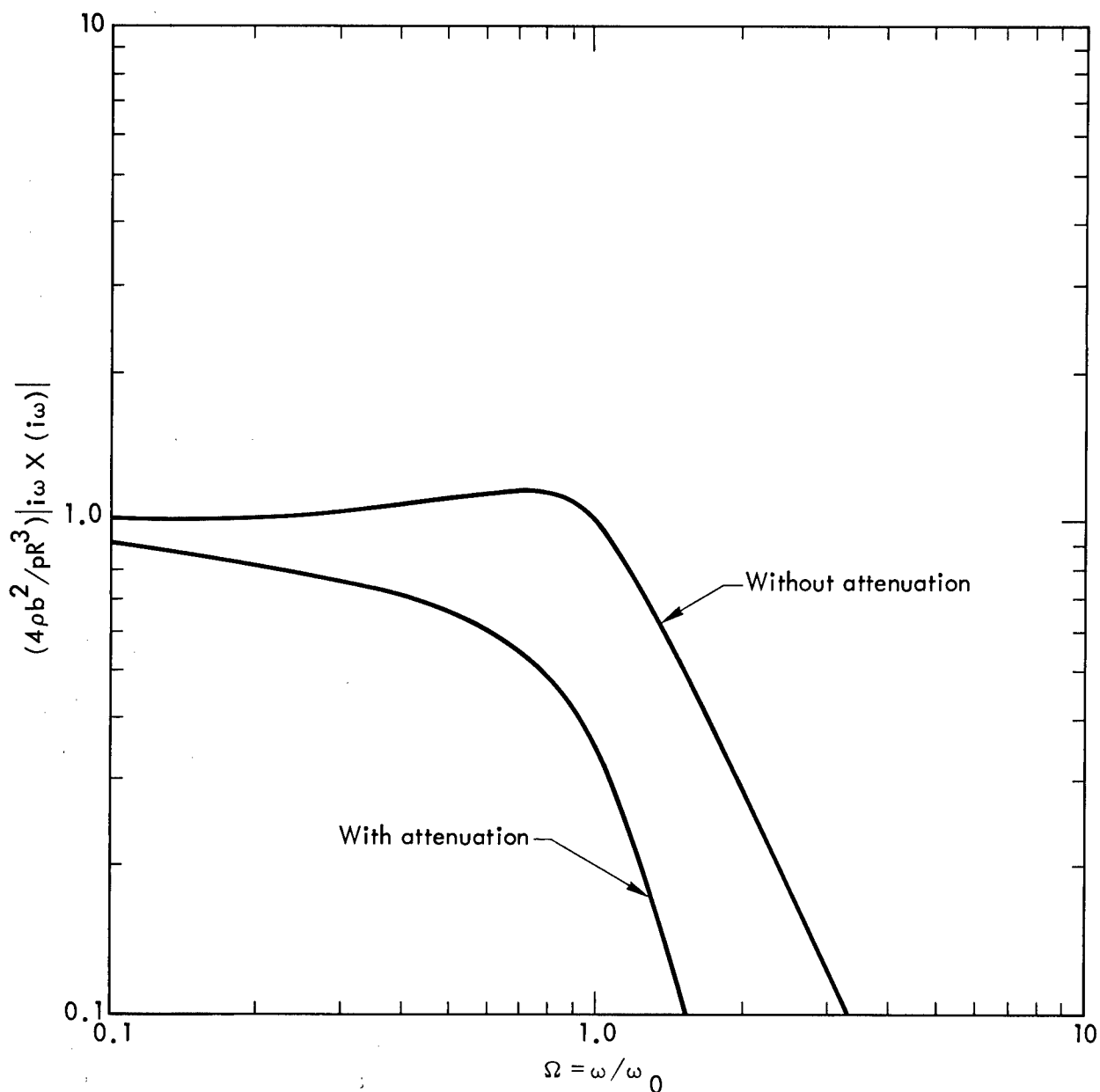


Fig. 11. Frequency domain (Fourier amplitude) solution of a P-wave equation.

Fig. 12 indicates that a step function of applied stress at the elastic radius (the equivalent of a cavity pressure p and cavity radius R) is a principal part of the driving function for these explosions.

A "flat earth" model is a reasonable approximation for the distances of tens and hundreds of kilometers at which seismic hazards must be evaluated. If such an earth is also isotropic and homogeneous, a buried spherical P-wave source (representing an explosion) produces three types of waves at the free surface which propagate at different velocities and consequently have different arrival times: the direct P wave, the R wave which appears and begins to develop some distance from the epicenter, and the surface-S wave* which is

*The surface-S wave is probably not significant to the seismic damage problem.

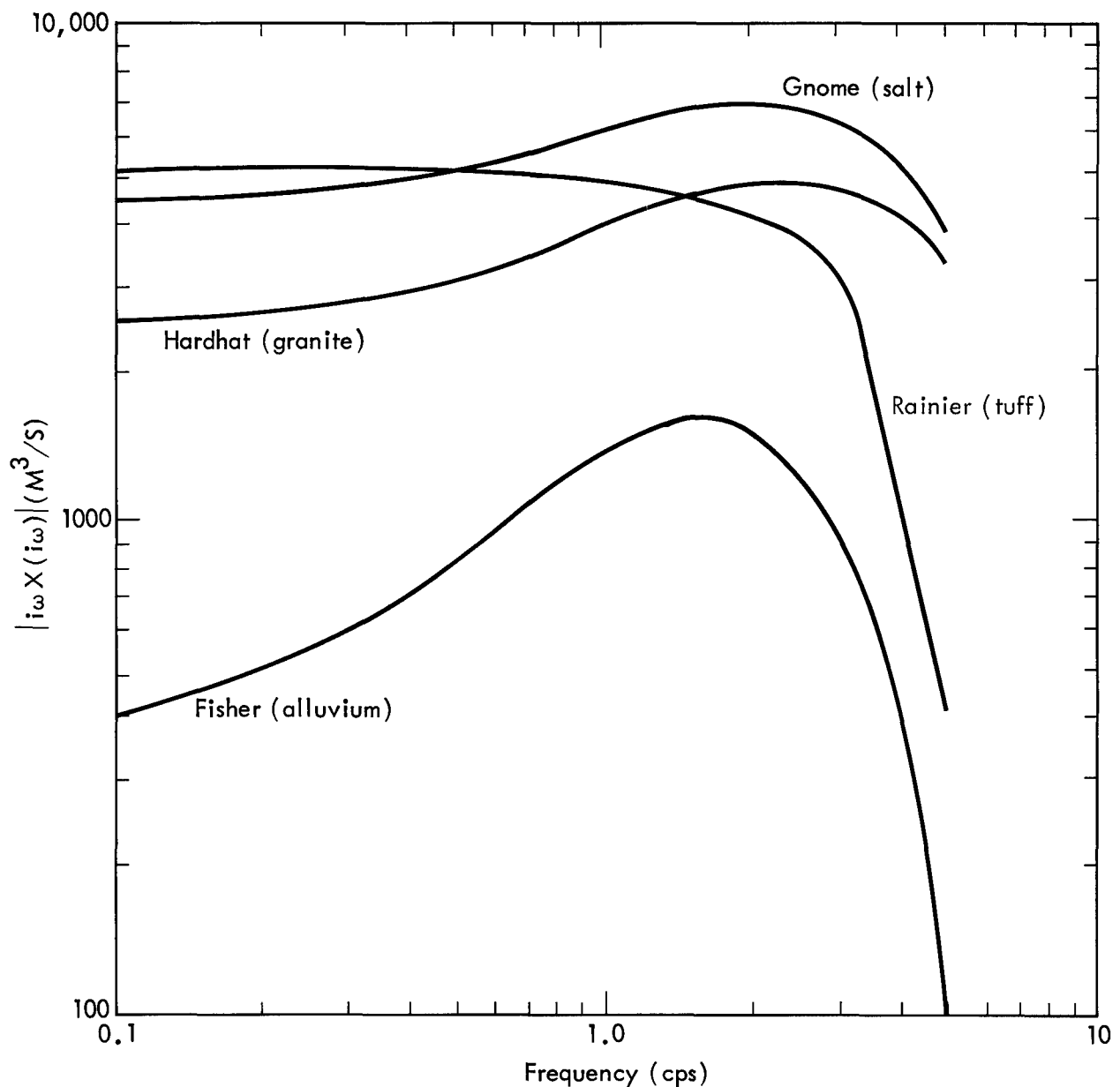


Fig. 12. Fourier amplitudes of reduced displacement potentials for four explosions.

much smaller than the R wave and develops at a greater distance from the epicenter.^{16, 38, 39} But the earth is not isotropic and homogeneous, and a better approximation is a layered half-space. As demonstrated by the model experiments conducted by Press *et al.*,⁴⁰ the analysis of seismograph recordings for such an earth model is more difficult because the recorded signal generally consists of superimposed and overlapping direct, reflected and refracted P and S waves as well as R waves. A further refinement of an earth model is that of (1) a small number of major discontinuities in physical properties (e.g., layers), and (2) a large number of random small inhomogeneities.⁴¹ The mathematical analysis of such a two-part model is very complex; one method for layered systems involves the solution of matrices;^{42, 43} a statistical approach is necessary in the case of many small discontinuities.^{41, 44}

A comprehensive experimental-theoretical study of an underground nuclear event from explosive detonation to distant seismic signal has been published for only one experiment, Salmon.^{45,46,47} This work concerned only the first P-wave arrival in the first zone, the head wave that is critically refracted at the Mohorovicic discontinuity. Other experimental-theoretical studies beginning with the measured reduced displacement potential (instead of the explosive detonation) and ending with the head wave arrival have been made.^{8,28} Toksöz et al.⁴⁸ used R-wave measurements from several nuclear explosions together with an appropriate layered geological model to calculate a seismic source function (equivalent to a reduced displacement potential) for the explosion. It is doubtful if any comprehensive experimental-theoretical study of an entire explosion-produced wave train has been accomplished.

These experimental-theoretical studies are necessary in order to obtain an understanding of the physical phenomena involved. However, it is not possible at present to base predictions of ground motion for seismic damage assessment only on calculations from the first principles of mechanics. This is because all the necessary calculational techniques have not been sufficiently developed in detail. If such techniques were in existence and proven, it would not be feasible to rely on calculations alone because it is impractical, at present, to determine all pertinent details of the geology from the explosion to sites where seismic damage may be of concern. Therefore, the prediction of ground motion for seismic damage assessment is presently based on interpolations and extrapolations of experimental data using theory as a guide: e.g., identification of elastic wave types,⁴⁹ statistical analysis of peak amplitudes close to⁵⁰ and farther from⁵¹ explosions, amplitude and frequency analysis of seismic waves from specific events,^{10,52} and development of frequency- and yield-dependent ground motion predictions.⁵³ The peak amplitude data for the wave train^{10,50-53} may be expressed in the form

$$A = KW^\alpha R^\beta \quad (3)$$

where A is the peak value of particle acceleration, velocity or displacement, K is an empirical geology-dependent factor, W is explosion yield, R is distance from the explosion, α is a yield-scaling exponent, and β is an attenuation exponent. Statistical techniques may be used, if sufficient data are available, to develop confidence limits for use with Eq. (3) in the case of "calibrated" areas like the Nevada Test Site and vicinity. Obviously, there is more uncertainty in applying Eq. (3) to areas where there is no prior experience, a normal situation in the Plowshare Program (see the papers on the Rulison event in this session). However, as discussed in the subsequent section on ground motion and property damage, it is not sufficient to predict only the peak values in the manner of Eq. (3). It is necessary to predict ground motion* as a function of frequency (as illustrated in Fig. 20).⁵³ These curves are derived from statistical analysis of ground motion measurements at the Nevada Test Site and vicinity. It is interesting to note that a shift toward lower frequencies with increasing yield is indicated, in accord with the expected variation of the cutoff frequency $\omega_0 = 2b/R$ as an inverse cube-root function of the yield [see the discussion associated with Eq. (2) and Fig. 11].

These experimental data from explosions are a function of both the ground motion and the response of the measuring instruments to this motion, so a discussion of measurement techniques is in order. The history of seismic measurements, particularly the beginning, concerns seismology from the geophysical, not the safety point of view. The initial interest was in the

* Actually, Fig. 20 is a plot of a function of ground motion called the pseudo relative velocity, not the motion itself.

detection of distant events against a background of seismic noise which tends to peak at periods of less than 1 sec and at about 7 sec.⁵⁴ As a consequence of this noise background and the physical processes of generation, propagation and attenuation for P, S and R waves, the "window" for maximum signal-to-noise ratio in the case of P waves occurs at periods ranging from 0.5 to 4 sec and that for R waves is at periods of 15 to 20 sec.¹⁹ The peak frequency range for S waves overlaps the short-period maximum in the seismic noise;¹⁹ most S waves from large-magnitude earthquakes are detected at periods of 2 to 4 sec.⁵⁵ As a consequence, both short-period (for P waves)⁵⁶ and long-period (for R waves)⁵⁷ instruments have been developed. The problem of signal-to-noise ratio obviously does not exist for the short-range measurements for seismic safety, so continuous band width (from short-period to long-period) measurements are feasible. Furthermore, the low-pass filtering effect of high-frequency attenuation in the earth is not as significant at short ranges. Measurements of seismic signals produced by nuclear explosions at the Nevada Test Site consequently indicate peak amplitudes at somewhat different and higher frequencies: 1 to 1.25 sec for P waves, 1.5 to 3 sec for S waves, and 2 to 4 sec for R waves.⁵² Many of the instruments used for routine measurements in the vicinity of the Nevada Test Site are described in the report by Navarro;⁵⁸ strong motion (generally perceptible zone), intermediate range (perceptible to teleseismic zone), and long-range (teleseismic which include the previously-mentioned short- and long-period seismometers). These appear to cover the amplitudes and frequencies of importance, including the high frequencies that are significantly attenuated at long ranges.

GROUND MOTION AND PROPERTY DAMAGE

Earthquake- and explosion-produced ground motion can cause a great variety of property damage, ranging from the catastrophic (major structural failure) to the annoying (cracked plaster, stucco or masonry). The possibility of a catastrophe cannot be overlooked; for example, the structural integrity of earth-fill dams was of concern in the safety evaluation of the Gasbuggy and Rulison events. However, the principal damage claims associated with nuclear explosions to date involve minor architectural, not major structural damage. Much has been learned about the conditions causing such minor damage since the Third Plowshare Symposium.

At that meeting, Cauthen⁴ reviewed the available information (based for the most part on experience with chemical explosives) and concluded that the threshold for architectural damage to residences (cracked plaster, stucco or masonry) is a peak surface velocity of 10 cm/sec independent of frequency. Several months later, the 5-kt Salmon experiment was executed near Hattiesburg, Mississippi. As illustrated in Fig. 13, many unexpected claims of such architectural damage were received from residents living where the ground motion was at least an order of magnitude smaller than the 10 cm/sec threshold.⁵⁹ One of the obvious conclusions is that the damage threshold cannot be considered to be a function of peak surface velocity alone. A controlled experiment was subsequently initiated with 43 relatively new masonry structures at Mercury, Nevada, the service community for the Nevada Test Site.⁶⁰ These buildings were inspected at intervals during periods of no testing, and before and after nuclear tests conducted at distances of about 30 to 80 km. It was found that an average of 2.5 cracks per day formed in these buildings during inactive periods, and that an average of 24 new cracks were found immediately after nuclear explosions that produced peak surface velocities ranging from 0.1 to 0.3 cm/sec (Fig. 14). The explosion-produced cracks were no more severe than those occurring naturally. These results confirmed the experience in Mississippi that 10-cm/sec peak surface velocity is not a satisfactory criterion for damage prediction. Nadolski⁶¹ proposed that all minor residential damage experience (chemical explosives, the Salmon event in Mississippi,

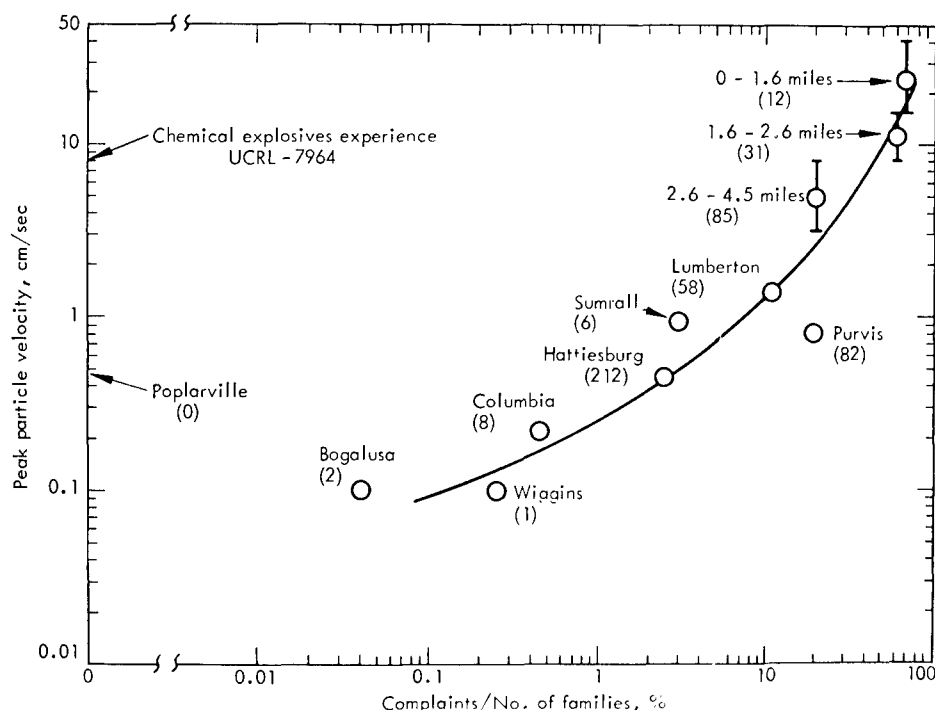


Fig. 13. Complaints resulting from the Salmon underground nuclear explosion. Note that these numbers are not actual damage or claims of damage but only initial complaints of damage. Numbers in parenthesis are complaints within specified areas (city limits for communities) received by January 15, 1965 (Ref. 59).

the Mercury study, and experience in Las Vegas) be plotted in terms of the probability of complaints versus the pseudo-absolute acceleration (Fig. 15). It appears that there may be a real—but empirical—relation between pseudo-absolute acceleration and the probability of damage claims. Work is presently underway to bring the data in Fig. 15 up to date in order to see whether or not subsequent experience confirms this hypothesis.

PHYSICAL MEANING OF RESPONSE SPECTRA

In view of the promise that (to paraphrase Richter²³ on seismic magnitude) the use of pseudo-absolute acceleration may be useful in making sense out of seismic damage statistics, it is in order to review the origin of this parameter and to define its physical meaning.

The ground motion produced at a given surface location by a specific event (earthquake or explosion) is a complex function of time. It is also a complex function of the geometry and physical properties of the source-transmission path-receiver system. The response of a structure is a function of both its mechanical oscillator properties and the ground motion to which it is subjected. The oscillator characteristics of a structure are a complex function of its design, construction, materials, foundation, etc. Consequently, a statistical or probabilistic approach is required, as indicated by the use of damage claim percentage in Fig. 15, as well as the use of a random function for ground motion.⁶²

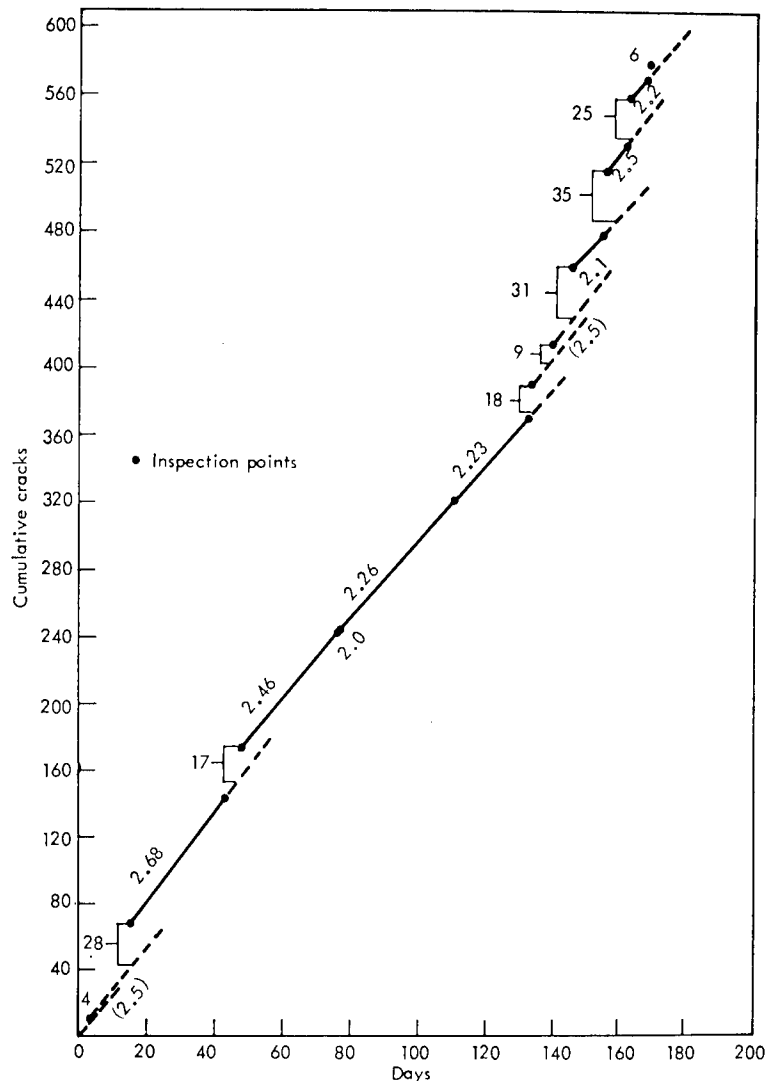


Fig. 14. Cumulative cracks and natural cracking rates for masonry buildings at Mercury, Nevada (Ref. 60).

It appears that Benioff⁶³ was the first to suggest that the destructive potential of an earthquake (or an explosion in the present case) be defined in terms of the peak response of a series of mechanical oscillators (identical except for resonant frequency which ranges over the bandwidth of interest) to the ground motion produced by the event. In his work, "...suppose we substitute for the... structures a series of undamped pendulum seismometers having frequencies ranging from the lowest fundamental frequency of... [these] structures to the highest significant overtones. ... the maximum recorded deflection of each pendulum against its frequency [gives] a curve which may be termed the undamped pendular spectrum of the earthquake." Subsequently, the "undamped pendulum seismometers" were replaced by linear, single-degree-of-freedom, mass-spring-dashpot oscillators and the term "pendulum spectrum" by "shock spectrum"⁶⁴ or "response spectrum."⁶⁵ A response spectrum provides... an envelope of the theoretical maximum responses of several single-degree-of-freedom systems excited by a base motion.⁶¹ The key assumption is that the actual structures are modeled by a simple mechanical oscillator.

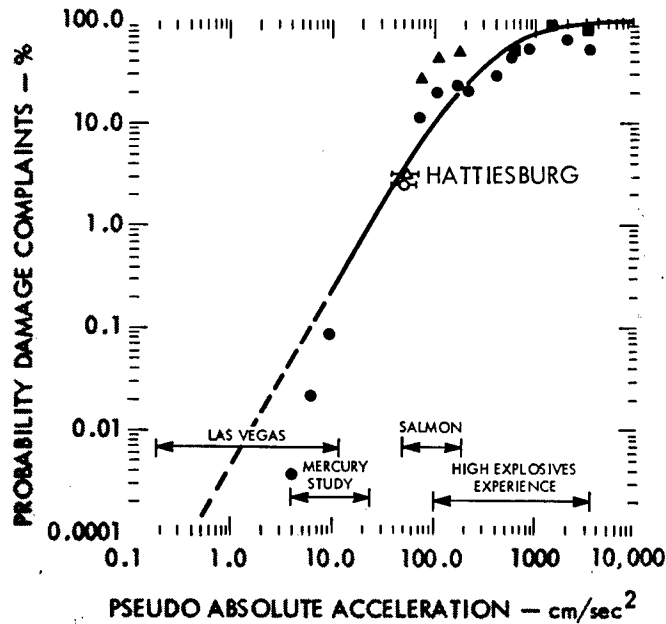


Fig. 15. Damage percentage versus pseudo-absolute acceleration for a damping ratio of 10% (Ref. 61).

These oscillators are defined by the equation

$$\frac{d^2x}{dt^2} + 2\zeta\omega_0 \frac{dx}{dt} + \omega_0^2 x = -\frac{d^2y}{dt^2} \quad (4)$$

where x is the relative displacement of the oscillator mass and y is the ground motion. This equation is mathematically identical to Eqs. (1) and (2), including the use of the undamped natural frequency ω_0 and the damping ratio ζ which are defined in terms of the mass, spring and dashpot properties instead of the elastic body parameters a , b and R as in Eqs. (1) and (2).^{62,66} Given a history of ground motion for a specific event, the envelope of peak relative displacements $x(\omega_0)$, defined as $RD(\omega_0)$, plotted versus oscillator natural frequency ω_0 is defined as the relative displacement spectrum (Fig. 16). The pseudo relative velocity is defined as the product of the peak relative displacement for a given oscillator frequency times that frequency:⁶⁴

$$PSRV(\omega_0) = \omega_0 RD(\omega_0). \quad (5)$$

Therefore, it is possible to define a pseudo-relative velocity spectrum (Fig. 17), which is proportional to the square root of the upper bound for the total kinetic energy of a vibrating structure.⁶⁴ The pseudo-relative acceleration is defined as

$$PSAA(\omega_0) = \omega_0 PSRV(\omega_0) = \omega_0^2 RD(\omega_0), \quad (6)$$

and is the greatest value of elastic spring force per unit of mass during the time history of input motion.⁶⁷ The corresponding pseudo-relative acceleration

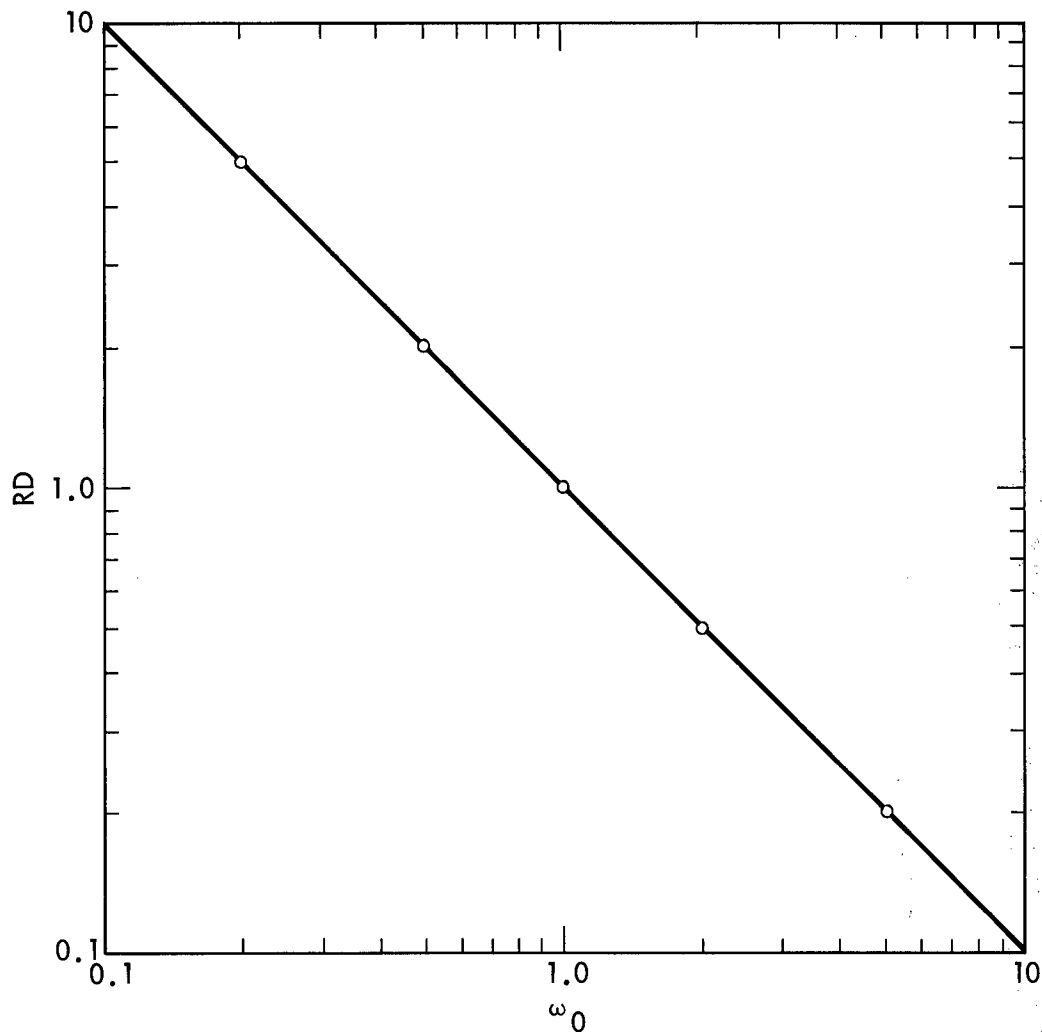


Fig. 16. Simplified example of a relative displacement spectrum.

spectrum is illustrated in Fig. 18. The curves of Figs. 16-18 are replotted as a single curve in Fig. 19 on a four-coordinate plot of RD, PSRV and PSAA versus ω_0 , a convenient form commonly used in shock and vibration studies.

Similar ground-motion data for a number of explosions may be used to generate predicted response spectra at a given distance as a function of yield, as illustrated in Fig. 20.⁵³ In this case, the abscissa is the period T where $T = 2\pi/\omega_0$.

SUMMARY

Seismic hazards, not airblast or radioactivity, can impose the principal constraints on some Plowshare operations, especially those involving contained rather than cratering nuclear explosions.

Three sources of seismic signals may be associated with underground nuclear explosions: the explosion itself, chimney collapse, and aftershocks. The signals from the latter two sources are at least an order of magnitude weaker than those directly produced by the explosion.

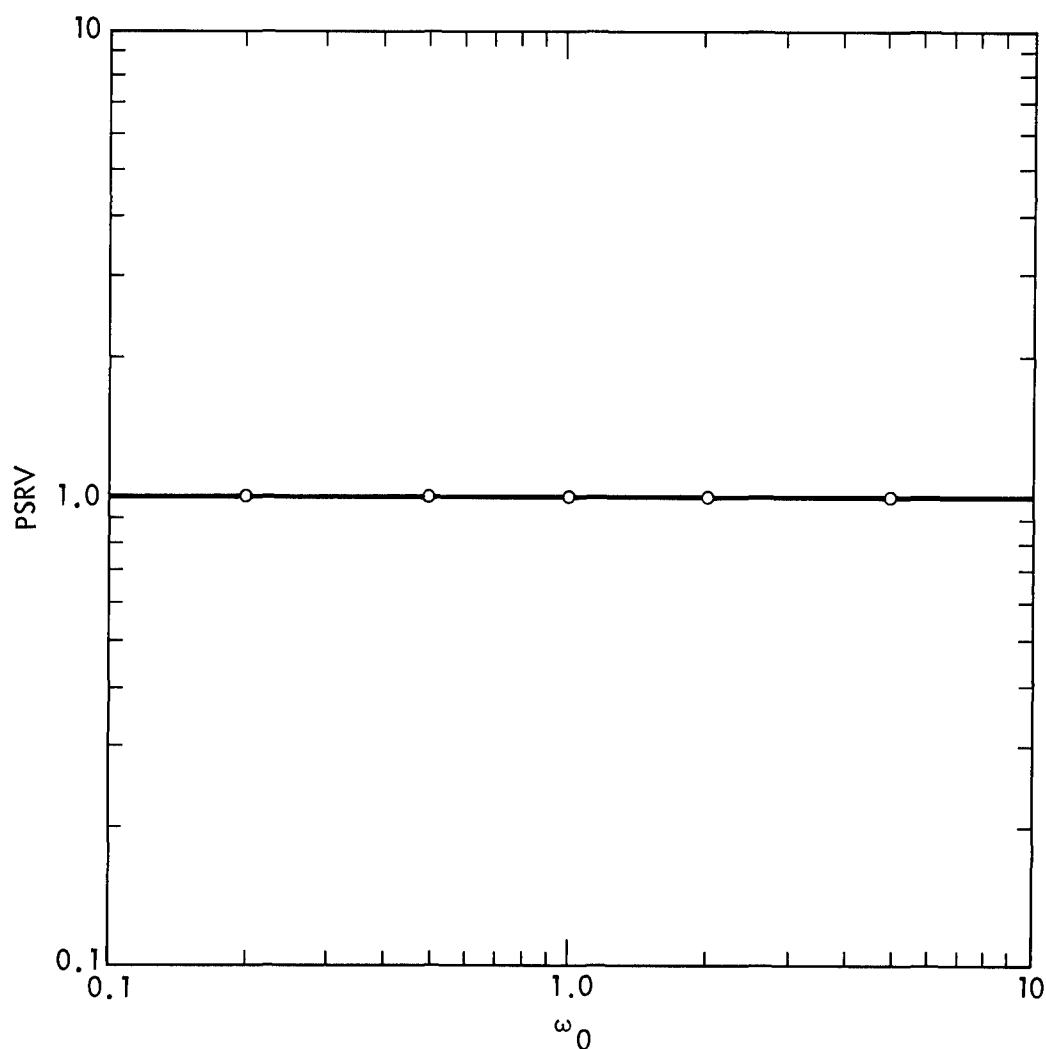


Fig. 17. Simplified example of a pseudo-relative velocity spectrum.

The energy of the seismic waves produced by an earthquake is at least an order of magnitude greater than that by an explosion with equal body-wave magnitude.

Explosions are inefficient seismic wave generators with the seismic energy fraction ranging from about 0.01 to 1%, depending upon the physical and chemical properties of the rock surrounding the explosive. The physical properties of the rock along the transmission path and at the receiver also affect the strength of seismic signals.

An ideal elastic medium has the characteristics of a low-pass filter. The inelastic attenuation within the earth enhances these low-pass filter characteristics.

It is not presently possible to base predictions of ground motion for seismic damage assessment on only theoretical calculations. This is because not all the necessary mathematical techniques have been developed or proven. Furthermore, it is not feasible to determine all pertinent details of the geology from the explosion to where seismic damage may be of concern. Therefore, the prediction of ground motion is based on interpolation and extrapolation of experimental data using theory as a guide.

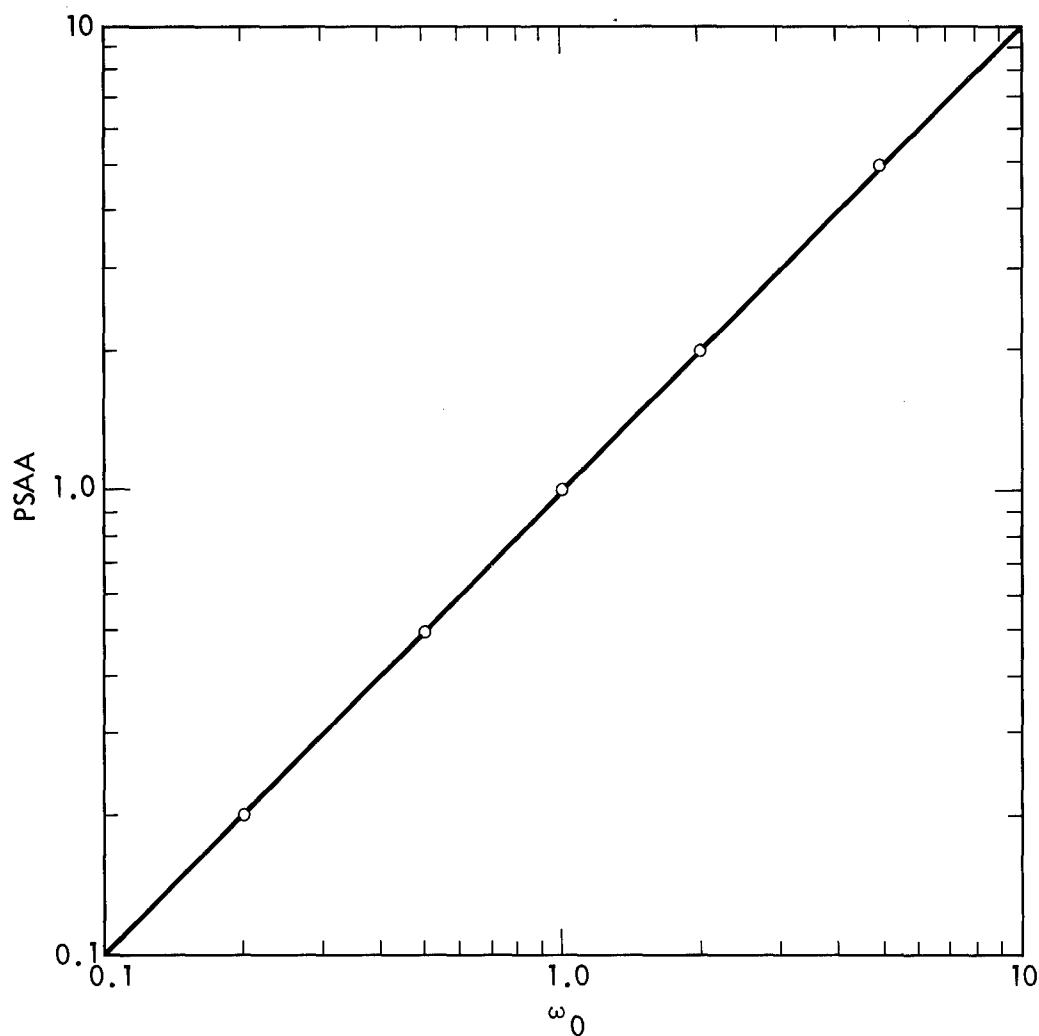


Fig. 18. Simplified example of a pseudo-absolute acceleration spectrum.

A promising criterion for correlating ground motion with property damage is an empirical relation between pseudo-absolute acceleration and probability of damage claims. The pseudo-absolute acceleration is derived as a response spectrum defined by an envelope of the theoretical maximum response of single-degree-of-freedom oscillators (each with a different natural frequency) to the motion generated by an earthquake or explosion. The key assumption is that the actual structures are modeled by a simple mechanical oscillator.

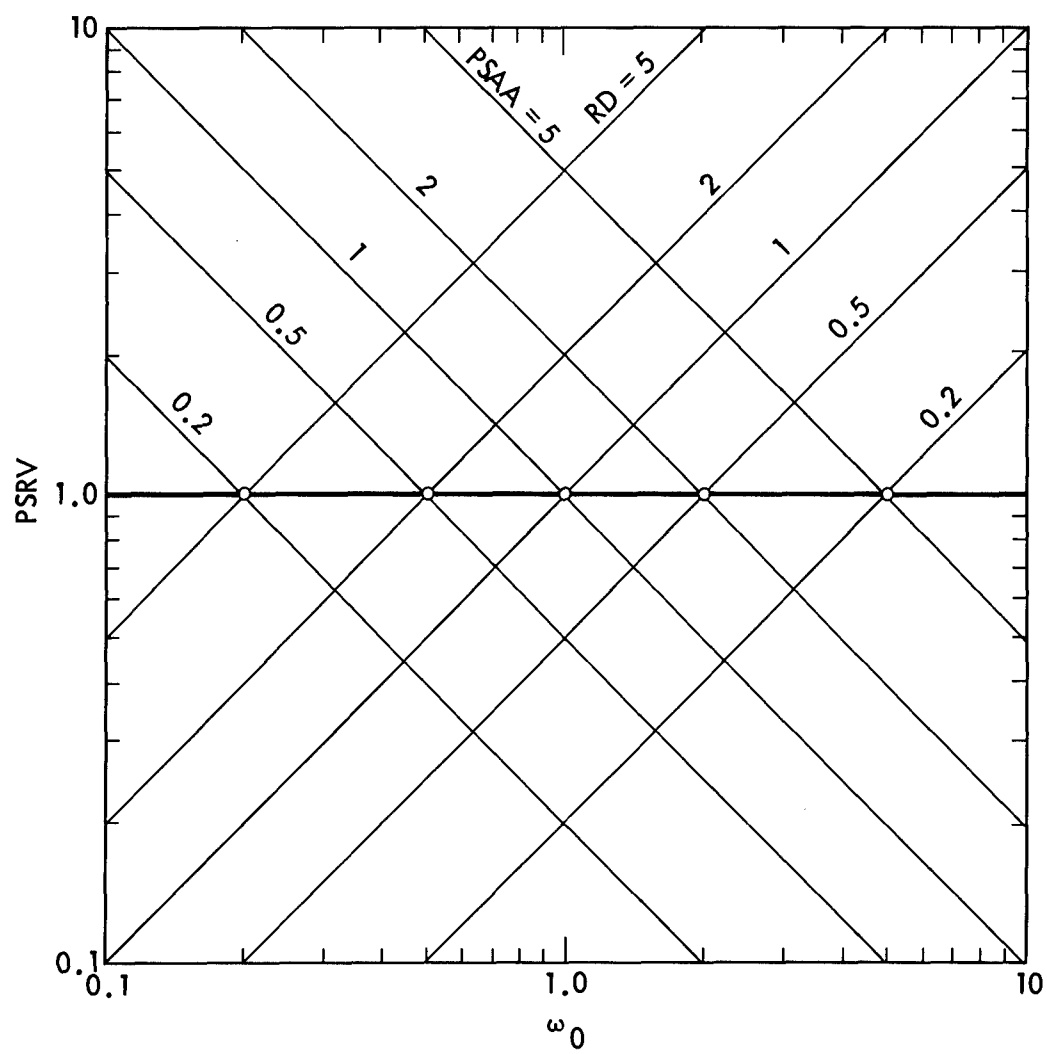


Fig. 19. Four-coordinate plot of RD, PSRV and PSAA spectra.

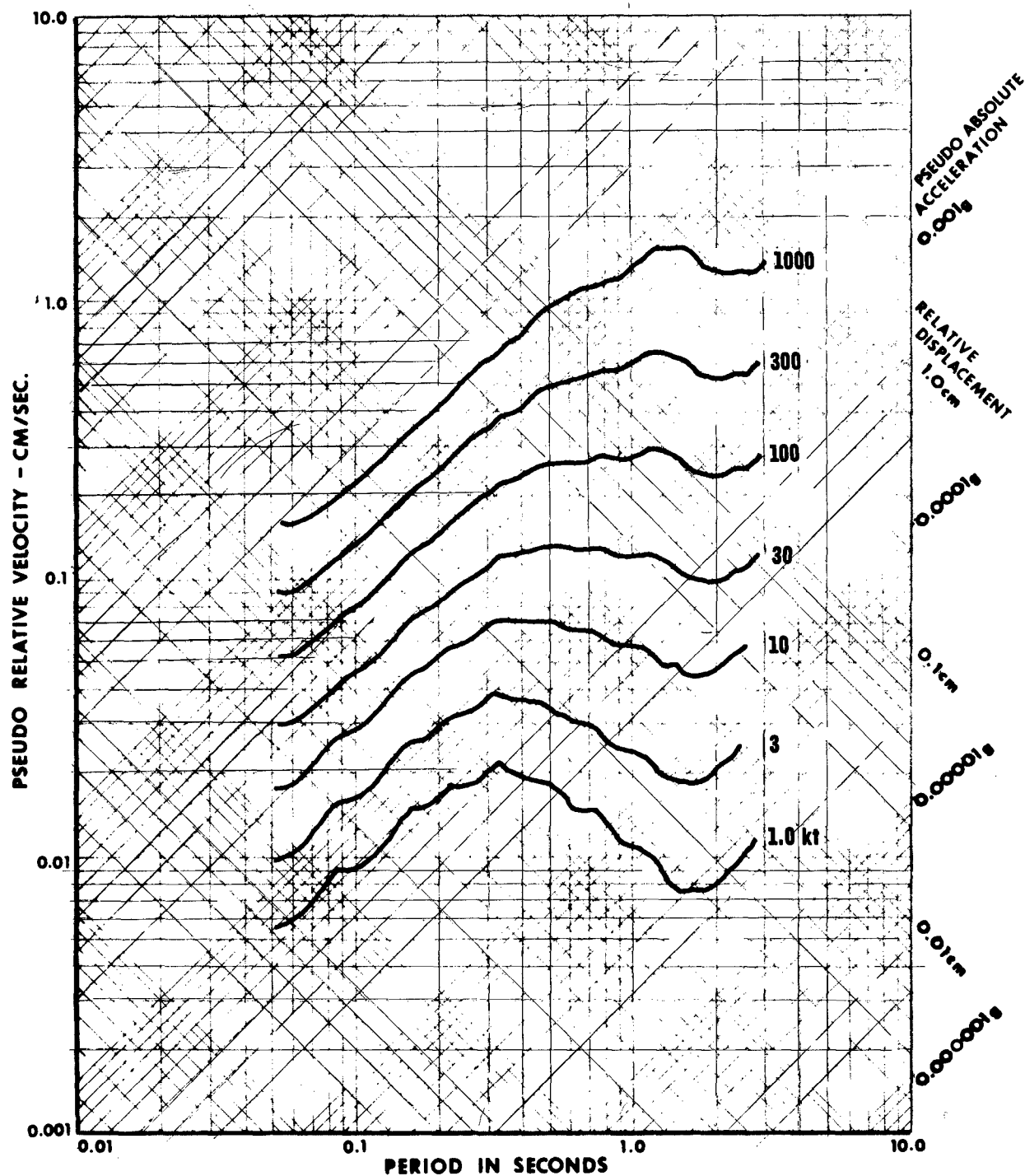


Fig. 20. A family of predicted mean PSRV curves with 5% damping for seven yields at a distance of 100 km (Ref. 53).

REFERENCES

1. C. Romney, and W. Helterbran, "Progress and Promise in the Study of the Earth Using Nuclear Explosives," in Proc. Third Plowshare Symp., U. S. Atomic Energy Commission, TID-7965, 1964.
2. W. V. Mickey, "Seismic Wave Propagation," in Proc. Third Plowshare Symp., U. S. Atomic Energy Commission, TID-7695, 1964.
3. D. M. Hankins, "Seismic Amplitudes at an Intermediate Range from Explosions," in Proc. Third Plowshare Symp., U. S. Atomic Energy Commission, TID-7965, 1964.
4. L. J. Cauthen, Jr., "The Effects of Seismic Waves on Structures and Other Facilities," in Proc. Third Plowshare Symp., U. S. Atomic Energy Commission, TID-7965, 1964.
5. G. Boucher, A. Ryall, and A. E. Jones, J. Geophys. Res., 74, 3808 (1969).
6. A. Ryall, and W. U. Savage, J. Geophys. Res., 74, 4281 (1969).
7. S. W. Smith, J. Geophys. Res. 68, 1477 (1963).
8. G. C. Werth, R. F. Herbst, and D. L. Springer, J. Geophys. Res. 67, 1587 (1962).
9. E. W. Carpenter, Proc. Roy. Soc. London, A290, 396 (1966).
10. R. W. Klepinger, and R. A. Mueller, "Analysis of Ground Motion from Cratering and Contained Events (Cabriolet Event)," Environmental Research Corporation Rept., Alexandria, Virginia, 1969.
11. K. Fuchs, Bull. Seismol. Soc. Am., 56, 75 (1966).
12. F. G. Blake, Jr., J. Acoust. Soc. Am, 24, 211 (1952).
13. P. Hazebrock, Proc. Roy. Soc. London, A294, 38 (1966).
14. W. R. Perret, Bull. Seismol. Soc. Am., 58, 2043 (1968).
15. A. E. H. Love, Some Problems of Geodynamics (Cambridge University Press, 1911); reprinted in 1967 by Dover Publications, Inc., New York, pp. 154-165.
16. H. Nakano, Japan J. Astron. Geophys. 2, 233 (1925).
17. Y. Sato, Bull. Earthquake Res. Inst., 30, 101 (1952).
18. SIPRI, Seismic Methods for Monitoring Underground Explosions, International Institute for Peace and Conflict Research (SIPRI), Stockholm, 1968.
19. H. I. S. Thirlaway, Contemp. Phys., 9, 17 (1968).
20. P. W. Basham, Geophys. J. Roy. Astron. Soc., 17, 1 (1969).
21. R. C. Liebermann, and P. W. Pomeroy, J. Geophys. Res., 74, 1575 (1969)

22. Z. Alterman, and F. Abramovici, *Geophys. J. Roy. Astron. Soc.*, 13, 117 (1967)
23. C. F. Richter, *Elementary Seismology* (W. H. Freeman and Company, San Francisco, 1958), p. 364.
24. J. F. Evernden, *Bull. Seismol. Soc. Am.*, 57, 591 (1967).
25. M. Bath, "Earthquake Energy and Magnitude," in *Physics and Chemistry of the Earth*, Vol. 7 (Pergamon Press, Ltd., Oxford, 1966).
26. E. D. Alcock, *Bull. Seismol. Soc. Am.*, 59, 245 (1969).
27. F. Holzer, *Proc. Roy. Soc. London*, A290, 408 (1966).
28. G. C. Werth, and R. F. Herbst, *J. Geophys. Res.*, 68, 1463 (1963).
29. C. Romney, *J. Geophys. Res.*, 64, 1489 (1959).
30. R. A. Heckman, "Deposition of Thermal Energy by Nuclear Explosives," in *Proc. Third Plowshare Symp.*, U.S. Atomic Energy Commission, TID-7965, 1964.
31. D. E. Rawson, R. W. Taylor, and D. L. Springer, *Naturwissenschaften*, 54, 525 (1967).
32. N. A. Haskell, *J. Geophys. Res.*, 72, 2583 (1967).
33. Reference 18, pp. 83, 86.
34. I. I. Gurvich, *Izv. Akad. Nauk. SSSR Fiz. Zemli.*, No. 10, 45 (1965) [*Bull. Acad. Sci. USSR, Earth Phys.*, No. 10, 684 (1965)].
35. J. C. Gillé, M. J. Pelgrin, and P. Decaulne, *Feedback Control Systems* (McGraw-Hill Book Company, Inc., New York, 1959), Chapt. 6.
36. A. Papoulis, *The Fourier Integral and its Applications* (McGraw-Hill Book Company, Inc., New York, 1962), p. 118.
37. L. Knopoff, *Quart. Rev. Geophys.*, 2, 625 (1964).
38. E. R. Lapwood, *Phil. Trans. Roy. Soc. London*, A242, 63 (1949).
39. W. W. Garvin, *Proc. Roy. Soc. London*, A234, 528 (1956).
40. F. Press, J. Oliver, and M. Ewing, *Geophysics*, 19, 388 (1954).
41. J. A. Hudson, and L. Knopoff, *Proc. Roy. Soc. London*, A290, 290 (1966).
42. W. T. Thompson, *J. Appl. Phys.*, 21, 89 (1950).
43. F. Gilbert, and G. E. Backus, *Geophysics*, 31, 326 (1966).
44. J. W. Dunkin, *Geophysics*, 34, 357 (1969).
45. L. A. Rogers, *J. Geophys. Res.*, 71, 3415 (1966).
46. D. W. Patterson, *J. Geophys. Res.*, 71, 3427 (1966).
47. D. L. Springer, *J. Geophys. Res.*, 71, 3459 (1966).

48. M. N. Toksoz, A. Ben-Menahem, and D. G. Harkrider, J. Geophys. Res. 69, 4355 (1964).
49. W. W. Hays, "Identification of Elastic Wave Types on Seismograms from Underground Nuclear Explosions," Environmental Research Corporation Rept. NVO-1163-157, Alexandria, Virginia, 1968.
50. V. E. Wheeler, and R. G. Preston, "Scaled Free-Field Particle Motions from Underground Nuclear Explosions," Lawrence Radiation Laboratory, Livermore, Rept. UCRL-50563, 1968.
51. J. R. Murphy, and J. A. Lahoud, "Analysis of Seismic Peak Amplitudes from Underground Nuclear Explosions, Environmental Research Corporation Rept. NVO-1163-166, Alexandria, Virginia, 1968.
52. W. W. Hays, and J. R. Murphy, "Amplitude and Frequency Characteristics of Elastic Wave Types Generated by Underground Nuclear Explosions," Environmental Research Corporation Rept. NVO-1163-181, Alexandria, Virginia, 1969.
53. R. D. Lynch, "PSRV Prediction Equations for Pahute Mesa Events," Environmental Research Corporation Rept. NVO-1163-TM-8, Alexandria, Virginia, 1969.
54. R. A. Frosch, and P. E. Green, Jr., Proc. Roy. Soc. London, A290, 368 (1966).
55. J. M. DeNoyer, Proc. Roy. Soc. London, A290, 448 (1966).
56. R. A. Savill, E. W. Carpenter, and J. K. Wright, Geophys. J. Roy. Astron. Soc., 6, 409 (1962).
57. F. Press, M. Ewing, and F. Lehner, Trans. Am. Geophys. Union, 39, 106 (1958).
58. R. Navarro, "Seismograph Systems," U. S. Coast and Geodetic Survey Rept. CGS-C-106, Rockville, Maryland, 1967.
59. D. V. Power, Bull. Seismol. Soc. Am., 56, 1413 (1966).
60. J. F. Wall, Bull. Seismol. Soc. Am., 57, 991 (1967).
61. M. E. Nadolski, Bull. Seismol. Soc. Am., 59, 487 (1969).
62. T. K. Caughey, and H. J. Stumpf, J. Appl. Mech., 28, 563 (1961).
63. H. Benioff, Bull. Seismol. Soc. Am., 24, 398 (1934).
64. Y. C. Fung, "Shock Loading and Response Spectra," in Shock and Structural Response (American Society of Mechanical Engineers, New York, 1960).
65. D. E. Hudson, Bull. Seismol. Soc. Am., 52, 417 (1962).
66. Reference 35, p. 89.
67. V. Jenschke, J. Penzien, and R. W. Clough, "Analysis of Earth Motion Accelerograms, Institute of Engineering Research Rept. SESM 64-1, University of California, Berkeley, California; Lawrence Radiation Laboratory Rept. UCRL-13109, Livermore, California, 1964.

ABSTRACT

PREDICTION OF SEISMIC MOTION FROM CONTAINED AND EXCAVATION NUCLEAR DETONATIONS

by

R. A. Mueller

Capability to predict ground motions from nuclear events is developed on empirical and theoretical bases. Analyses of the experimental data provide basic predictions of peak particle motions and spectra which follow a $(\text{yield})^m \text{ times } (\text{distance})^{-n}$ relationship. The exponents on yield and distance are frequency dependent and derived from experiment and theory. Theory provides a physical understanding of the phenomena which allows extrapolation to off-NTS and atypical events. For example, yield scaling theory predicts significantly higher frequency motions and consequently larger ground accelerations for overburied events such as Gasbuggy, Rulison, Wasp and Wagon Wheel. These conclusions are observed from Gasbuggy (26 kt) which generated ground accelerations comparable to a normal buried event of 200 kt. This result is important in avoiding personal injury and assessing the probability of property damage. Conversely, theory predicts lower ground accelerations and seismic efficiencies for excavation events; these effects are observed from the Cabriole and Schooner events and consequently predicted for the Sturtevant and Yawl events.

With regard to the distance exponent, scattering theory determines a distance exponent which predicts greater attenuation effects on higher frequency motions. This trend is verified experimentally by regression analyses on a large number of data points which determine the distance exponent to range from -1.1 at low frequencies to -1.6 at high frequencies. Results indicate that cube root similarity scaling is not appropriate in the far field except possibly for peak particle displacements at the low frequency end of the spectrum.

In addition to the source and transmission factors, current ground motion prediction techniques, on and off-NTS, take into account local site characteristics. Experimental evidence and theoretical models--layered media elastic theory, finite element modeling, and building response modeling--demonstrate local geology and structural amplifications of ground motions.

PREDICTION OF SEISMIC MOTION FROM CONTAINED AND EXCAVATION NUCLEAR DETONATIONS

by

Richard A. Mueller, Senior Member of the Technical Staff
Environmental Research Corporation

Introduction

Capability to predict ground motions resulting from underground nuclear detonations requires an intimate combination of empirical and theoretical studies. Environmental Research Corporation under contract with AEC's Nevada Operations Office provides a continuing effort in this direction. The theoretical studies provide an understanding of the physical phenomena and form the basis for correlating data with various physical properties and extending prediction capability to new areas and atypical events.

Empirical Studies

Peak Motions

The basic regression equation used in many empirical analyses is the power law dependence of the form

$$A = A_0 W^m R^{-n} \quad (1)$$

where A is the dependent variable (peak ground motion or spectral amplitude), and the independent variables considered most important are yield (W) and distance (R).

Murphy and Lahoud (1969) have applied equation (1) to the peak resultant vector of ground motions. The data sample includes more than 2,900 points of acceleration, velocity, and displacement measured from 99 underground nuclear events ranging in yield from 1 to 1200 kilotons over a recording distance of less than 1 to 600 kilometers. Separate analyses are performed on "hard rock" stations only and alluvium stations only. This division is dictated by experience which indicates that the next most important variable to yield and distance is the local station geology (Davis and Murphy, 1967), where alluvial layers generally give rise to amplification effects. This phenomenon will be dealt with in greater detail later on. Comparison of the prediction equations with the observed Boxcar (1.2 megaton) peak acceleration data is shown in Figure 1. The distinction between hard rock and alluvium stations is made displaying the

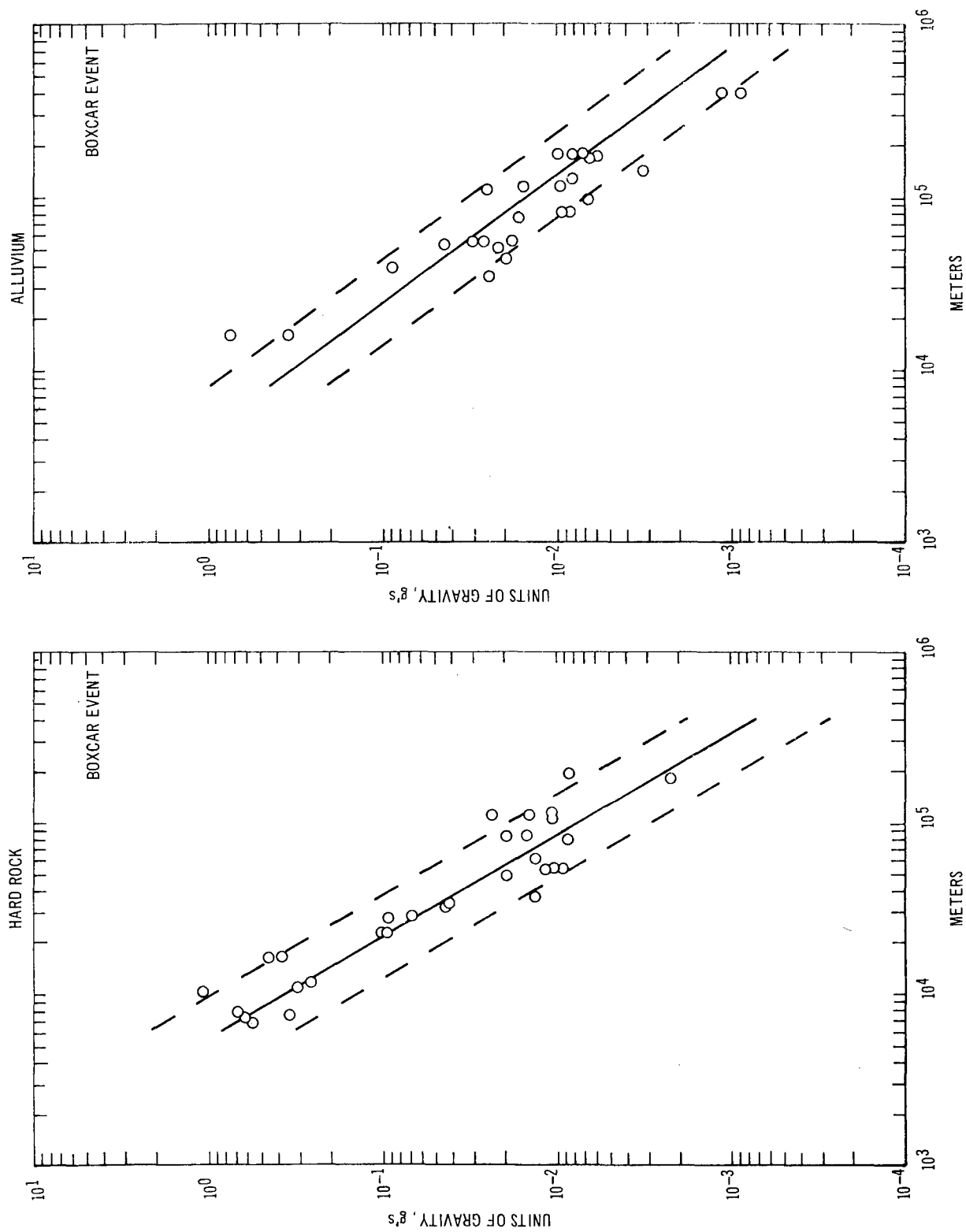


Figure 1. Comparison of Observed Peak Acceleration Data from Boxcar Event

amplification effects of the alluvial layers. The dashed lines represent the standard error of estimate.

Ground Motion Spectra

Returning to the complete seismogram, in order to completely specify a time signal, the Fourier amplitude and phase spectra are needed. Experimentally, it is found that the amplitude spectrum behaves in a somewhat regular fashion, whereas the phase spectrum is quite erratic with parametric variations. The amplitude spectrum is therefore more amenable to a statistical analysis in which the major independent variables are considered. Lynch (1969a) has performed a general regression analysis of peak response spectra of a single degree of freedom system from 11 Pahute Mesa events, recording at 64 seismic stations. The data sample spans a yield range of about 20 kt to 1200 kt and a distance range of 4.4 km to 551 km. The same basic equation (1) forms the nucleus for the analysis at 40 separate periods or frequencies. Figure 2 demonstrates a typical prediction from this study for the Boxcar Event (1.2 mt) at Las Vegas. Note the dotted curves which indicate the standard error of estimate, varying from 2.5 to 3.

This error can be substantially reduced by eliminating the distance variable in equation (1). By studying ground motions at a single station, the transmission and local station transfer functions are essentially eliminated. In this procedure one is effectively looking at variations in the source, and the major variable of the source region is the yield. Second order source parameters would be depth of burial, emplacement hole, and the physical properties of the medium. Lynch (1969b) has performed a single station analysis at individual stations of PSRV data from 12 Pahute Mesa events. Figure 3 shows the results of this study for the Boxcar Event at a station in Las Vegas. Again note the dotted curves which indicate the standard error of estimate. It varies from 1.3 to 1.8, which is substantially lower than obtained from the general regression analysis, which ranged from 2.5 to 3.0.

Theoretical

Source Scaling

Concerning the source related ground motion scaling, a theoretical model and associated analysis have been developed (Mueller, 1969) which correlate observations from typical and atypical events detonated in various media.

The basic ideas are the following: (1) by considering observations at some common distant station, the transmission and station transfer functions can be conveniently eliminated, as indicated previously in the empirical studies; (2) a physically reasonable representation of the source consists of a spherically symmetric pressure function acting at an elastic radius, i.e., the radius at which the medium behaves elastically. By solving this mathematical boundary value problem and assuming from

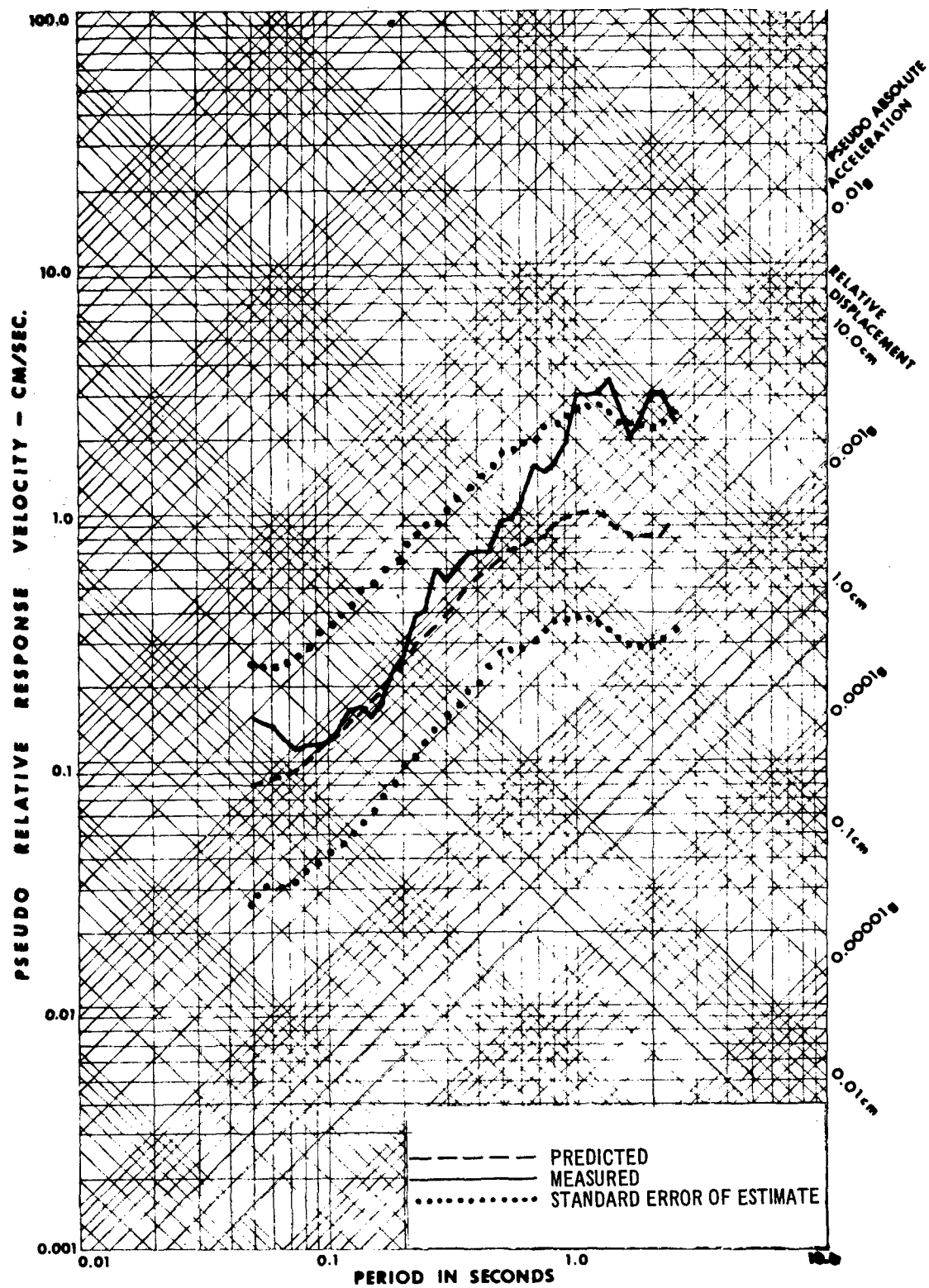


Figure 2. Comparison of Predicted and Measured PSRV Spectra,
Boxcar Event, Station SE-6, Radial Component,
Distance = 176.8 km

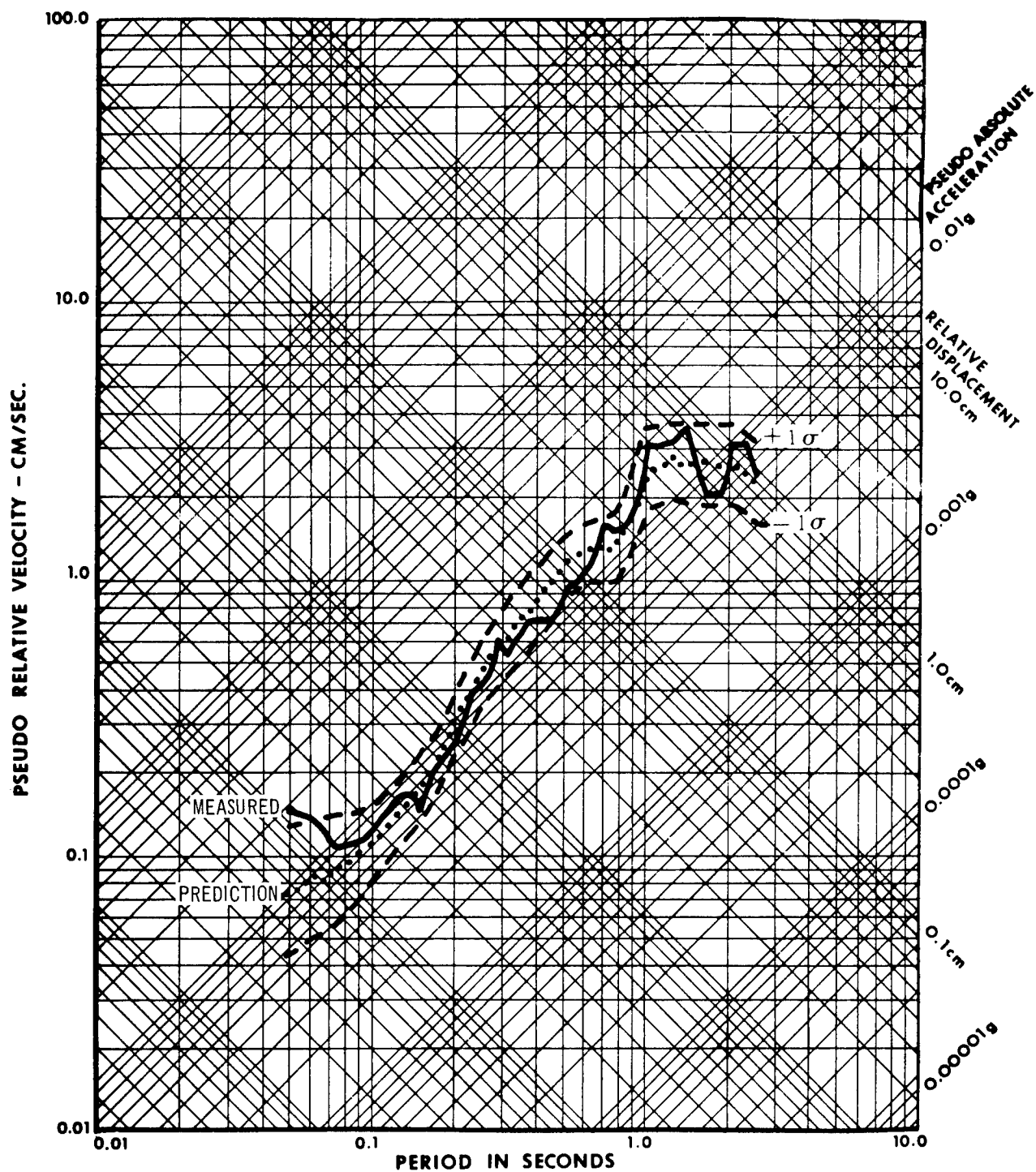


Figure 3. Comparison of Station Analysis Prediction and Measured PSRV Spectra, Boxcar Event, Station SE-6, Radial Component, Distance = 176.8 km

free-field observations a suitable forcing function, a full scaling scheme has been developed.

It is of interest to investigate the consequences of this scaling scheme for shots buried at a typical scaled depth for containment, since a large class of nuclear detonations fall into this category. A statistical determination of yield-scaling exponents from many shots, mostly in tuff, has been made (Lynch, 1969b). Figure 4 shows the resulting empirical and theoretical yield-scaling exponents. The theoretical study analytically simulated the same least squares criterion and averaging process that was utilized in the empirical study. It can be seen that the theoretically derived yield exponents are in good agreement with those obtained from the measured data. The one sigma levels of the experimental data are also shown.

Encouraged by this result, the scaling scheme is utilized on atypical events such as excavation and overburied events.

In the excavation class of events, Figure 5 shows the seismic spectrum from the Cabriole excavation event detonated in Pahute Mesa and recorded in Las Vegas--182 km away. Also shown is the contained event Knickerbocker, scaled to the same yield but at a different depth of burial. Taking into account the difference in depths of burial through the scaling scheme described here gives the dashed curve which is seen to present good agreement. Scaling to the shallower depth of burial reduces the level of motion and shifts the dominant seismic energy to lower frequencies or longer periods.

The row charge array falls into the category of excavation events. Although no theoretical model has completely explained the ground motion effects of such an event, it is of interest to look at its characteristics. In the Buggy I experiment, which consisted of five individual 1.1 kt nuclear charges separated 150 feet apart, the ground motion spectrum at Las Vegas is shown in Figure 6 (Cassity, 1969). Also shown is Cabriole scaled to an individual charge (1.1 kt and 135 feet) and Cabriole scaled to the total row charge (5.5 kt and 135 feet). It is observed that at the low frequency portion of the spectrum, Buggy I generated ground motions comparable to a single charge and at the high frequency portion it generated ground motions comparable to the total row charge. This phenomenon is also observed at other stations. The total spectrum is actually comparable to the ground motion generated by a contained single charge event of 1.1 kt, as shown in Figure 7.

A study of overburied events such as the Gasbuggy and Rulison events shows that they generate seismic motions of significantly higher frequency content and ground accelerations than normally buried events. Figure 8 shows the spectra at 80 km of the overburied off-NTS Gasbuggy Event and a typical contained NTS event at the same yield. Scaling the typical contained event spectrum for the large difference in depths of burial gives the scaled curve which is in good agreement with the observed Gasbuggy data. The dominant energy is shifted to higher frequencies which significantly affects the resulting peak

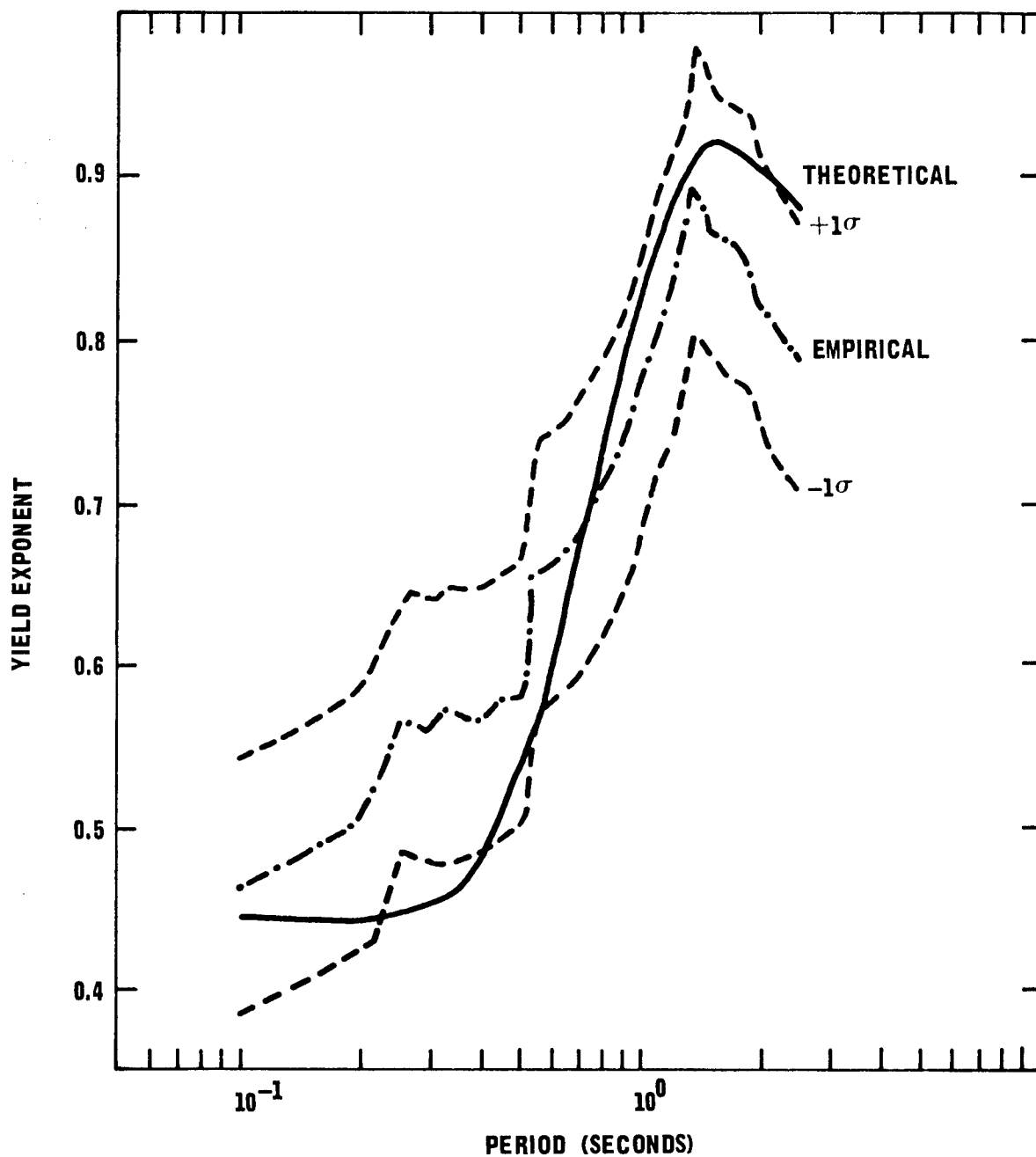


Figure 4. Comparison of Theoretical and Empirical Yield Scaling Exponents Derived from Eight Single Station PSRV Analysis

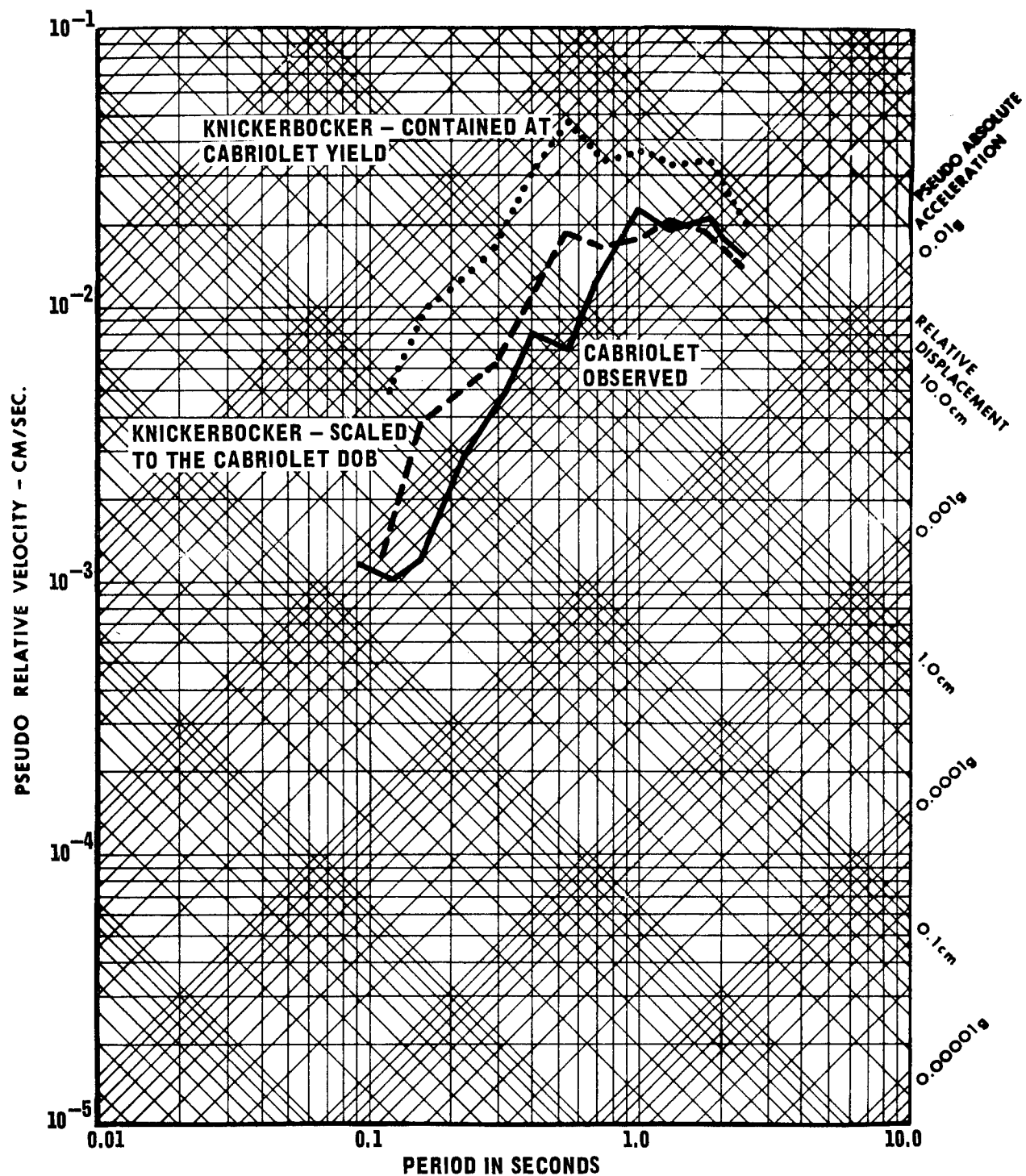


Figure 5. Comparison of PSRV from Knickerbocker and Cabriolet Events

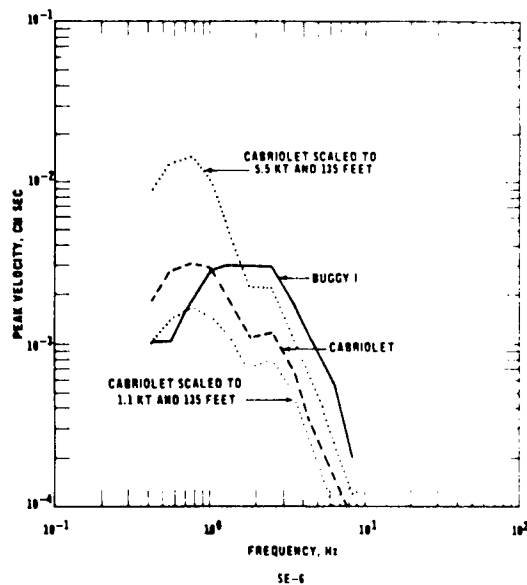


Figure 6. Comparison of Buggy I (Solid Line), Cabriolet (Dashed Line) and Scaled Cabriolet (Dotted Line) BPF Curves

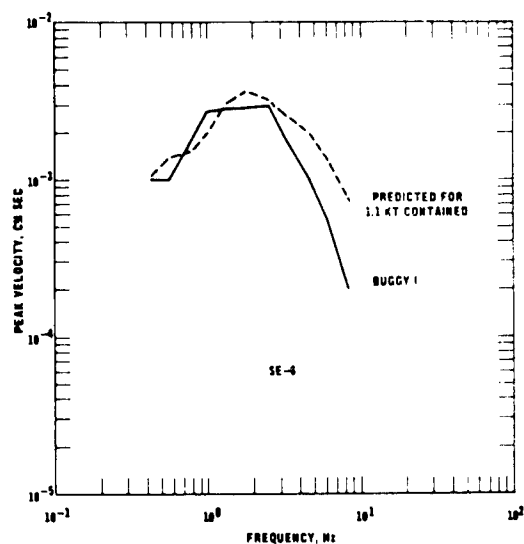


Figure 7. Comparison of Observed Buggy I BPF Curves with BPF Predictions for a 1.1 kt Single-Contained Event, Stations SE-6 and Tonopah Church

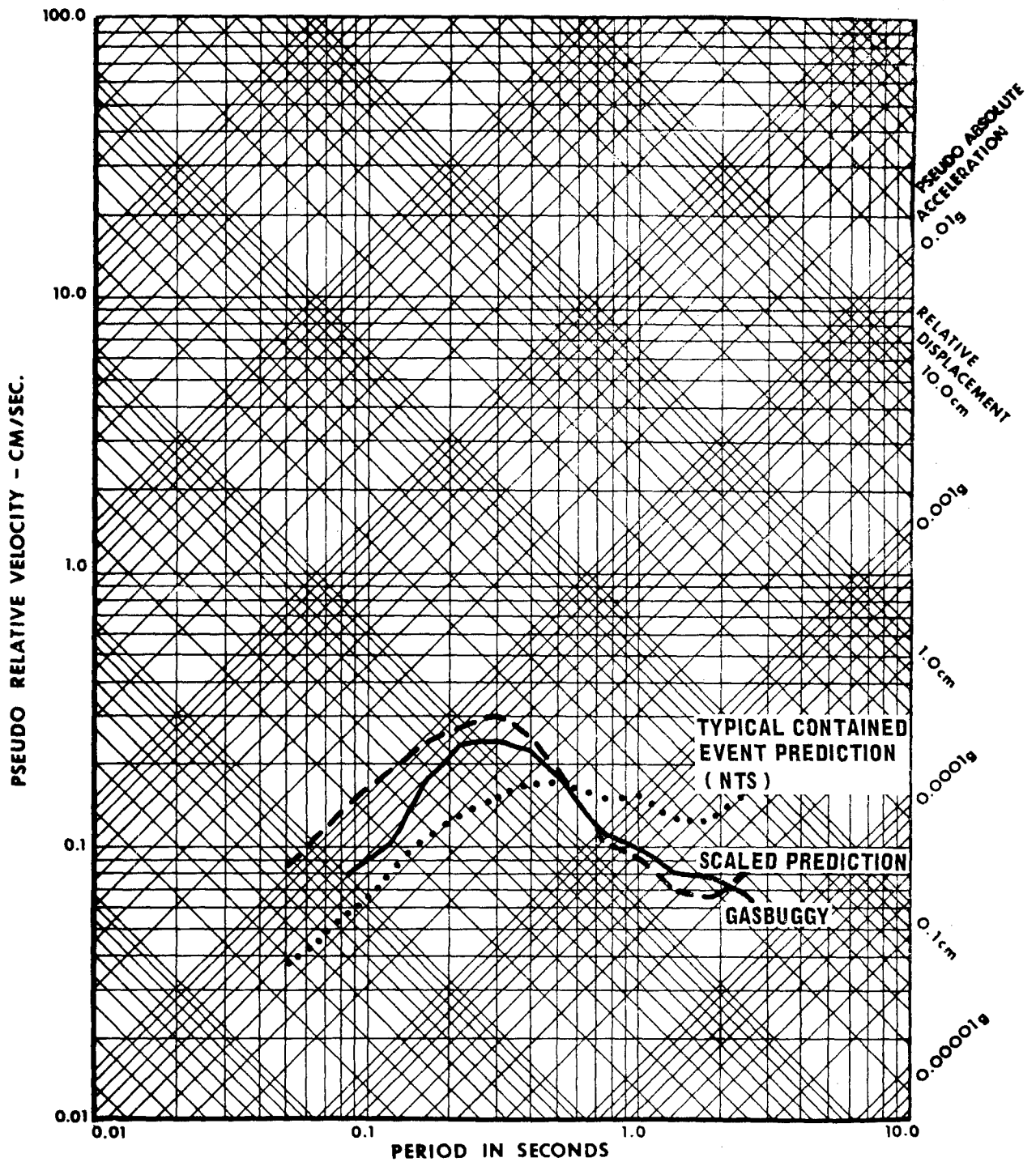


Figure 8. Comparison of Gasbuggy (26 kt) and Predicted PSRV (5% Damping) at 80 km

accelerations. Figure 9 displays peak accelerations from the Gasbuggy Event and a typical contained event at the same yield. Gasbuggy at 26 kt generated peak particle accelerations comparable to a typical contained event of 200 kt. Scaling for depth of burial gives the scaled prediction.

Distance Scaling

As is well known in seismology, higher frequency waves attenuate more rapidly than lower frequency waves. Lynch (1969a), as previously indicated, has performed a general regression analysis on seismic motion which shows that one cycle motion attenuates with a distance exponent of about -1.0 while ten cycle motion attenuates at about -1.6. Beaudet (1970) used a heterogeneous model of the earth to explain this phenomenon. In this model the Lamé constants and the density are considered to have random fluctuations. A correlation length, characteristic of the heterogeneous medium, enters into the model. The problem is essentially a scattering problem with the correlation length controlling the phenomena. For wavelengths large compared to the correlation length, the medium "appears" homogeneous. However, for wavelengths comparable to the correlation length, a significant amount of scattering occurs which is frequency dependent. From the experimental data cited above, an estimation of 215 meters for the correlation length is made. Figure 10 shows the agreement between theory and experiment in the frequency range applicable.

Station Response

In determining the response at a particular location, the local geology underlying the station must be taken into account. It is found that alluvial layers with significantly different elastic constants than the underlying hard rock will give rise to amplification effects.

A specific example of this effect is demonstrated in Figure 11. The site is Tonopah and the curves indicate the observed and theoretically calculated amplification factors as a function of frequency for shear horizontal waves. The single layer model is also shown in the figure. The theoretical infinite layer and finite element models give good agreement to the observed data in the frequency range of interest. Computational errors arise in the finite element model at low frequencies, producing the erroneously high amplification factor in this portion of the spectrum.

It is quite clear, therefore, that local geology effects must be accounted for in making adequate ground motion predictions. For example, in the Rulison Event refraction surveys were conducted to determine underlying layers that were subsequently used in the theoretical amplification model for prediction purposes.

Finally, given the input ground motion, structural amplification response may be simulated by a number of models. The finite element code represents a powerful tool and is

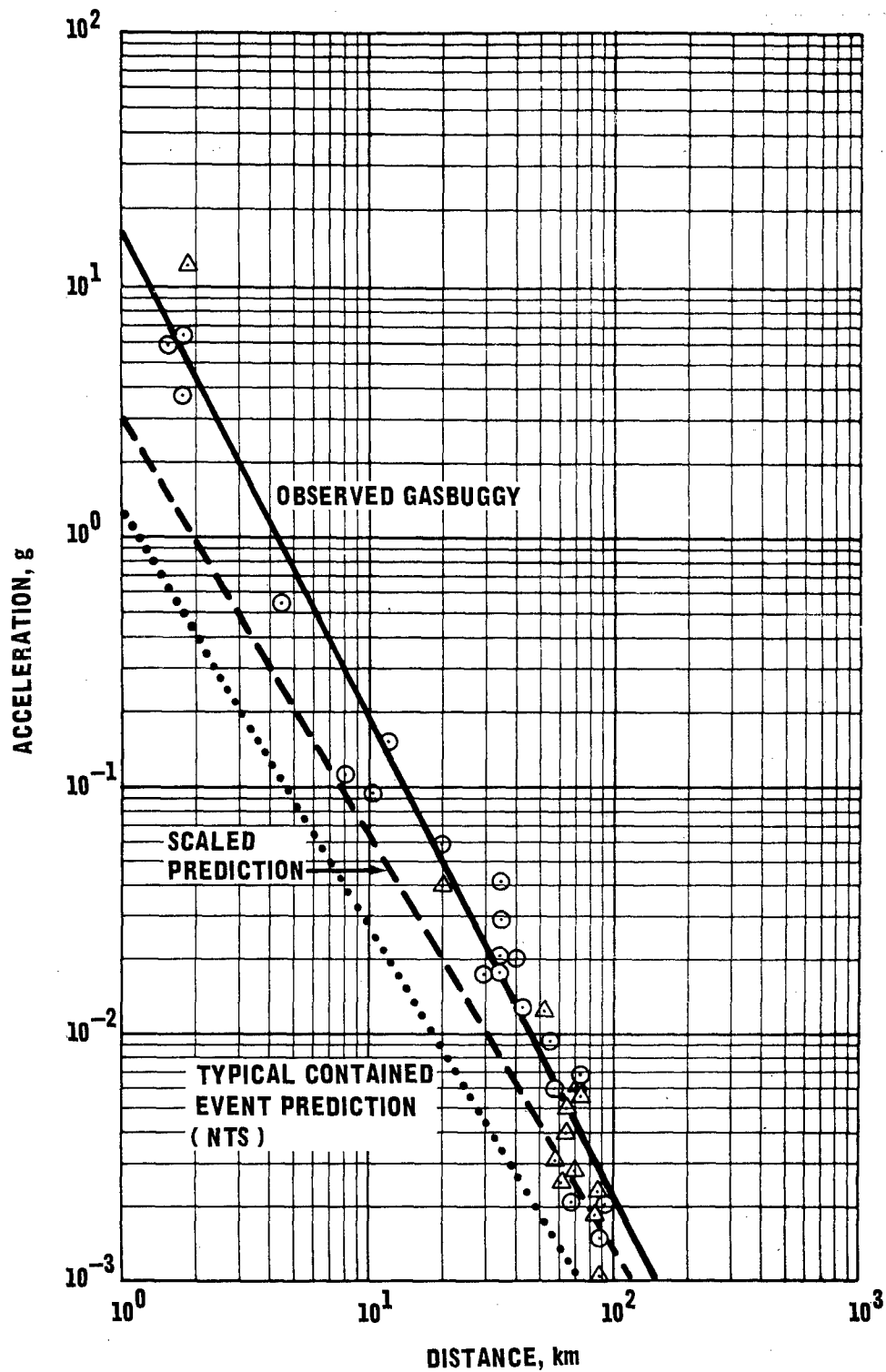


Figure 9. Comparison of Observed Gasbuggy and Predicted Peak Particle Accelerations

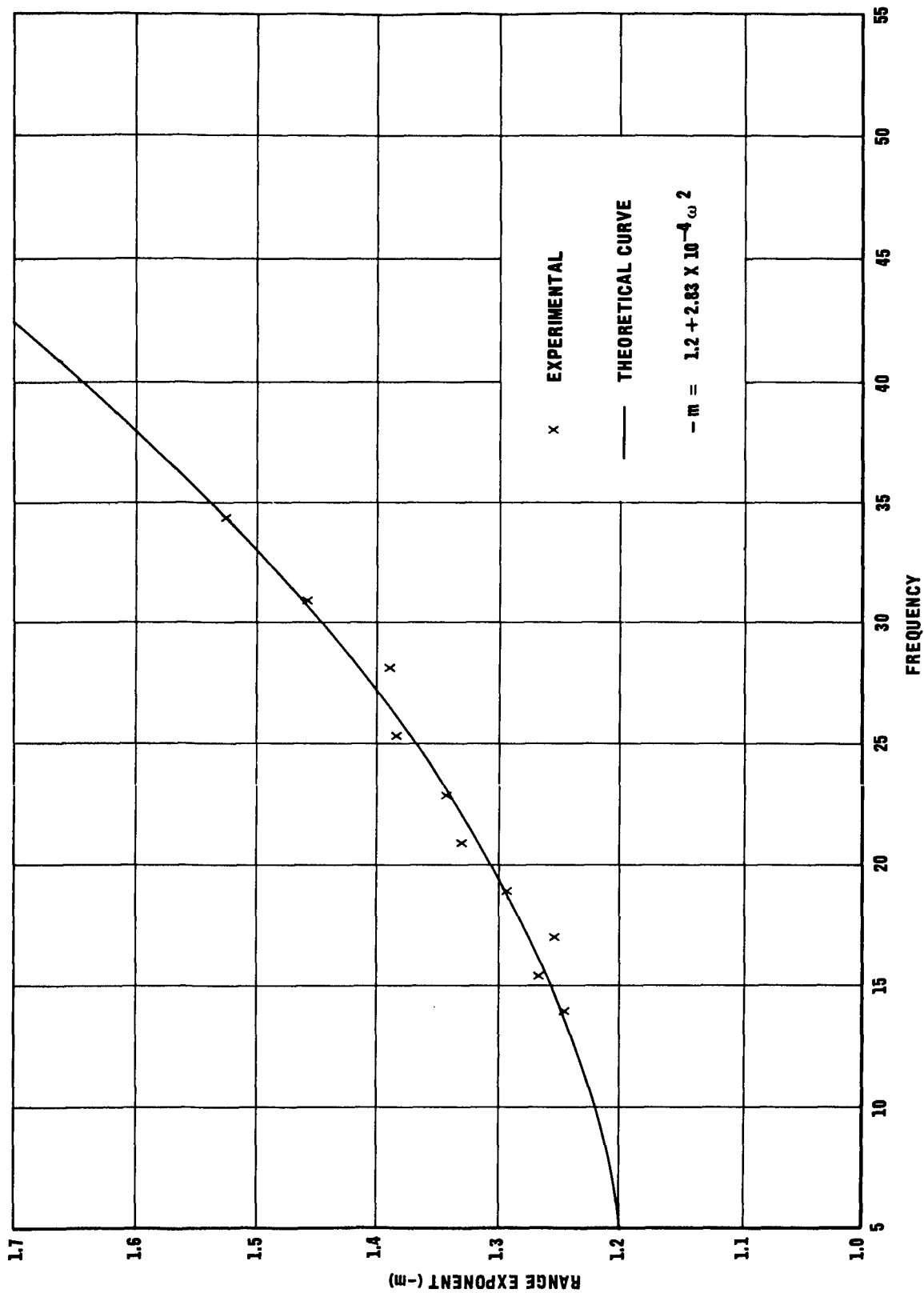


Figure 10. Range Exponent versus Frequency (Angular)

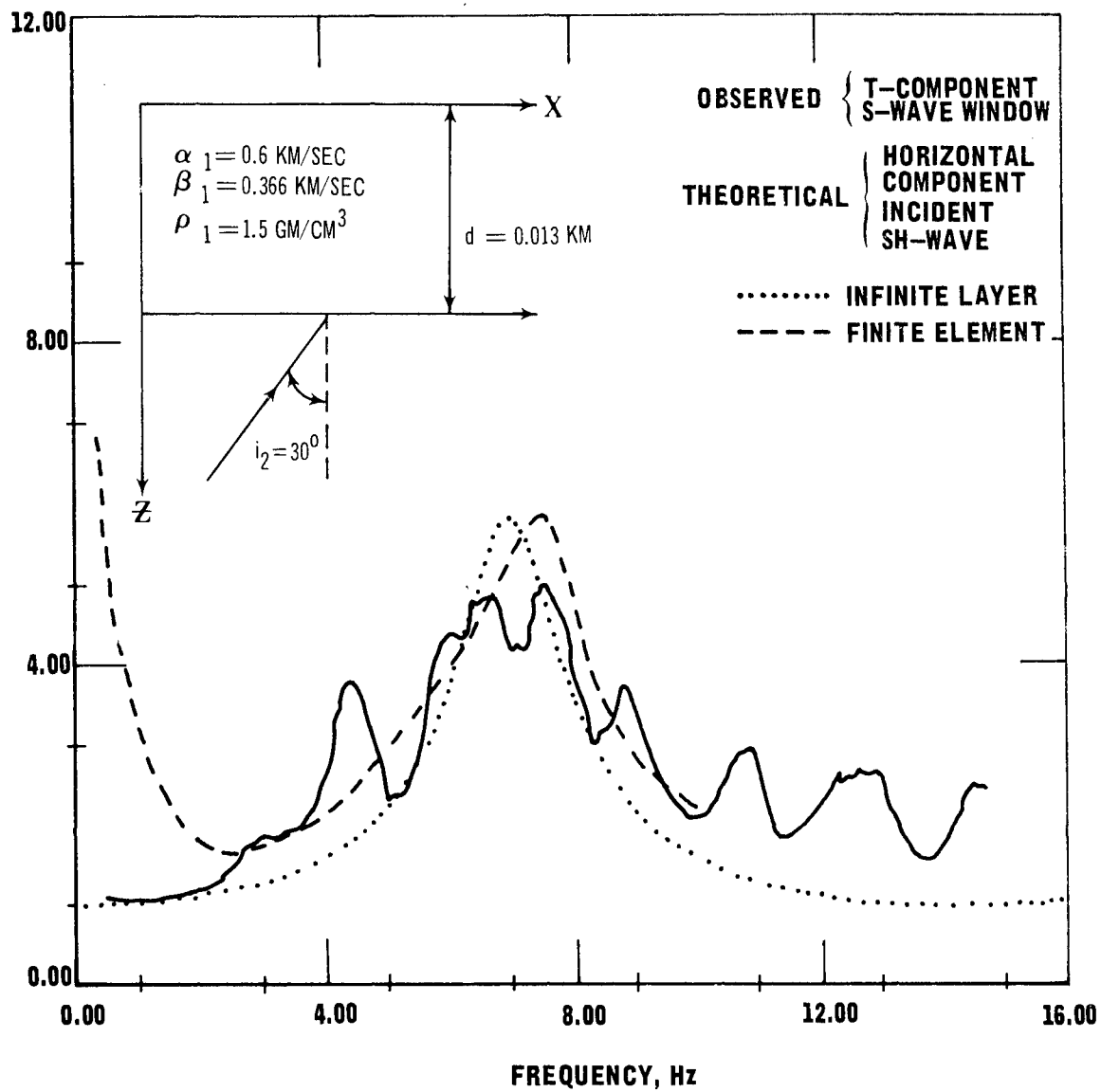
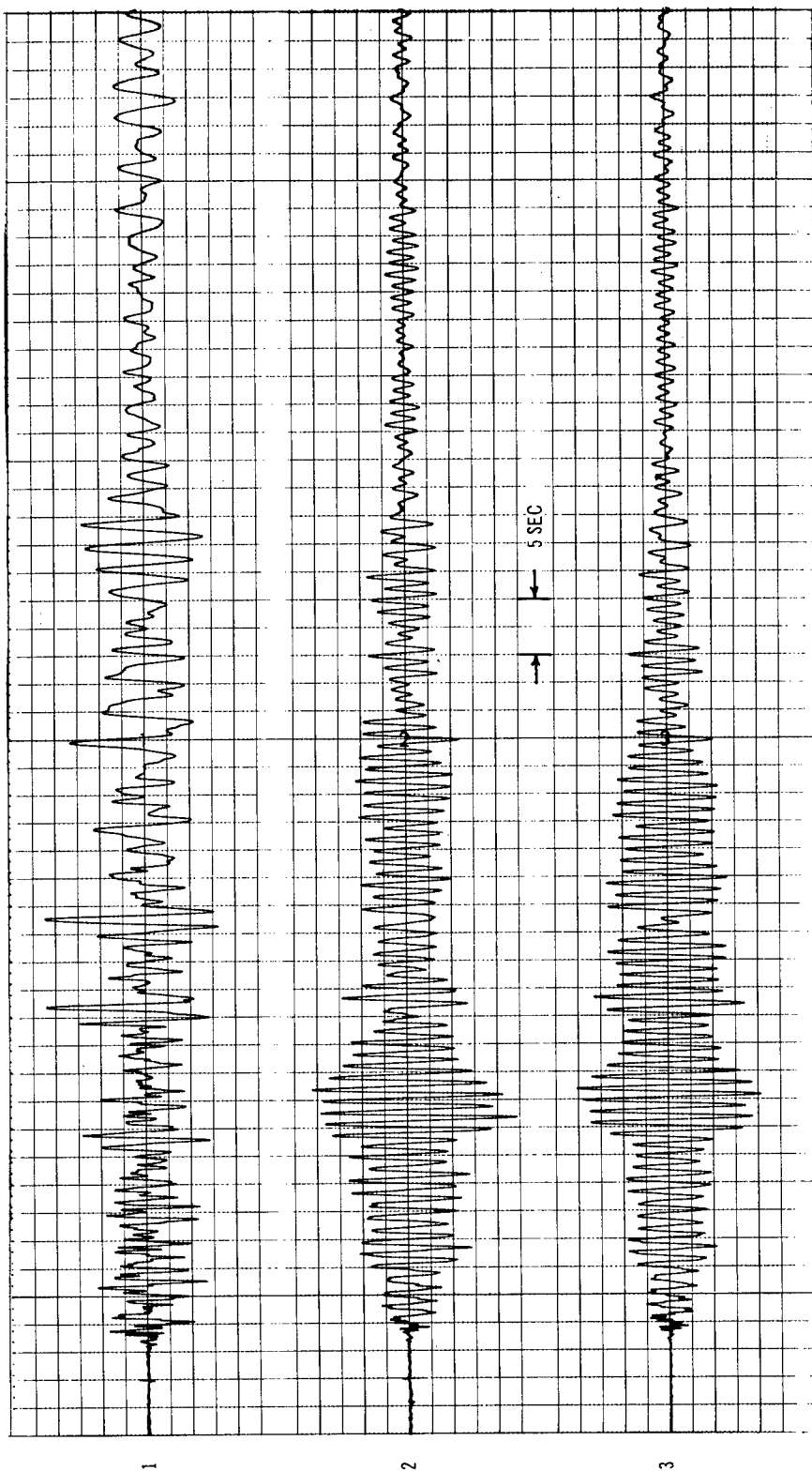


Figure 11. Tonopah Amplification Factor (T Component, S-Wave Window)

presently under development. Lynch (1965) found that the dynamic response of top level high-rise structures, such as found in Las Vegas, may be simulated on an analog computer by the linear superposition of two transfer functions. Upon examination of individual top level seismograms from five high-rise structures, the presence of two well-defined oscillatory wave trains was indicated--a dominant low frequency contribution and a minor high frequency contribution. Figure 12 shows the result of simulating a high-rise structure in Las Vegas by this double transfer function to ground motions induced by the Halfbeak event.

In conclusion, all of the studies and techniques outlined in this paper are utilized in present ground motion predictions. As indicated, special considerations and studies must and have been given to atypical events such as overburied events, single charge excavation events, and multiple row charge events.



- 1 BASE VELOCITY, v
- 2 TOP VELOCITY, v_T
- 3 SIMULATED TOP VELOCITY, v_T

EVENT	HALFBEAK	COMPONENT	L

Figure 12. Example of Simulation

REFERENCES

- Beaudet, P.R., 1970, Elastic Wave Propagation in Heterogeneous Media, Environmental Research Corporation, NVO-1163-202, AEC.
- Davis, A.H., and Murphy, J.R., 1967, Amplification of Seismic Body Waves by Low Velocity Surface Layers, Environmental Research Corporation, NVO-1163-130, AEC.
- Lynch, R.D., 1965, Analog Computer Study of Building Response to Ground Motion, Environmental Research Corporation, NVO-1163-67, AEC.
- Lynch, R.D., 1969a, Response Spectra for Pahute Mesa Nuclear Events, BSSA59, 2295-2309.
- Lynch, R.D., 1969b, Single Station Analysis of PSRV Data from Pahute Mesa Events, Environmental Research Corporation, NVO-1163-TM-14, AEC.
- Mueller, R.A., and Murphy, J.R., 1970, Seismic Spectrum Scaling of Underground Detonations, Environmental Research Corporation, NVO-1163-195, AEC.
- Murphy, J.R., and Lahoud, J.A., 1969, Analysis of Seismic Amplitudes from Underground Nuclear Explosions, BSSA59, 2325-2341.

ABSTRACT

SEISMIC MOTIONS FROM PROJECT RULISON

by

P. C. Loux

In the range from a few to a few hundred km, seismic measurements from the Rulison event are shown and compared with experimentally and analytically derived pre-event estimates. Seismograms, peak accelerations, and response spectra are given along with a description of the associated geologic environment.

Techniques used for the pre-event estimates are identified with emphasis on supportive data and on Rulison results. Of particular interest is the close-in seismic frequency content which is expected to contain stronger high frequency components. This higher frequency content translates into stronger accelerations within the first tens of km, which in turn affect safety preparations.

Additionally, the local geologic structure at nearby population centers must be considered. Pre-event reverse profile refraction surveys are used to delineate the geology at Rifle, Rulison, Grand Valley, and other sites. The geologic parameters are then used as input to seismic amplification models which deliver estimates of local resonant frequencies. Prediction of such resonances allows improved safety assurance against seismic effects hazards.

SEISMIC MOTIONS FROM PROJECT RULISON

Peter C. Loux, Associate Technical Director
Environmental Research Corporation

Introduction

Environmental Research Corporation provides scientific and engineering support to AEC's nuclear test program by predicting seismic motions from nuclear detonations. Predicting the motions for Rulison, the second Plowshare gas stimulation experiment, is one example of such support which we shall explore here.

Directly induced nuclear generated ground motions are strongly dependent on several factors: device energy release, source medium, device depth of burial, distance to the observation point, geology surrounding the observation point and geologic and geophysical parameters between the device and the area of interest.* Current ground motion predictive technology quantitatively accounts for all these factors except the last one--the transmission path geology. Although studies to delineate the effect of the parameter are in progress, the problem remains that even if this structure is known, satisfactory models are not always available to describe the detailed effect on the seismic motion.

Accurate prediction of the ground motion is imperative, because associated seismic hazards may well limit future Plowshare activity. We will have to assess accurately the probability of damage to property and certainly preclude the possibility of personal injury.

After a brief geographical, geological, and seismic instrument orientation, I propose to complete this presentation by showing you Rulison seismic data compared with pre-event estimates. Then we can explore methodology used for making estimates, and touch on the question of future seismic predictions for the Rulison area.

The first slide (Figure 1) shows the location of the seismic stations operated by the U.S. Coast & Geodetic Survey. Station locations were chosen for safety documentation, seismic wave propagation studies in this type of environment, and for calibration data for future Plowshare activity in this area. Generally, radial, vertical, and transverse components of ground velocity as a function of time were recorded at some 36 sites; with acceleration and displacement subsequently derived from these data. I believe it fair to summarize that USC&GS did a tremendous job in obtaining the seismograms.

*See References 1, 2, 3, 4, 5, and 6.

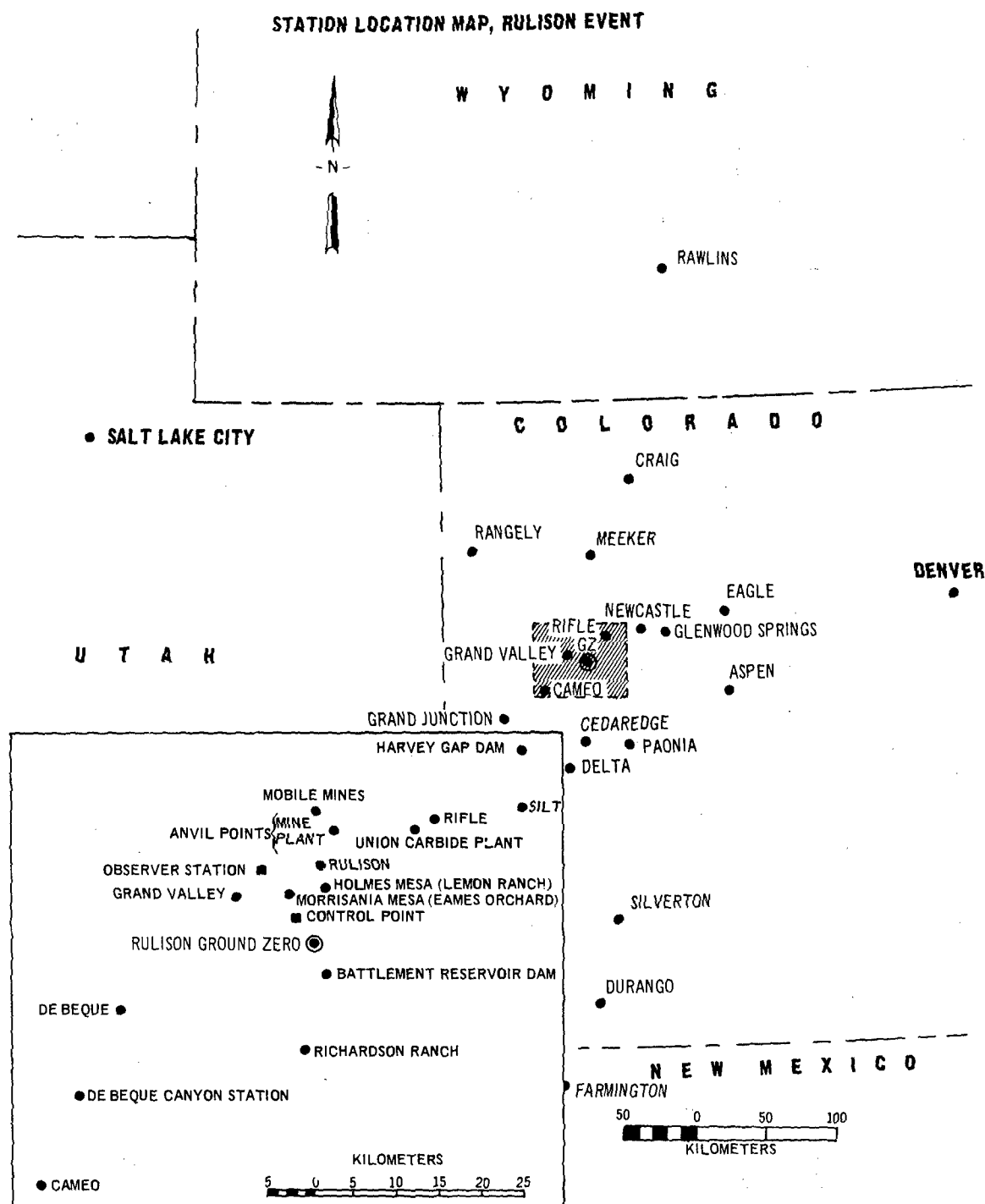


Figure 1. Station Location Map, Rulison Event

The insert in this map shows the emphasis on seismic instrumentation within the first 25 km or so. Of particular interest are the populated areas such as Grand Valley, Rulison, and local home sites, as well as industrial sites and earth structures.

The device was fired at a depth of some 8400 ft. in the Rulison gas field of the Piceance Creek Basin. With the seismic motions in mind, I would like to highlight the fact that this Basin is geologically comparable to the San Juan Basin of New Mexico where a similar experiment, called "Gasbuggy" was performed. Essentially flat-lying beds of shales, siltstones, and sandstones predominate in the geologic columns at both sites. As we shall see in a moment, this similarity in source medium and geology was one factor utilized for the Rulison ground motion predictions.

Data and Predictions

Let's now look at some of the Rulison seismic data. The next slide (Figure 2) depicts the seismic motion measured in the town of Rulison. Shown are the radial, transverse, and vertical components of surface motion, as a function of time. At the bottom of the figure we see the amplitude as a function of time of the instantaneous vector amplitude. From this curve you will note that the peak motion is 7/10 g; in the three following slides we will be discussing peak motion defined in this manner.

A conspicuous feature at the Rulison station is the strong 0.07 second vertical motion (with a wave velocity of about 5.5 km/sec) at the beginning of the trace, as compared with the horizontal-radial component. Other identifiable waves are seen at the right side of the figure. Appearing on the radial and vertical traces is a 0.15 to 0.2 second Rayleigh (surface) wave whose velocity is in the order of 2 km/sec. At the same time, on the transverse trace, is either a love or a horizontal (SH) shear wave. We note that this SH wave appears to be rather large, recalling our expectation that the nuclear source ought primarily to generate compressional waves. Coincidentally, this same phenomenon has recently come under study at the Nevada Test Site, where we are investigating physical mechanisms that might be generating the shear motion.

We will also be concerned with the seismic frequency content, because of its potential effect on structures such as houses, and other buildings, industrial plants, dams, etc. When we later view the response spectrum for each of these seismograms, we will be particularly interested in spectral peaks that may occur at resonant frequencies of nearby structures.

Recalling that the peak motion will be defined as the peak of the vector trace, let's look at Rulison peak motions as a function of distance from the detonation. May I have the next slide, please. (Figure 3.) Ignoring the solid lines for a moment, we have the vector displacement peaks (circled points) plotted as a function of the straight line, or slant, distance from the shot point. The first observation is the rather well behaved decrease in amplitude, that is attenuation, with distance.

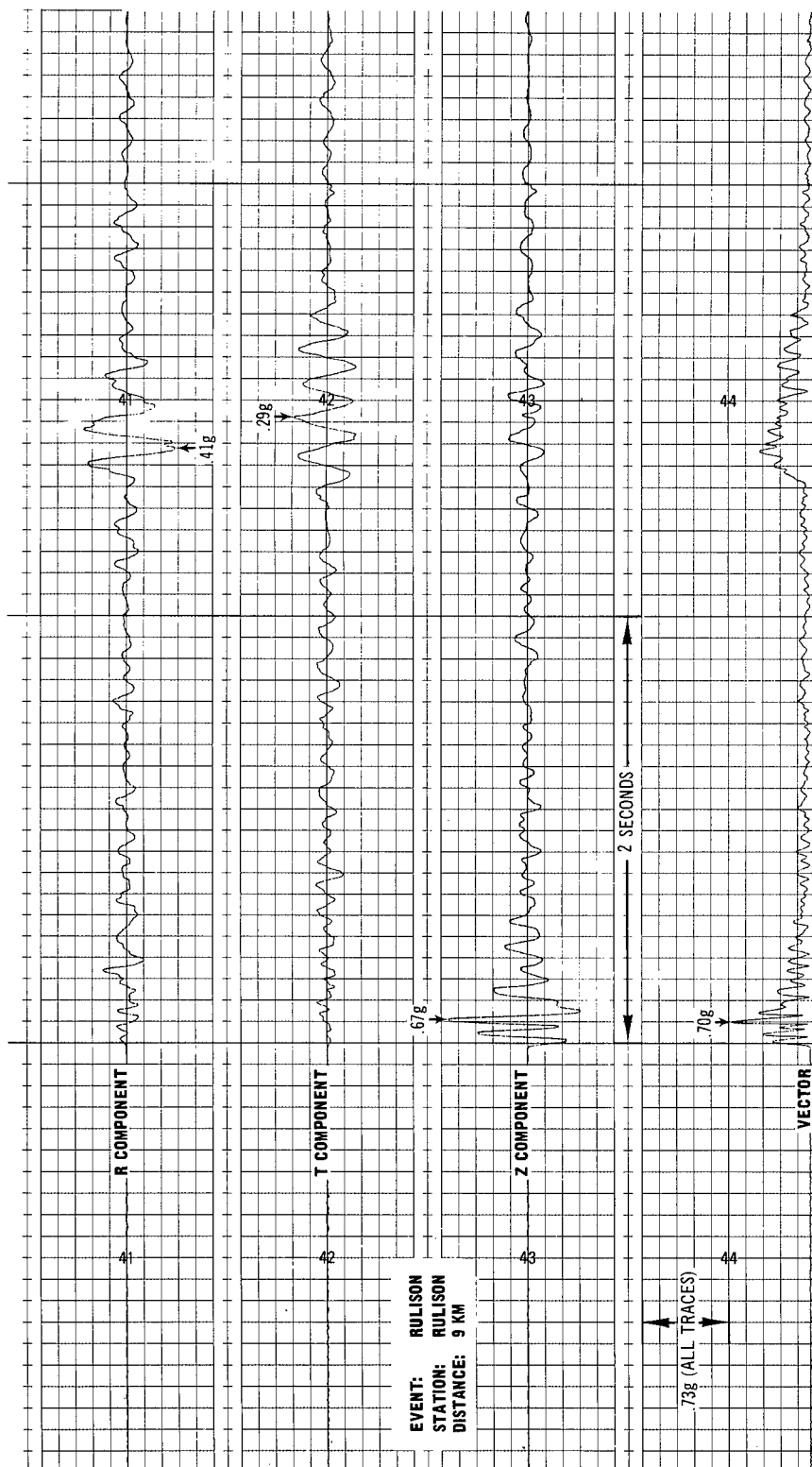


Figure 2. Rulison Station Seismogram

Those familiar with seismic motions know that this is often not the case, so that for Plowshare activity in particular, one has to be concerned with accurate prediction of amplitudes that depart on the high side of the average behavior. This average behavior is shown by the solid line labelled "observed data." For comparison we show the line labelled "40 kt NTS experience," which represents the average attenuation observed from over 95 experiments at the Nevada Test Site.⁵ Compared with both the observed Rulison data and our NTS experience is the third line, called the "prediction." You will immediately see that the prediction is apparently not based on the average NTS experience. As a matter of fact it is based on the seismic data from the Gasbuggy Event. Briefly, the rationale for this is the unusual behavior of the Gasbuggy seismic data compared with our NTS experience, and also the similarity of the Gasbuggy and Rulison geologic environment. We shall see in a moment that unusual behavior appears in the velocity and acceleration data, and that Dr. Mueller's depth of burial and medium scaling analysis offers a good explanation.¹

The next slide (Figure 4) shows the same type of information for the velocity peak amplitudes as a function of distance. Again, the prediction agrees quite well with the observed data, but for the velocities, we now see a significant departure from NTS experience with serious implications if NTS experience alone were used for the predictions. Assuming roughly that the energy in the seismogram is proportional to the peak velocity squared (not necessarily true) there would have been 25 times as much energy incident on structures at 10 km than would be predicted from NTS experience (from Figure 4, at 10 km the measured peak velocity is 5 times the NTS experience). A miscalculation in the damage assessment, such as this would cause, could have a permanently damaging influence on Plowshare activity.

On the next slide are shown the Rulison accelerations as a function of distance; again, good agreement between observed data and the prediction is obtained. The departure of the observed data from NTS experience is even more pronounced here than for the velocities. For example, at 10 km the measured acceleration is about 8 times higher than would have been estimated from NTS experience. Another way of expressing this is to note that the NTS yield that would have produced this acceleration (0.4 g) at 10 km, is not 40 kt but rather more than 1000 kt!

As indicated by Dr. Mueller in the preceding talk,¹ the predominant factors causing this departure from NTS experience, are the large depth of burial for Rulison, and the shale, siltstone geologic source environment. The effect of the large depth of burial is to enrich the high frequency seismic motion, a situation which finds expression in higher velocities and still higher accelerations. Sponsors of underground engineering applications (deep burial) will have to be concerned with high acceleration, especially at locations within the first 5 or 10 miles from the source, because of potential hazards to people and property. For cratering applications, no special problems arise, in that Mueller's theory predicts lower seismic amplitudes (attended by a shift toward lower frequencies) than are experienced from fully contained shots.

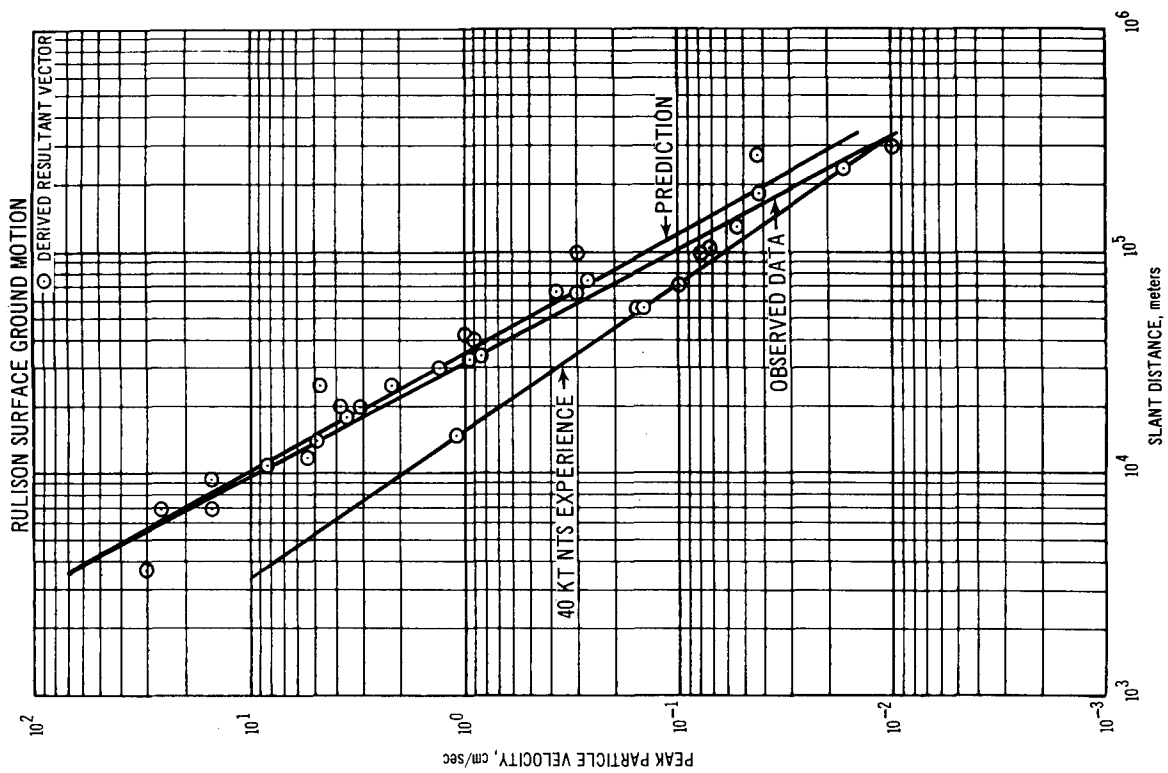


Figure 3. Observed Peak Particle Resultant Vector Displacement

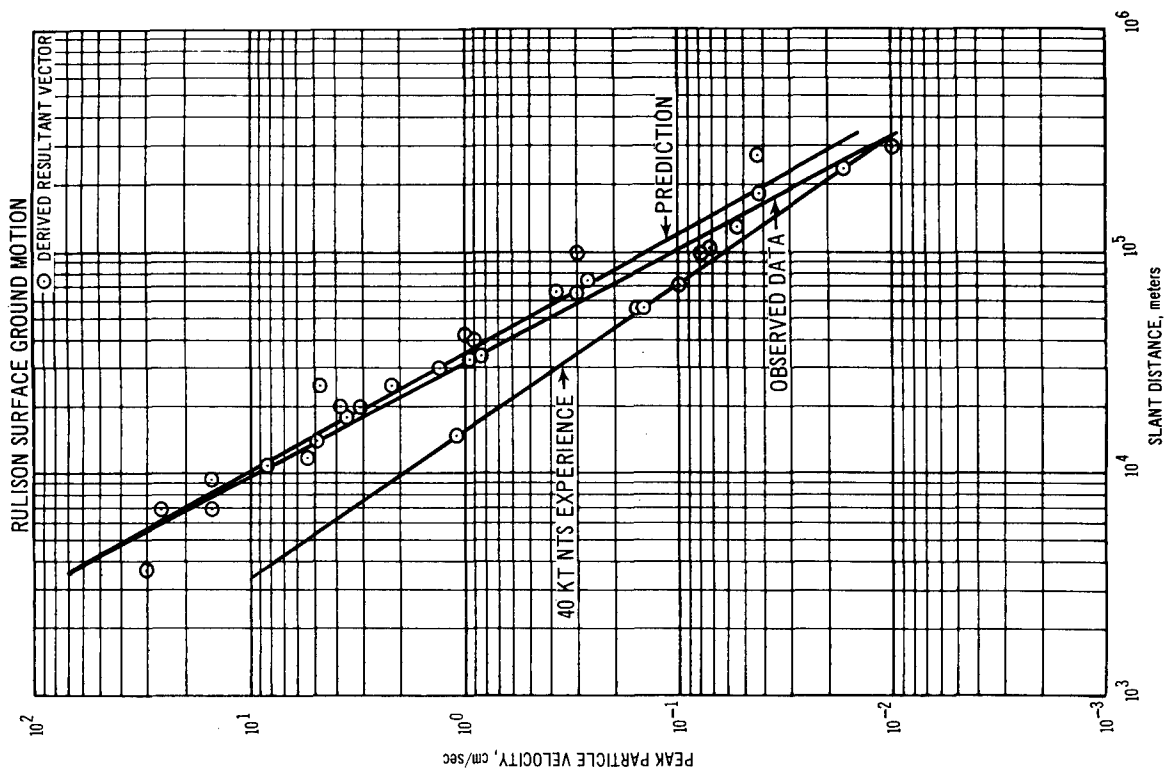


Figure 4. Observed Peak Particle Resultant Vector Velocity

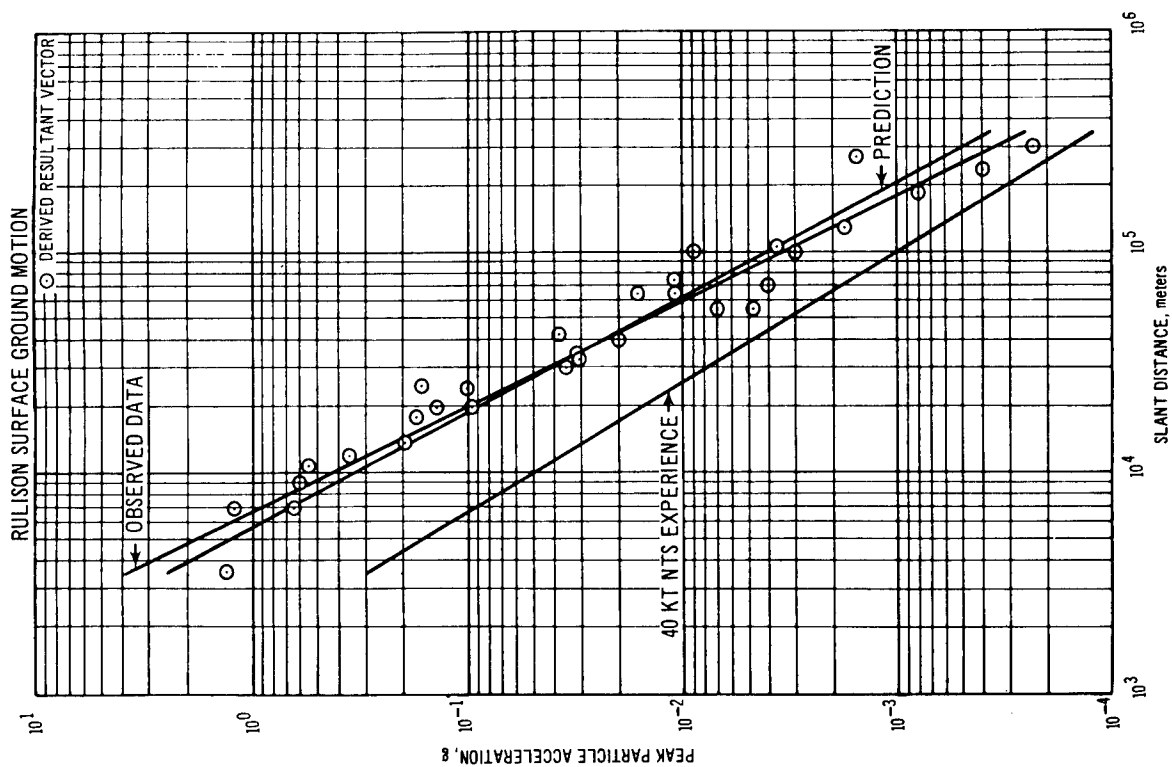


Figure 5. Observed Peak Particle Resultant Vector Acceleration

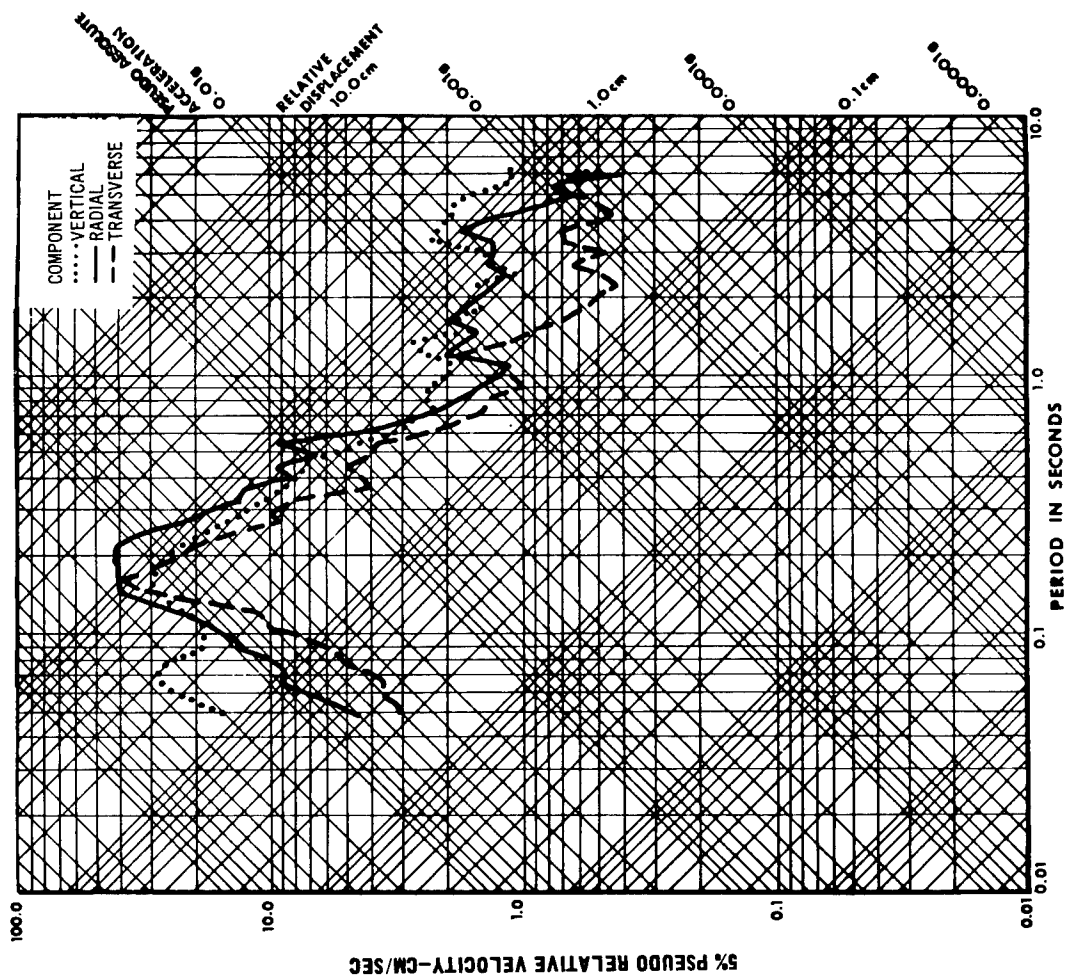


Figure 6. Station Rulison, Distance 9 km

Next slide please (Figure 6). As promised earlier, here are the response spectra for the Rulison station radial, transverse, and vertical seismograms shown in an earlier slide (Figure 2). Each spectrum represents the approximate velocity response of a simple, damped oscillator to the seismogram, as a function of the resonant period of the oscillator. In this case, the oscillator is damped at 5%. For those familiar with frequency domain representations of time histories (such as seismograms), the response spectrum turns out to be similar to the Fourier amplitude spectrum of the seismogram. The utility of the response spectrum lies in its analogy with the response of real structures to the ground motion. I'm sure that in a following paper, Dr. Blume will explore this point in more detail.

On the vertical component spectrum we see a spectral peak at about 0.07 seconds, caused by the strong primary wave on the vertical seismogram viewed earlier. The remaining predominant energy in the seismograms is contained in the surface wave motion (Rayleigh and SH) and this is evidenced by the spectral peaks in the neighborhood of 0.17 seconds.

I would now like to turn your attention to the prediction of the response spectrum for a few of the important locations in the vicinity of the Rulison experiment. The next slide (Figure 7) compares observed and predicted spectra, with the predicted spectrum based on the Gasbuggy Event spectra, depth of burial correction and also on estimates of seismic amplification caused by impedance contrasts in the near-surface geologic layering. The amplification is computed from analytical models describing seismic wave propagation through the layered system, underlying the station. Input parameters for the model, namely layer thicknesses and seismic velocities, were determined from standard reverse profile refraction surveys.

Also shown in this figure is the spectrum that would be expected on the basis of average Nevada Test Site (NTS) experience,³ noticeably different from the Gasbuggy and Rulison data. In subsequent slides you will see that the prediction accuracy for the Rulison Event improved with distance. After the fact, we are now in a position to improve the close-in spectral predictions, in general, and in particular for this Rulison area. We can expect to be able to predict this shift in spectral period (in this case from 0.25 second to less than 0.2 seconds) as well as the higher amplitude (40 cm/sec versus 20 cm/sec) of the response spectrum peak. Indeed, further scrutiny of the Gasbuggy, Rulison, and other data should lead to explanation of this close-in seismic behavior which, until now, has not required careful study for safety purposes.

The next slide (Figure 8) gives the comparison for the town of Grand Valley, about 11 km from the source. Again the prediction of the spectral peak is within a factor of two for both the period and the amplitude of the peak.

In the next slide (Figure 9) the same type of information is shown for a station at Rifle, this time with very satisfactory agreement between the observed and predicted spectrum. We mentioned earlier that seismic amplification caused by near-surface

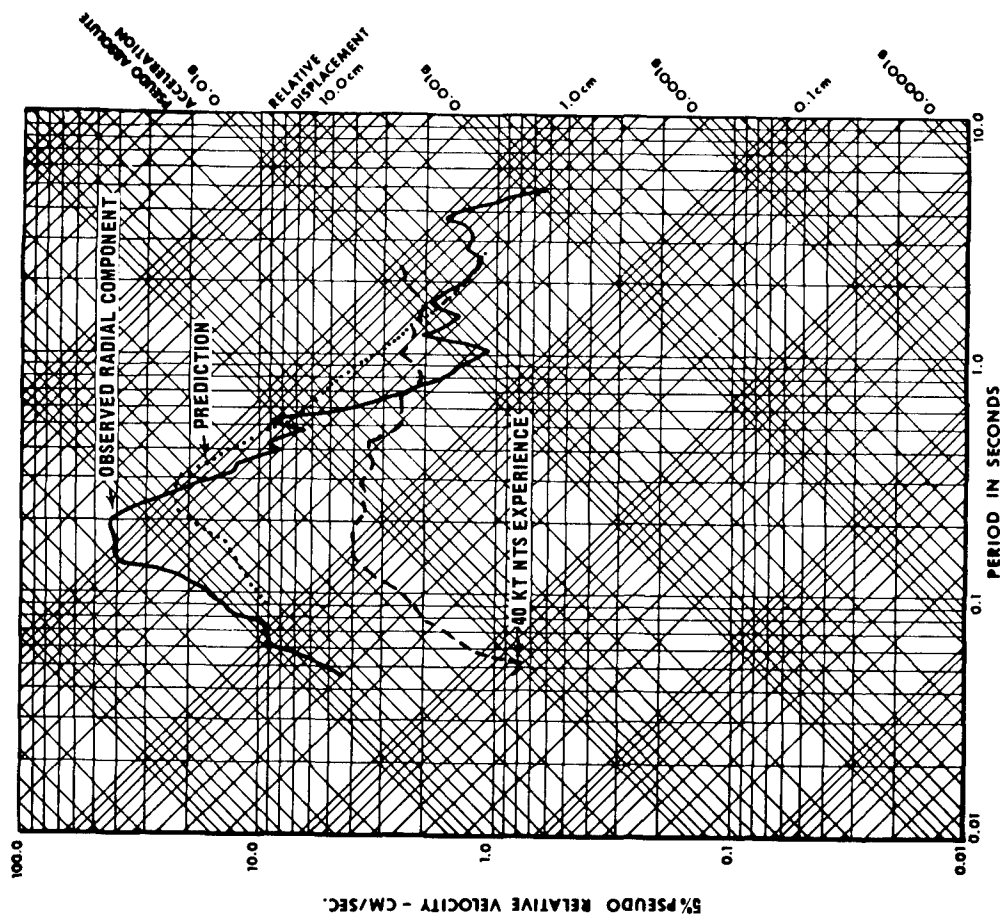


Figure 7. Response Spectra, Station Rulison, Distance 9 km

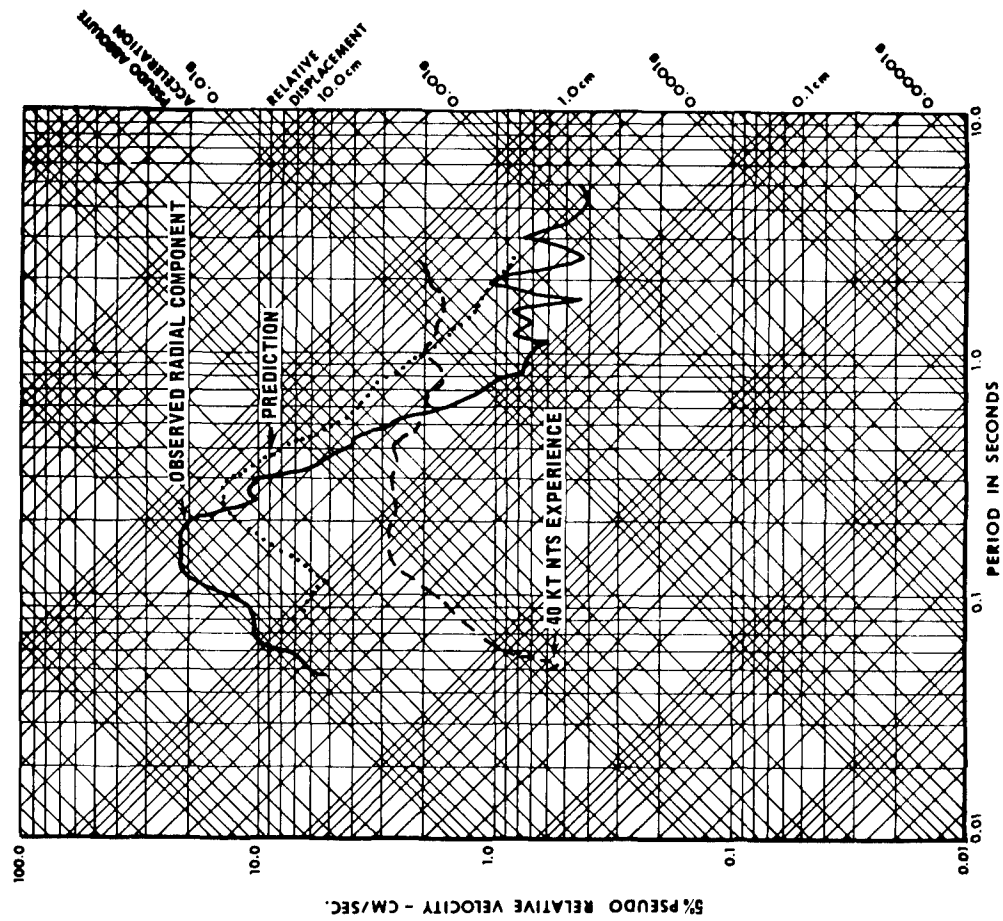


Figure 8. Response Spectra, Grand Valley, Distance 11 km

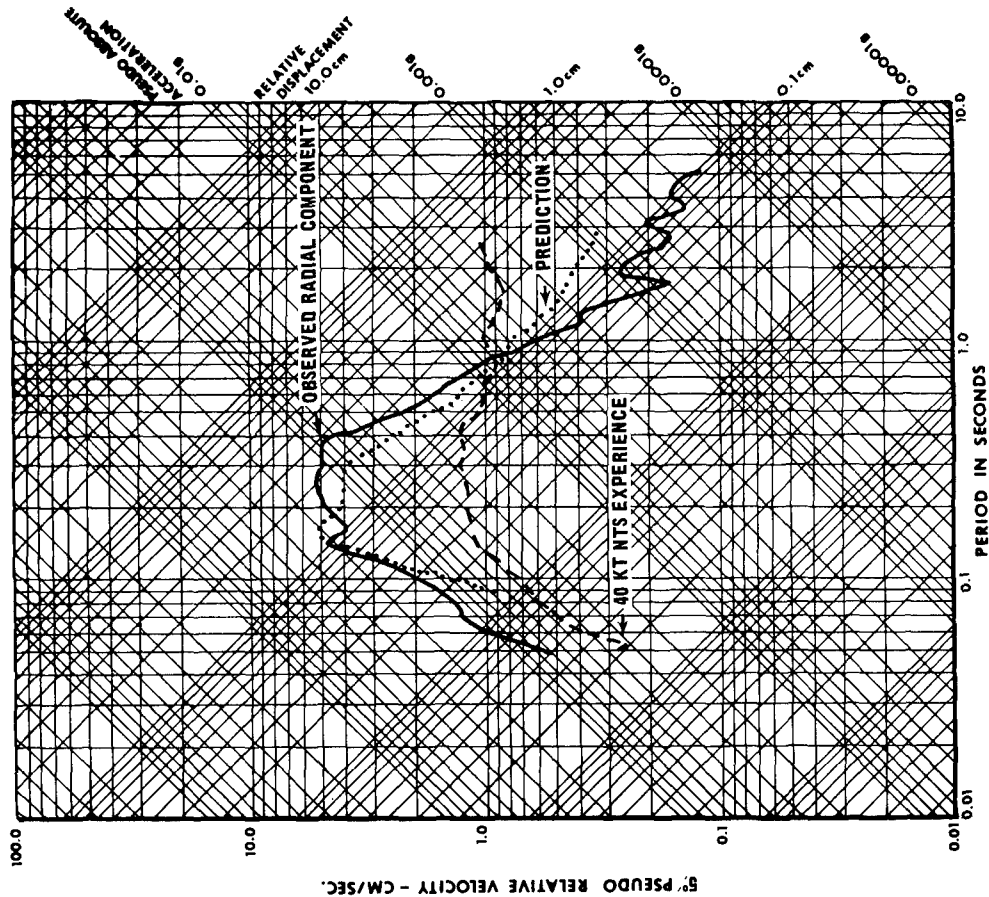


Figure 9. Response Spectra, Rifle (Top of Hill), Distance 20 km

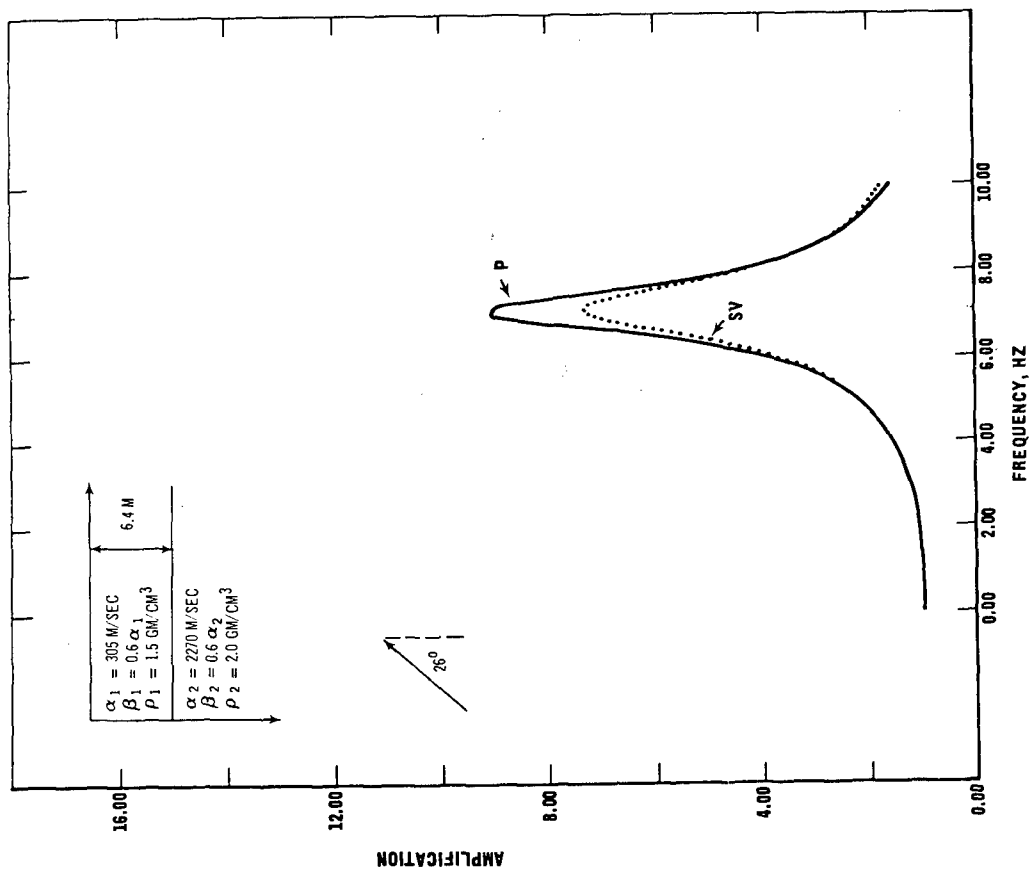


Figure 10. Horizontal Amplification versus Frequency, Rifle

layering was taken into account in the prediction of the response spectrum. To give you a feel for the amount of spectrum change caused by the station amplification we can look at the amplification correction curve for Rifle. Next slide please (Figure 10).

The layer thicknesses and elastic constants determined by a refraction survey are shown in the upper part of the figure. Using this information, the amplification computer models for compressional (P) and shear vertical (SV) waves deliver spectral amplifications that peak at about 0.14 second period (7 Hz). That this seismic amplification actually occurred is evident in the successful prediction of the response spectrum at this site.

In the next slide (Figure 11) we have the computed station resonance for the base of Harvey Gap Dam. This resonance enhances the response spectrum in the 0.1 to 0.16 period range (10 Hz to 6 Hz), and we can see that this is the case in the next slide (Figure 12). Our prediction is slightly higher than the observed data in this period range (0.1 to 0.16 sec), but it would have been significantly lower than the observed data without the station amplification correction.

Summary

Predicted seismic peak amplitudes and response spectra from the Rulison experiment are well verified by the observed data. Future seismic predictions for this area can be expected to be very accurate for single detonations of larger yield nuclear devices, with the provision that nuclear yield, shot depth of burial and geologic medium, site amplification effects and the close-in behavior of the (Gasbuggy and) Rulison data are all taken into account. Accurate estimates of seismic hazards are then possible.

Two additional points might be mentioned in connection with the ground motions from future detonations in this area. The first is the question of the reliability of the seismic prediction especially as it enters estimates of damage to structures. Much of the associated analysis that I, and Dr. Mueller in more detail, have touched upon, is performed on a statistical basis that includes a measure of the seismic data scatter. For a rough idea of the behavior of the data to be anticipated at Rulison sites, with the condition that the factors we have discussed are taken into account, one can expect seismic prediction accuracy to remain comfortably within a factor of two.

Another point is the question of multiple detonations at the Rulison site. The behavior of seismic motions from row charges is expected to differ from single bursts, and future studies will have to address this situation. Until this behavior is more completely understood, less confidence in seismic predictions from multiple charges will have to be tolerated.

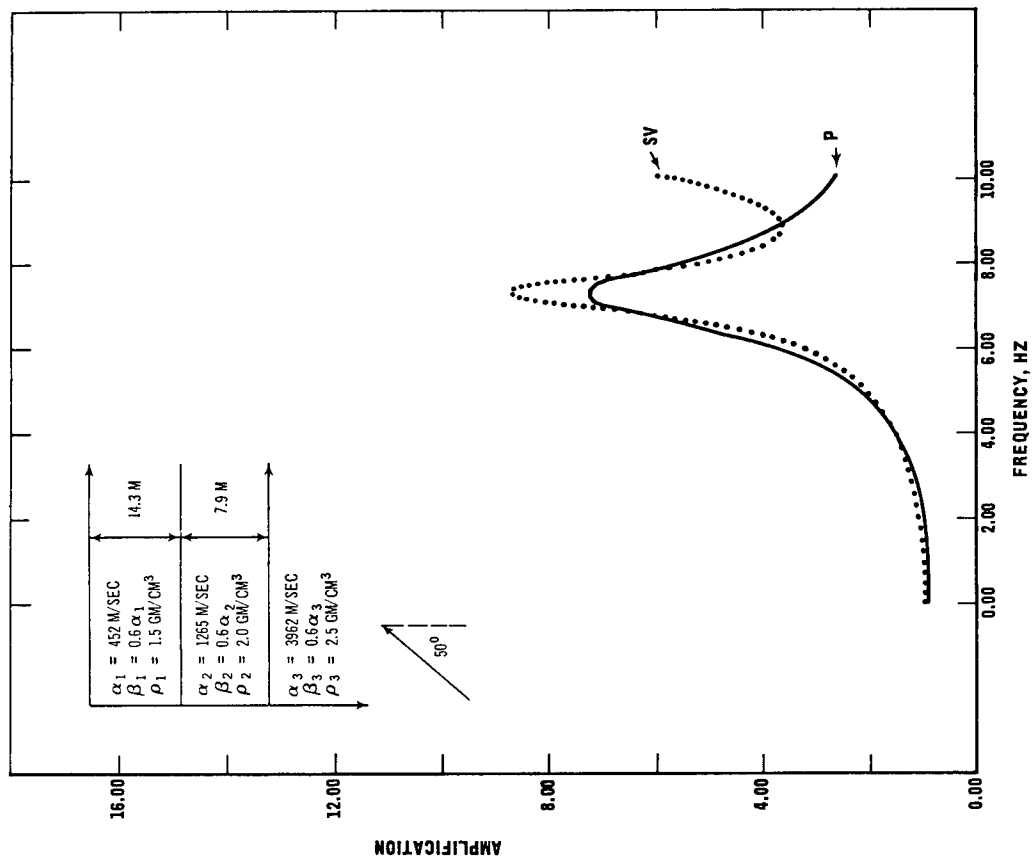


Figure 11. Horizontal Amplification versus Frequency, Harvey Gap Dam

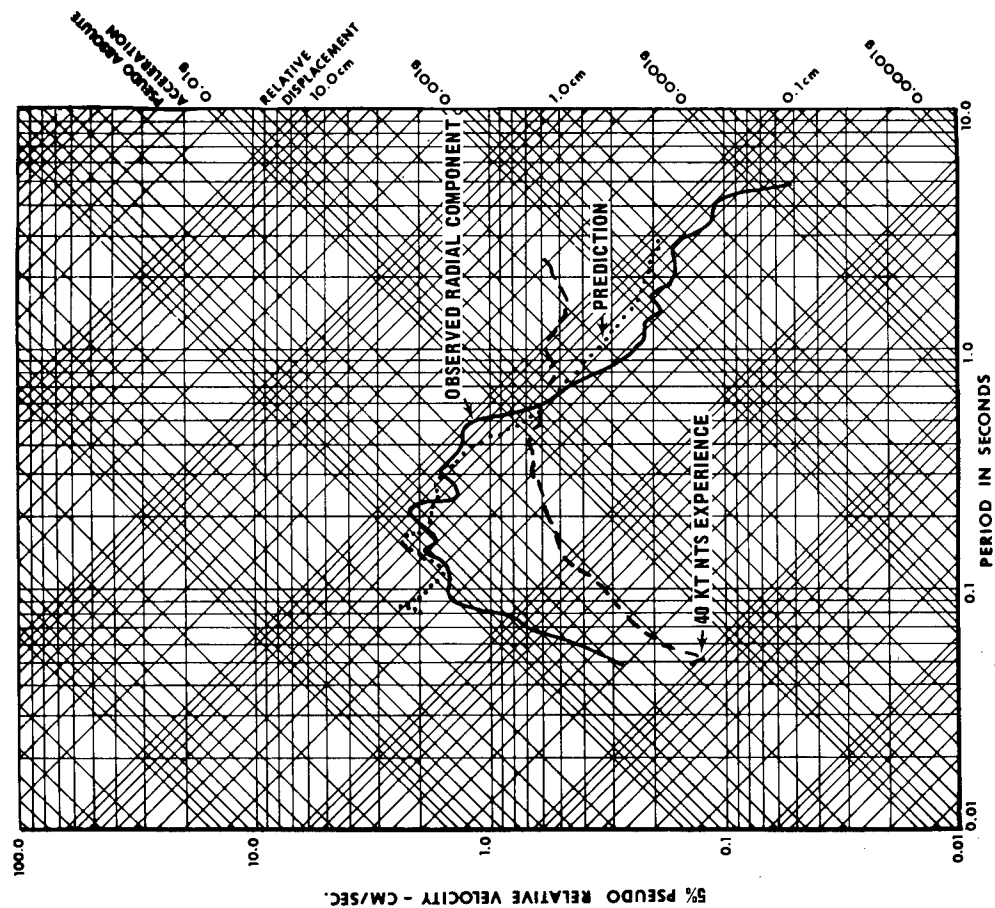


Figure 12. Response Spectra, Harvey Gap Dam, Distance 33 km

REFERENCES

1. Mueller, R.A., Prediction of Seismic Motion from Contained and Excavation Nuclear Detonations, National Topical Meeting on Plowshare (Fourth Plowshare Symposium), 1970.
2. Hays, W.W., Amplitude and Frequency Characteristics of Elastic Wave Types Generated by the Underground Nuclear Detonation, BOXCAR, BSSA 50, 2283-2293, 1969.
3. Lynch, R.D., Response Spectra for Pahute Mesa Nuclear Events, BSSA 59, 2295-2309, 1969.
4. Mueller, R.A., Seismic Energy Efficiency of Underground Nuclear Detonations, BSSA 59, 2311-2323, 1969.
5. Murphy, J.R., and Lahoud, J.A., Analysis of Seismic Peak Amplitudes from Underground Nuclear Explosions, BSSA 59 2325-2341, 1969.
6. Davis, A.H., and Murphy, J.R., Amplification of Seismic Body Waves by Low Velocity Surface Layers, Environmental Research Corporation, NVO-1163-130, AEC, 1967.

THE EFFECTS OF THE RULISON EVENT
ON BUILDINGS AND OTHER SURFACE STRUCTURES

Lloyd A. Lee and Roger E. Skjei
John A. Blume & Associates Research Division
San Francisco, California

INTRODUCTION

Project RULISON is a joint experiment sponsored by Austral Oil Company Incorporated, Houston, Texas, the U.S. Atomic Energy Commission and the Department of the Interior, with the Program Management provided by CER Geonuclear Corporation of Las Vegas, Nevada under contract to Austral. Its purpose is to study the economic and technical feasibility of using underground nuclear explosions to stimulate production of natural gas from the low productivity, gas bearing Mesaverde formation in the RULISON Field.

The nuclear explosive for Project RULISON was detonated successfully at 3:00 P.M. plus 0.1 seconds Mountain Daylight Time, September 10, 1969, at a depth of 8425.5 feet below ground level and was completely contained. Preliminary results indicate that the RULISON device behaved about as expected; i.e., with a yield of about 40 kt. The wellhead of the emplacement well, Hayward 25-95A, is at an elevation of 8154 feet above mean sea level (MSL) and is located 1976.31 feet east of west line and 1813.19 feet north of south line of Section 25, Township 7 South, Range 95 west of 6th P.M., Garfield County, Colorado which corresponds to geodetic coordinates of longitude 107°56'53" west and latitude 39°24'21" north.

John A. Blume & Associates Research Division, under contract with the Nevada Operations Office of the U.S. Atomic Energy Commission, has been assigned responsibility for structural inventories in the range of probable damage, structural response and damage predictions, surface earth structure hazard evaluations, and recommendations for safety measures in these particular aspects. The predictions were based on field data, office studies, ground motion predictions from the Environmental Research Corporation (ERC), and pertinent published information.

This paper is essentially an interim report of currently available data. Studies are continuing to further develop the relationship of ground motion, structural properties, and damage.

STRUCTURAL RESPONSE

The geographical distribution of towns, dams, and major population centers with regard to RULISON Ground Zero (GZ) is shown in Figure 1. Major industrial facilities within 35 kilometers include the Oil Shale Research Center at Anvil

Points, the Union Carbide Plant at Rifle, and the Public Service Company Steam Plant at Cameo. The major dams are Rifle Gap Dam, Harvey Gap Dam, and Vega Dam. Smaller dams are located on Battlement Mesa, approximately 3 kilometers south of GZ. Several of the Battlement Mesa dams have been inoperative for a considerable number of years, and of those that do contain water the outlet control works are inoperative. Consequently, the flow that reaches Battlement Creek is normal overflow from the reservoir surface water, sustained by seepage through the ground from the reservoirs' areas in late summer. Of the other three major dams, Harvey Gap above the town of Silt presented an apparent hazard in view of its age, obvious disrepair of outlet works, and because of the high water levels in the reservoir in early spring. However, when the shot detonation time was extended to September, the reservoir was predicted to be nearly empty and no hazard was then presented.

Within the range of 0 to 5 kilometers from GZ there are 3 log cabins and 3 wood-frame cabins generally used during the summer. There is also a television relay station with guyed television antennas and a small metal shack housing the electronic equipment.

Within the range of 5 to 10 kilometers there are approximately 184 locations with 28 log houses, 145 wood-frame houses and 20 masonry houses. There are also 558 minor outbuildings. Most of the structures within this 5 to 10 kilometer range are associated with farms or summer cabins.

The area from 10 to 15 kilometers includes the town of Grand Valley, population 245, and the Anvil Points Oil Shale Research Station. Also included within this range are the steel truss bridges over the Colorado River at Grand Valley and at Rulison. Table I indicates that there are approximately 146 locations in this range which could be the source of damage complaints. The structures include 143 residences and 269 outbuildings associated with these residences.

From 15 to 20 kilometers there are many small ranches, the town of Collbran, and the large Union Carbide Plant near Rifle. Generally, the structures located here are again as found in Table I with 209 locations, 218 houses, and 614 associated outbuildings.

The range of 20 to 25 kilometers includes the towns of Rifle with a population of 2135, the town of De Beque with a population of 173, and Vega Dam. With the many small ranches and the houses in Rifle and De Beque, there are 893 locations with 935 associated outbuildings. The Oil Shale Company of America, a consortium of several oil companies, has a facility approximately 25 kilometers northwest of GZ in the Parachute Canyon area known as the TOSCO Facility. The structures are conspicuous and there is a large tower approximately 200 feet high which is situated in the Canyon.

Major locations within the range of 25 to 30 kilometers include the small town of Silt just east of Rifle, and Rifle Gap Dam as well as many small ranches. There are 184 locations with 177 houses and 601 associated outbuildings.

The final ring in the area of interest covers the range from 30 to 35 kilometers and includes the town of Mesa, many small ranches, and Harvey Gap Dam. At the 265 locations in this range there are 266 houses with 519 associated outbuildings.

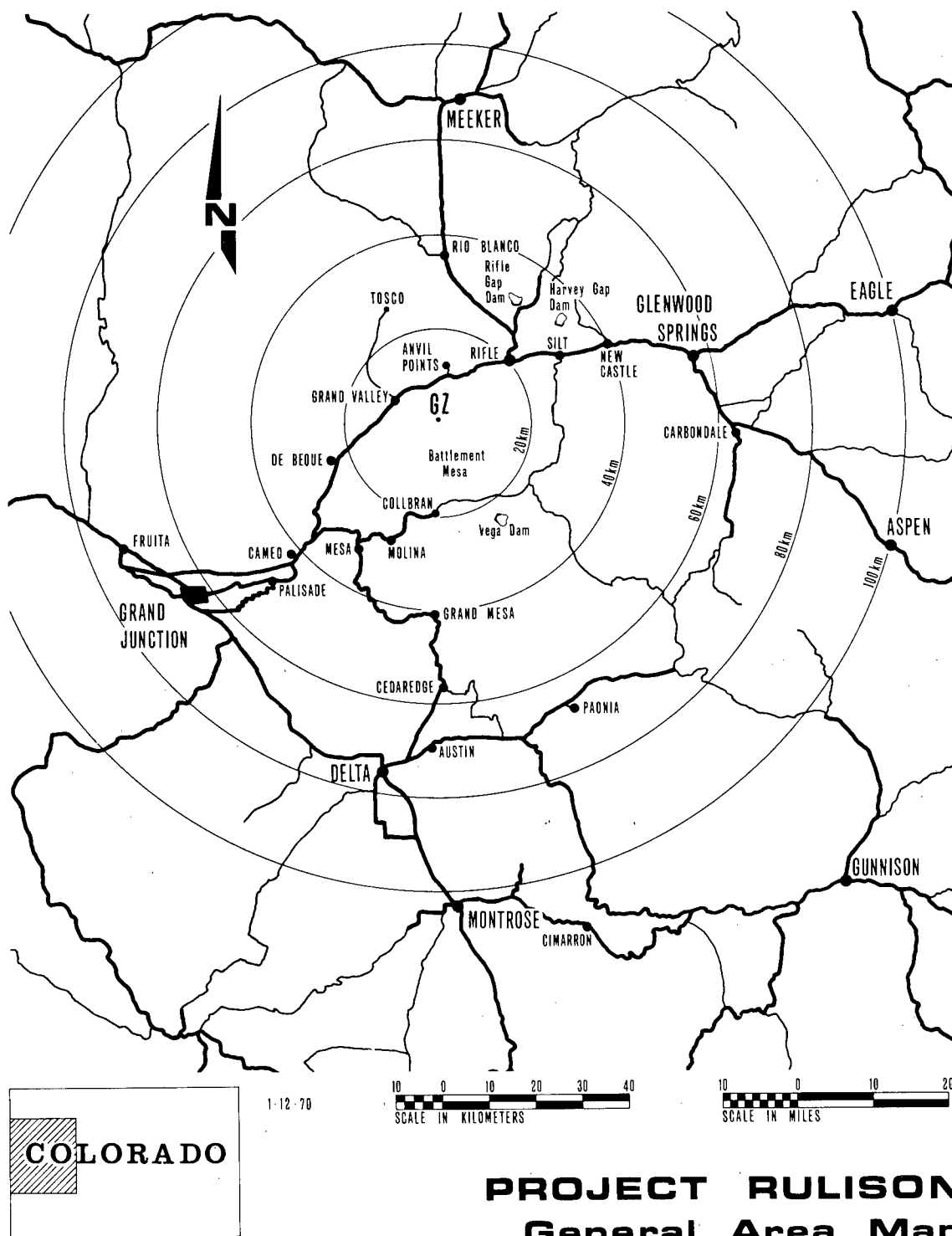


Figure 1

TABLE I - STRUCTURE DISTRIBUTION

Distance (kilometers)	No. of Locations	House Type			Outbuildings
		Log	Wood	Masonry	
0-5	6	3	3		1
5-10	184	28	145	20	558
10-15	146	20	108	15	269
15-20	209	25	170	23	614
20-25	893	33	576	226	935
25-30	184	26	126	25	601
30-35	265	11	217	38	519
TOTAL	1887	146	1345	347	3497

DAMAGE PREDICTIONS AND SAFETY RECOMMENDATIONS

Ground motion predictions for the maximum credible yield and corresponding predictions of 5% damped Pseudo Relative Response Velocity Spectra (PSRV) were provided by ERC. These data were then used in developing the damage predictions and safety recommendations.

Hazards to personnel were predicted to exist within 7.4 kilometers as a consequence of predicted ground motion in excess of 0.3g and evacuation and other appropriate safety measures were taken. In the area from 7.4 to 14 kilometers lesser hazards to personnel were predicted to exist as a consequence of ground motion between 0.1 to 0.3g. Inhabitants in this area were requested to be outside and clear of their structures to avoid hazards resulting from possible damage to the structure. These criteria for the safety of non-participating personnel have been used extensively for previous AEC events. School buildings were also temporarily evacuated in Rifle, Collbran, and Plateau Valley during the event to eliminate the possible hazard which could be created by over-response of school children to structural motion.

Rockfalls are a normal hazard in many areas surrounding GZ. As a result of extensive investigation, these potential rockfall areas were identified. Ranch occupants, and highway and railroad traffic were kept clear of these areas.

Based on ground motion forecasts and spectra, a distance of 35 kilometers was selected as the range of potentially damaging ground motion. Within this area of 35 kilometers from GZ all structures were located, inventoried, and evaluated for possible damage. Towns were treated as separate units. Outside of the 35 kilometer radius and to a distance of about 100 kilometers, where ground motion was predicted to exceed 0.001g, all areas were visited and particularly vulnerable structures were noted and evaluated for possible damage.

Following the period of reconnaissance, inventory, and evaluation of structures, a pre-shot report was prepared and submitted. This report summarizes

safety recommendations and structure damage predictions. Recommended structural revisions to specific structures were also included in the pre-shot report. These involved brick chimney removal, undercribbing of structures, anchorage and bracing, and the placement of safety guys on tall chimneys to guide their direction of fall in the event of failure. Removal of the chimneys was based on an analysis of response under median ground motion and considered the present condition and the consequences of further damage to the structure in the event of failure.

Damage predictions were arrived at by the use of the Blume-developed Spectral Matrix Method of Damage Prediction, and separately confirmed by an engineering judgment prediction. The damage predictions in the pre-shot report involved a qualitative prediction of damage at various locations, as presented here in Table II. Repair costs were also predicted and presented in the pre-shot report.

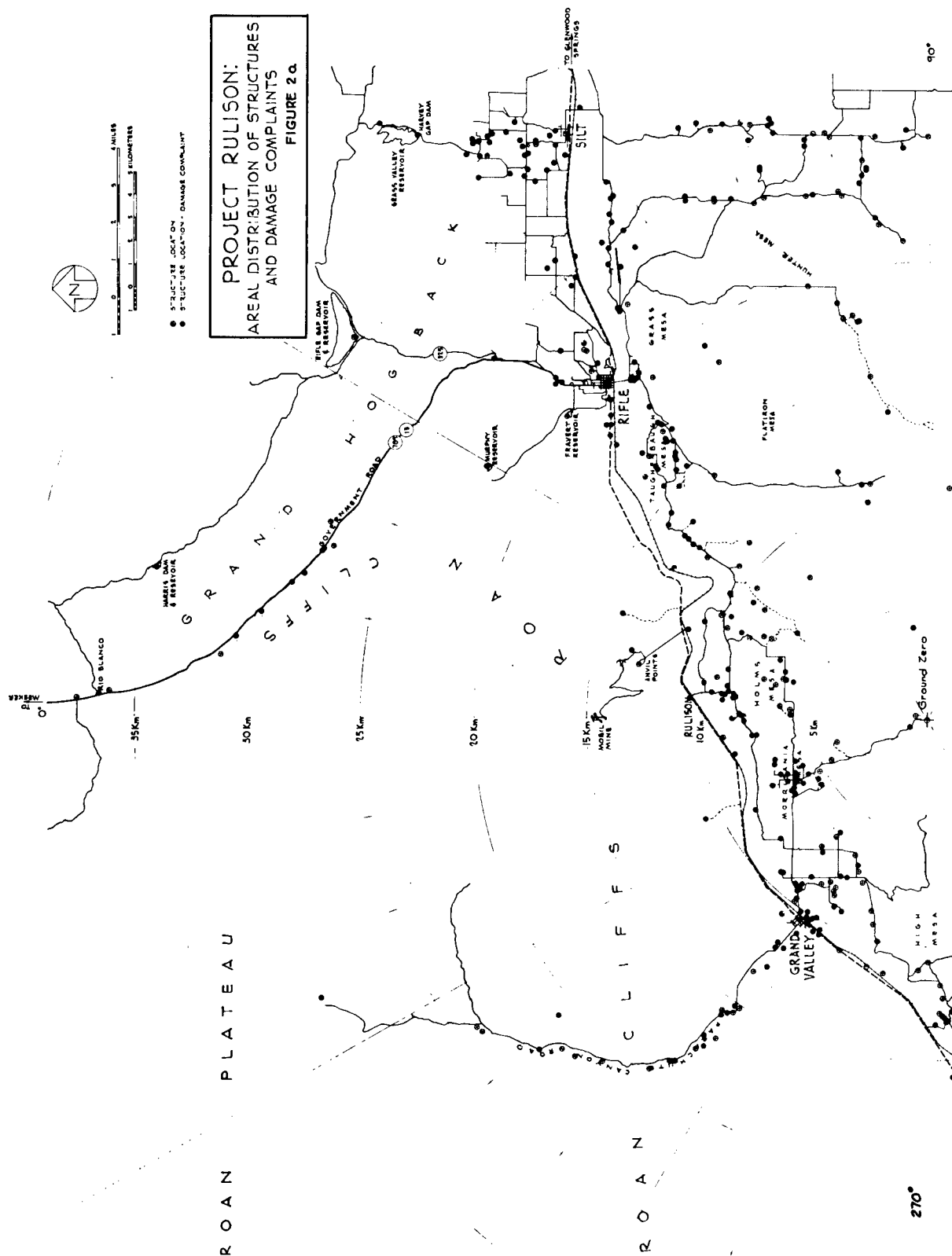
By the end of 1969, more than 90% of the damage claims had been settled at a total cost of approximately \$55,000. This figure is less than the predicted repair costs and may be explained in part by the fact that the prediction was based on cost figures for actual professional repairs. Many claimants, however, preferred to accept lesser cash settlements and either make their own repairs or simply accept the damage.

ANALYSIS OF COMPLAINTS

As of the first week of January 1970, 251 damage complaints have been analyzed from the area within 35 kilometers of GZ. A few other complaints, minor in nature, have been received from outlying areas and are not included in this presentation. Table III summarizes the various types of damage claims grouped in 5-kilometer increments from GZ. Many of the complaints are multiple types involving two or more different kinds of damage at the same location.

Table IV presents a breakdown, again by 5-kilometer increments, of the total number of structure locations versus damage complaints. A structure location as used here is a house or cabin location with or without outbuildings. Thus, a ranch is a structure location and a house in Grand Valley is also a structure location. The areal distribution of structure locations and damage complaints outside of the towns is shown in Figure 2. The 69 complaints in Grand Valley and the 74 complaints in Rifle are not shown in this Figure.

Table V presents a comparison of complaints in the three main categories (chimneys, interior plaster, and masonry walls) with the inventoried number of chimneys and the estimated number of interior plastered walls and exterior masonry walls. Also presented is the approximate peak 5% damped spectral response in the horizontal and vertical direction and for the corresponding distance increment. These peaks represent the upper envelope of measured spectra in that distance band.



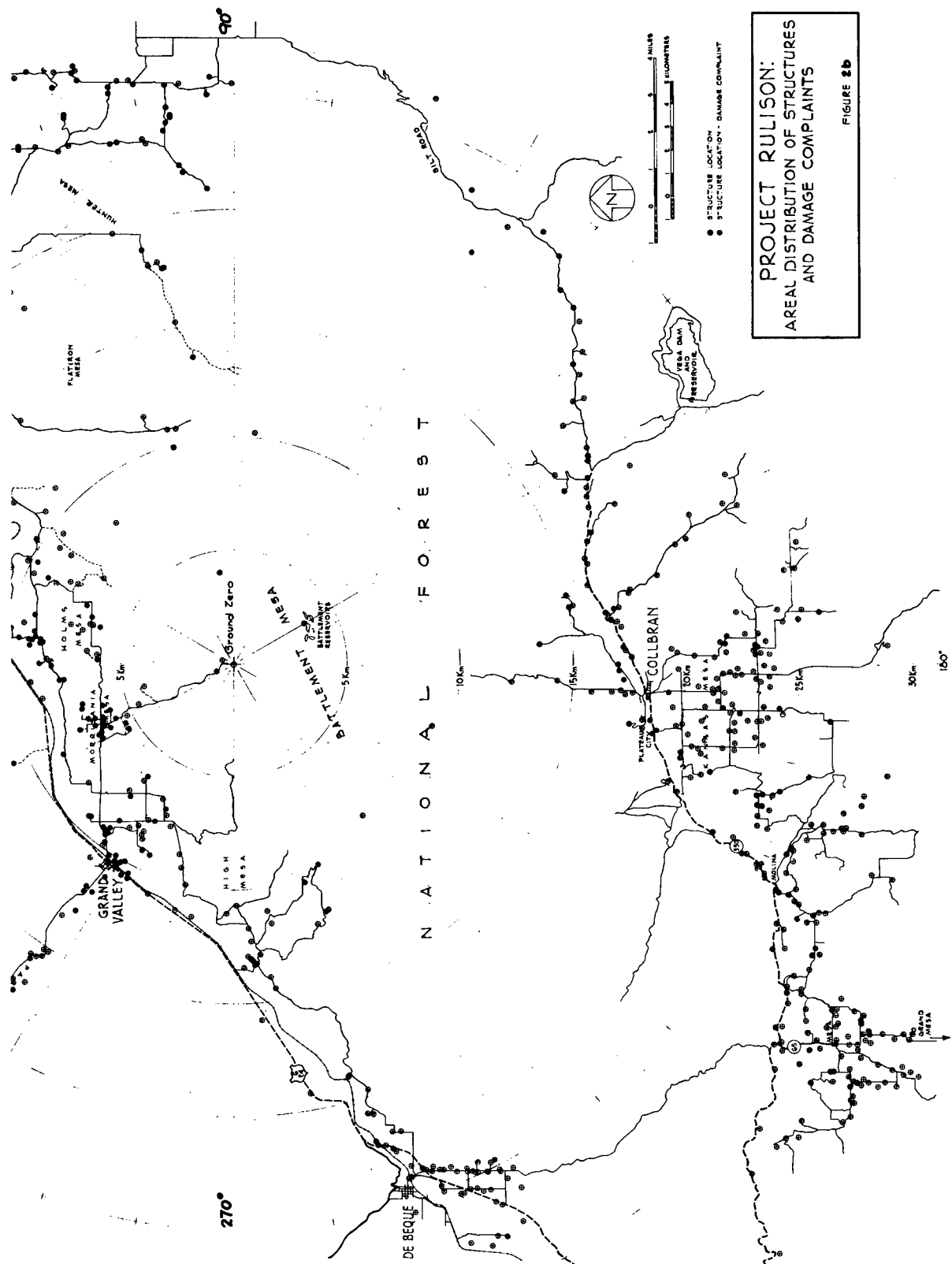


TABLE IICOMPARISON OF DAMAGE PREDICTIONS AND ACTUAL EFFECTS

(Based on predicted PSRV at design yield of 40 kilotons)

<u>Name</u>	<u>Distance & Direction From GZ (km)</u>	<u>Predicted Effect</u>	<u>Actual Effect</u>
Rulison	8(-) N	Moderate damage	Moderate damage
Grand Valley	10 NW	Moderate damage	Moderate damage
Anvil Points	12 N	Moderate to minor damage	Possible minor road damage
Microwave	14 W	No damage	No damage
Ranches	14(+) SE	Minor damage	Minor damage
Union Carbide	18 NE	Minor damage	Minor damage
Collbran	19 S	Minor damage	Minor damage
Rifle	20 NE	Minor damage	Minor damage
De Beque	25 SW	Minor damage	Minor damage
TOSCO	25 NW	No damage	No damage
Vega Dam	25 SE	No damage	No damage
Rifle Gap Dam	30 NE	No damage	No damage
Silt	30 NE	Minor damage	Minor damage
Mesa	32 SW	Minor damage	Minor damage
Harvey Gap Dam	34 NE	No prediction	No damage
New Castle	40 NE	No damage	No damage
Glenwood Springs	58 E	No damage	No damage
Grand Junction	64 SW	No damage	Several minor complaints
Delta	76 S	No damage	No damage

TABLE III - SUMMARY OF DAMAGE COMPLAINTS

Type of Damage	Distance in Kilometers from GZ							Total
	0-5	5-10	10-15	15-20	20-25	25-30	30-35	
Chimney	-	31	56	4	23	-	-	114
Interior Plaster	-	17	44	12	50	2	1	126
Window	-	5	1	2	5	1	1	15
Fireplace	-	2	-	2	4	-	-	8
Foundations	-	8	4	7	9	1	-	29
Masonry Walls	-	4	14	1	16	2	1	38
Other Exterior Walls	1	1	3	2	1	-	1	9
Roof	-	3	1	-	-	-	-	4
TV Sets	-	2	-	-	-	-	-	2
Household Items	-	4	-	2	2	-	1	9
Cisterns	-	15	1	1	2	-	-	19
Wells	-	1	-	-	-	-	-	1
Earth Slides	-	2	1	2	1	-	-	6
Utility Lines	-	1	-	-	2	-	-	3
Other Damage	1	7	17	2	15	-	-	42

TABLE IV - COMPARISON OF STRUCTURE LOCATIONS AND COMPLAINTS

Distance (Kilometers)	Number of Structure Locations	Damage Complaints
0-5	6	1
5-10	184	54
10-15	146	87
15-20	209	17
20-25	893	84
25-30	184	3
30-35	265	5
TOTAL	1887	251

TABLE V - COMPLAINT COMPARISON VERSUS APPROXIMATE PEAK PSRV RESPONSE

Distance (Kilometers)	Ratio of Complaints to Inventory			Approximate Peak 5% Damped Spectral Response					
				Vertical			Horizontal		
				Sa (g)	Sv (cm/sec)	Sd (cm)	Sa (g)	Sv (cm/sec)	Sd (cm)
0-5	0/0	0/0	0/0	*	*	*	*	*	*
5-10	31/175	17/41	4/20	3.5	56	1.3	2.3	42	1.3
10-15	56/107	44/54	14/15	1.6	16	0.4	1.0	21	0.60
15-20	4/159	12/71	1/23	0.37	7.0	0.20	0.40	8.2	0.26
20-25	23/449	50/350	16/226	0.62	12	0.27	0.36	13	0.46
25-30	0/121	2/44	2/25	*	*	*	0.13	7.0	0.36
30-35	0/201	1/87	1/38	0.12	3.0	0.10	0.13	3.7	0.10

*Data not available.

CONCLUSIONS

The precautions taken in having people evacuated from the area or outside of the house and two building heights away from the house were well advised as was the care taken during the pre-shot activity in removing or re-building chimneys at close-in locations. At these locations none of the remaining chimneys fell, although some loose bricks on the tops of small chimneys did fall as was predicted. Chimneys in most old homes in rural areas are unlined and because of repeated heating and cooling, and freezing and thawing cycles during the years, the mortar joints near the brick cap become loose to the point that none of the bricks are bonded. Many of these chimneys which were damaged were noted in the original inventory as being a hazard because of the loose bricks or badly deteriorated condition.

Ground motions from the event were quite close to predicted motions, and as shown in Table 2, damage occurred in the locations and generally to the extent predicted. It is easier to predict damage to structures on a qualitative basis than to predict the actual cost of damage settlements. This is demonstrated by the difference between settlement costs and predicted damage repair costs. The latter is intended to cover all damage, even that which may not be discovered or claimed. Predicted damage costs will therefore very likely never be actually attained.

Further study of RULISON damage claims will hopefully lead to understanding of relationships between settlement costs to predicted damage repair costs for use on future Plowshare projects.

Origins of Displacements Caused by Underground Nuclear Explosions*

by

John S. Rinehart
ESSA Research Laboratories, and
Department of Mechanical Engineering, University of Colorado
Boulder, Colorado 80302

ABSTRACT

Elastic theory has been used to calculate the relative displacement that will occur between the two sides of a loose boundary when a plane wave strikes the boundary obliquely. The calculations suggest that the displacements produced along loose fractures and faults close in to the underground nuclear explosions are a direct consequence of reflection of the transient stress wave at this loose boundary. Quantitatively the results agree fairly well with the limited data that are available.

INTRODUCTION

A common effect of an underground nuclear explosion is the development at the time of the explosion of displacements along jointed rock structures and preexisting faults as illustrated for the Boxcar event in Fig. 1. Such displacements have been extensively described (Barosh, 1968; Buckman, 1969; Dickey, 1968; Dickey, Jenkins, McKeown, and Lee, 1967; Dickey, McKeown, and Ellis, 1968; Hamilton, McKeown, and Healy, 1969; McKeown and Dickey, 1969). Both vertical and right lateral displacements occur out to a few thousand meters from ground zero, the displacements being of the order of tens of centimeters.

The purpose of this paper is to show that these displacements are the anticipated consequence of the interaction of the generated elastic transient stress wave with a loose interface obliquely inclined to the front of the wave.

*Work partially supported by a grant from the American Petroleum Institute to the University of Colorado.

PARTICLE VELOCITY MAGNITUDES

Consider two flat blocks of similar material juxtaposed and loosely connected. When a transient compressional stress wave strikes obliquely such a boundary, the interface, considered perfectly lubricated, can sustain no shear stress. Only normal stresses can be transmitted. The four boundary conditions that must be met at all times during the interaction of the wave with the boundary are: continuity of normal stress across the interface; continuity of normal particle velocity, or displacement, across the interface; and zero shear stresses on both surfaces forming the interface.

When these conditions are applied to an advancing elastic dilatational compression wave, the five waves shown in Fig. 2 become involved in the interaction: the incident longitudinal wave (A); a reflected longitudinal wave (C); a reflected shear wave (D); a transmitted longitudinal wave (E); and a transmitted shear wave (F).

If the particle velocity in the incident is V_A (Fig. 2), the particle velocities in the four new waves will be given by

$$V_B/V_A = (\sin 2\alpha \sin 2\beta) / (K^2 \cos^2 2\beta \sin 2\beta)$$

$$V_C/V_A = (K \cos 2\beta \sin^2 \alpha) / (K^2 \cos^2 2\beta + \sin 2\alpha \sin 2\beta)$$

$$V_D/V_A = (K \cos 2\beta \sin 2\alpha) / (K^2 \cos^2 2\beta + \sin 2\alpha \sin 2\beta)$$

$$V_E/V_A = (K^2 \cos^2 2\beta) / (K^2 \cos^2 2\beta + \sin 2\alpha \sin 2\beta)$$

where α is the angle of incidence of the advancing wave (Fig. 2) and β is the angle the two shear waves make with the interface. The constant K is the ratio of the longitudinal wave velocity C_L to the shear wave velocity C_S . The angles α and β and K are related by the expression

$$\sin \alpha / \sin \beta = C_L / C_S = K = \left[2(1-\nu)/(1-2\nu) \right]^{\frac{1}{2}}$$

where ν is the Poisson's ratio. Thus the respective particle velocities in the several waves are functions both of the angle of incidence and Poisson's ratio.

Relative particle velocities for each of the five waves are plotted as a function of angle of wave incidence for several Poisson's ratios in the series of curves, Figs. 3 through 6. At low Poisson's ratios, proportionately more of the momentum of the original wave ends up in the reflected and transmitted shear waves, which in accordance with the above equations are equal.

Using values from these curves, it is a straightforward matter to calculate the relative velocity with which the two faces of the interface move with respect to one another. The right hand face (cd, Fig. 7) will move only perpendicular to itself. Its velocity will be the vector sum of V_D and V_E (Fig. 2). The face ab will also have the same component of velocity in the same direction but in addition will have a

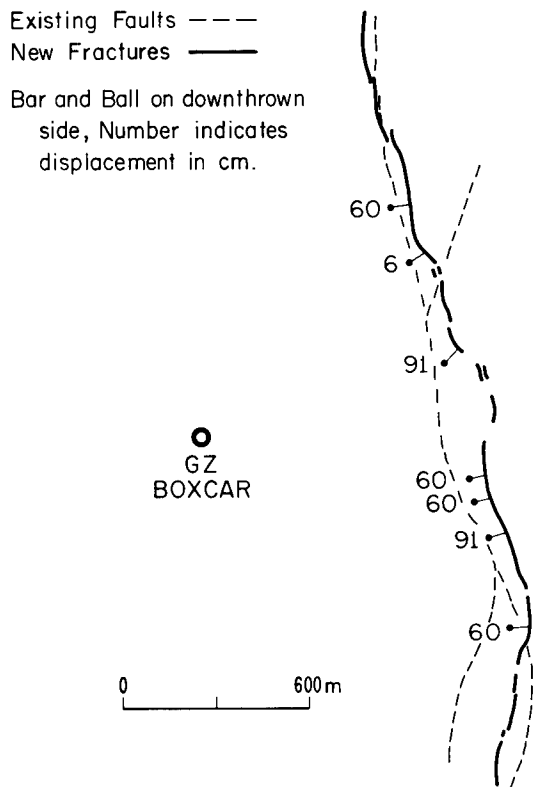


Fig. 1. Fractures generated along existing faults by Boxcar event (after Dickey, McKeown and Ellis, 1968).

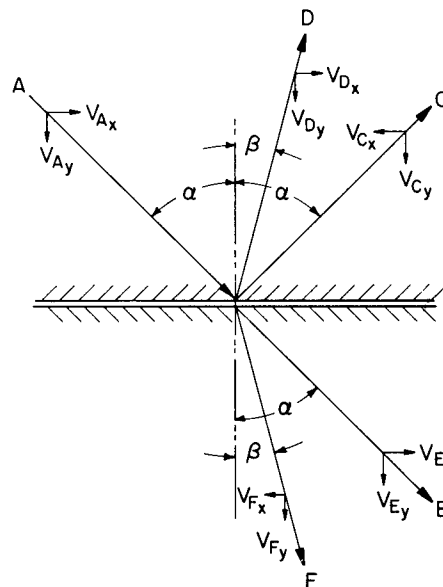


Fig. 2. Waves involved in interaction of a longitudinal wave at a loose interface. A, C, and E are longitudinal waves; D and F are shear waves.

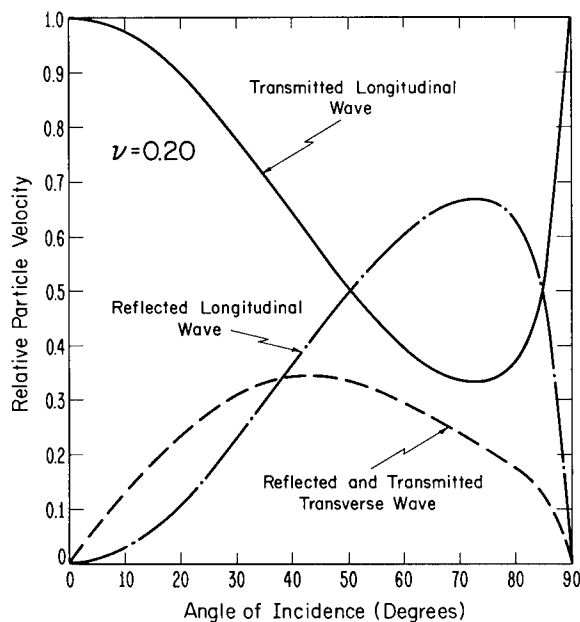


Fig. 3. Particle velocities associated with the five waves shown in Fig. 2 as a function of angle of incidence. $\nu = 0.20$.

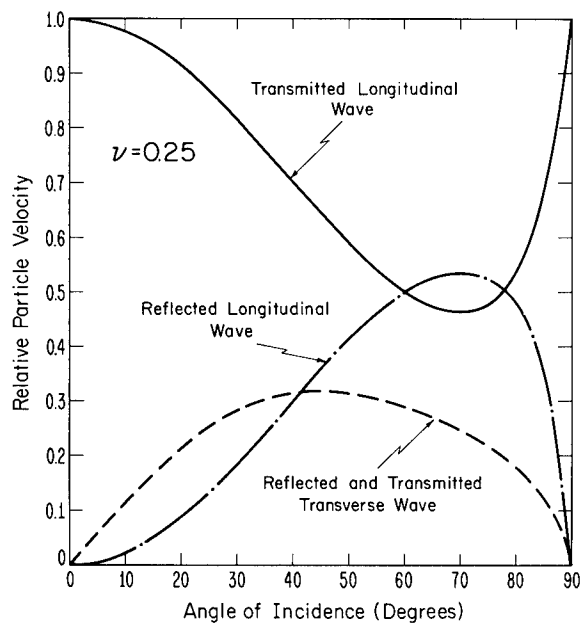


Fig. 4. Same as Fig. 3 except $\nu = 0.25$.

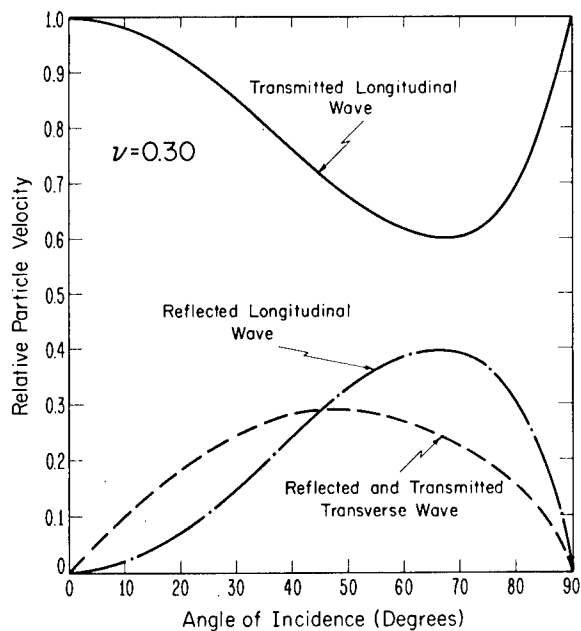


Fig. 5. Same as Fig. 3 except $\nu = 0.30$.

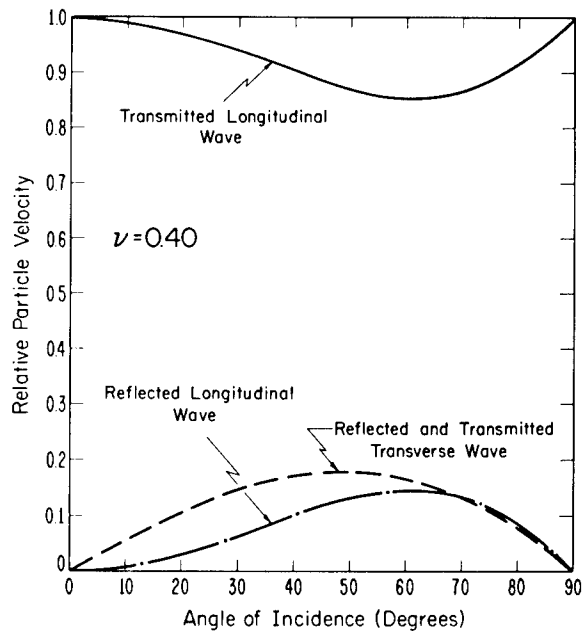


Fig. 6. Same as Fig. 3 except $\nu = 0.40$.

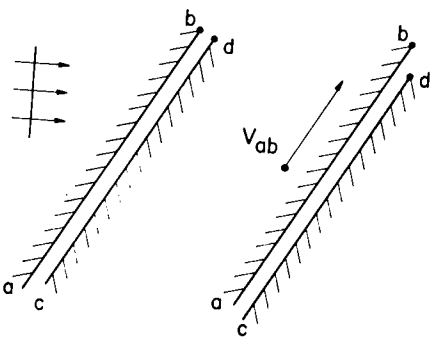


Fig. 7. Movement generated by interaction of transient stress wave with loose boundary.

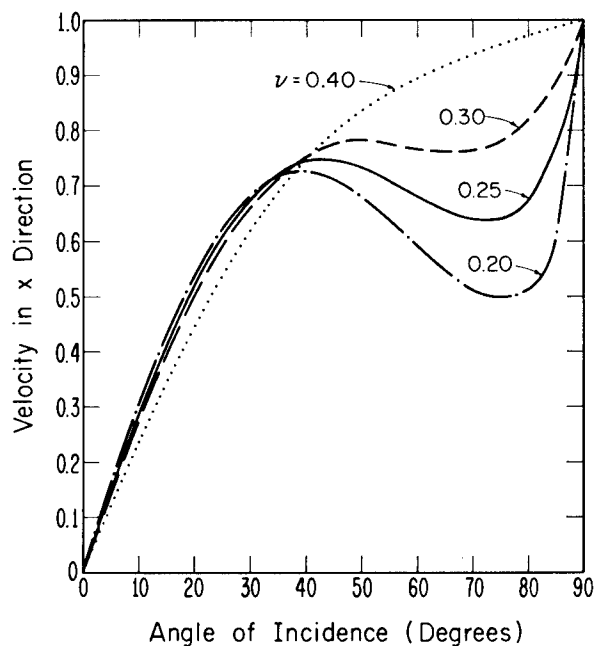


Fig. 8. Velocity of face ab (Fig. 7) with respect to face cd (Fig. 7) for several Poisson's ratios as a function of angle of incidence.

component of velocity parallel to the interface. This parallel component V_{ab} will be given by the expression

$$V_{ab} = V_A \sin \alpha + V_D \cos \beta - V_C \sin \alpha$$

where the right hand side is the sum of the particle velocity components along the interface of each of the three waves involved in the interaction. The velocity V_{ab} has been plotted in Fig. 8 for several Poisson's ratios as a function of angle of incidence.

For a transient compressional wave, the total displacement d of the face ab with respect to the face cd will be given by

$$d = \int V_{ab}(t) dt \quad (1)$$

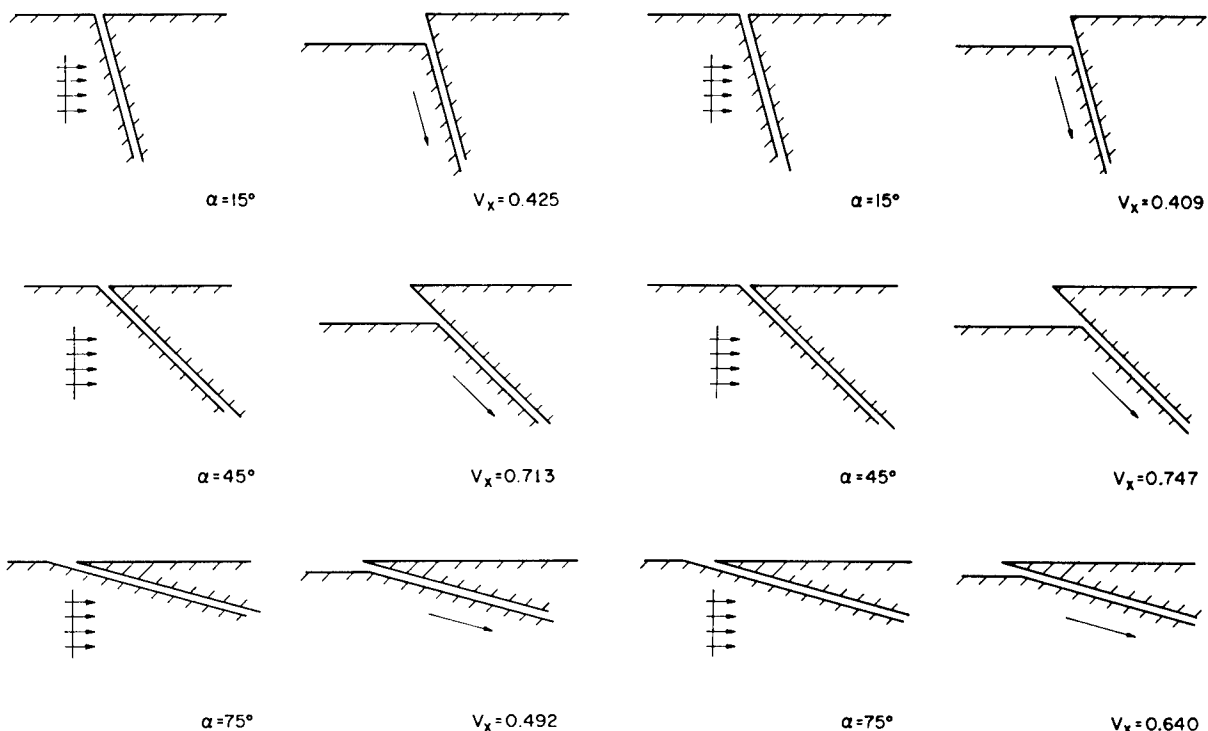
where the integration is taken over the duration of the wave. Assuming that the transient wave is square topped and of unit duration, the relative surface displacements that would accompany the impingement of the wave against a loose fracture or fault at various angles of incidence are illustrated for several Poisson's ratios in Figs. 9 through 12. Only a few cases are shown and these are ones in which the fault has a negative dip and its near side is thrown downward. When the dip of the fault is positive, the near side will be thrown upward.

In the examples shown thus far, it has been assumed that the wave front is plane and parallel to the plane of the interface. Usually neither is the case. For a non parallel plane wave front, the slippage can be resolved into components at right angles, one relating to vertical displacement and the other to horizontal displacement. At a ground surface, the displacements would manifest themselves at combined right lateral and vertical slips.

SOME SAMPLE CALCULATIONS

Unfortunately very little quantitative data have yet been made available on the magnitudes and durations of the particle velocities developed around underground nuclear explosions so that it is not possible to make accurate and detailed calculations regarding the displacements to be expected along fractures and faults. However, it is known that the observed particle velocity versus time distributions are generally "N" shaped, which at distances of 1000 to 2000 m from the explosions have durations of the order of one quarter to one second and maximum amplitudes of a meter or two per second (Perrett, personal communication). While the Poisson's ratios of the materials in which the detonations were set off is not known precisely, they are in the neighborhood of 0.20.

As an example, consider an explosion located at a one kilometer distance from a vertical fault and buried at a one kilometer depth. The angle of incidence between the wave front and the plane of the fault near the ground zero would be 45° . From Fig. 8 it is seen that at ground level the near surface of the fault would move upward with respect to the far surface at a velocity of 0.75 times the particle velocity in the incident wave. Applying

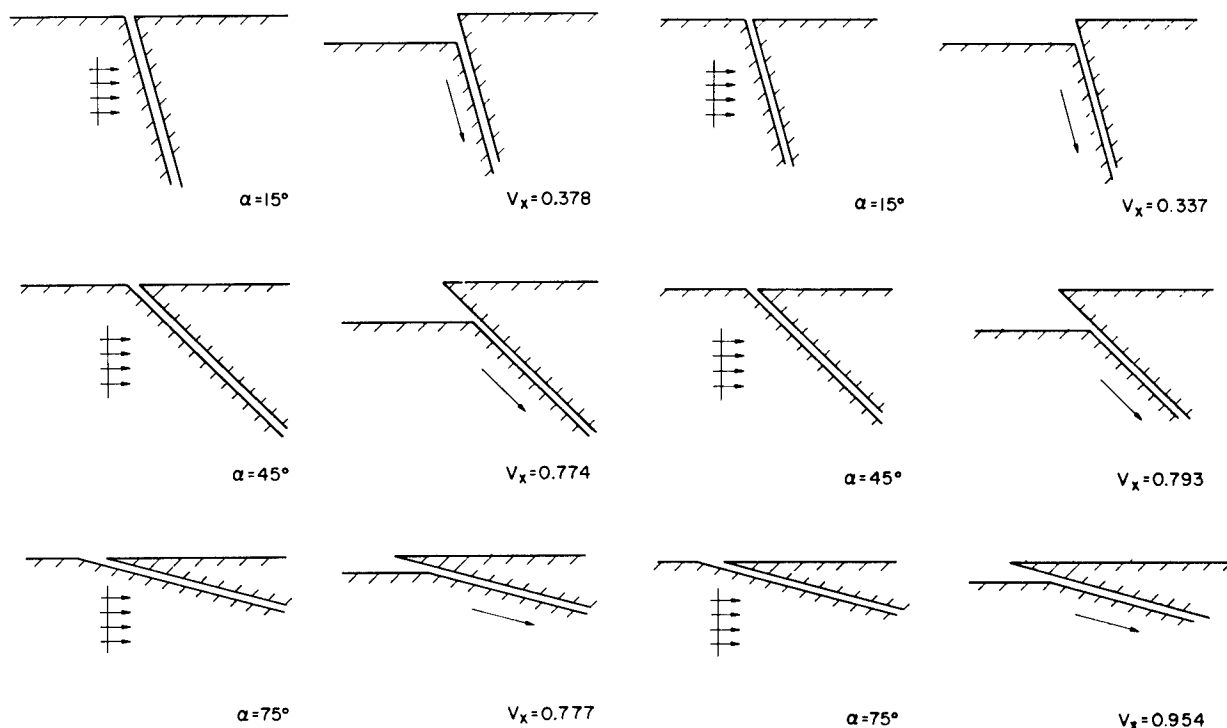


$\nu = 0.20$

Fig. 9. Surface displacements caused by a square topped transient stress wave impinging against a loose fracture or fault. $\nu = 0.20$.

$\nu = 0.25$

Fig. 10. Same as Fig. 9 except $\nu = 0.25$.



$\nu = 0.30$

Fig. 11. Same as Fig. 9 except $\nu = 0.30$.

$\nu = 0.40$

Fig. 12. Same as Fig. 9 except $\nu = 0.40$.

Eq. (1), the displacement produced by a wave of amplitude 3m/sec and the duration of positive phase of 0.25 sec results in 28 cm, a value quite compatible with those observed in the field (Fig. 1).

In a recent Amchitka Island event, an abrupt, about 30 percent, decrease in particle velocity occurred across the nearby Rifle Range Fault (Perrett, personal communication). This fault is so located with respect to ground zero that the wave inclination assuming that the fault is vertical, would be about 45° . However, the dip of the fault has not been established. The curve for $\nu = 0.20$ in Fig. 3 for the intensity of the transmitted longitudinal wave indicates that if the fault were vertical, the particle velocity should be reduced even more, by as much as 50 percent. The actual change in particle velocity suggests that the fault may have a positive dip of about 30° , making the angle of incidence 70° , and hence increasing the intensity (Fig. 3) of the transmitted wave to 70 percent of the intensity of the incident wave.

BIBLIOGRAPHY

Barosh, P.G., 1968. "Relationships of Explosion-Produced Fracture Patterns to Geologic Structures in Yucca Flat, Nevada, Test Site". Geol. Soc. Amer., Mem. 110, 199-217.

Bucknam, R. C., 1969. "Geologic Effects of the BENHAM Underground Nuclear Explosion". Bull. Seis. Soc. Amer. 59, 2209-2219.

Dickey, D.D., 1968. "Fault Displacement as a Result of Underground Nuclear Explosions". Geol. Soc. Amer., Mem. 110, 219-232.

Dickey, D.D., E.C. Jenkins, F.A. McKeown, and W.H. Lee, 1967. "Geologic Effects of the Greeley Event". Nevada Test Site Technical Letter: NTS-196, U.S. Geol. Surv. Open File Report.

Dickey, D.D., F.A. McKeown, and W.L. Ellis, 1968. "Summary of Geologic Effects of the Boxcar Event, Nevada Test Site". Technical Letter: Special Studies -65, U.S. Geol. Surv. Open File Report.

Hamilton, R.M., F.A. McKeown, and J.H. Healy, 1969. "Seismic Activity and Faulting Associated with a Large Underground Nuclear Explosion" Science 166, 601-604.

McKeown, F.A. and D.D. Dickey, 1969. "Fault Displacements and Motion Related to Nuclear Explosions". Bull. Seis. Soc. Amer. 59 2253-2269.

ON THE PREDICTION OF BUILDING DAMAGE FROM GROUND MOTION

John A. Blume
John A. Blume & Associates Research Division
San Francisco, California

ABSTRACT

In the planning of a nuclear event it is essential to consider the effects of the expected ground motion on all exposed buildings and other structures. There are various steps and procedures in this process which generally increase in scope and refinement as the preparations advance. Initial, rough estimates, based upon rules-of-thumb and preliminary predictions of ground motion and structural response, may be adequate to show general feasibility of the project. Subsequent work is done in both the field and analysis phases, to estimate the total structure exposure, to isolate special hazards, and to make damage cost estimates. Finally, specific analyses are made of special buildings or structures to identify safety problems and to make recommendations for safety measures during the proposed event. Because the ground motion and the structural response both involve many random variables and therefore some uncertainties in prediction, the probabilistic aspects must be considered, both on a broad statistical basis and for specific safety considerations. Decisions must be made as to the acceptability or non-acceptability of the risks and any indicated procedures before and during the event to reduce or to eliminate the risks.

The paper discusses various techniques involved in these operations including the Spectral Matrix Method of damage prediction, the Threshold Evaluation Scale for specific building analysis, and the inelastic and probabilistic aspects of the problem.

INTRODUCTION

In order for a new field of effort such as engineering with nuclear explosives to progress, it is essential that satisfactory predictions be made of the various effects. In recent years it has become clear that the prediction of structural response to ground motion is a very important -- and often controlling -- factor not only for safety but in overall planning and feasibility determinations of proposed nuclear events.

Very important decisions may have to be made on the basis of structural response predictions. These decisions include yield limitations, safety precautions, evacuation of persons, and the effects of these factors and damage costs on the economic and technical feasibility of a project. In view of the importance of these predictions it is essential that they be reliable, not be unduly conservative, and that the probabilities of possible variations be provided in addition to the mean prediction. Conservatism should be

reserved for the decision making stages, and not be injected all along the way and thus unduly limit or restrict a proposed project.

In the development of reliable prediction techniques it is important not only to obtain, analyze and document empirical data but to fully recognize its limitations and conditions so that it will not be applied where it should not be. Moreover, it is basic that theory be developed, tested, reconciled with reliable data, and used to recognize and to evaluate important parameters. It is also important to recognize random variables in the problem and to develop reliable probabilistic models of the important parameters.

Many disciplines are involved in the detailed study and prediction of building response to ground motion. These include dynamics, structural engineering, earthquake engineering, architectural engineering, soil mechanics, engineering geology, mechanics, mathematics, statistics and probability theory, and a sound knowledge of how real buildings are designed, are constructed, and respond to ground motion. Of course, the ground motion per se involves disciplines such as seismology, geophysics, mechanics, and mathematics.

There is not time in this short presentation to cover the various prediction techniques in detail. Instead, a broad overview will be provided with general descriptions and discussion of how and where the methods would be applied. Detailed papers are being developed and will be published as soon as feasible and as data become available.

BACKGROUND

There are many prediction techniques, some of which are relatively new and some of which are still being developed or improved. John A. Blume & Associates Research Division, under contract to the United States Atomic Energy Commission, Nevada Operations Office (USAEC-NVVO), has not only been providing actual predictions for test-site and off test-site events, but has been compiling and analyzing data and developing techniques for improved reliability and efficiency. Only recently, however, has there been enough real damage to provide some of the data points needed and to test the methods in service. More data is needed as is more time for detailed analysis. However, the results thus far are encouraging.

The field of effort has suffered from lack of extensive data on real damage, from the use of various rules-of-thumb and empirical constants without identification of important parameters, and from oversimplification of a complex subject. For example, the use of peak particle ground acceleration, velocity, or displacement without identification of the frequency content relative to that of the structures has been common in blasting, in early nuclear explosive engineering, and in some phases of earthquake engineering. This can lead to erroneous results and is not recommended for nuclear engineering except as a tentative, initial approach to a problem, or on a very broad statistical basis. A few early experiments in the blasting field have led to extensive use of limited data sometimes without adequate regard to the type or condition of the structures, the type or condition of the soil, of the frequency of the ground motion, or of the dynamic characteristics and strengths of the buildings. With these very important parameters neglected, the results can only be very doubtful when applied to specific areas. The damage resistance of low buildings, for example, may vary from essentially nothing (if other damaging processes are already on hand) to acceleration values of one g or more.

The response spectrum is valuable in damage studies and predictions in that it defines the ground motion as it would affect idealized oscillators of various natural periods and damping ratios. It is thus of much greater significance insofar as response and damage are concerned than the peak ground motion per se. The response spectrum has been used in certain areas of earthquake engineering for some time, and as part of the USAEC-NV00 structural response program since early 1965. A spectrum is developed by mathematically subjecting an idealized one-degree-of-freedom oscillator of a particular period and damping to the entire time history of recorded ground motion in the component under consideration. The maximum response, in terms of acceleration, velocity, or displacement is plotted against the natural period. By repeating the above computation for a whole array of oscillator periods using the same damping ratio, enough points of maximum response are obtained to plot the response spectrum. The whole process can be repeated for other damping values and a family of curves can be constructed. Figure 1 shows such plots for acceleration, relative velocity, and relative displacement. Figure 2 shows another useful device wherein the plotting is done on 4-way logarithmic paper. In such plotting there is the generally acceptable assumption that the response is harmonic or sinusoidal in nature so that the acceleration, velocity, and displacement are simply related, as follows:

$$S_a g = \omega S_v = \omega^2 S_d \quad (1)$$

$$\omega = \frac{2\pi}{T} \quad (2)$$

wherein

S_a = spectral value of the absolute acceleration of the oscillator mass, fraction of gravity

S_v = spectral value of the oscillator mass velocity relative to the ground, cm/sec

S_d = spectral value of the oscillator mass displacement relative to the ground, cm

ω = the angular velocity of the oscillator, radians per second

T = the natural period of the oscillator, seconds

g = acceleration of gravity, taken as 981 cm/sec²

In Figures 1 and 2 the accelerations are generally greater in the short period range, the relative velocities in the middle period range, and the relative displacements in the long period range. It may be seen that the structures are sensitive to not only peak spectral response but to period. However, equation (1) provides a simple relationship under which acceleration, velocity, or displacement may be used interchangeably. The short period response acceleration approaches the maximum ground acceleration, and the long period response displacement approaches the maximum ground displacement.

The kinetic energy input to a vibrating system may be related to the square of the pseudo relative velocity. If the response is elastic the energy is stored, but if inelastic response occurs, some of the energy does work in the system and is thus not returned. Spectral response velocity squared is therefore a useful index.

It is obvious that spectral response is more meaningful in response than peak particle motion. Fourier spectra are also useful, but generally the response spectrum is satisfactory and somewhat simpler in use for most response purposes.

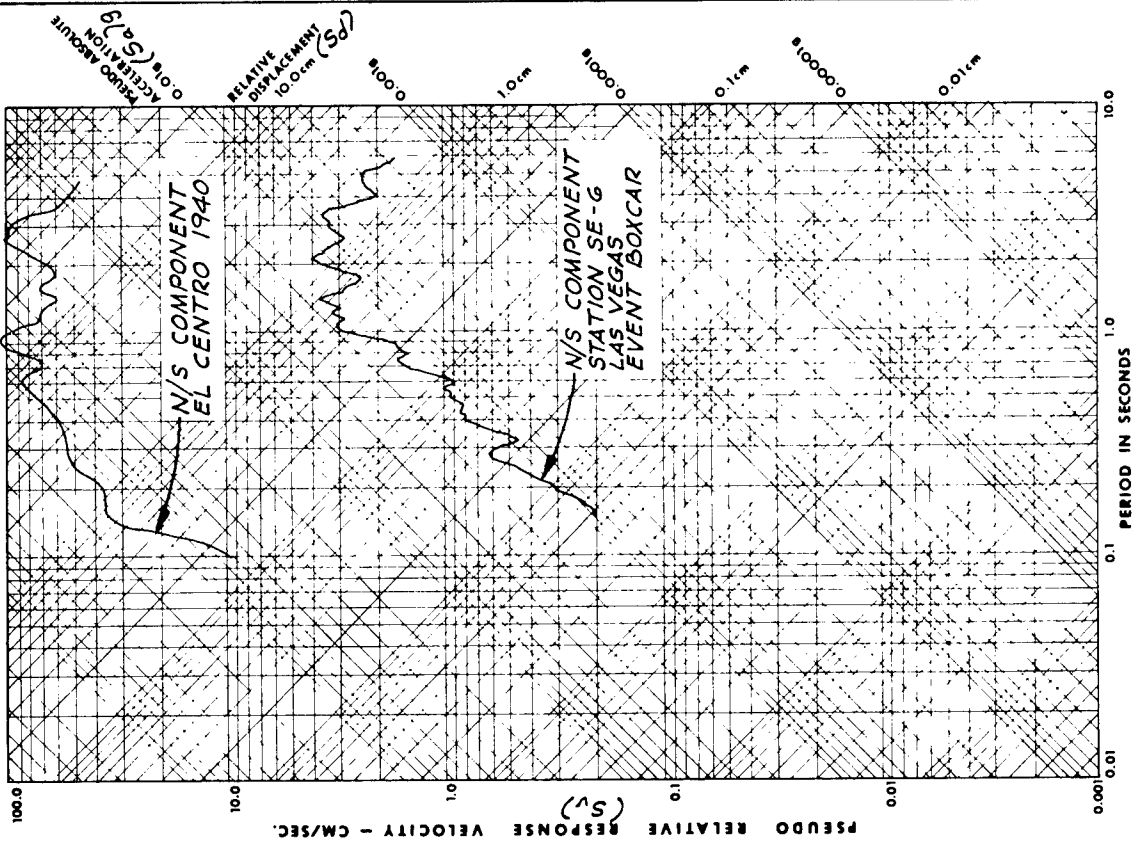


FIG.2 - 5% DAMPED SPECTRAL RESPONSE

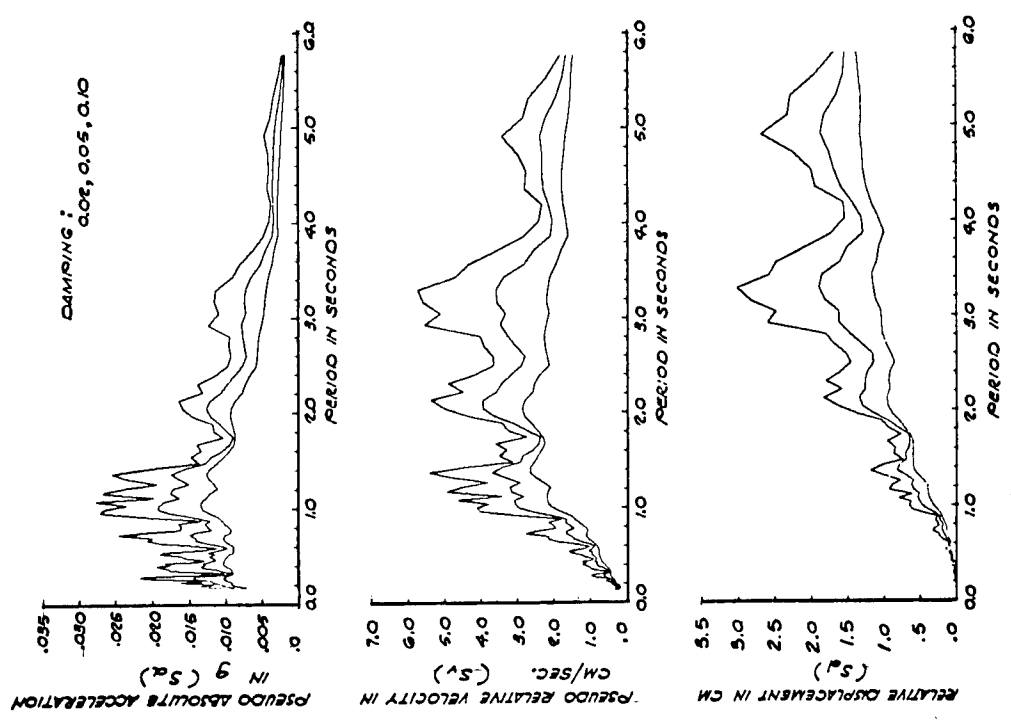


FIG.1 - SPECTRAL RESPONSE TO GROUND MOTION AT STATION SE-G, N/S COMPONENT, LAS VEGAS, EVENT BOXCAR (L-7 INSTRUMENT)

However, there are vast differences between the idealized oscillator of the spectrum and real buildings. Many of these have been discussed in some of our AEC reports. (1)(2)

Recent papers (3)(4) have shown the use of pseudo absolute acceleration, PSAA, as an index in estimating the number of damage complaints. It should be noted that S_a (which is the same as PSAA) has been used in the USAEC-NVOO structural response program for many years. The results -- although better than those obtained by using peak particle motion -- are not expected to be reliable for specific damage predictions unless related to the natural periods of the buildings under consideration. If the buildings happen to all be in the short period range where S_a tends to peak, spectral acceleration may be a good index. However, this does not preclude the use of S_v or even S_d for convenience if proper adjustments are made as in the above equations.

There has been some expression recently that the spectral response diagram may not always be a good indicator of damage. (5) This is largely based on the fact that there was little or no damage from local sharp earthquake motion and high spectral response values close to the moving fault in the Parkfield earthquake of 1966 and the assumption that buildings have only Uniform Building Code minimum values. Our studies have clearly shown in this program (6) and elsewhere (7) that many low buildings have much greater resistance to ground motion than the building codes require. The real resistance may be many times that specified, usually because of the building geometry and the use of strong walls. In addition, it is often the case that the spectral peaks do not occur at natural building periods. The spectral response diagram is thus a generally good, simple indicator of damage onset when all the parameters are considered. The degree of damage is better approached with inelastic reserve energy analyses which are included as part of the Spectral Matrix Method of damage prediction and in the Reserve Energy Technique. (8)

It has been our experience that there may be poor correlation between the number of damage complaints and the extent of real damage. The number of complaints is not only some function of motion intensity but also of the condition of the buildings and their foundation materials, latent potentially damaging conditions of many possible types as for example shrinkage stress, and of publicity before and after the shot. The real ground-motion induced damage is a function of motion intensity as most simply defined by spectral response, but it bears no relationship to publicity, and only very nebulous and complex relationships to the twenty or more latent conditions that may exist. Objective complaint investigations may clearly show the damage to be from old, pre-existing conditions. It must not be overlooked, however, that investigations cost money even where the complaint lacks validity.

The methods being used for specific response and damage predictions in the USAEC-NVOO structural response program include:

- | | |
|----------------------------------|--|
| Peak Values | - for early reconnaissance only |
| Extrapolated Motion | - for general information |
| Judgment Estimate | - as a part of survey procedure |
| Spectral Matrix Method (SMM) | - for damage estimation over large areas |
| Threshold Evaluation Scale (TES) | - for safety investigation of large or key buildings |
| Reserve Energy Technique (RET) | - investigation of special risk buildings in the inelastic range |
| Time History Analysis | - special studies where time history of ground motion is available |

Not all methods are needed for each event. Generally, only the Judgment Estimate and the SMM results are reported on a routine basis. Any significant difference in results between these two methods is investigated to improve knowledge and values of constants for building capacities. After an event the SMM procedure may be redone, using the actual response spectra rather than predicted response spectra, in order to compare the results to any actual damage and to improve data on real building capacities.

In all cases, pre-event field surveys are conducted to obtain data on the number, types, sizes and values of buildings; on the soil conditions; and on the condition of the buildings. Any special risks or typical sample buildings are examined again after the shot, and all complaints are investigated promptly, carefully, and courteously.

A brief, general description of these methods and procedures will be given. For more details reference is made to published material and to material that will be published as soon as feasible and adequate data become available.

PEAK VALUES

Peak values of predicted response spectra are useful as a guide for preliminary reconnaissance purposes. They are much more useful than predicted peak horizontal ground motion which may have to be used instead if predicted response spectra are not available early in the investigation period. The spectral response may be in terms of acceleration or velocity although acceleration is generally used. For this purpose we have used a standardized damping value of 5% of critical.

Surveys are conducted in order to obtain information on the structures of various types that fall within various spectral or ground motion values. These surveys often start near the proposed surface zero and work outward. Use is made of all available maps, assessment records, geologic maps, and any other existing information that might be helpful in determining the number of structures of various types that exist within the area of the survey.

As the investigator makes this early reconnaissance, he looks for any structures that might be particularly vulnerable to ground motion because of poor condition, location, or geometry. Experience is essential in this regard.

The objectives of preliminary reconnaissance are to make very rough estimates of potential damage for a proposed yield, to discover any particularly vulnerable structures or safety problems, and to obtain information essential for the planning of more detailed surveys should the project go ahead.

Following are the values below which surveys have not been made or generally should not be considered necessary, at least during the initial field effort.

	<u>Low Buildings</u>	<u>Tall Buildings, Stacks, etc. of Long Period</u>
Peak horizontal ground motion	0.01 g	0.001 g
Peak vector ground motion	0.02 g	0.002 g
5% damped spectral acceleration, S_a	0.02 g	0.003 g

EXTRAPOLATED MOTION

In an area where building response has been measured under ground motion from previous detonations, plots are made of the actual measured response, often taken at the top level of a building, versus various parameters such as peak horizontal ground motion in the direction under consideration, peak spectral response or preferably spectral response at the period of the fundamental mode of the building-component under consideration. Such plots can be extrapolated by judgment, or preferably by a least squares computation procedure.

These plots are not only useful to provide predictions of particular building motion for forthcoming events but they provide visual evidence of the variations from the mean values. Such variations must, of course, be taken into account when making predictions. Should the predicted motion appear to be in an amount that would lead to damage, special analyses are indicated. It may be the case that damage is not expected but the motion may be so severe that the Test Manager should be notified for his consideration of special safety precautions.

Extrapolations are not feasible in a new area except by analogy to other areas that may be applicable with some adjustments or normalizing of data. Obviously, it is not prudent to extrapolate too far beyond the available information.

There may also be cases where the yield or the range has changed in such manner that interpolation is possible. This, of course, can be done with greater confidence than extrapolation.

Figure 3 shows a plot of actual motion for a Las Vegas highrise building. In this case S_a is used as the index using the period of the fundamental mode of the building. There is little deviation in this example, largely due to the fact that this spectrum is developed from fairly close ground motion recordings. For other buildings there may be considerable variation and, often, the maximum top level acceleration is much greater than the spectral response, S_a .

THE JUDGMENT ESTIMATE

Along with the more detailed field surveys that are essential when the planning for a proposed event is advancing, engineers experienced with building resistance to ground motion can make on-the-spot judgment determinations of possible damage. To do this they must have in mind when inspecting a building or other structure, the predicted spectral response for the period of the fundamental mode. An experienced investigator determines and notes the condition of the building, any other apparent damaging processes, prior damage, any vulnerable elements, the soil conditions, and he mentally forms a picture of what would be expected to happen under the proposed ground motion. He may do this in terms of percentage of total cost, as for example he may estimate that the building is worth \$20,000 and would suffer about 5% or \$1,000 worth of damage. An alternate procedure is to visualize the type of damage such as cracked plaster, etc., and to estimate the probable repair costs.

Sketches and photographs are desirable as part of this operation. It is desirable to use suitable forms which not only lead to the orderly accumulation of data but are constant reminders of the various items of information that must be obtained in the field.

The data thus obtained are assembled, coordinated, and analyzed in the office and are combined to obtain a judgment estimate of the probable damage from the proposed nuclear event. Since the judgment estimate is largely subjective, it is not the only estimate made. It is used instead as a cross-check on the more exotic methods and in improving knowledge of building performance and characteristics.

THE SPECTRAL MATRIX METHOD (SMM)

The Spectral Matrix Method of damage estimation has been developed in the structural response program and is being improved as new data become available. It is a comprehensive analytical procedure which includes several important factors such as the estimated spectral response for the ground motion, the estimated statistical variations of the ground motion, the estimated dollar values and mean capacities of the various types of structures to resist ground motion, the spectral variations of the mean capacities, the periods of the structures, the soil conditions, and the inelastic characteristics of any structures that should enter a damaging region of response.

The method is comprehensive, and is best suited to large geographical areas which may have a multitude of estimated ground motions, building types, and other conditions. It has been applied to nuclear events in Nevada, Colorado, and elsewhere and has been used as a parameter study vehicle for proposed interoceanic canal crossings for which damage has been estimated over the area of an entire country. The Spectral Matrix Method is designed for computer operation although for small areas it could be processed manually.

The matrix is superimposed on a 4-way logarithmic spectral diagram such as that in Figure 2, with 9 period bands, j . Spectral response velocity lines can be used to define the rows of the matrix. The median expected spectral response velocity, \bar{S}_v , is utilized together with the probable deviations from the median value.

$$S_{v_j} = \bar{S}_{v_j} \beta_j^y \quad (3)$$

in which S_{v_j} = the 5%-damped spectral velocity relative to the ground; cm/sec

\bar{S}_{v_j} = the median value of S_{v_j} ; cm/sec

β_j = the geometric standard deviation of S_{v_j} ; dimensionless

y = the standardized normal variable having zero mean and unit variance; dimensionless

j = a subscript denoting the period band

The buildings are divided into categories by types of construction and by estimated fundamental period of vibration. The latter can in many cases be determined as a simple function of the number of stories. A particular type of building may in fact have a wide possible range of periods in which case this would be accounted for by a period vector which would extend into two or more period bands in the matrix. For convenience, the capacity of a building is defined as its "yield point", or a point at which assumed linear response would

become non-linear and cracking or other types of failure would commence. It is recognized, however, that the start of damage, or the yield point, is by no means, in most cases, the start of collapse. There are reserve capacities of most buildings to develop the energy demands of the continuing ground motion by doing work in cracking, yielding, etc. This too is taken care of in the Spectral Matrix Method by use of one of several inelastic models designed to represent the characteristics of the structure beyond the yield point.

The yield point capacity is a mean value and statistical variations and uncertainties are expected to cause fluctuations from this value. These may be modeled as any convenient probability distribution including the normal, lognormal, etc. Adjustments are made for the properties of real buildings as compared to simple oscillators.

There is a joint probability of any demand being associated with any capacity. This is a joint probability of two independent random variables. If the demand exceeds the capacity, damage starts. If the demand does not exceed the capacity, there is no damage whatsoever. The amount of damage depends upon how much the demand exceeds the capacity and the properties of the structures in the inelastic range.

The final result desired is the amount of damage in dollars. This is obtained as the product of the probability of exceeding the yield point, the total dollar cost of the structure, and the computed ratio of damage cost to total cost. The damage ratio is in turn a function of the inelastic properties and the amount that demand exceeds capacity.

As a byproduct of the output, high damage ratios may be used as a guide to safety recommendations. In other words, if damage should exceed a certain percent, such as say 5% or 10% of the total value, there may be some possibility of people in or near the structure being injured.

Figure 4 is a typical plot of estimated damage versus the probability of that damage not being exceeded for a proposed event.

Although theory and the technique are well advanced, there is much more to be learned about the capacities of various types of structures and about their properties in the inelastic range. Special papers are being developed in order to present the Spectral Matrix Method in detail and to provide estimates of structural capacities.

THE THRESHOLD EVALUATION SCALE (TES)

Another tool used in the structural response program is the Threshold Evaluation Scale (TES) procedure which provides a means of estimating the probability of the response of a particular building crossing various thresholds of interest. This method requires detailed knowledge about each building under consideration as well as the probable ground motion demands on the structure. TES has been developed in the structural response program as an aid in safety considerations.

Although the problems and the steps are similar regardless of the height or the size of the building, and it is fully recognized that all buildings are important, the highrise building problem is especially important because it may be difficult and costly to control people in and near large buildings if a relatively high probability of major damage were predicted. Moreover, tall buildings often have less capacity for lateral forces than smaller buildings, and they are more sensitive and responsive to ground motion resulting from

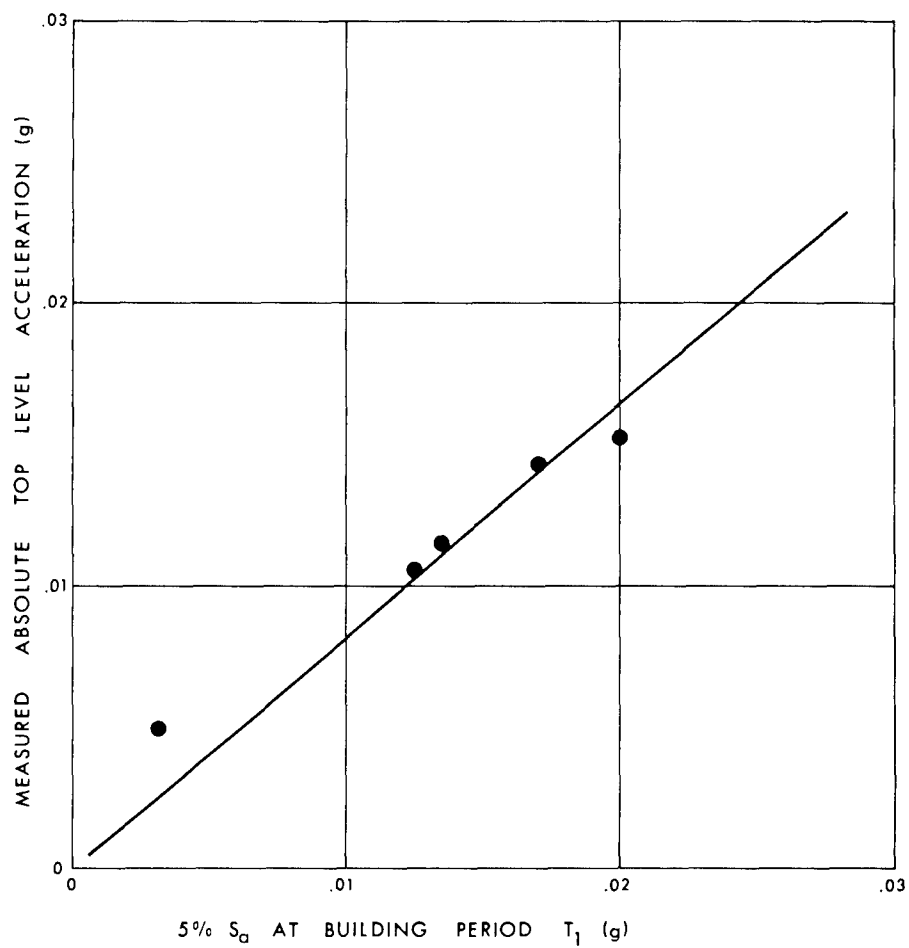


Figure 3 - Building Response vs S_a

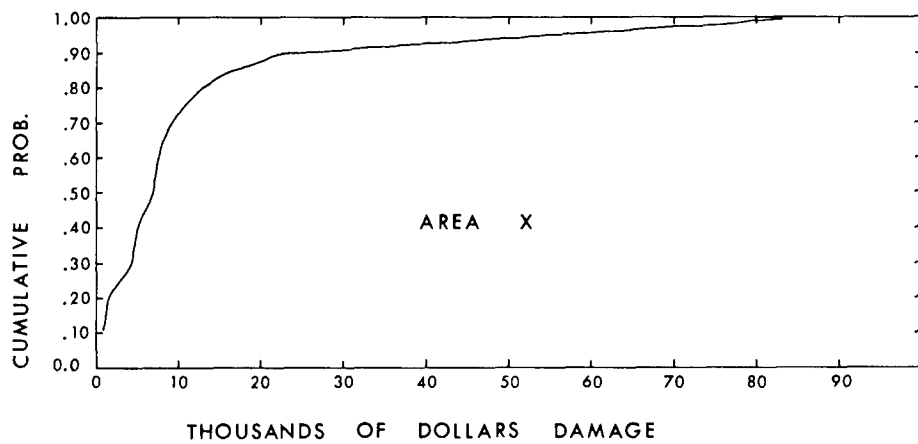


Figure 4 - Sample SMM Output

distant releases of energy. Thus, the TES procedure is often restricted to highrise building analysis.

Unfortunately, as in many such problems, the answers are not simply yes or no. The subject involves random variables, statistical variations and other problems. There is no absolute certainty about the ground motion, the building characteristics, the response to the ground motion or the building capacities at various thresholds. However, as more data become available or can be reliably estimated, the probabilities can be evaluated.

There are many thresholds that may be considered in a complex highrise building. It is essential either directly or implicitly to consider all of them. Some thresholds are more important than others. For example, an upper level beam overstressed in flexure is much less important than a lower story column overstressed in compression or in shear. A further consideration is redundancy in framing with which a local overstress merely causes the transference of force from an initial point to some other part of the structure, which part may offer greater or more sustained resistance.

In order to make the TES procedure simple and more useful, many of the less significant technical complications of structures and dynamics are omitted. It is assumed for example that the lateral inertial force distribution on the structure is in the general form of an inverted triangle. This condition is often close to reality since the fundamental mode usually dominates the response for energy releases at great distance, and the fundamental mode shape of many tall buildings is often close to the form of an inverted triangle. The base shear coefficient is used as a convenient and meaningful index or parameter. However, it is adjusted for the most critical stress condition which may exist anywhere in the building under the assumption of inverted-triangle force distribution.

The output of the TES analysis for a particular building is the probability under a proposed event of reaching various thresholds, such as the following:

- T1 - the building code required base shear value, at code unit stresses
- T2 - same as T1 except it is that value actually provided in the building
- T3 - the point at which a minor or redundant member first reaches its yield value
- T4 - the yield level of an important horizontal member such as a girder or beam
- T5 - the yield level of an important vertical element such as a column or a principal shear wall
- T6 - the shear, compression, or other ultimate value of an important vertical element such as a column or a principal shear wall
- T7 - the start of damage to non-structural materials or elements

It becomes a management decision as to what course to take given reliable estimates of yield or damage probabilities. Naturally, the acceptable risk varies with the seriousness of the consequences. Threshold T6, for example, would constitute serious damage and should have a much lower probability than say threshold T3. Thresholds T1 and T2 are merely guidelines and in themselves involve no damage. If a particular probability of a particular threshold should not be acceptable, there are several decision possibilities including

evacuate the building or portion of the building adjacent to the critical member at event time, strengthen the building, decrease the yield, change the shot location, or cancel the shot. If a particular problem becomes critical, the building may also be reanalyzed by even more rigorous methods. TES is valuable in smoking out possible trouble spots.

THE RESERVE ENERGY TECHNIQUE

If a particular threshold such as T5 or T6 in the TES procedure should present an unacceptable probability of being reached, a more detailed analysis may be conducted in the inelastic range in order to verify the results or to estimate the consequences of the threshold crossing in more detail. The Reserve Energy Technique (8) is ideal for this in that it takes into account energy absorption as well as strength, and provides information as to the mode and consequences of various levels of damage and the hazard resulting from such damage.

A story shear-deformation diagram is developed for the critical story. This takes into account all of the resisting materials and elements and the inelastic as well as elastic range properties of each. Figure 5 shows some common types of shear-deformation diagrams. It is necessary to know a great deal about a building to plot a reliable diagram.

In applying RET to the nuclear response problem it is assumed that the kinetic energy demand, KE, on a building above a certain level, z , is defined by equation (4).

$$KE_{iz} = \sum_{j=n}^z \frac{1}{2} m_j \dot{D}_{ij}^2 \quad (4)$$

in which

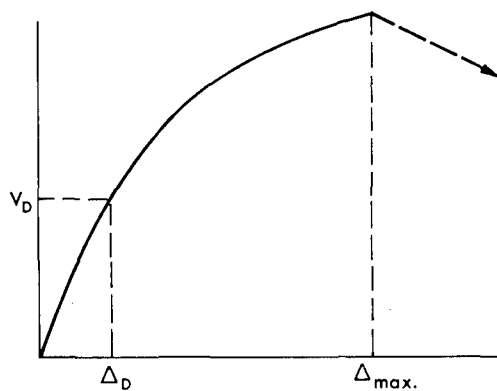
m_j = the mass of story j

\dot{D}_{ij} = the velocity of mass j in mode i , which may in turn be related to S_{vi} . (2)

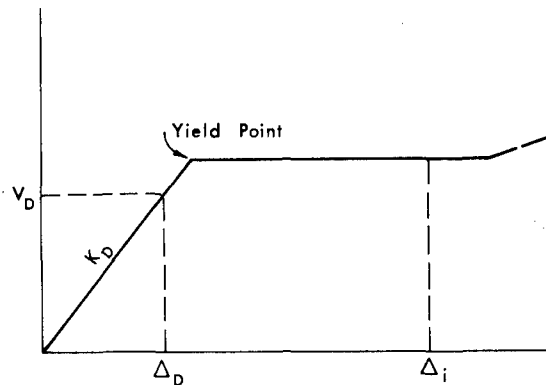
The total kinetic energy is equal to the sum of heat energy, stored energy, and work done, each in appropriate units. The heat energy may be represented by the damping term used to obtain S_v , and the sum of stored energy and work done by the sum of the integrals of the shear-deformation curves (for appropriate deformations) of stories n to z . Obtaining the appropriate deformations for the various stories involves consideration of the mode shape, the shear demands on each story, and the resistance of the story. Generally, this is best done by iteration. Often, only one or two stories may reach the inelastic range, and will thus account for most of the work done.

The procedure is to solve for the S_v value which can be developed when various points of interest are reached on the deformation scale of the shear-deformation diagram, and then to obtain the probability of this S_v value being developed by the ground motion. It may be necessary to consider alternate story shear-deformation diagrams in order to explore the possible range of real structural values in the story.

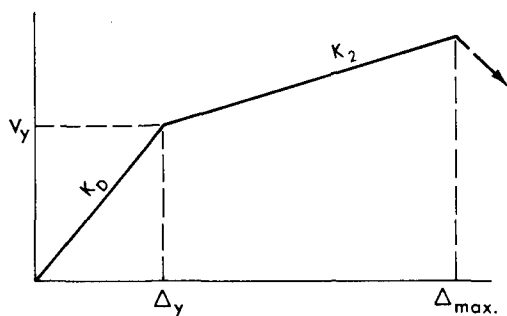
The output of the RET computation is the probability of reaching certain story deformations in the inelastic range, the corresponding degree and type of damage, and the risk to persons that may be associated with the damage. The information is used in the decision making process as to the course of action to be followed for the proposed event.



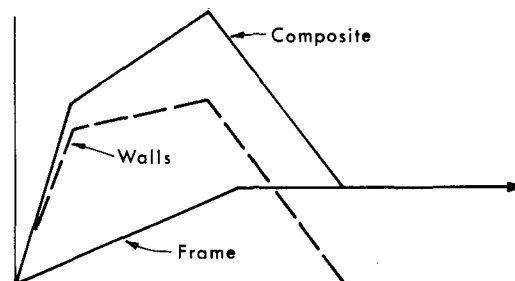
(a) Non-Linear, Softening



(b) Elasto-plastic



(c) Bilinear, Softening



(d) "Plateau" resistance

Figure 5 - Common Types of Shear - Deformation Diagrams

TIME HISTORY ANALYSIS

Any procedure that involves the use of response spectra in estimating damage includes some uncertainty as to modal combinations. However, for many situations, especially for highrise buildings some distance from the energy source as in Las Vegas, the fundamental mode dominates (9) and this modal uncertainty is of minor importance. An exact solution is entirely possible, with computer aid, for a specific time history of ground motion and a reliable model of a building. The entire response, at all levels, can be considered. The problem is that complete time-histories of ground motion are only available after the event and it is often extremely difficult to make an accurate model of a complex, real building.

Progress is being made, however, in developing realistic artificial time-histories of ground motion and in learning more about the properties of real buildings. In the meantime, time-history analysis is a valuable aid in research and in learning more about building properties.

ENGINEERING INTENSITY SCALE

An engineering intensity scale has recently been proposed. (10) It is a by-product of the structural response program, and provides an objective scale for the intensity of ground motion from any cause. It is based upon spectral response. It is believed that as more data become available, this scale will be very useful in the damage estimation problem. It will be possible, on a broad statistical basis, to correlate damage and lack of damage with spectral response in various period bands for various classes and types of buildings.

CONCLUSION

There are several techniques and procedures being used and being developed to predict building damage, or lack of damage, from ground motion. These include exotic methods with dynamic analysis and which require computer aid. Allowance is made for the frequency content of the motion and for the fact that the ground motion, the structural-dynamic characteristics, and the response are random variables with probabilistic variations. The selection of methods depends upon the particular problem at hand, and may advance into the more detailed operations only as the apparent risk indicates. Considerable confidence in damage prediction is possible today and it is expected to improve as more data on real building properties become available.

REFERENCES

- (1) Blume, John A., Chapter 10, "Structural Response to Nuclear Induced Ground Motion", of Report NVO-40 (Revision No. 2), "Technical Discussions of Off-site Safety Programs for Underground Nuclear Detonations", U. S. Atomic Energy Commission, Nevada Operations Office, May 1969.
- (2) Blume, John A., "The Motion and Damping of Buildings Relative to Seismic Response Spectra", Bulletin of the Seismological Society of America, February 1970.
- (3) Nadolski, M. E., "Architectural Damage to Residential Structures from Seismic Disturbances", Bulletin of the Seismological Society of America, April 1969.
- (4) Knox, Joseph B., "Nuclear Excavation: Theory and Applications", Nuclear Applications & Technology, Vol. 7, September 1969.
- (5) Housner, G. W., "Requirements of Seismic Analysis and Research Needs", paper presented at the ASCE Annual and Environmental Meeting, Chicago, Illinois, October 1969.
- (6) John A. Blume & Associates Research Division, "Structural Response of Residential-Type Test Structures in close Proximity to an Underground Nuclear Detonation", Vela Uniform Program, report VUF-1030, issued November 15, 1965.
- (7) Blume, John A., "The Earthquake Resistance of California School Buildings- Additional Analyses and Design Implications", Division of Architecture, California State Printing Division, Sacramento, California, 1962.
- (8) Blume, John A., "A Reserve Energy Technique for the Design and Rating of Structures in the Inelastic Range", Proceedings, Second World Conference on Earthquake Engineering, Japan, 1960.
- (9) Blume, John A., "Response of Highrise Buildings to Ground Motion from Underground Nuclear Detonations", Bulletin of the Seismological Society of America, December 1969.
- (10) Blume, John A., "An Engineering Intensity Scale for Earthquakes and Other Ground Motion", Bulletin of the Seismological Society of America, February 1970.

MAGNITUDE DETERMINATION FOR LARGE UNDERGROUND NUCLEAR EXPLOSIONS*

Lawrence D. Porter

Lawrence Radiation Laboratory, University of California
Livermore, California 94550

ABSTRACT

A method is presented for determining the local magnitudes for large underground nuclear explosions. The Gutenberg-Richter nomograph is applied to the peak amplitudes for 24 large underground nuclear explosions that took place in Nevada. The amplitudes were measured at 18 California Wood-Anderson stations located 150-810 km from the explosion epicenter. The variation of the individual station magnitudes and magnitude corrections and the variation of the average and rms error estimates in the magnitude determinations are examined with respect to distance, azimuth, and event location. The magnitude prediction capability of the Gutenberg-Richter nomograph is examined on the basis of these two criteria, and certain corrections are suggested. The azimuthal dependence of the individual station magnitudes is investigated, and corrections for the California stations are calculated. Statistical weighting schemes for two-component data are employed, and the assumptions and limitations in the use of peak amplitudes are discussed.

INTRODUCTION

It is well known that earthquakes and explosions differ appreciably in their local seismic effects. An inspection of a typical explosion seismogram recorded at a distance of about 100 km shows that there is considerably more compressional wave energy present in relation to the other wave energies than would be true for an earthquake. Consequently, one of the continuing problems in modern seismology is the evaluation of underground nuclear explosions in such a way that their seismic effects can be compared with those of earthquakes.

In this paper we investigate 24 of the larger underground nuclear explosions conducted in Nevada by the U.S. Atomic Energy Commission. Since the larger Nevada explosions are well recorded at almost all of the California seismic stations, it should be possible to compute magnitudes that are valid throughout California and hence over a range of several hundred kilometers. Furthermore, the variations due to azimuth and source locations can be investigated. Finally, station corrections can be computed for the California stations with respect to the Nevada explosions and from this result some feeling can be developed for the variations that can be expected in regions with complex geology.

Since some of the best recordings of local shocks are made on instruments with relatively low magnification, we turned to the Wood-Anderson

*Work performed under the auspices of the U.S. Atomic Energy Commission.

seismograph. This instrument has been used extensively throughout California for local shock studies. At some time between 1927 and the present 33 such instruments have been at 18 locations in California that were stations of regular seismic networks. The Wood-Anderson data offers an opportunity to exploit the considerable advantage of working with records from a single instrument, thus avoiding the obvious complications due to differences in frequency response and magnification that would arise with a variety of instruments.

In this paper we approach the problem of local magnitude determination for large underground nuclear explosions in much the same manner as Gutenberg and Richter¹ did for earthquakes. Individual station magnitudes for a given event are computed using an amplitude-distance relationship derived empirically from local earthquakes, and then statistical methods are used to compute weighted event magnitudes. Station corrections are calculated by reviewing an event catalog. The local magnitudes provide a useful complement to the teleseismic data that is included in the more general magnitude determinations for explosions such as that carried out by Evernden.²

In using the Gutenberg-Richter nomograph for relating Wood-Anderson amplitude and distance to magnitude, we assume that the peak horizontal amplitude is the most dominant feature of the records. Peak amplitudes are important because they are one of the principal factors in seismic-related damage.^{3,4} We make the further assumption that the decay rate of explosion peak amplitudes with distance does not differ appreciably from that for earthquakes. Such an assumption is probably true over a portion of the distance for which the Gutenberg-Richter nomograph is valid for local shocks. To make up for any deficiencies in the nomograph we introduce an iteration scheme that uses a first evaluation of the data as a calibration for the seismic stations.

The main conclusions of this investigation are that the Gutenberg-Richter nomograph may be used in the evaluation of underground explosions, but at least one iteration of the calculations must be performed to obtain uniform magnitudes. Station corrections as large as ± 0.8 magnitude units are possible. Furthermore, the nearer stations (closer than 300 km) sometimes show erratic variations, even when one attempts to calibrate them over a catalog of closely spaced events. Generally, for distances less than 10°, peak amplitudes for explosions attenuate less rapidly with distance than they do for earthquakes.

The measurements used in this investigation were supplied through the courtesy of Prof. Thomas V. McEvilly of the University of California, Berkeley, and Mr. John M. Nordquist of the California Institute of Technology.

STATISTICAL TREATMENT OF MULTICOMPONENT SEISMIC DATA

One of the characteristics of seismic data ensembles from a group of events is the absence of data from certain stations for some of the events. For a uniform event evaluation procedure a statistical approach must be adopted, and it is to this problem that the present section is devoted. In the case of multicomponent seismic data, variations in the number of components recorded at certain stations must also be taken into account.

The most general approach in seismic event evaluation is to use a magnitude scale such as the Gutenberg-Richter nomograph to convert the amplitudes recorded at various stations into station magnitudes. These magnitudes are examined for the entire set of stations at which the event was recorded, and an event magnitude is assigned. Station deviations for each event are the differences between the individual station magnitudes and the event magnitude. At the end of a series of events the station deviations may be averaged to give station corrections. Following such an approach to its ultimate development,

the station corrections can be used in an iterative process to determine adjusted magnitudes. The quality of the station corrections can be measured by the relative smallness of rms deviations for the station corrections.

To satisfy these aims we introduce the following statistical approach. Let W_{ik} be an element of the statistical weighting matrix W . W_{ik} has an integer value corresponding to the number of independent measurements made at a given station. The subscripts i and k refer to the fact that this weight is to be associated with the data recorded at the i th station from the k th event.

The individual station magnitudes, M_{ik} , for a given event are determined from an appropriate magnitude scale, which we shall denote by $F(\Delta_{ik}, B_{ik})$. Δ_{ik} and B_{ik} are the event-station epicentral distance and the representative station amplitude for the event, respectively. The method of determining the representative station amplitude is discussed at the beginning of the next section.

The weighted event magnitude \overline{M}_k for the k th event is given by the formula

$$\overline{M}_k = \frac{\sum_i W_{ik} M_{ik}}{\sum_i W_{ik}}, \quad (1)$$

where the summation with respect to i is carried out over the entire station catalog, since those stations with no usable records are assigned a weight of zero. The magnitude correction Mc_{ik} at the i th station for the k th event is

$$Mc_{ik} = \overline{M}_k - M_{ik}. \quad (2)$$

The weighted average magnitude correction \overline{Mc}_k for the k th event is

$$\overline{Mc}_k = \frac{\sum_k W_{ik} Mc_{ik}}{\sum_k W_{ik}}. \quad (3)$$

Substitution of Eq. 2 into Eq. 3 shows that $\overline{Mc}_i \equiv 0$. The weighted rms magnitude correction for the k th event is

$$\overline{Mc} \text{ rms}_k = \left| \left\{ \frac{\sum_k W_{ik} Mc_{ik}^2}{\sum_k W_{ik}} \right\}^{1/2} \right|, \quad (4)$$

where the absolute signs have been introduced to ensure that the square root is to be taken as positive. This positive definite quantity serves as a measure of the station magnitude variation for a given event.

From an ensemble of events it is possible to compute a weighted average station correction, \overline{Msc}_i , where

$$\overline{M}_{sc_i} = \frac{\sum_k W_{ik} M_{c_{ik}}}{\sum_k W_{ik}}. \quad (5)$$

The summation with respect to k is carried out over the complete event catalog, since, in a fashion analogous to the station catalog, the noncontributing events for a particular station are assigned zero weight. In addition, one may compute a weighted rms station correction, \overline{M}_{scrms_i} , which is given by

$$\overline{M}_{scrms_i} = \left[\frac{\left\{ \frac{\sum_k W_{ik} M_{c_{ik}}^2}{\sum_k W_{ik}} \right\}^{1/2}}{\sum_k W_{ik}} \right]. \quad (6)$$

Again, analogous to the case of Eq. 4, \overline{M}_{scrms_i} serves as a measure of the station correction variation for an ensemble of events.

The station corrections defined by Eq. 5 may be used as the starting point for an iterative scheme to compute higher-order station corrections as well as corrected values for all of the quantities mentioned in Eqs. 1 through 6. These terms may be ordered by the use of the superscript j , where j is an integer corresponding to the number of times that the iteration has been performed. The individual station magnitudes are determined by the relation

$$M_{ik}^{(j+i)} = M_{ik}^{(0)} + \overline{M}_{sc_i}^{(j)}. \quad (7)$$

With the aid of $M_{ik}^{(j+i)}$, higher-order corrected values for the quantities \overline{M}_k , $M_{c_{ik}}$, \overline{M}_{c_k} , \overline{M}_{crms_k} , \overline{M}_{sc_i} , and \overline{M}_{scrms_i} can be determined. The computation and interpretation of all of these quantities for an actual sequence of events and their corresponding station amplitudes is carried out in the next two sections.

EVALUATION OF CALIFORNIA SEISMIC DATA FOR LARGE UNDERGROUND NUCLEAR EXPLOSIONS

The data from the large underground nuclear explosions in Nevada consists of peak amplitude readings from Wood-Anderson seismographs recorded at a maximum of 18 stations that were in operation between 1962 and 1969. Seven of the stations were operated by the University of California, Berkeley, while the remaining 11 were operated by the California Institute of Technology. The names, symbols, networks, locations, and periods of operation of the stations are given in Table I. The map in Fig. 1 shows the geographic locations of the stations.

The seismic data was generated by 24 underground nuclear explosions that took place between 1962 and the first half of 1969. The events are identified in Table II by their names, origin times, and locations. Twenty-three of the explosions had their origins in the Nevada Test Site, with 13 of these being in Yucca Flats and the remaining 10 in Pahute Mesa. One explosion took place at the Supplementary Test Site in Central Nevada. The distance and station azimuths between the explosions and the two most well known seismic stations in California, Berkeley (BKS) and Pasadena (PAS), are given in Tables III and IV, respectively. Because of the relatively small distances between the events

Table I. Locations of seismic stations in California with Wood-Anderson seismographs.

No.	Station	Symbol	Network ^a	Latitude (N)	Longitude (W)	Component	Started	Ended
1	Arcata	ARC	UCB	40° 52.6'	124° 04.5'	N,E	1948	—
2	Barrett	BAR	CIT	32° 40.8'	116° 40.3'	N	1/17/52	—
3	Berkeley	BKS	UCB	37° 52.6'	122° 14.1'	S,W	1962	—
4	Cottonwood	CWC	CIT	36° 26.3'	118° 04.7'	N,E	10/13/65	—
5	El Centro ^b	ECC	CIT	32° 47.9'	115° 32.9'	N,E	11/28/56	—
6	Haiwee	HAI	CIT	36° 08.2'	117° 56.8'	N,E	9/11/29	10/27/65
7	Mineral	MIN	UCB	40° 20.7'	121° 36.3'	S,E	1938	—
8	Mt. Hamilton	MHC	UCB	37° 20.5'	121° 38.5'	S,E	1927	—
9	Palo Alto	PAC	UCB	37° 25.0'	122° 10.9'	N,E	1927	7/65
10	Pasadena	PAS	CIT	34° 08.9'	118° 10.3'	N,E	3/17/27	—
11	Riverside	RVR	CIT	33° 59.6'	117° 22.5'	N,E	10/19/26	—
12	San Francisco	SFB	UCB	37° 46.6'	122° 27.1'	N,E	1940	12/1/64
13	San Nicolas	SNC	CIT	33° 14.9'	119° 31.4'	E	7/24/57	1/24/68
14	Santa Barbara	SBC	CIT	34° 26.5'	119° 42.8'	N,E	5/10/27	—
15	Sawmill	SWM	CIT	34° 43.1'	118° 34.9'	N,E	3/7/66	—
16	Tinemaha	TIN	CIT	37° 03.3'	118° 13.7'	N,E	9/4/29	—
17	Vinyard	VIN	UCB	36° 45.6'	121° 23.1'	S,W	1959	3/9/66
18	Woody	WDY	CIT	35° 42.0'	118° 50.6'	E	8/5/52	—

^aUCB = University of California, Berkeley; CIT = California Institute of Technology.

^bStrong-motion instrument with Wood-Anderson frequency response but with magnification = 140. Wood-Anderson magnification = 2800.

Table II. Event catalog.

No.	Date	Origin time (GCT) hr:min:sec	Latitude	Longitude	Event	Region
1	10/5/62	17:00:00.2	37° 08.4'	116° 03.0'	Mississippi	Yucca Flats
2	9/13/63	17:00:00.1	37° 03.6'	116° 01.3'	Bilby	Yucca Flats
3	1/16/64	15:00:00.1	37° 08.5'	116° 02.9'	Fore	Yucca Flats
4	4/24/64	20:10:00.2	37° 08.0'	116° 03.3'	Turf	Yucca Flats
5	3/26/65	15:24:08.2	37° 08.9'	116° 02.6'	Cup	Yucca Flats
6	12/3/65	15:13:02.1	37° 09.9'	116° 03.1'	Corduroy	Yucca Flats
7	5/19/66	13:56:28.4	37° 06.7'	116° 03.5'	Dumont	Yucca Flats
8	6/30/66	22:15:00.1	37° 18.9'	116° 17.9'	Halfbeak	Pahute Mesa
9	12/20/66	15:30:00.1	37° 18.1'	116° 24.5'	Greeley	Pahute Mesa
10	2/23/67	18:50:00.0	37° 07.6'	116° 04.0'	Agile	Yucca Flats
11	5/20/67	15:00:00.0	37° 07.8'	116° 03.8'	Commodore	Yucca Flats
12	5/23/67	14:00:00.0	37° 16.5'	116° 22.2'	Scotch	Pahute Mesa
13	9/27/67	17:00:00.0	37° 05.9'	116° 03.2'	Zaza	Yucca Flats
14	10/18/67	14:30:00.0	37° 06.9'	116° 03.5'	Lanpher	Yucca Flats
15	1/19/68	18:15:00.1	38° 38.1'	116° 12.9'	Faultless	Central Nevada
16	2/21/68	15:30:00.0	37° 07.0'	116° 03.2'	Knox	Yucca Flats
17	3/22/68	15:00:00.1	37° 20.0'	116° 18.6'	Stinger	Pahute Mesa
18	4/26/68	15:00:00.0	37° 17.7'	116° 27.3'	Boxcar	Pahute Mesa
19	6/15/68	14:00:00.0	37° 15.9'	116° 18.9'	Rickey	Pahute Mesa
20	6/28/68	12:22:00.0	37° 14.7'	116° 29.0'	Chateaugay	Pahute Mesa
21	8/29/68	22:45:00.0	37° 15.0'	116° 20.8'	Sled	Pahute Mesa
22	9/6/68	14:00:00.1	37° 08.2'	116° 02.8'	Noggin	Yucca Flats
23	12/19/68	16:30:38.8	37° 13.9'	116° 28.4'	Benham	Pahute Mesa
24	5/7/69	13:45:00.0	37° 16.9'	116° 30.0'	Purse	Pahute Mesa

located within a particular area at NTS, a specific event has been selected for each area as being a representative location for the computation of distance and azimuth to the various stations; the station distances and azimuths with respect to them are listed in Tables V, VI, and VII. All of the distances were computed according to Rudoe's formula,⁵ while the azimuths were obtained by

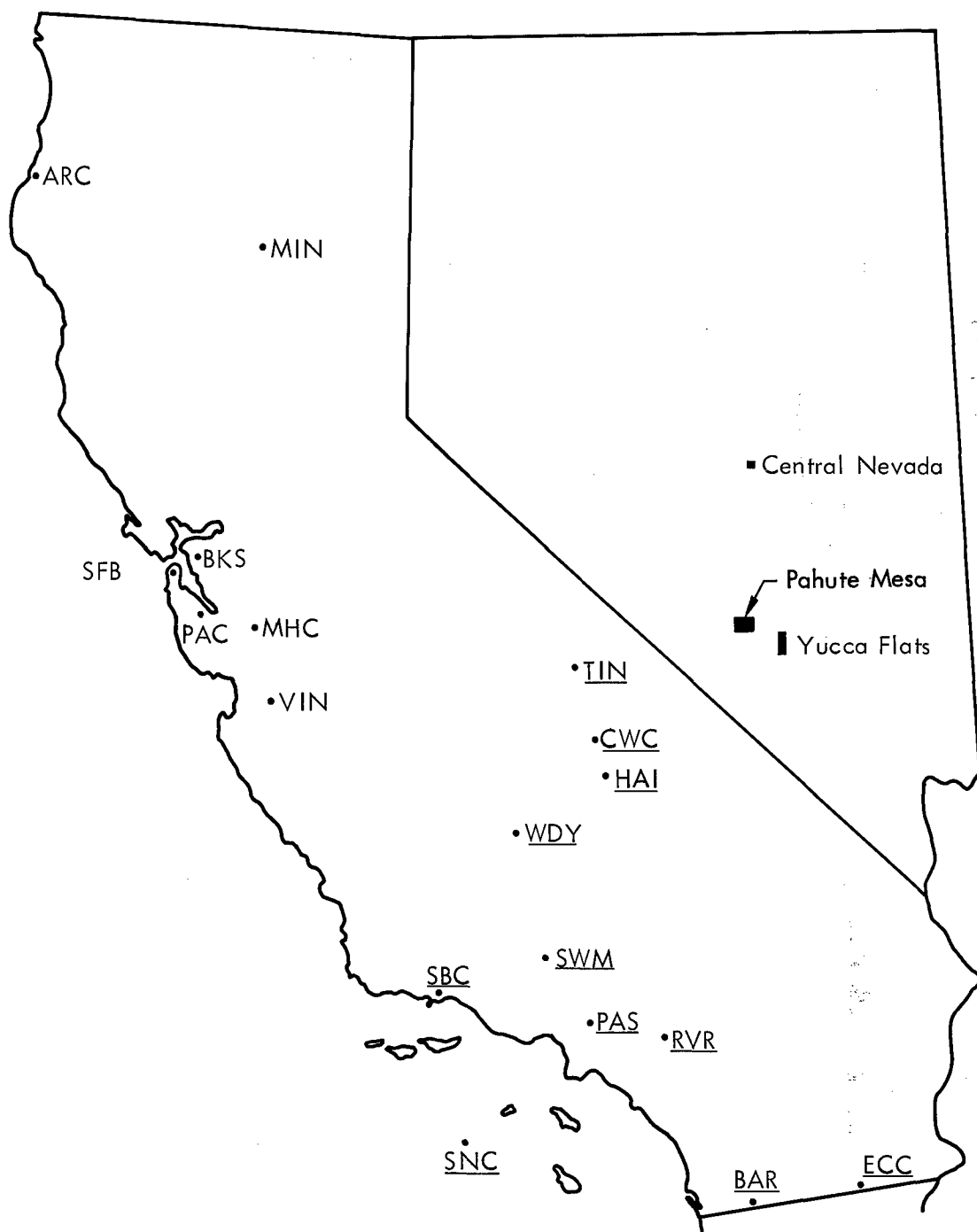


Fig. 1. Map of California and Nevada showing the locations of Wood-Anderson seismographs and the underground nuclear explosions. Stations reporting to the California Institute of Technology are underlined; the others are operated by the University of California, Berkeley.

Table III. Distance and azimuth from Berkeley to event locations.

Event	Latitude	Longitude	Distance (deg)	Distance (km)	Azimuth	Back Azimuth	Method
10/05/62	37.140	-116.050	4.972	552.8	96.619	280.371	RUDGE
09/13/63	37.060	-116.022	5.010	557.0	97.472	261.233	RUDGE
01/16/64	37.142	-116.048	4.973	553.0	96.597	280.351	RUDGE
04/24/64	37.133	-116.055	4.970	552.5	96.703	280.452	RUDGE
03/26/65	37.148	-116.043	4.976	553.3	96.513	280.270	RUDGE
12/03/65	37.165	-116.052	4.967	552.2	96.336	280.090	RUDGE
05/19/66	37.112	-116.058	4.971	552.7	96.954	280.700	RUDGE
06/30/66	37.315	-116.298	4.748	527.9	94.970	276.579	RUDGE
12/20/66	37.302	-116.408	4.663	518.5	95.293	278.634	RUDGE
02/23/67	37.127	-116.067	4.962	551.7	96.798	280.540	RUDGE
05/20/67	37.130	-116.063	4.964	551.9	96.755	280.493	RUDGE
05/23/67	37.275	-116.370	4.198	522.3	95.556	273.120	RUDGE
09/27/67	37.015	-116.053	4.994	555.2	98.034	261.779	RUDGE
10/18/67	37.115	-116.058	4.970	552.6	96.916	280.662	RUDGE
01/19/68	38.635	-116.215	4.794	533.5	79.075	262.769	RUDGE
02/21/68	37.117	-116.053	4.974	553.0	96.889	280.638	RUDGE
03/22/68	37.333	-116.310	4.736	526.6	94.768	278.370	RUDGE
04/26/68	37.295	-116.455	4.628	514.5	95.445	278.957	RUDGE
06/15/68	37.265	-116.315	4.743	527.3	95.531	279.132	RUDGE
06/28/68	37.245	-116.483	4.613	512.9	96.101	279.535	RUDGE
08/29/68	37.250	-116.347	4.720	524.8	95.820	279.396	RUDGE
09/06/68	37.137	-116.047	4.976	553.2	96.651	280.405	RUDGE
12/19/68	37.232	-116.473	4.623	514.1	96.248	279.747	RUDGE
05/07/69	37.283	-116.500	4.594	510.8	95.658	279.143	RUDGE

Table IV. Distance and azimuth from Pasadena to event locations.

Event	Latitude	Longitude	Distance (deg)	Distance (km)	Azimuth	Back Azimuth	Method
10/05/62	37.140	-116.050	3.449	363.5	29.457	210.698	RUDGE
09/13/63	37.060	-116.022	3.392	377.2	30.475	211.721	RUDGE
01/16/64	37.142	-116.048	3.451	363.6	29.462	210.694	RUDGE
04/24/64	37.133	-116.055	3.441	362.7	29.456	210.684	RUDGE
03/26/65	37.148	-116.043	3.459	364.6	29.462	210.698	RUDGE
12/03/65	37.165	-116.052	3.470	365.6	29.227	210.458	RUDGE
05/19/66	37.112	-116.058	3.421	360.4	29.602	210.629	RUDGE
06/30/66	37.315	-116.298	3.506	390.1	25.211	206.301	RUDGE
12/20/66	37.302	-116.408	3.458	364.5	24.005	205.030	RUDGE
02/23/67	37.127	-116.067	3.431	361.5	29.379	210.600	RUDGE
05/20/67	37.130	-116.063	3.435	362.0	29.389	210.612	RUDGE
05/23/67	37.275	-116.370	3.447	363.3	24.653	205.700	RUDGE
09/27/67	37.015	-116.053	3.341	371.5	30.510	211.733	RUDGE
10/18/67	37.115	-116.058	3.424	360.8	29.574	210.800	RUDGE
01/19/68	38.635	-116.215	4.747	527.9	18.650	200.007	RUDGE
02/21/68	37.117	-116.053	3.426	361.1	29.617	210.646	RUDGE
03/22/68	37.333	-116.310	3.520	391.4	24.943	206.026	RUDGE
04/26/68	37.295	-116.455	3.436	362.1	23.489	204.487	RUDGE
06/15/68	37.265	-116.315	3.457	364.5	25.380	206.459	RUDGE
06/28/68	37.245	-116.483	3.382	376.0	23.491	204.472	RUDGE
08/29/68	37.250	-116.347	3.433	361.7	25.114	206.174	RUDGE
09/06/68	37.137	-116.047	3.448	363.4	29.523	210.756	RUDGE
12/19/68	37.232	-116.473	3.373	375.0	23.708	204.645	RUDGE
05/07/69	37.283	-116.500	3.411	379.3	23.021	203.993	RUDGE

Table V. Distance and azimuth from Yucca Flats to California seismic stations.

Station	Latitude	Longitude	Distance (deg)	Distance (km)	Azimuth	Back Azimuth	Method
ARC	40.877	-124.075	7.277	809.0	303.302	118.263	RUDOE
EKS	37.877	-122.235	4.972	552.8	280.371	96.619	RUDOE
MHC	37.342	-121.642	4.466	496.6	274.266	90.895	RUDOE
MIN	40.345	-121.605	5.394	599.7	308.086	124.621	RUDOE
PAC	37.417	-122.182	4.898	544.6	275.079	91.378	RUDOE
SFB	37.777	-122.452	5.133	570.7	279.044	95.164	RUDOE
VIN	36.750	-121.385	4.291	477.1	266.397	83.203	RUDOE
BAR	32.680	-116.672	4.479	498.0	186.729	6.375	RUDOE
CNC	36.438	-118.078	1.772	197.1	247.335	66.125	RUDOE
ECG	32.798	-115.548	4.351	483.8	174.422	354.709	RUDOE
HAI	36.137	-117.947	1.825	202.9	237.286	56.159	RUDOE
PAS	34.148	-118.172	3.449	383.5	210.688	29.457	RUDOE
KVR	33.943	-117.375	3.320	369.2	199.373	18.605	RUDOE
SNC	33.248	-119.523	4.813	535.2	217.239	35.245	RUDOE
SBG	34.442	-119.713	4.014	446.4	228.965	46.631	RUDOE
SWM	34.718	-118.582	3.172	352.7	221.120	39.641	RUDOE
TIN	37.055	-118.228	1.744	193.9	267.866	86.537	RUDOE
WDY	35.700	-118.843	2.672	297.1	238.300	56.649	RUDOE

Table VI. Distance and azimuth from Pahute Mesa to California seismic stations.

Station	Latitude	Longitude	Distance (deg)	Distance (km)	Azimuth	Back Azimuth	Method
ARC	40.877	-124.075	6.922	769.5	303.448	118.657	RUDOE
EKS	37.877	-122.235	4.628	514.5	278.957	95.445	RUDOE
MHC	37.342	-121.642	4.135	459.7	272.211	89.079	RUDOE
MIN	40.345	-121.605	5.044	560.8	308.713	125.496	RUDOE
PAC	37.417	-122.182	4.564	507.5	273.254	89.792	RUDOE
SFB	37.777	-122.452	4.790	532.6	277.574	93.934	RUDOE
VIN	36.750	-121.385	3.983	442.8	263.634	80.677	RUDOE
BAR	32.680	-116.672	4.608	512.4	182.275	2.151	RUDOE
CNC	36.438	-118.078	1.558	173.2	237.191	56.221	RUDOE
ECG	32.798	-115.548	4.547	505.7	170.323	350.842	RUDOE
HAI	36.137	-117.947	1.665	185.2	226.481	45.593	RUDOE
PAS	34.148	-118.172	3.436	382.1	204.487	23.489	RUDOE
KVR	33.943	-117.375	3.379	375.7	193.083	12.549	RUDOE
SNC	33.248	-119.523	4.754	528.6	212.769	31.004	RUDOE
SBG	34.442	-119.713	3.587	432.2	223.869	41.967	RUDOE
SWM	34.718	-118.582	3.096	344.2	214.475	33.230	RUDOE
TIN	37.055	-118.228	1.437	159.7	260.935	79.868	RUDOE
WDY	35.700	-118.843	2.497	277.7	231.117	49.702	RUDOE

Table VII. Distance and azimuth from Central Nevada to California seismic stations.

Station	Latitude	Longitude	Distance (deg)	Distance (km)	Azimuth	Back Azimuth	Method
ARC	40.877	-124.075	6.457	717.8	292.755	107.743	RUDOE
EKS	37.877	-122.235	4.799	535.5	262.789	79.075	RUDOE
MHC	37.342	-121.642	4.477	497.8	254.918	71.590	RUDOE
MIN	40.345	-121.605	4.506	500.9	293.959	110.543	RUDOE
PAC	37.417	-122.182	4.866	541.0	257.370	73.709	RUDOE
SFB	37.777	-122.452	4.986	554.4	262.039	78.194	RUDOE
VIN	36.750	-121.385	4.511	501.6	246.944	63.795	RUDOE
BAR	32.680	-116.672	5.954	662.0	183.716	3.450	RUDOE
CNC	36.438	-118.078	2.646	294.2	214.608	33.478	RUDOE
ECG	32.798	-115.548	5.849	650.4	174.482	354.670	RUDOE
HAI	36.137	-117.947	2.550	316.9	209.474	28.427	RUDOE
PAS	34.148	-118.172	4.747	527.9	200.007	18.850	RUDOE
KVR	33.943	-117.375	4.726	525.5	191.780	11.095	RUDOE
SNC	33.248	-119.523	6.007	668.0	207.522	25.586	RUDOE
SBG	34.442	-119.713	5.044	560.9	215.001	32.926	RUDOE
SWM	34.718	-118.582	4.547	483.4	206.666	25.257	RUDOE
TIN	37.055	-118.228	2.242	249.3	225.918	44.688	RUDOE
WDY	35.700	-118.843	3.604	400.7	216.427	34.845	RUDOE

applying the spherical trigonometric formulae from Bullen⁶ to the event and station locations in geocentric coordinates.

The number of peak amplitudes recorded for each event varies between 15 and 23 for the entire event series. The individual station magnitudes were determined with the aid of the Gutenberg-Richter nomograph. The Appendix describes a tabulated version of the nomograph that is particularly suited to numerical computation. To reveal the presence of any azimuthal dependence in the determination of the magnitudes, two representative amplitudes were used for each station. First, the magnitude was computed in the conventional manner; that is, from the average of the north-south and east-west components. A second magnitude was computed from the rms value (in a horizontal vector sense)

$$B_{\text{rms}} = \left[\frac{1}{2} (B_{\text{EW}}^2 + B_{\text{NS}}^2) \right]^{1/2} - \frac{|B|_{\text{horizontal}}}{2} \quad (8)$$

of the peak amplitudes for these two perpendicular components. This latter calculation was made on the assumption that the peak amplitudes were recorded simultaneously on the two perpendicularly oriented seismometers. Even though this condition may not have been fulfilled for all the two-component station recordings, the difference in magnitudes obtained by the two methods never exceeded 0.02 for the entire event series. Data from the stations with only one instrument or one usable recording were weighted as discussed in the previous section. From this result one may conclude that the Gutenberg-Richter nomograph is insensitive to the direction of the waves incident upon a given station. In this paper we therefore quote only the magnitude determined in the conventional manner.

The magnitude calculations are carried out in two successive steps. The first step is to begin without station corrections and compute all of the quantities defined in Eqs. 1 through 6. Since $\overline{M}_{\text{sc}_i} = 0$ in Eq. 7, for this calculation we label the quantities with superscript zero and refer to them as zero iteration quantities. For each of the 24 events we calculate the individual station magnitudes $M_{ik}^{(0)}$ according to Eq. A-1 in the Appendix, the weighted event magnitude $\overline{M}_k^{(0)}$ from Eq. 1, the magnitude corrections $\overline{M}_{c_{ik}}^{(0)}$ from Eq. 2, the weighted average event magnitude correction $\overline{M}_{c_k}^{(0)}$ defined by Eq. 3, and the weighted rms event magnitude correction $\overline{M}_{\text{crms}_k}^{(0)}$ from Eq. 4. Calculations of these quantities for the events typical of the three areas are given in Tables VIII, IX, and X. The weighted event magnitudes for the entire event catalog are summarized in Table XI. By averaging the individual magnitude corrections over the event catalog, as indicated in Eqs. 5 and 6, we obtain the station corrections listed in Table XII.

The second step in the magnitude determination scheme is to repeat all of the above-mentioned computations, this time with the aid of the station corrections given by $\overline{M}_{\text{sc}_i}^{(0)}$. For this purpose we calculate the individual magnitudes $M_{ik}^{(1)}$ according to Eq. 7 written in the form

$$M_{ik}^{(1)} = M_{ik}^{(0)} + \overline{M}_{\text{sc}_i}^{(0)}. \quad (9)$$

All of the quantities in Eqs. 1 through 6 are labelled with superscript 1 and referred to in the text as first iteration calculations. The convergence rate of the iteration scheme is shown by comparing the weighted rms event magnitude corrections $\overline{M}_{\text{crms}_k}^{(0)}$ with $\overline{M}_{\text{crms}_k}^{(1)}$ in Table IX and the weighted station corrections $\overline{M}_{\text{sc}_i}^{(0)}$ with $\overline{M}_{\text{sc}_i}^{(1)}$. In general, the station corrections decrease by an order of magnitude in going from zero to first iteration, while $\overline{M}_{\text{crms}_k}$ decreases by a factor of 2 to 4.

Table VIII. Magnitude determination representative of Yucca Flats.

Station	Distance (km)	Amp (EW)	Amp (NS)	Amp (av)	Amp (vec)	$M_{ik}^{(0)}$	$Mc_{ik}^{(0)}$	$M_{ik}^{(1)}$	$Mc_{ik}^{(1)}$	Weight
ARC	809.0	0.	0.	0.	0.	0.	0.	0.	0.	0
BKS	552.8	1.5	1.2	1.35	1.36	5.00	0.07	4.87	0.13	2
MHC	496.6	5.7	6.5	6.10	6.11	5.50	-0.42	5.07	-0.07	2
MIN	599.7	1.1	1.2	1.15	1.15	5.05	0.02	4.87	0.13	2
PAC	544.6	4.0	3.0	3.50	3.54	5.39	-0.32	5.00	-0.01	2
SFB	570.7	2.5	1.5	2.00	2.06	5.22	-0.14	5.12	-0.12	2
VIN	477.1	8.2	9.1	8.65	8.66	5.60	-0.53	5.07	-0.07	2
BAR	498.0	0.	0.6	0.60	0.60	4.49	0.58	5.10	-0.10	1
CNC	197.1	0.	0.	0.	0.	0.	0.	0.	0.	0
ECC	485.8	0.	0.	0.	0.	0.	0.	0.	0.	0
HAI	202.9	0.	0.	0.	0.	0.	0.	0.	0.	0
PAS	383.5	2.3	2.4	2.35	2.35	4.74	0.33	4.47	0.03	2
RVR	369.2	2.4	0.	2.40	2.40	4.70	0.37	5.09	-0.10	1
SNC	525.2	0.7	0.	0.70	0.70	4.67	0.41	4.89	0.11	1
SBC	446.4	5.0	9.0	7.00	7.28	5.42	-0.35	5.09	-0.09	2
SMM	352.7	0.	0.	0.	0.	0.	0.	0.	0.	0
TIN	195.9	19.3	14.3	16.80	16.98	4.72	0.36	4.77	0.23	2
WDY	297.1	3.0	0.	3.00	3.00	4.47	0.61	5.21	-0.21	1

	Weighted magnitude	Sum (av)	\overline{Mc}	Sum (rms)	\overline{Mc}_{rms}	Data points
$\overline{M}^{(0)}$ (zero iteration)	5.07	-0.00	-0.00	2.90	0.36	22
$\overline{M}^{(1)}$ (first iteration)	4.99	-0.00	-0.00	0.31	0.12	22

Table IX. Magnitude determination representative of Pahute Mesa.

Station	Distance (km)	Amp (EW)	Amp (NS)	Amp (av)	Amp (vec)	$M_{ik}^{(0)}$	$Mc_{ik}^{(0)}$	$M_{ik}^{(1)}$	$Mc_{ik}^{(1)}$	Weight
ARC	769.5	9.5	9.0	9.25	9.25	6.29	-0.34	6.15	-0.14	2
BKS	514.5	24.0	29.5	26.75	26.69	6.19	-0.24	6.06	-0.05	2
MHC	459.7	43.2	58.8	51.00	51.59	6.32	-0.37	5.90	0.11	2
MIN	560.8	33.2	35.6	33.40	33.40	6.41	-0.46	6.23	-0.22	2
PAC	507.5	0.	0.	0.	0.	0.	0.	0.	0.	0
SFB	532.6	0.	0.	0.	0.	0.	0.	0.	0.	0
VIN	442.8	0.	0.	0.	0.	0.	0.	0.	0.	0
BAR	512.4	0.	3.0	3.00	3.00	5.23	0.72	5.84	0.17	1
CNC	173.2	0.	0.	0.	0.	0.	0.	0.	0.	0
ECC	506.7	0.	0.	0.	0.	0.	0.	0.	0.	0
HAI	185.2	0.	0.	0.	0.	0.	0.	0.	0.	0
PAS	382.1	16.0	21.4	18.70	18.69	5.64	0.31	5.87	0.14	2
RVR	375.7	23.3	16.0	19.65	19.99	5.64	0.31	6.04	-0.02	2
SNC	528.6	0.	0.	0.	0.	0.	0.	0.	0.	0
SBC	432.2	0.	0.	0.	0.	0.	0.	0.	0.	0
SMM	344.2	0.	0.	0.	0.	0.	0.	0.	0.	0
TIN	159.7	0.	0.	0.	0.	0.	0.	0.	0.	0
WDY	277.7	15.3	0.	15.30	15.30	5.09	0.96	5.83	0.18	1

	Weighted magnitude	Sum (av)	\overline{Mc}	Sum (rms)	\overline{Mc}_{rms}	Data points
$\overline{M}^{(0)}$ (zero iteration)	5.95	-0.00	-0.00	2.70	0.44	14
$\overline{M}^{(1)}$ (first iteration)	6.01	-0.00	-0.00	0.28	0.14	14

Table X. Magnitude determination representative of Central Nevada.

Station	Distance (km)	Amp (EW)	Amp (NS)	Amp (av)	Amp (vec)	$M_{ik}^{(0)}$	$Mc_{ik}^{(0)}$	$M_{ik}^{(1)}$	$Mc_{ik}^{(1)}$	Weight
ARC	717.8	4.5	3.7	4.10	4.12	5.85	0.06	5.71	0.20	2
BKS	533.5	16.5	17.3	16.90	16.90	6.04	-0.14	5.91	-0.01	2
MHC	497.8	15.5	27.8	21.65	22.51	6.05	-0.15	5.64	0.27	2
MIN	500.9	22.2	37.7	29.95	30.94	6.20	-0.30	6.03	-0.13	2
PAC	541.0	0.	0.	0.	0.	0.	0.	0.	0.	0
SFB	554.4	0.	0.	0.	0.	0.	0.	0.	0.	0
VIN	501.6	0.	0.	0.	0.	0.	0.	0.	0.	0
BAR	662.0	0.	1.7	1.70	1.70	5.35	0.55	5.96	-0.06	1
CNC	244.2	0.	0.	0.	0.	0.	0.	0.	0.	0
ECC	650.4	0.	0.	0.	0.	0.	0.	0.	0.	0
HAI	316.9	0.	0.	0.	0.	0.	0.	0.	0.	0
PAS	527.9	10.0	8.4	9.20	9.23	5.76	0.14	6.00	-0.09	2
RVR	525.5	7.1	4.9	6.00	6.10	5.57	0.33	5.97	-0.06	2
SNC	668.0	0.	0.	0.	0.	0.	0.	0.	0.	0
SBC	560.9	23.0	0.	23.00	23.00	6.25	-0.35	5.90	0.01	1
SMM	483.4	43.0	56.0	49.50	49.92	6.37	-0.47	6.13	-0.22	2
TIN	249.3	0.	0.	0.	0.	0.	0.	0.	0.	0
WDY	400.7	4.3	0.	4.30	4.30	5.06	0.85	5.80	0.11	1

	Weighted magnitude	Sum (av)	\overline{Mc}	Sum (rms)	\overline{Mc}_{rms}	Data points
$\overline{M}^{(0)}$ (zero iteration)	5.90	-0.00	-0.00	2.10	0.35	17
$\overline{M}^{(1)}$ (first iteration)	5.90	-0.00	-0.00	0.40	0.15	17

Table XI. Summary of weighted event magnitudes and corrections.

Event	$\bar{M}_k^{(0)}$	$\bar{M}_{crms_k}^{(0)}$	$\bar{M}_k^{(1)}$	$\bar{M}_{crms_k}^{(1)}$	Data points
10/05/62	5.07	0.36	4.29	0.12	22
09/17/63	5.57	0.31	5.56	0.09	21
01/16/64	5.02	0.41	5.01	0.15	23
04/24/64	5.00	0.33	4.99	0.29	27
07/26/65	4.97	0.33	5.00	0.11	20
12/03/65	5.23	0.34	5.25	0.15	17
05/10/66	5.39	0.50	5.37	0.09	23
06/30/66	5.70	0.51	5.68	0.11	23
12/20/66	5.91	0.41	5.87	0.12	21
02/27/67	5.28	0.45	5.31	0.09	21
05/20/67	5.37	0.45	5.45	0.08	19
05/23/67	5.26	0.40	5.34	0.09	19
09/27/67	5.31	0.46	5.38	0.14	20
10/18/67	5.51	0.45	5.34	0.09	19
01/10/68	5.90	0.35	5.90	0.15	17
02/21/68	5.34	0.51	5.31	0.11	22
03/22/68	5.41	0.45	5.39	0.20	20
04/26/68	5.95	0.44	6.01	0.14	14
06/15/68	5.49	0.51	5.46	0.12	22
06/20/68	5.05	0.33	5.06	0.07	15
08/20/68	5.47	0.42	5.49	0.09	19
09/06/68	5.26	0.52	5.24	0.09	20
12/10/68	6.02	0.46	5.96	0.12	16
05/07/69	5.37	0.39	5.43	0.10	21

Table XII. Summary of weighted station corrections.

Station	$\bar{M}_{sc_i}^{(0)}$	$\bar{M}_{scrms_i}^{(0)}$	$\bar{M}_{sc_i}^{(1)}$	$\bar{M}_{scrms_i}^{(1)}$	Data points
ARC	-0.14	0.21	0.01	0.11	30
EKS	-0.13	0.16	0.00	0.09	47
MHC	-0.43	0.45	0.00	0.12	48
MIN	-0.18	0.24	0.00	0.15	46
PAC	-0.39	0.40	-0.02	0.03	6
SFR	-0.11	0.14	-0.04	0.11	6
VIN	-0.53	0.54	-0.04	0.05	6
PAP	0.61	0.64	0.01	0.18	23
CWC	0.66	0.66	0.02	0.06	26
ECC	-0.84	0.85	-0.04	0.09	18
HAI	0.11	0.15	-0.00	0.11	8
PAS	0.22	0.25	0.00	0.09	48
PVR	0.40	0.42	0.01	0.11	46
SNC	0.21	0.23	0.00	0.05	10
SPC	-0.35	0.36	-0.00	0.09	41
SWH	-0.25	0.27	-0.02	0.09	28
TIN	0.05	0.23	0.00	0.21	13
WDY	0.74	0.81	-0.00	0.33	24

INTERPRETATION OF THE CALIFORNIA SEISMIC DATA FOR LARGE UNDERGROUND EXPLOSIONS

Two aspects of the California seismic data for large underground explosions can be examined with the aid of the evaluations carried out in the preceding section. First, we inspect the magnitudes as determined with the aid of the Gutenberg-Richter nomograph and the statistical weighting procedure described earlier. The fit of the data is judged in terms of the various error estimates. Second, we attempt to correlate the magnitude variations in terms of the geographic locations of the stations and the events.

The basic objective in devising a magnitude determination scheme is to make magnitude independent of distance and azimuth. To see how appropriate the Gutenberg-Richter magnitude scale is for underground explosions we examine the individual station magnitude for the selected events from each of the three areas. For the zero iteration calculations in Tables VIII, IX, and X the extreme values of the individual station corrections $\overline{Mc}_{ik}^{(0)}$ have the extreme values +0.86 and -0.47. The rms error $\overline{Mcrms}_k^{(0)}$ in the determination of the event magnitudes $\overline{M}_k^{(0)}$ in Table XI fluctuates between 0.31 and 0.52 and bears no apparent connection to the event magnitude. The station corrections $\overline{Msc}_i^{(0)}$ in Table XII range from -0.84 for El Centro (ECC) to 0.74 for Woody (WDY), with a corresponding rms station corrects $\overline{Mscrms}_i^{(0)}$ of 0.85 and 0.81. Convergence of the iteration scheme and thus an enhancement of the fit of the data is shown by the decrease in the values for all of the quantities mentioned above. In the case of the first iteration calculations, $\overline{Mc}_{ik}^{(1)}$ has the extreme values +0.28 and -0.22 for the three selected events in Tables VIII, IX, and X. $\overline{Mcrms}_k^{(1)}$, given by Table XI, fluctuates between 0.08 and 0.29. In Table XII, $\overline{Msc}_i^{(1)}$ ranges from -0.04 to +0.02. The extreme values for $\overline{Mscrms}_i^{(1)}$ are 0.03 and 0.33. The extreme values for all the statistical quantities are summarized in Table XIII. The consistency of the seismic stations is found by examining $\overline{Mscrms}_i^{(0)}$ and $\overline{Mscrms}_i^{(1)}$. These results are presented in Table XIV, and $\overline{Mscrms}_i^{(1)}$ shows clearly that Woody is by far the least reliable of the California Wood-Anderson stations.

Table XIII. Extreme values for quantities used in magnitude determination.

	Upper value	Lower value
Individual magnitude correction for a given event:		
$\overline{Mc}_{ik}^{(0)}$	1.08 (WDY, 1/16/64)	-1.09 (ECC, 2/23/67)
$\overline{Mc}_{ik}^{(1)}$	0.44 (MIN, 4/24/64)	-1.17 (WDY, 4/24/64)
Rms error in magnitude determination:		
$\overline{Mcrms}_k^{(0)}$	0.52 (9/6/68)	0.31 (9/13/63)
$\overline{Mcrms}_k^{(1)}$	0.29 (4/24/64)	0.07 (6/28/68)
Average station correction:		
$\overline{Msc}_i^{(0)}$	0.74 (WDY)	-0.84 (ECC)
$\overline{Msc}_i^{(1)}$	0.02 (CWC)	-0.04 (SFB, VIN, ECC)
Rms station correction:		
$\overline{Mscrms}_i^{(0)}$	0.85 (ECC)	0.14 (SFB)
$\overline{Mscrms}_i^{(1)}$	0.33 (WDY)	0.03 (PAS)

Table XIV. Seismic station reliability.

Station	Distance (km)			$\overline{M}_{scrms}^{(0)}$	$\overline{M}_{scrms}^{(1)}$	$\overline{M}_{sc}^{(0)}$	Data points
	Yucca Flats	Pahute Mesa	Central Nevada				
TIN	193.9	159.7	249.3	0.23	0.21	0.05	13
CWC	197.1	173.2	294.2	0.66	0.06	0.66	26
HAI	202.9	185.2	316.9	0.15	0.11	0.11	8
WDY	297.1	277.7	400.7	0.81	0.33	0.74	24
SWM	352.7	344.2	483.4	0.27	0.09	-0.25	28
RVR	369.2	375.7	525.5	0.42	0.11	0.40	46
PAS	383.5	382.1	527.9	0.25	0.09	0.22	48
SBC	446.4	432.2	560.9	0.36	0.09	-0.35	41
VIN	477.1	442.8	501.6	0.54	0.05	-0.53	6
ECC	483.8	505.7	650.4	0.85	0.09	-0.84	18
MHC	496.6	459.7	497.8	0.45	0.12	-0.43	48
BAR	498.0	512.4	662.0	0.64	0.18	0.61	23
SNC	535.2	528.6	668.0	0.23	0.05	0.21	10
PAC	544.6	507.5	541.0	0.40	0.03	-0.39	6
BKS	552.8	514.5	533.5	0.16	0.09	-0.13	47
SFB	570.7	532.6	554.4	0.14	0.11	-0.11	6
MIN	599.7	560.8	500.9	0.24	0.15	-0.18	46
ARC	809.0	769.5	717.8	0.21	0.11	-0.14	30

Because of the inherent variations between seismic stations it is not legitimate to use magnitude determinations that have been made without the aid of station corrections. The effect of station corrections can be seen by comparing the zero iteration calculations for a given event with those of first iteration. The differences are shown even more clearly by comparing Fig. 2 with 3, 4 with 5, and 6 with 7. The scatter of the points with respect to distance is greatly reduced in going from zero to first iteration. From these figures one can refine the requirements for an acceptable magnitude determination method by noting that the slope should be zero for a line passing through the individual station magnitudes. The first iteration station magnitudes in Fig. 5 show a slight positive slope, which implies that the Gutenberg-Richter nomograph should attenuate less rapidly with distance for it to be valid in the case of Pahute Mesa. The scatter in the data for the first iteration calculations must be regarded as a measure of the complex geology in Nevada, because the variations can occur with only very small changes in event locations.

In addition to this feature there is another aspect that must be taken into account—one that makes the checking of the validity of the Gutenberg-Richter nomograph for explosions much more difficult. Note in Figs. 2, 4, and 6 that all the underlined stations, which are operated by the California Institute of Technology, lie in southern California. The individual station magnitudes for these stations are for the most part below the weighted event magnitudes. Since the northern California stations are generally further away from both Yucca Flats and Pahute Mesa than are the southern California stations (see Fig. 1), one would expect just the reverse situation. It turns out, however, that there is a regional effect associated with southern California that makes that area appear to be seismically less well-coupled than northern California for Nevada events. In fact, it is not unusual for explosions in Pahute Mesa to produce larger amplitudes at Berkeley (510 km) than at Pasadena (390 km). This azimuthal dependence is shown in Fig. 8, in which the station corrections $\overline{M}_{sc}^{(0)}$ are plotted as a function of distance. (Distances from Pahute Mesa are used because they are representative values, as may be seen from Table XIV.) Because of the geographical configuration of the station and event locations it is impossible to separate the distance variations from the azimuthal effects.

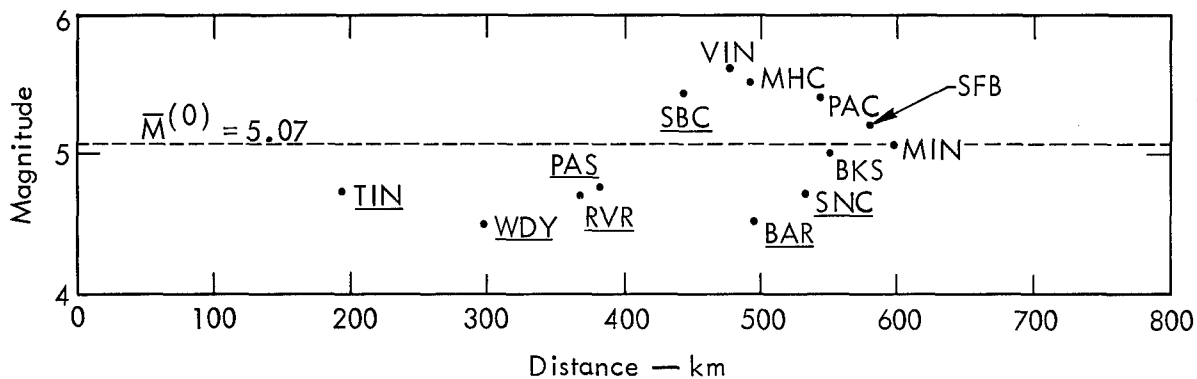


Fig. 2. Magnitude vs distance for Yucca Flats, zero iteration.

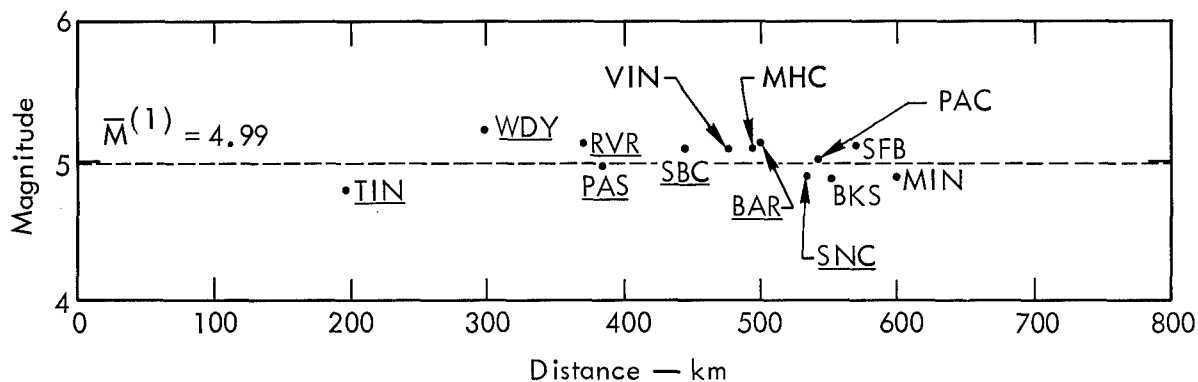


Fig. 3. Magnitude vs distance for Yucca Flats, first iteration.

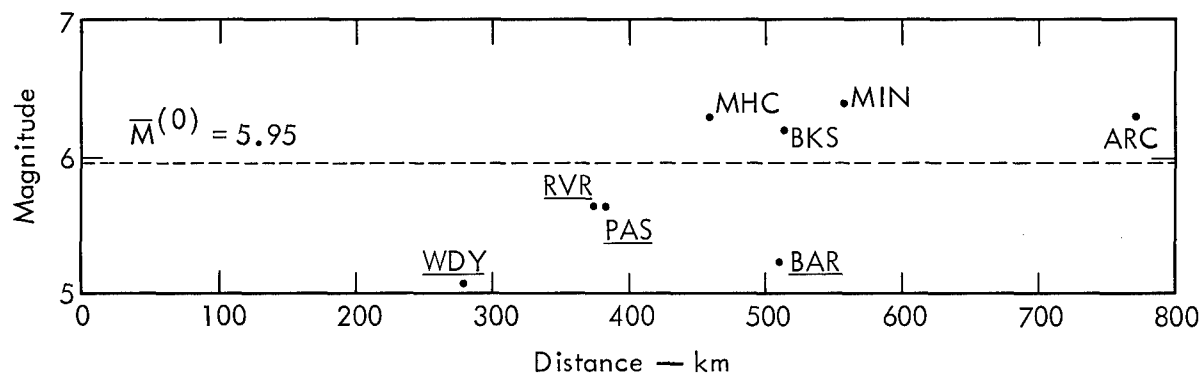


Fig. 4. Magnitude vs distance for Pahute Mesa, zero iteration.

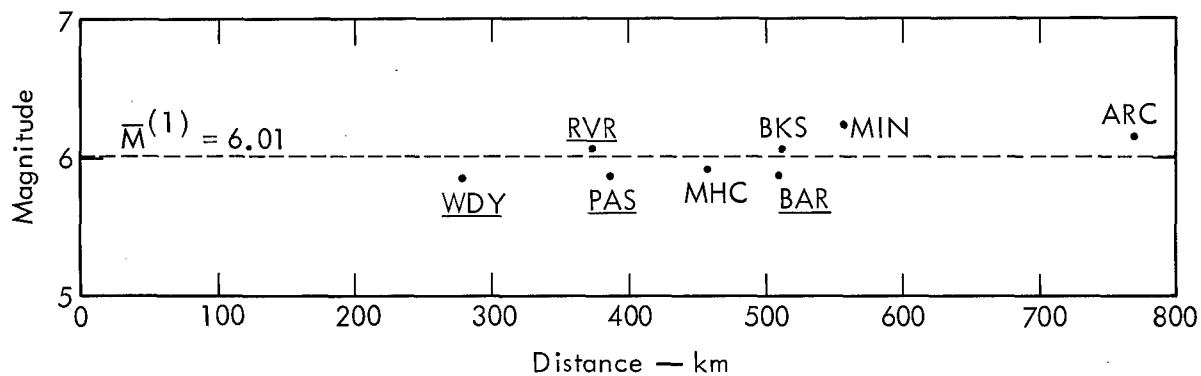


Fig. 5. Magnitude vs distance for Pahute Mesa, first iteration.

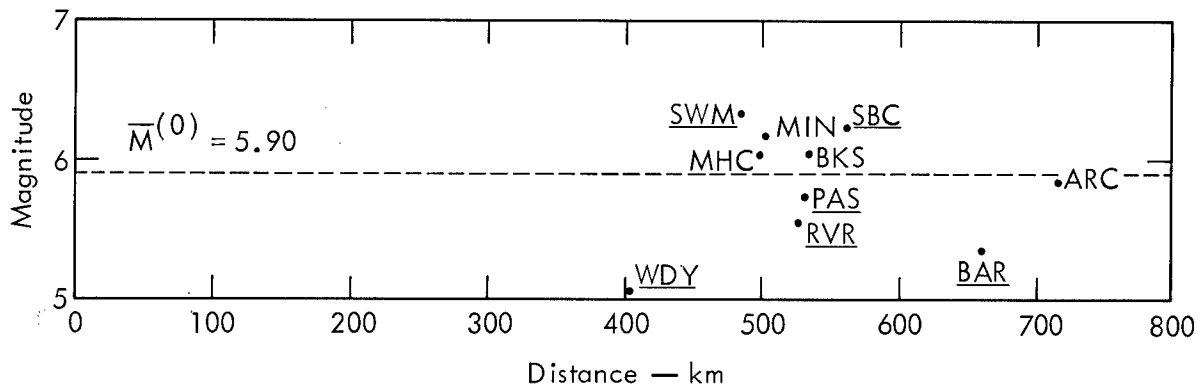


Fig. 6. Magnitude vs distance for Central Nevada, zero iteration.

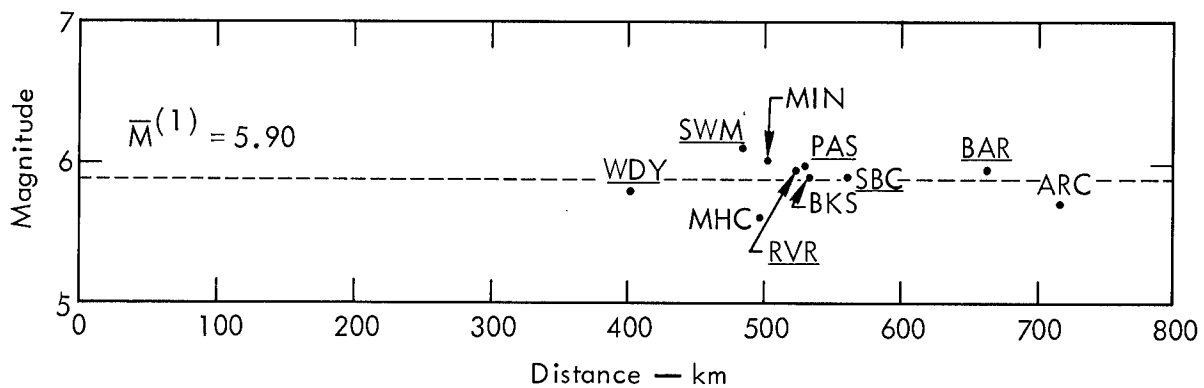


Fig. 7. Magnitude vs distance for Central Nevada, first iteration.

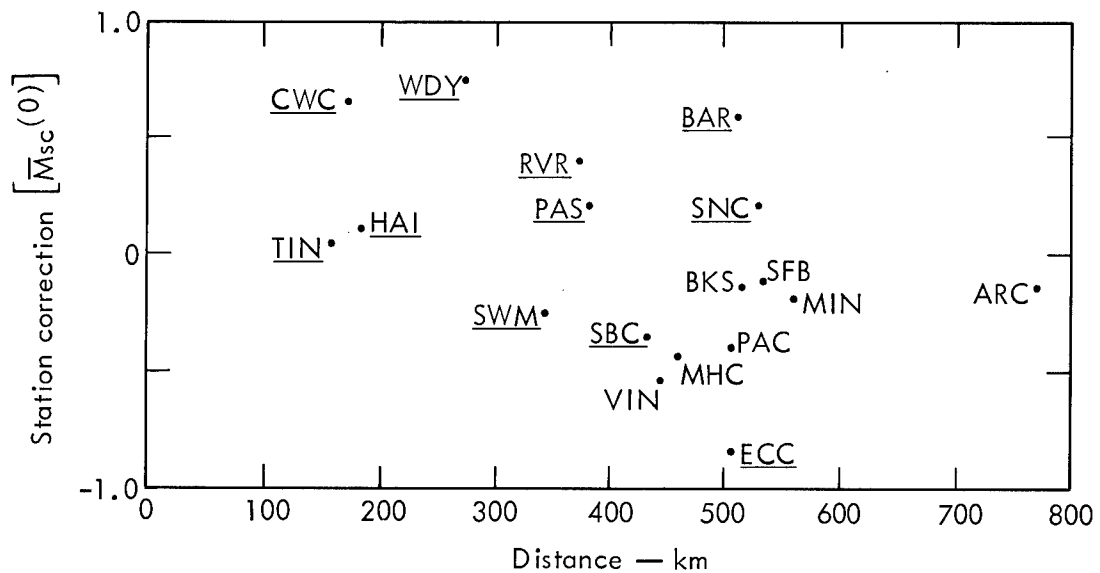


Fig. 8. Station correction vs distance (from Pahute Mesa).

In reviewing the application of the Gutenberg-Richter scale to the evaluation of explosion data, mention should be made of the assumptions under which the scale was constructed. Gutenberg and Richter assumed that the direct shear waves, which are the primary elastic wave radiations from a shallow focus earthquake, are responsible for the peak amplitudes at distances

up to 100 km. At about 100 km there is a transition to dominance by other crustal modes, which continues out to about 1000 km, beyond which the surface waves are the source of the peak amplitudes. Furthermore, Gutenberg and Richter limited both the event and station locations to southern California.

In the case of underground nuclear explosions the primary seismic radiation is a compressional wave, which would attenuate in the same manner as the direct shear wave from an earthquake if reflection and refraction phenomena could be excluded. Observations supporting this prediction have been reported in detail by Romney^{7,8} for some of the smaller underground nuclear explosions in Nevada. Even though the individual reflected and refracted wave amplitudes differ between earthquakes and explosions because of the difference in wave type for the primary seismic radiation, one still would expect the attenuation rate for the peak amplitudes to be much the same. The California Wood-Anderson data verifies this fact, even though it represents peak horizontal amplitudes that are measurements not of the compressional waves but rather of the shear, Lg, and other crustal waves resulting from the complicated conversions that take place when the primary compressional wave is incident upon the various media interfaces.

The basic conclusion that may be drawn from this study is that the Gutenberg-Richter scale may be used for the magnitude determination of large underground nuclear explosions in the distance range 200 to 800 km, provided that the local station variations are removed with the aid of station corrections. Allowance should also be made for a constant correction that may have to be applied to all local magnitudes to make them compatible with teleseismic magnitudes.²

APPENDIX

Numerical Computation of Magnitudes According to the Gutenberg-Richter Nomograph

The Gutenberg-Richter nomograph¹ may be represented mathematically in the form

$$M = F(\Delta, B_0) + \log_{10}(B/B_0), \quad (A-1)$$

where M is the magnitude, B the Wood-Anderson peak amplitude in millimeters, and Δ the epicentral distance in kilometers. B_0 has a value of 1 mm. For $B = B_0$ we obtain M_1 , the magnitude for 1 mm:

$$M_1 = F(\Delta, B_0). \quad (A-2)$$

The expression $F(\Delta, B_0)$ is given by Table A-I. The relationship in Table A-I is essentially the same as that given by Richter,⁹ where the values may be interpreted as being either the values of $\log_{10}A$ (A = amplitude) as a function of distance for magnitude zero or the magnitude as a function of distance for an amplitude of 1 mm.

Table A-I is depicted graphically in Figs. A-1 and A-2. Figure A-1 covers the distance range 0 to 100 km, while Fig. A-2 covers the interval 10 to 1500 km. Figure A-1 is linear in distance so that the near epicentral dependence of magnitude on distance can be displayed in detail. Figure A-2 is logarithmic in distance so that a larger interval may be accommodated.

Figure A-2 also shows a basic feature of the Gutenberg-Richter nomograph that may be used to interpolate between values in Table A-I. By

Table A-I. Gutenberg-Richter scale—magnitude vs distance for a Wood-Anderson amplitude of 1 mm.

Distance (km)	Magnitude	Distance (km)	Magnitude	Distance (km)	Magnitude
0	1.42	70	2.81	500	4.72
10	1.48	80	2.88	600	4.99
15	1.55	90	2.93	700	5.20
20	1.7	100	3.0	800	5.38
25	1.93	150	3.29	900	5.52
30	2.15	200	3.52	1000	5.68
35	2.32	250	3.78	1100	5.79
40	2.42	300	4.00	1200	5.88
45	2.53	350	4.26	1300	5.97
50	2.60	400	4.42	1400	6.04
60	2.72	450	4.59	1500	6.10

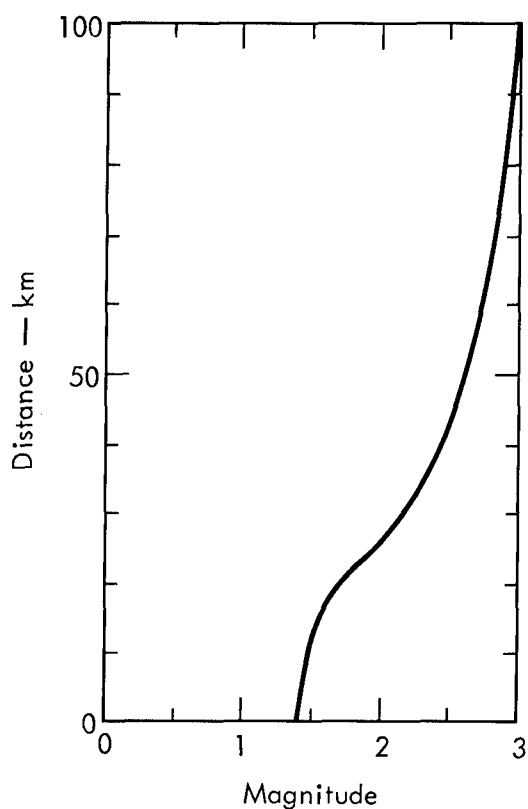


Fig. A-1. Gutenberg-Richter scale—magnitude vs distance for a Wood-Anderson amplitude of 1 mm. Range 0 to 100 km.

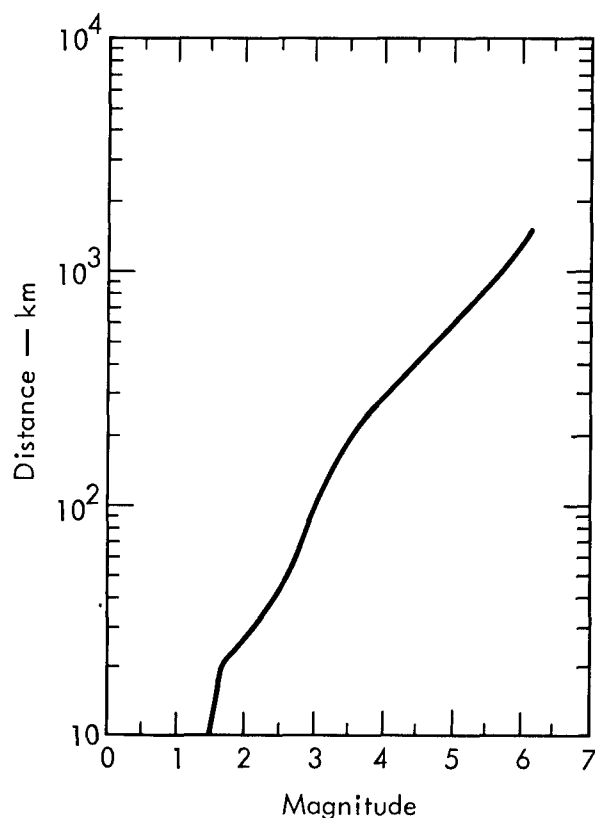


Fig. A-2. Gutenberg-Richter scale—magnitude vs distance for a Wood-Anderson amplitude of 1 mm. Range 10 to 1500 km.

inspection of Fig. A-2 it can be seen that the linear interpolation

$$\delta M = \frac{\Delta - \Delta_{\ell}}{\Delta_{\ell+1} - \Delta_{\ell}} (M_{\ell+1} - M_{\ell}) \quad (\text{A-3})$$

may be used for $0 \leq \Delta \leq 200$ km, whereas logarithmic interpolation

$$\delta M = \frac{\ln (\Delta / \Delta_{\ell})}{\ln (\Delta_{\ell+1} / \Delta_{\ell})} (M_{\ell+1} - M_{\ell}) \quad (\text{A-4})$$

should be used for $\Delta > 200$ km. The subscript ℓ refers to the ℓ th entry in Table A-I.

REFERENCES

1. B. Gutenberg and C. F. Richter, Bull. Seismol. Soc. Am. 32, 163 (1942).
2. J. F. Evernden, Bull. Seismol. Soc. Am. 57, 591 (1967).
3. P. J. Barosh, Use of Seismic Intensity Data to Predict the Effects of Earthquakes and Underground Nuclear Explosions in Various Geologic Settings, U.S. Geological Survey, Washington, D. C., Bulletin 1279 (1969).
4. J. R. Murphy and J. A. Lahoud, Analysis of Seismic Peak Amplitudes from Underground Nuclear Explosions, Environmental Research Corporation, Alexandria, Va., Rept. NVO-1163-166 (1968).
5. G. Bomford, Geodesy (Clarendon Press, Oxford, 1952), pp. 88-91.
6. K. E. Bullen, Introduction to the Theory of Seismology (Cambridge University Press, Cambridge, England, 1963).
7. C. F. Romney, Bull. Geol. Soc. Am. 70, 1743 (1959).
8. C. F. Romney, J. Geophys. Res. 64, 1489 (1959).
9. D. F. Richter, Elementary Seismology (W. H. Freeman and Co., San Francisco, 1958), p. 342.

COMPRESSIONAL SEISMIC WAVES RECORDED DURING UNDERGROUND NUCLEAR EXPLOSION TESTS IN HOGGAR

Henri FERRIEUX
Commissariat à l'Energie Atomique (France)
Centre d'Etudes de Bruyères-le-Châtel

ABSTRACT

The seismic measurement device was the following :

- a movable apparatus in the shot area,
- at larger distances, two stations at permanent places.

The radial compression wave is examined from the beginning of the pseudo-elastical behaviour of the medium to a distance of fifty kilometers.

The amplitude laws evolution is conformed to the theory predictions.

The shots energy and the observation distance influence on the amplitude spectra of the compression waves, is studied.

INTRODUCTION

The seismic effects of the contained nuclear explosions in HOGGAR (Sahara) have been measured at various distances from the shot points and each type of wave has been separately studied.

The purpose of this paper is to present the results relative to the radial compressional waves, which were examined in a more careful manner. As a matter of fact, they are the most easily connected to the original phenomenon, since their existence does not need medium heterogeneity.

The measure devices have allowed us to follow the evolution of these waves, from the beginning of the pseudo-elastical behaviour of the rock, up to about 50 kilometers.

The study essentially concerns measurements carried out at distances larger than 10 kilometers, with classical devices of seismic measurements ; these results are compared with those obtained in the close-in zone, to examine if the evolution of the seismic signal, when the distance increases, could be predicted. We shall not insist on the results of the close-in zone, which have been published elsewhere (1) (2).

1. DEVICES OF MEASUREMENTS

1.1. Close-in device (1)

Strong motions measurements were carried out in the mountain, in a zone extending from the end of the fractured zone up to a few thousands meters.

The following parameters were recorded :

- absolute displacement
- acceleration
- relative displacement
- displacement velocity of the "normal point" (point of the surface of the mountain which is the nearest to the shot-room). From the absolute displacement, the particle velocity was obtained by derivation.

Instruments were radially disposed with regard to the shot points at scaled distances :

$$0.06 < d/W^{1/3} < 1 \quad (d : \text{km}, \quad W : \text{kt})$$

At the same distances, seismographs were disposed to listen the microns of the mountain mass, after the nuclear explosions (3). Spectral studies of the direct seismic effect of the explosions have been made, by using the records of these seismographs.

1.2. Remote device

Two permanent stations, at mean distances respectively 15 kilometers (station 1) and 50 kilometers (station 2), far from the shot points, were used. Each of them has six locations aligned with the shot points in a N-S direction, the length of the device was a few kilometers.

All six locations of the station were equipped with vertical, longitudinal and transversal seismographs, with different resonance frequencies : 2 Hz, 4,5 Hz and 7,5 Hz.

Position and orientation of both stations were chosen after a geological and seismic study of the site.

Nuclear explosions were fired in a granite mountain relatively young (intrusive granite). This mountain is located in the midst of highly metamorphosed rocks which have a general structural North-South orientation (fig. 1).

The metamorphism is very intense and it is possible to consider that the physical characteristics of this metamorphosed rocks really differ from those of the granite only by the anisotropy with a preferential direction.

Measures of the seismic waves propagation velocity were made. Inside the mountain, the P waves have a very constant velocity (about 5 850 m/s). This confirms the petrographical homogeneity of the test site. Outside, the velocities of the P waves are lower in the E-W direction (5 700 m/s) and greater in the N-S direction (5 900 to 6 000 m/s). An estimate of the energy transmitted by the seismic waves has been made from the measured amplitudes. The "isoenergy" map shows a minimum of attenuation in the N-S direction. It is the direction of the geological structures.

The stations are set up in permanent locations in the compact outcropping rock. The coupling between the apparatus and the seismic body waves do not change very much from one explosion to another. In these conditions, the effect of some source parameters (particularly : energy of the explosion) upon the amplitudes, could be studied.

2. RESULTS

In the remote zone, seismic records have been calibrated (in velocity impulsions) and deconvolved.

The first half-cycle of the P waves was particularly studied, because it was, in the site conditions, free from all interferences coming from multiple reflections or from resonances in the ground layers of each station. This first half cycle, directly results from the transformation of the close-in zone signal.

2.1. Results in the close-in zone

More than 100 measurements of displacement, acceleration and particle velocity were made. Similitude relations for each of these parameters could be verified.

With regard to the radial particle velocities, the following relation is obtained :

$$(1) \quad V(\text{cm/s}) = 10 W(\text{kt})^{0.58} d(\text{km})^{-1.73}$$

$$\text{or} \quad V(\text{cm/s}) = 10 \left(\frac{d}{W^{1/3}} \right)^{-1.73}$$

$$0.06 < d/W^{1/3} < 1$$

The error corresponding to the standard deviation is from + 50 % to - 30 %.

2.2. Results in the remote zone

We see, for each shot, differences of amplitudes which can reach 50% between two seismographs recording the same component, in the same station. This variation remains constant for the different shots : therefore, the coupling between ground and gauges does not vary. An average of the amplitudes, always established with the same gauges, tends to eliminate the effects of a local resonance, and is representative of a shot.

The mean law of the radial velocities for the first half-cycle is :

$$(2) \quad V(\text{cm/s}) = (4.26 \pm 1.06) W_{(\text{kt})}^{+0.85} d(\text{km})^{-1.3 \pm 0.1}$$

for the contained explosions in HOGGAR, with an energy inferior to a few tens of kilotons.

It is valid for distances between 15 and 50 kilometers (and for the passing-band of the apparatus 2 to 64 Hz).

For the superior energies, the relation becomes :

$$(3) \quad V(\text{cm/s}) = 11.8 W(\text{kt})^{0.51} d(\text{km})^{-1.3}$$
$$15 < d < 52 \text{ km}$$

Figure (2) represents these relations, at station 2.

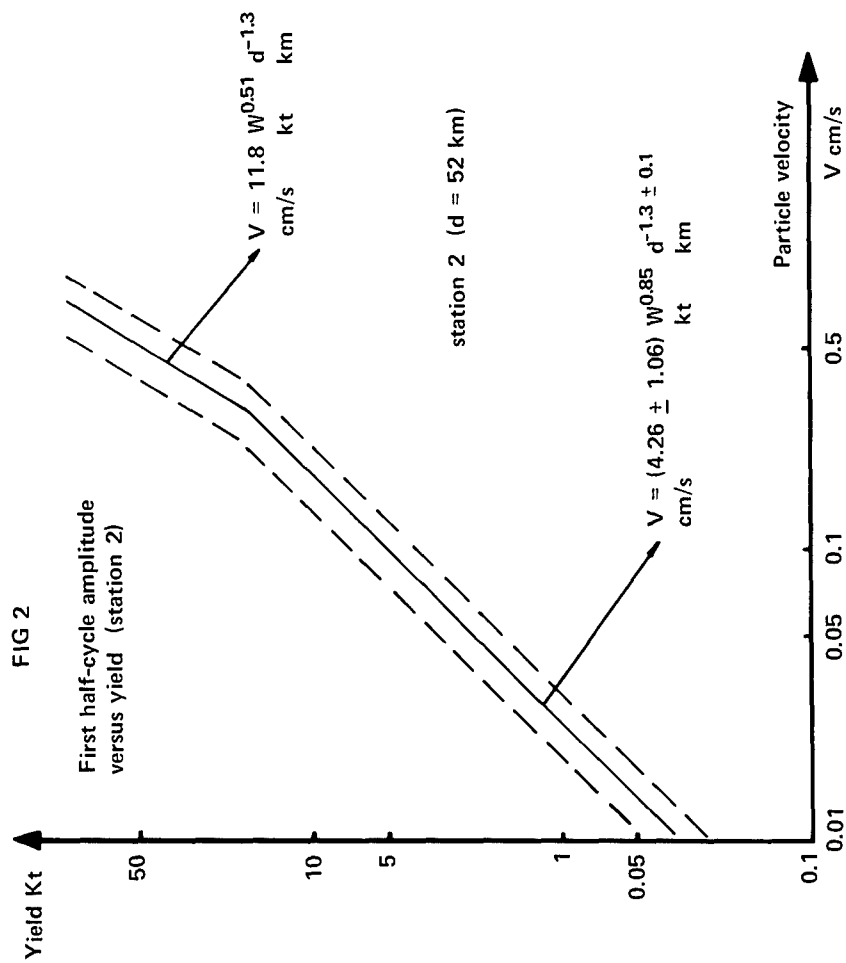
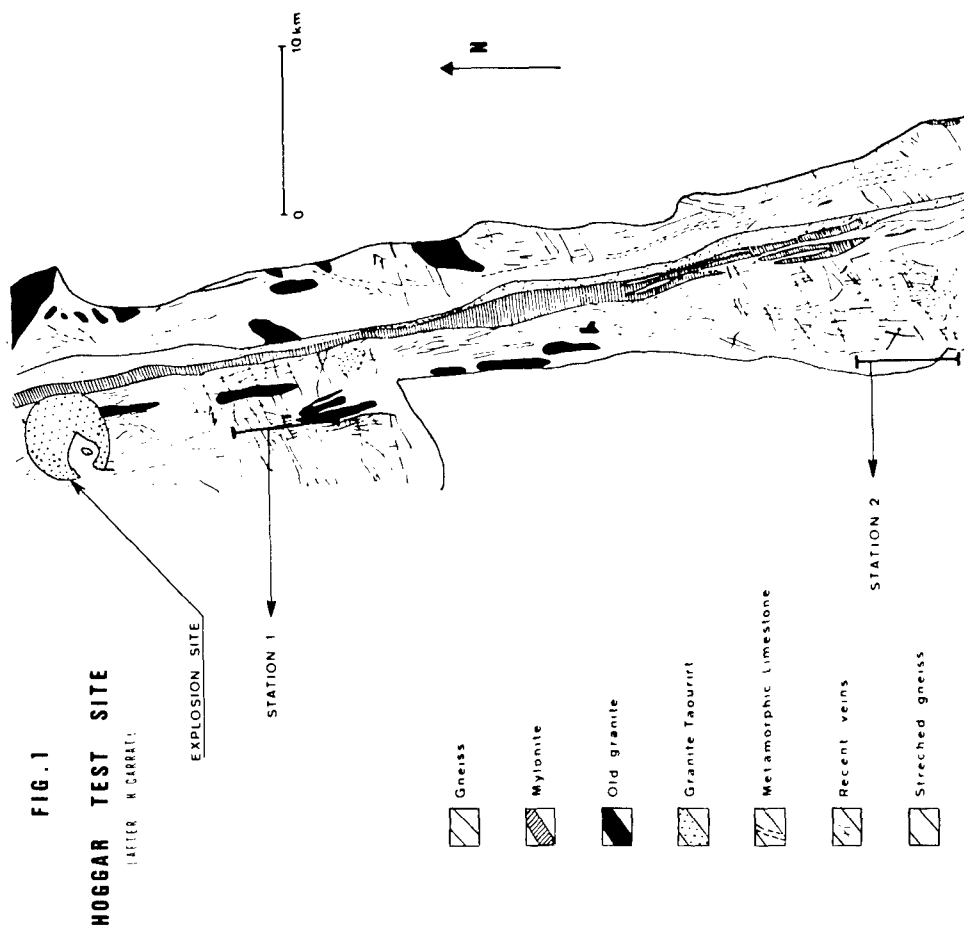
2.3. Remark about the dispersion of the law of the particle velocities in the remote zone

This dispersion is not a random one. We have determined in the shot mountain, three zones at which correspond different seismic efficiencies. According to whether the explosion takes place in one of these three zones, the representative point which corresponds to it is located on figure (2) on the left, on the right or near the middle straight line given by the above equations (2) and (3). A careful study of the possible causes of this dispersion, connected to the geographical situation in the mountain, has been carried out.

Two types of causes can be supposed :

- the medium conditions near the shot points can be different from one zone to the other (medium nature, state of stresses).

The study of the lithostatic pressure near the shot points, taking into account the form of the mountain (dihedron effect), shows that this lithostatic pressure allows us to define scaled overburden thickness, varying from zone to zone.



For great scaled overburden thickness, the seismic amplitudes measured at the remote zone, are relatively small and conversely, this is conformed to the theory and to the experience.

The differences between the scaled lithostatic pressures are small. Other hypothesis have been foreseen, which gives an account of source anomalies (4), and which could be applied to the measures in the remote zone.

Nevertheless, the close-in measures do not show this geographical dispersion.

We can think that these characteristics come from the wave propagation and more particularly from the energy dispersion, different according to the shot zone, owing to the mountain geology. Large faults cut up the mountain and their orientation with regard to the seismic rays, allows us to explain the stated phenomenon.

2.4. Comparison between the laws of the close-in zone and the remote zone

We have represented on figure (3) the laws corresponding to the equations (1) (2) (3), for three explosions, the yields of which are respectively : 1, 10 and 100 kt. It can be observed that if we extrapolate the close-in zone laws to distances of a few tens of kilometers, the amplitude of the first half-cycle, and all the more the waves which follow it, should be underestimated. This fact shows the importance of the propagation about the characteristics of the seismic waves.

Attenuation

It is much weaker in the remote zone

$$\begin{array}{ccc} (d^{-1.73} & \text{and} & d^{-1.3}) \\ \text{close-in} & & \text{remote} \\ \text{zone} & & \text{zone} \end{array}$$

The expression d^{-n} represents the product of the geometrical attenuation of the amplitudes d^{-1} , and of the unelastical absorption $e^{-\alpha d}$

$$d^{-n} \approx e^{-\alpha d} d^{-1}$$

The absorption coefficient α is consequently greater in the close-in zone.

The end of the unreversible zone, for radial stresses of about 500 bars, begins at a distance of about $0.15 W(kt)^{1/3}$ km.

The close-in measurements are thus executed in a zone where the rock behaviour is still quite unelastic which produces the stated strong absorption.

In the remote zone, the rock behaviour, even imperfectly elastic, corresponds to an absorption coefficient much weaker. We are in the so called "acoustic zone", where the deformations are infinitesimal.

Addendum

The close-in zone and the remote zone laws, relative to the radial compression wave, are given in the following table.

The results about the vertical components (undeconvolved traces) (8), are also reported in this table.

We notice that the absorption is more important than for the radial motion (convolved traces) for the following reasons :

1. the radial wave has a vertical component relatively weaker at the farthest station.
2. the deconvolution restitutes the low frequencies which are less absorbed by the ground.

The similitude relationships application on these laws, shows a great dispersion of the results, that is to say that the similitude relationships are not verified (it is the same for the radial motion).

Yield influence of the explosions

It can be stated that the relation with $W^{0.58}$ for the close-in region, which is valid for the whole yield range, is not far from that of the remote zone, which is valid for high yield. This fact was theoretically forecast if the ground has essentially a low-pass filter action.

As a matter of fact, the amplitude spectrum of a large yield explosion, is essentially a low frequency one and is consequently little deformed during the propagation.

For the explosion of smaller yields, the action of the ground low-pass filter was theoretically studied (5) (6).

It can be shown that the exponent n of W^n is higher in the case of a shot of small yield. Indeed we stated this fact experimentally.

2.5. Study of the amplitude peaks of the body waves

The systematic analysis of the maximal amplitudes A_M of the bodywaves has been carried out for many records of the far stations.

The ratio $\frac{A_M}{A_1}$ of these values with the amplitudes of the first half-cycles, has been calculated for each trace. This ratio does not apparently depend on the explosion yield.

Radial particle velocity

(V:cm/s ; d:km ; W:kt)

Close-in zone ($0,06 < d/w^{1/3} < 1$)	Remote zone ($15 < d < 50$)
$V = 10 W^{0,58} d^{-1,73}$ <p>Standard deviation +50% -30%</p> <p>For any yield</p>	<p>1) Undeconvolved P wave (vertical component)</p> $V = (9,0 \pm 1,0) W^{0,78 \pm 0,10} d^{-1,75 \pm 0,15}$ $V = (9 \pm 4) (RW^{-1/3})^{2,06}$ <p>For any yield</p> <hr/> <p>2) Deconvolved radial P wave</p> $V = (4,26 \pm 1,06) W^{0,85} d^{-1,3 \pm 0,1}$ <p>($W < 20$ kt)</p> <hr/> $V = 11,8 W^{0,51} d^{-1,3}$ <p>($W > 20$ kt)</p>

For station 1 $1 < \frac{AM}{A_1} < 4$

For station 2 $1 < \frac{AM}{A_1} < 5$ (a single value reaches 7)

These numbers are to be compared to the numerous results relative to the contained explosions of any nature, with different conditions and media.

With some chemical explosions in France, in a sedimentary layered region, the ratio $\frac{AM}{A_1}$ reached the value of 30.

This ratio essentially characterizes the nature of the underground in the vicinity of the station. The relative weakness of the numbers for the HOGGAR nuclear test site, shows a good enough homogeneity of the underground.

2.6. Spectral studies in the remote zone (7)

The Fourier analysis of the deconvolved seismic signals, has been made for the P waves. The apparatus has been calibrated in velocity impulsion.

The length of the analysed trace was chosen so that the signal is representative of the source phenomenon, and that the parasite effects corresponding to the various resonances or reflections, do not take too much importance.

The analysis was made with a spacing of 2 Hz ; we got material velocity spectra from 1 to 60 Hz (in the best cases).

In the test mountain : 18 spectral studies
In the remote zone : 108 spectral studies.

Methods of study

To compare two spectra, one can divide frequency by frequency the amplitudes of a spectrum with those of another.

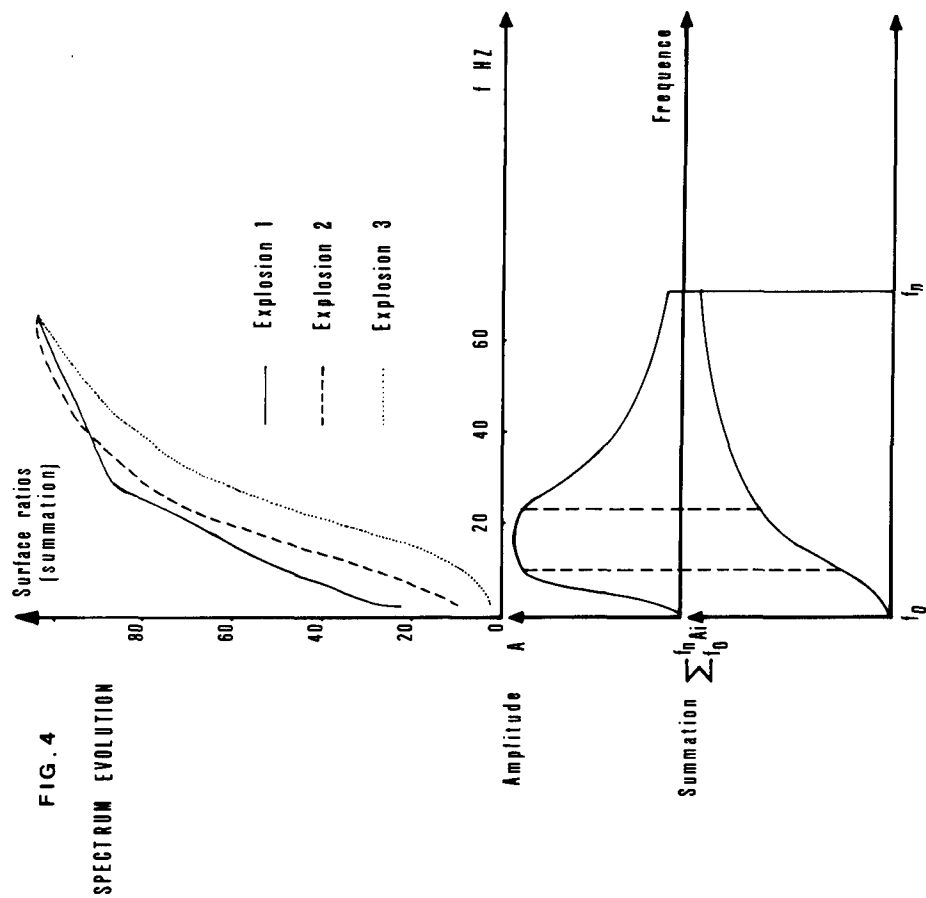
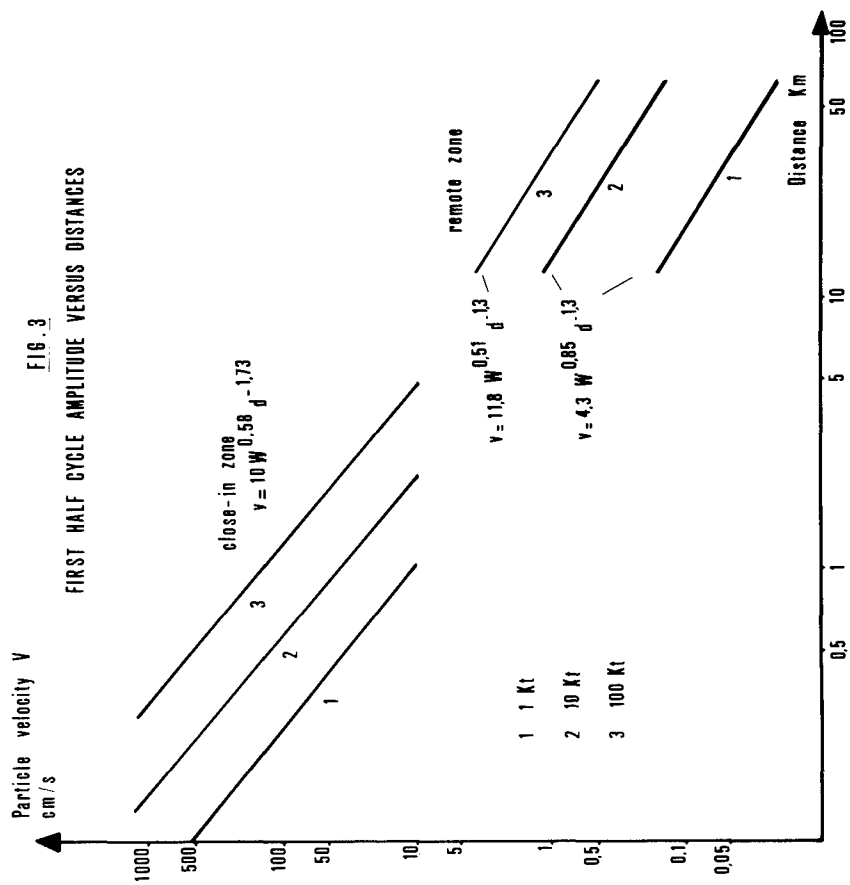
This method gives bad results in the parts of the spectra poor in energy.

The spectra have been smoothed by a "summation method", taking into account the spectral area variation.

The ordinate of the "summation" for the frequency f_n , is the sum $C_n = \sum_{f_0}^{f_n} A_i(f_i)$ of all the spectral amplitudes between f_0 and f_n (fig. 4).

This curve has the following characteristics :

- it is constantly increasing
- it is concave upwards, when the spectrum increases and convex in the opposite case



- it is a straight line when the spectral amplitude is constant.

Therefore, the slope of this curve characterizes the evolution of the spectrum.

If this curve is smoothed, only the essential variations are kept, eliminating local variations.

By fixing for C_n the maximal value 100 (corresponding to the greatest frequency studied), we shall have the evolution of the spectrum area, in percentage of its total area.

Influence of the explosion yield over the spectra

Figure 4 shows the "summation" curves for three explosions of decreasing yield ; 1, 2, 3 recorded at 15 km.

One can state the stronger the explosion, the richer the spectrum in low frequencies.

The spectra extend from 2 to 60 Hz ; for this example, the inferior limit of 2 Hz corresponds :

- to the increasing part of the spectrum in the case of the weak explosion (summation concave upwards).
- to the constant part of the spectrum (maximum) in the case of the intermediate explosion (summation curve rectilinear).
- to the decreasing part of the spectrum for the strong explosion.

The stronger the explosion yield, the lower the characteristic frequency of the spectral maximum.

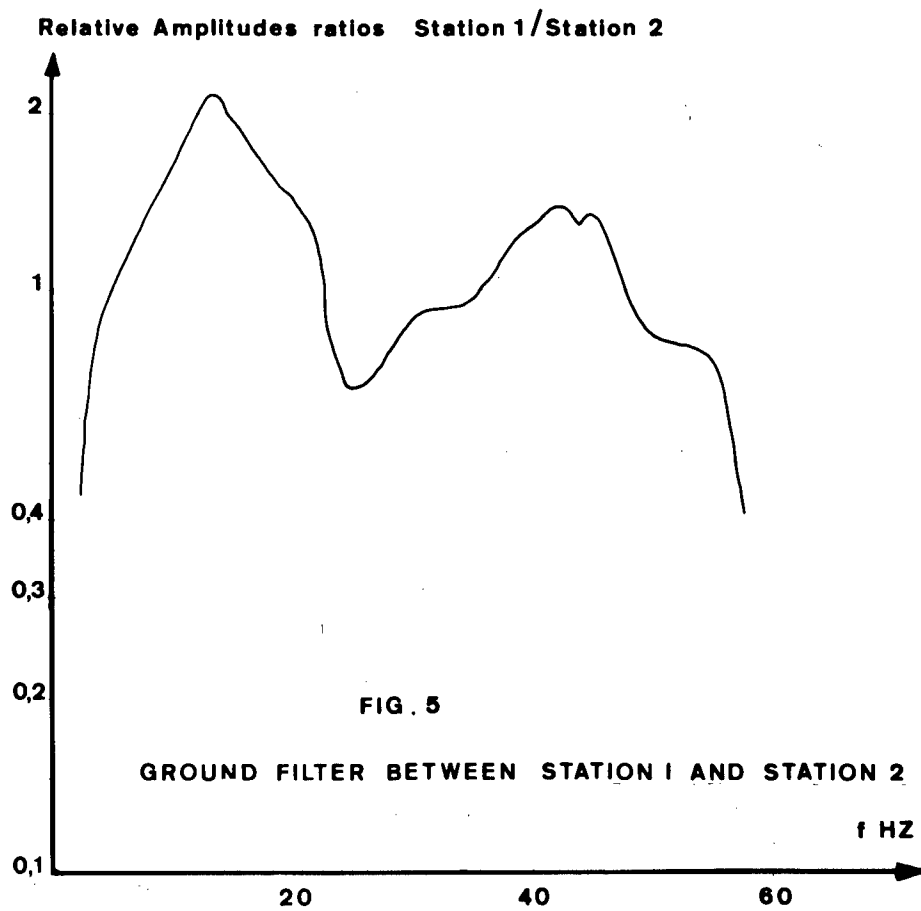
Influence of the observation distance

In the test site mountain, the pass-band of the apparatus extended from 6 to 100 Hz.

For these frequencies, at short distance from the zero point, the "summation" curve is almost linear (white spectrum). It appears that, in this frequency band, near the zone where the rock behaviour begins, the motion is nearly a velocity impulsion.

For each shot, with the help of the records at different distances, we could determine a ground-filter. Its aspect is constant enough (fig. 5). It cuts outright the high frequencies (25 dB/octave). It cuts moderately the low frequencies (5 dB/octave) below 10 Hz. Unfortunately the limit of 2 Hz does not allow us to see whether the very low frequencies are filtered.

Therefore, the ground-filter is apparently a pass-band (low frequencies) between 2 Hz and 60 Hz.



In the conditions of the experiments, that low-frequencies cutting action does not modify the previous conclusions which were supposing a purely low-pass filter.

Figure (5) only represents the selective effect of the ground for different frequencies expressed in percentage. It does not take into account geometrical attenuation, identical for all frequencies.

2.7. Calibration of the ground with chemical explosions

Contained nuclear explosions of the HOGGAR test site, were preceded by a series of three high-explosive shots of 50, 200 and 2000 kg of TNT.

The seismic effects of these shots were recorded with seismographs of 2 Hz, at distances from 3.4 to 9.4 km.

The studies of the first half-cycle amplitudes versus the yield W of the explosions, and versus the observation distance d , lead to the relationship

$$A = A_0 \quad W^{0.9} \quad d^{-1.3}$$

This relation is almost the same as for the nuclear explosion ($W < 20$ kilotons) apart the coefficient

$$A_0 = 1.7 A_1 \quad (A_1 : \text{coefficient of the nuclear explosion relation}).$$

This confirms the following known fact : the seismic efficiency of a chemical shot, is superior to that of a nuclear shot. It is therefore possible, save for a little factor, to calibrate a ground, for seismic measurements of later nuclear shots, with the help of a small number of chemical shots, of different yields.

CONCLUSION

The results show that a good choice of the seismical devices, based on geological and geotechnical studies, has given homogeneous results and precise quantitative laws. One can follow the evolution of the radial compressional wave (in particle velocity) versus the explosion yield and the observation distance. The spectral study has shown that, in the band-pass of the apparatus, the signal is near an impulsion, close by the shot point. With these methods, it is possible to obtain the signal at the origin, and to compare it with the results of the calculations starting from the shot point.

ACKNOWLEDGEMENTS

The author acknowledges the skilled assistance of Miss A. ALBARET and MM. C. GUERRINI and M. PERRIER, and particularly Mrs F. DUCLAUX (Chief Engineer of the Seismic Measurements), who directed this team work.

BIBLIOGRAPHY

1. C. GUERRINI - J.L. GARNIER
Mouvement matériel du milieu environnant une explosion nucléaire souterraine.
Rapport C.E.A. -R N° 3 885 (1969)
2. F. DELORT - C. GUERRINI
Dégâts dus aux explosions souterraines sur les habitations et les équipements.
Rapport C.E.A. -R N° 3 749 (1969)
3. F. DUCLAUX - S. DERLICH - J. FAURE - H. FERRIEUX - M. PERRIER
Liaison entre le rayon et la durée d'existence des cavités créées par les tirs nucléaires souterrains.
Compte-rendu de l'Académie des Sciences PARIS tome 264 - pp. 496-497 (1967)
4. L. MICHAUD
Explosions nucléaires souterraines. Etude des rayons de cavité.
Rapport C.E.A. -R N° 3 594 (1968)
5. W.E. PEET
A shock wave theory for the generation of the seismic signal around a spherical shot hole.
Geophysical Prospecting (1960) vol. 8 n° 41
6. A.L. LATTE - E.A. MARTINELLI - E. TELLER
A seismic scaling law for underground explosions.
Physics of fluids (1959) vol. 2 n° 5
7. A. ALBARET - F. DUCLAUX
Contenu spectral des mouvements sismiques dus aux explosions nucléaires souterraines.
Rapport C.E.A. -R N° 3 767 (1969)
8. F. DUCLAUX - A. ALBARET - H. FERRIEUX - M. PERRIER
Effets sismiques des tirs nucléaires souterrains au champ d'expérimentation du HOGGAR.
Annales de géophysique tome 25 - fasc. 3 pp. 681 - 692 (1969)
9. H. FERRIEUX
Ondes de compression liées aux explosions nucléaires souterraines.
Rapport C.E.A. - R (en cours de publication).

DIRECTIVITY OF SEISMIC RADIATION FROM A SERIES OF LINE CHARGES*

Thomas J. Ahrens**

ABSTRACT

A series of two-dimensional calculations describing the stress wave propagation from a row of line explosive sources, detonated sequentially at a supersonic phase velocity on the surface of various layered (half-space) crustal models, was carried out. Spectral ratios of the resulting free-surface velocities at a series of hypothetical seismic stations were used to calculate directivity functions. As in the case considered earlier by Ben-Menahem (where the source moved subsonically), strong enhancement of certain frequencies in the spectrum of the horizontal component of velocity was obtained. Directivity is especially prominent when the explosion-induced signals are generated in a medium in which the longitudinal elastic wave velocity is comparable to the detonation phase velocity and when the seismic signal being analyzed has been refracted from a higher-velocity, underlying layer.

INTRODUCTION AND BACKGROUND

It has been demonstrated by experiments with both chemical¹⁻³ and nuclear⁴ explosives that large trench-shaped excavations may be efficiently produced in rock and alluvium by nearly simultaneous detonation of a linear array or row of surface or near-surface explosive charges. Large-scale application of row-charge cratering excavation with nuclear explosives to the construction of canals and railroad and highway cuts has been proposed in detail.⁵ Advances in nuclear explosive technology^{5,6} and continuum mechanics calculational methods, permit the design of large-scale excavational programs in which choice of charge yields and their placement optimize cratering efficiency⁷ and concurrently minimize local fallout of radioactive debris.

The small-scale, row-charge cratering experiments carried out to date with chemical explosives and in one case, nuclear explosives (Project Buggy), have emphasized study of the interaction and enhancement effects resulting from simultaneous charge detonation. Simultaneous detonation of charges precludes the possible effect of damaging adjacent charges with the stress wave produced by a given charge. A theoretical study carried out by Ash and Eichler⁸ has dramatically demonstrated the enhancement in cratering efficiency resulting from symmetric interaction of shock waves and the associated particle-velocity motions when adjacent charges are fired simultaneously. Experiments with chemical explosives² indicate that when row charges are buried at or near the optimal cratering depth, the row-charge crater is about 10% wider and 20% deeper than that from an individual charge.

*Work done under the auspices of the U. S. Atomic Energy Commission.

**Consultant to Lawrence Radiation Laboratory, University of California, Livermore, California.

The inherent nonlinearity, and hence nonadditivity, of the response to the detonation of a single charge to the prediction of dynamic effects of a row-charge detonation has been recently demonstrated to extend to the seismic signals recorded at distances from 3 to over 100 km from the source.⁹ Cassity, et. al. have found that the direct signal recorded at distances of 3 to 11 km from the Buggy explosion (five 1.1-kt devices in a row configuration, fired simultaneously) showed little if any of the directivity in spectral amplitudes predicted from a simple linear (Huygens) interference model. Of special interest is their observation that the refracted signals recorded out to 150 km had Fourier amplitude spectra which were close to those expected from a single-charge (1.1 kt) member of the ensemble, rather than the 5.5-kt total.

Potential applications of nuclear cratering with row charges, such as canal excavation, require post-explosion crater widths (lip to lip) of about 0.5 km.⁵ Experimental cratering data indicate that individual charges of 0.2 to 2 Mt are required.¹⁰ A recent analysis of possible problems arising from the application of charges in this yield range by Rodean¹¹ points out that the seismic ground motion from these explosives may, under certain conditions, present significant hazards to structures and reposing slopes of unconsolidated earth.

Because of the potential seismic hazards associated with the near-surface detonation of explosives in the megaton range, the effect on seismic radiation of employing a judicious scheme of nonsimultaneous detonation of row charge is examined. It is of particular interest to investigate whether it is practicable, by such means, to attempt to focus a certain band of seismic frequency away from areas where unacceptable levels of seismic damage might result. Naturally, if a focusing scheme were proposed, the advantages accrued must be weighed against the concurrent losses in excavation efficiency.

SEISMIC RADIATION FROM A LINE CHARGE

The seismic body and surface-wave radiation pattern from a finite-length point source moving along a line near the earth's surface has been examined by Ben-Menahem, et. al.^{12,13} This previously studied case corresponds to one of waves radiating from the rupture of a fault in earth along some line or plane. The propagation of a rupture is always subsonic with respect to the medium and will, in general, take place at a velocity which is slightly less than the local shear-wave velocity.

In contrast to the earlier work, in the calculations described in Sec. II, the source always moves at a supersonic phase velocity with respect to the medium below, and hence, depending on the strength of the source, a downward traveling oblique shock wave or head wave will always result. The radiation from the steady-state supersonic surface source is described by Fung.¹⁴ A series of theoretical seismograms for hypothetical stations on the earth's surface are calculated by assuming a series of line charges, sequentially detonated on the surface of an appropriately structured earth. The calculational procedure for generating the theoretical seismograms and their Fourier analyses are described in Sec. III. The resulting asymmetries, or in a two-dimensional sense, the radiation patterns induced by sequential detonation are discussed in Sec. IV for two grossly different and extremely primitive crustal structures. The calculated results which appear pertinent to discussions of possible focusing of seismic radiation are summarized in Sec. V.

COMPUTATIONAL PROCEDURE

The stress and propagation from a series of line charges, chosen to obtain a two-dimensional representation of a series of point charges was calculated numerically using the Richtmeyer-von Neumann finite-difference code HEMP.¹⁵ A series of chemical explosives placed on the surface of a

computational net, representing a layered half-space, were detonated either at one end of the row (end detonation) as in Fig. 1, or detonated simultaneously (volume detonation) in the calculation. Because of the necessarily finite bounds of the computational net, configurations chosen for the calculations were such that stress waves arriving at a series of hypothetical seismic stations (Fig. 1) were unaffected by waves reflected from the net boundaries. Although the dimensions and times shown in subsequent figures are indicated in terms of millimeters and microseconds, if linear conditions apply, the results could be considered in terms of kilometers and seconds. However, a series of similarity calculations have not yet been performed. Hence, some caution should be exercised in attempting to scale or extrapolate the present calculational results.

In the stress wave-calculations, which were performed on the LRL 7030 (IBM-Stretch) computer, the horizontal and vertical components of particle velocity at a minimum of four hypothetical seismic stations, located on the free surface, were obtained as a function of time. For computational efficiency it is important to maximize the finite time step employed. In order to insure that intense material deformation in the vicinity of the explosive source would not seriously decrease a computational net element dimension, and hence decrease the time step, a relatively "weak" hypothetical explosive, having the detonation speed of Composition B3 (8 km/sec) but only 1/300th of its detonation energy, was assumed. For simple crustal structure, such as sketched in Figs. 2 and 10, the stress-wave calculations were carried out for 8 and 13 μ sec, respectively. For runs of this magnitude, Stretch computational times take 15 and 45 min, respectively.

After calculating the horizontal and vertical velocity profiles at each of the hypothetical stations, interpolated velocity values are reassigned so as to correspond to equal time intervals. The amplitude and phase spectra of the resulting velocity-time series were then obtained using a program written especially to handle seismic data on the LRL CDC 6600 computer. This program employs the Cooley-Tukey fast Fourier transform method and incorporates a version of the IBM Fourier SHARE subroutine written for the CDC compiler by C. F. Andrews.

In order to compare the seismic free-surface velocity as a function of frequency in the direction of successive explosive detonation and in the opposite direction, the ratio of amplitudes at each frequency is also calculated. This ratio, first constructed for free-surface displacements by Ben-Menahem,¹² is called the directivity function.

COMPUTATIONAL RESULTS

Initial calculations were carried out using a ten-layer crustal model in which successively deeper layers have higher elastic moduli and density (Fig. 2). This type of crustal structure, corresponding to a deep section of igneous rock, was designed in such a manner that seismic signals from the explosive source would be refracted along approximately semicircular ray paths to the hypothetical seismic stations 1, 1', 2, and 2'. Upon detonation of the line sources, beginning at the left-hand side, the horizontal component of refracted compressional wave at station 2 is calculated (Fig. 3). As can be seen in Figs. 3 and 4, this signal has significant energy bands at 2 and 4 MHz. The minor asymmetries of the Fourier amplitude spectrum about the midpoint frequency, 8.1 MHz arise from numerical errors in the Fourier analysis program. The signal, which is reconstructed from the Fourier amplitude and phase spectra, is shown in Fig. 5. The calculated horizontal component of velocity recorded at station 2' (Fig. 2), in the direction of explosive detonation, is shown in Fig. 6. The calculated first motion is of opposite sign (positive) with respect to that of station 2, because the origin of the Cartesian coordinate system in the HEMP calculation was placed in the center of the explosive. Both the time and frequency representation (Fig. 7) of this signal indicate a marked enhancement of higher frequencies.

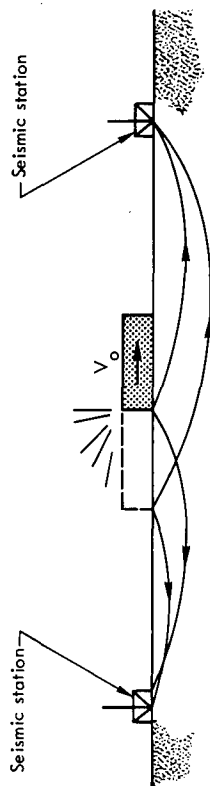


Fig. 1—Geometry employed in numerical calculations. Phase velocity, V_0 , of detonating explosive is supersonic with respect to longitudinal velocity in underlying medium. Hypothetical ray paths to seismic stations are indicated.

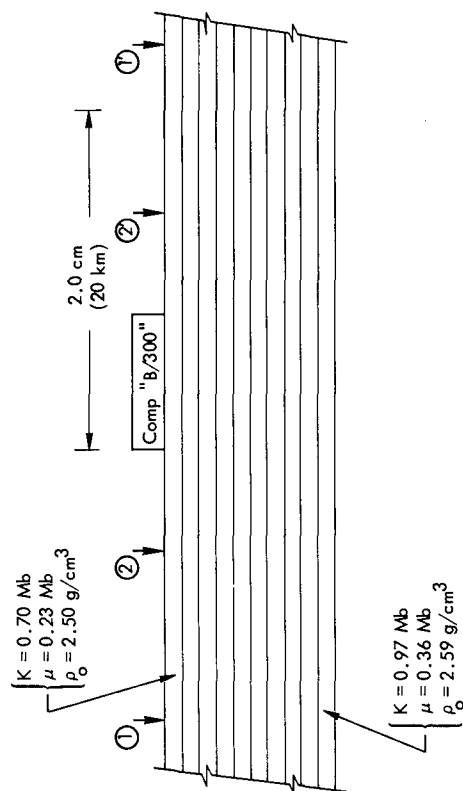


Fig. 2—Crustal configuration used to calculate relative enhancement of spectral amplitudes at stations 1' and 2' relative to 1 and 2. Elastic moduli and density increase with depth. These are chosen to yield approximately semicircular compressional wave ray paths. Vertical and horizontal scales are the same.

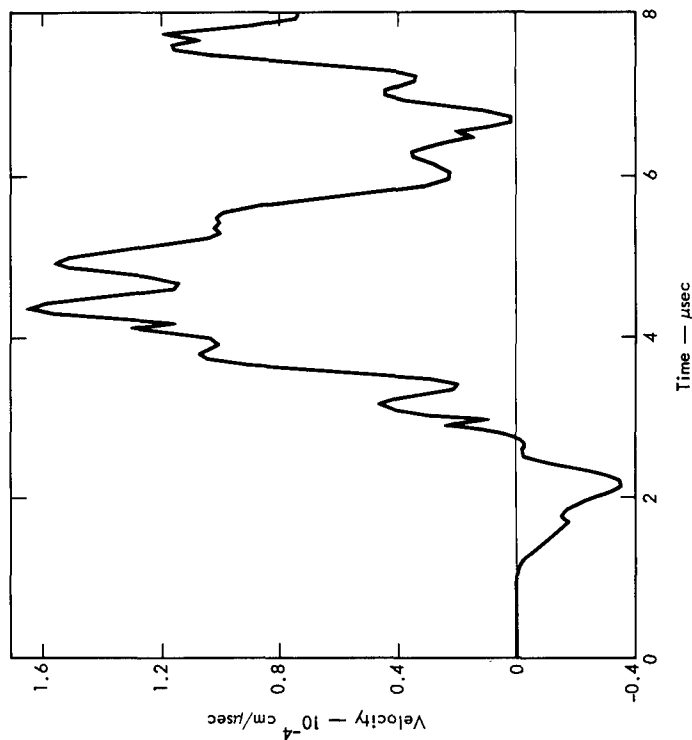


Fig. 3—Horizontal velocity vs time calculated for station 2 of Fig. 2.

Fig. 4—Spectral amplitude vs frequency for time series (horizontal velocity) shown in Fig. 3.

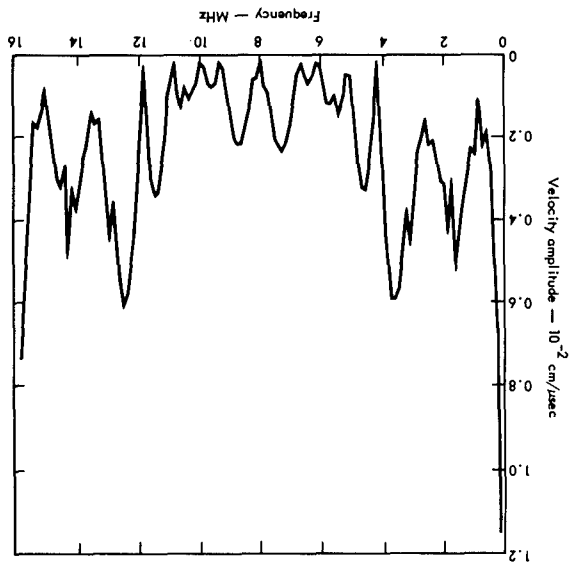


Fig. 5—Horizontal velocity vs time recovered from Fourier spectrum of Fig. 4.

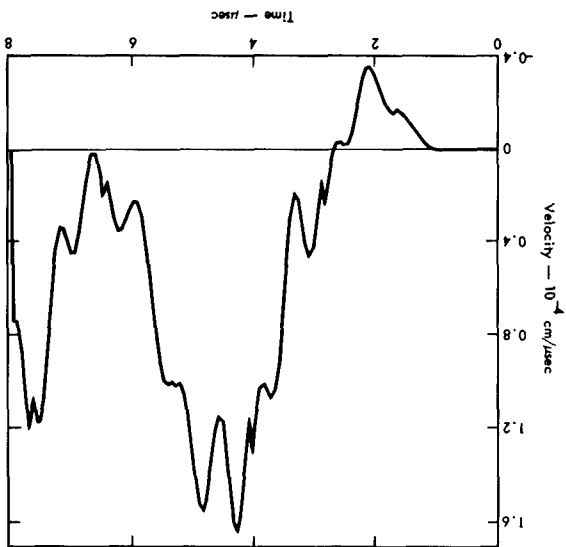


Fig. 6—Horizontal velocity vs time calculated for station 2' of Fig. 2.

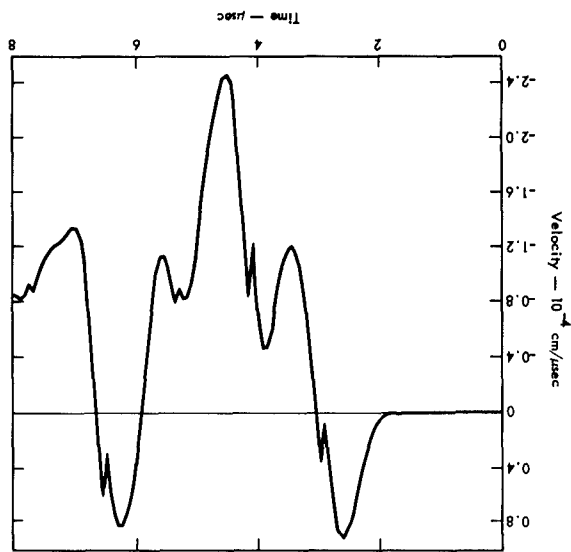
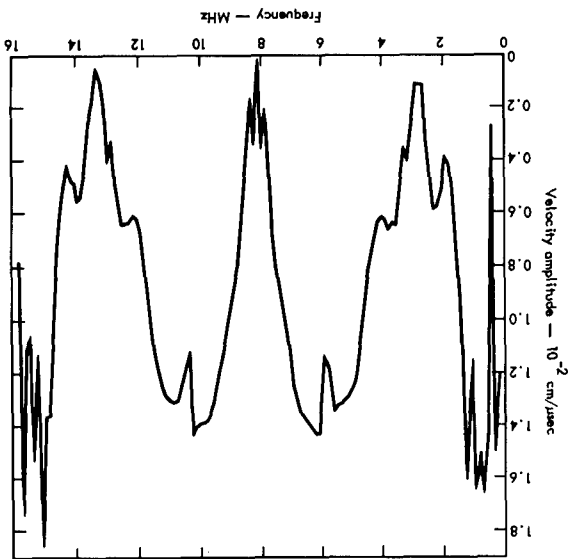


Fig. 7—Spectral amplitude vs frequency for time series (horizontal velocity) shown in Fig. 6.



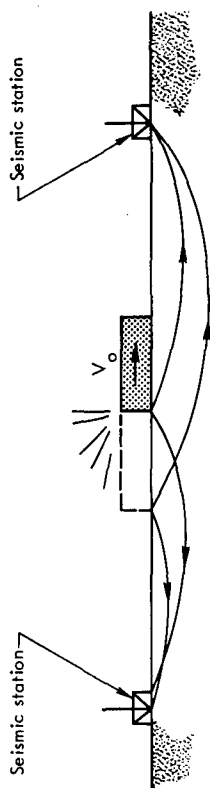


Fig. 1—Geometry employed in numerical calculations. Phase velocity, V_0 , of detonating explosive is supersonic with respect to longitudinal velocity in underlying medium. Hypothetical ray paths to seismic stations are indicated.

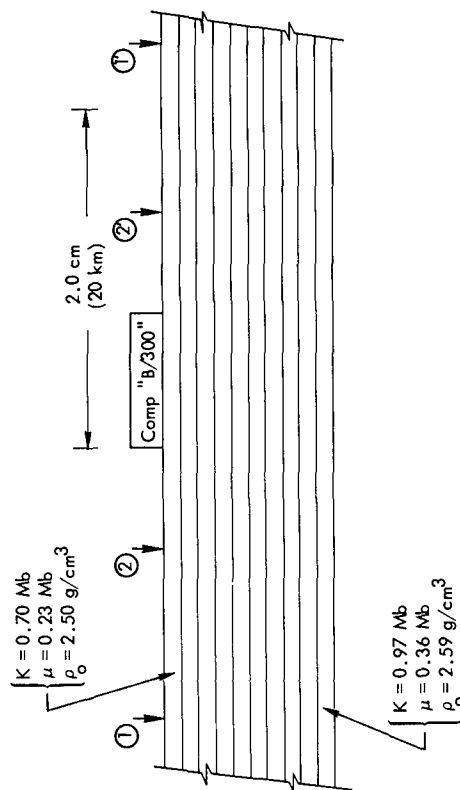


Fig. 2—Crustal configuration used to calculate relative enhancement of spectral amplitudes at stations 1' and 2' relative to 1 and 2. Elastic moduli and density increase with depth. These are chosen to yield approximately semicircular compressional wave ray paths. Vertical and horizontal scales are the same.

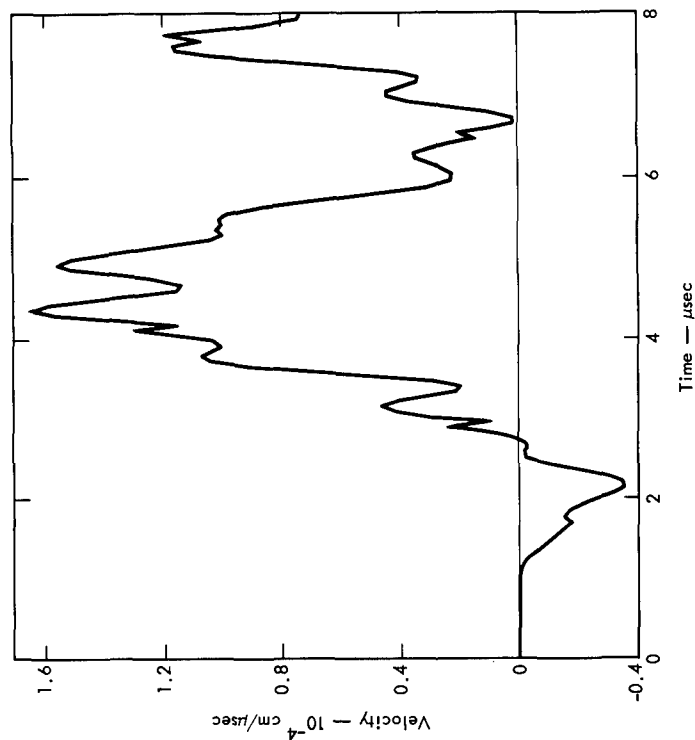


Fig. 3—Horizontal velocity vs time calculated for station 2 of Fig. 2.

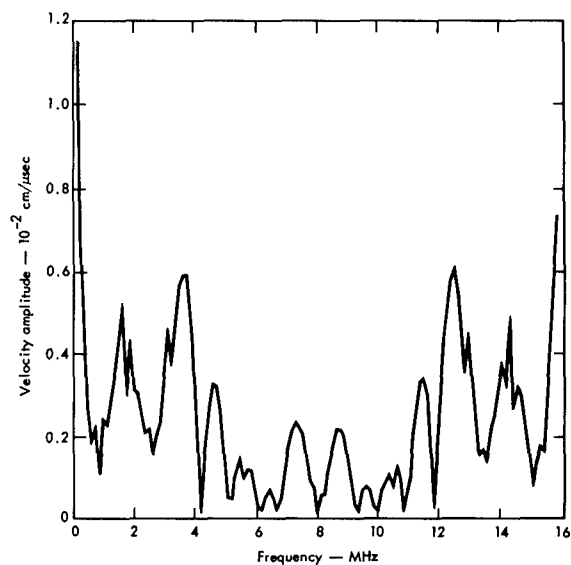


Fig. 4—Spectral amplitude vs frequency for time series (horizontal velocity) shown in Fig. 3.

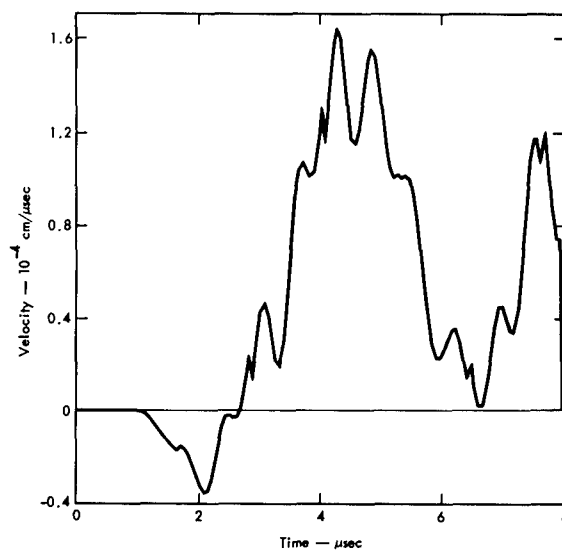


Fig. 5—Horizontal velocity vs time recovered from Fourier spectrum of Fig. 4.

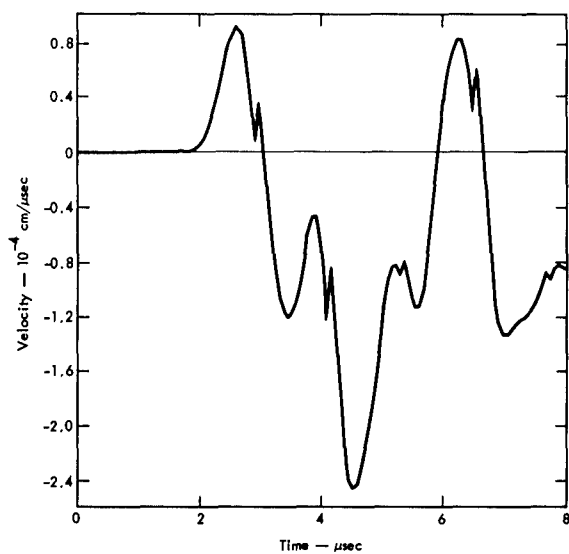


Fig. 6—Horizontal velocity vs time calculated for station 2' of Fig. 2.

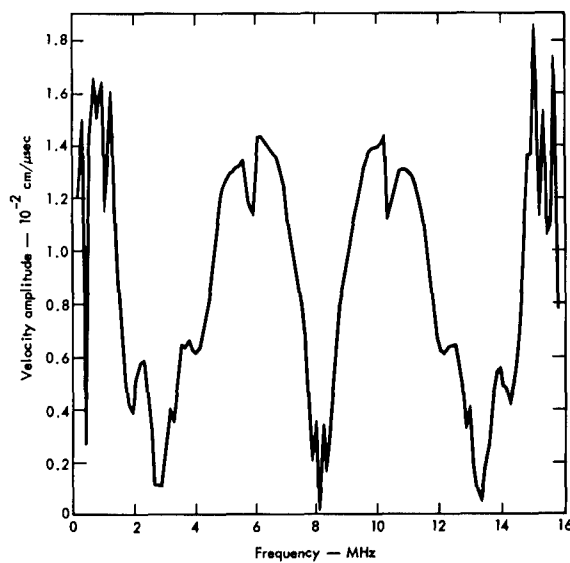


Fig. 7—Spectral amplitude vs frequency for time series (horizontal velocity) shown in Fig. 6.

Whether the increase in amplitude in the ~ 0.6 -MHz radiation, over that in Fig. 5, is significant is not yet clear. The signal which is reconstructed from the Fourier spectrum is shown in Fig. 8. A comparison of Figs. 6 and 8 demonstrates that numerical errors shifted the time series of the reconstructed signal ahead by about $0.1 \mu\text{sec}$.

The Fourier amplitude ratios of the horizontal velocity signal calculated for station 2' with respect to 2, are shown in Fig. 9. The enhancement of the signal in the direction of detonation in the vicinity of 6 MHz, and to a lesser extent at ~ 0.6 MHz, is evident. Similar results were obtained upon comparing calculated signals for stations 1' and 1. The directivities, as a function of frequency, calculated for the vertical velocity components for this and subsequent cases, were markedly less well defined.

Calculations were carried out in a second geometry (Fig. 10) for which both direct and refracted signals from the source could be observed along the free surface. This configuration, which is meant to simulate a crust with a thick cover of sedimentary rock overlying a dense igneous basement rock, incorporates a considerably larger number of cells in the computational net than the configuration of Fig. 2.

The calculated horizontal signal at station 1, which contains both direct (P) and refracted (P_n) compressional wave energy, is shown in Fig. 11. Because of the limited number of data points handled in the calculation, the time resolution in this profile is poorer than in the previous calculation. In spite of the deficiency in time resolution, a marked increase in high-frequency energy, as well as in maximum amplitude, is calculated at the station 1' on the right-hand side of the explosive in the direction of detonation (Fig. 12). The amplitude spectrum, which again shows a peak at ~ 6 MHz, is shown in Fig. 13. Because of the short time duration of the velocity profile, the frequency resolution in the calculated spectrum is sharply limited.

The ratio of Fourier amplitudes for station 1', relative to station 1, is shown in Fig. 14. Although frequency resolution is low, enhancement of energy at ~ 6 , ~ 12 , and ~ 18 MHz in the direction of detonation is easily detected.

The configuration of Fig. 10 was also used to calculate seismic signals for the case in which the upper, 3-km/sec layer was replaced by a very low shock-impedance gravel layer. The equation of state used for this gravel layer material is shown in Fig. 15. The low initial density of 1.332 g/cm^3 indicates a porosity of at least $\sim 50\%$, if the material which makes up the gravel consists primarily of silicate minerals. The equation of state for gravel, as used in the HEMP code (#28), employed an irreversible compaction routine. This routine constrains material, which upon being shocked into Regime II, III, or IV, to revert, upon pressure release, to a zero-pressure density of 2.1 g/cm^3 rather than the initial, 1.332-g/cm^3 value. Thus, a very pronounced intrinsic material attenuation mechanism is built into the equation of state. At zero pressure, the bulk sound speed in the gravel is 0.4 km/sec .

When gravel (#28) was employed as the upper medium in the configuration of Fig. 10, the calculated free-surface velocity profiles and the Fourier spectra for simultaneous and end detonation of the explosive were symmetric about the source and virtually identical. This result might have been expected, since in the gravel the wave velocity outside of the source region is extremely low as compared to the detonation phase velocity (8 km/sec). The stress wave forming in the gravel propagates so slowly that it effectively moves a negligibly small distance, compared to the length of the source region, and thus cannot differentiate an end from a volume detonation.

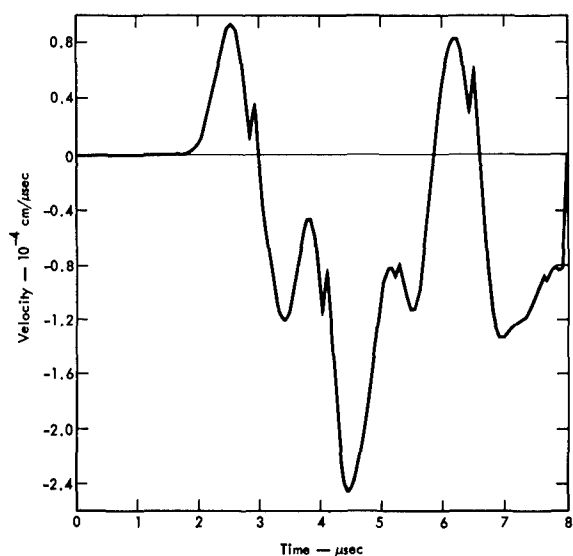


Fig. 8—Horizontal velocity vs time recovered from Fourier spectrum of Fig. 7.

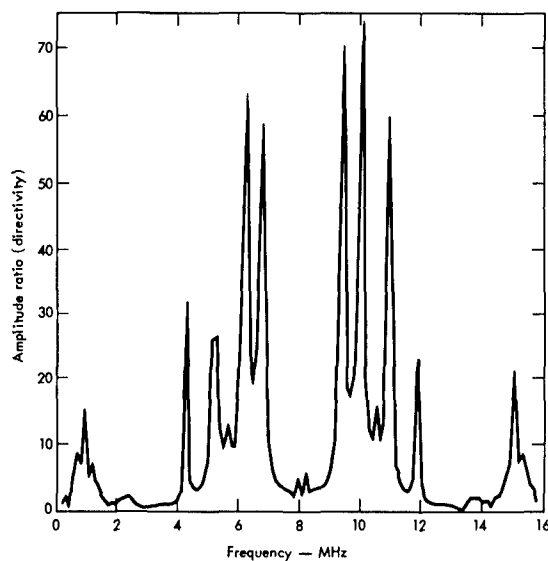


Fig. 9—Spectral amplitude ratio vs frequency for horizontal velocity calculated at station 2' relative to station 2 (see Fig. 2).

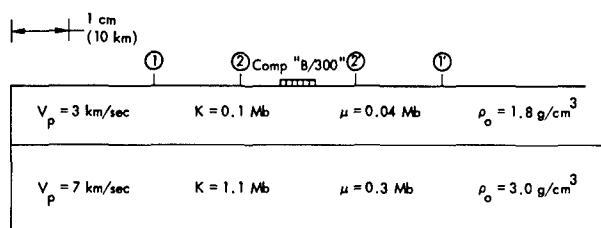


Fig. 10—Crustal configuration used to calculate spectral directivities. For the computational time interval, stations 1 and 1' receive both direct and refracted energy. Stations 2 and 2' receive primarily the direct compressional wave upon detonation of explosive source. Vertical and horizontal scales are the same.

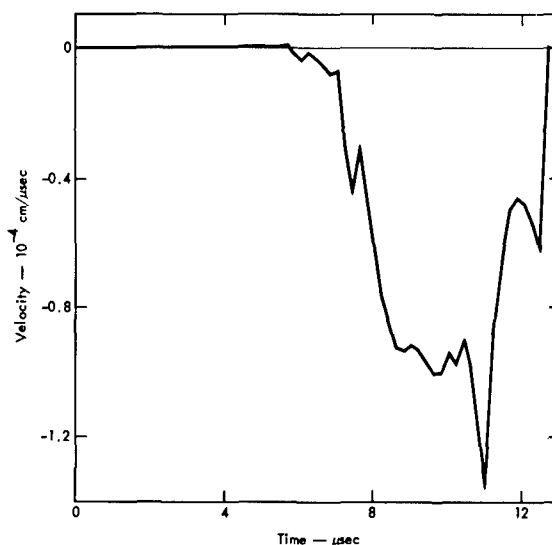


Fig. 11—Horizontal velocity vs time, calculated for station 1 of Fig. 10.

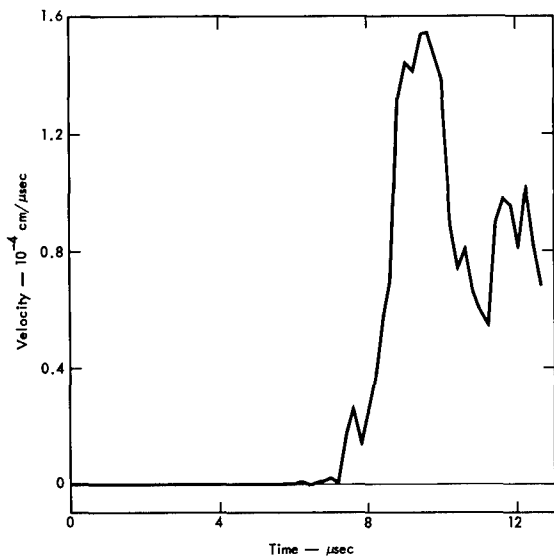


Fig. 12—Horizontal velocity vs time, calculated for station 1' of Fig. 10.

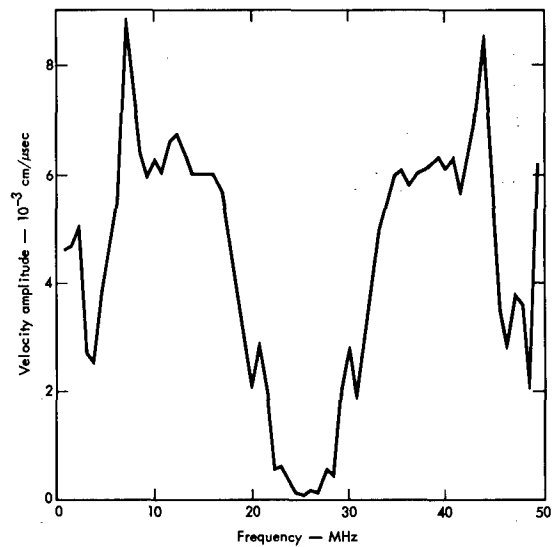


Fig. 13—Spectral amplitude vs frequency for time series (horizontal velocity) shown in Fig. 12.

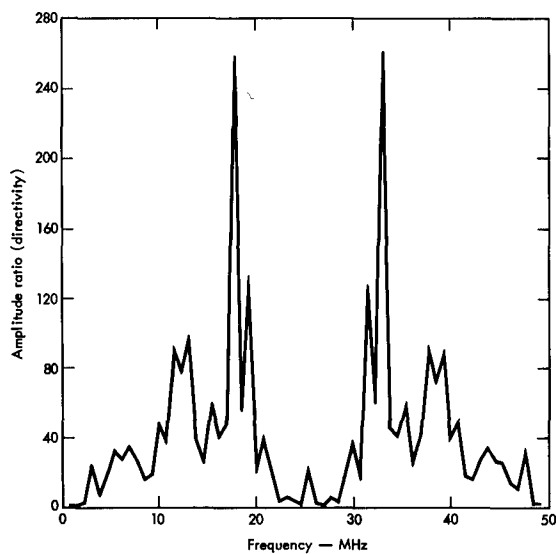


Fig. 14—Spectral amplitude ratio vs frequency for horizontal velocity calculated at station 1' relative to station 1 (see Fig. 10).

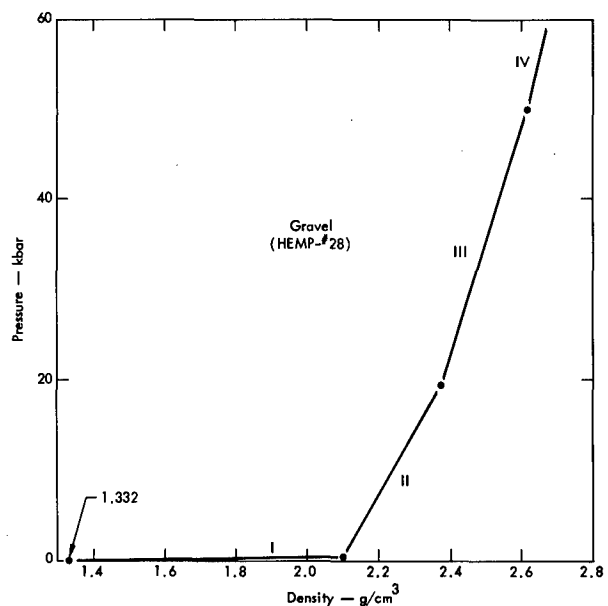


Fig. 15—Pressure-density equations of state for gravel used as upper material in crustal configuration shown in Fig. 10. Initial density of 1.332 g/cm^3 is not recovered after material is shocked above Regime I. Compacted density is then 2.1 g/cm^3 .

DISCUSSION AND CONCLUSION

Although very limited in scope, the present calculational results indicate that when surface explosive sources are sequentially detonated at a supersonic phase velocity, they produce a frequency-dependent, seismic radiation pattern. As in Ben-Menahem's subsonic case, certain frequencies which arrive at the free surface via different paths, such that they constructively interfere, will be enhanced in the direction of sequential detonation. The converse is true for the balance of the spectrum. For a surface disturbance, the directivity effects are more pronounced for the horizontal component of free-surface velocity. It also appears that greater directivity is associated with the P_n (refracted) signal than with the P (direct) wave. This probably occurs because the P_n wave "sees" interference from the entire source region, whereas the direct P wave signal is effectively controlled by the portion of the explosive source closest to the recording station.

The results of one numerical experiment performed with a very low-impedance gravel material indicate that the directivity effects will be seen in cases where the phase velocity of the sequential detonation is comparable in magnitude to the longitudinal elastic velocity of the underlying medium. This result suggests that in certain cases the usual constraint that the phase velocity of sequential detonation be supersonic with respect to the underlying earth material might be relaxed. Placing adjacent charges within small near-surface cavities could effectively permit a subsonic sequential detonation velocity to be achieved.

The questions of scaling the present calculations of seismic frequency spectra and directivities to nuclear explosive-type yields, as well as carrying over the results from two to three dimensions, have not been considered. The effects on the resulting stress waves of various assumed rock rheologies within the region immediately around the explosive source, and the effect of surface vs subsurface charge placement should also be examined. These areas are of critical importance in any thorough examination of the possible advantages of sequentially firing row charges for excavation applications.

ACKNOWLEDGMENTS

This research was performed under the auspices of the U.S. Atomic Energy Commission. I am indebted to Mark Wilkins and his staff for their efforts in running the HEMP code calculations. Discussions with Lawrence Porter were helpful in evaluating the present calculational results.

REFERENCES

1. A. D. Rooke, Jr. and L. K. Davis, Emplacement and Firing of High-Explosive Charges and Crater Measurements, Final Rept. PNE 302 (1965).
2. J. L. Spruill and F. F. Videon, Studies of the Pre-Buggy II Apparent Craters, Final Rept. PNE 315F (1965).
3. M. K. Kurtz, Jr. and W. C. Day, A Report of the Scope and Preliminary Results of Project Pre-Gondola II, NCG Technical Memorandum 67-9, (1967).
4. J. Toman, A Nuclear Row Excavation Experiment, UCRL-71280 (1968).
5. E. Teller, W. K. Talley, G. H. Higgins, and G. W. Johnson, The Constructive Uses of Nuclear Explosives, McGraw-Hill, New York, (1968).
6. H. C. Rodean, Understanding and Constructively Using the Effects of Underground Nuclear Explosions, Rev. Geophys. 6, 401 (1968).
7. J. T. Cherry, Computer Calculations of Explosion-Produced Craters, Int. J. Rock. Mech. Min. Sci. 4, 1 (1967).
8. J. E. Ash and T. V. Eichler, A Theory of Cratering for Multiple Nuclear Underground Explosions, IIT Research Inst. Final Rept., Task I, T6094, (1964).
9. C. R. Cassity, R. W. Klepinger, J. A. Lahoud, and J. R. Murphy, Analysis of Ground Motion, Buggy I Event, (TID-4500), PNE-326, (1969).
10. M. D. Nordyke, On Cratering. A Brief History, Analysis and Theory of Cratering, Lawrence Radiation Laboratory, Livermore, UCRL-6578, (1961).
11. H. C. Rodean, Explosion-Produced Ground Motion: Technical Summary with Respect to Seismic Hazards, Proc. Engineering with Nuclear Explosives, ANS Meeting, Las Vegas (1970).
12. A. Ben-Menahem, Radiation of Seismic Body Waves from a Finite Moving Source in the Earth, J. Geophys. Res. 67, 345 (1962).
13. A. Ben-Menahem, S. W. Smith, and T. Teng, A Procedure for Source Studies from Spectrums of Long-Period Seismic Body Waves, Bull. Seism. Soc. Am. 55, 203 (1965).
14. Y. C. Fung, Foundations of Solid Mechanics, Prentice-Hall, Englewood Cliffs, N. J., 1965.
15. M. L. Wilkins, "Calculation of Elastic-Plastic Flow," in Methods in Computational Physics, 3, Academic Press, New York (1964).

WATER RESOURCES DEVELOPMENT

Review — Water Resources Development

by

David K. Todd
Professor of Civil Engineering
University of California, Berkeley

Introduction

For the past 15 years the possibilities of employing nuclear explosives to develop and manage water resources for the benefit of man have been studied. Experimental and theoretical studies of many types have been undertaken. Numerous applications have been considered including site studies for particular projects. Attention has been given to the economics of specific applications, to hazards and safety problems, to legal limitations, to geologic and hydrologic considerations, and to effects on water quality.

The net result of this effort has been the development of a large body of knowledge ready to be drawn upon wherever and whenever needed. Nuclear explosives are important tools for water resources development; they must be carefully selected so as to serve their intended purpose at minimum cost with few side effects.

Applications

Water resources management as we know it today embraces an ever-expanding field including supplying water for municipal, industrial, and agricultural needs, controlling too much water, overcoming problems of too little water, and regulating bacterial, chemical, and physical quality of water. In addition, there are concerns of water for power, water for navigation, and water for recreation. With a constant world supply of water facing multiplying and competing demands for water, the water resources engineer often feels like the circus juggler with too many china plates up in the air at one time.

Much of the responsibility for identifying potential applications of nuclear explosives to water resources has been carried by the U. S. Geological Survey. And of that organization my colleagues on this program, Mr. Arthur M. Piper and Mr. Frank W. Stead, stand out as the recognized national leaders in that effort. Their studies and publications in recent years on the principles, problems, and national canvass of projects relating to nuclear explosives applications are the guides we have today for interpreting and planning for the future.

A listing of the principal applications of nuclear explosives to the water resources field would include the following:

(a) Harbors. A series of cratering explosions, properly spaced according to known scaling curves, could create a harbor having an orientation perpendicular to the coast line. Precise predictions of crater or channel geometry are not essential for the functional success of such a harbor.

(b) Off-Channel Reservoirs. By one or more cratering explosions a surface reservoir could be formed near a stream or aqueduct and could be connected by a channel, weir, and control gates. The reservoir could be operated as a storage volume for flood control or for seasonal irrigation. An important advantage of such a reservoir is the fact that it could be constructed in a level area without the usual geologic and hydrologic constraints of a normal dam and reservoir system.

(c) Dams. With the selection of a favorable topographic site a row charge can be fired to create by upthrust and mass ejection an embankment to form a dam. Such a "crater-lip" dam is a relatively new engineering concept so that the conversion of an embankment produced by a nuclear explosive to an essentially watertight dam will require further study concerning its permeability and stability.

A second type of dam can be constructed by detonating nuclear explosives in the side of a steep valley to create a dam embankment either by gravitational flow or by directed bulking across the valley. Sealing of the new dam would be required, perhaps by sluicing of the rock structure with a sand, silt, or clay mixture. Under proper siting conditions such construction techniques can introduce substantial savings as compared to the cost of conventional dams.

(d) Canals. As in the harbors application a line of properly spaced cratering explosions can be employed to construct a canal for water supply or navigational purposes.

(e) Drainage. For small drainage basins where disposal of occasional runoff may present a local problem, a crater could provide the small volume of temporary storage required.

(f) Ground-Water Recharge. A nuclear crater filled with water which is permitted to infiltrate into the ground serves as an excellent structure for artificially recharging the underlying ground water. Because of the relatively large volume of a crater as compared to a conventional basin or pit, water can be stored intermittently and recharged more or less continuously. A further advantage of a crater is by its formation impermeable geologic strata which inhibit the downward percolation of water are fractured and thereby rendered more permeable. A rubble chimney resulting from a contained explosion can serve the same purpose.

(g) Waste Storage or Disposal. Concentrated wastes which cannot be discharged into streams and for which treatment may not be economically justified can be stored temporarily or permanently, depending upon local circumstances, in nuclear craters or rubble chimneys. Such wastes may include oil-field wastes, natural salt springs, radioactive wastes, harmful industrial wastes, and concentrates of treatment processes.

(h) Recreation. The demand for water-based recreation in arid and semi-arid regions of the United States is extremely high. To meet this need nuclear craters designed for surface storage of water could provide an attractive environment for boating, swimming, water skiing, fishing, and picnicking. With proper location and design a group of craters could be supplied by water from a nearby aqueduct and also return the water to the same source at a point farther downstream. The chief water loss would be by evaporation as seepage from the craters could be minimized by installing impermeable blankets.

Problems

A primary question of concern in applying nuclear explosives for water resources development is that of safety. Evaluation of hazards, including ground motion, earthquake generation, air blast, and atmospheric fallout, is a matter of common concern to all nuclear explosives engineering. Because these problems

have been studied extensively and are not generally regarded as insurmountable for specified site conditions, they do not require discussion here.

A second important problem is that of the cost of nuclear explosives relative to conventional construction techniques. Definitive cost data are difficult to obtain because of the lack of a commercial market for nuclear explosives at present and also because the AEC will cooperate financially in any initial demonstration projects. Limited economic studies of creating dams or craters for water storage have indicated that nuclear explosives can be feasible in many situations.

Finally, a most important problem in water resources applications is that of ground water contamination. Radionuclides released from large underground nuclear explosions are distributed initially by direct action in the immediate vicinity of the explosion. If the shot point is near or below the water table, the nuclides may be transported by ground water in possibly hazardous concentrations.

Because ground water generally moves at velocities measured in terms of feet per year, only long-lived radionuclides are important in water transport. The biologically significant radionuclides in this category include H^3 (tritium), Ca^{45} , Co^{60} , Sr^{90} , Cs^{137} , Ru^{106} , and Ce^{144} . Laboratory and field experiences have demonstrated that all of these nuclides except tritium are strongly adsorbed by exchange with cations on the surfaces of clay materials; consequently, their movement is only an insignificant fraction of that of the ground water with the result that their concentrations fall below the maximum permissible concentration (MPC) within a short distance from ground zero. However, the disposition of radionuclides in limestone or dolomite is more complex and in these rocks the adsorption may be substantially less than in volcanic rock. For tritium, a negligible exchange between tritiated water and the rock matrix must be assumed. Thus, in terms of curies of activity tritium represents the most abundant nuclide in ground water from a large fusion-fission explosion and becomes the primary contaminant in ground water.

Assuming tritium moves as an ideal tracer with ground water, it will travel in the direction of the local water table gradient and at a velocity governed by the magnitude of the gradient and the permeability of the aquifer. Although average values of gradients and permeabilities in a particular medium can be determined from well data, movements of tritium one to two orders of magnitude greater than the average ground water velocity can be expected as a result of 1) local heterogeneities in aquifers, particularly openings such as solution tubes, fractures, and faults, and 2) dispersion resulting from hydrodynamic mixing as water travels through an actual porous media. Transport can be most rapid through formations such as limestones, basalts, and coarse-grained alluvial deposits which contain large openings.

Experience gained from waste disposal operations at Hanford shows that maximum ground water velocities can be several-fold greater than the average velocity and that without extensive subsurface information the location and direction of these high-velocity tongues are impossible to predict. Similarly post-shot field tests at Project Gnome revealed velocities some 25 times greater than expected values.

At the Nevada Test Site subsurface hydrological investigations have defined the regional ground water flow pattern and average rates of flow. Water tables in the area are deep, exceeding 1600 feet, because of drainage to the south through underlying carbonate formations. Although permeabilities are large, water table gradients are low and consequently velocities are small. Exploratory well data have thus far revealed no evidence of continuous underground conduits which could permit high ground water velocities; nevertheless, the possibility of such heterogeneities must be recognized and an active program of testing

maintained. There is no reason, based upon evidences collected to date, to believe that tritiated ground water will reach the discharge areas, some 50 miles south of NTS, at concentrations above the maximum permissible concentration (MPC).

Conclusions

(1) Although there are important environmental limitations, no major technical obstacles exist to the creation of properly located nuclear craters or chimneys for water resources management.

(2) Nuclear craters and chimneys have potentially important applications for a variety of water resources purposes.

(3) The economic feasibility of constructing nuclear craters and chimneys for water resources projects can be demonstrated in many situations.

(4) More definitive information should derive with time from test detonations and related studies which are underway in fields other than water resources.

References

(1) Graves, E., Jr., Nuclear excavation of a sea-level Isthmian canal, Civil Engineering, pp. 48-55, October 1954.

(2) Knox, J. B., Nuclear excavation: theory and applications, Nuclear Applications and Technology, v. 7, pp. 189-231, September 1969.

(3) Piper, A. M., Potential applications of nuclear explosives in development and management of water resources -- Preliminary canvass of the ground-water environment, Rept. TEI-873, U. S. Geological Survey, 173 pp., 1968.

(4) Piper, A. M., and F. W. Stead, Potential applications of nuclear explosives in development and management of water resources -- Principles, Rept. TEI-857, U. S. Geological Survey, 128 pp., March 1965.

(5) Todd, D. K., Nuclear craters for ground water recharge, Jour. Amer. Water Works Assoc., v. 57, pp. 429-436, April 1965.

(6) Todd, D. K., Nuclear craters for water resources development and management, Civil Engineering, pp. 64-67, June 1965.

NUCLEAR EXPLOSIVES IN WATER-RESOURCE MANAGEMENT

By Arthur M. Piper
United States Department of the Interior
Geological Survey

PERSPECTIVE

Nuclear explosives afford diverse tools for managing our water resources. These include principally: the rubble column of a fully contained underground detonation, the similar rubble column of a retarc, the crater by subsidence, the throwout crater of maximum volume (the latter either singly or in-line), and the ejecta of a valley-slope crater. By these tools, one can create space in which to store water, either underground or on the land surface--in the latter instance, to a considerable degree independently of the topography. Underground, one can accelerate movement of water by breaching a confining bed, a partition of a compartmented aquifer, or some other obstruction in the natural "plumbing system." Finally, on the land surface, one can modify the natural pattern of water flow, by canals excavated with in-line detonation. In all these applications, the potential advantage of a nuclear explosive rests chiefly in undertakings of large scale, under a consequent small cost per unit of mechanical work accomplished.

WATER STORAGE

Space created underground by a fully contained nuclear detonation is slightly less than 3 million gallons or 9 acre-feet (11,000 cubic meters) per kiloton of yield. Such is the volume of an initial cavity of detonation, of void spaces in rubble of a collapse chimney, and (approximately) of a subsidence crater. In most situations the present overall cost of such space would grossly exceed that of conventional land-surface storage, commonly by about an order of magnitude. However, the underground space would be free from loss by evaporation, the ever-present "tax" on water stored in land-surface reservoirs. Practically, underground storage space by nuclear detonation seems limited to special circumstances, such as (1) an urgent water requirement in a region whose rocks are massive and of inconsequential natural water content, but where infrequent surface runoff could be intercepted; or (2) a need to dispose of an especially noxious waste fluid which would be intolerable in the biosphere.

Storage space on the land surface, in a maximum-volume throwout crater, is several-fold greater than that in an underground cavity or rubble chimney, per kiloton of yield. Specifically, the crater space is about 8-fold greater than the chimney space at a yield of 1 kiloton, 6-fold greater at 10 kilotons, and 5-fold greater at 100 kilotons.

As a reservoir for water storage, the throwout crater is virtually independent of land form; generally, therefore, such storage can be sited principally or exclusively for maximum hydraulic efficiency. Costwise, crater space would be potentially competitive with conventional dam-and-reservoir

space for volumes more than 5,000 to 10,000 acre-feet (about 10 million cubic meters), assuming all the apparent volume of the crater were usable. However, unless charging or evacuating is by pumping, the usable space may be only a small fraction of aggregate space--usable space being limited upward by the highest hydraulic grade line at which water feasibly can be diverted into the crater by gravity flow, and limited downward by the lowest hydraulic grade line at which the crater can be evacuated by gravity. Space above the upper limit would be inaccessible; that below the lower limit would be "dead." Either the upper limit or the lower limit might be fixed by the position of the natural water table.

As a tool for creating space, the throwout crater has two potential applications that are somewhat uncommon: in or alongside a stream channel, to trap sediment; and, off-channel and above hydraulic grade line, to provide storage for on-peak hydroelectric capacity.

Potentially the most efficacious nuclear means of creating space for water storage appears to be the slide dam, or the dam by ejection from a valley-side crater. Practical limitations on this means would rest largely in competitive engineering design, nuclear v. conventional, which is beyond the scope of this paper.

WATER MOVEMENT UNDERGROUND

Compared to most natural water bearing materials, the rubble column of a fully contained underground detonation, likewise that of a retarc, is very highly permeable indeed. Thus, suitably sized and placed to breach a confining bed, partition, or other obstruction to ground-water movement, the rubble column becomes a potential means for (1) under-draining a perched water body into the regional aquifer system; (2) discharging a confined water body, upward or downward, into any other aquifer of less head (hydrodynamic potential); or (3) integrating a compartmented aquifer system. The general purpose would be to accelerate recharge, or to increase or prolong the potential yield of developed or developable aquifers.

In all such applications, overall hydraulic performance is most likely to be limited, not by transmissibility of the rubble chimney, rather by natural transmissibilities elsewhere in the aquifer system. Thus, an adequate forecast of performance would require, prior to detonation, that natural hydrologic conditions be appraised widely and possibly exhaustively. The results of appraisal could be inconclusive. A further practical limitation is a potentially common necessity that the vertical run of a rubble column be matched closely to thickness and succession of the rock strata, with no more than nominal over-break beyond some certain stratigraphic zone. A sufficiently nice fit of rubble-column height and stratigraphic thicknesses may not be attainable.

An additional potential advantage of a rubble column is its so-called big-well aspect in massive rocks through which water moves "arterially" in rather widely spaced fractures or ramifying solution channels. Under such conditions the rubble column may intersect several such fractures or channels, and thereby increase the potential rate of water withdrawal (but not the perennial yield). Alternatively, in the big-well aspect, the rubble column would tend to accelerate recharge of, or dissipation of waste fluid into, an aquifer whose natural permeability is small.

Movement of water into the ground--that is, recharge--would tend to be accelerated by the rubble column of a retarc, by the dilated and up-turned wall rocks of a throwout crater, or possibly by the non-dilated collapse column of a subsidence crater. Determinative factors would include the permeabilities, thicknesses, and succession of strata in relation to depth reached by the retarc column or the crater, as well as depth to the aquifer.

WATER TRANSPORT ON THE LAND SURFACE

Effective re-distribution of the natural streamflow is the common requirement of water-resource management. Major works to such an end--canals for intra- or inter-basin diversion--conceivably can be constructed by simultaneous detonation of several nuclear explosives buried in line at a suitable spacing. Practicality of this nuclear application would appear to rest mainly in cuts at least a few hundred feet deep; a 1,000-foot depth of cut appears not impossibly large. Thus, for a major stream diversion, a straight rather than circuitous alinement commonly becomes feasible, independent of all except major land-form barriers.

PRACTICAL LIMITATIONS ON DETONATION

Beyond aspects of engineering design, which are much too complex to be summarized here, feasibility of any particular nuclear detonation is restricted by (1) moderate uncertainty as to dimensions of rubble column or crater produced by a given yield of energy; (2) side effects of detonation--ground motion, air blast (if any), and dispersal of radionuclides produced by the detonation; (3) comparative economics of nuclear v. conventional methods; and (4) legal considerations. The stringency of such limitations would be peculiar to environmental features at and surrounding each proposed detonation site; accordingly, comprehensive pre-shot assessment of the surroundings, possibly very widely, becomes necessary. Some perspective can be summarized here, in the inverse order of the categories just listed.

A nuclear detonation for a water-management purpose involves not only the obvious risk of liability for immediate injury to persons or damage to structures, but also the additional risk that might arise from delayed or prolonged infringement on the rights of individuals in water bodies whose natural behavior was modified. The immediate risk relates to ground motion in the case of a non-venting detonation; to air blast or dispersal of air-borne detonation products in the case of a venting detonation. Reasonably definitive criteria are at hand by which to minimize these immediate risks, in terms of remoteness of a detonation from centers of population or from structures. However, assuming a detonation of 100 kilotons or more, the ideal remoteness commonly may not be possible and some minor injury or damage might be inevitable. In this situation, standards by which to measure the injury or damage are currently neither universal nor reasonably precise. Thus, magnitude of the liability would at this time be difficult to ascertain. In regard to the delayed risk of infringed water rights, the minimum requirement would be a comprehensive and exhaustive appraisal of hydrologic conditions both before and after detonation. Even so, the kind or degree of infringement could be inconclusive and the magnitude of liability not determinable.

As to comparative economics, nuclear v. conventional, the speaker takes the present overall cost of a single nuclear detonation not exceeding 100 kilotons to be in the general order of \$2 million; that of a detonation of greater yield only nominally more. This is the basis for the preceding generalizations that (1) water-storage space in a rubble column or in a standard crater-by-subsidence would not compete economically with space in a conventional reservoir on the land surface, and (2) storage space in a throwout crater would not compete in volumes less than 5,000 to 10,000 acre-feet (about 10 million cubic meters). Thus, the smaller storage spaces by nuclear detonation seem justifiable only by an urgency or an advantage that overrides non-economic cost. (On another hand, the larger nuclear undertakings involve potentially limiting side effects, which will be summarized.)

Comparative efficacy and economics of a rubble column v. a conventional drilled hole should be assessed carefully, be the scale of the project large or small. Take, for example, the concept that the classic Dakota artesian basin might be re-pressurized by breaching confining beds that intervene between the Dakota and Lakota aquifers, also, between these aquifers and the underlying Madison limestone. The concept derives from the recent showing by Swenson that the Dakota-Lakota overlap the Madison and, in the belt of overlap, are charged from the Madison. It appears technically feasible to breach the particular confining beds with rubble columns generated by nuclear detonations, each from a few hundred kilotons to possibly a few megatons. Even with population centers dispersed as in central and eastern South Dakota, sites that would both accommodate detonations so large and satisfy hydrologic requirements are not readily identifiable. On the other hand, the hydrologic effect of each rubble column could be duplicated by two conventional drilled holes of the diameter necessary for emplacing the nuclear explosive. The drilled holes would cost substantially less and would avoid both the uncertainties and the side effects of nuclear detonation.

In regard to radionuclides dispersed by a non-venting detonation in the ground-water environment, early and close-in concentration might greatly exceed the so-called maximum permissible. However, considering rates of radioactive decay, velocities of ground-water movement, and the degree to which specific nuclides would be adsorbed onto the water-bearing medium, concentration of all nuclides except tritium would generally not exceed "permissible" in water withdrawn several miles down-gradient from shot point. For each proposed nuclear detonation, however, a specific radiation-protection guide would need be determined for the particular environment. The specific guide might be less stringent than the "permissible" concentrations of Handbook 69, especially if none of the water would enter food or drink.

In a fission-fusion detonation, tritium becomes the critical and diagnostic nuclide. If it could enter the food chain, tritiated ground water generally should be withdrawn only from an aquifer of small permeability, with the point of withdrawal tens of miles down-gradient from shot point, so that residence time of the water in the aquifer would be at least a century. If use of the tritiated water were wholly separate from the food chain, a shorter residence time in the aquifer might be acceptable but the waste fluid resulting from the use would require disposal under acceptable public-health standards. Obviously, expected concentration and dispersal history of tritium would need be appraised with great care in the planning stage of each proposed fission-fusion detonation.

A venting detonation for a throwout crater or trench (for water storage, recharge, or transport) adds the complication of air-borne radionuclides dispersed by the wind. Seriousness of such dispersal would of course be peculiar to each detonation, to environmental features of the site, and to meteorologic conditions at shot time. Dispersal might be wide if nuclides fall into a major flowing stream, or greatly prolonged if nuclides fall first onto the land surface but subsequently are transported to streams by overland runoff. Complexities are many and beyond the scope of this paper.

Public acceptability of a nuclear detonation for a water-management purpose would depend to a considerable degree on severity of the attendant ground motion. As has been alluded to under the preceding discussion of liability, reasonably definitive criteria are at hand by which such severity can be anticipated. Assuming, however, that the feasible water-management detonation will be on the order of 100 kilotons or more, distance from shot point to centers of population or vulnerable structures might need be in the order of a few tens of miles. Sites so remote, but at the same time effective for a common water-management purpose, are unlikely to be widely available.

Allusion has been made to the common requirement for a nice fit between dimensions of an underground rubble column and stratigraphic dimensions of the environment. Again assuming that the feasible water-management detonation will be of moderately large yield, rather than small yield, even the moderate present uncertainty in dimensions of rubble column or crater appears commonly to preclude the nice fit required.

CONCLUSION

Considering both the practical and the technical limitations that have been outlined, it seems that nuclear detonation for water-resource management is likely to be practicable only in unusual hydrologic settings, or under an urgency that overrides economic or technical disadvantage.

The concepts here summarized briefly have been developed at length in two antecedent documented papers, as follows:

Piper, A. M., and Stead, F. W., 1965, Potential applications of nuclear explosives in development and management of water resources--Principles: U.S. Geol. Survey rept. TEI-857, 128 p.

Piper, A. M., 1968, Potential applications of nuclear explosives in development and management of water resources--Preliminary canvass of the ground-water environment: U.S. Geol. Survey rept. TEI-873, 173 p.

PROJECT AQUARIUS
CONTROL OF RADIOISOTOPES AND SAFETY

Dr. Roy G. Post
Department of Nuclear Engineering
University of Arizona

I. Introduction

The potential application of nuclear explosives to the development of water resources provides real hope for substantial increases in the availability of water from our natural water supplies. A wide range, exploratory project sponsored by the United States Atomic Energy Commission, the Bureau of Reclamation, the Arizona Atomic Energy Commission, and The University of Arizona was conducted by the Hydrology and Water Resources Office, the Department of Nuclear Engineering, and various state and federal governmental agencies in exploring the potential applications of nuclear explosives for developing water resources in the State of Arizona. The primary objective of the project was of a scouting nature, a reconnaissance effort to assess the potential for Arizona. This work, Project Aquarius, is at an early state and any significant conclusions are certainly premature. Since this is a survey, detailed analyses are not justified. Our purpose is to define limiting problems and estimate our ability to solve them. We do not seek to formulate a detailed solution until the project has been defined better.

In all of the plowshare activities the primary responsibility of the Atomic Energy Commission for safety and control of not only radiological but all hazards has been well defined and documented. Thus, the work here does not reflect any opinion or voice of the Atomic Energy Commission but is based on my own views and conclusions. I have referred to the work of the various laboratories, offices, and contractors of the Atomic Energy Commission.

By way of orientation, let us consider the map of Arizona shown in Figure 1. There are many relatively remote areas in Arizona but to develop water resources either yields of present water systems must be increased or we must develop presently unappropriated water. The latter are almost nonexistent. Indeed, in many areas there are more legally justified claims to water than there is water. These considerations exceed the scope of our papers but they were a factor in restricting the areas to be considered. We will look at the Cave Creek area in southeastern Arizona, near the New Mexico border, and the Clear Creek area near the Mogollon Rim in east central Arizona.

First, let us consider the range of concern. Using the formula defined by Joe Knox⁽¹⁾ in his paper in the September 1969 special issue of *Nuclear Applications and Technology* for the seismic response parameter, pseudo acceleration:

$$A_g = 5.03 \times 10^5 W^{0.7} R^{-2.0}$$

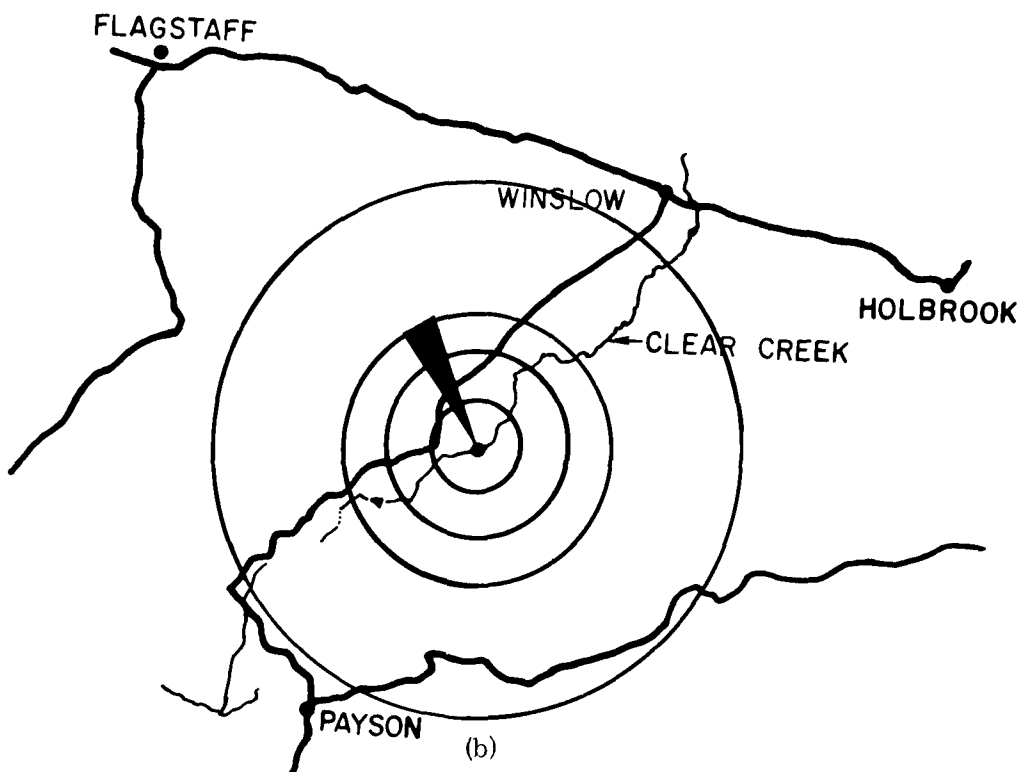
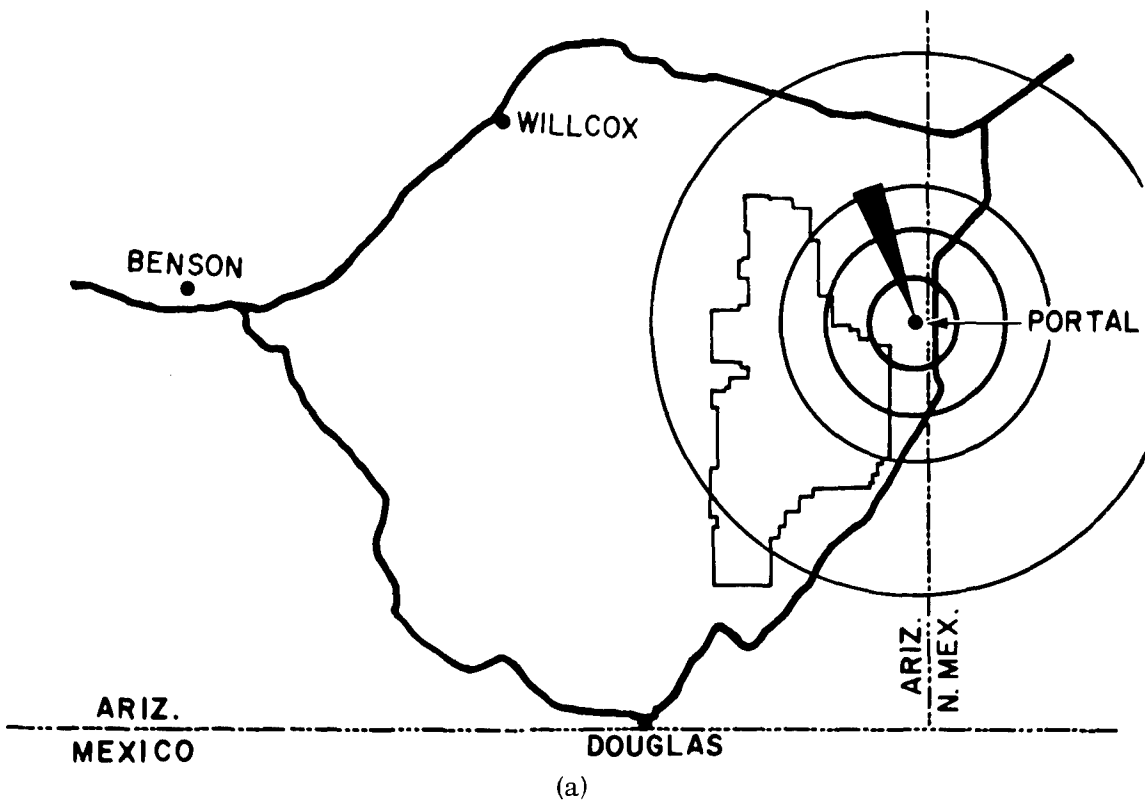


Figure 1

where A_g is the pseudo acceleration in gravity units,

W is the yield in kilotons

and

R is the range in meters

and solving for R , we have

$$R = 7.1 \times 10^2 W^{0.35} A_g^{-0.5}$$

for $A_g = 10 \text{ cm/sec.}^2$

$$R = 7.0 \times W^{0.35} \text{ km}$$

and

$$= 4.35 W^{0.35} \text{ miles.}$$

for the explosive yields of interest, as reported by R. F. Griffin in these proceedings, we calculate the ranges shown in Table 1.

Table 1.

Range of Minimum Seismic Effect

Yield	Range, $A_g = 10$	
	<u>Km</u>	<u>Miles</u>
15	17.8	11.1
75	31.6	19.6
100	35.0	21.7

Five, ten, and thirty mile ranges are plotted on the Arizona map and as you can see covers a very small area, largely unpopulated. Thus, no seismic damage should be expected.

Looking at air blast, depending on conditions, about 5 miles to 10 miles should be considered as a possible range for a 2 mb overpressure. Again no serious hazard exists.

Turning now to the question of radioactivity, we have a more serious problem. Again using Knox's report in the September issue of *Nuclear Applications and Technology*, for a 50 KT cratering or retarc shot, about 10 miles are needed for the limiting 0.17 rad/year of external gamma exposure and 25 miles for iodine in milk. There are no milksheds of consequence in these areas so although these need further careful evaluation, these early conclusions indicate no need for concern. The crater volume of 2,250 acre-feet for a 50 KT explosive would be dispersed by evaporation from a 200 acre pond in about a year and a half. If this mixes in a 30° mixing cone, then within 10 miles the tritium is diluted by a factor of about 30,000 with respect to the water capacity of the air. Thus, after 10 miles, the humidity due to the pond water is only 1/30,000 saturated. This will reduce the tritium well below mpc. Thus, if the experiment permits filling the crater and disposing of the water by evaporation, there would be no tritium problem for the crater or the aggregate production.

The dispersal of tritium by dilution within the aquifer is more doubtful since about 13,400 acre-feet of water are needed for dilution to mpc limits. This is about 6 cavity volumes.

If the water flows into the cavity and then into the aquifer, the complete mixing implicit in the example just presented is not probable. One should expect relatively little mixing so that the tritiated water would move as a front. Monitoring water at a point very close to the source should show a very rapid rise in tritium concentration followed by a gradual drop.

The inventory of tritium will be carried in a relatively small quantity of water - probably less than a cavity volume. The reduction in concentration by some factor - probably greater than six may be realized by at least two other means - radioactive decay and dilution with water from the aquifer. The first will require a residence time of about 33 years which isn't really long for most aquifers but would preclude charging and immediate recovery, an essential part of one water conservation scheme.

In this method one would trap flash floods with a retarc or crater dam, designed so that the water would percolate to an unsaturated aquifer. It would then be pumped out as required. The second reduction in concentration would require some sort of conical mixing in the aquifer. If the circumferential dispersion angle and the thickness of the aquifer is known, the distance the front must move before the tritiated water becomes sufficiently dilute, can be calculated. A slight modification of this scheme might be in order for the aquifer charge-pump scheme. One could let the front pass and use the water behind it or pump out and evaporate water too high in tritium. As shown earlier, disposal of tritium by evaporation looks quite reasonable.

The important question of the overall desirability of Aquarius or any project can only be resolved following the thorough understanding of behavior of all potentially hazardous isotopes produced by the use of nuclear explosives. These radioisotopes will be subjected to the movement of groundwaters. Thus, it is important to understand the behavior of all of the isotopes in those formations which will carry water away from the site of a nuclear detonation.

Considerable work has been done both in the delineation of the behavior of trace elements in the movement of water through various aquifer materials and in the hydraulics of aquifers similar to those found in Arizona. Indeed rather extensive investigations of the properties of aquifers in the Tucson basin have been conducted over the years. The references citing the works in these two important fields are too numerous for a complete listing but samples are indicated in the Selected Bibliography. Some of these works have been directed to the definition and solution of specific problems of dispersal of radioactive elements. The work at Chalk River and at Hanford was directed toward the behavior of fission products from nuclear fuels processed by the chemical plants separating plutonium and uranium. The soils and groundwater movements were studied extensively and much data obtained. In addition, considerable work has been done on the Nevada Test Site and much of this has been reported in the open literature.

The objectives of these earlier studies did not include the possibility of using the groundwaters as a source of potable water. Although the Nevada Test Site does provide some variation in geology the aquifers may not include the types that are of potential interest in development of Arizona water resources by nuclear explosive engineering. In general, the work has been restricted to rather empirical treatment of the data and the published works have indicated that the radionuclei are well retained by those aquifers which have been studied. The full confidence of good behavior of all radioisotopes

potentially hazardous to health, and the confident extrapolation of this observation to those aquifer formations with significantly different chemical and physical properties requires a much more sophisticated understanding and accurate prediction than is currently available. A first step in this process is the formulation of a realistic mathematical model which will reflect not only the observed behavior but will be based on a sound picture of the physical system so that the extrapolation can be done with a high degree of confidence. In the movement of groundwater, one assumes conventionally that the radioisotopes are in equilibrium with the solid material. This is a reasonable assumption in large distances and relatively uniform ground materials. In a particular formation there may be cavities. The exchange equilibria and kinetics for the specific formation and soils that are representative of the test areas must be studied to assure the accuracy of the predictions for exchange. There is very little possibility of a significant variation in the conclusion that all isotopes other than tritium will be readily contained in the soils. Nonetheless, specific data are needed to confirm this. The action of the porosity and conduits through the limestone formations must be evaluated since this is an area that has not been very carefully analyzed in previous work.

The public response to nuclear experiments is often surprising and always of dominant importance. Every reasonable effort must be made to inform the public and to assure them that the planning of the experiment is done with a high degree of confidence and due regard for all hazards and impact on the ecology, the environment, and the general public. They must be sure that the benefits to be gained by the experiment justify the risk to be taken and that these risks are as small as can be reasonably provided. We cannot expect the people in authority who must make most of the decisions for these kinds of experiments, particularly on the state and local levels to be knowledgeable in these areas or even to have advisory groups that are knowledgeable in nuclear explosion technology. Detailed competent analysis by interested persons not directly responsible for the project can have a beneficial and reassuring influence for not only the political figures but the local nongovernmental public figures such as newspapers and civic organizations. Failure to provide this assurance to the general public and the spokesmen and opinion makers in the area can lead to failure of the project regardless of the technical and economic potential and value. We cannot afford to take such risks in the early stages of this most promising technology.

Project Aquarius--Geohydrologic Investigation

William J. Ganus
University of Arizona

Abstract

Piper and Stead (1965) suggested several potential applications of nuclear explosives in the development and management of water resources. The Aquarius study began with an investigation of these potential applications in Arizona.

The three district physiographic provinces of Arizona offered a wide range of geohydrologic settings for study of modification by nuclear explosives. Damming of surface water by bulking techniques including rock quarrying, was considered the most favorable application for analysis. A general discussion of geologic and hydrologic conditions for a canyon site in North-central Arizona is given. Groundwater recharge by cratering in alluvial materials is rated as the second most favorable application and a site in Southeastern Arizona, representative of a typical alluvial fan setting, is discussed. Other applications are presented but hold less promise due to lack of geohydrologic and nuclear explosion data necessary for proper evaluation.

In the review of potential sites for study, primary consideration was given to distance of site from population centers and to the quantity of water that could be developed and managed. For surface water resource development by nuclear explosions, additional considerations for site selection included canyon shape for landslide, throw-out or rock-fill techniques, canyon meanders necessary for diversion channels, low permeable rock types for minimizing problems of radioisotope migration, and a clear identification of any groundwater system that could be affected. In the site selection for recharge craters, considerations included adequate subsurface storage space, aquifer characteristics favorable to recharge and recovery, subsurface lithologic type and distribution that would permit control of radioisotopes by either monitoring or removal, suspended sediment load of water source, and estimated increased efficiency of artificial recharge over natural recharge.

Introduction

With the technology of his time, man continually strives to exercise control of his water resources. Today he is on the threshold of employing the newest and most dramatic technique--nuclear explosives-- to water resource development and management.

In 1965, Piper and Stead (1) presented several imaginative concepts for modifying the geohydrologic system by nuclear explosives. Harshbarger, et al (2), in 1967, with the support of the Arizona Atomic Energy Commission,

prepared a preliminary report on potential sites in Arizona for nuclear cratering related to water management. This preliminary investigation was expanded in 1968 into the Aquarius Project. The initial phase of this project, as reported here, consisted of a general inventory of the geohydrologic environments in the state in regards to the possible modification for water resource development and the selection of two sites for detailed analyses.

Physiography and Geology of Arizona

The state of Arizona may be divided into three geographic provinces: (1) the Plateau Uplands, (2) the Central Highlands, and (3) the Basin and Range Lowlands. (Figure 1)

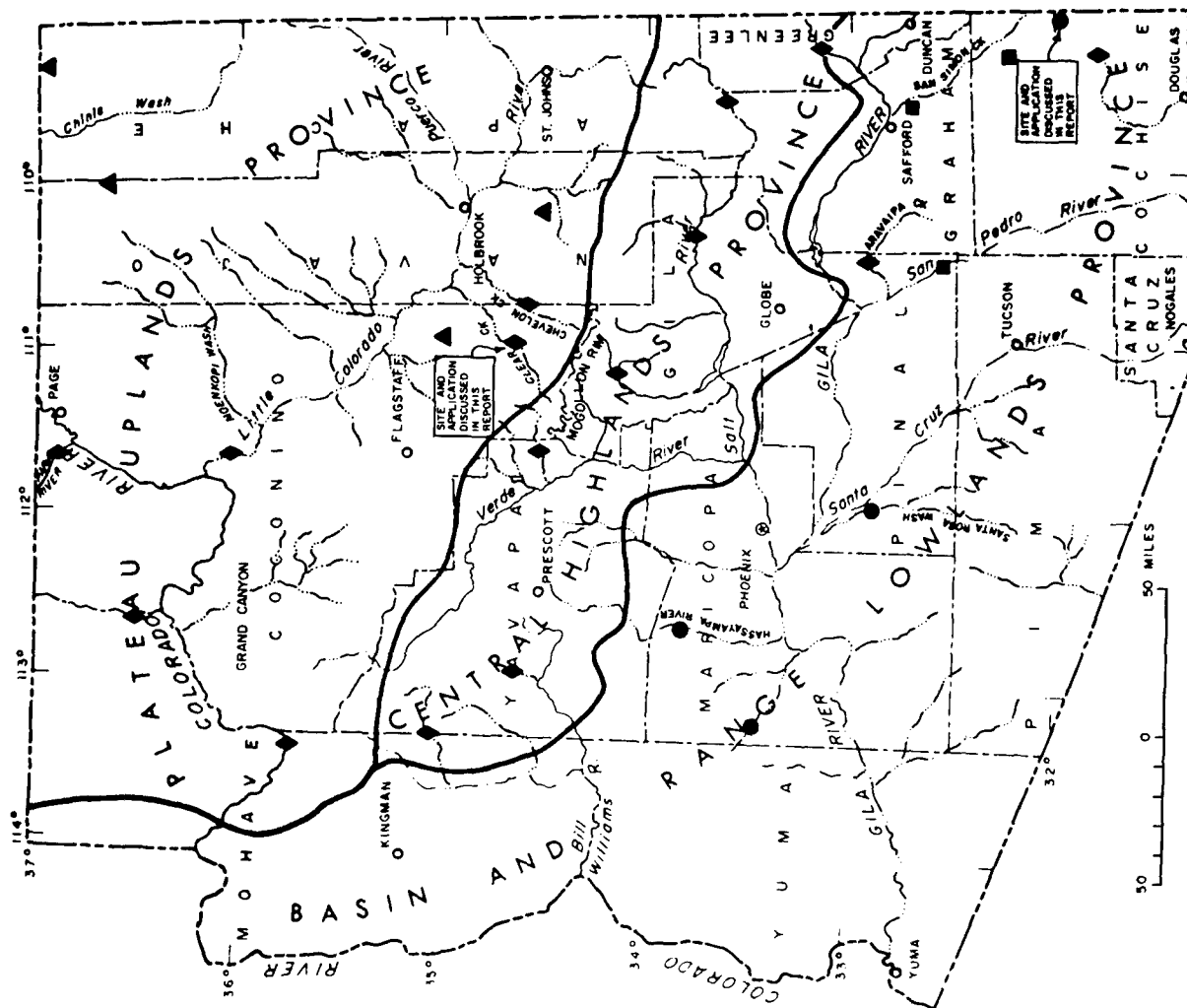
The Plateau Uplands are characterized by buttes, mesas, and gently sloping mountains which have formed on predominantly sedimentary rock sequences. The combination of low precipitation (less than 10 inches annually) and high potential evapotranspiration results in very small surface runoff in the area north of the Little Colorado River. South of this river the Plateau slopes upward to the Mogollon Rim where relatively high precipitation and runoff have created a number of canyons along streams tributary to the Little Colorado River. The northwest portion of the province is marked by a major through-flowing stream, the Colorado River, which has formed the Grand Canyon. In the eastern half of the province from the Mogollon Rim to the northern state boundary, sandstone formations provide considerable storage for groundwater; however, the fine grained nature of these units restrains water recovery by wells except in areas where secondary permeability has been created by fracturing.

The Central Highlands, which separate the Plateau Uplands from the Basin and Range Lowlands, consist of rugged mountains of predominantly igneous rocks. The combination of the high precipitation, (10 to 35 inches annually) due to the altitude of the highlands, and the impervious character of the rock comprise conditions for this province to yield the greatest amount of surface runoff in the state. The occurrence of groundwater is limited to small alluvial basins and fracture zones within the bedrock, and therefore is of minor importance in the area.

The Basin and Range Lowlands are dominated by isolated mountain blocks partially buried by their own detritus and broad alluvial basins. Precipitation is variable and closely related to topography. The higher precipitation in the mountains provides the source of some surface runoff into the valleys where a portion is consumed by evapotranspiration and the remainder comprises infiltration. Large storms or local thunderstorms may produce substantial surface flow in the valley streams; however, this type of flow is ephemeral and highly variable. The rock materials in the alluvial basins provide a vast storage reservoir for groundwater. The variations of permeability of the alluvial material result in a wide range of yields from water wells.

Possible Uses of Nuclear Explosives for Water Management in Arizona

From a detailed study of the many different types of geologic and hydrologic environments in the state, one could find numerous sites where nuclear explosive concepts would have potential application in water management programs. However, because of the many unknown factors both in nuclear



engineering applications and in the geologic and hydrologic systems, the sites and concepts must be considered as being preliminary in nature. The overall technical, safety, and economic feasibility of a project would have to be demonstrated by an in-depth study. With this provision, a general description of possible concepts for suggested potential sites in each physiographic province is presented.

In the review of potential sites for study, primary consideration was given to the distance of site from population centers for safety reasons. From a hydrologic standpoint the primary consideration was quantity of water that could be developed and managed. (A cursory examination of the cost factors related to the use of nuclear explosives indicates that economics are generally more favorable for the larger projects.)

In the Plateau Uplands, high evapotranspiration losses and general geomorphology combine to make large scale damming unrealistic in the area northeast of the Little Colorado River. South and west of the Little Colorado River the high precipitation and runoff and the through-flowing Colorado River with its many tributaries have created a vast and varied system of canyons in the generally flat-lying or gently sloping sedimentary rock sequences. These canyons are predominantly steep-walled and present large variations in depth. Bulk dam concepts, using either retarc, throw-out, or landslide techniques, which are applicable in the many canyon sizes in the area, offer a wide range of potential nuclear explosives for use in surface water management. Possible concepts for any particular site would have to be evaluated from the standpoint of the purpose and use of the dam. Several sites shown in Figure 1 are suggested for feasibility study. A proposed dam site on Clear Creek, located near the southern boundary of the Plateau Uplands, was selected for an in-depth analysis of a nuclear engineering application. In the area of modification of groundwater systems, nuclear explosives appear to have a limited potential in the Plateau Uplands. Current information on the effects of nuclear explosives in a consolidated media indicates that induced fracturing in the vicinity of the explosion does not extend radially outward at sufficient distances to produce a significant increase in yield from a low-permeability aquifer. However, the fine grained sandstone aquifers of the Plateau Uplands have undergone some tectonic modifications which have produced anomalous zones of fracture permeability and have significantly increased groundwater storage potential. Wells in these areas, where they intercept one or more major fractures, yield substantially more than wells in the unfractured aquifer. The rubble chimney concept could have an application in such a situation where a number of large fractures may be intercepted by the chimney and result in significantly greater recovery from wells drilled into the chimney. This type of well-chimney-aquifer system could offer decided advantages for a range of operations involving recharge, storage, or recovery. Approximate locations for potential applications of this concept are shown in Figure 1.

In the Central Highlands province, the high precipitation and runoff have carved a complex system of canyons in predominantly igneous type rocks. Although many of the streams of this area have been dammed by conventional methods for a variety of purposes, many potential sites remain where nuclear engineering concepts would be feasible. Although the Clear Creek site mentioned above is located in a canyon of sedimentary rock in the Plateau Uplands, it is believed that the method of concept analysis would be very similar to potential nuclear engineering applications in the Central Highlands.

The occurrence and development of groundwater is of minor importance in the Central Highlands and therefore no study of nuclear engineering concepts appears warranted for this area. When more data on groundwater and fractured rock areas are obtained, nuclear engineering techniques may be appropriately considered.

In the wide valleys of the Basin and Range Lowlands surface flow characteristics, evapotranspiration losses, and general geomorphology make surface water damming by conventional methods unattractive. However, where major streams have cut across the mountain blocks steep walled canyons are present. In these areas bulk dam concepts may hold promise. (Figure 1)

The higher amounts of precipitation on the larger mountain blocks of the province contribute significant runoff in many small streams which drain into the alluvial basins. This flow is quickly dissipated by evapotranspiration and infiltration losses. Although the part of the infiltration that results in groundwater recharge may be desirable, it is believed that evapotranspiration often greatly exceeds infiltration in many areas. In order to capture most of this surface flow before it reaches the basins a number of small dams would be required. A nuclear quarry concept may show that a centrally located quarry could provide aggregate at a low cost to a number of small nearby damsites. The west side of the Chiricahua Mountains is an area where this concept may apply.

The importance of groundwater in the Basin and Range Lowlands and its widespread occurrence justify the careful study of any technique of groundwater system modification and management. The lithologic variations and dimensions of most basins are not fully defined; however, geological events during the formation of the Basin and Range structures indicate that a number of basins underwent alternating periods of interior and exterior drainage, resulting in depositional combinations of sand, gravel, silt and clay beds in various local and basin-wide depositional patterns. Groundwater in these deposits may be found in a range of water table, semiconfined and confined conditions. The potential yield and chemical characteristics of the deeper aquifers generally have been unexplored and therefore have been unappraised as to their present or potential importance in the development and management of the shallower aquifers.

In applying nuclear engineering concepts to the groundwater system, the principal objective would be to induce recharge to the aquifer that is suffering a loss in hydrostatic head due to pumping by man. The nuclear explosive concept of greatest potential appears to be a surficial feature, like a single crater or row charge crater in a stream bed, which could facilitate recharging the groundwater system, especially where impermeable strata may be retarding natural recharge. In effect, the natural line source (groundwater recharge) and line sink (evapotranspiration losses) would be replaced by a point source (groundwater recharge) and point sink (evaporation losses). Controlling factors for recharge effectiveness would be the permeabilities of materials in the crater vicinity, both vertical and horizontal, and the available groundwater storage space in the area of recharging. If the topography of the stream channel is pronounced, the upstream lip of the single crater or row charge crater may be used as a detention basin for desilting purposes. One site for study of the recharge concept has been selected on a tributary to the San Simon Creek. Other potential sites for similar applications are shown in Figure 1.

When the feasibility of this recharge concept is demonstrated, an additional use of this application may be considered. Along the route of a canal aqueduct there may be areas of alluvial sediments of favorable permeability and storage potential. In such areas, single craters or row charge craters could be used for recharging and storing water underground during periods of surplus flows.

In some alluvial basins water table aquifers that are undergoing depletion are underlain by an aquiclude and artesian aquifer with a hydrostatic head higher than the water table aquifer. The concept of aquiclude breaching by nuclear explosives may apply in such a groundwater situation. The desired effect would be to utilize the high head of the artesian aquifer for recharging the water table aquifer from below, through a rubble zone in the aquiclude. Also, the chemical characteristics of the deeper water may make it marginally acceptable for use and the flow into the water table aquifer through the rubble zone could be an effective aid in mixing. Depending on the depth of the aquiclude and the competence of the overlying material, this application could result in a subsidence crater at the surface which could serve as a recharge point for the surface waters. Potential sites for the aquifer breaching concept are shown in Figure 1. Better definition of the deeper aquifer systems is definitely needed to evaluate properly the potential of this application.

Rating of Nuclear Explosive Applications to Water Management in Arizona

A combined analysis of available information on nuclear explosive engineering and geologic-hydrologic systems throughout the state permit a rating of applications which warrant continued study of technical, safety and economic feasibility.

Because of the numerous canyon environments in various rock media, it is believed that dam concepts, either by bulking techniques at the site or by nuclear quarrying nearby, hold the most promise for nuclear explosive use in water management. Therefore this application is ranked first and has been studied in detail for a site in the Plateau Uplands province.

The importance of groundwater in the southern part of the state makes the recharge concept by cratering worthy of continued study. Natural flows as well as surplus imported flows could be better managed by utilizing the subsurface for storage, transmission and purification. This application is rated second and has been studied for a site in the Basin and Range Lowlands province.

Aquifer modification by rubble chimney or aquiclude breaching appears to have only limited application and to be somewhat uncertain in effectiveness. Better definition of certain hydrologic-geologic conditions may eventually indicate ideal sites for these applications. Until then, these applications must be rated third.

Rubble chimneys for waste disposal purposes have not been considered in this study because no major disposal problems of relatively low volume and high contamination were noted in the State. When and if such a problem arises, the rubble chimney concept for disposal should be given consideration.

Description of Sites

Mogollon Mesa - Clear Creek Area* - Dam Site

The southwestern margin of the Plateau Province is marked by the Mogollon Rim, a spectacular fault scarp. The Mogollon slope dips gently northward from the Mogollon Rim to the Little Colorado River Valley. The region is marked by rugged canyons in the upper reaches of most major streams. The Clear Creek area of study lies within the upper portion of the Mogollon slope.

Clear Creek is an intermittent stream that discharges snowmelt in the spring and is normally dry during the early summer months. It flows again during the late summer from typical Arizona summer high-intensity storms. Stream flow records at the proposed damsite from 1948 to 1965 indicate a mean annual flow from 321 square miles of watershed of 55,770 acre-feet. During this period an annual high of 142,400 acre-feet and low of 12,610 acre-feet were recorded.

Pertinent stratigraphic units in the subject area include, in descending order, the Kaibab limestone, Coconino sandstone, and Supai formation. The Permian Kaibab limestone forms the surface over much of the Mogollon slope. Along the Mogollon Rim it is about 300 feet thick, and consists of thin to thick-bedded gray limestone interbedded with fine grained, lime-cemented sandstone. The lower Kaibab member consists of massive, interbedded limestone and limey sandstone with sporadic beds of nodular and cherty limestone. Bedding planes are open, clay filled, and exhibit solution channels. Solution cavities along the Kaibab-Coconino contact are common. The permian Coconino sandstone of aeolian origin is white to buff, fine to medium grained, quartzitic, and ranges in thickness from 250 to about 1,000 feet in northern Arizona. The grains are well sorted, subangular to subrounded, and moderately to firmly bonded by dominantly siliceous cement. The Supai formation of Pennsylvanian-Permian age consists of 1,500 to 2,000 feet of red to brown, interbedded sandstone, conglomerate, siltstone, limestone, and evaporites. In some areas an upper sandstone member is difficult to distinguish from the overlying Coconino.

The gently dipping Mogollon slope roughly conforms to the dip of the underlying formations, about 3° to 5° to the north and northeast. Numerous transverse northwest and northeast trending low-dip and plunging anticlines and synclines occur on the slope. Faults on the Mogollon slope similarly trend northeast and northwest, are generally of small displacement and nearly vertical. The regional joint system includes two principal sets which are generally vertical and strike about north 55° west and north 30° east.

Groundwater near the southern, or upper, end of the Mogollon slope occurs in the Coconino sandstone and underlying aquifers. Commonly, water levels occur about 200 feet below the Kaibab-Coconino contact. Except for the upper sandstone member, the Supai formation is essentially impermeable and serves as an effective barrier, except where fractured, to all vertical movement of water to rock units below the Supai.

*This section is summarized largely from U.S. Bureau of Reclamation, preliminary investigation of the Wilkins Damsite. (3)

The permeability of the unfractured Coconino sandstone is inherently low; however, the permeability can be increased significantly by jointing and fracturing.

Recharge to the Coconino sandstone occurs primarily along the Mogollon slope. Direct precipitation, stream flow and snow melt percolate downward through interconnected solution cavities and other openings in the highly jointed and fractured Kaibab limestone, as well as through the Coconino where it is exposed. This water may move downward through the Supai and other underlying formations in areas of intense fracturing.

The proposed reservoir would lie within a narrow, nearly vertical-walled canyon about 500 feet deep which exposes about 300 feet of the Kaibab limestone and about 200 feet of the Coconino sandstone. There is little to no alluvium within the canyon floor. Data from surrounding oil tests and water wells indicate a total Coconino thickness at the site of about 600 feet.

As the concepts of dam construction by nuclear explosives were developed in the study, it became apparent that certain considerations would weigh heavily in future site selections. The canyon geometry--width, depth, and angle of walls-- plays a major role in the determination of the concept, whether it be landslide, throw-out, or rock-fill. Also, the presence of meanders in the stream can greatly facilitate the construction of diversion canals. In order to reduce the potential problems of radioisotope migration in the subsurface, ideally the canyon rock should be impermeable and not be a part of an aquifer system. If a ground water system does exist, it must be clearly defined.

San Simon Basin - Cave Creek Area - Recharge Site

The Sam Simon Basin, in the southeast corner of Arizona, is part of a structural trough that extends northwestward from Rodeo, New Mexico to Globe, Arizona. (4) The particular area of interest in the study, the Cave Creek area, is located on the western slope of the basin near the southern boundary. Cave Creek drains about 40 square miles of watershed in the Chiricahua Mountains and enters the basin near the small community of Portal, Arizona. The watershed is about 6500 feet in average elevation and receives about 20 inches of rainfall annually. Stream flow measurements made near Portal from 1919 to 1925 indicate a high of 13,540 acre-feet per year and a low of less than 1,000 acre-feet per year with an average annual flow of about 6,000 acre-feet. The predominant rock in the watershed is rhyolite which produces a low suspended sediment load in the runoff.

As the runoff leaves the mountains and enters the basin it flows in a somewhat poorly defined channel in the alluvium for about 10 miles before it reaches the major stream in the basin, the San Simon Creek. Upon entering the basin, the stream flow decreases as the water is lost to infiltration and evapotranspiration.

The groundwater environment in the study area cannot be clearly defined from the few wells drilled in the area. Lithologies from drillers' logs (5) appear to be typical of alluvial fan deposits--gravels, sands, silts and clays in beds of highly variable lateral and vertical extent. The over-all groundwater body in the area is considered to be under water table conditions, however, several miles to the north the clay beds increase in thickness and lateral extent, creating artesian conditions. From meager and widely scattered data, the general groundwater system in the study area comprises recharge near the mountain front and northeasterly movement to the discharge

points in the San Simon Creek and in wells near the Creek. There is a significant volume of unsaturated alluvial material in the upper reaches of the fan similar to many alluvial fan environments in southern Arizona. This unsaturated zone offers attractive possibilities for recharging surface flows near the source and before the high evapotranspiration losses are incurred. The advantages of the subsurface porous and permeable media for storage, transmission and purification have been extolled many times.

A site for study of a recharge crater created by a nuclear explosion has been selected on Cave Creek in the eastern half of section 8, Township 17 South, Range 32 East. At this location, the static water table altitude occurs at approximately 3950, about 300 feet below the ground surface. Detailed subsurface exploration by wells would be required to properly predict radioisotope movement in the heterogeneous deposits of sand, gravel and clay. Pumping tests from wells several miles to the north of the site show transmissivity values in a confined aquifer to be about 20,000 gallons per day per foot. The nature of the sediments described by drillers' logs near the site suggests that an average specific yield value of 15 per cent may be realistic for long term drainage and recharge calculations.

The most important parameter in the determination of the proper crater size for a particular recharge rate is the value of the effective coefficient of permeability. The heterogeneous nature of the alluvial material that will be exposed as the recharging surface in the crater will permit a wide range of infiltration rates to occur as the crater is being filled with water. Lateral movement of water into sands and gravels may be expected to account for the greater infiltration rates.

A major hydrologic factor that must be considered in any artificial recharge project such as this is the possible improvement in the system. Natural recharge to some extent occurs on all similar alluvial fans; however, data necessary for estimating this quantity is seldom available. Therefore, to realistically assess the benefits of an artificial recharge project, recharge under natural conditions should be determined first.

Summary and Conclusions

The hydrogeologic environments of Arizona are quite varied and offer numerous sites for which nuclear explosives may have potential use in water development and management schemes. In the central and northwestern portion of the state, surface water damming in canyons by landslide, throw-out or rock-fill techniques appear to hold the most promise for nuclear explosive application. In the southern portion of the state, where groundwater in the alluvial basins is a major resource, nuclear craters could significantly enhance the recharge capability of the fan material.

For any concept of nuclear explosive use in the modification of the hydrogeologic system it is apparent that considerably more data, for both nuclear explosive effects and the particular hydrogeologic environment, must be obtained before realistic in-depth economic and prediction analyses can be performed.

REFERENCES

1. Piper, A. M., and Stead, F. W., 1965, Potential Applications of Nuclear Explosives in Development and Management of Water Resources--Principles, U.S. Department of Interior, Geological Survey, Report TEI-857.
2. Harshbarger, J. W., Supkow, D. J., and Johnson, R. B., 1967, Potential Site Investigation for Nuclear Energy Crater Experiment and Water Management in Arizona: Hydrology and Water Resources Office and Engineering Experiment Station, The University of Arizona.
3. U. S. Bureau of Reclamation, 1967, Preliminary Wilkins Damsite Investigation.
4. White, N. D., 1963, Analysis and Evaluation of Available Hydrologic Data for San Simon Basin, Cochise and Graham Counties, Arizona: U. S. Geological Survey Water Supply Paper, 1619-DD.
5. White, N. D., and Smith, D. R., 1965, Basic Hydrologic Data for San Simon Basin, Cochise and Graham Counties, Arizona, and Hidalgo County, New Mexico: Arizona State Land Department Water-Resources Report. Number Twenty-one.

AQUARIUS STUDY - ENGINEERING AND ECONOMIC CONSIDERATIONS

Roger F. Griffin
Bechtel Corporation

The two previous papers described the scope of the Aquarius Study and the various applications considered in evaluating the use of nuclear explosives for the development of water resources in Arizona. Surface storage behind a dam created with the use of nuclear explosives was selected for the major effort, primarily because it could afford the most valid direct comparison between nuclear and conventional methods. In this paper I will focus on the engineering and economic considerations involved in developing and evaluating three concepts for constructing a rockfill dam using nuclear explosives. Engineering development and economic evaluation of the concepts was the principal responsibility of Bechtel Corporation as a consultant in the study to the Arizona Atomic Energy Commission. We depended heavily on information supplied by the Federal participants, notably the U.S. Bureau of Reclamation for site data and the U.S. AEC's Lawrence Radiation Laboratory for information on nuclear explosives effects. Since the study report has not yet been published and additional material is still forthcoming, some of the information I will present, such as the cost estimates, may be subject to change and should be considered preliminary.

Clear Creek Site

The site selected for the study of dam construction techniques is on Clear Creek in northern Arizona. One reason for selecting this site was the availability of site data previously obtained by the U.S. Bureau of Reclamation for the preliminary design and cost estimate of a conventional dam in the same area. This site also is relatively remote and has a number of favorable physical features which make it suitable for a nuclear dam. The main drawback with this site, or any other available site in Arizona, from a nuclear explosives standpoint, is the relatively small dam and reservoir which can be constructed.

The first slide (Figure 1) is a simplified topographic map of the site and immediate vicinity. Clear Creek flows in a northerly direction. The site for the conventional dam is just

downstream from the confluence of Willow Creek and Clear Creek. Further downstream the creek makes a right angle bend to the left followed by a hairpin turn to the right. The canyon is relatively steep-walled and averages about 500 feet in depth from the stream bed to the flat plateau above the canyon rim. The height of the dam would be about 220 feet above the canyon floor, providing a reservoir capacity of 45,000 acre feet. Dam height and reservoir volume are limited by the fractured nature of the limestone formation (Kaibab) extending from about the middle of the canyon to the plateau surface. Beneath this is a sandstone formation (Coconino) which is quite impermeable. Mean annual flow at the site is about 55,000 acre feet with a design flood of 57,500 cubic feet per second. The next slide (Figure 2) is a simplified perspective of the site.

Several techniques for constructing a dam at this site were considered initially. Of these, the nuclear quarrying, throwout dam, and retarc dam concepts appeared to be appropriate for the site and were investigated further. Nuclear quarrying was selected as the reference concept for the study for the following reasons: (1) it requires the lowest device yield (and thus has least severe yield-related problems such as ground shock and airborne radioactivity release); (2) it has minimum potential for surface water contamination; (3) it has fewest uncertainties affecting the design concept and cost estimate; and (4) technical feasibility and cost are least sensitive to the assumptions which must be made. On the other hand, this concept may be considered relatively unimaginative since it fails to take advantage of the material movement effect of the nuclear explosive. Therefore, I will also describe the other two concepts and the problems we had with them, some of which are site-related.

Nuclear Quarrying Concept

In the nuclear quarrying concept, the nuclear explosive is used only to produce fill material while hauling and placing are done in a conventional manner. The explosive is emplaced at a depth which will produce a retarc (or nuclear rubble mound) and thus provide a maximum of fill material above ground with minimum device yield. The retarc can be located at any convenient site in the vicinity of the dam in order to adapt to local conditions and safety considerations.

Approximately 725,000 cubic yards of rockfill would be required for the dam embankment. The next slide (Figure 3) shows the assumed cross-section of the nuclear quarry retarc. To minimize loading and hauling costs, the retarc was sized to produce sufficient fill material above the original ground surface. Based on size distribution data from nuclear shots in other media, it was assumed that 75 per cent of the broken material would be less than the three-foot size considered maximum for this application. Assuming that another 25 per cent of the above-ground material is inaccessible or otherwise unusable, about 1.4 million cubic yards of material as bulked would be required above the original ground surface. Extrapolating the rather limited data on retarcs and assuming the data are applicable to the sandstone medium at the site, a device yield of 15 kt at a depth of 500 feet would be required.

CLEAR CREEK SITE

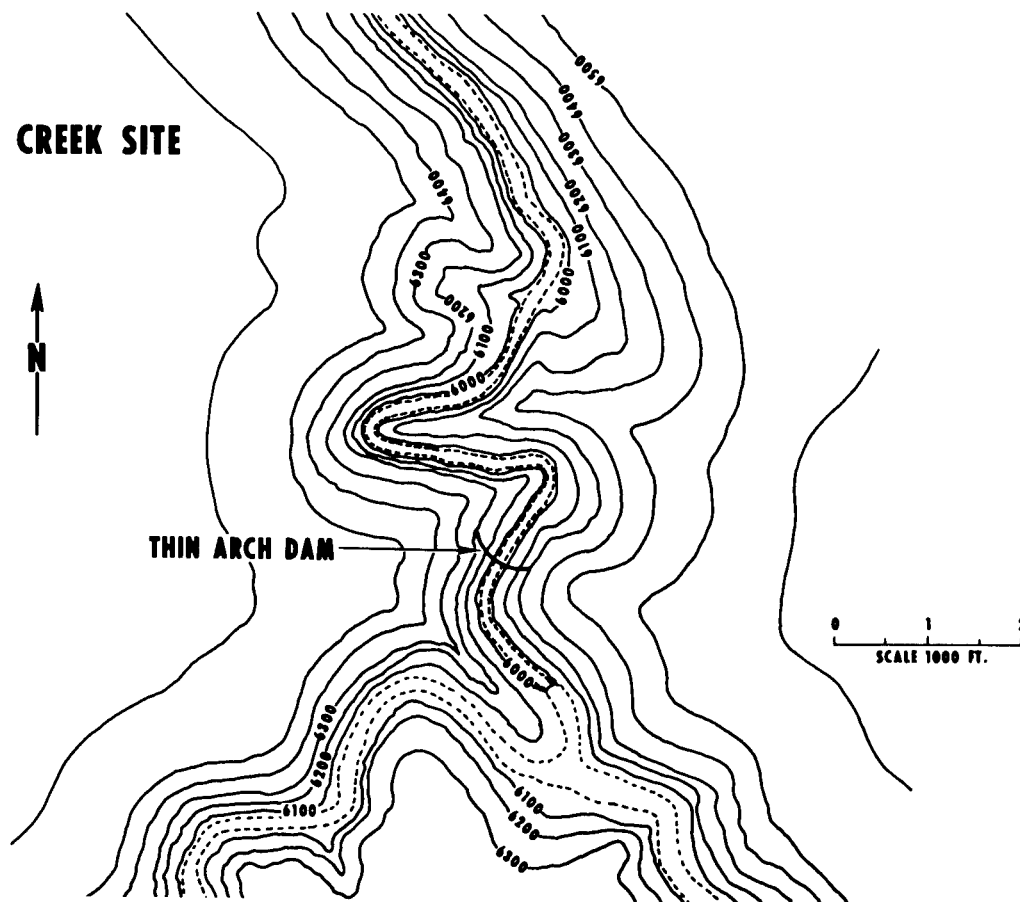
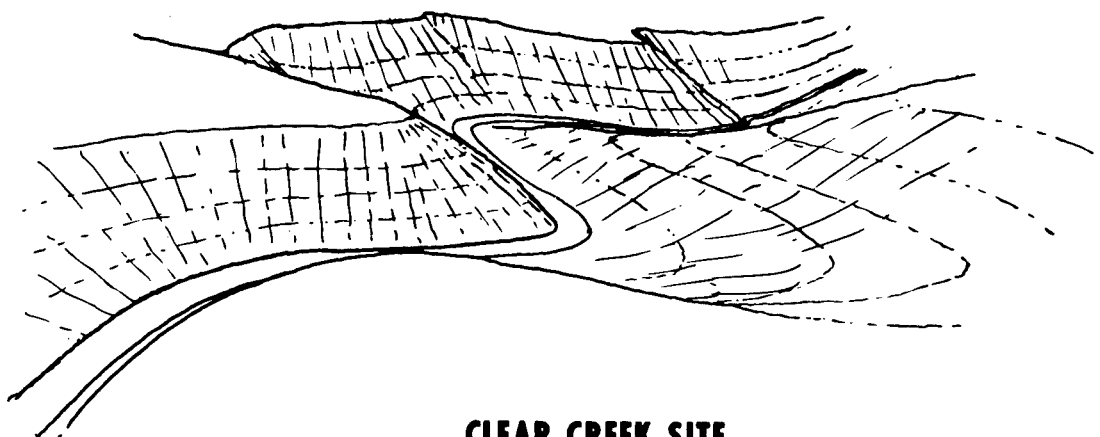


Figure 1



CLEAR CREEK SITE

Figure 2

The next slide (Figure 4) shows the location of various features associated with this concept. A point about 4,000 feet east of the damsite and on the plateau well back from the canyon rim was selected for the site of the nuclear quarry. This location results in a maximum haul distance of about two miles, all downhill, and also permits gravity drainage of contaminated wash water to the evaporation pond to the north. The quarry location was selected away from the canyon to avoid the possibility of base surge fallout on the canyon walls or stream bed and to assure that no contaminated water could flow from the retarder to the stream, either on the surface or through subsurface fractures. The east bank location was selected to be downwind from the stream and work site with the prevailing wind direction assumed to be from the west or southwest.

Immediately following detonation, upstream and downstream rockfill coffer dams and a diversion tunnel would be constructed. These provisions would be the same as for a conventional rockfill dam. The tunnel would provide a diversion capacity of about 10,000 cfs which is adequate to pass the maximum flood normally expected during the construction period. There is some probability that a flood would exceed this diversion capacity and flood the construction area, but this calculated risk is normal for conventional construction.

After initial preparations (such as building a haul road and clearing and excavating to provide a competent foundation), hauling and placement of the fill would be carried out in a conventional manner except for washing of the fill material to remove radioactive contamination as discussed in subsequent paragraphs.

Grouting of the canyon floor and walls up to the elevation of the reservoir surface would be required at this site for any type of dam to seal cracks and fissures and minimize leakage around the dam. The upstream face of the embankment would be covered with a waterproof barrier, assumed in this study to be reinforced concrete, which would be tied to the grout curtain at the canyon floor and walls. A 400-foot long spillway crest would be provided along the ridge at the north abutment of the dam. This spillway, together with the diversion tunnel modified to provide normal reservoir regulation, would have sufficient capacity to pass the design flood of 57,500 cfs.

The possibility of contaminating surface water with radioactive debris probably is the main concern associated with using nuclear explosives for dam construction. Suitable provisions must be made to ensure that complete control would be maintained over all potentially contaminated water and that downstream contamination levels would be kept well within allowable limits. Three potential sources of water contamination must be considered: (1) base surge fallout in the immediate vicinity of the nuclear explosion, particularly that falling on the stream bed or canyon walls where it could be washed into the stream; (2) contamination on the rubble within the true crater which could be leached off and washed into the groundwater; and (3) contamination, primarily tritium, deposited on the surface of the rubble which is used for the fill material.

CROSS SECTION-NUCLEAR QUARRY 15 KT DEVICE

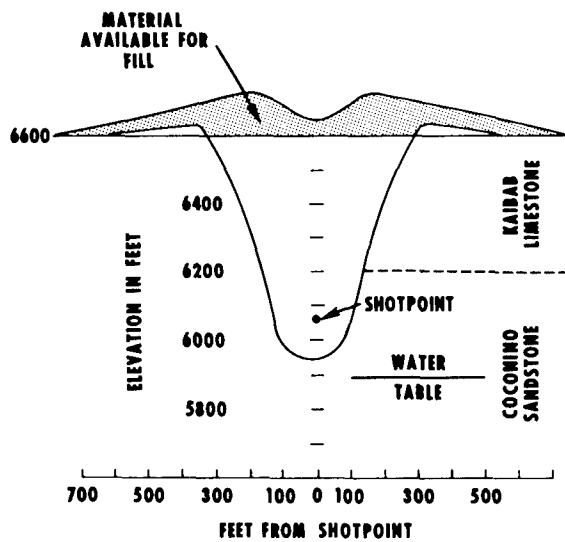


Figure 3

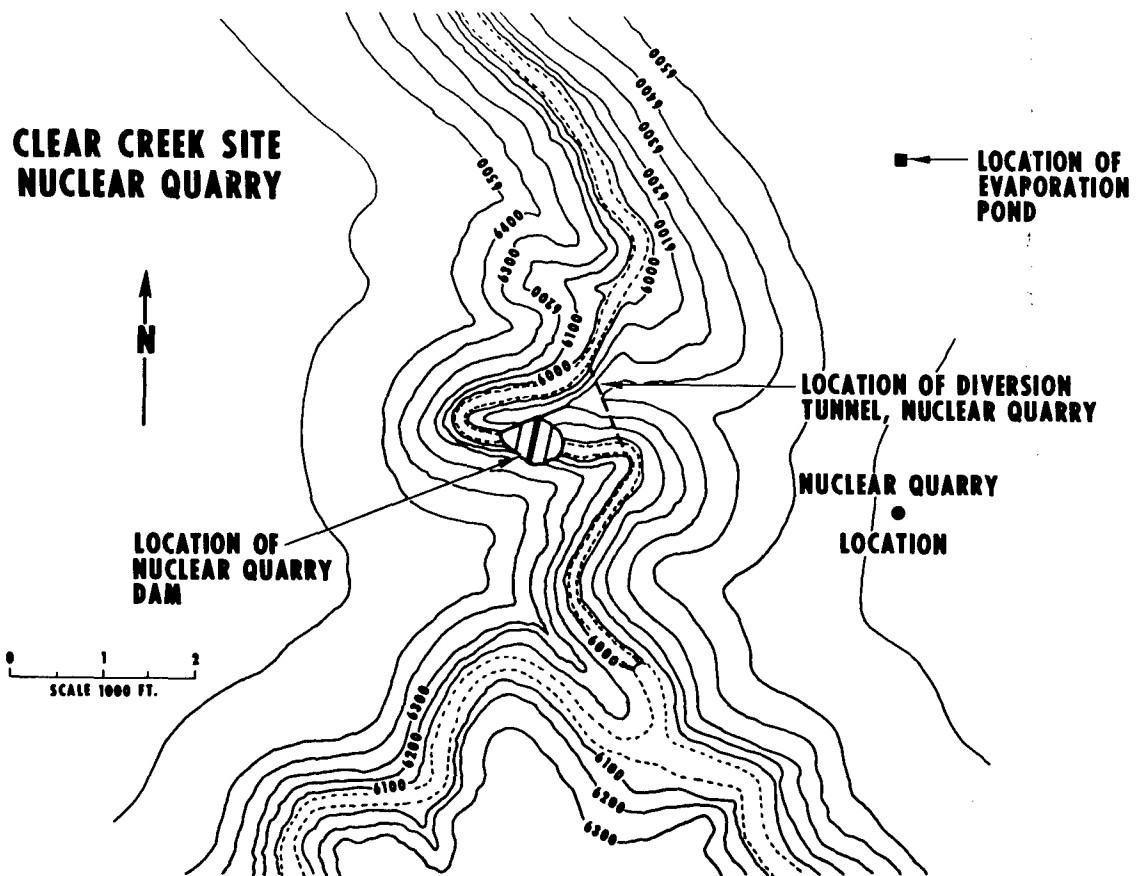


Figure 4

Base surge fallout is considered minimal for a retarc but, in any case, should not present a serious problem for this concept since the quarry can be located so that there will be no fallout within the canyon. Contamination of groundwater does not appear to be a major concern at this site because of the very low groundwater flow rate. Nevertheless, it is assumed that special wells for monitoring groundwater flow in the vicinity of the shotpoint would be provided and that production wells in the general area would be monitored periodically.

The contamination deposited on the surface of the retarc rubble to be used for fill material would be washed off before the fill is put in place. This would control the contamination close to its source and eliminate the possibility of contaminating the stream in the event of a flood during construction which exceeds diversion tunnel capacity. The contaminated wash water would be collected and disposed of by controlled evaporation to the atmosphere and by controlled release to the stream. To minimize the possibility that evaporation of this water would result in excessive airborne tritium concentrations in work areas, the evaporation pond was located to provide an exclusion distance of one kilometer and to be downwind from the quarry and dam sites. Evaporation pond area would be limited in order to limit airborne tritium concentration under conditions of high evaporation rate or unfavorable atmospheric diffusion. Additional evaporation when conditions permit could be provided by a system of sprinklers.

Throwout Dam Concept

In the throwout dam concept, shown in the next slide (Figure 5), the nuclear device is emplaced in the canyon wall downstream from the desired dam location and the rockfill material is ejected upstream to form the embankment. The steep canyon wall overlooking the horseshoe bend in the creek downstream from the rockfill dam site is a favorable location for using this technique.

Since directed blasting of earth and rock has not been demonstrated on a large scale, a simplified conservative approximation was used to estimate the deposition of the ejecta as a function of device yield and location. Assuming a 100 kt device as a practical upper limit, the post-shot configuration was determined to be as shown. As can be seen, the ejecta pattern falls far short of producing an embankment of sufficient height for the dam. The embankment would be completed by mechanically placing the additional material required - - about half of the total embankment volume. The effective downstream toe of the dam was located at the lip of the true crater and relatively flat slopes were assumed for both the upstream and downstream faces of the dam because of the uncertainty concerning the degree of compaction and resulting embankment stability which could be achieved.

The next slide (Figure 6) shows the location of the throwout dam and associated features.

Since all of the rubble would be contaminated by radionuclides (notably tritium) which presumably could be readily

CLEAR CREEK SITE CROSS SECTION-THROWOUT DAM 100 KT DEVICE

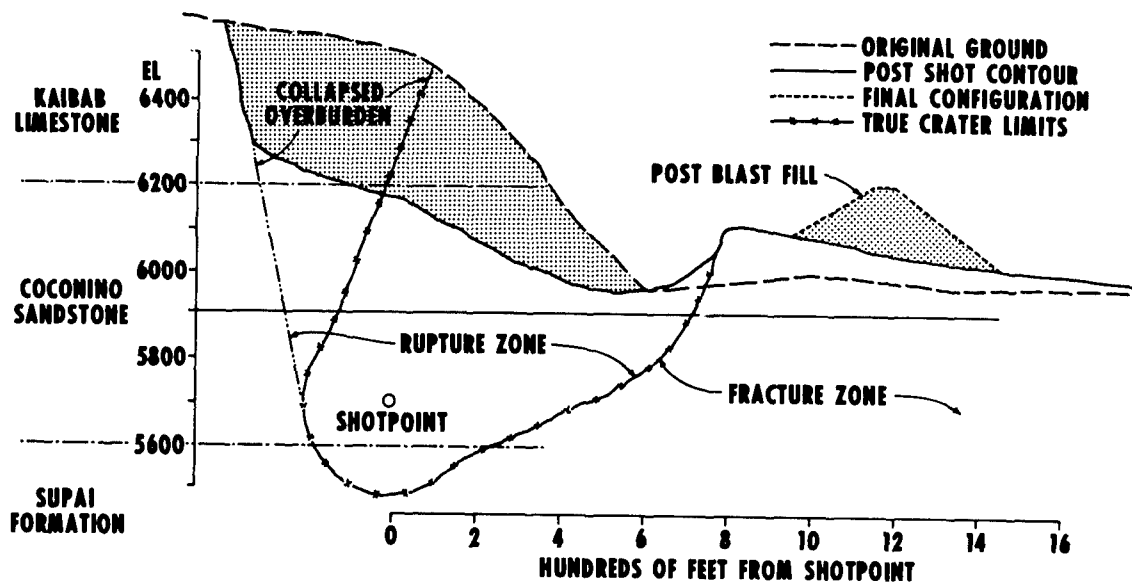


Figure 5

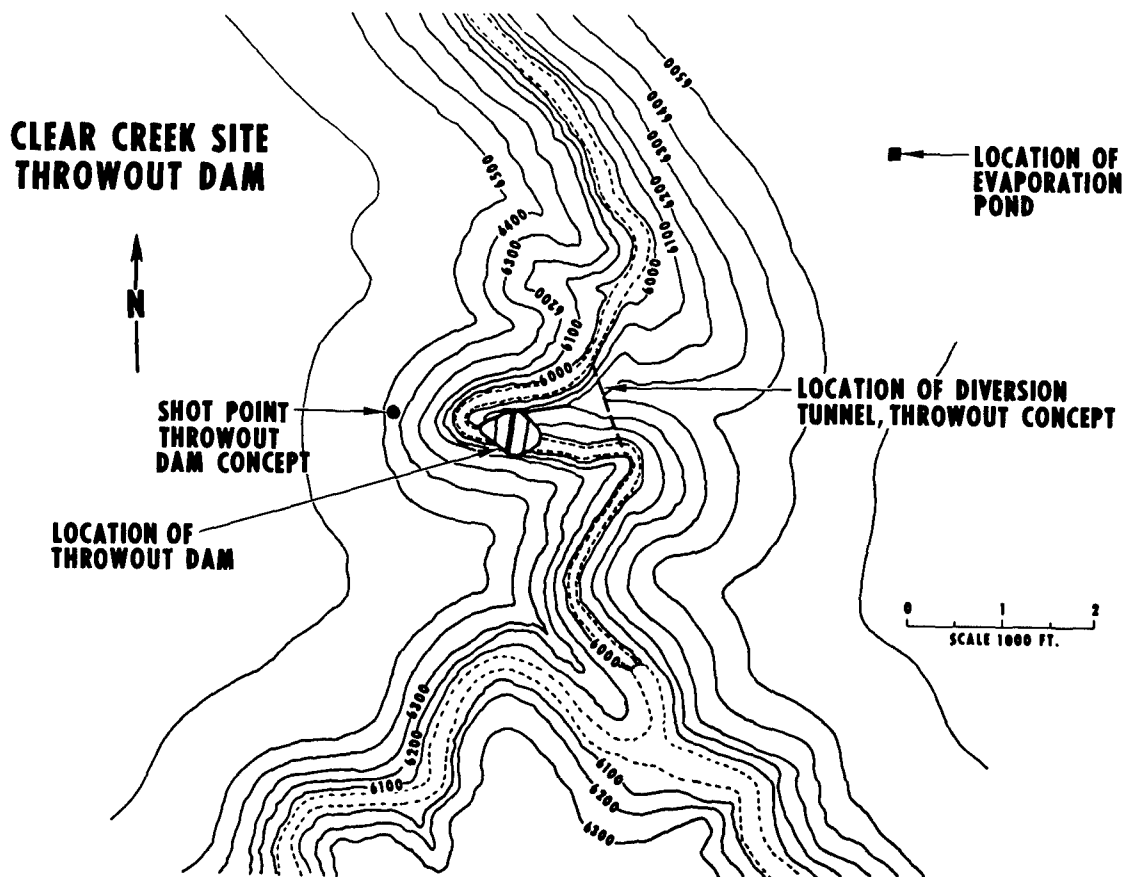


Figure 6

washed off and contaminate any water flowing through it, all stream flow would have to be diverted around the rubble even under the most adverse conditions. This requires that the diversion tunnel capacity be adequate for the maximum flood which could occur during the construction period. At this site, six 20-foot diameter diversion tunnels would be required, representing a significant penalty for this concept. Furthermore, upstream and downstream coffer dams and at least one of the diversion tunnels would have to be in place before the detonation and possible damage to these structures from ground shock would have to be considered.

The fracture zone might extend as much as 2,000 feet outward from the shotpoint, thus increasing the potential for leakage around the dam and increasing grouting requirements. Perhaps as much as ten to twenty times as much grouting would be required for this concept as for a conventional rockfill dam or for the nuclear quarry dam. This requirement is another major penalty associated with this concept.

A concrete dam facing and a spillway would be required much as for the nuclear quarry case. However, since the diversion tunnels must provide capacity for the design flood, it is possible that they could be modified to serve as a permanent spillway and that no additional spillway would be required.

Minimizing the amount of water which could become contaminated and providing positive means of assuring that contaminated water would not flow downstream uncontrolled present particularly difficult problems for this concept. Base surge fallout on the stream bed and canyon walls may be a severe limitation. Since this is a cratering shot, some fallout in the immediate vicinity is certain and there are no obvious remedial measures which can be taken easily and cheaply if such fallout could lead to unacceptably high levels of water contamination. As with the nuclear quarrying concept, contamination of groundwater is not considered a particular problem at this site because of the low groundwater flow rate, even though this shot is considerably larger than the quarry shot and is below the water table.

Contamination of surface water by contact with the rubble is a particular concern with this concept since the detonation point and most of the resulting rubble would be located within the confines of the canyon. This requires that extensive precautions be taken to prevent the stream from flowing into the rubble and to collect and dispose of any water which does contact the rubble. As described above, diversion capacity is required for the entire design flood during the construction period. In addition, rain water flowing through the rubble pile and any leakage through the dam after it is completed would have to be collected and pumped to an evaporation pond. A much greater quantity of contamination would have to be disposed of than in the nuclear quarrying case (about 2,000 vs. about 50 kilocuries of tritium) and the pumping and evaporation would have to continue for several years.

Retarc Dam Concept

In the retarc dam concept the dam embankment is formed from the upstream lip of a retarc produced in the floor of the canyon. The desired embankment height is achieved by bulking of the fractured material above the initial ground surface. In order to provide sufficient material in the immediate vicinity of the desired dam axis, a 75 kt device was selected for the evaluation. The next slide (Figure 7) shows the assumed cross-section through the retarc. The device would be emplaced approximately 1,000 feet downstream from the dam axis and at a depth of 1,350 feet below the canyon floor. As with the throwout concept, only a small fraction of the total broken material produced is used for the dam embankment. Because of the likelihood of settlement of the rubble within the retarc itself, the embankment would be designed so that the effective downstream slope would intercept the point of maximum uplift at the rim of the true crater. To produce the desired embankment would then require that about 100,000 cubic yards of fill material be moved conventionally after the shot. This amount of material is readily available in the immediate vicinity of the embankment.

The next slide (Figure 8) indicates the assumed location of the retarc dam shotpoint and embankment. The dam location was moved upstream close to the site of the conventional dam because of the likelihood that the ridge within the hairpin curve would be highly fractured in this concept. This imposes a considerable additional penalty because it requires that the diversion tunnels be about three times as long as for the other two concepts. As with the throwout dam concept, six 20-foot diameter diversion tunnels would be required to pass the entire design flood to preclude any possibility of flood waters passing through the retarc area. Upstream and downstream coffer dams and at least one of the tunnels would be required before the shot and possible damage from ground shock would have to be considered.

Somewhat more grouting would be required for this concept than for the throwout dam concept, or perhaps ten to twenty times that required for a conventional dam, since the dam axis is located closer to the shotpoint and fracturing of the dam foundation would be expected to be greater. A concrete facing such as that provided for the other concepts also would be required. Since there is no convenient location for a conventional overflow spillway at this site as at the downstream site used for the other concepts, it is assumed that the diversion tunnels would be adapted to provide the entire spillway capacity.

Water contamination control problems are essentially the same for this concept as for the throwout dam concept. Base surge fallout should be significantly less, however, and the concentration of tritium on the rubble and in the wash water should be about half of that for the throwout concept. Furthermore, it is likely that much of the total contamination would remain in the retarc well below the canyon floor and not have to be removed and evaporated.

Comparative Costs of Nuclear and Conventional Dams

The principal cost comparison made in the study is between the cost of nuclear quarrying and conventional methods of

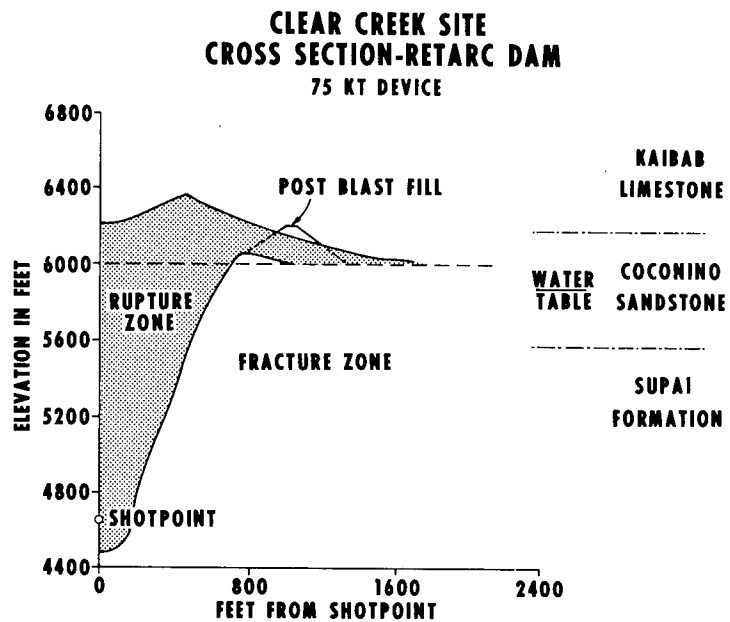


Figure 7

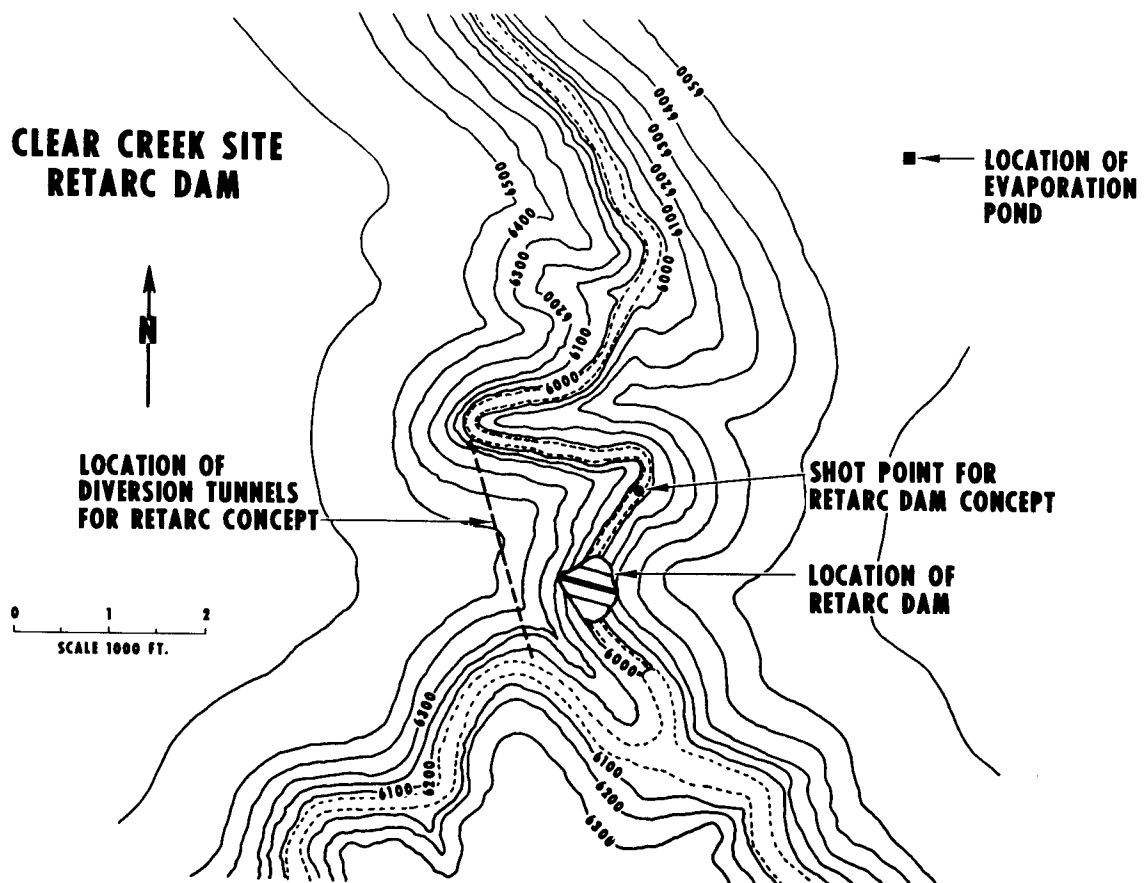


Figure 8

constructing a rockfill dam at the Clear Creek site. Since these two dams are essentially identical, the only difference in cost would be in producing the rockfill material. The cost of a comparable thin-arch concrete dam, previously estimated for this site by the U.S. Bureau of Reclamation, is also included for general comparison. Cost comparisons for the throwout and retarc dam concepts were not made because of the large uncertainties in certain aspects of these concepts.

The cost estimates are based on the following conditions:

1. No development costs are included. It is assumed that the nuclear explosives technology required for the nuclear quarrying concept will have been demonstrated beforehand.
2. Construction wage rates for the Flagstaff, Arizona area are used.
3. No premium or hazard pay is included for possible exposure to radiation or handling of radioactive materials.
4. It is assumed that construction bids would be taken only after the prospective contractors have had the opportunity to inspect the rock produced at the nuclear quarry. A contingency is included to cover the possible need for secondary blasting to produce rock of suitable size.
5. Current (1969) unit prices are used with no escalation.
6. No land costs are included.
7. Adequate commercial power is assumed to be available within one mile of the site.
8. Access roads are assumed to be available with no more than a minimum of improvement required to permit them to handle heavy equipment.

The next slide (Figure 9) gives cost breakdowns for the nuclear quarry and conventional rockfill dams and for the concrete thin-arch dam. The first item, "Preparation", includes diversion tunnels and coffer dams, haul road for the two rockfill dams, and excavation for the dam and spillway. "Embankment" for the nuclear quarry concept covers the cost of washing, loading, hauling, placing and compacting the rock produced by the nuclear detonation. Also included are the costs of delivering wash water and controlling and disposing of contaminated wash water. For the conventional rockfill dam this item includes not only the cleaning, hauling, placing and compaction of the rock but also the production of the fill material by conventional explosives.

"Concrete" includes the cost of the concrete for the thin-arch dam structure and for the facing and spillways of the rockfill dams. It also includes the cooling system required to control the temperature rise of the concrete in the thin-arch dam during curing and the reinforcing for the facing and spillways of the rockfill dams. "Grouting" includes all costs associated with the sealing of the cracks and fissures in the canyon floor and

CLEAR CREEK SITE DAM COSTS
(THOUSANDS OF DOLLARS)

<u>ITEM</u>	<u>THIN ARCH</u>	<u>NUCLEAR QUARRY</u>	<u>CONVENTIONAL ROCKFILL</u>
PREPARATION	\$ 1,134	\$ 1,062	\$ 1,062
EMBANKMENT	—	2,351	2,682
CONCRETE	5,022	985	985
GROUTING	215	640	640
OTHER	201	260	260
	<hr/>	<hr/>	<hr/>
SUBTOTAL	6,572	5,298	5,629
ALLOWANCE AND CONTINGENCIES	2,468	2,502	2,114
NUCLEAR COSTS	—	1,600	—
	<hr/>	<hr/>	<hr/>
DIRECT FIELD COST	\$ 9,040	\$ 9,400	\$ 7,743

Figure 9

walls and tying in with the dam structure or facing.

"Other" costs include the outlet structure, the electrical system, and the mechanical system to control routine releases of water from the reservoir.

An allowance of ten per cent was added to each estimate to cover unlisted items and an additional 25 per cent was included for contingencies. To this was added, for the nuclear quarry concept, \$1,600,000 for costs associated with the nuclear explosive and its effects. These "Nuclear Costs" include exploratory holes and the device emplacement hole, ground zero and control point facilities, support services and security, instrumentation, observation and communications systems, the nuclear device charge, the cost of the entire safety program, and an allowance for other charges. Due to the inability at the present time to accurately predict the size distribution of the rock in the aboveground portion of the retarc, an additional contingency of \$500,000 was included to cover the possibility of a substantial amount of secondary shooting. Experiments in production of rock by retarcs may make it possible to reduce or eliminate this item.

The total costs represent direct field costs or the expected bid prices, since each total contains reasonable overhead and markup. Additional costs for the total dam project would include engineering, procurement, supervision, administration, interest during construction, and land.

As shown in the table, the conventional rockfill dam would be the least expensive of the alternatives considered, based upon the assumptions previously discussed and upon the order of magnitude cost estimates prepared for this site at this time. It is not surprising that the nuclear quarry dam is somewhat more expensive, since nuclear costs are relatively insensitive to yield and the unit cost of rock produced by nuclear detonation would be relatively high for a small dam such as this.

Although the costs of the throwout and retarc dam concepts were not estimated, it is clear that they would be much more costly because of the measures which would have to be taken to minimize the problems associated with these concepts. However, future developments could make one or both competitive. For example, proof of the ability to efficiently place the ejecta from a throwout crater in a desired configuration might reduce the costs of shaping and grouting enough to offset the cost of the six diversion tunnels. Eliminating or substantially reducing the problem of radioactive contamination of the rubble might eliminate the need for five of the six diversion tunnels in both the retarc and throwout concepts. Diversion tunnel costs are roughly \$8 million and \$2 million for the retarc and throwout concepts respectively as developed in this study.

Conclusions

Because of the many participants and widely divided responsibilities in the Aquarius Study, I am not in a position to draw general conclusions reflecting the entire study. Moreover, the study was directed specifically toward applications in Arizona and the concepts developed are quite site-dependent. However, recognizing the more general applicability of much of

this work, it is possible to make the following observations based on our portion of the study:

1. Based on currently available data, it appears to be technically feasible to use nuclear explosives to produce material suitable for constructing a rockfill dam. This applies to a wide range of site conditions, provided safety criteria can be satisfied.
2. Economic feasibility of the nuclear quarry technique of dam construction is highly site-dependent. As with most applications, the larger the volume of rock to be broken or moved, the greater the advantage of the nuclear method. Extrapolation of the results of this study would indicate that for a dam embankment volume greater than about 2 1/2 million cubic yards, the cost of the nuclear quarry dam would be less than that of a conventional rockfill dam, all other conditions being equal.
3. Significant improvements in the economies of nuclear techniques of dam construction should be possible if future developments reduce the uncertainties and solve some of the problems associated with the throwout and retard dam techniques. For example, in the throwout technique, efficient placement of the ejecta into the desired configuration would reduce the device yield required and the need for grouting and shaping. Eliminating or greatly reducing radioactive contamination on the rubble would remove the need for elaborate precautions to prevent contamination of the stream. Even with the nuclear quarry technique, costs below those estimated in this study may be possible if the uncertainties are reduced and less conservative assumptions and allowances can be used.
4. The potential for the use of nuclear explosives in dam construction is sufficiently attractive to warrant further development, including experiments aimed specifically at some of the questions identified in this study. With relatively little additional knowledge, nuclear quarrying should be considered along with conventional techniques in selecting a method of constructing any moderate to large rockfill dam (or other structure requiring a comparable amount of rockfill) at a fairly remote site.

MECHANICS OF SLIDE DAMS

by G. A. Young*

INTRODUCTION

Studies which promote the use of nuclear energy for peaceful projects in engineering are sponsored by the Atomic Energy Commission under the Plowshare program. Specific projects being considered include the construction of harbors, canals, and dams. Of these projects, perhaps the most difficult to accomplish will be the latter.

This paper which is in two parts considers the problems which are associated with the construction of slide dams with nuclear explosives. It examines first the characteristics of conventional earth and rock-fill dams which are based upon proven techniques developed after many years of experience. The characteristics of natural landslide dams are also briefly considered to identify potential problems that must be overcome by slide dam construction techniques. Second, the mechanics of slide dams as determined from small-scale laboratory studies are presented. It is concluded that slide dams can be constructed and that small-scale field tests and additional laboratory studies are justified.

CHARACTERISTICS OF CONVENTIONAL EARTH- AND ROCK-FILL DAMS

Earth-Fill Dams

Today most earth-fill dams are constructed by rolled-fill methods. Modern practice¹ requires that fill material of carefully controlled moisture content be placed in layers, usually less than 1 foot thick. After being placed, each layer is thoroughly compacted by an appropriate roller to provide the maximum relative density. A nearly uniform gradation of material may be used throughout the dam or, when materials permit, zones with different gradations of material and different permeabilities may be created (Figures 1 and 2). An arrangement in which the less permeable zone is placed near the upstream face provides good drainage and prevents a build up of seepage pressure near the downstream toe of the embankment. However, the upstream face is susceptible to failure during reservoir drawdown conditions.

An important element in all earth-fill dams is the graded filter drain shown at the downstream toe in Figures 1 and 2. The filter drain improves the stability of the downstream face. Without a filter,² fills of nearly uniform permeability become almost entirely saturated, and the seepage line intersects the downstream slope, as illustrated by the broken line in Figure 1. This condition develops regardless of the base width. A properly designed filter drain, however, draws the seepage line well down into the fill and greatly increases stability (see Figure 1). The filter is constructed of layers of pervious material, each layer having a different range of particle sizes,

*Director of Engineering, Agbabian-Jacobsen Associates, Los Angeles

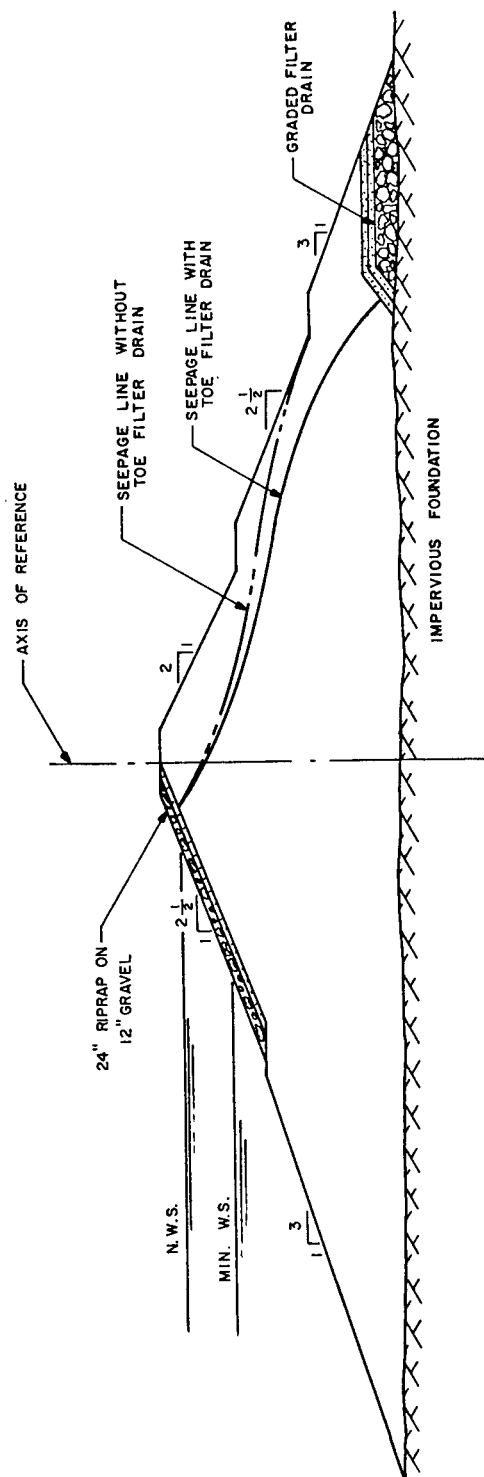


Figure 1. Typical Section of a Rolled Earth-fill Dam Built with Uniform Materials

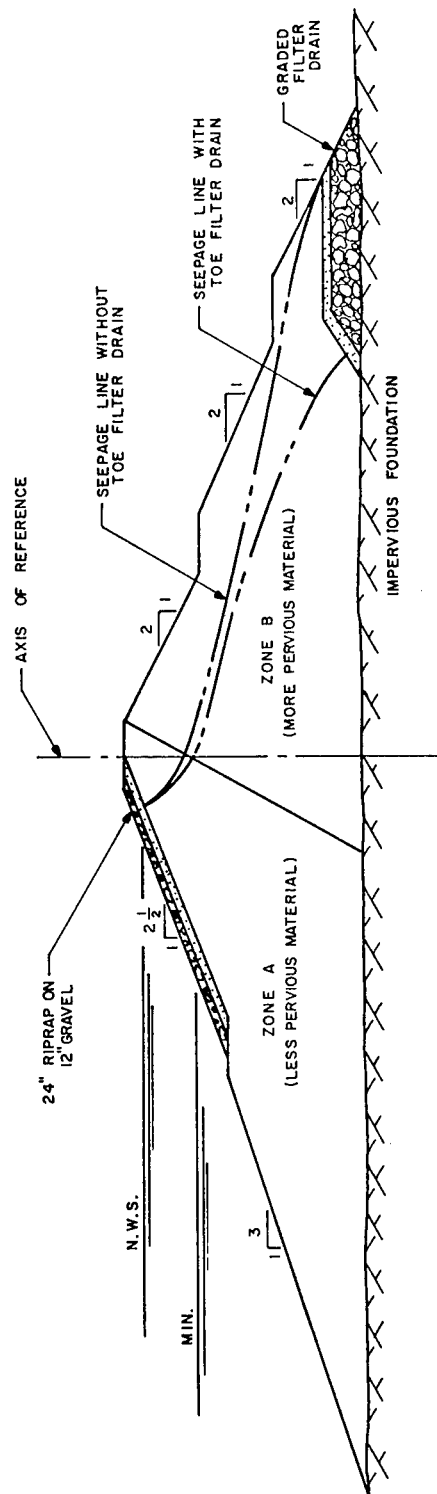


Figure 2. Typical Section of a Rolled Earth-fill Dam Built with Zoned Materials

selected such that the void diameter of each layer is smaller than the diameter of the finer particles of the preceding layer. The layer immediately adjacent to the fill has the smallest particle and void diameters and retains the fine particles in the fill. Without a filter, fine particles are washed out of the fill, thereby increasing the velocity of the seepage flow. Still larger particles are then eroded, until eventually a free-flowing passageway or "pipe" develops through the dam and causes failure. This phenomenon is called "piping." The exact filter drain arrangement required depends greatly upon the relative permeabilities of the fill and the foundation. The arrangements shown in Figures 1 and 2 assume a relatively impervious foundation.

Slopes of earth-fill dams are normally determined by the shearing strength of either the foundation or the fill material. As a result, earth dams usually have a downstream slope of about 2.5 to 1 and an upstream slope of about 2.5-3 to 1. However, if the foundation is poor, the slopes may be flatter. Provisions for slope protection are important for earth-fill dams. The upstream slope must be protected from wave action, (see Reference 3) and the downstream slope must include provisions for the drainage of surface storm water. The former normally requires slope paving of 2 to 3 feet of riprap. Even though riprap is provided, fluctuations of the reservoir water surface and wave action will gradually erode the fine particles from the fill, unless a graded filter is placed between the riprap and the fill. A normal arrangement is shown in Figures 1 and 2.

Rock-Fill Dams

Rock-fill dams are classified according to the type of core or surface used to retain the reservoir water. In general, modern rock-fill dams fall into one of three classes: those with a concrete upstream face, those with a central vertical earth core, and those with an internal earth core which slopes upstream.

Examples of rock-fill dams utilizing a reinforced-concrete upstream face are the Salt Springs Dam⁴ (328 feet high) and the Bear River Dam⁵ (233 feet high). A section of the latter, completed in 1952, is shown in Figure 3. This type of rock-fill dam is characterized by relatively steep slopes both upstream and downstream and by a thin, reinforced-concrete upstream-face slab supported by a 10- to 20-foot-thick layer of rubble (mortarless) masonry. The remainder of the rock fill is dumped in place from high lifts and sluiced with high-velocity water jets³. Because of the upstream location of the water barrier, the entire fill remains unsaturated. As a result, stable slopes as steep as 1.3-1.4 to 1 can be attained and a big saving in material realized over other types of rock-fill dams. Objections sometimes made to this arrangement are that the concrete slab is susceptible to damage during settlement of the fill and that too much labor is required to place the rubble masonry layer.

The central, vertical earth-core arrangements is perhaps the type most frequently used in recent years. The Ambuklao Dam⁶ (413 feet high) and the Derbendi-Khan Dam⁷ (440 feet high) are two examples. A section of the latter is shown in Figure 4. In this arrangement, the central earth core is placed by conventional rolled-fill procedures, while the rock-fill shell is placed by dumping in the manner described above. The earth core is protected by graded filter drains on both the upstream and downstream surfaces (see Figure 4). Because the shell is pervious, the upstream slope is quite stable, even though reservoir operation may permit a sudden drawdown. As a result of this stability, slopes on both the upstream and downstream surfaces can frequently be 1.75 to 1.

The sloping earth core is an arrangement intermediate between the two previously discussed. The Nantahala Dam³ (230 feet high) and the Brownlee Dam⁸ (407 feet high) are typical of this arrangement (see Figure 5). A comparison

of Figures 3 and 5 shows that the downstream slope of the Brownlee Dam is as steep as that of the Bear River Dam. Because the sloping upstream core is susceptible to sliding during sudden reservoir drawdown conditions, a flatter upstream slope was provided for the Brownlee Dam.

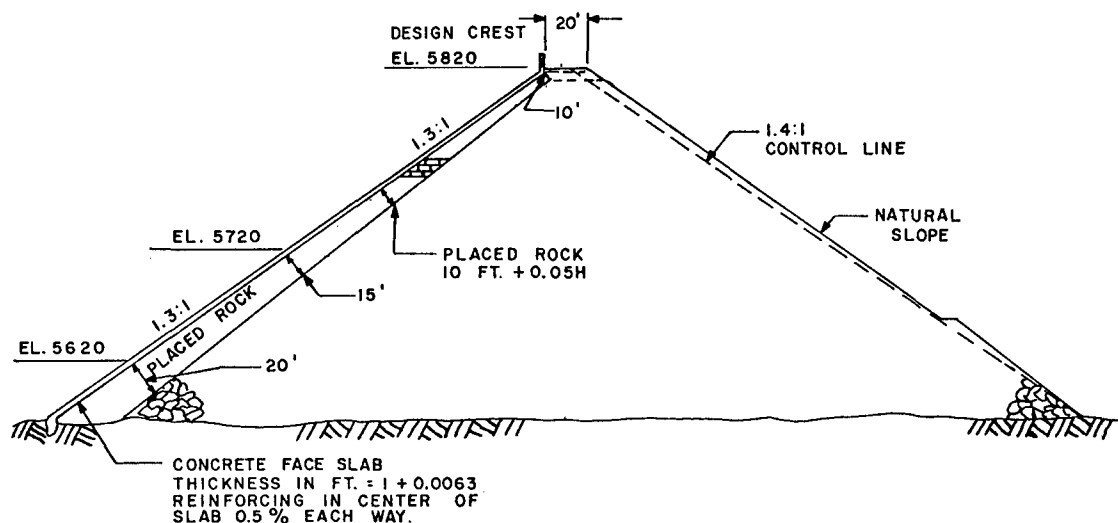


Figure 3. Section of the Bear River Rock-fill Dam

(After I. C. Steele and J. B. Cooke, "Rockfill Dams: Salt Spring and Lower Bear River Concrete Face Dams," *Journal of the Power Division of the ASCE*, August 1958, p. 1737-25.)

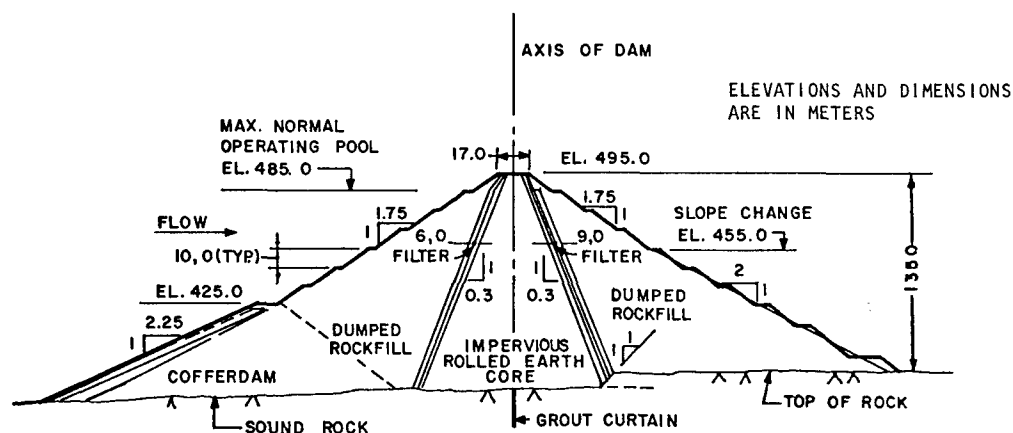


Figure 4. Section of the Derbendi-Kahn Dam

(From C. V. Davis, "Rockfill Dams: the Derbendi Khan Dam," *Journal of the Power Division of the ASCE*, August 1958, p. 1741-16.)

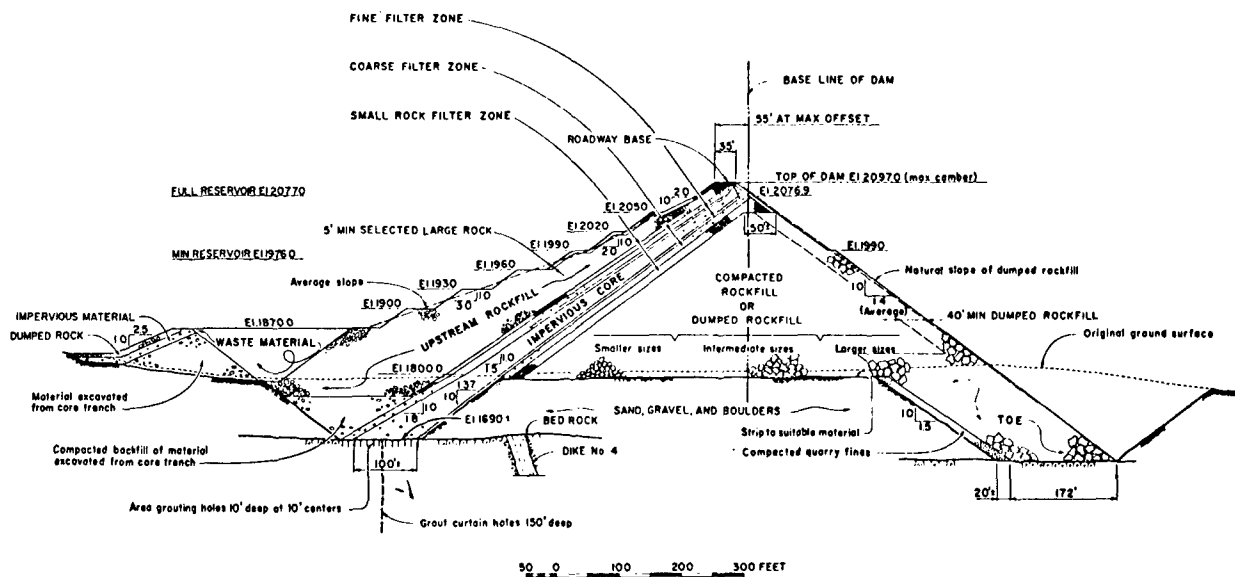


Figure 5. Maximum Section of the Brownlee Project Rock-fill Dam
 (From T. Murdal, "Rock-fill Dams: Brownlee Sloping Core Dam,"
Journal of the Power Division of the ASCE, August 1958, p. 1734-7.)

To control seepage, a cutoff which makes a junction with the core in the dam is usually grouted in the rock foundation. On high dams, the cutoff frequently extends more than 100 feet into the foundation. The object of grouting is to seal open joints, cracks, fissures, and seams in the foundation rock. Weathered zones and solution channels often have to be cleaned out and backfilled with concrete before being grouted. Both the importance and the cost of these operations are frequently underestimated. This type of cutoff is shown in Figure 5. When an earth core is placed on a rock foundation, there is always considerable danger that compaction will not be uniform at the rock-earth contact because of the uneven rock surface and that, as a consequence, piping may occur through a loosely compacted zone. Two procedures are followed to prevent this possibility. In the first, one or more shallow, reinforced-concrete cutoff walls are placed nearly parallel to the longitudinal axis of the dam; the walls project 5 to 10 feet up into the earth fill and down into the rock foundation. When a reinforced-concrete upstream face slab is used to retain the water, the slab ties into a shallow cutoff wall which extends 10 to 25 feet into the foundation (Figure 3). In the second approach to this problem, the rock surface is paved with concrete or gunite to provide a smooth surface upon which the earth fill can be uniformly compacted. The foundation is also grouted as noted above.

It will be pointed out in the next section that natural landslide dams have frequently failed because of piping or because of other phenomena resulting from a lack of drainage or a lack of other provisions typical of conventional fill dams. It is well, therefore, to recognize that provisions for settlement and for seepage, slope protection, and slope stability are as essential for slide dams as for conventional fill dams.

CHARACTERISTICS OF NATURAL LANDSLIDE DAMS

Technical and scientific journals record numerous natural landslides in the past few decades, of which some have created huge natural dams. The volumes of some slides have approached the volumes of the largest embankments constructed by man. Landslide events producing these huge embankments have normally been initiated and completed in a matter of minutes in contrast to the years of effort required for equivalent man-made embankments. Unfortunately, in many cases the natural embankments have later failed and released floods which have taken human lives and caused considerable property damage. Because of both the manner in which natural dams have been produced and the manner in which some have failed, a review of the characteristics of natural landslides is essential.

CAUSES OF LANDSLIDES

Terzaghi⁹ has indicated that natural landslides result from either internal or external causes. With the former, no change in shearing stress occurs along the plane of ultimate sliding; rather, sliding occurs because some internal action causes a reduction in the shearing resistance of the material. With the latter, some external action causes an increase in shearing stress, but the shearing resistance of the material along the surface of sliding remains unaltered. Terzaghi has further classified the processes which result in landslides as:

1. Construction operations or erosion
2. Tectonic movements
3. Earthquakes or blasting
4. Creep in a weak stratum below the slope
5. Rains or melting snow, causing
 - a. Increase in pore water pressure
 - b. Loss of apparent cohesion
 - c. Swelling
 - d. Chemical weathering
6. Frost action
7. Shrinkage in clays, causing cracks and loss of cohesion
8. Rapid changes of water level in lakes or of the water table in the ground
9. Slow rise of the water table or a slow increase in artesian pressure
10. Seepage from lakes, canals, etc.

It is significant that all but the first four processes listed involve the action of water in one manner or another. Also, while slides frequently take place in a very short period of time, most of the processes listed are of a continuing nature and are probably in action long before a slide occurs. Actually, none of these processes are typical of the action most likely to be utilized to initiate a slide or rock fall through the use of nuclear explosions. Indeed, some of the causes indicate conditions unfavorable to dam construction. A study of actual case histories of landslides makes this fact more evident.

CASE HISTORIES

Although several natural landslide events reported in the technical and scientific literature should prove of interest to most readers, not too much

of the information is directly transferable to the problem being considered. Consequently, only four representative examples will be presented.

Gohna Slide^{10,11}

This slide occurred in northern India in 1893 and is of significance because of its size and because of the manner in which the dam formed by the slide ultimately failed. The slide was initiated at an elevation of 4000 feet above the stream bed in a region where limestone beds dip toward the river at an angle of 45 to 50 degrees. Possible processes contributing to the slide were increased pore water pressure between rock layers, undercutting of the toe of the slope by the river, and a weakening of the limestone beds due to dolomitization. The slide created a dam 900 feet high with a crest length of 3000 feet and a base width of 11,000 feet (Figure 6). The initial slopes were relatively flat, on the average about 5 to 1. The volume of the slide exceeded 50 million cubic yards, and the volume of the lake ultimately impounded was slightly less than 400,000 acrefeet.

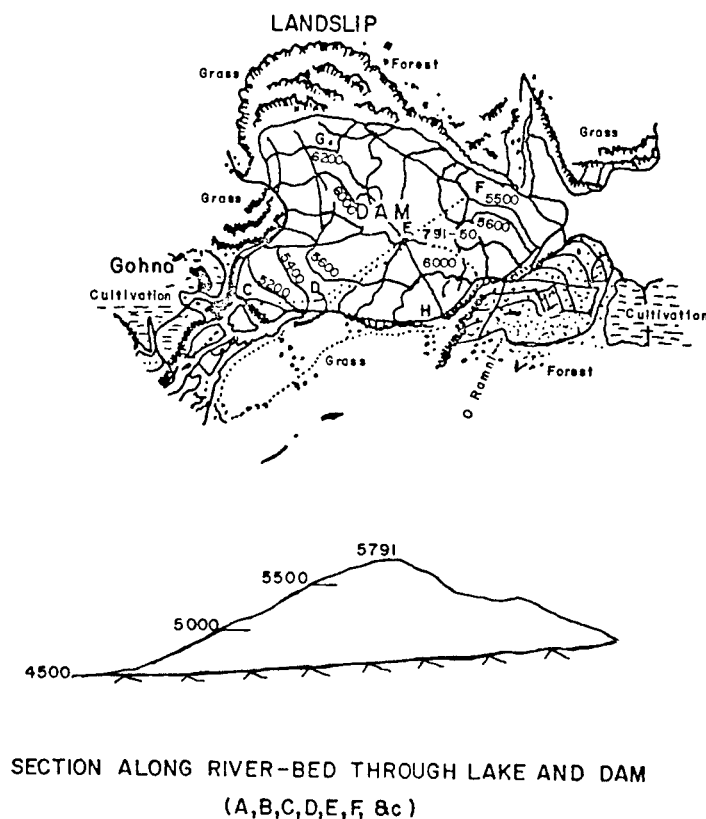


Figure 6. Plan and Profile of the Gohna Slide

(From J. H. Glass, "The Great Landslip of Gohna...", *Journal of the Society of Arts*, London, March 27, 1896, p. 432.)

The slide occurred in September, and the resulting dam was breached in August of the following year. The dam was rather closely observed, for it early was recognized that the dam would be overtopped and would probably fail. In early July, leakage from the dam was estimated as about 50 cubic feet per second. As the reservoir filled, the rate rapidly increased and was estimated by mid-August to be about 350 cubic feet per second. Following a heavy rain which occurred about this time at the dam site, a large portion of the dam slipped

downstream, leaving a nearly perpendicular wall about 400 feet high. Although huge stones were also present, the slide revealed very finely ground rock material, approaching rock flour. This slide occurred when the reservoir water surface was within 80 feet of the crest of the dam.

Prior to failure, the seepage rate increased still further, and only a few hours after the crest was lightly overtopped during another rain, approximately 400 feet of the top of the embankment swept away. Failure was apparently due to piping, although failure would no doubt also have resulted from overtopping.

Gros Ventre Dam^{12,13}

A slide occurred in Wyoming on the Gros Ventre River in 1925. The slide dam created is also of significance because of both its size and the manner in which it failed. In the region of the slide, beds of limestone, sandstone, and clay shales dip toward the river at an angle of about 20 degrees. The instability of the general region, particularly to the north, had been long recognized.¹⁴

On the day of the slide, a mass of 50 million cubic yards of material slid down a 2100-foot scarp and created a dam about 250 feet high. As shown in Figure 7, the slide was oriented upstream at an appreciable angle. Because of this orientation and also because of the low shear strength of the material, very flat slopes resulted; the base width of the dam approached 10,000 feet, and the average slopes were about 15 to 1.

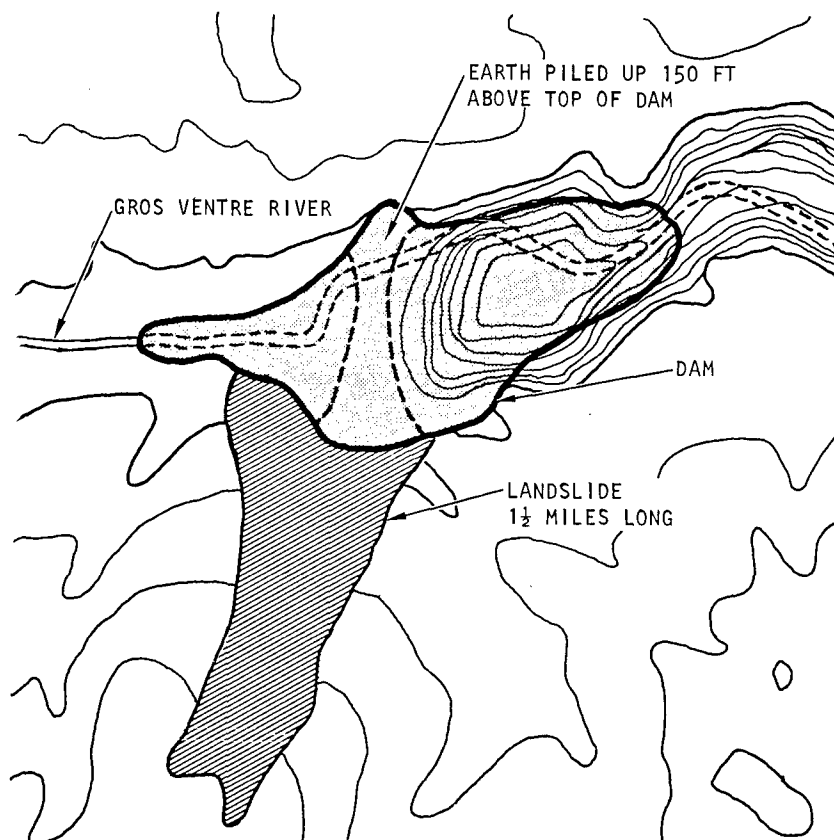


Figure 7. Gros Ventre Landslide Dam

(From R. H. Carlson, *Nuclear Explosives and Landslide Dams*, SC-4403(RR), Sandia Corporation, 1960, p. 58.)

Because the river was in flood at the time of the slide, the lake reached a depth of 200 feet within 3 weeks. No leakage appeared below the dam for about 12 days, but once seepage broke through the downstream face, its rate increased until it equaled the flow rate of the stream. At this point, the lake level stabilized at a depth of about 200 feet and later dropped. Seepage was estimated to have reached a rate of about 500 cubic feet per second.

Considerable confidence developed that the dam would not fail, but during the flood runoff 2 years later, it was overtopped, and a channel 100 feet deep and 300 feet wide was scoured across its crest. The lake had impounded about 165,000 acre-feet of water when the dam was overtopped, approximately half of which was released in only a few hours. The result was heavy damage and the loss of several lives downstream. The failure can be attributed to overtopping, but piping may also have been a factor, since the channel scoured down to the depth where the leakage was greatest.

Frank, Alberta, Slide¹⁵

This slide, which occurred in April 1903, destroyed a part of the town and killed about 70 people. The river valley in the region of the slide was more than 1/2 mile wide and was filled with boulder clay and gravel, above which projected several sandstone ridges and knolls. The valley was flanked on each side by low terraces, above which (on the side from which the slide was initiated) a talus slope extended at an angle of about 30 degrees. The cliff slope consisted of limestone beds which dipped into the hillside at an angle of 50 degrees. The limestone beds and the talus slope overlay shales and sandstones which also dipped into the hillside, but at a steeper angle of about 82 degrees.

Due to creep in the shale beds, which may have been aggravated by coal-mining operations at the foot of the slope, a huge mass 1/2 mile square and 400 to 500 feet thick sheared across the limestone beds (Figure 8), plowed through the boulder clays and gravel in the valley, and climbed the opposite slope to a height of 400 feet. In some places, sandstone ridges deflected the slide by as much as 90 degrees. In the valley, the slide spread over more than one square mile to a depth which varied from 3 to 150 feet, with an average of about 65 feet. Although small ponds were formed, no effective dam was created.

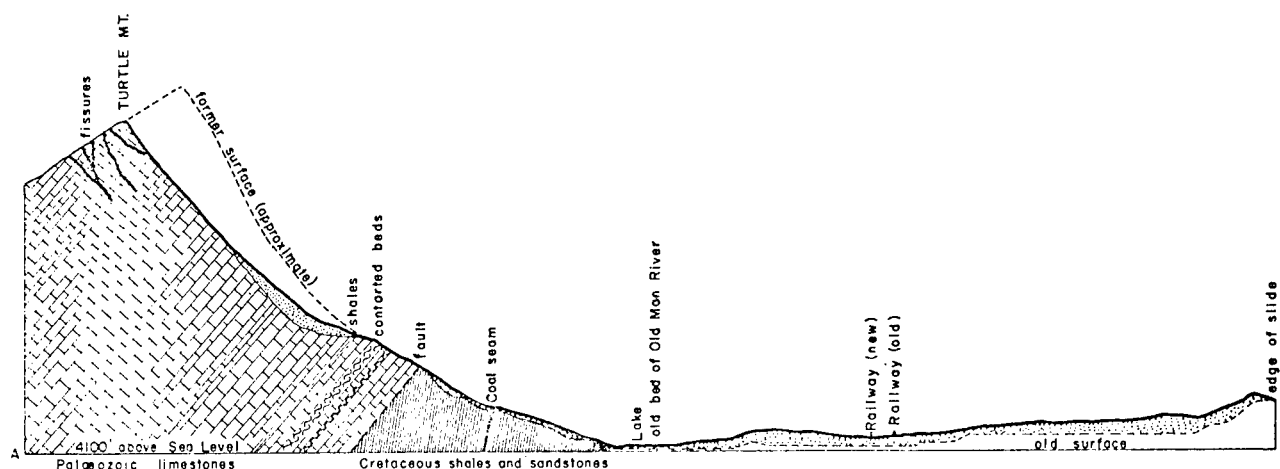


Figure 8. Section Along the Frank, Alberta, Slide

(From R. G. McConnel and R. W. Brock, *Report on the Great Landslide at Frank, Alberta*, Extract from Part VIII, Annual Report, 1903, Department of the Interior, Dominion of Canada)

Madison Canyon Slide^{16,17,18}

This slide, initiated by a severe earthquake near the Montana-Wyoming border in August 1959, occurred about 7 miles below Hebgen Dam and completely blocked the Madison valley. The main portion of the slide consisted of micaceous schist and gneiss which were weathered to a depth of about 100 feet. This material was held in place by a tapered buttress of dolomite at the base of the slope. The earthquake motion caused the dolomite buttress to shear, releasing the unstable mass of schist and gneiss. The volume of the slide was more than 30 million cubic yards.

The dam formed by the slide had a base width of about 4500 feet (measured along the valley) and a height of about 200 feet above the river bed. The average slopes exceeded 10 to 1 (Figure 9). The volume of the lake which would have formed was estimated at about 80,000 acre-feet. Because it was recognized that there was danger of a flood wave downstream if the dam should be overtopped in its natural condition, steps were taken to reduce the crest height by 50 feet by a process of hydraulic degradation controlled by excavating equipment. This action reduced the lake volume by more than one-half and provided a channel approximately 3500 feet long and with a controlled slope across the crest of the dam. The great length of the channel made a sudden failure no longer possible. Also, the smaller lake volume reduced the magnitude of any potential flood. In all probability, the channel across the dam will continue to degrade slowly until the channel is stabilized and a much smaller permanent lake is created.

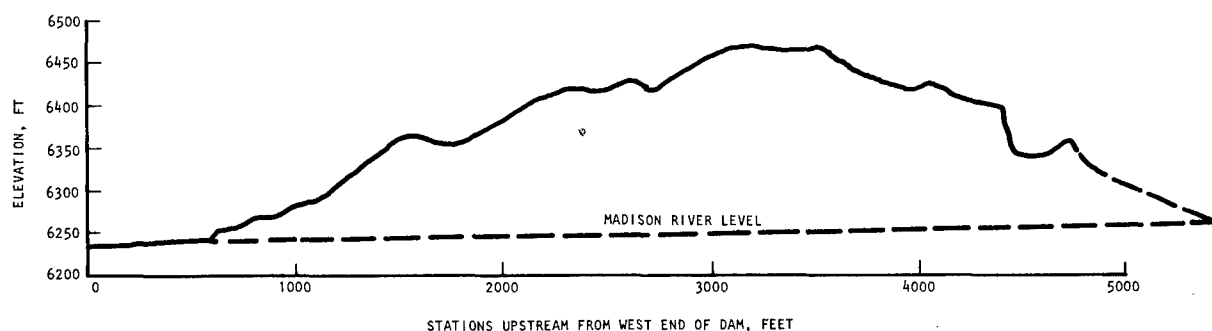


Figure 9. Profile of the Madison Canyon Slide

(From R. H. Carlson, *Nuclear Explosives and Landslide Dams*, SC-4403(RR), Sandia Corporation, 1960, p. 68.)

OBSERVATIONS FROM NATURAL LANDSLIDES

As mentioned previously, many natural landslides can be studied, but not too much can be learned which is directly applicable to the problem being considered. The following represent observations which appear pertinent.

Materials

A great variety of materials have produced notable slides, as indicated by Terzaghi⁹ and by the case histories presented. Also, the materials incorporated into the slide are usually not the types of materials which would be used for fill-dam construction. Weathered schist and gneiss (Madison Canyon), unstable clays and weathered shales (Gros Ventre) are examples of such unsuitable materials.

Even when competent materials have been incorporated, the height of fall has in some instances been more than optimum. As a result, the kinetic energy imparted to the slide has caused materials as hard as limestone to be ground into fine powder (Gohna and Frank, Alberta, slides). In conventional rock-fill dam construction, it has been found that less settlement occurs when the rock is dropped from high lifts. Lifts as high as 100 to 200 feet have given good results. The reason is that settlement largely occurs in rock-fill dams when the reservoir is filled, because the increased pressure causes sharp points of contact between rocks to break off, thereby developing larger areas of contact and allowing the rocks to move closer together. When rock is dropped from high lifts, impact and sliding tend to break off sharp points and produce more rounded particles. But slides from heights of several thousand feet appear to impart too much kinetic energy; the result is flat slopes and perhaps an over-grinding of the particles. The latter is not too objectionable, but it does result in a lower angle of internal friction for the rock mass. Also fine particles are more susceptible to piping.

Because of the impact and grinding action which takes place in drops from a favorable height, it cannot be assumed that a slide in hard, sound rock would not have a favorable relative density or that settlement would not be of acceptable proportions. Judgment suggests that favorable conditions could develop for rock. Whether this statement is also true for earth-slide embankments is uncertain. Research is obviously needed to establish the relationship between height of fall and the resulting relative density of the slide embankments in both rock and earth materials.

Natural slides have all been characterized by a wide variation in the particle sizes produced. In rock slides from great heights, the gradation has ranged from rock flour to boulders with a volume of several cubic yards. Even though such embankments may be relatively dense, slides such as Gohna and Gros Ventre show that they have a marked susceptibility to piping. This would be expected; even though a rolled-fill dam is carefully controlled and placed, seepage problems will result unless proper provisions are made for drainage. Thus, experience with both natural slide dams and man-made, rolled-fill dams indicates that slide dams produced by nuclear explosives will have to be provided with an earth core or an impervious face slab to control seepage or provisions will have to be made for adequate drainage to prevent piping.

Sites

The sites of many large landslide dams have been unfavorable. At Frank, Alberta, the valley was extremely broad and was deeply covered with boulder clay and gravel--certainly an unfavorable site for either a conventional or a slide dam. While the Gohna slide occurred in a valley having a reasonable foundation, some treatment would obviously have been provided before the placement of a conventional or a slide dam. Indeed, experience with conventional dams indicates that, for either conventional or slide dams, sites should be given some treatment before placement of fill.

Spillway, diversion, and outlet arrangements for high earth- and rock-fill dams present problems which can be satisfactorily solved only by some initial construction prior to placement of the fill material. Because the foundation must also be prepared and treated before the fill is placed, natural slide dams are almost foredoomed to failure because of these omissions. Experience would indicate that a procedure for constructing slide dams by the use of nuclear explosives must also include provisions for diversion and proper spillway and outlet capacity. Some construction for these items must be provided before initiation of the slide.

Slide Profiles

A study of the cross sections or profiles of natural slide dams reveals the same general characteristics. Slopes are usually very flat, varying from 5 to 1 to as much as 10 or 15 to 1. The crest is usually quite wide and rounded. The net result is a dam with a much broader base than those of conventional dams. This is not a favorable characteristic, as will be shown later.

The flat slopes are apparently caused by more than one factor. In some cases, the slide has not been oriented normal to the valley (for example, Gros Ventre and Madison Canyon). In other cases, such as Frank, Alberta, the valley was quite broad but contained ridges which deflected the slide. Other important factors are the kinetic energy of the material in motion and its internal resistance to flow. These are probably quite variable. For example, the saturated clays at Gros Ventre may have been extremely sensitive and may have experienced spontaneous liquification. However, at the present time, not much is known about the mechanics of the slide motion. Certainly the kinetic energy of the slide particles, which can be variable with depth as well as with the lateral extent of the slide, and the kinematic viscosity of the flowing mass are factors which influence the slope at which the slide ultimately comes to rest. Thus, in contrast to conventional construction, the static shear strength of the material is not a satisfactory parameter for predicting the slope angles of a slide.

In many cases, earth- and rock-fill dams have proved feasible because it was possible to provide spillway and outlet structures at some location other than in the valley containing the fill dam. In such cases, flat earth slopes would not be objectionable. Frequently, however, the spillway, diversion, and outlet works must be in the same valley as the fill dam. This usually means that a shaft, side channel, or chute spillway must be provided and that diversion and outlet releases must be furnished by driving tunnels through the abutments around the base of the fill. In such cases, flat dam slopes are expensive; 5 or 10 to 1 slopes double or quadruple the cost of these items in comparison with 2.5 or 3 to 1 slopes. Thus, techniques that ensure satisfactory slopes for slide dams produced by nuclear explosives must be developed.

Observation Summary

From the preceding considerations, the following observations are important and indicate the requirements of slide dams:

1. The first requirement is an adequate site, one which has a good foundation and good slide materials suitably located. The site must also permit construction of economical spillway, diversion, and outlet structures.
2. It should be anticipated that foundation treatment will be required for all foundations and that this work must normally be done before initiation of the slide.
3. Theory and experience with both conventional dams and natural slide dams show the importance of adequate provisions for drainage and seepage control. Graded filter drains will be required in some cases; an impervious membrane or core adequately protected by filters may be required in others.
4. In many cases, it will be desirable to create slopes steeper than those occurring in natural slides. Techniques for achieving this objective are needed.
5. The settlement and drainage characteristics of slide dams may be influenced by the kinetic energy imparted to the slide. Thus,

relationships should be established between valley and slide geometry; rock properties; and the geometry, relative density, and permeability of the resulting slide dam.

SLIDE MECHANICS

The two previous sections are based upon a literature search and theoretical study by the author which was reported in Reference 19. This study concluded that although it is possible to develop a nuclear-induced slide dam at an ideally chosen site, a better understanding of the slide initiation techniques and of the mechanics of the slide are required to develop efficient designs. Laboratory studies were also recommended to establish the effects of valley and slide geometry, rock properties and foundation conditions upon the geometry, permeability, and settlement characteristics of the resulting slide dams.

Pilot studies consisting of small-scale laboratory experiments have been performed to provide information on the general phenomena of rock slides and to determine whether this type of behavior can be scaled. The results of these studies have been reported in Reference 20. A brief review of some of the results are of interest.

Importance of Valley Geometry

In planning the slide mechanics experiments, consideration was given to the influence of the geometry of the valley cross section. Two limiting valley cross sections are illustrated in Figure 10. In Figure 10a, the valley side slopes are nearly vertical. If, as indicated, the canyon is deep and narrow relative to the dam dimensions, the slide phenomenon becomes almost a rock fall, particularly when slides are initiated high on each side slope. For this geometry, the rock will fall nearly vertically downward until contact is made with the foundation, after which it will move laterally outward normal to the longitudinal axis of the dam. The rock particles, therefore, will have almost plane motion.

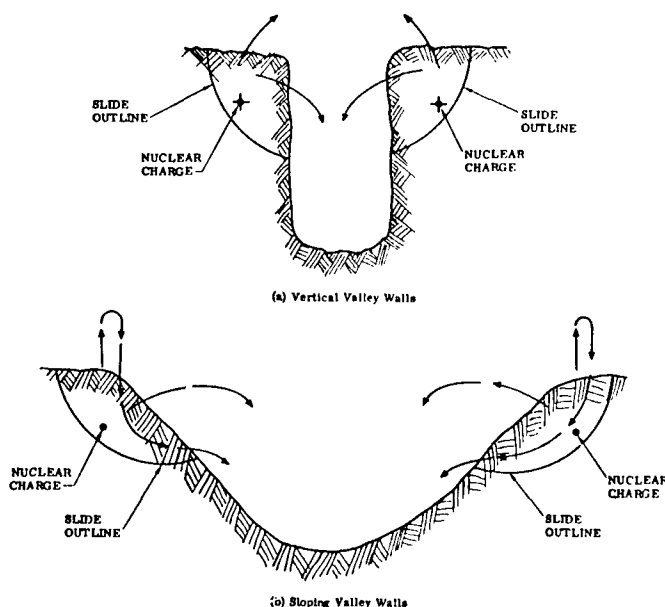


Figure 10. Valley Wall Profiles

Figure 10b represents the other limiting cross-section geometry. In this case, the slope is the flattest upon which a slide can be maintained by gravity. To initiate a slide on such a valley wall, rock would have to be heaved from the crater, after which it would fall back to the crater and slope before sliding to the valley floor. Rock particles, after falling back to the slope, would have three-dimensional motion. That is, most rock particles would have one vertical and two horizontal components as they move down the slope and onto the valley floor.

Experimental Models

Most valleys provide cross-section geometries intermediate between the two extremes described above. However, the plane motion example represents a real condition and is the simpler to consider experimentally. Because of this, it was selected for the initial studies. After some success was achieved with the plane motion studies, general phenomena were observed on a three-dimensional model. In both cases, the models were simplified idealizations of actual field conditions.

The plane motion model is shown in Figure 11a. An ideal plane motion resulted when a granular, cohesionless material, sand, was dropped vertically from a hopper to a flat concrete surface. The controlled variables were the volume of granular material (Q), the width of the hopper (b) and the height of the fall (h). The primary test objective was to observe general phenomena as the model dam was formed. Relationships were established between the controlled variables and the X and Y dimensions of the profile. Attempts were also made to produce geometrically similar profiles to establish the feasibility of scaling.

Figure 11b shows the general features of the three-dimensional model. This model, even when restricted to a consideration of geometric factors, is much more complex than the one used in the plane motion study. Only observation of general phenomena and a limited effort to produce geometrically similar profiles was attempted with this model. Controlled variables were the volume of granular material (Q), the hopper width (b), the shape of hopper cross section (b/b'), the slope angle (θ), the length of slope (K), and the width of the valley (w_v).

Dimensional Relationships

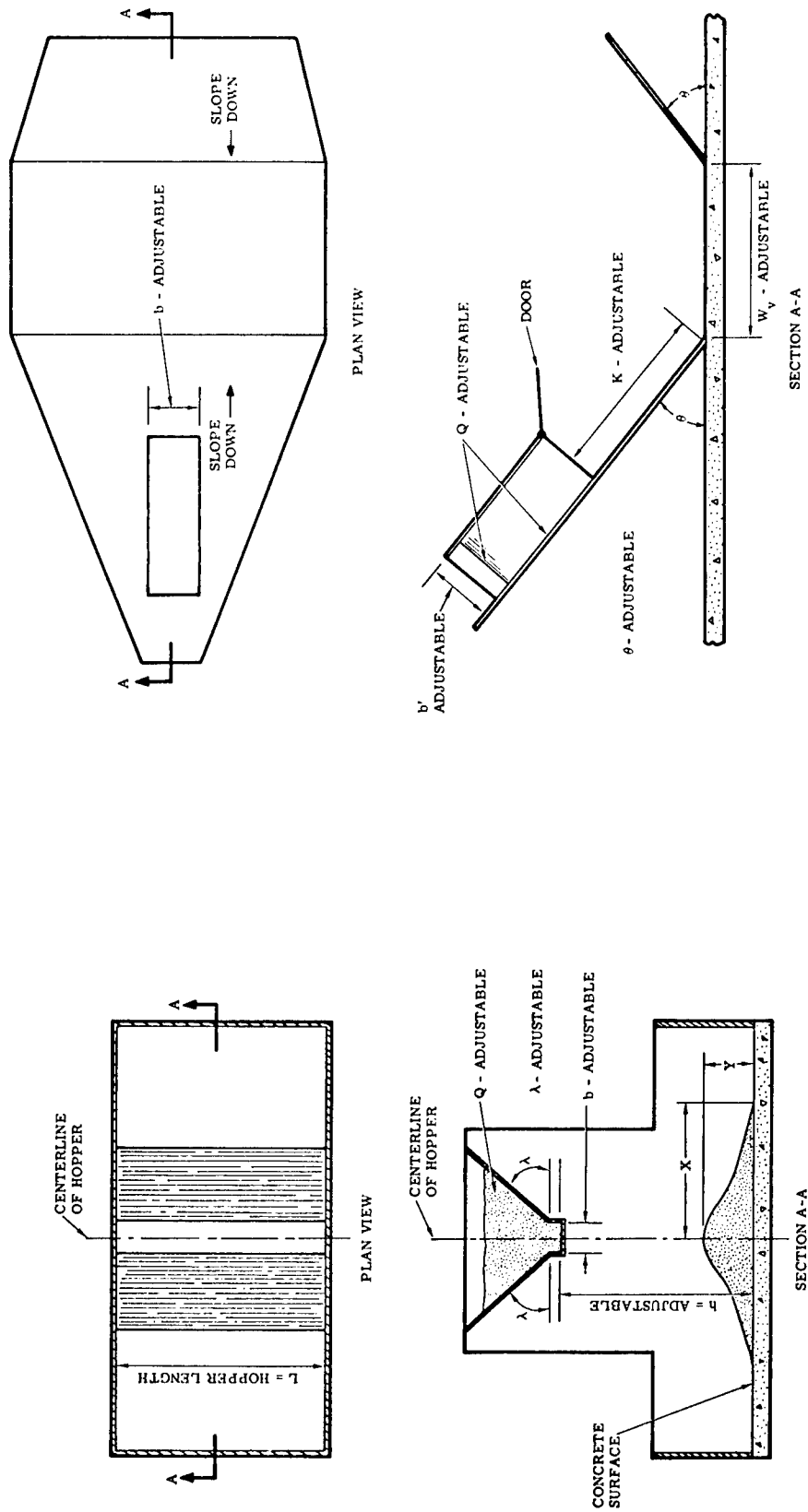
A consideration of the dimensional relationships associated with the plane motion model identified eighteen dimensionless products (π terms) of which four terms involved slide and hopper geometry, four introduced properties of the flowing materials, and ten represented ratios of the physical properties of the dam and foundation materials. By using the same slide and foundation material (i.e., Ottawa sand and a concrete floor), similarity was guaranteed for the ten π terms relating the material properties of the dam and foundation. Thus, only the following π terms were significant in the plane motion model experiments:

$$\begin{array}{ll} \pi_1 = X/b \text{ or } Y/b & \pi_5 = Vb/v \\ \pi_2 = h/b \text{ or } V^2/gb & \pi_6 = \gamma V^2/gE \\ \pi_3 = b/d & \pi_7 = \mu V/dE \\ \pi_4 = Q/Lb^2 = q/b^2 & \pi_8 = \phi \end{array}$$

Nomenclature not previously defined in the text or in Figure 11 is as follows:

g = acceleration of gravity

V = average velocity of falling particles, computed from $V = \sqrt{2gh}$



(a) Plane Motion Model

(b) Three-Dimensional Model

Figure 11. Schematic Views of Slide Mechanics Models

- d = particle diameter of slide material
 q = volume of slide material in hopper per foot of hopper length, $q = Q/L$
 ν = kinematic coefficient of viscosity of slide material
 γ = unit weight of slide material in hopper
 E = elastic modulus of slide material
 μ = strain rate modulus of slide material
 ϕ = angle of internal friction of slide material.

Two of the terms, π_5 and π_7 , involve properties of flowing material which to date have not been satisfactorily measured or controlled. Therefore, no attempt was made to control these terms in any of the experiments and some model distortion resulted. It is well to note that it would be extremely difficult, if not impossible, to provide geometric scaling without a distortion in these two terms since the velocity appears to the second power in π_2 and π_6 but is a first power quantity in π_5 and π_7 .

Slide Geometry Tests

As stated earlier, the primary objective of the plane motion experiments was to observe the effects of hopper geometry upon the model dam profile. Ottawa sand was selected as the principal test material. A series of tests were conducted which provided variations in the quantity of slide material, Q , the width of hopper opening, b , and the height of drop, h . The hopper configurations and heights of drop considered are indicated in Figure 12.

A limited number of experiments were performed in which the physical properties of the slide materials were varied to obtain some indication of the importance of these properties. Variations in particle density, particle size, and angle of internal friction of the granular slide material were provided. Magnetite and quartz blast sands were used to provide the variations in physical properties. A few experiments were also made to determine whether revetments could be used effectively to improve slide dam profiles. The reader should refer to Reference 20 for discussion of these studies.

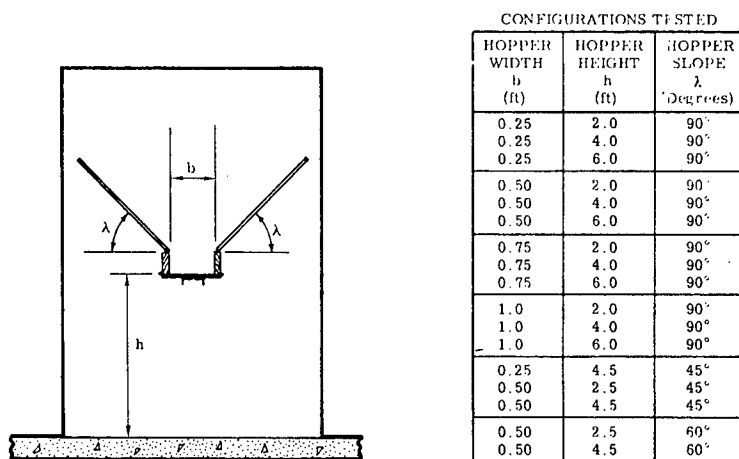


Figure 12. Hopper Configurations Tested

General Slide Behavior

An explanation of the general slide behavior was not possible until an end wall of the test apparatus was replaced with a glass plate and high-speed photographs were taken of test runs. Visual observation through the glass and study of the pictures indicates that the behavior of the slide material upon impact with the foundation is somewhat similar to that of a water jet impinging upon a flat plate. Sand particles are first deflected outwardly parallel to the foundation surface at a high velocity. The first particles travel a great distance, and a few even travel beyond the width of the base of the final plotted profile. If the quantity of slide material is small, that is, the duration of the flow is short, the resulting profile is very flat as shown in Figure 13a for $q/b^2 = 6$ and 8. The slopes for these particular examples are about 17:1.

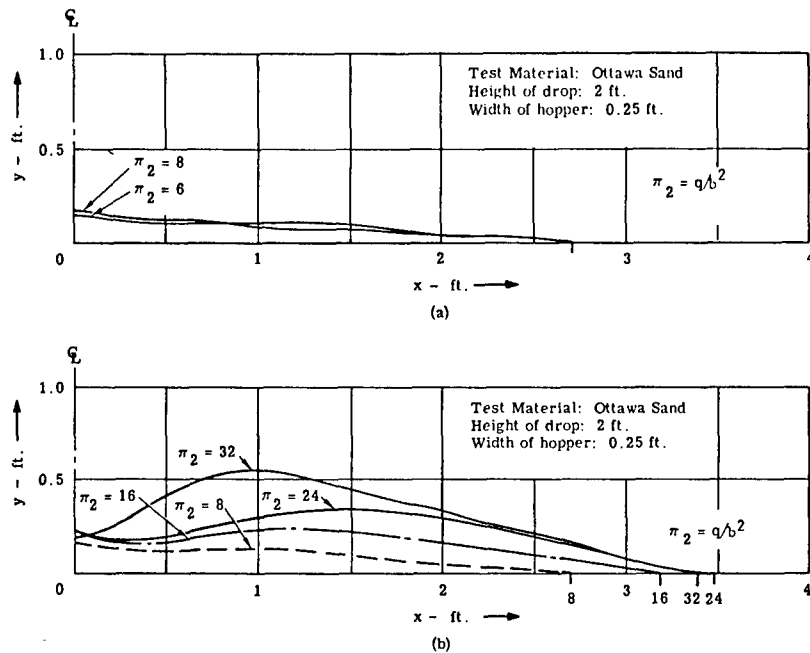


Figure 13. Comparison of Half Profiles; Quantity of Slide Material Variable

If the flow continues for a longer time, as is the case for a larger volume of slide materials (width of hopper (b) remaining the same), the lateral deflection pattern of the particles changes, and a thin stream of particles starts to flow upward and outward over previously deposited particles. A cup-like depression forms on each side of the vertical stream of particles falling from the hopper. If the flow of particles from the hopper ceases at this point, profiles similar to those shown in Figure 13b for $q/b^2 = 24$ and 32 result. The final slopes for the latter are slightly flatter than 4:1. When the flow of particles continues still longer, the pattern is much the same, but steeper final slopes result. While the flow of materials is in progress, the slopes are very steep near the crest of the model profile, but after the flow stops, the stream of material continues to move down the slopes and flatter final slopes result. The flow pattern at two different stages of profile construction is represented in Figure 14. It will be noted that the depth of the flowing material decreases outwardly from a maximum near the crest. Maximum final slopes achieved with a large volume of hopper material were approximately 2:1 with Ottawa sand.

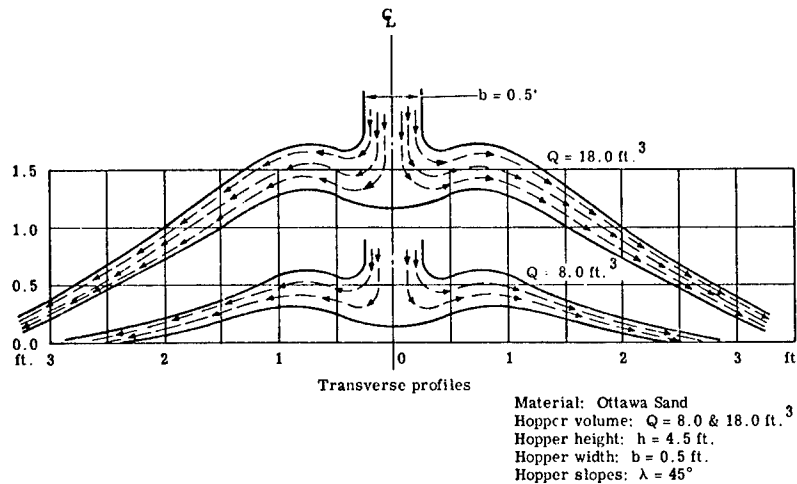


Figure 14. Flow Patterns

Effect of Hopper Width

The above discussion considered only the effect of the volume of slide material. Actually, similar profile variations can be produced by holding the volume of slide material constant and changing the hopper width. Figure 15 indicates the influence of the width of opening (b). Figure 15a suggests that decreasing the width of the hopper decreases the maximum height of dam profile. This is true, however, for only small relative quantities of slide material. When the quantity of material is doubled, as represented in Figure 15b, the maximum profile height for $b = 0.25$ foot is slightly greater than for $b = 0.50$ foot. Increasing the quantity of slide material further will cause the smaller hopper opening to have the greater maximum height of profile and the steeper slopes. These effects are more clearly depicted in Figure 16a. It should be noted that for the larger quantities of slide materials, the maximum height of profile does not occur at the centerline.

Effect of Hopper Height

Figure 16b provides two examples of constant volume slide material and width of opening, but variable height of drop. As expected, flatter profiles are experienced with the greater heights of drop.

Geometric Scaling

Two types of geometric scaling were attempted. In the first, the geometry of the hopper and the height of drop were scaled but particle size of the granular material was kept constant. Figure 17, 18, and 19 provide typical results for the normalized profiles. Excellent agreement was demonstrated in Figures 18 and 19, but the very small hopper opening of 0.25 feet appeared to introduce some model distortion in Figure 17. However, a comparison was then made between the normalized profile for the 0.25 feet hopper opening and a normalized profile for a geometrically similar test having a hopper opening of 0.5 feet which utilized a blast sand having a larger particle size. The results are shown in Figure 20. Obviously much better scaling resulted, and particle size is considered to be a factor in scaling.

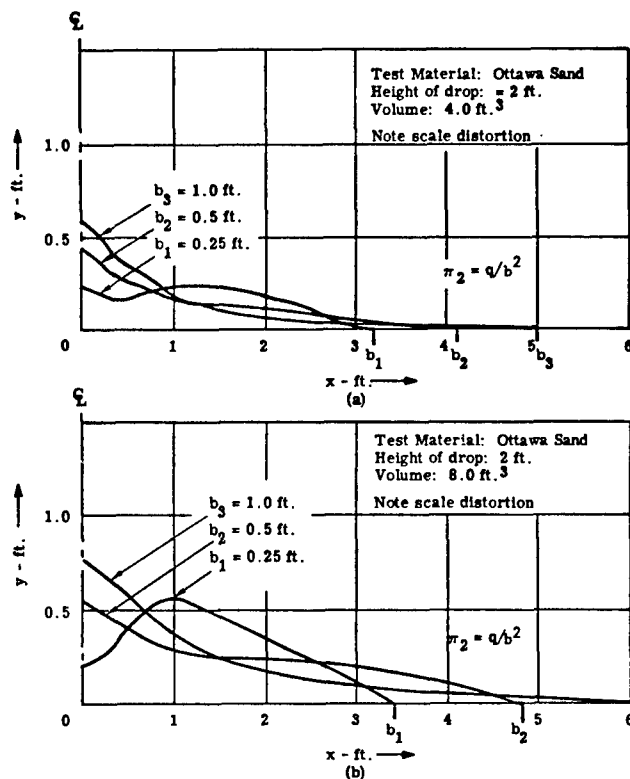
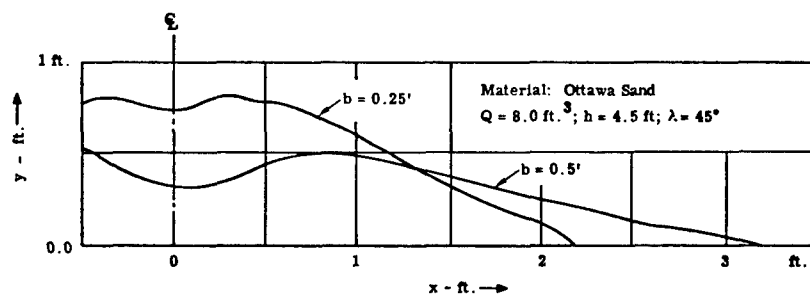
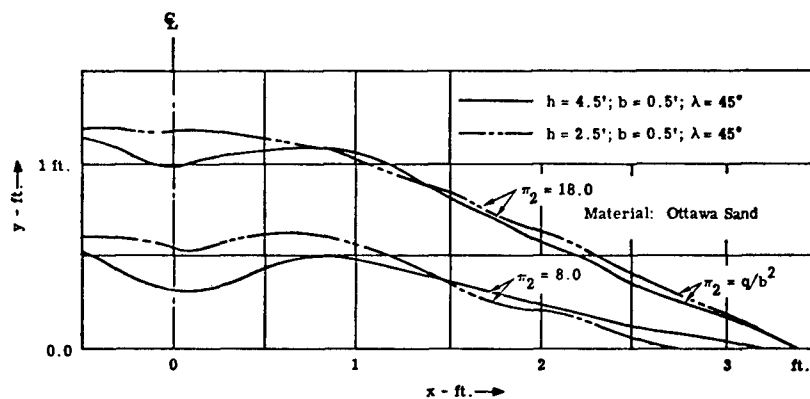


Figure 15.
Comparison of Half Profiles
with Vertical Hopper, Width
of Hopper Variable



(a) Half Profiles Showing Effect of Width of Hopper Opening

Figure 16.
Comparison of Test
Profiles



(b) Half Profiles Showing Effect of Hopper Height

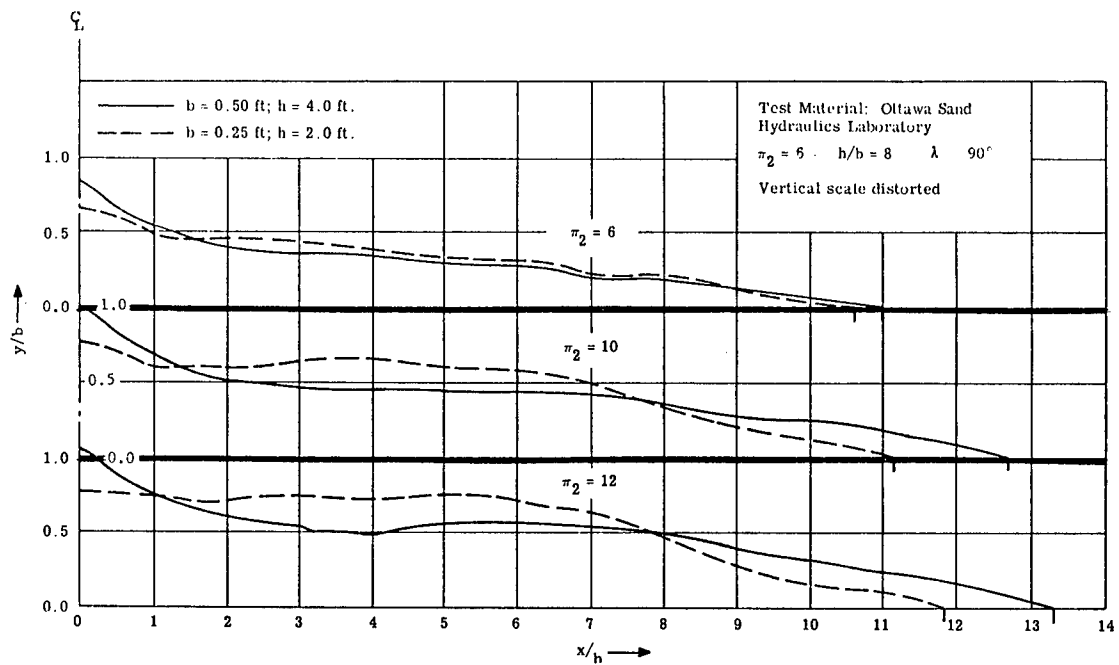


Figure 17. Comparison of Geometrically Scaled Profiles

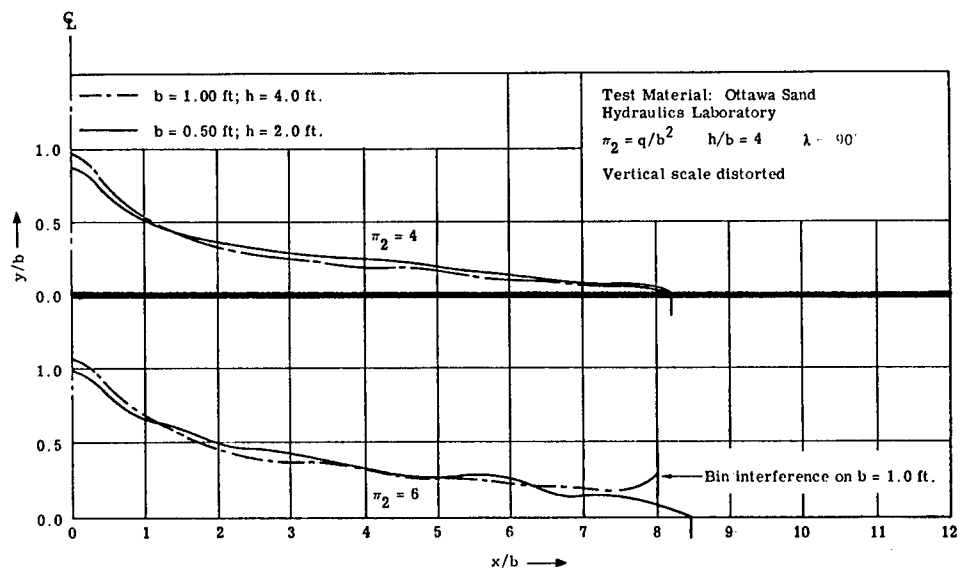


Figure 18. Comparison of Geometrically Scaled Profiles

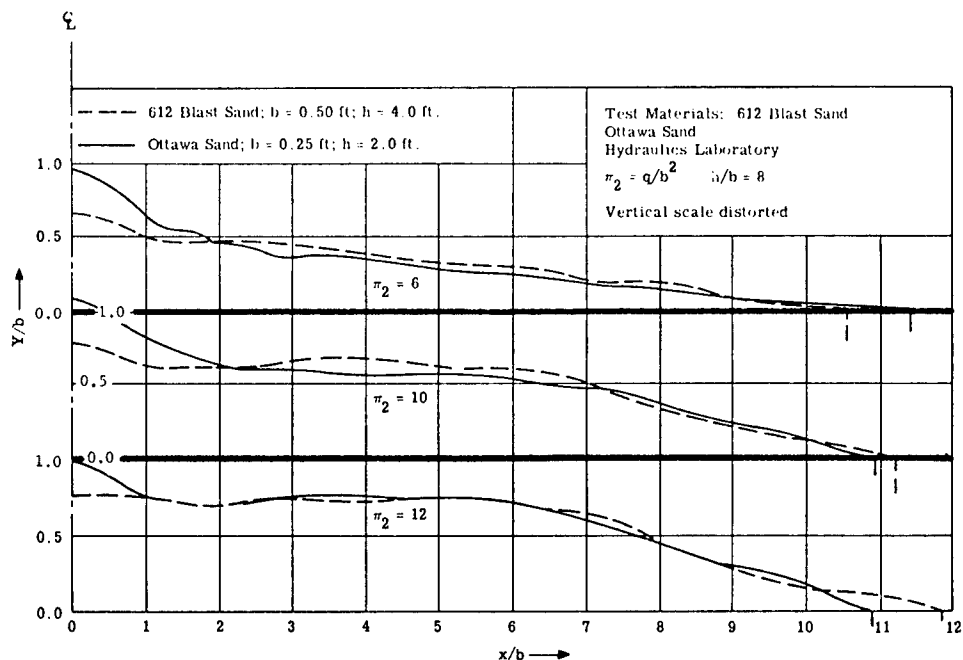


Figure 19. Normalized Half Profiles; Particle Size Scaled Geometrically

Three-Dimensional Motion Model Results

It is not possible to elaborate upon the three-dimensional motion model results, but it is important to indicate that the same general type of phenomena was observed with this model as discussed above for the plane motion studies. Figures 20 and 21 are provided to demonstrate that geometric scaling was also successfully achieved with this model.

SUMMARY AND RECOMMENDATIONS

In this paper it has been demonstrated that there are many important features of conventional dams that must be incorporated into the designs for slide dams. For example, foundation treatment and adequate diversion and spillway capacity must be provided. Also, adequate provisions must be made to control seepage and prevent piping. Important lessons can be learned from observing the characteristics of natural landslides. Slide dams created by man, however, must provide better results than have been observed in nature. Limited laboratory studies have helped define the general phenomena of the mechanics of slides and gives indications that the phenomena can be scaled. The information obtained is useful in planning more extensive laboratory experiments and small-scale field tests. In the field tests, it is assumed that the slides will be initiated with high explosives. Such experiments are now justified and would help develop a more complete understanding of slide dam mechanisms.

ACKNOWLEDGEMENT

This paper is based upon studies conducted by the author which were sponsored by the Sandia Corporation, Albuquerque, New Mexico. Mr. Luke Vortman served as technical adviser for the Sandia Corporation.

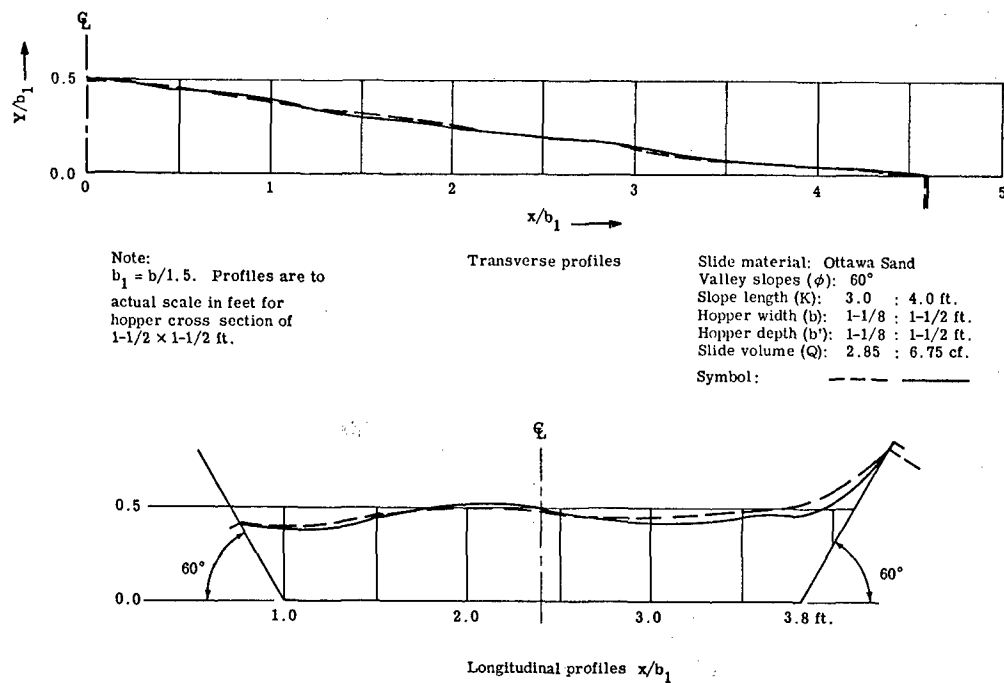


Figure 20. Comparison of Geometrically Scaled Profiles

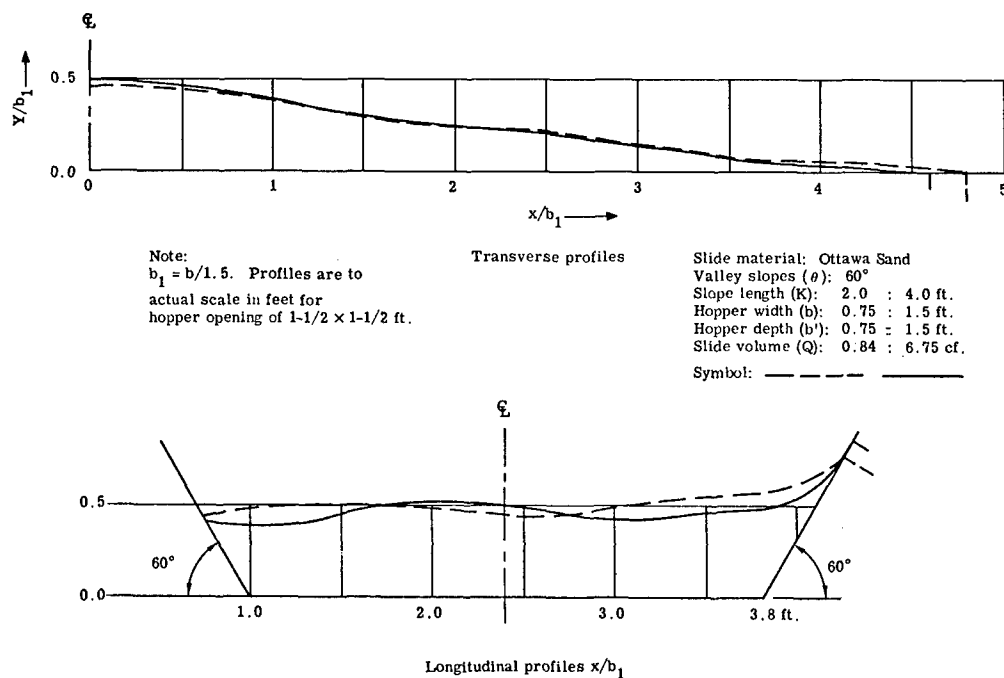


Figure 21. Comparison of Geometrically Scaled Profiles

REFERENCES

1. Justin, J. D., Hinds, J., and Creager, W. P., *Engineering for Dams*, Vol. III, John Wiley and Sons.
2. Taylor, D. W., *Fundamental Soil Mechanics*, John Wiley and Sons.
3. Davis, C. V., *Handbook of Applied Hydraulics*, Second Edition, McGraw-Hill (1952).
4. Steele, I. C., "High Rockfill Dam Designed with Jointed Concrete Face," *Engineering News-Record*, Vol. 104, No. 3, (January 16, 1930), pp. 92-95.
5. Steele, I. C., and Cooke, J. B., "Rockfill Dams: Salt Springs and Lower Bear River Concrete Face Dams," *Journal Power Division, Proc. Am. Soc. Civil Engineers*, Paper 1737, (August 1958).
6. Fucik, E. M., and Edbrooke, R. F., "Design and Construction of Ambuklao Rock Fill Dam," *Proc. Am. Soc. Civil Engineers*, Vol. 84, No. SM5, Pt. 1, Paper 1864, (Dec. 1958), 28 pages.
7. Davis, C. V., "Rockfill Dams: The Derbendi-Khan Dam," *Journal Power Division, Proc. Am. Soc. Civil Engineers*, Paper 1741, (August 1958).
8. Mundal, T., "Rockfill Dams: Brownlee Sloping Core Dam," *Journal Power Division, Proc. Am. Soc. Civil Engineers*, Paper 1734, (August 1958).
9. Terzaghi, K., "Mechanism of Landslides," *Berkey Volume*, Geological Society of America, (November 1950), pp. 83-123.
10. Strachey, R., "The Landslip at Gohna, in British Garwhal," *Geographical Journal*, Vol. 4, (August 1894), pp. 162-170.
11. Glass, J. H., "The Great Landslip of Gohna, in Garhwal, and Measures Adopted to Prevent Serious Loss of Life," *J. Soc. of Arts*, (March 27, 1896), pp. 431-445.
12. Alden, W. C., "Landslip and Flood at Gros Ventre, Wyoming," *American Institute of Mining and Metallurgical Engineering*, Volume 76, pp. 347-361.
13. Emerson, F. B., "180-Ft Dam Formed by Landslide in Gros Ventre Canyon," *Engineering News-Record*, Vol. 95, No. 12, (Sept. 17, 1925), pp. 467-468.
14. Blackwelder, E., "The Gros Ventre Slide, An Active Earth Flow," *Geological Soc. Am. Bull.*, Vol. 23, (Oct. 21, 1912), pp. 487-492.
15. McConnel, R. G., and Brock, R. W., *Report on the Great Landslide at Frank, Alta.*, Extract from Part VIII, Annual Report 1903, Department of the Interior, Dominion of Canada, Ottawa Government Printing Office.
16. Hadley, Jarvis B., "The Madison Canyon Landslide," *Geotimes*, Vol. 14, No. 3, (October 1959), published by the American Geological Institute.
17. *Flood Emergency, Madison River Slide, Volumes I and II*, Report by U.S. Army Engineer District, Omaha, Corps of Engineers, Omaha, Nebraska, (Sept. 1960).
18. Carlson, R. H., *Nuclear Explosives and Landslide Dams*, SC-4403(RR), Sandia Corporation, (April 1960).

19. Young, G. A., *Slide Dam Construction Employing Nuclear Explosives*, SC-4781(RR) Sandia Corporation, Albuquerque, New Mexico, May 1963.
20. Young, G. A., *A Study of the Mechanics of Slide Dams with Sand Models*, SC-RR-67-24, Sandia Corporation, Albuquerque, New Mexico, April 1967.

THE USE OF A RUBBLE CHIMNEY FOR DENITRIFICATION OF IRRIGATION RETURN WATERS

Roy B. Evans* and Paul Kruger
Civil Engineering Department
Stanford University

Biological denitrification has been proposed as a means of removing nitrates from waste waters to control eutrophication in receiving waters. A potential use for this method is the treatment of irrigation return waters containing high concentrations of nitrate-nitrogen, since direct discharge of such wastes may cause objectionable algal growth in the receiving waters. For example, the process may be used to treat agricultural waste waters in the San Joaquin Valley in California, where an estimated 580,000 acre-feet/year of return waters, containing 20 mg/l of nitrate-nitrogen, will require disposal by A.D. 2020. Two methods of biological denitrification are presently under study for possible use in the San Joaquin Valley. In one method nitrates are reduced to nitrogen gas by bacterial action in deep ponds; in the other method bacterial denitrification takes place in biological filters. In biological filters, bacteria are grown on columns of submerged stones. A possible alternative to the conventional construction of these filters is the creation of a rubble chimney by a contained nuclear explosion. This paper presents the results of a preliminary investigation of the feasibility of using a rubble chimney as a biological filter for denitrification.

IRRIGATION RETURN FLOWS AND WATER QUALITY

Arid regions which import large quantities of water for irrigation are sometimes faced with the problem of salt build-up. The imported water contains dissolved salts which accumulate in soils as the irrigation water evaporates, reducing the productivity of the soils. These salts can also find their way into ground water through infiltration, degrading the ground water quality. The salt build-up problem can be avoided by providing drainage facilities to convey agricultural return flows to suitable disposal sites, but disposal of the return flows can cause secondary water quality problems.

Use of water for irrigation seriously reduces the quality of the water. Irrigation return water may have high concentrations of salts, pesticides, and plant nutrients, and discharge of the return flows into rivers or other receiving waters can seriously affect the quality of the receiving waters. The increased availability of cheap fertilizers has had the undesirable side-effect of increasing concentrations of nitrogen and phosphorus in irrigation return flows. The presence of these elements can be troublesome. Both are nutrients necessary for the growth of algae, and in some situations their presence may result in severe algal blooms in the receiving waters. Their removal from waste water is considered difficult and expensive. Biological denitrification may be a relatively simple means of removing nitrates. No comparable solution is presently available for removal of phosphates.

* now at the Southwestern Radiological Health Laboratory, U.S. Public Health Service, Las Vegas, Nevada.

The optimum means of disposing irrigation return flows depends on the geography of the particular problem area. Possible solutions include discharge to an ocean, evaporation of the waters in evaporation pans where the salts can be removed periodically, or treatment of the return flows to remove specific objectionable contaminants before discharge to non-saline receiving waters. Where economics permit, the return flows might be desalinized and reclaimed.

BIOLOGICAL TREATMENT FOR NITRATE REMOVAL

Two biological treatment processes have been suggested for removing nitrate-nitrogen from irrigation return flows. The first, algae stripping, involves growing algae in shallow, aerobic ponds and harvesting the algae crop to remove assimilated nitrogen.

The second is biological denitrification. Two methods for biological denitrification have been proposed, one using deep ponds and another using biological filters. In the deep pond process, organic material such as methanol is added to the return water to provide a source of energy and carbon for anaerobic bacteria. The waste is then routed through a deep reservoir with sufficient capacity to provide a hydraulic detention time of about ten days. During passage through the reservoir dissolved oxygen in the water is depleted by bacterial oxidation of the organic materials. Under such anaerobic conditions, denitrifying bacteria reduce nitrate-nitrogen to nitrogen gas which evolves to the atmosphere. After passing through the reservoir, the water is reaerated and discharged. Nitrogen removal efficiencies of 90 per cent or more have been obtained in pilot plant studies using this method [9]. The process is illustrated in Figure 1.

The biological filter consists of a large mass of denitrifying bacteria grown in a column filled with rocks or other suitable material. Models tested in pilot plant studies are similar in design to the aerobic trickling filters common in sewage treatment plants, but flow is upward in the anaerobic filter to keep the matrix rocks completely submerged. This process is illustrated in Figure 2.

The advantage of this configuration is the long biological solids retention time possible. Microorganisms consuming the organic material added to the waste water multiply rapidly and accumulate in the matrix void spaces, clinging loosely to the surfaces of the matrix rock. Large masses of biological solids are concentrated in the filter, stabilizing the wastes with much shorter hydraulic detention times than are available in the pond process. In the pond process a large fraction of the bacteria produced is wasted in the effluent. The fraction of organisms wasted from the biological filter is much smaller.

CHEMISTRY OF ANAEROBIC DENITRIFICATION

The chemistry of biological denitrification has been described by McCarty [9] and McCarty, Beck, and St. Amant [11]. The process involves the reduction of nitrates and nitrites to nitrogen gas by a variety of common facultative bacteria, including the genera *Pseudomonas*, *Achromobacter*, and *Bacillus*. In the absence of oxygen, these organisms use nitrates as terminal electron acceptors while oxidizing organic matter for energy. The nitrates and nitrites serve essentially the same purpose as oxygen does under aerobic conditions. Thus denitrification can take place only if organic material is available as an energy source and only under anaerobic conditions. Most investigations have used methanol as the energy source because it is relatively inexpensive.

The reduction of nitrates to nitrogen gas is described as a two-stage process: the nitrates are first reduced to nitrites, then nitrites are reduced to nitrogen gas. The nitrogen gas is eliminated by release to the atmosphere. For a process using methanol as the energy source, the overall reaction can be represented as follows:

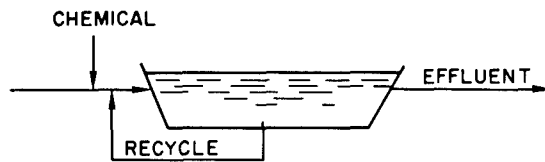


Figure 1. Anaerobic pond

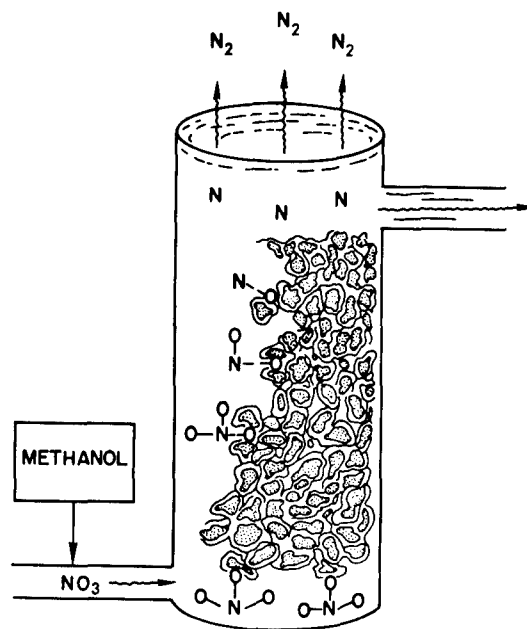
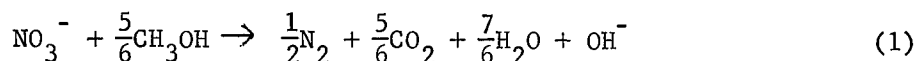
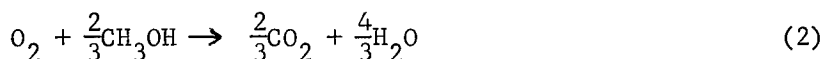


Figure 2. Removal of Nitrogen by bacterial action--filter method



The stoichiometry of the reaction indicates that 1.9 mg/l of methanol is required for each 1.0 mg/l of nitrate-nitrogen present in the waste-water. If less methanol were added, the reaction would not go to completion, and the resulting effluent would be high in nitrite-nitrogen.

In addition to the material required to provide an energy source for the reduction reaction, sufficient organic material must be added to allow the bacteria to deplete the dissolved oxygen present in the influent water to create anaerobic conditions and to supply carbon which is assimilated to form new cells. The amount of methanol necessary for the biological removal of the dissolved oxygen is given by



At least 0.67 mg/l methanol would be required for each 1.0 mg/l dissolved oxygen present in the influent.

McCarty, Beck, and St. Amant [11] experimentally determined the amount of methanol required for bacterial growth and found that an additional amount of approximately 30 per cent of the methanol needed for oxygen depletion and denitrification had to be added for this purpose. The total amount of methanol required is given by

$$C_m = 2.47 N_o + 1.53 N_1 + 0.87 D_o \quad (3)$$

where:

C_m = required methanol concentration, mg/l

N_o = initial nitrate-nitrogen concentration, mg/l

N_1 = initial nitrite-nitrogen concentration, mg/l

D_o = initial dissolved oxygen concentration, mg/l

The rate of biomass production, C_b , in mg/l is given by McCarty, et al., as

$$C_b = 0.53 N_o + 0.32 N_1 + 0.19 D_o \quad (4)$$

RESULTS OF BIOLOGICAL FILTER PILOT PLANT STUDIES

Tambllyn and Sword [13] and St. Amant and McCarty [12] have reported on pilot plant studies of anaerobic filter denitrification. These studies investigated the hydraulic detention times necessary for satisfactory nitrate-nitrogen removal with filters constructed of different matrix materials. Matrix media investigated included sand, activated carbon, volcanic cinders, gravel, coal, and a commercially-produced plastic trickling filter material. Media sizes ranged from coarse sand to three-inch diameter gravels, and hydraulic detention times ranged from one-half hour to two hours.

The sand filters were initially satisfactory but soon clogged as biological solids filled the void spaces. Removal efficiencies of 80 to 100 per cent were obtained at hydraulic detention times of one-half hour to two hours with all matrix media except the three-inch gravel, which attained 58 to 76 per cent removal at three to six-hour detention times [47]. Apparently the void spaces in the

three-inch gravel were too large to provide good biological solids retention.

St. Amant and McCarty [12] recommended that rounded stones, 1 to 2 inches in diameter, be used as the matrix media for practical systems for denitrification of municipal drinking water. They advised that hydraulic detention times of about one hour would be required to ensure complete denitrification at water temperatures of at least 12°C. Longer detention times would be required at lower temperatures, while correspondingly shorter times might be satisfactory at higher temperatures.

Most of these studies have been conducted with relatively small filters of 36-inch diameter or less. The largest filter yet constructed is ten feet square and six feet high. No provision was made for removal of biological solids from this filter, but it is expected that excess biological solids can be flushed out by sharply increasing the flow-rate through the filter for a short period of time.

USE OF A RUBBLE CHIMNEY AS A BIOLOGICAL FILTER

The use of a rubble-filled chimney as a biological filter may offer several attractions over alternative methods of denitrification. These include lower construction costs, faster construction, and a smaller physical plant aesthetically more acceptable than conventional treatment plants. The essential element in a biological filter is a large volume of crushed rock in an impervious container. A contained nuclear explosion would provide a relatively inexpensive means of constructing such a structure. A nuclear explosive could be detonated in a suitable geologic formation at the desired filter location to produce a rubble chimney. Methanol would be added to the waste waters and the mixture would be pumped to the bottom of the chimney and forced upward through the rubble. Large masses of denitrifying bacteria would accumulate in the rubble material. The concept is represented schematically in Figure 3.

The considerations involved in the engineering use of a nuclear explosion include the mechanical and radioactivity effects produced by the detonation. In the use of a rubble chimney as a biological filter, further consideration must be given to the effect of rubble size distribution on biological solids retention, the effects of temperature and hydrostatic pressures on bacterial nitrate reduction, and the long-term geochemical reactions between the rock matrix and the waste waters.

The parameter most convenient for the design of a biological filter appears to be the hydraulic detention time necessary for satisfactory nitrate removal. The hydraulic detention time depends strongly on the retention of bacteria (biological solids) within the filter. There appears to be an optimum matrix particle size for good solids retention. In pilot plant studies, best results were obtained with round stones 1 to 2 inches in diameter. With smaller diameters, filter clogging produced high back pressures and short-circuiting, causing low nitrogen removal efficiencies. With three-inch gravel, biological solids retention was poor, apparently because the void spaces were too large. Young [10] suggested that the effective biological solids are retained in the filter both as a layer of solids attached to the stones and as large flocculated particles loosely held in the void spaces. To some extent, therefore, solids retention should be proportional to matrix surface area.

The pilot plant filters contained smooth, round stones of nearly uniform size, but the rubble in a chimney produced by a contained nuclear explosion has a distribution of particle diameters ranging from less than a centimeter to more than a meter. Surfaces of the rubble are rough and irregular and should yield more surface area per unit volume and better solids retention than smooth stones of similar size. The particle size distributions of rubble observed in experiments in granite and dolomite are given in Table I. Particle diameters are

apparently larger than the 1 to 2 inch stones recommended for filter construction by St. Amant and McCarty. Data on the size distribution of the void spaces is required to estimate the extent of solids retention, but these data are not generally available. Void spaces in the rubble should be smaller than would be found in crushed rock from quarries because there should be less displacement of particles relative to their neighbors. As the chimney collapses after the detonation, particles in the same geologic bedding plane tend to downwarp simultaneously, and the collapse may produce little actual mixing of strata. To obtain quantitative estimates of solids retention in rubble material, pilot plant studies with filters constructed from rubble material are recommended.

The rock chosen for the chimney location must be resistant to decomposition by water. Soft, friable rock such as mudstone or siltstone would tend to slump and might form a slurry or mud with water, clogging the interstitial voids. Shale might react in a similar fashion. The choice of media is probably restricted to igneous rock, metamorphosed sedimentary rock, and possibly competent sandstones resistant to decomposition by water.

EFFECTS OF PRESSURE ON BACTERIAL NITRATE REDUCTION

Conventional biological waste treatment processes normally operate at pressures corresponding to a few feet of water. However the pressures in a submerged rubble chimney with a depth of burial of 3,000 feet would be of the order of one hundred atmospheres. Hydrostatic pressure seems to affect metabolic chemical reactions of organisms, possibly through the effect of volume changes in these reactions. Terrestrial bacterial species generally will not grow at 600 atmospheres and may be killed at even lower pressures [27]. Reports by several investigators [28,29,30] indicate that growth is severely retarded at pressures greater than 300 atmospheres for most surface-dwelling species. One investigator reported vigorous growth of several members of each of the genera Pseudomonas, Achrombacter, and Bacillus at pressures of 200 atmospheres [29], though growth of some species was retarded at only 50 atmospheres. Nitrate reduction by most surface-dwelling bacteria is completely inhibited at 400 to 600 atmospheres [30].

There is insufficient evidence to support a firm conclusion about biological denitrification at high pressures, but from the references cited it appears that many bacteria are capable of multiplication and denitrification at 200 atmospheres and that a denitrifying process operating at less than 200 atmospheres would probably be successful. This pressure is equivalent to a water inlet depth of 6800 feet. Since the economics of drilling and casing the inlet and outlet tubes would probably prohibit the construction of a filter at this depth, the effects of hydrostatic pressure can probably be disregarded for most practical filters. However, this conclusion should be experimentally verified.

EFFECTS OF TEMPERATURE ON REACTION RATES

The kinetics of biological waste treatment are strongly affected by temperature. Within broad limits, the rate of denitrification would be expected to increase exponentially with temperature. Increasing the reaction rate would decrease the required detention time. The bacteria may be destroyed at temperatures in excess of about 50°C. Although energy deposited by the nuclear explosion would cause elevated temperatures in the rubble immediately after the detonation, flooding of the chimney would quickly cool the rubble.

The steady-state temperature of the filter will be approximately that of the inflow. The flow-rate through a filter of practical size will be sufficient to nullify the effects of the geothermal gradient, which might be of the order of 1°C per 200 feet of depth. The operating temperature of the filter will vary seasonally with the temperature of the inflow.

AN EXAMPLE--THE SAN JOAQUIN VALLEY DRAINAGE PROBLEM

An example of the possible use of an underground nuclear rubble chimney as a biological filter for anaerobic denitrification is for treatment of irrigation return waters in the San Joaquin Valley of California. The San Joaquin Valley drainage water problem offers an opportunity to compare the economics of a rubble chimney filter with costs of conventional denitrification processes in a typical application.

The San Joaquin Valley is a north-south structural trough about 250 miles long, bounded by the Sierra Nevadas on the east, the Coast Ranges on the west, and the Tehachapi Mountains on the south, comprising the southern part of the Central Valley of California. The topography of this area is illustrated in Figure 4. The climate is semi-arid; annual rainfall varies from approximately 4 inches in the south to 9 inches in the north. Near Hanford a low east-west ridge divides the valley into two separate basins; the southern basin has no surface outlet, and the northern basin drains via the San Joaquin River into the Sacramento-San Joaquin Delta and subsequently into San Francisco Bay.

Much of the valley is productive farmland, but the combination of low rainfall and high potential evapo-transpiration (40-70 inches/year) makes irrigation essential. Little water flows into the valley from the Coast Ranges on the west but several large streams originate in the Sierra Nevada on the east and are diverted for irrigation by a system of dams and canals. As agricultural production increased in the 1940's, the combined yield of pumpage from ground water and diversion of the eastern streams fell short of the demand and the Central Valley Project was developed by the U.S. Bureau of Reclamation (USBR) to import water from the Sacramento Valley. The Delta-Mendota Canal, the first link in this system, was placed in operation in 1951; the proposed network, when completed, will include import canals on both eastern and western slopes of the valley.

Before the construction of the Delta-Mendota Canal only high quality water from the eastern tributaries was used for surface diversion, and salt build-up in the soil was not a general problem. Water imported from the Sacramento River contains agricultural return flows from areas upstream from the canal's intake point and consequently carries a higher salt content than the Sierra runoff; this higher salt content and other factors have caused the deterioration of ground water quality in the west side of the valley. Water quality in the lower San Joaquin River was reduced to levels which caused damage to crops irrigated with the water, and localized highly saline bodies of perched ground water developed. Tile drainage systems had to be installed in some areas.

Increased water imports from the Sacramento Valley via the San Luis Canal and the California Aqueduct are expected to aggravate the salt build-up problem, and, consequently, both the California Water Plan and enabling legislation for the San Luis Project include requirements for tile drainage and return water disposal to remove salts. The USBR has already begun construction of the San Luis Drain, which will serve the Federal San Luis Unit. The location of the drain is shown in Figure 5. The California Department of Water Resources (CDWR) is continuing its studies to construct a drain for the rest of the valley, with the possibility that construction of drain facilities may be postponed until 1980 [1].

When completed, the San Luis Drain will be a concrete-lined canal extending from Kettleman City in the south to a discharge point on the western edge of the Delta near Antioch. The first reach of the canal from Tranquility to a shallow holding reservoir near Gustine (Kesterson Reservoir) is to be completed by January, 1970. The second reach, from Kettleman City to Tranquility, will be completed before January, 1971. The third reach, from Kesterson Regulating Reservoir to Antioch, is scheduled to be completed by January, 1972. Drainage waters will be accumulated in Kesterson Reservoir for the first two years until the third

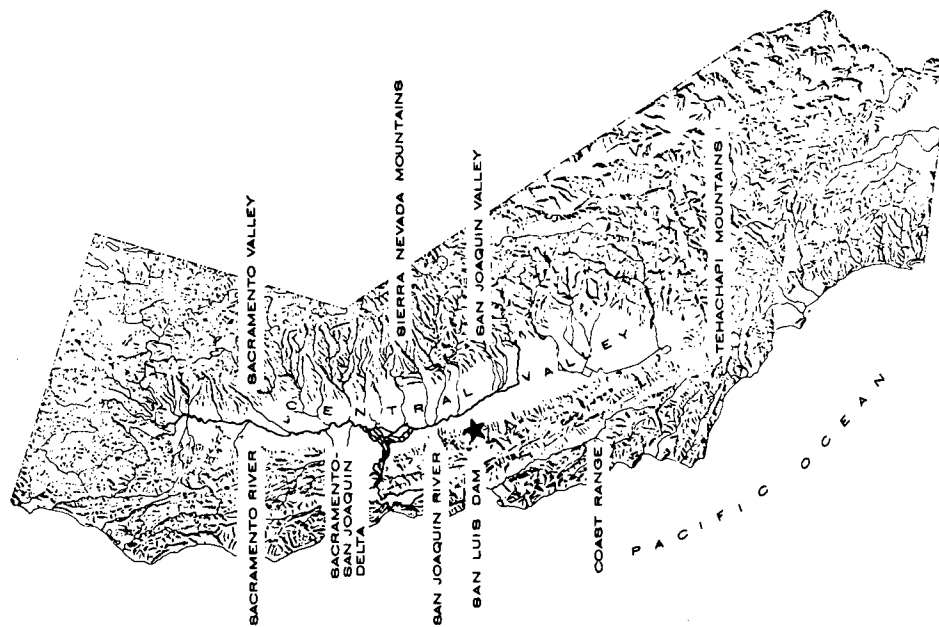


Figure 4. The Central Valley of California

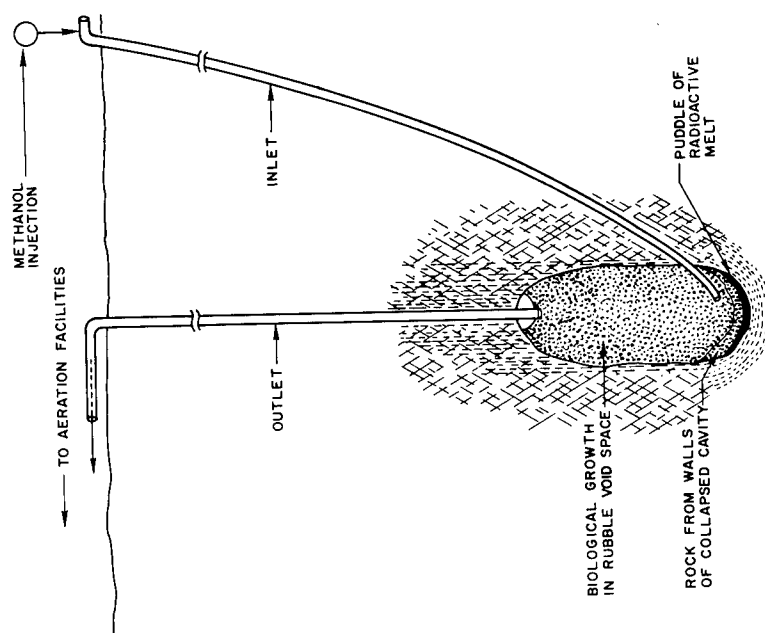


Figure 3. Diagram of a Rubble Chimney Biological Filter

reach to Antioch is completed. The total cost of the drain construction program is between \$50 and \$60 million; this figure includes contingencies for construction of facilities for denitrification and for providing additional reservoir space.

Several possible methods have been suggested for the disposal of San Joaquin Valley return waters. These include pumping the water over the Coast Range into the Pacific Ocean, evaporating the water, and treatment before discharge into the San Francisco Bay - Delta system. The least expensive solution appears to be discharge of the waters into Suisun Bay, part of the San Francisco Bay - Delta system. However, direct discharge of the water into Suisun Bay without treatment may degrade the quality of the receiving waters. The average concentration of nitrate-nitrogen in the return water is expected to be about 20 mg/l, and studies by the Federal Water Pollution Control Administration (FWPCA) indicate that this added nitrogen might cause severe algae blooms in Suisun Bay [3,4].

Investigations of the possible effects of discharging the San Joaquin Master Drain at Antioch indicated that the concentration of nitrogen in the receiving waters would be approximately doubled [3]. It was concluded that such concentrations might cause severe algal growth. The blooms, if they occur, would cause objectionable smells and discoloration of Suisun Bay water. Potential detriments from nutrient enrichment may be prevented if the total nitrogen concentration in the waters of Suisun Bay is maintained below 2 mg/l, but freshwater reaches of the Delta may require a lower limit to prevent blooms of blue-green algae under minimum flow conditions. It was recommended that at least 90 per cent of the nitrogen in the drain waters be removed to meet these limits [3,4].

Table II gives the estimated annual requirements for irrigation return water disposal in the San Joaquin Valley between 1970 and 2050. Available estimates indicate that the amount of brackish agricultural waste waters that will require safe disposal in the valley is 85,000 acre-feet/year in 1970, 440,000 acre-feet/year in 1990, and 580,000 acre-feet/year in 2020. Table III gives USBR estimates of certain water quality factors expected in the San Luis Drain return flows in 1970 and 2020. Initial salt concentrations will be higher because large quantities of salt already present in valley soils will have to be removed by leaching the soils and draining shallow ground water.

The feasibility of using biological treatment for removing nitrogen from the drain waters is being investigated in a joint program by the Federal Water Pollution Control Administration, the California Department of Water Resources, and the U.S. Bureau of Reclamation. Pilot plant studies of both algae stripping and anaerobic denitrification have been performed. Feasibility of the algae stripping process seems to depend on finding a commercial use for the harvested algae, such as livestock feed. Pilot plant studies of both the deep pond process and the anaerobic filter have been performed, and both processes appear technically feasible.

Design of a rubble chimney filter for this application is based on an assumed hydraulic detention time of ten hours. This value has been increased by an order of magnitude over the one-hour detention time recommended by St. Amant and McCarty to allow for uncertainties in the extent of biological solids retention. The void volume required to accommodate the expected ultimate San Joaquin return flow of 580,000 acre-feet/year would then be about $8.2 \times 10^5 \text{ m}^3$, the volume of a sphere of radius 58 m.

Possible locations for a rubble chimney filter in the San Joaquin Valley are severely restricted by the alignment of the San Luis Drain, shown in Figure 5, and the geology of the west side of the valley. Any treatment process for the drain waters should be located downstream from the last return water inflow. Figure 6 indicates that the northernmost drainage problem area is in Contra Costa

TABLE I

PARTICLE SIZE DISTRIBUTIONS FOR CHIMNEYS IN GRANITE AND DOLOMITE

<u>Particle Diameter</u>	<u>Percentage of Chimney Volume</u>	
	<u>Granite [32] (Hardhat)</u>	<u>Dolomite [33] (Handcar)</u>
over 0.3 m.	10%	28.3%
0.15-0.3 m.	40%	38.5%
less than 0.15 m.	50%	33.2%

TABLE II

ESTIMATED ANNUAL AGRICULTURAL WASTE WATER DISPOSAL REQUIREMENT*

Year ¹	Annual Requirement (1000 A-F)		
	San Luis Unit ²	Other parts of valley ³	Total
1970, 1975	5	82	87
1980, 1990	53	200	253
1990, 2005	123	318	441
2000, 2020	155	401	556
2010, 2035	162	414	576
2020, 2050	162	421	583

¹Earliest and latest estimated dates.

²USBR estimate.

³DWR estimates include a requirement for Kern County and a maximum of 40,000 A-F/year for Tulare Lakebed.

*From "Final Report," San Joaquin Valley Drainage Advisory Group, January, 1969, a report to the DWR.

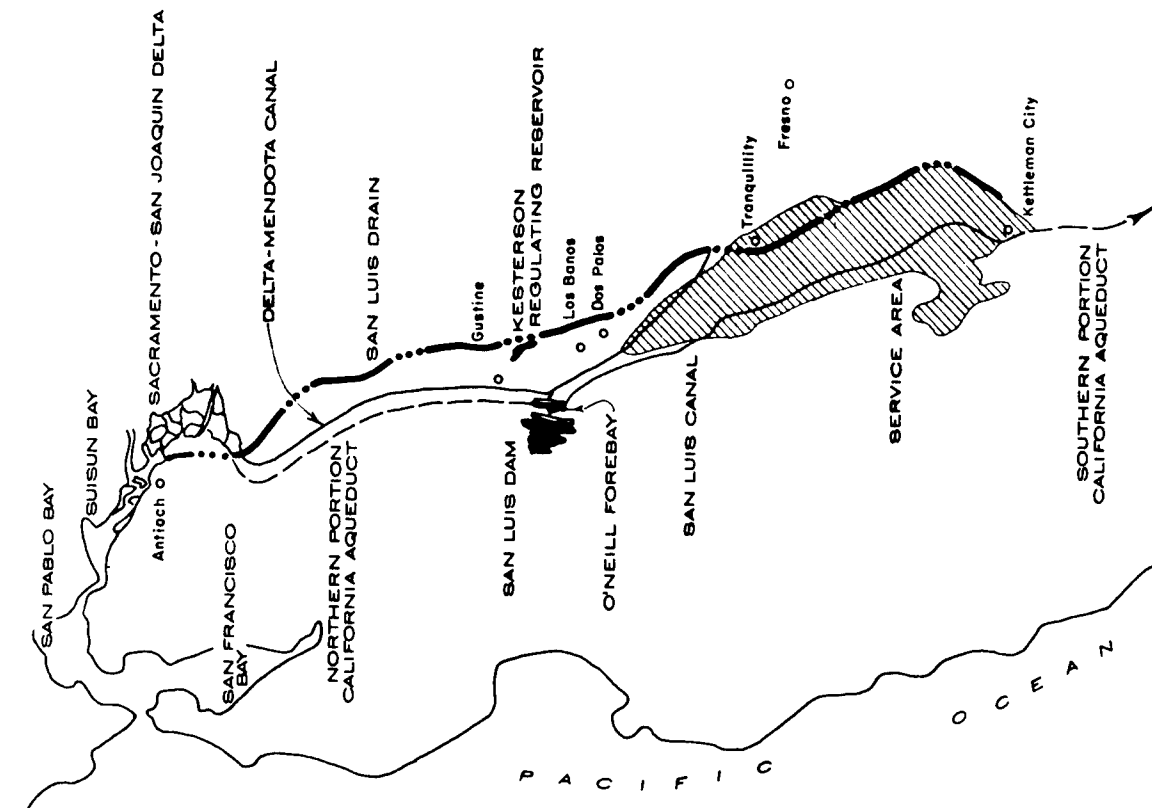


Figure 5. The San Luis Unit and related facilities

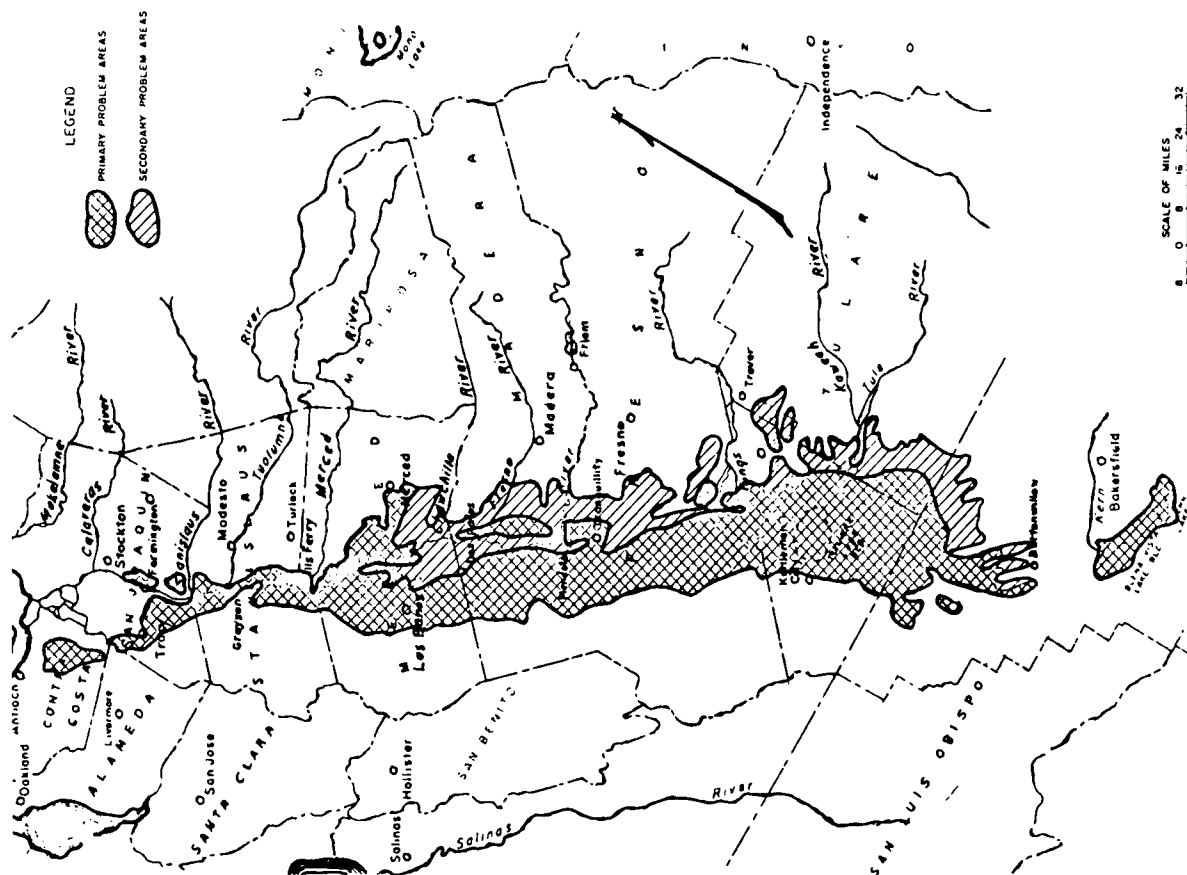


Figure 6. Primary and secondary drainage disposal problem areas

County, close to the discharge point. However, this isolated area would produce only an estimated 10,000 acre-feet/year, or about 1.7% of the expected ultimate flow from the entire valley, according to the San Joaquin Valley Drainage Advisory Group [7]. In terms of the total nitrogen load, this amount is less than the variation in treatment efficiency for the process and can probably safely be left untreated.

The filter would have to be located as close to the drain alignment as possible to minimize pumping costs. Reasonably hard rock which does not decompose upon submersion in water would be necessary. A location which may satisfy these requirements lies in the extreme southeastern corner of Contra Costa County, at a point on the canal alignment about four miles south of the town of Byron. An emplacement hole at this point would contact the upper portion of the Panoche Group, an Upper Cretaceous sedimentary formation. The uppermost formation likely to be encountered in the area is the Moreno Shale. Conformably underlying the Moreno Shale is the Panoche Group, a complex of massive, concretionary sandstones, shale, siltstones, and conglomerate lenses. In the Pacheco Pass Quadrangle, fifty miles to the south, the Moreno Formation is about 1000 feet thick and the Panoche Group is about 25,000 feet thick. In the Pacheco Pass area, the Panoche Group contains a few massive sandstones that might serve as matrix rock for a rubble chimney filter.

Schilling reports that the Panoche Group in the Pacheco Pass area contains two sandstone members at least 850 feet thick and two others over 3000 feet thick [19]. These are located in the upper portion of the Panoche, in what Schilling calls Formation B. He describes the sandstone as arkosic, well-cemented, concretionary, and generally quite solid though friable in places. The composition of this sandstone is 29% quartz, 12% plagioclase, 16% K-feldspar, 17% lithic grains (quartzite, chert, and volcanics), and 5% fine silt and clay matrix, with variable amounts of calcite cement.

The reaction of the sandstone to immersion in water is a problem in geochemical equilibria. Disintegration of the rock will depend on the rate of dissolution of calcium, magnesium, and carbonate ions in the drain water, temperature of the rubble filter, and the hydrostatic pressure. No simple analytic solution can be given. However, the sandstones could be easily tested by immersing samples in drain water.

Figure 7 is an idealized cross-section through the proposed filter site based on the mapping of Pampeyan [21] and the columnar section of the Panoche Group given by Schilling [19] for the Pacheco Pass area. This assumed geology places the bottom of the uppermost sandstone of Formation B about 4500 feet below the surface at the filter location.

The geologic environment of Project Gasbuggy more closely resembles the Panoche Group than does the geology of any other experiment for which adequate data have been published. Experience from Gasbuggy can be used to predict chimney height and void volume for a detonation in Panoche sandstones. The nuclear device would be detonated just below the bottom of the sandstone member, as shown on Figure 7. The chimney void volume would be approximately the volume of the spherical cavity formed by the explosion. The radius of this cavity is given by [34]

$$R_c = C \frac{W^{1/3}}{(\rho h)^{1/4}} \quad (5)$$

where:

R_c = cavity radius, in meters;

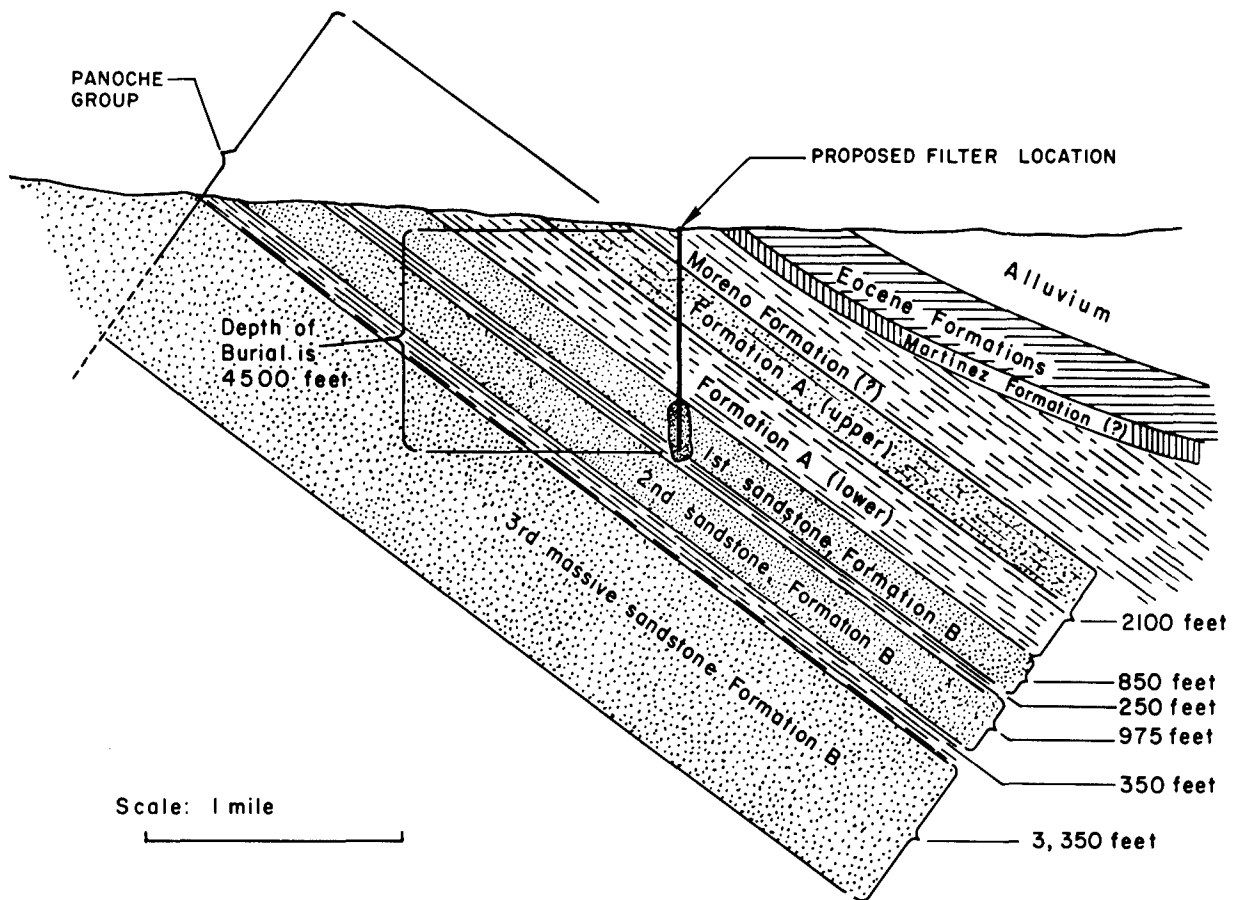


Figure 7. A cross-section through the geological formation at the filter site

- W = energy yield of nuclear device, kilotons;
 ρ = average overburden density, grams/cm³;
 C = empirical constant for a given type of rock.

Higgins and Butkovich [37] have considered the effect of water vapor in estimating the cavity expansion following an underground nuclear explosion, but sufficient experimental data on water content are not available for this purpose.

Substitution of the appropriate values for the proposed site:

- R_c = 58 m,
 ρ = 2.3 g/cm³,
 h = 4500 feet = 1370 m,
 C = 61,

into Eq. (5) indicates that the required energy yield would be about 370 kilotons. The assumptions regarding overburden density and depth of burial strongly influence this estimate. Scaling from Gasbuggy, the chimney height would be approximately 245 meters.

RATE OF BIOMASS PRODUCTION

The rate of biomass production can be estimated from Eq. (4) by assuming that the nitrate-nitrogen concentration is 20 mg/l, the nitrite-nitrogen concentration is negligible, and the initial dissolved oxygen, present in the inflow to the filter is 8.0 mg/l. Complete nitrate removal would produce approximately 12.1 mg/l of cells, corresponding to a mass production of about 990 kg/hr when operating at full capacity. The volume rate of production would be about 5 cubic meters per hour, assuming that solidly packed cells displace a volume of approximately 0.5 per cent per gram of volatile suspended solids per liter [10].

Some small fraction of the biomass produced will escape from the filter but most of the biological solids should be retained, at least during the initial stages of filter operation. Assuming that all biological solids produced are retained in the filter, the time required to fill half of the void volume of the filter would be approximately ten years. If accumulating biomass clogged the filter and interfered with its operation, it is expected that an increased flow-rate through the filter would flush out the excess organisms. The flushed biomass could then be removed from the effluent with appropriate filters and discarded. Since pilot plant studies have not yet confirmed that excess biomass can be satisfactorily removed by flushing, further experimental study of this topic is recommended.

ENVIRONMENTAL EFFECTS

An evaluation of the feasibility of a rubble chimney for waste water treatment must include consideration of the environmental effects of radioactivity produced by the explosion. The concentrations of radionuclides expected in the chimney water after flooding may be estimated by the methods given by Stead [40] and Knox [41,42].

Radioactivity will be created in the explosion by three processes: fission, fusion, and neutron activation. The radioactive fission products include many different radionuclides, but most of these are relatively short-lived and will not be of long-term interest. Of biological significance are the relatively few

long-lived fission products, such as Sr-90 and Cs-137. The required device yield is estimated to be 370 kt. If the device used is one of the family of Flowshare explosives announced in 1964, the fraction of the total yield contributed by fission could be relatively small, on the order of three kilotons. Most of the device energy may be derived from fusion, which produces tritium in amounts of the order of 20 kilocuries per kiloton. Activation products of the explosion will depend on the chemical composition of the device itself, the casing of the emplacement hole, and the surrounding rock.

Quantities of selected radionuclides which would be produced by a 370 kt explosion with 3 kt of fission yield are given in Table IV. Also listed are the fraction of the radionuclides which would be found in the rubble and concentration guides for water recommended by the NCRP in NBS Handbook 69.

It is assumed that radionuclides are distributed throughout the zone of intense dynamic fracturing by direct explosive action. Stead [40] assumed a spherical geometry for the zone of fracturing, and the discussion presented here will also assume a spherical crushed zone. Porosity and grain density of the sandstone are assumed to be 10 per cent and 2.5 grams/cm^3 , respectively.

Experience from the Gasbuggy experiment indicates that tritium will rapidly form HTO and that tritium ion exchange with the sandstone is negligible [45]. Assuming that the Panoche Sandstone will fracture to 4.2 times the initial cavity radius, similar to conservative estimates of fracturing produced by the Gasbuggy detonation, the 7.4×10^6 curies of tritium produced will be diluted in approximately $6.8 \times 10^{12} \text{ ml}$ of water, resulting in a tritium concentration of the order of $1.1 \text{ } \mu\text{Ci/ml}$, about 1100 times the NCRP standard. Two methods are considered for reducing tritium concentrations to acceptable levels.

One is to purge the chimney by forcing water through the rubble in normal operating fashion. This water would be removed at the outlet and disposed of by diluting to reduce the tritium concentration to the required concentration. The volume of water would also depend on the hydraulic detention time used for purging. If long hydraulic detention times are used, the water in the chimney will mix with influent water and concentrations will decrease nearly exponentially with the total volume of water passed through the chimney [38]. In this case, a purging volume of water equal to nine times the void volume of the chimney would reduce the concentration of tritium by about four orders of magnitude. If short hydraulic detention times were used, water in the chimney would be displaced in a piston-like fashion, and purging would require less water.

The other method of purging the chimney of tritium could be used if the surrounding formation were sufficiently permeable and if the hydraulic head of the ground water were less than the hydraulic head in the chimney. In this case, water would flow from the flooded chimney into the formation. For a case where the chimney completely penetrates a confined aquifer, the flowrate into the formation would depend on the formation permeability and thickness, the radius of intense dynamic fracturing, the difference in hydraulic heads between the chimney and the formation, and on time. Assuming a formation thickness of about 800 feet, a formation permeability of 50 millidarcies, and a difference in hydraulic heads of 1,000 feet between the chimney and the formation, flowrates out of the chimney during the first several months might average about 2.4×10^4 cubic meters/day, or 34 days per chimney void volume. Thus, if the chimney were allowed to stand while adding water to balance the flow into the formation, tritium levels would be reduced below $1.0 \times 10^{-3} \text{ } \mu\text{Ci/ml}$ within 10 months.

Ion exchange will be significant for radionuclides other than tritium. Some portion of the Sr-90 will be adsorbed onto the rubble material, and an ion exchange equilibrium will be reached between the water and the solids. Assuming that 520 curies of Sr-90 will equilibrate with about 1.3×10^{14} grams of solids

TABLE III
ESTIMATED CONCENTRATIONS OF SUBSTANCES IN SAN LUIS DRAIN WATERS

Substance	1970 Conditions (mg/l)	2020 Conditions (mg/l)
Total Dissolved Solids	7,000	3,000
Salts:		
Sulfate	3,000	700
Sodium	1,500	700
Chloride	1,200	900
Calcium	300	100
Magnesium	200	50
Bicarbonate	200	100
Potassium	20	10
Boron	10	3
Nutrients:		
Total Nitrogen*	20	20
Total Phosphate	0.15	0.15

*Virtually all of the nitrogen is expected to be present as nitrate nitrogen.

TABLE IV
SELECTED RADIONUCLIDES PRODUCED BY 3 KT OF FISSION (U-235)
AND 370 KT OF FUSION

Nuclide	Amount Produced (Ci) [41]	Half-Life	Tolerance Level Recommended by NCRP* (μ Ci/ml)
Sr-90	520	28 yr	3×10^{-8}
Cs-137	510	30 yr	7×10^{-6}
Ru-106	960	365 days	3×10^{-6}
Ce-144	1.8×10^4	290 days	3×10^{-6}
Tritium	7.4×10^6	12.3 yr	1×10^{-3}

*Recommended values for the general population in an uncontrolled area. These values were obtained by dividing occupational concentration guides (for a 168-hour week) recommended by the National Council on Radiation Protection in NBS Handbook 69 by a factor of 10 for the general population and by another factor of 3 recommended by the Federal Radiation Council to allow for deviations of individuals from the sample average.

and 6.8×10^{12} ml of water and that the distribution coefficient for Sr-90 for the combination of drain water and sandstone will be on the order of $10 \text{ cm}^3/\text{gm}$, the initial concentration of Sr-90 in the water might be about one order of magnitude above the concentration guide of $3 \times 10^{-8} \text{ } \mu\text{Ci/ml}$. For a distribution coefficient for Cs-137 of about $100 \text{ cm}^3/\text{gm}$, the initial concentration of Cs-137 might be two orders of magnitude below the concentration guide of $7 \times 10^{-6} \text{ } \mu\text{Ci/ml}$.

Concentrations of Sr-90, Cs-137, and other radionuclides affected by ion exchange would be reduced by purging the chimney with water, but their rate of removal from the chimney would not equal that of tritium. Ion exchange would alter the dynamics of purging from the perfect mixing model applicable to tritium. Rabb [39] has reported on small-scale batch-leaching tests of granite rubble from the Piledriver chimney. These tests indicated that about one-third of the gamma-ray emitting activity in the rubble would be removed with the initial volume of water through the chimney. Rabb indicated that further dissolution and extraction would proceed at a slower rate, so that years might be required to attain 60 to 75 per cent extraction from the rubble.

The presence of large masses of bacteria in the chimney would add to the total mass available for ion exchange. The bacteria would have effective distribution coefficients much higher than those of the sandstone, and large masses of biological solids in the chimney would significantly reduce the fraction of radionuclides released to the water. The effects of the presence of biological solids on leaching of radioactivity from the chimney should be investigated.

While tritium cannot be removed from the filter effluent, radionuclides affected by ion exchange could be removed by filter beds with appropriate ion-exchange properties. Water used in the purging phase of filter construction could be passed through such filters to avoid the necessity of discharging these radionuclides to the receiving waters.

COMPARISON OF COSTS WITH ALTERNATIVE PROCESSES

The main operating expense for anaerobic denitrification will be the cost of the injected methanol. Eq. (3) with an assumed nitrate-nitrogen concentration of 20 mg/l , a dissolved oxygen concentration of 8 mg/l , and a cost of \$0.25 per gallon for methanol indicates the annual cost for methanol to treat the design capacity would be about \$3,350,000.

Electric power for pumping is another important operating expense. McCarty [9] estimated pumping power costs for the anaerobic ponds at about \$150,000, assuming a price of \$0.01 per kilowatt hour. The total hydraulic head loss for the rubble chimney process is the sum of the head loss through the chimney plus the head loss through the inlet and outlet tubes. Assuming a rubble particle size distribution similar to that reported by Boardman, *et. al.*, [33] for the Handcar experiment in dolomite, calculations (using standard techniques for predicting head losses through graded crushed rock) indicate that head losses through the chimney will be less than one foot. Head loss through the inlet and outlet tubes will be much greater than head loss through the rubble for any feasible tube size. Losses through tubes of seven-foot diameter would be approximately 80 feet, assuming tube lining with approximately the same roughness as commercial iron pipe. At a power cost of \$0.01 per kilowatt-hour, this head loss would result in annual pumping costs of about \$600,000 when operating at design capacity. For ten-foot diameter tubes, total head losses would be about 15 feet and annual pumping costs would be about \$115,000.

Preliminary estimates of construction costs for the rubble chimney filter compare favorably with estimated construction costs of the alternative treatment processes. The estimates given here do not include the cost of auxiliary facilities such as equipment for methanol injection, effluent re-aeration, and

finishing. However, auxiliary equipment required for the rubble chimney filter will be essentially the same as required for the two conventional anaerobic treatment processes.

Device and emplacement costs listed in Table V-a are based on device cost estimates released by the Atomic Energy Commission in 1964 [34] and on published estimates of the Gasbuggy operations costs [35]. Costs of the ten-foot diameter inlet and outlet tubes are based on drilling costs for the emplacement of large-diameter nuclear devices published by Hair [36]. Construction costs for the inlet and outlet tubes account for more than 80% of the total estimated cost of \$16,000,000.

Tables V-a and V-b show that the rubble chimney filter might cost about \$1,900,000 less than a conventionally-constructed anaerobic filter at the same location, \$10,000,000 less than the anaerobic pond process, and about \$28,000,000 less than the algae stripping process. The indicated cost advantage of the rubble chimney filter is very significant compared with the anaerobic pond and algae stripping processes but less significant compared with the conventional filter.

The estimates quoted for the rubble chimney filter should be viewed with caution because the largest single item, construction of the inlet and outlet tubes, is based on questionable projections of costs for drilling slightly smaller holes. The casing or lining of these holes comprises about 85% of their estimated cost. A steel casing with two-inch walls and steel-rib reinforcing was assumed. Some less expensive way of lining the tubes might be found. The cost advantage of the rubble chimney filter in this application depends primarily on the cost of the tube lining, not on the cost of the nuclear operations phase.

CONCLUSIONS

The San Joaquin example points out certain conclusions which apply to the general concept of using rubble chimneys for biological treatment. Because a filter constructed at the Byron location would have to be located 4500 feet beneath the surface, the estimated cost of constructing the inlet and outlet tubes is very high compared to other phases of the construction. Inlet and outlet tubes for a chimney at a shallower depth of burial would cost much less. The large depth of burial at the Byron location also dictates a much larger device yield than would be required at a shallower depth to produce the same chimney void volume. A smaller device producing the same void volume at a shallower depth would produce lower initial radioactivity concentrations, and the initial phase of radioactivity purging would require less time.

In any application of a rubble chimney filter, the most significant cost is likely to be the construction of the inlet and outlet tubes. Their cost can be minimized by locating the filter at as shallow a depth as permitted by the geology of the locale. Cost of the device emplacement hole will increase with both diameter and depth, but costs of other phases of filter construction are likely to remain nearly constant regardless of filter capacity. The cost of the nuclear operations phase will vary little with device yield. The concept of waste water treatment with rubble chimney filters appears to be economically feasible provided shallow depths of burial can be used.

Waste water treatment with rubble chimney filters also appears technically feasible, but certain aspects of the concept should receive further experimental investigation. Experiments to determine biological solids retention in rubble material are indicated. If the necessary hydraulic detention time could be reduced to one hour, both the void volume and the device yield could be reduced by a factor of ten below the values assumed in the discussion above. Reduction of the device yield would reduce the initial concentrations of radioactivity correspondingly.

TABLE V-a
COSTS FOR NUCLEAR CONSTRUCTION

ITEM	ESTIMATED COST
Geologic Test Hole	\$ 70,000
Emplacement Hole	450,000
Device Cost (370 kilotons)	500,000
Safety	425,000
Support	910,000
Inlet and outlet tubes (2 holes, 10-foot inside dia., lined, 4500 feet deep)	13,000,000
Engineering and inspection	200,000
Contingency	400,000
5 acre construction site (\$2200/acre plus acquisition costs)	15,000
TOTAL	\$15,970,000

TABLE V-b
CONSTRUCTION COSTS FOR ALTERNATIVE PROCESSES

<u>Algae Stripping Ponds</u>	
ITEM	ESTIMATED COST
Purchase of land (9000 acres between Delta and Bethany at \$2200/acre plus acquisition costs)	\$19,900,000
Land Development and Piping (9000 acres at \$2650/acre)	23,850,000
TOTAL	\$43,750,000
<u>Anaerobic Denitrification Ponds</u>	
Purchase of land (1,500 acres between Delta and Bethany at \$2200/acre plus acquisition costs)	\$ 4,425,000
Land Development and Piping (1,500 acres at \$2650/acre plus 30¢/sq.ft. for pond covers)	23,625,000
TOTAL	\$26,950,000

Conventionally Constructed Anaerobic Denitrification Filters

ITEM	ESTIMATED COST
Purchase of land (200 acres between Delta and Bethany at \$2200/acre plus acquisition costs)	\$ 450,000
Filter Construction* (8.7 million cubic feet of stone at \$2.00 per cubic foot)	17,000,000
<u>TOTAL</u>	<u>\$17,850,000</u>

*Based on a one-hour detention time for the design capacity, 33% void volume in the stones, and a cost of \$2.00 per cubic foot for the stones in place, as estimated by St. Amant and McCarty [12].

Costs quoted in Table V-b are based on [9,12,46,47].

The effects of temperature and pressure on the denitrification process should be verified by experiment. The rate of leaching of radioactivity from a chimney containing large amounts of biological solids should be further investigated. The concept appears sufficiently promising to justify further attention.

Preliminary estimates of construction costs for the rubble chimney filter in the San Joaquin Valley example compare favorably with estimated construction costs for the alternative treatment processes. If another location permitting a shallower depth of burial could be found, the rubble chimney filter would offer significant cost advantages over the alternatives in this particular application. The rubble chimney filter also offers aesthetic advantages over the conventional alternatives. All of the conventional treatment processes require larger physical plants covering many acres, and the anaerobic pond and algae stripping processes are likely to produce unpleasant odors. The rubble chimney filter would produce no odors and would require only a few acres of land for housing auxiliary equipment.

ACKNOWLEDGEMENTS

The authors acknowledge the support of Roy B. Evans at Stanford University by the U.S. Public Health Service and the training grant from the U.S. Atomic Energy Commission, Division of Peaceful Nuclear Explosives.

BIBLIOGRAPHY

DRAINAGE WATER PROBLEM

1. California State Department of Water Resources, "Current Status of Drainage Facilities for the San Joaquin Valley," (February, 1968).
2. Pafford, R.J., Jr., and Price, E.P., "A Disposal System for Agricultural Waste Waters in the San Joaquin Valley of California," proceedings of the Fourth Technical Conference, U.S. Committee on Irrigation, Drainage, and Flood Control, Phoenix, Arizona (March, 1968).
3. Federal Water Pollution Control Administration, Southwest Region, "San Joaquin Master Drain: Effects on Water Quality of San Francisco Bay and Delta; Appendix, Part C: Nutrients and Biological Response," (August, 1968).
4. Federal Water Pollution Control Administration, Southwest Region, "San Joaquin Master Drain: Effects on Water Quality of San Francisco Bay and Delta (January, 1967).
5. Huffman, Elmo W., "Waste Water Disposal: San Joaquin Valley, California," Journal of the Irrigation and Drainage Division, Proceedings of the ASCE, 4847, IR-2 (June, 1966).
6. California State Department of Water Resources, "Bulletin No. 127: San Joaquin Valley Drainage Investigation," Preliminary Edition (January, 1965).
7. San Joaquin Valley Drainage Advisory Group, "Final Report," Fresno (January, 1969).
8. Johnston, William R., "Drainage Problems and the Proposed Solution for a Large Irrigated Area in the San Joaquin Valley of California (USA)," proceedings of the Seventh International Congress of the International Commission on Irrigation and Drainage, Mexico City (April, 1969).

ANAEROBIC FILTER

9. McCarty, P.L., "Feasibility of the Denitrification Process for Removal of Nitrate-Nitrogen from Agricultural Drainage Water," report to the San Joaquin District, California State Department of Water Resources (1966).
10. Young, James C., and McCarty, P.L., "The Anaerobic Filter for Waste Treatment," Technical Report No. 87, Department of Civil Engineering, Stanford University (March, 1968).
11. McCarty, P.L., Beck, Louis, and St. Amant, Percy, "Biological Denitrification of Wastewaters by Addition of Organic Materials," proceedings of the 24th Annual Purdue Industrial Waste Conference, Purdue University (May, 1969).
12. St. Amant, Percy, and McCarty, P.L., "Treatment of High Nitrate Waters," proceedings of the 89th Annual Conference, American Water Works Association, San Diego, California (May, 1969).
13. Tambllyn, Thomas A., and Sword, Brian R., "The Anaerobic Filter for Denitrification of Agricultural Sub-surface Drainage," proceedings of the 24th Annual Purdue Industrial Waste Conference, Purdue University (May, 1969).
14. Tambllyn, Thomas A., Personal Communication, (July, 1969).

HYDROLOGY OF SAN JOAQUIN VALLEY

15. Davis, G.H., Green, J.H., Olmsted, F.H., and Brown, D.W., "Groundwater Conditions and Storage Capacity in the San Joaquin Valley, California," U.S.G.S. Water Supply Paper No. 1469 (1959).
16. Davis, G.H., Lofgren, B.E., and Mack, Seymour, "Use of Groundwater Reservoirs for Storage of Surface Waters in the San Joaquin Valley, California," U.S.G.S. Water Supply Paper No. 1618 (1964).

GEOLOGY

17. California State Department of Natural Resources, "San Jose Sheet," Geologic Atlas of California (1966).
18. Page, Ben M., "Geology of the Coast Ranges of California," Geology of Northern California, Bulletin 190, California Division of Mines and Geology (1966).
19. Schilling, F.A., The Upper Cretaceous Stratigraphy of the Pacheco Pass Quadrangle, California, unpublished Ph.D. thesis, Stanford University (1962).
20. Davis, F.F., and Goldman, H.B., "Mines and Mineral Resources of Contra Costa County, California," California Journal of Mines and Geology, vol. 54, no. 2 (October, 1958).
21. Pampeyan, Earl H., Geology and Mineral Resources of Mount Diablo, Contra Costa County, California, Special Report No. 80, California Division of Mines and Geology (1964).
22. Geological Society of Sacramento, Guidebook to The Mount Diablo Field Trip, Sacramento (1964).
23. Bishop, Charles C., personal communication (July, 1969). Geologist, California Division of Mines and Geology.

24. Remson, Irwin, Ph.D., Professor of Geology, Stanford University, personal communication (July, 1969).
25. Rich, Ernest I., Asst. Dean, School of Earth Sciences, Stanford University, personal communication (July, 1969).
26. Dickinson, William R., Ph.D., Professor of Geology, Stanford University, personal communication (July, 1969).

EFFECTS OF PRESSURE

27. Lamanna, Carl, and Mallette, M. Frank, Basic Bacteriology, second edition, p. 444ff, Williams and Wilkins Co., Baltimore (1959).
28. ZoBell, C.E., and Johnson, F.H., "The Influence of Hydrostatic Pressure on the Growth and Viability of Terrestrial and Marine Bacteria," Journal of Bacteriology, 57:179-189 (1949).
29. ZoBell, C.E., and Oppenheimer, C.H., "Some Effects of Hydrostatic Pressure on the Multiplication and Morphology of Marine Bacteria," Journal of Bacteriology, 60:771-781 (1950).
30. ZoBell, C.E., and Morita, R.Y., "Barophilic Bacteria in Some Deep Sea Sediments," Journal of Bacteriology, 73:563-568 (1957).

NUCLEAR EXPLOSION TECHNOLOGY

31. Rawson, D.E., Korver, J.A., Pritchard, R.L., and Martin, W., "Gasbuggy Postshot Geologic Investigations," AEC Report PNE-G-11 (UCRL-71354), (November, 1968).
32. Boardman, Charles R., Rabb, David D., and McArthur, Richard D., "Contained Nuclear Explosions in Four Media--Geologic Factors in Cavity and Chimney Formation," Engineering with Nuclear Explosives, Proceedings of the Third Powshare Symposium, U.S.A.E.C., TID-7695, p. 109ff (1964).
33. Boardman, Charles R., Meyer, G. Lewis, Rabb, David D., "Macrodeformation Resulting from the Handcar Event," AEC Technical Report UCRL-50149 (December, 1966).
34. Teller, Edward, Talley, Wilson K., Higgins, Gary H., Johnson, Gerald W., The Constructive Uses of Nuclear Explosives, McGraw-Hill, San Francisco, (1968).
35. El Paso Natural Gas Company, U.S. Atomic Energy Commission, U.S. Bureau of Mines, Lawrence Radiation Laboratory, "Project Gasbuggy," AEC Report PNE-1000, El Paso, May 14, 1965.
36. Hair, J.L., "Construction Techniques and Costs for Underground Emplacement of Nuclear Explosives," U.S. Army Engineer Nuclear Cratering Group, Livermore, AEC Report PNE-5004F, April 1969.
37. Higgins, G.H., and Butkovich, T.R., "Effect of Water Content, Yield, Medium, and Depth of Burst on Cavity Radii," Lawrence Radiation Laboratory, Livermore, February 21, 1967 (AEC report UCRL-50203).
38. Higgins, G.H., Rabb, David D., and Rodean, H.C., "Theoretical and Experimental Studies Relating to the Purging of Radioactivity from a Gas Well Stimulated by a Nuclear Explosion," Lawrence Radiation Laboratory, Livermore, December 24, 1968 (AEC report UCRL-50519).

39. Rabb, David D., "Size Distribution Study of Piledriver Particles," Lawrence Radiation Laboratory, Livermore, October 1, 1968 (AEC report UCRL-50489).
40. Stead, Frank W., "Distribution in Groundwater of Radionuclides from Underground Nuclear Explosions," in Engineering with Nuclear Explosives, Proceedings of the Third Plowshare Symposium, AEC report TID-7695.
41. Knox, J.B., "Water Quality in Flooded Nuclear Craters," Lawrence Radiation Laboratory, Livermore, December 9, 1968, (AEC report UCRL-51531).
42. Knox, J.B., Groundwater Safety Appendix to UCRL-7350 Rev. I, "Characteristic Effects of Contained Nuclear Explosives for Evaluation of Mining Applications," Livermore (1963).
43. Batzel, Roger E., "Radioactivity Associated with Underground Nuclear Explosions," Lawrence Radiation Laboratory, Livermore (June 23, 1959). (AEC Report UCRL-5623).
44. Korver, J.A., "Fluid Flow from Nuclear Chimneys," Water Resources Research, Vol. 2, no. 2 (second Quarter 1966).
45. Smith, C.F., and Momyer, F.F., "Studies of Chemical and Radiochemical Composition of Natural Gas from the Cavity Produced by the Project Gasbuggy Nuclear Shot," Radiological Health Data and Reports, vol. 10, no. 7, July 1969.

COST ESTIMATES

46. Powell, W.H., "San Joaquin Valley Drainage Facilities Land Aquisition Estimates," DWR Memorandum, 18 November, 1968.
47. Tamblyn, Thomas A., FWPCA, Fresno, personal communication, July, 1969.

SCIENTIFIC APPLICATIONS

THE PRESENT STATUS OF SCIENTIFIC APPLICATIONS OF NUCLEAR EXPLOSIONS*

G. A. Cowan and B. C. Diven

Los Alamos Scientific Laboratory, University of California
Los Alamos, New Mexico

This is the fourth in a series of symposia which started in 1957 at Livermore with the purpose of examining the peaceful uses of nuclear explosives.¹ Although principal emphasis has been placed on technological applications, the discussions have, from the outset, included the fascinating question of scientific uses. Of the possible scientific applications which were mentioned at the 1957 meeting, the proposals which attracted most attention involved uses of nuclear explosions for research in seismology. It is interesting to note that since then a very large and stimulating body of data in the field of seismology has been collected from nuclear tests. Since a parallel session of this conference is devoted to seismology, it will not be discussed further in this session.

Ideas for scientific applications of nuclear explosions go back considerably further than 1957. During the war days Otto Frisch at Los Alamos suggested that a fission bomb would provide an excellent source of fast neutrons which could be led down a vacuum pipe and used for experiments in a relatively unscattered state.² This idea, reinvented, modified, and elaborated upon in the ensuing twenty-five years, provides the basis for much of the research discussed in this morning's program.

In 1952 a somewhat different property of nuclear explosions, their ability to produce intense neutron exposures on internal targets and to synthesize large quantities of multiple neutron capture products, was dramatically brought to our attention by analysis of debris from the first large thermonuclear explosion (Mike) in which the elements einsteinium and fermium were observed for the first time.³ Most of the remainder of this morning's program will be devoted to reports on experiments whose origin can be traced back to this observation.

The reports of the next two Plowshare symposia in 1959 and 1964^{4,5} help record the fascinating development of the scientific uses of neutrons in nuclear explosions. Starting with two "wheel" experiments in 1958 to measure symmetry of fission in ^{235}U resonances, the use of external beams of energy-resolved neutrons was expanded on the "Gnome" experiment in 1961 to include the measurement of neutron capture excitation functions for ^{238}U , ^{232}Th , ^{197}Au , and ^{180}Hf by M. Lindner at Livermore. The list of experiments grew longer in 1964 with the addition of several fission cross-section measurements, marking the beginning of the physics cross-section measurement program at Los Alamos. Since then four more nuclear tests with energy-resolved neutron beams have been used for physics and nuclear chemistry experiments, one each in 1965, 1967, 1968, and 1969. The major developments during this period include successive

* Work performed under the auspices of the U. S. Atomic Energy Commission.

large increases in numbers of measurements on each new test, a steady improvement in our ability to prepare and to measure the neutron cross sections of very small samples and very radioactive samples, an expansion in the capacity to record and analyze enormous numbers of data points, and a better understanding of the techniques for shaping the neutron spectrum to best satisfy the varying demands of a large number of experimentalists.⁶⁻²⁰ By 1969 the number of experiments on a single test had grown to thirty-two (Table I) accommodated in a five-story tower mounted on rails so that all equipment could be removed from the immediate area of the explosion before ground collapse.

TABLE I

Measurements Performed on Physics Experiment, NTS, Summer, 1969

<u>Fission</u>	<u>Capture</u>	<u>Scattering</u>	<u>Transmission</u>
Am-243	Au-197	Yt-89	Pu-239
Bk-249	Th-232	Ta-181	
Cf-249, 252	U-238	Pu-239	
Cm-243, 4, 5, 6, 7, 8	Cm-244, 6		
Es-253	Pu-239		
Np-237			
Pu-239, 242, 4			
U-232, 4, 6, 8			

Other:

Further investigation of the symmetry of fission at resonances in ^{235}U

Ratio of neutron capture cross sections for production of isomers of ^{134}Cs at resonances

Neutron polarization by transmission through LMN polarized proton crystal at 1°K

A particularly striking illustration of the improvement in energy resolution and collimation of the neutron beam in "wheel" experiments is available from comparison of autoradiographs of exposed ^{235}U in the 1958 "Quay" experiment, the 1961 "Gnome" experiment, and in the recent 1969 experiment (Figs. 1, 2, and 3).

The external neutron beam is uniquely suitable for the measurement of cross sections of small, frequently highly radioactive nuclides and its application to such measurements will continue to increase. A number of such measurements have been done but a large number remain.

Fission cross sections of twenty-eight nuclides have been measured using nuclear explosion sources. Some of these experiments could have been performed in the laboratory but others are impossible using laboratory techniques. Nearly as many remain with lifetimes suitable for nuclear explosion work. As might be expected, the remaining nuclides present formidable problems of sample preparation; the fact that very small samples are usable with our intense sources is in many cases the deciding factor in determination of practicability of the measurement.

Capture cross-section measurements have been made on several nuclides including some such as ^{147}Pm , ^{152}Eu , and ^{154}Eu that are extremely radioactive.

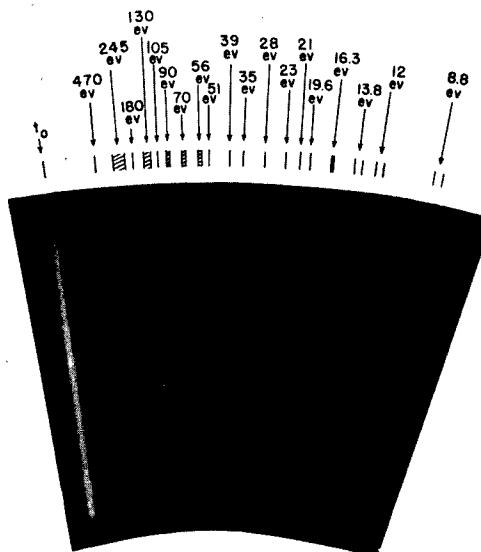


Fig. 1. Autoradiograph of ^{235}U wheel, 1958 experiment.

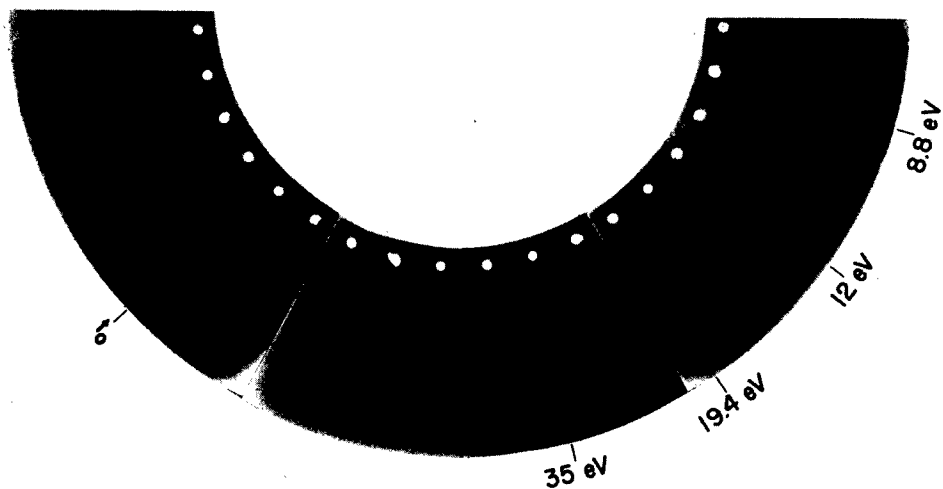


Fig. 2. Autoradiograph of ^{235}U wheel, 1961 experiment.

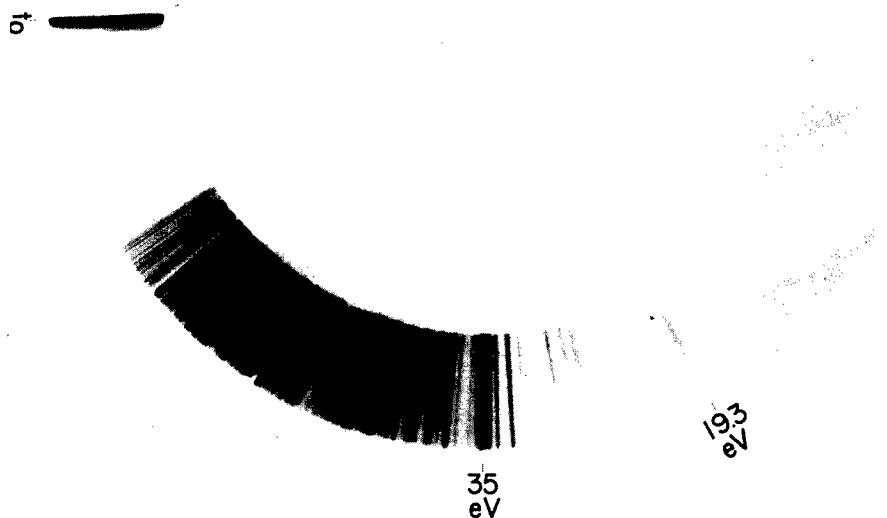


Fig. 3. Autoradiograph of ^{235}U wheel, 1969 experiment.

Both the fission products and the heavy elements provide many examples of radioactive materials whose neutron capture cross section is needed for practical purposes but whose radioactivity precludes the measurement except with the intense beam of neutrons from an explosion source.

Measurements of neutrons resonantly scattered from nuclei have been plagued with intensity problems. We shall hear later in the program of the elegant experiments that can be performed when lack of intensity in the neutron beam poses no difficulty.

Finally, it was demonstrated in the 1969 experiment that the neutron beam from a nuclear explosion can be polarized and this has opened up an entirely new set of experiments for us to consider. Polarization experiments have always been famous for their low counting rates. The combination of our intense beams of neutrons and an efficient method for polarization of those neutrons is certain to result in many very interesting research efforts on future shots.

Like the external beam experiments, the multiple neutron capture experiments have established an impressive record of development and improvement. The principal advance in the experimental technique has been in the neutron source. A figure of merit in these experiments is the size of the term $\int n v dt$, the time-integrated neutron flux or exposure of the target expressed in neutrons per cm^2 or per barn. In a review of this subject in early 1967²¹ we plotted the highest exposure achieved by the end of each year for the years 1963-1966 and extrapolated this curve through 1967. However, no new devices were tested until the "Hutch" event conducted by Livermore last summer. Nevertheless, the 1967 extrapolation nearly fits on our actual experience curve from which we might draw the conclusion that designs with computers evolve and improve with time independently of the frequency of actual tests (Fig. 4).

Another figure of merit in these experiments is the total amount of ^{257}Fm made in recent devices, a figure which has increased dramatically between 1964 and 1969 (Fig. 5). Despite this enormous increase, no nuclides heavier than ^{257}Fm have been identified in the "Hutch" debris. Accordingly, we now hypothesize that there are short-lived spontaneous fissioning species (half-lives of less than one day) in every mass chain through mass 265 which lead to the disappearance of these chains before the debris is recovered and chemistry is completed. This explanation is supported by empirical extrapolations of the known spontaneous fission half-lives to this mass region but, unfortunately, we still have no certain guidance as to what may occur in even heavier regions.

There is some reason to believe that a mere repetition of the "Hutch" experiment with the addition of a prompt sample recovery system would lead to the identification of new short-lived heavy nuclides. It can also be argued, somewhat more optimistically, that a new device should be tested at the limit of the present state-of-the-art in the hope that a region of greater stability would be reached. However, the highest mass number made in such an advanced experiment might be 275 or 280. Consequently, it would be rash to predict that the capture chain in such an experiment would pass through the short-lived region above mass 257 and reach a predicted island of stability which is presently thought to exist in the neighborhood of mass 298.

Perhaps a more promising prospect for achieving the kind of experimental information we need to guide our further efforts lies in the direction of large-scale recovery and extraction of products from a "Hutch" type device. For the first time in "Hutch" it has been demonstrated that macroscopic quantities of ^{257}Fm can be made. Other uniquely heavy and neutron-rich products include ^{250}Cm and ^{254}Cf . The ^{257}Fm can be used to determine the properties of its immediate neighbors ^{258}Fm , ^{259}Fm , ^{259}Md , ^{259}No , ^{260}No , and ^{257}Es . By heavy ion bombardments, neutron evaporation products can be obtained from each of the

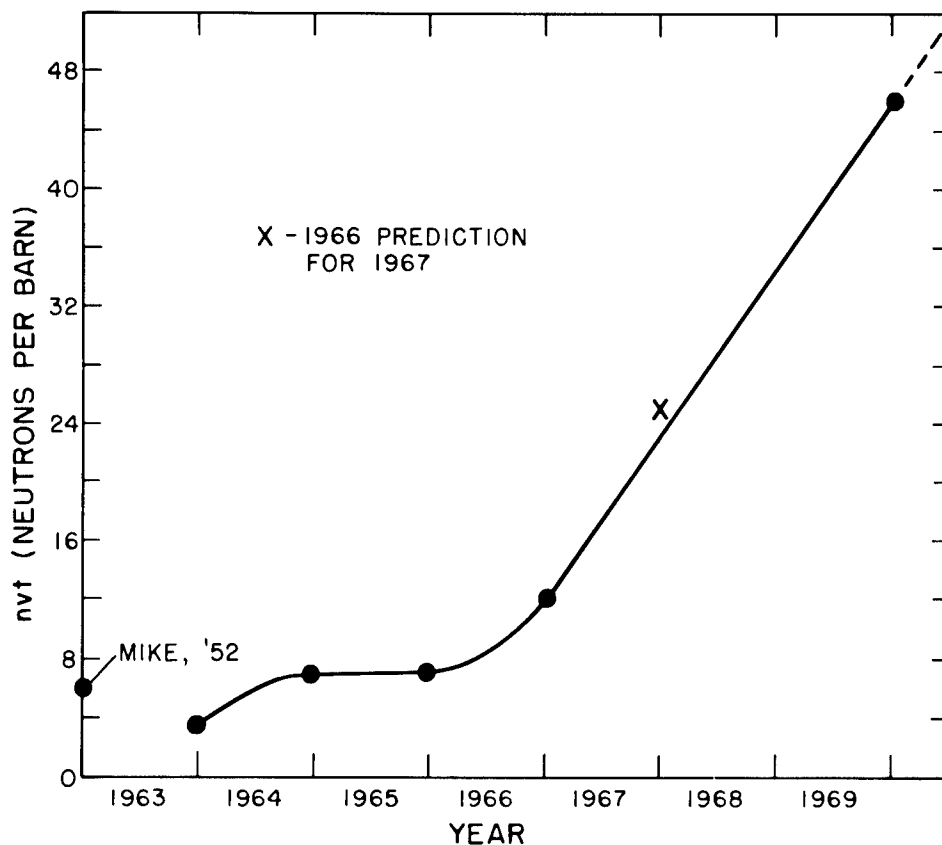


Fig. 4. Improvement in neutron exposure since 1963.

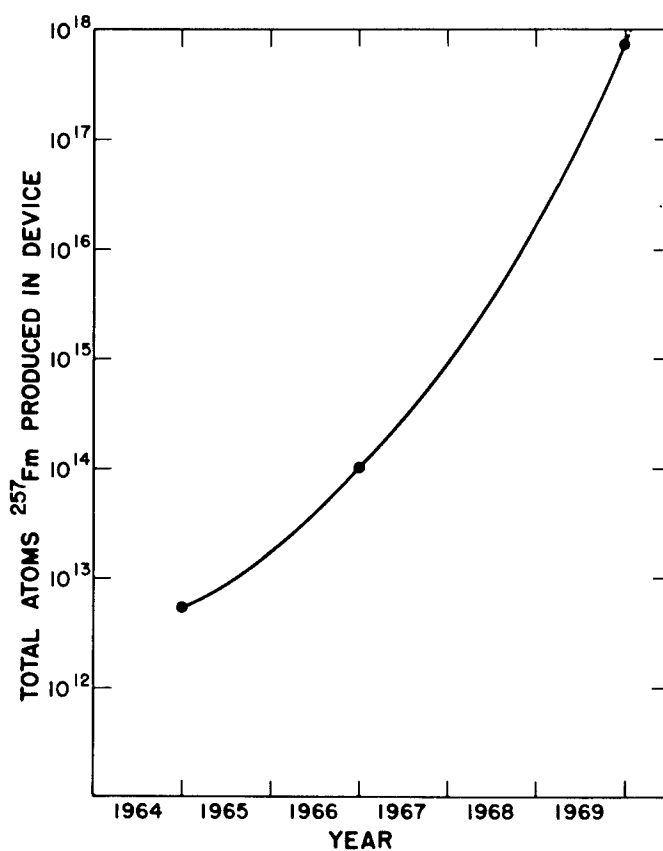


Fig. 5. Increase in ^{257}Fm produced in multiple neutron capture experiments since 1964.

very neutron-rich targets which will be closer to the line of beta-stability and presumably longer-lived than can be produced from presently available heavy plutonium and curium isotopes. Presumably the same general result should be obtained from more exotic reactions which may occur in heavy ion bombardment such as $^{18}\text{Ar}^{40} + ^{96}\text{Cm}^{250} \rightarrow ^{10}\text{Ne}^{20} + ^{104}\text{Zr}^{270}$. The status of efforts to recover these valuable materials from the "Hutch" debris will be described later in this program.

Succeeding presentations in this session will cover the subject matter in more detail than has been attempted here. The points of principal emphasis in this summary are that a considerable effort has been devoted over the past several years to the further development and enrichment of scientific research with nuclear explosions, that new and highly useful nuclear data have resulted from such investigations, and that the outlook for the future should be at least as bright as the realizations of the immediate past.

REFERENCES

1. Plowshare Report No. 1, Feb. 6-8, 1957, Industrial Uses of Nuclear Explosives, H. Zodtner, Ed., UCRL-5253.
2. Ibid, E. Teller, p. 4.
3. A. Ghiorso et. al., Phys. Rev. 99, 1048 (1955).
4. Proceedings of the Second Plowshare Symposium, May 13-15, 1959, Part V, Scientific Uses of Nuclear Explosions, UCRL-5679.
5. Proceedings of the Third Plowshare Symposium, April 21-23, 1964, Engineering with Nuclear Explosives, TID-7695.
6. A. Hemmendinger et. al., Los Alamos Scientific Laboratory Report LA-3478, Part I (1967).
7. P. A. Seeger and D. W. Bergen, Los Alamos Scientific Laboratory Report LA-3478, Part II (1967).
8. CONF-660303, Books 1 and 2, "Proceedings of the Conference on Neutron Cross Section Technology," Washington, D. C., March 22-24, 1966.
 - a. D. W. Bergen, M. G. Silbert, and R. C. Perisho, "The Fission Cross Section of ^{235}U , 20 eV - 2 MeV," p. 895, Book 2.
 - b. Wilbur K. Brown, D. W. Bergen, and J. D. Cramer, "Fission Cross Section of ^{235}U , 20 eV - 2 MeV," p. 971, Book 2.
 - c. N. W. Glass, J. K. Theobald, A. D. Schelberg, J. H. Warren, and L. D. Tatro, "Measurements on the Capture Cross Section of ^{238}U with Bomb Source Neutrons," p. 766, Book 2.
 - d. Edward R. Shunk, W. K. Brown, and R. LaBauve, "Fission Cross Section of ^{239}Pu , 20 eV - 2 MeV," p. 979, Book 2.
 - e. D. H. Byers, B. C. Diven, and M. G. Silbert, "Capture and Fission Cross Sections of ^{240}Pu ," p. 903, Book 2.
 - f. O. D. Simpson, R. G. Fluharty, M. S. Moore, N. H. Marshall, B. C. Diven, and A. Hemmendinger, "The Fission Cross Section of ^{241}Pu from 20 - 200 eV as Determined from a Nuclear Explosion, p. 910, Book 2.
9. NBS Special Publication 299, Vols. I and II, "Proceedings of a Conference on Neutron Cross Sections and Technology," Washington, D. C., March 4-7, 1968.
 - a. M. V. Harlow, A. D. Schelberg, L. D. Tatro, J. H. Warren, and N. W. Glass, "Capture Cross Section Measurements for Lu, ^{151}Eu , ^{153}Eu and the Total Cross Section of Eu," p. 837, Volume II.
 - b. N. W. Glass, A. D. Schelberg, L. D. Tatro, and J. H. Warren, " ^{238}U Neutron Capture Results from Bomb Source Neutrons," p. 573, Volume I.
 - c. R. R. Fullwood, J. H. McNally, and E. R. Shunk, "Neutron Induced Fission Cross Section Measurements in ^{244}Cm ," p. 567, Volume I.

10. Los Alamos Scientific Laboratory Report LA-3586, "Fission Cross Sections from Petrel," (Dec. 9, 1966).
 - a. ^{233}U , D. W. Bergen, M. G. Silbert, and R. C. Perisho, p. 16.
 - b. ^{235}U , Wilbur K. Brown, D. W. Bergen, and J. D. Cramer, p. 31.
 - c. ^{239}Pu , Edward R. Shunk, W. K. Brown, and R. LaBauve, p. 45.
 - d. ^{240}Pu , D. H. Byers, B. C. Diven, and M. G. Silbert, p. 59.
 - e. ^{241}Pu , O. D. Simpson, R. G. Fluharty, M. S. Moore, N. H. Marshall, B. C. Diven, and A. Hemmendinger, p. 72.
 - f. ^{241}Am , P. A. Seeger, A. Hemmendinger, and B. C. Diven, p. 86.
 - g. ^{242}Am , P. A. Seeger, A. Hemmendinger, and B. C. Diven, p. 99.
11. D. W. Bergen and M. G. Silbert, "Resonance Analysis of the ^{233}U Fission Cross Section," Phys. Rev. 166, 1178 (1968).
12. J. D. Cramer, "A Multilevel Analysis of the ^{235}U Fission Cross Section," Los Alamos Scientific Laboratory Report LA-3917-MS (1968).
13. J. A. Farrell, "The Fission Cross Section of ^{232}U ," Bull. Am. Phys. Soc., II, 13, 1409 (1968).
14. J. A. Farrell, "Multilevel Analysis of the ^{239}Pu Fission Cross Section from 14 to 90 eV," Phys. Rev. 165, 1371 (1968).
15. J. H. McNally, K. Wolfsberg, B. J. Dropesky, and J. W. Barnes, Bull. Am. Phys. Soc., II, 13, 1665 (1968).
16. P. A. Seeger, A. Hemmendinger, and B. C. Diven, "Fission Cross Sections of ^{241}Am and ^{242m}Am ," Nucl. Phys. A96, 605 (1967).
17. G. A. Cowan, B. P. Bayhurst, R. J. Prestwood, J. S. Gilmore, and G. W. Knobeloch, "Symmetry of Neutron-Induced ^{239}Pu Fission at Individual Resonances," Phys. Rev. 144, 979 (1966).
18. J. G. Berry and J. W. Coddington, Jr., "Measurement of Capture Cross Section of ^{147}Pm in the Energy Range 20 eV to 10 keV," Bull. Am. Phys. Soc., II, 13, 1391 (1968).
19. N. W. Glass, A. D. Schelberg, J. H. Warren, and L. D. Tatro, "Some Petrel Results on ^{238}U ," Reports to NCSAG, WASH-1074, p. 67 (April 1967).
20. W. K. Brown, P. A. Seeger, and M. G. Silbert, Los Alamos Scientific Laboratory Report LA-4095 (1969).
21. G. A. Cowan, "Synthesis of Neutron-Rich Nuclides," Los Alamos Scientific Report LA-3738, Talk presented at A.C.S. meeting, Miami, Fla., April 11-14, 1967.

USE OF NUCLEAR EXPLOSIVES IN MEASUREMENT OF NUCLEAR PROPERTIES OF FISSIONABLE MATERIALS

B. C. Diven

University of California, Los Alamos Scientific Laboratory
Los Alamos, New Mexico

Nuclear explosives have been used as sources of neutrons for measurement of the several cross sections for interaction of neutrons with fissionable materials.^{1,2} Because most of the very heavy nuclides are highly radioactive and short-lived, the intense single burst of neutrons is ideal for such measurements. Over two dozen of these nuclides have been investigated with this technique.

Those heavy materials that are thermally fissionable are frequently available only in very small quantities because they are "burned out" by fission in the reactors used to produce them. Fortunately, the large numbers of neutrons from a nuclear explosion make possible the measurement of a fission cross section with only a few micrograms of material. Frequently the available sample is not only small but also short-lived. For example, on the Pomard experiment we measured the fission cross section of ^{237}U (one week half-life) with an 18-microgram sample. This measurement extended in neutron energy from 40 electron volts to a few million electron volts. This example serves to demonstrate several useful features of nuclear explosion sources that we wish to exploit. First, the high intensity of neutrons in the beam allows us to produce nuclear reactions at such a high rate in the sample material that backgrounds produced in nuclear reaction detectors by sample radioactivity are trivial in comparison to signals from the reactions being studied. Highly radioactive materials are therefore appropriate subjects for study with bomb neutrons. The second advantage of the explosion source over conventional laboratory neutron sources lies in the very short time scale of the experiment. Only a few milliseconds are required for the entire experiment so that sample decay during the course of the measurement is not important. Thirdly, only a very small quantity of material is required to make a satisfactory measurement of many types of reactions, a few micrograms being sufficient for a fission cross section measurement of a thermally fissionable nuclide. Even with such small quantities the measurement can extend over a wide range of neutron energies.

The method we employ to make our measurement is the familiar time-of-flight method. A small underground nuclear explosion produces 10^{24} neutrons in less than 10^{-7} seconds. The energy spectrum of these neutrons can be modified by causing them to scatter in a hydrogenous material near the bomb. The design of this moderator is tailored to produce the spectrum desired by the experimenters. The time scale of slowing down of neutrons in the moderator is sufficiently short that all neutrons are emitted within a few microseconds. We now place an evacuated pipe between the moderator and the surface of the

ground. The neutrons all leave the moderator at essentially the same time. A few travel up the pipe and reach the surface of the ground at a time that depends on their velocity. In other words, they are sorted out according to their energies by their time of flight. Several small beams are formed just below the ground surface by suitable collimators and the various beams are assigned to different groups of experimenters. Samples of materials to be studied are placed in these beams and nearby detectors catch nuclear reaction products. If a fission cross section is being measured the sample of fissionable material can be very thin and deposited on a thin backing so that a negligible fraction of the neutrons is disturbed but a large number of fissions occur in the sample. Some of the fission fragments strike a solid state detector placed out of the beam, an inch or two from the sample. The reaction rate is so high that individual fission events are not observed. The enormous number per microsecond of fission fragments striking the detector produces a current from the detector whose amplitude is proportional to the product of the fission cross section and the neutron intensity. At any one time neutrons of only one energy are striking the sample since they have been sorted out by time of flight. The current as a function of time then measures the cross section as a function of energy.

Most of the nuclear reactions that can be produced in fissionable materials with neutrons available from nuclear explosions can be satisfactorily measured with methods analogous to those used in the laboratory. If we confine our attention to reactions with neutrons of energies below the threshold for inelastic scattering, then the available reactions are fission, radiative capture and elastic scattering. All of these types of reactions are measured in laboratory experiments. It must be emphasized that the uniqueness of the measurements does not lie in the kind of reactions studied but rather in the ability to use small, short-lived, highly radioactive samples. Fission measurements have already been described. The experimental setup was quite similar to a laboratory measurement of a fission cross section except that currents are observed from the fission detectors rather than individual pulses.

Cross sections for radiative capture are similarly measured using detectors for capture gamma rays in the current mode. We use an adaptation of the Moxon-Rae gamma-ray detector that is commonly used in laboratory cross section measurements. The detector consists of a solid state detector surrounded by a graphite converter that removes any charged particles such as fission fragments that may be produced in the sample and that converts some of the gamma rays into Compton-scattered electrons to produce the detector current. Of course the detector is sensitive to gamma rays from any reaction so that fission gamma rays are detected along with capture gamma rays and the fission cross section must be measured simultaneously so that this effect can be subtracted.

One of the most difficult measurements to make with low energy neutrons is the scattering cross section. The scattered neutrons have too little energy to make use of recoiling charged particles as they collide with detector atoms. Instead we rely upon neutron reactions that produce energetic charged particles. One of these reactions that has been used is the ${}^3\text{He}(n,\alpha)\text{T}$ reaction. The ${}^3\text{He}$ is used as a high pressure gas and the tritons and alpha particles are detected either in solid state detectors placed in the gas chamber or light produced in the helium gas by the charged particles is collected and converted to current by photomultipliers.³ Unfortunately, the detectors are sensitive both to fission neutrons and gamma rays from fission and capture so again it is necessary to measure simultaneously the fission and capture cross sections so these effects can be subtracted.

At low neutron energy, these three reactions, fission capture and scattering, are the only possible reactions and their sum is the total cross section. The total cross section can be measured separately by a transmission

measurement to provide a redundant set of cross section values for each neutron energy. In laboratory measurements the transmission of a sample is determined by measuring the intensity of a neutron beam that passes through the sample and then in a separate exposure, the intensity of the beam when the sample is removed. Since we have only one beam pulse and therefore cannot do a sample in-sample out measurement, we must measure the beam intensity on each side of the sample, a procedure that introduces some additional error because the relative efficiencies of the two flux monitors must be known in our case.

We have learned, as described above, to measure all of the reactions between low energy neutrons and the fissionable materials using bombs as neutron sources. One further bit of important information concerning nuclear reactions in the neutron energy region where resonances are resolved is the spin of the resonance. This could be determined if we could polarize a sample of fissionable material and also polarize the neutron beam so that all atoms in the sample are spinning in the same sense and for example all neutrons in the beam are spinning in the same sense as those in the sample. Under these conditions, reactions will be observed only in those resonances that have a spin that is the sum of the neutron and target spin whereas those resonances corresponding to the difference of target and neutron spin will disappear. In this manner the spin of the compound nuclear state corresponding to the resonance is identified. We have successfully completed our first step of this experiment by polarizing the neutron beam from a nuclear explosion and expect to have a polarized target to use on our next shot.

One of the most interesting recent developments in fission theory arose from the observation of a measurable amount of fission in resonances far below the fission barrier where it was once assumed no detectable fission would occur. A theoretical explanation has been obtained by assuming a double-humped fission barrier whose details are far from complete. A very desirable set of measurements would consist of a survey of the subthreshold fission of a large number of even-even and odd-even nuclei extending over as great a range of the periodic table as possible. We have begun this survey using nuclear explosions and have extended it in atomic number from uranium to einsteinium. We shall also cover as large a range of neutron number as possible. For instance on a recent experiment we measured fission in all isotopes of curium from mass number 243 to 248. It is expected that this survey will have a very useful influence on the theory of fission. We shall also measure other properties of the fissionable nuclides including capture, scattering and resonance spins, concentrating on those nuclides whose radioactivity or availability make measurements with conventional methods impractical.

REFERENCES

1. Diven, B. C., "Proceedings of the Third Plowshare Symposium" (Davis, California, 1964), AEC Technical Information Division Report 7695, pp.25-30.
2. CONF-660303, Books 1 and 2, "Proceedings of the Conference on Neutron Cross Section Technology," Washington, D. C., March 22-24, 1966:
 - a) Bergen, D. W., Silbert, M. G., Perisho, R. C., "The Fission Cross Section of ^{233}U , 20 eV-2 MeV," p. 895, Book 2.
 - b) Brown, W. K., Bergen, D. W., Cramer, J. D., "Fission Cross Section of ^{235}U , 20 eV-2 MeV," p. 971, Book 2.
 - c) Glass, N. W., Theobald, J. K., Schelberg, A. D., Warren, J. H., Tatiro, L. D., "Measurements on the Capture Cross Section of ^{238}U with Bomb Source Neutrons," p. 766, Book 2.
 - d) Shunk, E. R., Brown, W. K., LaBauve, R., "Fission Cross Section of ^{239}Pu , 20 eV-2 MeV," p. 979, Book 2.

- e) Byers, D. H., Diven, B. C., Silbert, M. G., "Capture and Fission Cross Sections of ^{240}Pu ," p. 903, Book 2.
- f) Simpson, O. D., Fluharty, R. G., Moore, M. S., Marshall, N. H., Diven, B. C., Hemmendinger, A., "The Fission Cross Section of ^{241}Pu from 20-200 eV as Determined from a Nuclear Explosion," p. 910, Book 2.
- 3. Hoffman, M. M., "Proceedings of the Fourth Plowshare Symposium" (Las Vegas, Nevada, 1970), "Elastic Neutron Interaction Measurements with a Moderated Bomb Source," next paper.

ELASTIC NEUTRON INTERACTION MEASUREMENTS WITH
A MODERATED BOMB SOURCE SPECTRUM*

submitted by

Marvin M. Hoffman
Los Alamos Scientific Laboratory
of the University of California

Abstract

Experimental measurements of the neutron flux elastically scattered from medium and high mass nuclei have yielded excellent cross section data over a wide range of neutron energies. The moderated bomb spectrum which comprises our neutron source function provides ample flux for cross section measurements between energies of 60 eV and 3 MeV. Analyses of the compound elastic scattering data show that the time dependence of the neutron source function contributes to a time-of-flight energy distribution which is approximately Poisson. The full width of the distribution at half the peak value exceeds one percent of the time-of-flight energy.

Area analyses of the measured elastic cross sections yield resonance parameters for energies up to the 100 keV region. A careful study of the applicability of shape analysis to these data reveals that a reduction in the width of the neutron source function would be highly advantageous and has led to additional calculations of moderator design. Results of some data analysis, moderator design and shielding calculations will be presented.

* Work performed under the auspices of the U. S. Atomic Energy Commission.

Introduction

During the past few years, several authors have called attention to the usefulness of nuclear explosions as neutron sources. In so doing they have emphasized the large yield of neutrons per event and the consequently high flux over long flight paths. It has also been emphasized that the neutron spectrum could be tailored to the desires of the users. A neutron moderator, composed largely of hydrogenous material, which stores neutrons for release at a later time and a lower energy is the principle component which determines the energy dependence of the neutron source function. The moderator is also a significant factor in determining the time dependence of the neutron source function. Although previous applications of nuclear device neutrons have required that the neutron energy distribution receive primary consideration, there are many applications which demand that the time coordinate of the source function be carefully controlled. I shall discuss some aspects of the neutron source functions relevant to neutron scattering experiments which have been performed as a part of the Plowshare program.

Discussion of Experiments and Calculations

Essentially all available information dealing with elastic scattering of neutrons by nuclei is either calculated or deduced from measurements of the total neutron cross section and whatever partial cross sections are available for neutron reactions. Nuclear device neutron sources enable one to determine scattering cross sections by making direct, energy resolved measurements of scattered neutrons using a ^3He cell and photomultiplier type neutron detector having good time response and low x-ray sensitivity. Examples of elastically scattered neutron cross sections measured on the Physics 7 and Physics 8 shots are shown in Figs. 1 and 2 respectively. These data are the result of a direct measurement of scattered neutrons with little or no background corrections required. These scattering cross sections are very similar to the total inasmuch as elastic scattering is the principle component of the total neutron cross-section. Direct measurements of elastic scatter data such as these are quite desirable for they permit more accurate determination of the scattering parameters than is possible using total cross sections. Also, in addition to the scattering cross section it would be highly desirable to measure the (n,γ) , and (n,f) cross sections, if fission does occur, and then apply shape analysis methods to extract the maximum possible information. This approach seems quite within the realm of possibility since excellent methods for the measurement of (n,γ) and (n,f) cross sections have been developed by other groups at Los Alamos. Also, a priori calculations of the experimental energy resolution indicate that it should be possible to obtain data which is good enough for shape analysis. Unfortunately, the application of our shape analysis program to the scattering data shows that the energy resolution is inadequate for this approach. Since the instrument response is shown to be adequate, the poor resolution is attributed to the neutron source. The alternative to our approach is to analyze the data by area analysis methods, the details of which are given by several authors ^{1,2}. In principle this can easily be done and should yield somewhat more accurate resonance parameters than is possible by analyzing total cross section data. There is, however, a very serious practical difficulty which arises from the need for multiple sets of data taken with scattering foils having different thicknesses, and for best results one signal should be from a foil thick enough so that very few of the incident neutrons pass through the foil without being scattered. In a way this makes up in quantity what is lacking in quality. While scattering cross section measurements are rather easy, the simultaneous collection of data from two or more thick scattering foils is not easily adapted to Plowshare physics experiments for two principle reasons. Since all data is collected simultaneously, each additional data channel re-

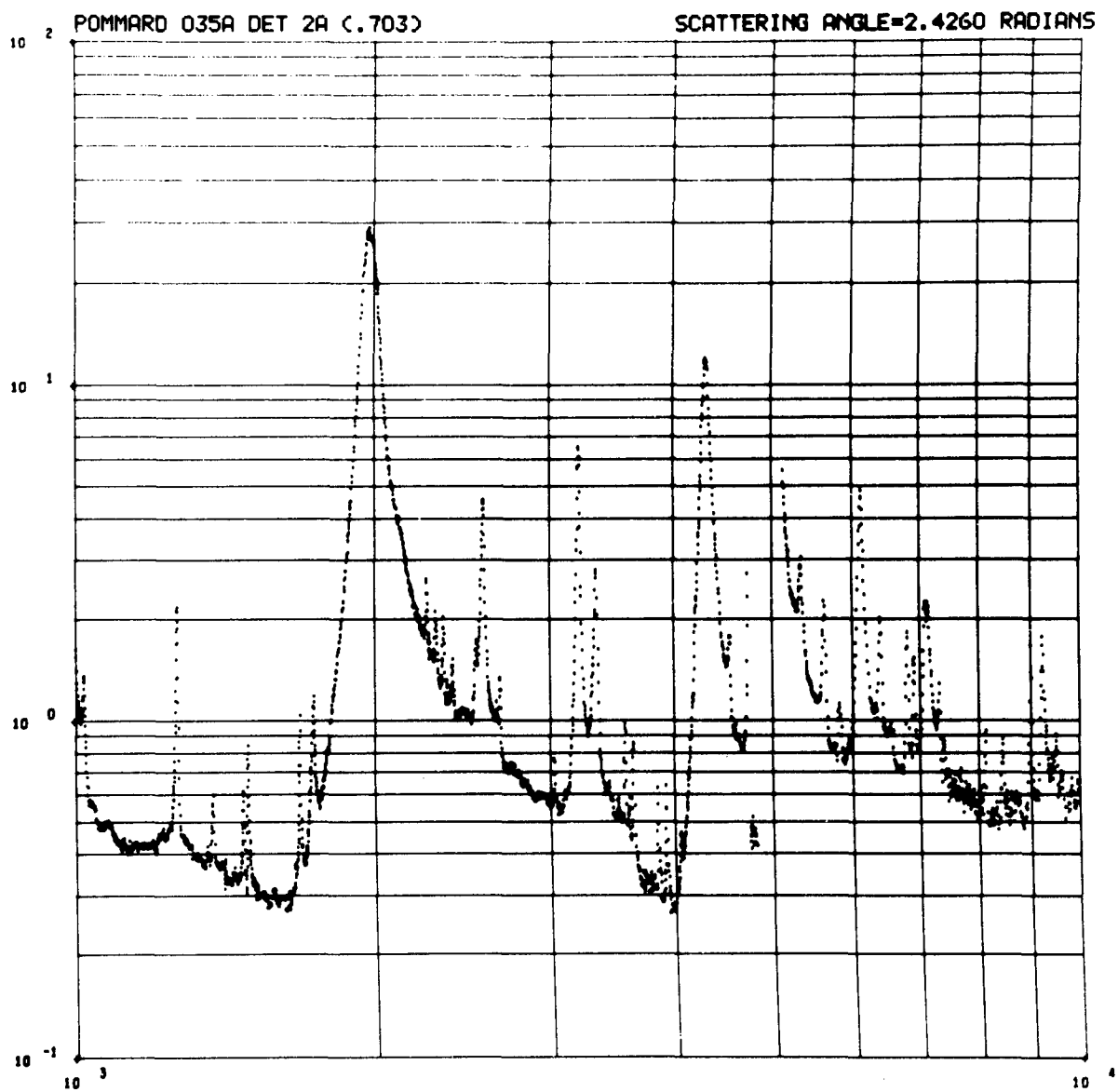
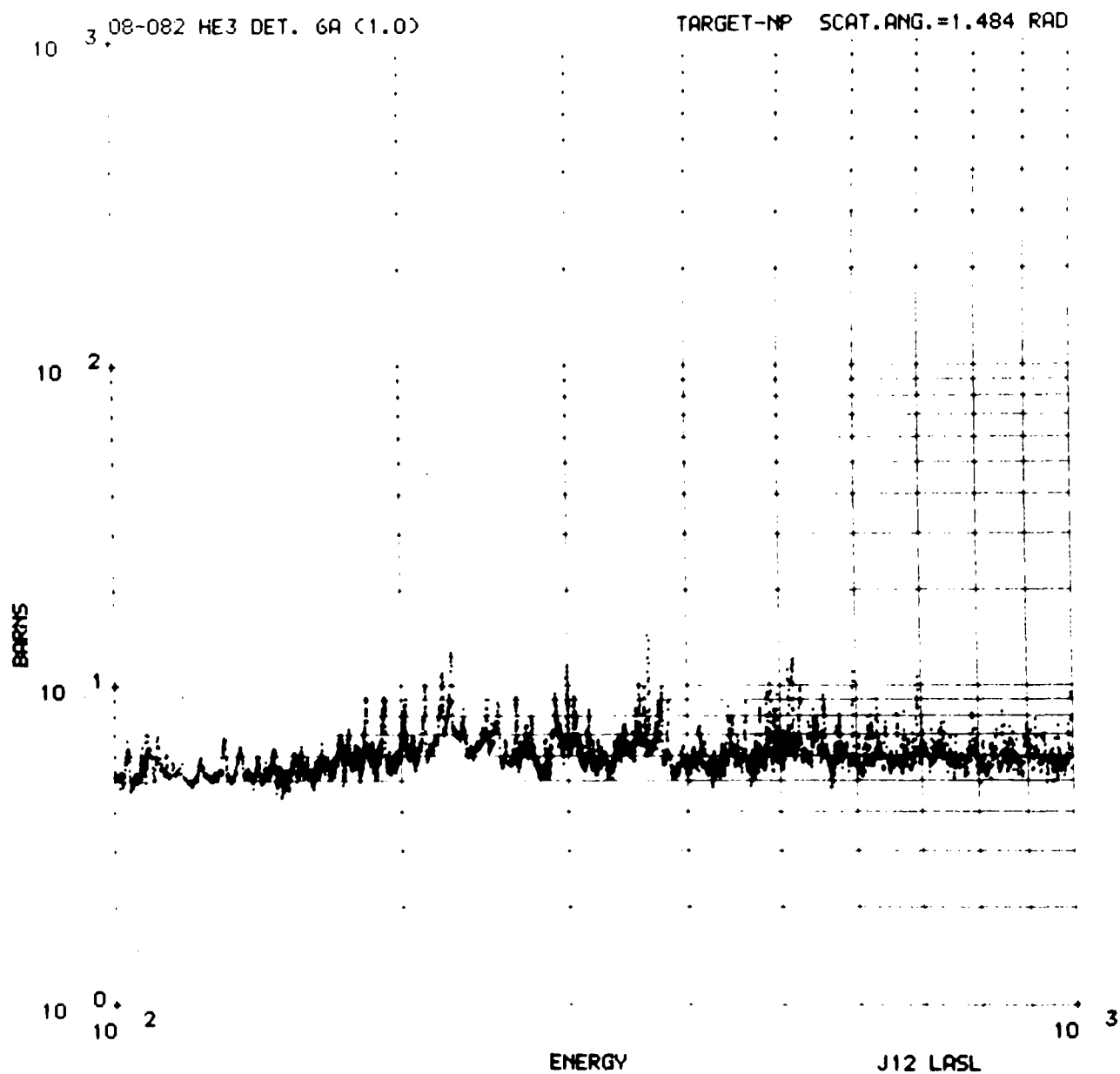


Fig. 1 — Cross section for the elastic scattering of neutrons by selenium from 1 keV to 10 keV as measured on the Physics 7 experiment.



SCATTERING XSECT (BARN'S) VS NEUTRON ENERGY (eV)

Fig. 2—Cross section for the elastic scattering of neutrons by neptunium from 100 eV to 1 keV as measured on the Physics 8 experiment.

quires a duplication of all detecting and recording equipment. Thus, the expense of the apparatus required for collection of a complete set of data for area analysis is approximately a factor of four larger than is required for a simple cross section measurement or for an experiment which lends itself to shape analysis. Secondly, the presence of thick foils in the incident beam alters the spectral composition of the beam and creates a very troublesome neutron background problem. These two difficulties are of such a magnitude that one is inclined to reconsider the problems involved with taking data which is satisfactory for shape analysis to see if one can make this an attractive Plowshare-type measurement. Our shape analysis of the nuclear resonance data relies on the assumption of a single level interaction as formulated by the Breit-Wigner cross section expression. For S-wave elastic scattering of neutrons in the vicinity of a resonance, the shape formula is:

$$\sigma_n = \frac{\sigma_{on}}{1 + X^2} + \left(\frac{2a \sigma_o}{\lambda_r} \right) X + 4\pi R^2 \quad (1)$$

$$\text{in which } X = \frac{E - E_r}{\Gamma/2}, \quad \sigma_{on} = \sigma_o \frac{\Gamma_n}{\Gamma},$$

$$\sigma_o = 4\pi g \lambda_r \frac{\Gamma_n}{\Gamma}, \quad g = 1/2 \left(\frac{2J+1}{2I+1} \right)$$

λ_r is the neutron de Broglie wave length at resonance in the center of mass system, I and J are the spins of target nucleus and of the compound state respectively, and the "scattering length" is given by a . The neutron width Γ_n , the total width Γ and the resonant energy E_r are the parameters by which the Breit-Wigner formula is fitted to experimental cross sections. In this expression one must allow for modification of the resonant shape resulting from thermal motion of the target nuclei. Subject to the assumption that incident neutron velocities are always much larger than nuclear thermal velocities, the modified cross section is a convolution of Equation 1 and the Maxwellian distribution in energy

$$W(E') dE' = 1/2 \left(\frac{M}{\pi m E k T_e} \right)^{1/2} \exp \left(\frac{-M(E' - E)^2}{4 m E k T_e} \right) dE'$$

to give:

$$\sigma_A(E') = \frac{\int_0^\infty dE' \sigma_n(E') W(E')}{\int_0^\infty dE' W(E')} \quad (2)$$

This expression is generally written in terms of two Doppler integrals³:

$$\psi(\beta, X) = \frac{1}{\beta \sqrt{\pi}} \int_{-\infty}^{\infty} dX' \frac{1}{1 + (X')^2} \exp \left(\frac{-(X' - X)^2}{\beta^2} \right)$$

and

$$\varphi(\beta, X) = \frac{1}{\beta \sqrt{\pi}} \int_{-\infty}^{\infty} dX' \frac{X'}{1 + (X')^2} \exp \left(-\frac{(X' - X)^2}{\beta^2} \right)$$

in which

$$\beta = 4 \left(\frac{m E k T_0}{M \Gamma^2} \right)^{1/2}, \quad X' = \frac{2(E' - E_r)}{\Gamma}, \quad X = \frac{2(E - E_r)}{\Gamma}$$

and T_0 is an effective target temperature derived by the Lamb ⁴ formula. The Breit-Wigner cross section in terms of the Doppler integrals is:

$$\sigma_{\Delta}(E) = \sigma_{on} \psi(\beta, X) + \left(\frac{2a \sigma_0}{\lambda_r} \right) \varphi(\beta, X) + 4\pi R^2 \quad (3)$$

To arrive at a calculated cross section which can be compared with experimental data it is necessary to convolute $\sigma_{\Delta}(E)$ with the experimental resolution function $R(E', E)$ to get the theoretical cross section

$$\sigma_{th}(E) = \int_0^{\infty} dE' \sigma_{\Delta}(E') R(E', E) \quad (4)$$

Ideally one would seek a system in which the experimental resolution is so sharply peaked at all energies that it is possible to replace $R(E', E)$ with $\delta(E' - E)$ or in lieu of this have precise knowledge of the resolution function. Herein was the source of difficulty in our shape analysis of Physics 7 data.

A combination of electronic instrumentation response and the neutron source function determine the resolution function $R(E', E)$. The neutron source function is the predominant factor for energies lower than 30 keV. Results of a calculation of neutron flux emitted by the moderator as a function of time with energy as a parameter are shown in Fig. 3. A source function determined from these calculations and experimental measurements of the system response was used for a test analysis of two isolated resonances in selenium at 683 eV and 988 eV for which resonance parameters are available from BNL-325. The source function constructed to correspond to the results of Fig. 3 is represented by:

$$R(t) = \frac{1}{1 + \frac{4K^2}{W^2} \left(\frac{1}{t^2} - \frac{1}{t'^2} \right)^2}$$

or in terms of energy,

$$R(E) = \frac{1}{1 + \left(\frac{(E - E')}{2/W} \right)^2}$$

This is a Lorentzian representation in which $k = Et^2$ is determined by the path length and W is the width at half maximum of the resolution function $R(E)$.

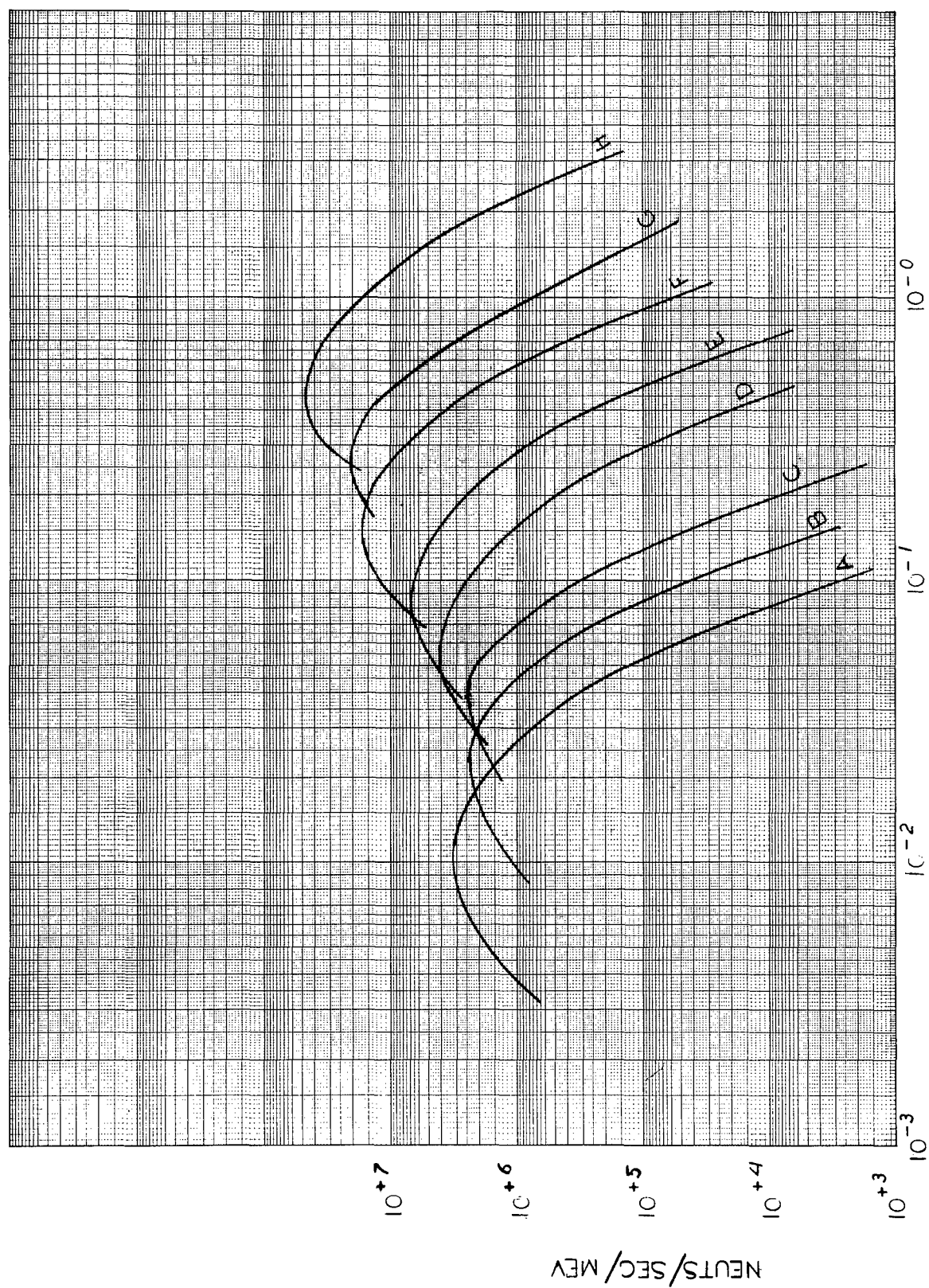


Fig. 3—Calculated flux of neutrons from the Physics 7 moderator in eight energy regions. Curve A represents 500 keV, B is 225 keV, C is 50 keV, D is 22.5 keV, E is 5 keV, F is 2.25 keV, G is 500 eV, and H is 225 eV.

With this resolution function the least squares fit of the theoretical cross section given by Equation 4 results in larger values of Γ and Γ_n than reported previously. One is forced to conclude that these elastic resonance peaks of the Physics 7 experiment have been broadened by a neutron source function appreciably wider than expected. To investigate this further the least squares program was modified to fit the experimental data to a theoretical cross section in which the resonance parameters Γ , Γ_n and E_r were fixed at the values reported in the literature and the width of the resolution function was the variable parameter. To effect a reasonable fit it was necessary to allow for asymmetries as large as 1 to 10 for the high to low energy half widths and for total widths as much as 3 times as wide as calculated. The source function estimated from the cross section data is shown in Fig. 4 together with the function calculated with the neutron transport code. We surmise that the discrepancy between the calculated source function and that deduced from experimental resonance shapes should be attributed to material in the vicinity of the moderator which acts as an appreciable source of neutrons, but which has not been included in our source function calculation. A similar although more exaggerated example of this phenomenon is shown in Fig. 5. In this case sharp isolated resonances in bismuth reveal the shape of the neutron source function at two different energies from the Physics 6 event. Details of the actual neutron source which can give rise to a significant flux over a period of 7 μ sec are not understood. Certainly that moderator was more than the simple lead and polyethylene structure which was intended. The results of these studies of selenium resonances data indicate that the same was true to a lesser extent for the Physics 7 shot.

Some calculations have been performed for moderator geometries selected primarily for shorter duration pulses bought at the expense of reduced neutron flux. Results of one such calculation are shown in Fig. 6. In this case the lead which serves to shield the moderator from gamma-ray heating and from debris has been moved out of the line of sight. The sheet of CH_2 has been thinned to 2.5 cm, half as thick as that used for Physics 7, and moved further from the neutron source. As a result of these changes the time for neutron emission has been reduced by about a factor of five. The net flux from this moderator is calculated to be about 20% of that from Physics 7.

Conclusion.

The energy resolution realized in previous elastic neutron experiments has been in the neighborhood of 5 ns/m in the energy region most interesting for resonance reactions. Thus, while nuclear explosions allow the direct measurements of elastic neutron interactions, the energy resolution is inferior to the pulsed-accelerator neutron generators with long flight paths. Calculations indicate that moderator configurations chosen to emphasize short duration neutron pulses instead of maximum low energy neutron yield could result in time-of-flight energy resolution at least equal to that realized at the best pulsed neutron laboratory facilities. The resulting beam flux degradation is not a serious problem for elastic scattering reactions if ample target material is available. Experiments placing emphasis on the energy region below 100 eV are seen to require a neutron moderator which is incompatible with that designed for high resolution experiments. Both types of experiments can, of course be performed simultaneously with neutrons from the same nuclear device, but with separate moderators and flight paths. The cost and difficulties inherent in collecting elastic neutron data suitable for area analysis indicate that effort should be directed toward high resolution experiments.

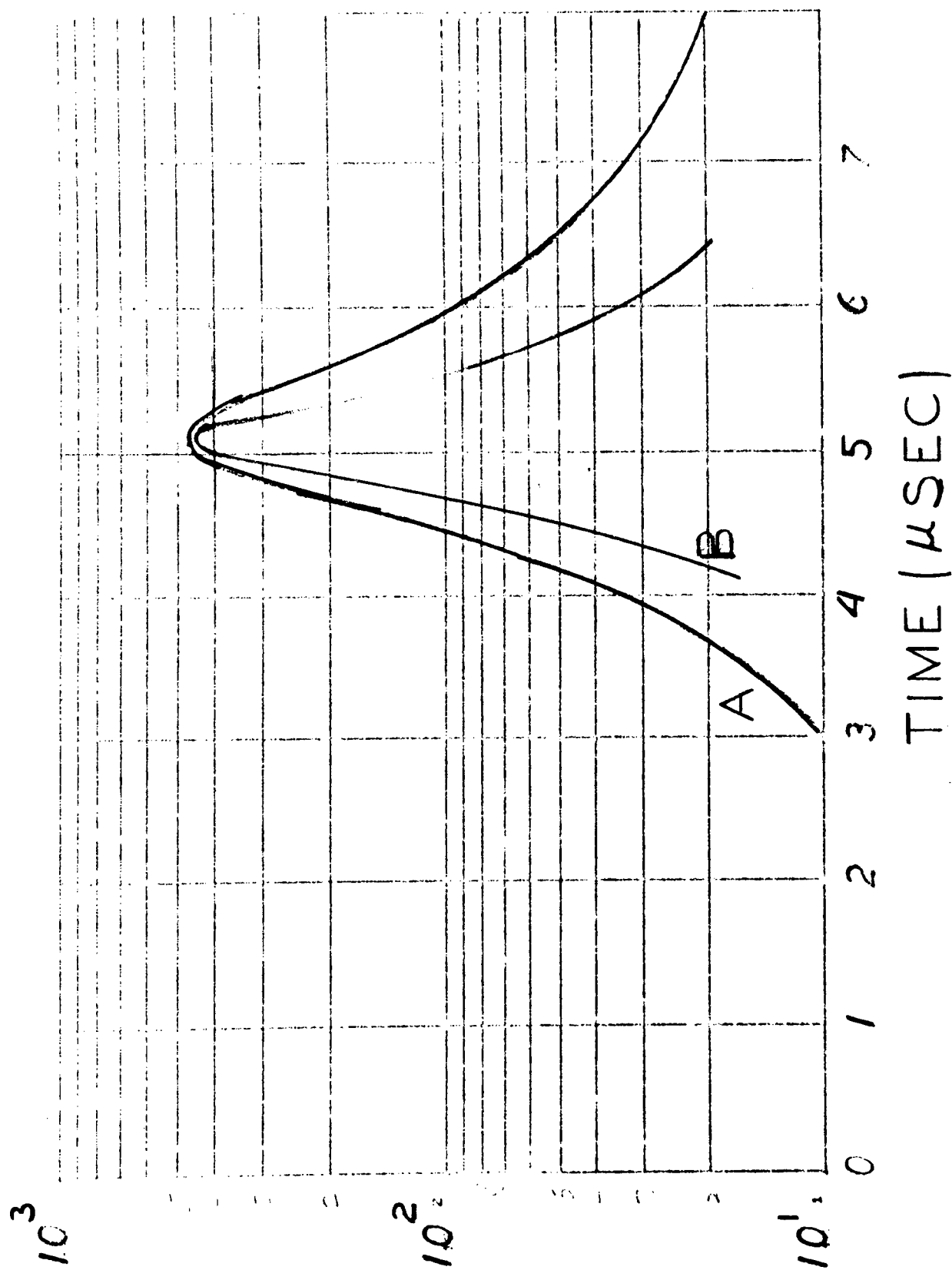


Fig. 4—Curve B represents the calculated resolution function of the Physics 7 experiment at 683 eV. Curve A is the actual resolution function as deduced by fitting the 683 eV resonance in selenium with the previously reported parameters for this level.

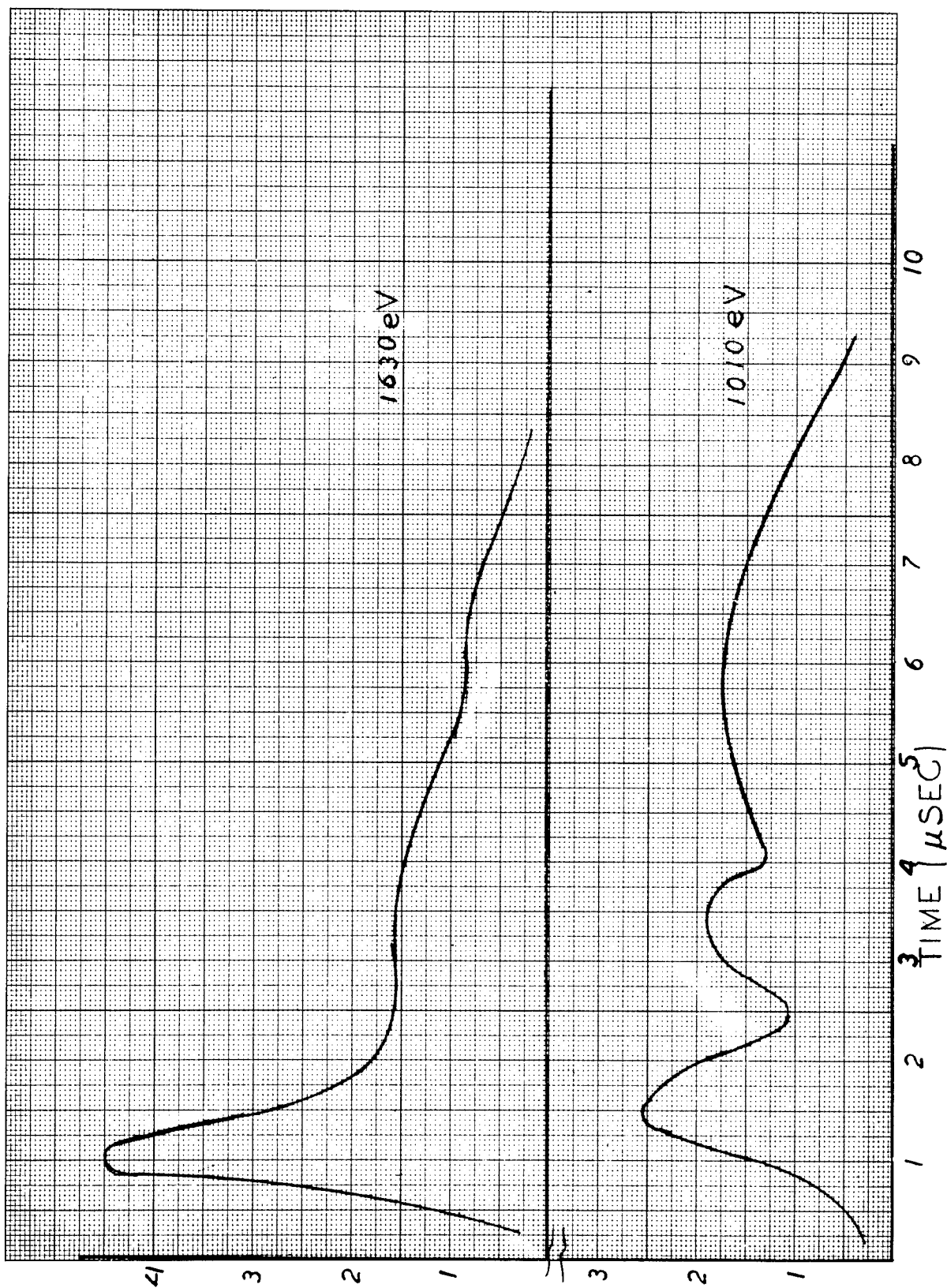


Fig. 5—Examples of the unusual neutron source function observed for the Physics 6 event at 1.63 keV and 1.01 keV.

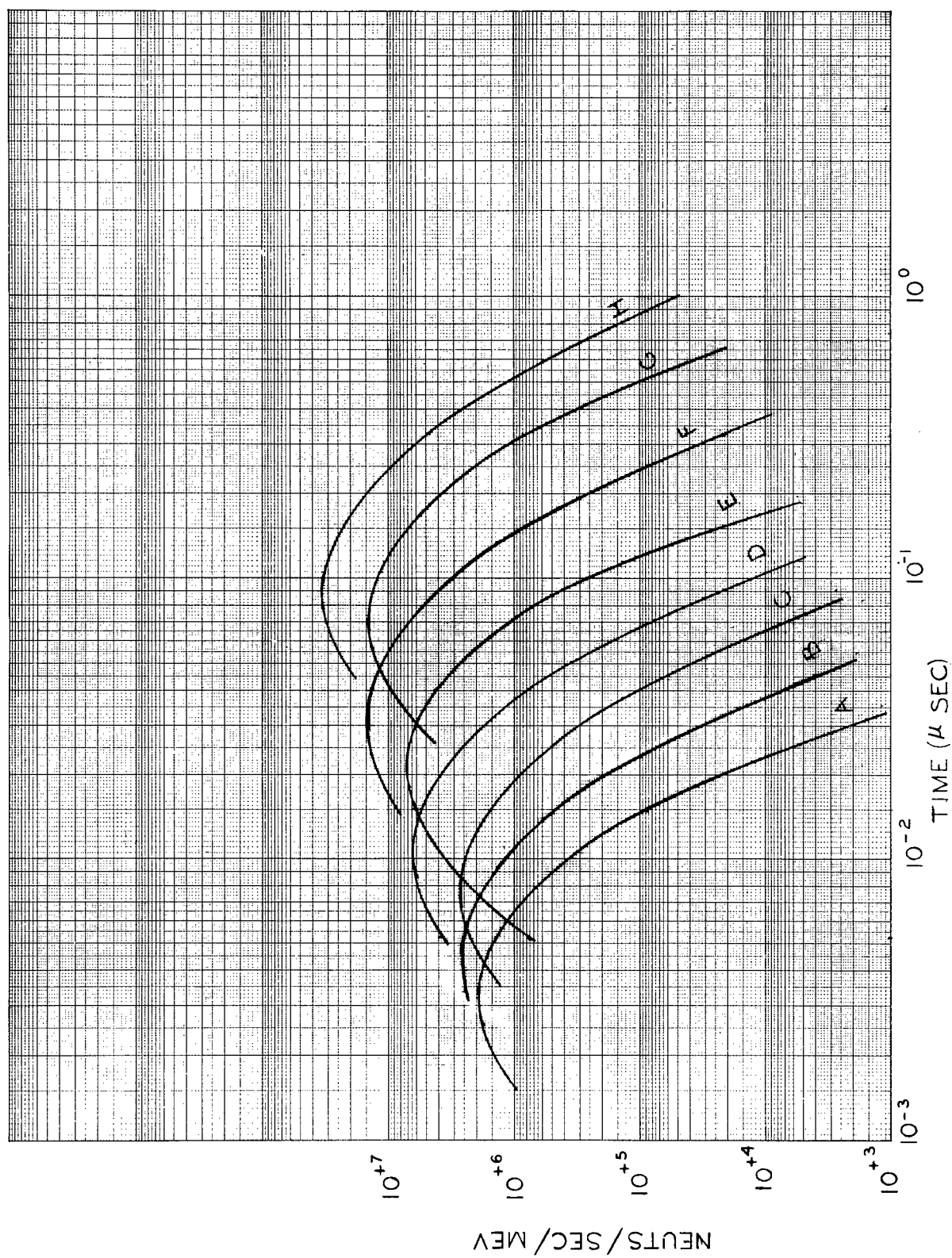


Fig. 6—The calculated flux of neutrons from a moderator designed for a source time 20% as long as the Physics 7 moderator. Curves A, B, C, D, E, F, G, and H represent the 500 keV, 225 keV, 50 keV, 22.5 keV, 5 keV, 2.25 keV, 500 eV, and 225 eV energy regions respectively.

REFERENCES

- (1) W. W. Havens, Jr., and L. J. Rainwater, Phys. Rev. 70, 154 (1946).
- (2) Edward Melkonian, Proceedings of the International Conference on Peaceful Uses of Atomic Energy, Vol. 4, P/583.
- (3) H. Bethe, Rev. Mod. Phys., 2, 140 (1937).
- (4) W. E. Lamb, Jr., Phys. Rev. 55, 190 (1939).

PRODUCTION OF HEAVY NUCLIDES IN NUCLEAR DEVICES*

Samuel F. Eccles

Lawrence Radiation Laboratory, University of California
Livermore, California 94550

ABSTRACT

Since the last Plowshare Symposium in 1964 a number of experiments have been carried out to study the production of heavy nuclei by rapid multiple neutron capture in specially designed nuclear devices. These experiments listed below were conducted underground at the Nevada Test Site and data were obtained radiochemically after sample recovery by drillback:

<u>Event Name</u>	<u>Laboratory</u>	<u>Date</u>	<u>Flux[†]</u>
Par	LRL	10/64	11
Barbel	LASL	10/64	11
Tweed	LRL	5/65	12
Cyclamen	LASL	5/66	18
Kankakee	LRL	6/66	12
Vulcan	LRL	6/66	12
Hutch	LRL	7/69	>35 ^{††}

The main characteristics of these experiments are 1) higher neutron fluxes than in the early events, 2) a variety of targets, including ^{238}U , ^{242}Pu , ^{237}Np , ^{243}Am , ^{232}Th , 3) the occurrence of an interesting "reversal of the odd-even effect" in the mass yield curves, and 4) the absence of nuclei in the debris with (Z,A) greater than (100,257). Analysis of data from these experiments have led to capture cross sections for neutron-rich uranium isotopes (out to ^{249}U), and capture-to-fission ratios for the odd-A neutron-rich plutonium isotopes (out to ^{253}Pu). General studies of the fission process in neutron-rich nuclei have also been undertaken using the data from these experiments. The large amounts of ^{250}Cm and ^{257}Fm made in the recent Hutch experiment ($\sim 1 \times 10^{20}$ and $\sim 5 \times 10^{17}$ atoms, respectively) make it scientifically exciting, and economically feasible, to mine and recover enough material to produce laboratory targets of these isotopes. These targets would be used in investigations of yet-undiscovered, short-lived isotopes of Fm, Md, and No, as well as the possible production of new isotopes of element 104 and even element 105.

*Work performed under the auspices of the U.S. Atomic Energy Commission.

[†]Implied 20 keV time integrated neutron flux (moles neutrons/cm²).

^{††}Based on preliminary analysis.

THE METHOD OF PROMPT MULTIPLE NEUTRON CAPTURE

The method of prompt multiple neutron capture should be clearly contrasted to the well known laboratory process of heavy-ion bombardment of a heavy target to produce very heavy nuclides. In heavy ion bombardment, the heavy ion plus the target produce nuclides on the proton-rich side of the line of beta stability, which then electron-capture to the line of stability or decay by alpha emission or spontaneous fission. Most of the elements above plutonium have been discovered by this method.¹ The multiple neutron capture technique differs, whether it takes place in a fission reactor or in a thermonuclear device, in that neutron-rich products are formed which then generally beta-decay to the line of stability.

An examination of a chart of the nuclides shows that little is known about these heavy neutron-rich nuclides. The main reason is that nuclear reactors produce nuclides close to the line of beta stability, and nuclear-explosive experiments have the disadvantage of the products being buried deep underground with long times (compared to beta half lives) needed to recover and identify the products. Thus what are finally obtained for study in both techniques are nuclides close to the line of beta stability.

In Fig. 1 we compare some details of four multiple neutron capture processes: a thermonuclear explosion, the High Flux Isotope Reactor (HFIR) at Oak Ridge National Laboratory, and two stellar processes. The exposure (time-integrated neutron flux) is more or less the same for these different processes; but the average flux, time scales, and neutron energies differ by many orders of magnitude. the high-flux reactor can be compared to the stellar S-process, wherein targets are emersed in low neutron fluxes for long periods of time. The big difference is in the energy of the neutrons, and therefore the capture cross sections are much larger in general for neutron capture in the HFIR.

TYPE OF EXPOSURE	FLUX ($n\bar{v}$)	Time Interval (Δt)	Exposure ($n\bar{v}\Delta t$)	Temperature
"HFIR"	$5 \times 10^{15}/\text{cm}^2\text{-Sec}$	0.5 YEAR	$\sim 10^{23}/\text{cm}^2$	2.5×10^{-5} KeV
STELLAR S-PROCESS	$\sim 10^{16}/\text{cm}^2\text{-Sec}$	$\sim 10^3$ YEAR	$\sim 10^{26}/\text{cm}^2$	~ 10 KeV
STELLAR R-PROCESS	$\geq 10^{27}/\text{cm}^2\text{-Sec}$	1-100 Sec	$> 10^{27}/\text{cm}^2$	~ 100 KeV
NUCLEAR EXPLOSION	$> 10^{31}/\text{cm}^2\text{-Sec}$	$< 10^{-6}$ Sec	$\sim 10^{25}/\text{cm}^2$	~ 10 KeV

Fig. 1. Neutron exposures in stellar processes, the High Flux Isotope Reactor, and thermonuclear devices.

The nuclear-explosive technique, on the other hand, is like the stellar R-process, with high average flux and relatively short capture times. Two important differences are the time scales and the energy of the neutrons. With a factor of ten higher neutron energy, the average cross sections for capture in the R-process are lower by a factor of about three. Since the important thing for production of nuclides by multiple neutron capture is the product of exposure and cross section, i. e.,

$$\sigma(E) \int_0^T \phi(E,t) dt = \sigma(E) \Phi(E),$$

where T is the lifetime of the process, the production of nuclides will be smaller than in a corresponding nuclear explosion with the same neutron exposure. That this is a large effect can be seen by the following expression for the number of atoms made, starting with N_0 :

$$N = N_0 \frac{(\sigma\Phi)^n e^{-\sigma\Phi}}{n!}$$

where n is the number of captures. This assumes that all the cross sections in a chain (at a given energy) are equal and only capture reactions take place.

In a nuclear explosion, essentially no beta decays can take place during the capture process, while in the R-process there is some competition to capture by electron emission. Thus the R-process would take a zig-zag path up to higher mass numbers, but the path would lie in the region of neutron-rich nuclei somewhat away from the line of beta stability. The nuclear explosion path is straight out from the target nucleus at constant Z to very neutron-rich isotopes. This is then followed by beta decay after the capture reactions have taken place. Figure 2 shows this schematically and lists the observed and predicted isotopes that should be produced along the line of beta stability.

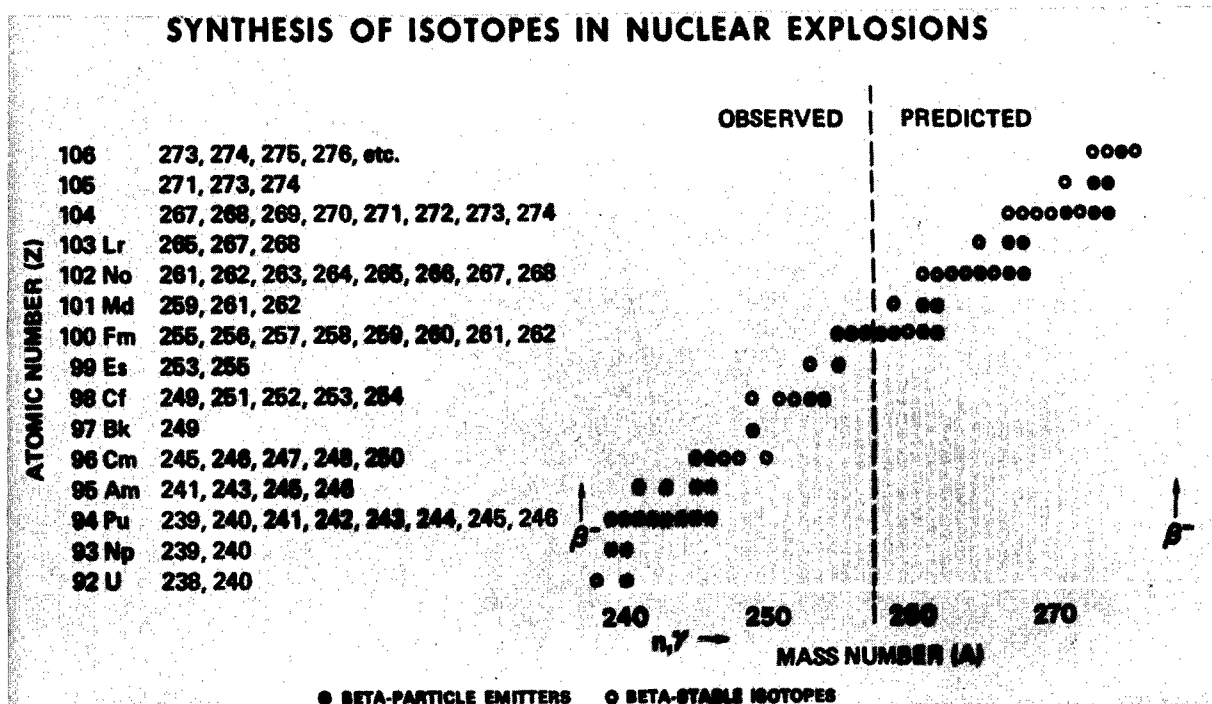


Fig. 2. Paths for synthesis of isotopes in nuclear explosions showing observed and predicted isotopes along line of beta stability.

The important point is that each of these processes measures to some degree the physical properties, such as capture and fission cross sections, and half lives for beta decay and spontaneous fission, of a different group of nuclides. Of the four processes, the nuclear explosive is the only means of obtaining physical properties of the very neutron-rich nuclei. In addition, because of the unique paths taken by the capture chains, certain isotopes can be formed only by this technique and the R-process technique. Some examples are ^{250}Cm , ^{254}Cf , and ^{257}Fm , which are discussed below and in the following two papers of this symposium.

REVIEW OF PROMPT NEUTRON CAPTURE TECHNIQUE

Table I shows a number of experiments undertaken since the last Plowshare Symposium. These experiments were conducted to achieve as high a neutron exposure as possible in order to produce and study extremely heavy isotopes and to understand from a nuclear-device design point of view the important parameters necessary to achieve this exposure. An important study has been the determination of the optimum target for this technique—for example, a heavy target has the advantage of requiring less captures, but the disadvantages of high fission competition and less availability. The targets that were used are listed in the table.

Table I. Experiments to achieve high neutron exposures.

Event Name	Laboratory	Date	Exposure ^(c)	Target
Par	LRL ^(a)	10/64	11	^{238}U
Barbel	LASL ^(b)	10/64	11	^{238}U
Tweed	LRL	5/65	12	$^{242}\text{Pu} + ^{237}\text{Np}$
Cyclamen	LASL	5/66	18	$^{238}\text{U} + ^{243}\text{Am}$
Kankakee	LRL	6/66	12	^{238}U
Vulcan	LRL	6/66	12	^{238}U
Hutch	LRL	7/69	$\approx 40^{(d)}$	$^{238}\text{U} + ^{232}\text{Th}$

^aLawrence Radiation Laboratory, Livermore, California.

^bLos Alamos Scientific Laboratory, Los Alamos, New Mexico.

^cEquivalent 20 keV time integrated neutron flux in moles of neutrons/cm². All the exposures except Hutch were determined as a consistent set by Ingley¹ and are relatively good to $\sim 10\%$.

^dThe Hutch number is preliminary with an accuracy of about ± 10 .

One striking result of these experiments is that the highest (Z,A) nuclide found in the debris has been ^{257}Fm ; and this is especially significant in the case of Hutch, where the exposure was significantly larger than in the previous experiments. Another interesting thing was the "reversal of the odd-even variation" in the mass yield curves at a mass number of about 250. This reversal is present in all yield curves but the Hutch one and is explained as being due to capture taking place in an odd-Z target and this odd-Z capture chain dominating the yield curve above mass 252. The source of this odd-Z chain is most probably a high-energy (n,p) reaction on ^{238}U leading to protactinium;* and because

*The (n,p) and (n, α) cross sections have recently been measured to be respectively 1.5 ± 0.4 and 0.6 ± 0.15 m barns³ at a neutron energy of 14.8 MeV.

of higher average capture cross sections for the Pa isotopes, this chain could dominate at higher A values. This effect is, of course, dependent on the neutron exposure as well as cross sections; and, because of the large increase of flux in Hutch, the Pa contribution would not dominate the yield curve until around mass 260, well beyond the end of the observed nuclides. Thus the Hutch results are consistent with this explanation of the odd-even reversals.

The use of targets of Np, Pu, and Am showed that each of these higher-Z capture chains suffered from fission to a rather high degree.^{2,4} In particular, the use of ^{242}Pu as a target in the Tweed experiment gave a mass yield curve much depressed from a similar exposure of a ^{238}U target. In the Cyclamen experiment, no contribution from ^{243}Am was required to explain the mass yield curve, indicating that severe fission was occurring in this capture chain. Even the uranium capture chain suffers from some fission competition, particularly at mass 239 and perhaps at 241. At mass 249 and 251, Ingley² has found fission to capture ratios of about 5.

For the Hutch experiment we thus decided to include, in addition to ^{238}U , a target with lower Z, even though many more captures would be needed. Since ^{238}Pa is made from the ^{238}U target, and the stable isotope, ^{231}Pa , is seven captures removed, this was not an interesting new target. We chose ^{232}Th as a target to supplement uranium, since this would be a new lower-Z target and since very little ^{235}Th is made from the (n,α) reaction on ^{238}U .^{*} Thorium should suffer less from fission than uranium, and the ^{232}Ac produced by the fast flux from thorium should provide a further interesting capture chain in case the uranium and/or protactinium should be depleted by fission. The calculated protactinium and actinium capture cross sections are generally 2 to 4 times as large as those of uranium and thorium.

Capture cross sections for the neutron-rich nuclei have been experimentally determined from the pre-Hutch data for uranium² and for plutonium.^{2,4} Figure 3 shows Ingley's comparison of experimental uranium cross sections to those calculated by Truran and Cameron. The agreement is seen to be quite good. We hope to extend this work and to extract cross sections for the uranium isotopes out to mass 257 from the Hutch data. The results of the Hutch experiment are described below.

THE HUTCH EXPERIMENT

The Hutch experiment[†] was the most recent in this series, and was designed to produce isotopes of transuranic elements by exposing heavy element targets to a very high neutron exposure from a thermonuclear explosion. In this experiment, we expected at least to double the neutron exposure of the target by among other things increasing the yield of the explosive over past experiments (see Table I). Since the synthesis of very-heavy nuclides requires the successive capture of about twenty neutrons, and since the amount of any nuclide produced varies roughly as the exposure to the n^{th} power, where n is the number of captures (see the equation given earlier), this modest increase in exposure would result in a very large increase in the amounts of the very heavy isotopes produced.

^{*}See previous footnote.

[†]Some early results and conclusions from the Hutch experiment have previously been described by Eccles and Hulet.⁵

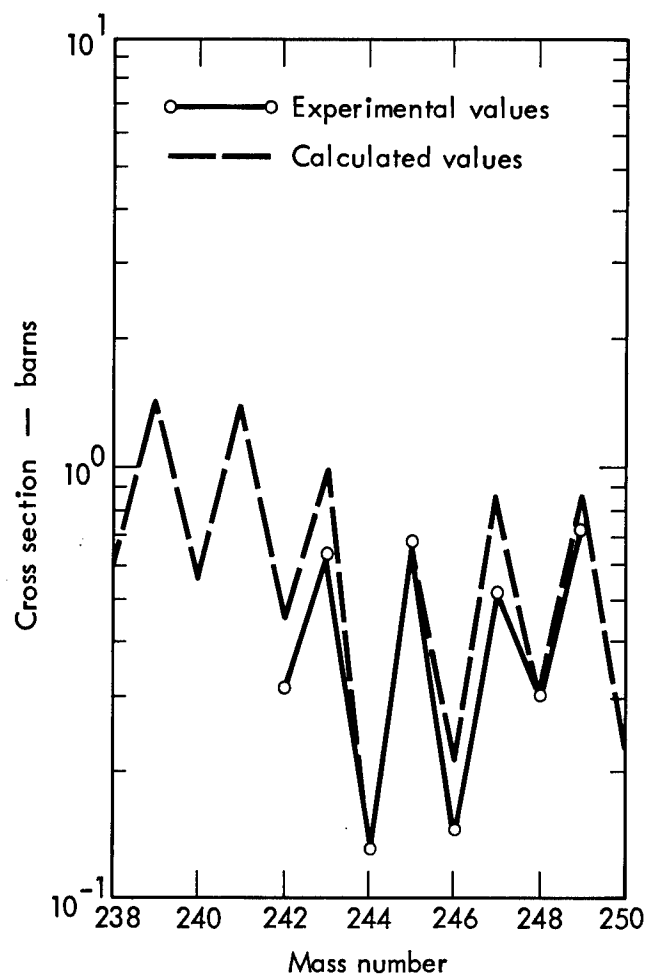
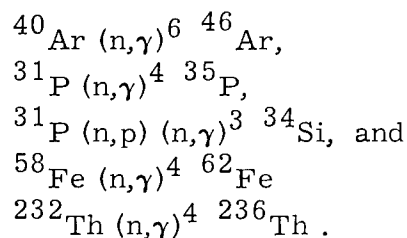


Fig. 3. Comparison of calculated and experimental 20-keV uranium cross sections (from Ingley²).

The results of the Cyclamen experiment⁶ showed that the neutron exposure of the ^{238}U target was sufficient to have made detectable amounts of ^{259}Fm or ^{259}Md , although these were not observed. Therefore, the primary objective of this experiment was to examine the production of heavy nuclides in an integrated neutron flux that was at least twice as great as that produced by the Cyclamen device.

Our specific objective were 1) to produce nuclides with mass numbers greater than 257, the upper limit of previous experiments; 2) to test ^{232}Th as a target for multiple neutron capture; 3) to produce appreciable quantities of ^{250}Cm and ^{257}Fm , so that after recovery they could be used as targets for accelerator bombardments to synthesize isotopes of mass greater than 257; and 4) to determine if detectable amounts of ^{35}P , ^{34}Si , ^{46}Ar , ^{62}Fe , and ^{236}Th could be produced through the following reactions, using the high neutron flux:



The target that was exposed to the intense neutron flux produced by the Hutch device consisted of 17.8 g of ^{238}U and 8.8 g of ^{232}Th . Neutron capture was expected to take place in four separate chains—the uranium chain starting from ^{238}U , the protactinium chain from ^{238}Pa , the thorium chain from ^{232}Th , and the actinium chain from ^{232}Ac . Detonation of the device 1800 ft underground, in tuff, at the Nevada Test Site occurred on 16 July 1969. The explosion produced an unusually large rubble zone and subsidence crater which was approximately 900 ft in diameter and 200 ft deep in the center (see Fig. 4; the drill-rig used for recovery of samples is also shown in this photograph).

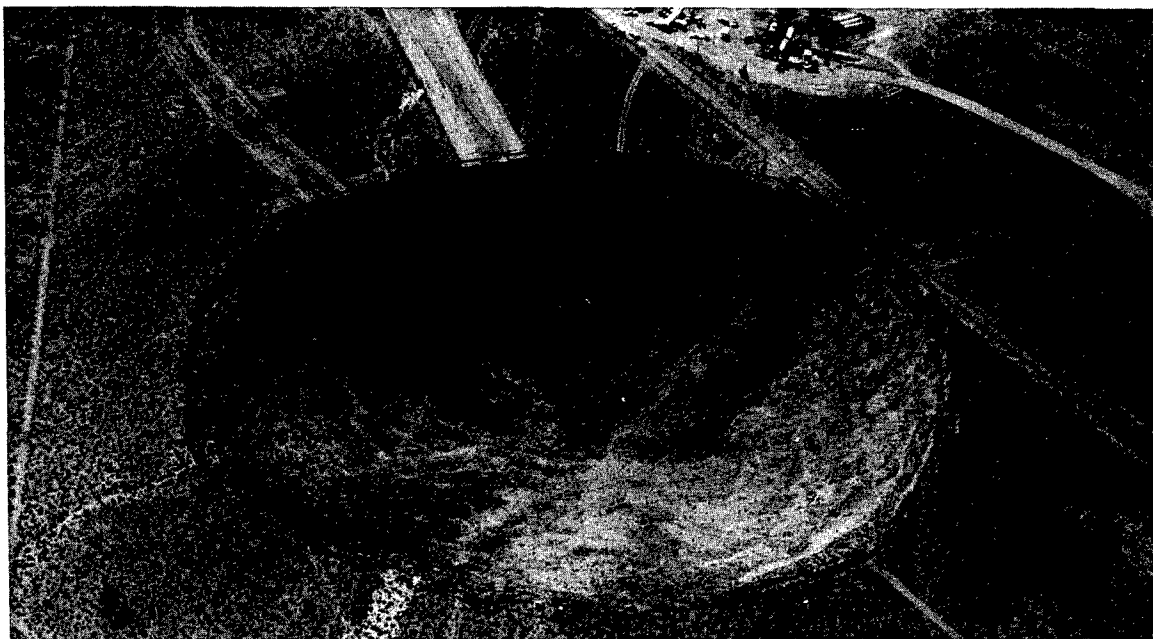


Fig. 4. The Hutch subsidence crater at the Atomic Energy Commission's Nevada Test Site with recovery drill rig in place.

Experimental data were obtained primarily by the methods of nuclear chemistry. Samples of rock containing the explosion debris were recovered by deep drilling (~2000 ft), which was followed by chemical processing to isolate individual transplutonium elements. Details are described in Ref. 5 and in the following paper, by Hoff and Hulet, in this symposium.

The entire experimental mass distribution above mass 241 is shown in Fig. 5 and compared with the mass-yields from Cyclamen, previously the most successful heavy-element test. As stated above, an effect of the higher neutron exposure is that the odd-even reversal noted in previous experiments does not occur in the Hutch data. This thus implies that capture has taken place in an even-Z chain, in this case either uranium or thorium (or both).

It is of interest to attempt to account for the detailed shape of the mass yield curve. What is determined in such a fit to the data is the product of cross section and integrated flux, $\sigma\Phi$, for each isotope, but we hope that in this case the actual neutron exposure can be determined. The uranium cross sections have previously been determined out to mass 249,² and for Hutch it may be possible to extend the U cross section determinations to mass 257 since the protactinium (actinium) contribution to the yield curve is insignificant which is unique to the Hutch experiment.

In order to fit the Hutch data, the following model was used. We assumed the targets of ^{238}U and ^{232}Th saw a flux of high-energy neutrons followed in time by a bomb thermal flux (taken to be at a temperature of 20 keV). Known

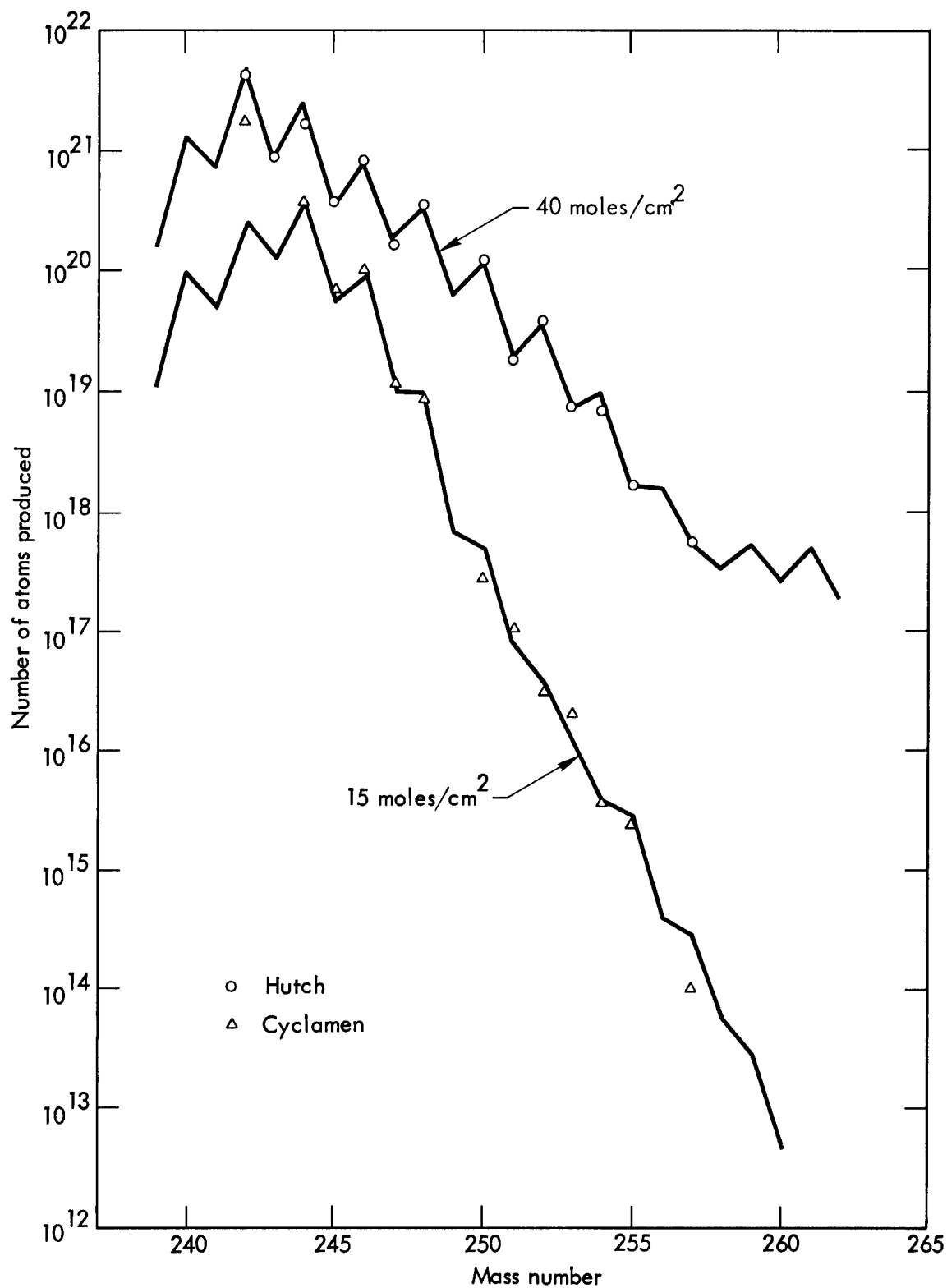


Fig. 5. The Hutch and Cyclamen mass yield curves. The solid lines are the result of calculational fits assuming neutron exposures of 40 moles/cm² and 15 moles/cm².

neutron cross sections were used for the fast-flux phase; and capture cross sections, calculated on a statistical model using Cameron's exponential mass formula,⁷ were used for the thermal flux phase. The latter are given in Table II. In the thermal phase, only neutron capture and fission reactions were allowed, and it was assumed that all captures took place before any beta decays. No spontaneous fission was allowed in the beta-decay chains, and thus the total amounts of the uranium isotopes made would appear as progeny along the line of beta stability. The variables that we hoped to determine were the thermal neutron exposure, Φ , and the fission cross sections in the uranium and thorium chains.

Table II. Truran's and Cameron's 20-keV neutron capture cross sections (barns).⁷

Mass Number	Actinium	Thorium	Protactinium	Uranium
230	3.81	0.738	—	—
231	2.07	1.75	—	—
232	3.71	0.562	—	—
233	2.06	1.49	—	—
234	3.43	0.471	—	—
235	1.91	1.01	—	—
236	3.34	0.340	2.91	0.705
237	1.79	0.886	1.58	1.40
238	3.31	0.312	2.78	0.530
239	1.73	0.882	1.52	1.26
240	2.95	0.257	2.75	0.490
241	1.18	0.576	1.31	1.26
242	2.81	0.0945	2.14	0.399
243	1.07	0.541	0.620	0.887
244	2.73	0.0823	2.13	0.165
245	1.33	0.542	0.591	0.840
246	2.56	0.180	2.19	0.150
247	1.13	0.488	1.10	0.839
248	2.24	0.140	2.06	0.298
249	0.951	0.377	0.897	0.770
250	1.89	0.107	1.74	0.230
251	0.790	0.299	0.733	0.615
252	1.60	0.0826	1.43	0.183
253	0.653	0.230	0.600	0.474
254	1.33	0.0647	1.20	0.144
255	0.525	0.180	0.484	0.374
256	1.067	0.0503	0.983	0.113
257	0.412	0.137	0.394	0.291
258	0.840	0.0397	0.798	0.0876
259	0.322	0.107	0.317	0.233
260	0.656	0.0311	0.651	0.0689

We are able to fit the Hutch data within the experimental accuracy of ~10% with the set of parameters in Table III, and in Fig. 5 the solid lines are the calculated curves for 40 moles/cm² and 15 moles/cm². (The fits for 30 and 50 moles/cm² are equally good.) Interestingly, thorium contributes to the yield curve only out to mass 245, and fission competition is absent in the thorium capture chain.

Table III. Uranium fission cross sections (barns).

Φ (moles/cm ²)	σ 239	σ 249	σ 251	σ 253	σ 255
30	3.3	0.70	0.45	—	—
40	6.5	1.0	0.75	0.30	0.30
50	6.5	2.6	1.2	0.30	0.40

It was impossible to achieve reasonable agreement with the data for an exposure less than about 30 moles/cm² and greater than about 50 moles/cm². On the basis of the Hutch data alone it does not seem possible to pin down the neutron exposure to better than 40 ± 10 moles/cm².

In order to determine the exposure more accurately as well as the magnitude of fission competition in the chains, the same method of analysis is being applied to the Vulcan and Cyclamen data. The solid line through the Cyclamen data points in Fig. 5 is a preliminary fit for 15 moles/cm². This work is still in progress, but we hope to be able to explain the three sets of data in terms of uniform fission cross sections, and fluxes appropriate to the particular experiment. We have found that the magnitude of the cross sections for protactinium (and probably actinium) in Table II are too large and will have to be uniformly reduced by a factor of 0.6 in order to fit the Vulcan and Cyclamen data.

In the subsidiary experiments, techniques from gamma-ray spectroscopy were used in searching for possible long-lived isotopes of P, Si, Ar, Fe, and Th. At the time of the measurements, some 9 days after the detonation, no evidence was found for any of the nuclides of interest. Half-life limits have not been determined because the amounts produced require a knowledge of the formation cross sections, and these are not yet available. Estimates of the half lives for these nuclides will be available in the future.

WHAT IS THE FUTURE OF THIS TECHNIQUE?

The disappointing results of not finding nuclides above ²⁵⁷Fm, apparently because of their short half lives, requires a critical analysis, which one should now undertake. On the basis of the systematics of spontaneous-fission half lives (shown in Fig. 6) and the Hutch results, further attempts to find new isotopes or elements just past ²⁵⁷Fm using these same techniques should be abandoned. Prompt sampling and/or fast recovery looks very difficult and costly at this time, and therefore not promising. There will have to be marked improvements in current drilling and recovery techniques even to realize the tremendous amounts of ²⁵⁷Fm now available through using present nuclear devices.

There are, however, two avenues of approach that should be studied. The first, attempting to reach the "island of stability" postulated by many theorists,⁸ is quite speculative but intriguing. The second approach is to use the current proven "Hutch technique" for production of certain known heavy elements. This is a more straightforward approach, and I shall discuss it first.

Figure 7 shows the production as a function of flux of two interesting isotopes: ²⁵⁰Cm and ²⁵⁷Fm. (The scientific interest in these and other heavy isotopes is discussed in the next paper in this symposium.) The Hutch device produced large quantities of these isotopes (Table IV).

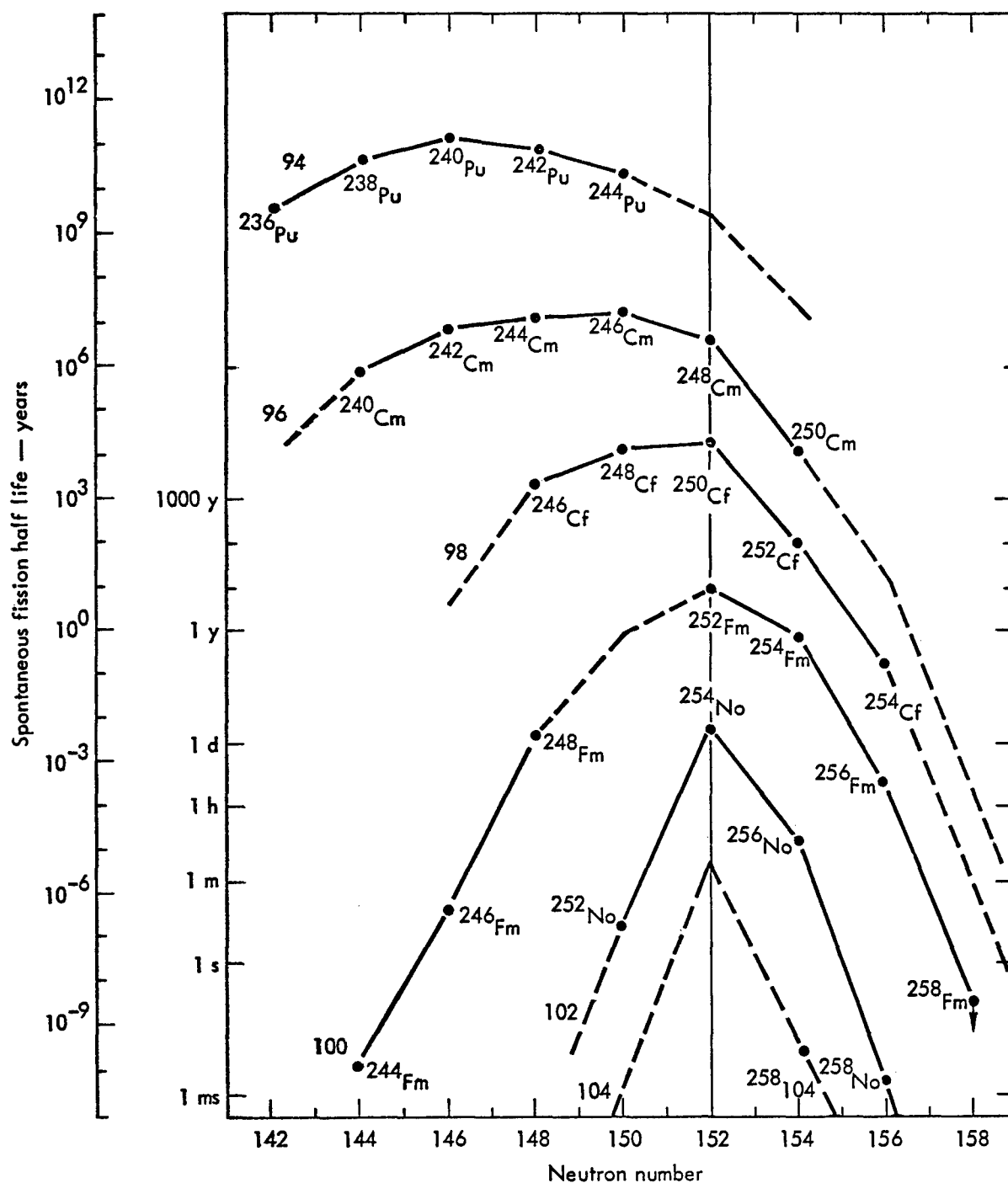


Fig. 6. Spontaneous fission half lives for the even-mass nuclei versus neutron number.

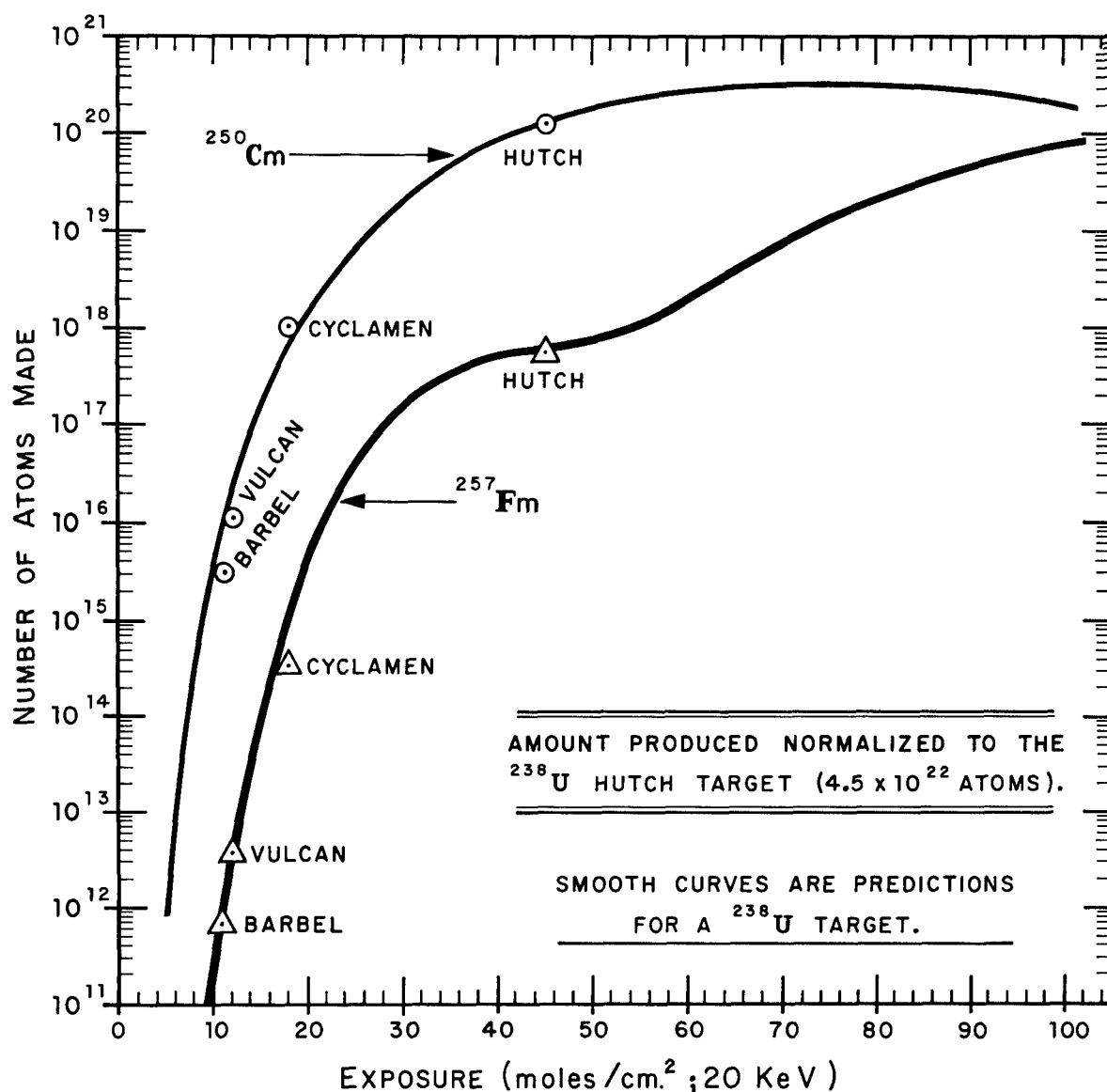


Fig. 7. Amounts of ^{250}Cm and ^{257}Fm made in various experiments as a function of neutron exposure.

Table IV. Isotopes produced in the Hutch event.

Isotope	Decay	Amount produced in Hutch
^{250}Cm	S. F. 17,000 year	40 mg (1.0×10^{20} atoms)
^{257}Fm	S. F., α decay 94 days	0.25 mg (6×10^{17} atoms)

An important point is that for the production of ^{250}Cm we now have the almost optimum machine! An increase of a factor of two in exposure over Hutch would nearly optimize the production of ^{257}Fm . (Higher fluxes would merely burn up the quantity of these isotopes already produced.) Thus the Hutch device, or some modification of it, could be used as a source for isotopes unattainable (or attainable in extremely small quantities) by other means. The only problem is in recovery of the rare isotopes from underground, and

this may be a formidable engineering problem. (The problems associated with the recovery of large amounts of these isotopes are discussed in an accompanying paper by R. Heckman of this symposium.)

The more interesting possibility, from a scientific point of view, is that of trying to reach the hypothesized "island of stability" using prompt neutron capture. Figure 8 schematically shows what would be involved in such a process. The current, proven technique exposes a target of ^{238}U ; 19 neutron captures take place, followed by 8 β -decays, finally producing ^{257}Fm . To reach the "island" would involve 60 neutron captures followed by 22 β -decays, and the path would lead through an unknown region of very neutron-rich nuclei. For example, current mass formulae do not extend very far into the neutron-rich nuclei (away from the line of β -stability), and therefore little is known of neutron binding energies and spontaneous-fission half lives. No theoretical data are available on neutron capture cross sections or fission cross sections in this region. Reactions such as (γ, n) with the thermal radiation can probably compete with neutron capture; and, in the β -decay chain, such reactions as $(\beta^-, \text{fission})$, as well as spontaneous fission could be possible. On the other hand, estimates of half lives for spontaneous fission and alpha decay for nuclides in the island seem to be reasonably long,⁹ so that the current drill-back technique could probably be used.

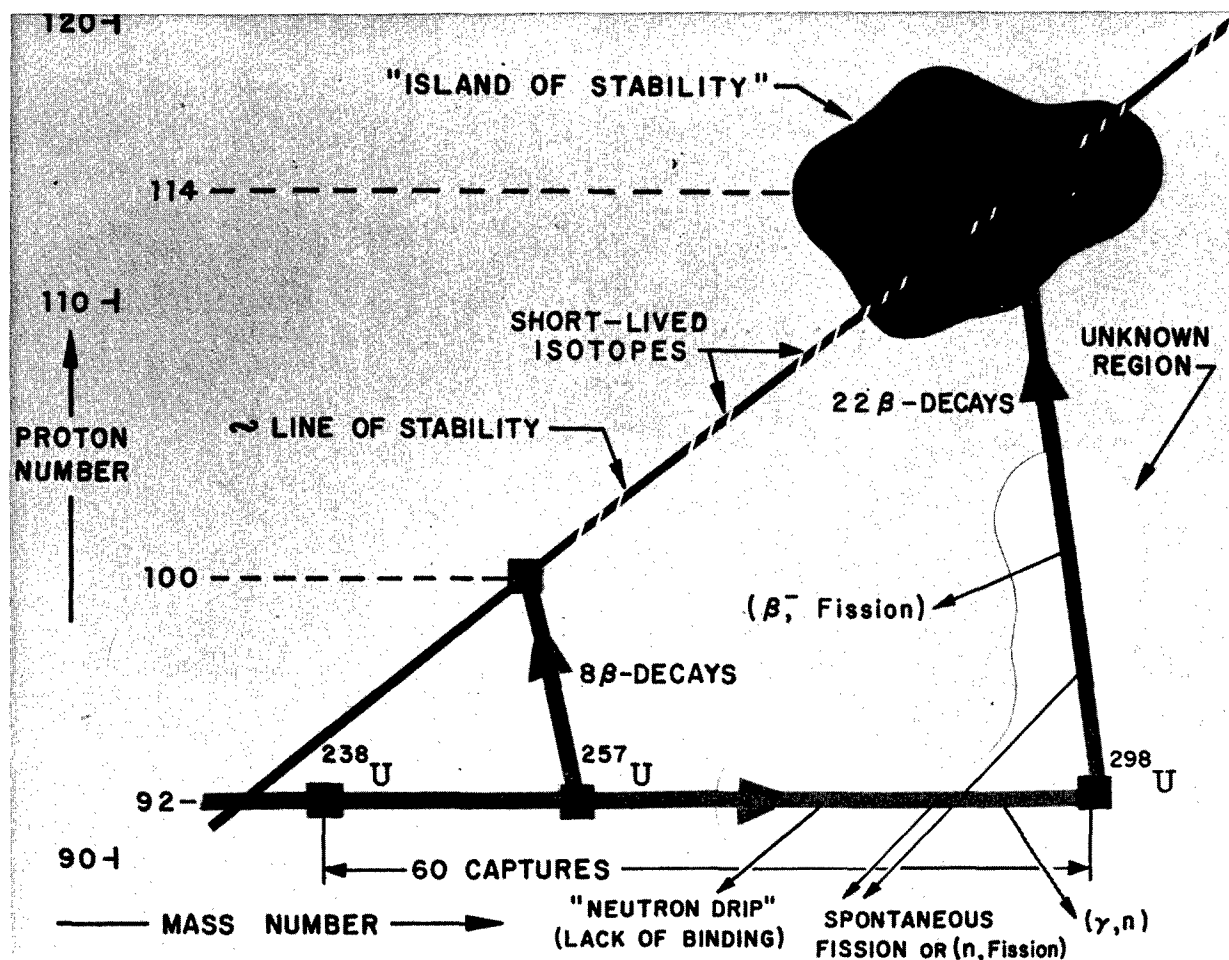


Fig. 8. Hypothesised path for reaching the "island of stability" by use of the prompt neutron capture technique.

There is also the other question, which will remain unanswered here, of whether a nuclear device can be designed to give an integrated neutron flux large enough to allow 60 captures. This would require a flux of at least 100 moles/cm² in order to produce a significant number of mass 298 atoms.

At the current time there is no way to reach this curious island by any technique (the necessary new heavy-ion accelerators will not be available for at least another two years). The rewards of reaching the island are great, and the thought of reaching out this far past the known nuclides is intriguing indeed.

REFERENCES

1. G. T. Seaborg, Man-Made Transuranium Elements (Prentice-Hall, Inc., Englewood Cliffs, N. J., 1964); and Ann. Rev. Nucl. Sci. 18, 53 (1968).
2. J. S. Ingley, Nucl. Phys. A124, 130 (1969).
3. N. Troutmann, et al. Universität Mainz, Germany, private communication. Naturforsch. 23a, 2127 (1968), and submitted to Radiochimica Acta (1969).
4. G. I. Bell, Phys. Rev. 139, B1207 (1965); ibid., 158, 1127 (1967).
5. S. F. Eccles and E. K. Hulet, Lawrence Radiation Laboratory, Livermore, Rept. UCRL-50767 (October 1969), unpublished.
6. D. C. Hoffman, Arkiv Fysik 36, 533 (1966).
7. J. W. Truran and A. G. W. Cameron, private communication; and Arkiv Fysik 36, 509 (1966).
8. See, for example, H. Meldner, Arkiv Fysik 36, 593 (1966); or V. M. Strutinski, Kurchatov Atomic Energy Institute Preprint IAE-1108, ANL-translation 353 (1966); or S. G. Nilsson, et al., Nucl. Phys. A131, 1 (1969).
9. There is currently some spirited discussion of the life times of the nuclei in the island. See, for example, conference proceedings of The Transuranium Elements—The Mendeleev Centennial (The Robert A. Welch Foundation, Houston, Texas, November 1969).

THE RECOVERY AND STUDY OF HEAVY NUCLIDES PRODUCED IN A NUCLEAR EXPLOSION—THE HUTCH EVENT*

R. W. Hoff and E. K. Hulet
Lawrence Radiation Laboratory, University of California
Livermore, California 94550

ABSTRACT

During the explosion of the Hutch device, the target (^{238}U and ^{232}Th) was subjected to a very high neutron exposure, 2.4×10^{25} neutrons/cm². Multiple neutron capture reactions resulted in the production of heavy nuclides, up to and including ^{257}Fm . Results of the search for species with $A > 257$ were negative. The recovery and chemical processing of kilograms of Hutch debris has resulted in the isolation of 10^{10} atoms of ^{257}Fm , which is 10^2 times more material than has been available for experimentation in the past. Experimentally significant amounts of other rare nuclides, e.g., ^{254}Cf , ^{251}Cf , ^{255}Es , and ^{250}Cm , have also been separated from the Hutch debris. The production of these nuclides in thermonuclear explosions is shown to be a valuable supplement to the AEC program for reactor production of transplutonium elements. The neutron flux achieved in Hutch was insufficient to even approach production of nuclides in the region of $^{298}114$. A much more intense neutron flux is required. In future experiments, considerable attention must be given to the problem of adequate sample recovery, in order to properly use the ability to subject targets to an exceedingly intense time-integrated neutron flux.

HEAVY ELEMENT PRODUCTION—NUCLIDES WITH $A \leq 257$

Explosion of the Hutch device resulted in irradiation of a mixed ^{238}U and ^{232}Th target to a total exposure of 40 moles neutrons/cm² (equivalent 20 keV neutron flux) and consequent production of appreciable amounts of certain heavy nuclides. This production was discussed by S. F. Eccles¹ and is summarized in a plot of logarithm of total atoms produced versus mass number in Fig. 1. The same data are given in Table I, where the nuclide listed for each mass number is usually the final (and longest-lived) member of each beta-decay chain. Early results and conclusions from the Hutch experiment have also been described in an earlier report by Eccles and Hulet.²

To obtain these experimental data, samples of rock containing explosion debris were recovered by drilling 2,000 ft below the surface of the ground at the Nevada Test Site. The first debris from the drilling was returned to our laboratory 7 days after the explosion. A 100-g sample of this material was processed immediately and a second 100-g sample that was especially rich in actinides was treated a day later. Hundred-gram samples were also sent to groups at Los Alamos Scientific Laboratory and Argonne National Laboratory for analysis. The rock was dissolved and the transcurium actinides were chemically isolated. Weightless samples of each element were electrodeposited and then carefully counted for alpha and spontaneous fission radioactivity. We found that the second 100 g of debris, representing 8.4×10^{-10} fraction of

*Work performed under the auspices of the U. S. Atomic Energy Commission.

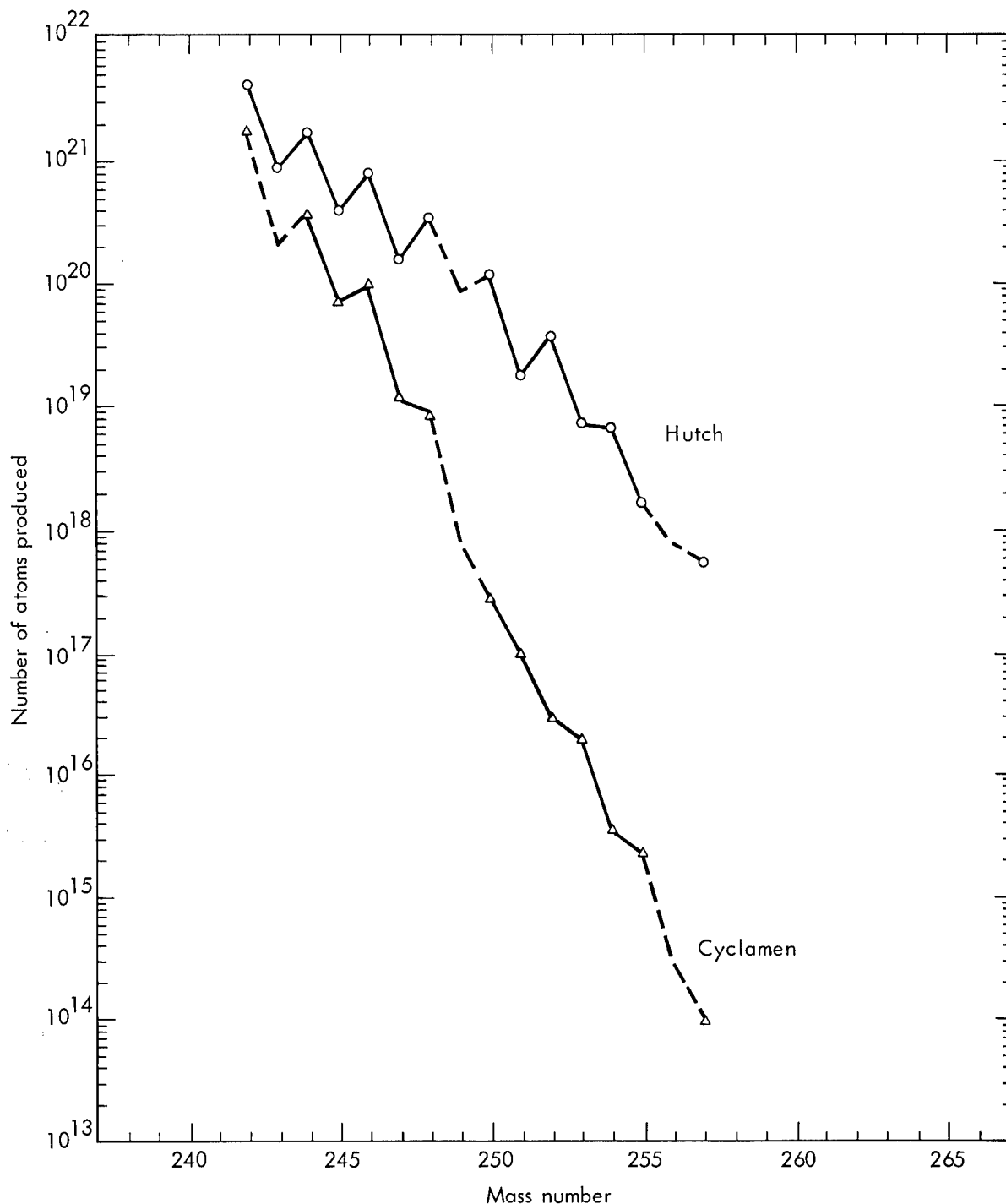


Fig. 1. Heavy element yields from the Hutch and Cyclamen experiments.

the total, contained 4×10^8 atoms of ^{257}Fm , or about seven times the quantity of this scarce isotope ever before isolated. The abundances of other known isotopes were equally impressive.

SEARCH FOR NUCLIDES WITH $A > 257$

In the analyzing of the Hutch samples, one of the most urgent problems was the search for new isotopes with mass numbers greater than 257. Extrapolating the data of Fig. 1, we estimate it should have been possible to detect nuclides with mass numbers as high as 265, provided the following conditions were satisfied: 1) the species with $A > 257$ do not experience a sudden increase in probability for neutron-induced fission, 2) the members of the

Table I. Total atoms for each mass number chain produced in the Hutch experiment

Nuclide	Half-life and decay mode	Total atoms (t_0 , 7/16/69)	Total atoms (1/1/70)
^{242}Pu	$3.9 \times 10^5 \text{ y } \alpha$	4.22×10^{21}	Same
^{243}Am	$8.0 \times 10^3 \text{ y } \alpha$	9.03×10^{20}	Same
^{244}Pu	$8.3 \times 10^7 \text{ y } \alpha$	1.71×10^{21}	Same
^{245}Cm	$8.3 \times 10^3 \text{ y } \alpha$	3.92×10^{20}	Same
^{246}Cm	$4.7 \times 10^3 \text{ y } \alpha$	8.54×10^{20}	Same
^{247}Cm	$1.6 \times 10^7 \text{ y } \alpha$	1.60×10^{20}	Same
^{248}Cm	$3.8 \times 10^5 \text{ y } \alpha$	3.54×10^{20}	Same
^{249}Bk	314 d β^-	(not measured)	(not measured)
^{249}Cf	352 y α	—	—
^{250}Cm	$1.1 \times 10^4 \text{ y SF}$	1.21×10^{20}	Same
^{251}Cf	900 y α	1.82×10^{19}	Same
^{252}Cf	2.7 y α	3.82×10^{19}	3.4×10^{19}
^{253}Cf	18 d β^-	7.20×10^{18}	1.1×10^{16}
^{253}Es	20 d α	—	2.1×10^{16}
^{254}Cf	60 d SF	6.82×10^{18}	9.7×10^{17}
^{255}Es	40 d β^-	1.66×10^{18}	8.9×10^{16}
^{255}Fm	20 h α	—	1.8×10^{15}
^{256}Fm	2.6 h SF	(too short-lived)	—
^{257}Fm	95 d α	5.56×10^{17}	1.6×10^{17}

beta-decay chains were not consumed rapidly by spontaneous fission decay, and 3) the final member(s) of the beta-decay chain survive(s) long enough to be detected 8 days after the Hutch explosion.

The unknown nuclides ^{259}Fm and ^{259}Md , end products of the mass-259 beta-decay chain, offer a good chance for detection because at formation time they would presumably be only a little less abundant than ^{257}Fm . The predicted decay modes, energies, and half-lives for ^{259}Fm and ^{259}Md are given in Table II. Our estimates of the spontaneous fission half-lives were

Table II. Estimated decay characteristics of ^{259}Fm and ^{259}Md

Nuclide	SF $t_{1/2}$	Alpha particle energy (MeV)	Alpha $t_{1/2}$	Beta decay energy (MeV)	Beta $t_{1/2}$
^{259}Fm	0.1 - 1 h	6.4	2 y	0.4	0.1 - 3 d
^{259}Md	0.1 - 1 h	6.8	33 y	0	stable

made by extrapolating from data shown in Fig. 2, experimentally-measured SF half-lives plotted as a function of neutron and proton number. In the region above $N = 152$, SF lifetimes are decreasing rapidly, amounting to nearly 10^5 reduction upon adding two neutrons or two protons. Indeed, these short lifetimes severely restrict the chances for the formation and identification of

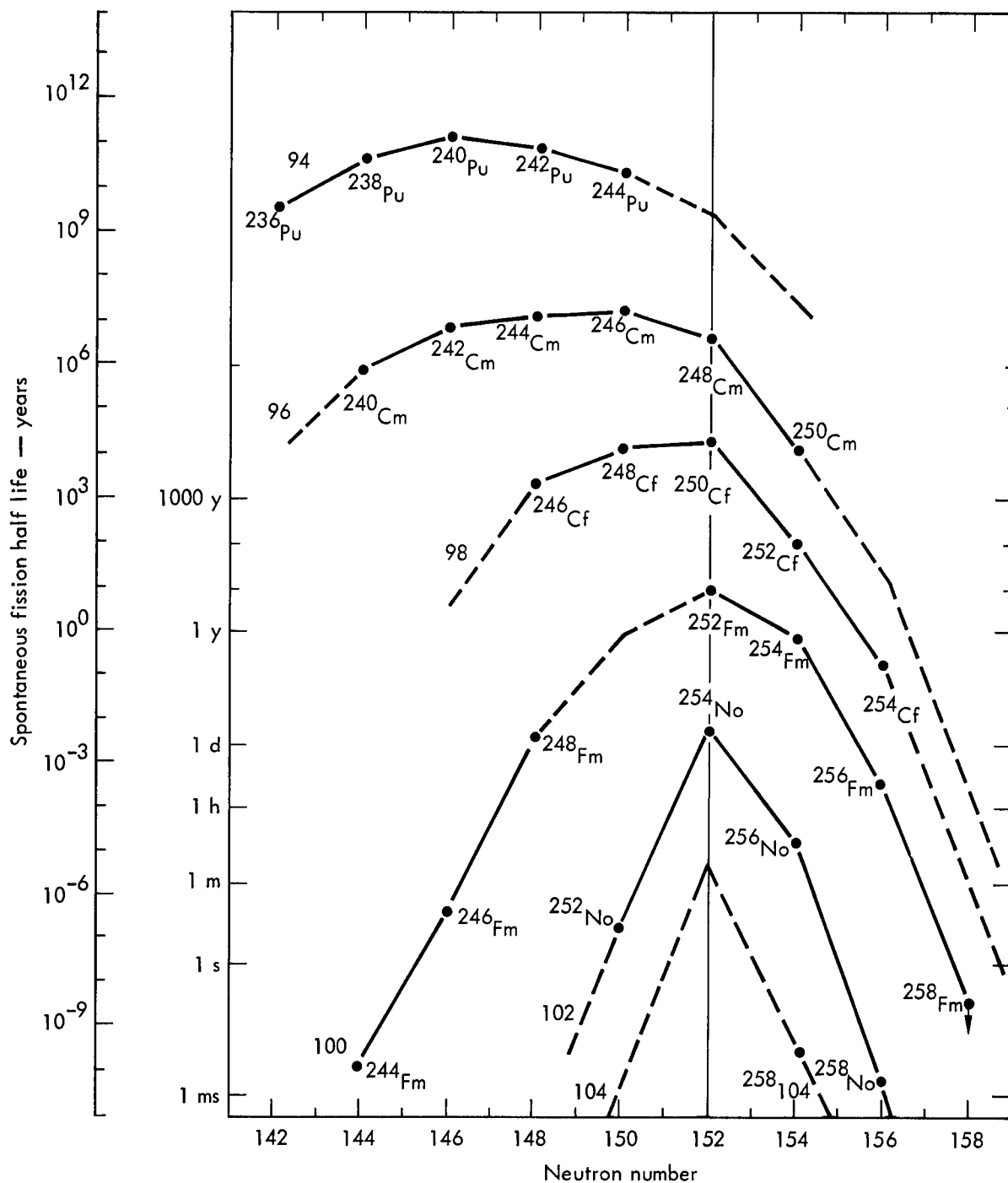


Fig. 2. Spontaneous fission half-life trends for even-even nuclei in the heavy elements.

nuclei with $A > 257$. One result is that the even-numbered mass chains with $A > 254$ are consumed by SF, leaving only the odd-numbered chains to survive because of hindrance to spontaneous fission rates associated with an odd neutron or proton. These predictions of spontaneous fission half-lives are sufficiently uncertain that there was a reasonable possibility of survival of a detectable number of atoms with $A = 259$ (~100 atoms are required) in our samples.

Counting of alpha particles and fission fragments from the first pure sample of fermium began ~8.5 days after the test. At that time the ratio of alpha to fission disintegration rates of ^{257}Fm in the sample was 470 ± 25 .

By comparing this value to an average ratio of 495 ± 15 measured later and to a ratio of 510 ± 25 for reactor-produced ^{257}Fm ,³ we find no excess fissions attributable to ^{259}Fm . Similarly, in two samples of a combined Md-Lw fraction there was no evidence for ^{259}Md in the alpha spectra, nor was there unassigned spontaneous fission activity. After counting alpha particles from the Md-Lw samples for 20 days in a Frisch-grid ionization counter, we noted only 24 events in the expected alpha-energy range for ^{259}Md of 6.7 to 7.0 MeV; these were shown to be random background. In addition, we have not observed any growth of 7.03 MeV ^{255}Fm alpha particles, a product of the alpha decay of either ^{259}Fm or ^{259}Md . Thus, we have no positive evidence for the presence of ^{259}Fm or ^{259}Md in our samples from Hutch.

Half-life limits for ^{259}Fm and ^{259}Md were calculated from the observed alpha and fission rates of our samples and are listed in Table III. Essential assumptions are that neutron capture proceeded from ^{257}U to ^{259}U without serious fission competition and that the mass-259 beta decay chain was not terminated by SF before reaching ^{259}Fm . On that basis we expected a total of 10^{17} atoms of ^{259}Fm or ^{259}Md product.

Table III. Half-life limits for ^{259}Fm and ^{259}Md

^{259}Fm :	$T_{1/2} \leq 0.5 \text{ d (SF) or } \geq 250 \text{ y } (\alpha)$
^{259}Md :	$T_{1/2} \leq 0.5 \text{ d (SF) or } \geq 1.25 \times 10^4 \text{ y } (\alpha \text{ or SF})$

In the upper range, the half-life limits for either nuclide are much too long to be credible, particularly when related to systematic trends in this region of nuclei. We can only conclude that one or more members of the mass-259 chain is shorter lived than our limits. The shortest half-life limits measured in this experiment and Cyclamen ($\leq 5.5 \text{ hr}$)^{4,5} are still well above the predicted lifetimes for SF. Clearly, because of the long drilling time needed to recover debris samples in underground nuclear experiments, it is impossible to use this technique when trying to identify heavy species with half-lives shorter than several hours. In view of the hour or less half-lives expected, we must find new methods for the faster recovery of debris in future experiments.

We might have also expected to see alpha decay from ^{265}Lw or ^{267}Lw , providing these nuclides were produced and survived long enough to be detected. In the energy region above 7.0 MeV where one would expect to observe the alpha groups of these nuclides, we found no evidence for their existence. The intermediate odd-A mass chains probably terminate at ^{261}No and ^{263}No . The LRL analyses did not include isolation of a nobelium fraction, but studies at LASL and ANL failed to produce any evidence for the existence of these nuclides.⁶

A search was also made for long-lived isotopes of element 104. Chemical isolation followed carrier-free Hf chemistry since the chemical properties of element 104 are expected to resemble those of Hf and Zr. There was no evidence for spontaneous fission or alpha activity in the final sample. Either element 104 was not produced in Hutch or the half-lives (spontaneous fission) are too short to allow observation in this experiment. Since the lightest isotope that might have been detected is $^{269}\text{104}$, production and detection of this nuclide was marginal at best.

One of the more intriguing postulates of recent years in the study of heavy elements has been the suggestion that nuclides in the region of $^{298}114$ may be long-lived enough to be detected if one can derive a means of producing them.⁷ Although the predicted half-lives and the extent of this "island of stability" are quite uncertain, it appears that one must produce nuclei with

$A > 294$ in order to reach a region of half-lives longer than a few hours. The neutron flux achieved in Hutch was insufficient to even approach production of atoms of mass number 294. A much more intense neutron flux is required. In addition to the question of whether there are ways to produce the necessary neutron exposure, one can ask whether the problems that prevented detection of nuclides with $A = 258-265$ in the Hutch debris will also prevent formation and detection of heavier nuclides. If this problem lies mainly in the destruction of heavy nuclei by neutron-induced fission during the capture phase, then one is doomed to failure in attempting to produce even higher fluxes and heavier products. If, however, the Hutch explosion resulted in the production of reasonable amounts of nuclides with $A = 258-265$ and these nuclides were then consumed in spontaneous fission decay of certain members of each beta-decay chain, there is still a mechanism available for producing heavier products if one finds a way to increase the total neutron exposure. Unfortunately, there are no direct clues in the data as to which mechanism is responsible for the fruitless search for heavier species.

LARGE-SCALE RECOVERY AND PROCESSING OF HUTCH DEBRIS

Perhaps the most important gain scored by the Hutch test is the opening of a new path for synthesizing useful quantities of rare nuclides. The debris offers a unique source of ^{250}Cm and ^{257}Fm , both of which can serve as target materials for charged particle bombardments to produce hitherto unobserved isotopes and possibly new elements. The ^{250}Cm and ^{257}Fm are rare enough that it was considered attractive to attempt to recover 500 kg of debris for chemical processing and recovery of the heavy actinides.

Accordingly, the Phase II, large-scale sample recovery operation was carried out during the period August 22 to September 14, 1969. The recovery technique involved enlarging a drill hole, initially 10 in. in diameter, to a 15-in. diameter by reaming and collecting the loosened rock in a basket mounted below the reaming tool. A total of eleven baskets, each full of rocks and drilling mud, were recovered from three holes drilled in various positions in the debris distribution. The total weight of material recovered in this manner was approximately 1100 lb or 500 kg.

During the initial attempts to recover samples immediately following the explosion, the recovery of debris from the 2000-ft depth was accomplished by sidewall sampling. With this technique a 100- to 200-g sample is obtained by forcing a hollow sampling tool into the side of the hole and recovering a sample from the rock lodged in the tool. Early Hutch samples obtained in this manner showed relatively good concentrations, e.g., the second 100-g sample studied had a concentration of 8×10^{-12} of the device per gram of rock in the sample. During Phase I sampling, a total of approximately 10 kg of sample was recovered. A few kg were dissolved for the early studies and the remainder was saved for later dissolution.

Analysis of the 500 kg of sample recovered in Phase II showed that the concentration of device debris in this rock was much lower than expected. In fact, the average concentration in the 500 kg was $\leq 3\%$ of that in the sidewall samples recovered during Phase I. Thus, we had the remainder of the sidewall samples, 6 kg that contained 5×10^{-8} of the device, and 500 kg of sample that contained $< 12 \times 10^{-8}$ of the device. Unless this latter batch could be enriched to some high degree through a "high-grading" technique, it was unattractive to process this material.

We have investigated the question of high-grading the 500 kg of material. After washing to remove drilling mud, the rock was screened to produce fractions classified according to particle size. The specific gamma activity of these fractions remains essentially constant. Thus, there was no gain in merely

sorting the rock according to size. In the larger-sized fractions, one can pick out pieces of fused rock which exhibit relatively high specific gamma activity. However, the yield from this operation is extremely low, e.g., 15 kg of material yields less than 100 g of fused rock.

A more promising high-grading technique has been to sort the more finely-divided material according to magnetic properties. In preliminary experiments, a factor of 4 enrichment has been obtained in a fraction that contains 87% of the spontaneous fission activity. Further study may allow us to improve this factor. Another approach which looks promising is the use of flotation processes for enriching the debris. These high-grading techniques are being further developed.

Inasmuch as we have not yet developed a high-grading technique that will give the desired degree of enrichment, we have proceeded to process a total of 10 kg of rich sample, leaving the remaining 500 kg of material for possible later treatment. Our chemical processing equipment is designed to operate on a 5-kg batch size.⁸ The process flowsheet, subject of an earlier report,⁹ involves leaching the actinide elements from finely-ground rock samples with a mixture of HNO_3 -HF. Following the leach step, the actinides are extracted directly into dioctylpyrophoric acid (DOPP). Following back extraction, an actinide lanthanide separation is accomplished with a LiCl-Dowex 1 anion exchange column. The final step is the production of pure elemental fractions of Fm, Es, Cf, Bk, and Cm. The processing of this 10 kg, which is nearly completed, will yield about 4×10^{-8} of the total device production. In terms of the key nuclides, this represents about 1×10^{10} atoms of ^{257}Fm and 5×10^{12} atoms of ^{250}Cm at this time.

RARE NUCLIDES PRODUCED IN THERMONUCLEAR EXPLOSIONS

In this section we wish to discuss some of the more rare heavy actinide isotopes produced in thermonuclear explosions and to contrast their production and availability with that for these same nuclides in reactor production. There are at least five nuclides that are most advantageously produced in thermonuclear explosions: ^{257}Fm , ^{255}Es , ^{251}Cf , ^{254}Cf , and ^{250}Cm . The first three of these nuclides exhibit large fission (and/or capture) cross sections for thermal neutrons; hence, they are rapidly destroyed in a high-flux reactor. In thermonuclear explosions, the average neutron energy during the capture process is tens of kilovolts and consequently the destruction cross sections for the entire series of multiple neutron capture products tend to be relatively uniform. The result is that certain elemental fractions, e.g., Es, Cf, and Cm, exhibit considerably less variation in isotopic composition when recovered from thermonuclear explosions as compared with reactor-produced material. Our intent is to show that production of these nuclides in thermonuclear explosions serves as a valuable supplement to the already enormously productive AEC production program centered about the High Flux Isotopes Reactor (HFIR) and the Transuranium Processing Plant (TRU) at Oak Ridge National Laboratory.

The most obvious advance in the Hutch experiment was the production of 6×10^{17} atoms of ^{257}Fm . This nuclide, the longest-lived isotope of fermium, has a 95-day half-life and decays predominantly by alpha emission with spontaneous fission branching ratio, SF/α , of 2×10^{-3} . Semiannual production of ^{257}Fm in the HFIR-TRU complex at Oak Ridge has been $\sim 8 \times 10^7$ atoms per batch, recently.¹⁰ Future production is predicted to increase to an annual rate of approximately 2×10^9 atoms by 1971. Thus, the amount of ^{257}Fm produced in the Hutch explosion exceeded current reactor production capacity by a factor of almost 10^{10} .

Much of the interest in ^{257}Fm for experimental purposes lies in the possibility of recovering enough material to serve as a target for charged-particle

and neutron irradiations. As has been already discussed by Cowan,⁵ a list of laboratory-produced nuclides one might produce with a ^{257}Fm target is shown in Table IV.

Table IV. Reactions for producing new nuclides with a ^{257}Fm target.

^{257}Fm	(n, γ)	^{258}Fm
	(d, p)	^{258}Fm
	(t, p)	^{259}Fm
	(t, n)	^{259}Md
	(α, n)	^{260}No
	$(\alpha, 2n)$	^{259}No

The goal here is to produce nuclides with neutron numbers greater than 157. To date, no heavy species has been observed that contains more than 157 neutrons in its nucleus, in spite of repeated attempts to identify ^{258}Fm from the $^{257}\text{Fm}(n, \gamma)$ reaction. It has been concluded that the half-life of ^{258}Fm is probably shorter than 200 msec where the decay is predominantly spontaneous.¹¹ Of importance in the experimental program for the ^{257}Fm target outlined in Table IV is that one can repeat the experiments many times, an essential feature when one is searching for and studying short-lived nuclides. In contrast, if one is constrained to search for nuclides such as ^{259}Fm , ^{259}Md , and ^{260}No only in the debris following the explosion of a heavy-element-producing device, the opportunities for repeated experiments are limited.

Another nuclide of interest in the Hutch debris is the 39-day alpha emitter ^{255}Es . In Table V we see that einsteinium produced in the High Flux Isotope Reactor contains 0.06 at.% ^{255}Es . To produce higher isotopic purity for experimental purposes, we have enriched these samples in the Livermore isotope separator with resultant purity as high as 90 at.% ^{255}Es . The ^{255}Es abundance in the Hutch Es is 20 at.% (see Table V), intermediate in concentration between the raw HFIR product and the same material following isotope separation. A significant feature of the Hutch Es is that ^{254m}Es is entirely absent, since the beta decay for mass 254 stops at the beta-stable ^{254}Cf . As an example, ^{254m}Es is an objectionable impurity in samples where one is studying ^{255}Es alpha decay because the lower-energy ^{254m}Es alpha groups tend to overlap the alpha groups of ^{255}Es . Thus, Hutch Es, if further enriched in an isotope separator, offers good prospects for very pure samples of ^{255}Es for experimentation.

Table V. Comparison of reactor-produced and Hutch einsteinium

Half-life, type of decay	HFIR Es ^(a)		Hutch Es	
	A	Atom ratio	A	Atom ratio
20.5 d α	253	1.00	253	1.00
276 d α	254m	0.003	254m	0
39 d β^- , α	255	0.0006	255	0.231

^aThe isotope ratios listed are typical for material directly from the HFIR reactor. The composition of HFIR Es changes rapidly with time because of the short half-lives of the isotopes.

The californium fraction in the Hutch debris is significantly richer in two isotopes, ^{251}Cf and ^{254}Cf , than is reactor-produced Cf. The comparison is made in Table VI. As feed material for isotopic enrichment, the Hutch Cf presents an opportunity to produce ^{251}Cf samples of high purity. In addition, the Hutch Cf offers an excellent opportunity to study the spontaneous fission of ^{254}Cf . When the first samples were recovered, 98% of the spontaneous fission rate of the Cf sample was due to ^{254}Cf ; even now the ^{254}Cf is 93% of the total rate. Wolfsberg and others¹² have used the Hutch Cf to make a radiochemical study of the distribution of fission products from the spontaneous fission of ^{254}Cf .

Table VI. Comparison of reactor-produced and Hutch californium

Half-life, type of decay	HFIR Cf ^a		Hutch Cf	
	A	Atom ratio	A	Atom ratio
352 y α	249	0.0012	249	—
13 y α	250	0.0083	250	—
900 y α	251	—	251	0.48
2.65 y α , SF	252	1.000	252	1.00
18 d β^-	253	0.0069	253	0.19
60 d SF	254	0.0007	254	0.18

^aCalifornium of differing isotopic compositions can be produced in the HFIR, depending upon total neutron exposure, target material, etc. The composition listed here is that for ^{252}Cf , which had been irradiated for 70 days at 3×10^{15} n/cm² - sec and had served as feed material for isotopic enrichment of ^{253}Cf and ^{254}Cf .

The Hutch curium is an invaluable source of the rare isotope, ^{250}Cm . Reactor production of heavy curium isotopes does not produce appreciable (or even detectable) amounts of ^{250}Cm , since its production depends upon competition between beta decay of 64-min ^{249}Cm and neutron capture by ^{249}Cm . The 2200 m/s capture cross section for ^{249}Cm is reported to be 2.8 barns (see p. 32 of Ref. 10). Even at the flux level of the HFIR (5×10^{15} n/cm² sec), a very large fraction of the ^{249}Cm atoms beta-decay (or are destroyed by neutron-induced fission), and only the minutest amount are converted to ^{250}Cm . The Hutch Cm contains 6.4 at.% ^{250}Cm (Table VII). This isotope is particularly attractive for use as a target material in heavy-ion bombardments because of its high ratio of neutrons to protons. It is often desirable to use neutron-rich targets in heavy-ion bombardments, since the products tend to be on the neutron-deficient side of beta stability. As an example, recent studies of the isotopes of elements 104 and 102 involved the bombardment of a ^{248}Cm target with oxygen ions.¹³ The half-life of ^{250}Cm , about 10^4 yr, is long enough that the debris can be mined and chemically processed long after the majority of fission products have decayed.

FUTURE EXPERIMENTS

From the preceeding discussion, it is clear that in future experiments considerable attention should be paid to insuring adequate sample recovery. There are two aspects of the problem that require development: rapid sample recovery and large-scale sample recovery.

In the search for short-lived species in previous experiments, a limit of ≤ 5.5 hr was set for the half-life of ^{259}Fm in the Cyclamen event.⁴ In this

Table VII. Comparison of reactor-produced and Hutch curium

Half-life, type of decay	HFIR Cm ^a		Hutch Cm	
	A	Atom ratio	A	Atom ratio
18 y α	244	5.11	244	—
8300 y α	245	0.043	245	1.00
4700 y α	246	1.000	246	1.00
1.6×10^7 y α	247	0.030	247	0.41
3.8×10^5 y α	248	0.058	248	0.91
1.1×10^4 y SF	250	—	250	0.31

^aThe isotopic content of curium from HFIR will depend upon the circumstances of its irradiation. The isotopic composition listed here is for material that has received intense neutron exposure and is considered a useful source of isotopes with A > 244.

work a sample had been recovered, processed chemically, and was ready for counting 36 hr after the explosion. To improve upon this limit, a means of delivering and processing samples much more rapidly must be devised. Technology does exist whereby samples are brought to the surface through a fluid-filled pipe immediately following the explosion. A report by J. D. Brady¹⁴ describes the results of analyses of the contents of tanks containing the prompt sample and fluid (a dilute starch solution in water) in two separate experiments. In the Anacostia experiment, the prompt sampling system collected 10 to 40 kg of solids with a specific Pu content nearly equal to that of good puddle glass samples. These solids were dispersed throughout 6.4 m³ of starch. There remains the development of a system that will successfully retrieve a small part of the solids collected in the tank, process the material chemically, and provide a sample for counting within 1 or 2 hr after zero time. Other techniques for retrieving prompt samples that may eliminate the need for extensive chemical purification are under study at our laboratory.

Perhaps the most vital need in the entire program is the development of a reliable, economical system for large-scale recovery of device debris. While the concentration of samples recovered in the latter phases of Hutch sampling was disappointing, the reaming of the sample hole did allow the retrieval of 500 kg of material. It is likely that additional work on this technique will produce a reliable method for recovering large samples.

Another factor in this problem is the medium in which the device is exploded. A promising approach would be to detonate the next experiment in salt, as was done in the Salmon event.¹⁵ In Salmon, the 5-kt explosion melted 5000 tons of salt. However, the debris was efficiently scavenged from the molten salt by the oxides (CaO, SiO₂, Na₂O, Fe₂O₃) present. Hence, the radioactive products from Salmon were contained in about 50 tons of solids. Sample concentrations were at least two orders of magnitude higher than one finds in the ordinary shots in NTS alluvium. An important feature here is that the spherical cavity produced during the explosion does not collapse; the debris is contained in molten salt that runs down to form a lake in the bottom of the cavity and eventually solidifies. Since there is no collapse of the cavity, the molten puddle is not diluted by inert material that falls from the ceiling. Although an explosion in a salt medium would produce the most concentrated debris, as well as material that is particularly amenable to large-scale

chemical processing,¹⁶ problems with doing experiments other than at NTS are so severe that other possibilities should be considered. Areas do exist within the Test Site where an experiment can be performed in dolomite rock (a mineral consisting primarily of Ca and Mg carbonate), a medium which offers some advantages in chemical processing.

In reviewing the current situation, we see that the device development phase of this program has reached a stage where it is possible to create quantities of certain nuclides that exceed reactor production by as much as ten orders of magnitude. Yet the development of a technology to recover these materials has not proceeded to where satisfactory amounts of this "ore" can be delivered to a chemical processing plant. In planning and executing future experiments, this imbalance will have to be corrected in order to obtain maximum benefits from the program.

ACKNOWLEDGMENTS

The authors wish to acknowledge the efforts of many co-workers at the Lawrence Radiation Laboratory, Livermore, Los Alamos Scientific Laboratory, and Argonne National Laboratory in analyzing samples and recovering actinides from the Hutch debris. We also wish to thank S. F. Eccles, and R. A. Heckman for their helpful discussions in preparing this manuscript.

REFERENCES

1. S. F. Eccles, "Production of Heavy Nuclides in Nuclear Devices," to be presented at the ANS Topical Meeting, Engineering with Nuclear Explosives, January 14-16, 1970, Las Vegas, Nevada.
2. S. F. Eccles and E. K. Hulet, Lawrence Radiation Laboratory, Livermore, Rept. UCRL-50767 (October 1969), unpublished.
3. E. K. Hulet, R. W. Lougheed, and B. J. Qualheim, Lawrence Radiation Laboratory, Livermore, private communication.
4. D. C. Hoffman, Arkiv Fysik 36, 533 (1966).
5. G. A. Cowan, Synthesis of Neutron-Rich Nuclides, Los Alamos Scientific Laboratory Report LA-3738 (1967); presented at American Chemical Society Meeting, Miami, Florida, April 1967.
6. G. A. Cowan, Los Alamos National Laboratory, Los Alamos, New Mexico, and P. R. Fields, Argonne National Laboratory, Argonne, Illinois; private communication.
7. S. G. Nilsson, et al., Nucl. Phys. A131, 1 (1969); H. Meldner, Arkiv Fysik 36, 593 (1967); and W. J. Swiatecki and W. D. Meyers, Nucl. Phys. 81, 1 (1966).
8. R. Quong and J. R. McNabb, Chemical Processing Facility to Recover Actinide Isotopes Produced in Underground Nuclear Explosions, Lawrence Radiation Laboratory, Livermore, Rept. UCRL-50499 (October 1968).
9. E. K. Hulet, J. E. Evans, R. Quong, and B. J. Qualheim, The Chemical Recovery of Heavy Elements from Underground Nuclear Explosions, Lawrence Radiation Laboratory, Livermore, Rept. UCRL-14838 (1968) Abstract; presented at American Chemical Society Meeting, San Francisco, March-April 1968.
10. W. D. Burch, J. E. Bigelow, and L. J. King, Oak Ridge National Laboratory Rept. ORNL-4428 (November 1969) unpublished.
11. E. K. Hulet, C. E. Bemis, Jr., and R. W. Lougheed, Lawrence Radiation Laboratory, Livermore, private communication.
12. K. Wolfsberg, et al., Los Alamos Scientific Laboratory, Los Alamos, New Mexico, private communication.
13. A. Ghiorso, M. Nurmi, J. Harris, K. Eskola, and P. Eskola, Phys. Rev. Letters 22, 1317 (1969).

14. J. D. Brady, Evaluation of the Prompt Sample Systems Used for the Anacostia and Kennebec Experiments, Lawrence Radiation Laboratory, Livermore, Rept. UCRL-50441 (March 1968).
15. D. Rawson, P. Randolph, C. Boardman, and V. Wheeler, J. Geophys. Res. 71, 3507 (1966).
16. R. Elson, et al., Coach Processing, A Study of Processes for Concentrating Actinides Formed in a Nuclear Detonation in a Salt Medium, Lawrence Radiation Laboratory, Livermore, Rept. UCRL-14494 (May 1965).

THERMONUCLEAR NEUTRON SOURCES—A NEW ISOTOPE PRODUCTION TECHNOLOGY*

Richard A. Heckman
Lawrence Radiation Laboratory, University of California
Livermore, California 94550

ABSTRACT

With the successful detonation of the Hutch device, we have demonstrated the feasibility of a new isotope production technique. The exposure of a ^{238}U and ^{232}Th target to an extremely large neutron flux, 1.8×10^{25} neutrons/cm², produced super-heavy nuclides up to ^{257}Fm by the multiple neutron capture process. Kilogram quantities of Hutch debris were recovered by a modification of standard drilling techniques. A semicontinuous batch process was used to concentrate approximately 10^{10} atoms of ^{257}Fm from approximately 50 kg of debris.

Experience from the Hutch debris recovery efforts indicates that significant engineering advances in recovery techniques and subsequent cost reductions are possible. The demonstrated success of the device clearly justifies an engineering development program. Comparing debris recovery by underground mining operations with recovery using possible advances in drilling technology does not indicate an obvious cost advantage of one system over the other.

Possible advances in mining technology could change this tentative conclusion. Any novel schemes for debris concentration that might be possible through an understanding of underground nuclear detonation phenomenology would also radically affect recovery and processing economics.

A preliminary process engineering design of a large-scale (a few hundred to a few thousand kilograms) processing facility located at the Nevada Test Site will be discussed. Cost estimates for isotopes produced in this facility will be described. The effects of debris concentration, "ore" beneficiation, and total debris processed on unit costs will be discussed. These preliminary estimates show that this new isotope "production" scheme would be competitive with existing reactor facilities.

INTRODUCTION

With the successful detonation of the Hutch device, an extremely large neutron flux, 1.8×10^{25} neutron/cm², was achieved. Exposing a ^{238}U and ^{232}Th mixed target to this neutron flux produced large quantities of super-heavy elements (see Fig. 1). Previous papers of this symposium^{1,2} have discussed this production and the subsequent search for nuclides with mass number (A) greater than 257 as well as possible future experimental searches for these nuclides.

*Work performed under the auspices of the U.S. Atomic Energy Commission.

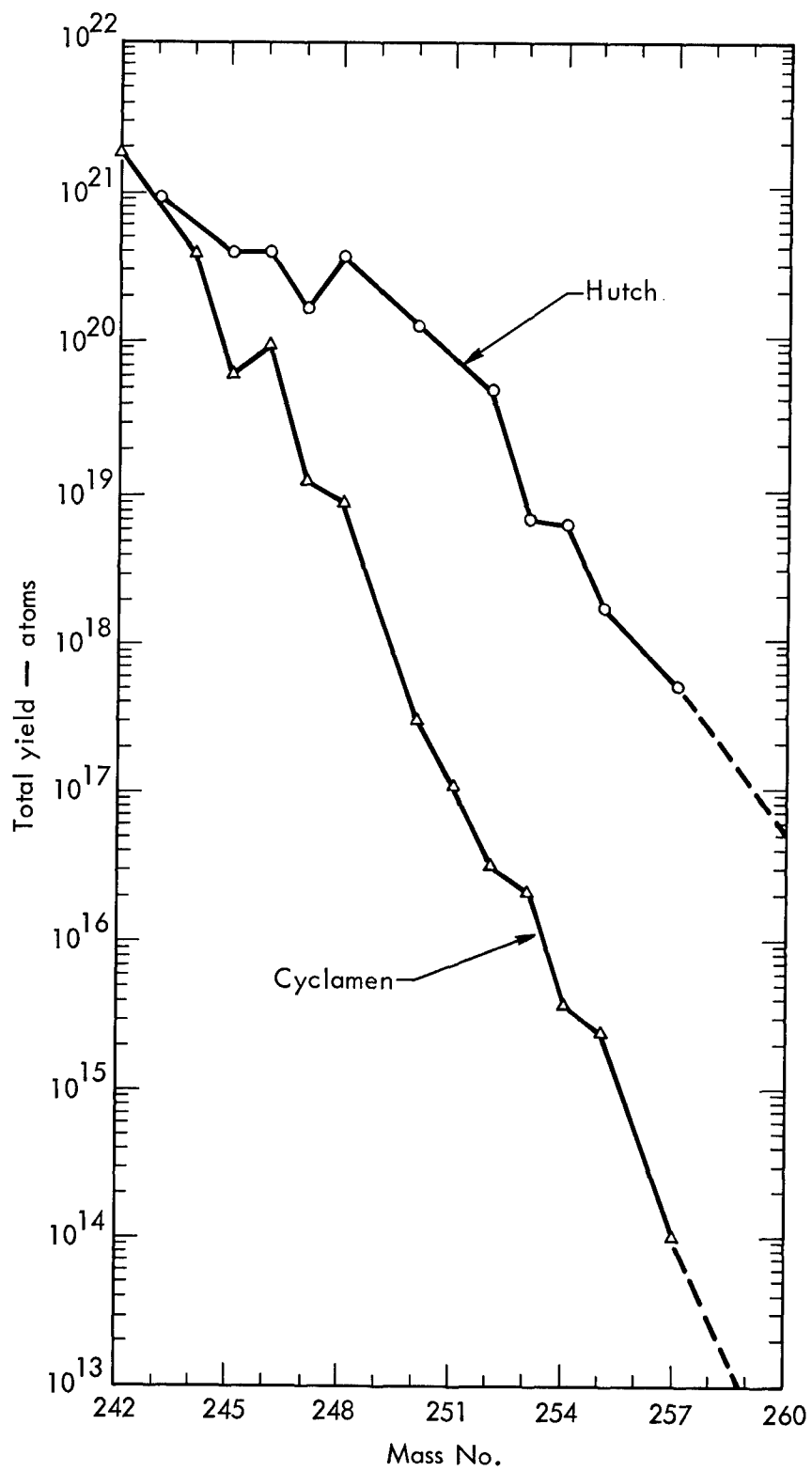


Fig. 1. Yield of transuranium elements from the Hutch and Cyclamen Events.

This paper will discuss the engineering feasibility of using thermonuclear neutron sources as part of a viable isotope production technique. The economics of this proposed technique will be discussed in some detail.

HUTCH DEBRIS RECOVERY OPERATIONS

Using a modification of standard postshot sampling techniques developed at the Nevada Test Site, approximately 1100 lb (500 kg) of Hutch debris was recovered between August 22, 1969, and September 14, 1969. To do this, a 10-in. hole was directionally drilled into the cavity region. The drilling bit and its string were removed and a directional log of the hole obtained by inserting a survey tool and running it up and down the hole. Then a gamma survey was run using a gamma logging tool. This technique locates the "ore."

Then a modified under-reamer tool capable of reaming to a total hole diameter of 15 in. was lowered to the desired sampling depth. The under-reamer arm was extended and the reaming operation done until the tool's chip-collection basket was filled. Then the under-reamer was brought back to the surface to dump the basket into the transportation caskets. Under-reams approximately 2 ft long per pass were possible. There is a practical limit to the length of the recovery basket because it must be able to pass through the dogleg produced by the whip-stocking operation (see below).

After a hole was under-reamed through the "hot" region (as determined by gamma logging), a new drilling string was run into the hole and a dogleg whip-stocked off the original hole. The directional and gamma logging steps were repeated, and the whole sampling process was repeated. Only a limited number of whip-stocks may be drilled in a single hole. It is then necessary to return the surface, reset the drill rig, and start a new hole from the surface. The insertion and removal of the strings during the drilling, surveying, gamma logging, and sampling operations around the doglegs associated with whip-stocking leads to the finite probability of hole collapse in the whip-stock region. Then the whole process starts again. Luck does play a significant role in the success of a postshot drilling operation.

Three surface holes were drilled on Hutch. Several whip-stocks were made off each hole. Eleven baskets (1100 lb) of debris were recovered.

Clearly, an engineering development program to significantly improve the reliability of postshot drilling recovery of very large quantities of debris is justified. The development of survey and gamma logging tools that can be installed directly in the drilling string would drastically improve the situation. This is no mean project, because of the very hostile environment—high temperatures, steam, and radiation fields—associated with an underground nuclear detonation.

ALTERNATIVE RECOVERY COMPARISON

An alternate recovery scheme would be the use of underground mining operations. Figure 2 is a schematic layout comparing the two systems.

A 60-in.-diam hole would be drilled and cased to the working-point elevation. A drift would be mined to the cavity edge. Using mining techniques developed during the Rainier Event exploration³ to minimize radiation exposure to the miners, the desired amount of debris could be safely recovered. Judicious location of the recovery operation shaft would allow use of the facilities for several events. For example, the several device emplacement holes could be arrayed in a circle with the recovery shaft at the center. Indeed, it would be possible to eventually use this shaft as a device emplacement hole itself.

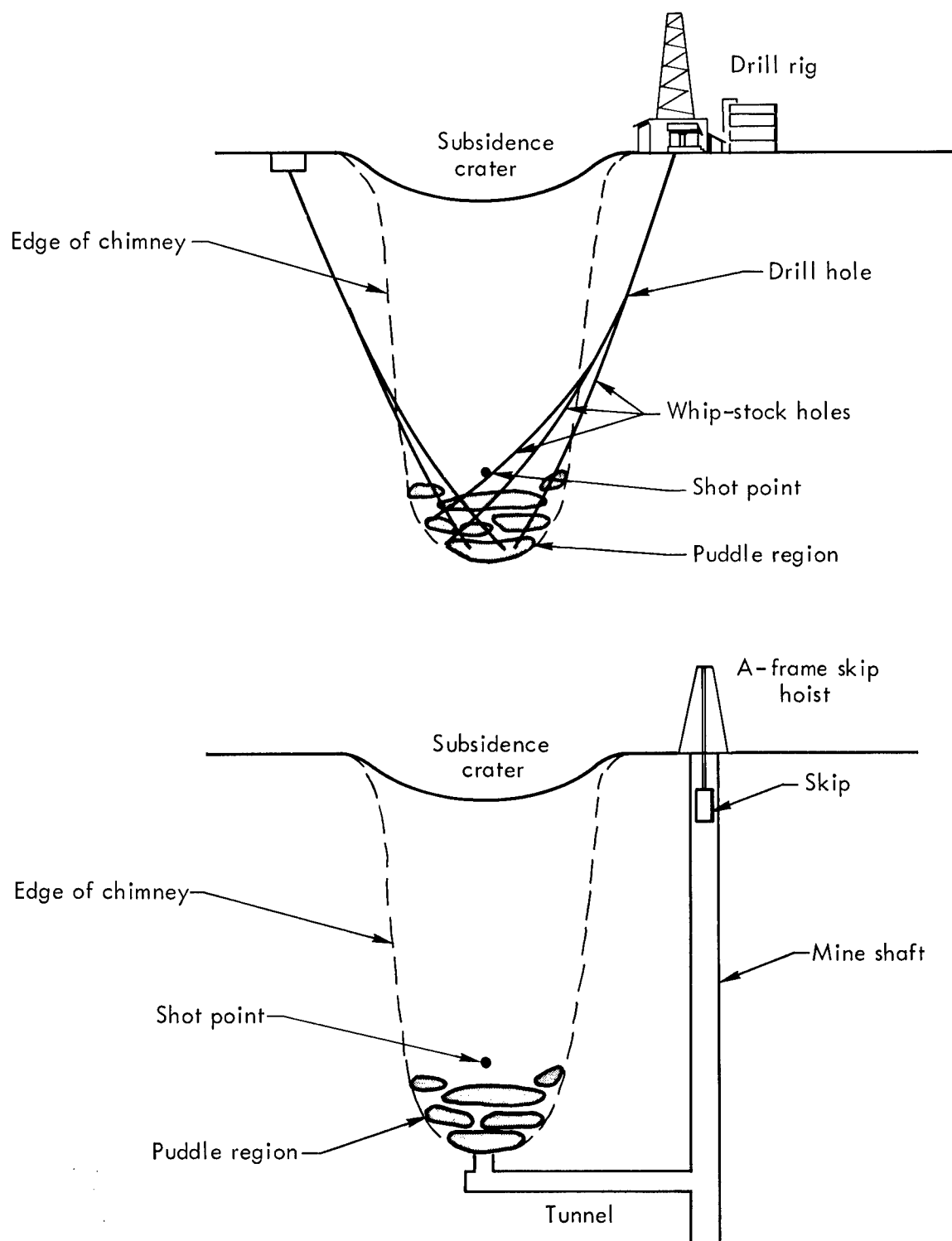


Fig. 2. Debris recovery methods: conventional postshot drilling (top) and underground mining (bottom).

Tables I and II summarize the cost estimates for each type of operation. This is no clear economic advantage for either system. Neither operation can recover a very large fraction of the debris because the removal of a large fraction of the chimney rubble causes the chimney to collapse.

Table I. Cost estimates of postshot drilling recovery operation.

3 each 10-in. drill holes at \$40/ft, 2000-ft long with 2 whip-stocks per hole	\$240,000
Radioactive shielding and handling tools (includes Rad-Safe operations, well-head containment unit, blooie line absorber units)	25,000
Total	\$265,000

Table II. Cost estimates of underground mining operation.

60-in. cased hole 2200-ft long at \$100/ft	(\$220,000)
Drift 6 ft X 4 ft X 2000-ft long at \$75/ft	150,000
Frame and hoist	50,000
Ventilation and filters	20,000
Radioactivity shield and handling tool	15,000
Sampling recovery operations	20,000
Total (not including 60-in. hole)	\$255,000

PROPOSED DEBRIS ENRICHMENT SCHEME

The Marvel Event was a nuclear shock tube experiment⁴ to study the hydrodynamic flow of energy down a circular tunnel from a nuclear explosion at one end of the tunnel. An appreciable fraction of the debris was deposited near the end of the tunnel. The Salmon Event was a nuclear detonation in a salt dome.⁵ Late-time chemical fractionation of the debris was observed at the bottom of the molten puddle formed at the bottom of the cavity. Combination of these two experimental observations of phenomenology associated with an underground nuclear detonation leads to the debris enrichment scheme shown in Fig. 3.

The thermonuclear neutron source is installed at the bottom of the emplacement hole. A horizontal tunnel extends to the debris zone. A large hole has been excavated by mining and filled with salt. Shortly after detonation and exposure to the high neutron flux, the target debris is ejected into the horizontal tunnel and travels to the salt zone, where it is stopped. The energy associated with the transfer process melts a portion of the salt. The debris is insoluble in the molten salt and settles to the bottom of the salt puddle. After the system cools to ambient temperature—a few weeks after the detonation—the salt zone can be re-entered and the highly enriched debris recovered and concentrated for processing.

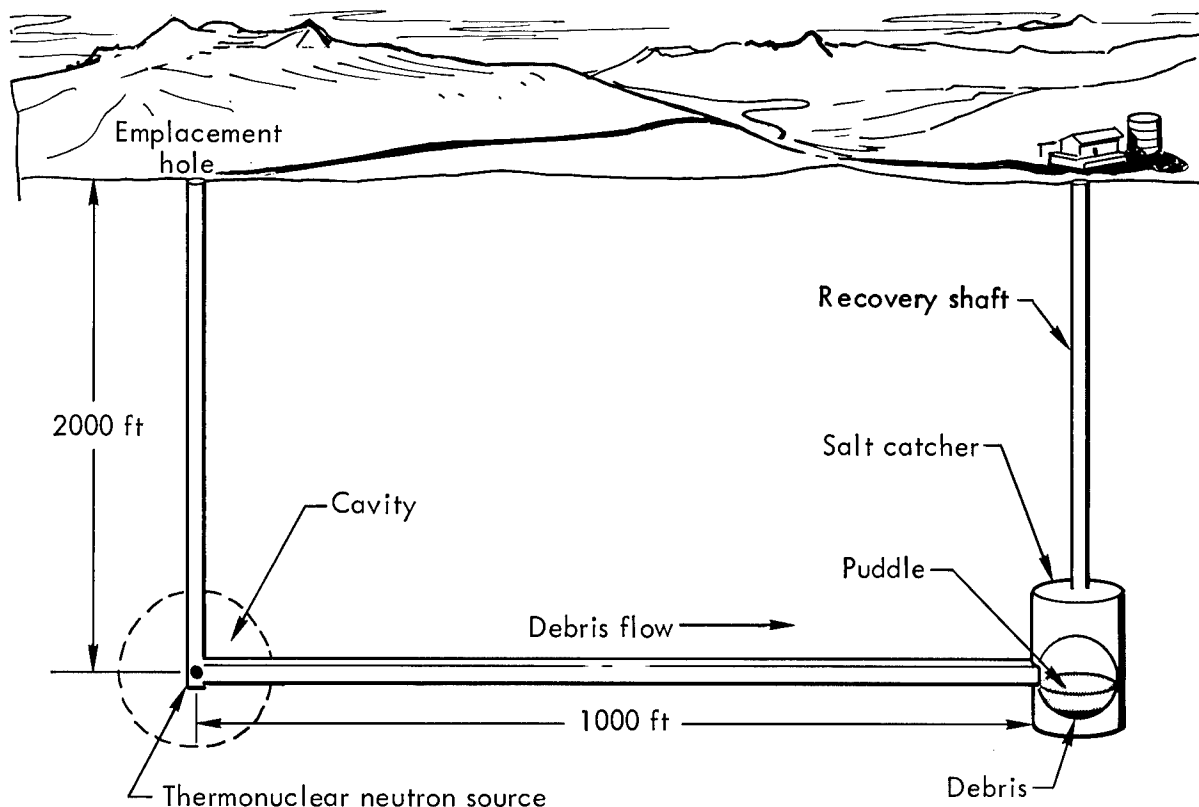


Fig. 3. Proposed debris enrichment scheme.

PROCESS ENGINEERING CONCEPT OF LARGE SCALE RECOVERY FACILITY

The block diagram of a heavy elements processing plant is shown in Fig. 4.⁶ A semicontinuous batch processing facility capable of handling up to 500 kg of ore was built and operated on Hutch debris.⁷ It should be noted that the final product is only about 0.5 g; we have reduced the debris mass from 5 kg to 0.5 g, a factor of 10^4 .

Table III summarizes the preliminary estimates of facility construction costs for a 1000 kg/wk plant. Operating costs include operating personnel, maintenance personnel, and chemicals.

For three-shift operation six people are required per shift (five operators and one maintenance engineer), or 18 people per day. At an average cost of \$10 per hour per man (including overhead burdens) the daily personnel operating costs are \$1440. Table IV summarizes costs per kilogram of raw "ore."

DEBRIS CONCENTRATION AND PROCESSING COSTS

If we were able to obtain "ore" for plant feed as concentrated as was obtained from Hutch (8×10^{-12} of the target yield per gram of rock), we would have to process at least 1.5×10^8 kg of material. A processing rate of 1000 kg/wk is clearly too slow to handle this fantastic quantity of material.

To handle the processing job in 10 weeks (assuming we want isotopes with half-lives greater than 30 to 60 days) we would need a processing rate of 1.5×10^7 kg/wk. This plant is estimated to cost \$115,000,000 (0.6 power capacity scaling factor). Chemical costs would be \$450,000,000.

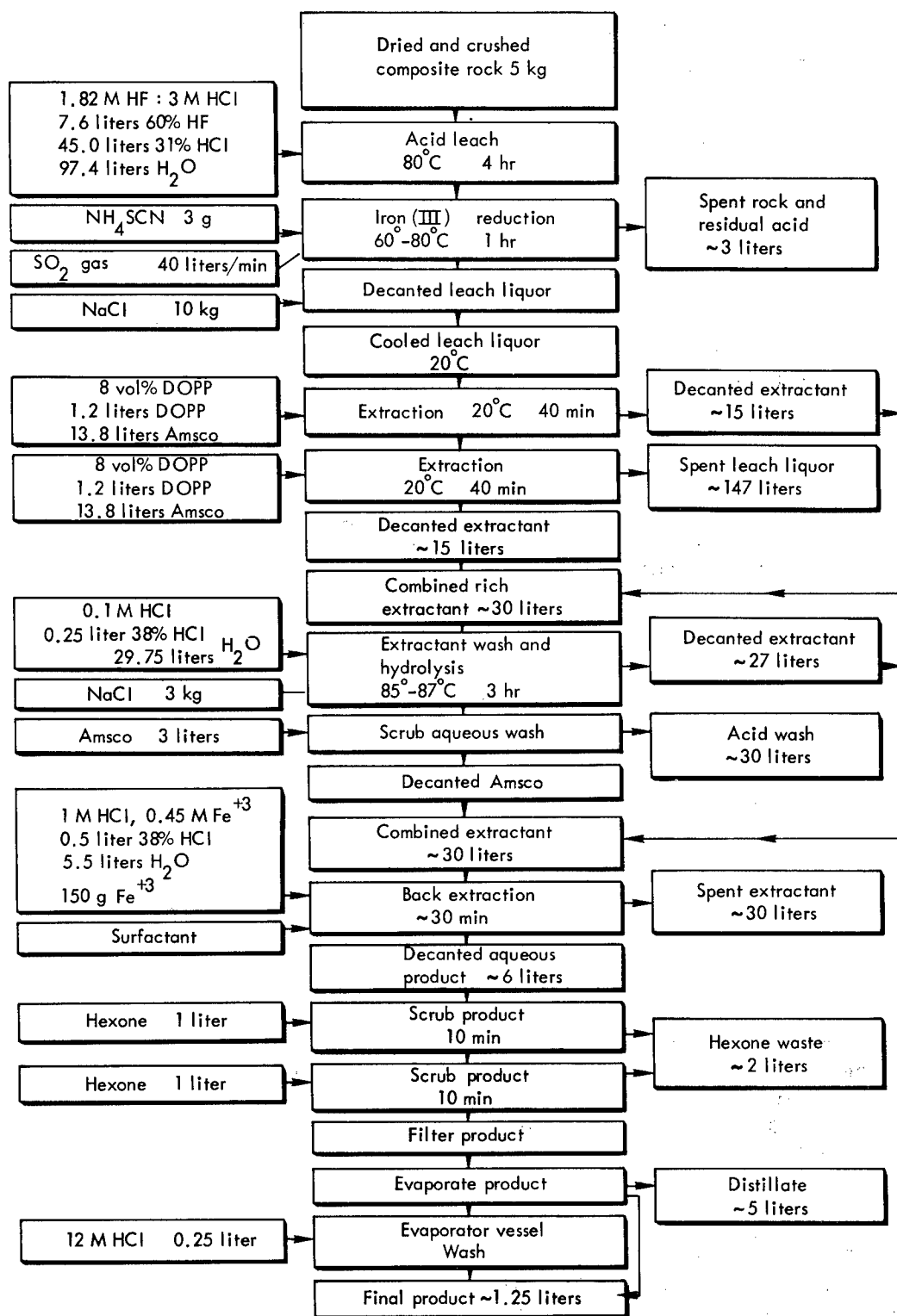


Fig. 4. Block diagram of heavy-elements processing plant.

Table III. Preliminary cost estimates for 100 kg/wk processing rate.

Processing tanks	\$ 40,000
Storage tanks	25,000
Piping, valves, pumps	10,000
Process equipment	20,000
Installation	75,000
Total equipment subtotal	\$170,000
Instrumentation	20,000
Electrical, utilities	35,000
Building, yard	25,000
Engineering and inspection	50,000
Subtotal	130,000
Contingency	60,000
Total plant cost	\$360,000

Table IV. Operating costs.

Direct chemical costs (per kg of rock debris):	
DOPP	\$0.20
HCl	0.50
HF	1.50
Amsco	0.15
Hexone	0.05
SO ₂	0.50
NaCl	0.05
Oil	0.05
Total	\$3.00

However, the material recovered during phase II on Hutch was only 3% of the concentration on which the above figures were based.² And, using a magnetic beneficiation technique, only a factor of 4 enrichment was achieved. Clearly, any massive recovery scheme based on this processing concept is doomed to economic failure.

However, let us consider the economics of the proposed novel enrichment scheme. Table V summarizes emplacement costs. These include construction of the nuclear device emplacement hole and tunnel complex, excavating the debris "catcher" room, filling it with bulk salt, and installing a 12-in.-diam recovery pipe containing a dilatant fluid. This recovery system has been described elsewhere.⁸ The dilatant fluid is pumped out of the pipe after the shot, and the "catcher" room is re-entered through this system.

Table V. Underground emplacement cost estimates.

60-in. cased hole 2000 ft deep at \$100/ft	\$ 200,000
60-in.-diam X 60-ft-long "debris catcher" room at \$1.50/ft ³	300,000
48-in. uncased device-emplacement hole 2000 ft deep at \$50/ft	100,000
Drift 6 ft X 4 ft X 1000 ft long at \$75/ft	75,000
Frame and hoist	50,000
Tunnel liner and installation in drift	75,000
Bulk salt crystal and installation in room (10,000 tons at \$20/ton)	200,000
Recovery pipe system and installation	50,000
Security transport and emplacement costs of nuclear device	50,000
Total	\$1,100,000

Table VI summarizes cost estimates for the neutron source target fabrication and direct postshot debris recovery. We will assume 5000 kg of debris has to be processed. We will operate the plant for 5 weeks at a cost of \$36,000 for operating and maintenance personnel. Chemical costs would be \$15,000 (5000 kg X \$3.00/kg). Table VII summarizes these cost estimates and shows a total project cost of \$2,366,000.

Table VI. Estimated costs for neutron source and debris recovery.

AEC projected service charge for a nuclear explosive ⁹ (including arming and firing)	\$550,000
Target (fabrication and material costs)	200,000
Re-entry of recovery pipe system (includes rig setup costs and radiological safety services)	55,000
Recovery of 1000 to 5000 kg of debris (at bottom of salt puddle)	25,000
Magnetic beneficiation	
Equipment	10,000
Operating costs	5,000
Packaging and transportation to processing plant	10,000
Total	\$855,000

Table VII. Summary of estimated costs.

Underground emplacement costs	\$1,100,000
Neutron source, target, and debris recovery	855,000
Processing plant	360,000
Plant operating expenses	
Personnel	36,000
Chemicals	15,000
Total	\$2,366,000

Table VIII summarizes the production of super heavy elements in the Hutch experiment. We will assume a 50% overall yield. Losses must include transmission down the tunnel to the debris "catcher" zone, recovery losses during post-detonation operations in the salt puddle, and processing plant losses.

Table VIII. Total atoms for each mass number chain produced in the Hutch experiment.

Nuclide	Half-life and decay mode	Total atoms (to 7/16/69)	Total atoms (to 1/1/70)
^{242}Pu	$3.9 \times 10^5 \text{ y } \alpha$	4.22×10^{21}	4.22×10^{21}
^{243}Am	$8.0 \times 10^3 \text{ y } \alpha$	9.03×10^{20}	9.03×10^{20}
^{244}Pu	$8.3 \times 10^7 \text{ y } \alpha$	1.71×10^{21}	1.71×10^{21}
^{245}Cm	$8.3 \times 10^3 \text{ y } \alpha$	3.92×10^{20}	3.92×10^{20}
^{246}Cm	$4.7 \times 10^3 \text{ y } \alpha$	8.54×10^{20}	8.54×10^{20}
^{247}Cm	$1.6 \times 10^7 \text{ y } \alpha$	1.60×10^{20}	1.60×10^{20}
^{248}Cm	$3.8 \times 10^5 \text{ y } \alpha$	3.54×10^{20}	3.54×10^{20}
^{249}Bk	$314 \text{ d } \beta^-$	(not measured)	(not measured)
^{249}Cf	$352 \text{ y } \alpha$	—	—
^{250}Cm	$1.1 \times 10^4 \text{ y SF}$	1.21×10^{20}	1.21×10^{20}
^{251}Cf	$900 \text{ y } \alpha$	1.82×10^{19}	1.82×10^{19}
^{252}Cf	$2.7 \text{ y } \alpha$	3.82×10^{19}	3.4×10^{19}
^{253}Cf	$18 \text{ d } \beta^-$	7.20×10^{18}	1.1×10^{16}
^{253}Es	$20 \text{ d } \alpha$	—	2.1×10^{16}
^{254}Cf	60 d SF	6.82×10^{18}	9.7×10^{17}
^{255}Es	$40 \text{ d } \beta^-$	1.66×10^{18}	8.9×10^{16}
^{255}Fm	$20 \text{ h } \alpha$	—	1.8×10^{15}
^{256}Fm	2.6 h SF	(too short-lived)	—
^{257}Fm	$95 \text{ d } \alpha$	5.56×10^{17}	1.6×10^{17}

We can compute unit costs in several ways. First, we can look at unit costs based on total target yield:

$$C_{\text{MT}} = \frac{\sum (\$_{\text{E}} + \$_{\text{O}} + \$_{\text{C}})}{\sum_{\text{A}=242}^{257} Y_{\text{A}}},$$

where C_{MT} = unit costs based on total target yield (\$/μg),
 Y_{A} = mass yield of isotope A (μg),
 $\$_{\text{E}}$ = plant equipment costs (\$),
 $\$_{\text{O}}$ = manpower operating expenses (\$),
 $\$_{\text{C}}$ = material operating expenses (\$).

We can also express costs for target yield above $A = 250$:

$$C_M = \frac{\sum_{A=250}^{257} (\$E + \$O + \$C)}{\sum_{A=250}^{257} Y_A},$$

where C_M = unit costs based on target yields $A \geq 250$ (\$/ μ g). Substituting data from Table VIII gives:

$$C_{MT} = \frac{\$2.36 \times 10^6}{(3.48 \times 10^6 \mu\text{g}) (50\%)} = \$1.35/\mu\text{g}$$

and

$$C_M = \frac{\$2.36 \times 10^6}{(7.2) (10^4) (50\%) \mu\text{g}} = \$65.50/\mu\text{g}.$$

Thus the proposed isotope production scheme is very competitive with existing reactor production methods.

REFERENCES

1. S. F. Eccles, "Production of Heavy Nuclides in Nuclear Devices," these Proceedings.
2. R. W. Hoff and E. K. Hulet, "The Recovery and Study of Heavy Nuclides Produced in a Nuclear Explosion—The Hutch Event," these Proceedings.
3. G. W. Johnson and C. E. Violet, Phenomenology of Underground Nuclear Explosions, Lawrence Radiation Laboratory, Livermore, Rept. UCRL-5124 Rev. I (1958).
4. H. D. Glenn and B. K. Crowley, Marvel—Nuclear-Driven Shock Tube Experiment, Lawrence Radiation Laboratory, Livermore, Rept. UCRL-71266 (1968).
5. D. E. Rawson, R. W. Taylor, and D. L. Springer, Naturwissenschaften **20**, 525 (1967).
6. R. Quong and J. R. McNabb, A Chemical Processing Facility to Recover Actinide Isotopes Produced in Underground Nuclear Explosions, Lawrence Radiation Laboratory, Livermore, Rept. UCRL-50499 (1968).
7. R. Quong and J. C. Cowles, Chemical Processing of Hutch Debris, Lawrence Radiation Laboratory, Livermore, Rept. to be published.
8. R. Heckman, Isotope Production with Nuclear Explosives, Lawrence Radiation Laboratory, Livermore, Rept. UCRL-7963 (1964).
9. Engineering with Nuclear Explosives (Proc. 3rd Plowshare Symp.), Division of Technical Information Extension, Oak Ridge, Tennessee, Rept. TID-7695 (1964).

SYMMETRY OF NEUTRON-INDUCED ^{235}U FISSION AT INDIVIDUAL RESONANCES. III*

G. A. Cowan, B. P. Bayhurst, R. J. Prestwood, J. S. Gilmore, and G. W. Knobeloch

Los Alamos Scientific Laboratory, University of California
Los Alamos, New Mexico

INTRODUCTION

A number of experiments have been described in recent years which document variations in the yields of symmetric or near-symmetric fission products at resonances in ^{235}U and ^{239}Pu neutron-induced fission. In the case of ^{239}Pu fission it has been demonstrated in a statistically significant sample of s-wave neutron resonances ($J^\pi = 0^+$ or 1^+) that the 0^+ levels have a characteristic ^{115}Cd yield which is a factor of four higher than the yield at 1^+ levels.¹ The fission widths of the $J = 0$ levels are larger than the $J = 1$ levels by a factor of ten. The populations of the two groups are in reasonable agreement with the expected $(2J + 1)$ distributions. Previous efforts to obtain equally detailed data in ^{235}U fission² and ^{233}U fission by the "wheel" technique have not been entirely successful due in large part to the high level densities in the epithermal excitation functions of these nuclides and the consequent difficulty in characterizing fission yields in a sufficiently large and well-resolved sample of levels. In a recent "wheel" experiment (late summer, 1969) with a ^{235}U target the energy resolution was sufficiently improved in the region 20 eV - 60 eV to allow characterization of a sample of 38 reasonably well-resolved levels by their relative symmetry of fission.

EXPERIMENTAL PROCEDURES AND RESULTS

The details of the experimental technique have been described previously.¹ In this experiment the flight path was 240.11-m long; the collimating slit was 0.2 cm wide at the rim and 7.1 cm long, the or alloy metal target ($\sim 93.3\%$ ^{235}U) was 0.381-mm thick; the wheel speed was 1.496×10^4 cm/sec at the rim; and the exposure time for a given atom on the target was 13.37 μsec , corresponding to an energy resolution of 0.0557 $\mu\text{sec}/\text{m}$ (the pulse width in time of the emergent neutrons at the moderated source is neglected). Neutrons were moderated at the source to a broad epithermal distribution peaking at $\sim 10^{12}/\text{cm}^2$ in 13.37 μsec in the 40- to 70-eV energy region (Fig. 1).³ The neutron flux on the wheel was terminated before the wheel had turned a full revolution when ground shock initiated by the nuclear explosion collapsed the line-of-sight pipe.

The autoradiographs of the three 60° metal sectors exposed to neutrons are shown in Fig. 2. Dark bands caused by resonance fission are observed at each of the neutron energies identified in Table I. These bands of exposed metal were cut in narrow radial strips of 0.5 - 1 g weight, dissolved, and analyzed for ^{99}Mo , ^{111}Ag , and ^{115}Cd . The ratio of 2.3-day ^{115}Cd activity to 2.7-day ^{99}Mo is

* Work performed under the auspices of the U. S. Atomic Energy Commission.

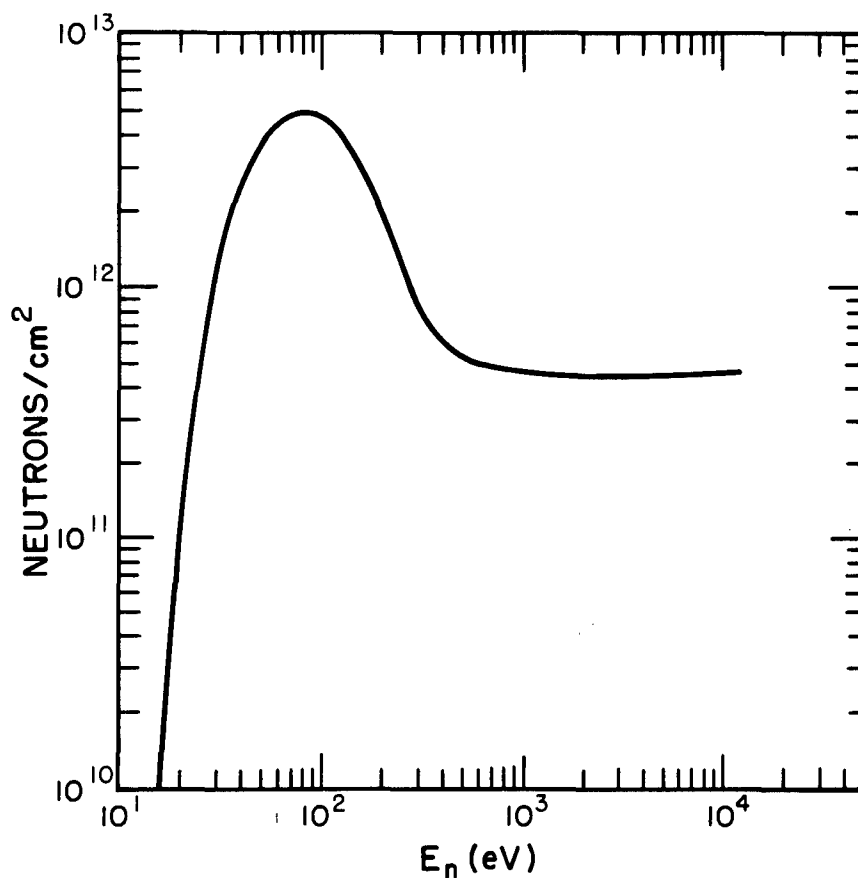


Fig. 1. Neutron exposure at ^{235}U target in $[E_n][\text{neutrons}/(\text{cm}^2)(\text{eV})]$ vs. E_n .

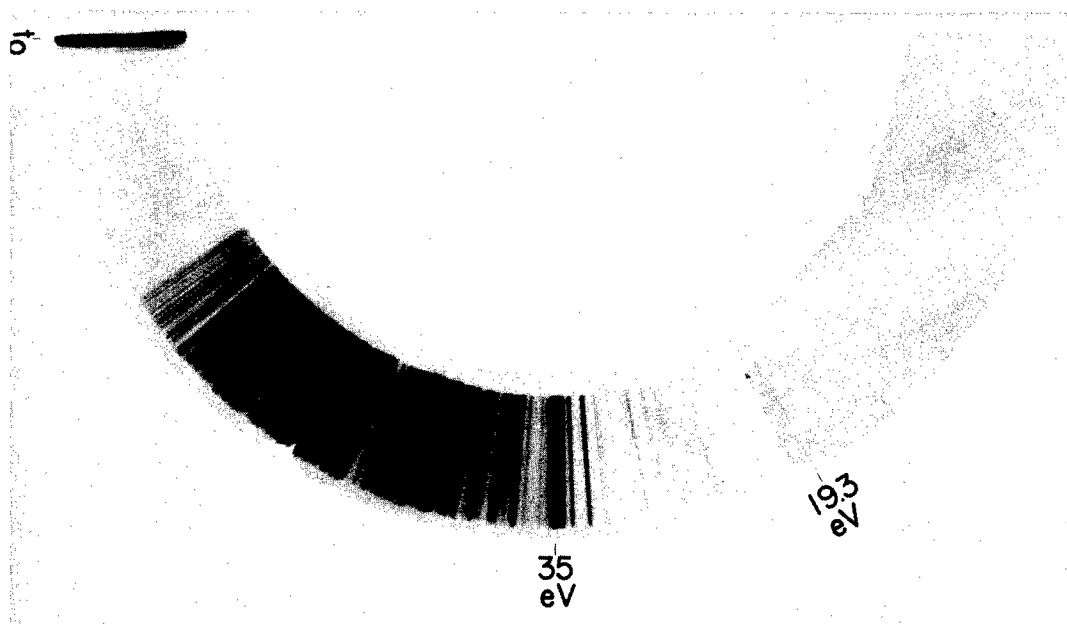


Fig. 2. Autoradiograph of uranium metal produced by contact exposure to fission products induced at resonances in target. An energy scale is provided by identification of the t_0 , 35.2 and 19.3 eV lines.

TABLE I. Sampled energy intervals, specific fissions in sample, $R_{\text{Cd/Mo}}$, and related resonance parameters.

Energy interval		Corrected fissions/gm (units of 10^9)	Corrected $R_{\text{Cd/Mo}}$	Major resonance energy ⁴ (eV)	ν (meV) ^a
E_1 (eV)	E_2 (eV)				
19.33	19.60	0.112	$0.402 \pm 26.3\%$	19.30	70
19.86	20.07	0.036	$0.426 \pm 35.4\%$		
21.03	21.17	0.105	$0.517 \pm 22.5\%$	21.07	50
21.17	22.90	0.017	$0.658 \pm 43.5\%$		
22.90	23.05	0.090	$0.374 \pm 24.7\%$	22.94	60
23.05	23.55	0.085	$0.631 \pm 9.9\%$		
23.55	23.74	0.204	$0.328 \pm 24.6\%$	23.63	120
23.74	24.19	0.066	$0.806 \pm 65.6\%$		
24.19	24.34	0.110	$1.100 \pm 9.6\%$	24.23	80
24.34	25.19	0.070	$1.167 \pm 3.5\%$		
25.19	25.47	0.183	$1.032 \pm 5.0\%$	25.65	350
25.47	25.65				
26.40	26.61	0.197	$0.619 \pm 19.9\%$	26.44	160
27.71	27.89	0.348	$0.554 \pm 14.3\%$	27.81	100
28.23	28.42	0.104	$1.250 \pm 10.4\%$	28.35	110
28.42	29.60	0.024	$0.323 \pm 26.9\%$		
29.60	29.78	0.055	$0.943 \pm 70.0\%$		
30.71	30.88	0.261	$0.441 \pm 18.3\%$	30.91	70
30.88	31.91	0.137	$0.518 \pm 7.7\%$		
31.91	32.13	1.010	$0.708 \pm 7.6\%$	32.10	80
33.31	33.59	0.874	$0.401 \pm 9.5\%$	33.55	70
34.21	34.52	1.260	$1.038 \pm 4.5\%$	34.39	90
34.52	34.83	1.280	$0.823 \pm 5.6\%$		
34.83	35.02	2.060	$0.830 \pm 4.9\%$	34.85	140
35.02	35.32	2.570	$1.027 \pm 4.3\%$	35.21	110
35.32	36.50	0.476	$1.326 \pm 3.6\%$	35.75	490
36.50	36.79	0.191	$1.362 \pm 5.4\%$	36.64	120
36.79	38.20	0.148	$1.385 \pm 3.1\%$		
38.20	38.51	0.342	$1.038 \pm 5.4\%$	38.42	190
39.18	39.54	1.960	$1.008 \pm 4.2\%$	39.44	90
40.48	40.76	0.537	$0.675 \pm 8.8\%$	40.51	150
41.33	41.74	0.828	$0.757 \pm 8.3\%$		
41.74	42.06	0.856	$0.693 \pm 6.8\%$	41.91	80
43.23	43.64	0.500	$0.544 \pm 4.0\%$	43.41	40
43.91	44.16	0.807	$0.633 \pm 3.9\%$	44.04	40
44.51	45.01	1.140	$1.060 \pm 4.0\%$	44.75	150
45.55	46.01	0.342	$0.574 \pm 8.1\%$	45.79	170
46.74	47.29	1.360	$0.620 \pm 5.1\%$	46.93	80
48.00	48.51	1.480	$0.769 \pm 4.5\%$	48.06	120
48.77	49.07	1.090	$0.875 \pm 5.0\%$	48.82	30
49.07	49.44	0.730	$0.784 \pm 7.6\%$		
49.44	49.79	0.677	$0.967 \pm 10.9\%$	49.51	60
50.37	50.79	1.530	$0.838 \pm 5.9\%$		
50.79	51.10	1.760	$0.928 \pm 4.7\%$		
51.10	51.55	3.370	$0.760 \pm 4.4\%$	51.37	130
52.12	52.68	2.380	$1.141 \pm 4.0\%$	52.27	250
53.34	53.73	0.900	$1.042 \pm 14.5\%$	53.56	140
55.41	55.78	2.630	$0.816 \pm 5.2\%$		
56.38	57.07	3.920	$0.480 \pm 4.7\%$	56.58	70
57.07	57.91	1.160	$0.572 \pm 6.3\%$	57.83	100
57.91	58.46	2.200	$0.603 \pm 5.4\%$	58.15	80
58.46	59.13	1.700	$1.151 \pm 4.2\%$	58.68	120

TABLE I. CONTINUED.

Energy interval		Corrected fissions/gm (units of 10^9)	Corrected $R_{Cd/Mo}$	Major resonance energy ⁴ (eV)	ν (meV) ^a
E_1 (eV)	E_2 (eV)				
59.13	60.16	0.723	$0.723 \pm 5.6\%$		
60.16	60.96	1.320	$0.613 \pm 5.4\%$	60.25	100
60.96	61.48	1.050	$0.649 \pm 8.9\%$	61.10	120
61.48	63.58	0.502	$0.982 \pm 4.0\%$		
63.58	64.41	0.800	$1.145 \pm 4.3\%$		
64.41	65.17	0.127	$1.189 \pm 10.0\%$		
65.17	66.03	0.131	$1.011 \pm 10.0\%$		
66.03	66.70	0.291	$1.085 \pm 16.9\%$		
66.70	70.34	0.346	$1.163 \pm 4.7\%$		
70.34	71.26	3.810	$0.585 \pm 8.9\%$		
71.26	72.34	1.220	$0.713 \pm 10.8\%$		
72.34	73.11	2.790	$0.406 \pm 17.6\%$		
73.11	74.57	0.585	$0.947 \pm 7.4\%$		
74.57	75.48	2.710	$0.607 \pm 11.6\%$		
75.48	76.14	1.790	$0.979 \pm 8.3\%$		
84.05	85.25	3.150	$0.962 \pm 5.7\%$		
85.25	86.30	1.400	$0.868 \pm 11.5\%$		

^aParameters of Ref. 4 were used except for those derived from Reich-Moore-type parameters of Cramer at 36.64 eV and 46.93 eV as listed in Ref. 5.

normalized to the thermal neutron value of this ratio and defined as $R_{Cd/Mo}$.

The ^{111}Ag data are converted to corresponding ^{115}Cd equivalents and included in the weighted mean values of $R_{Cd/Mo}$ which are listed in Table I. Where the values fail to agree within statistics, the result with the smallest statistical error is chosen. We assume that the yield of ^{99}Mo is constant and that changes in the value of $R_{Cd/Mo}$ are a measure of changes in the yield of ^{115}Cd .

The measured fission densities, based on ^{99}Mo analyses, are plotted in Fig. 3. The smoothed estimated background is shown as a dashed line. Part of the background is due to the 0.8 - 1.0 cm of tapered aluminum wheel immediately behind the target. Another part is due to scattered neutrons in the line of sight. An additional component is due to fission neutrons produced in the target and is enhanced in the neighborhood of large resonances. An additional "background", in a practical sense, is due to the contribution of tails of nearby resonances which may have a different ^{115}Cd yield than the resonance which is being examined. We have not attempted to evaluate this component, partly because a single-level formula is inadequate to make the corrections at these level densities and the corrections vary widely depending on how a choice is made of resonance parameters from a large number of differing values available from multi-level fits. However, we believe that the smoothed background correction applied to our data is generally accurate to 10 - 15%. This uncertainty has apparently introduced no significant effect on the qualitative separation of the resonances into characteristic groups.

Values of $R_{Cd/Mo}$ at resolved resonances are listed in Table II. A few visible resonances are not included in Table II for one or more reasons which are discussed at greater length later. The multilevel fit we have used to correlate with our data is that of Derrien and de Saussure,⁴ and their assigned resonance widths ($\nu = \Gamma_{tot}/2$) are listed in Table I.

TABLE II. Values of $R_{Cd/Mo}$ at resolved resonances.

$E_o^{(4)}$ (eV)	\bar{E}_{sample} (eV)	$R_{Cd/Mo}$	Γ_f (meV) ^a
19.30	19.46	$0.402 \pm 26.3\%$	100
21.07	21.10	$0.517 \pm 22.5\%$	60
22.94	22.98	$0.374 \pm 24.7\%$	80
23.63	23.64	$0.328 \pm 24.6\%$	200
24.23	24.26	$1.100 \pm 9.6\%$	120
25.65	25.42	$1.032 \pm 5.0\%$	660
26.44	26.50	$0.619 \pm 19.9\%$	280
27.81	27.80	$0.554 \pm 14.3\%$	160
28.35	28.32	$1.250 \pm 10.4\%$	180
30.91	30.80	$0.441 \pm 18.3\%$	100
32.10	32.01	$0.708 \pm 7.6\%$	120
33.55	33.45	$0.401 \pm 9.5\%$	100
34.39	34.36	$1.038 \pm 4.5\%$	140
34.85	34.92	$0.830 \pm 4.9\%$	240
35.21	35.17	$1.027 \pm 4.3\%$	180
35.75	35.91	$1.326 \pm 3.6\%$	940
36.64	36.54	$1.362 \pm 5.4\%$	200
38.42	38.36	$1.038 \pm 5.4\%$	340
39.44	39.36	$1.008 \pm 4.2\%$	140
40.51	40.62	$0.675 \pm 8.8\%$	260
41.91	41.90	$0.693 \pm 6.8\%$	120
43.41	43.44	$0.544 \pm 4.0\%$	40
44.04	44.04	$0.633 \pm 3.9\%$	40
44.75	44.76	$1.060 \pm 4.0\%$	260
45.79	45.78	$0.574 \pm 8.1\%$	300
46.93	47.02	$0.620 \pm 5.1\%$	120
48.06	48.26	$0.769 \pm 4.5\%$	200
48.82	48.92	$0.875 \pm 5.0\%$	20
49.51	49.62	$0.967 \pm 10.9\%$	80
51.37	51.32	$0.760 \pm 4.4\%$	220
52.27	52.40	$1.141 \pm 4.0\%$	460
53.56	53.54	$1.042 \pm 14.5\%$	240
56.58	56.72	$0.480 \pm 4.7\%$	100
57.83	57.49	$0.572 \pm 6.3\%$	160
58.15	58.18	$0.603 \pm 5.4\%$	120
58.68	58.80	$1.151 \pm 4.2\%$	200
60.25	60.56	$0.613 \pm 5.4\%$	160
61.10	61.22	$0.649 \pm 8.9\%$	200

^a Γ_f is derived from ν from equation $\Gamma_f = (2\nu) - (40 \text{ meV})$.

The frequency distribution of all corrected values for $R_{Cd/Mo}$ is plotted in Fig. 4. Two groups are apparent with peak frequencies in the 0.6 - 0.7 bracket and in the 1.0 - 1.1 bracket. There are 24 levels in Group I, hereinafter referred to as I, and 14 levels in Group II, hereinafter referred to as II. The frequency of levels as a function of values of Γ_f (derived from values of ν assigned by Derrien and de Saussure) is also plotted for I and II. It seems evident that these groups have somewhat different distributions in fission width. These distributions resemble those observed for I and II populations identified in the ^{239}Pu measurements of fission symmetry.¹ From Porter-Thomas arguments⁶ they indicate that several channels (three or more) are available for fission in both groups.

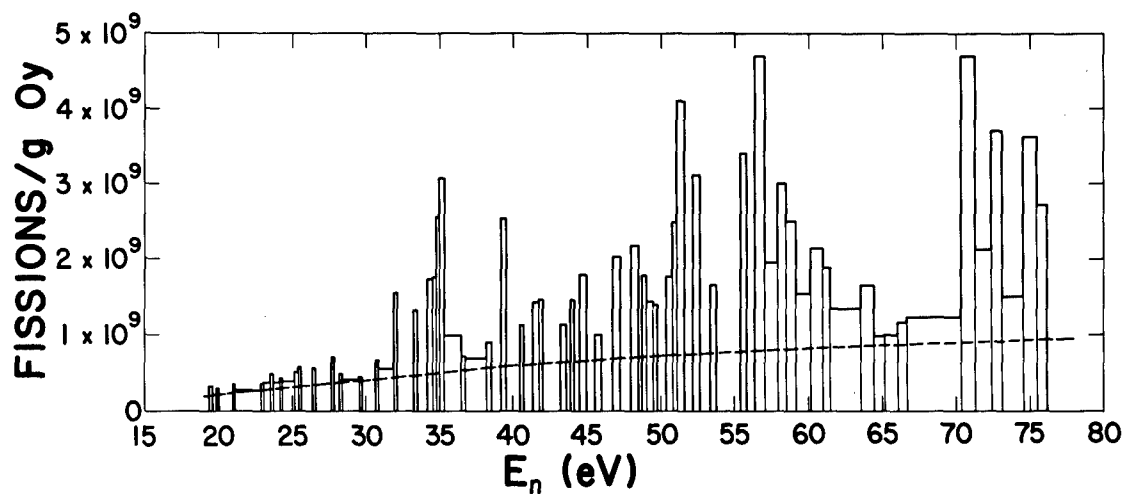


Fig. 3. Experimental results on fission density. Width of bar represents width of sample cut.

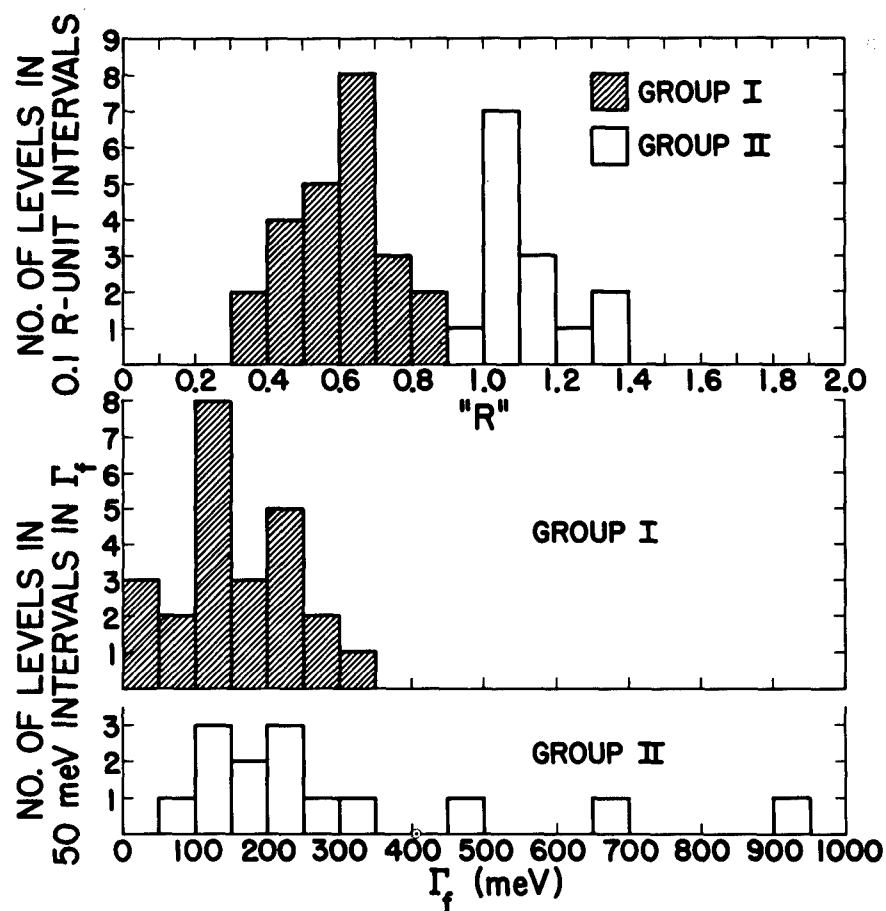


Fig. 4. The frequency distributions in $R_{Cd/Mo}$ at resonances and in associated fission widths.

The relative populations of levels assigned to I and II are 63% and 37% respectively. If $J = 4$ in I and 3 in II, the prediction for the relative populations is 56.2% and 43.8% respectively. The average value of Γ_f in I is 146 meV and in II it is 296 meV. The average value of R in I is 0.593 and in II it is 1.110. These average values can be used to calculate that thermal ^{235}U fission is predominantly of type II (22% of I and 78% of II).

Fission resonances in the 20 - 60 eV region which are not included in Table II were omitted for one or more of the following reasons:

1. The resonance is too weak to be seen and was not sampled.
2. The background correction is 80% or more of the total activity in the analyzed sample.
3. The resonance is much weaker than a closely adjoining resonance from which it is not resolved.
4. Two adjoining resonances of comparable size are not resolved from one another and are both excluded.
5. The sample was not analyzed due to time limitations (applies above 50 eV).

The omitted levels are at the following energies: 20.21, 20.61, 23.43, 27.21, 28.77, 29.68, 30.59, 37.06, 39.92, 41.39, 41.64, 42.16, 42.70, 44.97, 46.98, 48.35, 50.24, 50.45, 51.68, 53.98, 55.16, 55.87, 59.75, and 60.76. The fission widths of the omitted levels average 200 meV compared to an overall average fission width for the analyzed samples of 201 meV. We conclude that since the widths of the omitted samples are not noticeably different from those in the population of analyzed samples, the omissions probably do not affect the relative distributions. The level assignments in I and II are summarized in Table III. A tendency for levels in II to cluster is evident.

TABLE III. Summary of level assignments in Group I and II.

Group I	Group II
E_0	E_0
(eV)	(eV)
19.30	
21.07	
22.94	
23.63	
	24.23
	25.65
26.44	
27.81	
	28.35
30.91	
32.10	
33.55	
	34.39
34.85	
	35.21
	35.75
	36.64
	38.42

TABLE III. CONTINUED.

Group I	Group II
E_0	E_0
(eV)	(eV)
	39.44
40.51	
41.91	
43.41	
44.04	
	44.75
45.79	
46.93	
48.06	
48.82	
	49.51
51.37	
	52.27
	53.56
56.58	
57.83	
58.15	
	58.68
60.25	
61.10	

DISCUSSION

The relative populations of levels assigned to I are in reasonable agreement with the prediction from $2J + 1$ statistics of $J = 4$ in I and 3 in II. However, we can not establish a correlation between these assignments and various published sets of ^{235}U spin assignments.^{7,8,9}

Based 1) on the fact that in ^{238}Pu the pattern of symmetry and fission width distribution is demonstrated to be related to spin, 2) on the measured values of the relative populations of I and II levels in ^{235}U , and 3) on the observation that the broader levels occur in II as might be expected if fission in these levels generally occurs through lower-lying channels than in I, we are inclined to favor the hypothesis that $J = 4$ in I and 3 in II. However, it is obvious that unambiguous spin assignments to several of these levels are required to affirm or disprove this conjecture.

ACKNOWLEDGMENTS

The assistance of numerous laboratory theoretical, engineering, metal fabrication, and photographic groups was essential to the success of this experiment. In particular, the cooperation and assistance of F. G. Berry, R. A. Cosimi, B. C. Diven, P. F. Moore, J. M. Taub, and W. G. Warren were indispensable. The alignment and monitoring of the neutron beam were performed with the kind offices of a number of other experimental groups involved in time-of-flight measurements on the same device. Many helpful conversations occurred with M. S. Moore in the course of preparation of this paper.

REFERENCES

1. G. A. Cowan, B. P. Bayhurst, R. J. Prestwood, J. S. Gilmore, and G. W. Knobeloch, Phys. Rev. 144, No. 3, 979 (1966).
2. G. A. Cowan, B. P. Bayhurst, and R. J. Prestwood, Phys. Rev. 130, 2380 (1963).
3. P. Seeger (private communication).
4. H. Derrien and G. de Saussure, ORNL-4280, Neutron Phys. Div. Annual Progress Report, 1 (1968).
5. G. de Saussure and R. B. Perez, ORNL-TM-2599, (1969).
6. C. E. Porter and R. G. Thomas, Phys. Rev. 104, 483 (1956).
7. J. D. Cramer, Nuc. Phys., A126, 471 (1969) No. 2.
8. M. Asghar, A. Michaudon, and D. Paya, Phys. Lett. 26B, No. 11, 644 (1968).
9. H. Weigmann, J. Winter, and M. Heske, Nuc. Phys. A134, 535 (1969).

UNDERGROUND ENGINEERING APPLICATIONS

REVIEW OF POSSIBLE PEACEFUL APPLICATIONS OF NUCLEAR EXPLOSIONS IN THE NATIONAL ECONOMY OF THE SOVIET UNION

By

Paul A. Witherspoon
University of California, Berkeley

ABSTRACT

The following review will give some of the current thinking of Soviet scientists and engineers on the possibilities of using nuclear explosions for peaceful purposes in the Soviet Union. This review is taken from a more detailed report that was presented under the same title by Soviet participants at an information-exchange meeting that was held in Vienna between the Soviet Union and the United States in April, 1969. Aside from a very brief review of one explosion in salt, the report does not give details on nuclear explosion effects (mechanical, seismic, radiation, or thermal). Rather, the report summarizes the results of design calculations and indicates the direction of Soviet planning for a variety of industrial applications. A complete translation of this report will be published by the Division of Technical Information and Education of AEC at Oakridge.

INTRODUCTION

It is evident from their Vienna report that Soviet workers have been investigating the industrial application of nuclear explosives for a considerable length of time. After a period of theoretical investigation, they pursued experimental studies to solve certain engineering and scientific research problems. These studies proceeded through three separate phases: (1) laboratory modeling studies, (2) field experiments with chemical explosives, and (3) field experiments with nuclear explosives.

The overall purpose of these theoretical and experimental investigations was to define the basic parameters that control the effects of nuclear explosions. Information on mechanical, seismic and radiation effects was obtained as well as the engineering properties of rocks that have undergone such explosions. At the same time, the Soviets also sought to develop the technological background necessary for engineering applications. They have worked on such problems as: (1) the optimal methods of utilizing nuclear explosions, (2) the stability of structures created by these explosions, and (3) the effect of seismic waves from such explosions on the stability of surface and underground structures.

As a result of all this work which included economic projections as well, the Soviets concluded that nuclear explosives have a very definite potential within the planned

economy of the USSR. They have established that a significant number of industrial applications should be possible. Investigations and work on specific projects are now underway along the following lines. Excavation shots are being planned for: (1) open pit mining operations, (2) building canals, (3) constructing rock-fill dams, (4) constructing storage pits for water supply, (5) excavating trenches and embankments for railroads and highways, (6) excavating harbors for seaports, and (7) constructing storage pits for mine-concentrate tailings. Underground explosives are being planned for: (1) improving oil and gas recovery, (2) constructing underground storage facilities, (3) developing subsurface facilities for disposing of industrial wastes, (4) underground mining operations, and (5) controlling subsurface pressures in mines and petroleum reservoirs. More attention has been paid to underground than to excavation explosives because the former are much safer.

The following briefly describes the results of one underground explosion in salt and examples of the kind of projections that the Soviets are making for both underground explosions and excavation shots.

UNDERGROUND EXPLOSIONS

Experimental Results in Salt

An experimental underground explosion was set off in salt (site not given) in order: (1) to investigate the possibility of creating an underground cavity that could be used for storage purposes, (2) to determine the configuration and dimensions of the cavity as well as the zones of deformation, (3) to investigate the seismic effect from the explosion on surface and subsurface structures, and (4) to investigate the distribution of radioactive products in the salt mass as well as on the land surface. The shot was a 1.1 kiloton explosive at a depth to charge ratio of 160 m/kt $1/3.4$.

The explosive was set off in a large dome-shaped mass of salt that extends to within 7-8m of the surface at the location of the emplacement well. The halite is composed of medium to large crystals ranging in size up to 2-3cm and exhibits a clearly expressed lamination. The salt laminae dip at an angle of 70° in a northwest direction (280°) and range from 2-15cm in thickness with interlayers 0.1 - 0.3 cm thick. The laminae are interspersed with carbonates and sulfates.

This explosion was completely contained. Heaving at the surface over the epicenter was 2m and in general was observed over an area about 60m out from shotpoint. Subsequent to the explosion, six exploratory holes were drilled to determine cavity configuration, dimensions and volume. The cavity was found to be slightly elliptical in cross-section with a vertical extent from shotpoint of about 18m and a horizontal extent, about 14m. Total volume of the cavity is $1.42 \times 10^4 \text{ m}^3$, and the lower one-third ($0.4 \times 10^4 \text{ m}^3$) is filled with fused salt and rock debris. The cavity is bordered by a zone of crushed halite 1.5 - 6.5m thick. The fissured zone can be traced 83m vertically upward, 29m downward, and 35m horizontally outward from shotpoint. Individual fissures extend for 150-200m.

Investigations of seismic effects were grouped in three categories of distance from shotpoint: (1) up to 2.3 km, (2) 7.5 to 45 km, and (3) up to 270 km. On the basis of computations, it was concluded that the seismic effect on structures in the closest zone was equivalent to the destructive force of a 6 to 7 Richter magnitude earthquake.

No release of radioactive products into the atmosphere was observed. After the explosion, the presence of noble gases in observation wells was measured at $t + 12$ minutes, $t + 24$ hours, and $t + 35$ hours. The amount detected did not exceed one percent of the total formed during the explosion. Other radioactive products were detected from their penetration into the salt mass along fissures. Strontium-89 and cesium-137 spread the farthest away with strontium-90, yttrium-91 and antimony found closer to the cavity. Zirconium-95, cerium-144 and ruthenium-106 were found within the cavity.

The Soviets concluded from this experiment that the results confirmed earlier work indicating the expediency of using nuclear explosions to create underground storage cavities in rock salt.

Improving Oil and Gas Recovery

According to the Soviets, their investigations indicate that the application of underground nuclear explosions to oil and gas reservoirs should substantially increase rates of production and thereby shorten the time needed for exploitation. They cite two methods of utilizing nuclear explosions for such purposes.

The first project will be aimed at improving gas production from a reef-type structure where a substantial gas cap overlies a relatively thin oil saturated zone that is underlain by water. The reef gas extends from a minimum depth of 1,000m to a gas-oil contact at 1,800m, which is isolated from underlying water by an oil zone, 85m thick. The caprock over the gas is composed of about 1,000m of anhydrite, salt, and near-surface deposits of Tertiary sandstones and clays, about 480m thick.

The project plan calls for three 40 kt, almost equilaterally spaced, explosives to be detonated at a depth of 1,600m, or about 600m below the top of reef gas. An intensely fractured zone around each shotpoint with a radius of 270m is predicted. Spacing between explosives will be approximately twice this radial distance. Emplacement wells will be reopened for production purposes unless this proves impractical, in which case new wells will be drilled.

It is anticipated that a very large increase in gas and gas condensate production will be realized. Individual well productions are predicted to increase from a conventional $0.25 \times 10^6 \text{ m}^3/\text{day}$ ($\sim 9 \text{ MMCFD}$) to $3 \times 10^6 \text{ m}^3/\text{day}$ ($\sim 103 \text{ MMCFD}$), or a 10-fold increase. Exploitation time will be shortened eleven times, and annual savings should be of the order of 5-6 million rubles.

The second project will be aimed at improving oil production from a small dome-shaped structure at a depth of about 1,400m. The most productive part of this structure is a sandstone about 100m thick overlying a dense, low permeability limestone. Beneath this oil-saturated limestone is a water-bearing limestone 70 to 200m thick. The caprock over the oil saturated sandstone is an argillaceous carbonate that is 90-150m thick and practically impervious.

Because of poor communication across the dense oil-saturated limestone, it is proposed to enhance the water drive potential of this field by detonating three nuclear explosives, of 20 to 30 kt each, in the center of the limestone aquifer beneath the oil-water contact. The resulting fracture pattern will greatly enhance water movement into the oil producing zones and stabilize oil production at a high level. Without stimulation, the field is predicted to reach a peak oil production of 350,000 t/yr ($\sim 6,700 \text{ BPD}$) for a two

year period and then require some 32 years to reach depletion. With stimulation, this peak level can be maintained over an eight-year period. The net result is that the production life can be shortened to 19 years and the cumulative recovery can be increased by about one-third.

Constructing Underground Storage Facilities

As a result of various investigations including field studies, the Soviets have concluded that underground nuclear explosions have three areas of application in building underground storage facilities: (1) creating cavities in salt deposits, (2) creating storage space in the broken rock and fissures associated with chimneys, and (3) improving the flow characteristics of natural storage reservoirs. Two examples are given to characterize the technology developed to date.

The first project will be designed to construct a storage cavity for gas condensate with a volume of $300,000 \text{ m}^3$ ($\sim 1,900,000 \text{ bbls}$) at a site where the geological cross-section consists of a thick bed of stratified salt beneath about 500m of sandstone. Two successive explosions of 35 kt each will be placed in the salt at a depth of 810m. To protect the first cavity from seismic damage during the second detonation, a minimum distance between shots of 528m has been prescribed. Exploitation wells will be drilled into these cavities one month after detonation. Experimental studies have indicated that 120 days after an explosion, cavity gas contained no radioactivity.

The second project will be designed to construct a storage space for natural gas with a volume of $1 \times 10^6 \text{ m}^3$ ($\sim 35 \times 10^6 \text{ ft}^3$) at a site where a thick section of tuff underlies 190m of permafrost. Three nuclear explosives, each 40 kt and 200m apart, will be detonated in the tuff at a depth of 710m. By storing gas in the resulting chimneys at pressures of 70 atm. ($\sim 1,050 \text{ psia}$), some $70 \times 10^6 \text{ m}^3$ ($\sim 2.5 \times 10^9 \text{ ft}^3$) of gas can be accommodated.

Preliminary economic studies show that the cost of nuclear storage will be six times less than surface storage of liquified natural gas, three times less than the cost of storing gas in solution cavities in salt, and under certain conditions about the same cost as conventional underground storage in aquifers.

Underground Mining

Nuclear explosives when used underground enable one to crush large ore deposits even with a considerable distance between shotpoints. As a result of experimental underground explosions in granite, it has been established: (1) 400,000 tons of granite can be crushed per kiloton of explosive, (2) the seismic waves cause complete crumbling at distances of 30 to 80m and rock falling, at distances of 60 to 150m, and (3) the radial dimensions of the different zones of destruction (R) in meters are related to yields in kilotons (Q) by the following relations:

- | | |
|--------------------|---------------------------|
| (a) Primary cavity | $R = (10-15) \sqrt[3]{Q}$ |
| (b) Crumbling zone | $R = (20-35) \sqrt[3]{Q}$ |
| (c) Fissure zone | $R = (50-70) \sqrt[3]{Q}$ |

The results obtained lead the Soviet workers to the conclusion that an efficient use of nuclear explosions in underground mining operations should substantially reduce the volume of drilling and shaft construction, simplify the mining process where mass breakage is required, and considerably improve the efficiency of mine work. They estimate that the cost of mining a ton of ore may be reduced 1.5 to 2 times using large-scale explosions. This would permit the exploitation of certain deposits that currently are not considered profitable.

EXCAVATION EXPLOSIONS

Constructing Water Reservoirs

The desert areas of the Central Asian republics of the Soviet Union have been in acute need of water for centuries. Lack of water in these regions has become a national economic problem because of the need for settling and developing these areas. Since the main volume of surface water discharge runs into rivers in the spring, the problem of an economic water supply for these areas may be solved by constructing a wide network of artificial reservoirs and water storage facilities. Such a network would allow regulation of the spring runoff and provide a water supply during the entire growing season.

Based on experience with excavation explosions in the U.S.S.R. and in the U.S.A., the application of nuclear explosives could considerably accelerate the solution of this water supply problem. An experimental water storage facility is planned that will consist of a conventional earth dam augmented by two non-overflow, rock-fill dams to be constructed using nuclear explosives. The facility is designed for a total capacity of $30 \times 10^6 \text{ m}^3$ ($\sim 24,000$ acre feet); the effective capacity will be $27 \times 10^6 \text{ m}^3$. With multiannual regulation, the water supply at a 75 percent guarantee level is projected at $10.8 \times 10^6 \text{ m}^3/\text{yr}$, and in periods of minimum runoff, at $20 \times 10^6 \text{ m}^3/\text{yr}$.

The non-overflow, rock-fill dams will be constructed first using two excavation explosions of 150 kt each. The nuclear explosives will be detonated at 185m depth in porphyrites. This depth was selected so as to maximize the height of ejecta on the lip of each crater and eliminate any further work on dam height. Computed parameters for each crater are as follows: (1) diameter - 180m, (2) depth - 105m, (3) maximum height of ejecta - 31.5m, (4) radius of rock destruction - 650m, and (5) volume of ejecta - $5.7 \times 10^6 \text{ m}^3$.

The area where the explosions will take place is very sparsely populated so that problems of seismic and radiation safety are not complicated. In addition, procedures to be followed in each explosion will be adjusted to prevailing meteorological conditions in order to meet prescribed safety levels. In computing dimensions of the danger zone from the standpoint of radiation safety, the quantity of radioactive products discharged during explosions was calculated using procedures given by G. W. Johnson and G. H. Higgins in their report "Engineering Applications of Nuclear Explosives: Project Plowshare", which was presented at the Third International Conference on Plowshare in Geneva, 1964, and also published by Lawrence Radiation Laboratory, University of California, Report UCRL-7634, May 19, 1964.

The construction of the rest of the facility using conventional methods will start two months after detonation of the nuclear explosives and will end five months thereafter. During this period, radiation exposure to personnel on the site will not exceed the maximum allowable of 5r/yr.

Upon completion of the facility, the concentration of strontium-90 in the storage water will, according to calculations, be much lower than the permissible safe levels. No mention is made by the Soviet authors of tritium in the storage water. Using nuclear excavation to construct the non-overflow, rock-fill dams will decrease capital investment for the water supply facility 1.5 times as compared to conventional methods.

Building Canals

Due to a climatic anomaly, increased water use and the creation of water reservoirs on the Volga, Kama and other rivers of the Caspian drainage basin, levels in the Caspian sea have fallen 2.5m over the past 35 years. This has caused considerable damage to the fish industry, sea transportation, and certain other branches of the economy along coastal areas of the Caspian. Predictions of an additional lowering of sea levels of 0.6m by 1980 and 1.7m by 2000, even under favorable climatic conditions, indicates the seriousness of this problem.

It is possible to offset the increased need for water in the central and southern regions of the European part of the U.S.S.R. and to stabilize Caspian Sea levels by diverting the discharge of northern rivers that carry an abundant supply of water to the Arctic. Specifically, it is planned to divert the discharge of the northward flowing Pechora river, at a point near its headwaters, into the Kolva river, which is a tributary of the Kama river that flows southward to join the Volga. In order to accomplish this diversion, it will be necessary to construct several dams and a deep canal across the Pechora-Kolva watershed, 112.5 km in total length. The north end of the canal will start near the town of Yaksha, whose approximate coordinates are 57°E longitude and 62°N latitude.

Along its total length, some 65 km of the canal will run through rocky terrain at higher elevations and is to be excavated by detonating groups of nuclear explosives. Conventional canal construction will be used elsewhere. The geologic section along the canal where nuclear excavation will be used consists of sandstone, siltstone and rock salt. The area is sparsely populated with a density of less than one person per square kilometer.

The canal has been designed with an effective cross-section of 5,000 m² and will be constructed in sections using a linear array and simultaneous explosion of 20 shots with a total capacity of three megatons. Approximately 250 explosives will be required in building the entire canal, or an average spacing between shots of about 260m. Computed depths to shotpoint range from 150-285m. The radius of the danger zone along the canal front will attain some 20 km.

The economics of this type of construction is very favorable. The use of nuclear excavation methods is expected to decrease costs 3 to 3.5 times as compared to conventional methods.

Open Pit Mining

In open pit mining of ore bodies, nuclear explosions may be used as an efficient means of removing overburden, building approach trenches, and crushing ore and rock. Depending on the stratification of the ore body and surface relief, group explosions can be used to obtain either a symmetric ejection of overburden or an asymmetric ejection by choosing appropriate locations for the shots.

One large non-ferrous metal deposit is being considered for nuclear open pit mining methods. The area has the characteristics of the Far North with a permafrost layer that reaches 650m, a high seismicity, and the possibility of avalanches. The region is almost uninhabited (one person per 20 square kilometers) and is far from existing railroads and highways.

The mineralization of this deposit occurs in a sandstone stratum with reserves stretching over a distance of 11 - 12 km. Ore can be found in the outcrop over an area 300 to 1800m in width and along a 400 to 1200m inclined plane. The ore vein varies in thickness from several meters to 150m. The country rock is composed of siltstone, argillite, and calcareous sandstone. Over 70 percent of the deposit will be mined by open pit methods, and the stripping operations will require the removal of $2.3 \times 10^9 \text{ m}^3$ (~6 billion tons) of overburden.

Because of the enormous stripping operation that will be required in mining this deposit, the application of nuclear explosions appears to be particularly well suited to this project. Such application is also indicated by the severe climatic conditions, lack of population, and distance from main lines of transportation and electric power supplies. The plan calls for the use of groups of excavation shots that will remove about 40 percent of the overburden ($900 \times 10^6 \text{ m}^3$) beyond the limits of the future open pit. The remaining debris and ejecta will be removed during mining. The savings from the reduced stripping operations are expected to reach one billion rubles.

A special experimental explosion is planned in order to develop a more precise understanding of the basic parameters controlling nuclear explosions under the specific conditions of this non-ferrous deposit.

WHY NUCLEAR GEOSTORAGE SYSTEMS FOR PETROLEUM?

L. van der Harst and C. F. Knutson
CER Geonuclear Corporation
Las Vegas, Nevada

The objective of any kind of storage system in general is to act as a buffer between cyclical changes in supply and demand of the stored commodities. Since the advent of nuclear explosives engineering the possibility of constructing large-scale underground storage systems by means of contained nuclear explosions, for which the name nuclear geostorage has been coined, should be regarded as a valid alternative to the conventional storage systems currently in existence.

Limiting this discussion to systems for storing crude oil, various options are available.

The choice of any particular storage method depends, of course, on the circumstances surrounding each particular storage requirement; however, in many cases and for a variety of reasons, nuclear geostorage can be preferable to conventional solutions.

Economic considerations are clearly among the most important ones. In this respect an increase in storage capacity will tend to favor the nuclear approach.

Besides the economics, however, other considerations are important and may in some cases swing the balance in favor of nuclear geostorage plants, for instance: safety and strategic values, aesthetics, ease of access, lack of suitable tank farm space or lack of suitable geologic conditions for natural reservoirs.

It should be borne in mind that the decision to use the nuclear approach to solve a storage problem can only be taken after satisfactory evaluation of the geological and geographical characteristics of the site, and when the technical, safety, political, and public relations factors can be handled adequately.

WHY NUCLEAR GEOSTORAGE SYSTEMS FOR PETROLEUM?

L. van der Harst and C. F. Knutson

CER Geonuclear Corporation

Las Vegas, Nevada

Introduction

The objective of any kind of storage system in general is to act as a buffer between cyclical changes in supply and demand. Large scale storage requirements have been met by a wide variety of reservoir systems. However, since the advent of nuclear explosives engineering, the possibility of constructing storage systems by means of fully contained nuclear explosions should be regarded as a valid alternative to the conventional methods, and in many cases will prove preferable. Nuclear Geostorage Systems (NGS) has been coined as the name of this particular Plowshare application and will be used in this report.

The gas industry was first to recognize the importance of the nuclear approach to creating underground storage space. This is not surprising in view of their familiarity with natural underground storage in various geological strata. Consequently, most of the published material on Nuclear Geostorage Systems deals with their use for gas storage. However, the void space in an underground nuclear chimney can be used equally well to store liquids, like petroleum, LPG and other petroleum products as well as water, sewage and liquid waste products. Oil storage has been selected as the example commodity for evaluation in this paper. In trying to analyze the use of NGS in crude oil storage, it is important to assess the relative storage capacities for which nuclear solutions might be acceptable. Figure 1 lists some possible combinations. 1) 2)

As most of the storage projects will be located fairly close to build-up areas, the explosive yield will usually be limited to about 100 kt or less. Economics in most cases will set a lower limit of about 25 kt. The most often employed charge sizes will, therefore, be within these limits. Taking a 50 kt option for this analysis, it follows that storage volumes of 1 to 1.5 million barrels capacity per unit will be produced. The biggest steel storage tanks for crude oil currently used have roughly a 1 million barrel capacity. Other conventional subsurface alternatives to NGS are leached salt cavities and mined caverns.

LIQUID STORAGE VOLUMES				
Charge Kt.	Depth in		Capacity in	
	Feet	Meters	1000 barrels	1000 m ³
10	2000	610	391	62
	3000	915	264	42
	4000	1220	200	32
25	2000	610	977	155
	3000	915	660	105
	4000	1220	500	79
50	2000	610	1957	311
	3000	915	1319	210
	4000	1220	998	159
100	3000	915	2639	419
	4000	1220	1995	317
	5000	1525	1606	255
200	4000	1220	3990	634
	5000	1525	3212	511
	6000	1830	2690	428
Based on $R_c = 580 \frac{W^{1/3}}{(ph)^{.324}}$ and $V_{CAV} = \frac{817.3 W}{(2.6 h)^{.972}}$				

Figure 1

Engineering Requirements

Geological-engineering techniques have been developed by industry to evaluate the subsurface conditions in the areas of proposed mined or leached storage sites. The techniques have been developed to reduce the probability of building expensive failures, and the actual occurrence of such failures provides an adequate incentive for this effort. The industrial techniques would be suitably modified for nuclear applications.

In general, the critical geological factors for storage are:

1. Permeability of storage area.
2. Strength of rocks.
3. Sensitivity of rock to chemical or physical attack by water or storage products.
4. Hydrology of the site area.

A generalized evaluation program is presented below to illustrate the recommended "practice". In any "real life" situation, the program would be modified to develop the maximum amount of information at a minimum cost for the specific situation encountered. It is important that the evaluation program be managed by professionals with prior experience in the field of underground storage problems.

1. Develop a preliminary subsurface geological model of the potential NGS site based on:
 - a. Geological information from private or government sources.
 - b. Compilation of all well data available .
 - c. Contact with local residents, industrial users and drillers to ascertain the quality and history of the groundwater.
2. Define potentially favorable areas on the basis of:
 - a. A relatively thick sequence of low permeability rock .
 - b. Inert rock in the chimney area .
 - c. Absence of aquifers in the fractures zones.
3. Evaluate the optimum location by a drilling and testing program:
 - a. Drill one to four vertical exploratory holes and core from at least 100 feet above to 100 feet below the maximum anticipated extent of the fractures zone .
 - b. Case the wells to within a few hundred feet of the coring point .
 - c. Drill with air or mist so that water influx rates can be measured while drilling.
 - d. Maintain accurate drilling logs for all wells .
 - e. Inspection and description of the core by a geologist immediately after removal from the core barrel. (The cores should be wrapped in plastic or preserved in a similar manner to minimize changes in rock and fluid properties).
 - f. Drill two or more slant holes to evaluate pre-existing open

fractures. These wells should be deflected in order to cover the lateral extent of the fractures zone. The horizontal projection of two holes should be roughly perpendicular to the major known regional fracture patterns.

- g. Evaluate in-situ permeability by fluid injection tests.
- h. Evaluate water quality and flow rates by aquifer flow tests.
- i. Make laboratory tests on representative core samples to evaluate:
 - 1) Air, product, and water permeability.
 - 2) Porosity and density.
 - 3) Compressive strength (parallel and perpendicular to the bedding).
 - 4) Chemical and physical sensitivity of the rock to water and storage product.
 - 5) Product threshold entry pressure.

The detailed findings on site suitability should be documented comprehensively and the site evaluation report should contain a recommendation as to the acceptability of the chosen site.

If the site evaluation turns out to be favorable, it should be reviewed and accepted by a competent control board before construction can be started.

The Nuclear Geostorage System Concept

To compare the merits of a nuclear solution with that of a conventional one, the description of a particular theoretical case will be useful. The example chosen is a crude oil NGS to be constructed about 12 miles off the coast and close to a major oil port. The total capacity of the system would be about 26 million barrels or about 4 million cubic meters. When ready, such an installation could belong to the port authorities, a private company, or a government agency specializing in storage of this kind.

Particularly in Europe, there appears to be widespread interest in this type of solution to the storage problem. In the first place, the trend toward the use of 300,000 to 600,000 ton supertankers makes it necessary to update numerous port facilities to cope with these giants. Then, practically all European governments require a strategic crude oil reserve, the capacity of which is based on the average consumption of the country involved. The areas close to existing major oil ports are usually very densely populated and the construction of large tankfarms will have to be done on relatively expensive land. An economic way to store large volumes of crude oil, without taking up large land areas is therefore a welcome solution.

Figure 2 shows a possible layout near a hypothetical harbor. The selection of this particular site has been based on the following parameters:

- 1. Favorable subsurface conditions.
- 2. Seismic effects acceptable with respect to existing onshore and offshore structures. 16) 17)
- 3. Harbor suitable for offshore unloading of tankers.
- 4. Site close to existing or planned tanker loading facilities.

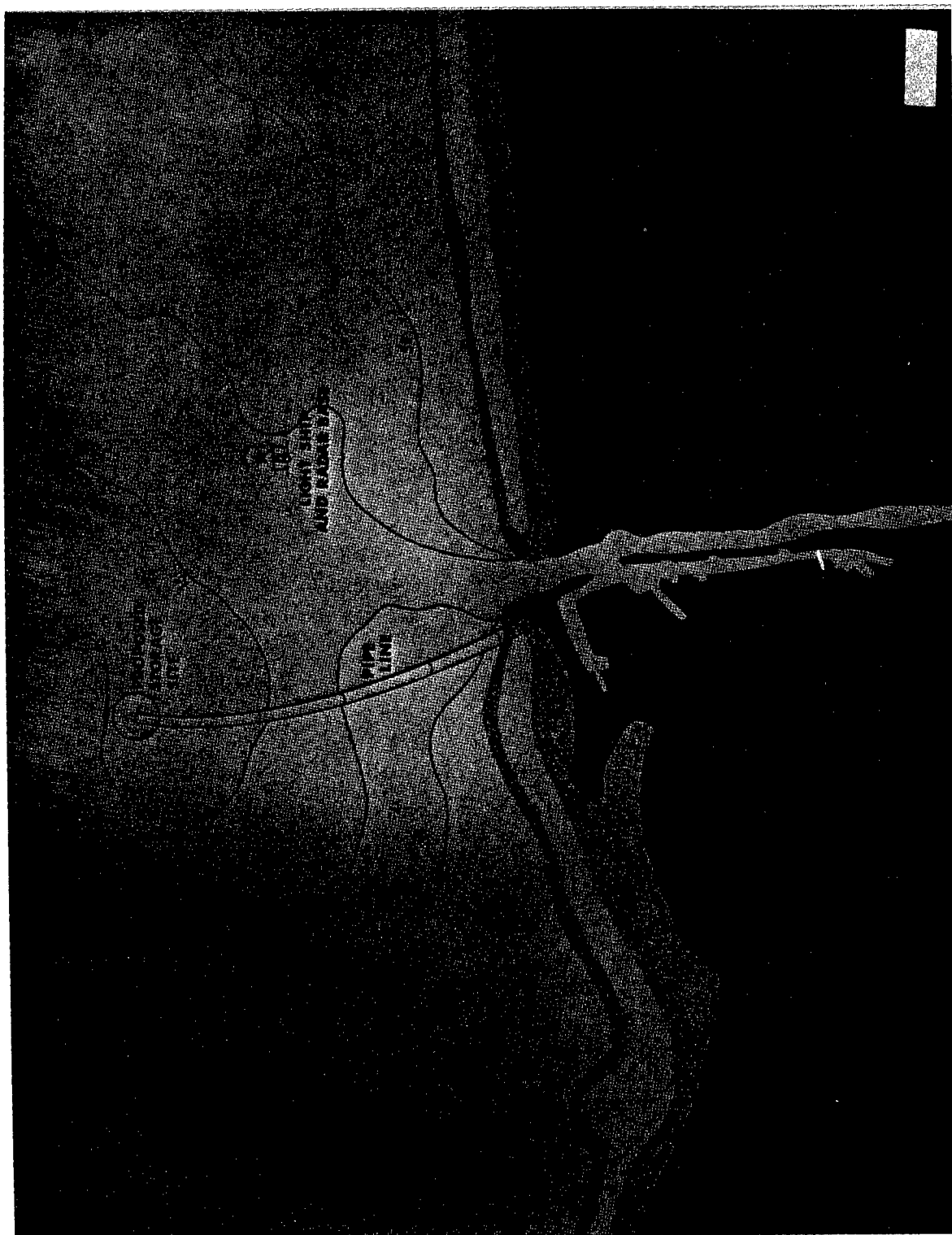


Figure 2

The water depth contours indicated on the map are characteristic of many harbor approach situations in the U. S. and Europe and point to another reason why offshore storage would be attractive.

A review of the Coast and Geodetic Survey Coast Pilots of the U. S. reveals that in the U. S. only 6 major harbors have authorized channel depths of 40 - 45 feet which will enable these ports to accept tankers below 100,000 tons. 3) Currently, loaded 300,000 ton supertankers have a draft of 80 feet or approximately 13 fathoms. 4) Larger tankers will tend to have an even deeper draft. Hence, approach and harbor channels will have to be dredged and maintained at 100 feet or more, to make it possible for these larger ships to enter the harbor. These operations will be costly if not physically impossible. Furthermore, it takes far more time and effort for these tankers to tie up at a dock than to moor and unload them offshore at a buoy station. Connecting an offshore terminal by pipeline to an onshore storage system is not an optimum solution either due to the high unloading rates of the supertankers. With pumping rates of 100,000 barrels per hour or more, the connecting pipeline will have to be large enough to accommodate these flow rates. Thus, 48" or larger pipeline probably will be needed, as in the case of the Gulf Oil terminal at Kuwait. 5) These high flow rates will not be needed elsewhere in the system. With the storage facility offshore, the size of the pipeline to the coast can be geared to the shore-based needs.

To obtain a storage capacity of about 26 million barrels, 20 separate units will be required using 50 kt explosions at about 3,000 feet depth. To avoid interlocking of the fractures surrounding each chimney, the distance between the units is kept to about 1,500 feet. An example of an offshore NGS is illustrated in Figure 3.

The construction time for a large NGS installation will take at least two or three years. Figure 4 shows an approximate time schedule for the drilling and construction effort. Seasonal weather problems may stretch the total construction time out over a longer period. In this particular example, a prototype unit is completed before starting the rest of the units.

It might be expedient to use a 25 kt charge for the prototype shot. This will make it possible to accurately scale the seismic effects for the full size shots. After successful completion of the first unit, the rest of the program goes on an assembly line basis. The emplacement holes probably are best drilled from a floating drillship. Two or more separate work barges and crews could handle the dummy runs, trial checkout, emplacement, stemming and preparation for firing. The firing itself probably will be done by radio from a shore-based operational headquarters.

The extensive safety measures that have to be taken at shot-time make this a costly part of the operation. For that reason in this example, it is assumed that groups of five shots will be fired with short delays on a single day. Although all five charges would be fired on a single day, a week-long firing "window" has been inserted in the planning schedule to absorb the influence of possible adverse sea and weather conditions.

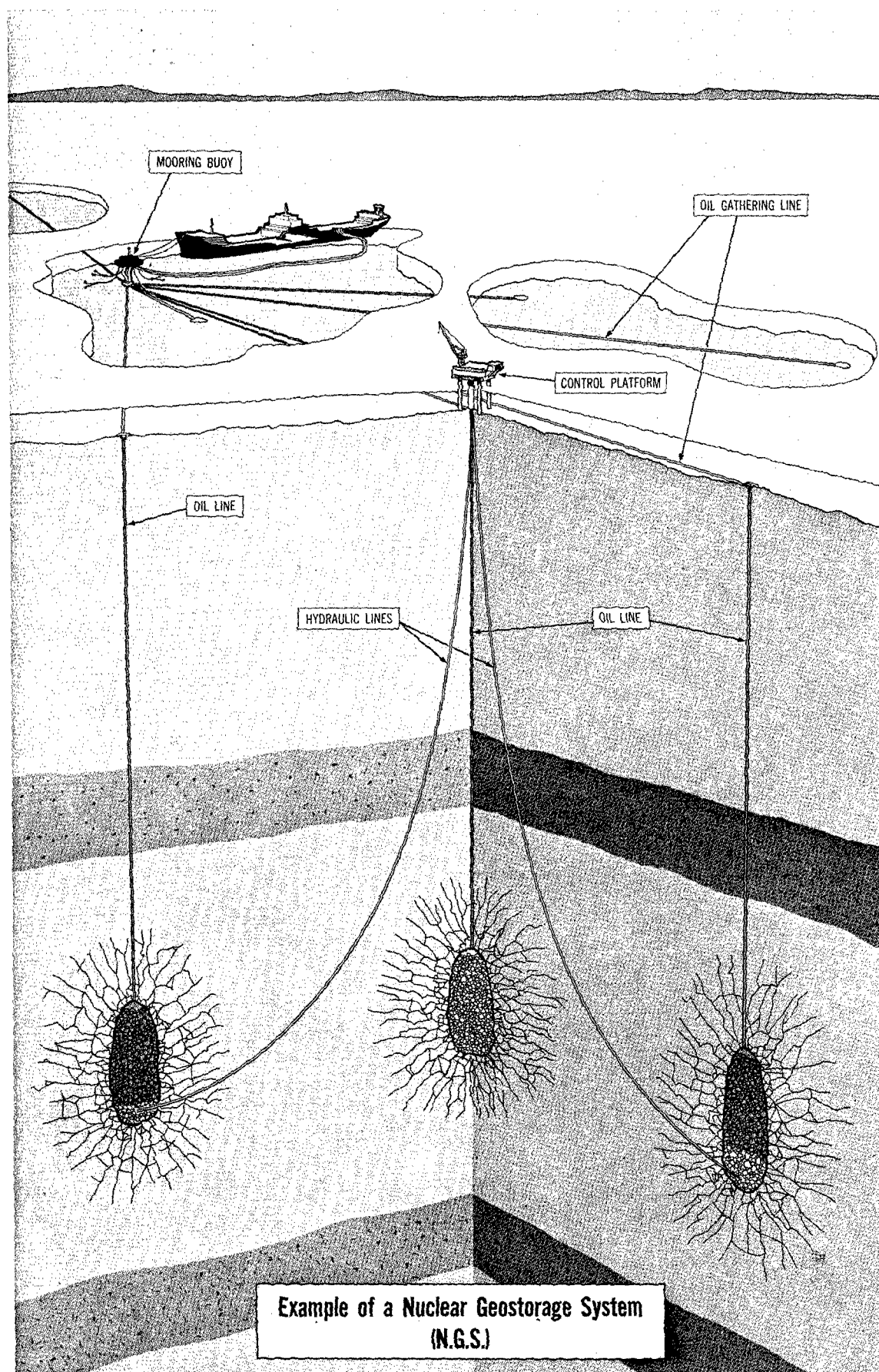


Figure 3

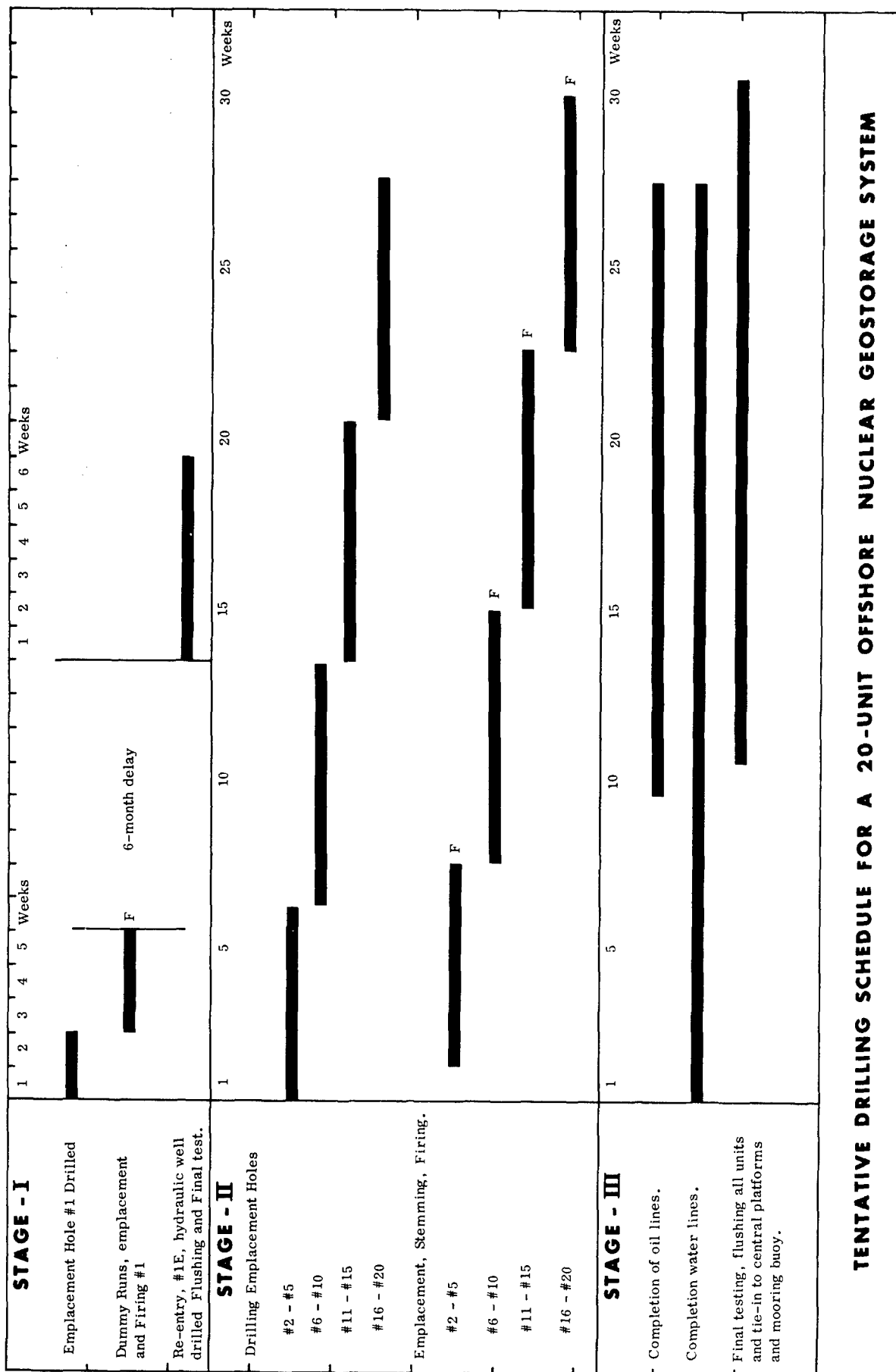


Figure 4

If explosives are available that can be left stemmed underground for as long as six months, all the shots after the prototype could be fired on a single day at the end of the preparatory drilling and stemming program. This would further reduce the cost of the total project.

In the case of firing in small groups, reentry drilling would be carried out in the same sequence as the firing to assure that a six-month time lag between the shot and reentry is maintained for each unit. The delay is scheduled to allow for the decay of short-lived radioactive material.

All units would be completed with two holes each. The well for the handling of the crude oil would be connected to the top of the chimney. The cased emplacement hole could be cleaned out and completed for this use. Another hole would be drilled to near the bottom of the chimney and would serve as a hydraulic line. These slant wells can be drilled from one or two permanent central platforms upon which would be located the booster pumps, oil-water separators, other needed equipment, and which could also house the loading crews. The same platform could also replace existing radar and light ships and serve as a sea base for harbor pilots.

Before putting the storage chimneys into operation, they have to be flushed thoroughly with seawater to remove the last remaining traces of mobile radioactive material. This flushing operation would have to be controlled carefully to assure that during all operations acceptably low radiation levels are maintained.

Filling the units would be accomplished by displacing the seawater in them with oil. This will generally be done by the tanker's loading pumps, the pumps on the platform or a combination of both. To avoid unacceptable pressure build up in the chimneys, due to the high pumping rates, it probably will be necessary, to maintain a minimum back pressure, to apply a certain amount of suction to the waterlines at the separator platforms.

The differential pressure of water and oil would aid in forcing the oil out of the reservoirs and into the pipeline or transfer hoses. A 24-inch line should prove adequate to connect the storage units with the shore stations. The booster pumps on the platform would provide the propulsive power by pumping seawater into the units via the hydraulic wells.

The project operation must be designed so that at no time pollution of the seawater can occur. It will be standard procedure to keep the oil-water interface within the confines of the chimney at all times and maintain safe chimney pressures. During loading operations, the water coming out of the chimney will be run through separators on the central platforms. The clean water will be returned to the sea, while oil-contaminated water could be pumped back to the tanker for ballast purposes. The large tankers must take on ballast to maintain at least a 40 feet draft at berth, to reduce the amount of hull exposed to the wind. These ships have on-board separators to remove oil from their ballast tanks. 4) If necessary, one of the NGS units can be used as a temporary storage for dirty ballast. To avoid any chance of an accidental release of oil from the reservoirs into the sea, all wells will be protected by storm valves.

The total cost of such an installation depends to a large extent on the circumstances peculiar to the chosen site. However, an estimate for a general case is presented in Figure 5. The emplacement and firing services are not included under the heading -- explosives, and the cost of a 50 kt device is estimated on the basis of the existing AEC schedule. It is hoped that eventually a 50 kt standard industrial nuclear explosive will be available for about \$150,000.

The example is based on a site where 3,000 feet holes can be drilled and cased in one week, and a daily drilling expense of \$14,000, including materials, has been used to arrive at drilling costs. Half a week was assumed to be needed to clean the cased reentry hole and complete it to the top of the chimney. Additional time has been allowed for rig moves. 6)

The post-shot construction costs of offshore terminal facilities and the pipeline to the coast are heavily dependent on local conditions, the existing facilities, and the ultimate owner's requirements. The cost of eventual shore-based installations are not considered in this estimate. The construction of the NGS itself amounts to \$0.77 per barrel. If the costs of the central platforms, equipped with separators and pumps, the mooring buoy and the pipeline to the coast are added, the cost per barrel would come to just over a dollar (\$1.08).

To put this in perspective, a comparison with a roughly 4.5 million barrel tank farm facility constructed for BP in Rotterdam is instructive. The total cost for this facility was reported as \$12.6 million or about \$2.80 per barrel.

The Rapid Access System Concept

A special application of the crude oil storage concept is that of one close to an offshore oil field that is so far from the nearest shore that a pipeline to the coast would not be an economical proposition. Loading tankers at a centrally located production platform straight from producing wells would generally be inefficient because of the extended loading times. An economical offshore storage system, which will be called a Rapid Access System, (RAS) would solve this problem.

According to Dr. Dunlap of Atlantic Richfield, 8) who advocated such a system a few years ago, a ten day storage capacity would be adequate in the case of Persian Gulf fields. In general, a RAS would have to have a capacity of about 1 to 10 million barrels, depending on the production rate of the field they would serve and the size of the tankers used.

As these fields are far away from shore, larger yield explosives can be used, if subsurface conditions are suitable. This would have a favorable influence on the cost per barrel of such an installation. Other cost reduction factors are: 1. the geology of the area is already well known, thus reducing the expense of site evaluation work, and 2. the absence of populated areas reduces the cost of the safety program and practically eliminates claim investigations and payment expenses.

COST-ESTIMATE FOR A 20-UNIT OFFSHORE N.G.S.

(Capacity - 26 million barrels or 4.2 million cubic meters.)

			<u>In 1,000 Dollar</u>
1.	Feasibility Studies and Pre-shot Expenses		1,000
2.	Emplacement Holes		2,900
3.	Explosives 20 @ 300		6,000
4.	Emplacement, Stemming, Firing		1,200
5.	Completion of all Oil and Water Lines		4,000
6.	Final Testing, Flushing of all Units		900
7.	Engineering Support and Logistics		4,000
Total Nuclear Operations			<hr/> \$20,000 (\$0.77/barrel)
8.	Gathering System	1,000	
9.	Production Platforms (2)	3,000	
10.	Single Point Mooring System	1,500	
11.	20 km 24" Diameter Pipeline to Shore	2,500	8,000
Total Project Cost		<hr/>	<hr/> \$28,000 (\$1.08/barrel)

Figure 5

Figure 6 presents a cost estimate for two solutions to a 6 million barrel Rapid Access System in Persian Gulf offshore conditions. The difference in the drilling costs between solution A and B is not only due to the difference in depth but also a result of the larger diameter required for the first solution. The diameter of the 200 kt emplacement holes does not only have to be larger to accommodate a slightly larger charge. However, as only two wells connect the loading platform with the reservoirs, the high tanker loading rates dictate a larger well diameter. In the second solution, five 12-inch lines are adequate for the loading function. Solution A leads to a \$1.28 per barrel cost for such an installation, while solution B comes to \$1.63 per barrel.

Recently a very interesting conventional storage equivalent to the RAS was constructed in the Persian Gulf by Chicago Bridge and Iron Corp. for a Continental Oil subsidiary. 9) It consisted of a large steel and concrete funnel-shaped container which was suspended in the water with the wide part of the funnel open and pointing down. Figure 7 shows this structure being towed to its final location. This 15,000 ton structure has a storage capacity of 500,000 barrels and has cost a total of \$7 million or \$14 per barrel. In this case, an equivalent onshore installation with pipelines to the field would have cost \$11 million or \$22 per barrel. In this particular location, the subsurface geological conditions were considered unsuitable for a nuclear solution. This is unfortunate, since about 1 to 1.5 million barrel storage capacity will ultimately be needed near the field under consideration, and costs for a nuclear Rapid Access System would have proved very competitive indeed. A submarine storage system consisting of prestressed concrete tanks moored on the seabottom has been suggested recently. 10) The cost of the storage alone was estimated at about \$10 per barrel.

Advantages of the Nuclear Approach

The choice of a particular storage method depends, of course, on the circumstances surrounding each particular case. Economic considerations are clearly among the most important ones. In this respect NGS appear to be very competitive compared with steel tank systems and mined caverns. Only salt dome storage systems are cheaper or similar in cost to the nuclear solution. However, salt domes are often not available in the most suitable locations. Figure 8 shows a general comparison of the cost of various possible storage options. 11), 12), 13)

However, other considerations can be of importance, and in some cases, where the economics are not clear cut, these may swing the balance to a choice for nuclear geostorage. Items to be considered are:

1. Economics
2. Safety
3. Strategic value
4. Aesthetics
5. More valuable land use needed
6. Ease of access

COST ESTIMATE FOR A 6-MILLION BARREL RAPID-ACCESS-SYSTEM

		SOLUTION A	SOLUTION B
		2 units 200 kt @ 5000 ft.	5 units 50 kt @ 3000 ft.
		In 1000 dollars	In 1000 dollars
1.	Preshot and Peripheral	600	800
2.	Emplacement Holes	1,000	2,000
3.	Explosives	800	1,500
4.	Emplacement Stemming, Firing	200	400
5.	Completion Oil and Water Lines	1,500	3,000
6.	Final Testing, Flushing	100	200
7.	Gathering Systems, Platform, Buoy	3,500	3,500
		7,700	11,400
Cost per barrel		\$1.28	\$1.63
Cost per cubic meter		\$8.05	\$10.25

(Based on Persian Gulf-type cost estimates.)

Figure 6

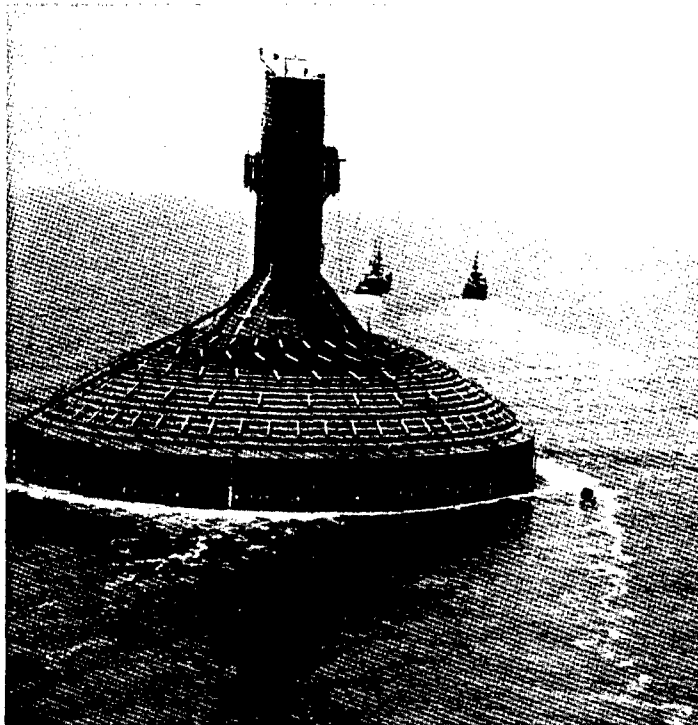
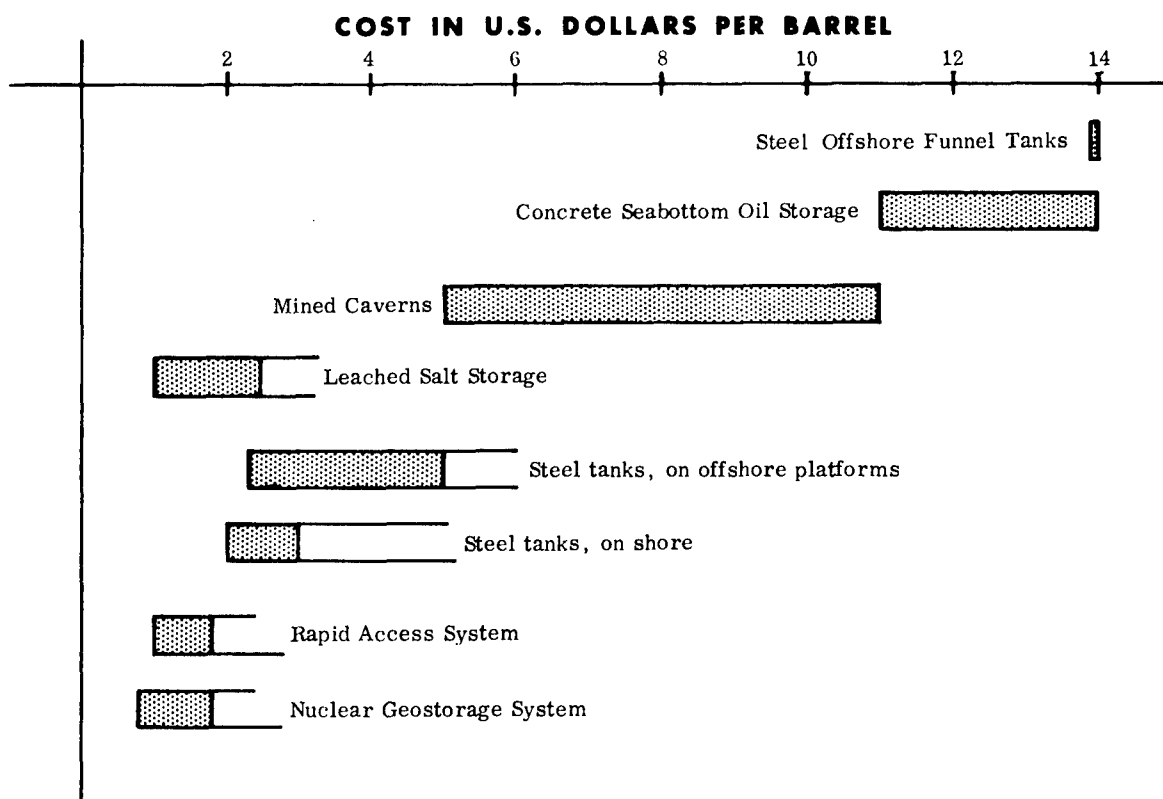


Figure 7



COST COMPARISON OF CRUDE OIL STORAGE SYSTEMS.

Figure 8

**WHY CHOOSE A NUCLEAR GEOSTORAGE
SYSTEM FOR CRUDE OIL?**

1. ECONOMICS.
2. SAFETY
3. STRATEGIC VALUE
4. AESTHETICS.
5. MORE VALUABLE LAND USE INDICATED.
6. EASE OF ACCESS.

Figure 9

The inherent safety of a nuclear geostorage system is obvious and of major importance. Too often fires occur in tank farms, and besides the possible loss of lives, the cost of such a fire can be tremendous. (Figure 10) In peacetime such fires occur by accident. However, under war conditions the adversary seeks to destroy tank farms as soon as possible, and sometimes the entire oil reserve of a country can be annihilated. The recent Middle East war has been a very vivid reminder of this. Obviously, nuclear geostorage systems are an ideal solution. With only some added defense features, the NGS site can be made to withstand conventional attacks.

Large tank farms are sometimes clustered in potentially very beautiful spots, near the shore of large bodies of water. They, certainly, do not contribute to the beauty of the landscape. The surface installations of onshore NGS can be made very small and inconspicuous and consequently would not clash with the natural surroundings (Figure 11). Placing the facility offshore would completely eliminate this problem. Modern offshore technology makes it possible to dispense completely with platform based facilities and is able to provide all needed systems on the seafloor or flush with it. In such a case only the mooring buoy would be visible at the surface.

In somewhat the same context, it may become more and more difficult to find the required space on land for extensive tank farms near old established harbor towns in the U. S. and Europe. Gulf's 8.2 million barrel Bantry Bay tank farm in Ireland takes up 325 acres for the tank emplacements alone. 4) Between Rotterdam and the sea, a rough estimate shows about 10,000 acres given over to tank farm storage systems with a total capacity of about 36 to 40 million barrels (Figure 12). This is about half the size of the actual city of Rotterdam, a town with approximately 1 million inhabitants. It is obvious that precious land space can often be put to much more valuable use than to serve as the foundation of a steel tank.

The ease of access of offshore NGS has been mentioned before. An example may illustrate this somewhat more clearly. At Bantry Bay the loading dock is situated in an ideal position. A large jetty has been constructed 1,200 feet offshore from the coast in amply deep water. In docking, the super-tankers have to approach the facility slowly and as nearly parallel as possible to the feeder system. Four powerful tugboats are then needed to assist in the final docking maneuver. 4) This may seem cumbersome, but it is nothing compared with the effort needed to berth such a ship in harbors like New York, Baytown, Long Beach, LeHavre, Liverpool, Rotterdam, Hamburg and many others.

If we compare this with the ease of mooring a tanker under its own power at a loading buoy in open water, (Figure 13) it becomes apparent that turn around time for these costly dockings can be cut drastically by avoiding the need for mooring at dock side. 14) 15)

Conclusion

A nuclear geostorage system should be considered a very attractive solution to petroleum storage problems. This especially is valid in situations where large volume storage facilities are required near harbors, offshore



Figure 10

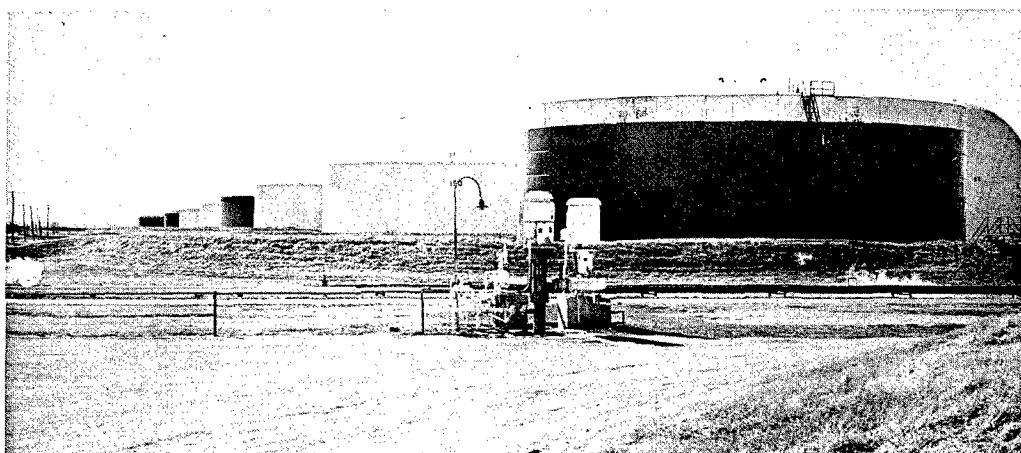


Figure 11: The pump installation in the foreground is the only surface equipment of a 5,000,000 barrel underground storage cavity for L.P.G. The tanks in the background have a capacity of 50,000 barrels each.

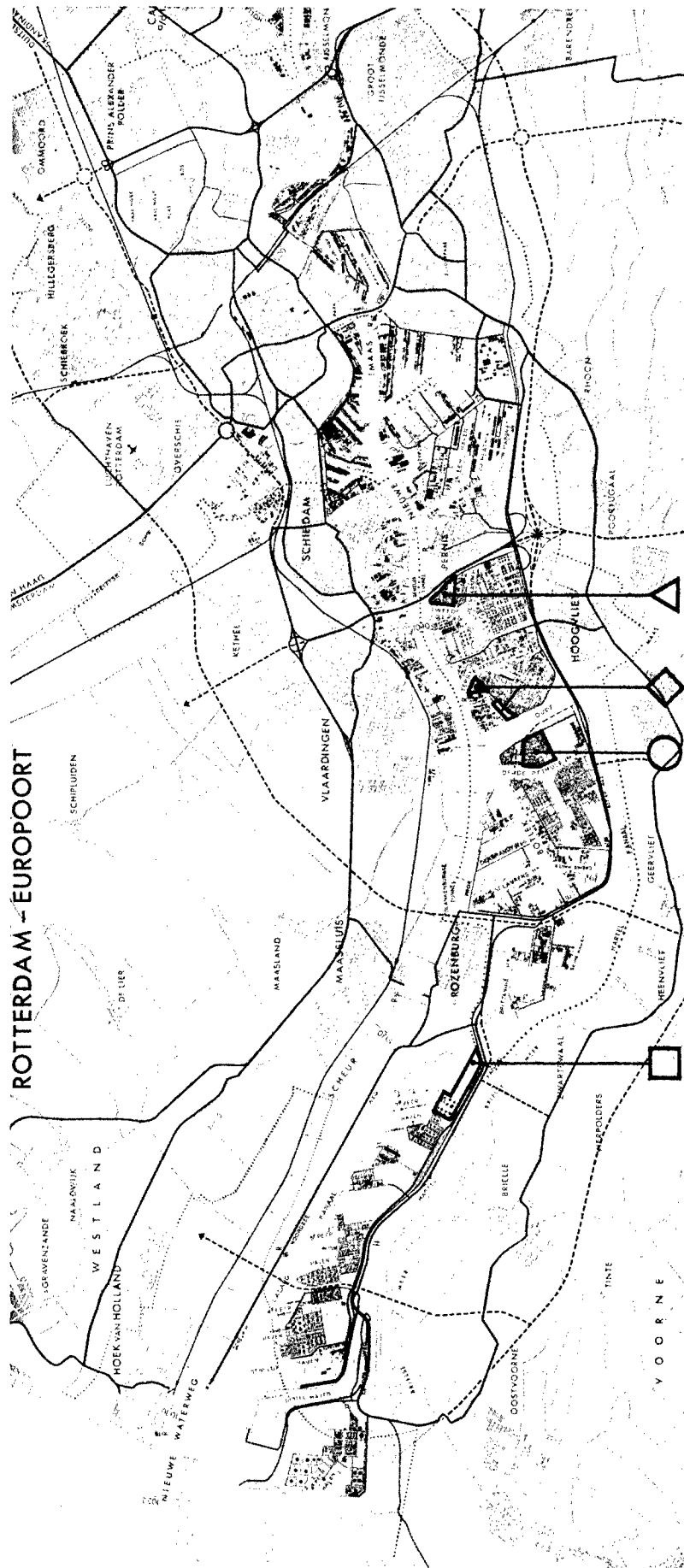


Figure 12: Tank Farms and refineries cover about half of the strip of land between the two rivers and stretching from the sea to the town of Rotterdam. A comparison with the area of the town itself and its closest suburbs brings out the tremendous size of these installations.

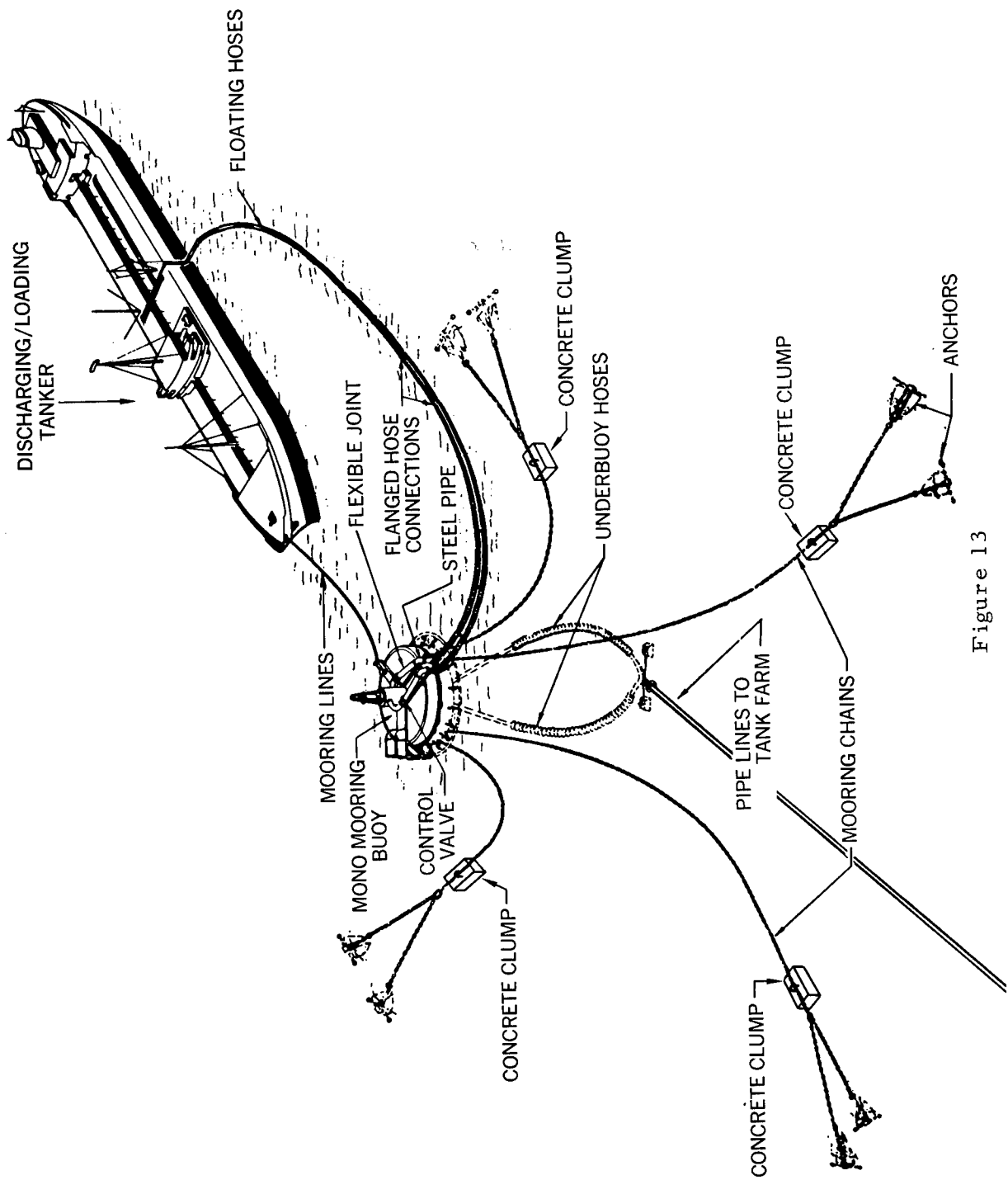


Figure 13

oilfields or strategically placed naval bunkering stations.

Potential NGS sites must be carefully evaluated. Not only must the rock properties, and structural and hydrological conditions be determined, but seismic effects, radiation and public and political response must be taken into consideration. In many cases economics and optimum land use considerations will make a nuclear geostorage system the first choice among various possible alternatives.

REFERENCES

- 1) Boardman, C. R. Engineering Effects of Underground Nuclear Explosions, Las Vegas, January 1970
- 2) Boardman, C. R. et all Responses of Four Mediums to Contained Nuclear Explosions, Journal Geoph. Res., Vol 69-#16, 1964
- 3) Frankel, B. Cmdr. Needed, Supertanker Sanctuaries, O & G Journal, April 17, 1961
- 4) Rogers, L. C. Gulf Aims for Full use of Mammoths, O & G Journal, May 19, 1969
- 5) --- Big Kuwait Tanker-Terminal Job Pushed, O & G Journal, April 22, 1968
- 6) Santa Fe Drilling Co. Private communication, December 1968
- 8) Dunlap, H. F. Use of Nuclear Explosives in Producing Operations, November 17, 1965
- 9) --- Dubai's Unique Storage Tank is Installed Without a Hitch, O & G Journal, Aug. 25, 1969
- 10) Kennedy, J. L. Offshore Total Project Approach is Best, O & G Journal, September 15, 1969
- 11) Phillips Petroleum Co. Methods and Costs of Storing L. P. G., March 1964
- 12) Pipkin, J. H. Communication on Cost of Crude Oil Storage in Salt Dome Caverns, October 1969
- 13) White, J. E. Economics of Scale Applies in Long Distance Pipeline Transport, O & G Journal, Jan. 27, '69
- 14) --- The Single Point Mooring, Marine Engr. -Log, July 1968
- 15) Black, John How to use Mono-Moorings, O & G Journal, September 1968 - Vol. 8 #9
- 16) Wiss, J. F. Effects of Blasting Vibrations on Buildings and People, Civil Engr., ASCE, July 1968
- 17) Cauthen, L. J. The Effects of Seismicwaves on Structures and Other Facilities, Proc. 3rd Plowshare Symposium, April 1964 TID 7695

NOTE: Reference 7 was deleted because photographic material originally intended for Figure 6 was not available.

TECHNICAL CONSIDERATIONS FOR PLOWSHARE APPLICATIONS TO OIL SHALE*

David B. Lombard
Lawrence Radiation Laboratory, University of California
Livermore, California 94550

Bruce G. Bray
CER Geonuclear Corporation
Las Vegas, Nevada

Harold W. Sohns
U.S. Bureau of Mines
Laramie, Wyoming

ABSTRACT

Nuclear explosions have been proposed for use in the recovery of oil from deep oil shale deposits. Before commercial feasibility can be established, a variety of technical problems must be examined. Some of these are related to nuclear explosion effects, others to the recovery of oil from the broken rock. Among the primary areas of interest are fracturing, chimney collapse, rubble size distribution, radioactivity, and retorting methods and variables.

To test the concept, nuclear explosion experiments will be needed. One such experiment, Project Bronco, has been designed in detail, and is used here to illustrate a possible direction of development. The design is based on the following objectives: to evaluate the overall feasibility of nuclear breaking, followed by in situ retorting; to investigate the gross physical effects of a nuclear explosion in oil shale, and to assess the role of radioactivities in the production of oil by in situ retorting. The experimental plan provides for the accomplishment of these objectives by appropriate preshot studies, a postshot examination of explosion effects, and experimental retorting of the nuclear chimney.

INTRODUCTION

A domestic hydrocarbon resource capable of supplementing U.S. energy needs for many decades would be an attractive target. Such a potential exists in the oil shale deposits of the Rocky Mountain region, but as yet there is no proven method for economic development.

The bulk of the resource is deeply buried and is not readily accessible with present mining technology; therefore, considerable attention has been devoted to a search for techniques for recovering the oil without mining. A lack of natural permeability in the oil shale deposits has stimulated research on means for creating permeability. It may be possible to provide the needed permeability by fracturing deep oil shale deposits with nuclear explosions.

*Work performed under the auspices of the U.S. Atomic Energy Commission; United States Department of the Interior, Bureau of Mines; and the CER Geonuclear Corporation.

The concept of nuclear explosion breakage as preparation for retorting in place has been under consideration for several years.¹ The technical feasibility of the concept is not fully established, and a program of research, including one or more nuclear explosion experiments, will be required to establish the technical as well as the economic potential of the method.

The feasibility of retorting the oil shale in place once it is broken has also been under examination.^{2,3} While results from preliminary research are encouraging, it is not yet certain how such retorting can best be accomplished.⁴ Several possible approaches have merit and are currently being investigated. A definitive design for retorting in the nuclear environment will depend on the results of current studies and the evaluation of the effects of actual nuclear explosions in oil shale.

Project Bronco has been proposed as an experiment to test the concepts discussed above.⁵ The technical design for the project has been carried as far as possible on the basis of available information. The Bronco design is presented here as an example of an experimental approach toward solution of some of the technical problems which have been identified.

EXPLOSION EFFECTS

The feasibility of using nuclear explosions in shale oil recovery can be established only with the aid of large-scale experiments. Because of the number and complexity of the technical problems, a first nuclear experiment would not result in a complete commercial technology. Such an experiment, however, should answer some of the key technical questions and point the way toward further development. Permanent changes in the surrounding rock created by the action of an explosion are of obvious interest because such effects may improve the retortability of oil shale. An objective of a first nuclear experiment would therefore be to measure some of the pertinent explosion effects.

Within microseconds, the detonation of a contained nuclear explosive creates a spherical cavity filled with gas and vaporized rock at very high temperatures and pressures. As the cavity expands and cools, its internal pressure drops. Expansion is complete when the cavity pressure is about equal to lithostatic stresses in the surrounding rock. The cavity expansion generates a very strong shock wave which moves rapidly out into the adjacent rock. The shock wave decreases in intensity as it recedes from the cavity boundary, and becomes the source of seismic disturbance when its amplitude has dropped below the elastic limit of the rock.

A nuclear explosion cavity may or may not be stable, depending upon its diameter and the strength of the rock above it. Typically, the ceilings of nuclear explosion cavities in hard rock have collapsed within a few minutes after detonation. Chunks of broken rock pour down into the cavity. The collapse proceeds upward for a distance of several cavity radii. The resulting rubble mass, called a nuclear chimney, commonly has an approximately cylindrical shape.

Fracturing

Both microscopic and macroscopic fracturing are found in the vicinity of underground nuclear explosions. Natural fractures, joints, bedding planes and other geological irregularities can be affected by the explosion and may contribute to the presence of fractures in a postshot environment. Figure 1 illustrates schematically several types of fracture which may occur as a result of underground nuclear explosions.

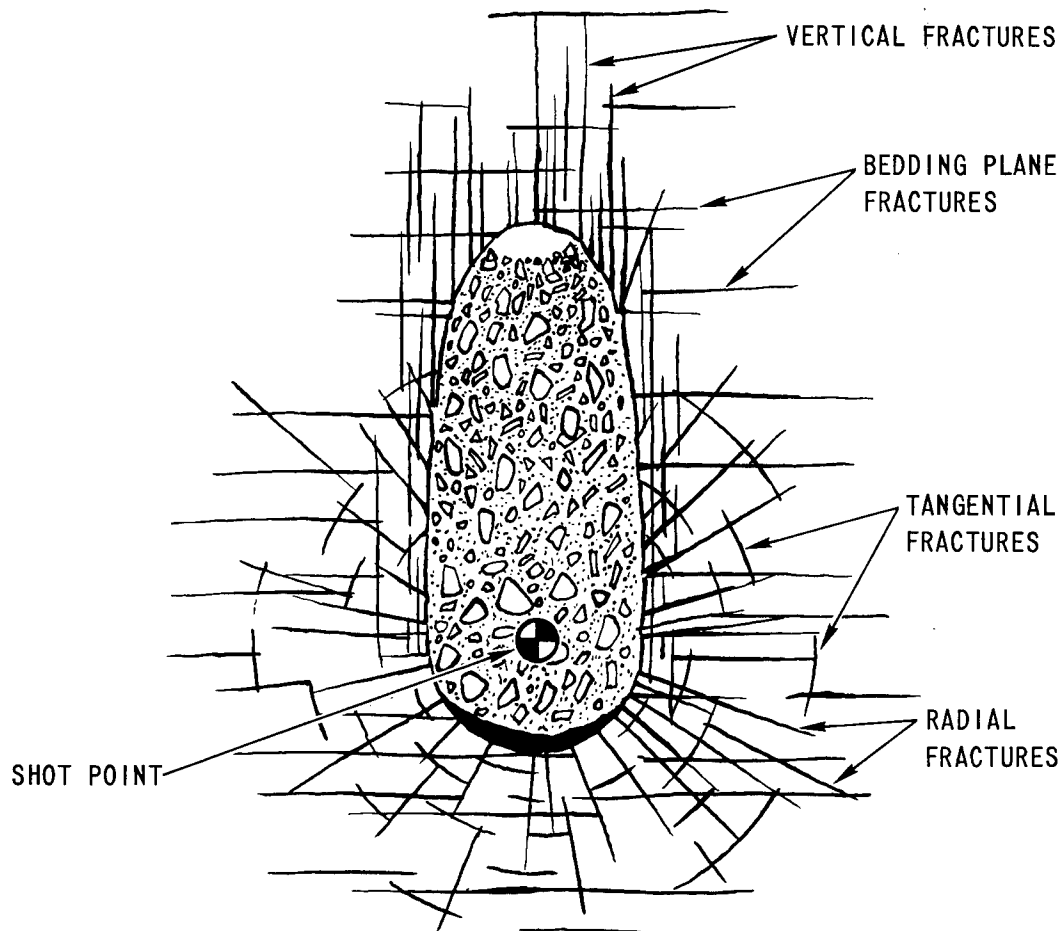


Fig. 1 Schematic illustration of possible types of fracturing near an underground nuclear chimney.

Chimney formation and size, rubble size distribution, bulk permeability of the rock outside chimneys, and the optimum placement of adjacent chimneys in the development of large oil shale tracts are currently believed to be related to fracturing. Fracturing to adjacent formations containing mobile water will probably be undesirable. An ability to predict the degree and extent of fracturing and permeability change due to an underground nuclear explosion in oil shale therefore should be a part of the technology of breaking oil shale with nuclear explosives.

Significant increases in bulk permeability of nuclear-fractured rock have been measured and correlated with distance from the chimney edge, but data are sparse.⁶ The effects of fracturing were detected more than 400 ft from the 26-kt, 4200-ft-deep Gasbuggy explosion.⁷

Although the cavity radius is not directly dependent on the extent or intensity of fracturing, the chimney height may be. In a rock as competent as Green River oil shale, the cavity may not collapse to form a chimney if the ceiling rock is not adequately fractured. Collapse will extend upward only as far as sufficient fracturing or bulking of the rubble permits. Thus the volume of rubble available for chimney retorting can be directly related to fracturing.

The size distribution of particles of oil shale rubble in a nuclear chimney will have a major influence on whether the chimney can be retorted at all, which of several possible methods is best, and whether that one can be employed efficiently enough to assure commercial feasibility. The nature and intensity of fracturing will affect the particle sizes and shapes which in turn

determine bulk permeability, bulk porosity, and specific surface in the rubble mass. Any retorting process is closely related to these quantities.

If shale oil is to be recovered by in situ retorting in the fractured but unfragmented region outside a nuclear chimney, the importance of fracture intensity, regularity and extent in that region is obvious. At depths of several kilometers, pressures and temperatures are great enough to cause plastic flow in many rock types. Because of its relatively plastic nature, there remains the question of whether oil shale at depths of 2000 to 3000 ft would retain fracture permeability. The oil shale grade would of course be an important factor.

Test drill holes in the Piceance Creek Basin of Colorado have revealed thick, rich oil shale deposits, as shown in Fig. 2.⁸ In many locations, water-bearing strata overlie and underlie the oil shale. In some circumstances, it will be desirable to adjust explosion energy yields and shot point locations in order to avoid fracturing to the water.

When large tracts of oil shale are prepared for in situ retorting by nuclear explosion fracturing, the spacing of the explosions will be critical. If the shot points are too close together, fracturing expense may be unnecessarily high. If they are too far apart, insufficient permeability may exist between chimneys, and associated retorting costs may be unnecessarily high. Those designing such tract developments will have to be aware of the degree of fracture enhancement between adjacent chimneys.

The question of inter-chimney fracturing will affect not only the spacing of shots but also their timing, energy yields, and burial depths. In arriving at the most effective plan for nuclear explosion shale oil recovery in a given tract, the designers will be influenced by the following factors:

1. The cost of each nuclear explosive is expected to be approximately independent of the yield.⁹
2. The volume of rock fractured by a nuclear explosion is expected to be approximately proportional to the yield.¹⁰
3. At a given site, the total yield that can be fired at one time will be limited by seismic considerations.
4. The yield of each individual explosive may be limited by the oil shale thickness and/or the overburden thickness.

Thus the sequential firing of single explosions, each at the seismic limit of yield, may appear to give the greatest economy. In some cases, however, simultaneous firings might be preferable. For example, the interaction of shock waves may prove to enhance fracturing enough to overcome the cost advantage of one explosive over two. The enhanced fracturing concept is illustrated schematically in Fig. 3. In exceptionally thick deposits, one shot above another might be fired in tandem to achieve an adequately tall chimney. Thin oil shale, reduced overburden, or local geologic conditions, on the other hand, might result in a single explosive yield limit significantly less than the maximum dictated by seismic considerations. In such cases the simultaneous detonation of an array of two or more explosives might be the most attractive plan.

The complexity of the design problem is apparent, as is the necessity for developing technical data about the fracturing and the retortability of the fractures. It is clear that adjacent nuclear explosions in oil shale will have to be studied before optimum design criteria can be established.

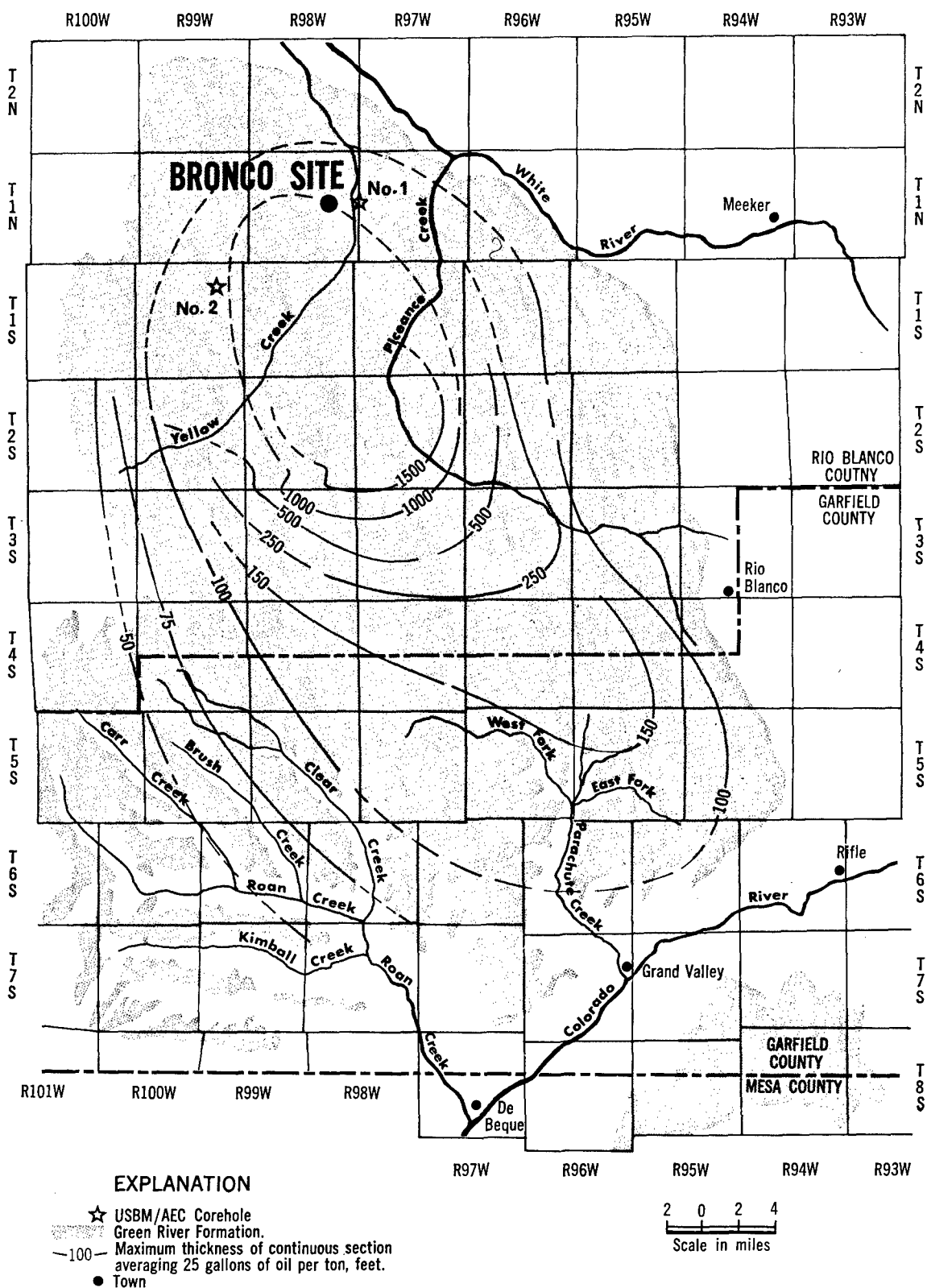


Fig. 2. Isopachous map of 25 gal/ton oil shale, Piceance Creek Basin, Colorado.

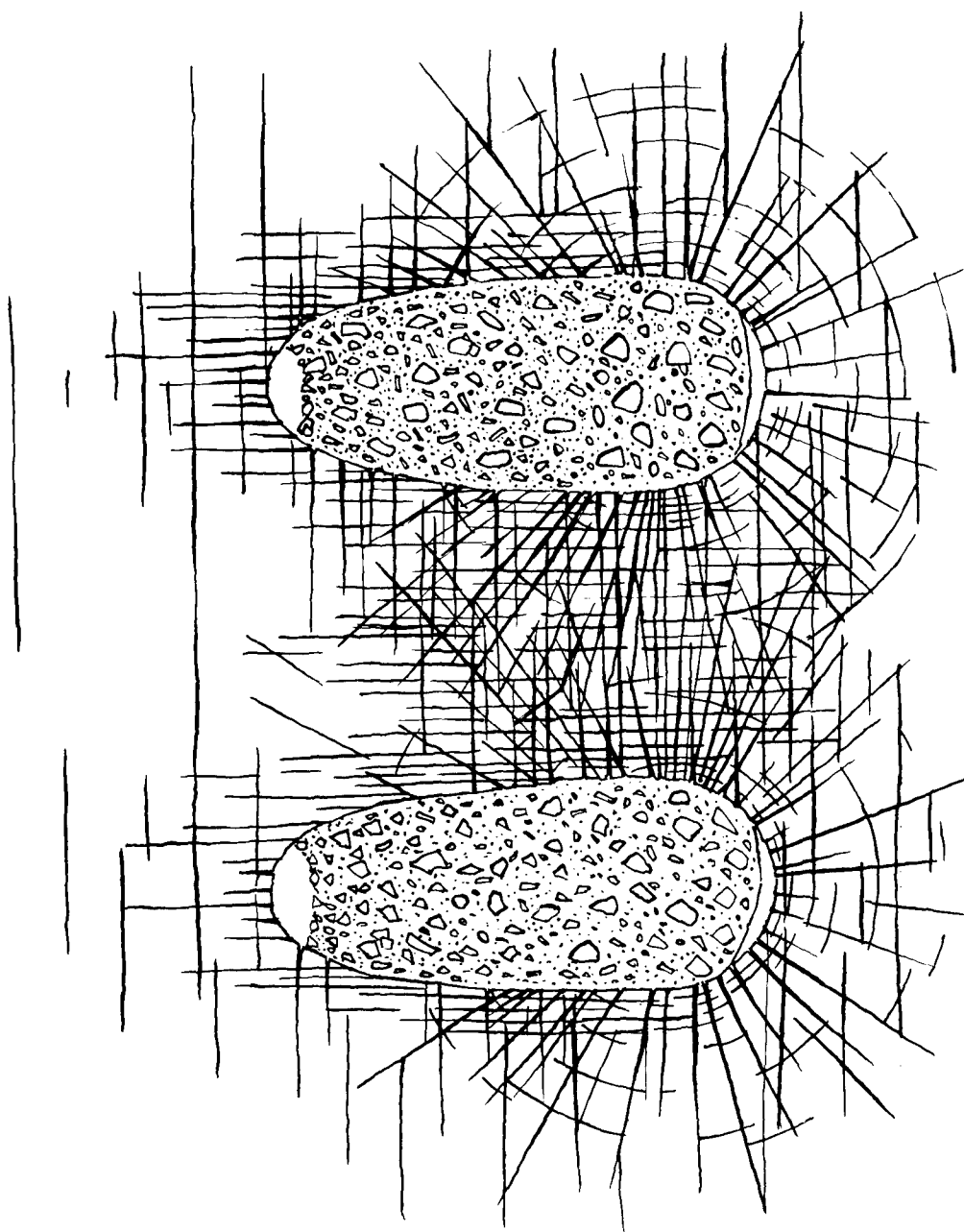


Fig. 3. Concept of enhanced fracturing between nuclear chimneys

Predictions of Fracturing

A needed development is the ability to predict the intensity, permeability, and extent of fractures that will be produced at a particular site by a single nuclear explosion of a given energy yield and emplacement depth. This predictive capability for fracturing cannot be developed on either a purely theoretical basis or a purely empirical basis, but must be founded on a combination of the two. If a mathematical model of the fracturing process is to be developed, it must be verified by experimental observation. On the other hand, the fracture pattern caused by a particular explosion cannot be extrapolated in entirety to other sites or energy yields without an underlying comprehension of the processes involved in the creation of fractures by underground explosions.

A mathematical model has been developed, based on the assumption that fracturing is a response of the rock to the outgoing shock wave.¹¹ In the model, fracturing occurs in a spherical zone about the detonation point; chimney height is determined by the radius of the fracture zone. The magnitude of the fracture radius depends upon the shock wave amplitude as a function of distance, and upon the brittle-ductile characteristics of the material. The physical properties of the rock are measured in the laboratory and fed into the calculation, which predicts cavity radius, fracture radius, and shock wave characteristics.

The model has predicted chimney height and radii of effects from several underground nuclear explosions (see Fig. 4).¹² Much more checking, however, remains to be done before the model is considered reliable.

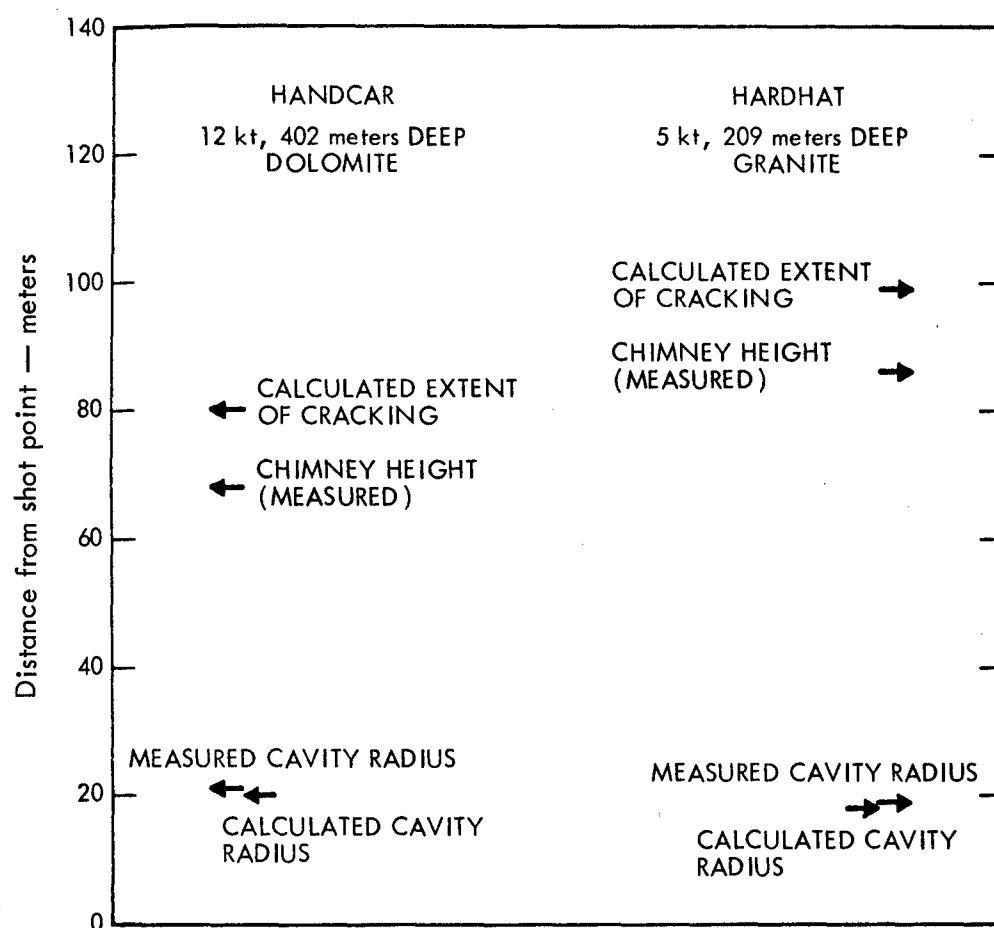


Fig. 4. Calculated cavity radii for Handcar and Hardhat, compared with observed dimensions.¹²

A long-recognized problem with fracture prediction is the influence of geologic irregularities. Since the present model is one-dimensional, it assumes a uniform medium. Natural rock formations are not so uniform; thus the differences between the model and the natural world result in differences between predicted and observed fracturing effects. Relative movement of formations along common boundaries was observed at Gasbuggy⁷ at ranges well beyond the predicted radius of intense fracturing. Data from dynamic instrumentation demonstrated clearly that the displacement was caused by the explosion.¹³ Geologic irregularities have been identified with other occurrences of fracture caused by nuclear explosions.

Green River oil shale is horizontally bedded in the deep, thick part of the Piceance Basin. Typical sections of the formation show great variations in oil shale grade over short vertical intervals. Such variations in grade are associated with large variations in those physical properties important in fracturing. It has been found that the stress at which brittle-ductile transition occurs is a strong function of oil shale grade, and also varies significantly between the principal directions, at least in the 18 to 25 gal/ton range.¹⁴ Because the variations are present only in a vertical plan and because the intervals of uniformity are exceedingly small, it will be difficult to develop a mathematical model for the oil shale.

Fracturing, then, is a key process in the use of nuclear explosions to aid in recovering oil from oil shale. A capability to predict the degree and extent of fractures is needed.

Rubble Characteristics

The time required to retort a block of oil shale varies as the square of its diameter. Therefore, the size distribution of the particles of fragmented oil shale in a nuclear chimney will have an appreciable effect on the rate and the efficiency of the oil recovery method. Post-shot investigations in Hardhat and Piledriver, nuclear explosions in granite, included mining into the chimneys to obtain information on particle size distribution. In Hardhat, an on-the-spot visual estimate of particle size distribution was made; in Piledriver, rubble samples were taken and analyzed.^{15,16} Mining to gather samples from nuclear chimneys is very expensive because of the weight and large numbers of samples needed. In oil shale, hot from a nuclear explosion, the presence of noxious and combustible gases would make a sampling operation even more expensive.

A camera, lowered into the apical void at the top of a chimney, can be used to photograph the top of the rubble (Fig. 5). This method, although simple and inexpensive, yields data of limited reliability because the size distribution of the top layer of fragments may not represent the distribution in the rest of the chimney. The particles at the top of the chimney are further from the detonation point, and may be larger than average because they have been subjected to the weaker part of the shock wave, have not fallen as far, and have not been broken by rubble falling from above. A better method for determining particle size distribution throughout the chimney is needed.

Yield Limits

Since the amount of rock broken by an underground nuclear explosion is proportional to the energy yield, and since the cost directly associated with a detonation will be roughly independent of the yield, it follows that the larger the yield, the more economical will be the breakage. There are two fundamental limitations on the maximum energy yield that might be used in breaking oil shale. One is geology of the site; yield might be restricted in a particular location by oil shale thickness, limited overburden, or the proximity of water-bearing strata.



Fig. 5. Top of fragmented rubble in Handcar chimney (dolomite). Large block in foreground has maximum dimension of about 3 ft.

The other yield limitation is seismic. The seismic waves from very large explosions might be felt in neighboring population centers and could cause damage in man-made structures. At some point, for a given site, the benefits of increased yield will be more than offset by potential damage. Because the effect of a seismic wave depends upon geological details and to some extent upon local architectural techniques and building standards, it is not now possible to predict accurately the maximum acceptable yield for a given

location. Data from well-documented nuclear explosion experiments will lead to significant improvements in the reliability of seismic damage prediction.

Explosive Design

If nuclear explosives are to be used on a large scale in the development of oil shale, the design of special explosives, with characteristics matched to the job, may be justified. Nuclear explosives can be designed to achieve relatively small diameter, to reduce some types of radioactive contamination, or to minimize cost. However, specifying one of these factors in the design criteria may limit the extent to which the other two can be adjusted. Several years are required to design, test, and produce special explosives. Therefore, the explosives ultimately designed for commercial use will be better adapted to the job than those available at the outset.

Mineral Recovery

A factor in the long-range commercial development of oil shale may be the ease with which other minerals can be extracted from the chimney after oil recovery is completed. For example, aluminum from dawsonite might find a market if it could be produced cheaply. Laboratory tests on the extraction of aluminum from retorted oil shale and oil shale ash are currently being conducted by the Bureau of Mines at College Park, Maryland.

Radioactivity

The amounts and kinds of radioisotopes produced directly and by neutron activations by a given nuclear explosion in a given rock medium can be predicted accurately.^{17,18} The chemical forms and spatial distribution of these isotopes and their decay products, however, are more difficult to calculate. In a carbonate rock such as dolomite, most of the fission product radioactivity is confined to the base of the chimney, and this is also expected to be the case in oil shale. Some gaseous or volatile radioactivities—and some with gaseous or volatile precursors—may be distributed through the chimney in low concentrations.

Tritium may be present in the chimney partly because some of the explosive energy may be derived from a fusion reaction and partly because of neutron activation of the oil shale itself. During its growth phase a nuclear cavity in oil shale will contain ions of carbon, oxygen, hydrogen, and tritium—which is chemically identical to hydrogen. These ions may recombine into organic compounds and water as the cavity temperature and pressure drop; the high radiation field may influence such reactions. It is not yet possible to forecast on a theoretical basis just what organic compounds will be formed, or just how the tritium will be distributed among them. An empirical approach must be employed. Measurements of radioactivity postshot and during retorting in experimental nuclear chimneys can be expected to define any problems which might exist. But prior to such experiments, bench scale work with radioisotopes and oil shale samples should provide much worthwhile information. Such work has already begun.¹⁹

Air and Water Pollution

In the eventual development of a commercial shale oil industry, the questions of air and water pollution must be considered. No matter what method is used for retorting, some gases will have to be disposed of. The most common method of disposal of unwanted gases is to stack them to the atmosphere. However, for a commercial shale oil retorting industry, alternative methods should be considered, e.g., treatment of effluent gases, storage or disposal in burnt-out chimneys, and re-use in the retorting cycle.

An evaluation of these potential problems and a search for solutions should be an integral part of research and development aimed at commercializing the production of oil from oil shale.

Such studies should also consider the possible effects of excess heat created during the retorting process. The question is not important for a single experimental chimney, but eventually several hundred chimneys per year may be involved. When retorting is complete, the retorted oil shale itself will be warm. Much of the heat might be used in preheating new chimneys and in exchange with gases injected into the chimneys being retorted, but some heat will remain. The atmosphere and local streams are commonly used as heat sinks, but on the proposed scale of shale-oil production, heat disposal must be considered carefully. Again, selection of the best commercial retorting method may be affected by these considerations.

RETORT ENGINEERING

In addition to technical questions related to the effects of underground nuclear explosions, there are several concerning the recovery of oil from the nuclear environment. The system consists of basically two parts, the chimney and the surrounding fractured zone. Because the characteristics of the zones are dissimilar, each may require a different retorting process. These differences may increase the complexity of in situ retorting.

The distinction between the explosion effects problems and those related to retorting is not always well-defined, but in general the latter are amenable to direct laboratory investigation, whereas explosion effects must be examined in nuclear explosion environments.

Methods of Retorting

Several methods for in situ recovery of oil from oil shale in a nuclear chimney have been proposed.⁵ In one, the heat required for retorting is supplied by the combustion of carbonaceous residues in retorted oil shale. Other methods involve passing preheated inert or reactive gases through the oil shale.

The combustion technique has the advantage of being thermally self-sufficient and of requiring only air as a raw material—except possibly at start-up. The products of combustion, mixed with other gases, carry heat energy through a zone of retorted but unburnt shale to the region where retorting is underway. The gases produced in retorting are added to the stream that preheats the raw oil shale. Part of the exhaust gas may be mixed with air to make up injection gas, and some of the heat carried by the exhaust gas may be delivered to the injection gas via a heat exchanger. The combustion process is shown schematically in Fig. 6.

In the hot gas methods, the gases would be heated prior to being injected into the chimney. The gases might be inert, serving only to carry heat energy to the oil shale, or reactive, entering into chemical reactions with the oil shale or shale oil to improve the efficiency of the retorting process or the quality of the oil.

The hot gas methods may also have an advantage over the combustion process by leaving the retorted oil shale in a stronger, less friable condition. The feasibility of the non-combustion techniques may depend on the long-term availability of suitable raw materials in the Piceance Creek Basin.

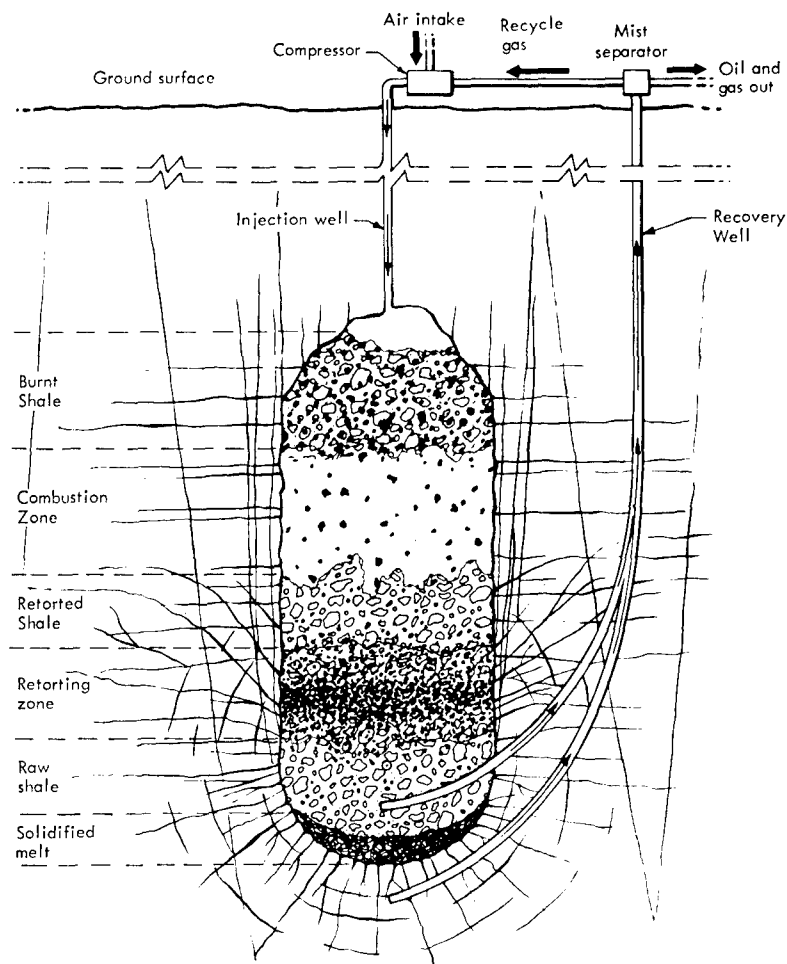


Fig. 6. Concept of retorting a nuclear chimney in oil shale by the combustion process.

Retorting Variables

The experimental retorting of a nuclear chimney will be an expensive procedure. To be of value, it should yield more than just a cursory understanding that if certain conditions are set up, a certain amount of oil is produced. The experiment should reveal some technical details of the response of the retorting process to variations in the controllable parameters. Similar information is needed to establish the optimum set of operating conditions for any of the suggested retorting methods. Acquiring direct knowledge of what is going on in the chimney may be complicated by the problems of installing appropriate instrumentation in the postshot chimney environment.

Three kinds of data would be helpful: pressure, gas composition and temperature, each as a function of time and position in the chimney. However, pressure in the chimney can be estimated with more than adequate accuracy. Gas composition is being examined in experimental retorts prior to the Bronco retorting, and can probably be correlated with temperature.

The bulk permeability of chimney rubble is directly related to the efficiency of various proposed recovery processes. If the particle size distribution and bulk porosity of the rubble vary from place to place within the chimney, the permeability of the rubble column will also be a function of position. The

fingering of gases in high permeability zones during retorting may result in the bypassing of a significant portion of the oil shale.

Permeability and particle size distribution may have an effect on combustion front stability if the combustion process is utilized. An unstable combustion front might reach and consume significant quantities of unretorted oil shale. In addition, the relationship of particle sizes to the efficiency of any proposed retorting process must be understood before an efficient recovery experiment for a nuclear chimney can be designed.

Many of these relationships can be investigated in a laboratory situation prior to the nuclear experiment. For this purpose, a 10-ton retort capable of handling shale pieces as large as 20 in. in two dimensions has been in operation at the Laramie Petroleum Research Center for the past two years.² A larger unit capable of handling 4-ft pieces of oil shale has been designed and has recently been placed in operation. Figure 7 is a schematic diagram of the larger retort.

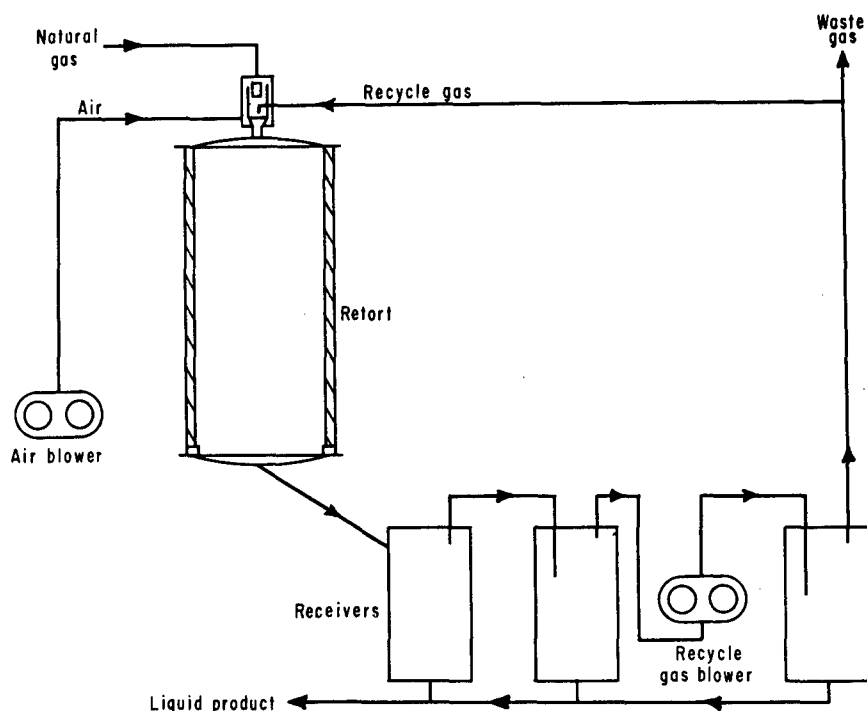


Fig. 7. Schematic diagram of the 150-ton retort.

Yields as high as 80% of Fischer assay have been obtained from the smaller unit.⁴ Statistical evaluation of data obtained from this unit indicates that oil yield is influenced mainly by recycle gas rates, shale bed temperatures, and grade of shale. These parameters and their squares and cross products accounted for 91% of the variability in oil yield. Although air rate and particle size of the charge had some effect on oil yield, these variables were not highly significant for the ranges investigated.

Thermocouple records from four runs in the 10-ton retort have been subjected to additional analysis. Ahead of the combustion front, in the temperature range 700°F to 1000°F, the cooler isotherms were found to be advancing more rapidly than the warmer ones (see Fig. 8). These results are consistent with the chimney retorting model illustrated in Fig. 6. It appears that endothermic decomposition of carbonate components of the oil shale does not seriously impede the retorting process in this temperature range.

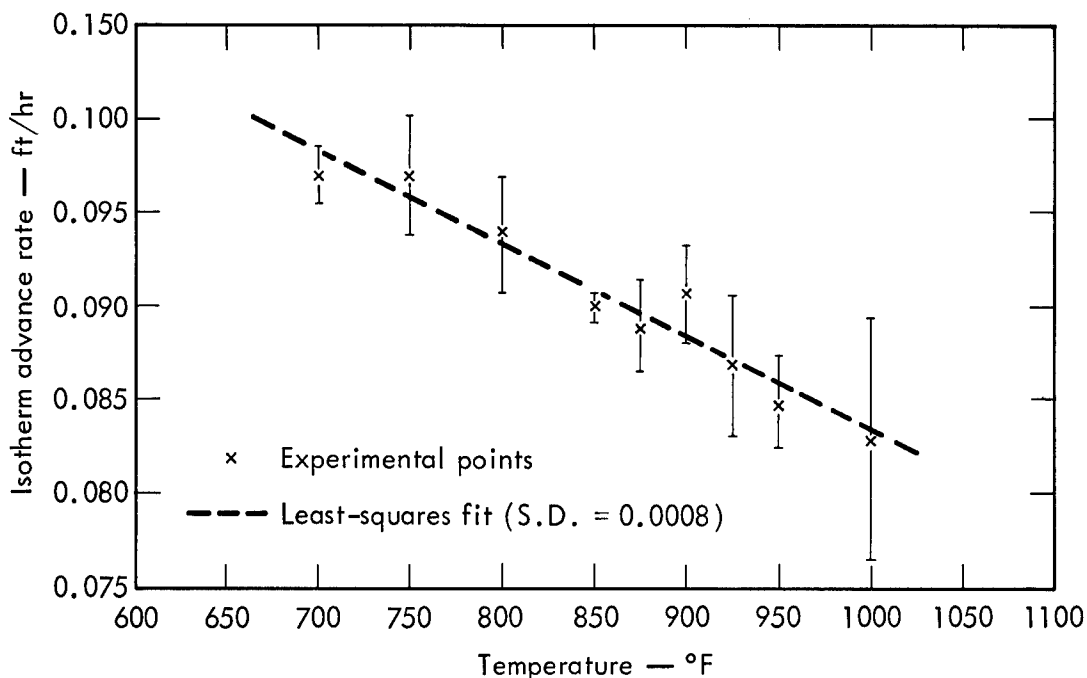


Fig. 8. Isotherm advance rates: Average of Laramie 10-ton retort runs 8, 9, 10, 11.

Laboratory work at the Laramie center has shown that settling and compaction of the shale bed during retorting, due to pressures such as those which might exist near the bottom of a nuclear chimney, reduce bulk permeability. Compaction at pressures corresponding to rubble column heights of 400 ft or more was evident at temperatures as low as 600°F.²⁰

A related question involves the retorted or retorted-and-burnt oil shale farther up in the chimney. The strength properties of the oil shale before and after retorting, and before and after combustion, are known to be different. Retorting removes the bulk of the kerogen which serves to bind the mineral particles. But there remain sufficient organics to cement the matrix. After combustion has removed essentially all carbonaceous residue, the resulting burnt shale is relatively friable. If the burnt oil shale crushes to any degree, the fine particles may tend to form a dense mass having relatively low bulk permeability that subsequently would block the flow of gases. Laboratory studies of the strength properties of retorted and burnt oil shale are underway at the Bureau of Mines' Laramie Station.

Enough energy remains in the vicinity of a nuclear explosion, in the form of heat, to retort some oil shale, perhaps as much as 10% of the fragmented material in the chimney.² If such retorting occurs, it will probably be at the base of the chimney where the heat is initially concentrated. The presence of water or organic fluids (including retorted oil) will serve to distribute heat energy more uniformly throughout the chimney, by a refluxing action, at a temperature below the retorting threshold.

Because the amount and composition of fluids that the chimney would contain are unknown, it is difficult to predict chimney temperature as a function of position and time. Yet the temperature distribution may very well be an important factor in properly conducting the retorting. If instrumentation can be installed in a chimney for retorting experiments, it will also be possible to measure the temperature distribution before retorting begins. It may also be possible to measure the amount of any fluid shale oil that may have collected at the bottom of the chimney by this time.

PROJECT BRONCO DESIGN

In order to evaluate some of the explosive effects in oil shale and also to study some of the variables of retorting in an explosion-created environment, Project Bronco was conceived and proposed⁵ as a fully contained nuclear explosion, approximately 3000 ft deep in the Green River oil shale deposit in the Piceance Basin of Colorado. An energy yield of 50 kt was chosen because it was considered to be large enough to assure chimney collapse. It was also considered to be of the same order of magnitude as potential commercial shots in oil shale. At the same time, 50 kt was small enough that full containment could be expected with a high degree of certainty at the planned depth of burial.

The technical plan for Project Bronco was developed with the following objectives:

1. To assess the technical and economic feasibility of in situ retorting as a method of recovering oil from oil shale fragmented and fractured by an underground nuclear explosion.
2. To confirm and refine the capability to predict physical properties and geometry of the cavity, chimney, and the fractured region produced by a nuclear explosion in oil shale.
3. To investigate the form and distribution of radioactivities left by the detonation, and to assess their behavior during in situ retorting.

The experiment was designed with full consideration for public health and safety. Extensive studies at the proposed site during the initial Site Confirmation phase were envisioned to assure that safety criteria were met.

Extensive geologic information on the proposed Piceance Basin site was available from the USBM-AEC Colorado Core Hole No. 1.^{21,22} In addition, Core Hole No. 3 was completed at the proposed site.²³ On the basis of preliminary data from No. 3 and taking into account the regional geology, the oil shale at the nominated site is estimated to be about 2250 ft thick, with an additional 950 ft of overburden.

Site Confirmation

In order to confirm and further evaluate geologic and hydrologic conditions and to establish whether safety criteria were met, three preshot wells were planned. Data to be obtained from the wells were: overburden thickness; oil shale thickness, grade, and uniformity; fracture occurrence and orientation; presence of other minerals; and the existence and characteristics of aquifers. Location of the wells in relation to the proposed explosive emplacement well are given in Fig. 9.

The first exploratory well was planned approximately 400 ft from the tentative shot location. Core was to be taken from the top of the oil shale to total depth, and a complete suite of logs was to be run. An extensive hydrologic testing program was planned.

The second well was planned as a geologic confirmation well and to conduct hydrologic tests, both transmissibility and capacity, in conjunction with the first. The wells were to be located several hundred feet apart on opposite sides of the proposed nuclear explosive emplacement hole.

A third well was planned as a whipstock to pass through the region above where the chimney was expected. Its principal purpose was fracture definition.

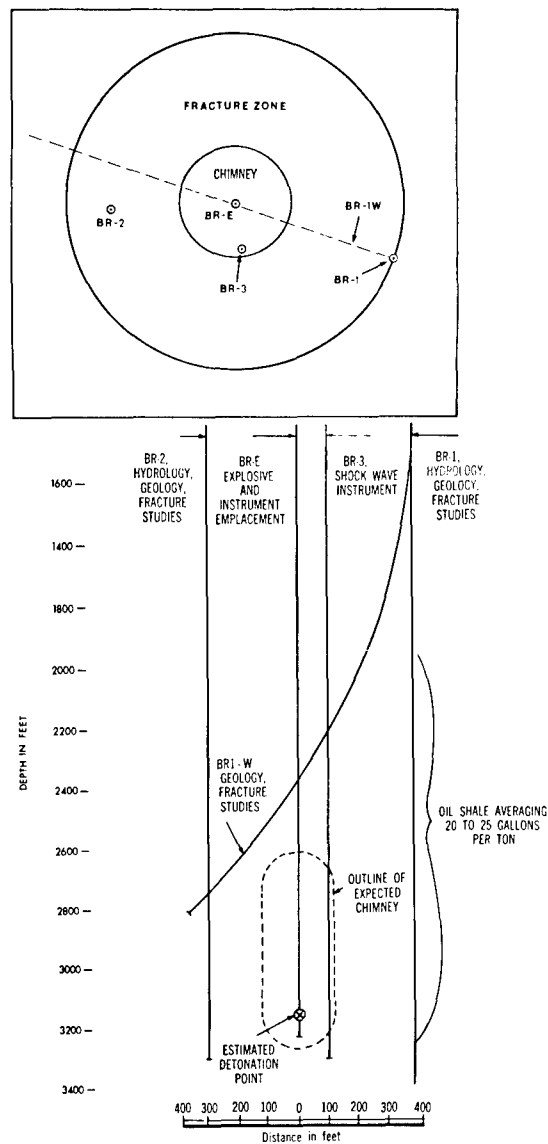


Fig. 9. Preshot well plan.

If any major fracture was encountered in the well, it would be thoroughly tested to determine its extent and capacity.

Should such a fracture exist in the immediate vicinity of the detonation, it could provide a path for water in overlying aquifers to migrate into the chimney. A copious flow of water into the nuclear chimney would complicate the subsequent retorting experiment. In addition, an extensive fracture system communicating to an overlying aquifer or to the ground surface would involve additional safety considerations.

Construction, Detonation, and Evaluation

When preliminary studies had assured that an acceptable site had been found, construction of roads, cableways, trailer pads, etc., were to start. In addition, an instrument well and the explosive emplacement well were to be drilled. Relative locations of these wells are also shown in Fig. 9.

An instrument well to provide dynamic explosive effects information was planned at a distance of 100 ft from the explosive emplacement hole. Instruments for measuring shock-wave phenomena associated with the explosion were to be placed at various levels in the well.

The emplacement well for the nuclear explosive was to be drilled to accept the explosive canister. It was proposed to emplace the explosive at approximately 3000 ft, near the bottom of the oil shale sequence. The well was to be stemmed to prevent the release of radioactivity. The scaled depth of burial for the explosion was about twice that of most completely contained explosions at the Nevada Test Site.

The nuclear chimney would be about 230 ft across and 520 ft high (measured up from the shot point).⁵ Fractures would extend as far as 460 ft laterally beyond the chimney edge. Such a chimney would contain about 1.2 million tons of fragmented oil shale, and the surrounding fractured region would contain considerably more. The oil content of the chimney alone, assuming 24 gal/ton average, would be about 660,000 barrels.

As soon as possible after detonation, a reentry well was to enter the top of the chimney near the emplacement hole, as shown in Fig. 10. The hole was to be cased through water-bearing zones and drilled dry below that, with core taken to aid in fracture studies. Pressures, temperatures, and radioactivities were to be monitored during drilling. Gas samples from the chimney would be analyzed for chemical composition and radioactivity. The chimney volume and effective fracture permeability were to be studied by gas injection and pressure fall-off techniques. Downhole photographs of the top of the chimney rubble would help define rubble size distribution.

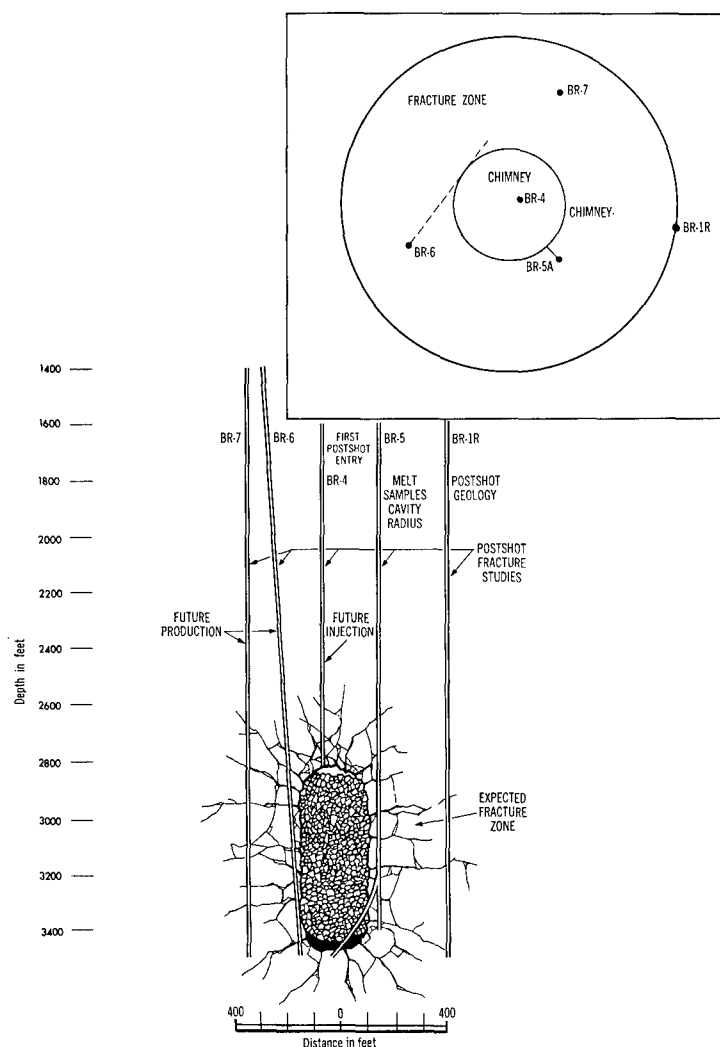


Fig. 10. Postshot environment evaluation plan.

A second reentry well, parallel to the sidewall of the chimney, was planned. Its major purposes were to study the fractures and the chimney boundary from a whipstock oriented to penetrate the bottom part of the chimney.

Three additional holes were to be drilled to further establish the nature and extent of fracturing outside the chimney. These holes also were to be modified later for use during the subsequent treatment phases. The wells would be cased through the upper aquifer and cored in the fractured region.

Isolation of water-bearing zones in all wells was planned to insure that the holes would not serve as paths for water entry to the chimney from the aquifer above and to prevent intermingling of different water zones.

In Situ Treatment

Most of the details for the retorting portion of the experiment are largely dependent upon the characteristics of the explosion environment defined by the postshot evaluation, and also upon results from retorting research currently in progress.

A retorting method that utilized the heat of combustion of retorted oil shale was planned as the basis for the recovery experiment. However, should research and development with preheated inert and reacting gases indicate greater commercial promise, one of these other methods could be selected for the experiment. In such a case there would be no change in the level of technical interest in such fundamental aspects as the amount of recoverable oil, the distribution of radioactivity in the oil, and the importance of variables such as injection rate, temperature, and pressure.

The chimney treatment plan, illustrated in Fig. 11, included three holes to the top of the nuclear chimney for the injection of a mixture of air and recycle gas. Each of these holes would serve, in addition, for the emplacement of pipe extending as far as possible into the chimney rubble for the purpose of installing instruments to monitor retorting process variables. A compressor system would be necessary to force gases into the chimney via the injection holes.

Three wells were to be used for production from the bottom part of the chimney. Tubing with downhole pumps in each of the wells would bring up liquid oil, with return gas and oil mist returning in the annuli.

Separation equipment at the surface would be needed to remove oil and water from the gas stream. A portion of the gas was to be returned to the chimney; the remainder was to be cleaned, if necessary, and flared. The production well fluids were to be monitored continuously for radioactivity and for composition. Because of the possibility of some contaminated water and oil, above-ground storage for water and oil was planned, as was temporary storage for disposable oil.

Upon completion of the recovery experiments in the chimney, the well adjacent to the chimney was to be reentered, and a new well beside the chimney drilled with whipstock or slant holes toward the chimney. The holes were to be cored to give material balance data on the chimney retort treatment.

The design of the fracture zone treatment outside the chimney is also highly dependent upon the results of the postshot evaluation. The extent, density, and permeability in the fractures would dictate the specific details and scope of the recovery treatment plan. Here again, research currently in progress would be utilized in the design. The extent of open fractures, the portion of oil recovered, and the occurrence of radioactivity are factors which should be investigated in such an experiment.

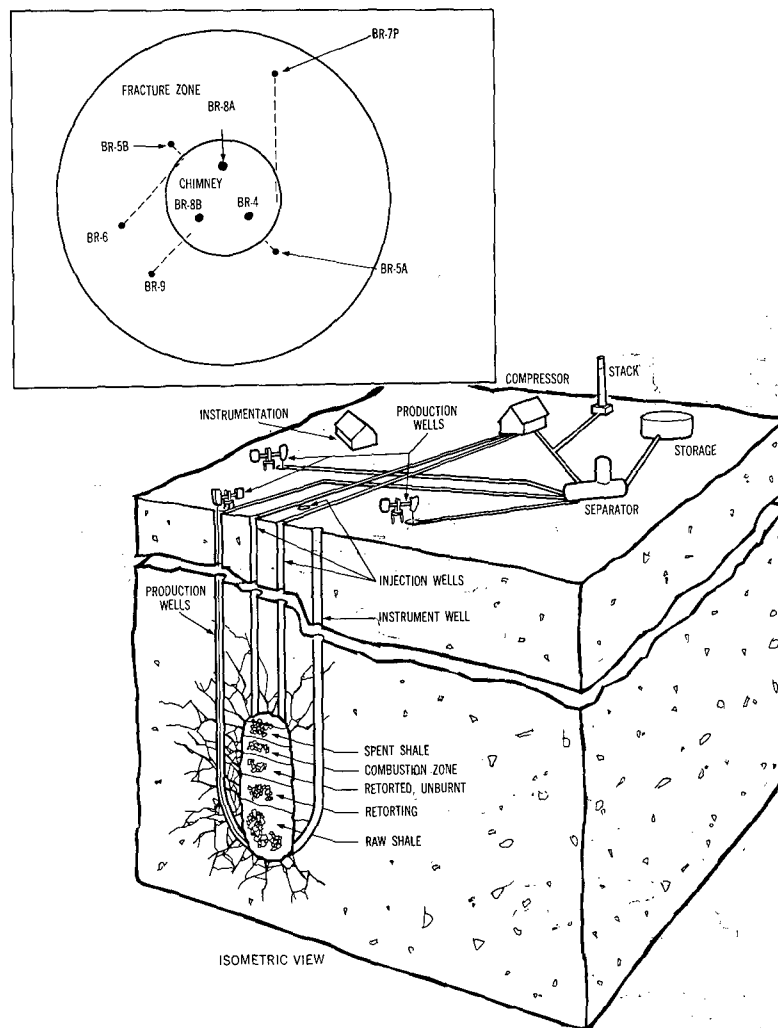


Fig. 11. Experimental chimney treatment concept.

As in the chimney treatment, in situ combustion was planned for the fracture treatment. The plan envisioned use of a 45° segment of the fracture zone with air or gas injection into the chimney. Air, recycle gas rates, oil shale grade, and explosion effects would be primary considerations in the specific experiment design. Figure 12 is a schematic concept of the fracture zone treatment wells.

SUMMARY

Nuclear explosions may be useful for introducing fracture permeability into deep oil shale deposits to prepare them for in situ retorting. The development of a commercial nuclear oil shale technology will involve the solution of several technical problems. A capability to predict explosion effects in oil shale will be needed, as will suitable retorting techniques and methods of controlling pollution. The Bronco design illustrates the key part nuclear explosion experiments will play in the development of this Plowshare application.

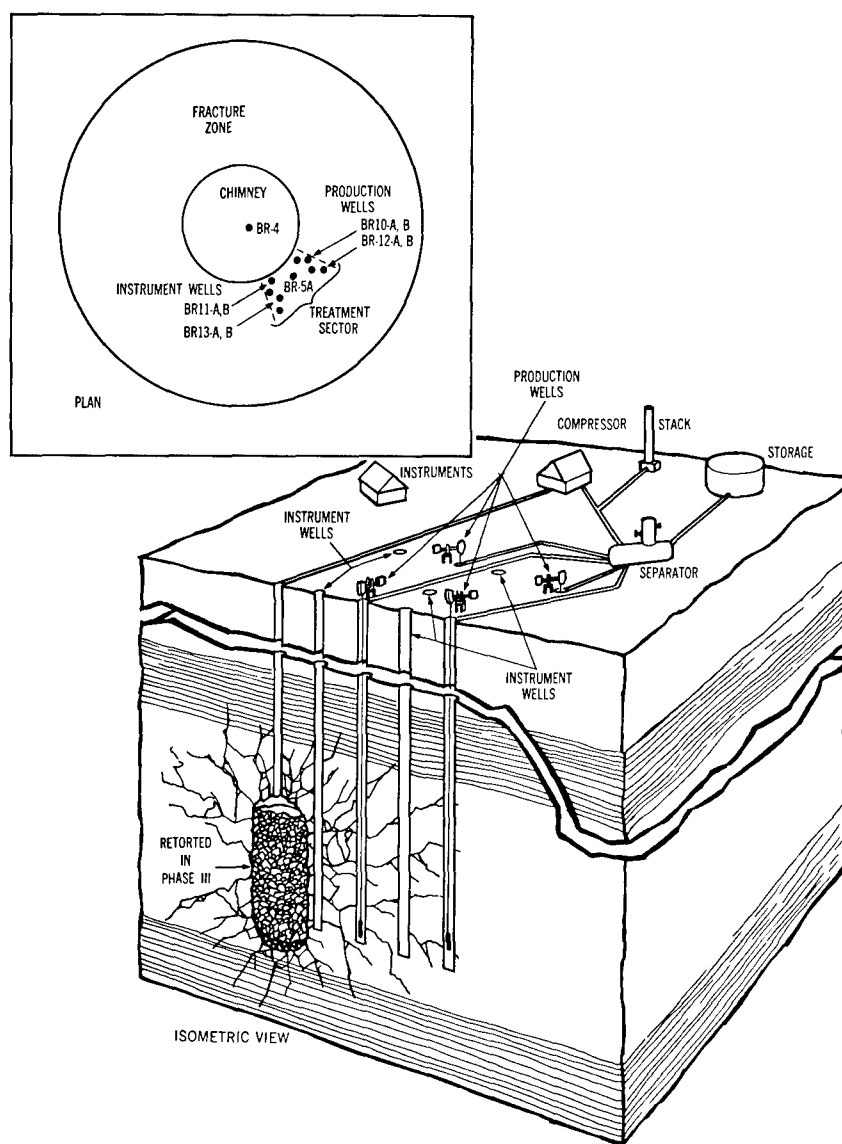


Fig. 12. Experimental fracture treatment concept.

REFERENCES

1. W. I. R. Murphy, "In Situ Shale Oil Production Problems," Proc. 2nd Plowshare Symp., Lawrence Radiation Laboratory, Livermore, UCRL-5678, May 1959, p. 80 ff.
2. D. B. Lombard and H. C. Carpenter, J. Petrol. Tech. 19, 727 (1967).
3. H. C. Carpenter, S. S. Tihen, and H. W. Sohns, "Retorting Ungraded Oil Shale as Related to In Situ Processing," Presented at Am. Chem. Soc. Natl. Meeting, San Francisco, California (April 1-5, 1968).
4. H. C. Carpenter and H. W. Sohns, "Application of Aboveground Retorting Variables to In Situ Oil Shale Processing," Proc. Fifth Symp. on Oil Shale, Quarterly of the Colorado School of Mines, 63, (4), 71-82 (1968).
5. "The Bronco Oil Shale Study," U.S.A.E.C. Report No. PNE-1400, 1967, prepared by USAEC, U.S. Bureau of Mines, CER Geonuclear Corp., and Lawrence Radiation Laboratory.
6. C. R. Boardman and J. Skrove, J. Petrol. Tech. 18, 619 (1966).

7. D. E. Rawson, J. A. Korver, R. L. Pritchard, and W. Martin, "Post-shot Geologic Investigations—Project Gasbuggy," Lawrence Radiation Laboratory, Livermore, Report No. UCRL-71354. Presented at Soc. Petrol. Engr. Meeting, Houston, Oct. 29, 1968.
8. J. R. Ege, "Locations of Potential Interest for Fracturing Oil Shale with Nuclear Explosives for In Situ Retorting, Piceance Creek Basin, Rio Blanco County, Colorado," U.S. Geol. Survey, TEI-868, 1967, 8 pgs., 8 plates.
9. W. J. Frank, "Characteristics of Nuclear Explosives," Proc. Third Plowshare Symp., USAEC TID-7695, (April 1964), pp. 7-10; also Lawrence Radiation Laboratory, Livermore, Report, UCRL-7878, 1964.
10. C. R. Boardman, D. D. Rabb, and R. D. McArthur, J. Geophys. Res. 64, 3457 (1964).
11. J. T. Cherry, D. B. Larson, and E. G. Rapp, Intern. J. Rock Mech. Min. Sci. 5, 455 (1968).
12. J. T. Cherry, D. B. Larson, and E. G. Rapp, "Computer Calculations of the Gasbuggy Event," Lawrence Radiation Laboratory, Livermore, Report UCRL-50419, 1968.
13. A. Holzer, "Gasbuggy: Preliminary Postshot Summary Report," U.S.A.E.C. Report PNE-1003, 1968.
14. H. C. Heard, Lawrence Radiation Laboratory, Livermore, to be published.
15. H. C. Rodean, Geophysics, 30, 616 (1965).
16. D. D. Rabb, "Size Distribution Study of Piledriver Particles," Lawrence Radiation Laboratory, Livermore, Report UCRL-50489, 1968.
17. H. A. Tewes, "Radioactivity Source Terms for Underground Engineering Applications," Proc. USPHS Symp. on Public Health Aspects of Peaceful Uses of Nuclear Explosives, Las Vegas, April 1969.
18. H. A. Tewes, "Radioactivity from Nuclear Cratering Explosives," to be published in Highway Research Record.
19. W. D. Arnold, and D. J. Crouse, "Radioactive Contamination of Oil Produced from Nuclear-Broken Shale", Proc. Symp. on Engineering with Nuclear Explosives, Las Vegas, January 1970.
20. S. S. Tihen, H. C. Carpenter, and H. W. Sohns, "Compaction of Broken Shale during Retorting," to be published as a U.S. Bureau of Mines Report of Investigations.
21. R. D. Carroll, D. W. Coffin, J. R. Ege, and F. A. Welder, "Preliminary Report on Bureau of Mines' Yellow Creek Core Hole No. 1, Rio Blanco County, Colorado," U.S. Department of the Interior, Geological Survey, Open File Report TEI-869, March 1967.
22. J. W. Smith, L. G. Trudell, and G. F. Dana, "Oil Yields of Green River Oil Shale from Colorado Core Hole No. 1," U.S. Bureau of Mines Report of Investigation 7071, January 1968.
23. G. F. Dana, "Bureau of Mines—Atomic Energy Commission Colorado Core Hole No. 3, Rio Blanco County, Colorado," Open File Report, Laramie Petroleum Research Center, 1968.

OIL SHALE RESEARCH RELATED TO PROPOSED NUCLEAR PROJECTS

By H. C. Carpenter, H. W. Sohns, and G. U. Dinneen

Laramie Petroleum Research Center, Bureau of Mines,
Department of the Interior, Laramie, Wyoming

ABSTRACT

The Bureau of Mines is conducting research to develop data pertinent to in situ retorting of oil shale fractured by a nuclear explosion or other means. Maximum utilization of the Green River oil shale found in Colorado, Utah, and Wyoming, at depths ranging from outcrops to several thousand feet, requires development of several methods of processing. Early research was devoted to developing processes for application to oil shale occurring at depths suitable for mining. In present research, the emphasis is on in situ retorting and recovery processes that would be more satisfactory for oil shales occurring at greater depths.

Development of an in situ process depends upon finding or establishing sufficient permeability in the oil shale beds for the passage of fluids which serve as a heat carrier in bringing the oil shale to retorting temperature. Use of a nuclear explosive seems to offer the best chance for successfully fracturing the thicker and more deeply buried portions of the deposit to give the required permeability. Processing the very large quantity of broken and fractured oil shale that would be produced presents many problems which require new background data for their solution. This paper describes research the Bureau of Mines is conducting to develop pertinent data. Primarily this research involves laboratory determination of properties of oil shale, pilot scale investigation of retorting characteristics of ungraded broken shale, and underground combustion of shale fractured by pressure and chemical explosives. Application of the research results should aid in designing the oil recovery phase and provide an estimate of the quantity of oil that may be obtained in a nuclear experiment in oil shale.

INTRODUCTION

Oil shale in the Green River Formation in Colorado, Utah, and Wyoming represents a tremendous energy resource and contains associated minerals that may be valuable. Research on methods for utilizing this resource has been conducted for many years, but has not yet resulted in commercial processing. Because the formation extends over a large area, approximately 16,500 square miles, in which the thickness and grade of shale as well as the amount of overburden vary greatly, many different combinations of mining and processing techniques will be required to fully utilize the deposit. The technique with which this paper deals is the utilization of an underground nuclear explosion to produce a chimney containing broken oil shale and a fractured zone around the chimney, and the subsequent processing of this oil shale in place to recover oil and possibly other minerals from it.

The possibility of using a nuclear explosive in oil shale has been actively considered for over 10 years, and numerous papers concerning it have been published (1-2)^{1/}. In these publications it has frequently been necessary to base much of the discussion on assumptions, as this is a new concept for which background data are not available. This is particularly true for underground processing because practically all of the extensive oil shale research in the past has been devoted to mining and aboveground retorting. Only in recent years has research designed to provide some of the background data required to evaluate the potential of the nuclear approach been undertaken. In this paper we will discuss the present research program of the Bureau of Mines to obtain this type of data, the results so far achieved, and the significance of these results to the nuclear approach for utilizing oil shale.

RESEARCH PROGRAM RELATED TO NUCLEAR EXPERIMENTS IN OIL SHALE

Two types of research are being conducted relating to the use of a nuclear explosive in oil shale. These are (1) resource evaluation to determine location, thickness and grade, physical properties, and chemical composition; and (2) engineering studies related to recovering shale oil from the deposit after it has been fractured by a nuclear explosive.

Resource Evaluation

Location

The Green River oil shale formation covers about 16,500 square miles in Colorado, Wyoming, and Utah, as shown in Figure 1. The thickness of the shale and the amount of overburden vary widely throughout this area. Until a few years ago, most of the information about the deposit had been obtained from coreholes drilled where the deposit would be amenable to mining or from cuttings from wells that passed through the formation, for example, during drilling of oil and gas wells. The results did not give adequate information about the thick, deep shales that might be suitable for fracturing by a nuclear explosive; therefore, during the last several years, the Bureau of Mines and the Atomic Energy Commission drilled three holes to obtain such information in the north-central portion of the Piceance Creek Basin in Colorado. These are shown on Figure 1 as Colorado Coreholes 1, 2, and 3. The conditions in the vicinity of Corehole 3 seem to be suitable for the use of a nuclear explosive. These have been discussed previously (1-3).

In addition to the coreholes in the Piceance Creek Basin, the Bureau of Mines has, during 1968-69, drilled Coreholes 1 and 1A in the Washakie Basin of southern Wyoming to see whether the deeper shales in this basin might be suitable for in situ recovery, using either nuclear or other fracturing techniques. Long sections of relatively low-grade oil shale were encountered. In general, the oil shales average only 10 to 15 gallons per ton. A selected 650-foot section has an assay averaging 11 gallons per ton. The leanness of the shales makes this site less attractive for initial development than other areas where the shales are richer.

Some support has also been given to an exploratory operation of the CER-Geonuclear Corporation and The Western Oil Shale Corporation in Utah. As a part of a feasibility study for the use of nuclear fracturing, these companies have drilled Utah EX-1 Corehole in the Uinta Basin. The Bureau's Laramie Petroleum Research Center cooperated by performing the assay work on the core. The data obtained are still being evaluated.

^{1/} Underlined numbers in parentheses refer to items in the list of references at the end of this report.

Physical Properties

Oil shale, as it occurs in nature, is a strong rock, having a compressive strength of about 10,000 psi. This is many times that required to withstand the stresses present in the column of rubble in a nuclear chimney. However, much of this strength, particularly in richer shales, comes from the organic material in the shale which will be altered or removed during the retorting process. Little is known regarding the structural response of oil shale as it is heated under compressive stress.

Research is being conducted, utilizing small cores and fragments, to evaluate the stress-strain-time-temperature relationships of oil shale under compressive stresses such as would exist in a nuclear chimney, and to study the effects of deformation on permeability (4). At present, the research has been on samples of richer-than-average material (35 to 64 gallons per ton), because it was thought that this type of material would be most troublesome in regard to structural changes. The results show that in these rich shales the organic matter is the predominant contributor to the oil shales' mechanical properties and structural response to heat and stress. For example, the compressive strength decreases from about 10,000 psi at ambient temperature to a few hundred psi at 725°F; samples can be sliced readily with a knife at 725°F, either perpendicular or parallel to the bedding plane; and the samples show extensive structural breakdown on heating in a stress-free environment. Although structural response of large masses of rubble cannot be predicted quantitatively from results on small specimens, these preliminary results do indicate that heat produces major structural responses in rich oil shales. The possible effects of these should be considered in designing underground processing experiments, both for a nuclear chimney and for the fractured area surrounding it.

Composition

Green River oil shale is an organically rich, dolomitic limestone that was deposited in the beds of Eocene lakes. Much research has been conducted on the composition of the organic material in the shale, and most past efforts have been directed toward utilizing the resource by obtaining oil from it. Recently it has been found that several minerals occur in quantity in certain areas of the Piceance Creek Basin in the deeper-lying shales that might be suitable for exploitation using nuclear fracturing. At the present time, nahcolite (sodium bicarbonate) and dawsonite (sodium aluminum dihydroxy carbonate) appear to be the most significant of these minerals, and the possibility of recovering them needs to be considered in evaluating the nuclear approach. Pertinent research is still in the early stages since the occurrence of dawsonite in quantity was not reported until 1966 (5). The preliminary nature of such research is illustrated further by the fact that there has been a reliable method for quantitatively determining nahcolite and dawsonite only since publication of a paper by Smith and Young in August 1969 (6).

Engineering Studies

Oil Production

Production of oil from oil shale requires application of heat to raise the shale to retorting temperature, generally about 900°F, and to supply the heat of retorting (7). When heated to retorting temperatures, the organic materials in the oil shale are converted to about 65 percent liquid products, about 10 percent gas, and about 25 percent carbonaceous residue which remains behind on the inorganic portion of the shale. Combustion of the carbonaceous residue generally can provide adequate energy for the retorting process.

During the last 25 years, the Bureau of Mines has conducted numerous investigations that gave results which can be directly related to retorting oil shale fractured by nuclear methods. The research includes the following studies which are of particular interest: (1) Aboveground retorting operations using the N-T-U retort at the Anvil Points, Colo., facility in the late 1940's and the current operation of the 10- and 150-ton retorts at the Laramie Petroleum Research Center; and (2) the present in situ field recovery experiments at Rock Springs, Wyo.

Aboveground Retorting

N-T-U Retort. The N-T-U retorts designed and constructed by the Bureau in 1947 (8) were used to investigate such retorting process variables as air rate, recycle gas rate, shale particle size, and shale grade. The retorts were cylindrical steel vessels with tapered, firebrick linings. The internal diameter decreased from 10 feet 4 inches at the bottom to 8 feet 8 inches at the top. Average cross-sectional area was 70.7 square feet. Height from the grate to the dome was approximately 16 feet. These retorts normally were charged with about 40 tons of shale.

Because of extreme pressure drops, gas channeling, and lower oil yield when using a wide particle size range of shale, charges to the N-T-U retorts were generally screened to provide minus 3 inch to plus 1/2 inch material. The charge was ignited at the top, the combustion zone passed downward through the shale bed, and all gaseous and liquid products were removed from the bottom of the retort. High air rates increased the retorting rate (pounds of shale processed per hour per square foot of retort cross section), but an optimum air rate somewhat lower than 5 scfm/ft² of cross-sectional area was required to produce the maximum quantity of oil per ton of shale. Use of recycle gas in the process was not found to be beneficial. Oil yield was also shown to be a function of the grade of shale processed; that is, the percentage of oil recovered, based on assay values, increased with increasing shale grade.

Because of the rather closely sized charge of the N-T-U retorts, the results of this early research do not give all the information necessary for designing a recovery experiment in rubble produced by a nuclear explosive because the rubble will have a large particle-size range. Hence, a project to study the retorting characteristics of this type of material was started in 1965. Subsequently, retorts large enough to contain 10 tons and 150 tons of shale, respectively, have been constructed at the Laramie Petroleum Research Center.

10-Ton Retort. The 10-ton retort (Figure 2) is a small batch unit, similar in principle to an N-T-U retort, consisting of a cylindrical steel shell 6 feet in diameter by 12 feet tall. This shell surrounds a tapered refractory lining 6 inches thick at the bottom and 9 inches thick at the top. The retort has been operated on shale charges made up of mine-run material containing pieces as large as 20 inches in two dimensions with the third dimension generally being between 12 and 18 inches, but occasionally being as large as 36 inches. The oil content of the shale charges ranged from 21 to 48 gallons per ton. Properties of three charges covering the range indicated above are shown in Table 1. Air rates used in these experiments ranged from 0.5 to about 4 scfm/ft² of retort cross section. Recycle gas-to-air ratios ranged from 0:1 to 1:1. The 10-ton retort has been operated for a total of 30 experiments. Oil yields from these experiments varied widely and ranged up to a maximum of about 80 percent of Fischer assay.

Least squares methods were used to derive linear models relating operating variables to shale oil recovery (9). Multiple regression analysis showed

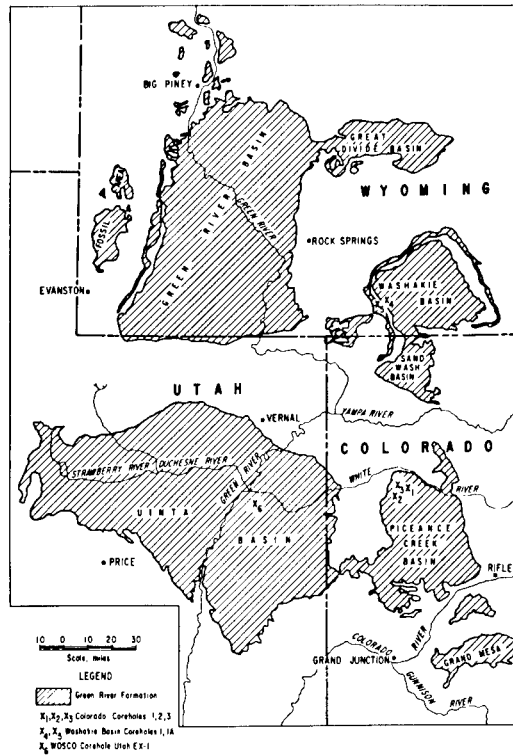


FIGURE 1. - Coreholes in the Green River Formation investigated for nuclear fracturing.



FIGURE 2. - 10-Ton retort.

Table I. - Properties of oil shale charges to 10-ton retort

	Charge number		
	1	2	3
Oil yield by Fischer assay, gal/ton	21.7	30.8	48.0
Water from Fischer assay, gal/ton	3.4	1.8	4.6
Organic ultimate analysis, wt pct			
Carbon	80.27	80.55	81.07
Hydrogen	12.86	11.79	11.30
Nitrogen	2.74	2.53	2.70
Sulfur	4.12	5.12	4.93
Shale particle size, wt pct			
+ 20 inches	-	29	17
12 to 20 inches	5	18	21
6 to 12 inches	22	16	10
<6 inches	73	37	52

that, over the ranges investigated, the most significant variables in the study were retorting temperature, recycle gas rate, and assay of the oil shale charge. Retorting temperature is not an independent variable, but depends on the primary variables as well as on heat lost to the surroundings. Further studies are planned to define these relationships.

150-Ton Retort. Because operation of the 10-ton retort on ungraded shale with a maximum size of approximately 20 inches gave recoveries approximately equivalent to those obtained on the N-T-U retort using closely graded shale, it was deemed advisable to determine the effect of scaling up the operation. To do this, a 150-ton retort (Figure 3) was constructed to operate on charges of ungraded material containing pieces up to a maximum of 4 feet on a side. The 150-ton retort is simply a larger version of the 10-ton retort and operates in the same manner with the combustion zone traveling downward through the shale bed. It has a cylindrical steel shell 12 feet in diameter by 45 feet tall, with a refractory lining consisting of 4 inches of insulating castable refractory next to the shell and 6 inches of high-density firebrick next to the charge.

One shakedown run has been made on the retort in which the charge consisted of mine-run, 25-gallon-per-ton shale, containing pieces as large as 3 feet on a side and weighing approximately 2 tons. In addition, the charge contained one 3-foot by 4-foot by 6-foot block of shale weighing 7500 pounds. Six thermocouples were imbedded in this block to permit comparing its heating rate with that of the surrounding bed. Retorting was completed after about $3\frac{1}{2}$ weeks of operation, and the bed was cooled with recycle gas prior to discharge. No operating difficulties were encountered, and temperature histories show that the retorting and combustion fronts advanced uniformly through the bed with little or no channeling or fingering. Because the run was made primarily for shakedown purposes to determine the operability of the unit, operating conditions were varied widely without any attempt at optimization. Oil yield amounted to more than 60 percent of Fischer assay, a most encouraging figure because optimization can be expected to result in substantial improvement in oil yield.

In Situ Processing

The rubble-filled chimney resulting from a nuclear explosion will be surrounded by a relatively large fractured area capable of yielding larger quantities of oil than the chimney. Development of successful methods to

process this fractured area will greatly enhance the possibility of successfully applying nuclear explosives to recovery of oil from oil shale. For several years the Bureau of Mines has been conducting in situ experiments near Rock Springs, Wyo., the primary purpose of which is to determine whether oil can be economically recovered from shale fractured by less drastic means than a nuclear explosion. The Rock Springs project was undertaken primarily to investigate non-nuclear approaches to in situ retorting of deposits that are too sparsely covered or too thin to be amenable to the nuclear approach; however the processing problems are closely related to those that can be expected in processing the fractured area surrounding a nuclear chimney.

Fracturing. In an effort to create sufficient permeability in a shale interval to allow ignition and support of a combustion zone, three techniques, used individually and in various combinations, were employed. These were (1) electrolinking, which is fracturing and/or weakening the formation with high-voltage electricity (10); (2) hydraulic fracturing with and without sand propping; and (3) fracturing with liquid and/or solid chemical explosives. Because these techniques in themselves are not of interest from the nuclear application standpoint, they are not discussed in detail in this paper.

Although no definitive method for evaluating the results of these fracturing treatments has been devised, flow testing with compressed air did give some information. It showed that electrolinking resulted in no substantial increase in permeability, but consecutive applications of hydraulic fracturing, sand propping, and explosive fracturing did. By injecting air into one of the wells fractured during this experiment, the following increases in permeability were observed:

<u>Stage of experiment</u>	<u>Injection pressure required to give flow rate of 700 mcfd</u>
After hydraulic fracturing	100.0 psig
After hydraulic fracturing and sand propping	34.8 psig
After explosive treatment	2.2 psig

Underground Retorting. An in situ retorting experiment was performed at the Rock Springs site in the Tipton member of the Green River oil shale formation in a 20-foot-thick section from 68 through 87 feet below the surface. Potential oil yield from this shale section was determined by coring and performing Fischer assays on 1-foot intervals of the core. The 20-foot section, which averages about 22 gallons per ton, was fractured by a combination of the techniques mentioned in the preceding section (10-11). The pattern of the wells utilized for the experiment is shown in Figure 4.

The oil shale formation was ignited in Well No. 5 by means of a propane burner. Air was injected into the well to supply oxygen for combustion of the propane and for combustion of the carbonaceous residue remaining on the retorted shale. After 2 weeks, the burner was shut off and combustion in the formation became self-sustaining, the organic material in the oil shale burning with air supplied from the surface. Combustion was then continued for an additional 4-week period. During the course of this retorting experiment, about 190 barrels of oil were recovered.

From this experiment it was concluded that (1) a combustion zone can be established in the fractured oil shale by use of air injection and a downhole burner; (2) this zone can be maintained and moved through the shale by injection of air; and (3) loss of permeability was not a major problem during this experiment at shallow depths and with the amount of permeability that had been created.



FIGURE 3. - 150-Ton retort.

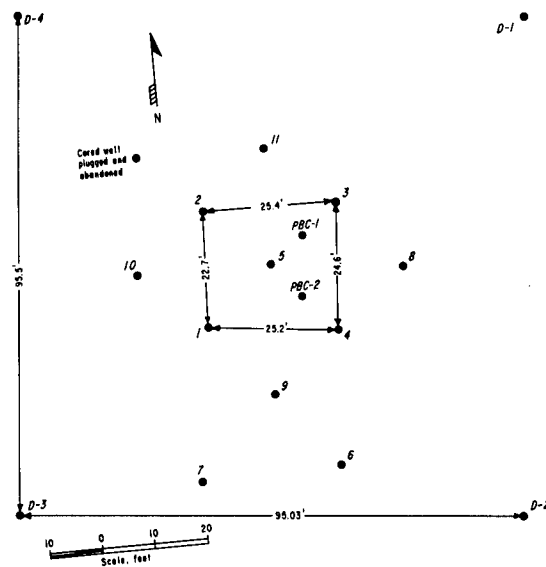


FIGURE 4. - Test well locations, Rock Springs Site 4.

Cores have been taken through the shale section in order to evaluate the areal and volumetric extent of the retorted zone. Examination of the cores is not complete, but preliminary results are given in Table II. These results

TABLE II. - Assays of cores from the in situ experiment

Depth, feet	Original assay, gal/ton	Post-burn assays	
		PBC-1, gal/ton	PBC-2, gal/ton
68	20.7	22.6	12.3
69	21.1	22.6	21.4
70	16.6	8.8	21.8
71	24.2	3.6	22.2
72	32.2	3.6	20.2
73	28.6	3.6	20.6
74	28.5	13.1	15.8
75	31.7	32.6	14.6
76	32.4	33.2	34.8
77	18.1	20.5	21.0
78	20.2	22.7	22.9
79	15.4	13.8	16.0
80	18.6	19.7	13.9
81	26.6	26.6	28.7
82	21.2	18.9	22.6
83	16.6	11.7	12.2
84	19.8	18.6	17.8
85	24.6	28.3	27.4
86	14.0	18.5	17.7
87	9.2	13.0	10.1

show that a thin but readily discernible retorted zone (70-74 feet) occurs at the location of one of the cores; a similar pattern is not evident at the other location, indicating that retorting did not proceed uniformly from the injection well.

Oil Yields and Properties

Yields and properties of oils obtained from the N-T-U, 10-ton, and in situ processes are given in Table III. The oil from the N-T-U retort has a

TABLE III. - Oil yield and properties

	N-T-U retort	10-ton retort	In situ experiment
Oil yield ^{1/} , vol pct of Fischer assay	79.7	80.4	<u>2/</u>
Selected oil properties:			
Specific gravity, 60°/60°F	0.932	0.915	0.874
Pour point, °F	90	70	20
Viscosity, SUS at 100°F	278	93	45
Nitrogen, wt pct	2.10	1.88	1.35
Sulfur, wt pct	0.79	0.76	0.68
Naphtha, vol pct of crude	2.7	6.7	12.4
Light distillate, vol pct of crude	16.5	18.5	43.4
Heavy distillate, vol pct of crude	31.2	38.2	29.2
Residuum, vol pct of crude	49.6	35.5	12.0

^{1/} Oil yield from the N-T-U retorts represents yield from a production run. Yield from the 10-ton retort represents approximately the maximum yield obtained.

^{2/} Not determined.

high pour point and viscosity and large contents of nitrogen and residuum. The oil from the 10-ton retort has somewhat lower values for these properties. The oil from the in situ experiment has more desirable properties than those from the other two processes, as the pour point, viscosity, and amounts of nitrogen and residuum are all substantially lower. These changes may be due in part to secondary thermal cracking reactions.

Minerals

In those areas where nahcolite and dawsonite occur, it appears that they are the principal minerals that should be considered in planning a nuclear experiment in oil shale. Nahcolite occurs in crystal masses from microscopic size to several feet in diameter and occasionally occurs in thin beds. Dawsonite, on the other hand, occurs in small crystals disseminated through the oil shale in continuous sections up to 800 feet thick.

Because of the large market for aluminum, the dawsonite, from which alumina has been produced in the laboratory, seems to be potentially the more valuable of the minerals. As discussed in a previous section, interest in dawsonite utilization is relatively new, and methods for economic processing are considered to be within the realm of possibility with further research. The rock in a nuclear chimney will be in fairly large pieces; hence, it will have relatively small surface area, and extraction of alumina before retorting to produce oil does not seem to offer much promise. Therefore, present research of interest from the nuclear application standpoint is directed toward determining what effect exposure to retorting temperatures has on the extractability of alumina and toward developing and evaluating extraction processes to see whether they may have potential economic value.

Waste Materials

All of the problems that will be encountered in disposal of organic and inorganic wastes from shale processing cannot be established until a processing scheme has been developed. For example, they will be quite different depending on whether or not leaching has been used to recover the associated minerals discussed in the preceding section. However, waters produced during retorting will probably be reasonably similar for all processing schemes, so detailed studies of retort waters are being made to determine what compounds are present, to demonstrate whether any of these can be recovered profitably to offset waste disposal costs, and to develop methods of treatment to render the water innocuous. Consideration is being afforded to both (1) the water that will have to be treated and disposed of aboveground, and (2) the water that will be left underground and that must be handled in such a way as to prevent contamination of ground waters. Waters presently being studied have been obtained from the 10- and 150-ton retorts at Laramie and the in situ combustion experiments at Rock Springs.

DISCUSSION AND CONCLUSIONS

Until the possibility of utilizing a nuclear explosive for fracturing oil shale was proposed some 10 years ago, most efforts to evaluate Green River formation oil shales were devoted to the portions that would be amenable to mining and aboveground retorting, as this was thought to be the only practical approach to the recovery of the resource. With the prospect of utilizing nuclear explosives, increased effort has been devoted during the last 10 years to examining the deeper-lying portions of the formation. Results obtained indicate that there is a very large quantity of oil potentially recoverable from portions of the formation that are sufficiently thick, deeply buried, and remote to be suitable for application of the nuclear approach.

Physical property determinations that have been made on the oil shale indicate that a nuclear explosive should produce a rubble-filled chimney and a surrounding fractured zone. The rubble, before retorting, will have sufficient strength to support itself and very high permeability. However, as the shale is heated toward retorting temperatures, it will have a tendency to become plastic, particularly in the case of higher-grade shales. Also, as the organic material is removed, the shale will lose much of its strength. Much additional information needs to be obtained concerning shale properties, as these properties will have to be considered in such contexts as placement of the nuclear device with relation to rich zones and design of the recovery system for the fractured area around the nuclear chimney.

The increased efforts of the last several years to evaluate the deeper-lying shales that would be suitable for a nuclear recovery process have indicated that certain of these shales contain associated minerals that may be recoverable along with the oil normally sought from oil shale. The presence of these minerals should not have any effect on the proposed experiments to determine whether or not nuclear fracturing and subsequent retorting offer promise as a means of recovering oil from oil shale. However, if these experiments indicate that this method has merit for the recovery of oil, economic recovery of the associated minerals, if suitable methods can be developed, could have a definite effect on the commercial application of the overall technique. Research has not yet progressed far enough to indicate how likely this possibility may be.

Experiments on the 10- and 150-ton retorts at Laramie are designed to give data which will indicate whether or not there is a reasonable chance of retorting successfully the ungraded rubble in a nuclear chimney. Results from the 10-ton retort showed that recoveries of approximately 80 percent of Fischer assay could be achieved on charges having pieces with maximum dimensions of 20 inches. Because of these encouraging results, the research has been scaled up to the 150-ton retort which has so far had only one shakedown run. However, this run was conducted without difficulty on a charge containing pieces as large as 3 feet by 4 feet by 6 feet, and weighing 7500 pounds, to give a recovery of about 60 percent of Fischer assay. Recoveries from the two retorts were achieved over a reasonably wide range of operating conditions, indicating that the process was not unduly sensitive to operating variables. Pressure drops across the beds in both retorts were less than 0.2 inch of water and did not increase appreciably during retorting, indicating that neither pressure drop nor pressure buildup in a nuclear chimney would be a problem in retorting the rubble column.

Research designed specifically to study problems involved in recovering oil from the fractured area surrounding the nuclear chimney is not in progress. However, in situ combustion experiments on shale fractured by combinations of electrolinking, hydraulic pressure, and chemical explosives are yielding data pertinent to the problems. Results indicate that combustion can be started and maintained in shale that has been fractured with some as-yet-undetermined degree of similarity to the broken material that presumably will surround a nuclear chimney. Although these results are encouraging, the present research is on a narrow shale interval (20 feet) at shallow depths, so results cannot be projected directly to the nuclear experiments. Planned research at depths of several hundred feet should yield more pertinent data.

LITERATURE CITED

1. The Bronco Oil Shale Study. PNE-1400, Clearinghouse for Scientific and Technical Information, Springfield, Va., October 1967, 64 pp.

2. Lombard, D. B., B. G. Bray, and H. W. Sohns. Technical Considerations for Plowshare Applications. Proceedings, Symposium on Engineering with Nuclear Explosives, January 1970, in press.
3. Dana, G. F. Bureau of Mines-Atomic Energy Commission Colorado Corehole No. 3, Rio Blanco County, Colorado. Bureau of Mines Open File Report, Laramie Petroleum Research Center, 1968.
4. Tisot, P. R., and H. W. Sohns. Structural Response of Rich Green River Oil Shales to Heat and Stress and Its Relationship to Induced Permeability. Preprints, Division of Petroleum, American Chemical Society, v. 14, No. 3, 1969, pp. B94-B104.
5. Smith, J. W., and Charles Milton. Dawsonite in the Green River Formation of Colorado. Economic Geology, v. 61, 1966, pp. 1029-42.
6. Smith, J. W., and N. B. Young. Determination of Dawsonite and Nahcolite in Green River Formation Oil Shales. Bureau of Mines Report of Investigations 7286, 1969, 20 pp.
7. Sohns, H. W., L. E. Mitchell, R. J. Cox, and W.I.R. Murphy. Heat Requirements for Retorting Oil Shale. Ind. Eng. Chem., v. 43, No. 1, 1951, pp. 33-36.
8. Ruark, J. R., K. L. Berry, and Boyd Guthrie. Description and Operation of the N-T-U Retort on Colorado Oil Shale. Bureau of Mines Report of Investigations 5279, 1956, 26 pp.
9. Carpenter, H. C., and H. W. Sohns. Application of Aboveground Retorting Variables to In Situ Oil Shale Processing. Colorado School of Mines Quarterly, v. 63, No. 4, October 1968, pp. 71-82.
10. Melton, N. M., and T. S. Cross. Fracturing Oil Shale with Electricity. J. of Petrol. Technol., v. 20, No. 1, January 1968, pp. 37-41.
11. Miller, J. S., and W. D. Howell. Explosive Fracturing Tested in Oil Shale. Colorado School of Mines Quarterly, v. 62, No. 3, July 1967, pp. 63-73.

THE ECONOMICS OF PLOWSHARE GEOTHERMAL POWER

J. B. Burnham

D. H. Stewart

Battelle-Northwest

INTRODUCTION

Geothermal energy is not a new concept. Naturally occurring hot water has been used for centuries in Iceland for heating purposes. About 20% of Klamath Falls, Oregon is today heated by hot water from geothermal wells.

The generation of electricity is a relatively new use for geothermal energy which has developed over the last half century. There are plants in operation in Italy, New Zealand and the U. S.; these have a total capacity of more than 700 MWe. Geothermal generation is being explored and developed today in Japan, USSR, Mexico, Nicaragua, El Salvador, and Guatemala. Whenever a favorable combination of recent magmatic intrusion and favorable groundwater conditions occurs to create the necessary steam conditions it is usually economic to build a generating plant. With fuel essentially free the plants are usually economically competitive even in small sizes.

Naturally occurring geothermal steam sites are rather limited. Witness to this statement can be found in the small number of plants (less than a dozen) in operation or under construction. On the other hand, geothermal anomalies are prevalent in every one of the world's continents. One writer describes geothermal areas in which the thermal gradient is $150^{\circ}\text{C}/\text{km}$ ($435^{\circ}\text{F}/\text{mile}$) to $180^{\circ}\text{C}/\text{km}$ ($522^{\circ}\text{F}/\text{mile}$). This may be compared to the world average gradient of $30\text{--}40^{\circ}\text{C}/\text{km}$ in non-geothermal areas.

In the United States, large areas of Oregon and northern California, as well as selected areas in Washington, Idaho, Montana, Nevada and Utah, are areas of recent intrusive activity and some have been drilled proving the existence of geothermal temperatures. It should be noted that most steam producing areas are relatively shallow, 400 to 2000 feet. In fact, most exploratory drilling ceases when hard rock is located as the chances for finding steam in these formations are limited. Temperatures as high as 750°F at 7900 feet have been found in the Niland area of California.

If a method could be found for recovering the energy in these areas without having to rely on the rare discoveries of large supplies of natural steam, the economic pay-off would be impressive. For example, the total energy in one cubic mile of hot rock is equivalent to that of a major oil field--300,000,000 bbls of oil worth \$600,000,000. A further example of the magnitude of this resource can be had by considering the recoverable energy in a single known geothermal area. One of the smallest of Oregon's areas is the Diamond Craters zone. This is shown in Figure 1. It is estimated that the energy available in this single area is roughly equivalent to that of the North Slope oil pool.

FLOWSHARE AND GEOTHERMAL POWER

The possible coupling of Plowshare with geothermal power to produce electricity first appeared in a paper by Professor George Kennedy of UCLA at the Second Plowshare Symposium in 1959. The idea is to use the rock crushing power of a nuclear device to produce a large cavity filled with broken rock from which the sensible heat can be removed. A simplified model of this concept is illustrated schematically in Figure 2. As will be seen later, an alternate arrangement can also be considered. The heat removal is accomplished by drilling a second hole into the bottom of the cavity and adding water. The resultant high pressure, high temperature superheated steam is removed from the top of the cavity. The steam is used to power a turbine generator, condensed, and returned to the cavity.

Since the detonation is deep, no venting will occur. As is characteristic of deep underground shots, most of the fission products are frozen in the molten rock of the cavity wall. The closed cycle nature of the plant assures minimal release to the environment during operation. These features make for a very clean method of power production.

Battelle-Northwest has carried out additional analysis of the potential of Plowshare augmented geothermal power and it appears extremely attractive.

If this approach is successful, many of the limitations which apply to the current geothermal plants are removed. It would no longer be necessary to find steam and live with the resultant limitations. Hot rock is the key requirement and a reasonable amount of surface or well water is required for condenser cooling. These characteristics would make possible production of high temperature (600-800°F), high pressure (up to 3,000 psi) steam.

The ideal Plowshare geothermal site would meet the following criteria:

1. Rock temperatures above 600°F at depths of 6,000 to 10,000 ft.
2. Large quantities of water for cooling the steam condenser.
3. An area remote from large population centers.
4. An area near major electrical transmission lines.

There are geothermal areas in Oregon, Nevada, Idaho, Montana, Utah and California which appear to meet all of these criteria. Some of the Oregon sites have already been noted in Figure 1.

If it is assumed that a 125°C/km gradient can be located, a temperature of 350°C (622°F) will lie 8,600 feet beneath the surface. After locating this temperature, the small exploratory hole would be enlarged to lower a 1 megaton nuclear device. On detonation, a cavity with a fractured volume of 1253×10^6 cu. ft. would be formed. Using a ΔT of 312°F, the sensible heat amounts to 14.7×10^{12} Btu's and the heat from the device is 3.8×10^{12} Btu's for a total of 18.5×10^{12} . It was thought that, as the cavity was cooled, the heat flow from the surrounding, nearly infinite, heat source would provide considerable additional energy. However, the transient heat analysis showed this effect to be negligible.

The calculations made here assume that a massive solid intrusion is involved. Professor A. R. McBirney of the University of Oregon has suggested that there may well exist lenses (laccoliths) of recent magmatic intrusions within a few thousand feet of the earth's surface. If these are recent enough, they may still contain a significant volume of liquid basalt. The liquid material contains considerably more heat per unit weight than the solid since it retains the

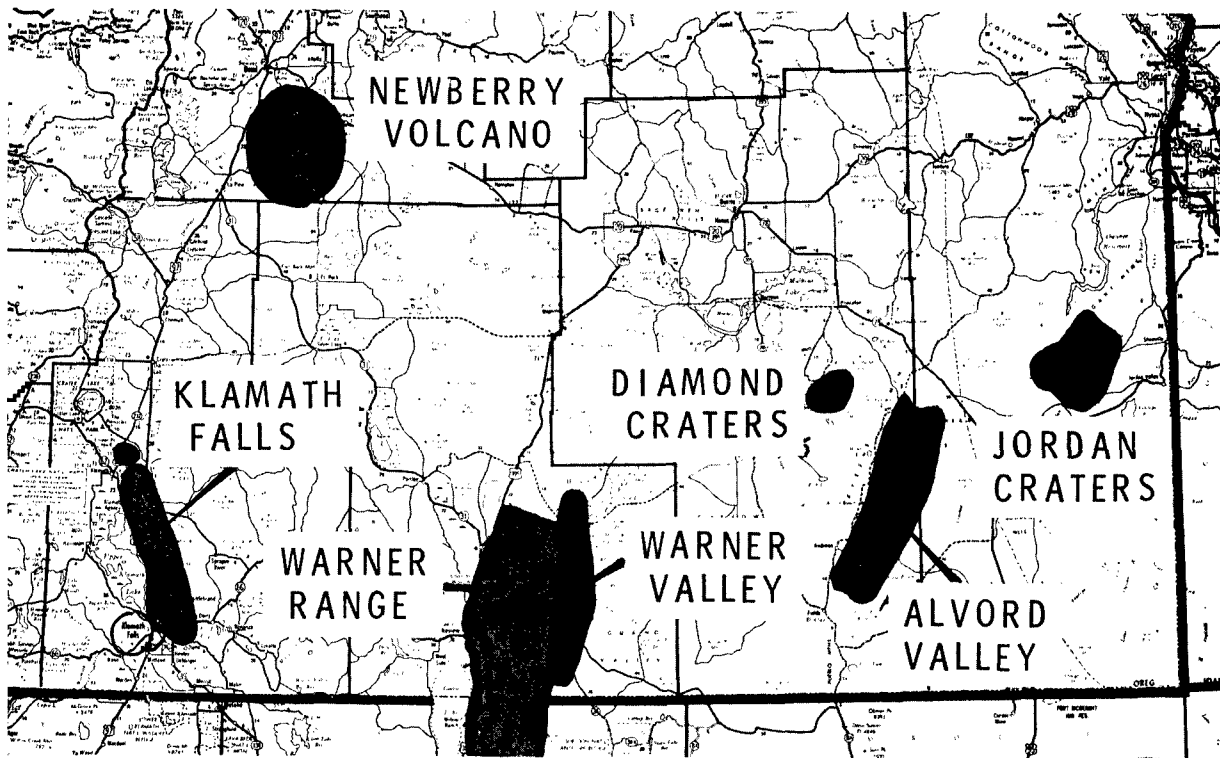


Figure 1. Geothermal Area for Southeast Oregon

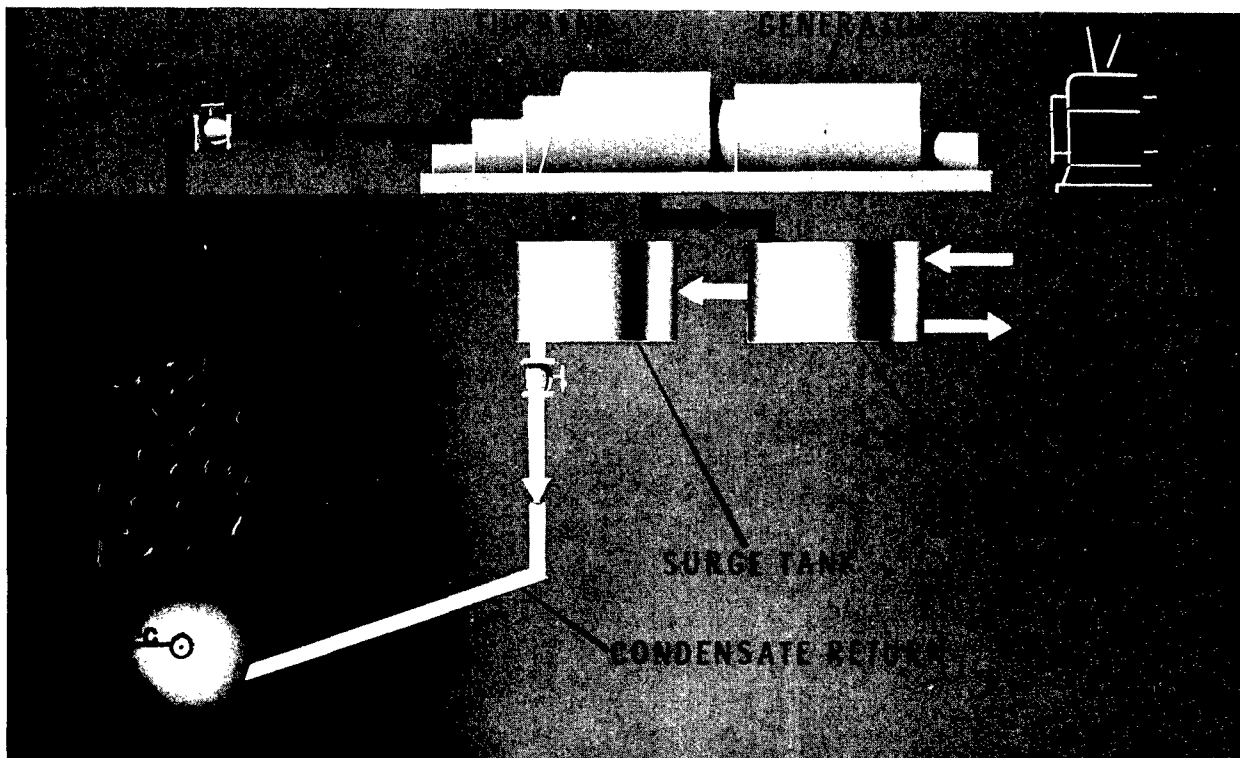


Figure 2. Plowshare-Geothermal Power Plant

latent heat of crystallization plus the sensible heat. If the techniques of "mining" such areas can be mastered, the heat values listed above are conservative by at least an order of magnitude.

It is interesting to speculate on the ultimate application of geothermal power. If slightly above normal thermal gradients of 50-60°C/km can be located, a hole of 5-6 kilometers in depth would produce interesting temperatures (300°C). Depths greater than this are often reached in oil exploration, and ARPA is exploring the feasibility of drilling to 50,000 ft. It does not seem too remote a possibility that with an incremental improvement in drilling technology in the larger diameter holes required, Plowshare geothermal power could find general application throughout the world. LRL has stated specially designed nuclear devices may be manufactured to fit through 12 to 14" holes, although to date large yield devices are much larger.

FEASIBILITY

The technical feasibility of the Plowshare created cavity has been demonstrated. Experience from several Plowshare devices and hundreds of underground weapons tests allow predictions of the cavity size and rubble produced with reasonable accuracy. The problems lie mainly in the engineering area. Perhaps the key problems in developing a Plowshare augmented geothermal plant will be adequate assurance of no unreasonable seismological disturbance and obtaining public acceptance. The seismic problem can be approached with seismic measurements and the evaluation of the results of a small nuclear device before development of the production size cavity.

There are a number of other problems which must be solved before this concept is reduced to practice. These include: development of a device which is operable at high temperatures; determination of the fracture volume from which heat can be extracted; design of a generating plant which will withstand the seismic shocks of these devices; and the determination of the radioisotope distribution in the system. Some of these questions are discussed at greater length in the following sections.

One of the most attractive features of a Plowshare geothermal project is that the area of highest uncertainty--the location of a suitable site--is the least expensive. Under present law a cooperative program would have to be developed with the AEC. An exploratory drilling program would be conducted. Once a suitable location was determined, a small device would be detonated and steam production tests made. If all turned out well, production size detonations would be fired and the power plant constructed.

ECONOMICS

As mentioned earlier it has been calculated that a one megaton device will fracture more than 10^9 ft³ of rock assuming the fracture radius is three times the cavity radius and the fracture height is a conservative 4.4 cavity radii. A transient heat analysis has shown that a modest heat transfer coefficient (10 Btu/hr/ft²/°F) is sufficient to allow the heat to be extracted from boulders as large as three feet in diameter. A total of 18.5×10^{12} Btu's is available from this fractured volume.

Figure 3 shows the costs involved in building this "boiler". Values are shown for 500 KT and 5 MT devices as well as the 1 MT one discussed above. In the present state of the art it seems highly unlikely that devices much larger than 1 MT can be fired in the U. S. As further experience is gained, as seismic decoupling techniques are developed, and as public acceptance improves, it is

conceivable that larger devices (2-3 MT) may be used. In any event, the calculations for a 5 MT device are included for illustrative purposes.

As can be seen in Figure 3, a major portion (about 54%) of the costs are included in the post-shot "plumbing." This immediately suggests the possibility of multiple-sequential shots in which these drillback costs would be spread over several holes. The yield of fractured rock per dollar of cost should go up with multiple-sequential patterns; further, and perhaps more important, the average heat rate of the turbines will be improved. Battelle-Northwest is currently studying for a private sponsor the economics of various shot patterns. When the results of this study are completed, it will be possible to calculate the power costs of a more sophisticated arrangement than the one presented here.

The first engineering studies completed on the steam cycle also indicate that there will be advantages in alternate patterns. Figure 4 shows the static and velocity head losses to be expected in the boiling water, single cavity pattern we are considering here. As can be seen from the curves, the steam pressure at the surface drops off rapidly as the temperature in the cavity decays. The original drop is caused by the gravity head. As the steam quality degrades, though, the demand goes up as does the velocity. At the end, the velocity head increases rapidly and the top-side pressure falls to zero.

This suggests an arrangement such as the one shown in Figure 5 where the boiling is allowed to occur in the cavity and steam is extracted. In this illustration a multiple-sequential vertical shot pattern has been used in which, presumably, a higher yield of fractured rock has been realized and only a single drillback expense has been encountered.

As the rock cools with time the water level in the chimney is raised. This will, in effect, make the bottom zone a preheater and the top a superheater. It should serve to keep the steam quality higher than the single cavity case. This will allow the turbine-generator to operate at a better average heat rate. When the calculations of fractured rock volumes are completed, a transient heat analysis will be run to test the validity of these assumptions and their impact on the economics of the system.

Another possible alternate system is shown in Figure 6. This incorporates a pressurized water system for heat removal. The shot array is a sequential-horizontal one. Such a pattern might be used to maximize the yield from a laccolith of limited thickness. The pressurized water heat removal has the advantage of better circulation in such a cavity. Since it is a pumped system, it will not be dependent on the pressure generated in the cavity to lift the steam to the surface. The pumping costs should not prove too high as the gravity head is compensated. It has attendant disadvantages, though, inasmuch as a primary pump, pressurizer, and steam generator will be required. The pickup of solubles and fission products from the cavity could also be a problem. Since the fission products are mostly trapped in the molten rock after it freezes and since the basaltic structures likely to be encountered are mostly silicates, both of these possibilities are fairly remote.

These alternate patterns with their larger fractured volumes will have an operational advantage over the single cavity case. The latter (with a 1 MT device) is estimated to provide steam for a 200 MW plant for only about a year; this estimate is based on an assumption that the fractured volume will be 6 cavity radii high (LRL estimates 6-8 R_c for the height) and 3 R_c in radius. The alternate patterns should power the same plant for 3-4 years.

The fractured volume of any of the shot patterns represents one of the major uncertainties of the system. In the multiple-sequential patterns the shock wave

	DEVICE YIELD (\$ IN MILLIONS)		
	500 KT	1 MT	5 MT
DEVICE, TIMING, FIRING	0.54	0.58	0.65
EMPLACEMENT COSTS	0.45	0.54	0.64
REENTRY DRILLBACK, PIPING, ETC.	1.40	1.40	1.40
ALLOCATED SAFETY COSTS	0.10	0.10	0.10
TOTAL PER SHOT	2.49	2.62	2.79

Figure 3. "Fuel and Boiler" Costs for a Plowshare-Geothermal Plant

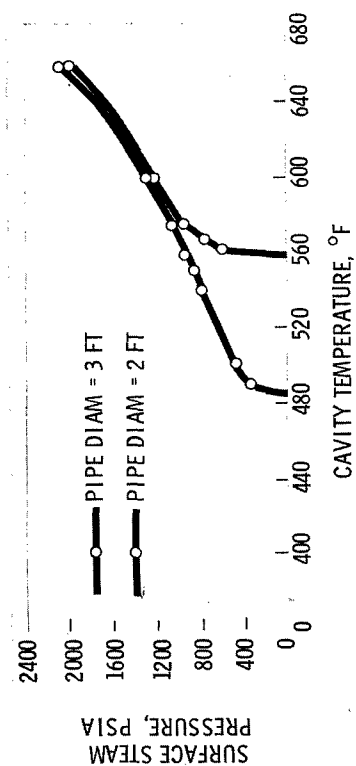


Figure 4. Surface Pressure as a Function of Temperature for an 8600-Foot Cavity

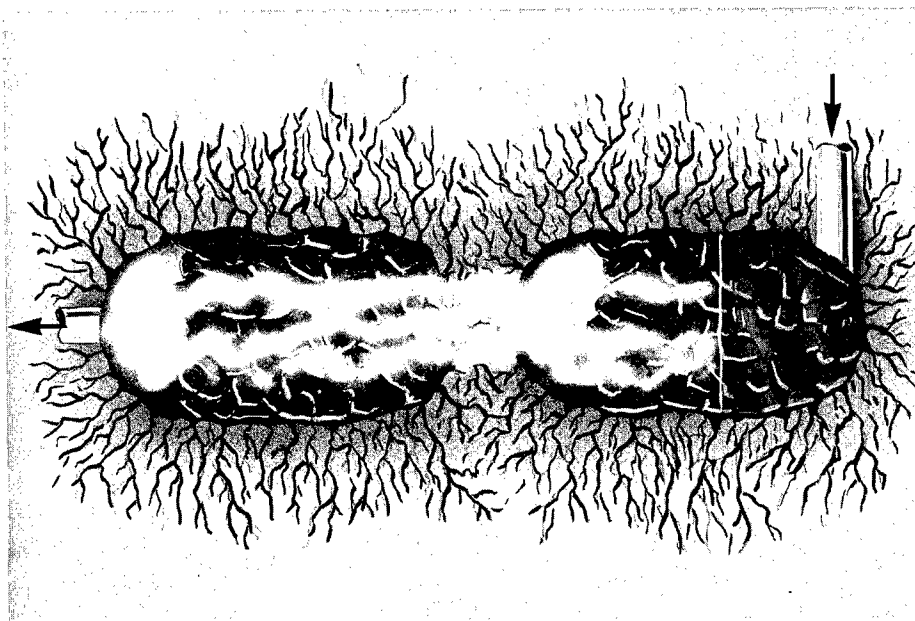


Figure 5. Boiling Water Sequential Pattern

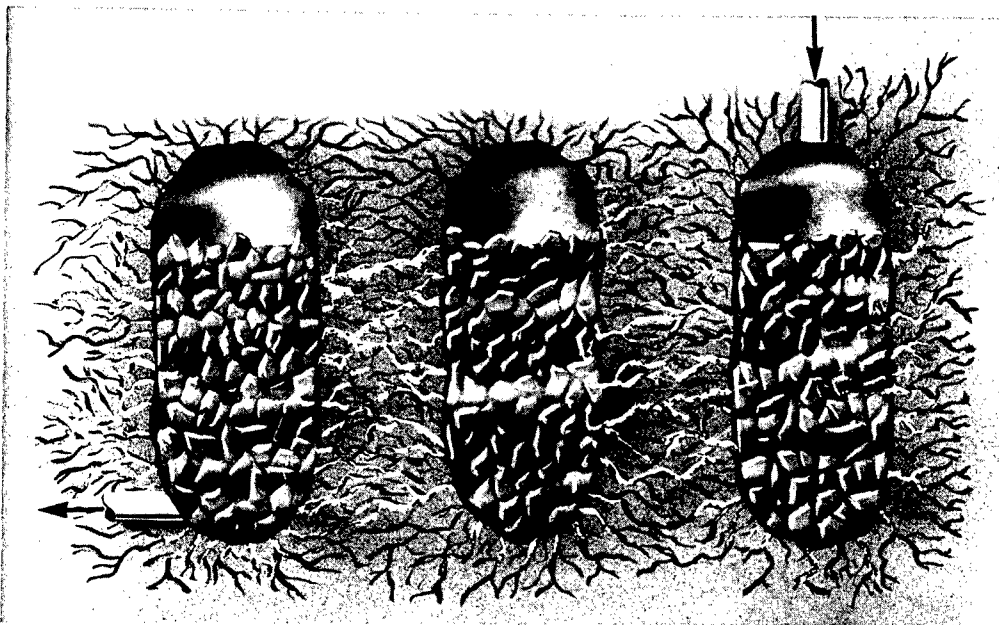


Figure 6. Pressurized Water Sequential Pattern

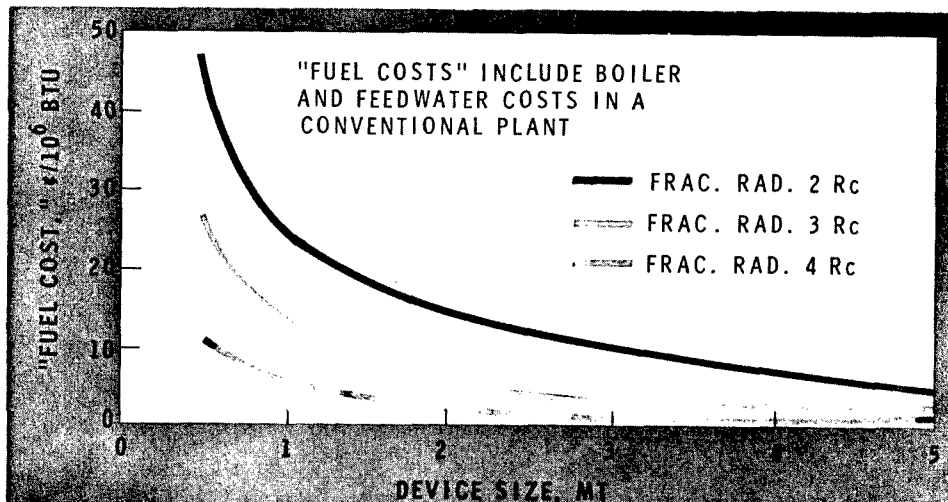


Figure 7. "Fuel and Boiler" Costs for a Plowshare-Geothermal Shot

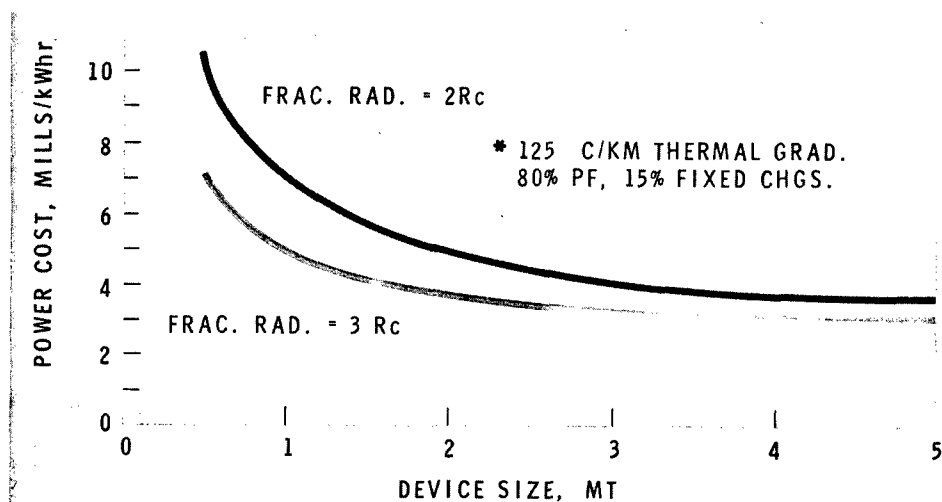


Figure 8. Total Power Costs for a 200 MW Plowshare-Geothermal Plant

interaction between cavities is still to be determined. There is a distinct possibility that thermal fracturing will occur under the system conditions; this might increase the fracture volume. Lithostatic pressure could act to close up fissures in time, which would have the opposite effect.

Fuel costs are reduced for single cavities to the common units of cents per million Btu's in Figure 7. In this case it should be remembered that the capital cost, and much of the maintenance costs, of the plant boiler are included in the Plowshare-geothermal "fuel costs." As is to be expected, these costs decrease as the fractured volume increases.

Rough estimates have been made of the generating capital costs for a 200 MW plant using the boiling water cycle. This size was picked somewhat arbitrarily. While this capacity is large enough to be of interest to a system, it is not so large as to require multiple shots to start operation. It can be anticipated that scaling the concept up in size will reduce power costs.

Capital costs of \$109/kW were estimated. These include a \$10/kW allowance for seismic hardening of the plant to withstand the shock of subsequent detonations. Although little data are available on plants of this type, these costs are thought to be conservative since no boiler system is required. In the more sophisticated cycles now being studied the added energy extraction of a pressurized water system will be balanced against the increased capital costs.

Total power costs are shown in Figure 8. A fixed charge rate of 15% has been assumed along with an 80% plant factor. As can be seen, the power costs even from such a small plant are highly competitive under these conditions. As the size of the device and the fractured volume increase, the power costs, of course, decrease.

CONCLUSIONS

This paper is based on preliminary analysis of the concept. It is recognized that a more in-depth feasibility study is required before firm conclusions can be drawn. Also, a demonstration experiment is required to prove out the concept in practical application. The large potential that geothermal power has as another major energy source warrants an in-depth study.

ACKNOWLEDGEMENTS

The authors gratefully acknowledge the aid of K. R. Wise for transient heat transfer calculations, D. W. Dragnich for the steam calculations, J. F. Fletcher for the capital cost estimates, and to R. E. Brown and Professor McBirney for advice on the geologic problems. The consultations with various members of the USGS at Menlo Park, California, and Oregon State Department of Minerals and Resources were also of great assistance.

ON THE USE OF NUCLEAR EXPLOSIVES FOR STIMULATION OF GEOTHERMAL HEAT

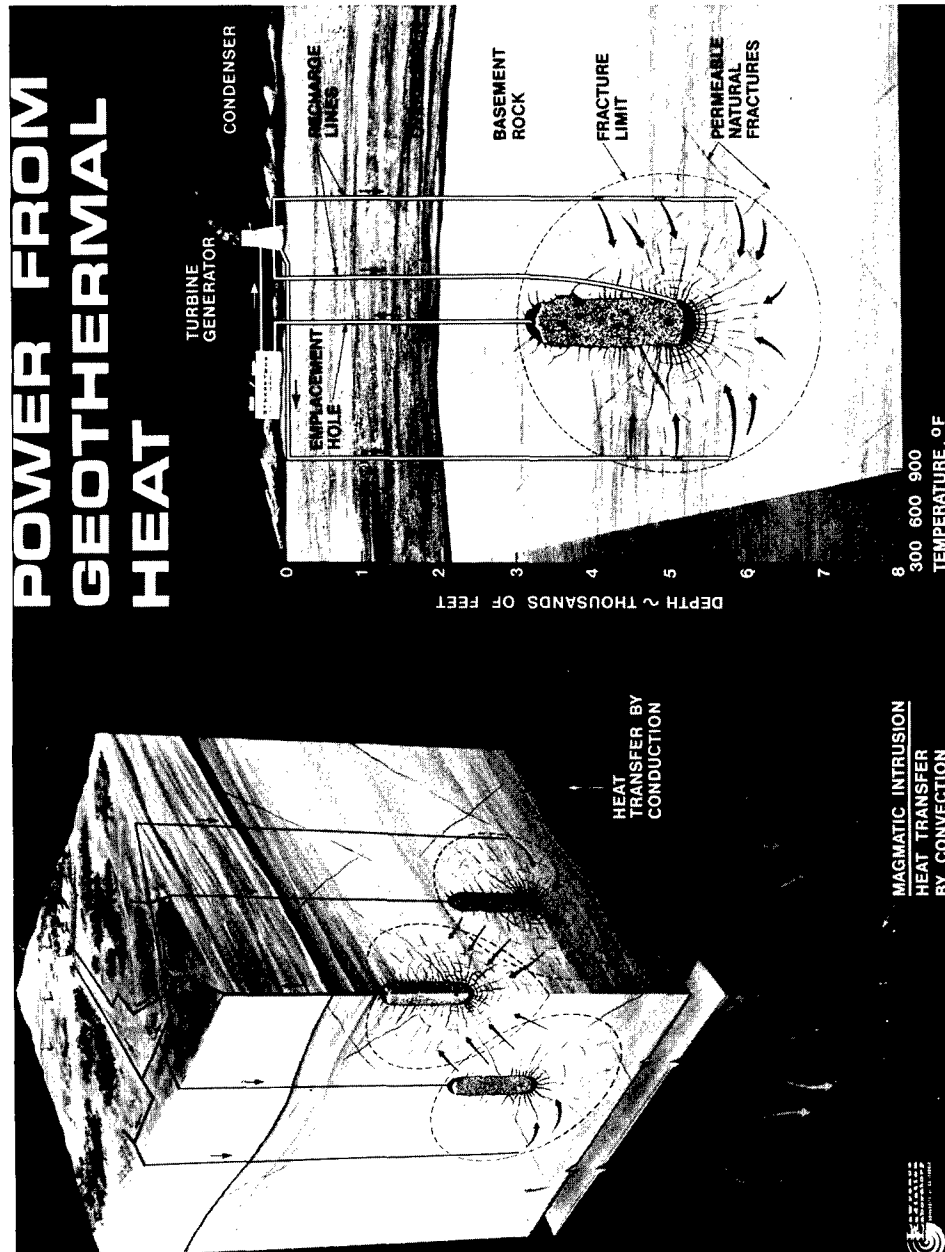
Milo D. Nordyke
Lawrence Radiation Laboratory, University of California
Livermore, California

Many areas of the world exist where high temperature isotherms supported by heat flow from the core of the earth occur very close to the surface of the earth. Commercial exploitation of these sources of energy has only recently become practical and is limited to those areas where a natural system of fracture acts to collect heat from a large volume of rock and sufficient natural water is available to act as a heat transfer agent. Recent studies have indicated many more areas of geothermal heat are available than had been identified previously.

The nuclear application envisages the creation of a chimney and associated fracture system with a nuclear explosion, introduction of water into the chimney-fracture system, and removal of superheated steam for the generation of electrical power. Three phenomena are considered: utilization of the heat content of the rock in the chimney and fracture zone; heat flow from the surrounding medium to the fracture zone or chimney by conductivity; and interconnection of a preexisting network of fracture by the highly permeable chimney and fracture zone.

A 1-Mt example is examined showing that over 10^9 kWh are available in the chimney, and over 10^{10} kWh in the central portion of the fracture zone. Using the current commercial value of 2 mills/kWh for such steam, the above heat has a worth of over \$30,000,000. In addition, heat flow into the fracture zone would represent over \$1 million per year additional value. Interconnection of fractures drawing heat from far removed volumes would be very site-dependent and difficult to estimate, and have not been included. Use of an array would permit circulation between chimneys with the resultant utilization of the heat energy contained in the intervening volume.

Ground shock associated with such an application would probably require development of a 30 to 50 year supply before the power plant is constructed. Radiological safety problems would be confined to operation of the power plant.



UNDERGROUND NUCLEAR EFFECTS III

DIMENSIONAL ANALYSIS FOR THE MECHANICAL EFFECTS OF SOME UNDERGROUND EXPLOSIONS

Francis DELORT

Commissariat à l'Energie Atomique (France)

Centre d'Etudes de Bruyères-le-Châtel

ABSTRACT

The influence of the medium properties upon the effects of underground nuclear and high explosive explosions is studied by dimensional analysis methods. A comparison is made with the experimental data from the Hoggar contained nuclear shots, specially with the particle motion data and the cavity radii. Furthermore, for example, crater data from explosions in Nevada have been examined by statistical methods.

I-INTRODUCTION

In order to predict what might be the effects of high yield explosions, it seems interesting to get, first, data from smaller yield tests, in similar conditions. At the same time, it is necessary to know how to pass from one result to the other.

Similitude brings solutions to that problem, either by dimensional analysis considerations, or by hydrodynamical equations.

We have examined these different methods and verified their range of validity with available experimental data, collected on the Hoggar (Sahara) nuclear test site or analysed on foreign reports (U. S. A.)

II-THEORETICAL DATA

Dimensional relationships are implicit in the shock wave propagation hydrodynamic equations :

$$\frac{\partial \rho}{\partial t} + \text{div.} (\rho v) = 0 \quad (\text{mass conservation})$$

$$\frac{\partial (\rho v_i)}{\partial t} + \frac{\partial (\rho v_i v_j + P_{ij})}{\partial x_j} = 0 \quad (\text{momentum conservation})$$

ρ density

t time

v velocity

p pressure

The same thing exists with the Hugoniot equations. But they do not take into account a few important effects - for example : viscosity, chemical reactions, external forces (gravity). Dimensional analysis, on the other hand, gives the opportunity to elaborate scaling rules which, in some cases, may better represent the influence of parameters like gravity.

Use of dimensional analysis

We consider that the explosion takes place in an homogeneous, isotropic medium, and that phenomena may be described by means of various quantities, such as :

- medium properties : c velocity
E elasticity modulus
- independent variables : R radius
W yield
H depth of burst
- dependent variables : d displacement
A acceleration

Matricial calculations (1) give complete series of dimensionless quantities between these variables and characteristics : so, when the gravity action, as an external force, is not used, we get

$$R \left(\frac{\rho c^2}{W} \right)^{\frac{1}{3}} ; \frac{E}{\rho c^2} ; t \left(\frac{\rho c^5}{W} \right)^{\frac{1}{3}} ; \frac{v}{c} ; A \left(\frac{W}{\rho c^8} \right)^{\frac{1}{3}}$$

Let us suppose that two explosions are made, with different yields W_1 and W_2 ; if similitude does exist, this means that all the dimensionless quantities for both shots are equal, and one will have the relationships, Table I

When the gravity factor g is included, we find identical groups of terms, and furthermore, the dimensionless product $\frac{C^2}{g L}$ which modifies a few relations - see table I.

An extensive study had already (2) been made for crater considerations which had shown the interest of such a work.

Range of validity

For a contained nuclear explosion, the hydrodynamical, plastic and crushing phases in the shock-wave propagation, are independent of the gravity factor, which acts through the atmospheric and lithostatic pressure. This is not true for the fracturation phase.

With the cratering explosions, it is the same but the ascensional earth-motion is submitted to the external gravity field - so, the final crater dimensions depend on the gravity influence on the ejection and the ballistic trajectory of the earth.

In table II are resumed these data.

TABLE 1

Dimensional analysis relationships

Without gravity	Gravity included
Distance	
$\frac{R_1}{R_2} = \left(\frac{\rho_2 C_2^2}{\rho_1 C_1^2} \right)^{\frac{1}{3}} \left(\frac{W_1}{W_2} \right)^{\frac{1}{3}}$	$\frac{R_1}{R_2} = \left(\frac{\rho_2 g_2}{\rho_1 g_1} \right)^{\frac{1}{4}} \left(\frac{W_1}{W_2} \right)^{\frac{1}{4}}$
Pressure	
$\frac{P_1}{P_2} = \frac{\rho_1 C_1^2}{\rho_2 C_2^2}$	$\frac{P_1}{P_2} = \left(\frac{\rho_1 g_1}{\rho_2 g_2} \right)^{\frac{3}{4}} \left(\frac{W_1}{W_2} \right)^{\frac{1}{4}}$
Velocity	
$\frac{V_1}{V_2} = \frac{C_1}{C_2}$	$\frac{V_1}{V_2} = \left(\frac{\rho_2 g_1^3}{\rho_1 g_2^3} \right)^{\frac{1}{8}} \left(\frac{W_1}{W_2} \right)^{\frac{1}{8}} = \frac{C_1}{C_2}$
Acceleration	
$\frac{A_1}{A_2} = \left(\frac{\rho_1 C_1^8}{\rho_2 C_2^8} \right) \left(\frac{W_2}{W_1} \right)^{\frac{1}{3}}$	$\frac{A_1}{A_2} = \frac{g_1}{g_2}$
ρ, C, P , may have constant values without similarity violation	ρ, C , may not have constant values without similarity violation

TABLE II
GRAVITY ACTION ON THE UNDERGROUND EXPLOSIONS EFFECTS

	negligible influence	Influence
Contained explosions	- shock-wave propagation - close ground motions - volume of vaporised, melted, and crushed zones.	- cavity dimensions - fractured zones dimensions.
Cratering explosions	- ditto contained tests	- apparent and true crater dimensions - lip heights - ejectas characteristics

Consequences for the particle motions

In the case of ground-motion due to the shock wave propagation, the gravity factor has no influence on the values of the particle acceleration, velocity and displacement.

So, we can write the following relationships

$$A \left(\frac{W}{\rho c^8} \right)^{\frac{1}{3}} = F_1 \left\{ R \left(\frac{\rho c^2}{W} \right)^{\frac{1}{3}}, \frac{E}{\rho c^2}, t \left(\frac{\rho c^5}{W} \right)^{\frac{1}{3}} \right\}^{\frac{1}{2}}$$

and similar equations for the quantities $\frac{v}{c}$, and $d \left(\frac{\rho c}{W} \right)^{\frac{1}{3}}$

If the explosions are in the same medium, we shall have $\rho_1 = \rho_2$; $C_1 = C_2$; $E_1 = E_2$ neglecting the viscosity, and for the shock-wave front, we can write table 3.

With the action of the gas expansion, the ground surface is deformed, and then, by taking into account the gravity field, we shall write other relationships - See Table 3.

Influence of the medium properties

In table 1, we have shown that for two scaled explosions, a few medium properties may also have to respect similitude relations.

As this is not generally observed, we have examined the influence of probable similitude violations upon the explosion characteristics.

Reaction to formation

By means of dimensional analysis, we have written the influence of the environnement = weight of overburden, field strength of the medium, atmospheric pressure

$$\frac{R_1}{R_2} = \left(\frac{\rho_2 c_2^2}{\rho_1 c_1^2} \right)^{\frac{1}{3}} \left(\frac{W_1}{W_2} \right)^{\frac{1}{3}} \text{ and } \frac{P_1}{P_2} = \frac{\rho_2 c_2^2}{\rho_1 c_1^2} = \frac{\rho_2 g_2 L_2}{\rho_1 g_1 L_1}$$

This last ratio shows that pressure needs to be scaled for the similarity requirement.

The interpretation to give to the dependent variables L_1 et L_2 leads to different results. Here, we consider that pressure P represents the reaction of the ground, which acts by the superposition of :

- the lithostatic pressure : $\rho \cdot g \cdot H$
- the atmospheric pressure, which can be expressed with a similar form : $\rho g k$ ($k \sim 4$ to 6 meters according to the medium type),
- the reaction of the earth due to the cohesive, tensile and compressive strength ; we may write it as $E = \rho g e$.

Finally, we have

$$P = \rho g (H + x), \text{ with } x = k + e \text{ (for sand, } x = k)$$

The former relations may be written

$$\frac{R_1}{R_2} = \left(\frac{\rho_2 g_2}{\rho_1 g_1} \right)^{\frac{1}{3}} \left(\frac{H_2 + x_2}{H_1 + x_1} \right)^{\frac{1}{3}} \left(\frac{W_1}{W_2} \right)^{\frac{1}{3}}$$

and is called "reaction scaling rule".

Different cases have been studied hereafter, which show the use of the dimensional analysis.

- a. For incoherent medium (soil, sand, alluvium...) we can write $e = 0$; we have, then, the overburden scaling rule (2). Two cases are analysed :

- $H \ll k$ = that is the case of low yield explosions ($W < a$ few hundreds of kilograms), and close to the surface since k is about 4 to 6 meters. Small craters are created.

We have the equation :

$$\frac{R_1}{R_2} = \left(\frac{\rho_2 g_2}{\rho_1 g_1} \right)^{\frac{1}{3}} \cdot \left(\frac{k_2}{k_1} \right)^{\frac{1}{3}} \cdot \left(\frac{W_1}{W_2} \right)^{\frac{1}{3}}$$

and finally, R is scaled by a cube-root rule.

-- $H \gg k$ = for the large depths of burst, large yields are necessary to form cratering explosions, whose dimensions may scale by the overburden rule. After transformation, the equation is reduced to

$$\frac{R_1}{R_2} = \left(\frac{\rho_2 g_2}{\rho_1 g_1} \right)^{\frac{1}{4}} \left(\frac{W_1}{W_2} \right)^{\frac{1}{4}}$$

This fourth-root scaling rule corresponds to the results shown table 4.

- b. With cohesive medium (rocks), "the yield strength scaling rule" would have the same form than the reaction scaling rule.

In table 4, this rule is used for effects prediction.

II-COMPARISON WITH EXPERIMENTAL RESULTS

We shall now compare the theoretical solutions to the experimental results observed during some nuclear and high - explosive (H. E) underground explosions.

1. Particle motions

For the ground motion associated with the shock-wave propagation, we have shown that the particle acceleration, velocity and displacement might be expressed with a cube-root scaling rule, that is to say, in a scaled distance $R/W^{1/3}$.

The use of logarithmic scales shows that the experimental data fit well a straight line, which, then, gives a good verification of the theoretical relationships.

In a relatively close-in zone, $0.03 < R < 2$ (km, $kt^{1/3}$) many data have been collected during the nuclear underground Saharian tests (3) and experimental laws have been determined, within 30 to 50 % per cent deviation.

The corresponding least squares fit straight lines are reported on the figures . 1-2-3.

For the seismic effects, studies of the frequency spectrum have been made (10) which lead to the relation.

$$p = 0,36 \left(\frac{R}{W^{1/3}} \right)^{0,43}$$

p = characteristic of the frequency spectrum, in the 10 to 30 Hz range.

In this range, the earth has no filtering action, so the source-signal is almost completely transmitted. Since it depends strictly on the initial shock-wave, it is not surprising that similitude is observed.

TABLE 3

Ground motion relationships

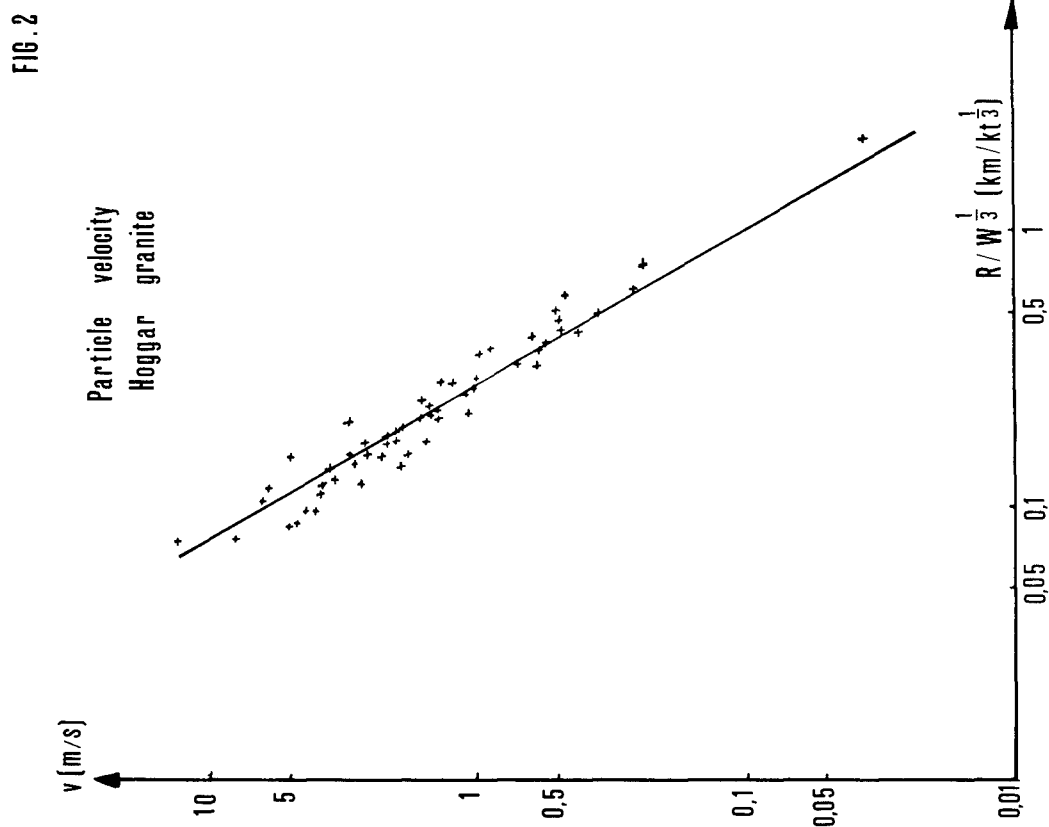
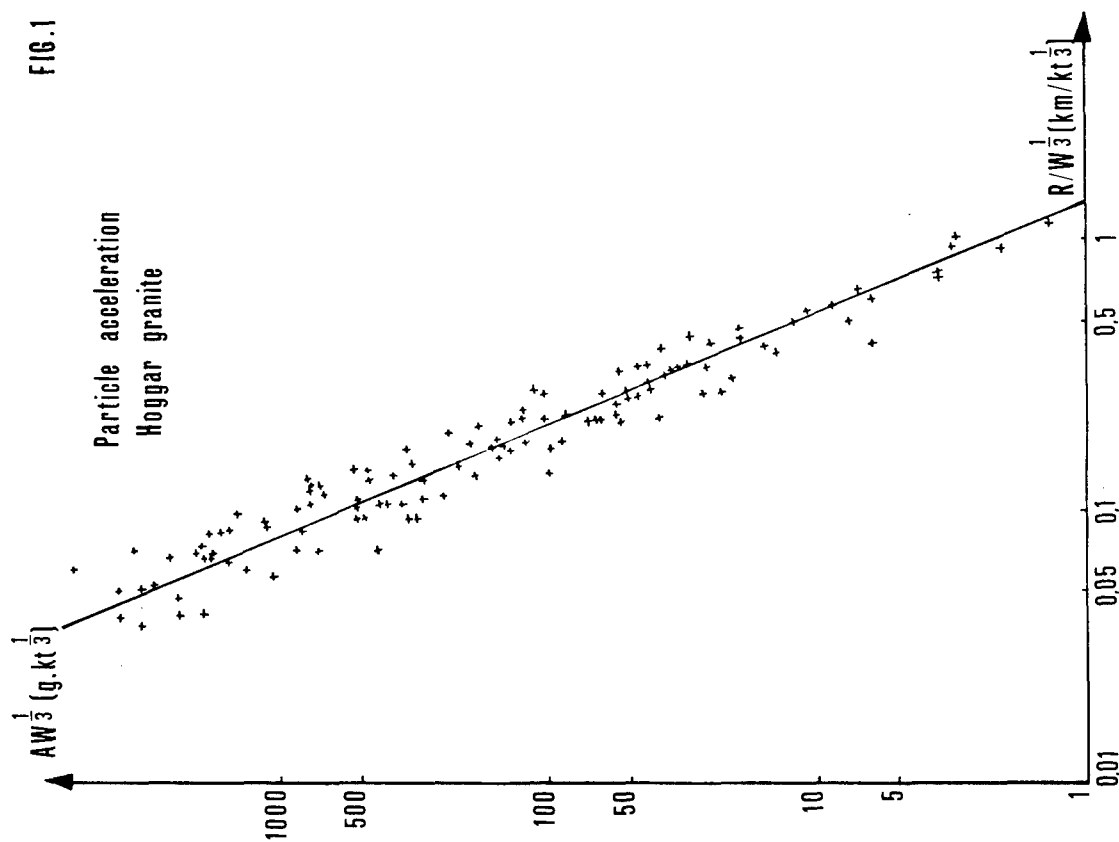
Without gravity	Gravity included
Acceleration	
$AW^{\frac{1}{3}} = f_1 (R/W^{\frac{1}{3}})$	$A = \phi_1 (R/W^{\frac{1}{3}})$
Velocity	
$v = f_2 (R/W^{\frac{1}{3}})$	$VW^{\frac{1}{3}} = \phi_2 (R/W^{\frac{1}{3}})$
Displacement	
$dW^{\frac{1}{3}} = f_3 (R/W^{\frac{1}{3}})$	$dW^{\frac{1}{3}} = \phi_3 (R/W^{\frac{1}{3}})$

TABLE 4

Predicted scaling exponents

$$r = RW^{-\frac{1}{n}}$$

	$n \sim 3$	$n \sim 4$
- Contained explosions		
$H > 100-150W^{\frac{1}{3}} (m, kt)$		
Soft ground: cavity radius		$W > 1kt$
rock: cavity radius,	$W < 0,030 kt$	
fractured zone		
- Cratering explosions		
$H \sim 40-50W^{\frac{1}{3}} (m, kt)$		
dimensions		
Soft ground	$W < 0,001 kt$	$W > 1.10 kt$
rock	$W < 1 kt$	$W > 10 MT$



2. Dimensions of the altered zones

We have distinguished the contained explosions from the cratering ones, and it is the influence of the earth-reaction which has been tested.

a. Cavity radii of nuclear contained tests

We have investigated if the cavity radius is related to a particular scaling rule so that the scaled radii ($R/W^{1/n}$) are identical for similar experiments.

The empirical relation of the cavity size is (4) :

$$R_c = 52 \frac{\alpha^{1/3} W^{1/3}}{(\rho g h + C_s)^{1/3} \gamma}$$

α = correcting factor ($\alpha = 1$ for devices in well)

h = height of overburden

C_s = coefficient of the medium

$C_s \sim 0^{(5)}$ for most media

γ = adiabatic gas expansion coefficient.

We have studied what might be the value of the scaling factor, n , so that the empirical equation can be verified.

A few calculations lead to the relation :

$$n = \frac{3\gamma + 1}{\gamma}$$

The values of γ , calculated for various media (dolomite, alluvium, tuff, granite, salt) lead to

$$3.88 > n > 3.97$$

This is close to the fourth-root scaling rule which has been predicted by dimensional analysis, including the gravity field.

The least-squares fit straight lines for Hoggar granite and Nevada alluvium and tuff are shown fig. 4, whose equations are explicit on table 5.

The use of these laws leads to a precision comparable and sometimes better, than when the former general relation is used.

2. Cratering explosions

The comparison of the dimensional results has been made with data from high-explosive and nuclear explosions (6) (7) in the U.S.A. for apparent radius and depth crater dimensions, and in France (11).

A statistical analysis has been made (8) with all the available data, in order to find the most representative scaling laws for basalt, alluvium and wet shale.

FIG. 3

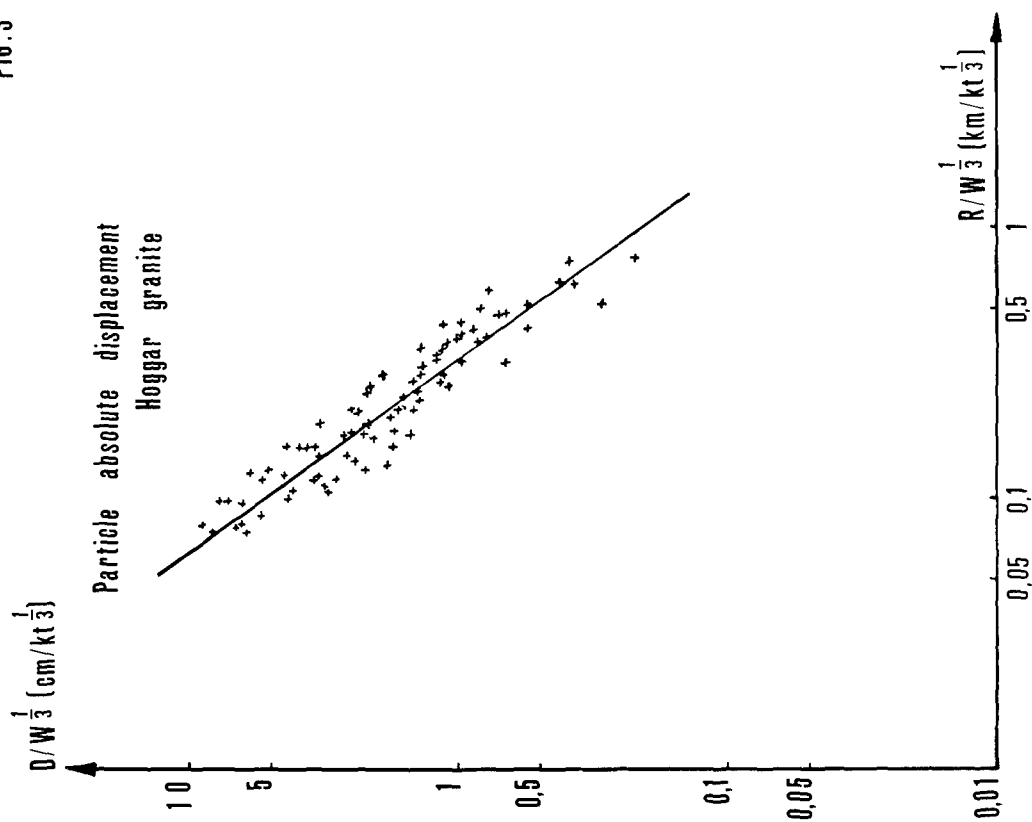
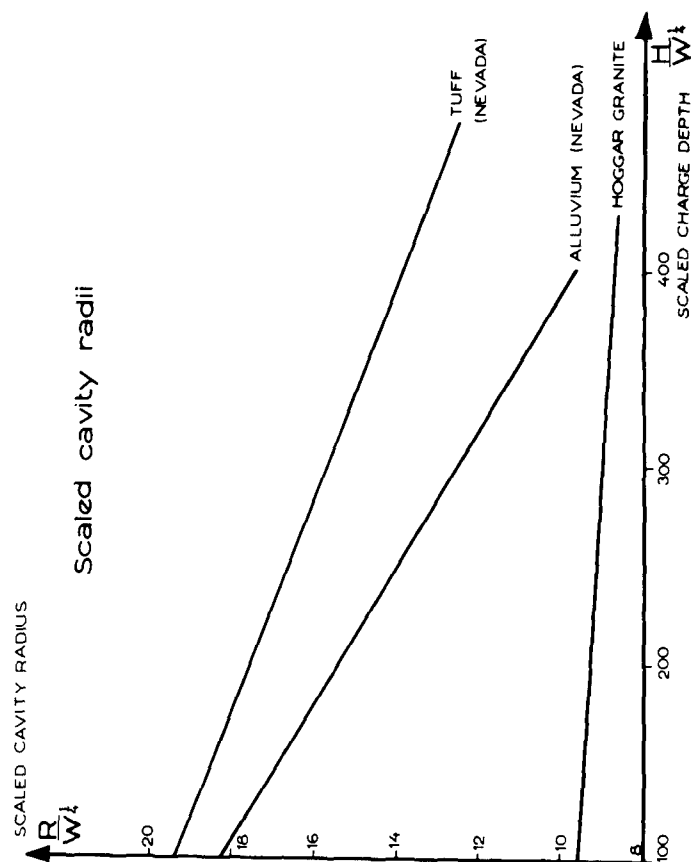


FIG. 4



In a first step, the scaled dimension I has been calculated

$$I = \frac{L}{W^{1/n}} \quad 3 < n < 8$$

When $n > 5$, the value of the correlation factor ϕ^2 increases since the scaled "standard deviations" are only comparable, for different yield explosions, with $2,5 < n < 5$.

In another study, the following scaled value has been used

$$I = \frac{L(H+x)^{\frac{1}{3}}}{W^{1/3}} \quad 0 < x < 10^4$$

For each case, we have made different groupings with the experimental data : all the nuclear and high-explosive tests, explosions with $W > 20$ tons; with $W < 20$ tons ; all the nuclear tests ; all the high-explosive tests.

The least squares fit lines have been calculated with the 2nd and 3rd order polynomial lines corresponding to the most physically representative shapes.

Data have been represented by both normal and logarithmic scales for alluvium and basalt. As for the regression straight lines, we have considered the positive-slope line corresponding to the depths of burst less than the optimum and a negative-slope straight line for the rest of the data.

The coefficients of correlation ϕ^2 (9) have been calculated. The closer to the line the points are, the nearer to one is the value of ϕ^2 . The deviations of the statistical distribution have also been computed.

Similar studies (2) (6) have been made in the U. S. A. and they had shown the interest of that kind of work.

b. Craters in Nevada alluvium

41 craters made by high-explosive testing (of which 31 are 126 kg-yield shots) and 4 with nuclear explosives have been analysed.

The analysis of the scaled dimensions $I = \frac{L}{W^{1/n}}$ has given the results reported on table 6 which is related to the 2nd order polynomial regression curves.

Fig. 5 shows that the coefficient of correlation ϕ^2 is maximum with $n = 3,9$ for the radius R and with $n = 3,4$ for the depth D, when the large-yield explosion dimensions are analysed ($W \geq 20$ tons with 9 explosions including 4 nuclear).

TABLE 5

Cavity radius scaling rules

$$R = aW^{\frac{1}{4}} + bH$$

Medium	a	b
Granite		
Tan Affela-sahara	9.72	-0.0023
Alluvium	21.25	-0.0289
Tuff	21.06	-0.0173

TABLE 6

Scaling rule representativity for alluvium craters

(decreasing value order of ϕ^2)Normal coordinates (2nd order polynomial regression curves)

Group of data	HE*+NE* W > 20T		All the HE+NE		All the HE		HE W < 20T	
Number of explosions	9		45		41		36	
Scaling rule	R*	D*	R	D	R	D	R	D
	H	34	H	34	H	H, 34	H	H°
	4	3	34	3	34	3	3	3, 34°
	34	H	3	H	3	4	34	
	3	4	4	4	4	3	4	4°

Logarithmic coordinates (regression straight lines)

Number of explosions	8		39		34		31	
Scaling rule	H°	H	H	H	H	H	H	H
	4°	34	4°	3°	4°	4°	3°	3°
	34	4	3°	4°	3°	3°	34°	34°
	3	3	34	34°	34°	34°	4°	4°

* HE : High explosive

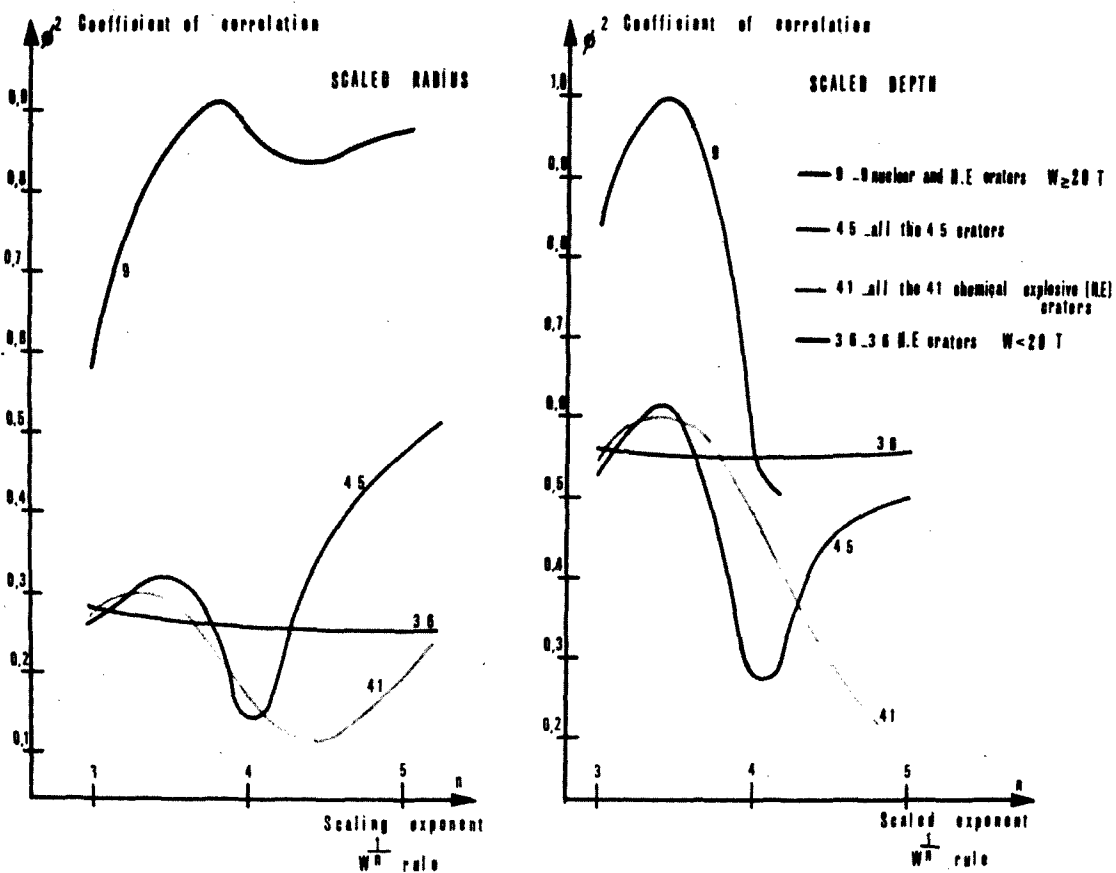
NE : Nuclear explosive

H : Depth scaling rule $\frac{LH^{\frac{1}{3}}}{W^{\frac{1}{3}}}$ 4,3;34 : Scaling exponent n of the $W^{\frac{1}{3}}$ scaling rule

R : Apparent crater radius ; D : Apparent crater depth

4° 3° sing : Close values of ϕ^2

FIG. 5
CORRELATION FOR SCALED CRATER DIMENSIONS
NEVADA ALLUVIUM



For the low-yield HE explosions ($W < 126$ kg), no rule looks better than another.

Similar results have been found with logarithmic coordinates.

Fig. 6 represents the regression curves for alluvium.

Table 6 shows the representativity of various scaling rules for alluvium, with a decreasing value order.

c. Craters in Nevada basalt

Less data for basalt than for alluvium is available and it comes from 15 shots with energy-yield $W > 500$ kg. Two nuclear explosions, $W = 92$ tons and $W = 420$ tons, are taken into account. The statistical analysis has been made in normal coordinates.

Fig. 7 shows that the coefficient of correlation ϕ^2 reaches a maximum for R and another for D. A precise examination of the 9 craters created by the 20 tons and more yield charges, made possible to select 7 of them which lead to a rather good correlation ($\phi^2 \sim 0,95$).

For the whole craters, it is the $n = 4,5$ value within $W^{1/n}$ which gives the best representativity. The study of the reaction scaling rule does not show that a particular value for x (earth strength) gives good coefficients of correlation.

If we consider the Sedan nuclear crater (7), with a 100 kt yield in alluvium, which is almost 400 m in diameter, it is possible to think that the $W^{1/3,4}$ scaling rule for basalt leads to more realistic results than the $W^{1/4,5}$ scaling law. This law would predict a 1000 to 1400 kt yield need for the same effect.

Finally, we can see that :

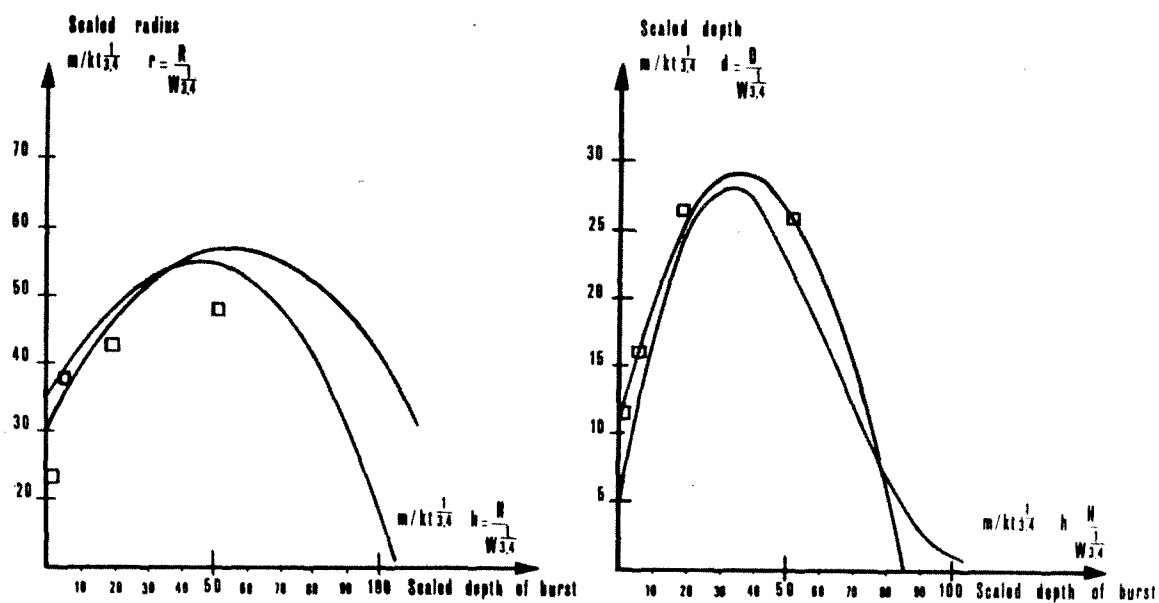
- for a body of small yield explosions $0,5 < W < 20$ tons, the most appropriate scaling rule is the $W^{1/4,5}$. The dimensional analysis leads to a similar result if it is admitted that the earth has its own strength and the gravity field has no influence.

Fig. 8 shows the corresponding experimental least squares-fit curves.

- for larger yields, especially nuclear craters, there are few available results. However, dimensional analysis shows that a scaling factor n $3 < n < 4$ would lead with a good precision, to the scaling rule. For the same yield, this factor n would be smaller for basalt than for alluvium.

The precision in the calculations made with the scaled curves is given in table 7.

FIG. 6
 SCALED APPARENT CRATER DIMENSIONS
 NEVADA ALLUVIUM $W^{1/3}$ SCALING RULE



- = $W > 20^T$ Nuclear and high explosive charges
- - - = High explosive charges
- = Nuclear explosions

FIG. 7

CORRELATION FOR SCALED CRATER DIMENSIONS
NEVADA BASALT

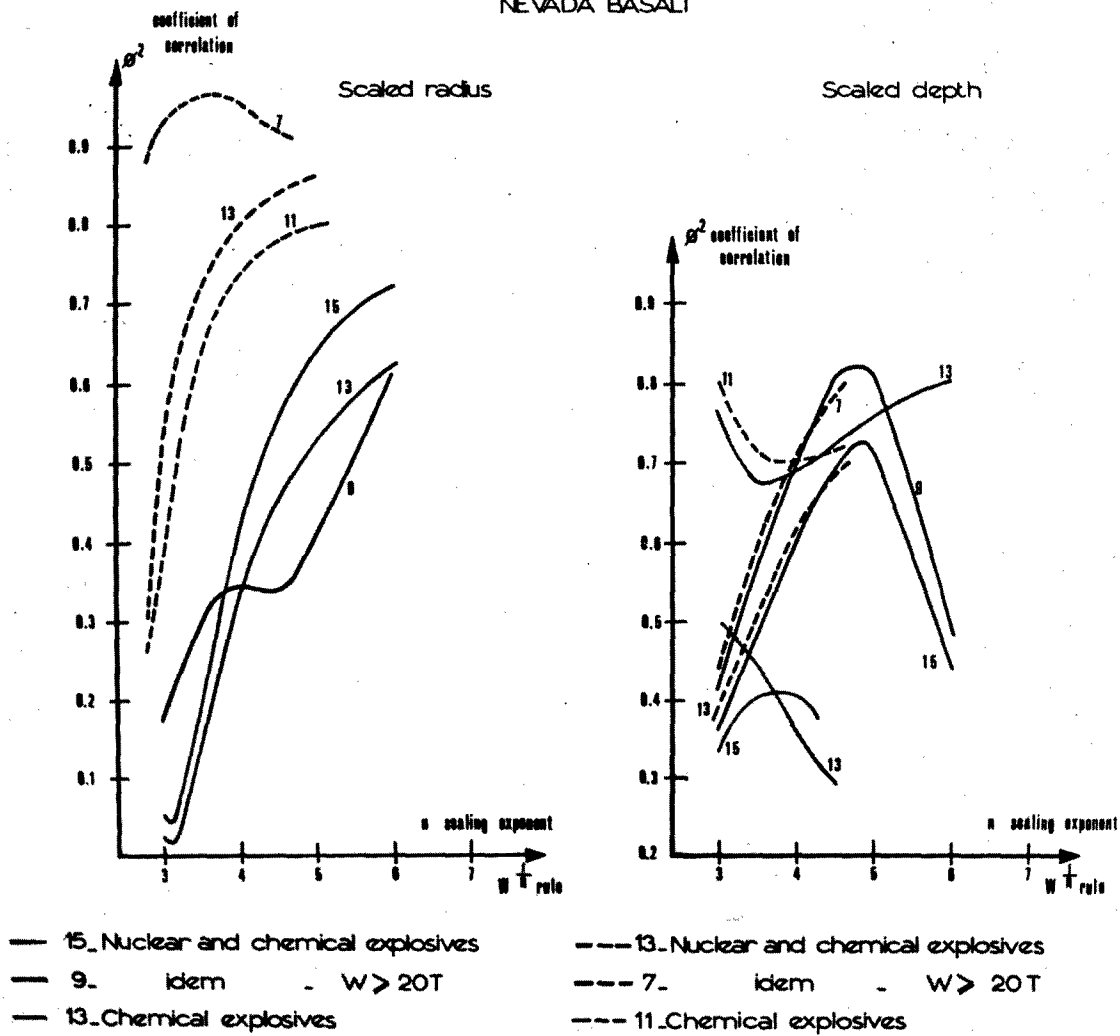


FIG. 8

APPARENT CRATER DIMENSIONS
NEVADA BASALT $W^{1/3}$ SCALING RULE

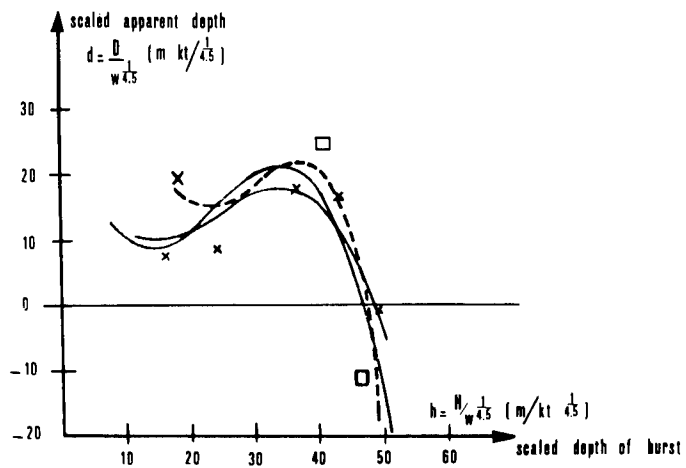
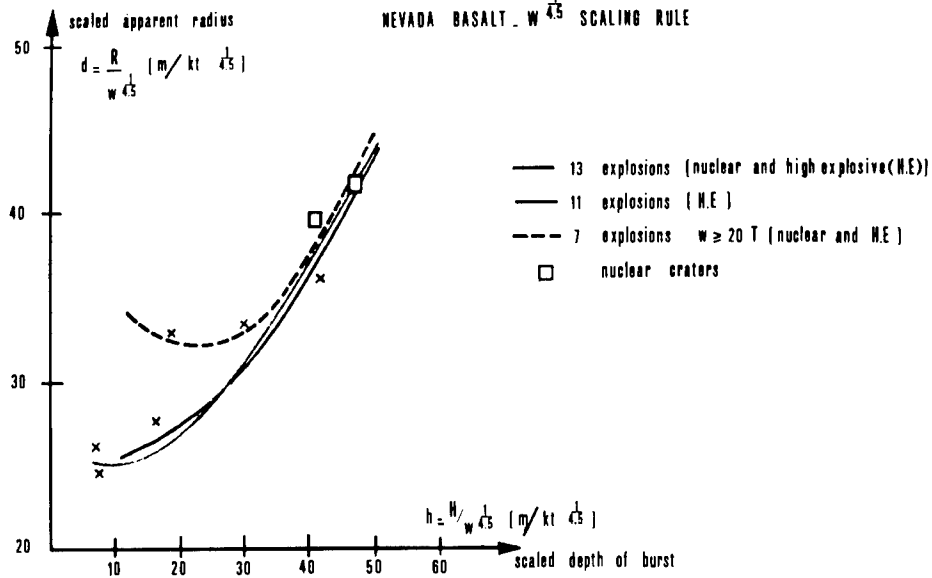


TABLE 7

Standard deviations of the scaled crater
dimensions
(per cent)

	High-explosive craters		Nuclear and high-explosive craters	
	$\frac{R}{W^{\frac{1}{n}}}$	$\frac{D}{W^{\frac{1}{n}}}$	$\frac{R}{W^{\frac{1}{n}}}$	$\frac{D}{W^{\frac{1}{n}}}$
Alluvium	$W \sim 0.126 T$ 20 25		$0.020 < W$ 10 10	
Basalt	$0.5 < W < 20 T$ 10 25			

CONCLUSION

The dimensionless relations which can be established by a theoretical analysis, have been described and a difference has been made when the gravity field is included.

The reaction of the earth to the formation of cavities and craters leads to the reaction scaling rule which takes into account the overburden, the atmospheric pressure and the strength of the medium. The interpretation shows that, for rocks, a fourth-root scaling law would be more representative for larger yields than for incoherent medium.

The particle and seismic ground motion characteristics are strictly related to scaling rules which are verified by experimental data with a deviation from 30 to 50 per cent.

The dimensions of cavities created by contained nuclear explosions correspond to a fourth-root scaling rule.

The statistical analysis of the correlation of the crater dimensions (nuclear and chemical explosives) in alluvium and basalt, shows that scaling rules in $W^{1/3,4}$, $W^{1/4}$ and $W^{1/4,5}$ are the most representative according to yield and medium conditions.

BIBLIOGRAPHY

- (1) Physique des explosifs solides
J. BERGER - J. VIARD - Ed. Dunod 1962
- (2) Scaling dimensions of craters produced by buried explosions
A.J. CHABAI SCRR 6570 - 1965
- (3) Mouvements mécaniques provoqués par des explosions nucléaires souterraines G. GUERRINI - J.L. GARNIER - Rapport CEA - R 3885-1969
- (4) Explosions nucléaires souterraines - Etude des rayons de cavité
L. MICHAUD Rapport CEA-R-3594-1968
- (5) Effect of water content, yield, medium and depth of burst on cavity radii G.H. HIGGINS - T.R. BUTKOVITCH - UCRL 50203-Feb.21.1967
- (6) Cratering experiment with large high explosive charges
L.J. VORTMAN TID 16739
- (7) Third Plowshare Symposium TID 7695 - 1964
- (8) Détermination statistique de relations expérimentales sur les dimensions des cratères F. DELORT - M. CENTENE - H. LARZILLIERE
CEA Rapport interne - 1968
- (9) Eléments de statistique mathématique - A MONJALLON - Lib. VUIBERT 1963.

(10) Contenu spectral des mouvements sismiques dus aux explosions nucléaires souterraines. Melle A. ALBARET - Mme F. DUCLAUX-Rapport CEA-R-3767-1969.

(11) Etude de synthèse sur les dimensions des cratères d'explosion. - 1ère partie - M. BOULON - J. GAUTIER - CENG/ASP 69-18-1969.

STUDY OF THE MINERALOGICAL TRANSFORMATIONS OF GRANITE BY UNDERGROUND NUCLEAR EXPLOSIONS

Jean FAURE

Commissariat à l' Energie Atomique (FRANCE)
Centre d'Etudes de BRUYERES-LE-CHATEL

ABSTRACT

The object of the following communication is to prove new data about the petrographic effects of the underground nuclear explosions. It is founded on the results of french tests in granite rock. The samples are collected by drilling and the temperature of the rock was measured in the hole. Four types of melted rocks can be sorted, grey-green glass and pumices, beige to red-brown pumices, dark lavas, dark veinlets and crushed granite. The distribution of these rocks is studied. Optical microscopy, X-rays and chemical analysis, study by electron probe, are made. The results complete previously published data. They are interesting as far as the use of nuclear explosions for industrial applications is concerned.

1 - INTRODUCTION

The object of the following communication is to prove new data about the petrographic effects of the underground nuclear explosions. The knowledge of rock transformations is indeed necessary to define exactly the useful effects of the explosions and their possible applications.

This study is founded on the results of french tests on the HOGGAR test site (Central Sahara). The shots were fired in a very homogeneous granite mountain mass the composition of which is well known (see Table 1).

The explosions took place at the end of horizontal tunnels and after the shot, the surrounding rocks we explored by drilling.

A short first part of this report gives the outline of this exploration. The second part describes the petrographic features of the rocks collected. The third part gives the results of the special study techniques used.

TABLE 1

Composition of the granite of the HOGGAR Test Site (2)

Chemical Analyses

SiO ₂	75,80	CaO	0,59
Al ₂ O ₃	12,49	Na ₂ O	3,80
Fe ₂ O ₃	1,30	K ₂ O	4,79
MnO	0,04	TiO ₂	0,08
MgO	0,03	P ₂ O ₅	0,01
	H ₂ O +	0,48	
	H ₂ O -	0,06	
	CO ₂	0,13	

Mineralogical Analyses

Quartz	35	Chaye's index	64
Microcline	37		
Plagioclase	25		
Biotite	2,1		
Muscovite	0,6		

2 - GENERAL DATA ON THE EXPLORATION

Three drilling methods are used :

- 1) A conventional rotary drilling method when the length of the bore-holes was under one hundred and sixty meters. The recovery of cores is generally good.
- 2) A turbo-drilling method for larger lengths ; the turbo-drilling used allows a better control of direction because of its great accuracy (about one or two meters in four hundred meters). But the rate of recovery is often low.
- 3) A composite method combining turbo-drilling and coring by rotary drilling in the most interesting areas.

By means of those methods, the rocks surrounding the shot point are explored in nearly every way, at all levels and in all directions. But every cavity was rarely studied by more than five or six holes. The use of dimensional analysis allows us to show the similitudes between different underground nuclear explosions and facilitates the generalizing of the observations. This method simplifies the comparison between several shots and eliminates local anomalies.

Figure 1 is drawn along these principles. Holes crossing near the shot point are shown in scaled coordinates (r scaled length from the shot point is equal to the quotient of R the true length by $W^{1/3}$, W being the energy yield of the device in kilotons). It shows the recovery rate of holes crossing the cavity. This rate is very unsteady but the exact study shows that the variations are due to technical reasons (slope or size of the hole) and the samples are representative of the rocks surrounding the shot point.

From the very first holes, the existence of important thermic effects was confirmed and temperature was measured. The heating of boring bits and water around the cavity is quite high. In several cases, an artificial geyser regime was produced when the shape of one or several holes was suited. The drilling waters gathered in pockets. They progressively became overheated and vaporized at the rock contact. When the pressure gets to an adequate value, a steam jet can be produced at the head of the hole.

Measurement afterwards allows us to study the distribution of temperature in space and time (1). Some weeks after shot, the following facts are recorded. The temperature of the cavity rocks is relatively uniform, included between five hundred and six hundred degrees Celsius. In the surrounding crushed zone (at the wall of the cavity), there is a very big thermic drop. At ten meters in scaled length of the shot point, temperature is almost the same as the one of the rocks before the explosion. In the chimney, the temperature is about seventy-five degrees Celsius. Except this last field, the isothermal lines are fairly spherical (fig. 2). The temperature evolution in time is rather slow. The recorded changes are about a hundred degrees Celsius per year.

3 - CLASSIFICATION OF ROCKS PRODUCED BY THE EXPLOSIONS

The detailed geological logs show the large variety of aspect of the melted granite products. They are very generally radioactive samples and their observations require care. They must often be examined in protected areas through leadglass bulls-eyes. The direct comparison of two samples is in practice unrealizable. Those conditions of study might induce us to regard any attempt to classifying as useless. Doing it is however necessary for the report to be clear. The here used classification is founded on the core features resolved by the naked eye. It also reflects their relative positions to the shot point (fig. 3 and 4).

The following types can be sorted (see also table 2)

- Type A - grey-green glass and pumices
- Type B - beige to red-brown pumices
- Type C - partially melted granite and dark lavas
- Type D - dark veinlets and crushed granite.

Let us now look at them in detail.

RECOVERY FOR HOLES CROSSING THE CAVITY

Recovery rate

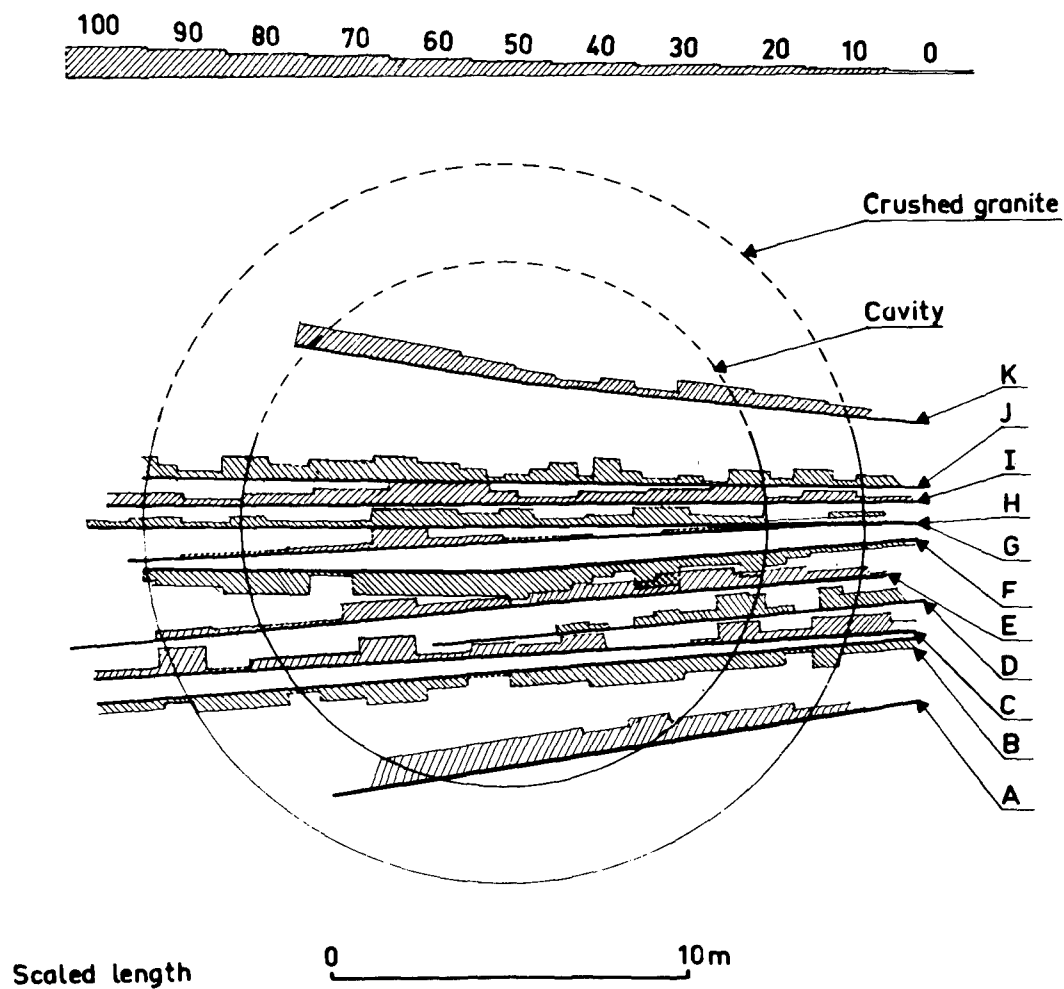


Fig. 1

EXAMPLE OF ISOTHERMS DRAWN ROUND A SHOT POINT

Results of C.E.N.G-degrees Celsius

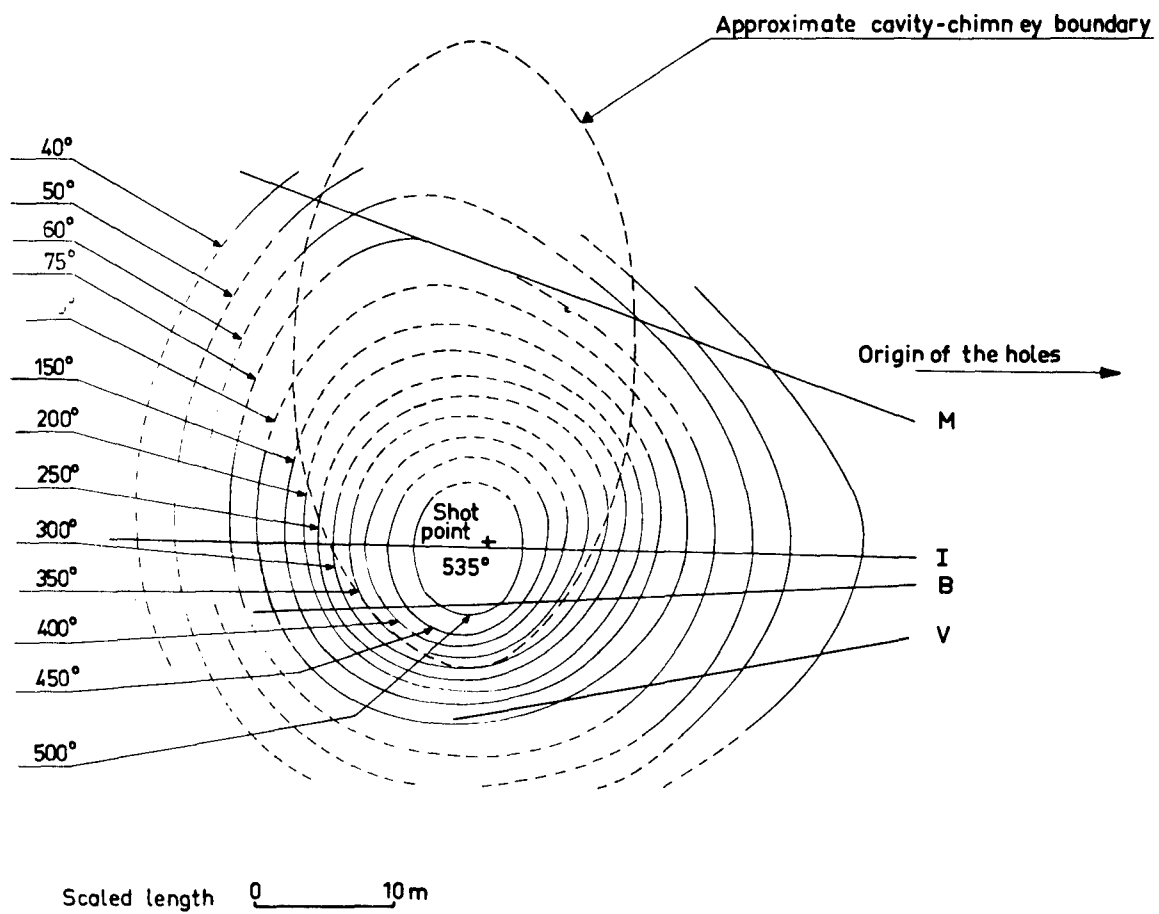


Fig. 2

GEOLOGICAL LOG OF A HOLE CROSSING THE CAVITY

Scaled length to shot point (m)

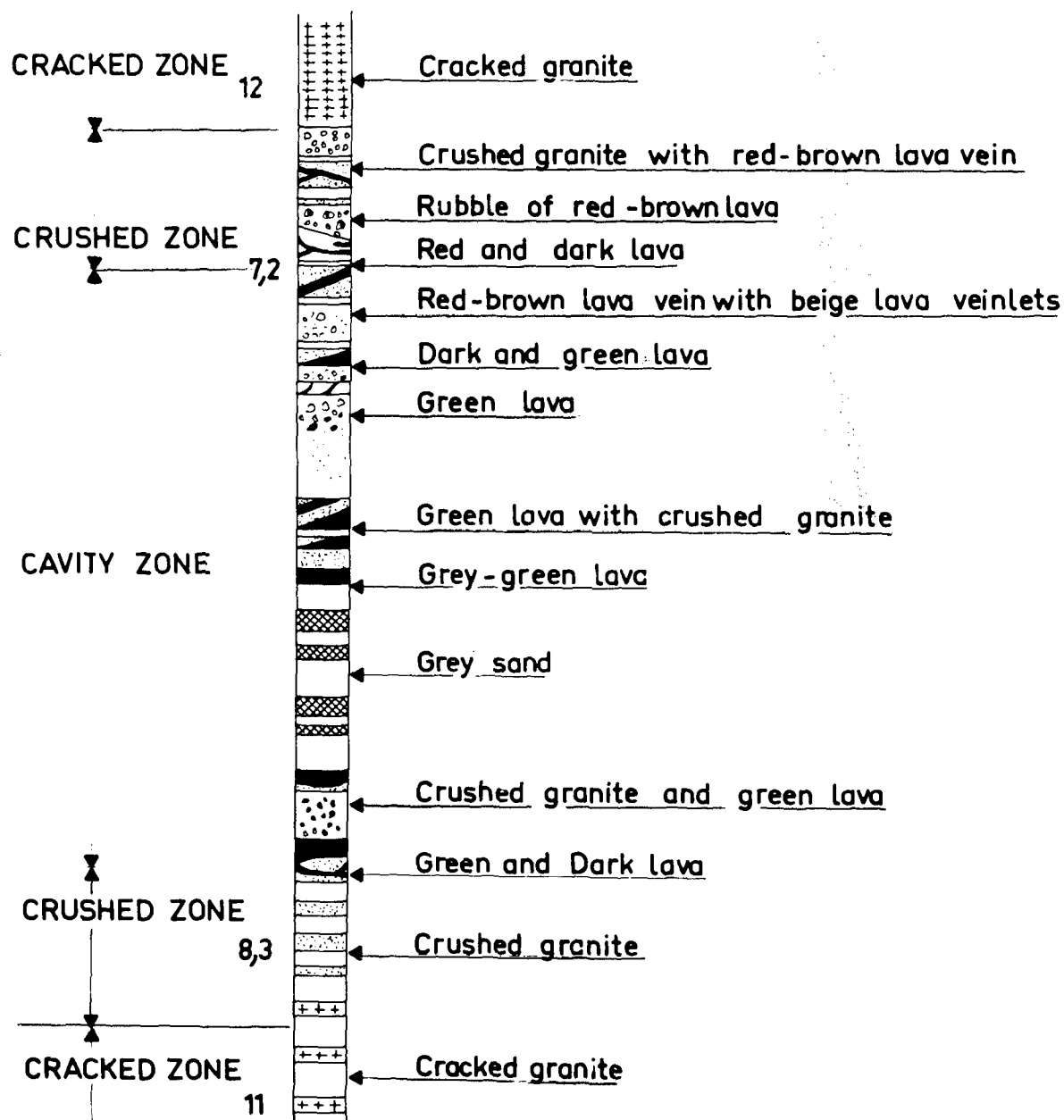


Fig. 3

DIFFERENT TYPES OF MELTED ROCKS

Scaled length to shot point (m)

Scaled length to shot point (m)

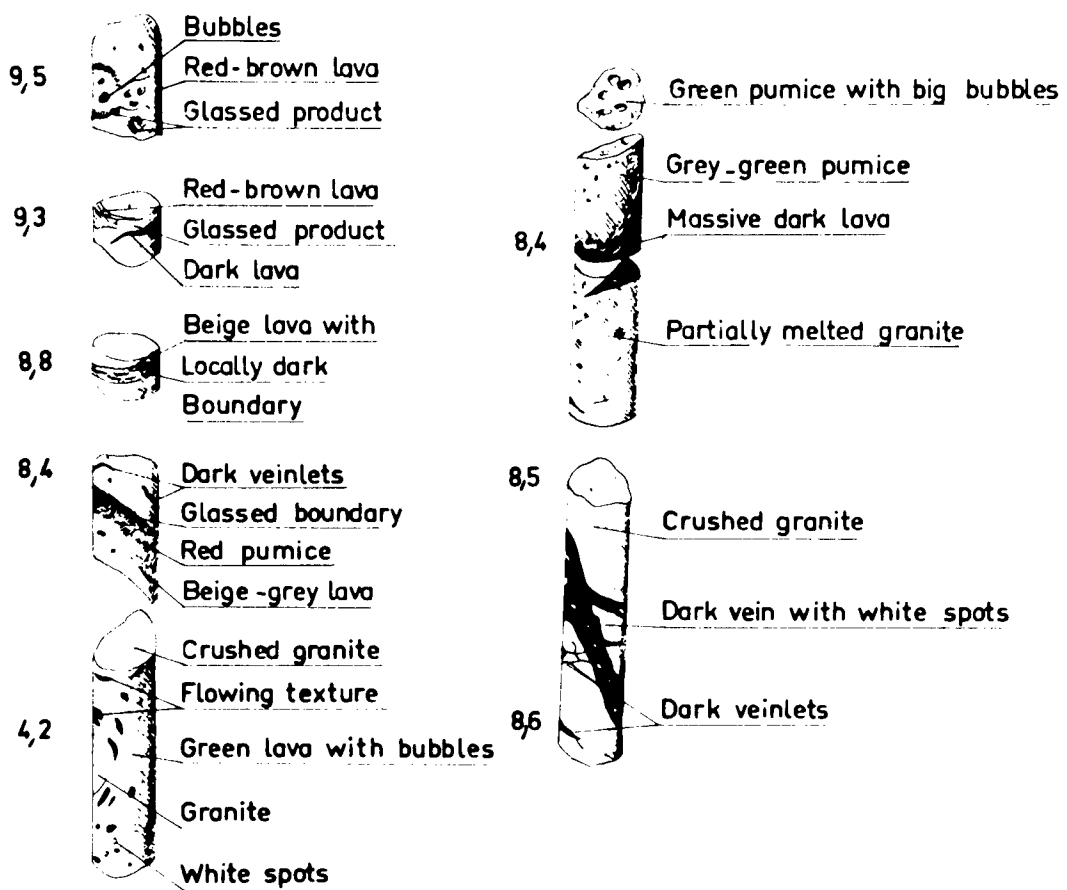


Fig. 4

3.1 - Grey-green glass and pumices

These are the majority of the melted rocks obtained. They represent about one half of the total amount of lavas encountered near the shot point. On massive sample resolved by the naked eye, their colour varies from a fairly dark dull green to a dark iron grey. Sometimes massive and porcelain looking, they are in some cases semi-transparent glass (fig. 5a). Generally, they have bubbles which diameter varies with the samples from one to eight millimeters (fig. 5b), reaching exceptionally several centimeters. Around the blocks fallen from the roof which are not entirely melted, the bubbles are very elongated and give a flowing texture. Some samples show here and there rectangular whity spots (perhaps cristobalite crystals).

The grey-green lavas seem to be typical of the cavity where there are nearly exclusively found. Inversely, this criterion can be used, in case of doubt, to determine the limit of the cavity. The grey-green lavas are very seldom connected with the still cristalline granite. Dark lavas and half melted granite separate them most often. Among the grey-green lavas, there seems to exist a certain classification. Pumices are often found above the shot point. The bubbles are then well developed and very elongated. In the lower part of the cavity, massive melted rocks are mostly found.

TABLE 2

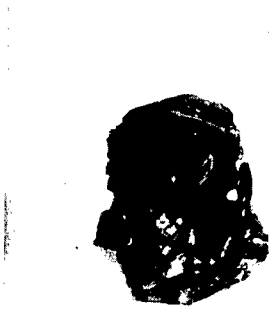
Types of melted rocks

Type	Rock pattern	Color	Localisation
A	Lava (Pumice) (Glass)	grey-green	in the cavity
B	Lava (Pumice)	beige to red-brown	veins out the cavity
C	Lava	dark	boundaries of the cavity and half-melted granite near the other types A and B.
D	Breccia (veinlets)	dark	crushed granite near the cavity boundaries.

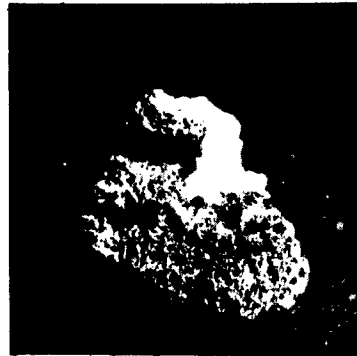
3.2 - Beige to red-brown pumices

These rocks look like the grey-green lavas. They differentiate from them by their distribution since they are found outside cavity and especially because they have other colors ranging from beige to dark brown with all kinds of red in between.

MELTED SAMPLES OF GRANITE



5a. GREEN GLASS TYPE A



5b. GREY-GREEN PUMICE TYPE A



5c. RED BROWN LAVA WITH WHITE
SPOTS TYPE B



5d. RED-BROWN LAVA WITH
LARGE BUBBLES



5e. DARK LAVA TYPE C



5f. BRECCIA WITH DARK VEINLETS

Fig. 5

Sometimes, they give light pumices constituted of a fibrous aggregate. Their flowing texture is marked and often accentuated in the most massive patterns by a change of colour according to the beds. White mineralisations and transparent inclusions are encountered now and then (fig. 5c and 5d).

The chemical analysis showed that the colour scale is not in connection with large changes in composition. Although these rocks generally are recovered far from the cavity, this result seems to be incompatible with both following assumptions :

- hybridation of the melted silicates with fortuitously crossing products or
- natural distillation of the volatile parts.

The most likely assumption is that the change in colour proceeds from an iron oxydation. In the cavity, the atmosphere would be reducing and iron in the state Fe^{++} . In the cracks around, the atmosphere would be oxydizing and iron in the state Fe^{+++} .

3.3 - Partially melted granite and dark lavas

The dark lavas are the second large whole of melted rocks to be found in the cavity. They appear making the transition between the grey-green lavas and the still cristalline rocks. Generally, they lie at the boundary of the blocks fallen from the cavity roof or along its wall. They look remarkably like glass produced by the melting of granite in a furnace. The whole range of states between undamaged granite and glass is indeed found :

- 1 - granite may be only whitened. The iron oxydes naturally coloring the rocks pink, gradually combine with feldspars crystals which are whitened. In contrast, biotite micas appear darker and darker.
- 2 - In some areas, the crystal boundaries become fuzzy and colour observed with the naked eye turns blue grey and then darkens. The micas vanish.
- 3 - There are only whity spots on a darker glass giving a "salmon skin" aspect to the rock. Finally the rock turns to a very dark lava as an obsidian (fig. 5e).

With binocular lens, the glassed areas generally appear most transparent. Their colour scale is between smoked yellow and grey.

3.4 - Dark veinlets and crushed granite

Rocks of this pattern make a special variety of breccia rocks. Amid a whity aggregate created by crushed crystals which are not resolved by the naked eye, dark veinlets are very visible (fig. 5f). They are seldom alone but frequently dividing and crossing one another. When they are very numerous, the rock comes to look like dark lava of entirely melted granite as described above. Dark veinlets do not rise by chance in the crushed rock. They cross very frequently the biotite crystals.

The rocks with dark veinlets shape a rim round the cavity. May be some rubble from its roof recovered near the shot point are also of this pattern but they are undistinguishable from the other half-melted rubbles. The rocks with dark veinlets are the most original type among rocks transformed by the nuclear explosion. Therefore, a large part of the special studies which have been made, concerns them.

4 - GEOLOGICAL AND MINERALOGICAL STUDIES OF ROCKS

4.1 - Distribution of melted rocks

As mentioned above, there is a connection between the different melted rock types and their position along the borehole. Thus, grey-green lavas lie in the depth of the cavity and dark lavas shape big accumulations at the boundary of the crushed granite rim. The amount of each of these two patterns is about the same. The beige to red-brown products are much less common and are almost exclusively to be found in veins along the cracks far from the cavity. The farther from the cavity-wall, the more the rocks tend to be red. The dark veinlets the amount of which is proportionally very small, lie only in the zone of crushed granite around the cavity.

In the cavity (fig. 6) lavas and rubbles are not homogeneously distributed. Detailed survey shows a certain grading. The upper level of lavas reaches about half the radius of the cavity above the shot point (hole K). There, melted rocks and rubbles are about fifty-fifty. But rubbles progressively become larger when the hole is bored lower in the cavity. From this result, it is possible to make a rule of thumb between the melted rocks rate and the sampling level in the cavity. It is a linear law and an integration gives an approximate value to the amount of melted rocks in the cavity : nearly forty per cent of the cavity volume before collapse or about one thousand and three hundred tons melted rocks for a standard explosion yielding one kiloton.

4.2 - Laboratory analysis

The samples which are not or very weakly radioactive are studied by detailed laboratory analysis especially concerning the melting phenomenology of crushed granite (2).

DISTRIBUTION OF MELTED ROCKS FROM HOLES CROSSING THE CAVITY

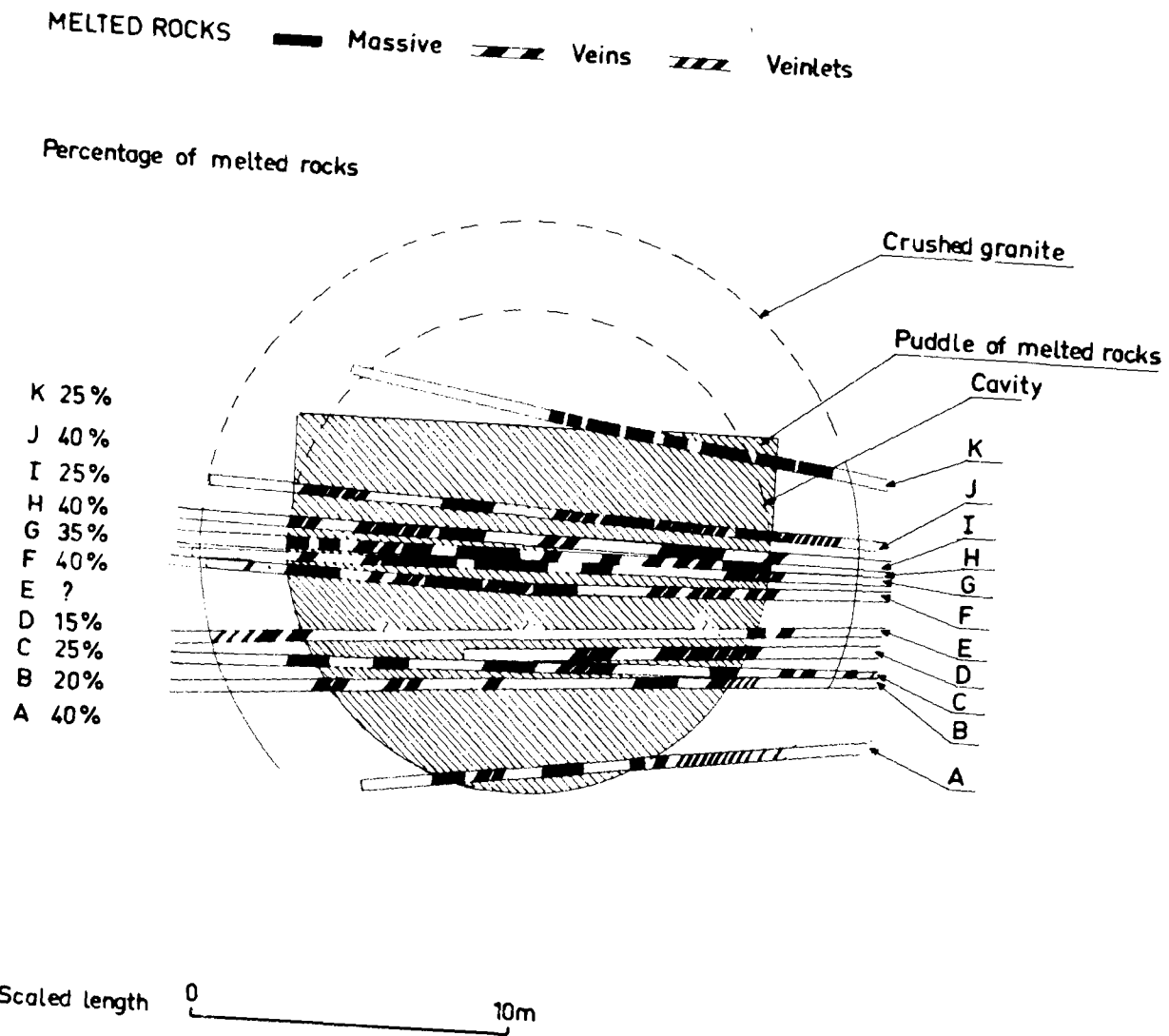


Fig. 6

4. 2. 1 - Optical microscopy

Thin plates survey shows that the glassed veinlets extend in a granite the crystals of which are profoundly altered. Quartz becomes optically biaxial and has many planar elements. Feldspars lose part of their lines of macle and of their birefringency. Biotite has many kink bands (fig. 7). In this aggregate, veinlets are constituted of a brownish glass matrix including many elements : little globular bubbles, round crystallizations, little white isotropic sticks, iron oxydes trails and clear minerals with often a marked relief. Crystals in connection with veinlets are sometimes corroded ; thus, on the boundary of a probably former microcline crystal, appears a big relief fringe. Biotites are surrounded by iron oxydes.

Under the microscope, it seems that grey-green lavas and pumices are made of homogeneous glass and dark lavas have an irregular distribution of the opaque iron oxydes.

4. 2. 2 - X-rays analysis

X-rays analysis was thought to allow :

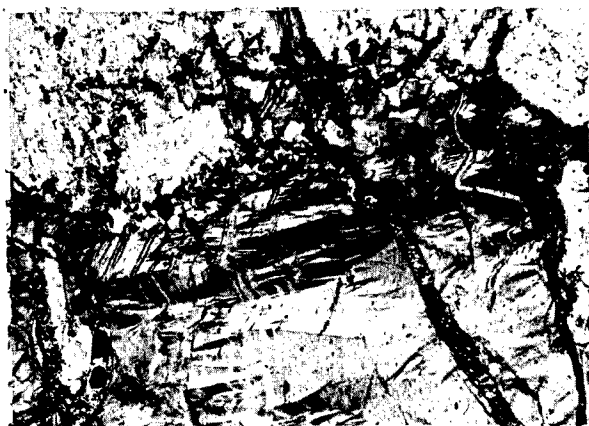
- showing possible alteration of mineral lattices in granite
- establishing the identity of new mineral species created.

About the first point, no difference has been observed between undamaged granite samples and granite altered by the explosion effects. The crystals parameters of quartz are the very same to a $2 \cdot 10^{-4}$ Å. Potash feldspars triclinism do not change : in all cases, it is a high microcline ($\alpha = 90^\circ 39'$ $\gamma = 87^\circ 47'$). No evolution is observed in the always pure albite perthites. Interreticular plagioclase lengths measurement always gives results corresponding to a five per cent anorthite plagioclase.

About the second point, X-rays analysis show the presence of two new species, sanidine and low cristobalite appearing in the crushed granite zone. At the cavity boundary the only minerals encountered are quartz, low cristobalite and sanidine. Low cristobalite is observed in small amounts in the white crushed granite part. Bigger amounts are to be found in the dark veinlets part and also in the totally melted samples. Sanidine is to be found in the crushed boundary but does not seem to appear in the cavity itself. Its concentration is also larger in dark veinlets than in white crushed granite (fig. 8).

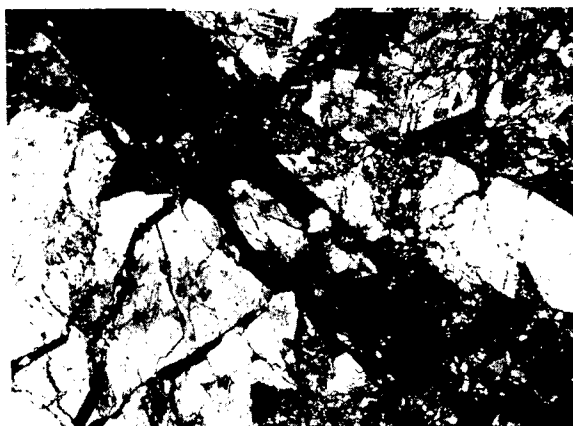
MELTING OF GRANITE OBSERVED UNDER MICROSCOPE

(polarized light)



7a. CRUSHED GRANITE WITH KINK BANDS

0 _____ 1mm



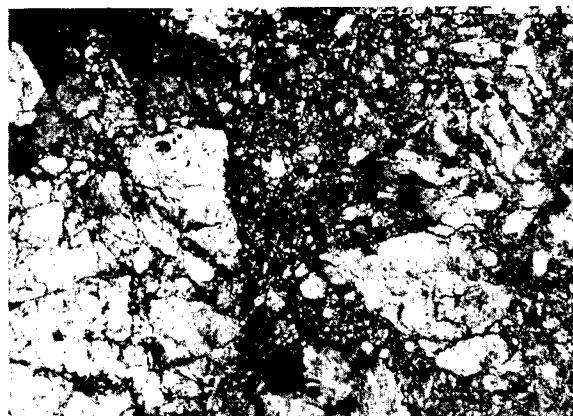
7b. VEINLET WITH MUCH GLASS

0 _____ 1mm



7c. VEINLET WITH RECRYSTALLIZED MATERIAL

0 _____ 1mm



7d. HALF MELTED GRANITE (LEFT)

CONNECTED WITH DARK LAVA (RIGHT)

0 _____ 1mm

Fig. 7

REPRESENTATION OF MINERALOGICAL CHANGES AT THE CAVITY BOUNDARY

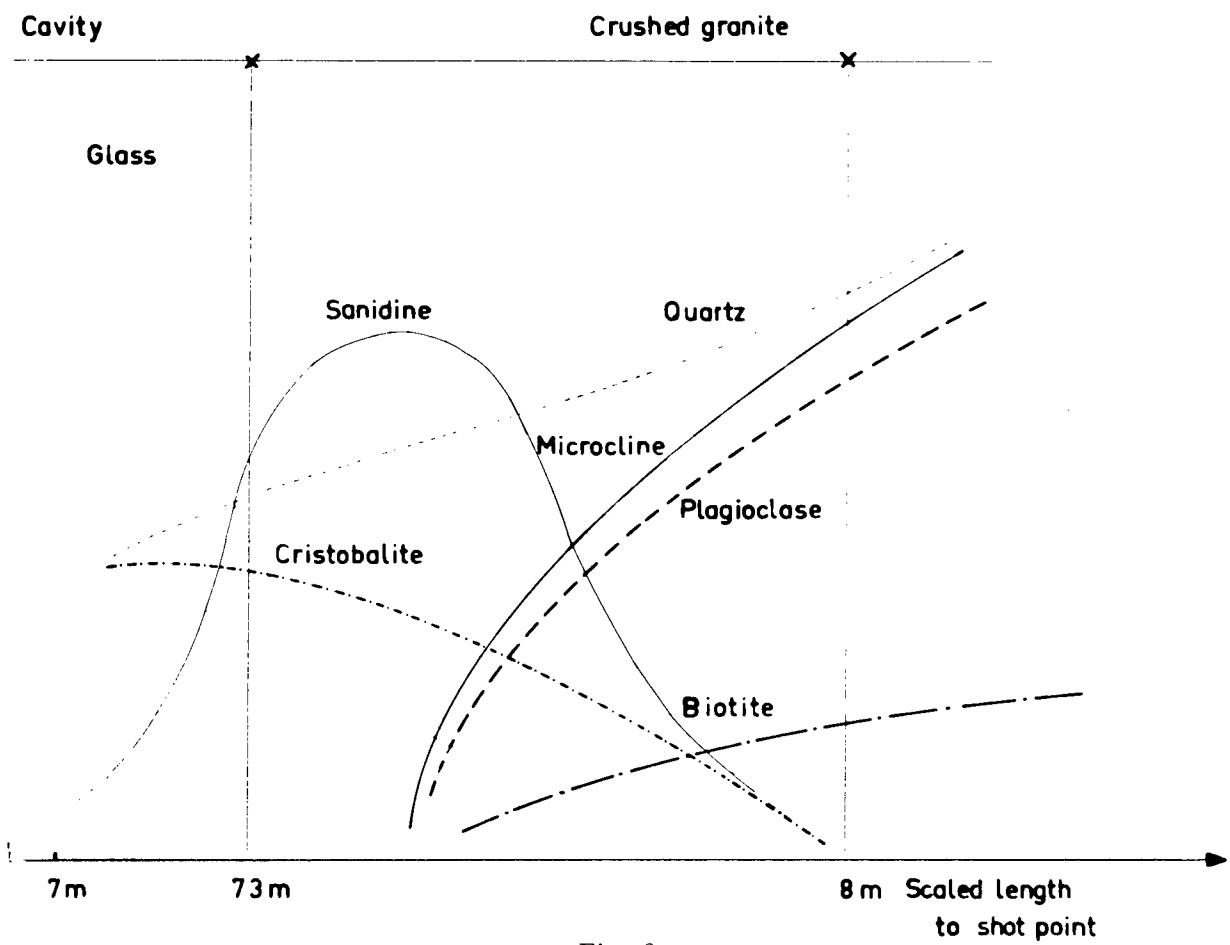


Fig. 8

The transformation pattern, in connection with the cavity boundary is typical of thermic effects. Shock effects are probably masked by them.

4.2.3 - Chemical study

In a parallel direction to the mineralogical analysis described above, granite samples have been studied by total chemical analysis. About one hundred chemical analyses were made on samples taken before explosion (see table 1). After shot, a first range of analysis were made on twenty-five samples recovered along the whole length of the explored areas. Figure 9 shows the results. There is no really significant change. But the survey of rocks bordering the cavity, is very interesting : samples can be divided in two parts. The white one is richer in silicium, the other one, which is created by the dark veinlets, has a higher rate in Al_2O_3 , Fe_2O_3 , MnO and K_2O . Thus, there is a kind of differentiation in this area.

The sanidine mineral which appears on the X-rays diagrams was analysed and this analysis shows that all the granite feldspars have newly crystallized creating a solid-solution potassium-sodium-calcium. There is also four point five per cent iron oxyde. This explains that sanidine did appear magnetic under mineral separation. But the parameters determined by X-rays show that the iron is not included in the lattice and may be in intergranulate state.

4.2.4 - Study by electron probe

The presence of a new mineral species as sanidine indicates a diffusion of the most volatile elements to reconstitue a new mineral. This induced us to try and find phenomena of element diffusion at microscope scale by observation with the electron probe. Using this instrument reveals that there is some iron oxyde in the cracks near the micas. Many analysis in the biotite specimens give large heterogeneity of iron, aluminium, silicium and potassium. But these changes can hardly be related to shock effect since the biotite of granite are already altering in the whole area. At the cavity boundary, for samples showing signs of a melting start, the electron probe still gives the mineral size. But in the same samples (fig. 10), some areas are clean whilst others show a more advanced stage of evolution. Potassium diffuses whilst iron, manganese or zirconium remain distinctly steady.

CHEMICAL ANALYSES OF CRUSHED GRANITE

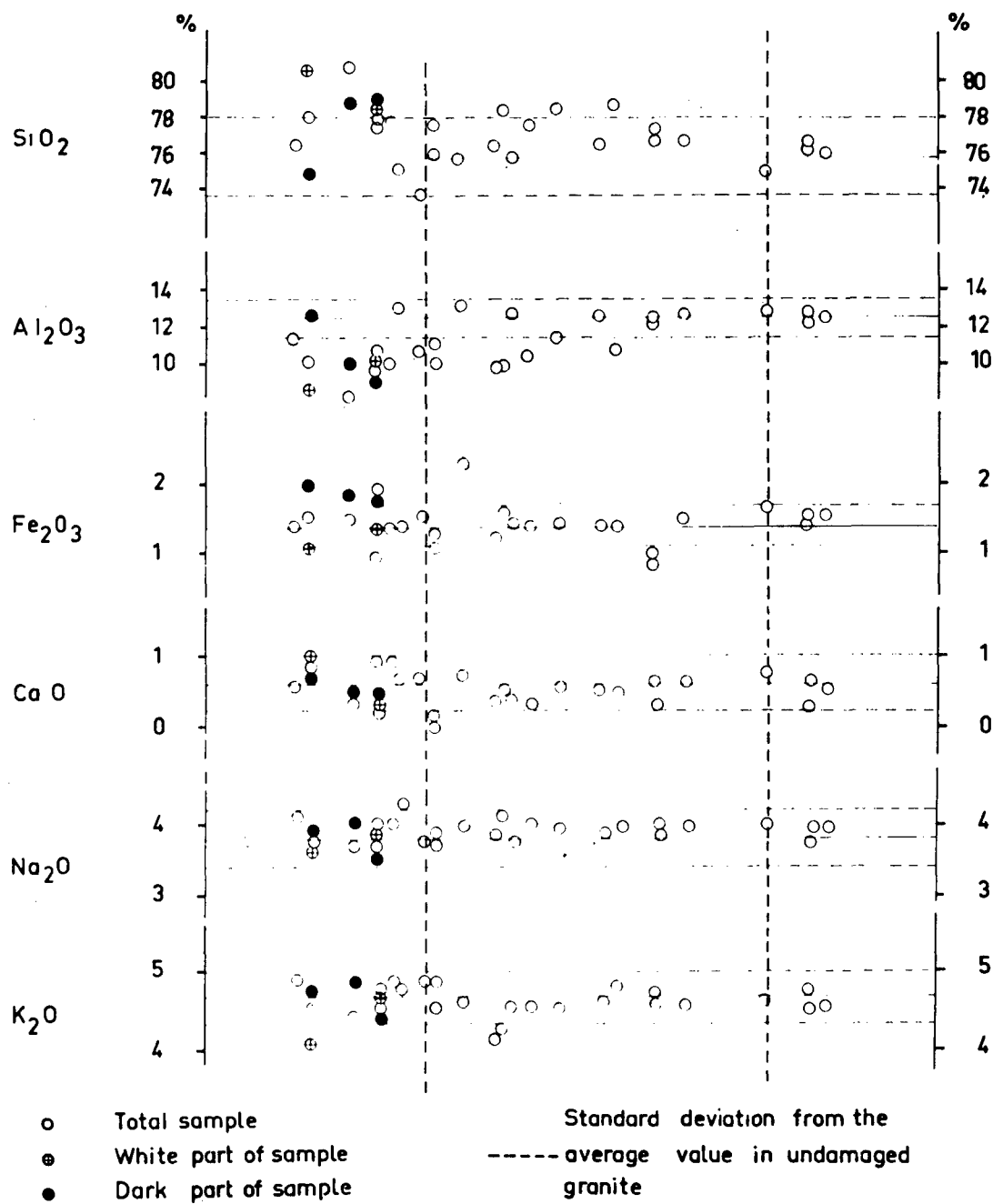


Fig. 9



DIFFUSION OF ELEMENTS OBSERVED WITH ELECTRON PROBE

A. Cristal boundaries are fuzzy potassium
especially diffuses.

B.size of minerals is always clean

Area A



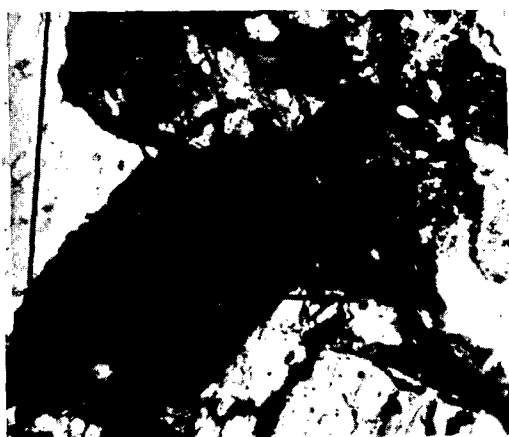
K



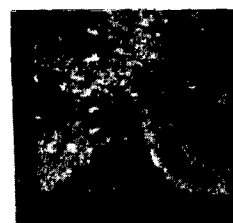
Si



Fe



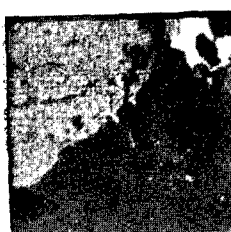
Area B



Mn



Zr



Al



Fe



Si

Fig. 10

TABLE 3

Comparison of different classifications of melted rocks		
SHORT (1964)	RAWSON (1966)	FAURE (1966)
Type 1 (dense usually dark glass represents puddle accumulation)	1 - Predominant phase (accumulated puddle droplets and injection into cracks)	Type A (grey-green pumices and lavas)
<hr/>		<hr/>
Type 5 (dense to vesicular melt injected into fractures)		Type B (beige to red-brown pumices).
<hr/>		<hr/>
Type 2 (light in color variably vesicular glass develops by super heat fusion)	2 - Border phase (interpreted as rep- resenting both rocks only partly melted by shock wave and melting by superheat)	Type C (dark lavas)
<hr/>		<hr/>
Type 3 (globules, blebs smears along fracture)	3 - Gas leakage phase (along cracks in permeable regions)	Type D (dark veinlets)
	4 - Condensed vap- or phase (observed on the surface of rocks or other phases)	
<hr/>		<hr/>
Type 4 (exclusive of craters shots).		
<hr/>		<hr/>

5 - CONCLUSIONS

The preceding results complete previously published data about the petrographic transformations in a granite under nuclear underground explosions. Account being taken of the different distribution of melted granite, temperature measurements are comparable in Nevada and in Hoggar. For the Shoal event, a six hundred degrees rocks puddle diffused the heat in the surrounding rocks (3).

Except for some particulars, the survey of melted products joins to the SHORT (4) and RAWSON (5) proposed classification after the Nevada test site nuclear explosions. The different rock patterns are in a fairly correct agreement save the radioactivity (table 3). However, the SHORT's type three and four are not commonly found in the Hoggar test site. The beige to red brown lavas belong to SHORT's type number five. One may wish to know whether there is a connection between RAWSON's phases three and four and the dark veinlets mentioned above.

In return, the distribution of melted products is clearly different on the two test sites (fig. 11). But calculation shows that most of these differences are due to the differences of cavity size and the respective amount of rubbles falling in the melt created by the shock wave.

The presence of low cristobalite (uncommon in the earth's natural materials, but found in the lunar samples collected by Apollo 11 (6) and sanidine and the diffusion of the elements in short length show the importance of thermic phenomena in rock transformation by an underground nuclear explosion.

Finally, we hope these results will contribute to accurate explosion phenomenology. In this regard, the data about the position of lavas in the cavity chimney unity, appear different from the published figures. This may be important in connection with problems of engineering explosions : the lavas area is the radioactive products area. It may for instance have to be untouched in the case of possible mining applications.

The results also accurate the mineralogical and thermic effects of explosions. Thus, for example, the high pressure quartz polymorphes coesite and stishovite do not appear. This fact is probably in connection with the transformation into high temperature species as cristobalite. A similar process may bring the secondary transformation into graphite of diamond created by a shock wave.

COMPARISON OF PUDDLE POSITION FOR UNDERGROUND NUCLEAR EXPLOSIONS IN GRANITE (HOGGAR AND NEVADA TEST SITES)

Yield energy : 1kt

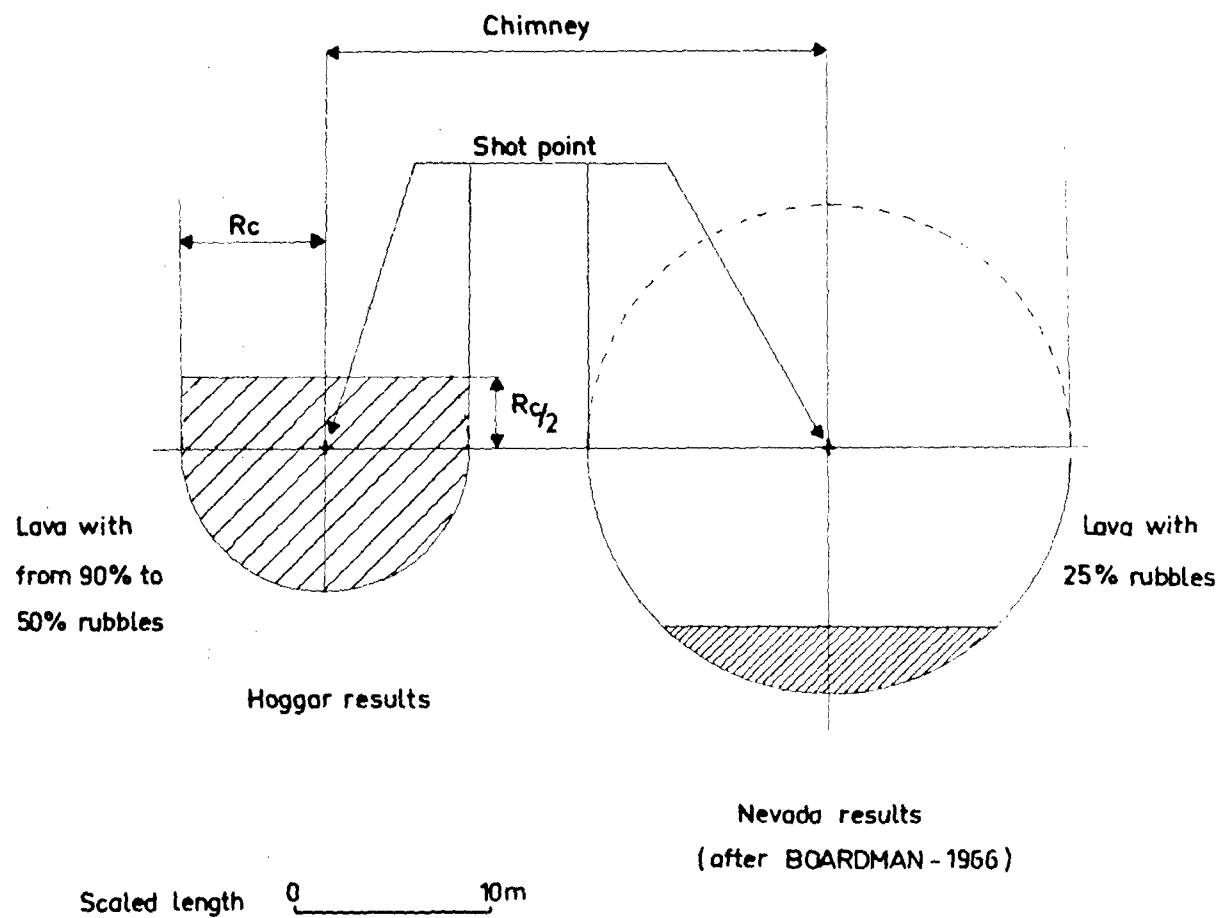


Fig. 11

6 - REFERENCES

- (1) - Results from P. PERROUD (1965)
Centre d' Etudes Nucléaires de GRENOBLE.
- (2) - Studies realized in collaboration with centre de Recherches
Pétrographiques et Géochimiques de NANCY
Director : Professor M. ROUBAULT.
- (3) - R. HECKMAN - Deposition of thermal energy by nuclear
explosives.
California Univ. Livermore, Lawrence Radiation Lab.
Rept. - UCRL-7 801 (1964).
- (4) - N. SHORT - Nuclear explosions craters, astroblemes and
crypto-explosions structures.
California Univ. Livermore, Lawrence Radiation Lab.
Rept. - UCRL - 7 787 (1964).
- (5) - D. RAWSON - Characteristics of glasses resulting from
nuclear explosions in silicate rock.
Abstract in Shock metamorphism of natural materials
Proceedings of the first Conference held at NASA,
Greenbelt (Maryland), April 1966.
Mono Book Corp. Baltimore - 1968.
- (6) - The lunar Sample Preliminary Examination Team
Preliminary Examination of Lunar Samples from Apollo 11.
Sciences, 19-9-1969, Vol. 165, n° 3 899, pp. 1211-1227.

ABSTRACT

SUBSIDENCE CAUSED BY AN UNDERGROUND NUCLEAR EXPLOSION

by

W. W. Hakala

An underground nuclear detonation creates a cavity, which may be followed by the formation of a rubble chimney and possibly by a surface subsidence crater. A knowledge of the mechanisms of surface and subsurface subsidence is valuable not only because of the potential engineering uses of the chimneys and craters that may form, but also for the prevention of surface damage.

Some of the parameters that are of interest in the subsidence phenomenon are the height and volume of the chimney, the porosity of the chimney, the crater size (depth and radius) and shape, and the time required after detonation for formation of the chimney or crater. The influence of the properties of the subsidence medium on the geometry of the subsidence crater must be considered. The conditions under which partial or complete subsidence is prevented must also be studied.

The applicability of the relations that have been developed for the flow of bulk solids for relatively small masses and low pressures to the subsidence problem associated with nuclear explosions is examined. Rational modifications are made to describe the subsidence problem. Sensitivity of the subsidence parameters to material properties and the prevailing geometry is shown. Comparison with observed results at the Nevada Test Site is made and the variations encountered are found to be within reasonable limits.

The chimney size and subsidence crater dimensions are found to be a function of the bulking characteristics of the medium, the strength parameters, the dimensions of the subsurface cavity, and the depth of the cavity. The great influence of the strength parameters on the collapse times is shown. For a given medium, the prevention of subsidence is dependent on the cavity size.

SUBSIDENCE CAUSED BY AN UNDERGROUND
NUCLEAR EXPLOSION

W. W. Hakala, Deputy Director for Engineering

Environmental Research Corporation
Alexandria, Virginia

The utility of subsidence craters for engineering purposes is questionable, since greater efficiency in producing surface depressions can be obtained with ejecta craters. Still, if containment of radioactivity is mandatory, subsidence craters may provide a solution for certain problems. Subsurface subsidence (e.g., permeable chimneys) does have immediate application in the Plow-share program. Independent of the engineering applications, it is necessary to determine the extent of surface subsidence for safety reasons. A knowledge of the subsidence mechanisms may even permit the control of subsidence to some degree.

This paper is a study of the subsidence associated with the collapse of underground spherical cavities (which were produced by underground nuclear detonations). The results are based on the work of Jenike and his colleagues, who have developed many of the concepts for the flow of bulk solids (bin-flow theory). Homogeneity, isotropy, and steady-state flow are usually assumed in Jenike's work.

Although deviations from homogeneity and isotropy are present in most of the subsidence cases, it is assumed that these effects are small. Of course, the presence of layered earth media having widely varying strength properties would affect the results significantly, and would require individual consideration.

In contrast to the fixed outlet dimensions in bin-flow theory, the material adjacent to the assumed spherical cavity is subject to collapse. However, it is assumed that the flow boundaries are close to the cavity walls and thus the outlet dimensions can be expressed in terms of the cavity radius, R_c .

This work also requires the cavity pressure to be approximately atmospheric. While the time to collapse will be dependent on the cavity pressure, it is not believed that the potential flow patterns will be affected significantly by this assumption. Because the type of subsidence being considered may involve vertical

movements of several hundred feet, it is quite likely that the steady-state flow patterns are reached in many instances.

The stresses and dimensions used in bin-flow theory are approximately two orders of magnitude less than those in the subsidence problem. However, the fundamental relations (equilibrium equations and yield criterion) remain valid.

A large portion of Jenike's work is concerned with the shape of the yield surface at small compressive stresses. Variations in the yield surface caused by consolidating pressures, temperatures, moisture, and time have been carefully examined, and a corresponding vocabulary of bulk solids flow has been developed. Jenike (1961) has provided strong physical arguments for a curved yield surface at small stress values. Because of the assumptions, the large pressures, and a lack of known material properties (in general), the present study does not warrant such refinement. Therefore, the linear Mohr-Coulomb yield criterion is assumed. Bin-flow theory is applied directly, if applicable, or modified to represent the physical situation.

THEORY OF SUBSIDENCE

Yield Criteria

Most of the stresses and strains encountered in the subsidence problem are compressive. Thus, it is convenient to assume compressive values as being positive and tension values as being negative. The collapsing medium has both cohesion (c) and internal friction (ϕ), and for purposes of analyses, is also assumed to be homogeneous, isotropic, and compressible.

The selection of the Mohr-Coulomb yield criterion as the failure mechanism requires only a knowledge of the major and minor principal stresses (σ_1 and σ_3 , respectively), and is independent of the intermediate principal stress (σ_2). Recent experimental work has found that the intermediate principal stress does affect the stress values at failure to a certain degree. However, this effect is quite small and will be neglected in this discussion. (it can also be argued that the selection of an angle of internal friction, ϕ , has taken into account the effect of σ_2 .)

The yield surface corresponding to the Mohr-Coulomb hypothesis in the principal stress space is shown in Figure 1. Neglecting the effect of σ_2 on yield results in a yield surface with sharp corners, which seems to violate one's intuition of expecting smooth transitions in physical processes. However, the rate of change of curvature at the edges is very large and thus the yield surface can be represented by a pyramid.

The usually assumed "open" yield surface used in soil mechanics was modified by Jenike and Shield (1959) to agree with the concept of normality and physical observations. This modification is the addition of a base that is perpendicular to the line equally inclined to each of the three principal stress axes. The position of the base depends on the mean stress, $\sigma'_m = (\sigma_1 + \sigma_2 + \sigma_3)/3$, during flow.

The concept of normality requires that the strain-rate vector ($\dot{\epsilon}$) be perpendicular to the yield surface. Inclusion of a base not only permits compression under a hydrostatic stress, but also allows either expansion or contraction if the stress state corresponds to a corner of the base, e.g., point "A" (the corresponding strains being plotted on the same axes as the stress). This model, then agrees with physical observations that either expansion or contraction takes place during flow. For failure stress states corresponding to points on the faces or edges of the pyramid, the normality requirement dictates material expansion.

Jenike (1961) found from laboratory tests on numerous materials that during "flow" (after incipient failure) the ratio of the principal stresses remains constant for a given material. The significance of this finding can be seen in a normal stress (σ) vs. shear stress (τ) plot (Figure 2). From the geometry it is readily seen that

$$\frac{\sigma_1}{\sigma_3} = \frac{1 + \sin \delta}{1 - \sin \delta}, \quad (1)$$

where δ is called the effective angle of friction. The envelope to the stress circles is called the effective yield locus (EYL). Because the stress circles at failure must also be tangent to the yield surface (or the yield locus, YL in Figure 2), it is then necessary for the yield surface to change in size as the principal stresses vary in the flowing medium (unless the yield locus coincides with the effective yield locus, i.e., no cohesive strength).

The linear Mohr-Coulomb yield locus together with a stress circle at failure are given in Figure 3. It is apparent from the geometry that the angle between the failure planes and the direction of the major principal stress is

$$\mu = 45^\circ - \phi/2 \quad (2)$$

The locus of points (in a plane) lying on the failure planes are called sliplines.

For the axially symmetric subsidence problem, it is convenient to work in the meridian plane and use either rectangular

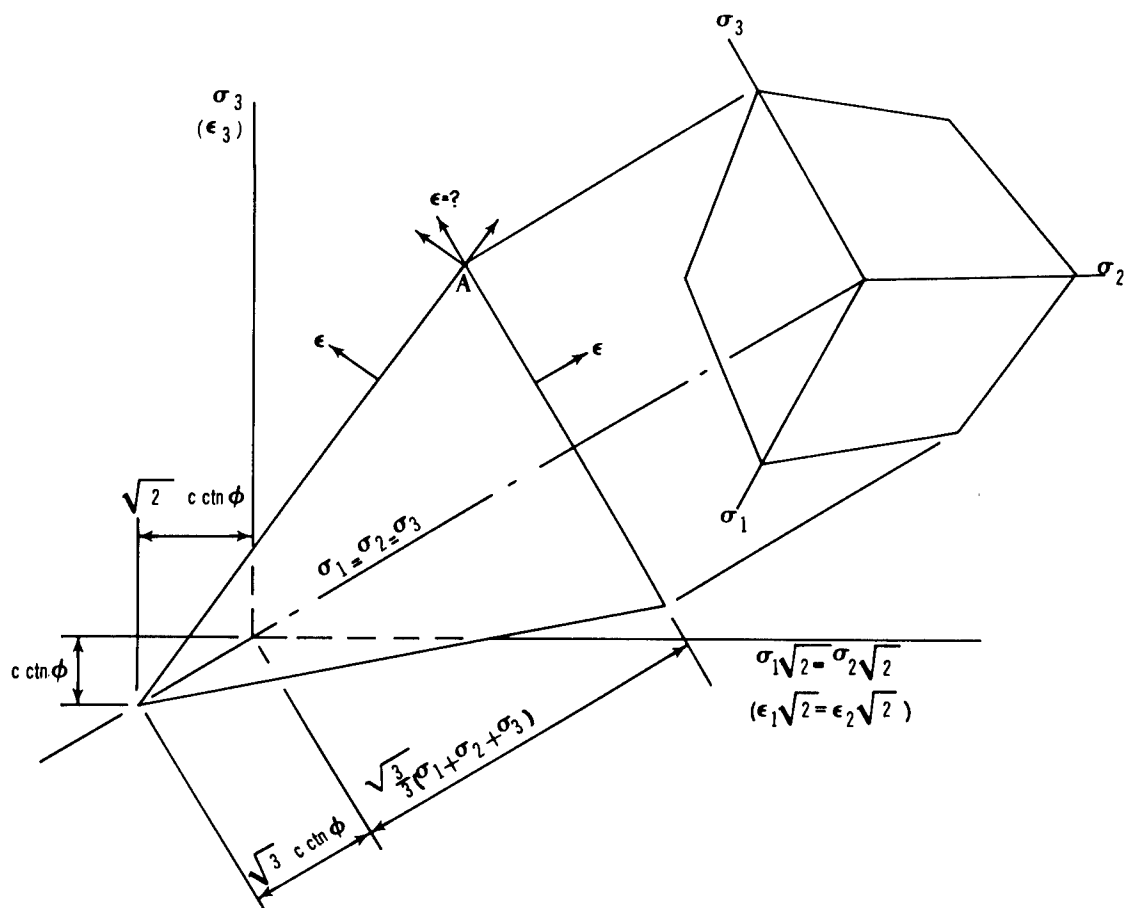


FIGURE 1. YIELD SURFACE IN PRINCIPAL STRESS SPACE

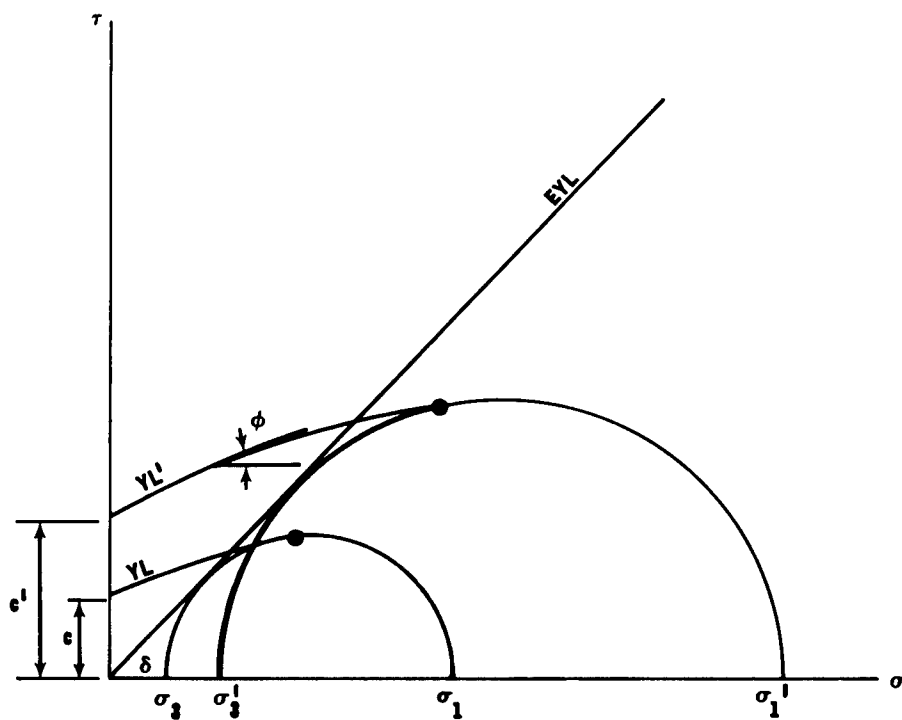


FIGURE 2. CHANGE OF YIELD LOCUS (YL) WITH CONSOLIDATION PRESSURE

or polar (or spherical) coordinates. Figure 4 shows these coordinate systems in the meridian plane.

The yield criterion in Figure 3 can be expressed as

$$\frac{1}{4} (\sigma_r - \sigma_\theta)^2 + \tau_{r\theta}^2 = \frac{\sin^2 \phi}{4} (\sigma_r + \sigma_\theta + 2\psi)^2, \quad (3a)$$

or

$$\frac{1}{4} (\sigma_x - \sigma_y)^2 + \tau_{xy}^2 = \frac{\sin^2 \phi}{4} (\sigma_x + \sigma_y + 2\psi)^2, \quad (3b)$$

where $\psi = c \cot \phi$.

Fundamental Relations

The two non-trivial differential equations of equilibrium for the stress state shown in Figure 5 expressed in spherical coordinates are (Sokolnikoff, 1956):

$$\frac{\partial \sigma_r}{\partial r} + \frac{1}{r} \frac{\partial \tau_{r\theta}}{\partial \theta} + \frac{1}{r} \left[2\sigma_r - \sigma_\theta - \sigma_\alpha + \tau_{r\theta} \cot \theta \right] + \gamma \cos \theta = 0, \quad (4a)$$

$$\frac{\partial \tau_{r\theta}}{\partial r} + \frac{1}{r} \frac{\partial \sigma_\theta}{\partial \theta} + \frac{1}{r} \left[(\sigma_\theta - \sigma_\alpha) \cot \theta + 3\tau_{r\theta} \right] - \gamma \sin \theta = 0,$$

where

$\sigma_r, \sigma_\theta, \sigma_\alpha, \tau_{r\theta}$ = stress components

r, θ, α = spherical coordinates

γ = density of medium.

If expressed in rectangular coordinates.....

$$\frac{\partial \sigma_x}{\partial x} + \frac{\partial \tau_{xy}}{\partial y} + \frac{\tau_{xy}}{y} = \gamma \quad (4b)$$

$$\frac{\partial \tau_{xy}}{\partial x} + \frac{\partial \sigma_y}{\partial y} + \frac{\sigma_y - \sigma_\alpha}{y} = 0.$$

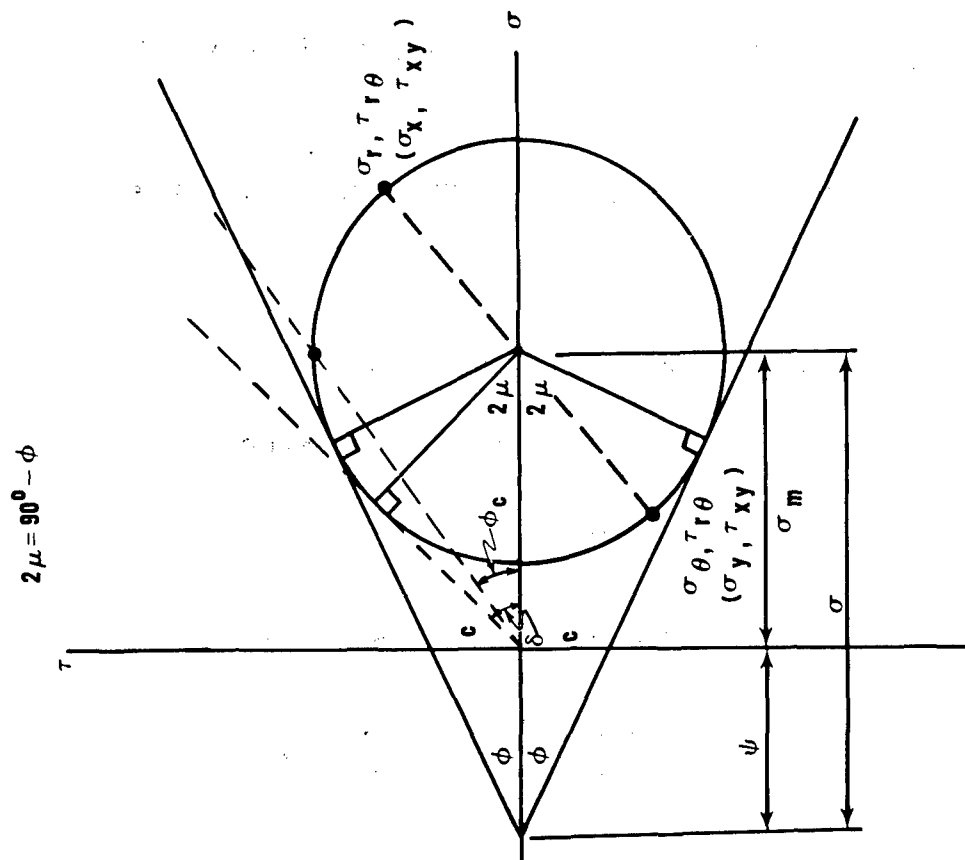


FIGURE 3. MOHR-COULOMB YIELD CRITERION

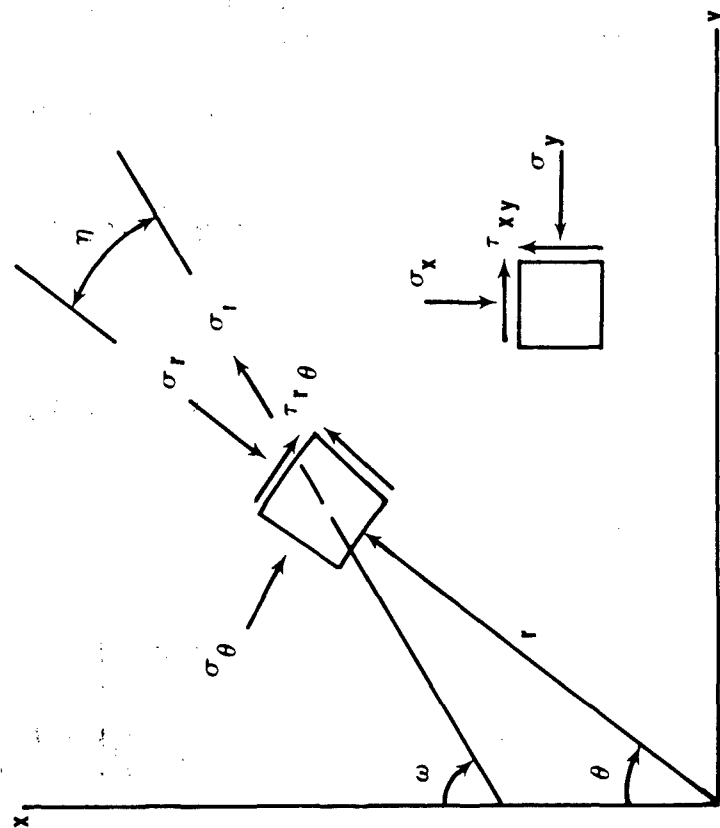


FIGURE 4. COORDINATE SYSTEMS IN MERIDIAN PLANE

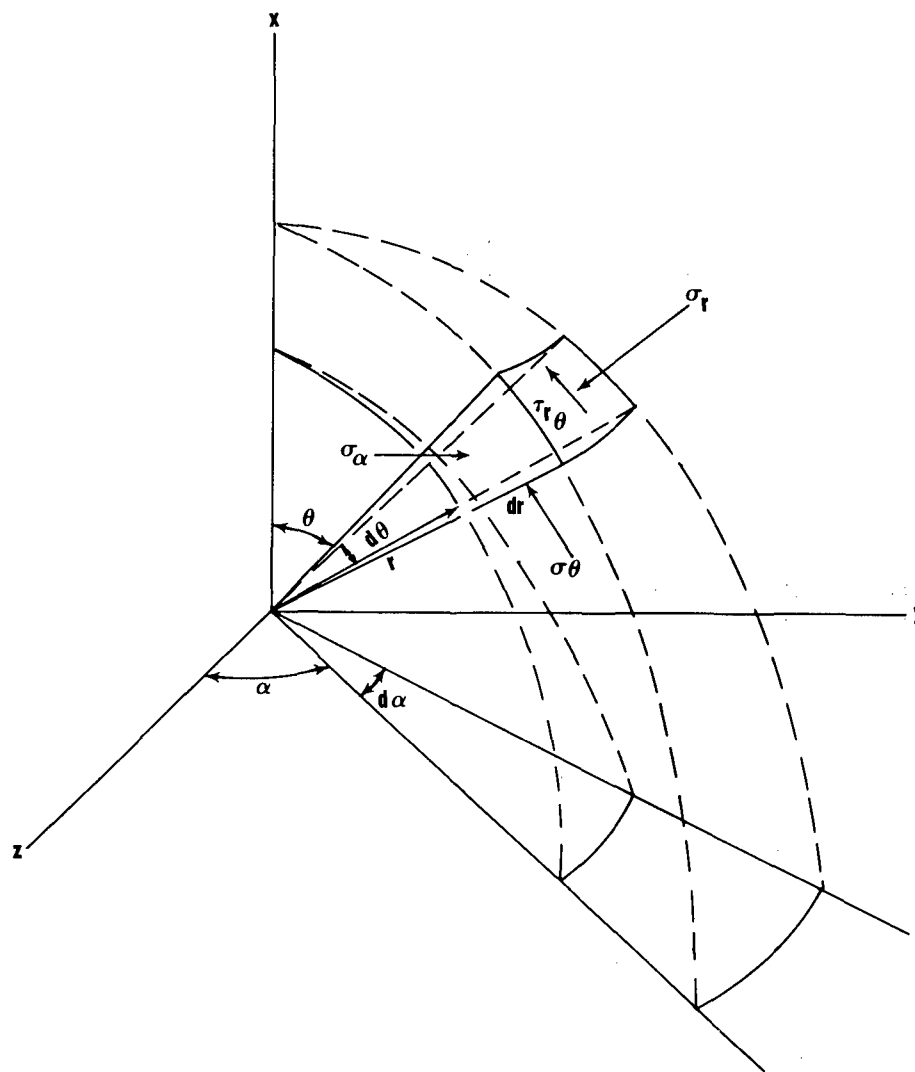


FIGURE 5. EQUILIBRIUM OF AN ELEMENT IN AXIALLY SYMMETRIC FLOW (SPHERICAL COORDINATES)

Assuming that every point in the collapsing material is in a state of limiting equilibrium, relations (3) and (4) provide three equations containing five unknowns (σ_r , σ_θ , σ_α , τ_{xy} , γ). During flow of bulk solids, Jenike (1961) found by experiment that the density could be expressed as a function of the mean stress in the meridian plane, $\sigma_m = (\sigma_r + \sigma_\theta)/2 = (\sigma_x + \sigma_y)/2$, i.e.,

$$\gamma = \gamma_0(1 + \sigma_m)^\beta \quad (5a)$$

where γ_0 and β are constants for a given material. If σ_m is expressed in pounds per square foot (psf), then Jenike found that β did not exceed .10 for any material that he tested. One would anticipate greater density changes than this for media containing large blocks. However, it can still be assumed that γ is a function of the mean stress, i.e.,

$$\gamma = \gamma_0 f(\sigma_m) \quad (5b)$$

The remaining relation is found from the Haar-von Karman hypothesis, which states that the circumferential stress, σ_α , is equal to the major principal stress in converging flow,

$$\sigma_\alpha = \sigma_1 \quad (\text{converging flow}), \quad (6a)$$

and the equal to the minor principal stress in diverging flow,

$$\sigma_\alpha = \sigma_3 \quad (\text{diverging flow}) \quad (6b)$$

Subject to the boundary conditions, it is theoretically possible to solve the subsidence problem from relations (3), (4), (5), and (6). The number of variables in these relations can be reduced by the substitution

$$\sigma = \psi + \sigma_m \quad (7)$$

If ω is the angle between the vertical axes and the direction of the major principal stress (Figure 4), the stresses at failure can be expressed as (see Figure 3)

$$\begin{aligned}
\sigma_x &= \sigma(1 + \sin\phi \cos 2\omega) - \psi, \\
\sigma_y &= \sigma(1 - \sin\phi \cos 2\omega) - \psi, \\
\sigma_\alpha &= \sigma(1 + \sin\phi) - \psi, \\
\tau_{xy} &= \sigma \sin\phi \sin 2\omega.
\end{aligned} \tag{8}$$

Replacement of ω by η results in similar relations for σ_r , σ_θ , and $\tau_{r\theta}$ (see Figure 4).

Characteristics

The stress characteristics (lines along which an infinity of solutions are possible) can be found by substituting equations (8) into (4b):

$$\begin{aligned}
(1 + \sin\phi \cos 2\omega) \frac{\partial \sigma}{\partial x} + \sin\phi \sin 2\omega \frac{\partial \sigma}{\partial y} - 2\sigma \sin\phi \sin 2\omega \frac{\partial \omega}{\partial x} \\
+ 2\sigma \sin\phi \sin 2\omega \frac{\partial \omega}{\partial y} = \gamma - \frac{\sigma}{y} \sin\phi \sin 2\omega, \\
\sin\phi \sin 2\omega \frac{\partial \sigma}{\partial x} + (1 - \sin\phi \cos 2\omega) \frac{\partial \sigma}{\partial y} + 2\sigma \sin\phi \cos 2\omega \frac{\partial \omega}{\partial x} \\
+ 2\sigma \sin\phi \sin 2\omega \frac{\partial \omega}{\partial y} = \frac{\sigma}{y} \sin\phi (1 + \cos 2\omega).
\end{aligned} \tag{9}$$

Sokolovsky (1960) found it convenient to define the quantity

$$S = \frac{\cot \phi}{2} \ln \frac{\sigma}{\sigma_0}, \tag{10}$$

where σ_0 is an arbitrary stress. Therefore,

$$\begin{aligned}
\frac{\partial \sigma}{\partial x} &= 2\sigma \tan \phi \frac{\partial S}{\partial x}, \\
\frac{\partial \sigma}{\partial y} &= 2\sigma \tan \phi \frac{\partial S}{\partial y}.
\end{aligned} \tag{11}$$

After replacement in equations (9) and some algebraic and trigonometric manipulations, the equilibrium equations become

$$\begin{aligned}\frac{\partial(S+\omega)}{\partial x} + \frac{\partial(S+\omega)}{\partial y} \tan(\omega+\mu) &= A, \\ \frac{\partial(S-\omega)}{\partial x} + \frac{\partial(S-\omega)}{\partial y} \tan(\omega-\mu) &= B,\end{aligned}\quad (12)$$

where

$$\begin{aligned}A &= \frac{\gamma \sin(\omega-\mu)}{2\sigma \sin\phi \cos(\omega+\mu)} + \frac{\cos(\omega+\mu) + \cos(\omega-\mu)}{2\gamma \cos(\omega+\mu)}, \\ B &= \frac{\gamma \sin(\omega+\mu)}{2\sigma \sin\phi \cos(\omega-\mu)} + \frac{\cos(\omega-\mu) + \cos(\omega+\mu)}{2\gamma \cos(\omega-\mu)}.\end{aligned}$$

Since

$$d(S\pm\omega) = \frac{\partial(S\pm\omega)}{\partial x} dx + \frac{\partial(S\pm\omega)}{\partial y} dy, \quad (13)$$

the four equations [(12), (13)] can be solved for the derivatives, $\partial(S\pm\omega)/\partial x$, $\partial(S\pm\omega)/\partial y$. It is found that these derivatives have an infinity of solutions when

$$\frac{dy}{dx} = \tan(\omega\pm\mu), \quad (14)$$

and the two families of curves defined by these slopes are called the stress characteristics. Thus, the stress characteristics coincide with the sliplines for incipient failure (see Figure 4).

During flow (assuming the validity of equation (1)) the stress characteristics have the slopes,

$$\frac{dy}{dx} = \tan\left[\omega\pm(45-\delta/2)\right], \quad (15)$$

and, in general, do not coincide with the sliplines.

The velocity field for steady flow is also found by determining its characteristics. If u and v are the velocity components in the x and y directions, respectively, the continuity equation for axi-symmetric flow becomes

$$\frac{\partial}{\partial x} (\gamma u y) + \frac{\partial}{\partial y} (\gamma v y) = 0 \quad . \quad (16)$$

After differentiating,

$$\frac{\partial u}{\partial x} + \frac{\partial v}{\partial y} + \frac{v}{y} + \frac{1}{\gamma} \left(u \frac{\partial \gamma}{\partial x} + v \frac{\partial \gamma}{\partial y} \right) = 0 \quad . \quad (17)$$

Assuming the collapsing medium to be isotropic requires that the directions of the principal strain rates coincide with those of the principal stresses. Since the normal strain rates (ϵ_x, ϵ_y) and the shear strain rates (ϵ_{xy}) are given by

$$\epsilon_x = \frac{\partial u}{\partial x}, \quad \epsilon_y = \frac{\partial v}{\partial y}, \quad \epsilon_{xy} = \frac{\partial u}{\partial y} + \frac{\partial v}{\partial x}, \quad , \quad (18)$$

then

$$\tan 2\omega = \frac{\frac{\partial u}{\partial y} + \frac{\partial v}{\partial x}}{\frac{\partial u}{\partial x} - \frac{\partial v}{\partial y}} \quad . \quad (19)$$

Equations (17) and (19) together with the total differentials du and dv , are solved for the derivatives, $\partial u/\partial x, \partial u/\partial y, \partial v/\partial x, \partial v/\partial y$. It is found that the characteristic directions are defined by the slopes

$$\frac{dy}{dx} = \tan (\omega \pm 45^\circ) \quad . \quad (20)$$

The velocity characteristics are orthogonal and coincide with the stress characteristics only if ϕ or $\delta = 0$. Coincidence with the sliplines occurs only when $\phi = 0$.

The above analyses show that the stress field can be computed independently of the velocity field.

Because of the isotropic requirement, the lines of maximum shear strain rate coincide with velocity characteristics. Physical conditions dictate that a line of infinite shear strain rate is possible only if the cohesion and internal friction are fully mobilized. Thus, lines of infinite shear strain rates must coincide with the sliplines. These lines are referred to as velocity discontinuities. A velocity discontinuity also includes jumps in the velocity magnitude.

The continuity equation in spherical coordinates is

$$\frac{\partial}{\partial r} \left[\gamma u_r r (\sin \theta) \right] + \frac{\partial}{\partial \theta} \left[\gamma u_\theta (r \sin \theta) \right] = 0 \quad , \quad (21)$$

while the isotropic condition is

$$\tan 2\eta(r, \theta) = \frac{\frac{\partial u_r}{r \partial \theta} + \frac{\partial u_\theta}{\partial r} - \frac{u_\theta}{r}}{\frac{\partial u_r}{\partial r} - \frac{u_r}{r} - \frac{\partial u_\theta}{r \partial \theta}} \quad . \quad (22)$$

For radial flow, $u_\theta = 0$, and the equations above reduce to:

$$r \frac{\partial u_r}{\partial r} + \left(2 + \frac{r}{\gamma} \cdot \frac{\partial \gamma}{\partial r} \right) u_r = 0 \quad , \quad (23)$$

$$\frac{\partial u_r}{\partial \theta} + \left(-r \frac{\partial u_r}{\partial r} + u_r \right) \tan 2\eta = 0 \quad . \quad (24)$$

Jenike (1961) has shown that the solution to these equations requires that η be only a function of θ , i.e.,

$$\eta = \eta(\theta) \quad . \quad (25)$$

Jenike has also shown that the radial velocity is zero and the rate of change of velocity with respect to θ is zero or infinite when $\eta = \pi/4, 3\pi/4$. Thus it is unlikely that a flow channel will develop beyond these limits. Observations of flow seem to verify this hypothesis. These limits happen to be velocity characteristics.

Radial Stress Fields

The equilibrium equations (4a) in spherical coordinates are useful in examining the stress state. Assuming the origin at the vertex of a converging flow channel, Jenike (1961) assumes that the mean stress (during flow, $\sigma_m = \sigma$) can be expressed as

$$\sigma = r \gamma(r, \theta) s(r, \theta) \quad . \quad (26)$$

Because a variable density has little influence on the results, $\gamma = \gamma_0$. Using analytical arguments and experimental observations of flow, Jenike finds that s is independent of r . Thus,

$$\sigma = r \gamma_0 s(\theta) \quad . \quad (27)$$

This result means that σ is linearly proportional to r along a ray from the vertex. This is called a radial stress field since it is compatible with a radial velocity field.

It is obvious that equation (27) is not valid up to a stress-free boundary. However, Johanson (1964) has shown that this stress field is valid to the near vicinity of such a boundary.

The limits placed on the boundaries of the flow channel by the radial velocity field require the walls of the channel to be both a velocity characteristic and a slipline. This requires that the wall yield locus pass through the point of maximum shear stress (see Figure 3). Therefore, the angle of friction at the wall (ϕ_c) must be lower than the effective angle of friction (δ), or (see Figure 3)

$$\tan \phi_c = \sin \delta \quad . \quad (28)$$

From numerical solutions of the stress and velocity fields, Jenike found that the angle of the flow channel cannot exceed the values in Table I.

TABLE I

δ	=	30°	40°	50°	60°	70°
Max. θ_c	=	15°	8.1°	4.4°	2.2°	0.5°

The values of δ in this table cover the normal range encountered in bulk solids.

Arching or Doming

Jenike and Leser (1963) determined the lower bound for the dimensions of an outlet opening that would prevent the formation

of a stable dome in the flow channel. This "critical" opening size, expressed in terms of the cavity radius, R_C , is given by

$$(R_C)_d = J(\theta_C) C_0/2\gamma \quad , \quad (29)$$

where C_0 is the unconfined compressive strength of the medium, and $J(\theta_C)$ depends upon the angle of the flow channel. For the limits of the flow angle given in Table I, $J(\theta_C)$ varies from 2.00 to 2.25 (for circular outlets). Within the limits of the approximations,

$$(R_C)_d \cong C_0/\gamma \quad . \quad (30)$$

Piping or Chimneying

A common occurrence in the flow of bulk solids is for a vertical cylinder (or well) to develop within the material, a phenomenon known as "piping." Jenike and Yen (1963) have performed an analysis similar to that for doming, resulting in the relation (the symbols modified for the subsidence problems)

$$(R_C)_p = C_0 M(\phi)/2\gamma \quad , \quad (31)$$

where

$(R_C)_p$ = minimum cavity radius to prevent piping,

$M(\phi)$ = piping function.

For the typical range of ϕ values, equation (31) takes the range of values

$$(R_C)_p \cong (1.2 \text{ to } 6) C_0/\gamma \quad . \quad (32)$$

Comparison of equations (30) and (32) shows that, for most values of ϕ , if the cavity radius is large enough to prevent piping, then doming will not occur.

In a homogeneous material, one then might anticipate that for very small cavity radii (i.e., $R_C < \sim C_0/\gamma$) no subsidence crater would form. With increasing cavity radius, a transition zone in which piping or "normal" flow may exist is reached. A range in

slope angles might be expected. At cavity radii larger than that given in equation (32), the slope should reach a constant value.

Excessive Bulking

In geologic materials where doming does not take place, surface subsidence may still be prevented if the material increases in volume upon collapse (bulks) so that the volume of the cavity is accounted for before the chimney propagates to the surface. The ratio of the bulked volume to the initial volume is called the bulking factor, N . It was shown by Berry and Hakala* that the maximum height to which a conically-shaped chimney will rise (H) can be found from the cubic equation (see Figure 6):

$$\left(\frac{R_c}{H}\right)^3 - \frac{3}{2} \frac{N-1}{N+1} \left(\frac{R_c}{H}\right)^2 - \frac{N-1}{N+1} \tan\theta_c \left(\frac{R_c}{H}\right) - \frac{1}{2} \frac{N-1}{N+1} \tan^2\theta_c = 0 \quad (33)$$

This equation is valid for (1) $H < \text{depth of burial, DOB}$, if $\theta_c \geq 0$, and (2) $R_c/H > R_c/\text{DOB} > -\tan\theta_c$ if $\theta_c < 0$.

Subject to these inequalities, the maximum chimney height results when θ_c is negative. However, for most contained explosions, θ_c algebraically must be larger than about -8° in order for the chimney to reach the surface.

For a vertical flow channel (i.e., $\theta_c = 0^\circ$), the expression (33) reduces to the simple relation (horizontal chimney top)

$$\frac{R_c}{H} = \frac{3}{2} \left(\frac{N-1}{N+1} \right) \quad , \quad (34)$$

or

$$H = \frac{2}{3} \left(\frac{N+1}{N-1} \right) (R_c) \quad . \quad (35)$$

The bulking factor (N) is not a constant for a given material, but depends on the initial porosity of the medium, the particle size produced during the initial yielding, and probably the energy absorbed by the solids during collapse. In general, the bulking factors for rock will be much larger than for soil. This is due

*This work is contained in a classified report to the U.S. Atomic Energy Commission and is available to those with the proper access clearance and a need to know.

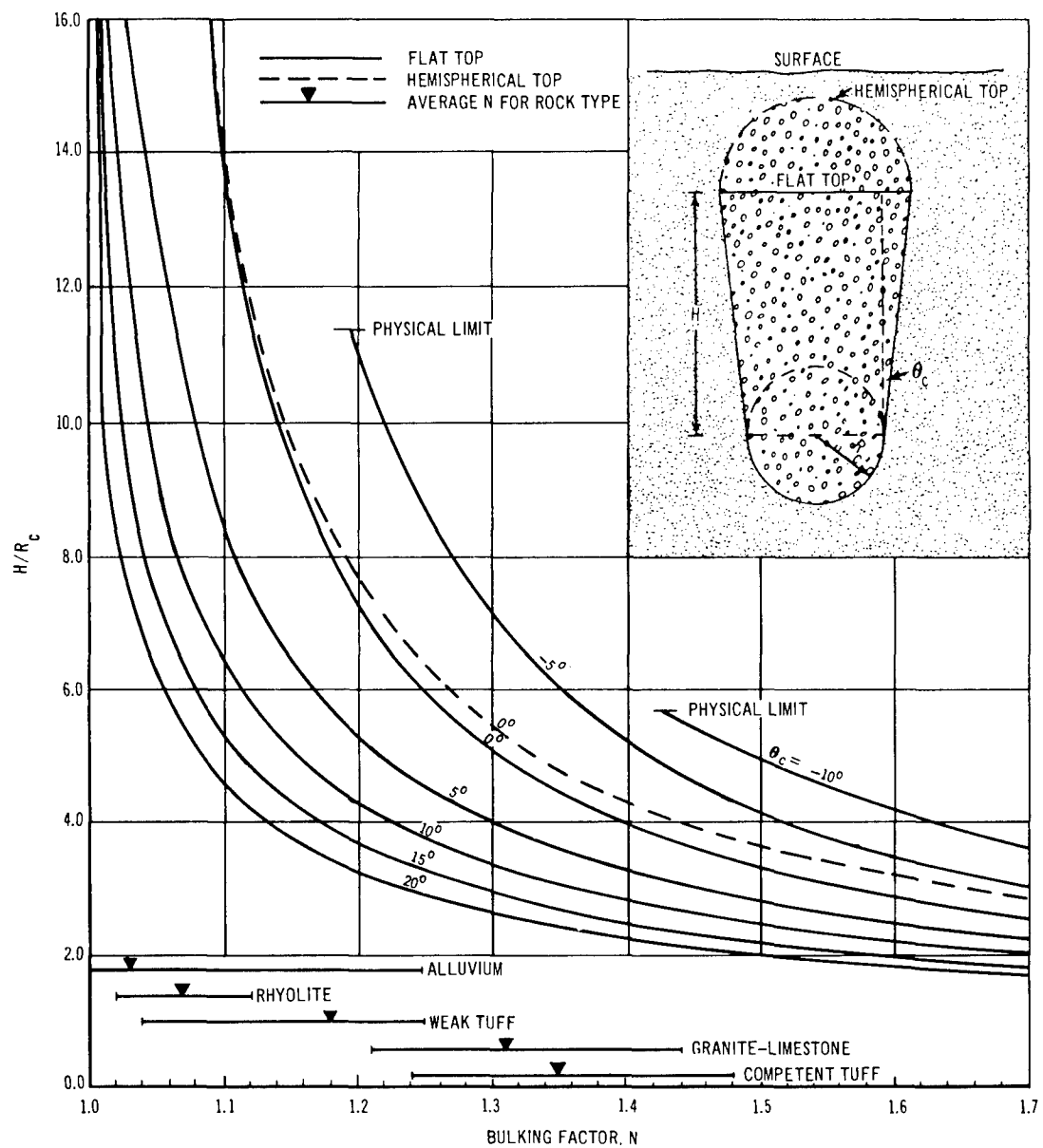


FIGURE 6. DIMENSIONLESS CHIMNEY HEIGHT AS A FUNCTION OF THE BULKING FACTOR

to the large fragments that are produced upon fracturing, resulting in a large percentage increase in the voids. Soils, on the other hand, have relatively lower bulking factors.

Graphical solutions of equation (33) are given in Figure 6. It can be seen that it is essential that an accurate value of N be found if the prediction of the chimney height for the excessive bulking condition is to be successful.

COMPARISON OF SUBSIDENCE AT THE NEVADA TEST SITE (NTS) WITH THEORY

A large number of contained underground nuclear detonation experiments have been conducted in the various test areas at the Nevada Test Site (NTS). Many of the explosions have produced subsidence craters, for which the cavity radius, and the radius, depth, volume, and time to collapse of the subsidence craters have been recorded. This information was compared with the theoretical principles discussed in the preceding sections. The assumed simplified geometry of a subsidence crater is shown in Figure 7. Very limited data are available for chimneys that do not reach the surface.

Subsidence Crater Radii

With the assumption of a conical-shaped chimney, the measured crater radius (R_{cr}) and cavity radius (R_c) can be used to compute the slope angle, (θ_c).

$$\tan \theta_c = \frac{R_{cr} - R_c}{DOB} \quad . \quad (36)$$

The procedures used in determining R_{cr} and R_c are given by Hakala.* Experimental verification of at least one conical-shaped chimney was found by Rawson and Rohrer.*

Values of θ_c obtained by equation (36) are plotted against the cavity radius in areas 2, 3, 9 and 10 at NTS in Figure 8. For classification purposes, the cavity radii have been reduced to dimensionless numbers. It appears that a tendency for piping (i.e., $\theta_c \approx 0^\circ$) exists for cavity radii less than about 1.0. For several events, θ_c is less than zero degrees. Numerous events with

*This work is contained in a classified report to the U.S. Atomic Energy Commission and is available to those with the proper access clearance and a need to know.

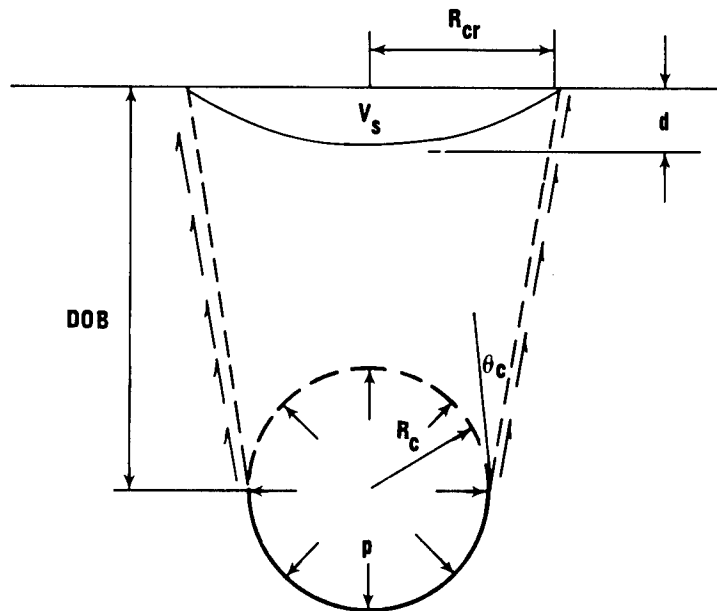


FIGURE 7. SUBSIDENCE CRATER GEOMETRY

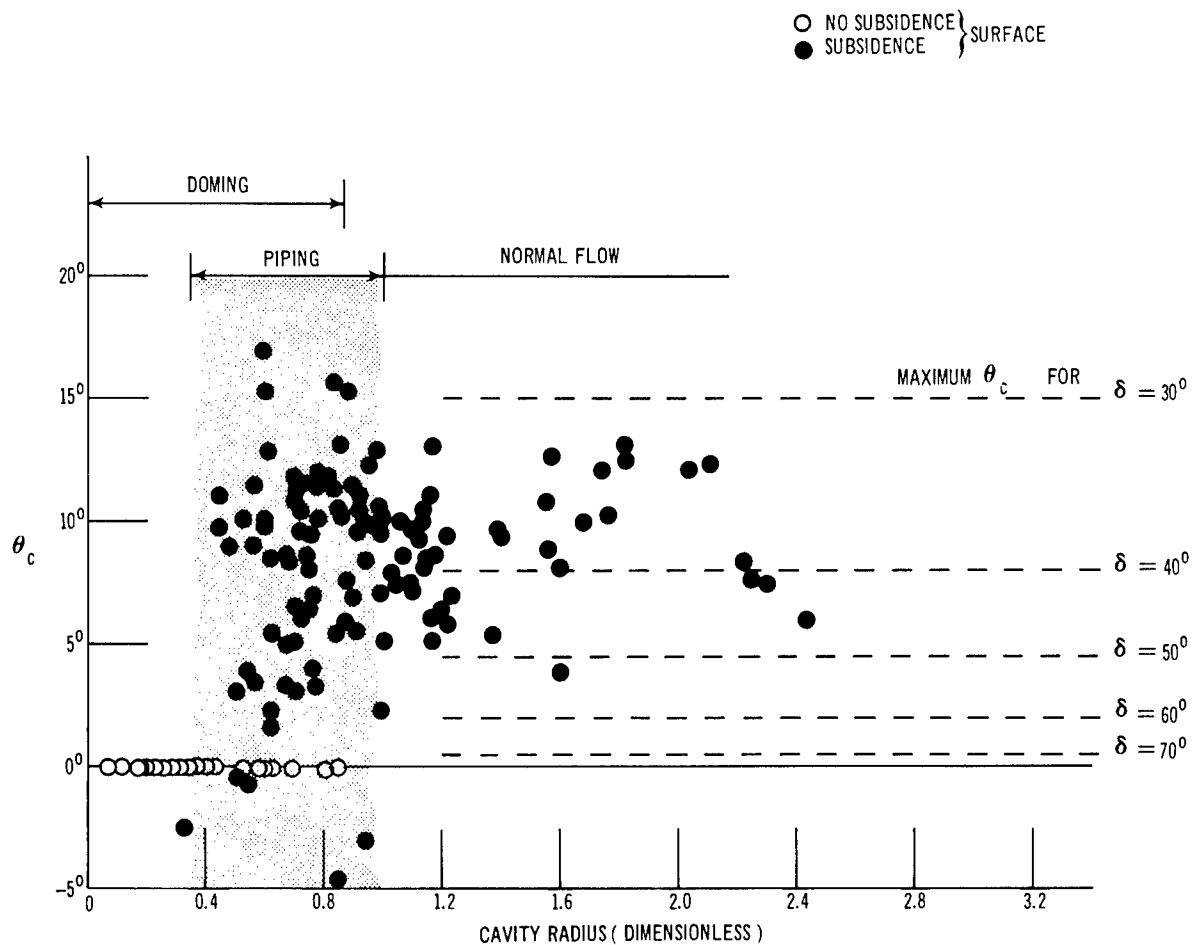


FIGURE 8 ANGLES OF FLOW CHANNEL (θ_c) vs CAVITY RADII IN ALLUVIUM IN AREAS 2, 3, 9, AND 10.

cavity radii less than about 0.6 (in all test areas) produce no surface subsidence, indicating the possibility of doming.

Approximate values of unconfined compressive strengths (C_0), as obtained from equations (30) and (32), are reasonable for the media being considered. A few observations of θ_c in rocks (not shown in Figure 8) indicate larger cavity radii at which piping results, which is to be expected for higher strength materials.

The scatter in Figure 8 is probably due to variations in the effective angle of friction, δ . However, almost all quantities lie within the theoretically predicted values for a normal range of δ (i.e., 30° - 70°), and all slope angles θ_c are less than 17° . There is a predominance of data points between $\delta = 30^\circ$ to 40° . This is less than the most common value of 50° observed for commercially handled materials (Johanson, 1964). [Jenike (1969) has recently found that the maximum slope angle for conical flow given in Table I can be exceeded for certain stress fields. Also, if the lower boundaries of the flow channel exceed the diameter of the cavity, this would appear in Figure 8 as larger θ_c 's for the smaller radii (since smaller radii are usually associated with shallow depths.)]

Assuming no doming or piping, if the value of δ is known, the slope angle (θ_c) can be found from Table I. The crater radius can then be predicted from (assuming R_c can be accurately predicted):

$$R_{cr} = R_c + DOB \tan \theta_c \quad . \quad (37)$$

Subsidence Crater Volumes

It was shown by Berry and Hakala* that the volume of a subsidence crater, V_{cr} , can be determined from

$$V_{cr} = \frac{2\pi}{3} DOB^3 (N + 1) \left(\frac{R_c}{DOB} \right)^3 - \frac{\pi}{3} DOB^3 (N - 1) \left[3 \left(\frac{R_c}{DOB} \right)^2 + \tan^2 \theta_c \left(\frac{R_c}{DOB} \right) + \tan^2 \theta_c \right] , \quad (38)$$

$$(V_{cr} \geq 0) ,$$

*This work is contained in a classified report to the U. S. Atomic Energy Commission and is available to those with the proper access clearance and a need to know.

which is based upon an assumed conical chimney above the cavity. Graphical solutions of Equation (38) are given in Figures 9 through 11. It is obvious from these curves that the crater volumes are very sensitive to the bulking factor, N , and to the angle of the flow channel, θ_c . These parameters, in turn, are functions of the material properties.

Berry and Hakala* used the measured values of V_{cr} and θ_c and relation (38) to evaluate bulking factors for the various test areas. The results are plotted in Figure 12 as a function of a dimensionless cavity radius. Figure 12 indicates that the computed bulking factor decreases with increasing cavity radius, approaching an asymptotic value of about unity at a cavity radius of approximately 1.0. (Bulking factors less than unity are unlikely in dense materials. Errors in volumes of craters, cavity radii, etc, would contribute to the scatter.)

A flow channel having $\theta_c = 0^\circ$ is the boundary between converging and diverging flow. Because there is a tendency for the intermediate principal stress (σ_α) to fluctuate between σ_1 and σ_3 under these conditions [see equations (6)], the flow is erratic and unsteady. This could produce variations in the bulking factors and, in general, give larger bulking factors. A cavity radius of about 1.0 does seem to agree with the upper limit of piping in Figure 8.

Subsidence Crater Depths

If the shape of the profile of a subsidence crater is known, the maximum depth of the crater, d , can be determined from a knowledge of the volume (V_{cr}) and the radius (R_{cr}).

For radial flow, Jenike (1961) found that the velocity u_r in an incompressible medium under axially symmetric conditions was

$$u_r = u_r^0 e^{-3 \int_0^\theta \tan 2\eta \, d\theta}, \quad (39)$$

where u_r^0 is the velocity along the axis of symmetry. Although the velocity field may not be unique, Equation (39) indicates that the radial velocity decreases from the axis of symmetry

*This work is contained in a classified report to the U. S. Atomic Energy Commission and is available to those with the proper access clearance and a need to know.

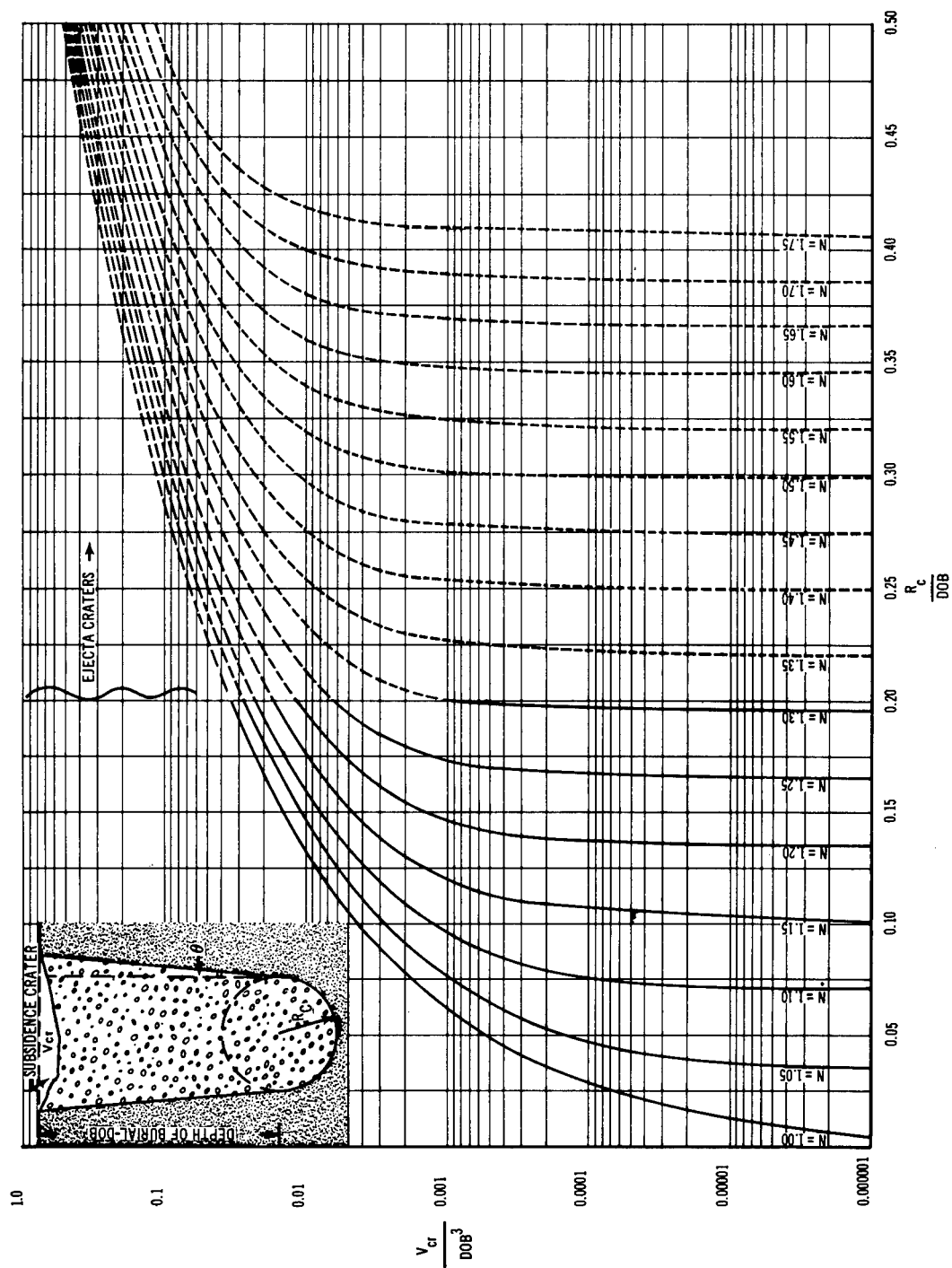


FIGURE 9. DIMENSIONLESS PLOT OF SUBSIDENCE CRATER VOLUMES ($\theta_c = 0^\circ$)

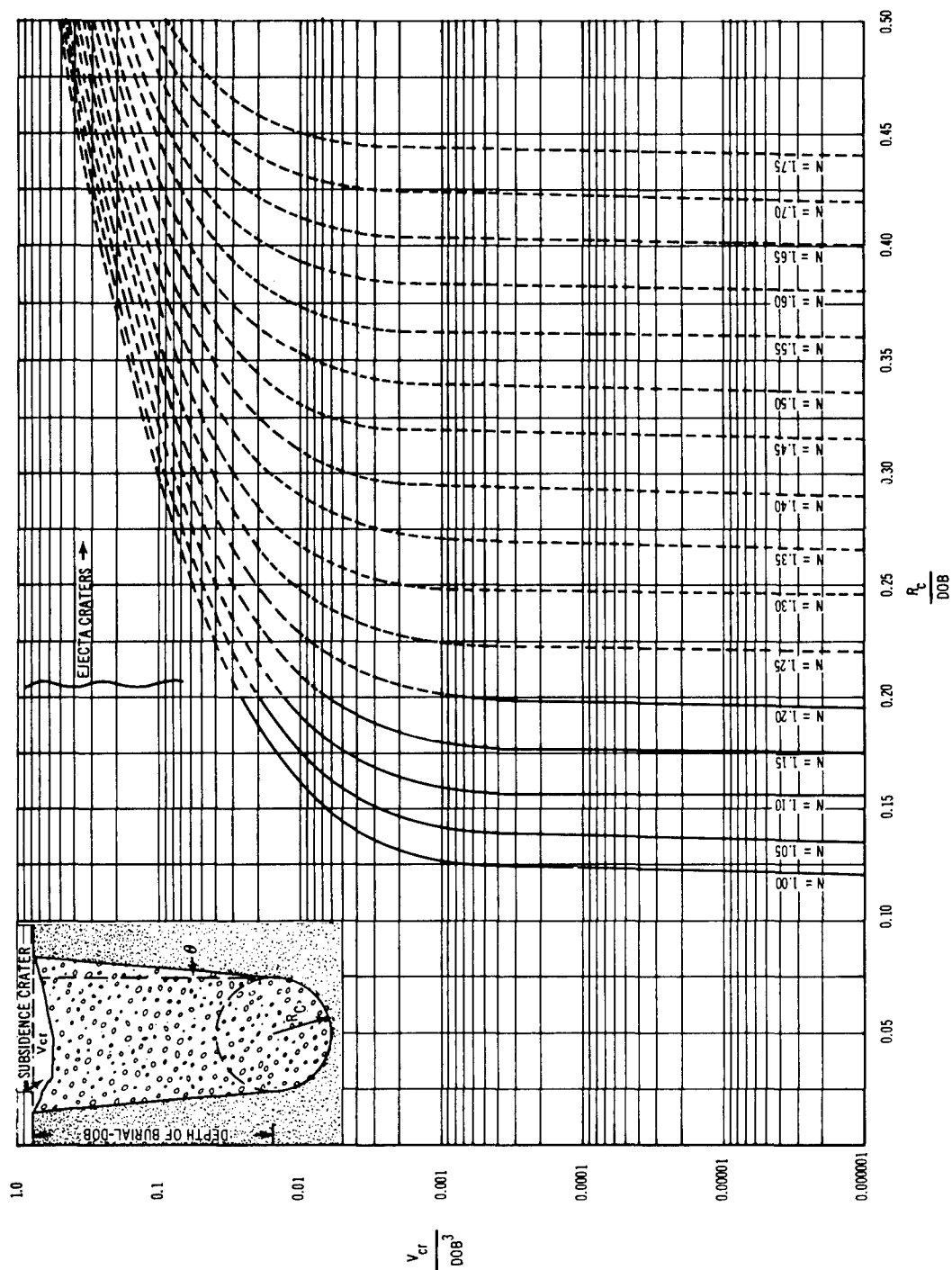


FIGURE 10. DIMENSIONLESS PLOT OF SUBSIDENCE CRATER VOLUMES ($\theta_c = 5^\circ$)

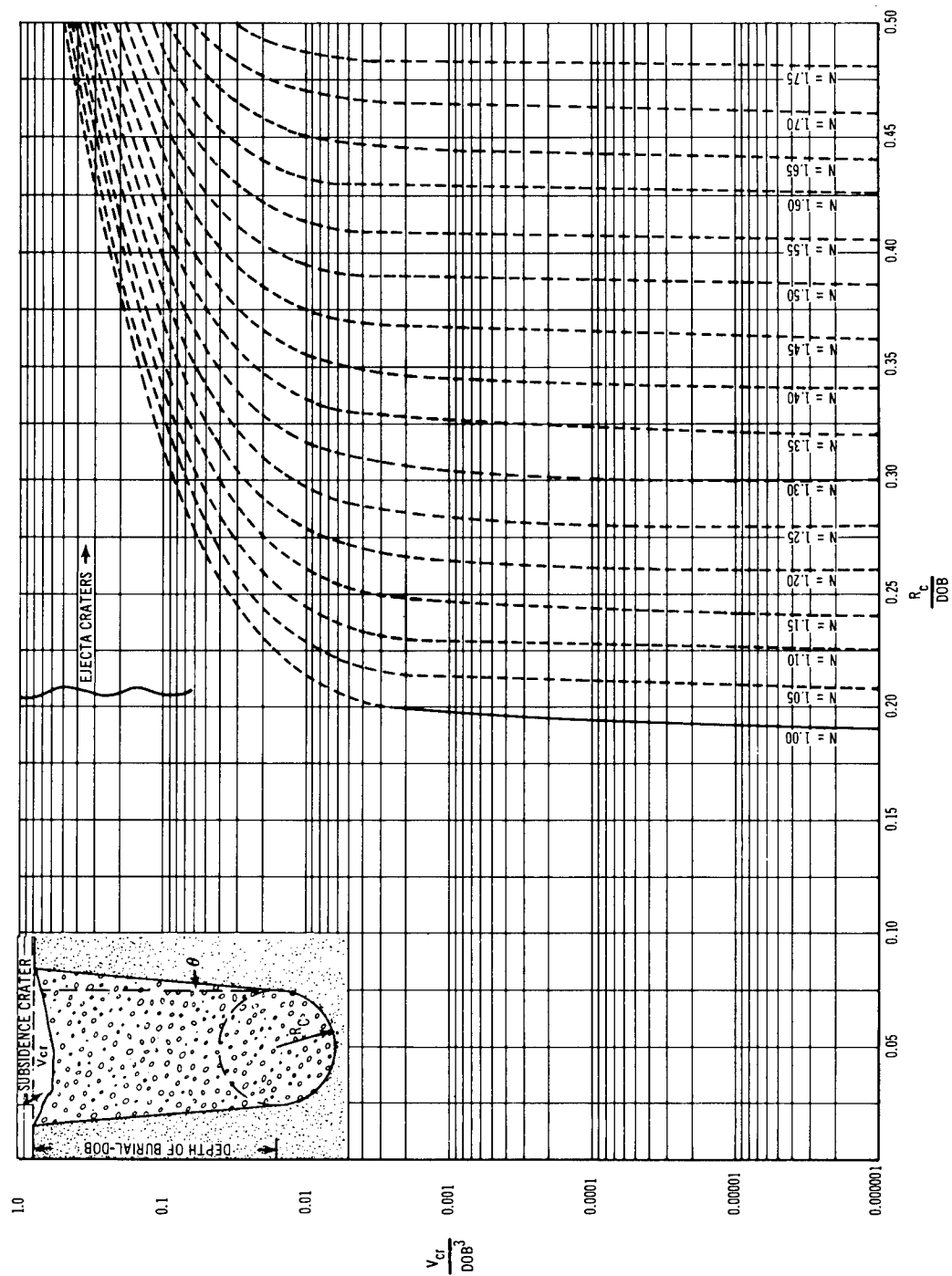


FIGURE 11. DIMENSIONLESS PLOT OF SUBSIDENCE CRATER VOLUMES ($\theta_c = 10^\circ$)

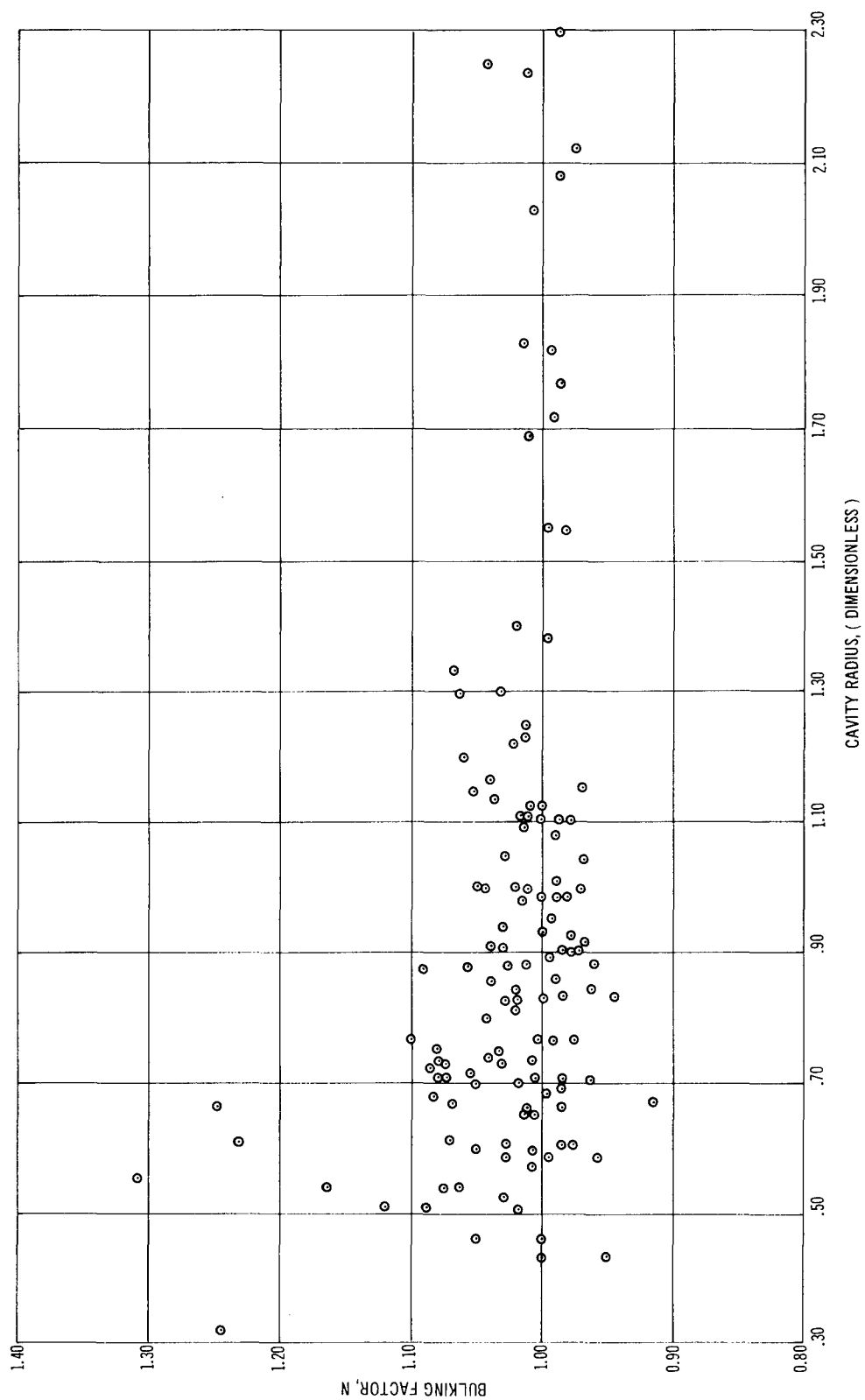


FIGURE 12. BULKING FACTORS FOR CHIMNEYS IN ALLUVIUM, AREAS 2, 3, 9, AND 10, NTS

toward the walls of the flow channel. (Cases do exist where a cylinder of material drops intact as a "plug.")

An approximate value for the maximum crater depth can be found from the relation:

$$d = \frac{m V_{cr}}{\pi R_{cr}^2} , \quad (40)$$

where $V_{cr} = V_{cr} (DOB, R_c, \theta_c, N)$, $R_{cr} = R_{cr} (DOB, R_c, \theta_c)$, and m is a shape factor defining the profile. Restricting the crater profile to be concave upward, m can vary within the range, $1 < m < 3$ (for a cylinder, $m = 1$; paraboloid, $m = 2$; cone, $m = 3$). For craters at the Nevada Test Site, it has been found that m decreases with increasing depths of burial (DOB) (Hakala, 1968).* [Using a stochastic model, Sweet and Bogdanoff (1965) determined that the profile for a small subsidence should be V-shaped in a dimensional model of a cohesionless soil, which was verified in laboratory tests.]

Substituting equations (37) and (38) into (40) gives

$$d = \frac{m DOB}{3 \left[\frac{R_c}{DOB} + \tan \theta_c \right]^2} \left\{ 2(N+1) \left(\frac{R_c}{DOB} \right)^3 - 3(N-1) \left(\frac{R_c}{DOB} \right)^2 \right. \\ \left. - 2(N-1) \tan \theta_c \left(\frac{R_c}{DOB} \right) - (N-1) \tan^2 \theta_c \right\} , \quad (41) \\ (d \geq 0) .$$

If the cavity radius is large enough to prevent piping, and $R_c/DOB \approx \tan \theta_c$, then for this case

$$d = \frac{m DOB}{12} \left\{ 2(N+1) \left(\frac{R_c}{DOB} \right) - 6(N-1) \right\} . \quad (42)$$

Making the additional assumption that the bulking factor (N) is near unity,

$$d \approx \frac{m}{3} (R_c) . \quad (43)$$

*This work is contained in a classified report to the U.S. Atomic Energy Commission and is available to those with the proper access clearance and a need to know.

Thus, the crater depth for low-bulking materials should lie in the range

$$\frac{1}{3} R_c < d < R_c \quad . \quad (44)$$

For craters that are concave upward, relation (44) has been verified (Hakala*).

Collapse Times

As discussed earlier, flow in vertical or nearly vertical channels is erratic because of the fluctuation of the circumferential stress. Jenike (1961) has also shown that zones of zero velocity are possible in steep flow channels if the velocity characteristics and sliplines do not coincide. It would then be anticipated that collapse times associated with subsidence in axially symmetric flow would be subject to large variations.

Approximate analyses by Hakala* have also shown the extreme sensitivity of the collapse time to the physical and mechanical properties of the medium. These analyses show that for a given scaled burial depth the time to collapse should increase with the size of the cavity. Although large deviations from a mean curve were found, there is a general increase in the collapse time as the cavity radius, yield of the explosion, and the depth of burial increases. (In general, all three of these parameters increase simultaneously.)

CONCLUSIONS

The subsidence associated with the collapse of an underground spherical cavity has been considered. Although the subsidence for many events has been controlled by geologic imperfections (faults, lineaments, etc.), most of the subsidence at NTS involves axially-symmetric conditions.

The fundamental equations and many of the concepts from bin-flow theory are applicable to the subsidence problem considered here. However, a knowledge of the strength properties, flow properties, and bulking characteristics is essential for the accurate prediction of subsidence values.

*This work is contained in a classified report to the U.S. Atomic Energy Commission and is available to those with the proper access clearance and a need to know.

REFERENCES

- Jenike, A. W., and Shield, R. T., "On the Plastic Flow of Coulomb Solids Beyond Original Failure," J. of Appl. Mech., V. 26, Trans. ASME, V. 81, Series E, December 1959, pp. 599-602.
- Jenike, A. W., Elsey, P. J., and Woolley, R. H., "Flow Properties of Bulk Solids," Proc. ASTM, 60, 1960, pp. 1168-1181.
- Jenike, A. W., "Gravity Flow of Bulk Solids," Bull. No. 108, Utah Engineering Experiment Station, October 1961.
- Jenike, Andrew W., and Yen, Bing Chen, "Slope Stability in Axial Symmetry," Proc. 5th Symp. on Rock Mech., Univ. of Minnesota, May, 1962, pp. 689-711.
- Jenike, Andrew W., and Leser, Tadeusz, "A Flow- No-Flow Criterion in the Gravity Flow of Powders in Converging Channels," 4th Int. Conf. Congress on Rheology, Brown Univ., August 1963, pp. 125-141.
- Jenike, Andrew W., Personal Communication, January 22, 1969.
- Johanson, J. R., "Stress and Velocity Fields in the Gravity Flow of Bulk Solids," J. of Appl. Mech., V. 31, Trans. ASME, V. 86, Series E., September 1964, pp. 499-506.
- Sokolnikoff, I. S., "Mathematical Theory of Elasticity," 2nd Edition, McGraw-Hill Book Company, Inc., 1956.
- Sokolovski, V. V., Statics of Soil Media, Butterworth's Scientific Publications, London, 1960.
- Sweet, Arnold L. and Bogdanoff, John L., "Stochastic Model for Predicting Subsidence," J. of the Engr. Mech. Div., ASCE, Vol. 91, No. EM2, Part 1, April, 1965, pp. 21-45.

Simulation of the Chemical Environment of a
Nuclear Explosion with Exploding Wires

Walter Meyer
Professor Nuclear Engineering
Kansas State University
Manhattan, Kansas

Oliver U. J. Block
NSF Trainee
Nuclear Engineering
Kansas State University

ABSTRACT

The chemical processes in an expanding underground cavity resulting from a nuclear explosion cannot be predicted or controlled as well as such physical characteristics as crater size, magnitude of the outgoing shock wave, or the extent of rock fracturing. However in most underground nuclear explosions it would be desirable to control the chemical and/or physical form and amount of radioactive fallout venting from the explosion.

The high temperatures and corresponding high energy densities produced by exploding wires are sufficient to produce in the wire and material immediately surrounding it the temperature (a few thousand degrees) required to simulate the chemical environment of a nuclear explosion in the time interval just preceding the venting of the cavity. The economics and the size of exploding wire apparatus make this type of experiment readily applicable to laboratory study.

Design of exploding wire circuits to obtain particular temperatures or energy densities can be completed using several different combinations of circuit and wire conditions. Since the circuit parameters, including charging voltage, capacitor bank capacitance and circuit inductance primarily determine the cost of the necessary laboratory equipment, these parameters should be selected by theoretical expressions while also considering economic factors. Wire parameters are then experimentally determined to produce the most energetic explosions with the selected circuit parameters.

A theoretical method applicable to designing exploding wire circuits to produce the desired high temperatures and energy densities in the wire and surrounding sample material has been obtained. The method assumes that a thermal spike of energy is deposited in a low conductivity material (typical of the earth's crust) surrounding the wire. From the assumed temperature distribution in the surrounding sample material the energy which must be deposited in the thermal spike to produce the desired temperature and energy density in a fixed amount of sample material can be calculated. The wire temperature corresponding to this energy is then calculated.

Assuming the maximum input power to the wire resistance (which is much greater than the resistance of the rest of the RLC circuit) is balanced by radiation energy losses from the wire, an estimate of the maximum temperature reached by the wire can also be obtained.

Experimental data show that about fifteen to forty percent of the energy initially stored in a capacitor bank is deposited in the wire before the wire bursts in the energetic type explosion needed to simulate the chemical environment of a nuclear explosion. Further, the experimental results show that if sufficient energy is available from the capacitor bank to satisfy the above efficiency constraint on energy transfer, then the circuit designed by the theoretical design method produces temperatures in the sample material within at least an order of magnitude of the design temperature.

Experimental results with bare wire explosions show that confining the wire after sufficient energy to vaporize the wire has been deposited will produce higher energy densities. A sample cell designed to make use of the magnetic pinch principle has been assembled and experimental results with it show that the cell does indeed confine the wire material while holding the sample material in close proximity around the wire.

1. Introduction

In most underground nuclear explosions it would be desirable to control the chemical and/or physical form and the amount of radioactive fallout venting from the explosion. Because of the size and expense of a nuclear explosion it would also be desirable to simulate the chemical effects of a nuclear explosion on a laboratory scale. Temperatures of a few thousand degrees are required to simulate the chemical environment of a nuclear explosion in the time interval just preceding the venting of the cavity. Meyer and Svensson of the Lawrence Radiation Laboratory have shown through experimental work that exploding wires can produce these temperatures in the wire and the material immediately surrounding the wire.¹ The economics and the size of exploding wire apparatus make this type of experiment readily applicable to laboratory study.

2. Exploding Wire Circuit Design

Exploding wire phenomena results from the deposition of a large amount of energy in a short period of time (microseconds or less) into a piece of metal of small cross sectional area. Design of exploding wire apparatus to produce the desired high energy densities in the wire and sample material must consider the energy source (e.g., capacitor bank), the circuit switch, the transmission lines, the wire, and the material surrounding the wire.

Design of exploding wire circuits to obtain particular temperatures can be completed using several different combinations of circuit and wire conditions. Since the circuit parameters (including charging voltage, capacitor bank capacitance and circuit inductance) primarily determine the cost of the necessary laboratory equipment, these parameters should be selected by theoretical expressions while also considering economic factors. Wire parameters are then experimentally determined to produce the most energetic explosions with the selected circuit parameters.

The thermal heating of the wire is described by the law of energy conservation which can be written as

$$(dU/dt) = P - \sigma \epsilon A T^4 - (dW/dt) - Q \quad (1)$$

where:

U is the internal energy in the wire,
P is the rate at which energy is deposited in the wire,
 $\sigma \epsilon A T^4$ is the radiative energy losses,
 dW/dt is the hydrodynamic energy losses, and
Q is the conductive and convective heat losses.

Thus, the amount of internal energy in the wire depends on the rate at which energy is deposited in the wire and the energy losses from the wire.

Assuming the capacitance, the resistance, and the inductance of the discharge circuit can be treated as lumped parameters, the discharge circuit is described by the circuit equation

$$L (di/dt) + R i + V_c = 0. \quad (2)$$

The inductance of the wire (L_w) is much less than the inductance of the remaining discharge circuit (L_c). Therefore, the inductance ($L = L_c + L_w$) is approximately equal to L_c . The discharge circuit is initially controlled by the RLC circuit parameters and the current rapidly increases. After a brief heating interval the resistance of the circuit is dominated by the wire resistance. Therefore R can be considered to be the wire resistance.

The high current density ($\sim 10^7$ to 10^{10} A/in²) heats the wire material to its melting point and the wire melts. The molten wire is heated further by the current which may be increasing or decreasing at this time. To discuss energetic wire explosions (necessary in simulating a nuclear explosion), let us consider only the increasing current case (Fig. 1). Since the entire exploding wire process occurs in microseconds or less, the physical shape of the wire is maintained by inertial and magnetic pressures. The wire continues to be heated by the current and reaches the normal boiling point near the current maximum. However pressure very significantly affects the boiling point and thus equilibrium boiling is not expected. Superheating occurs as the temperature of the wire rises past the atmospheric boiling point while the wire material is still in the liquid state.

At some time t_B , with the wire temperature above the normal boiling point, the voltage across the wire rapidly increases to a peak value and the wire (wholly or partially in a vapor state) actually explodes. Conduction through the metal ceases when the metal has expanded 2-5 times its initial diameter.²

With no current flowing there is no power input to the wire. Thus, in a wire explosion, it is only the energy added in the short time interval after the wire has exceeded the vaporization temperature but before it begins to expand that is effective in producing high temperatures ($\sim 10^6$ °K). The rate of radiative energy losses at high temperatures is of course very large ($\sim 10^{10}$ watts). Thus, high energy densities and high temperatures in the wire can only be obtained by depositing the energy from the electrical circuit very rapidly (in microseconds or less).

The maximum rate of energy delivery to the wire occurs if the wire is well matched to the circuit parameters. The wire is said to be well matched to the circuit parameters if the short time interval after the wire has exceeded the vaporization temperature but before it begins to expand occurs near the current peak (See Fig. 1). Bennett² has shown that a wire is well matched to the circuit parameters for an optimum mean value of wire resistance which satisfies the relation:

$$1.1 \leq R_{\text{opt}} (C/L)^{1/2} \leq 1.3 \quad (3)$$

The equations describing the exploding wire circuit could be solved analytically if the resistance, the cross sectional area, and the specific heat of the wire were constant. However these factors depend on the physical state of the wire, and for wire temperatures above the vaporization temperature they also depend on the rate of energy delivery to the wire. An equation of state is required for the different types of wire explosions if the equations are to be solved to obtain definite results. In addition, solutions of equations require as a corollary a relationship between resistance and the physical state of the wire. Neither an equation of state nor a quantitative relationship for the wire resistance is available. Thus a combined analytic and experimental approach must be used over limited temperature ranges and limited time intervals to solve the equations.

The wire resistance is calculated using the relation

$$R_w = \frac{V_w - L_w (di/dt)}{i} \quad (4)$$

where:

R_w is the wire resistance,
 V_w is the voltage across the wire,
 L_w is the inductance of the wire,
 i is the current through the wire, and
 (di/dt) is the time rate of change of current.

V_w , i , and (di/dt) are measured experimentally; L_w can be calculated from the physical properties of the wire.³

The energy deposited in the wire material at any time t after the start of the discharge of the capacitor bank can be computed by integrating the instantaneous power over the time interval from the start of the discharge until time t .

$$E_w = \int_0^t R_w i^2 dt' \quad (5)$$

Assuming the inductance of the wire is constant and substituting equation (4) into equation (5) gives

$$E_w = \left(\int_0^t V_w i dt' \right) - 1/2 L_w i^2(t). \quad (6)$$

Thus, the energy placed in the wire can be computed by integrating the product of the voltage and current, and subtracting the energy stored in the inductance of the wire gap at time t .

The internal energy of the wire is related to the temperature of the wire by the relation

$$\int_{U(T_0)}^{U(T)} dU' = \sum_{j=1}^n \lim_{\delta \rightarrow 0} \left[\int_{T_{j-1}+\delta}^{T_j-\delta} (dU'/dT) dT + \Delta U_j u(T-T_j) \right] + \lim_{\delta \rightarrow 0} \int_{T_n+\delta}^T (dU'/dT) dT \quad (7)$$

where:

T_0 is the initial temperature of the wire,
 T_j ; $j=1,2,\dots, n$ are transition temperatures,
 $U(T)$ is the internal energy and is a function of temperature,
 ΔU_j is the internal energy change at the j^{th} transition, and
 $u(T-T_j)$ is the unit step function.

An upper limit of the temperature reached by an exploding wire can be determined by equating the energy deposited in the wire with the change in internal energy of the wire. The energy deposited in the wire can be computed using equation (6). Substitution of this calculated energy into equation (7) and assuming no energy loss from the wire permits a determination of an upper temperature limit.

Another estimate of the maximum possible wire temperature is obtained by assuming the radiation energy losses are much greater than the conductive and convective energy losses. Also for fast energetic wire explosions the maximum temperature is reached before the hydrodynamic losses (dW/dt) become important. Therefore, for energetic explosions of interest in simulating the chemical environment of a nuclear explosion, equation (1) can be approximated by

$$(dU/dt) = P - \epsilon \sigma A T^4. \quad (8)$$

The maximum internal energy and the maximum temperature are reached when the rate of change of internal energy is zero ($dU/dt = 0$). Thus, from equation (8) the maximum power is

$$P_{\max} = \epsilon \sigma A T_{\max}^4. \quad (9)$$

Therefore to obtain high temperatures in an exploding wire it is necessary to have high peak powers and small radiating areas. An estimate of the maximum power, P_{\max} , delivered to a constant resistive load from an RLC circuit is⁴

$$P_{\max} = (V_0^2/2)(C/L)^{1/2}. \quad (10)$$

Substituting equation (10) into equation (9) and solving for T_{\max} gives

$$T_{\max} = [(C/L)^{1/2} (V_0^2/2 \epsilon \sigma A)]^{1/4}. \quad (11)$$

To obtain high temperatures in an exploding wire, therefore, it is necessary to have high initial charging voltage on the capacitor, appreciable capacitance, and low inductance.

To study the high temperature chemistry of the material surrounding an exploding wire, it is necessary to transfer the energy from the wire to the surrounding material. Little energy is lost from the wire material by any method other than radiation until after the wire bursts, and little energy is deposited in the wire after about one microsecond following the wire explosion. If energy is deposited instantaneously along a line, a thermal spike may be used to represent the system. Thus, the energy deposited in a system consisting of a thin

central wire and a low thermal conductivity surrounding medium, e.g., earth, can be represented by a thermal spike. If Q' is the energy released per unit length of wire, the temperature distribution in the surrounding medium is as follows⁵

$$T(r,t) = T_0 + (Q'/4\pi C_p \rho)(1/\alpha t) \exp(-r^2/4\alpha t) \quad (12)$$

where:

$T(r,t)$ is the time dependent temperature distribution,
 T_0 is the temperature before energy is deposited,
 C_p is the heat capacity of the surrounding material,
 ρ is the density of the surrounding material, and
 α is the thermal diffusivity of the surrounding material.

Thus the time dependent temperature distribution is just a function of Q' and the physical properties of the surrounding material.

Typically, materials such as those in the earth's crust have small thermal conductivities. Therefore essentially all of the energy would be deposited in a wire surrounded by earth before any energy would be conducted into the surrounding material. Hence, the thermal spike can be used to predict the time dependent temperature distribution in a sample of earth's crust surrounding an exploding wire.

In designing exploding wire apparatus, the temperature or the energy density necessary to study the high temperature chemistry of a nuclear explosion in a sample material is known or can be estimated. Knowing the temperature necessary to achieve the desired effect, the necessary circuit parameters of the exploding wire apparatus can be designed as follows:

1) Calculate the energy which must be deposited in the wire to raise the desired amount of sample material to the desired temperature. To complete this calculation, handbook or estimated values of thermal diffusivity, density, and heat capacity for the sample material are used in equation (12). Typical results are shown in Figure 2.

2) Calculate, using equation (7), the wire temperature at which the wire material will contain the energy calculated in step (1). Handbook values of the physical properties are used for the calculation when they are available. For the extremely high temperatures typical of wire explosions, the specific heat and latent heats usually must be estimated since they are considerably beyond handbook values. The results shown in Figure 3 were calculated assuming an ideal plasma gas and that the i^{th} electron was ionized from each atom when the kinetic energy ($3kT/2$) of the gas particles was equal to the ionization energy I_i , $i = 1, 2, \dots, Z$. Ionization energies tabulated by Moore⁶ were used for the calculations. (Rouse has calculated more accurate results by using the Saha equation.⁷)

3) Determine the rate of energy input to the wire which will balance the radiation losses from the wire at the necessary wire temperature. The power corresponding to a given temperature can be calculated using equation (9); typical results are shown in Figure 4. (The product of the wire diameter and the emissivity of the wire material is used as a parameter.)

4) Determine the electrical circuit parameters necessary to obtain the power calculated in Step (3). The maximum theoretical power available from an RLC network to a constant resistive load can be estimated using equation (10). Figure 5 shows the estimated maximum theoretical power available from an RLC network as a function of charging voltage with (C/L) as a parameter. This maximum power is available to an exploding wire if the wire is well matched to the circuit parameters. In determining the electrical circuit parameters, it is

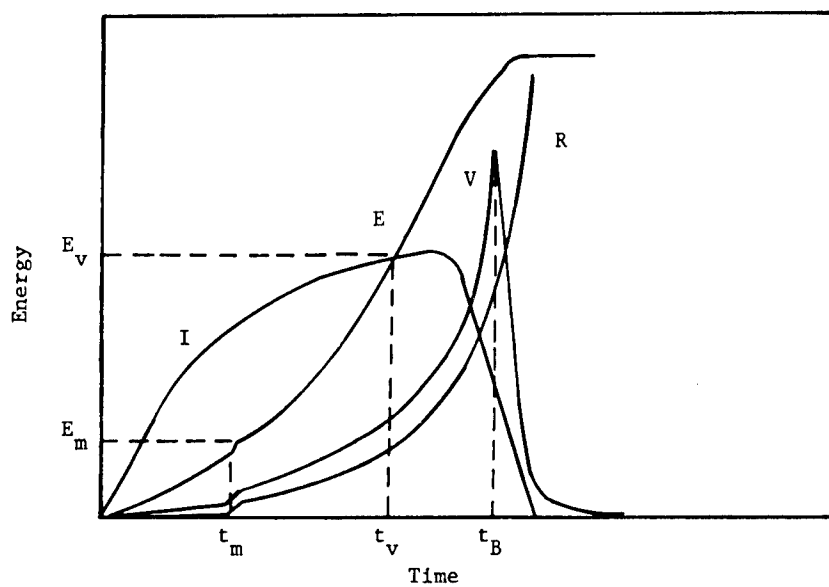


Figure 1. Curves for typical fast wire explosion.

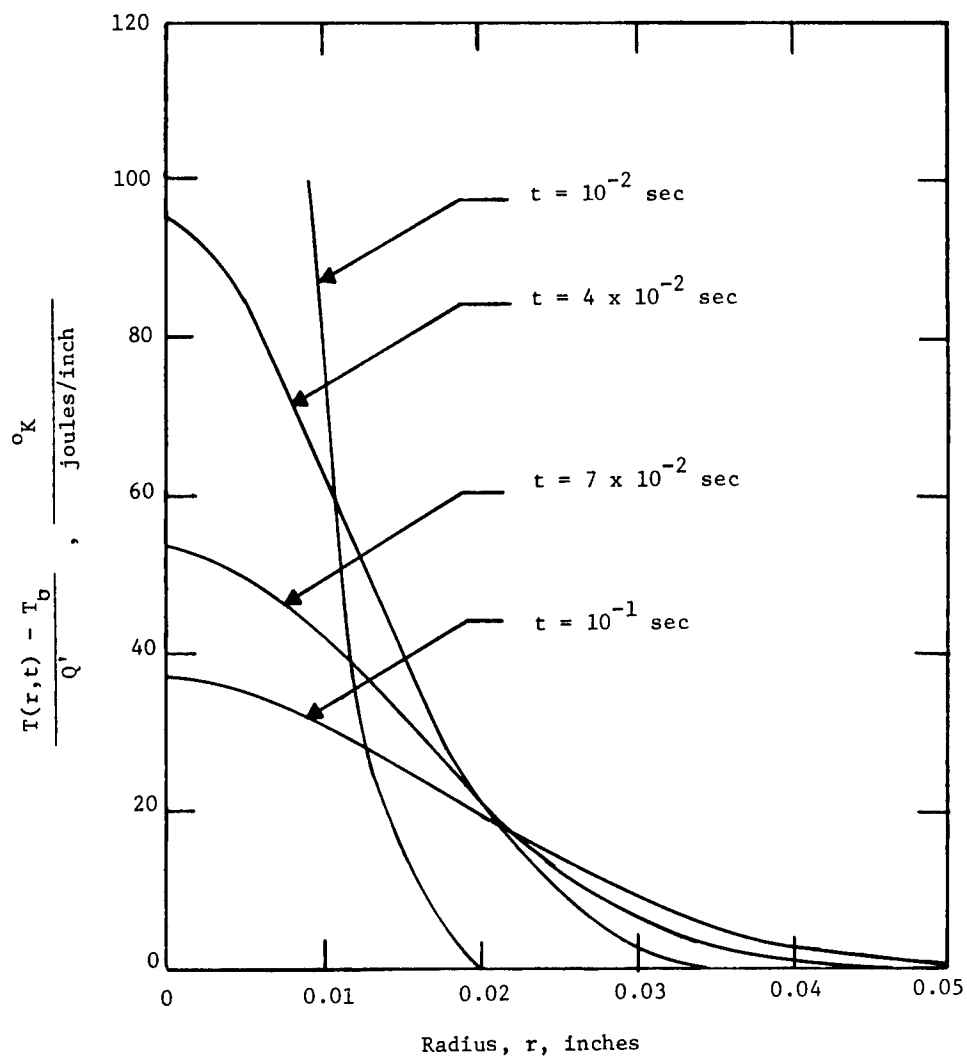


Figure 2. Temperature distributions in a cylindrical thermal spike at various times. Parameters typical of the earth crust were used. $C_p = 0.2 \text{ cal/g} \cdot ^\circ\text{K}$; $k = 0.005 \text{ cal/sec} \cdot \text{cm} \cdot ^\circ\text{K}$; $\rho = 2.24 \text{ g/cm}^3$.

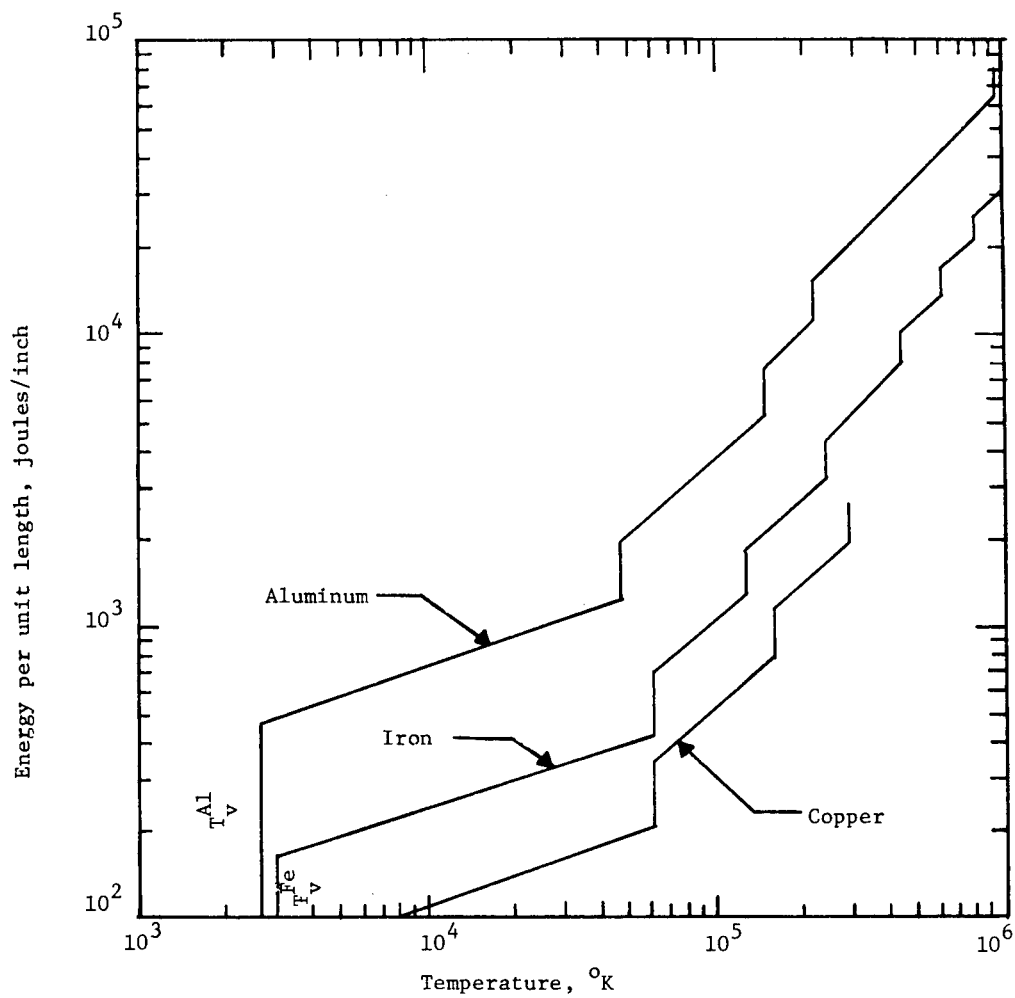


Figure 3. Energy per unit length as a function of wire temperature the first few ionization levels for 10 mil copper, 14 mil iron and 32 mil aluminum wire.

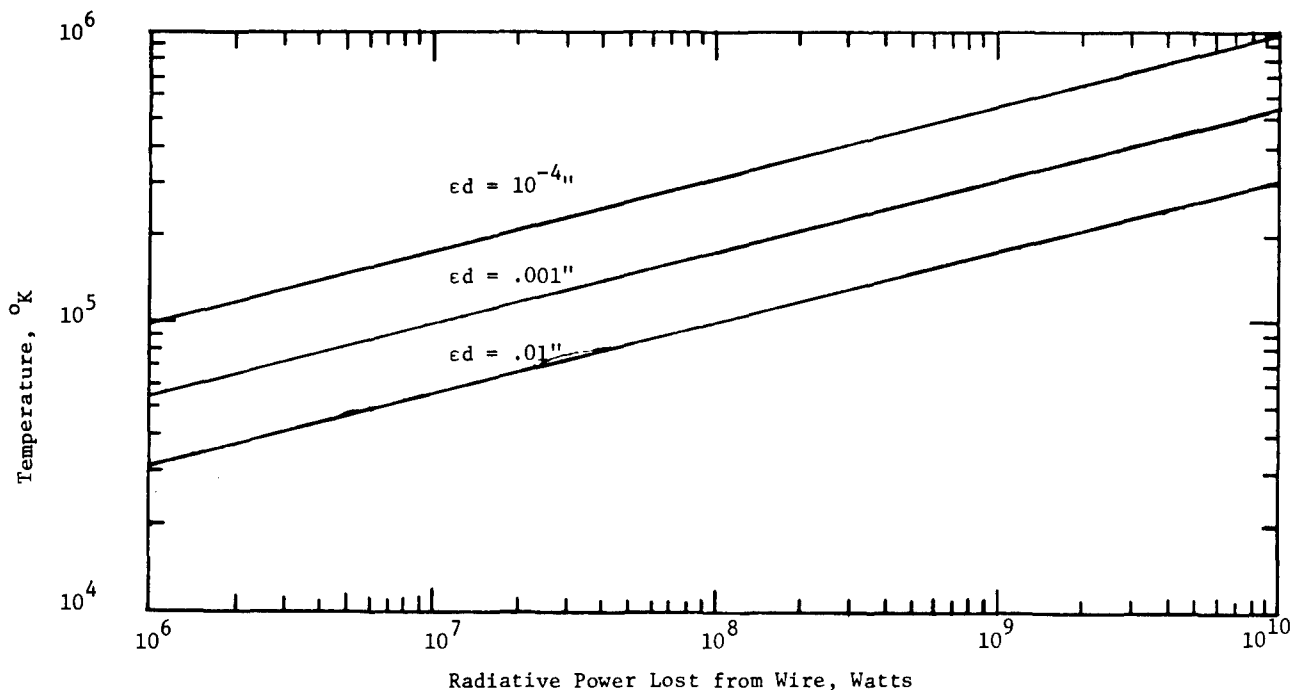


Figure 4. Rate of radiative energy losses from wire as a function of temperature. Product of the emissivity and wire diameter used as a parameter.

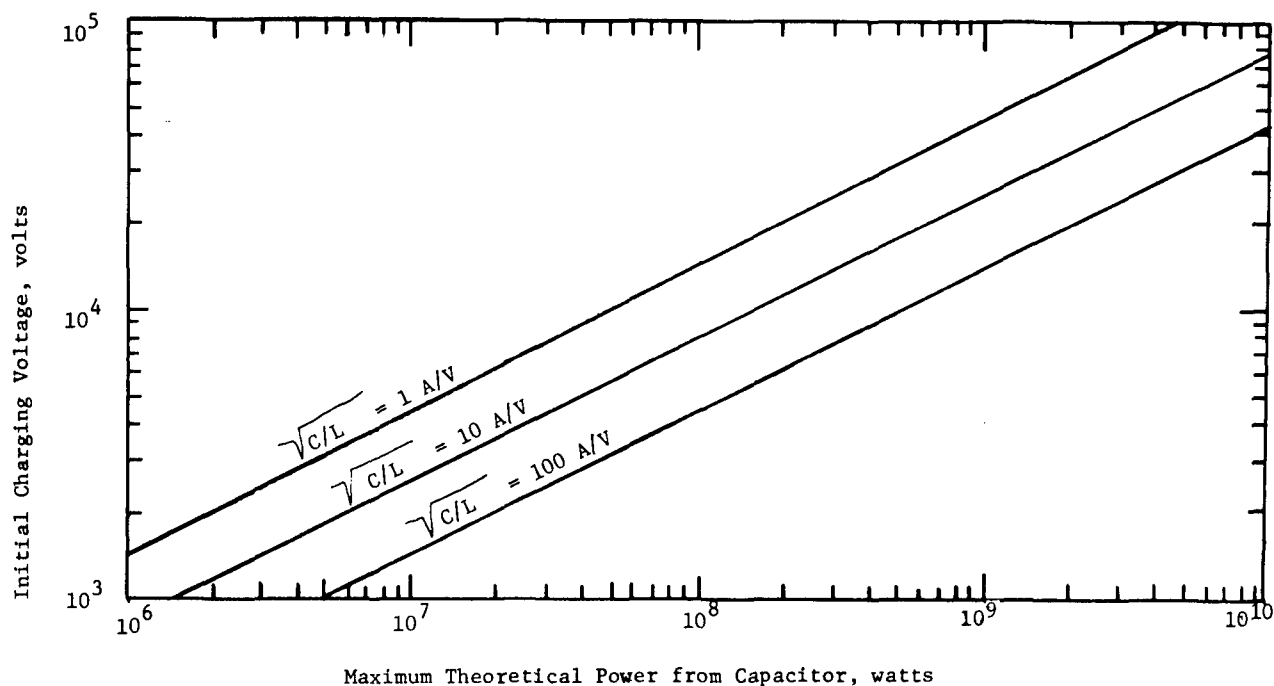


Figure 5. Maximum theoretical power than can be delivered to a constant resistive load from an RLS circuit as a function of potential to which the capacitor is charged.

necessary that the initial energy stored by the capacitor bank ($E_{co} = 1/2 CV_0^2$) be greater than the energy calculated in step (1).

3. Selection of Wire Parameters

After designing for the circuit parameters as described above, the wire parameters which will actually produce energetic explosions are experimentally determined. As previously mentioned the energetic explosions are obtained if the wire explodes near the current peak. The effect of wire parameters on exploding wire phenomena are known^{8,9,10}; thus it is only necessary to vary the wire parameters to obtain the desired energetic wire explosions.

The time to burst (time interval from initiation of discharge to the voltage peak) decreases with an increase in charging voltage of the capacitor bank, and increases with increasing wire diameter if other parameters are constant. Too thin wires are poorly matched to the discharge circuit because they explode in short times and use little of the stored energy. If the diameter of the wire is too large, the energy absorbed by the wire will not be sufficient to vaporize the wire. For maximum power and energy deposition, the wire diameter should be varied so that the wire explodes near the first current peak.

The power and the energy deposited in the wire also depend on the wire length. There is an optimum length for the maximum energy deposition and peak power. However, the peak power per unit length and the energy density increase with decreasing wire length if end effects are not important.⁹ Thus, the shortest wire, which does not have appreciable end effects, should be used.

Energy required to vaporize and to ionize the wire material does not increase the temperature of the wire material. Thus, to obtain high temperatures, a wire material which has low heat of vaporization and low ionization energies is desirable.

4. Experiments

Experiments were performed to verify that the circuit parameters designed for by theoretical equations did produce the predicted temperatures. Measurements of voltage, current, and current derivative were used to determine the rate of energy deposit and the total energy deposited in the wire. A schematic diagram of the discharge circuit and the measuring circuits is shown in Figure 6. Typical voltage, current, resistance, power, and energy results are shown in Figures 7 and 8. Estimated standard deviations were as follows: voltage - 5%, current - 5%, and calculated values - 10 to 15%. Larger deviations may occur when the current or the voltage curves are near the zeroline.

Data were obtained for various wire materials, wire sizes, circuit capacitances, and circuit charging voltages. The calculated results based on experimental measurements are summarized in Table I. The experimental results show that 15 to 40% of the energy initially stored in the capacitor bank was deposited in the wire before the wire bursts in the energetic type explosions needed to simulate the chemical environment of a nuclear explosion. Further, the experimental results indicate that if sufficient energy is available from the capacitor bank to satisfy the above efficiency constraint on energy transfer, then the circuit designed by the theoretical design method produces temperatures in the sample material within an order of magnitude of the design temperature.

Experimental results reported in Table I also show that wires well matched to the circuit parameters can have the maximum power greater than predicted using equation (10). Thus the resistance of the wire must vary in these cases so that energy is deposited at a higher rate than if the resistive load remained constant. If a wire is uniformly heated, then the rate of energy deposit to

Table I. Calculated experimental results of exploding wires

WIRE	PARAMETERS			CIRCUIT*			ENERGY			ENERGY DENSITY		
	Material	Size (in.)	C (μF)	V _C (kV)	Time to Burst (μsec)	Peak Power (MW)	Burst (joules)	Plateau (joules)	Burst (eV/atom)	Plateau (eV/atom)	Burst (eV/atom)	Plateau (eV/atom)
Wires exploded at ambient atmospheric conditions												
Al	.032 x 1		8	11	-	9	-	70	-			0.55
Al	.032 x 1		8	15	13.8	113	509	730	4.01			5.75
Cu	.020 x 1/2		8	11	-	9	-	81	-			2.32
Cu	.020 x 1		8	11	-	9	-	85	-			1.22
Cu	.020 x 2		8	11	-	21	-	157	-			1.12
Cu	.020 x 1/2		8	15	11.2	96	237	514	6.81			14.8
Cu	.020 x 1		8	15	11.8	187	305	543	4.38			7.80
Cu	.020 x 2		8	15	13.8	173	606	837	4.35			6.01
Cu	.020 x 3		8	15	13.8	179	586	810	2.81			3.88
Cu	.010 x 1		4	11	2.48	196	92	112	5.29			7.01
Cu	.010 x 1		4	15	1.96	472	107	202	6.15			11.6
Cu	.010 x 1		8	8	3.22	84	85	89	4.88			5.11
Cu	.010 x 1		8	11	2.52	280	92	122	5.28			7.01
Cu	.010 x 3		8	11	2.89	183	123	143	2.36			2.74
Cu	.010 x 1		8	15	2.04	543	151	221	8.68			12.7
Cu	.010 x 3		8	15	2.25	282	200	351	3.83			6.72
Fe	.014 x 1		4	11	3.53	65	124	129	3.62			3.77
Fe	.014 x 1		4	15	2.53	158	176	236	5.14			6.90
Fe	.014 x 1		8	8	4.46	54	101	105	2.95			3.07
Fe	.014 x 1		8	11	2.93	94	133	162	3.89			4.73
Fe	.014 x 3		8	11	6.06	74	159	225	1.55			2.19
Fe	.014 x 1		8	15	2.37	208	207	263	6.05			7.68
Ni-Cr	.028 x 1		8	11	-	19	-	182	-			1.24
Ni-Cr	.028 x 1		8	15	14.3	103	571	701	3.88			4.77
Wires exploded in sample cell geometry												
Cu	.020 x 1		8	11	12.1	42	172	226	2.47			3.25
Fe	.014 x 1		8	11	3.42	49	100	126	2.92			3.68

*Circuit inductance for all cases was 1.33 microhenrys.

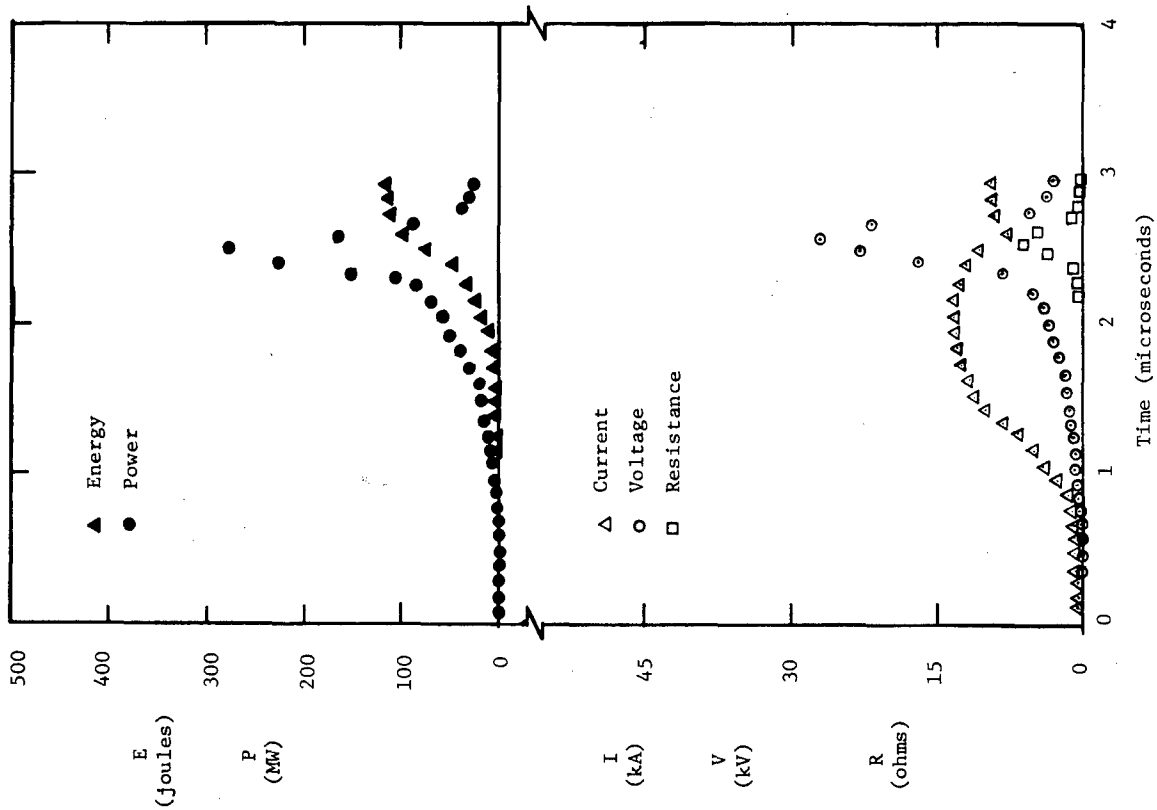


Figure 7. Curves for 10 mil x 1 inch copper wire exploded at 8 μ F and 11 kV.

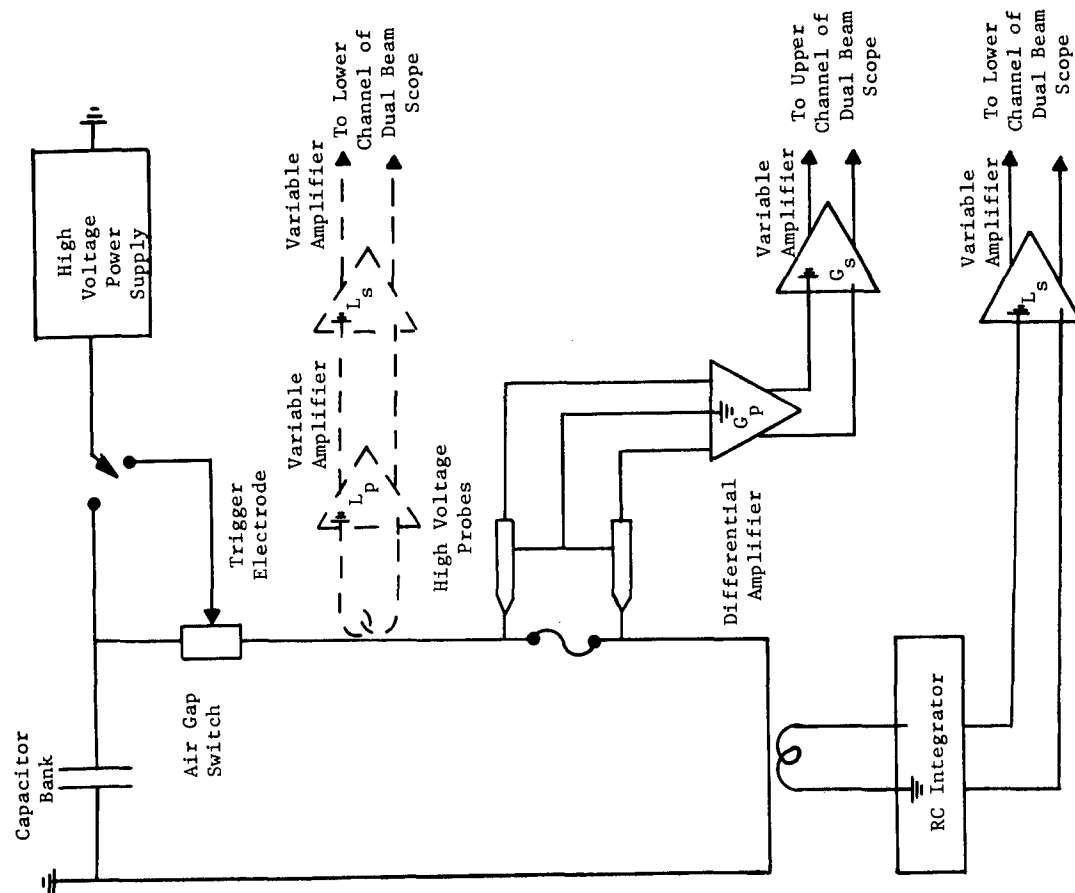


Figure 6. Schematic diagram of measuring circuits.

the wire is more than sufficient to balance the radiant energy losses near the peak of the power curve. Therefore it is desirable to develop a technique to contain the wire material for longer periods of time after the vaporization energy is deposited.

If the discharge circuit is designed so that the return current from the wire to the capacitor bank is distributed symmetrically about the wire, the magnetic pinch effect will tend to confine the wire material for a longer period of time.^{11,12} Figure 9 is a drawing of the cross-section of a sample cell developed during the course of this study to confine the wire material after the vaporization energy had been deposited. The cell can also be used to hold material in close proximity around the wire during the explosion. Confining the wire material by using the sample cell shown in Figure 9 results in more energy being deposited in both the wire and the material surrounding the wire than if the wire material is not confined.

Since voltages in the kilovolt range were used for wire explosions in the sample cell, voltage breakdown or arcking tended to occur between points of the current path in the sample cell. This voltage breakdown allowed the current to short circuit. Therefore, the pointed brass lead and the outside of the cell were covered with electrical tape to prevent arcking; in addition an insulator cap was used to prevent arcking from the brass lead to the cell wall. Three mylar disks, each .010 inch thick, made up the insulator cap.

Several materials (mylar, mica, polyethylene, plexiglas, teflon, and compressed CaCO_3) were tested for use as an insulator cap. However the energy density and pressure of the wire explosions either melted or shattered all tested materials except mylar. The melting or shattering of the insulator cap resulted in arcking from the brass lead to the cell wall and thus if the insulator cap melted or shattered before the time of burst, the amount of energy deposited in the wire was significantly reduced.

One inch long stainless steel tubes were used for the sample cell walls. The inside diameter of the tubes used were 1/16", 1/8", and 3/8". To provide insulation between the wire and the cell wall, a silicon based caulk was placed in the sample volume and allowed to dry at atmospheric conditions. However the caulk was insufficient insulation to prevent arcking from the central wire to the cell wall for the two smaller diameter tubes. Thus, consistent data were obtained only for the 3/8" diameter tube.

Voltage and current curves were measured for wires exploded in the sample cell environment. Typical experimental and calculated results are shown in Figure 10. As expected the peak of the power curve for the wire exploded in the sample cell geometry was broadened and flattened when compared with bare wire results (Figure 8). One of the reasons for lowering the power peak was sparkover from the central wire to the inner cell wall caused by the high voltage peak. Sparkover occurred because the insulation between the wire and the tube wall was insufficient. Limitation of the voltage peak by sparkover precluded the attainment of the energetic explosions needed to simulate a nuclear explosion in this early work. However, since the experimental results show that the sample cell geometry stabilized and confined the wires, redesign of the cell to prevent sparkover should produce explosions with the desired energy density.

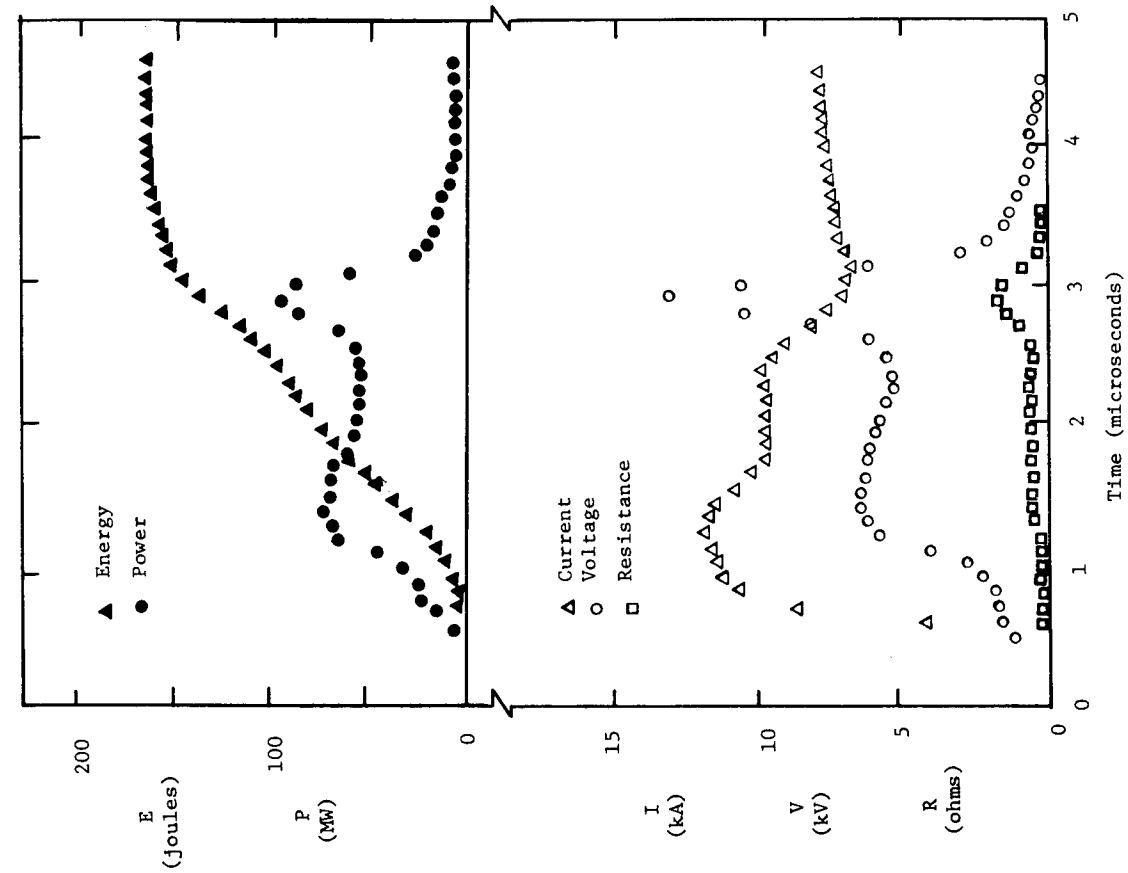


Figure 8. Curves for 14 mil x 1 inch iron wire exploded at 8 μ F and 11 kV.

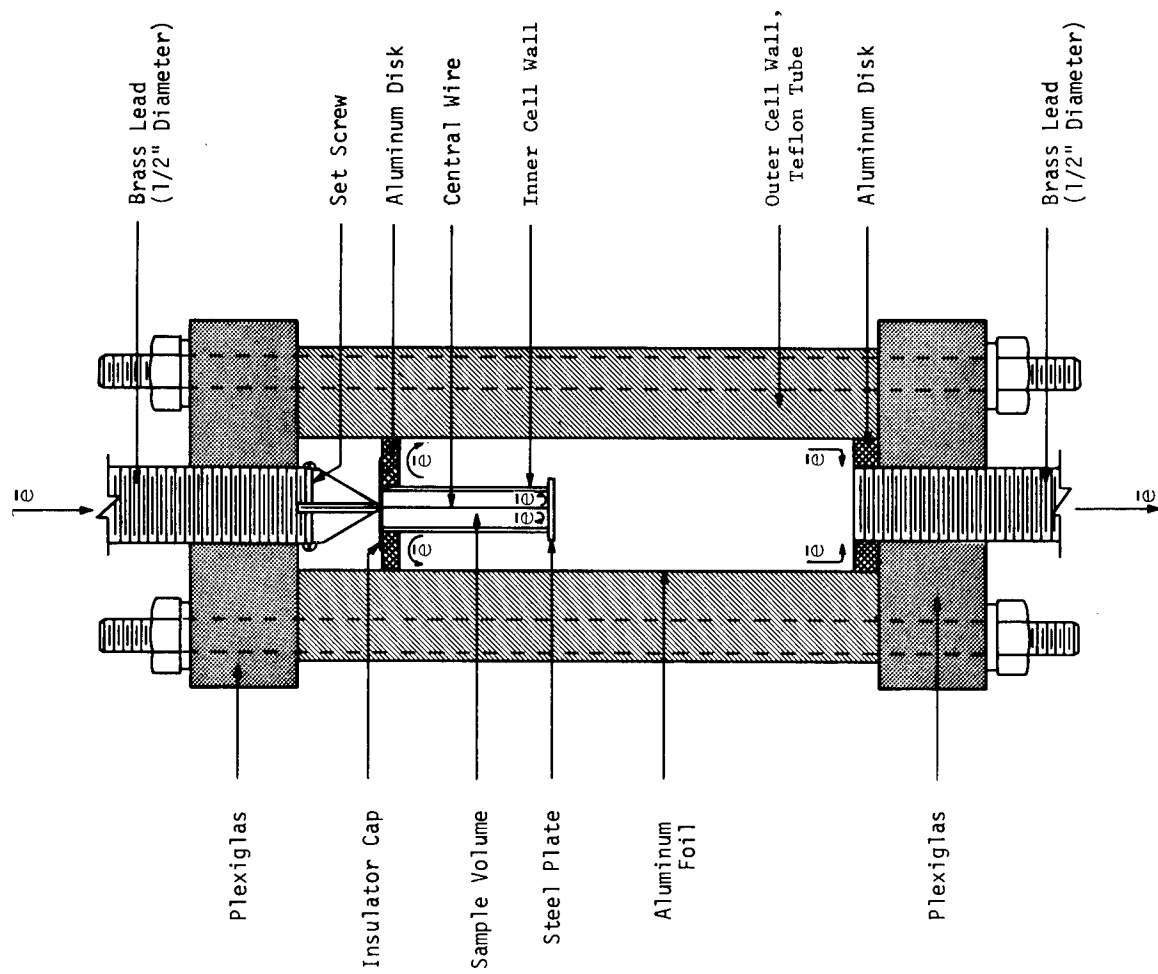


Figure 9. Schematic of Sample Cell Geometry (To scale).

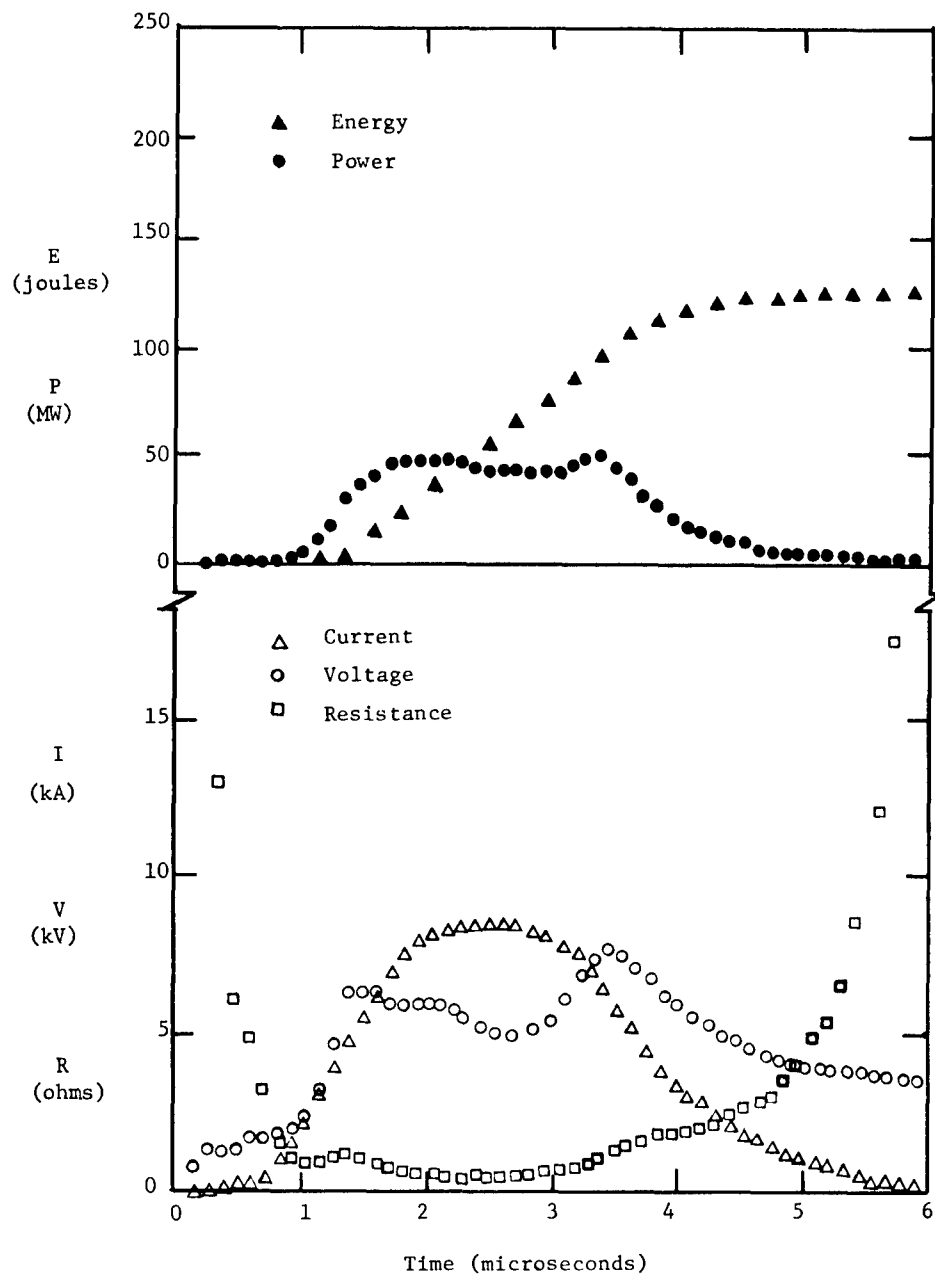


Figure 10. Curves for 14 mil x 1 inch iron wire exploded in sample cell geometry at 8 μ F and 11 kV.

5. Literature Cited

1. Walter Meyer and F. G. Svensson, August Monthly Report, Chemical Engineering Division, Lawrence Radiation Laboratory, (1964).
2. F. D. Bennett, "Energy Partition in Exploding Wire Phenomena," *Phys. Fluids* 1, 515-522 (1958).
3. Handbook of Chemistry and Physics, C. D. Hodgman, Editor in Chief, (Chemical Pub. Co., Cleveland, 1959), 40th ed., p. 3257.
4. V. E. Scherrer, "The NRL-AFSWP Exploded Wire Research Program," in *Exploding Wires*, Vol. 1, edited by W. G. Chace and H. K. Moore, pp. 118-134, Plenum Press, New York, (1959).
5. G. J. Dienes and G. H. Vineyard, *Radiation Effects in Solids* (Interscience Publishers, Inc., New York, 1957), Chap. 2, p. 35.
6. C. E. Moore, *Atomic Energy Levels*, U. S. National Bureau of Standards Circular, No. 467, Vol. III, Washington, (1958).
7. C. A. Rouse, "Ionization Equilibrium Equation of State," *Astrophys. J.* 134, 435-446 (1961).
8. O. U. J. Block, "Simulation of the Chemical Environment of a Nuclear Explosion by Exploding Wire Techniques," an M. S. Thesis, Kansas State University, 1969.
9. H. S. Leopold, "Effect of Bridgewire Parameters on Explosive Initiation," in *Exploding Wires*, Vol. 3, edited by W. G. Chace and H. K. Moore, pp. 125-152, Plenum Press, New York, (1964).
10. F. D. Bennett, H. S. Burden, and D. D. Shear, "Correlated Electrical and Optical Measurements of Exploding Wires," *Phys. Fluids* 5, 102-113 (1962).
11. Jack Katzenstein, "The Pinch Effect in the Exploding Wire Phenomena," in *Exploding Wires*, Vol. 1 edited by W. G. Chace and H. K. Moore, pp. 135-144, Plenum Press, New York, (1959).
12. A. Sakurai and T. Takao, "Effect of Applied Axial Magnetic Field on the Exploding Wire Phenomenon," in *Exploding Wires*, Vol. 3, edited by W. G. Chace and H. K. Moore, pp. 247-256, Plenum Press, New York, (1964).

6. Nomenclature

A	surface area of wire (in^2)
C	capacitance of capacitor bank (farads)
C_p	heat capacity (joules/gram $\cdot^\circ\text{K}$)
d	diameter of wire (in)
E	energy deposited in exploding wire (joules)
E_{co}	initial energy stored in capacitor bank (joules)
E_m	increase in energy density above standard conditions needed to melt wire material (eV/atom)
E_v	increase in energy density above standard conditions needed to vaporize wire material (eV/atom)
I_i	energy density required to ionize the i th electron from atom of wire material (eV/atom)
I	current (kA)
i	current (kA)
k	thermal conductivity (joules/meter $\cdot\text{sec}\cdot^\circ\text{K}$)
L	inductance of discharge circuit (henries)
L_w	inductance of wire (henries)
P	power (rate of energy deposited in wire), (megawatts)
Q	rate of conductive and convective heat losses from wire (joules/sec)
Q'	energy deposited per unit length of wire (joules/in)
R	resistance of discharge circuit (ohms)
R_w	resistance of wire (ohms)
r	radial distance from center of wire (in)
T	absolute temperature ($^\circ\text{K}$)
t	time (sec)
t_B	time from initiation of discharge until wire bursts (sec)
t_m	time from initiation of discharge until wire melts (sec)
t_v	time from initiation of discharge until wire vaporizes (sec)
U	internal energy of exploding wire (joules)
$u(T-T_j)$	unit step function

V	resistive voltage drop across wire (volts)
V_c	voltage on capacitor bank (volts)
V_o	initial charging voltage on capacitor (volts)
V_w	total voltage drop across wire (volts)
W	hydrodynamic energy of the wire (joules)
α	thermal diffusivity (in^2/sec)
ΔU_j	internal energy change at j^{th} transition (joules)
ϵ	emissivity
π	3.141592654
ρ	density (g/cm^3)
σ	Stefan-Boltzmann constant = $5.7 \times 10^{-5} \text{ erg}/\text{sec} \cdot \text{cm}^2 \cdot ^\circ\text{K}^4$

POSSIBLE HAZARD REDUCTION BY USING DISTRIBUTED
PHASED NUCLEAR EXPLOSIONS

Frank Chilton

Theoretical Physics Program, Stanford Research Institute, Menlo Park, California
and

Department of Applied Science, University of California, Davis, California

and

James A. Cheney

Department of Civil Engineering, University of California, Davis, California

Abstract

The use of two or more nuclear devices, phased together in order to constructively add their respective particle velocities, is proposed herein. By directing the seismic waves of the nuclear explosions to make them more efficient in accomplishing the intended construction, we hope to be able to reduce the radioactivity, seismic, and airblast hazards substantially. Experiments are being performed with one gram charges of PETN.

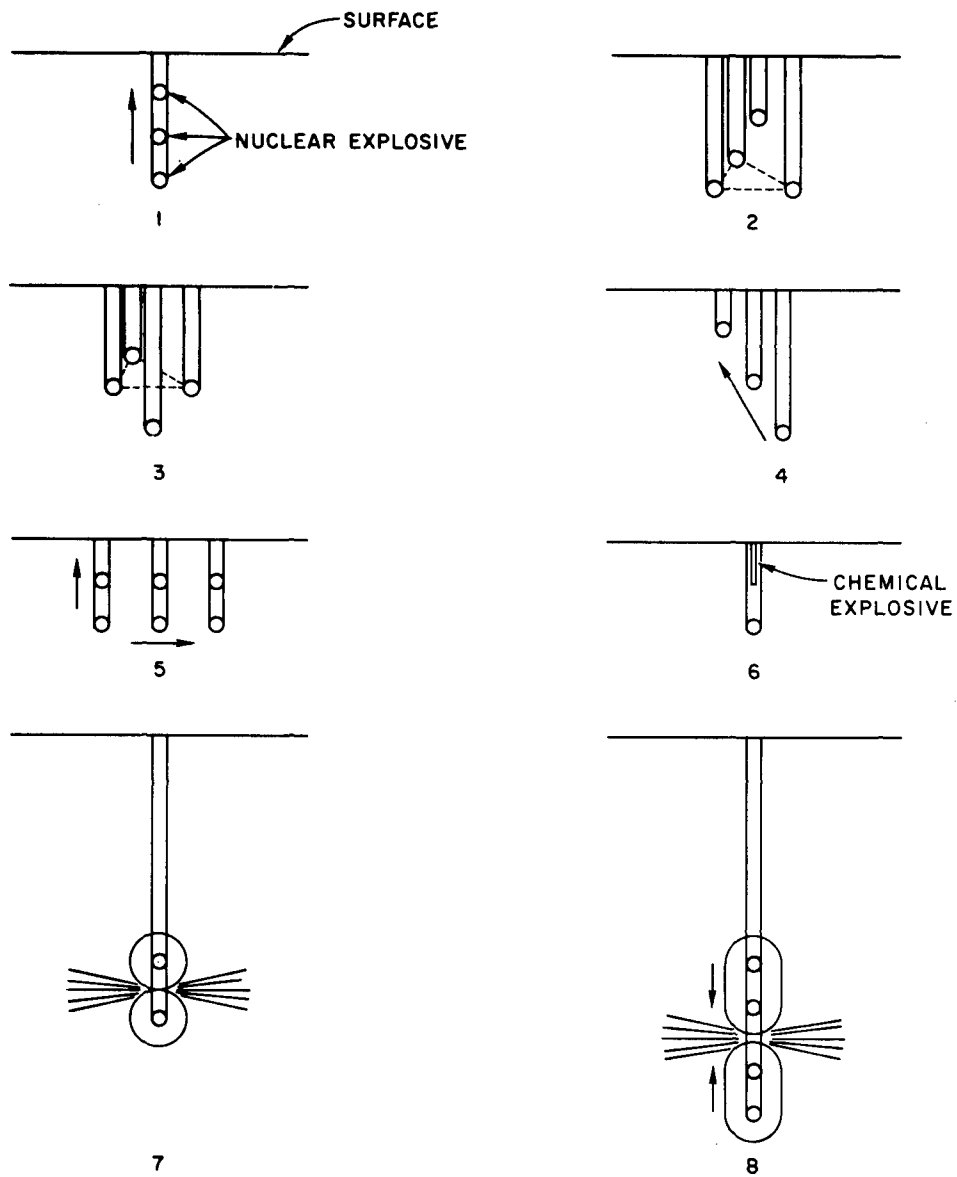


Fig. 1 — Configurations of Explosives.

Introduction

Hazards associated with nuclear explosions represent a serious obstacle to widespread engineering use. Even when it is known that no geophysical or physiological damage would occur, the thought of radioactive, seismic, or airblast hazards has been known to cause sufficient social and political controversy to delay or prevent particular nuclear explosion engineering projects.

It may be possible to reduce these hazards by making the distribution of energy far from the spherically symmetric distribution of a single explosion. A way to achieve a directed angular distribution of energy is to use distributed phased nuclear explosions (dpne).

For cratering, the basic configuration of dpne is shown in Fig 1.1. The explosives above the lowest one are detonated in phase with the shock wave arriving from below. It should be possible to place the uppermost explosive deep enough so that the cratering mechanism is spalling² alone.

Normally, cratering includes venting^{1,3} as one stage of its history. It is during venting that some radioactivity is released and much of the airblast is produced. Modification of venting may significantly reduce these hazards. The altered angular distribution of energy should affect a significant reduction in the seismic hazard.

The basic idea of dpne is rather similar to an explosive design used in seismic exploration,⁴ and can be used in a wide variety of geometries. Figures 1.2 to 1.4 show dpne concepts useful for special crater shaping. A non-vertical array such as that of Fig 1.5 shows a concept of two dimensional dpne as applied to canal construction.

There may be occasions where it is useful or economic to combine nuclear and chemical explosives in dpne configurations. One such concept is shown in Fig 1.6. The chemical explosive is used to impart horizontal velocity to the medium and thereby decrease the fallback in the crater.

For underground applications similar considerations lead to the concepts of Figs 1.7 and 1.8. The detonation of the explosives should be in simultaneous pairs. It may be possible to fracture a formation horizontally without the cavity intersecting the formation at all.

Results from Linear Theory

Although a rigorous calculation of multiple distributed phased nuclear explosions is quite beyond present analytical and numerical capability, much qualitative insight can be gained from linear wave theory. Such a model, with phenomenological correction, has been shown to be successful for spalling from underground nuclear explosions.²

In the forward direction N explosions with yield W and phased properly would give peak particle velocity approximately N times those of a single explosion with yield W . The width, in time of the first positive portion of the pulse, would be the same as that of a single explosion with yield W .

In the backward direction the peak particle velocity would remain the same as that of a single explosion but the width in time would be much increased.

That spalling due to deeply buried coherent explosions is capable of producing a crater is best illustrated by some sample numbers. The Danny Boy shot was buried at $\approx 40 \text{ m/kT}^{1/3.4}$ and gave surface velocities $\approx 45 \text{ m/sec}$. It was only a little deeper than optimum cratering depth and hence yielded a large crater. The Charlie shot was buried at $\approx 65 \text{ m/kT}^{1/3.4}$ and gave surface velocities $\approx 30 \text{ m/sec}$. It gave no crater at all (only a mound). Assuming that coherent detonation will result in an adding of the velocity waves in the upward direction, two devices in different holes, both with depths greater than $65 \text{ m/kT}^{1/3.4}$ would give velocities of $\sim 60 \text{ m/sec}$ at surface zero which would make a substantial crater. Even if the velocity waves do not completely add there appears to be adequate range for adjustment.

Nonlinear effects would be essential to a detailed theory of phased explosions because we want to add two stress waves in the vicinity of the explosion. Nevertheless, it may be possible to confine the theory to the quasi-linear region outside the explosion and take from experiment information on the extent and way in which waves add.

Precise timing of the successive explosions is important. Linear wave theories, particularly in electrodynamics, show that waves which have a dependence on distance such as r^{-e} , where $e \geq 1$ is an exponent, are altered when the source is moving to something like $(r - \underline{r} \cdot \underline{u}/c)^{-e}$ where \underline{u} is the velocity vector for the explosion source and c is the velocity of the formation.⁵ The exponent e would be of the order of three.⁶ In the forward direction the ratio of the

amplitudes for $u - c = \pm 0.01c$ and $u - c = \pm 0.10c$ would be 1000 meaning that 10% matching of the effective source velocity to the velocity of the formation is not satisfactory at all.

In the underground application of Fig 1.7 the improvement is predicted as a factor of N , the number of explosions, in a linear theory. Again the nonlinear effects would appear to be an essential complication. The shock-shock interaction would cause a much wider horizontal region of cracking than would be predicted by a linear theory.

Safety and Economics

Safety is presumably improved by using distributed phased nuclear explosions. However, not all of the effects of dpne are clearly going to make positive contributions to safety. Several aspects require further study. For example, the phasing does indeed reduce the peak particle velocity in the backward (downward) direction but it also spreads the pulse in time thus shifting its frequency spectrum toward lower frequencies. The earth transmits the lower frequencies better, which works against improved seismic safety. Likewise, cratering by spalling above, without venting, will certainly reduce airblast and radioactivity; however, the larger total cavity formed by several explosions may not permit a guarantee of no venting. These points would need to be studied before engineering use of dpne would be possible.

Use of several devices, instead of one, would also presumably increase the device cost for Plowshare projects. This cost increase may be partially or completely offset by being able to perform projects not otherwise possible, and by decreases in safety and monitoring costs.

Experimental Program

Small-scaled experiments are being carried out in the Explosion Engineering Laboratory at the University of California, Davis branch. The purpose of the experiments is to establish feasibility of the above proposals and experimental verification of theoretical predictions. Small amounts of PETN (one to seven grams) are being used, detonated by exploding-bridge-wires and with carefully controlled timing.

The duration of the positive phase of the traveling wave from a small PETN explosion is very much shorter (microseconds) than that of a nuclear device

(milliseconds); consequently the time is far more crucial in small-scale experiments than in full-scale experiments.

Equipment

The key piece of equipment in the test set up is a multi-pulse generator (Hewlett-Packard Spec. K02-5332A) capable of present output time from 1 μ sec to 10,000 μ sec from a given start time with each pulse being $3V \pm 1V$ into 1K ohm for 20 μ sec. This permits the necessary accuracy in timing the sequence of explosions. The multi-phase generator triggers a thyrotron firing circuit which discharges capacitors charged at 2000V across a bridge wire detonator.

To date experiments have been carried out in a steel box 6 ft. X 6 ft. X 2 ft. filled with ordinary construction sand. Figure 2 shows the laboratory control equipment and the sand box. The firing circuits rest on the top shelf, the lower shelf holds the multi-pulse generator, a 2000V power supply and a 30V power supply also part of the firing circuitry. The mylar screen assists in protecting the equipment from flying debris.

Calibration

The velocity of a traveling compression wave in the soil must be known with precision in order to phase the detonations properly. Experimental determination of this parameter is complicated by reflections off the side of the box and transmission around the box which can permit a signal to arrive at a distant pickup before it arrives at a near one. This latter phenomenon is due to the fact that the velocity of sound in steel is roughly 10 times that in the sand.

Nevertheless, the determination of velocity was made by the use of two piezoelectric transducers set 24 inches apart and subjected to a stress wave from an impact on the side of the box. A record of the resulting charge on the transducer was obtained by means of a Tectronix Storage Oscilloscope. Figure 3 shows a typical trace after one such experiment. The time ordinate is 5 msec per division. The top trace is from the sensor closest to the impact. The average of several shocks gave a velocity of the first peak compressive wave as 34 in/msec.

This means that explosives set 5 inches apart in a vertical array should be detonated 147 μ sec apart from bottom to top in order to have maximum vertical orientation.

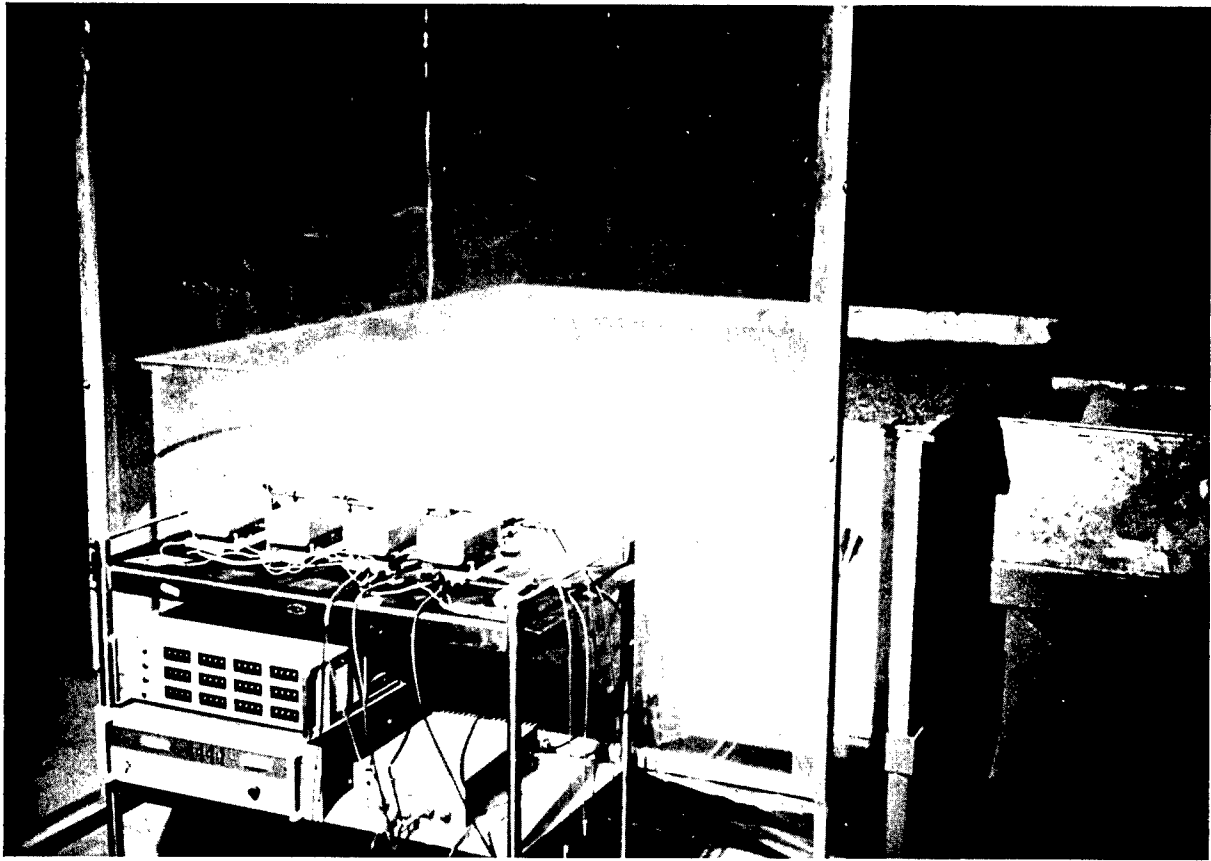


Fig. 2—Firing Control Equipment and Sand Box.

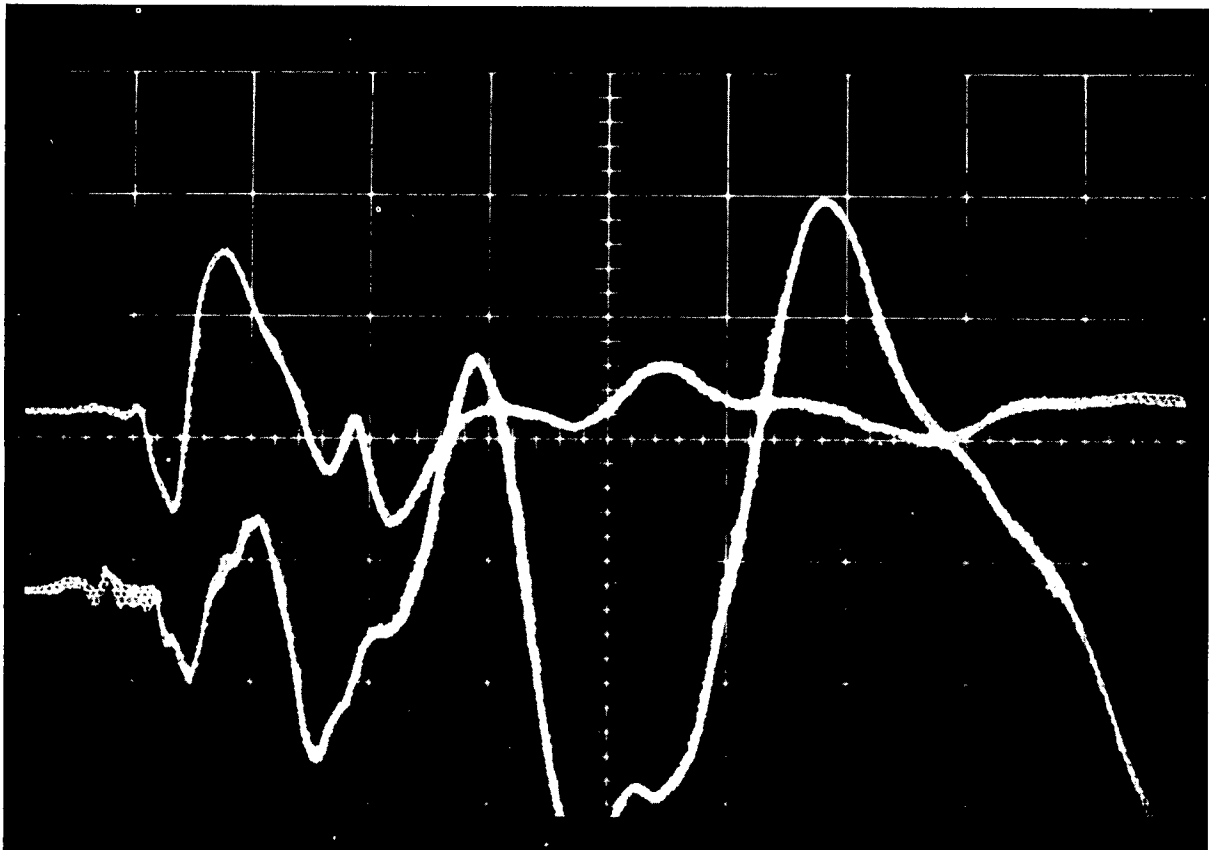


Fig. 3—Typical Stress Wave Traces.

Sand Box Experiments

The usual period of development of the equipment and the learning period of the experimentalist preceded any meaningful data. The early experiments included single shot, double array shots and triple array shots in hopes of establishing the depth of burial to prohibit venting. It became apparent, however, that in loose dry sand it is not easily determined whether the crater lip is formed by spalling or venting. The crater itself is formed to a large degree from subsidence caused by the compaction of the sand during the explosion. This is demonstrated in those cases where no lip is formed, implying that there was no ejecta. This is shown in Fig 4.

The pure subsidence case is interesting for itself, in that with the vertical phased distribution the compactive effort is localized to give a narrow vertical column of compacted soil. The following table gives the results of three subsidence crater shots with vertical arrays.

Depth of Burial	Number in Array	Depth of Subsidence	Diameter
6-3/8 in.	1	3/4 in.	8 in.
9, 14	2	1-5/16 in.	10 in.
10-5/8, 16-5/8, 22-5/8	3	2-1/4 in.	11-1/2

Table 1 Subsidence craters from vertical phased arrays of 1 gm charges

The depth of subsidence from a single shot of 3 gms, by the $1/3$ power scaling law, should be 1.42 times the depth of subsidence of a 1 gm charge, namely 1-1/16 in.

If the phasing is not correct or the depth of burial too shallow, spalling or venting may actually be detrimental in that bulking of the sand at the surface reduces the apparent crater depth. An example of this was a shot containing 3-1 gm charges arrayed vertically 6 inches apart from 7 in. below the surface and phased for half the true velocity. A crater depth of only 7/8 in. resulted.

Speculations from Preliminary Experiments

It is apparent that loose sand will vent the explosion gases regardless of the depth of burial due to the high inherent permeability of sand. The effect

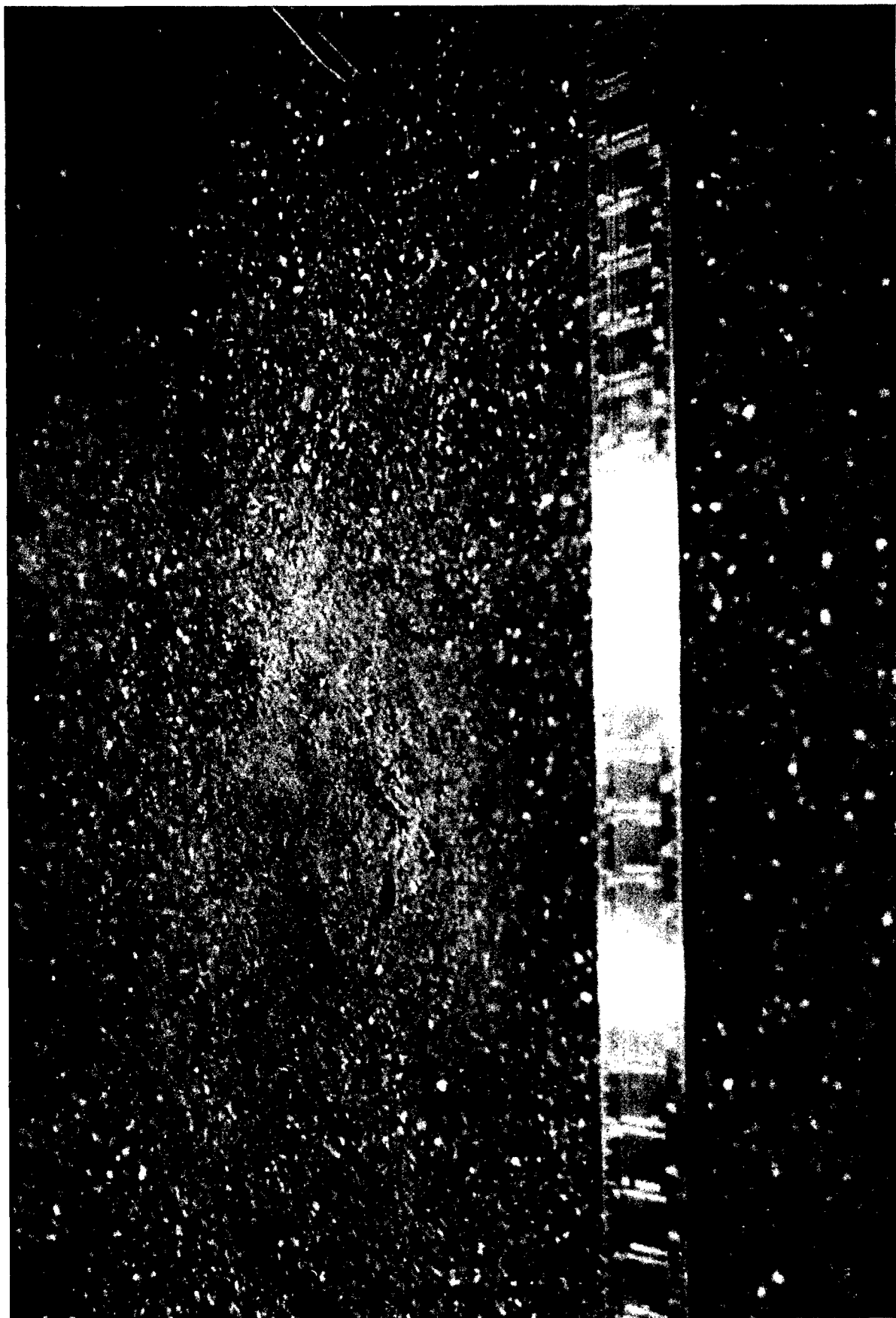


Fig. 4 — Typical Subsidence Crater.

of venting can be made negligible by making the flow path long so that the gas velocity is too small to move the surface particles. This is done by a deeper burial. It can also be done by decreasing the effective permeability by moistening and compacting the sand. The moisture can fill the flow paths and essentially eliminate gas flow provided the surface tension of the water is strong enough to prohibit water transport. This latter requirement can be satisfied by close particle spacing (compaction).

The moisture in the sand will provide an apparent tensile strength proportional to the surface-tension-strength of the water. This will reduce the velocity of spallation, namely

$$V_1 = 2V_o = \frac{2\sigma_{\max}}{\rho c}$$

for loose sand in the vertical direction, while for competent material having tensile strength σ_c ,

$$V_1 = 2V_o - \frac{\sigma_c}{\rho c} \left(1 + \frac{\gamma \lambda}{2\sigma_{\max} - \gamma \lambda} \right)$$

where $\gamma = \rho g$, the unit weight of the material

σ_{\max} = the wave front stress

ρ = density of the sand

c = velocity of the wave

λ = distance of positive pressure behind the shock front

However, the reduction in venting of the explosion gases may well result in a larger σ_{\max} which will more than offset the reduction in velocity from tensile strength.

Other suggestions for model materials which should solve the problem of inherent permeability to gas flow are paraffin wax and plaster of paris. Both of these can be easily handled in the laboratory, but are not as easily compared to real soils.

Conclusions

The concept of the distributed phased nuclear explosion (dpne) suggests a possibility of containing all, not most, of radioactive material below ground while still producing desired surface effects (cratering) as well as reducing undesired effects (airblast, seismic motion). It is suggested that the

feasibility of these proposals should be first demonstrated in the small scale laboratory experiments at relatively small cost before full scale tests are considered. Some of these tests have been initiated at the University of California, Davis.

Acknowledgment

The authors are grateful to Professor W. K. Talley and Mr. J. D. Eisler for many helpful discussions.

References

1. E. Teller, W. K. Talley, G. H. Higgins and G. W. Johnson, The Constructive Uses of Nuclear Explosives (McGraw-Hill, New York, 1968).
2. F. Chilton, J. D. Eisler and H. G. Heubach, "Dynamics of Spalling of the Earth's Surface by Underground Explosions," J. Geophys. Research 71, 5911 (1966).
3. J. Knox, "Nuclear Excavation: Theory and Applications," Nuc. App. and Tech. 7, 189 (1969).
4. S. T. Martner and D. Silverman, "Broomstick Distributed Charge," Geophysics 27, II, 1007 (1962).
5. J. D. Jackson, Classical Electrodynamics (Wiely, New York, 1962), Chap. 14 and 16.
6. Nuclear Geoplosics, Ed. F. M. Sauer, DASA-1285 (Stanford Research Institute, Menlo Park, California, 1964), Vol. IV, Chap. 1.

NUCLEAR EXCAVATION EFFECTS

Review: Airblast Effects

Jack W. Reed, Sandia Laboratories

I. Long Range Airblast Propagation

On February 2, 1951, the Atomic Energy Commission discovered that airblast from an 8-kt explosion could break many windows in Las Vegas at 60 miles range from Frenchman's Flat. Yet later, on February 6, only minor effects resulted from three times as large a yield. Atmospheric conditions were found to be responsible for this apparent anomaly. A weather watch was initiated under the direction of Everett Cox to help prevent recurrences during further atmospheric nuclear testing.

Our atmosphere with its stratifications of temperature and winds acts as an acoustic lens which may trap, duct, or even focus blast waves from explosions. The basic refraction mechanism is described by Figure 1. Sound speed is proportional to the square root of absolute temperature, as shown in Newton's Principia, so as temperature decreases with altitude, so does sound speed. The proper coefficient was found by Laplace, using adiabatic rather than Newton's isothermal compression. Sound or blast waves propagate through moving air with this wind added or subtracted from the sound speed. This affects an initially vertical plane wave to make it increasingly distorted with time. Wave normals, or rays, are bent upward, away from ground, in layers where net sound velocity decreases with altitude and are bent downward where sound velocity increases with altitude.

This bending, applied to a point sound source or explosion, gives ray paths typified by Figure 2. Where ducting is caused by a velocity inversion high above the ground, there is a zone of silence beyond the immediate range of the strong explosion wave, and a sound ring at some distance determined by the height and strength of the ducting layer.

Calculation of ray paths has evolved with the growth in needs and computer capabilities. A 1912 model by Fujiwhara, at the Tokyo Central Meteorological Observatory (1), was quite complete. Rothwell (2) in 1947 provided the system of equations used for the first nuclear test predictions, by desk calculator, in late 1951. Techniques were speeded up by hand calculation methods of Cox, et al (3), and used with an analogue computer built in 1955 at Sandia by Durham (4). Modern computer capabilities now allow a complete acoustic solution, without simplifying assumptions about wind effects, from Thompson's program (5,6), for 1° ray elevation angle increments, in several azimuth

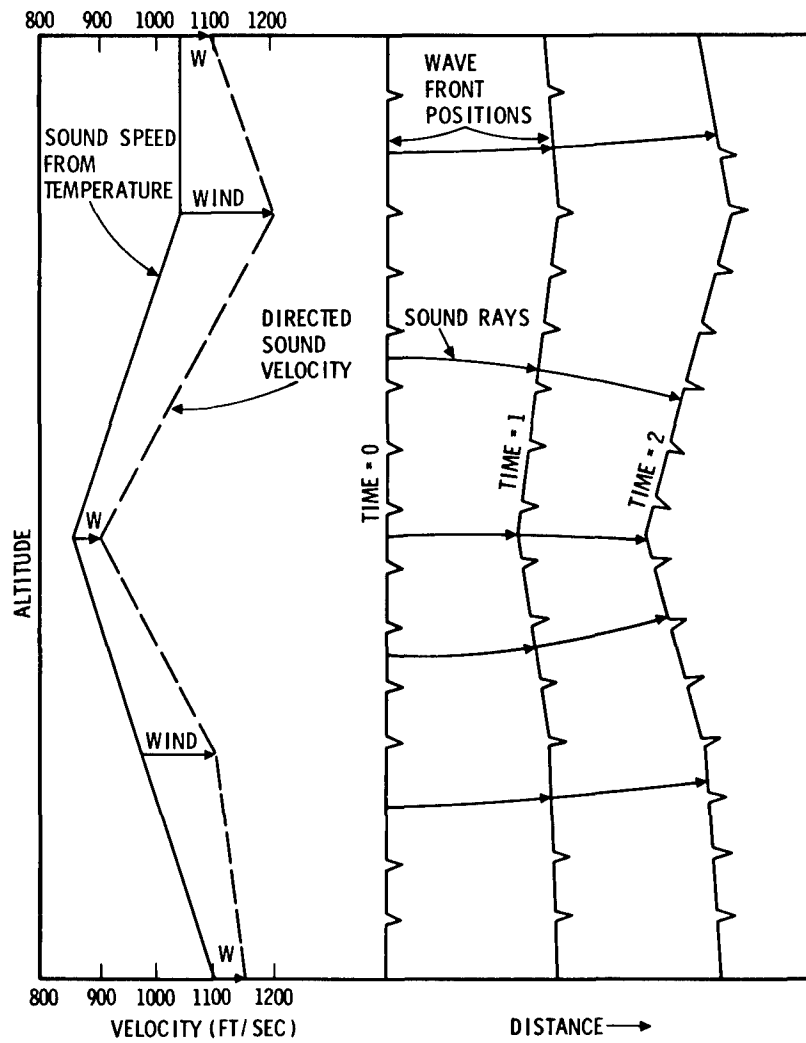


Fig. 1 Shock-Wave Distortion by Layered Atmospheric Temperature and Wind Structure.

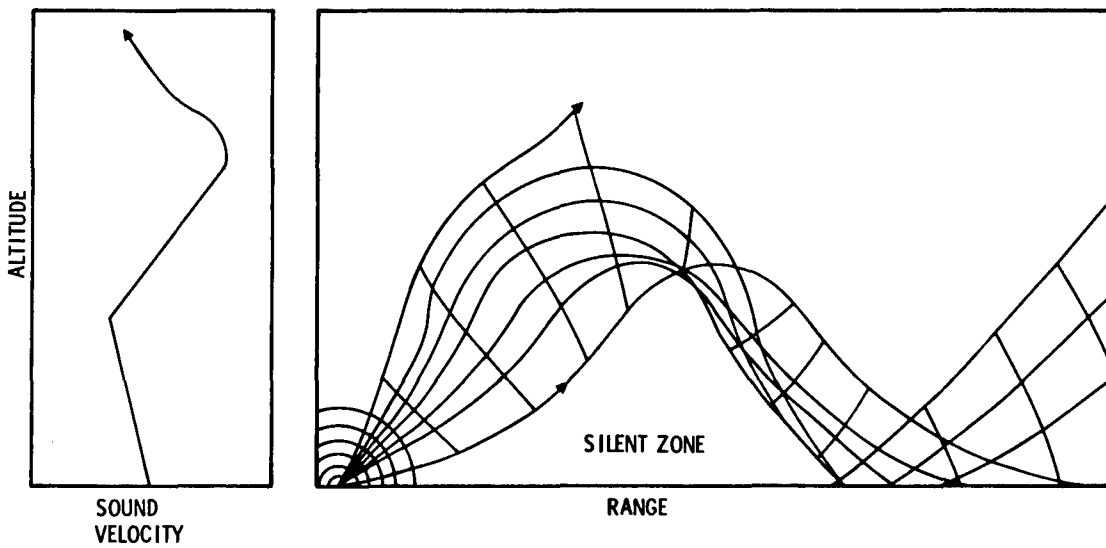


Fig. 2 Typical Explosion Ray Paths.

directions, through 200,000 ft. of observed atmospheric layers with gradients in both temperature and vector wind, in less than a minute on a CDC-3600. [Nevertheless, current periodicals contain several papers per year showing ray calculation programs which apparently were generated from digitizing the equations in the Dover Edition (7) of Lord Rayleigh's classical text. Most even assume homogeneous layers and overcome this deficiency by dividing the atmosphere into almost an infinity of infinitesimal layers, to fully use their computer capacity and help justify its acquisition.]

When there is a strong night-time temperature inversion, or equivalent low-level wind structure, as shown in Figure 3, there will be a continuous and enhanced blast pattern. Such inversions seldom extend beyond the 1500 ft. thick boundary layer. These propagations from NTS have been blocked or at least attenuated by the mountains which surround the test basins. Over flat terrain this inversion effect must be considered. A solution to the wave equations for this type of ducting has been obtained in the form of Airy Waves, by Byatt and Devault (8), but it has not been computer programmed or experimentally verified for lack of urgency in applications.

According to Cox, et al (9), the RANGER incident of 1951 was caused by jet stream winds, as shown by a similar pattern in Figure 4, which caused ducting above 20,000 ft. altitudes, and focusing at some range between 12 and 25 miles. This wave was almost perfectly reflected by the ground and repeated its atmospheric path several times until it struck Las Vegas. Only one other nuclear airburst was fired with strong northwest winds, on November 2, 1951, and results confirmed the theory. Four large plate windows were smashed, others were cracked, on Fremont Street, and boxes of china were knocked from shelves at the Desert Inn, according to newspaper accounts (10).

All other distant blast damages from later tests were caused by ducting at much higher altitudes, in the ozone-sphere near 150,000 ft. altitude, as shown by Figure 5. There is a warm layer centered near that altitude according to the U. S. Standard Atmosphere (11), so that even moderate wind speeds will cause ducting toward downwind directions. The blast ring usually strikes at 70 to 150 miles range. Fairly steady winds to 150 knots speed blow with seasonal directions at these high altitudes, from west in winter and from east in summer. Atmospheric magnifications and test yields were only occasionally both large enough to cause damage from this ducting. This was fortunate because sounding rockets were only developed in 1958 to measure these high-altitude conditions, after most of the large NTS atmospheric tests were completed. We could not have made predictions from measured atmospheric data and acoustic ray path calculations for earlier tests.

The pressure pulse signature from an explosion, at short range, is shown in Figure 6. After long travel through the atmosphere, with its various layers and turbulence, the

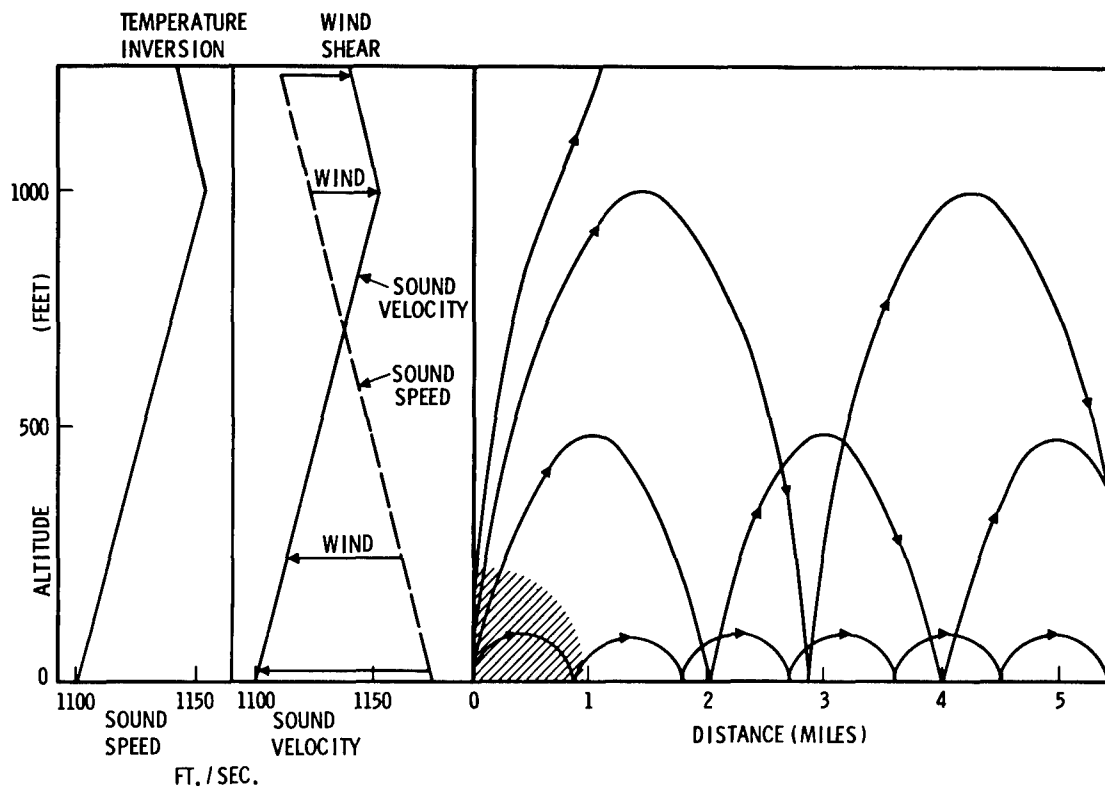


Fig. 3 Surface Inversion Sound Ducting.

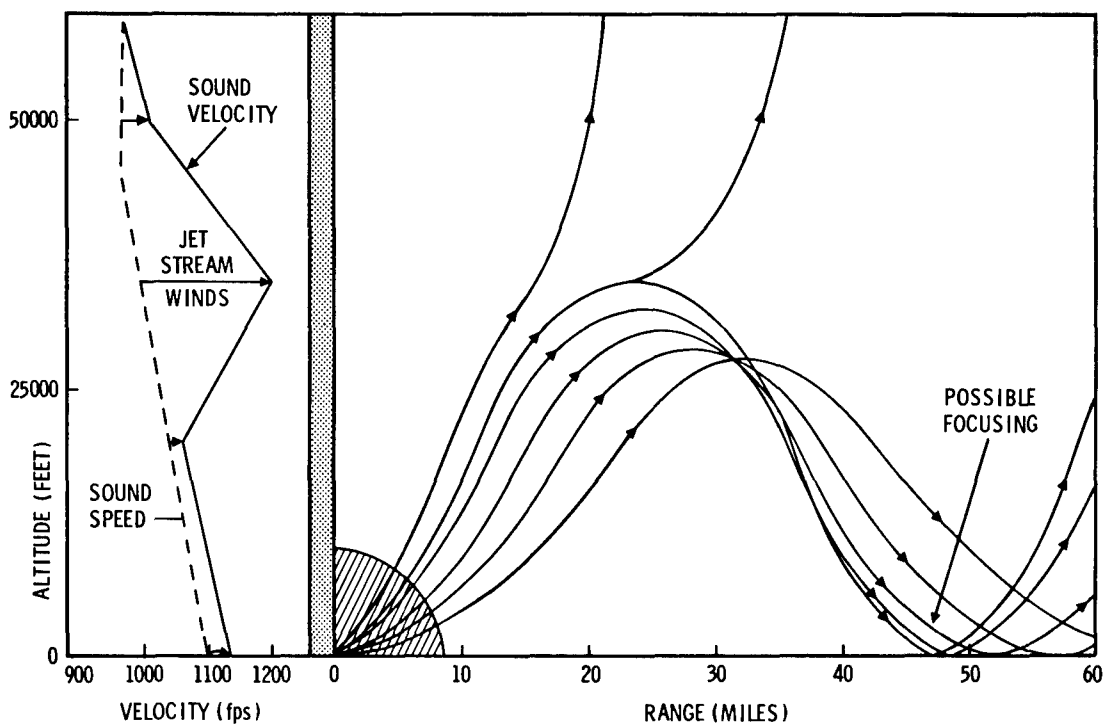


Fig. 4 Jet-Stream Sound Ducting.

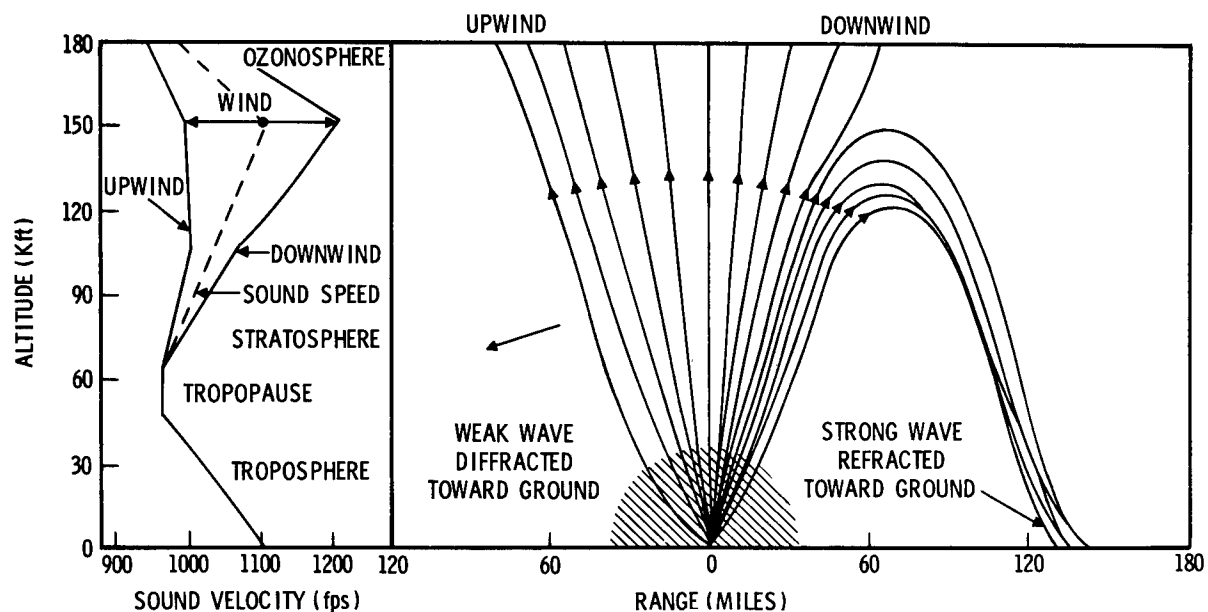


Fig. 5 Ozonosphere Wind Effect on Sound Ducting.

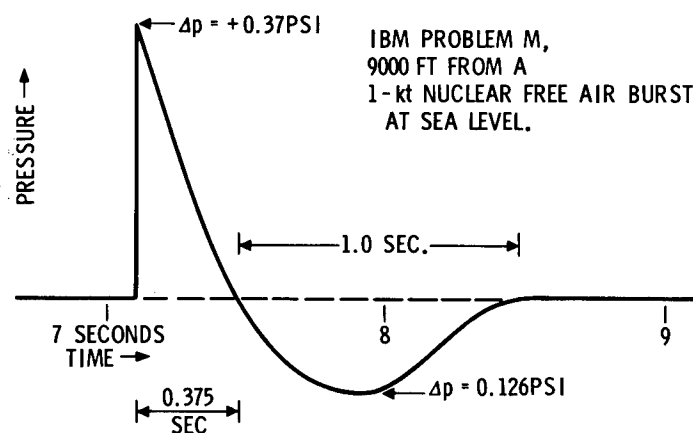


Fig. 6 Explosion Wave Pressure-Time Signature.

wave usually arrives as a rumbling of several cycles. Occasionally some of the classical waveform is preserved and loud bangs may be heard. Positive phase duration is usually two to four times as long as at close-in ranges, and near five seconds per cycle for 10 kt, but still in the range which may cause resonance in very large windows. Phase durations increase in proportion to the cube root of larger yields following Sachs (12) scaling, or A-scaling as described in The Effects of Nuclear Weapons (13).

Airblast standard overpressures are shown in Figure 7, for some distances of concern to off-site safety predictions. To 9000 ft. from 1-kt the hydrodynamic calculations, IBM Problem M, is used for a homogeneous, calm atmosphere at sea level pressure. This calculation was made at Los Alamos by Porzell, based on derivations by Bethe and Fuchs, but results are compiled in a report by Broyles (14). Scaling laws are shown for distance and time, with constant shock strength, $\Delta p/p$. These laws are used for adjustment to other yields and pressure altitudes. Beyond the hydro-calculation a power law decay is assumed, that $\Delta p \sim R^{-1.2}$, which also gives $\Delta p \sim W^{0.4}$ under the scaling laws. This decay was empirically determined from the Banshee experiments, at White Sands Missile Range in 1961 (15), with vertical propagations from 500 lb. HE bursts, and at Sandia with 1 lb. HE bursts. These were not distorted by refraction in the horizontally stratified atmosphere. It was also reasonably well confirmed by Reed (16) at PRAIRIE FLAT by comparison of propagations from different yields (1.2 ton and 500 ton HE) fired close in space and time to approximate equal atmospheric distortion. This experiment was conducted at Suffield Experiment Station, Alberta, Canada, in August 1968. We operated 18 microbarographs at one and two mile separations at ranges from 119 to 141 miles.

Recently more extensive hydro-calculation have been carried out to lower overpressures by Whittaker at AFWL (17) and by Lehto and Larson at NOL (18). These show lesser slopes like $\Delta p \sim R^{-1.12}$, but they still neglect attenuation of high frequencies by the low ozonosphere air densities, opposing reshocking effects, and air turbulence, so there is no overwhelming benefit to warrant making this minor change in prediction procedures at this time. There is concern with extrapolation to large Plowshare yields, so both theoretical and experimental refinements are being attempted to gain insight into the real decay laws, to provide more satisfying formulations for this important element of prediction.

Standard overpressures, scaled for planned yield, give amplitudes versus distance for propagation in a calm, homogeneous atmosphere. Acoustic calculation gives predictions of infinite magnification at caustics or foci, which cannot be correct, but the degree of reduction has not been satisfactorily obtained from theoretical analyses of the problem. Several attempts, by Viacelli at LRL (19), Seckler and Keller (20), and Barash (21), to name a few, have given differing results. The real atmosphere causes empirically determined refractive magnifications, or divergences, for

explosion waves, as shown in Figure 8, where values are multipliers on the standard overpressure. In practice, recorded peak-to-peak amplitude is usually reported for the noisy, quasi-sinusoidal waves at long range. For this, overpressure is multiplied by 1.35 to give peak-to-peak amplitude based on IBM Problem M, as shown earlier by Figure 6, and by another factor of two for ground reflection doubling as the wave strikes a ground level gage or a window pane near to ground level.

Recorded amplitude of troposphere signals versus distance curves for nuclear test series in the 1950's are shown in Figures 9-12. Amplitudes have been normalized to 1-kt free airbursts, and height-of-burst effects have been removed. The scatter results from differences in atmospheric refraction effects on propagation.

The annual cycling of ozonosphere signal amplitudes is best displayed by comparing records from St. George, Utah, and Bishop, California, in Figures 13 and 14. These data are also normalized for yield and height-of-burst. Maximum propagation goes east to St. George in winter, west to Bishop in summer. These stations were at about 135 miles range. At the shorter range of Boulder City, shown in Figure 15, seasonal cycling is not so pronounced. At Las Vegas, in Figure 16, it is hardly noticeable. These closer stations are usually in the calculated silence zone, short of the range of ray arrivals calculated by atmospheric ray tracing. What they do get is noise scattered or diffracted down from the stronger wave passing overhead. This scattering effect is probably caused by partial reflection from either atmospheric layers with locally large vertical sound velocity gradients and wind shears, or cells of turbulence, sometimes called turbulons, where temperature and wind may vary from the mean for the layer. It is not much influenced by the season or upper winds but appears to be mostly determined by the temperature inversion and associated wind shears and turbulence near 100,000 ft. altitudes, which apparently do not change much with season.

Seasonal direction patterns persist throughout temperate and polar latitudes but high altitude circulation over the equator and tropics is more complicated. From rocket data collected by the IOCS project, it was found by Buell (22) that about half of the high altitude wind variance is explained by very long secular waves, shown in Figure 17. The predominant wave at 150,000 ft., for ozonosphere propagation ducting, has six months periodicity in agreement with results by R. J. Reed (23) for Ascension Island at 9° south latitude. There is a significant annual periodicity superimposed and some influence of the quasi-biennial wave may also be found. The important conclusion for tropical latitudes is that there are usually four periods each year with nearly calm conditions and minimized distant airblast ducting. There are only two such periods in temperate latitudes.

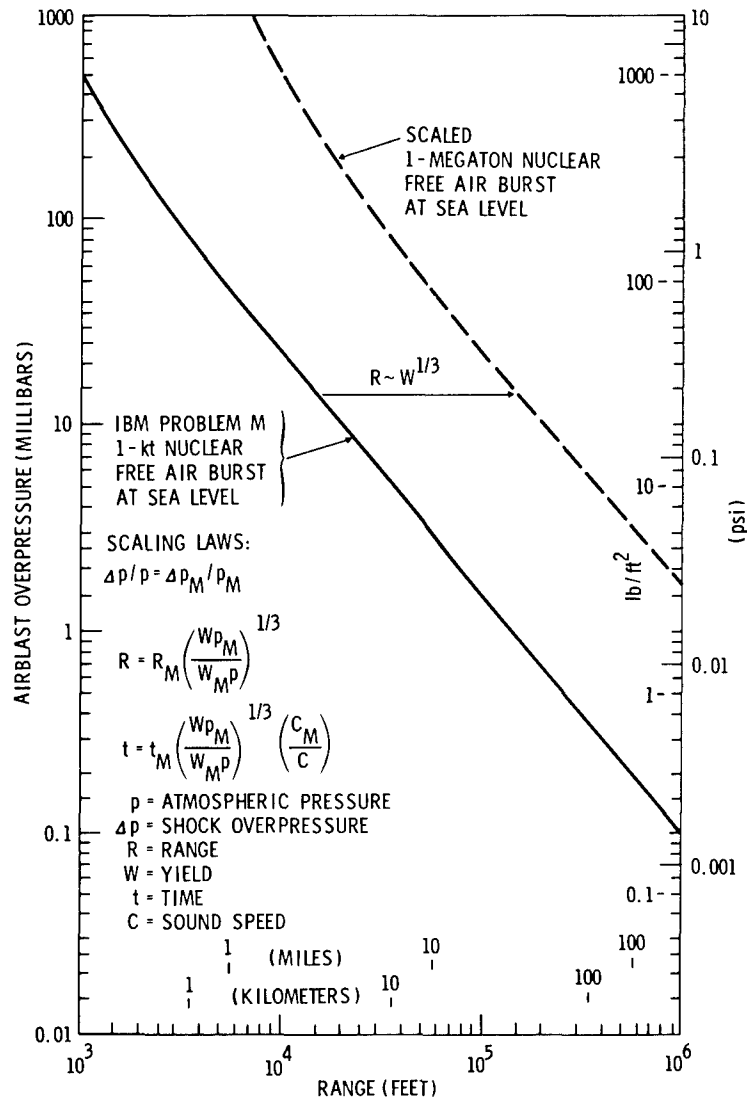


Fig. 7 Standard Explosive Overpressure-Distance Curves.

ATMOSPHERIC FOCUS FACTORS

$$F = \frac{\Delta p(W; \text{REAL ATMOSPHERE})}{\Delta p(W; \text{HOMOGENEOUS, CALM ATMOSPHERE})}$$

FOCUS FACTORS

<u>DUCTING</u>	<u>TYPICAL</u>	<u>EXTREME</u>
INVERSION	2	3
JET STREAM	1.6	4
OZONOSPHERE	1.5	3.5
IONOSPHERE	0.1	0.2

Fig. 8 Atmospheric Focus Factors.

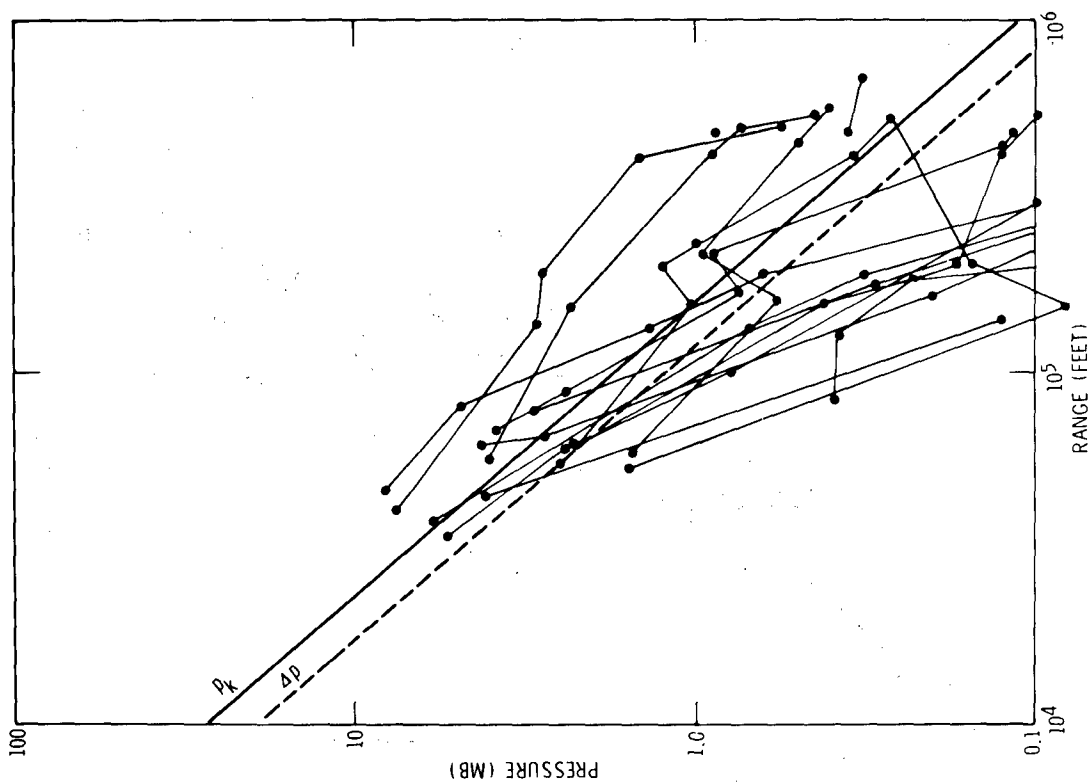


Fig. 10 Summary of Troposphere Propagations, Teapot, 2/18-5/15, 1955.

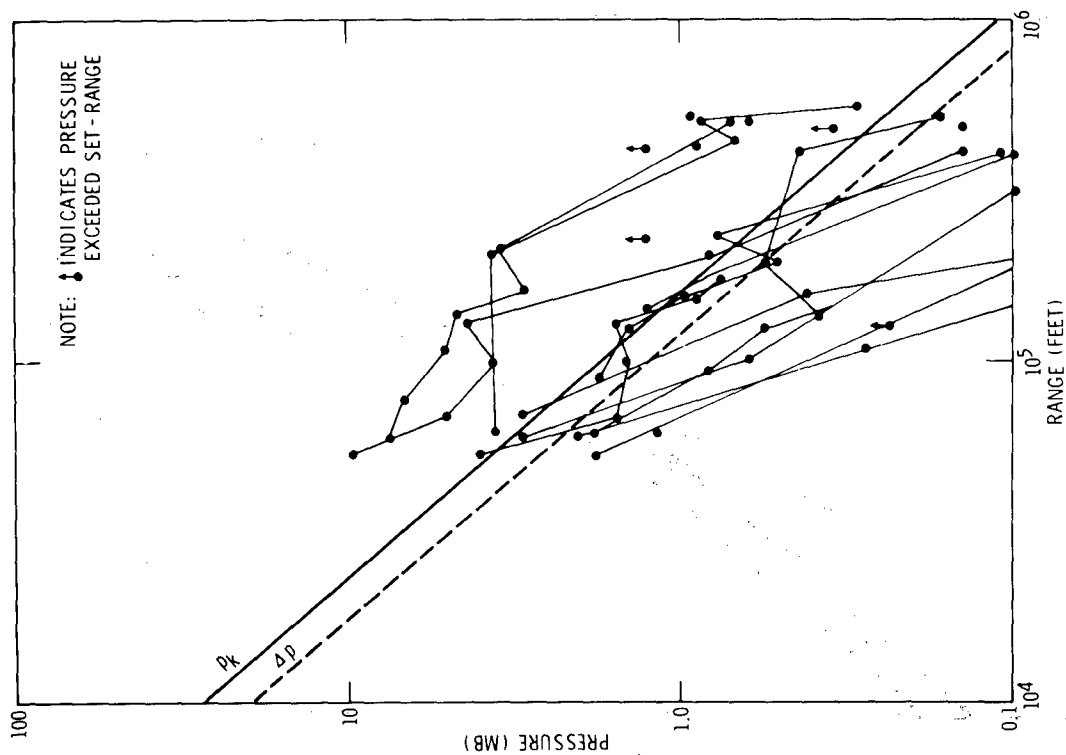


Fig. 9 Summary of Troposphere Propagations, Upshot-Knothole, 3/17-6/4, 1953.

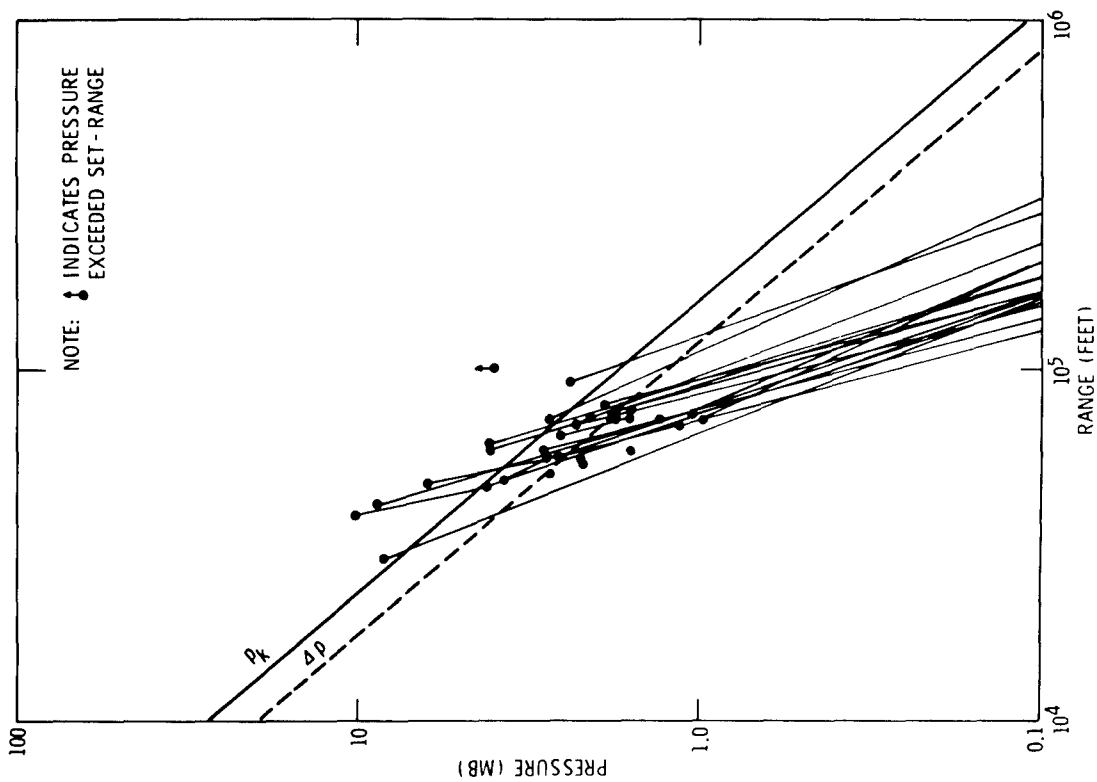


Fig. 11 Summary of Troposphere Propagations, Plumbob, 5/28 - 10/7, 1957.

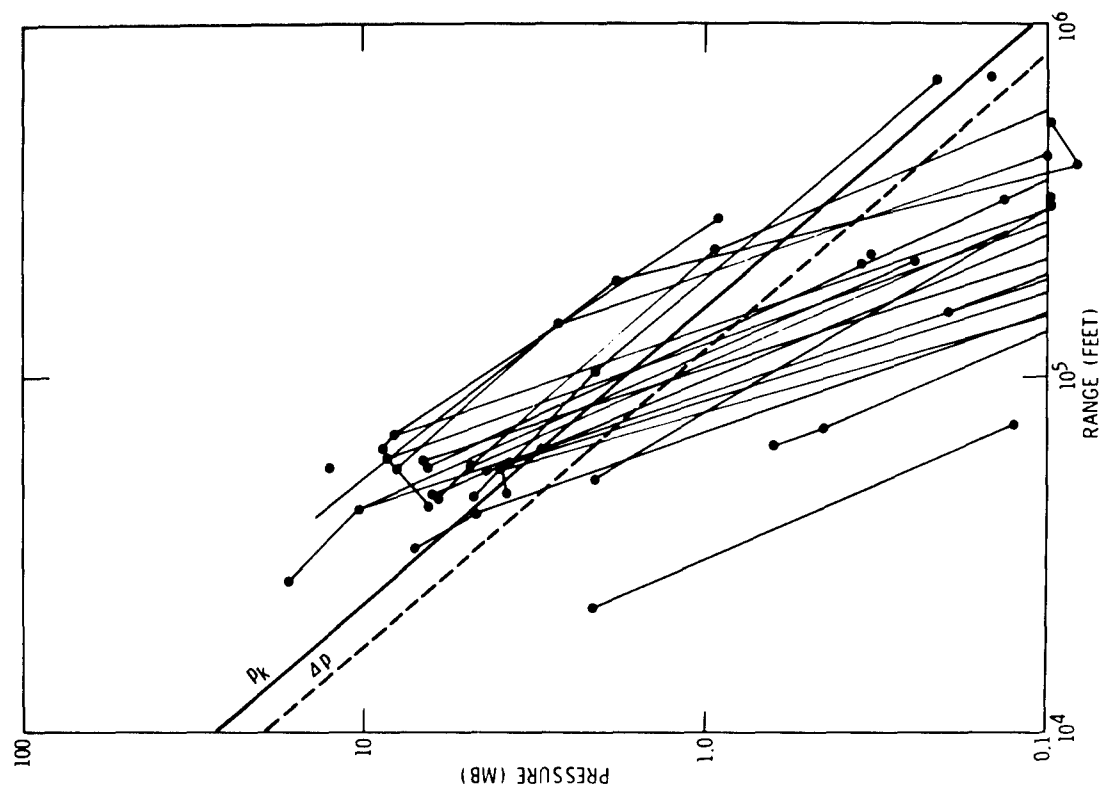


Fig. 12 Summary of Troposphere Propagations, Hardtack II, 9/19 - 10/29, 1958.

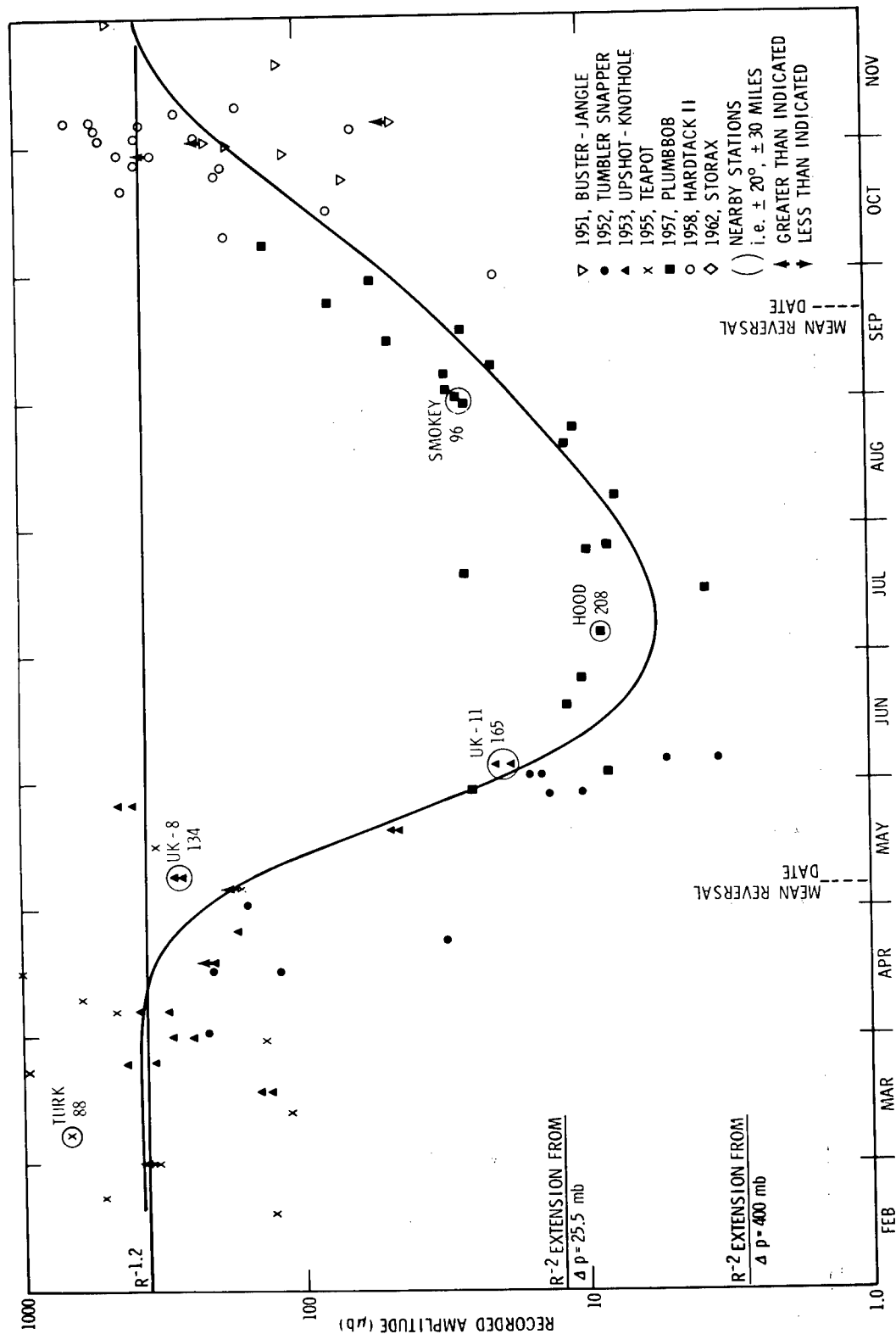


Fig. 13 Ozonosphere Signal Amplitudes, St. George, Utah.

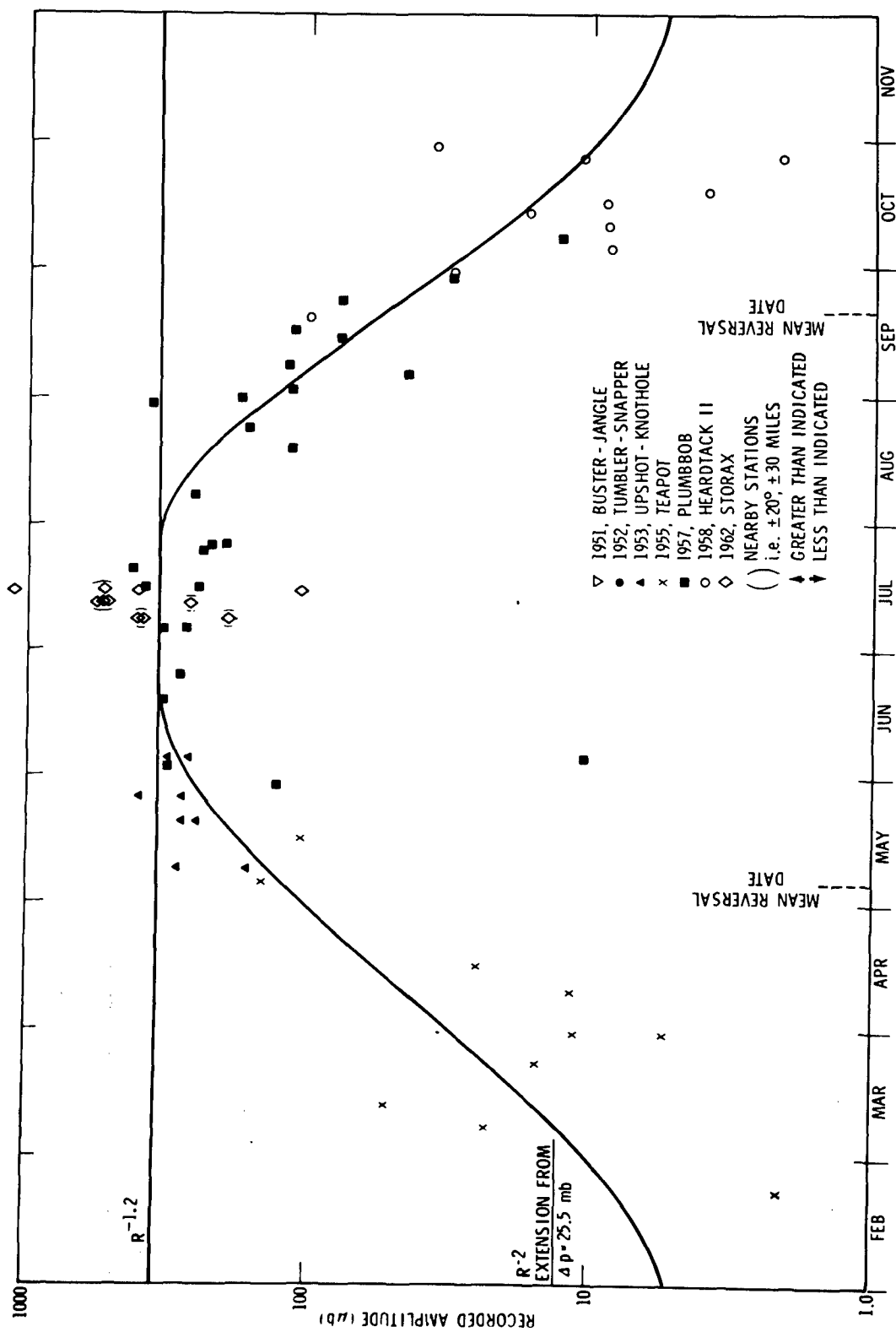


Fig. 14 Ozonosphere Signal Amplitudes, Bishop, California.

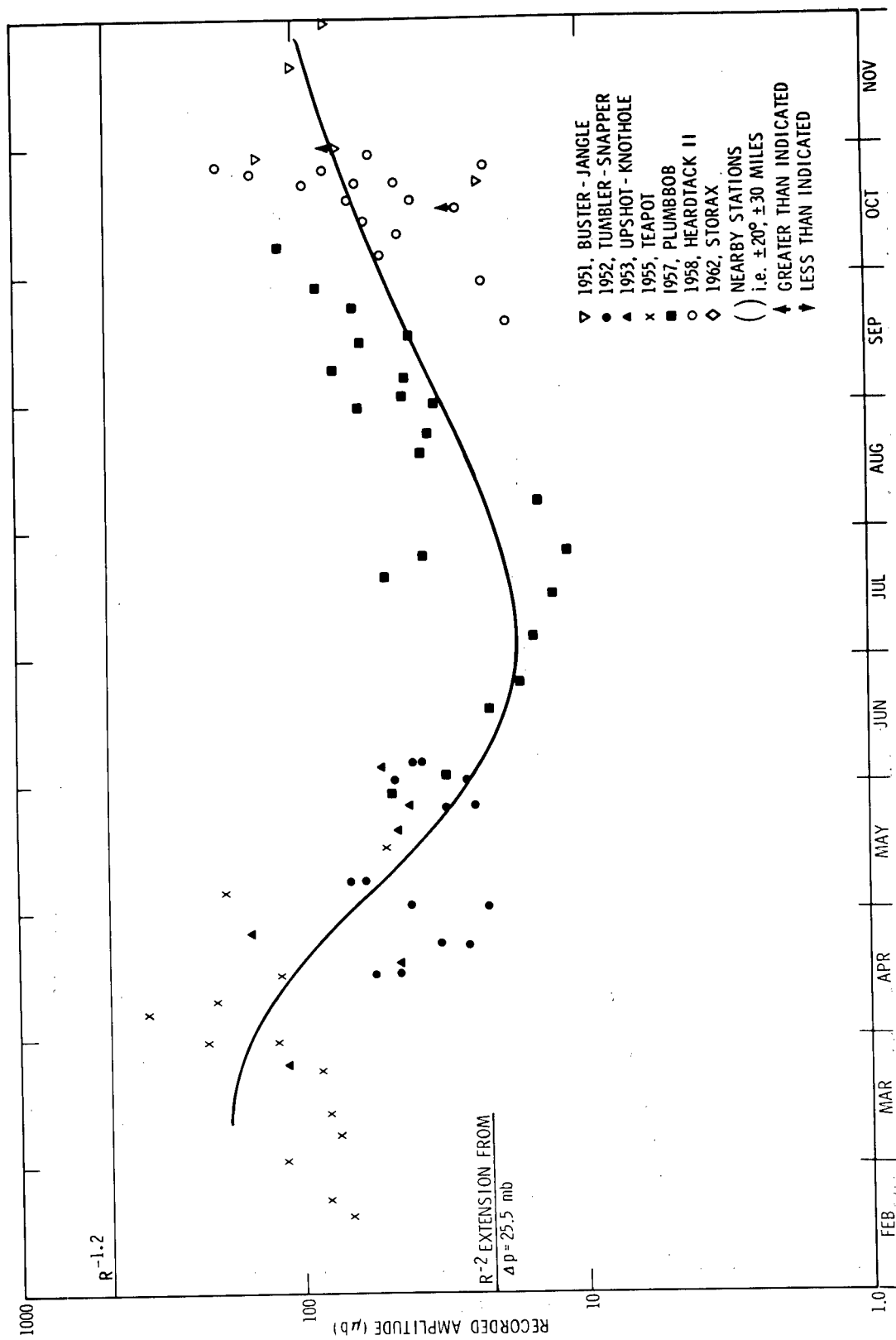


Fig. 15 Ozonosphere Signal Amplitudes, Boulder City, Nevada.

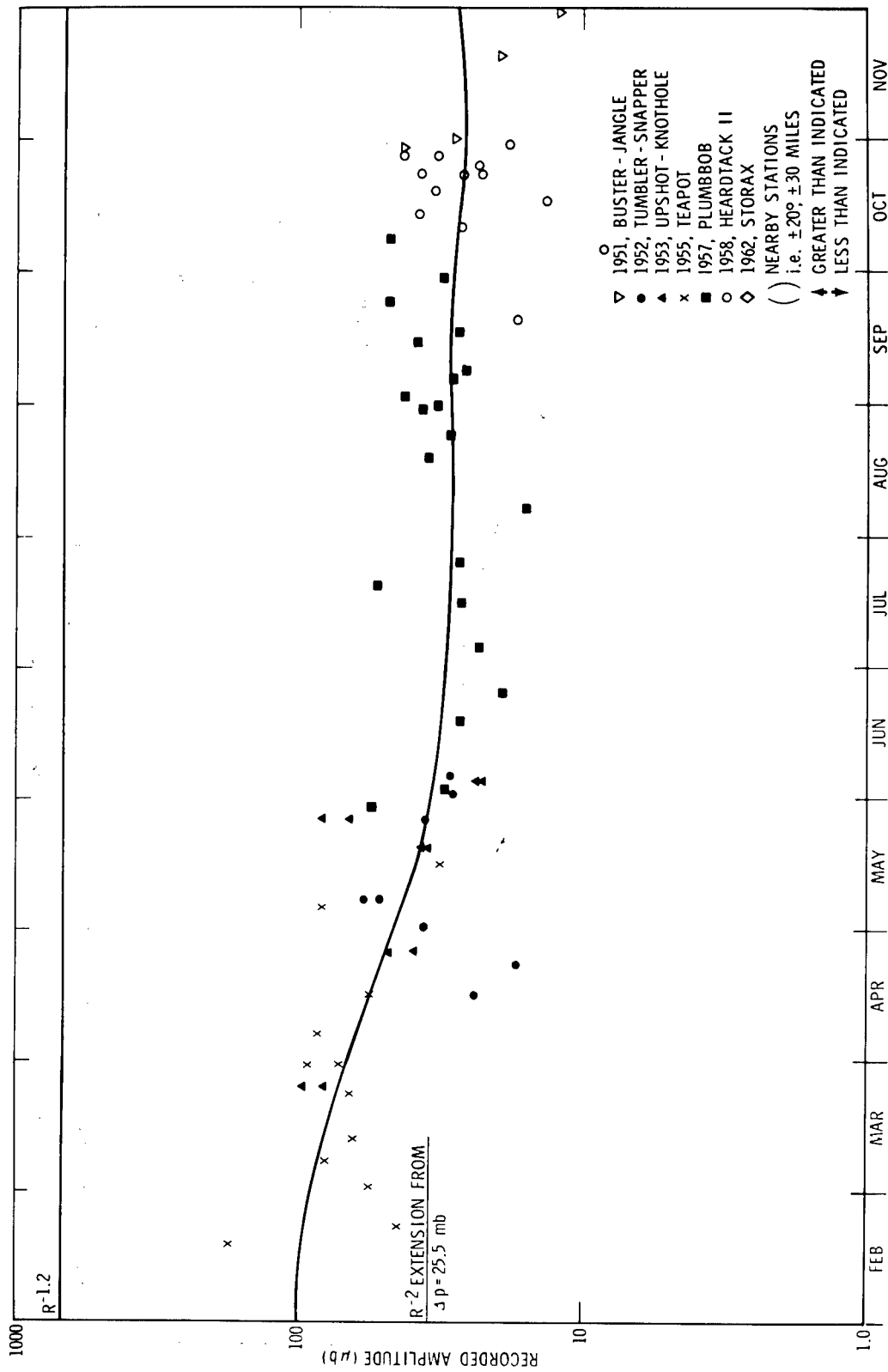


Fig. 16 Ozonosphere Signal Amplitudes, Las Vegas, Nevada.

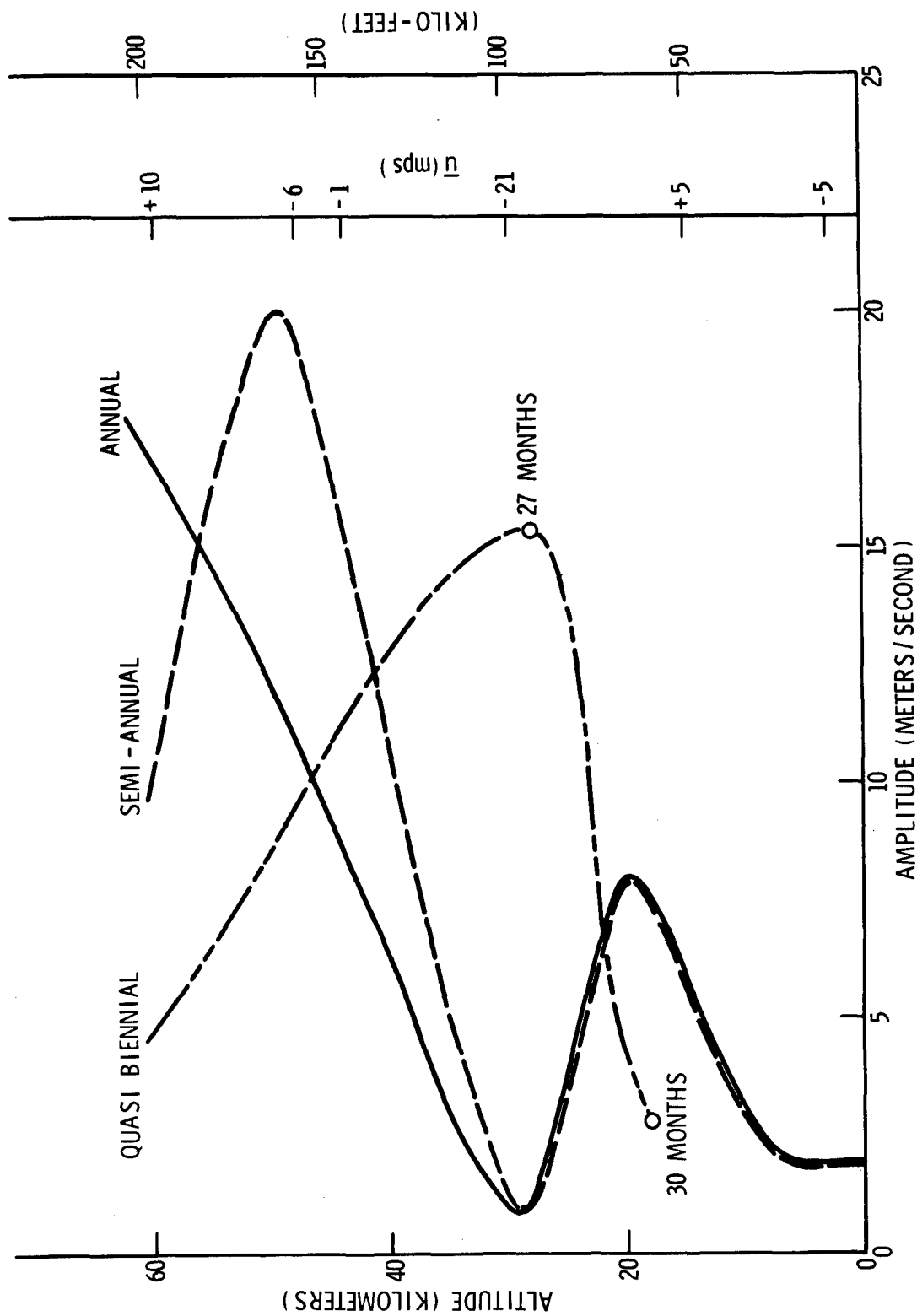


Fig. 17 Panama Zonal Wind Analysis—Secular Components per Buell, 6/23/69.

A computer movie of the three years of rocket soundings at Battery MacKenzie, Canal Zone, has been prepared to show the oscillatory nature of these ducting zonal wind speeds.

II. Plowshare Explosives

Underground bursts give airblast waves which are in varying degrees muffled and distorted by the shot environment. As shown in Figure 18, bursts at shallow depths are only slightly changed from the airburst character. At contained depths only a ground-shock-induced wave is coupled to the air by the piston-like mechanism of surface motion. At intermediate depths of burst, for cratering events, both ground-shock-induced and gas-venting pulses may be observed.

Piston theory reliably predicts air overpressures from contained bursts, assuming that ground motion velocities in the surface zero region are adequately predicted by the ground motion specialists--and they usually are. At minimum containment burst depths the airwave overpressure would not much exceed 1 psi at surface zero, compared to almost 100 psi at the same distance from an airburst, so the safety problems are much reduced. The main concern is with light aircraft observing the event for any of various reasons, and they must not be exposed to more than 0.2 psi. They are usually restricted to flying at or beyond about four burst depths, or a little less overhead where ambient pressure and shock strength decreases with altitude.

Cratering events, however, can cause large enough waves to give distant damages. Their muffling may be empirically expressed by a transmission factor, shown in Figure 19. Transmissivity is defined by the ratio of overpressure, or amplitude, from the underground burst, to that expected from the same device but airburst.

Some distant observed transmission factors, for various nuclear cratering test events, versus scaled burst depth, are shown in Figure 20. There is considerable scatter and uncertainty because of the difference in geological media between these events, because of non-uniformities with direction in the gas venting eruption, and because of atmospheric variability. This last causes differences in propagation when compared to the small airburst HE calibration shots used to establish atmospheric propagation patterns. Calibration shots have been found by Reed (24) to be non-repeatable in amplitude by factors of 1.6, geometric standard deviation, in time separations of only a few minutes. On the average, however, this variability smooths out.

Schooner results, indicating little attenuation from burial, are probably explained by the high water content of the burst environment which gave a very large steam bubble and enhanced the gas-venting pulse. Certain explanation must await our obtaining further data from future nuclear cratering experiments and more complete hydro-calculations such as are done at LRL (24a).

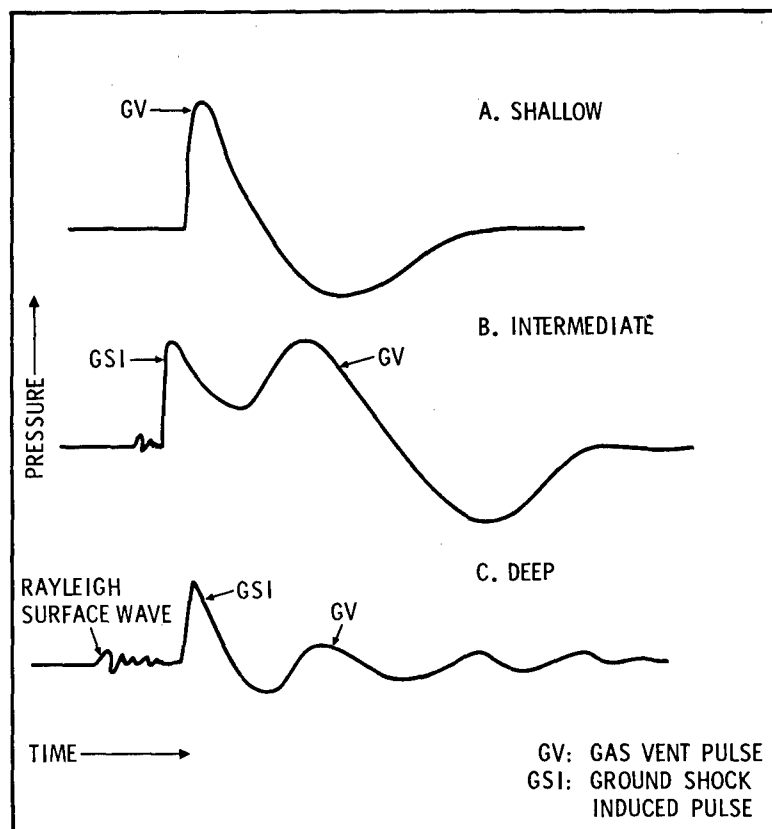


Fig. 18 Cratering Explosion Pressure-Time Signatures.

TRANSMISSIVITY DEFINITION

$$T = \frac{\Delta p(W, \text{UNDERGROUND BURST})}{\Delta p(W, \text{AIRBURST})}$$

Fig. 19 Transmissivity Definition.

Even with a source model based on Schooner, however, large Plowshare excavators could be fired during periods of minimum atmospheric propagation with negotiable effects. Figure 21 shows standard recorded amplitudes versus distance for single charge 1-Mt cratering bursts near sea level. Near 135 miles range standard amplitudes, typical of downwind ozonosphere propagation, would be 6 mb with a chance of magnification to 20 mb. This could give extensive nuisance damage, even without further increase necessary for a row charge salvo of many devices. To clearly control damage, firing during ozonosphere calm transition periods would give only 2 mb amplitudes.

Airblast from row charges, as shown in Figure 22, is considerably enhanced in directions perpendicular to the row. Empirical data, observed at close ranges by Vortman (25), show a compromise result, between $N^{0.4}$ increase with number of charges, N , which follows from yield addition, and N dependence from acoustic wave addition by interference. The exponent observed is $N^{0.7}$, so that a row of ten charges causes five times the amplitude emitted by a single charge. Exercises with burst depth variations, charge spacing, and timed intervals between detonations would help to refine this estimate if really needed.

III. Damage Predictions

Although there have been clear occasions where plaster walls were cracked at low amplitudes which did not break any windows, the latter damages are most spectacular, pose some hazard, any usually generate the largest repair bills. A rough rule of thumb is that total damage claims are 40 percent greater than the window claims bill. It remains to predict glass damage versus predicted airblast amplitude.

In theory glass panes are treated as simply supported thin plates, uniformly loaded, so that maximum stress occurs near the center of the pane. The load or pressure at failure should be proportional to the pane area, inversely proportional to the square of the thickness, and proportional to the breaking stress of the particular glass. Laboratory tests, by Ansevin (26) at the Pittsburgh Plate Glass Company, have shown mean breaking stresses for various glasses to range from about 6,000 psi to 30,000 psi for rapid loading as in explosion airblast waves or sonic booms. There is, however, appreciable scatter in test results which has been described by McKinley (27) as a 25 percent standard deviation around the mean breaking stress. This may be useful to designers, interested in safety factors of two, and recommended by the Pittsburgh Plate Glass Company (28), but it is not adequate for nuisance damage prediction where 10^{-4} failure probabilities can create a large reaction in a city with 10 million window panes. The Gaussian distribution with 25 percent standard deviation gives total failure, 4σ , with about 4×10^{-5} probability, under no load. There have not been enough glass test samples to adequately show just what the small probability distribution looks like, but a log-normal distribution assumption avoids the no-load breaking result. The distribution described by Weibull (29),

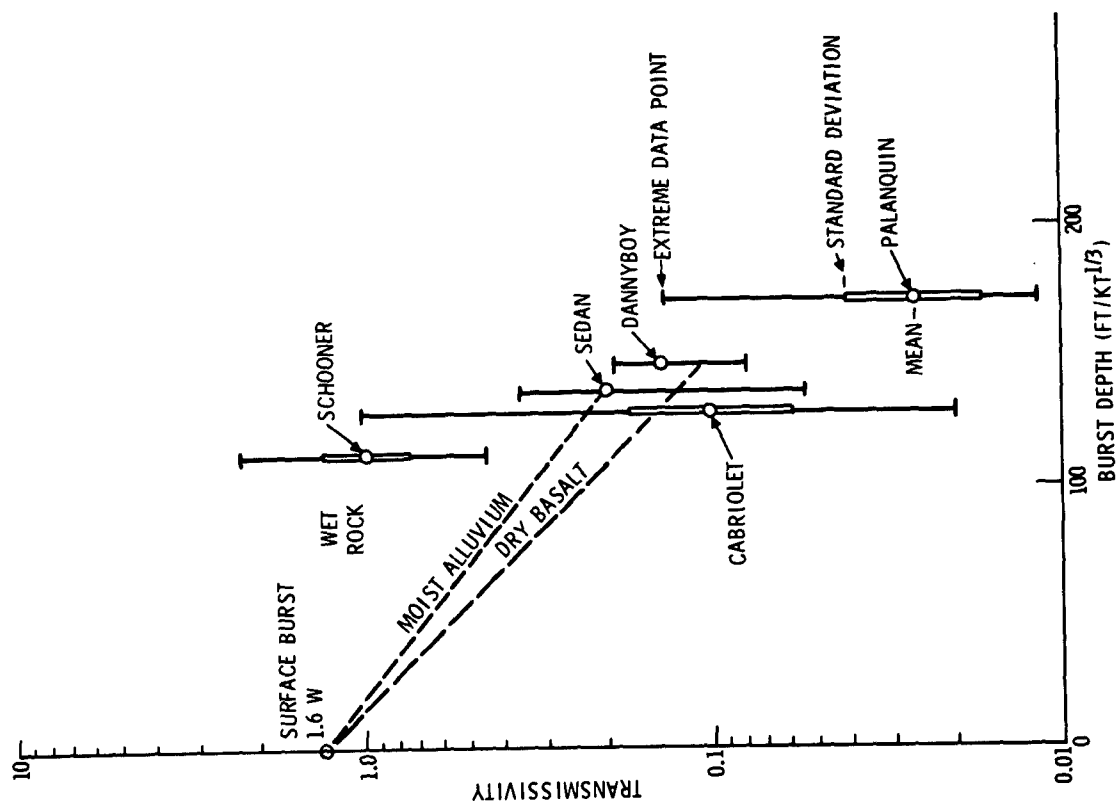


Fig. 20 Airblast Transmissivity from Underground Nuclear Tests.

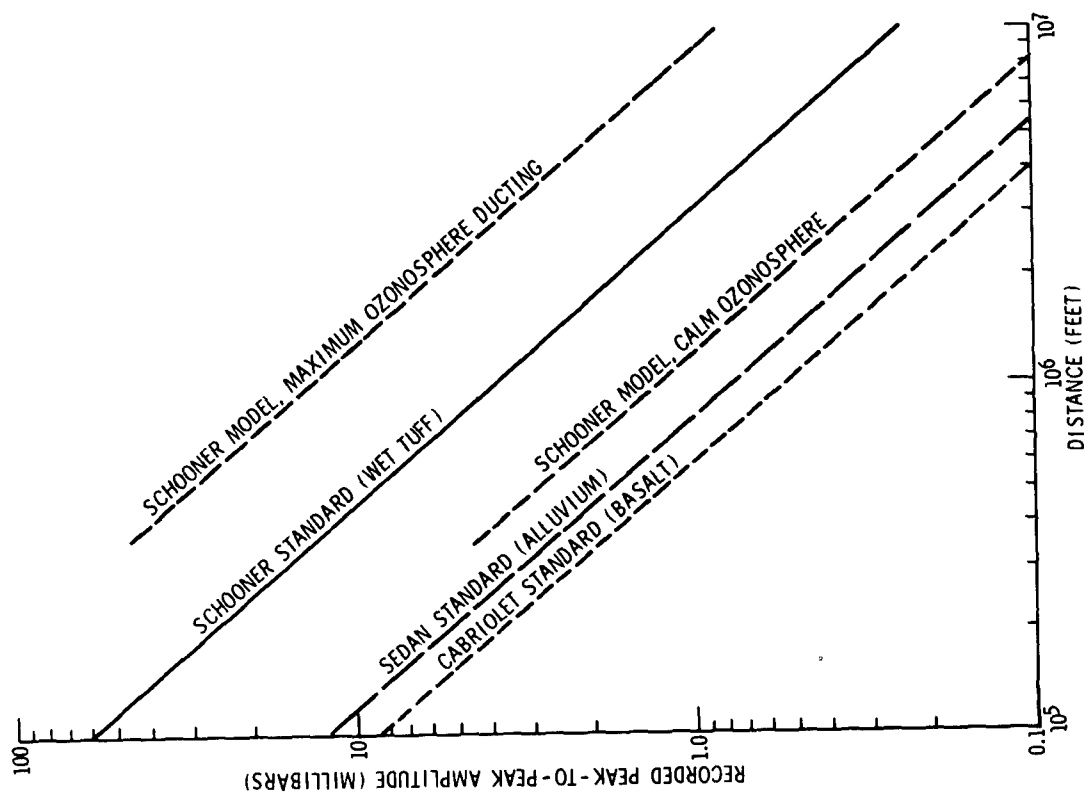


Fig. 21 Airblast Amplitudes for 1-Mt Crater Bursts.

a weakest link model, may also be assumed, but again, there are yet insufficient data to show a better fit than is given by the log-normal.

Large pane areas are most vulnerable and they are further affected by resonances with sonic boom or explosion waves. Maximum deflections and stresses occur on the rebound, as shown by Wiggins (30), sometimes synchronous with the negative pressure phase. This has been verified by the multitude of occasions where large store windows wound up on the sidewalk. Back-chamber Helmholtz resonance may also contribute significantly, according to Seshadri (31), depending on the room or building protected by the glass pane. Rather complete calculated estimates have been made for sonic booms by Blume, et al (32), and Wiggins (33), with consideration of these factors plus assumed damping and directional exposure effects, to explain various damage incidents. To date some have given the right order of magnitude for breakage but there have been inconsistencies and credibility limitations with the simplified theory.

At this time, while awaiting expected improvements, damage predictions for Plowshare purposes may be made from the results of the Medina explosion described by Reed, Pape, Minor, and DeHart (34). An accidental explosion of 115,000 lbs. of chemical explosives near San Antonio, Texas brought claims for 3,644 broken panes in that city. Special weather data were obtained and a blast prediction calculation for refracted waves was made, giving an overpressure pattern which resembled the claims patterns. A census of total exposed panes, by pane area categories, was made that allowed final calculation of breakage probability versus pane area and incident overpressure. This result is summarized in Figure 23, for the distribution of pane sizes as counted in San Antonio. Applied to other incidents, the Medina relation often appears to work quite well but occasionally misses. Further work on this problem continues to be sponsored by the SST project (35), for it is most important to predicting damage from sonic booms.

Recent calculation, with Latin-American window pane census data, indicates that nuclear excavation of a sea level canal in 1979 would probably break 6,000 to 10,000 panes, at a cost of about \$150,000, from either the Panama-Darien route or the Colombia-Atrato route. This damage level for the entire series of salvos, spread over whatever the construction period turns out to be, only totals two to three times the accidental damage to San Antonio in 1963.

No one was hurt by broken glass in San Antonio. Breaking glass may be a hazard, though, for a sonic boom at the Air Force Academy graduation in 1968 broke 300 panes, cut 15 people, hospitalizing one, according to news report (35). This extreme example points up needs for concern, warnings necessary, and public relations required to counter airblast effects from Plowshare.

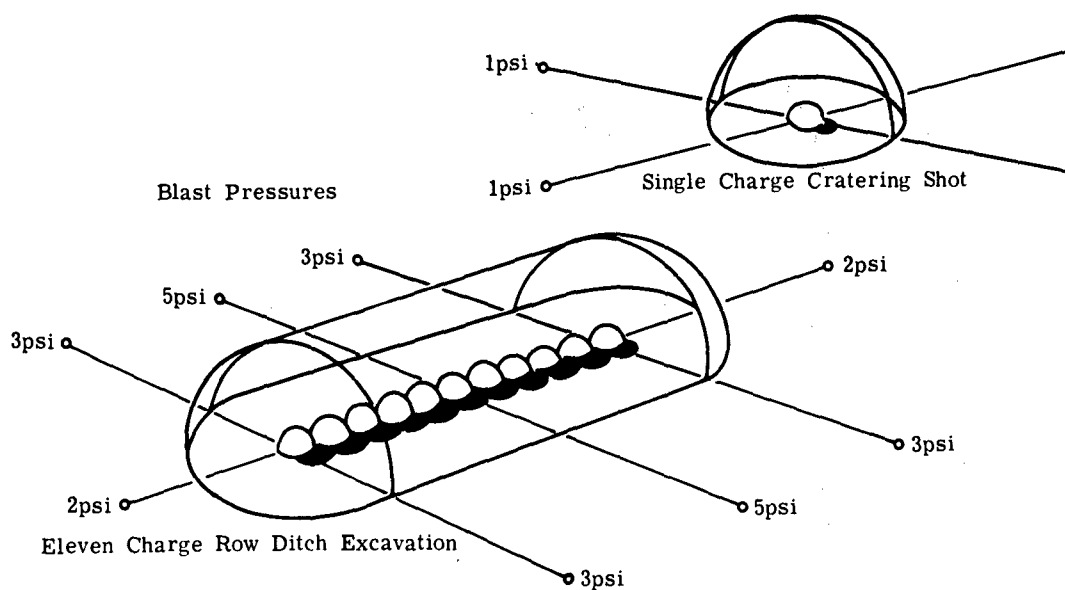


Fig. 22 Blast from Multiple Charges.

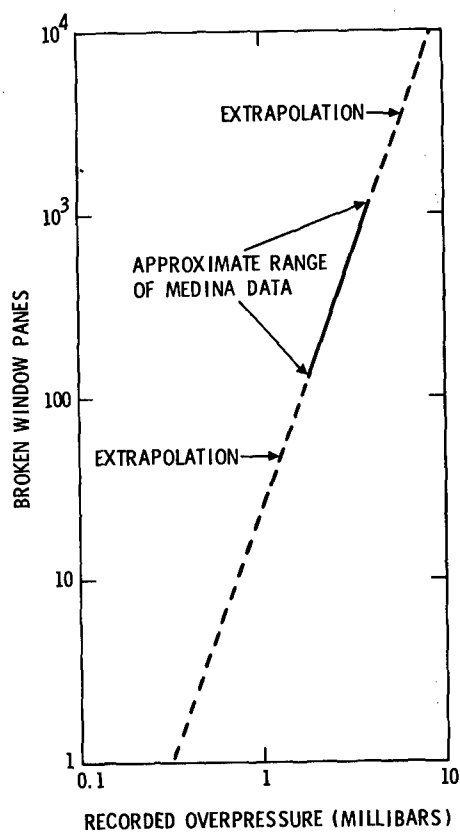


Fig. 23 Expected Window Damage versus Explosion Blast Overpressure, 100,000 People Exposed.

REFERENCES

1. Fujiwhara, S., "On the Abnormal Propagation of Sound," Bull. Cent. Meteor. Obs. Japan 2 (1) (1912).
2. Rothwell, P., "Calculation of Sound Rays in the Atmosphere," J. Acoust. Soc. Amer. 19, 205 (1947).
3. Cox, E. F., H. J. Plagge, and J. W. Reed, "Meteorology Directs Where Blast Will Strike," Bull. Am. Meteorol. Soc., Vol. 35, No. 3, pp. 95-103, March 1954.
4. Durham, H. B., "Raypac - A Special Purpose Analogue Computer," Sandia Corp. TM-46-55-54, March 24, 1955.
5. Thompson, R. J., "Sound Rays in the Atmosphere," Sandia Corp., SC-RR-64-1756, January 1965.
6. Thompson, R. J., "Computing Sound Ray Paths in the Presence of Wind," Sandia Corp., SC-RR-67-53, February 1967.
7. Lord Rayleigh, Theory of Sound, Sec. 270, Dover Publications, New York, 1945.
8. Byatt, W. J. and G. P. DeVault, "An Iteration Variation Method for Wave Propagation Problems," J. Geophys. Res., Vol. 66, June 1961.
9. Cox, E. F., H. J. Plagge, and J. W. Reed, "Damaging Air Shocks at Large Distances from Explosions, Operation Buster-Jangle," Sandia Corp., WT-303, April 24, 1952.
10. Yacenda, A., "Congress Trio Hails War Games," Las Vegas Morning Sun, November 2, 1951.
11. U. S. Standard Atmosphere, 1962, NASA-USAF-USWB, U. S. Government Printing Office, Washington, December 1962.
12. Sachs, R. G., "The Dependence of Blast on Ambient Pressure and Temperature," Report 466, Ballistic Research Laboratory, Aberdeen Proving Ground, Maryland, 1944.
13. The Effects of Nuclear Weapons, S. Glasstone, editor, Rev. Ed., DOD/AEC, U. S. Govt. Printing Office, Washington, D. C., April 1962.
14. Broyles, C. D., "IBM Problem M Curves," SCTM-268-56(61), Sandia Corp., December 1, 1956.
15. Kelso, J. R., G. Stalk, and C. C. Clifford, Jr., "Project Banshee Field Operations," (1961 and 1962), Preliminary Report, DASA-543, Defense Atomic Support Agency, May 1963.
16. Reed, J. W., "Distribution of Airblast Amplitudes in the Ozonosphere Sound Rings," SC-M-69-33, Sandia Laboratories, February 1969.
17. Whittaker, Maj. W. A., unpublished communication, U. S. Air Force Weapons Laboratory, Kirtland AFB, N. M., July 1969.
18. Lehto, D. L., and R. A. Larson, "Long Range Propagation of Spherical Shockwaves from Explosions in Air," NOLTR 69-88, U. S. Naval Ordnance Laboratory, to be published.
19. Viecelli, J., "Atmospheric Refraction and Focus of Blast Waves," J. Geophys. Res., Vol. 72, No. 10, May 15, 1967.
20. Seckler, B. D. and J. B. Keller, "Geometrical Theory of Diffraction in Inhomogeneous Media," J. Acoust. Soc. Amer., Vol. 31, pp. 192-216, 1959.
21. Barash, R. M., "Evidence of Phase Shift at Caustics," J. Acoust. Soc. Amer., Vol. 43, pp. 378-380, 1968.
22. Buell, C. E., unpublished communication, Kaman Nuclear, August 1969.
23. Reed, R. J., "Zonal Wind Behavior in the Equatorial Stratosphere and Lower Mesosphere," J. Geophys. Res., Vol. 71, September 15, 1966.
24. Reed, J. W., "Amplitude Variability of Explosion Waves at

- Long Ranges," J. Acoust. Soc. of Amer., Vol. 39, No. 5, Pt. 1, May 1966.
- 24a. Knox, J. B., and R. W. Terhune, "Calculation of Explosion Produced Craters-High Explosive Sources," UCRL-7738 (Rev. I), Lawrence Radiation Laboratory, Livermore, California, October 1964.
 25. Vortman, L. J., "Close-in Air Blast from a Row Charge in Basalt," Project Dugout Final Report, PNE-608F, Sandia Corporation, Albuquerque, New Mexico, August 4, 1965.
 26. Ansevin, R. W., "Correlation of the DSR with the Strength of Glass of Different Compositions and Configurations," Pittsburgh Plate Glass Company, Air Force Materials Laboratory, Wright-Patterson Air Force Base, Contract Report ML-TDR-04-180, August 1964.
 27. McKinley, R. W., "Response of Glass in Windows to Sonic Booms," Materials Research and Standards, Vol. 4, No. 11, November 1964.
 28. Glass Product Recommendations--Structural, Tech. Svc. Report, No. 101, Pittsburgh Plate Glass Company, 1964.
 29. Weibull, W., "A Statistical Distribution Function of Wide Applicability," J. of Appl. Mech., Vol. 18, No. 3, September 1951.
 30. Wiggins, J. H., Jr., Effects of Sonic Boom, J. H. Wiggins Company, Palos Verdes Estates, California, 1969.
 31. Seshadri, T. V., "Transient Response of Mechano-Acoustical Networks," Doctoral Dissertation, Univ. of Oklahoma, May 1968.
 32. Blume, J. A., R. L. Sharpe, J. Proulx, and E. G. Kost, "Response of Structures to Sonic Booms," Annex G, Part I, of NSBEO-1-67, National Sonic Boom Evaluation Office, July 28, 1967.
 33. Wiggins, J. H., Jr., "The Effects of Sonic Boom on Structural Behavior," SST Report No. 65-18, Federal Aviation Agency, J. A. Blume and Associates, San Francisco, October 1965.
 34. Reed, J. W., B. J. Pape, J. E. Minor, and R. C. DeHart, "Evaluation of Window Pane Damage Intensity in San Antonio Resulting from Medina Facility Explosion on 13 November 1963," Proceedings of Conference on Prevention and Protection Against Accidental Explosion of Munitions, Fuels and Other Hazardous Materials, (10-13 October 1966), Annals of the New York Academy of Sciences, October 28, 1968.
 35. Subcommittee on Physical Effects, Committee on SST-Sonic Boom, "Report on Physical Effects of the Sonic Boom," NAS-NRC, Washington, D. C., February 1968.
 36. Albuquerque Journal, "Boom Shatters 300 Windows," June 1, 1968.

ABSTRACT

CLOSE-IN AIRBLAST FROM UNDERGROUND EXPLOSIONS

Air overpressures as a function of time have been measured from surface zero to about $170 \text{ ft/lb}^{1/3}$ along the ground from nuclear and chemical explosions. Charge depths varied from the surface to depths below which explosion gases are contained. A ground-shock-induced air pressure pulse is clearly distinguishable from the pulse caused by venting gases. Measured peak overpressures show reasonable agreement with the theoretical treatment by Montan.* In a given medium the suppression of blast with explosion burial depth is a function of the relative distance at which the blast is observed. Rates of suppression of peak overpressure with charge burial are different for the two pulses. Rates are determined for each pulse over the range of distances at which measurements have been made of air overpressure from chemical explosions in several media. Nuclear data are available from too few shots for similar dependence on burial depth and distance to be developed, but it is clear that the gas venting peak overpressure from nuclear explosions is much more dependent on medium than that from chemical explosions.

For above-ground explosions, experiment has shown that airblast from a 1-kiloton nuclear explosion is equal to that from a 0.5-kiloton TNT explosion. Data on ground-shock-induced airblast is now sufficient to show that a similar relationship may exist for buried explosions. Because of medium dependence of the gas venting pulse from nuclear explosions, data from additional nuclear events will be required before a chemical/nuclear airblast equivalence can be determined for the gas-venting pulse.

*D. H. Montan, "Source of Airblast from an Underground Explosion," Transactions, American Nuclear Society, Vol. II, No. 2, November 1968, pp. 541, 542.

CLOSE-IN AIRBLAST FROM UNDERGROUND EXPLOSIONS

L. J. Vortman
Sandia Laboratories
Albuquerque, New Mexico

INTRODUCTION AND BACKGROUND

Airblast has been measured near the ground surface close to a large number of cratering detonations of buried chemical explosives in single-charge (Table 1), row-charge (Table 2), and horizontal-array (Table 3) configurations. The term "close-in" refers to distances sufficiently small that meteorological effects on blast propagation are not significant. Measurements have been made on a smaller number of detonations of single-charge nuclear explosions and on one row-charge nuclear explosion at charge burial depths at which craters are formed (Table 4), and on several single-charge nuclear explosions at charge burial depths great enough to contain explosion products (Table 5). Airblast is a function of the medium surrounding the explosion, explosion energy, type of explosive, charge burial depth, and distance from the epicenter; these parameters are included in the tables.

It is useful to identify principal characteristics of a typical overpressure-time history (Figure 1) for an explosion buried near the depth which produces maximum crater dimensions and to associate those characteristics with mechanisms causing them. The two major characteristics are the ground-shock-induced (GSI) pulse and the pulse from venting gases.

Neglecting gravity and layering effects, ground shock propagates essentially spherically until the surface is reached, and free-field ground particle velocity (u) can be defined by

$$u = c (R/W)^{1/3}^{-\beta} \quad (1)$$

where R is the radial distance in the ground, W is the explosion energy, and c and β are medium dependent. Particle velocity in the ground can be determined from hydrodynamic calculations or, since such calculations are not readily available, and tend to decrease in accuracy with increased R , ground particle velocities determined experimentally³² for several media may be used. The vertical component of free-surface particle velocity (u_{vfs}) at the

TABLE 1
HE Single Charges

Shot or Series	Date	Soil Type	Charge Weight ^a (lb)	Number of Shots	Range of Charge Burial Depth		Range of Distance Over Which Airblast was Measured		Ref.
					Actual (ft)	Scaled (ft/lb ^{1/3})	Actual (ft)	Scaled (ft/lb ^{1/3})	
UET-312	05/05/51	Dry Clay	2560	1	7	0.5	41-180	3.0-13.0	1
UET-315	05/10/51	Dry Clay	40,000	1	17	0.5	102.5-450	3.0-13	1
UET-318	05/22/51	Dry Clay	320,000	1	35	0.5	205-1230	3-18	1
Jangle HE 1, 3	08/25/51-09/15/51	Alluvium NTS	2560	2	1.9-6.9	0.15-0.5	28.4-1025	2.08-75	2
Jangle HE 2	09/03/51	Alluvium NTS	40,000	1	4.7	0.15	85.5-1025	2.49-30	2
Mole 100 Series	06/28/52-07/19/52	Dry Clay	256	4	1.6-6.4	0.26-1.0	12-80	1.89-12.6	3
Mole 200 Series	09/14/52-10/24/52	Alluvium NTS	256	5	0.8-6.4	0.13-1.00	12-80	1.89-12.6	3
Mole 300-309 Series	09/15/53-10/16/53	Wet Sand	256	6	0.8-4.8	0.13-0.75	15-80	2.36-12.6	3
Mole 311	10/20/53	Moist Clay	256	1	3.2	0.50	20-80	3.16-12.6	3
Mole 400 Series	10/23/54-11/04/54	Alluvium NTS	256	6	0.8-6.4	0.13-1.00	15-60	2.36-9.46	3
Sandia I Series	01/21/59-01/27/59	Alluvium NTS	256	7	6.4-19.0	1.0-3.0	60, 80	9.46, 12.6	4
Area 14 Series	04/10/59-04/21/59	Tuff NTS	256	9	6.0-18.7	1.00-2.94	25.5	4.02	5
Stagecoach 1, 2, 3	03/15/60-03/25/60	Alluvium NTS	40,000	3	17.1, 34.6, 80	0.5, 1.0, 2.3	80-5020	2.34-146.8	6
Buckboard 11, 12, 13	08/24/60-09/27/60	Basalt	40,000	3	25.5, 42.7, 58.8	0.75, 1.25, 1.72	59.5-480	1.74-14.0	7
Scooter	10/13/60	Alluvium NTS	987,410	1 ^e	125	1.25	300-6500	3-25	8
TTR-211-4, 5	05/22/64-05/26/64	Playa	64	2	5.5, 6.0	1.36, 1.50	50-1500	12.5-375	9, 10
TTR-211-6, 7, 8	06/01/64-06/18/64	Playa	700	3	6, 13	0.68, 1.50	50-1500	12.5-375	10
Sandia III (pre Capsa) 1 and 2	05/03/65-05/06/65	Alluvium ABQ	256	2 ^e	9.5	1.50	50, 150	7.85-23.6	10
Pre-Schooner II	09/30/65	Rhyolite	189,200 ^b	1 ^e	71	1.24	0-4000	0-69.7	11
Capsa 1-8	08/16/66-09/13/66	Alluvium ABQ	1000	8 ^e	10, 12.5, 15, 17.5	1, 1.25, 1.5, 1.75	0-700	0-70	10
TTR-211-42	10/25/66	Playa	64	1	6.9	1.73	50-1500	12.5-375	9
Capsa 9	05/21/68	Alluvium ABQ	1000	1 ^e	12.5	1.25	0-700	0-70	10
Capsa 10	05/29/68	Alluvium ABQ	1000 ^b	1 ^e	12.5	1.25	0-700	0-70	10
Capsa 11	10/13/68	Alluvium ABQ	30,478 ^c	1 ^e	47.9	1.53	0-2275	0-73	10
Capsa 12-13	07/25/68	Alluvium ABQ	979 ^b	2 ^e	12.5, 15.0	1.25, 1.50	0-200	0-70	10
Tugboat 1a, b, c, d	11/04/69-11/06/69	Water-Covered Coral	2000 ^d	4	17.33, 17.86, 21.72, 25.84	1.38, 1.42, 1.72, 2.05	259-8425	20.6-669	12
Tugboat 1e	11/07/69	Water-Covered Coral	20,000 ^d	1	42.9	1.58	277-8614	10.2-317	12

^a TNT unless otherwise noted

^b Nitromethane

^c Composition B

^d Aluminized ammonium nitrate

^e Measurements were also made at airborne stations well above ground level

TABLE 2

HE Row Charges

Shot or Series	Date	Soil Type	Charge Weight ^a (lb)	Number of Shots	Number of Charges in Each Row	Charge Burial Depth		Spacing Between Charges		Range of Distance Over Which Airblast was Measured ^b		Reference
						Actual (ft)	Scaled (ft/lb ^{1/3})	Actual (ft)	Scaled (ft/lb ^{1/3})	Actual (ft)	Scaled (ft/lb ^{1/3})	
Dugout	6/24/64	Basalt	40,000 ^c	1	5	58.8	1.72	45	1.31	170 - 5000	4.97 - 146	13
Pre-Capsa 3	5/27/65	Alluvium (Abq)	256	1 ^d	5	9.5	1.50	13.6	2.14	75 - 600	11.8 - 94.5	10
TTR-211-41	10/5/66	Playa	64	1	2	6	1.50	8	2	50 - 1500	12.5 - 375	9
TTR-211-44	11/22/66	Playa	64	1	5	6	1.50	8	2	50 - 1500	12.5 - 375	9
TTR-211-10,13	8/20/64 3/3/65	Playa	64	2	11	6	1.50	8	2	50 - 1500 ^e	12.5 - 375	9
TTR-211-43	11/18/66	Playa	64	1	25	6	1.50	8	2	50 - 1500	12.5 - 375	9
TTR-211-46	3/27/67	Playa	64	1	2	6.9	1.73	5.25	1.31	50 - 1500	12.5 - 375	9
TTR-211-16	5/27/65	Playa	64	1	5	6.9	1.73	5.25	1.31	19.9 - 567	5 - 142	9, 14
TTR-211-45	2/24/67	Playa	64	1	11	6.9	1.73	5.25	1.31	50 - 1500	12.5 - 375	9
Pre-Gondola II	6/28/67	Shale	E 77,200 ^c	1	5	59.7	1.40	105.5	2.48	225 - 5000	5.3 - 117	15
			F 39,400 ^c			49.4	1.45	79.8	2.35	225 - 5000	6.6 - 147	--
			G 39,100 ^c			48.8	1.44	79.9	2.88	225 - 5000	6.6 - 147	--
			H 79,120 ^c			59.9	1.40	79.9	1.86	225 - 5000	5.2 - 116	--
			I 40,000 ^c			48.8	1.43	79.9	2.34	225 - 5000	6.6 - 146	--

^aTNT unless otherwise noted^bMeasurements made perpendicular to and off end of row^cNitromethane^dMeasurements were also made at airborne stations above ground^eMeasurements were also made on line 45 degrees radially from end charges

TABLE 3

ARRAYS OF CHARGES

Shot or Series	Date	Soil Type	Charge Weight ^a	Number of Charges	Charge Burial Depth		Spacing Between Charges		Range of Distance Over Which Airblast was Measured		Reference
					Actual (ft)	Scaled (ft/lb ^{1/3})	Actual (ft)	Scaled (ft/lb ^{1/3})	Actual (ft)	Scaled (ft/lb ^{1/3})	
Quincuncial Arrays (Five Charge Square) ^b											
TTR-211-22	8/26/65	Playa	64	5	6	1.5	10	2.5	50 - 1500	12.5 - 375	16
TTR-211-27,	9/9/65	Playa	64	5	8	2	10	2.5	50 - 1500	12.5 - 375	16
TTR-211-28	9/10/65	Playa	64	5	10	2.5	10	2.5	50 - 1500	12.5 - 375	16
TTR-211-35	11/8/65	Playa	64	5	6	1.5	16	4	50 - 1500	12.5 - 375	16
TTR-211-32	11/9/65	Playa	64	5	8	2	16	4	50 - 1500	12.5 - 375	16
TTR-211-29	9/27/65	Playa	64	5	10	2.5	16	4	50 - 1500	12.5 - 375	16
Double Row (118.8 feet between rows)											
Pre-Gondola III, Phase I	Shale	2000 ^c	14	19.5	1.55	27	2.14	93 - 320	7.38 - 254	17	

^aTNT unless otherwise noted

^bMeasurements made perpendicular to one side of square

^cNitromethane

^aTNT unless otherwise noted^bMeasurements made perpendicular to one side of square^cNitromethane

TABLE 4
Nuclear Cratering Shots

Shot or Series	Date	Soil Type	Yield (kt)	Charge Burial Depth			Range of Distance Over Which Airblast was Measured			Reference
				Actual (ft)	Scaled (ft/kt ^{1/3})	Scaled (ft/lb ^{1/3})	Actual (ft)	Scaled (ft/kt ^{1/3})	Scaled (ft/lb ^{1/3})	
Jangle U	11/29/51	Alluvium (NTS)	1.2	17	16	0.13 ^a	314 - 3,100	295 - 2,917	2.35 - 31.4	18
Teapot ESS	3/23/55	Alluvium (NTS)	1.2	67	63	0.50	250 - 600	235 - 565	1.86 - 4.48	19
Danny Boy	3/5/62	Basalt	0.43	110	146	1.16	200 - 8,500	265 - 11,261	2.12 - 90.1	20
Sedan	7/6/62	Alluvium (NTS)	100	635	137	1.09	2,960 - 15,500	638 - 3,339	5.06 - 26.5	21
Johnie Boy	7/11/62	Alluvium (NTS)	0.5	2	2.5	0.02	65 - 16,126	82 - 20,317	0.65 - 161.3	22
Sulky	12/18/64	Basalt	0.085	90	205	1.62	165 - 3,772	375 - 8,579	6.77 - 155	23
Palanquin	4/14/65	Rhyolite	4.3	280	172	1.36	21 - 7,380	12.9 - 4,538	0.1 - 36	24
Cabriole	1/26/68	Rhyolite	2.3	171	130	1.03	3.35 - 6,000	2.5 - 4,545	0 - 36.1	25
Buggy I ^b	3/12/68	Basalt	Five 1.1	135	131	1.04	500 - 10,500 ^c	484 - 10,172	3.8 - 81	26
Schooner	12/8/68	Rhyolite	31	355	113	0.90	21 - 15,600	6.7 - 4,966	0 - 39.4	27

^aMeasurements were also made at airborne stations above ground

^bRow charge spacing between charges 150 feet

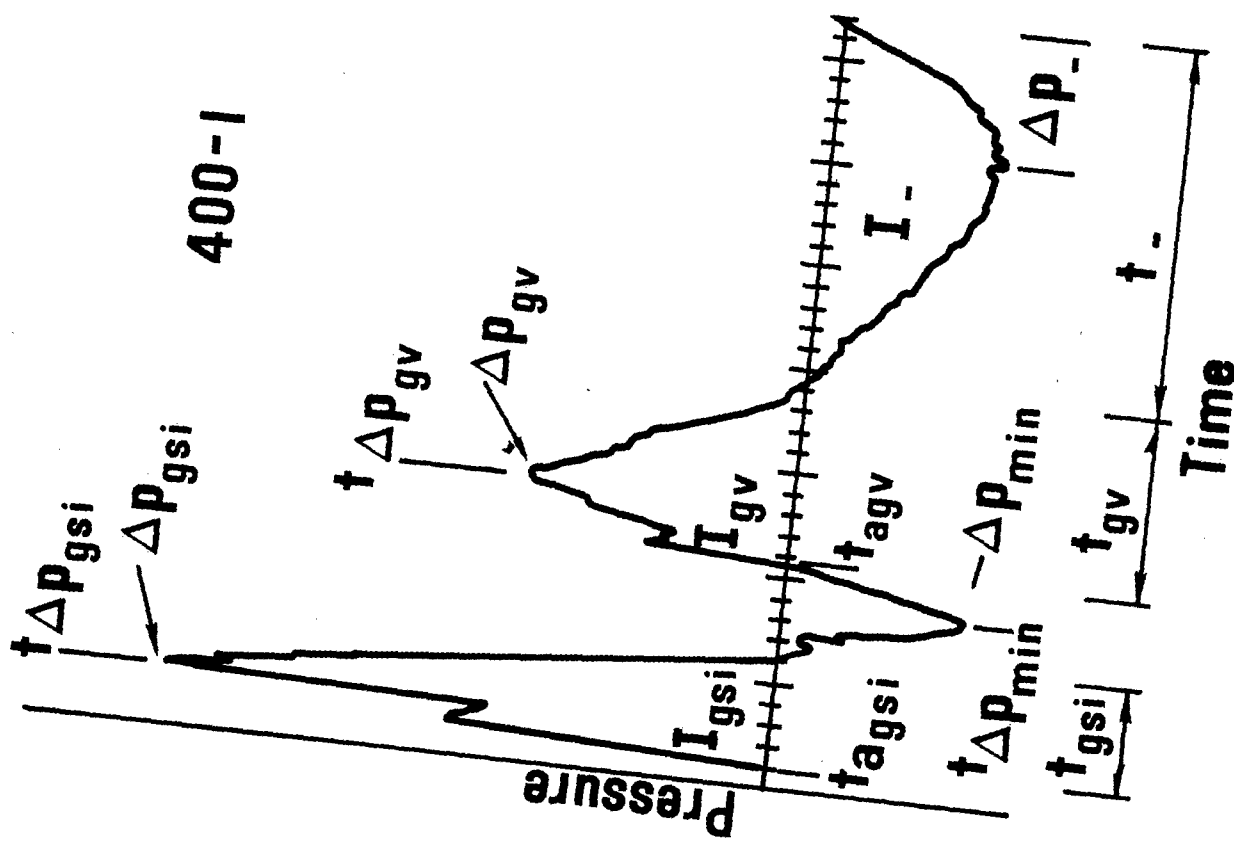
^cMeasurements made along four lines--two perpendicular to midpoint of rows, two off the ends of the row

TABLE 5

Nuclear Contained Shots

Shot or Series	Date	Soil Type	Yield (kt)	Charge Burial Depth		Which Airblast was Measured			Reference
				Actual (ft)	Scaled (ft/kt ^{1/3})	Actual (ft)	Scaled (ft/kt ^{1/3})	Scaled (ft/lb ^{1/3})	
Gnome	12/10/61	Halite	3	1184	821	40, 1,000, 2,500	28, 693, 1733	122, 5.5, 13.8	28
Dumont	5/19/66	Tuff	a	2201	a	0, 3,000, 6,000, 14,000, 30,000	a	a	10
Greeley	12/20/66	Saturated tuff	825	3991	426	50, 2,000, 4,000, 16,487, 32,853, 65,788	5.3, 213, 426, 1758, 3503, 7014	0.04, 1.69, 3.39, 14.0, 27.8, 55.7	10
Scotch	5/23/67	Tuff	150	3210	604	71, 7,515, 19,890	13.4, 1414, 3743	0.1, 11.2, 29.7	29
Faultless	1/19/68	Tuff	a	3200	a	1,500, 6,000	a	a	10
Boxcar	4/26/68	Rhyolite	1200	3822	360	75, 1,000, 11,504	7.1, 94, 1083	0.06, 2.75, 8.59	29, 30
Nilrow	10/2/69	Pillow lava	about 1000	3992	~39.9	300, 4,000	~30, ~400	~0.24, ~3.17	10, 32

^aYield is classified



Δp_{gsi} = peak positive overpressure of ground-shock-induced pulse
 Δp_{min} = minimum pressure between pulses; may be positive or negative
 Δp_{gv} = peak positive overpressure of venting gas pulse
 Δp_{-} = peak negative pressure
 I_{gsi} = positive impulse of ground shock pulse
 I_{gv} = positive impulse of venting gas pulse
 I_{+} = total positive impulse: $I_{gsi} + I_{gv}$
 I_{-} = negative impulse
 $t_{a_{gsi}}$ = time of arrival of ground-shock-induced pulse
 $t_{a_{gv}}$ = time of arrival of gas venting pulse; may coincide with $t_{\Delta p_{min}}$
 $t_{\Delta p_{gsi}}$ = time of peak positive overpressure of ground-shock-induced pulse
 $t_{\Delta p_{min}}$ = time of minimum pressure between pulses
 $t_{\Delta p_{gv}}$ = time of peak positive overpressure of gas venting pulse
 t_{gsi} = duration of ground-shock-induced pulse
 t_{gv} = duration of gas venting pulse
 t_{+} = duration of positive phase = $t_{gsi} + t_{gv}$
 t_{-} = duration of negative phase

Fig. 1—Typical airblast waveform for buried explosions.

air-ground interface at a horizontal distance (r) from the epicenter, is

$$u_{vfs} = 2u \left(\frac{DOB}{R} \right) \quad (2)$$

where DOB is the depth-of-burst to the charge center and r is $(R^2 - DOB^2)^{1/2}$. Where the air overpressure is induced at r by u_{vfs} and where r is also the point of observation or measurement, the overpressure pulse is defined here as a ground-transmitted GSI pulse, and can be identified by an arrival time associated with ground shock propagation velocity; e.g., the first peak overpressure in Figure 1. Where the horizontal distance to the point of observation or measurement is greater than the distance, r, at which the overpressure is induced, the arrival of the pulse is delayed by the slower propagation velocity in air from r to the point of observation. That pulse is defined here as the air-transmitted GSI pulse; e.g., the maximum peak in Figure 1. This pulse has an apparent source along the surface away from the epicenter. The ground-transmitted GSI pulse attenuates rapidly and is rarely observed at $r > 3 DOB$ because gages ordinarily are set to measure the larger air-transmitted GSI pulse.

At relatively large horizontal distances, a train of minor pulses can be observed in some media preceding the air-transmitted GSI pulse. The train is induced by the vertical component of ground motion of either surface waves, refracted body waves, or a combination of both.

The gas-venting pulse is the second major characteristic of the overpressure waveform from buried explosions. The overpressure transferred to the atmosphere is a function of the gas cavity volume and pressure at the time venting occurs, which are, in turn, dependent on burial depth, medium, and type of explosive. Sedan²¹, a nuclear detonation in alluvium, vented while the cavity was under high pressure, producing a relatively high overpressure, whereas cavities of Pre-Gondola II¹⁵ and Pre-Gondola III, Phase I¹⁷ (nitromethane detonations in shale) continued to expand until cavity pressure approached ambient, producing a gas-venting pulse that was barely identifiable.

There is one other contribution to the overpressure waveform. From the time of arrival of the ground shock at the surface, the ground shock, together with the expanding cavity, causes the surface of the ground to mound. Characteristic mound heights at time of venting are also dependent on burial depth, medium, and type of explosive. Mound growth provides a long-period contribution to the waveform between arrival of the GSI pulse and the peak of the gas-venting pulse. This contribution cannot be separated from the other pulses.

THEORY

Charge burial depths for cratering explosions usually are sufficiently deep that strong shocks are not induced in the air, and acoustic approximations suffice. Cole's³³ acoustic approxi-

mation of shock transmission across a water-air interface can be adapted to soil if shear in the ground is ignored:

$$\frac{\Delta p_a}{\Delta p_s} = \frac{2 \rho_a c_a \cos \theta_s}{\rho_a c_a \cos \theta_s + \rho_s c_s \cos \theta_a} \quad (3)$$

where subscripts refer to soil or air, Δp is overpressure, ρ is density, c is the sonic velocity, and θ is the angle between the advancing shock front and the surface. Cole's expression is applicable only to the initial peak overpressures in the air at the interface.

If shear in the ground is not to be ignored, an expression³⁴ for the vertical velocity (u_v) induced by the compression wave of unit amplitude incident upon the free surface is

$$\frac{1}{2} u_{vfs} = \frac{\sin \theta}{\cos 2 \phi \tan \theta + 2 \sin^2 \phi \tan 2 \phi} \quad (4)$$

where

$$\frac{\sin \theta}{\sin \phi} = \frac{\epsilon}{\eta} \quad (5)$$

and θ and ϕ are their angles of incidence, and where ϵ and η are velocities of compression and shear waves, respectively. Reference 34 presents a table of values of the denominator of Equation 4 for a range of values of Poisson's ratio.

From Equations 1, 2, and 4, u_{vfs} can be described as a function of distance from the epicenter and u_{vofs} the vertical velocity at the epicenter. The vertical component of velocity at the epicenter u_{vofs} can be measured or computed from shock strength incident at the surface. The vertical component of the free surface velocity can be set equal to the corresponding velocity in the air above the free boundary to derive the pressure induced in the air; i.e.

$$\Delta p = \frac{7 P_o u_{vfs}}{5 c_a} \quad (6)$$

where P_o is the ambient air pressure. GSI overpressure away from the epicenter can be determined by assuming the pressure profile varies with distance from the epicenter as the particle velocity profile varies with distance. Refinements have been devised^{35,36} to take into account both dissipation at the shock front in air, and divergence and crossfeed at the shock front. Crossfeed results from not having all parts of the front at the same strength.

Using an acoustic approximation and a simple source model, Montan³⁷ has related GSI peak overpressure in the far field (where distance is much larger than the radius of the source) to that at the source as a function of charge burial and distance to the point

of observation. Montan also considers gas-venting pressure produced by cavity pressure where cavity pressures at vent time are estimated from two-dimensional hydrodynamic calculations.

DATA

It is the objective of this paper to use available data as a basis for empirical models that can be used for estimating airblast. Such models can be used for estimating by those who do not have access to relatively expensive, elaborate hydrodynamic calculations. Empirical models are presented for GSI peak overpressure, gas-venting peak overpressure, and positive-phase impulse. Other purposes are to summarize work on close-in airblast from buried explosions and to compare Montan's acoustic model with measured overpressures.

Overpressures, impulses, and durations for most of the events listed in Tables 1 through 5 were available on IBM cards. All values were corrected to standard sea-level conditions ($P_0 = 14.7$ psi; $T_0 = 15^\circ\text{C}$). Measurements made over a period of 20 years involved several instrument systems, but the slow rise of pressure waveforms from buried explosions make instrument response an insignificant limitation on data quality, with the possible exceptions of surface bursts or the very shallowest charge burials. Measurements on the Sandia I series were recorded on Brush paper tape recorders and are below the quality of other measurements. Results from that series, however, enter into the data analysis only rarely. Otherwise, the quality of records was good and improved with time.

ANALYSIS

The data have been analyzed by examining separately (a) the GSI peak overpressure, (b) the peak overpressure from venting gas, and (c) the positive-phase impulse. In determining rates of attenuation with distance, power-law least-square fits have been used because neither the quality nor quantity of the data justifies the refinement of a higher-order fit.

Thus, for any given event, $\Delta p = r^{-m}$.

Rate of Attenuation of Airblast with Distance

Spherical attenuation of shock overpressure with distance might be assumed to be nearly r^{-1} as the acoustic region is approached, but theoretical treatments are inconsistent in this regard.

IBM Problem M³⁸ was not carried to the infinitesimal acoustic limit but in the region from 0.4 to 1 psi the peak overpressure

followed an attenuation rate of about $r^{-1.2}$. (A subsequent recalculation by Whitaker³⁹ gave $r^{-1.12}$ for overpressure levels of 0.01 to 0.02 psi). Positive-phase impulse followed an attenuation rate of $r^{-0.9}$.

The Kirkwood-Brinkley free-airburst curves for cast TNT⁴⁰ were carried only to about the 1-psi level. The region from 1 to 3 psi followed an attenuation rate of $r^{-1.35}$. The positive-phase impulse over the same region shows an attenuation rate of r^{-1} . A recent hydrocode calculation⁴¹ carried to 0.0001639 psi shows an attenuation rate of $r^{-1.0575}$ over the last distance increment of the calculation. Note that this overpressure corresponds to a scaled distance of 84,000 ft/lb^{1/3}. For the overpressure range of interest here, average attenuation rates of $r^{-1.22}$ were calculated for the 0.1 to 1.0 psi range, and of $r^{-1.126}$ for the 0.01 to 0.1 range. Thus, even in the spherical free-air case, there are differences between the attenuation rates of various models.

Experimental results from hemispherical surface-burst HE tests⁴² indicate that for the region from 0.01 to 0.1 psi the peak overpressure follows an attenuation rate of about $r^{-1.35}$. Positive-phase impulse follows $r^{-1.4}$ approximately.⁴³

Examination of the attenuation rates of the three parameters described below will make it clear that a great deal of variation occurs on experiments and that there are only a few consistencies to be found.

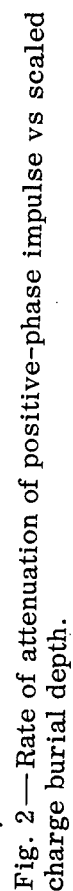
Attenuation rates greater than r^{-1} can occur if (a) winds blow toward ground zero from the end of the blast line, and/or (b) a temperature gradient exists, with warmer temperatures at ground level.

Attenuation rates would be less than r^{-1} if (a) winds blow toward the end of the blast line from ground zero; (b) temperature inversions exist, with the ground colder than the air above it; (c) gas-venting peak overpressures are less at closer distances where the wave must diffract down the surface of the mound through which gases vent; (d) waves starting with rounded peaks shock up with propagation over the distance range of the measurements, and/or (e) the size of the source (especially in the case of GSI peak overpressure from buried explosions) relative to the radius to the point of measurement may be important except at very large distances.

Information was not available for most HE events on winds, temperature gradients, or inversions, so those effects cannot be evaluated.

Impulse-HE -- Figure 2 shows m_I for experiments at several scaled burst depths in seven media where

$$I = c r^{-m_I}. \quad (7)$$



There is no consistent dependence of m_I on medium. The HE shots in playa and Albuquerque alluvium were fired under especially calm winds and were of a limited range of burial depth; those data show little variation in m_I . Shots in dry clay and NTS alluvium were fired under less ideal wind conditions and spanned a larger range of charge burial depths; those shots show greater variation in m_I . When charge burial depth is considered (Figure 2), a clear dependency of m_I on charge burial depth emerges. The reduction in m_I from theoretical spherical attenuation (r^{-1}) as the surface is approached could be due to a preferential upward direction of air-blast as the surface is approached. Under this condition, close gages receive less than for spherical attenuation, and the distant gages more, as blast flows downward along the blast front from upper regions to the ground. Over the burial depth range 0.15 to 2.0 ft/lb^{1/3}, the dependence of m_I scaled burial depth can be approximated within the accuracy indicated by the spread of data in Figure 2 by

$$m_I = \frac{\log_{10} \frac{DOB/W^{1/3}}{0.055}}{1.5} \quad (8)$$

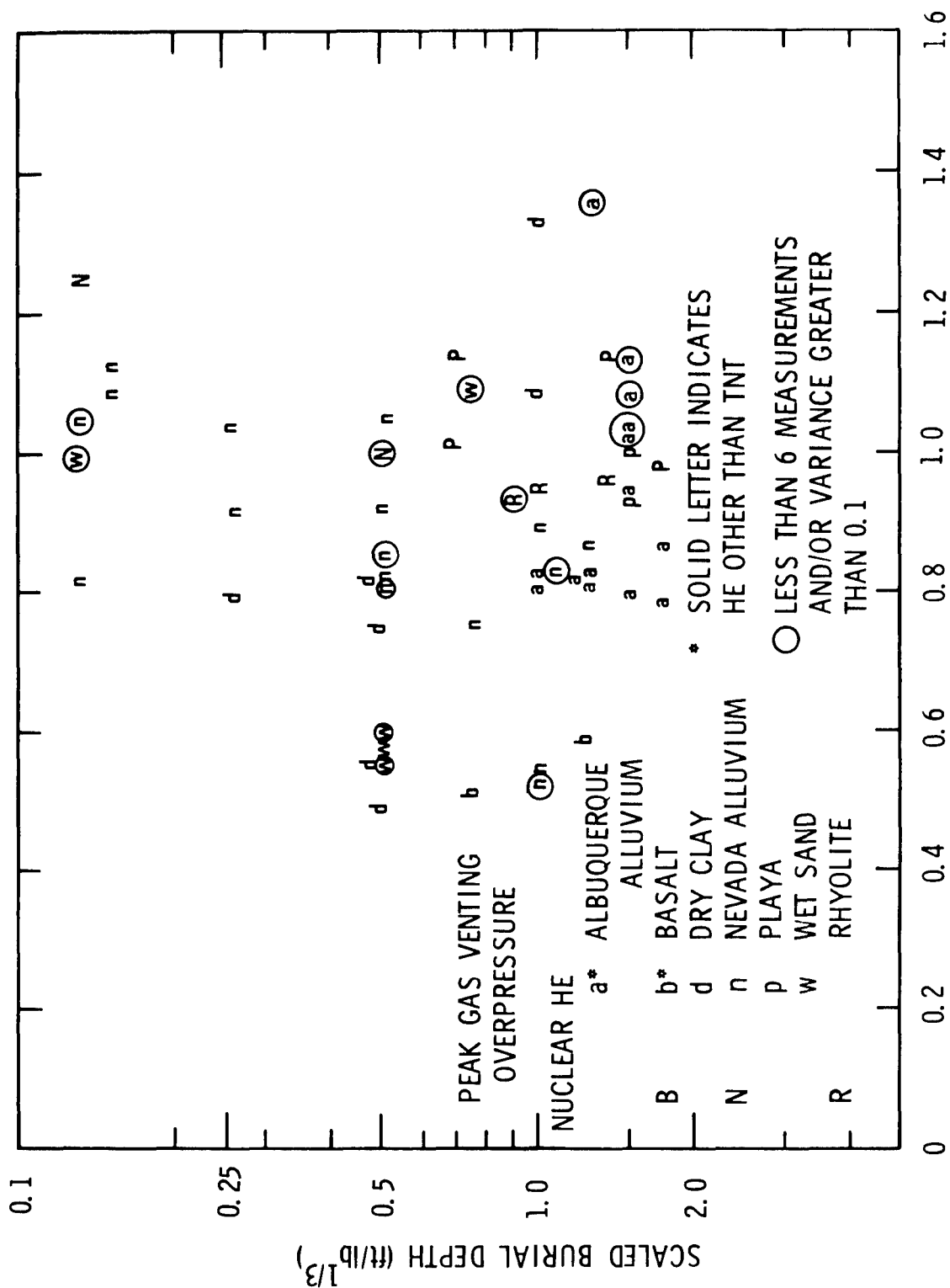
The figure includes data from one shot in basalt with nitromethane, three shots in Albuquerque alluvium where nitromethane was used, and one shot in Albuquerque alluvium with Composition B. With one exception, m_I for those five shots falls within the spread of data from nuclear and TNT shots.

Impulse-NE -- Impulse data for nuclear shots are limited to two shots in basalt (Danny Boy and Sulky), two in NTS alluvium (Jangle U and Teapot ESS) and three shots in rhyolite (Palanquin, Cabriolet and Schooner). The values of m_I for nuclear shots fall within the spread of values for shots in which chemical explosives were used. Although the data are sparse, they tend to confirm the trend shown by data from HE shots of decreasing m_I as the ground surface is approached.

Peak Overpressure-HE and NE -- There is no similar trend in reduction of attenuation rate with decreased burial depth for either gas venting or GSI peak overpressures (Figures 3 and 4). For the latter, there are no data for the shallow burial depths where the GSI pulse is overtaken by the stronger gas-venting pulse. Values of m_p for GSI peak overpressure were spread about the 1.0 to 1.25 region with four exceptions. Four of five nuclear shots have attenuation rates for GSI peak overpressure very close to 1.2.

Values of m_p for gas-venting peak overpressure show a greater scatter, and the center of the spread is decidedly lower than in the case of the GSI peak overpressure. Values for four of five nuclear shots fall in the region of 0.95 to 1.0.

In view of the scatter in values of m , a word is in order concerning variance. Variance is small for shots in which the number of measurements is relatively large; it is small also where special care was taken in gage calibration and where quality of



M_p - RATE OF OVERPRESSURE ATTENUATION WITH DISTANCE

Fig. 3—Rate of attenuation of ground-shock-induced peak overpressure vs scaled charge burial depth.

instrumentation was high; recent measurements, for example, show less variance than early measurements. Where variance was high or low for one blast parameter, it usually was the same for the other two parameters. This reflects the quality of the measurements on a particular shot or series. The following list is a generalization of the variance observed.

<u>Medium</u>	<u>Small variance (\pm)</u>	<u>Large variance (\pm)</u>
<u>HE</u>		
Albuquerque alluvium	CAPSA 10 (0.04-0.045)	CAPSA 11-13 (0.09-0.17) ^a
Basalt	CAPSA 1-9 (0.02-0.06)	Sandia III (not determinable)
	Buckboard & Pre-schooner II (0.02-0.07)	
Dry clay		UET (0.06-0.12)
NTS alluvium	Scooter, Stagecoach (0.02-0.06)	Mole 100 series (0.05-0.19)
		Sandia I (not determinable)
		Mole 200 (0.06-0.13)
		Mole 400 (0.04-0.15)
Playa	211 Series (0.015-0.06)	Jangle HE (0.03-0.09)
Wet sand		Mole 300 (0.03-0.2)
<u>NE</u>		
	Jangle U (0.03-0.06)	Teapot ESS (0.04-0.2)
	Cabriolet (0.02-0.05)	Danny Boy (0.90-0.36)
	Schooner (0.06-0.07)	Sulky (0.21-0.42)
		Palanquin (0.06-0.12)

^aThese were nitromethane or Composition B shots with values of m usually well over 1.0.

It is worth noting that the fact that the variances of m are as small as 0.02 for shots in several media indicates that first-order fit to measured data is quite adequate and lends credence to the argument that much of the variation has to do with quality of measurement.

Rate of Suppression of Airblast with Charge Burial

HE Experiments -- Airblast is attenuated (suppressed) also by charge burial. Analysis done in connection with the Cabriolet event²⁵ suggested that, within the accuracy of the data, airblast suppression at a constant scaled range could be expressed by

$$\Delta p = k \left(\frac{DOB}{W^{1/3}} \right)^{-n} \quad (9)$$

A custom has evolved in which charge burial depths have been chosen such that scaled burial depth increases by specified increments. The scaled burial depths most frequently used are:

0.13 ft/lb^{1/3} (Top of TNT sphere tangent to ground surface)
 0.25
 0.50
 0.75
 1.00
 1.25
 1.50

This custom led to the distribution of charge burial depths illustrated in Figure 5 for gas-venting peak overpressure at a scaled distance of 5 ft/lb^{1/3} for HE shots in NTS desert alluvium. The data points represent values given at 5 ft/lb^{1/3} by equations of the type of Equation 7 for each shot. As indicated in Figure 5, it appeared that in the case of gas-venting peak overpressure (and also for positive-phase impulse) there were two separate rates of airblast attenuation--one rate for shots shallower than 0.5 ft/lb^{1/3} and one for deeper shots. In three of the six media (NTS alluvium, dry clay, and wet sand) for which there are HE data spanning both ranges of scaled burial depth, there were similar suggestions of differences in attenuation rates. Further analysis has shown that airblast suppression may be represented better by semi-log presentation than by log-log presentation, and moreover that the two-slope characteristic of Figure 5 results from a combination of the customary burial depths and the log-log presentation. Thus, a better expression for blast suppression with charge burial is

$$I, \Delta p = \frac{k}{10 \exp \left[n \left(\frac{DOB}{W^{1/3}} \right) \right]} \quad (10)$$

Using equations for airblast ($I, \Delta p$) versus distance for each shot, values of k and n (Equation 10) were determined for all HE shots in six media at scaled ranges of 5, 7, 10, 20, and 50 ft/lb^{1/3}. In no case were data extrapolated beyond the scaled distance at which measurements were made, although, if the variance in rate of attenuation with distance was small, little error would be involved in doing so. As a result, there are less data for 20 ft/lb^{1/3}, and still less for 50 ft/lb^{1/3}. Accordingly, variance of k and n is always larger for 20 ft/lb^{1/3} than for closer ranges, and is even larger for 50 ft/lb^{1/3}.

Airblast suppression at a single scaled range (7 ft/lb^{1/3}) for HE shots in six media is illustrated for impulse (Figure 6), gas venting peak overpressure (Figure 7) and GSI peak overpressure (Figure 8). Points plotted in each figure represent a value for a constant scaled range from a calculated airblast-distance relationship (Equation 7) for each shot. For each medium and scaled

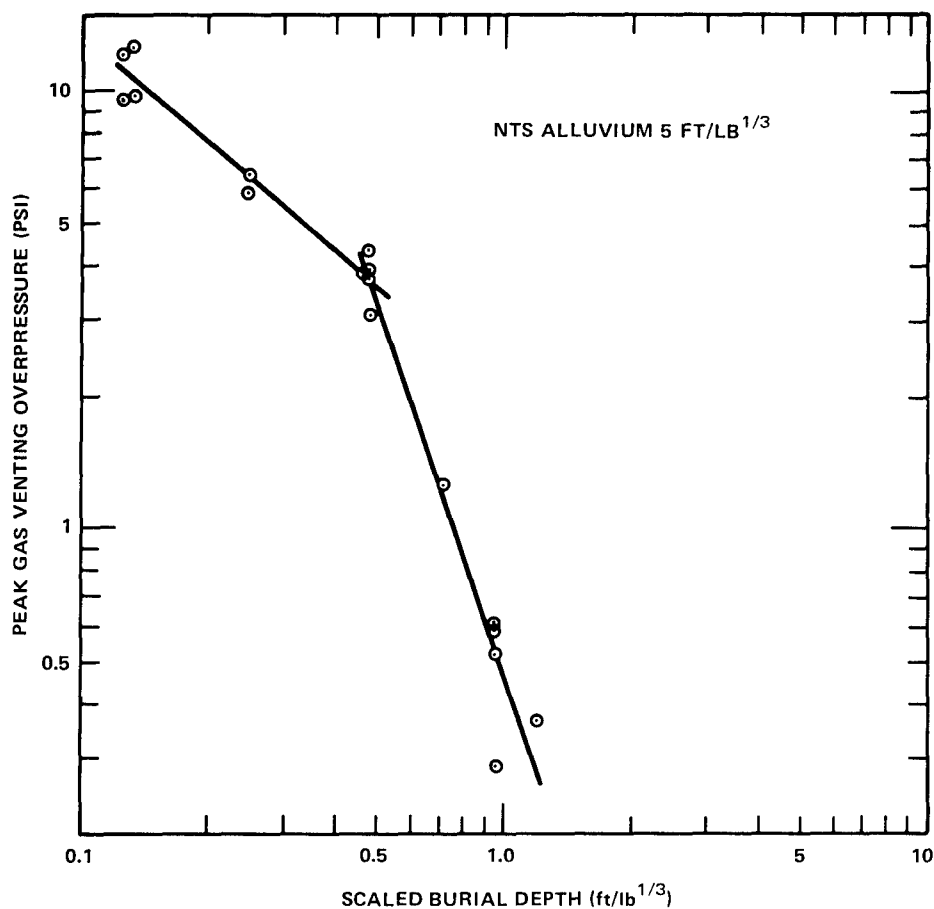


Fig. 5 — Peak gas-venting overpressure vs scaled charge burial depth.

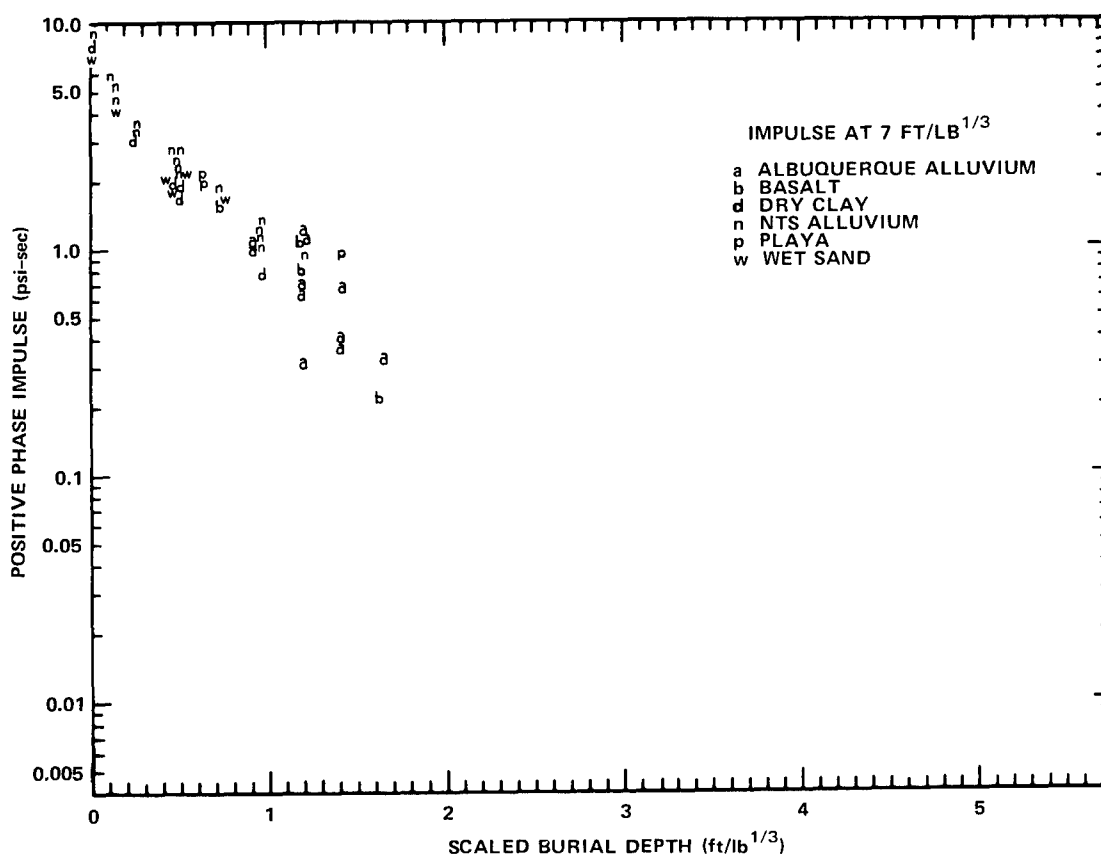


Fig. 6 — Positive-phase impulse data vs scaled charge burial depth for six media.

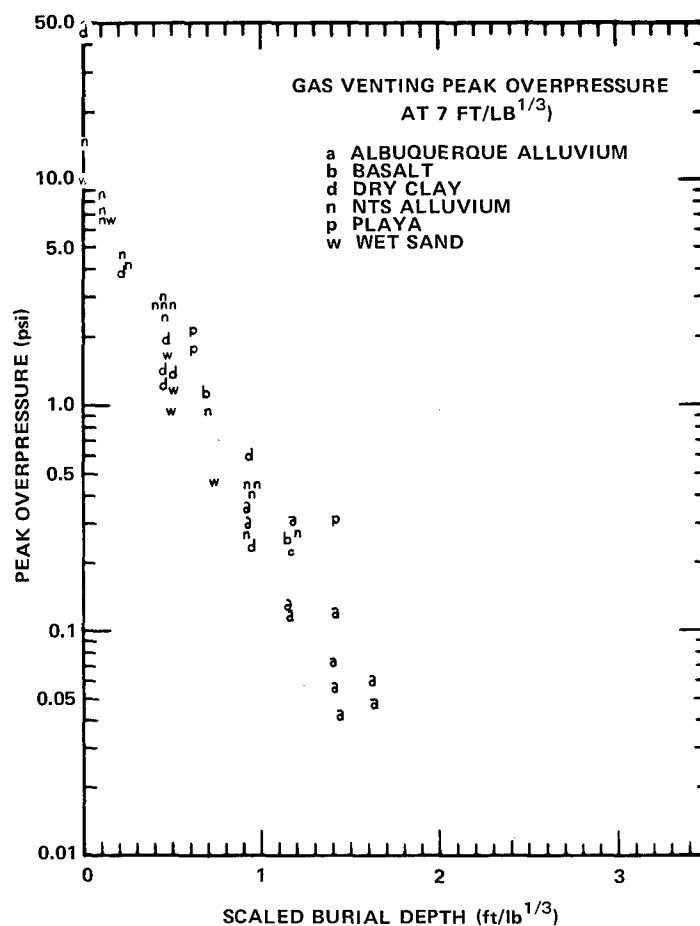


Fig. 7—Gas-venting peak overpressure data vs scaled charge burial depth for six media.

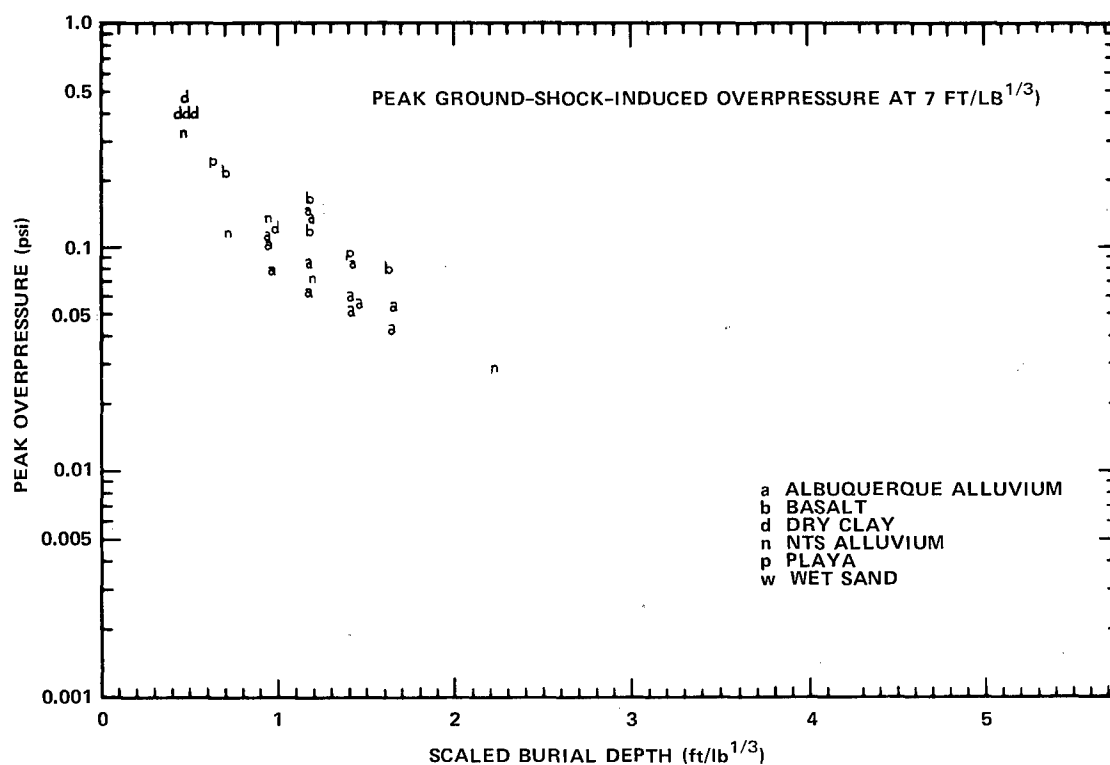


Fig. 8—Peak ground-shock-induced overpressure data vs scaled charge burial depth for six media.

distance, suppression expressions (Equation 10) were determined. Examining the expressions (Table 6) shows that n is either constant or exhibits a slight dependence on scaled range. The dependence may be a result of too few shots in a given medium. The constant k always shows a dependence on scaled range

$$k = c'r^{-m'} \quad (11)$$

where m' constitutes a synthesized rate of attenuation with distance of the blast parameter for a given medium (so long as n is constant for that medium).

Table 6 lists the equations for each medium and each parameter, developed from fits to data of Figures 6 through 8. Results of these fits are illustrated in Figures 9 through 11 for a single scaled range (7 ft/lb^{1/3}). Using the equations of Table 6 it is possible to predict any of the three parameters of airblast from buried HE shots over the depth of burst and distance spans of the data for any of the six media within the accuracy of the measured parameters.

An attempt was made to correlate k and n or c' and m' with known physical characteristics of the media, either singly or in combination. The attempt was completely unsuccessful. Nonetheless, if predictions are necessary for explosions in media for which there are no data, one alternative is to use that one of the six for which results are presented here, that qualitatively compares best with the medium under consideration. Another alternative is to use the last expression in Table 6, which was obtained using all data without regard for medium.

Nuclear Events - Adequate expressions for airblast as a function of distance cannot be developed for all of the nuclear cratering events for any of the blast parameters. There was no measured GSI pulse for the Jangle U, Teapot ESS, or Sedan events. Gas-venting pulses were not measurable for the Sulky and Danny Boy events. These pulses, of course, were non-existent for the contained nuclear explosions (Table 5). The number of measurements on contained events other than Dumont and Greely was small, and airblast-distance relationships must be used cautiously. Accordingly, a spread is used for contained nuclear events in Figures 9 through 11.

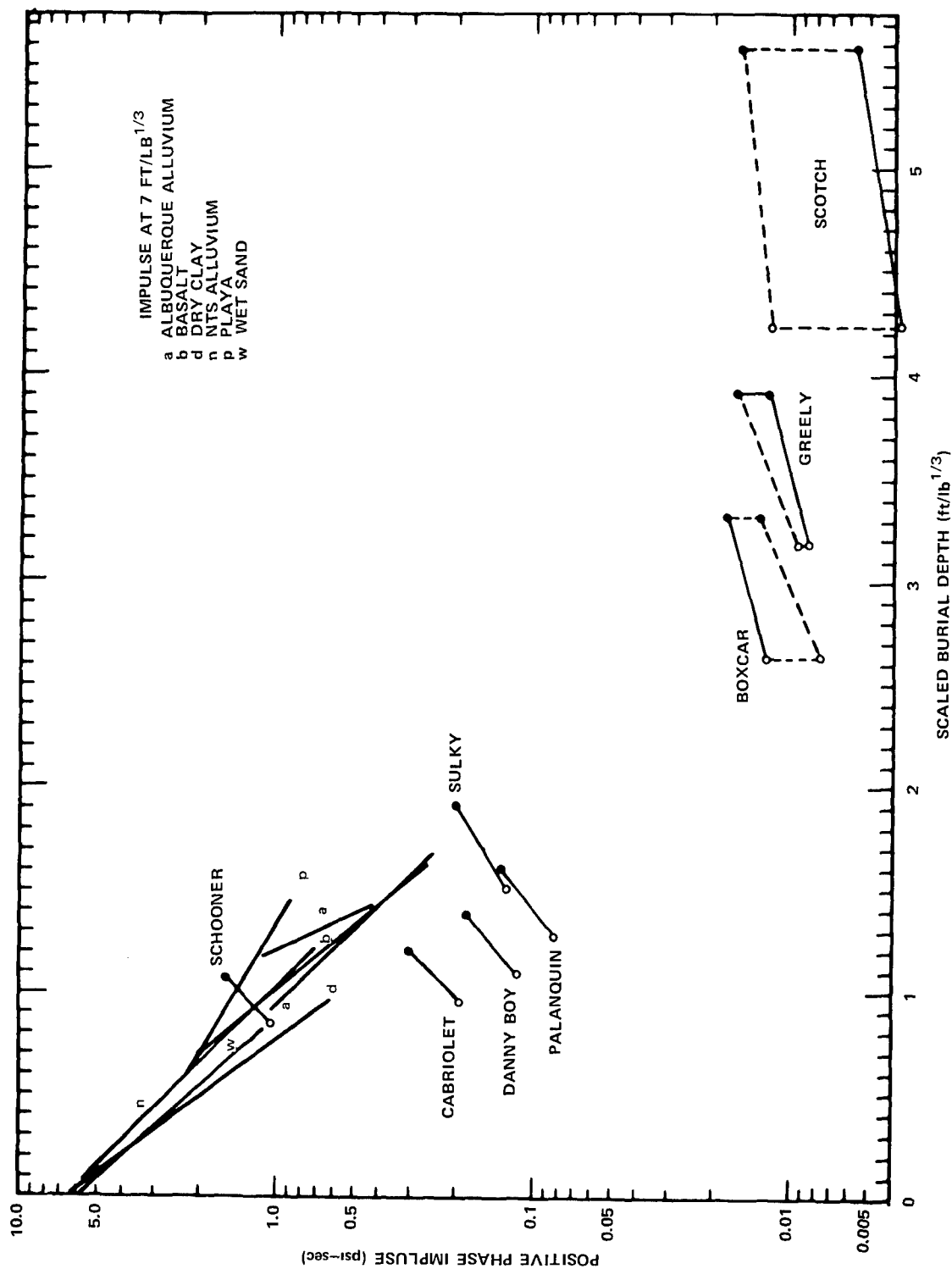
The nuclear events are few, and are spread over four media (alluvium, basalt, rhyolite, and tuff), preventing development of meaningful relationships for airblast suppression with charge burial. Consequently, a different means is used here for presenting blast suppression as a function of burial depth, and for comparing suppression for nuclear events with that for HE shots. In Figures 9 through 11 blast suppression versus burial depth for each of the three airblast parameters at a scaled distance of 7 ft/lb^{1/3} is presented. Nuclear data are presented separately for each event.

TABLE 6
Equations for Airblast Predictions

	Ground-Shock-Induced Peak Overpressure (psi)	Gas Venting Peak Overpressure (psi)	Positive Phase Impulse (psi-sec)
Albuquerque Alluvium - TNT	$\Delta P = \frac{2.5 \left(\frac{r}{w^{1/3}} \right)^{-1.1}}{10 \exp \left[0.5 \left(\frac{DOB}{w^{1/3}} \right) \right]}$ (c)	$\Delta P = \frac{13 \left(\frac{r}{w^{1/3}} \right)^{-0.74}}{10 \exp \left[1.15 \left(\frac{DOB}{w^{1/3}} \right) \right]}$ (c)	$I = \frac{20 \left(\frac{r}{w^{1/3}} \right)^{-0.65}}{10 \exp \left[0.8 \left(\frac{DOB}{w^{1/3}} \right) \right]}$ (a)
NTS Alluvium	$\Delta P = \frac{8.5 \left(\frac{r}{w^{1/3}} \right)^{-1.6}}{10 \exp \left[0.58 \left(\frac{DOB}{w^{1/3}} \right) \right]}$	$\Delta P = \frac{110 \left(\frac{r}{w^{1/3}} \right)^{-1.13}}{10 \exp \left[2 \left(\frac{r}{w^{1/3}} \right)^{-0.15} \left(\frac{DOB}{w^{1/3}} \right) \right]}$	$I = \frac{13.5 \left(\frac{r}{w^{1/3}} \right)^{-0.38}}{10 \exp \left[0.38 \left(\frac{r}{w^{1/3}} \right)^{0.3} \left(\frac{DOB}{w^{1/3}} \right) \right]}$ (a)
Basalt	$\Delta P = \frac{3.5 \left(\frac{r}{w^{1/3}} \right)^{-1.03}}{10 \exp \left[0.47 \left(\frac{DOB}{w^{1/3}} \right) \right]}$ (a)	$\Delta P = \frac{23 \left(\frac{r}{w^{1/3}} \right)^{-0.39}}{10 \exp \left[1.4 \left(\frac{DOB}{w^{1/3}} \right) \right]}$ (a)	$I = \frac{11 \left(\frac{r}{w^{1/3}} \right)^{-0.12}}{10 \exp \left[0.54 \left(\frac{r}{w^{1/3}} \right)^{0.28} \left(\frac{DOB}{w^{1/3}} \right) \right]}$ (a)
Albuquerque Alluvium - Other Than TNT	$\Delta P = \frac{900 \left(\frac{r}{w^{1/3}} \right)^{-1.59}}{10 \exp \left[1.25 \left(\frac{DOB}{w^{1/3}} \right) \right]}$ (b)	$\Delta P = \frac{950 \left(\frac{r}{w^{1/3}} \right)^{-0.93}}{10 \exp \left[2.35 \left(\frac{DOB}{w^{1/3}} \right) \right]}$ (b)	$I = \frac{720 \left(\frac{r}{w^{1/3}} \right)^{-1.08}}{10 \exp \left[1.65 \left(\frac{DOB}{w^{1/3}} \right) \right]}$ (b)
Dry Clay	$\Delta P = \frac{20 \left(\frac{r}{w^{1/3}} \right)^{-1.32}}{10 \exp \left[1.2 \left(\frac{DOB}{w^{1/3}} \right) \right]}$ (a)	$\Delta P = \frac{24 \left(\frac{r}{w^{1/3}} \right)^{-0.17}}{10 \exp \left[1.3 \left(\frac{r}{w^{1/3}} \right)^{0.2} \left(\frac{DOB}{w^{1/3}} \right) \right]}$ (a)	$I = \frac{12 \left(\frac{r}{w^{1/3}} \right)^{-0.34}}{10 \exp \left[0.7 \left(\frac{r}{w^{1/3}} \right)^{0.21} \left(\frac{DOB}{w^{1/3}} \right) \right]}$ (a)
Wet Sand	No data	$\Delta P = \frac{135 \left(\frac{r}{w^{1/3}} \right)^{-1.33}}{10 \exp \left[3.1 \left(\frac{r}{w^{1/3}} \right)^{-0.27} \left(\frac{DOB}{w^{1/3}} \right) \right]}$ (a)	$I = \frac{20 \left(\frac{r}{w^{1/3}} \right)^{-0.63}}{10 \exp \left[0.72 \left(\frac{r}{w^{1/3}} \right)^{0.11} \left(\frac{DOB}{w^{1/3}} \right) \right]}$ (a)
Plays	$\Delta P = \frac{5.6 \left(\frac{r}{w^{1/3}} \right)^{-1.2}}{10 \exp \left[0.54 \left(\frac{DOB}{w^{1/3}} \right) \right]}$ (d)	$\Delta P = \frac{80 \left(\frac{r}{w^{1/3}} \right)^{-1.13}}{10 \exp \left[1.01 \left(\frac{DOB}{w^{1/3}} \right) \right]}$ (d)	$I = \frac{23 \left(\frac{r}{w^{1/3}} \right)^{-0.89}}{10 \exp \left[0.46 \left(\frac{DOB}{w^{1/3}} \right) \right]}$ (d)
	$\Delta P = \frac{3.5 \left(\frac{r}{w^{1/3}} \right)^{-0.93}}{10 \exp \left[0.59 \left(\frac{DOB}{w^{1/3}} \right) \right]}$ (e)	$\Delta P = \frac{160 \left(\frac{r}{w^{1/3}} \right)^{-1.15}}{10 \exp \left[1.3 \left(\frac{DOB}{w^{1/3}} \right) \right]}$ (e)	$I = \frac{27 \left(\frac{r}{w^{1/3}} \right)^{-0.88}}{10 \exp \left[0.58 \left(\frac{DOB}{w^{1/3}} \right) \right]}$ (e)
All Media	$\Delta P = \frac{5 \left(\frac{r}{w^{1/3}} \right)^{-1.05}}{10 \exp \left[0.6 \left(\frac{DOB}{w^{1/3}} \right) \right]}$ (b)	$\Delta P = \frac{70 \left(\frac{r}{w^{1/3}} \right)^{-0.93}}{10 \exp \left[1.5 \left(\frac{DOB}{w^{1/3}} \right) \right]}$ (b)	$I = \frac{15 \left(\frac{r}{w^{1/3}} \right)^{-0.5}}{10 \exp \left[0.56 \left(\frac{r}{w^{1/3}} \right)^{0.17} \left(\frac{DOB}{w^{1/3}} \right) \right]}$ (c)

$$\Delta P = \frac{C \left(\frac{r}{w^{1/3}} \right)^{-m}}{10 \exp \left[n \left(\frac{DOB}{w^{1/3}} \right) \right]}$$

NOTES: (a) Valid for $r = 5$ to $10 \text{ ft/lb}^{1/3}$
 (b) Valid for $r = 5$ to $20 \text{ ft/lb}^{1/3}$
 (c) Valid for $r = 5$ to $50 \text{ ft/lb}^{1/3}$
 (d) Valid for $r = 7$ to $10 \text{ ft/lb}^{1/3}$
 (e) Valid for $r = 20$ to $50 \text{ ft/lb}^{1/3}$



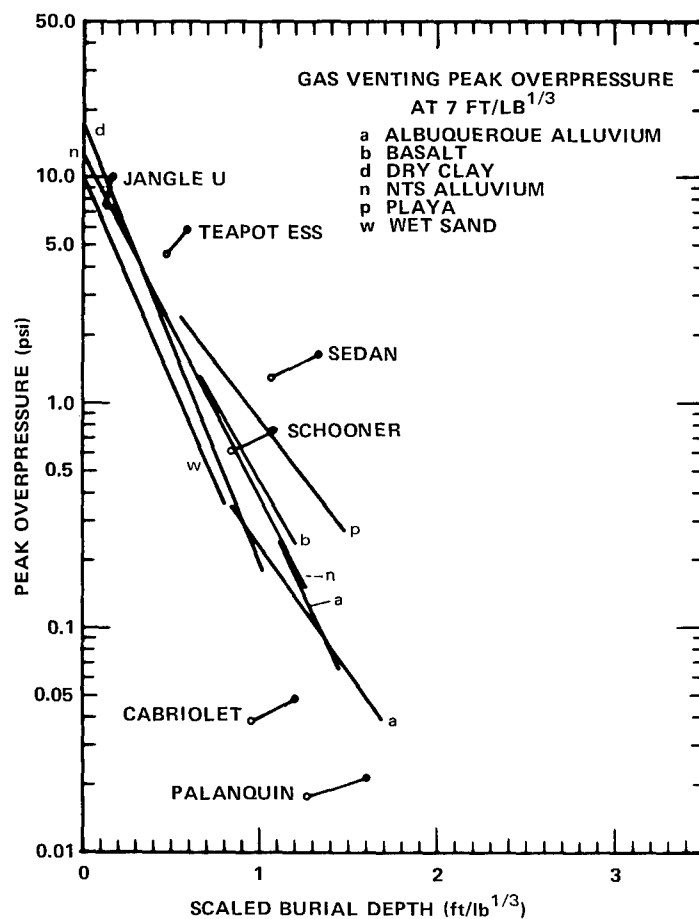


Fig. 10—Gas-venting peak overpressure vs scaled charge burial depth; HE relationships compared with nuclear data.

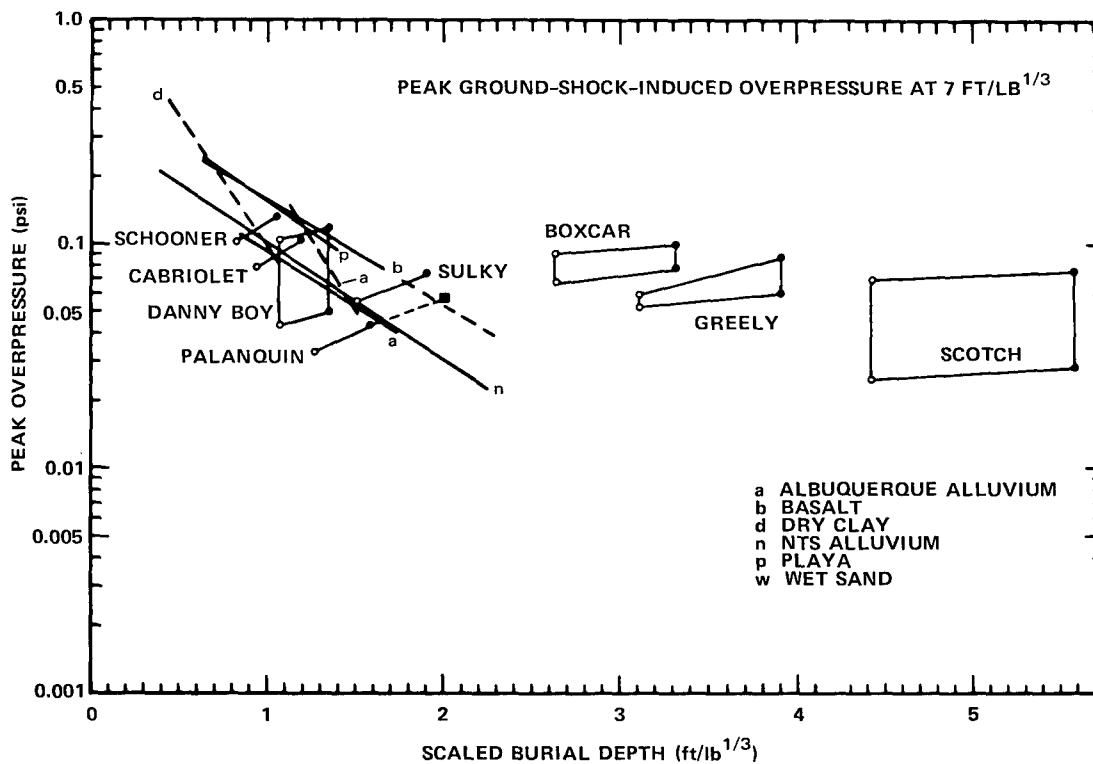


Fig. 11—Peak ground-shock-induced overpressure vs scaled charge burial depth; HE relationships compared with nuclear data.

Scaling - Cube-root scaling, i.e., linear dimensions and times for two events proportional to the cube roots of their charge weights, has been applied throughout the foregoing to HE events. No indication of any departure from cube root scaling is suggested by any of the HE data. For above-ground explosions, airblast measurements on nuclear explosions agree with measurements from TNT explosions only if the nuclear explosion is considered to have a TNT equivalent energy yield of half its nominal yield.*

While there is no a priori reason to expect the same equivalence for buried explosions,** the opportunity to examine the possibility has been provided in Figures 9 through 11 by presenting each airblast parameter scaled to one pound TNT equivalent on the basis of both the nominal yield (the open circles) and one-half the nominal yield (filled circles).

The positive-phase impulse from nuclear shots shows a continuation from HE data of decrease with increased burial depth (Figure 9). The trend is reasonably uniform even though impulse from Boxcar, Greely, Scotch, Danny Boy, and Sulky is entirely from the GSI pulse while that from Palanquin, Cabriolet, and Schooner is from both the GSI and gas-venting pulses--as is impulse from the HE shots. There is no consistent clue to nuclear-HE equivalence.

Peak gas-venting overpressure (Figure 10) shows the decrease in overpressure with increased burial depth for the HE shots. Nuclear events in alluvium (Teapot ESS and Sedan) produced gas-venting overpressures greater than in HE shots, while two of the cratering events in rhyolite (Cabriolet and Palanquin) produced less. The Schooner event produces about the same as would be expected from HE shots. This attests to the greater dependence of gas-venting peak overpressure on medium (and especially its moisture content) in the case of the nuclear events than in the HE shots. It attests further to a consequent inapplicability of HE shots as a source of predicting gas-venting peak overpressure from nuclear events.

Suppression with burial depth of GSI peak overpressure (Figure 11) presents a different picture. No GSI pulse is observed for burial depths shallower than about $0.5 \text{ ft/lb}^{1/3}$. From four of the nuclear cratering shots there is consistently better agreement with HE basalt data on the basis of one-half nominal yield. Palanquin would have to have a nominal yield of 2 kt to agree with the other four events. It is this observation for

*The equivalence actually varies with overpressure, but is close to half for most of the overpressure range from which it has been derived. Recent calculations⁴¹ suggest an equivalence of 0.7 for the lower overpressure range for free-air explosions.

**Nuclear energy is deposited locally, and afterburning of HE gases is less (if, in fact, afterburn exists at all for buried explosions).

these five nuclear cratering shots that is taken as evidence that the nuclear-HE equivalence observed for airblast from above-ground explosions is also applicable to that from cratering explosions. This observation is possible only for the GSI peak overpressure, where medium and moisture content effects are not an overriding factor.

GSI peak overpressure from contained explosions, either separately or together with the cratering nuclear explosions, appears to follow a law of blast suppression with charge burial depth quite different from that of the HE shots. The suggestion is that GSI airblast from contained nuclear explosions is suppressed less effectively by charge burial. Data from HE shots at comparable burial depths are not available to show whether this is a characteristic of nuclear shots only. The larger area source of the GSI pulse from contained nuclear explosions may be a possible explanation.

Comparison with Montan's Acoustic Approximation

Montan has shown³⁷ that ground surface motion can be described by

$$\frac{U_{vfs}}{U_{ovfs}} = \left(\frac{DOB}{S} \right)^{n_m} \quad (12)$$

where S is slant range. He shows further that overpressure as a function of horizontal range (r) would have the form

$$\frac{\Delta p}{\Delta p_0} = \alpha \left(\frac{r}{DOB} \right)^{-\mu} \quad (13)$$

Values for n_m of about 3 for alluvium and rhyolite and about 6 for hard rock were found from experiment results, corresponding to α of 0.318 and 0.188 respectively. The latter were evaluated for four HE shots in alluvium, as well as for three HE shots and two NE shots in basalt.

The availability of pressure data from a larger number of shots permits similar evaluations to be made easily. These questions were asked:

1. Is the exponent μ precisely -1; if not, what is it?
2. What are values of α for $\mu = -1$, and for the exponent evaluated from the data?

Of course, $\mu = m$ (m from Eq. 7) for the GSI pulse and μ departs from 1 for precisely the same reasons that m departs from 1 (see Figure 3). Since the departure is biased on the higher side, the acoustic approximation departs from reality accordingly.

Tables 7 and 8 list values for μ and α indicated by the data, and α indicated by the data where μ is held equal to 1 according to an acoustic assumption. Values of n_m are listed also, derived from α .

One unique feature of the HE data of Table 7 is the large values of α (low n_m) for the Albuquerque alluvium, a feature that carries over into some shots in NTS alluvium. Alluvial soils appear as nearly elastic media since for elastic media $n_m = 2$ (Ref. 44). Large values of α can be attributed to either a unique characteristic of the medium or to a measurement which failed to record a Δp_0 as large as actually occurred (in the case of the CAPSA series); in the case of NTS alluvium Δp_0 was not measured in any instance, but was calculated (using Equation 6 and ambient conditions) from a surface zero velocity versus depth of burst relationship or from measured surface zero velocity.

Several shots were used to evaluate the acoustic theory further. Two of the better of these are shown in Figure 12 (Scooter) and Figure 13 (Cabriolet). Note that for Scooter there are four separate values shown for α and n_m :

1. From n_m derived from measured surface motion data,
 $\alpha = 0.252-0.268$
 $n_m = 3.65-3.95$
2. From Reference 37, $\alpha = 0.318$
 $n_m = 3.00$
3. From measured pressure data, $(\frac{r}{DOB})^{1.147}$, $\alpha = 0.381$
 $n_m = 2.55$
4. From measured pressure data, $(\frac{r}{DOB})^{-1}$, $\alpha = 0.286$
 $n_m = 3.35$

These observations can be made: (1) none of the four approaches departs appreciably from measured data; (2) the acoustic (r^{-1}) attenuation, although approximate, is not realistic; (3) the range of both α and n_m exhibited does not depart appreciably from the data, and (4) failure to account for actual rates of attenuation is as important as uncertainties or variations of ± 25 percent or more in α or n_m .

Similar observations can be made concerning Cabriolet (Figure 10). Similar comparisons were made for other shots, resulting in these additional observations: (1) uncertainties or variations in measured surface velocity profiles often detract from the accuracy of n_m and hence the utility of acoustic theory, and (2) Δp_0 derived from measured surface velocity or surface velocity relationships can also introduce variations or uncertainty in evaluation of the acoustic approximation.

TABLE 7
Single HE Shots

			μ	α	n_m	$\mu = 1$	
						α	n_m
<u>NTS Desert Alluvium</u>							
Jangle HE	3	c	0.978	0.517	<2.0	0.541	<2.0
Mole 402		c	1.248	0.462	2.15	0.288	3.35
404		c	1.423	0.605	<2.0	0.305	3.15
Sandia I	-9	c	1.142	0.272	3.55	0.205	5.30
Stagecoach	1	b	1.038	0.285	3.35	0.277	3.50
	2	b	1.063	0.502	2.00	0.435	2.30
	3	b	1.114	0.536	<2.00	0.400	2.45
Scooter		b	1.147	0.381	2.55	0.286	3.35
<u>All NTS Alluvium</u>							
<u>Albuquerque Alluvium</u>							
Sandia III	-1	d	1.104	0.543	<2.0	0.432	2.30
Sandia III	-2	d	1.150	0.729	<2.0	0.523	<2.0
Capsa	1	a	1.133	0.633	<2.0	0.489	2.05
	2	a	0.986	0.467	2.15	0.480	2.10
	3	a	1.091	0.883	<2.0	0.714	<2.0
	4	a	1.021	0.548	<2.0	0.528	<2.0
	5	a	1.063	0.649	<2.0	0.607	<2.0
	6	a	0.987	0.430	2.30	0.442	2.25
	7	a	1.065	0.674	<2.0	0.565	<2.0
	9	a	1.011	0.404	2.40	0.395	2.50
	10	a	1.115	1.033	<2.0	0.810	<2.0
	11	a	1.238	0.599	<2.0	0.376	2.55
	12	a	1.550	0.492	2.05	1.318	<2.0
	13	a	1.300	0.979	<2.0	0.594	<2.0
<u>Basalt</u>							
Buckboard	11	b	0.961	0.218	4.80	0.237	4.25
	12	b	1.050	0.278	3.50	0.257	3.85
	13	b	0.943	0.238	4.25	0.259	3.80
<u>Rhyolite</u>							
Pre-Schooner II		a	1.076	0.456	2.20	0.401	2.45
<u>Playa</u>							
TTR 211-4		b	0.973	0.397	2.45	0.436	2.30
TTR 211-7			1.073	0.461	2.20	0.422	2.35
a - P_o measured b - P_o derived from measured surface velocity and ambient conditions c - P_o derived from relation for surface velocity versus DOB and ambient conditions for HE shots d - P_o assumed same as measured for other shots in same medium at same scaled burial depth							

TABLE 8
Contained Nuclear Shots
and Nuclear Cratering Shots

		$\mu = 1$				
		μ	α	n^1	α	n_m
Dumont	a	1.137	0.475 to 0.746	<2.0 to 2.10	0.381 to 0.60	<2.0 to 2.55
Greely	a	1.143	0.341	2.80	0.299	3.20
<u>Basalt</u>						
Danny Boy	b	0.785	0.201	5.45	0.292	3.30
Sulky	b	1.220	0.393	2.50	0.243	4.15
<u>Rhyolite</u>						
Palanquin	a	1.236	0.349	2.75	0.231	4.45
Cabriolet	a	1.240	0.511	<2.0	0.314	3.05
Schooner	a	1.203	0.328	2.90	0.219	4.75

a - P_o measured

b - P_o derived from relation for surface velocity versus DOB
and ambient conditions using yield of nuclear shot
1 kt = 10^6 lb HE

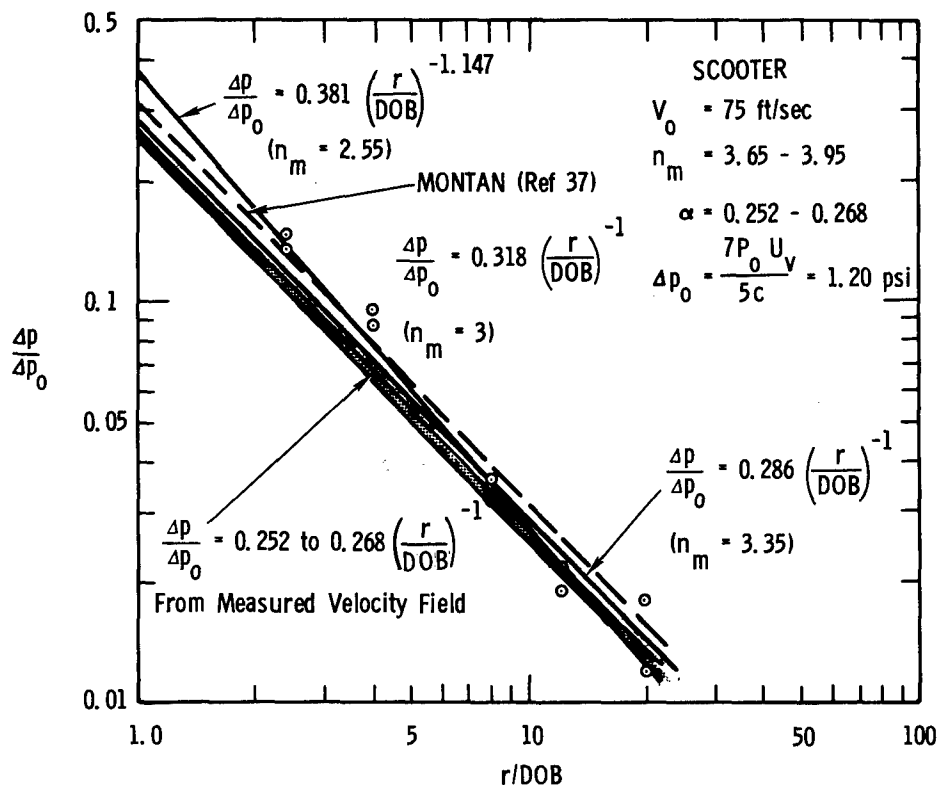


Fig. 12 — Comparison of acoustic approximation with Scooter measurements.

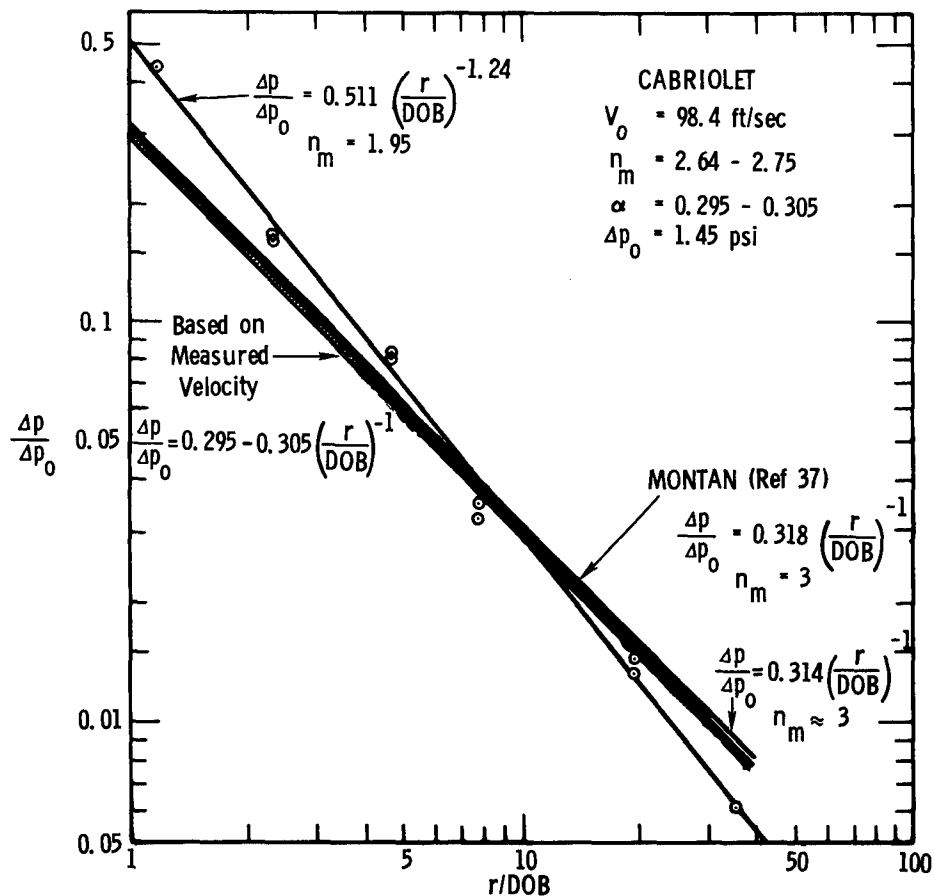


Fig. 13 — Comparison of acoustic approximation with Cabriolet measurements.

Figure 3 showed that attenuation rates observed on experiments averaged well above r^{-1} . While there are almost certainly some meteorological effects contributory to the scatter, it is difficult to see how shot conditions could have been chosen to provide the bias illustrated by the figure. This, together with calculated attenuation rates, suggests that while the acoustic case may be approximated, it is not achieved precisely.

Rows and Arrays

Airblast parameters from row charges were found to approximately equal N^α times the same parameter for a single charge, where N is the number of charges. The power α was different for each parameter; it was a function of charge spacing, and increased as spacing between charges in the row decreased. The power was always greater perpendicular to the row (but always less than 1) than off the end of the row.

Pressure and impulse were always greater perpendicular to the row than off the end of the row, and the difference increased as the number of charges increased. The increase was also a function of charge spacing. The shots listed in Table 2 suggest that there also are medium dependencies, but the data are too sparse to suggest their nature. Rates of airblast attenuation with distance for row charges exhibited about the same variation for each parameter and from one parameter to another as did single charges.

Similar variations were observed also for quincuncial (symmetrical five-charge) arrays. There GSI peak overpressures were about 2.25 and 1.7 times those of a single charge at the same burial depth for 10- and 16-ft. spacing respectively. Corresponding ratios for gas-venting peak overpressures were reversed, i.e., 1.7 and 2.25 times respectively. For positive-phase impulse, the ratio was 3.3 for both spacings. GSI peak overpressures were in agreement with those to be expected perpendicular to a row of five such charges. Gas-venting peak overpressures from the array were larger by comparison.

CONCLUSIONS

Rate of attenuation of airblast with distance is affected by local meteorology and gage performance. There is no consistent dependence of attenuation rate on medium. Attenuation rates are different for GSI peak overpressures, gas-venting peak overpressure, and positive-phase impulse. The latter is the only parameter in which a clear dependence of attenuation rate on scaled burial depth is demonstrated.

It has been possible, using the high-explosive data, to provide relationships with which to predict any of three components of airblast from the buried HE shots. The relationships are, of course, applicable only for the media from which data were

obtained, only over the range of charge burial depth in those media, and over the range of distances from the charges at which measurements were made. The accuracy of the prediction is comparable to scatter in the measured airblast parameter. No GSI overpressures were observed for explosions where the charge burial depth was less than $0.50 \text{ ft/lb}^{1/3}$.

In the case of nuclear explosions the number of events is too small, considering medium effects, to permit derivation of similar relationships. Gas-venting peak overpressures for the Teapot ESS and Sedan nuclear cratering explosions in NTS alluvium were larger than would be predicted from HE shots; that of the Schooner event in rhyolite was about equal, whereas the remaining events in basalt or rhyolite had peak gas-venting pressures lower than would be predicted from results of chemical explosions. This stresses the importance of the medium, and particularly its moisture, in the determination of gas-venting peak overpressure.

Impulses from nuclear explosions are generally comparable with those from chemical explosions and continue the trend of blast suppression with charge burial established by the chemical explosions.

The GSI peak overpressures for completely contained explosions decrease less rapidly with increased charge burial depth than is indicated by the HE data. For the nuclear cratering explosions, the peak GSI overpressures are in better agreement with results from chemical explosions if the nuclear explosions are considered to have a TNT energy equivalence equal to half their nominal yield. This makes equivalence for underground nuclear events agree with the equivalence observed for above-ground explosions.

Availability of data from a large number of chemical and nuclear explosions has permitted a comparison of experiment results with Montan's acoustic approximation. His acoustic prediction is generally comparable with measured overpressures. The most obvious departure from the acoustic approximation occurs because the rate of overpressure attenuation with distances is greater than the r^{-1} predicted by acoustic theory. It was found that a major source of uncertainty in applying acoustic theory results from uncertainties or inaccuracies in measurement of the ground surface velocity profile.

ACKNOWLEDGMENTS

This work was supported by the Division of Peaceful Nuclear Explosives, U. S. Atomic Energy Commission. The author recognizes the cooperation of the Dikewood Corporation in providing airblast data cards, and of J. W. Long in programming all computations.

REFERENCES

1. Vaile, R. B., Jr., Surface Structure Program, Underground Explosion Tests At Dugway, AFSWP-298, Stanford Research Institute, Menlo Park, California, March 1952
2. Doll, E. B., High Explosive Tests, Operation Jangle, WT-365, Armed Forces Special Weapons Project, October-November 1951
3. Sachs, D. C. and L. M. Swift, Small Explosion Tests, Project MOLE, Vols. I and II, AFSWP-291, Stanford Research Institute, Menlo Park, California, December, 1955
4. Murphey, B. F. and E. S. Ames, Air Pressure Versus Depth of Burst, SC-TM-42-59(51), Sandia Laboratories, Albuquerque, New Mexico, February 1959
5. Murphey, B. F., High Explosive Crater Studies: Tuff, SC-4574(RR), Sandia Laboratories, Albuquerque, New Mexico, April 1961
6. Vortman, L. J., et al, 20-Ton HE Cratering Experiment in Desert Alluvium, Project STAGECOACH, SC-4596(RR), Sandia Laboratories, Albuquerque, New Mexico, May 1962
7. Vortman, L. J., et al, 20-Ton and 1/2-Ton High Explosive Cratering Experiments in Basalt Rock, Project BUCKBOARD, SC-4675(RR), Sandia Laboratories, Albuquerque, New Mexico, November 1960
8. Perret, W. R., et al, Project SCOOTER Final Report, SC-4602(RR), Sandia Laboratories, Albuquerque, New Mexico, October 1963
9. Vortman, L. J., Airblast and Craters from Rows of Two to Twenty-five Charges, SC-RR-68-655, Sandia Laboratories, Albuquerque, New Mexico, January 1969
10. Unpublished data, Sandia Laboratories, Albuquerque, New Mexico
11. Reed, J. W. and L. J. Vortman, Airblast Measurements, Project PRE-SCHOONER II, PNE-512F, Sandia Laboratories, Albuquerque, New Mexico, February 1968
12. Unpublished data, Sandia Laboratories, Albuquerque, New Mexico and U. S. Corps of Engineers, Nuclear Cratering Group, Livermore, California

13. Vortman, L. J., Close-in Airblast From a Row Charge in Basalt, PNE-608F, Sandia Laboratories, Albuquerque, New Mexico, August 4, 1965
14. Vortman, L. J., Comparison of Airblast from Two Sizes of Row Charges, SC-RR-66-415, Sandia Laboratories, Albuquerque, New Mexico, October 1966
15. Keefer, J. M., W. F. Jackson, and D. P. Lefevre, "Close-in Air Blast from a Row of Buried Charges," Ballistic Research Laboratories, Aberdeen Proving Ground, Maryland, Chapter in Project Pre-Gondola II, Summary Report, U. S. Corps of Engineers, Nuclear Cratering Group, Livermore, California, to be published
16. Rappleyea, C. Annette, Crater, Ejecta, and Air-Blast Studies from Five High-Explosive Charges in a Horizontal Square Array, SC-RR-66-480, Sandia Laboratories, Albuquerque, New Mexico, April 1967
17. Vortman, L. J., "Close-in Airblast Measurements," Sandia Laboratories, Albuquerque, New Mexico, Chapter in Project Pre-Gondola III, Phase I, Summary Report, PNE-1114, U. S. Corps of Engineers, Nuclear Cratering Group, Livermore, California, to be published
18. Gannon, W. F., et al, Blast and Shock Measurements II, Operation Jangle, WT-367, Armed Forces Special Weapons Project, Washington, D. C., October-November 1951
19. Sachs, D. C. and L. M. Swift, Underground Explosion Effects, Operation Teapot, Project 1.7, WT-1106, Armed Forces Special Weapons Project, Washington, D. C., March 3, 1958
20. Vortman, L. J., Close-in Airblast from a Nuclear Detonation in Basalt, Project DANNY BOY, POR-1810, Sandia Laboratories, Albuquerque, New Mexico, June 1962
21. Vortman, L. J., Close-in Airblast from a Nuclear Event in NTS Desert Alluvium, Project SEDAN, PNE-211F, Sandia Laboratories, Albuquerque, New Mexico, October 2, 1964
22. Keefer, J. H., Free-air and Free-field Blast Phenomena from a Small Yield Device, Operation Sunbeam, Shot Johnie Boy, POR-2280, Ballistic Research Laboratory, Aberdeen Proving Ground, Aberdeen, Maryland, November 27, 1963
23. Vortman, L. J., Close-in Air Blast from a Relatively Deep Low-Yield Nuclear Detonation in Basalt, Project SULKY, PNE-711F, Sandia Laboratories, Albuquerque, New Mexico, May 1965
24. Vortman, L. J., Close-in Air Blast from a Cratering Nuclear Detonation in Rhyolite, Project Palanquin, PNE-902F, Sandia Laboratories, Albuquerque, New Mexico, April 1966

25. Vortman, L. J., Close-in Air Blast from the Cabriolet Event, PNE-951, Sandia Laboratories, Albuquerque, New Mexico, October 25, 1968
26. Vortman, L. J., Close-in Airblast from the Buggy I Event, PNE-320, Sandia Laboratories, Albuquerque, New Mexico, to be published
27. Vortman, L. J., Close-in Airblast from the Schooner Event, PNE-521, Sandia Laboratories, Albuquerque, New Mexico, to be published
28. Reed, J. W. and H. W. Church, Microbarograph Measurement, Project Gnome, VUP-2001, Sandia Laboratories, Albuquerque, New Mexico, January 1962
29. Perret, W. R., Personal Communication
30. Reed J. W., Personal Communication
31. Preliminary Report on Effects of Milrow Detonation, Amchitka Island, Alaska, October 2, 1969, Press Release, U. S. Atomic Energy Commission, October 22, 1969
32. Wheeler, V. E. and R. G. Preston, Scaled Free-Field Particle Motions from Underground Nuclear Explosions, UCRL-50563, Lawrence Radiation Laboratory, Livermore, California, August 1, 1968
33. Cole, R. H., Underwater Explosions, Princeton University Press, Princeton, New Jersey, 1948
34. Knopoff, L., R. W. Fredricks, A. F. Gangs, and L. D. Porter, "Surface Amplitudes of Reflected Body Waves," Geophysics, Vol. SSII, No. 4., October 1957, pp. 842-847
35. Merritt, M. L., Airpressures from a Deep Underwater Burst; Operation Wigwam, WT-1035, Sandia Laboratories, Albuquerque, New Mexico, May 1955
36. Merritt, M. L. and C. R. Mehl, Airpressures from Deep Underwater Explosion, II, Crossfeed, SC-TM-274-55 (51), Sandia Laboratories, Albuquerque, New Mexico, December 1955
37. Montan, D. N., "Source of Airblast from the Underground Explosion," Transactions, American Nuclear Society, Vol. II, No. 2, November 1968, pp. 541-542
38. Bethe, H., et al, Blast Wave, LA-2000, Los Alamos Scientific Laboratory, Los Alamos, New Mexico, March 27, 1958
39. Whitaker, W. A., Air Force Weapons Laboratory, Personal Communication
40. Kirkwood, J. G. and S. R. Brinkley, Jr., Theoretical Blast-Wave Curves for Cast TNT, OSRD 5481, NDRL A-341, Office of Scientific Research and Development, Washington 25, D. C., August 23, 1945

41. Lehto, D. L. and R. A. Larson, Long Range Propagation of Spherical Shockwaves from Explosions in Air, NOLTR 69-88, U. S. Naval Ordnance Laboratory, Explosions Research Department, White Oak, Maryland, July 1969
42. Kingery, C. H. and B. F. Pannill, Peak Overpressure versus Scaled Distance for TNT Surface Bursts (Hemispherical Charges), BRL Memorandum Report No. 1518, Ballistic Research Laboratories, Aberdeen Proving Ground, Maryland, April 1964
43. Kingery, C. H., Airblast Parameters versus Distance for Hemispherical TNT Surface Burst, BRL Report 1344, Ballistic Research Laboratories, Aberdeen Proving Ground, Maryland, September 1966
44. Montan, D. N., Personal Communication

PREDICTION OF GAMMA EXPOSURE RATES IN LARGE NUCLEAR CRATERS

Thomas M. Tami and Walter C. Day
U. S. Army Engineer Nuclear Cratering Group
Lawrence Radiation Laboratory
Livermore, California

INTRODUCTION

In many civil engineering applications of nuclear explosives there is the need to reenter the crater and lip area as soon as possible after the detonation to carry out conventional construction activities. These construction activities, however, must be delayed until the gamma dose rate, or exposure rate, in and around the crater decays to acceptable levels. To estimate the time of reentry for post-detonation construction activities, the exposure rate in the crater and lip areas must be predicted as a function of time after detonation. An accurate prediction permits a project planner to effectively schedule post-detonation activities.

Method of Approach

In developing a means to predict the exposure rate in the crater and lip area, it became apparent that the radioactive debris was volume distributed rather than plane distributed as occurs in fallout fields. This meant that methods designed to predict the exposure rate in a fallout field could not be used to predict the exposure rate in the crater and lip area. The succeeding steps were followed in developing a technique for predicting the crater and lip exposure rate: (1) a uniform distribution of the radioactive debris in the upper portions of the fallback and ejecta was assumed; (2) a uniform infinite slab source was used to analytically calculate the exposure rate and was shown to be applicable in the crater and lip area; (3) this calculated exposure rate was then normalized to previously measured values of the exposure rate in and around several nuclear craters; (4) and finally, exposure rates in and around future nuclear craters were calculated. These four steps are developed and discussed in the remainder of this paper.

DISTRIBUTION OF RADIONUCLIDES IN CRATER EJECTA AND FALLBACK

The distribution of the radionuclides in the post-detonation environment must be known or inferred before a workable model could be developed for predicting the exposure rate in the crater and lip area. When our predictive model was developed, little empirical data describing the distribution of gamma-emitting radionuclides in the fallback and ejecta of nuclear craters were available. Hence, from a qualitative understanding of the nuclear cratering process (and from considerations of an infinite slab source), we assumed that the gamma-emitting radionuclides in the upper 2 feet of the ejecta and fallback were uniformly distributed. (1, 2). Koranda (3) has since shown that in 4 out of 5 locations on the lip of the SEDAN Crater, the gamma-emitting radionuclides indeed approximate a uniform distribution in the upper 2 to 3 feet of ejecta.

It should be noted that the distribution of radionuclides in the ejecta and fallback is influenced by many factors: for example, the yield of the device, the depth of burst, and the geological and chemical properties of the medium in which the device is detonated. Not all cratering events have or are expected to produce a uniform distribution of radionuclides in the upper 2 feet of the ejecta and fallback. However, for these cratering events we are able to predict the exposure rate by using a normalization factor, based on an event's scaled depth of burst, which takes into account this nonuniform distribution.

MATHEMATICAL MODEL FOR CALCULATION OF THE CRATER AND LIP EXPOSURE RATE

Since we have assumed that the gamma-emitting radionuclides are approximately uniformly distributed in the upper 2 feet of ejecta, a mathematical model for calculating the exposure rate in the crater and lip area can be developed.

The exposure rate from a source emitting mono-energetic photons is directly proportional to the magnitude of the gamma photon flux, the photon energy, and the energy absorption properties of air. This relationship is given by

$$ER = k \mu_a E \phi \quad (R/hr) \quad (1)$$

where

ER = exposure rate (R/hr)

ϕ = gamma photon flux (photons/cm²-sec)

E = energy per photon (Mev/photon)

μ_a = linear energy absorption coefficient of air
for photons of energy E (cm⁻¹)

$k = 5.33 \times 10^{-2} (R/hr)/(Mev/cm^3\text{-sec}).$

For a flux composed of photons of different energies, the exposure rate is simply the sum of the exposure rates due to each photon energy. Except for the flux, the quantities in equation (1) are well known. Thus, the problem of calculating the exposure rate becomes one of calculating the gamma photon flux.

Flux Above an Infinite Slab Source of Finite Thickness

If radionuclides are distributed uniformly throughout an infinite slab, the source density (i.e., the number of gamma photons emitted per unit time per unit source volume) may be treated as a constant at a specified time. The photon flux at a specified distance above such a source configuration has been derived by Rockwell. (4). Rockwell's derivation was modified to include a build-up factor which depends linearly on the number of mean-free paths from the source to a point at which the flux is to be calculated. (5). The flux at point P above this source configuration (see Figure 1) is given by

$$\phi_s = \frac{\lambda_s S_v}{2} \left[E_2(\mu_0 h) - E_2(\mu_0 h + \mu_s z) + \exp(-\mu_0 h) - \exp(-\mu_0 h - \mu_s z) \right] \text{ (photons/cm}^2\text{-sec)} \quad (2)$$

in which

ϕ_s = gamma photon flux above the slab at point p (photons/cm²-sec)

h = distance from the slab to point P (cm)

- S_v = uniform source density (photons/sec -cm³)
- λ_s = relaxation length of the slab material (cm). (1). This quantity is plotted in Figure 2 for a material having an average atomic number of 12 (i.e., typical ejecta and fallback)
- μ_s = linear attenuation coefficient of the slab material (cm⁻¹). This quantity is the reciprocal of the relaxation length, i.e., $\mu_s = 1/\lambda_s$
- μ_0 = linear attenuation coefficient of air (cm⁻¹). The mass attenuation coefficient, μ_0/ρ , which is equal to μ_0 divided by the density of air, ρ , is plotted in Figure 3.
- z = thickness of the slab (cm)
- $E_2(t)$ = second order exponential integral function with argument t . (4).

The flux above a uniform infinite slab source depends on the concentration of radionuclides comprising the slab source, the density of the slab material, the energy of the photons emitted by the radionuclides, the height above the slab where the flux is calculated, and the thickness of the slab.

Application to the Crater and Lip Area

It was assumed that an infinite slab source approximates the source configuration found in the nuclear crater and lip area. In order to verify this assumption, equation (2) is evaluated for three photon energies: 0.1, 1 and 2 Mev. The flux is evaluated at a point 3 feet ($h = 91.4$ cm) above the slab which is composed of a material with average atomic number of 12 and with a density of 1.5 gm/cm³. The exposure rate in the crater and lip area is usually measured at a height of 3 feet above ground surface. The variables in equation (2), evaluated at the given photon energies, were determined from Figures 2 and 3 and are tabulated in Table I.

TABLE I
Variables used to evaluate equation (2)

	<u>Flux composed of photons with energy</u>		
	<u>.1 Mev</u>	<u>1 Mev</u>	<u>2 Mev</u>
μ_0	2.0 (-4)	8.1 (-5)	5.7 (-5)
$\mu_0 h$	1.8 (-2)	7.4 (-3)	5.2 (-3)
λ_s	4.2	10.5	15.2
μ_s	2.4 (-1)	9.5 (-2)	6.6 (-2)

The values in Table I were used to evaluate terms containing z in equation (2). The results are given in Table II for three values of z .

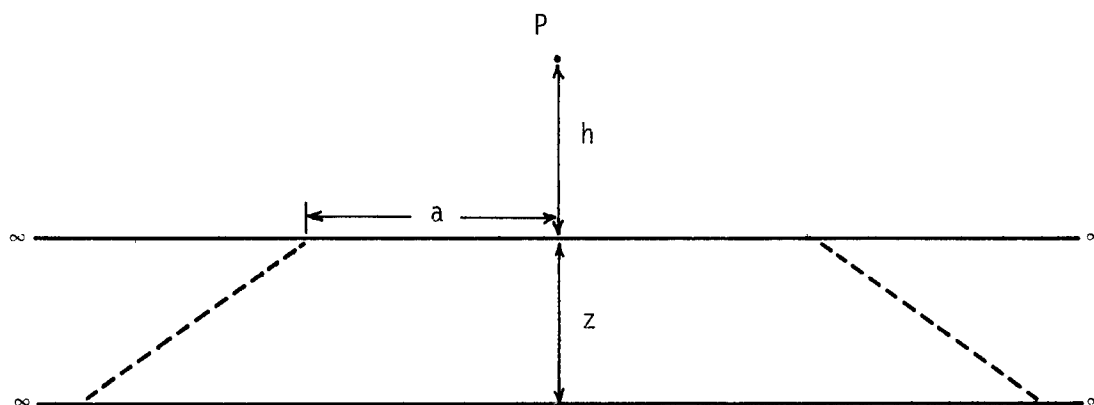


Figure 1. Crosssectional view of both an infinite slab source (solid lines) of thickness " z " and a truncated cone source (broken and solid lines) with an upper radius of " a ".

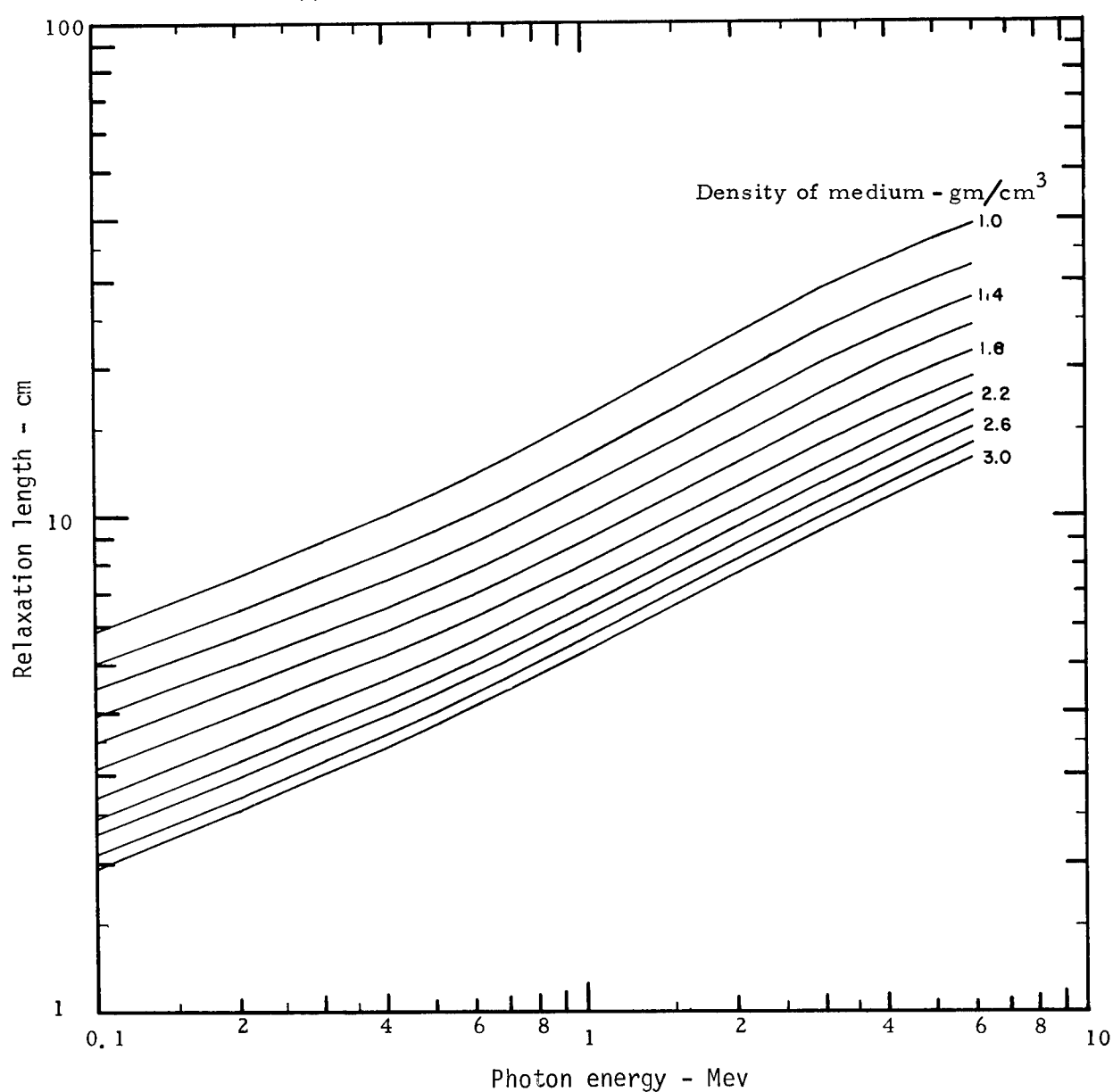


Figure 2. Relaxation length as a function of photon energy and density of the medium having an atomic number of 121.

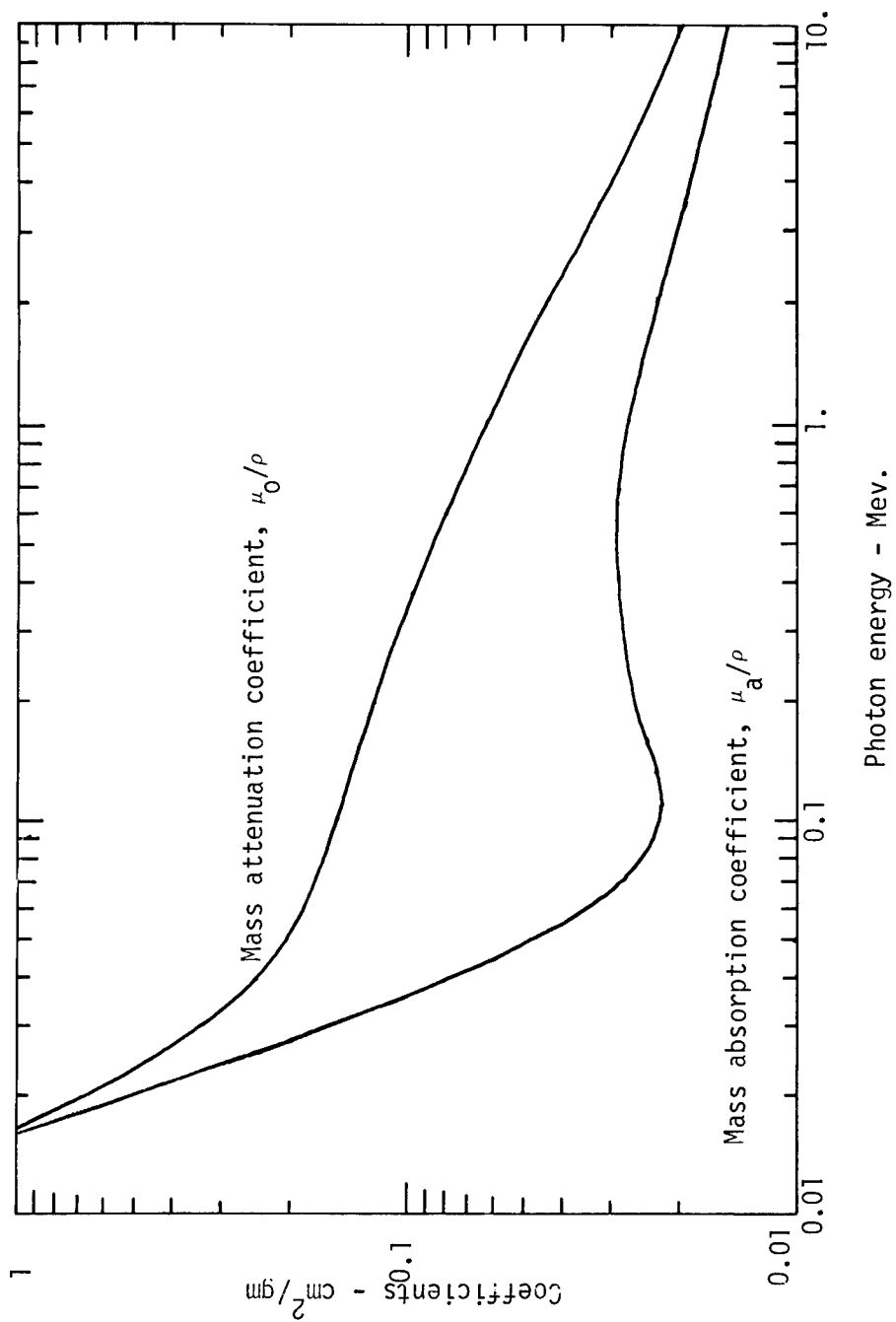


Figure 3. Mass attenuation and absorption coefficients in air as a function of photon energy.⁴

TABLE II

Evaluation of terms containing z in equation (2) for:

Slab thickness z (cm)	Term	Source emitting photons with energy		
		.1 Mev	1 Mev	2 Mev
30	$E_2 (\mu_0 h + \mu_s z)$	8.0 (-5)	1.3 (-2)	3.7 (-2)
30	$\exp (-\mu_0 h - \mu_s z)$	7.4 (-4)	6.1 (-2)	1.4 (-1)
60	$E_2 (\mu_0 h + \mu_s z)$	3.8 (-8)	4.2 (-4)	3.4 (-3)
60	$\exp (-\mu_0 h - \mu_s z)$	6. (-7)	3. (-3)	2. (-2)
∞	$E_2 (\mu_0 h + \mu_s z)$	0	0	0
∞	$\exp (-\mu_0 h - \mu_s z)$	0	0	0

It can be seen in Table II that as z increases, the exponential and the E_2 function decrease rapidly. When z is 60 cm the terms containing z are quite small. The flux from a slab 60 cm thick differs from the flux from an infinitely thick slab by only 2%. Therefore, with little loss in accuracy, equation (2) can be approximated by

$$\phi = \frac{\lambda_s S_v}{2} \left[E_2 (\mu_0 h) + \exp (-\mu_0 h) \right] \text{ (photons/cm}^2 \text{ -sec)} \quad (3)$$

Thus the flux at a point 3 feet above the slab ($h = 91.4$ cm) is essentially insensitive to the source material below the first 60 cm of slab thickness. In the first 60 cm of SEDAN ejecta, the radionuclides were uniformly distributed. Consequently, the vertical distribution of the source in the lip area approximates that of an infinite slab source.

Comparison of the flux from a truncated cone source, shown by the dashed lines in Figure 1, with the flux from an infinite slab source of equal thickness, indicates that over 95% of the flux at point P comes from the source contained in the truncated cone whose upper radius "a" (Figure 1) is approximately 35 feet. The source distribution in the crater and lip area of large craters approximates this lateral distribution.

Thus, we have indicated that the flux in the crater and lip area can be calculated by equation (3).

Equation (3) could be simplified further by noting that $E_2 (\mu_0 h)$ and $\exp (-\mu_0 h)$ are both approximately equal to 1 for photon energies between 0.1 and 2 Mev. An approximate value for the flux above the slab source would then be given by

$$\phi = \lambda_s S_v \quad \text{(photons/cm}^2 \text{ - sec)} \quad (4)$$

However, for photon energies less than .1 Mev, significant error would be introduced by the use of equation (4) because the linear attenuation coefficient, μ_0 , for these energies becomes relatively large and $E_2 (\mu_0 h)$ and $\exp (-\mu_0 h)$ are no longer approximately 1. For this reason, equation (3) is used to calculate the flux used in the model. From equations (1) and (3), the exposure rate for a mono-energetic photon source in the crater and lip area of large nuclear

craters is given by

$$ER = 2.67 \cdot 10^{-2} \mu_a E_{\lambda_s} S_v \left[(E_2 (\mu_0 h) + \exp (-\mu_0 h)) \right] \quad (R/hr) \quad (5)$$

For an exposure rate resulting from a source emitting photons of many energies, the summation of the relative contribution to the exposure rate from each photon energy can be obtained with ease. To apply equation (5) to the crater and lip environment, the source density S_v must be determined.

DETERMINATION OF THE SOURCE DENSITY

The equation for calculating the exposure rate in the crater and lip area was derived assuming the source density, S_v , was uniform in the upper 2 feet of the volume distributed source. This quantity, S_v , depends both on the amount of gamma activity, S , present in the cratered material and the volume of material containing these radionuclides. Therefore, the source density, S_v , can be defined by the following expression:

$$S_v = S / \delta V_t \quad (\text{photons/sec-cm}^3) \quad (6)$$

where

S_v = source density (photons/sec-cm³)

S = gamma activity remaining in the ejecta and fallback (photons/sec)

V_t = true crater volume (cm³)

δ = normalizing factor (unitless).

These quantities are discussed below in detail.

Definition of the Source

If the total gamma activity due to the radionuclides produced by the nuclear explosive is represented by S_T , then the source, S , is given by

$$S = S_T(1-f_v) \quad (\text{photons/sec}) \quad (7)$$

in which

f_v = fraction of the total produced activity vented into the atmosphere and deposited as local fallout (fraction vented).

This equation assumes that all radionuclides are vented into the atmosphere to the same degree. This is a fair approximation for many of the radionuclides. However, fractionation (the process which causes different species of radionuclides to be vented to varying degrees) effects should be considered in the future when more information dealing with this process becomes available.

The total gamma activity produced, S_T , can be considered to be composed of two groups: the first group, S_f , is composed of the gamma activity from the fission products; and the second, S_i , is composed of the gamma activity from the neutron-induced radionuclides. Representing this division symbolically

$$S_T = S_f + \sum_{i=1}^I S_i \quad (\text{photons/sec}) \quad (8)$$

where

S_T = total gamma activity from the radionuclides produced by the nuclear explosive

S_f = gamma activity from fission products

S_i = gamma activity from the i^{th} neutron-induced radionuclide

I = total number of significant gamma emitting neutron-induced radionuclides

From equations (8) and (7), the source can be expressed as:

$$S = (S_f + \sum_{i=1}^I S_i) (1-f_v) \quad (\text{photons/sec}) \quad (9)$$

This equation expresses the source as a function of the fraction of the total activity vented into the atmosphere, the gamma activity from the fission process, and the gamma activity from the induced radionuclides.

In most nuclear crater applications at optimum depth of burst, it can be expected that f_v will be very small. Without introducing any significant error, f_v may be set equal to zero. As a result, the source can be approximated as

$$S = S_f + \sum_{i=1}^I S_i \quad (\text{photons/sec}) \quad (10)$$

This approximation will permit predictions of the exposure rate without specifying the vent fraction, f_v .

True Crater Volume

The calculation of the true crater volume V_t is based on a simple geometrical model. For single charge craters, the model consists of a truncated cone and a hemisphere. The volume of the truncated cone depends on the yield W (kt), the scaled apparent crater radius r_a ($\text{cm}/\text{kt}^{1/3.4}$), the scaled cavity radius r ($\text{cm}/\text{kt}^{1/3.4}$), and the scaled depth of burst dob ($\text{cm}/\text{kt}^{1/3.4}$). (6). The volume of the hemisphere depends only on the scaled cavity radius. Using this geometrical configuration, the true crater volume is given by

$$V_t = \frac{\pi}{3} \left\{ 2r_a^3 W + \left[\text{dob } r_a^2 + \text{dob } r_a r + \text{dob } r^2 \right] W^{3/3.4} \right\} (\text{cm}^3) \quad (11)$$

where the terms are as defined above. For row craters, other geometries must be used to estimate the true crater volume.

Normalizing Factor - δ

Values of the normalizing factor, δ , as a function of the scaled depth of burst of an event are given in a later section of this paper. Before presenting a discussion of the manner in which values of δ were determined, the time behavior of the source density and also the exposure rate is given.

PREDICTION OF THE EXPOSURE RATE AS A FUNCTION OF TIME

In previously developed equations, the time dependence of the exposure rate was not considered. In this section, the equations for the exposure rate as a function of time are developed. This development separates the total exposure rate in the crater and lip areas into two parts: (1) the exposure rate from individual induced radionuclides, and (2) the exposure rate from fission products. This separation is expressed by

$$ER(t) = ER_f(t) + \sum_{i=1}^I ER_i(t) \quad (\text{R/hr}) \quad (12)$$

where

$ER(t)$ = total exposure rate as a function of time after detonation (R/hr)

t = time after detonation

$ER_f(t)$ = exposure rate as a function of time from fission products (R/hr)

I = number of significant induced radionuclides

$ER_i(t)$ = exposure rate as a function of time from the i^{th} induced radionuclide (R/hr)

The time dependence of this exposure rate considers only radioactive decay. (7). Other processes, such as weathering, leaching, and groundwater transport of radionuclides which affect the decrease of the crater and lip exposure rate, have been ignored.

Exposure Rate from Induced Radionuclides

The type and quantities of induced radionuclides comprising the source determine the time behavior of the exposure rate. Since most neutron-induced radionuclides decay directly to stable nuclides, the amount of these radionuclides present in the fallback and ejecta is simply a function of exponential radioactive decay. The exposure rate given by equation (5) is summed for each type of radionuclide present in the cratered material and an exponential decay term is included to give the time dependence. Thus the exposure rate from the i^{th} radionuclide is given by

$$ER_i(t) = 2.67 \times 10^{-2} (\lambda_i N_i \exp(-\lambda_i t) / \delta V_t) \times \left\{ \sum_{j=1}^J \mu_{a_{ij}} f_{ij} E_{ij} \lambda_{s_{ij}} \left[E_2(\mu_{o_{ij}} h) + \exp(-\mu_{o_{ij}} h) \right] \right\} \text{ (R/hr)} \quad (13)$$

where

ER_i = exposure rate produced by the i^{th} radionuclide (R/hr)

h = height above ground level where ER_i is calculated (91.4 cm)

N_i = number of atoms of the i^{th} radionuclide remaining in the ejecta and fallback immediately after detonation

λ_i = radioactive decay constant (sec^{-1})

t = time after detonation (sec)

δ = normalizing factor

V_t = true crater volume (cm^3)

J = number of different characteristic photons emitted by the i^{th} radionuclide

E_{ij} = energy of the j^{th} characteristic photon (Mev)

f_{ij} = fraction per disintegration resulting in a photon of energy E_{ij}

$\mu_{a_{ij}}$ = linear energy absorption coefficient in air for the j^{th} photon (cm^{-1})

$\mu_{o_{ij}}$ = linear attenuation coefficient in air for the j^{th} photon (cm^{-1})

$\lambda_{s_{ij}}$ = relaxation length of the ejecta and fallback for the j^{th} photon (cm).

Equation (13) is evaluated for all significant neutron-induced radionuclides present in the ejecta and fallback. If the induced radionuclide doesn't decay directly to a stable nuclide, the exponential decay term in equation (13) can

easily be modified to calculate the contribution to the exposure rate from the growth and decay of daughter radionuclides.

Exposure Rate from Fission Products

There are, at one hour after detonation (H+1), approximately 250 radionuclides that were produced by the fission process. A description of the time behavior of these radionuclides would be complex. This complexity arises from the fact that fission products decay and grow by complicated pathways. If one were to apply equation (13) to fission products, the following information would have to be known: (1) the number of atoms of a fission product at all times after detonation at which the exposure rate from that fission product was to be calculated; (2) the gamma decay scheme of all fission products; and (3) the fractionation of each fission product.

Because Plowshare nuclear explosives are designed to minimize the fission process and because fractionation effects from fission products are not well understood, the exposure rate from the fission products was treated in a simplified manner. The exposure rate from the fission products at H+1 hour was estimated, and this value was decayed according to a function which approximates the well-known $t^{-1.2}$ decay rate for fission products. Therefore, the exposure rate from the fission products is expressed as

$$ER_f(t) = ER_f(H+1) f(t) \quad (R/hr) \quad (14)$$

where

$ER_f(t)$ = exposure rate from fission products as a function of time (R/hr)

$f(t)$ = the approximate $t^{-1.2}$ decay rate (see Figure 4)

Fleming (8) has shown that the total activity for 1 kiloton of unfractionated fission products at H+1 hours is 4.20×10^5 kilocuries per kiloton (KCi/kt) and the infinite plane exposure rate is 2700 roentgens per hour per kiloton per square mile (R/hr/kt/mi²). By considering only gamma emitters in Fleming's data, the activity for 1 hour old gamma emitting fission products was determined to be 3.61×10^5 KCi/kt. Crocker, Connors, and Wong (9) give an equation for calculating the exposure rate 3 feet above an infinite-plane source. An average gamma energy, 1.06 Mev, per photon is found by solving this equation when the exposure rate is 2700 R/hr/kt/mi² and the gamma activity is 3.61×10^5 KCi/kt/mi². Knowing the average energy per gamma disintegration (1.06 Mev) and the gamma activity per kiloton of unfractionated fission products (3.61×10^5 KCi/kt) at H+1 hours, $ER_f(H+1)$ in equation (13) becomes

$$ER_f(H+1) = 2.56 \times 10^{13} \lambda_{s_f} kt_f / \delta V_t \quad (R/hr) \quad (15)$$

where

λ_{s_f} = relaxation length which depends on the postshot density of the cratered material and the average gamma energy, 1.06 Mev, (cm) (see Figure 2)

kt_f = fission yield (kt)

V_t = true crater volume (cm³)

δ = normalizing factor (unitless)

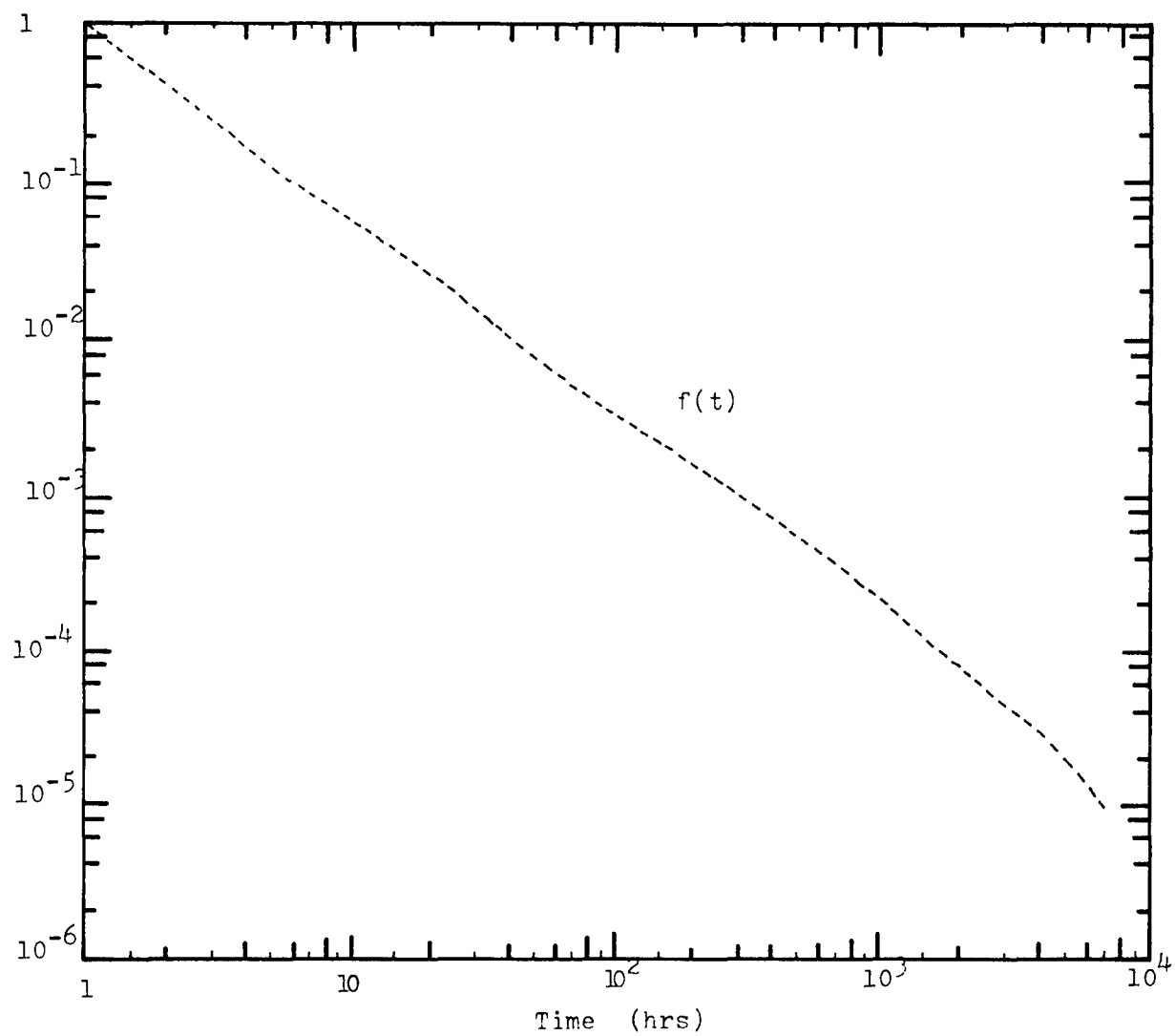


Figure 4. Time dependence of the exposure rate from fission products.

Total Exposure Rate as a Function of Time

The equation for predicting the exposure rate as a function of time is given by simply substituting equations (13) and (14) into (12).

$$\begin{aligned} ER(t) = & 2.67 \times 10^{-2} (\lambda_i N_i \exp(-\lambda_i t) / \delta V_t) \times \left\{ \sum_{j=1}^J \mu_{a_{ij}} f_{ij} E_{ij} \lambda_{s_{ij}} \right. \\ & \left. \left[E_2(\mu_{o_{ij}} h) + \exp(-\mu_{o_{ij}} h) \right] \right\} \\ & + 2.56 \times 10^{13} \lambda_{s_f} (kt_f / \delta V_t) f(t) \text{ (R/hr)} \end{aligned} \quad (16)$$

where all the terms are as defined above.

NORMALIZATION OF THE MODEL

All the terms in equation (16), except for the normalization factor δ , have been discussed. In this section, the method by which δ was determined is given.

The exposure rate was calculated for several previous cratering events using equation (16) with δ set equal to 1. Experimentally measured values of the exposure rate for these past cratering events were found in the literature. Then the calculated exposure rate, $ER_C(\delta=1)$, was fitted to the measured exposure rate, ER_m , so that

$$\delta = \frac{ER_C(\delta=1)}{ER_m}$$

The normalizing factor, δ , determined in this manner, was plotted as a function of the event's scaled depth of burst, and a smooth curve was fitted to the values of δ (see Figure 5). Not enough data were available to distinguish any media dependence of δ .

The region of the curve for which δ is relatively flat indicates that the assumption of a uniform distribution of gamma activity in the upper two feet of ejecta and fallback is probably good. When the slope of δ is steep, this assumption is not correct. For example, if the scaled depth of burst is around $180 \text{ ft}/kt^{1/3.4}$, a region of bulked material, rather than a crater, is produced. For this scaled depth of burst, most of the radioactive debris remains near the detonation point. The radioactivity which reaches the upper portion of the bulked material has been shown to be unevenly distributed. For shallow depths of burst, the slope of δ is again steep. For these scaled depths of burst, the gamma activity in the ejecta decreases very rapidly with depth below ground surface (i.e., the source density is a function of depth). Therefore δ must become small so that an equivalent uniform distribution results. A model to predict the exposure rate, which uses a source density term which is a function of depth below the surface, could be developed for craters produced by a shallow depth of burst. This model would more accurately describe the actual physical distribution of gamma activity in the ejecta and fallback.

However, most proposed applications of nuclear craters will be at optimum depth of burst where the slope of δ is relatively flat and where this model is especially designed to predict the exposure rate.

Application of the Model to the SCHOONER Event

The exposure rate for the SCHOONER event was calculated by equation (16) with δ set to 1. Measured values of the maximum and minimum exposure rates at

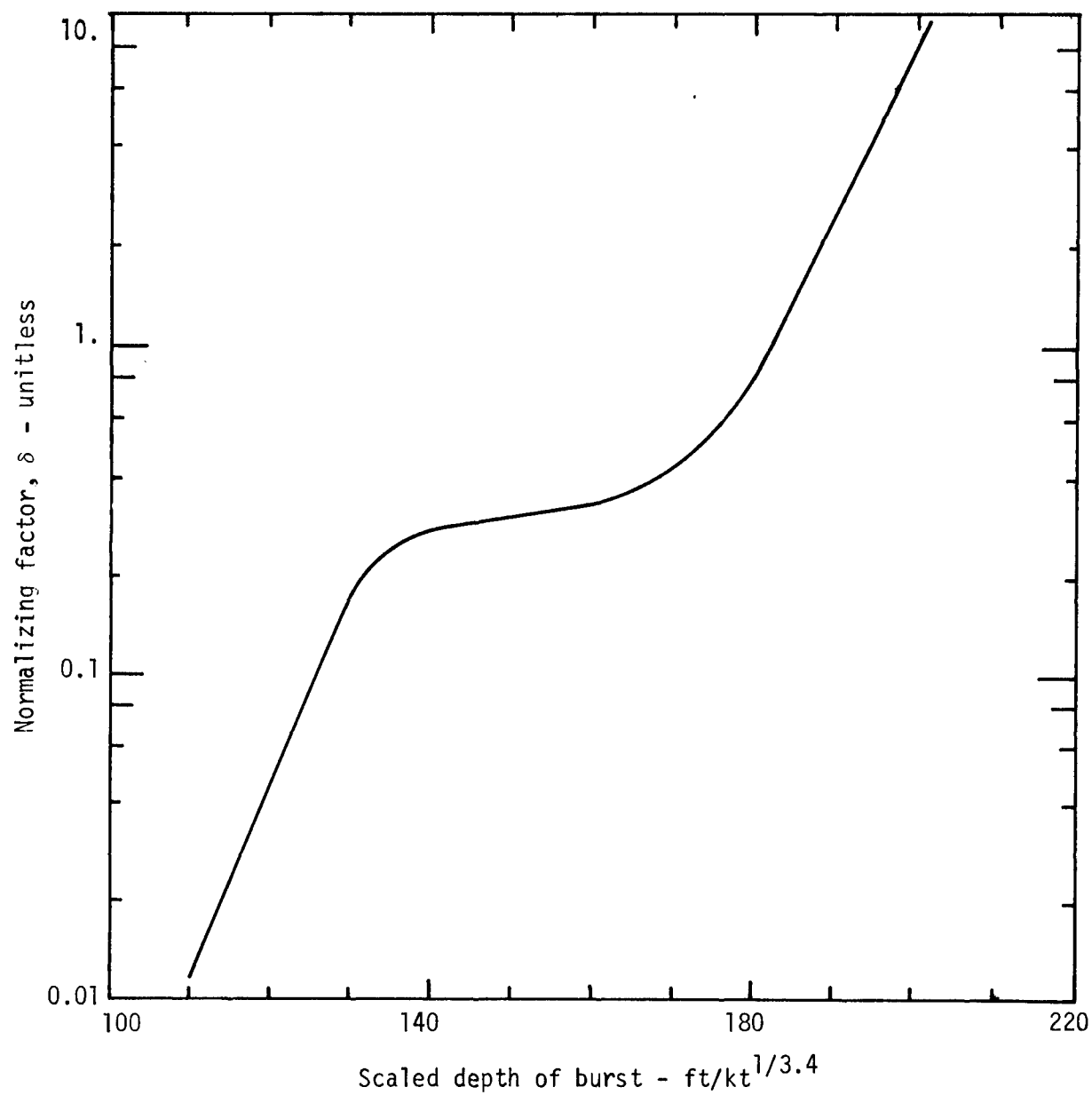


Figure 5. Normalizing factor, δ , as a function of scaled depth of burst.²

eight locations on the SCHOONER lip (10) were plotted as a function of time. The calculated exposure rate was then fitted to the measured values (see Figure 6). Therefore, the model calculates an exposure rate which, when fitted to measured values of the exposure rate, correctly estimated the SCHOONER exposure rate for over a period of a year, the limit of experimental data. This, we believe, certainly demonstrates the capability of the model, after it has been normalized, to accurately predict the crater and lip exposure rate.

APPLICATION OF THE MODEL

The exposure rate for future nuclear cratering detonations may be estimated using data released to the public by the AEC and assumptions consistent with that data. The AEC has stated that it may be assumed that no more than a few kilotons of energy produced by a high-yield Plowshare excavation device will result from the fission process. The balance of the energy will be produced by the fusion process. The AEC has also stated that for each individual nuclear explosive detonated, the sum of fission products airborne in the radioactive cloud and in the fallout can be expected to be as low as the equivalent of 20 tons (11). In addition, the sum of the activation products airborne in the radioactive cloud and in the fallout may be expected to be as low as the amounts shown in Table III.

TABLE III
Representative Set of Gamma-Emitting Induced Radioactivities
at Detonation Time (11)
(Total in Cloud and Fallout)

Nuclide	Nuclide Production, Kilocuries for Yield of		
	100 kt	1 Mt	10 Mt
Na ²⁴	200	800	2000
Mn ⁵⁴	0.1	0.3	0.7
Mn ⁵⁶	600	2000	5000
Fe ⁵⁹	0.4	.15	0.3
W ¹⁸⁷	300	500	700
Pb ²⁰³	1000	7000	20,000

If it is assumed that the fission trigger has a yield of 3 kt, then the ratio of the fission yield to the fission products in the cloud and fallout is 150. It is also assumed that the ratio of the amount of radioactivities produced to the amount in the cloud and fallout is 150. Using these assumptions and the information in Table III together with equation (16), the exposure rate has been calculated for five explosive yields (10 kt, 100 kt, 500 kt, 1 Mt, and 10 Mt) detonated at a scaled depth of burst of $145 \text{ ft/kt}^{1/3.4}$ ($\delta = 0.3$). The results are shown graphically in Figure 7.

It is obvious from Figure 7 that the exposure rate in the crater and lip area decreases as the explosive yield increases. This decrease is due to lower concentrations of radionuclides in the fallback and ejecta. This lower concentration results from (1) a decrease in the amount of radioactivity produced per unit yield with increasing yield (i.e., the constant fission trigger), and (2) the amount of material which contains the radioactivity increases

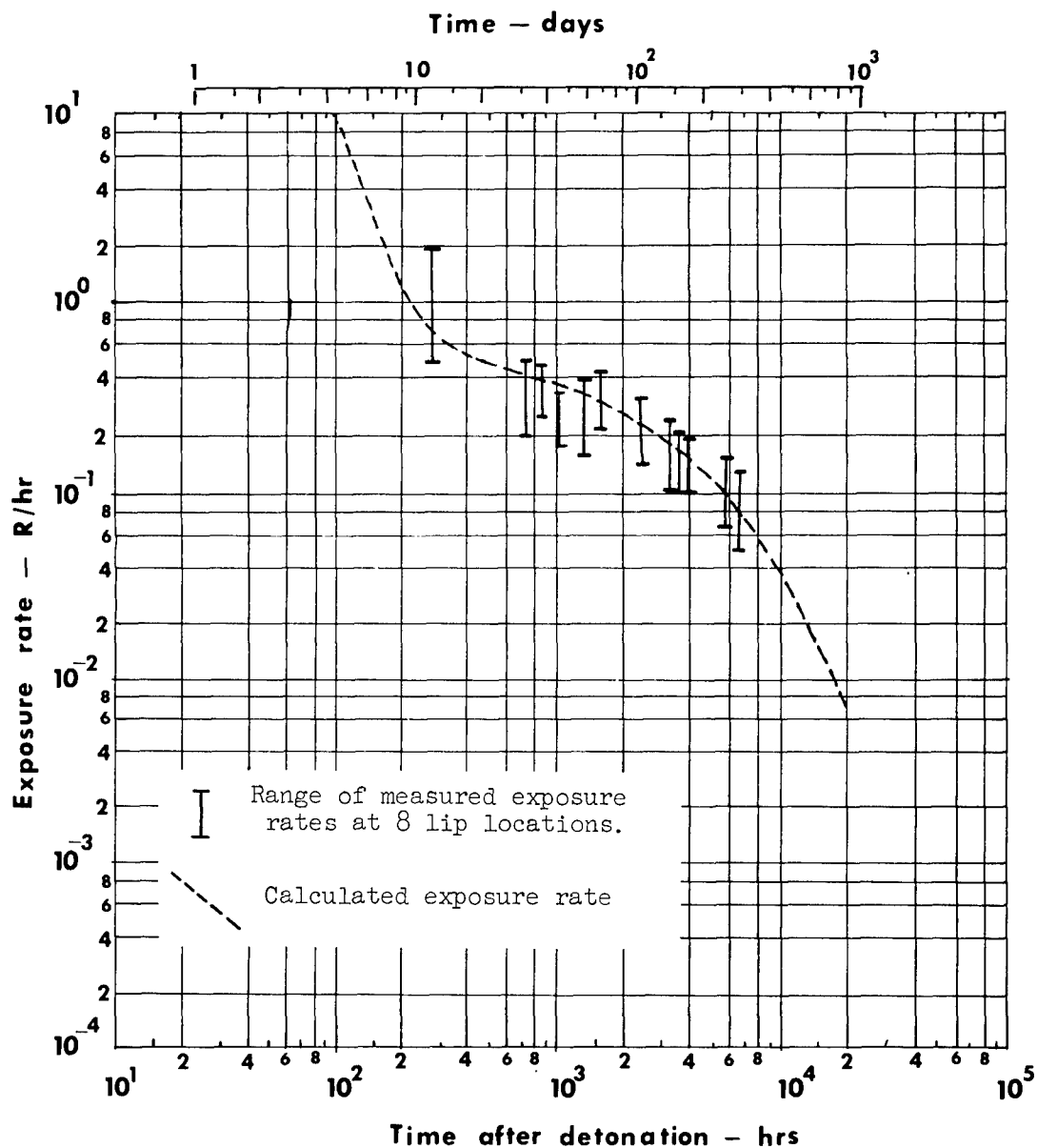


Figure 6. Measured and calculated exposure rates for Project SCHOONER as a function of time.

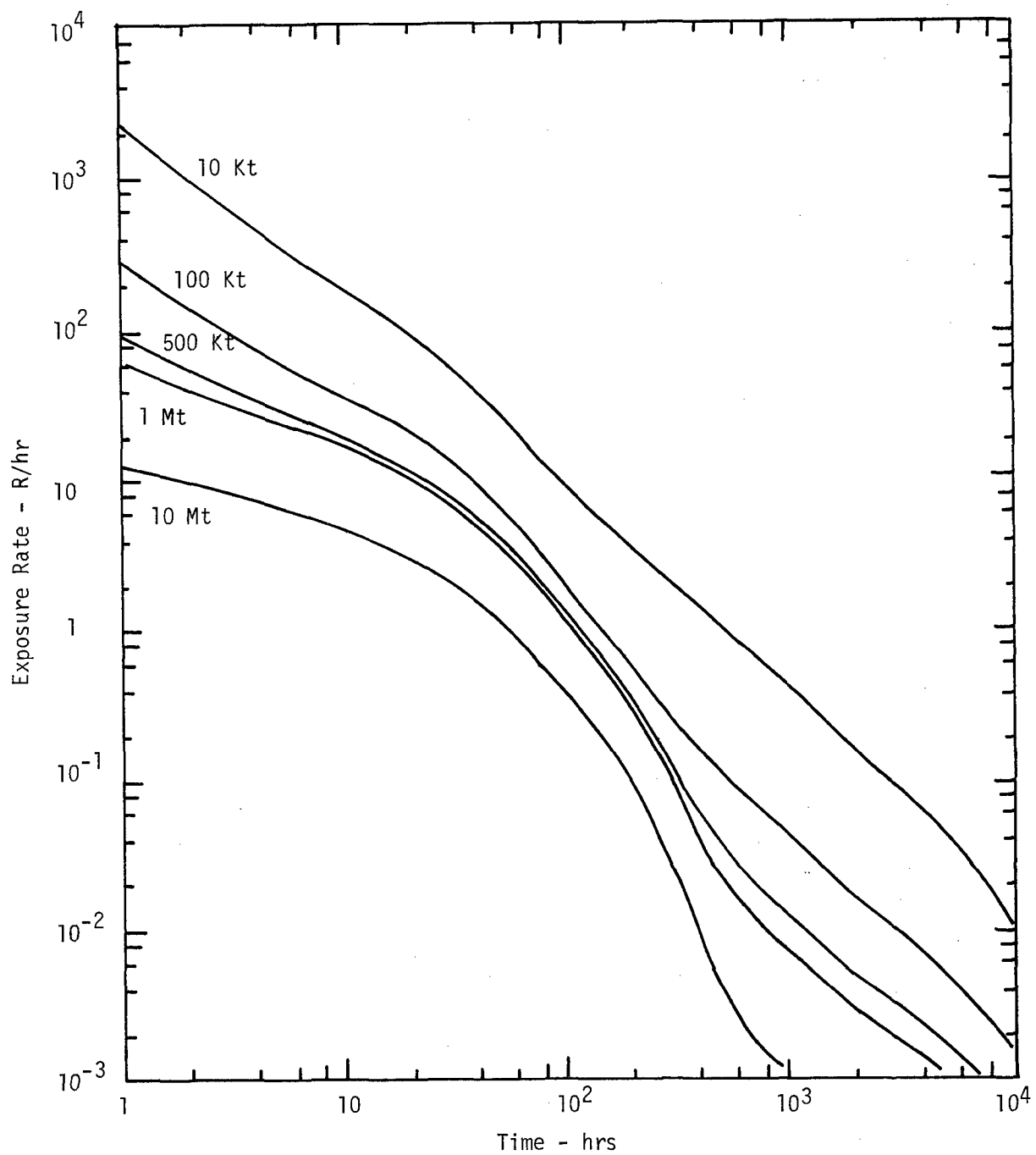


Figure 7. Exposure rate in the crater and lip area for 5 explosive yields as a function of time for a scaled depth of burst of $145 \text{ ft/kt}^{1/3.4}$.

directly with yield. The shapes of the curves change with yield because, as the yield increases, the induced radionuclides become more significant than the fission products in producing the exposure rate.

For a quarrying event ($\text{dob} = 190 \text{ ft/kt}^{1/3.4}$) the value of the normalizing factor δ is 3 instead of the 0.3 value used for a scaled depth of burst of $145 \text{ ft/kt}^{1/3.4}$ (see Figure 5). Therefore, the exposure rate in the bulked region of a quarrying detonation would be 1/10 the values of the exposure rate given in Figure 7. The difference in the true crater volume for a quarrying detonation as opposed to a cratering detonation has been ignored in order to provide conservative estimates of the quarry exposure rate.

Reentry Time to the Crater and Lip Area

Reentry to the crater and lip area for construction activities will be determined by an acceptable level of the exposure rate. Standards have been established for the maximum dose that occupational workers can receive. These standards are given in Table IV.

TABLE IV

Recommended Maximum Permissible Radiation Doses (12)

	<u>Occupational Worker Dose</u> (rem)
Whole body radiation dose in 13 weeks	3
Whole body radiation dose in 1 year	5

If the dose received by personnel in the crater and lip area is due only to the external gamma radiation field, then the exposure rate should not exceed 2.5 mR/hr for a 40-hour work week over a one-year period. This is equivalent to a dose of 5 rem in one year. The time necessary for the exposure rate to decrease to 2.5 mR/hr as a function of yield is given in Figure 8. This figure will provide the project planner with a conservative estimate of the time of reentry for construction activities.

SUMMARY AND CONCLUSIONS

The mathematical model to predict the crater and lip exposure rate is based on calculating the exposure rate above an infinite slab source with a uniform source density. This configuration was shown to be applicable in the crater and lip area. The source has been divided into two groups: (1) the radionuclides from neutron activation, and (2) the fission products. The model has been applied to several past nuclear cratering events and a normalization factor found which depends on the event's scaled depth of burst. The time dependence of the exposure rate was determined by considering only radioactive decay. Finally, conservative estimates of the exposure rate as a function of time after the detonation were given for five nuclear explosive yields.

The calculated exposure rate for the SCHOONER event, fitted to the experimental values of the exposure rate, certainly demonstrates that the model has the capability to predict accurately. Documentation of the exposure rate in and around future nuclear craters will provide a means of testing this model and should increase the model's reliability.

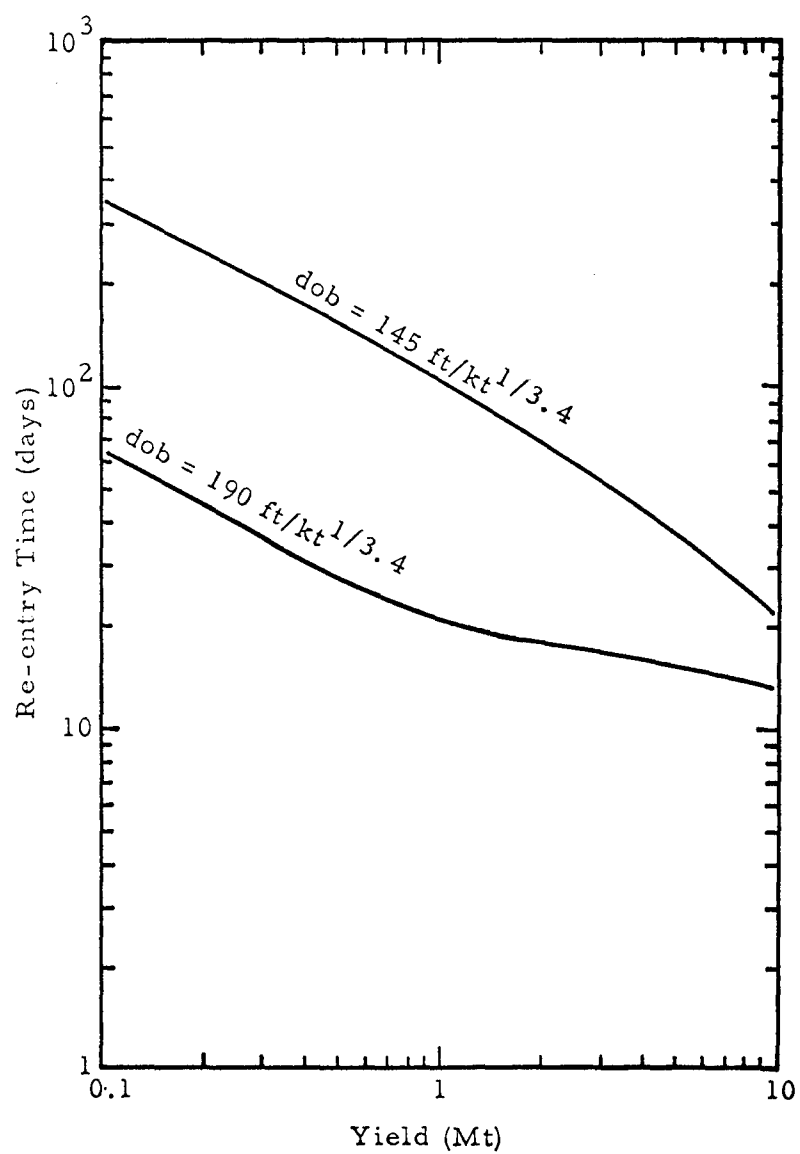


Figure 8. Reentry time as function of yield and scaled depth of burst.

An important aspect of the model is that it can be used for craters produced with any nuclear device. Only predetonation estimates of the radio-nuclides produced by the detonated device are required. However, since an approximation was made for the exposure rate from fission products, the model should predict more accurately as the ratio of the fission yield to the total yield of a device decreases.

The scaled depth of burst of an event is the most important factor in determining what the resulting exposure rate will be. Estimates show that for large yield Plowshare cratering events, at a constant scaled depth of burst, that the exposure rate will decrease with increasing yield.

REFERENCES

1. Day, W. C.; Predicted Dose Rates Within the Nuclear Crater and Lip Area, U. S. Army Engineer Nuclear Cratering Group, Livermore, Rept. NCG/TM 67-1 (1967).
2. Tami, T. M., Day, W. C.; Predicted Exposure Rates Within the Nuclear Crater and Lip Area; U. S. Army Engineer Nuclear Cratering Group, Livermore, Rept. NCG/TM 69-7 (1969).
3. Koranda, J. J., Martin, J. R., and Wikkerink, R. W.; Leaching of Radio-nuclides at SEDAN Crater; Lawrence Radiation Laboratory, Livermore, Rept. UCRL-70630; March, 1968.
4. Rockwell, T.; Reactor Shielding Design Manual; (D. VanNostrand Company, Inc., Princeton, New Jersey, 1956) 1st ed.
5. Blizard, E. P., Abbott, L. S.; Reactor Handbook, Volume III, Part B, Shielding; (Interscience Publishers, New York, 1962) 2nd ed.
6. Hughes, B. C.; Nuclear Construction Engineering Technology; U. S. Army Engineer Nuclear Cratering Group, Livermore, Rept. 2, September 1968.
7. Evans, R. D.; The Atomic Nucleus; (McGraw-Hill, Inc., New York, 1955).
8. Fleming, E. H., Jr.; The Fission Product Decay Chains; Lawrence Radiation Laboratory, Livermore, California, Rept. UCRL-50243, Vol I, II, and III; March 1967.
9. Crocker, G. R., et. al.; Some Factors for the Calculation of Infinite-Plane Exposure Rates from Gamma Radiation; (U. S. Naval Radiological Defense Laboratory, San Francisco) Health Physics, Vol 12; (1966).
10. Gibson, T. A.; private communication.
11. AEC Classification Bulletin WNP-11.
12. "Report of ICRP Committee II on Permissible Dose for Internal Radiation (1959) with Bibliography for Biological, Mathematical and Physical Data," Health Phys. 3 (1960).

RADIOACTIVITY III

REDUCTION OF RADIOACTIVITY PRODUCED BY NUCLEAR EXPLOSIVES*

Richard M. Lessler
Lawrence Radiation Laboratory, University of California
Livermore, California 94550

Four main sources contribute to the radioactivity produced by a nuclear explosive:

1. Fission products from the nuclear explosive,
2. Fusion products from the nuclear explosive,
3. Induced radioactivity in the nuclear explosive,
4. Induced radioactivity in the environment.

This paper will summarize some of the work done at the Lawrence Radiation Laboratory at Livermore to reduce the radioactivity from these sources to levels acceptable for peaceful applications.

Although it is theoretically possible to have no radioactivity produced by nuclear explosives, this goal has not been achieved.

The fusion of a deuteron reacting with a triton to give a neutron and helium nucleus plus energy does not lead to the production of radionuclides if the neutron is moderated and then captured by a nucleus which goes to a stable product (such as B^{10} going to Li^7). However, in present thermonuclear explosives, radioactive products result from a number of processes: (1) Energy from a fission "trigger" is needed to initiate the fusion reaction, leaving a residue of fission products; (2) there is also some residual tritium; (3) side reactions occur in the thermonuclear fuel leading to radioactive products; and (4) some neutrons are captured by other materials present before they are moderated and absorbed by the shielding materials, and some escape through the shield into the environment. Careful study of these processes leads to modifications in the design of Plowshare nuclear explosives that minimize the production of radionuclides by these various mechanisms. Typical modifications are enumerated as follows:

First, the yield of the fission trigger is being reduced. Second, materials in and around the explosive which produce radioactive products of particular biological objectionability can be replaced by materials which give less undesirable products. Thus, plastics and vanadium can be substituted for much of the steel and aluminum in structural materials. Much of the tungsten radioactivity recently observed in nuclear debris can be reduced by selective substitution of lead. These changes will result in a large reduction in the amounts of radioactive sodium, manganese, iron, and tungsten isotopes formed by the detonation of the redesigned explosive.

Third, shielding materials such as polyethylene (CH_2) and boric acid (H_3BO_3) can be used. These materials moderate and/or absorb neutrons so

*This work was performed under the auspices of the United States Atomic Energy Commission.

that the external activation of surrounding materials and soil can be reduced significantly.

This shielding around the device effectively moderates high-energy neutrons so that the ratio of high-energy neutron reaction products from $(n,2n)$, (n,p) and (n,α) reactions to low-energy neutron reaction products from (n,γ) reactions may markedly decrease relative to what would be observed if no shielding were present.

When these precautions are taken the amount of radioactivity produced is not only less, but the radioactive products can be very different from those observed in past nuclear weapons testing.

Different Plowshare applications will require different types of explosives. For excavation applications, one will want an explosive that is very low in fission products and induced activities. For contained underground applications, where the nuclear debris is predominantly trapped in insoluble form, one could use an all-fission explosive. This explosive would yield only small amounts of diffusable gases, such as tritium, which would result in some product contamination. However, if boron is used to absorb neutrons, thereby reducing the quantity of tritium formed in the surroundings as from the Li in the soil, the neutrons should be moderated to reduce their energy below the (n,T) threshold before they are captured to prevent formation of tritium from boron.

When a fission explosive is detonated, about 2×10^{23} neutrons are emitted from the fissioning material for each kiloton of fission yield. Similarly, fusion neutrons are produced by both D-D and D-T reactions. For example, about 1.5×10^{24} D-T reactions will produce a kiloton of energy, and each D-T reaction produces a neutron. The value of 1.5×10^{24} neutrons per kiloton of fusion will be used in this paper to illustrate the relatively small fraction of neutrons produced that are captured in the surroundings. The number of neutrons that will be produced per kt of fusion in a Plowshare explosive is equal to or greater than 1.5×10^{24} due to other fusion reactions that may occur. Since the number of neutrons emitted per kiloton of fission yield is only a small fraction of the number of neutrons formed per kiloton of fusion yield, the neutron activation problem could be much more severe for the "cleaner" nuclear explosive without neutron shielding. A related problem is the formation of residual tritium by neutron capture by Li in the explosive. On the order of 2 g (20,000 Ci) of residual tritium per kiloton of fusion yield can result from this process.

As noted previously, to decrease the radioactivity of fission-fusion explosive, not only must the yield of the fission "trigger" be minimized, but also the neutrons available to produce radioactive products must be reduced.

Monte Carlo calculations have been made to determine the number and energy spectra of the neutrons escaping from untested 100-kt, 1/2-Mt, and 1-Mt thermonuclear Plowshare explosives. These calculations were done on the CDC-6600, using a static, two-dimensional Monte Carlo Code, called SORS. The geometry from a hydrodynamic neutronics calculation of the exploding device at the time most neutrons are escaping into the surroundings, together with a corresponding energy spectrum of those neutrons which have escaped from the neutron-producing region, are used as input to the Monte Carlo calculation. This neutron source term is then followed by the Monte Carlo Code until the neutrons have all been absorbed by materials outside the neutron-producing region. Neutron fluxes as a function of energy and region are obtained from this calculation. In addition, this information can be used as input to a simple "bookkeeping" code called ACTIVE which calculates the radioactive isotopes produced in a region of given composition by a particular time-integrated flux with a known energy distribution.

Several assumptions are made in these calculations. Only one geometry is used to approximate a dynamic situation. This geometry must be approximated by a combination of spheres, slabs, cylinders, or cones. The estimated temperature of each material region is taken as the minimum energy which neutrons in the region of interest will be allowed to attain. When the neutrons are greatly attenuated by shielding, Monte Carlo calculations performed with a reasonable sample size of neutrons give results with large statistical deviations.

These calculations cannot be more accurate than the cross sections employed in the codes. A small inaccuracy in a cross section can make a significant difference in calculational results—especially where large amounts of shielding are involved. Factor-of-two uncertainties are not unlikely. In the case of high-neutron flux regions, where second-order reactions occur, order-of-magnitude errors are possible, since the cross sections for these second-order reactions can only be estimated. Internal induced radioactivity in the nuclear explosives due to multiple reactions is calculated by the ACT code.

For soil activation (a region of low neutron flux), the elemental composition must be measured to at least the accuracy one wishes to obtain from the calculation. Thus, if the sodium abundance is in error by a factor of 2, then the calculation will be off by this amount. The calculation also assumes that the soil is homogeneous in composition.

When all these sources of error are taken into account, the absolute value given for the total number of neutrons escaping should be considered accurate only to about a factor of 3.

The results of the Monte Carlo portion of these calculations are shown in the following tables. Table 1 shows the initial number of neutrons in moles (6×10^{23} neutrons) escaping into the soil as a function of energy for 100-kt, 1/2-Mt, and 1-Mt explosives. These explosives were assumed to have been emplaced in a 60-in.-diam hole, with all available space between the explosive and the soil filled with boric acid. The calculations on the 100-kt explosive showed 1.7×10^{21} neutrons per kiloton escaped into the soil, but only 4.4×10^{20} neutrons per kiloton were captured by the soil. These numbers were obtained by running the problem twice; once with soil, and once with the soil replaced by a vacuum. Evidently, many of the neutrons escaping into the soil are reflected back to the H_3BO_3 where they are subsequently captured.

Table 1. Neutron spectra escaping into soil (in moles) (1 mole = 6×10^{23} neutrons).

E (MeV)	100 kt	1/2 Mt	1 Mt
11-15	0.019	0.17	0.80
7.5-11	0.032	0.22	0.87
4.7-7.5	0.034	0.19	0.88
2.5-4.7	0.029	0.27	0.35
1.2-2.5	0.040	0.17	0.56
0.43-1.2	0.018	0.23	0.34
0.034-0.43	0.028	0.12	0.38
0.003-0.034	0.017	0.050	1.17
<0.003	0.066	0.36	0.70
Totals	0.283	1.78	6.05
Total per kt	0.0028	0.0036	0.0061
Total captured in soil	0.073	0.425	1.57

Based on an initial neutron production of about 1.5×10^{24} neutrons/kt, only about 1 in 1000 neutrons escaped into the soil, and only 1 in 3400 was captured in the soil.

The calculations on the 1-Mt explosive showed 3.6×10^{21} neutrons/kt escaped into the soil, and 9.4×10^{20} neutrons/kt were captured by the soil. A larger number of neutrons per kiloton escaped from the 1-Mt explosive than from the 100-kt one, since the larger dimensions of the 1-Mt explosive resulted in less space being available for the boric acid because both explosives were assumed to be emplaced in a 60-in.-diam hole. The lowest energy group of neutrons are mostly in the range of 1 to 3 keV, as the shielding has been heated to this temperature.

The number of neutrons escaping are orders of magnitude lower than those currently being used in the unclassified literature primarily because these neutrons have been moderated and absorbed by large amounts of shielding. This is the first time the neutron spectrum escaping a Plowshare excavation explosive has been disclosed. With this information, a more realistic evaluation may be made of the amount of external neutron-induced radioactivity produced by Plowshare excavation explosives. For example, the radioactivity produced in the soil by a Plowshare explosive can be estimated by combining the spectra given in Table 1 with the results of the neutron-induced soil activation calculations given by Lessler and Guy^{1,2} for surface and contained explosions respectively.

Table 2 summarizes the results given in Table 1. One sees that only about one-fourth the neutrons reaching the soil are captured in it, and that only 1 neutron in 1600-3400 assumed to be produced is actually captured in the soil.

Table 2. Neutron history.

	100 kt	1/2 Mt	1 Mt
Total neutrons escaping into the soil (moles)	0.283	1.78	6.05
Total neutrons captured in the soil (moles)	0.073	0.425	1.57
Albedo $\left(\frac{\text{neutrons captured}}{\text{neutrons escaping}}\right)$	0.26	0.24	0.26
Initial neutrons produced (2.5 moles/kt)	250	1250	2500
Attenuation factor $\left(\frac{\text{initial neutrons}}{\text{neutrons captured}}\right)$	3400	2900	1600

Tables 3 and 4 give an indication of the time and distance at which neutrons escaping from these three explosives are captured. Our calculations indicate that these times and distances are similar for all three explosives, so only one set of numbers is given. From this, it is seen that about 1% of the neutrons are still uncaptured at 1 msec, and that about one-sixth of them have penetrated through more than 64 cm of soil.

¹R. M. Lessler and F. W. Guy, Gamma Dose Rates and Integrated Doses from Neutron-Induced Residual Radioactivity in Soil, UCRL-12339, Lawrence Radiation Laboratory, Livermore, March 1965.

²R. M. Lessler and F. W. Guy, Neutron-Induced Activity in Earth and Sea Water from Buried and Surface Neutron Sources, UCRL-12407, Lawrence Radiation Laboratory, Livermore, April 1965.

Table 3. Distribution of capture times of neutrons in soil.

< 10 μ sec	40%
10-100 μ sec	40%
0.1-1 msec	20%
>1 msec	1%

Table 4. Distribution of distance in soil at which neutrons are captured.

0-24 cm	50%
24-64 cm	33%
>64 cm	17%

Other calculations using a Moving Boundary Monte Carlo Code show that, within limits, about a factor-of-10 reduction in soil activation is obtained for every 15 cm of boric acid shielding. Thus, shielding factors larger than 3400 can be obtained if more shielding is used. These shielding calculations were done for a dynamic geometry, where the radii and temperatures of the regions are changing with time. Thus, these results are better than those obtained using the static Monte Carlo Code. The main disadvantage is that the dynamic code is only one-dimensional and cannot calculate a non-spherical emplacement environment. The effect of allowing the shielding to expand and heat up is that fewer neutrons are absorbed by the shielding than in the static case. This correction varies with the conditions assumed, and for the problems we have run, it can make a difference of as much as a factor of 2 in the results. In these calculations, Mn^{56} and Na^{24} gave the largest contribution to the soil-induced radioactivity at early times.

When examining the problem of using nuclear explosives for excavation, one should not look primarily at the amount of radioactivity made by current explosives, as they do not represent future excavation explosives. Instead, a set of safety criteria should be established and then the explosive should be designed to satisfy or surpass these criteria before it is used for excavation. In other words even before the best possible explosive is used, it should satisfy all health and safety criteria.

The radioactivity per unit yield from Plowshare explosives has been decreasing as changes have been made in the explosive and its emplacement environment. For example, in 1967, the AEC issued a planning statement giving the estimated amount of radioactivity released to the environment by future nuclear cratering explosives. There have been some changes in our estimates of anticipated radionuclide release; consequently, the 1967 release estimates should be used only for order-of-magnitude planning. Also, the assumptions used as they relate to emplacement techniques, neutron shielding, scavenging, and significant nuclides released to the environment do not necessarily represent the current state of the art.

Since it is the only Plowshare Model released, I will use it to illustrate the decrease of radioactivity that might be expected from future nuclear explosives. According to this model, it is possible for planning purposes to use a total radioactivity release in cloud and fallout from a 100-kt explosive which is equivalent to the radiation from 60 tons of fission. In contrast, back in 1962 the radioactivity in the fallout field from the "clean" 100-kt Sedan explosive was equivalent to that produced by 2000 tons of fission. A comparison of

these activation products is given in Table 5. Thus considerable progress has been made in reducing radioactivity from a nuclear explosive, and it is anticipated that continuing progress will be made in the future.

Table 5. Gamma exposure from fallout (in equivalent tons of fission integrated from H+1 hr to infinity).

	Sedan	1967 Planning model
Total fission products	1400	20
Activation products		
Na ²⁴	20	12
Mn ⁵⁴	—	1
Mn ⁵⁶	3	2
Fe ⁵⁹	—	0.1
W ¹⁸⁷	500	5
Pb ²⁰³	—	20
Others (Be ⁷ , Sc ⁴⁴ , Sc ⁴⁶ , Y ⁸⁸ , Rh ¹⁰² , W ¹⁸⁸)	102	small
TOTAL	~2000	~60

Note: Nuclei such as P³², Ca⁴⁵, Fe⁵⁵, W¹⁸⁵, have no γ radiation, so give no significant γ dose. In the 1967 model, they show 0.1, 0.01, 0.04, and 6 kilocuries, respectively.

ACKNOWLEDGMENTS

The author wishes to thank Dr. Howard Tewes and Richard Pond for discussions on this paper and W. Edward Alley and Richard Gell for programming and executing the calculations presented in this paper. Thanks are also due to Robert Andrews and Roger Moore for furnishing the input used in these calculations.

RADIOACTIVE CONTAMINATION OF COPPER PRODUCED USING
NUCLEAR EXPLOSIVES

D. J. Crouse
W. D. Arnold
F. J. Hurst

ABSTRACT

Laboratory tests simulating the processing of copper ore after fracturing with nuclear explosives indicate that only very small fractions of the radioactive fission products will be dissolved on leaching with dilute sulfuric acid. Tritium (as tritiated water) will be by far the dominant radionuclide in the circulating leach liquor, assuming use of a fusion device.

Only ^{106}Ru appears of significant importance with respect to contamination of the cement copper. It is rejected effectively in electrolytic purification and, therefore, the final copper product should be very low in radiocontamination and not hazardous to the customer. The activity level may be high enough, however, to make the copper unsuitable for some specific uses. If necessary, solvent extraction can be used as an alternative to the cementation process to reduce the radioactivity of the copper products.

The tritium in the circulating liquor and the ^{106}Ru in the cement copper are potential hazards at the plant site and must be given consideration in designing and operating the facility. However since the activity levels will be low, the protection necessary to ensure safety of the operating personnel should be neither difficult nor costly to provide.

Research sponsored by the U. S. Atomic Energy Commission under contract with the Union Carbide Corporation.

Introduction

Fracturing copper-bearing ore bodies with nuclear explosives and leaching the copper from the ore in place has been proposed as a potential low-cost method for recovering copper from deep deposits that cannot be mined economically in the usual manner. The technical and economical feasibility of this proposal is being investigated by the Division of Peaceful Nuclear Explosives of the AEC in cooperation with associated contractors and with the Kennecott Copper Corporation. An experiment (Project Sloop) has been designed to field test the application.¹ The Chemical Technology Division of the Oak Ridge National Laboratory is cooperating in this program by studying potential problems that might arise from the presence of radioactive contaminants in the processing cycle.

The nuclear shot will produce an approximately cylindrical chimney of broken ore several hundred feet high and containing several million tons of ore rubble. The proposed process flowsheet involves percolating dilute sulfuric acid down through the broken ore to dissolve the copper, collection of the leach liquor at the bottom of the chimney and pumping it to the surface, recovery of a copper concentrate from the solution by cementation on scrap iron, and recycling of the copper-barren solution to leaching after fortifying it with acid. The cement copper concentrate from this operation will be purified by electrolysis before being marketed as copper metal.

We have grouped the potential problems arising from the presence of radionuclides in the system under three main categories, first, evaluation of radiation hazards to operating personnel in the processing complex, second, possible radiocontamination of the copper product which, of course, could affect its marketability, and third, potential radiation hazards to the general public associated with process release or underground migration of radionuclides to the off-site environment. The last, which is outside the scope of the present studies, is not of apparent significance with respect to Project Sloop but would require careful study and evaluation prior to extensive development of a particular ore body.

Assessment of these problems requires some knowledge of the quantities of the different radionuclides that would be present, their leachability under expected flowsheet conditions, and their behavior in certain processing steps, for example, the copper cementation step. The quantities of each of the fission products and tritium produced by a detonation of a given yield depends, of course, on the type of device used. Fig. 1 gives a rough estimate of the amounts of the more important fission products and tritium as a function of time following an arbitrarily assumed 50-kiloton shot in which 90% of the energy is derived from fusion and 10% from plutonium fission. The estimated tritium production of 25,000 curies per kiloton of fusion is the approximate mid-point of the 7,000 to 50,000 curies per kiloton range specified by Miskel.² Isotopes such as ^{140}Ba , ^{147}Nd , and ^{143}Pr , with half-lives in the range of 11 to 14 days are present in large amounts shortly after the detonation but would essentially disappear prior to the start of leaching at the expected 250 to 300 days. Other isotopes such as ^{103}Ru , ^{91}Y , and $^{95}\text{Zr-Nb}$ with half-lives of intermediate range, would be present in significant amounts at the start of leaching but would rapidly diminish in importance over the 1-to 2-yr period of leaching. At 300 days, the tritium activity would be more than an order of magnitude higher than the total fission product activities. Choice of an all-fission device for use would, of course, greatly increase the relative importance of the fission products compared to tritium. In addition, radionuclides formed by neutron activation would be present. The quantities of these produced would depend on the composition of the ore and certain conditions of the experiment. We have concluded that, compared to the fission products, the neutron activation products will not be an important

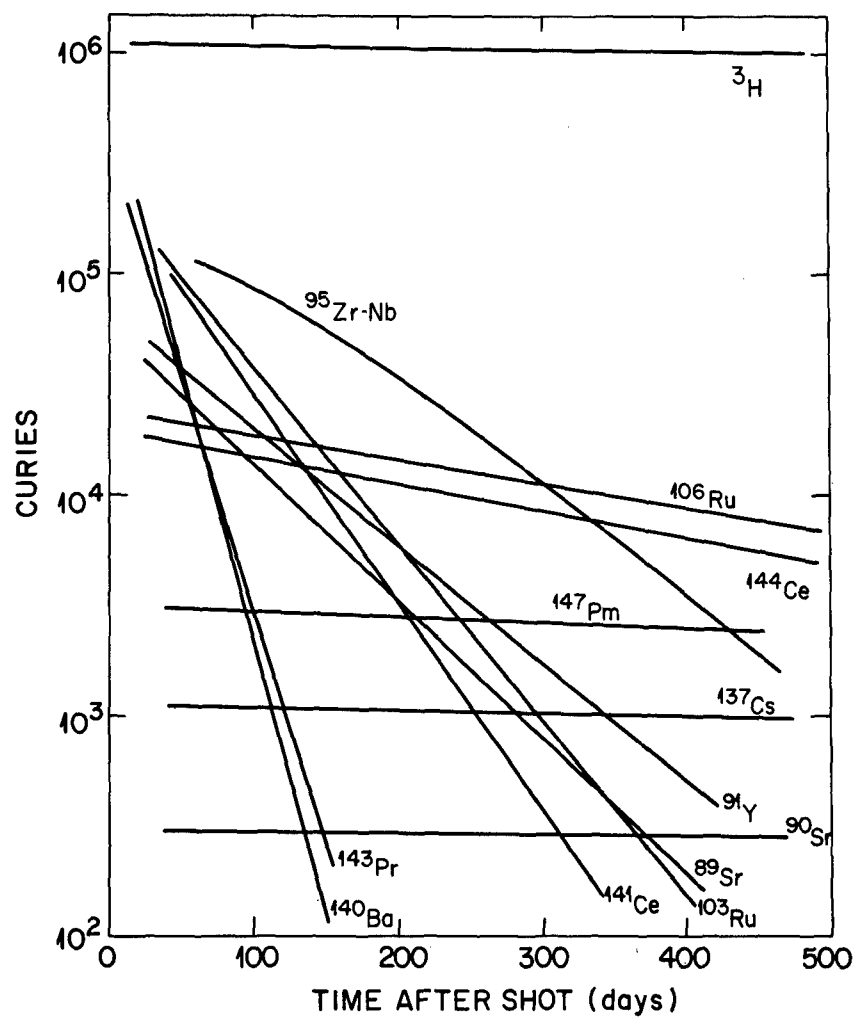


Fig. 1 — Estimated Amounts of Radioactive Fission Products and Tritium Resulting from a Fifty Kiloton Shot (90% fusion--10% Pu fission).

consideration in applying nuclear explosives to copper ore recovery.

It is known from earlier Flowshare experience that, with contained underground nuclear explosions, most of the fission products and induced radionuclides are trapped fairly efficiently in the melted rock that accumulates at the bottom of the ore chimney. It is also known that this fused material is not very leachable. However, appreciable amounts of certain fission products, for example ^{90}Sr and ^{137}Cs , which have gaseous precursors, and ^{106}Ru and ^{125}Sb , which form volatile compounds, move up into the chimney and are deposited on the ore rubble in a more leachable form. The tritium should be present as tritiated water and, therefore, in a completely soluble form.

Because copper ore that has been broken by nuclear explosives is not available for leaching tests, we have studied the behavior of the radionuclides in the processing cycle by dosing copper ore with soluble isotopes, with radioactive debris from one of the Nevada test site shots, and with reactor-irradiated copper ore.

Leaching of Radioactive Debris

Under expected flowsheet leaching conditions (pH 2-3), less than 2% of any of the long-lived radionuclides were dissolved from a sample of puddle glass (melted rock) from a Nevada test site shot (Fig. 2). However about 50% of the ^{90}Sr , 20% of the ^{144}Ce , and 5-10% of the ^{106}Ru were dissolved in this pH range from ore rubble that was sampled in the vicinity of the melted rock. These debris samples were about 3.5 yrs old at the time of leaching and thus did not contain detectable amounts of some radioisotopes, e.g. $^{95}\text{Zr-Nb}$, that would be of importance at the time of processing (Table I).

Similar leaching tests were made with ore rubble from a different test shot. In this case the sample was 2 yrs old and was taken about 200 feet above the shot point. The gross gamma activity of the sample was about 10^4 counts $\text{min}^{-1}\text{g}^{-1}$, due principally to ^{106}Ru and ^{137}Cs (Table I). Samples of the debris were leached for 6 days at room temperature with simulated copper ore leach liquors. Sulfuric acid was added during the leach to maintain the pH approximately constant at levels of 1.0, 2.0, or 3.6. About 50% of the ^{90}Sr and 30-35% of the ^{106}Ru were dissolved in the pH range of 1 to 2 (Fig. 3). The amounts of ^{125}Sb and ^{137}Cs that were leached decreased from about 12% at pH 1 to 2-4% at pH 2. In the test at pH 3.6, the gross gamma activity of the leach solution was only 1% of that obtained at pH 1 and too low to analyze for the individual radionuclides.

Adsorption of Radionuclides by Copper Ore

The ion exchange properties of the copper ore would be highly important in regulating the quantities of certain radionuclides that would be dissolved and carried to the surface processing operation. Batch distribution tests with soluble radionuclides showed that some are adsorbed very strongly by the ore from acid leach solutions (Fig. 4). In these tests, soluble radioisotopes were added to a copper ore leach liquor that was adjusted to various pH levels and the solutions were then contacted with copper ore from the Safford, Arizona deposit of the Kennecott Copper Corporation. Certain of the fission products such as ^{137}Cs and $^{95}\text{Zr-Nb}$ were adsorbed strongly, with distribution coefficients (K_D) values of 50 or higher. Strontium was adsorbed much less, although still significantly. Even distribution coefficients considerably lower than 1 would result in appreciable ion-exchange retention of the radionuclide by the ore because of the relatively large ore to solution ratio (possibly 10 to 1) that would prevail in the system. In other adsorption tests with ore from the Safford deposit and with solution prepared by leaching radioactive debris, cesium adsorption was strong and ruthenium and strontium

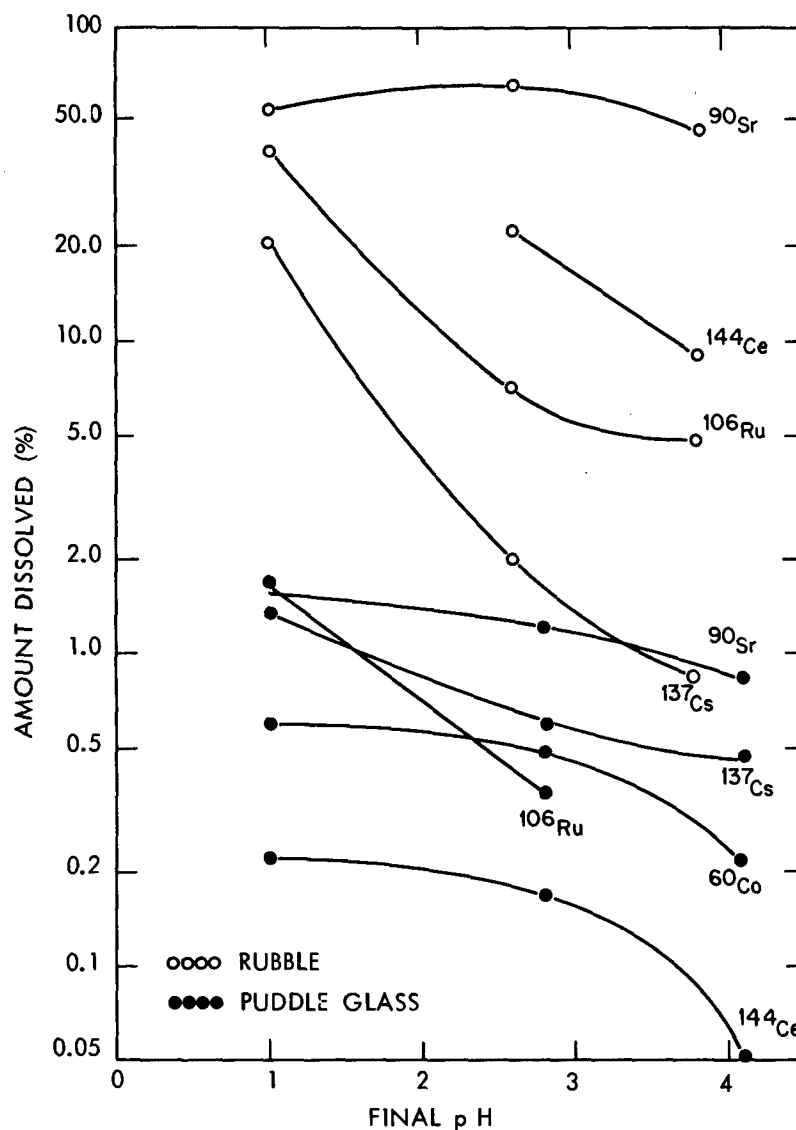


Fig. 2 — Leaching of Test Shot Debris with Sulfuric Acid. Procedure: 10-g samples of minus 4-mesh debris (test shot No. 1, analyses in Table I) leached for two days at room temperature with 20 ml dilute H_2SO_4 ; acid added during the leach to maintain the pH approximately constant at 1.0, 2.5, or 4. The supernate was analyzed for the various radionuclides.

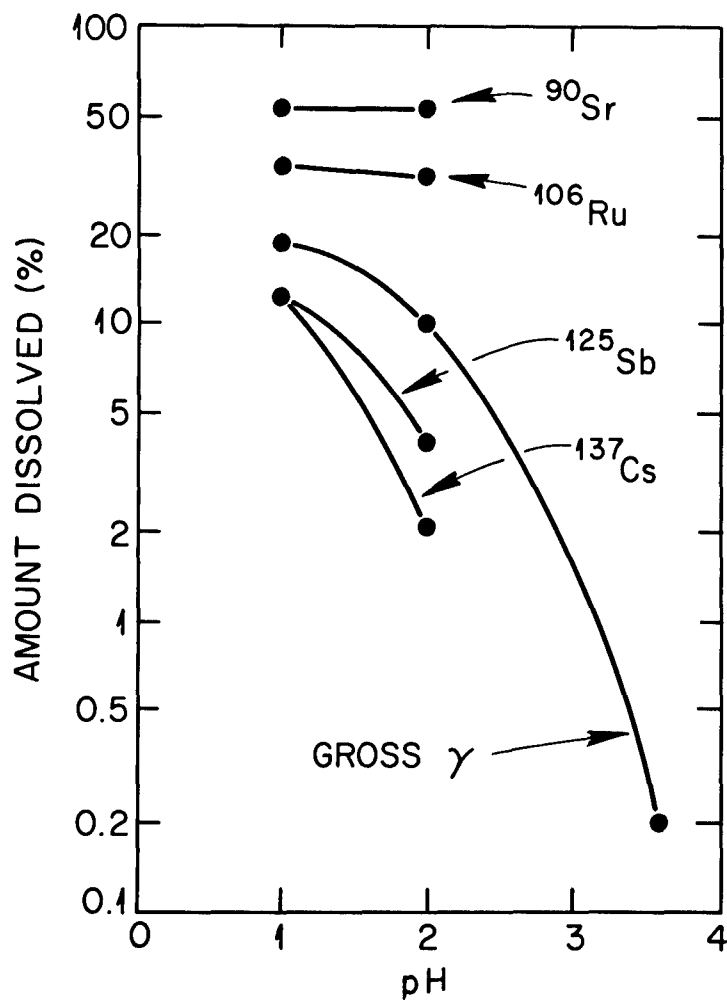


Fig. 3 — Leaching of Test Shot Debris. Procedure: 100-g samples of test shot debris (Nevada test shot No. 2) leached 6 days with 200 ml of synthetic copper ore leach liquor (2 g Cu^{2+} , 1 g Fe^{3+} , and 3 g Fe^{2+} per liter as sulfates). Sulfuric acid added during the leach to maintain the pH approximately constant at 1.0, 2.0, or 3.6. Amounts dissolved are based on the original debris and the supernate analyses.

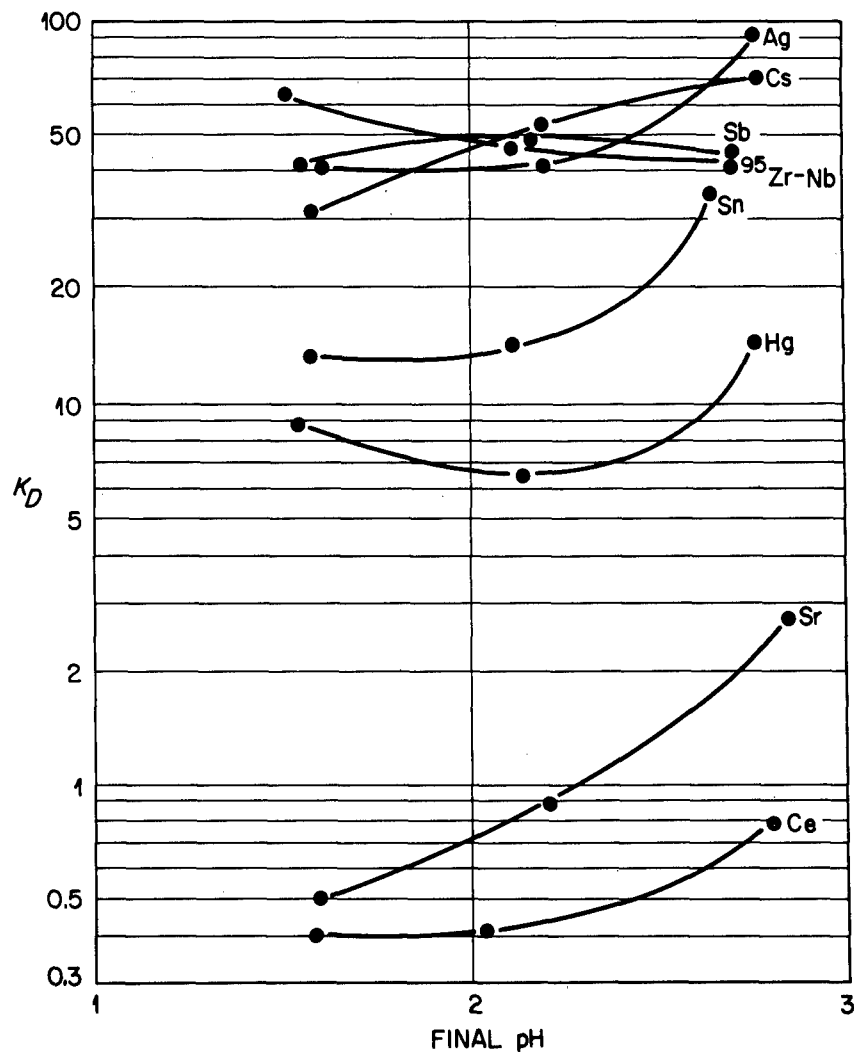


Fig. 4 — Adsorption of Radionuclides by Safford Copper Ore. Procedure: 5 ml of Safford copper ore leach liquor (adjusted to different pH levels and spiked with the appropriate radioisotope) contacted 16 hr with 1 g of -20 mesh ore tailings; amount adsorbed calculated on basis of head solution and supernate analyses. Less than 4% ($K_D < 0.25$) of ruthenium, iron, europium, scandium, yttrium, chromium, cobalt, zinc, and cadmium were adsorbed in the pH range of 1.5 to 2.8.

Table I. Test Shot Debris Samples

Radionuclide	Concentration (dis min ⁻¹ g ⁻¹ x 10 ⁴)		
	Test Shot No. 1		Test Shot No. 2
	Puddle Glass	Rubble	Rubble ^a
¹³⁷ Cs	1.4	2.2	2.1
¹⁴⁴ Ce	2.2	0.04	<0.03
⁹⁰ Sr	4.1	0.09	0.2
¹⁰⁶ Ru	2.0	0.12	1.4
⁶⁰ Co	3.7	0.01	b
¹²⁵ Sb	b	b	0.4

^aSampled 200 feet above the shot point.

^bNot detected.

adsorption coefficients were similar to those obtained by adding radioisotopes in solution form to the liquor. Antimony, however, was not strongly adsorbed as before, suggesting that the chemical form of the antimony in solution was different for the two experiments. In an actual leaching operation, the chimney of broken-ore would function as an ion-exchange column several hundred feet high. Radionuclides dissolved from the ore in the bottom of the chimney in the early phases of the leaching cycle would tend to be adsorbed on the ore as the leach solution was recycled through the ore column. This would limit the build-up in concentrations of radionuclides in the leach liquor to levels far below those that would be predicted on the basis of simple batch leach test results such as those shown in Figs. 1 and 2.

Cementation Tests

Cementation tests were run with a simulated copper ore leach liquor that was dosed with radioisotopes to determine which of these might contaminate the cement copper. As expected, the more noble metals such as silver cemented almost quantitatively with the copper (Fig. 5). Also, about 25 to 40% of the tin, antimony, and ⁹⁵Zr-Nb and 15% of the ¹⁰⁶Ru were removed with 95% of the copper from the solution over the 90-min cementation period. No cementation of ¹³⁴Cs, ⁵¹Cr, ⁴⁶Sc, ⁵⁹Fe, ¹⁴⁴Ce, ¹⁵²⁻¹⁵⁴Eu, ⁸⁶Sr, ⁶⁵Zn, or ⁶⁰Co was detected.

Because ¹²⁵Sb has exhibited anomalous behavior in some tests, additional cementation tests were made with this isotope under a variety of conditions. The fraction of ¹²⁵Sb that cemented with the copper in 60-min tracer tests decreased from about 40% to 15% when the initial activity of ¹²⁵Sb in the liquor was decreased from 10⁵ to 10³ dis min⁻¹ ml⁻¹. With a liquor derived from leaching radioactive debris and in which the ¹²⁵Sb activity was only 70 dis min⁻¹ ml⁻¹, no cementation of ¹²⁵Sb was detected (Table II). As in the tracer tests, there was no significant cementation of ⁹⁰Sr or ¹³⁷Cs. The amounts of ¹⁰⁶Ru cemented were 14% at pH 1 and 8% at pH 2, results that are in the approximate range of 10 to 25% usually obtained with ¹⁰⁶Ru.

Table II. Cementation Tests

Leach Liquors: Synthetic copper ore leach liquor after leaching of rubble from test shot No. 2.

Procedure: 100 ml samples of liquor (initial pH 1.0 or 2.0)^a contacted with 0.35 g sheet iron (detinned cans) for 1 hr.

Radionuclide	Liquor from pH 1.0 Leach Test		Liquor from pH 2.0 Leach Test	
	Conc. in Liquor (dis min ⁻¹ ml ⁻¹)	Amount Cemented (%)	Conc. in Liquor (dis min ⁻¹ ml ⁻¹)	Amount Cemented (%)
⁹⁰ Sr	460	<2	420	<2
¹⁰⁶ Ru	2130	14	2040	8
¹²⁵ Sb	215	<2	70	<2
¹³⁷ Cs	1160	<2	210	<2
Gross γ	890 ^b	7.5	490 ^b	7.5

^a60 to 70% of the copper cemented in these tests.

^bGross γ activity measured in counts min⁻¹ ml⁻¹.

In studies of variables affecting ¹⁰⁶Ru contamination of cement copper, little change in the amount of contamination occurred as the pH or iron concentration of the liquor or the rate of agitation during cementation were changed. Although some of these variables affected the rate of copper cementation, there was usually a corresponding change in the rate of ¹⁰⁶Ru cementation so that the ¹⁰⁶Ru concentration in the copper product was relatively constant. As expected, the ruthenium contamination of the cement copper increased when the initial concentration of ruthenium in the leach liquor was increased while maintaining the copper concentration constant, but the effect was not linear. In the range of ¹⁰⁶Ru concentrations studied (1000 to 40,000 counts min⁻¹ ml⁻¹, equivalent to about 0.001 to 0.05 μ C/ml), increasing the initial ¹⁰⁶Ru concentration by a factor of 10 increased the ¹⁰⁶Ru concentration in the cement copper by a factor of about 20 (Fig. 6). About 95% of the copper was cemented in all tests, whereas the amount of ¹⁰⁶Ru cemented increased from 7.5% for the liquor containing the lowest concentration of ¹⁰⁶Ru to 33% for the highest. We have estimated that the ¹⁰⁶Ru in the circulating leach liquor would probably not exceed 0.001 μ C/ml which is about the lowest of the concentrations examined in this experiment.

Although certain potential radioactive activation products such as the silver and mercury isotopes cement quantitatively with copper, they should be present in extremely small amounts and that present, even if in leachable form, would be held tenaciously by the ore through ion-exchange mechanisms. Fission products such as ⁹⁵Zr-Nb and tin isotopes, both of which cement appreciably with the copper, are also adsorbed efficiently by the ore and, therefore, should not be present in significant amounts in the circulating leach liquor.

After considering the quantities of each of the various radionuclides that we would expect to be present in the leach liquor and their behavior in the cementation process, we conclude that ¹⁰⁶Ru is the only radioisotope

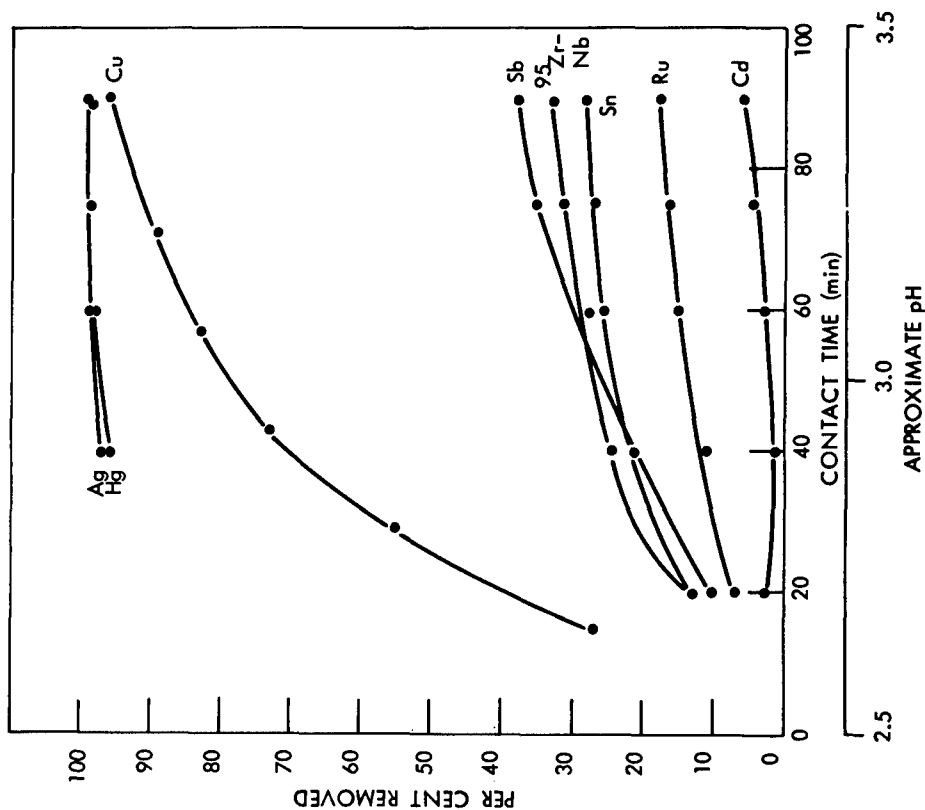


Fig. 5 — Contamination of Copper Cementation Product. Procedure: 200 ml copper leach liquor (2 g Cu/liter, pH 2.5) contacted with 0.7 g detinned cans for 90 min. Amount of radioisotope removed from solution was calculated on basis of head solution and supernate analyses. Less than 2% of ^{134}Cs , ^{51}Cr , ^{46}Sc , ^{59}Fe , ^{144}Ce , $^{152-154}\text{Eu}$, ^{85}Sr , ^{65}Zn , and ^{60}Co were removed with the copper.

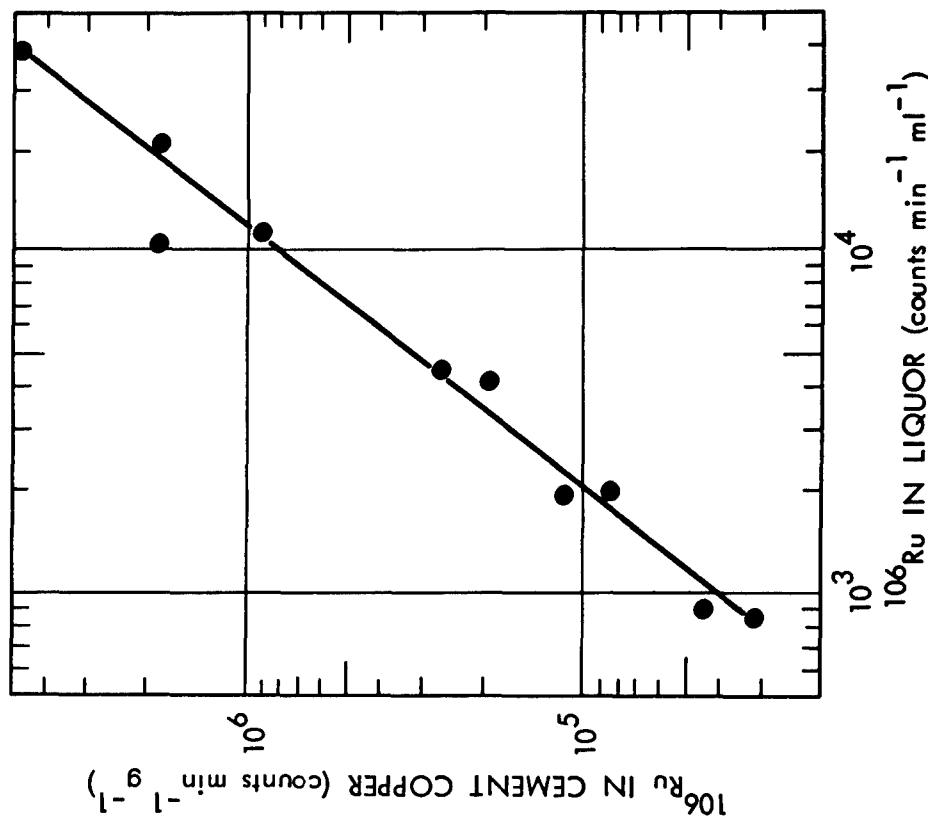


Fig. 6 — Effect of Initial ^{106}Ru Concentration on ^{106}Ru Contamination of Cement Copper. Solutions: Synthetic leach liquor (pH 2.0) containing 0.15 M SO_4^{2-} and in grams per liter, 2.0 Cu^{2+} , 1.0 Fe^{3+} , 3.0 Fe^{2+} and 0.5 NaCl ; spiked with 1000 to 40,000 counts $\text{min}^{-1} \text{ml}^{-1}$ of ^{106}Ru . Procedure: 200 ml of solution stirred at $\sim 25^\circ\text{C}$ with 0.7 g detinned cans for 45 min.

that appears important with respect to radiocontamination of the cement copper. Attempts were made to remove ^{106}Ru from the leach liquor with various types of ion exchange and other adsorbents but none of these were very effective. Most of the ^{106}Ru can be removed from the recycle liquor by partial neutralization with lime to a pH of about 4.5, and this method could be used to decrease, but not eliminate, the ^{106}Ru contamination. Fortunately, as described later, the ^{106}Ru is efficiently separated from the copper during electrolytic purification.

Column Leaching Tests

Several test runs were made in which a 4-in.-diam column of copper ore (from the Safford, Arizona deposit) was leached with sulfuric acid by the open drainage--trickle leach method. In the first run, 2000 g of rubble from Nevada test shot No. 1 was interdispersed with 2500 g of ore in the column. The dissolved copper was recovered from the column effluent by cementation on detinned cans and the depleted solution was fortified with sulfuric acid and recycled to the column. Initially, the solution pumped to the column was adjusted to pH 1.2. The rubble contained considerable acid-consuming material since over 5 liters of solution were passed through the column before the effluent pH dropped below 7. The pH of the incoming solution was adjusted to higher and higher values (in the range of 1.2 to 1.8) as the run progressed so that the effluent pH never was lower than 2.0. Throughout the run, the gamma activity of the leach solution was less than 20% of the background activity. The ore was leached until about 80% of the copper was recovered.

Fifteen batch cementations were made during the test. As before, ^{106}Ru was the only radionuclide found in the products. The combined products contained about 8% of the total ^{106}Ru added to the column; another 1% was in solution at the end of the test. The ruthenium concentration of the copper products increased fairly steadily with each cementation through the first eight (Fig. 7). The ^{106}Ru concentration of the column effluent was in the range of 25 to 45 $\text{dis min}^{-1} \text{ ml}^{-1}$ which was very close to the limit of detection. About 10-20% of the dissolved ruthenium cemented with copper in each cementation. Following cementations eight through eleven, the barren effluent was adjusted with lime to pH 4 to 5 to remove ruthenium before being acidified and recycled to the column. The effect of this treatment is evident in the decreased ruthenium concentration of subsequent products. When the lime treatment was discontinued, the ruthenium contamination again increased steadily. About 3 g of $\text{Ca}(\text{OH})_2$ per liter of solution was required for adjustment to pH 4 and 9 g for adjustment to pH 5.

In order to better follow the paths of some of the more important fission product elements in the extraction cycle, another column run was made in which the ore, before being added to the column, was wetted with a small volume of solution containing about 2×10^7 counts min^{-1} each of ^{144}Ce , ^{134}Cs , ^{106}Ru , ^{85}Sr , and $^{95}\text{Zr-Nb}$. Appreciable fractions (10 to 30%) of the ^{85}Sr , ^{144}Ce , and ^{106}Ru were leached from the ore column. However, almost none of the ^{134}Cs and $^{95}\text{Zr-Nb}$ were found in the column effluent owing to their strong adsorption by the ore. The initial portions of effluent contained principally ^{90}Sr but its concentration slowly decreased as the solution was recycled through the column. The concentrations of ^{106}Ru and ^{144}Ce in the effluent, however, increased slowly as the effluent pH decreased to about 2 and then did not change greatly thereafter. Near the end of the run about 54% of the total activity of the effluent was due to ^{144}Ce , 42% to ^{106}Ru , and 3% to ^{85}Sr . Only ^{106}Ru was found in the cement copper in appreciable amounts. The ^{106}Ru contamination of the copper increased with each successive product batch.

Still another column leaching run was made with 4000 g of ore that had been blended with 2.4 grams of reactor-irradiated ore (cooled 52 days,

Table III. Analysis of Irradiated Safford Copper Ore
(Cooled 52 days)

Isotope	Half-Life	Concentration ($\mu\text{c/g}$)	Calculated Conc. after 300 days of cooling ($\mu\text{c/g}$)
^{46}Sc	84 d	109 ± 3.2	14.1
^{54}Mn	314 d	11.9 ± 1.4	6.9
^{59}Fe	45 d	77.8 ± 6.4	1.7
^{60}Co	5.3 y	13.5 ± 1.3	12.3
^{65}Zn	245 d	11.0 ± 6.3	5.5
^{75}Se	120 d	6.9 ± 0.5	1.6
^{95}Zr	65 d	1.4 ± 0.6	0.1

analysis in Table III). Only small fractions (1 to 10%) of the radioisotopes present were dissolved during leaching and < 3% of that dissolved reported to the copper cementation product. It appears that, in copper processing, the neutron activation products will be a much less important consideration than the fission products.

Removal of Tritium - To determine the manner in which tritium (which should be present as tritiated water) would be washed from the ore column, the ore was wetted with a small volume of tritiated water and heated at 85°C for 1 week in a closed system to allow equilibration of the tritiated water with any bound water in the ore. About 80% of the tritium initially present on the ore column was removed in the first 0.4 bed volume of effluent (Fig. 8). This test suggests that the tritium concentration in the circulating liquor, and correspondingly the tritium hazard to the plant workers, could be appreciably decreased by discarding rather than recycling some of the initial effluent which would contain most of the tritium but little or no copper.

Electrolytic Purification of Copper

The cement copper will probably be melted to produce impure copper metal in the form of a consumable anode and converted to pure copper metal by electrolysis. Alternatively, the cement copper could be purified by dissolving it in sulfuric acid and recovering copper metal from the solution by electro-winning. Small-scale tests demonstrated that both procedures give efficient separation of copper from ^{106}Ru .

In determining the separation achieved by the melting-electrolysis route, cement copper that was contaminated with 0.7 μc of ^{106}Ru per gram of copper was melted in a graphite crucible at 1300-1350°C in the presence of CaO , SiO_2 , and carbon. This level of ^{106}Ru contamination is probably at least 1 or 2 orders of magnitude higher than would be expected in process practice. The molten copper was cooled, separated from the slag, and then remelted and cast into two anodes. No separation of ^{106}Ru from the copper was obtained in the melting process. The two copper anodes were electrolyzed in consecutive runs in the same electrolyte at a current density of about 13 amps/ft² and a cell voltage of 0.2 volt. The ^{106}Ru concentration in the electrolyte increased at

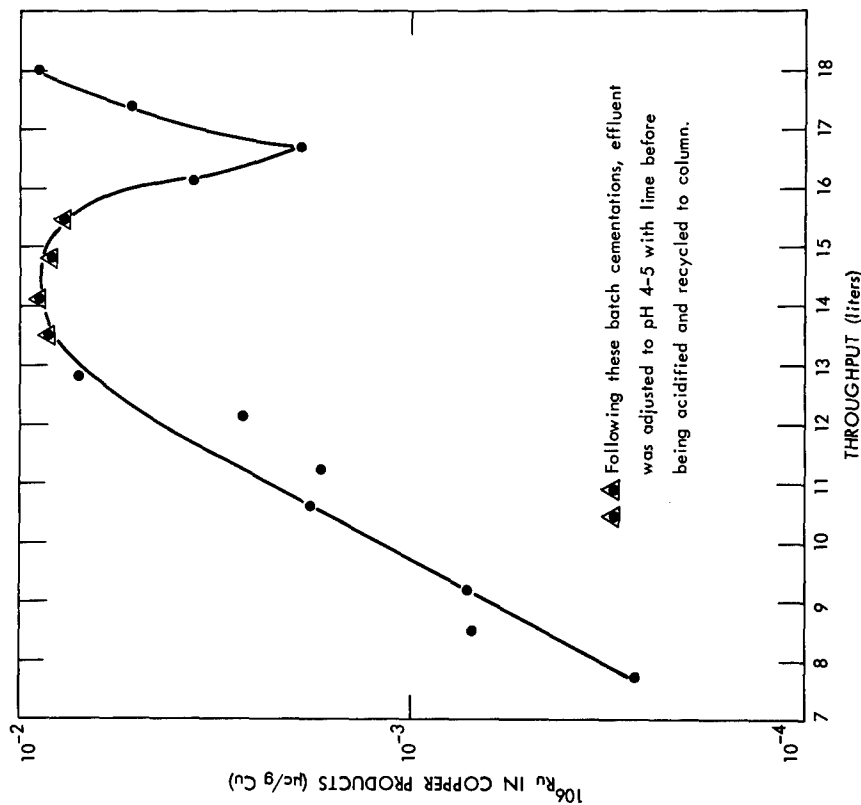


Fig. 7 — Ruthenium Contamination of Cement Copper Products. Procedure: 2500 g of minus 0.5-in. Safford copper ore and 2000 g of test shot rubble mixed and placed in 4-in.-diam column; leached at 0.5 ml/min with recycle liquor; copper recovered from column effluent by cementation on detinned cans; barren cementation solution acidified with H_2SO_4 to pH 1.2-1.8 and recycled to column.

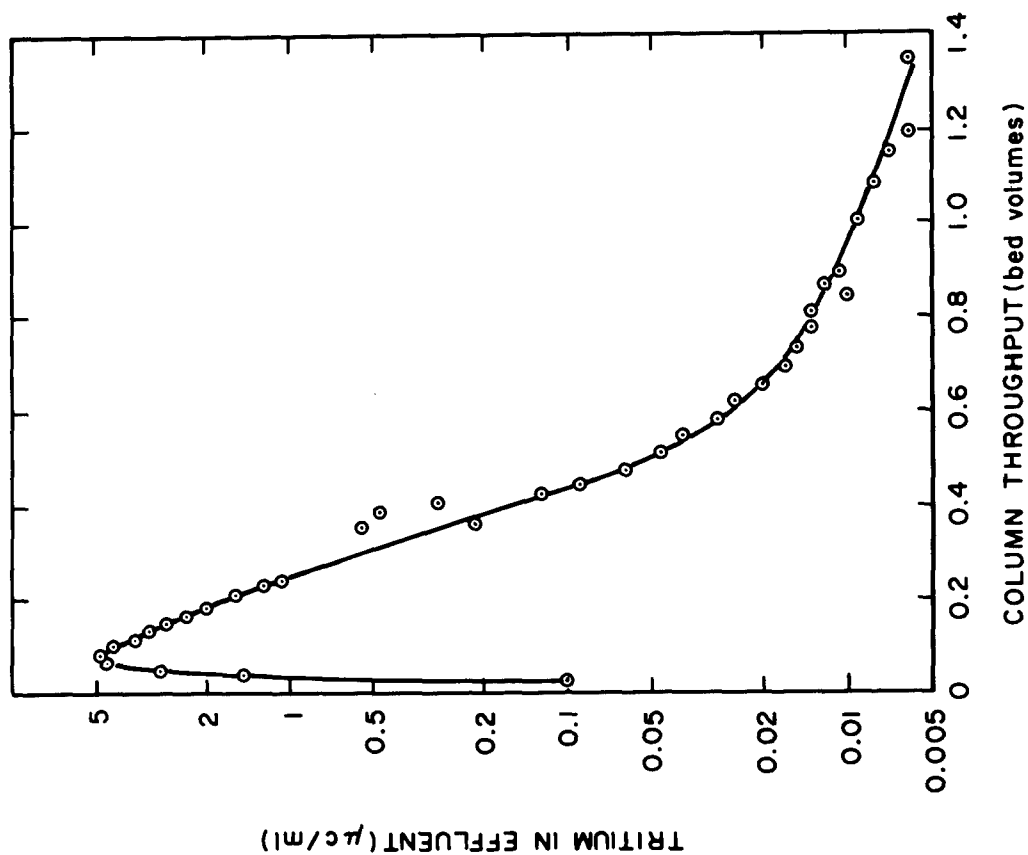


Fig. 8 — Tritium Elution from an Ore Column. Procedure: 300 g of Safford ore and 3 ml H_2O containing 180 μc of tritiated water were heated at 85°C in a stoppered 1-in.-diam column for one week. The ore was then leached with dilute H_2SO_4 (pH 1.8) at a flow rate of 0.12 ml/min.

a constant rate throughout the run, indicating that the ^{106}Ru was uniformly dispersed (alloyed with the copper) in the anodes (Fig. 9). About two-thirds of the ^{106}Ru released from the anode was found in the electrolyte and one-third was found in the "anode mud" that settled to the bottom of the electrolytic cell. Only 1-2% was found in the cathode copper.

Some provision in the process would be required to handle the radioactive anode mud. Also, it would be necessary to prevent excessive build-up of ^{106}Ru in the cell electrolyte since the solution would eventually become a radiation hazard and also since there was some increase in the ^{106}Ru contamination of the cement copper as the ^{106}Ru concentration in the electrolyte increased. The ^{106}Ru was removed from simulated $\text{CuSO}_4\text{--H}_2\text{SO}_4$ electrolyte solutions by bubbling ozonized air through the solution at 90°C . In a continuous run, increasing the solution residence time in the reactor from 5 min to 15 min increased the amount of ^{106}Ru volatilized from 47 to 72%. The ^{106}Ru was removed from the gas stream on activated carbon which had a saturation loading capacity of more than 2 millicuries of ^{106}Ru per gram. These tests suggest that the ^{106}Ru concentration in the cell electrolyte could be controlled at a tolerable level by continuously withdrawing cell electrolyte at a low rate (possibly 10% of the electrolyte inventory per day) for a ruthenium removal treatment and then returning the partially decontaminated solution to the cell.

Solvent Extraction of Copper

Recovery of copper from the leach liquor by solvent extraction with LLX-64 is a potential alternative to the cementation process. The extracted copper can be stripped from the solvent with sulfuric acid and fed directly to an electrowinning operation. This solvent extraction process³ is currently used in the copper industry.

Of eleven radionuclides tested, only $^{95}\text{Zr-Nb}$, ^{59}Fe , and ^{110}Ag had extraction coefficients higher than 0.01 in extractions from simulated copper ore leach liquors (pH range of 1.5 to 2.5) with varsol containing 100 g of LLX-64 per liter (Fig. 10). Copper extraction coefficients were 10 or higher in all tests. Ruthenium-106, the most troublesome radiocontaminant in the cementation process, had extraction coefficients of less than 0.005 over this pH range, as did ^{134}Cs , ^{85}Sr , ^{60}Co , ^{46}Sc , ^{66}Zn , and ^{144}Ce . Further study of the extraction of $^{95}\text{Zr-Nb}$, ^{59}Fe , and ^{110}Ag showed extractions of the first two to be time dependent (Fig. 11). Essentially all of the ^{59}Fe but only about 30% of the ^{110}Ag and 20% of the $^{95}\text{Zr-Nb}$ were stripped from the extracts with 2 M H_2SO_4 in a 10-min contact at a phase ratio of 1/1.

Fortunately, it is anticipated that the concentrations of $^{95}\text{Zr-Nb}$, ^{59}Fe , and ^{110}Ag in the leach liquors obtained by in-situ leaching of nuclear-broken ore will be very low. Solvent extraction of copper with LLX-64, therefore, should produce a copper product solution essentially free of radionuclides.

Hazards to Operating Personnel

Assuming the amounts of radionuclides present in the system as shown in Fig. 1, a rough estimate was made of the concentrations of each that might be present in the circulating leach liquor (Table IV). The estimates of the fractions of each radionuclide that would be dissolved are based on our leaching data and general Plowshare experience that fission product elements not having gaseous precursors are trapped efficiently in the melted rock in insoluble form. Consideration was also given to the fact that a large portion of the soluble fraction of some isotopes, e.g. ^{137}Cs , would be held firmly by the ore through ion exchange mechanisms. These calculations indicate that the expected activity levels would be sufficiently low that shielding of the

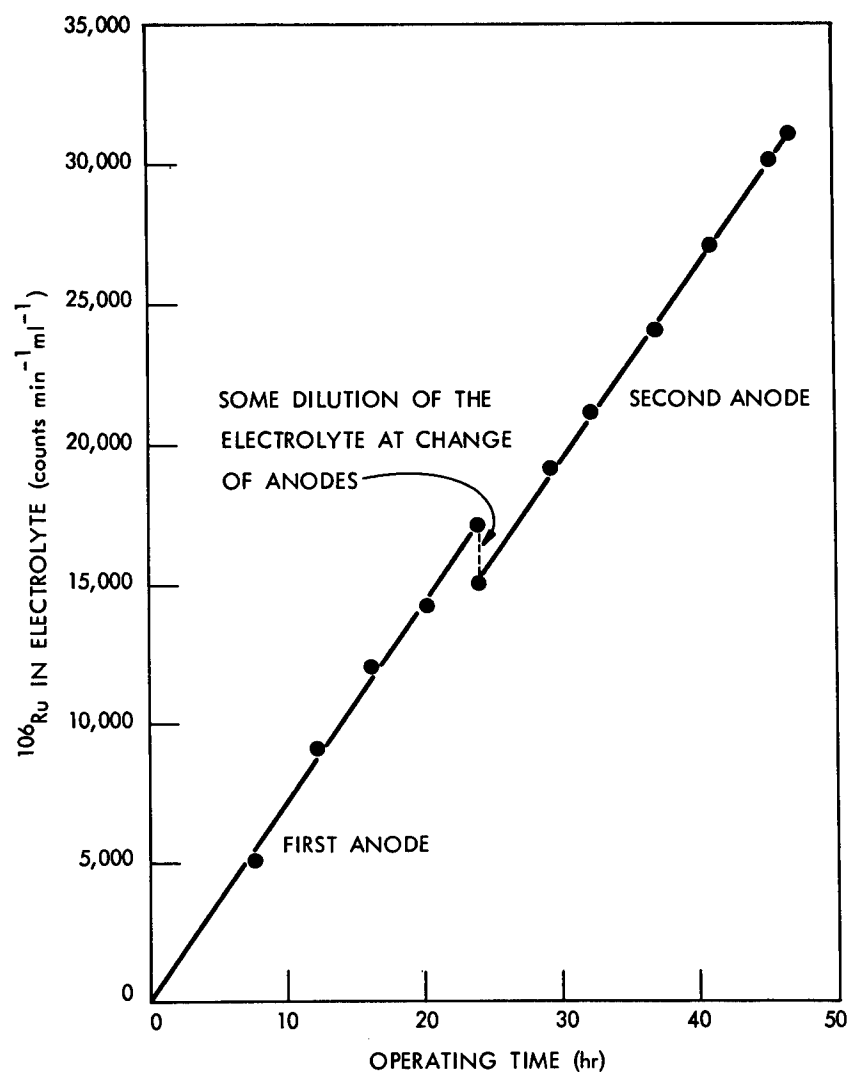


Fig. 9 — Accumulation of ^{106}Ru in the Cell Electrolyte. Anodes containing 8.2×10^5 counts of ^{106}Ru per gram were electrolyzed in a solution containing 45 g of Cu and 200 g of H_2SO_4 per liter.

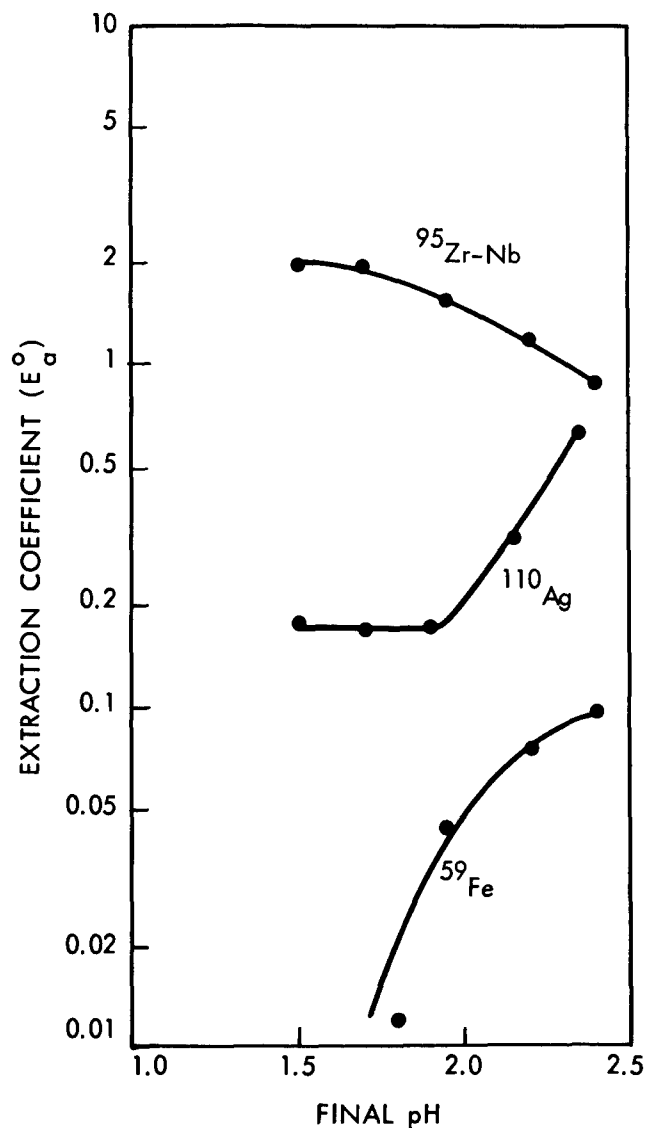


Fig. 10 — Effect of pH on Extraction of Radioactive Contaminants with LIX-64. Organic phase: 10^W/v% LIX-64 in varsol. Aqueous phase: synthetic copper ore leach liquor containing 0.1 M SO_4^{2-} and, in g/liter, 0.2 Cu, 1.0 Fe^{3+} , 3.0 Fe^{2+} , and 0.5 NaCl; traced with the radioactive contaminants. Contact: 5 min at phase ratio of 1/1. Radionuclides that had extraction coefficients less than 0.005 were ^{106}Ru , ^{134}Cs , ^{85}Sr , ^{144}Ce , ^{60}Co , ^{65}Zn , ^{46}Sc and ^3H .

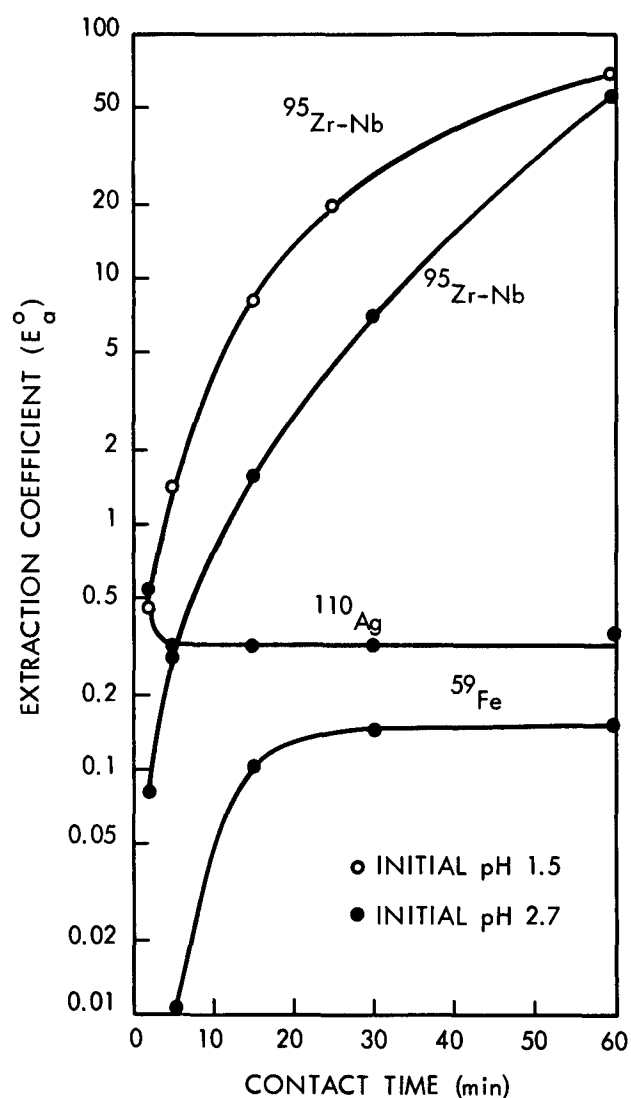


Fig. 11 — Effect of Contact Time on Extraction of Radionuclides with LIX-64. Organic phase: $10^w/v\%$ LIX-64 in varsol. Aqueous phase: synthetic copper ore leach liquor traced with the radionuclides. Phase ratio: 1/1. Temp.: $\sim 23^\circ\text{C}$. Negligible amounts of ^{59}Fe were extracted from the pH 1.5 solution in 1 hr; extractions of ^{110}Ag from this solution were not measured.

Table IV. Estimated Concentrations of Radionuclides in Circulating Leach Liquor

- Assumptions: 1) No migration of radionuclides from the site
 2) Leaching at 8 months after the shot
 3) Uniform distribution of the dissolved radionuclides in 45 million gallons of circulating leach liquor.

Isotope	Assumed % Dissolution	Concentration in Leach Liquor ($\mu\text{c/ml}$)
$^{95}\text{Zr-Nb}$	0.01 - 1	1×10^{-5} - 1×10^{-3}
^{144}Ce	0.01 - 1	6×10^{-6} - 6×10^{-4}
^{141}Ce	0.1 - 2	9×10^{-6} - 2×10^{-4}
^{106}Ru	0.1 - 2	7×10^{-5} - 1×10^{-3}
^{103}Ru	0.1 - 2	1×10^{-5} - 2×10^{-4}
^{137}Cs	0.1 - 2	7×10^{-6} - 1×10^{-4}
^{90}Sr	0.5 - 5	1×10^{-5} - 1×10^{-4}
^{89}Sr	0.5 - 5	6×10^{-5} - 6×10^{-4}
^{91}Y	0.5 - 5	1×10^{-4} - 1×10^{-3}
^{147}Pm	0.001- 0.1	1×10^{-7} - 1×10^{-5}
^3H	100	6

processing equipment to prevent excessive exposure of personnel to radiation would not be required. With the exception of tritium, the potential hazards due to radioactivity appear to be of the same order as those in the uranium ore processing industry.

Since tritium would be in volatile form, it requires special consideration. It does not appear to be a serious hazard except possibly in certain underground operations such as the servicing of pumps that pump leach liquor to the surface. For these operations special precautions could be taken to prevent excessive exposure. The processing tanks should be covered to prevent excessive exposure of the personnel to process vapors. As mentioned previously, the tritium concentration is expected to be high in the initial leach effluent and the tritium hazard could be appreciably lessened by discarding rather than recycling this solution. The ^{90}Sr concentration in the solution is expected to be at its highest value in the initial leach effluent and discard of this solution would have the additional advantage of decreasing the ^{90}Sr concentration in the circulating liquor.

The expected level of contamination of the cement copper with ^{106}Ru is highly uncertain primarily because it is not known what fraction of the ^{106}Ru will be present in the chimney in a leachable form. Our column leaching tests indicate that the copper to ^{106}Ru ratio in the leach liquor will be considerably higher in the initial stages of the leaching cycle (high pH effluent) than in the later stages and so the ^{106}Ru concentration in the cement copper should increase as leaching proceeds. However, this will be counteracted to some extent by loss of some leach solution from the system and by decay of the ^{106}Ru . Considering all of these factors, we estimate that the ^{106}Ru content of

the cement copper will probably not exceed 0.05 μc per gram at any time over the period of processing and, for most of the copper recovered, will be considerably lower than this value. Although not high, this level of contamination dictates that care be taken in design of the facility to minimize contact of the operating personnel with the cement copper.

To obtain a rough idea of the maximum γ -radiation dose that operating personnel conceivably could receive in handling the cement copper, calculations were made of the dose that would be received in a room in which impure copper anodes (cast from the cement copper) were stored prior to electrolytic purification. It was assumed that the worker would be situated in a corridor between copper anodes stacked to a height of 10 ft. The estimated γ -radiation dose rates under these conditions are 0.2 and 10 mr/hr, respectively, for assumed concentrations of ^{106}Ru in the copper of 0.001 and 0.05 μc per gram. The higher dose rate would require that the worker's time in this area be limited to about 10 hr per week in order not to exceed acceptable dose limits. As described previously, a ^{106}Ru concentration of 0.05 $\mu\text{c/g}$ is expected to be the highest level of contamination that we estimate will occur and the concentration should usually be much lower than this value. In any case, with proper monitoring, it should not be difficult to control exposures at acceptable levels.

Estimates of the β -dose to the hands that would occur on contact of bare hands with the copper anodes are 4 and 200 mr/hr, respectively, for assumed ^{106}Ru concentrations in the copper of 0.001 and 0.05 μc per gram. Use of gloves, which would certainly be required if hand contact with the anodes was needed at all, would greatly reduce the dose rates. With proper equipment design and operational procedures, control of β -exposures to acceptable limits should not be difficult.

In summary, expected potential radiation hazards to operating personnel are significant enough that the facility would have to be considered a radiochemical processing facility and, therefore, be licensed and monitored. It appears, however, that the protection necessary to ensure safety of the operating personnel should be neither difficult nor costly to provide.

Copper Product Suitability

Because of the expected efficient separation of copper from ^{106}Ru during electrolytic purification, the radioactivity of the final copper product should be very low and not hazardous to the customer. The activity level, however, could be sufficiently high so as possibly to make the copper unsuitable for certain specialized uses, e.g., in radiometric counting instruments, in the photographic industry, for copper cooking equipment. If necessary, solvent extraction of the copper could be used as an alternative to the cementation process to reduce the radioactivity of the copper product.

Acknowledgements

The authors thank W. B. Howerton and J. S. Shveima for technical assistance and LRL personnel for providing samples of radioactive test shot debris. Wet chemical analyses and some of the radiochemical analyses were provided by the ORNL Analytical Chemistry Division.

References

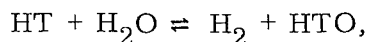
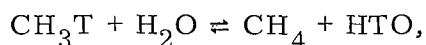
1. Sloop, edited by Peter F. Zimmer and M. A. Lekas, PNE-1300 (June 1, 1967).
2. J. A. Miskel, Characteristics of Radioactivity Produced by Nuclear Explosives, Third Plowshare Symposium, TID-7695 (April, 1964).
3. H. J. McGarr, N. H. Berlin, and W. F. A. Stolk, Engineering and Mining Journal, 170, No. 12, pp 66-67 (December, 1969).

POSSIBLE TECHNIQUES FOR DECONTAMINATION
OF NATURAL GAS FROM GAS WELLS STIMULATED
BY A NUCLEAR EXPLOSION

John A. Wethington, Jr.*
Lawrence Radiation Laboratory, University of California
Livermore, California 94550

ABSTRACT

Decontamination of the products from gas wells stimulated by nuclear explosions requires the removal of T, present as HT, CH₃T, C₂H₅T, etc., and ⁸⁵Kr from the production stream. Flaring of large volumes of gas from the Gasbuggy well led to the replacement of radioactive cavity gas with inactive formation gas, but this would not be a satisfactory production procedure because it releases T and ⁸⁵Kr into the atmosphere and wastes large amounts of product gas. Exchange reactions appear to offer promise for removing the tritium. For example, water or steam flowing countercurrent to tritiated gas in the presence of a suitable catalyst can participate in the exchange reactions



resulting in the transfer of T from gas into water. Other possibilities for utilizing exchange reactions include exchange of the gas with ethylene glycol used in the gas dryer, with silicate rocks introduced into the gas stream, or with a countercurrent stream of NH₃ or H₂S. As another approach, use of the contaminated gas for the manufacture of ammonia synthesis gas has potential for removal of both T and ⁸⁵Kr.

INTRODUCTION

Radiochemical data on gas obtained from the Gasbuggy well after nuclear stimulation have been compiled by Smith¹; these data show that the only significant radioactive contamination results from T and ⁸⁵Kr. The former is present mainly as HT and CH₃T with lesser amounts of C₂H₅T and C₃H₇T. Flaring of the well has produced significant decreases in the radioactivity level of the gases, but this procedure is undesirable on a production scale since it releases radioactivity into the biosphere, wastes large quantities of marketable gas, and interrupts the normal production in the distribution system. Better methods of decontaminating the gas are needed.

The quantities of gas involved and the economic structure of the industry seem to require that any chemical or physical process used for decontamination have a large throughput and employ inexpensive or reusable process materials. These requirements suggest using some combination of the isotope effect, exchange reactions, and/or gas-liquid extraction processes. This report examines some possible decontamination techniques and outlines a proposed program of studies aimed at developing a satisfactory production procedure.

*Permanent address: University of Florida, Gainesville, Florida 32601.

TRITIUM REMOVAL

The Isotope Effect

Equilibrium

Mass differences affect the energy of molecules, and for the hydrogen isotopes, these energy differences are large; consequently, the distribution of hydrogen isotopes among several molecular species at equilibrium is far from random. Isotopes of heavier elements, on the other hand, tend to be randomly distributed among the various possible molecular species. Representative values are shown in Table I.

Table I. Equilibrium distribution of selected isotopes, illustrating large departure from random distribution in isotopes of lighter elements.

Reaction	(K/K') ^a at 298.1°K
HT + H ₂ O ⇌ H ₂ + HTO	6.194
HD + H ₂ O ⇌ H ₂ + HDO	3.703
HCl + DI ⇌ DCI + HI	1.527
¹³ CO ₂ + ¹² CO ₃ ⇌ ¹² CO ₂ + ¹³ CO ₃	1.012
¹²⁷ I ¹²⁹ I + ¹²⁷ I O ₃ ⁻ ⇌ ¹²⁷ I ₂ + ¹²⁹ I O ₃ ⁻	1.002

^aK is the true equilibrium constant calculated from Urey's² summary of partition functions, and K' is the equilibrium constant from random distribution of isotopes.

Kinetics

Isotopic molecules also undergo chemical transformation at different rates, and Bigeleisen³ has estimated from statistical rate theory the maximum isotope effect on rate constants. These results, summarized in Table II, show clearly that separation of the hydrogen isotopes by differences in reaction rate is highly favored over such separation methods for heavier molecules; consequently a separation can be accomplished by using equilibrium values, kinetic effects, or a combination of the two.

Table II. Ratio of specific rate constants (k₁/k₂) at 25°C for selected isotope pairs (abstracted from Ref. 4).

Isotope 1	Isotope 2	k ₁ /k ₂
H	D	18
¹² H	¹³ T	60
¹² C	¹³ C	1.25
¹⁶ O	¹⁸ O	1.19
¹²⁷ I	¹³¹ I	1.02

Exchange Reactions

Mechanism

Why do exchange reactions take place? The mechanism for many such reactions is not known, but in general, the rate-determining step is one of the following:

1. The reversible dissociation of one reactant to give a product that may exchange rapidly with the second reactant.

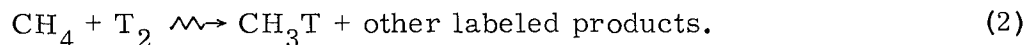
2. The decomposition of a transition state in which one or more electrons may be transferred from one reactant to the other.

3. The decomposition of a transition state in which one or more atoms may be transferred from one reactant to another.

This study is concerned with mechanism 3, illustrated by the exchange between halide ion and halogen, the trihalide ion presumably being the transition state as shown in the reaction



It should be clearly understood that this work is not concerned with the Wilzbach⁵ labeling which is commonly used to label organic compounds with T by means of the following radiation-induced reaction:

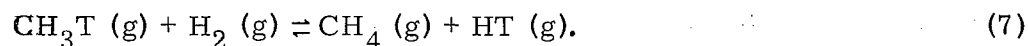
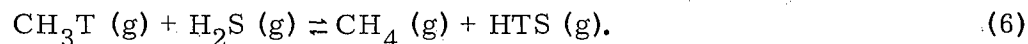


Certainly reaction (2) will take place in addition to the expected exchange reactions, but it will not be considered here.

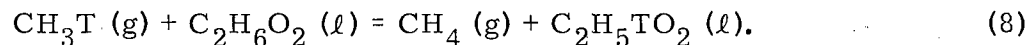
Application to Tritium Removal

Clearly, an exchange reaction, if it will proceed at a reasonable rate, can remove T from the gas produced from a nuclearly stimulated gas well. Data from the Gasbuggy Experiment¹ showed that, during the initial shut-in period, two of the main gaseous components were CH₄ (30-40%) and H₂ (10-20%). The corresponding radioactive species, CH₃T and HT, accounted for the majority of the T contamination. Consequently, subsequent discussions are concerned with these two gases, with the main emphasis placed on CH₃T.

Exchange reactions (3)-(7) below, which involve only common chemicals, are worth considering for gas decontamination. Analogous reactions (except for reaction (7)), where HT replaces CH₃T should also be considered for decontamination. Both sets of reactions must be considered in a thorough decontamination study.



Glycol dryers,⁶ as used in natural gas processing, might be used in decontamination procedures by employing the ethylene glycol as a reactant:



Reactions of a similar nature where the gas stream is passed through a bed of silicate rocks or through rocks containing metal hydroxides might also be employed. These reactions will not be considered further in this paper.

Flow Requirements for Separation

If an exchange reaction proceeds at a reasonable rate, then separation can be accomplished by contacting the flowing gas with a stream of the other component moving in the opposite direction. Consider reaction (3); what water flow would be required?

Let

$A = \mu\text{Ci of CH}_3\text{T per ml of produced gas,}$

$G = \text{gas flow rate, ft}^3/\text{day,}$

$W = \text{water flow rate, ft}^3/\text{day,}$

$(\text{RPG})_g = \text{amount of T in gas, } \mu\text{Ci/cc,}$

$(\text{RPG})_w = \text{amount of T in water, } \mu\text{Ci/cc,}$

where (RPG) denotes Radiation Protection Guide.* Conservation of radioactivity shows that

$$W = \frac{[A - (\text{RPG})_g]G}{(\text{RPG})_w}. \quad (9)$$

The order of magnitude of CH_3T in the gas during the shut-in period was $\sim 15 \mu\text{Ci/ft}^3$ or $\sim 5.3 \times 10^{-4} \mu\text{Ci/cc}$. The required water flow is, of course, a function of the values taken for $(\text{RPG})_g$ and $(\text{RPG})_w$. Since no values have been tabulated for natural gas, $(\text{RPG})_g$ was taken as $(\text{RPG})_a$, the value for air, with T as HTO and no dilution with uncontaminated gas or combustion products. No dilution of the waste water was considered. Results are tabulated in Table III.

Table III. Water flow required for production of 1 million cubic feet gas per day.

Condition of exposure	$(\text{RPG})_g$, $\mu\text{Ci/cc}$	$(\text{RPG})_w$, $\mu\text{Ci/cc}$	Water flow, ft^3/day
168-hr week, general population, gas as HTO	7×10^{-8}	1×10^{-3}	5.3×10^5
40-hr week, occupational, gas as HTO	5×10^{-6}	1×10^{-1}	5.3×10^3

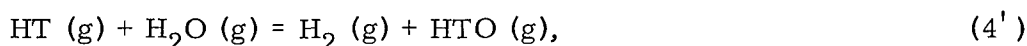
Number of Stages Required

Clearly, the gas can be decontaminated by countercurrent equilibrium between the gas and water, and a logical question is how many stages might be required for extraction of T into H_2O ?

Exchange processes can be considered in terms of the single-stage separation factor, α , defined as the abundance ratio (atoms desired isotope/atoms undesired isotope) in the heads (product) stream divided by the isotope abundance ratio in the tails (waste) stream. The separation factor can be related to the equilibrium constant, K_{eq} , as shown below. If one considers reaction (3), defines T as the "desired" isotope, and replaces activities by molar concentrations, he finds that

$$\alpha(3) = \frac{[\text{HTO}]}{2[\text{H}_2\text{O}]} \bigg/ \frac{[\text{CH}_3\text{T}]}{4[\text{CH}_4]} = 2 K_{\text{eq}}. \quad (10)$$

On the other hand, replacement of CH_3T by HT in reaction (4) gives reaction (4'):



* (RPG) values taken from Standards for Protection Against Radiation, Code of Federal Regulations, Title 10, Chapter 1, Part 20 (U.S. Govt. Printing Office, Washington, D.C.) (Revised Jan. 1, 1969).

and

$$\alpha(4') = K_{eq} . \quad (11)$$

Alpha is then related to but not necessarily equal to K_{eq} .

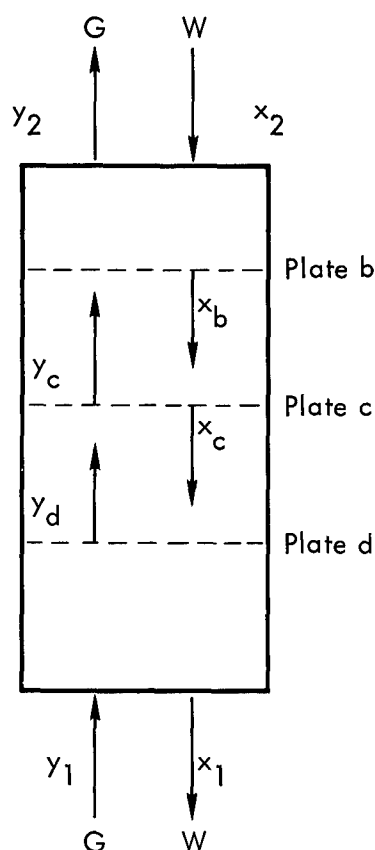
Values of α for many T-containing compounds have been published,⁷ and some appropriate values are listed in Table IV.

Table IV. Single-stage separation factors (α) for selected reactions involving tritium compounds (abstracted from Ref. 7).

Reaction	α
$\text{CH}_3\text{T} + \text{H}_2\text{O} \rightleftharpoons \text{CH}_4 + \text{HTO}$	1.14
$\text{CH}_3\text{T} + \text{NH}_3 \rightleftharpoons \text{CH}_4 + \text{NH}_2\text{T}$	1
$\text{CH}_3\text{T} + \text{H}_2\text{S} \rightleftharpoons \text{CH}_4 + \text{HTS}$	1
$\text{CH}_3\text{T} + \text{H}_2 \rightleftharpoons \text{CH}_4 + \text{HT}$	0.17

Consider the liquid-gas extraction unit shown in Fig. 1 and the cases listed in Table III. It can be shown that m of Fig. 1 and α are related by the formula

$$m = \frac{1.6 \times 10^{-3}}{\alpha} \quad (12)$$



G = volume of CH_4 flowing upward
(cu ft per day per unit area),

y = concentration of desired component
in gas stream at any stage (μCi of
 CH_3T per cu ft),

W = volume of H_2O flowing downward
(cu ft per day per unit area),

x = concentration of desired component in
liquid stream (μCi of HTO per cu ft).

Fig. 1. Symbols and parameters used in column design. (Treatment based on Sherwood and Pigford.⁸)

for this particular reaction and system of units. Substitution of these data into equation (13) shows that only three or four plates are required in the cases considered.

Referring to Fig. 1, one sees that a material balance applied below plate c requires that

$$W(x_1 - x_c) = G(y_1 - y_d),$$

and a linear equilibrium relationship states that at any stage

$$y_n = mx_n.$$

The solution for the required number of plates, N_p , can be expressed as:

$$N_p = \frac{\ln \left[\left(1 - \frac{mG}{W} \right) \left(\frac{y_1 - mx_2}{y_2 - mx_2} \right) + \frac{mG}{W} \right]}{\ln (W/mG)}. \quad (13)$$

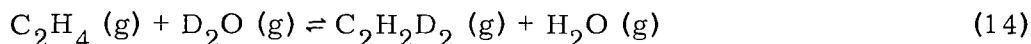
Similar considerations apply to HT, C_2H_5T , etc., but these reactions were not studied because of lack of time.

Reaction Rates

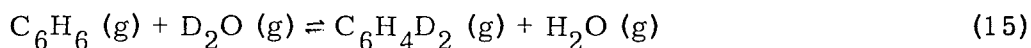
These results show that if the previously discussed exchange reactions proceed at an acceptable rate, tritium decontamination is possible; however, the real question is whether or not the reactions proceed at a reasonable rate. A literature search showed no evidence for the homogeneous gas-phase exchange of either D or T between H_2O and CH_4 . Recent data⁹ have verified that this homogeneous exchange does not occur in a mixture standing for 24 hours at $450^\circ C$. These results are not surprising when the possible rate-determining steps mentioned earlier are considered.

The exchange should occur by atomic interchange in the transition complex, and this behavior requires that the reaction take place either in aqueous solution with a homogeneous catalyst or in the gas phase with a heterogeneous catalyst.

Horiuti and Polanyi,¹⁰ using Pt black or active Ni catalysts, found that the reaction



reached equilibrium in 24 hours at $80^\circ C$. The reaction



reached equilibrium after 2 hours at $200^\circ C$, and the exchange between C_6H_6 and H_2O was found to be 10^5 times slower than C_6H_6 and H_2 when both reactions were carried out over a Ni catalyst.

Extensive exchange studies with CH_4 were conducted by Morikawa et al.¹¹⁻¹⁴ who reported that CH_4 exchanged with D_2 , CD_4 , and D_2O at $140^\circ C$ and higher over an active Ni catalyst. The rates were in the order $CD_4 > D_2 > D_2O$. Clearly, H_2O vapor and CH_4 gas undergo catalytically induced H atom exchange.

The preparation of deuterated or tritiated organic compounds by direct exchange of the compound with H_2O was pioneered by Garnett.¹⁵ Platinum (II) oxide was employed as a catalyst; the procedure was most successful with aromatic compounds, but exchange occurred between T_2O and a wide variety of alicyclic, aromatic, and aliphatic compounds. Rapid exchange was

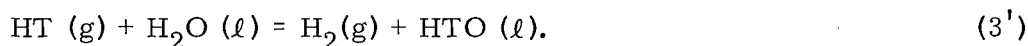
attributed to interaction between π -bonds of the aromatic molecules and d-orbitals of the Pt^{+2} . Aliphatic hydrocarbons, containing only σ -bonds, underwent much slower exchange on the platinum surface. This procedure has now been extended to homogeneous systems¹⁶ using Na_2PtCl_4 as a homogeneous catalyst, and compounds which are difficult to label in the heterogeneous system (e.g., nitrobenzene, bromobenzene, naphthalene, and acetophenone) have been labeled by the homogeneous method. A review of these methods has been published.¹⁷

KRYPTON REMOVAL

Possible methods for ^{85}Kr removal include (1) solution of ^{85}Kr in H_2O , (2) chemical synthesis of a clathrate or a fluorine compound, and (3) use of the contaminated gas as feed material for ammonia synthesis.

The first of these is ruled out because the solubility¹⁸ of Kr in water is too small for effective removal during the exchange process. The second appears unpromising for the following reasons: Although the placing of large amounts of a fluorine-containing compound around the nuclear explosive used for gas well stimulation might have some potential for forming krypton fluorides, the compounds KrF_2 and KrF_4 lack stability.¹⁹ Clathrate compounds of Kr with phenol²⁰ and with β -hydroquinone^{21,22} have been described, but in general these compounds have been made under high Kr pressures. Nothing is known about the stability of possible Kr compounds in the postshot environment.

The third method, use of the contaminated gas for ammonia synthesis, seems to have real potential. The normal process²³ for manufacturing ammonia synthesis gas starts with the partial oxidation of a hydrocarbon to a mixture of CO and H_2 . An iron catalyst then converts steam and CO to H_2 and CO_2 ; the gas is subsequently washed with water to remove CO_2 . Tritium can be removed from the H_2 in this step by the reaction



The gas is then passed through a tower countercurrent to liquid N_2 which condenses Ar, CO, and residual CH_4 and adds the required amount of N_2 to the process stream. The ^{85}Kr will be removed from the process stream at this point; however, it may be necessary to add inert Kr as a carrier.

RECOMMENDATIONS

The use of exchange reactions seems to have potential for decontamination of product gas, but this potential needs verification. A program to confirm the usefulness of this technique should include the following:

1. Equilibrium constants should be calculated for reactions (3) through (8), and their H_2 counterparts, which offer potential means of removing the tritium.
2. Equilibrium data plus reasonable flow data should be employed in preparing a preliminary reference design for such a possible separation plant. A cost estimate should be made.
3. Use of the gas for ammonia synthesis should be examined carefully, since this appears to be a promising way to remove the ^{85}Kr .
4. Experimental work on the rates of these reactions should be started. Can the reaction be made to go with liquid water? Is a catalyst necessary? Is the catalyst poisoned by liquid water, thereby requiring that the reactions be run in the vapor phase?
5. An effort should be made to set some standards for radioactivity in natural gas. This is a difficult question, but without standards it is impossible to do practical planning for nuclear stimulation of gas wells.

ACKNOWLEDGMENTS

This work was done under the auspices of the U. S. Atomic Energy Commission, while the author was a summer employee at Lawrence Radiation Laboratory. It is a pleasure to acknowledge the aid of R. W. Taylor, Charles F. Smith, Howard A. Tewes, and Edward L. Lee. Norman Bonner, Howard Tewes, and Albert E. Sherwood reviewed this manuscript; the author is grateful for their aid.

REFERENCES

1. Charles F. Smith, Jr., Project Gasbuggy Gas Quality Analysis and Evaluation Program Tabulation of Radiochemical and Chemical Analytical Results, Lawrence Radiation Laboratory, Livermore, Report UCRL-50635 (April 22, 1969).
2. H. Urey, J. Chem. Soc., 562 (1947).
3. J. Bigeleisen, J. Chem. Phys. 17, 675 (1949).
4. J. Bigeleisen, Isotopic Exchange Reactions and Chemical Kinetics — Brookhaven Conference Report, Brookhaven National Laboratory Rept. 53 (1948).
5. K. E. Wilzbach, J. Am. Chem. Soc. 79, 1013 (1957).
6. Charles Bowman, El Paso Natural Gas Co., private communication (July 23, 1969).
7. Ya. M. Barshabskii, in Tritium in the Physical and Biological Sciences (International Atomic Energy Agency, Vienna, 1962), vol. 1, pp. 169-177.
8. Thomas K. Sherwood and Robert L. Pigford, Absorption and Extraction (McGraw-Hill Book Co., New York, 1952), 2nd ed., pp. 144-148.
9. Preston Gant and Kim Yang, Continental Oil Co., private communication (July 24, 1969).
10. Jumo Horiuti and M. Polanyi, Trans. Faraday Soc. 30, 1164 (1934).
11. K. Morikawa, W. S. Benedict, and H. S. Taylor, J. Am. Chem. Soc. 57, 592 (1935).
12. K. Morikawa, W. S. Benedict, and H. S. Taylor, J. Am. Chem. Soc. 58, 1445 (1936).
13. K. Morikawa, W. S. Benedict, and H. S. Taylor, J. Am. Chem. Soc. 58, 1795 (1936).
14. K. Morikawa, N. R. Trenner, and H. S. Taylor, J. Am. Chem. Soc. 59, 1103 (1937).
15. J. L. Garnett, Nucleonics 20 (12), 86 (1962).
16. J. L. Garnett and R. J. Hodges, Chemical Communications, 1001 (1967).
17. J. L. Garnett and W. A. Sollich-Baumgartner, Advances in Catalysis (Academic Press, New York, 1966), vol. 16, p. 95.
18. Handbook of Chemistry and Physics, Charles D. Hodgman, Editor (Chemical Rubber Publishing Co., Cleveland, Ohio, 1955), 37th ed., p. 1608.
19. G. J. Moody and J. D. R. Thomas, Noble Gases and Their Compounds (Macmillan, New York, 1964).
20. P. H. Lahr and H. L. Williams, J. Phys. Chem. 63, 1432 (1959).
21. M. M. Hagan, J. Chem. Educ. 40, 643 (1963).
22. J. W. McClain and W. S. Diethorn, J. Appl. Radiation Isotopes 14 (10), 527 (1963).
23. Marshall Sihig, Inorganic Chemical and Metallurgical Process Encyclopedia (Noyes Development Corp., Park Ridge, New Jersey, 1968), p. 56.

RADIOACTIVE CONTAMINATION OF OIL PRODUCED FROM
NUCLEAR-BROKEN SHALE

W. D. Arnold
D. J. Crouse

ABSTRACT

The results of small-scale exposure and retorting tests indicate that oil recovered from shale that has been broken with nuclear explosives will be contaminated with tritium. When oil shale was heated in sealed flasks with tritiated water vapor or with tritiated hydrogen, both the shale and the oil subsequently retorted from the shale contained tritium. There was much less contamination of the shale or oil, however, when the shale was exposed to tritiated methane and ethane. Contamination of shale and oil with tritium, as the result of exposure to tritiated water, increased as the exposure temperature, exposure pressure, and the tritium concentration in the water were increased. This contamination also increased as the exposure time was increased up to 25 days, but not significantly thereafter. More than 90% of the tritium was removed from contaminated shale by treating the shale with moist air at elevated temperatures. Only small amounts of the tritium were removed from crude oil by contacting it with solid drying agents or with water. When tritium-contaminated shale oil was distilled, the tritium contents of the recovered fractions were found to be approximately equal.

After being heated with a sample of underground test-shot debris, liquid shale oil became contaminated with radioactive fission products. Most of the radioactivity of the oil was due to finely dispersed solids rather than to dissolved radionuclides. Filtration of the oil removed a major fraction of the radioactive material. When the contaminated oil was distilled, more than 99% of the radionuclides remained in the pot residue.

Research sponsored by the U. S. Atomic Energy Commission under contract with the Union Carbide Corporation.

Introduction

Oil shale is a fine-grained sedimentary rock that contains kerogen, a solid hydrocarbon. This organic material is distributed among the inorganic particles, with little or none of it bonded either chemically or physically to the mineral constituents.¹ When kerogen is heated to temperatures above 350°C, it decomposes to gas, water, and a liquid hydrocarbon mixture similar to crude petroleum, leaving a carbonaceous residue. The Colorado oil shales, which are located in Colorado, Utah, and Wyoming, are estimated to contain up to two trillion barrels of oil^{2,3} and represent one of the world's major undeveloped hydrocarbon resources.

The Atomic Energy Commission, in cooperation with several government agencies and commercial organizations, is studying the possibility of breaking deeply buried shale with contained nuclear explosions and subsequently recovering the oil by retorting in place. The shale would be ignited at the top of the nuclear-broken chimney, and combustion would be maintained by introducing air. The hot combustion gases, preceding the burning front, would decompose the kerogen into vaporized shale oil, which would condense in the lower part of the chimney and be pumped to the surface. The carbon residue that remains after the retorting of the oil would provide fuel to the advancing fire front. If successful, this concept would allow the development of the oil shale resources while avoiding the problems associated with mining the shale and with disposal of the spent shale after above-ground retorting. Large-scale operations would be possible with a minimum disturbance of the natural landscape.

Project Bronco is a proposed 50-kiloton experiment to study the feasibility of this concept. The anticipated blast, about 3000 ft below the surface, should break more than a million tons of shale in a chimney 230 ft in diameter and 520 ft high.⁴ In-situ retorting to recover the 660,000 barrels of oil from the broken shale will begin about 15 months after the detonation. This report describes the results of laboratory tests that are being made at the Oak Ridge National Laboratory to study the behavior, in the oil recovery system, of the radioactive contaminants that would be released in the nuclear detonation.

Radionuclides of Concern

The amounts of individual fission products and tritium that are produced in a detonation of a given yield depend on the type of device used. In our initial assessment of the potential problems of radioactive contamination of the shale, we have assumed that most of the energy of the device will be derived from fusion. In this case, when oil recovery is started about 15 months after the detonation, the tritium in the chimney will represent more than 95% of the total radioactivity present. If, however, tritium should prove to be more troublesome than the fission products in this application, it may prove advantageous (as in the case of the natural gas stimulation application) to use a fission device to break the shale.

The shale rubble will be contaminated with certain fission products, principally ⁹⁰Sr and ¹³⁷Cs, which have gaseous precursors, and ¹⁰⁶Ru and ¹²⁵Sb, which form volatile compounds. After the cavity formed by the detonation has collapsed, these radionuclides will be deposited on the rubble throughout the chimney and could contaminate the oil as it flows down the chimney. Most of the other long-lived fission products will be trapped in the glassy melt at the bottom of the chimney in a relatively inaccessible form.

Radioactive material will also be formed by neutron activation of the shale immediately surrounding the nuclear device. The principal induced radionuclide present in a shale sample after irradiation in the Oak Ridge Research Reactor was ^{46}Sc . Smaller amounts of ^{54}Mn and ^{59}Fe along with traces of ^{51}Cr , ^{65}Zn , and ^{124}Sb , were also detected in the irradiated shale. Except for the ^{54}Mn and ^{65}Zn , these radionuclides have relatively short half-lives and will decay to only a few percent of their initial concentrations by the time oil recovery is started. In addition, the bulk of these activation products will be captured with most of the fission products in the glassy melt, and therefore, should be in a relatively innocuous form.

Tritium

Assuming that a total of about 25,000 curies of tritium is produced per kiloton of fusion (the approximate mid-point of the 7,000- to 50,000 curies-per-kiloton range specified by Miskel⁴), the detonation will release about $1\mu\text{c}$ of tritium per gram of broken shale in the chimney. Conceivably, the tritium could be present as tritiated water, tritiated hydrogen, or tritiated hydrocarbons. Results of our small-scale equilibration and retorting tests indicate that appreciable contamination of the shale oil will occur from tritiated water or tritiated hydrogen, while contamination from tritiated hydrocarbons should be much less severe (Table I).

The shale used in these tests was obtained from the Bureau of Mines shale mine near Rifle, Colorado. This shale assayed at 32 gal of oil and 2.5 gal of water per ton. A sized fraction containing pieces of shale 4.8 to 8.0 mm in diameter was used. Samples of shale weighing 120 g, and tritium (as tritiated compounds) were heated in steel pressure vessels with volumes of about 300 cm³ each. The tritiated water that was added consisted of 1.2 ml of water containing about 120 μc of tritiated water, and the gases that were added consisted of 130 ml of hydrogen, methane, or ethane containing about 100 μc of the corresponding tritiated gas. The vessels were heated under nitrogen pressure for 6 to 7 days at 85°C and 560 psig. At the end of the heating period, the pressure was released and the shale was washed with water and dried with warm (65°C) air. Oil was recovered from a 100-g sample of the dried shale in a small retort composed of two electric furnaces (Fig. 1). The shale sample was held in the lower furnace in a crucible with a perforated bottom. The oil was retorted by increasing the temperature of the shale from 25°C to about 430°C over a period of 5 to 6 hr. A mixture of nitrogen (24 ml/min) and carbon dioxide (24 ml/min) was preheated in the upper furnace and passed through the shale to a condenser at 38°C and a cold trap at 0°C. The gas was routed through a bed of cupric oxide at 700 to 750°C to burn the hydrocarbon gases released by the shale and to convert the hydrogen to water. The water was frozen from the gas stream, which exited from the system through a flowmeter. In a typical run, slightly more than 11 g of oil and 1.2 ml of water were collected in the 38°C receiver; an additional 0.5 ml of water was collected in the 0°C trap. The depleted shale weighed about 85 g.

Factors Affecting Tritium Contamination

A series of equilibration and retorting tests was made to study some of the variables that affect tritium contamination of the shale and oil when the tritium source is tritiated water. The exposure tests were made at atmospheric pressure in 1-liter glass flasks, using 120-g shale samples and 1.2 ml of water containing about 120 μc of tritiated water.

The contamination occurred rapidly (Fig. 2). The tritium concentration of the oil increased from 0.56 $\mu\text{c/g}$ to 0.92 $\mu\text{c/g}$ when the exposure time of the shale to tritiated water vapor at 85°C was increased from 1 day to 29 days. A

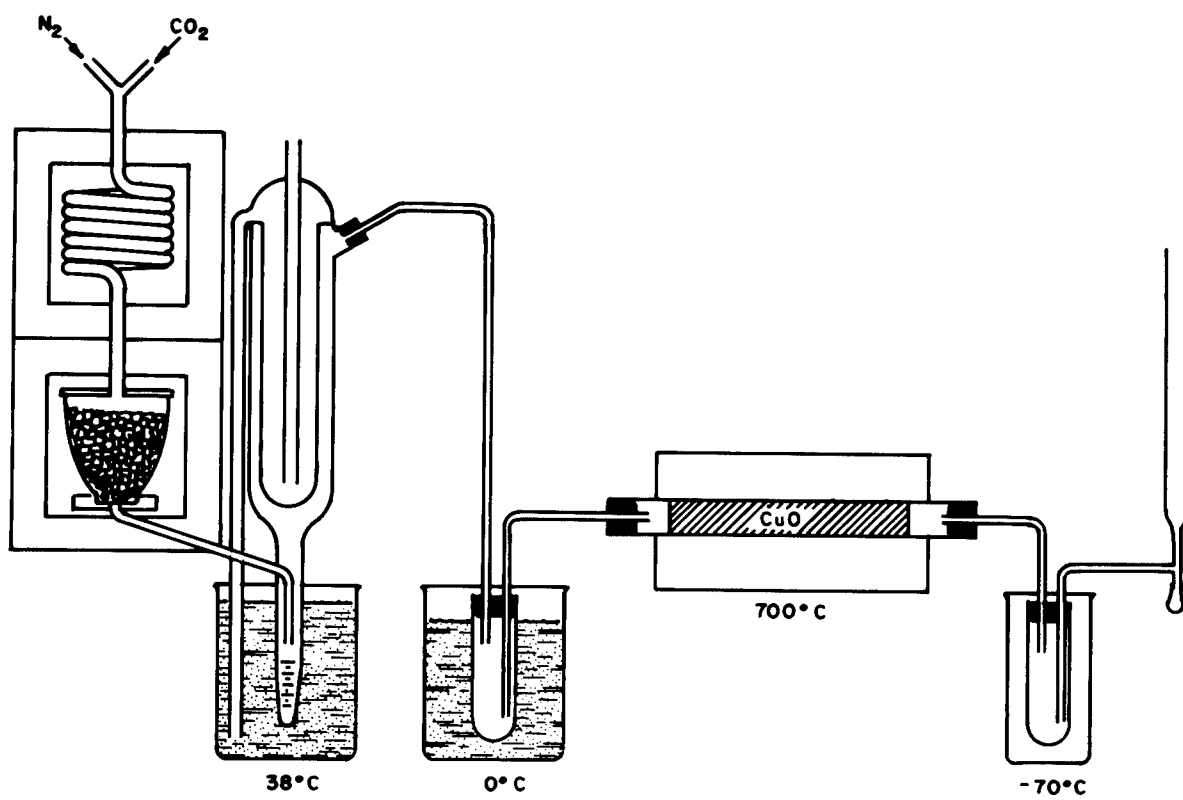


Fig. 1. Bench Scale Retort.

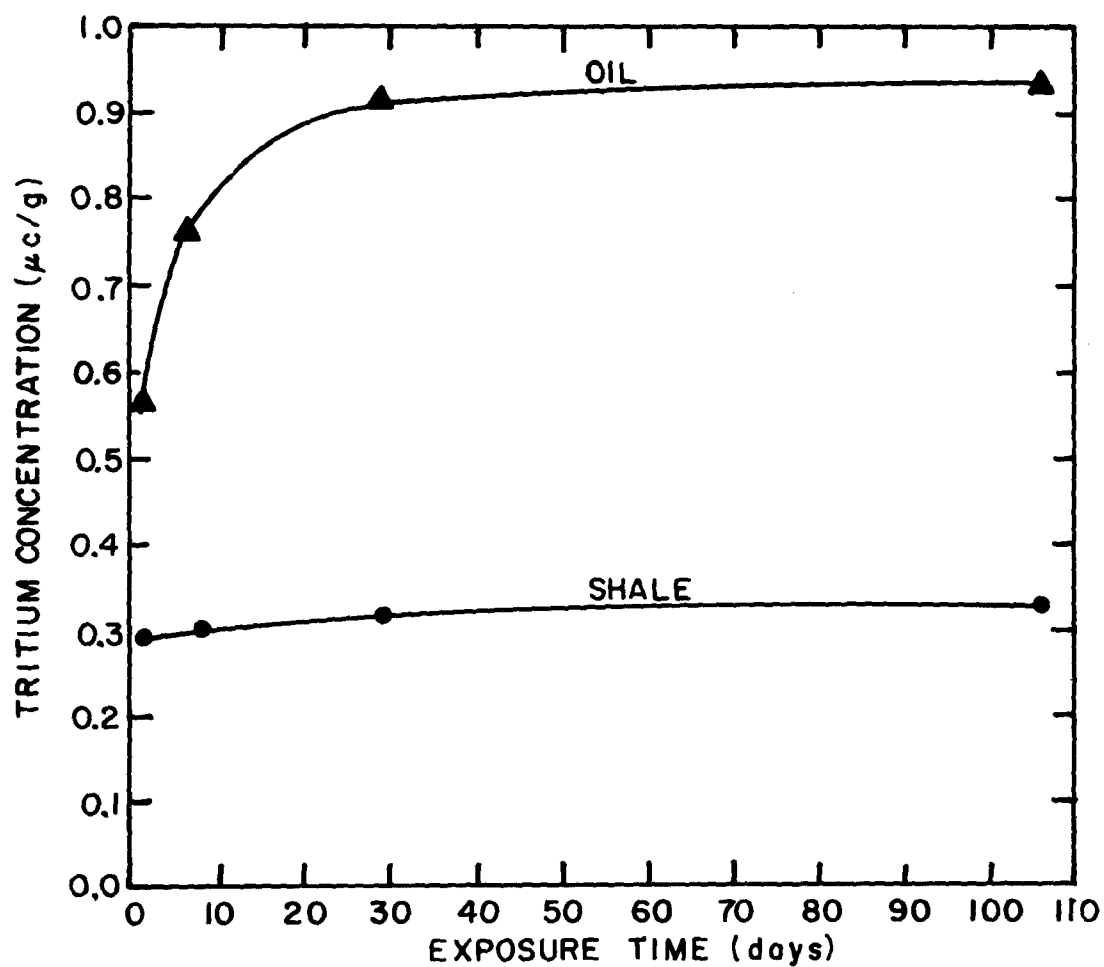


Fig. 2. Effect of Exposure Time on Tritium Contamination of Shale and Oil. Procedure: 120g of shale was heated in a sealed flask at 85°C with 1.2 ml of water containing about 120 μc of tritiated water. After the shale was washed with water and dried with air at 65°C, oil was retorted from a 100-g sample.

Table I. Tritium Contamination of Shale and Oil

Procedure: 120 g of oil shale was heated for 6 to 7 days at 85°C and 560 psig with (a) 1.2 ml of water containing about 120 μc of tritiated water or (b) 130 ml of hydrogen, methane, or ethane containing about 100 μc of the corresponding tritiated gas. After the shale was washed and dried with air at 65°C, oil was retorted from a 100-g sample.

Tritiated Compound Added	Tritium Concentration ($\mu\text{c/g}$)	
	In Dried Shale	In Oil
Water	0.37	0.57
Hydrogen	0.19	0.24
Methane	0.013	0.023
Ethane	0.037	0.024

further increase in exposure time to 106 days increased the tritium concentration of the oil to only 0.93 $\mu\text{c/g}$.

The contamination of the shale and oil was directly proportional to the tritium concentration of the water added to the exposure flask (Fig. 3). The tritium concentration of the water was varied by a factor of 100, resulting in equivalent variations in the tritium concentrations in the shale and in the oil. The exposure time at 85°C was 25 to 29 days.

The tritium contamination of the oil retorted from shale after the shale had been exposed to tritiated water vapor for 25 days increased with increasing temperature in the sealed exposure flask (Fig. 4). The oil contained 0.48 μc of tritium per gram at a flask temperature of 45°C, 0.67 $\mu\text{c/g}$ at 65°C, 0.92 $\mu\text{c/g}$ at 85°C, and 1.0 $\mu\text{c/g}$ at 95°C.

In tests with shale fractions both coarser and finer than the 4.8- to 8.0-mm fraction, the tritium contamination of both the shale and the oil increased as the shale particle size was increased (Table II). The oil from the coarsest shale fraction (8 to 26 mm in diameter) contained almost three times as much tritium as the oil from the finest fraction (1.2 to 2.0 mm in diameter). The surface area and the porosity of the shale samples increased with decreasing particle size, possibly the result of fractures introduced by crushing the shale. Measurements of the pore size distribution indicated that the pores in the 8- to 26-mm shale were small, usually less than 1 micron diameter. The other three samples of shale contained pores or fractures up to 17 microns in diameter. Tritiated water penetrated to the center of a shale cube that measured 28 mm on a side when the cube was heated with tritiated water for 25 days at 85°C. The tritium concentration increased with depth, from 0.46 $\mu\text{c/g}$ in the outer 4-mm layer to 0.22 $\mu\text{c/g}$ in the 5- to 8-mm-deep layer, and to 0.13 $\mu\text{c/g}$ in the center 10-mm cube. The center cube represented 6% of the initial shale weight and contained about 2% of the total tritium in the shale block.

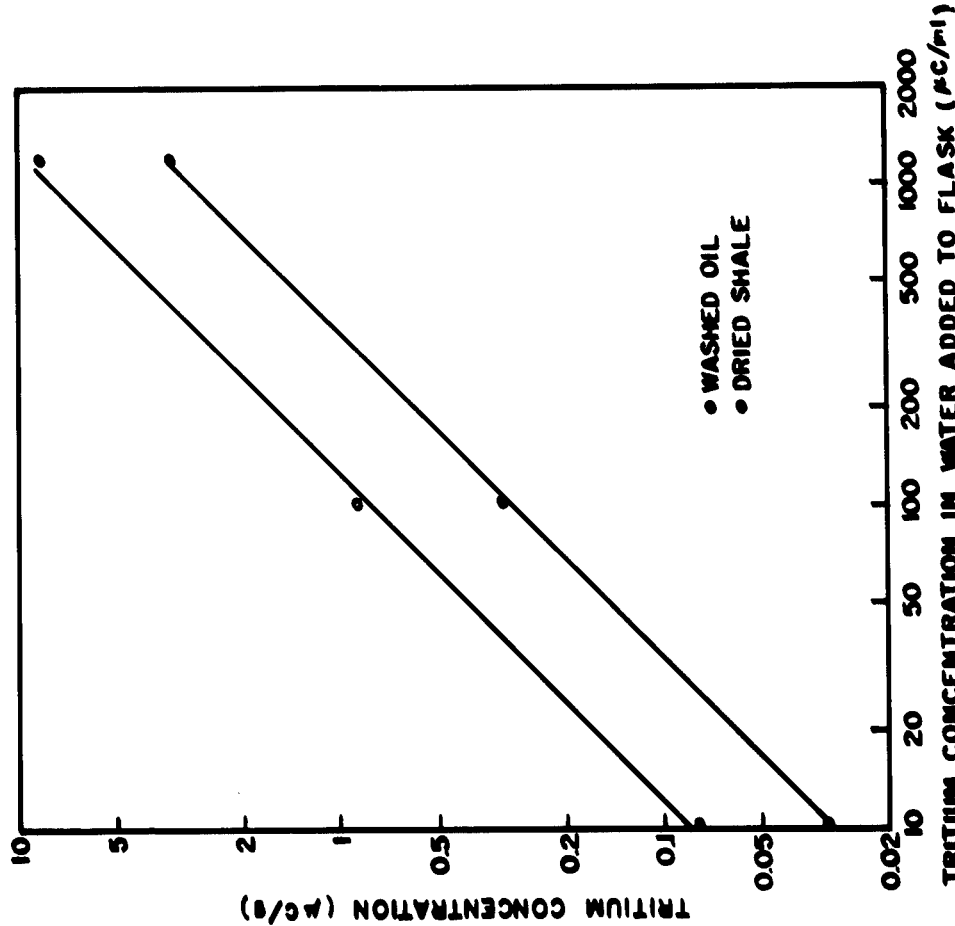


Fig. 3. Effect of Tritium Concentration in Water Added to Reaction Flask on Tritium Contamination of Shale and Oil. Procedure: 120g of shale and 1.2 ml of water, containing the indicated concentration of tritiated water, were heated in a sealed flask at 85°C for 25 to 29 days. After the shale was washed with water and dried with air at 65°C, oil was retorted from a 100-g sample.

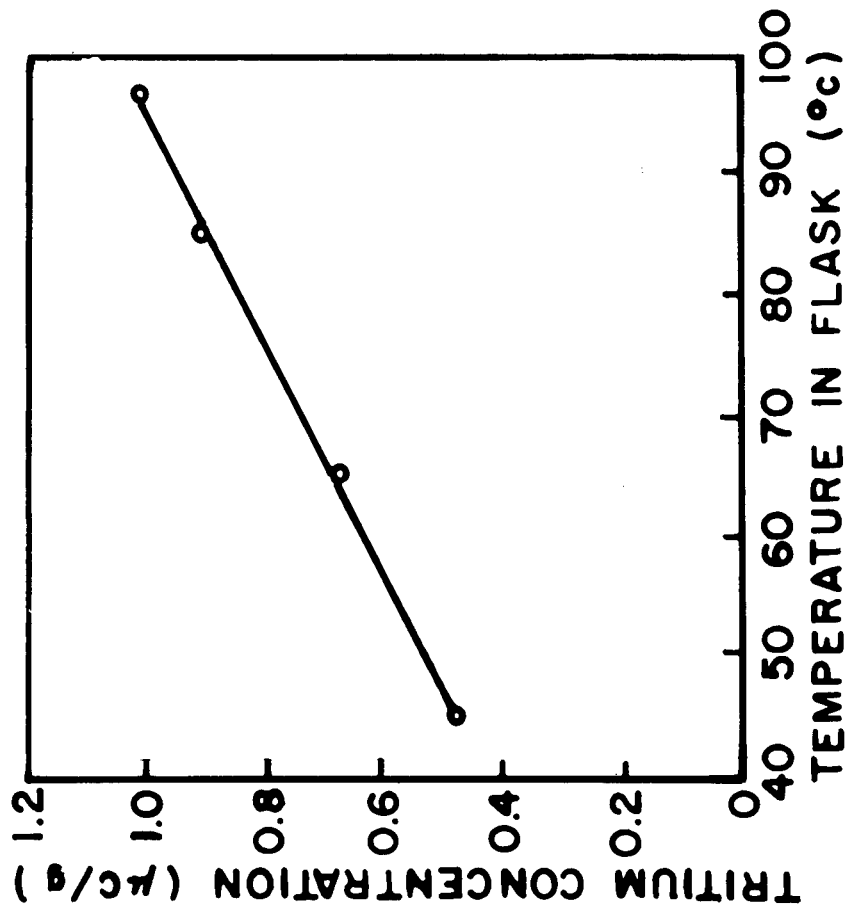


Fig. 4. Effect of Reaction Temperature on Tritium Contamination of Oil. Procedure: 120g of shale and 1.2 ml of water containing 120 μc of tritiated water were heated in a sealed flask for 25 days at the indicated temperatures. After the shale was washed with water and dried with air at 65°C, oil was retorted from a 100-g sample.

Table II. Effect of Shale Particle Size on Tritium Contamination of Shale and Retorted Oil

Procedure: 120-g samples of Green River oil shale were heated at 85°C for 25 days in sealed 1-liter flasks with 1.20 ml of water containing about 120 μc of tritiated water. Oil was retorted from 100 g of the washed and dried shale samples.

Range of Shale Particle Sizes (mm)	Surface Area (m^2/g)	Porosity (%)	Tritium In Shale ($\mu\text{c/g}$)	Tritium In Retorted Oil ($\mu\text{c/g}$)
1.2-2.0	0.165	4.7	0.14	0.52
2.0-4.8	0.127	3.2	0.17	0.51
4.8-8.0	0.092	1.7	0.32	0.92
8.0-26	0.004	0.5	0.36	1.42

Increasing the pressure during exposure of oil shale to tritiated water vapor increased the tritium contamination of the shale and the oil (Fig. 5). The tritium concentration of the oil recovered from shale after being exposed to tritiated water vapor for 25 days measured from 0.48 $\mu\text{c/g}$ to 0.73 $\mu\text{c/g}$ when the exposure pressure at 85°C was increased from 50 psig to 860 psig. Increasing the exposure time at 85°C and 560 psig increased the tritium contamination of the oil, but the increases were smaller than those measured at atmospheric pressure. The oil retorted from a shale sample that had been exposed for 1 day contained 0.47 μc of tritium per gram. The contamination was 20% and 35% higher for shale exposed 6 days and 26 days, respectively.

In one test, the oil recovered on retorting a sample of tritium-contaminated shale was collected in increments. The tritium concentration was essentially the same in the three oil fractions:

<u>Oil Fraction</u>	<u>Retort Temperature Range (°C)</u>	<u>Oil Volume (ml)</u>	<u>Tritium In Oil ($\mu\text{c/ml}$)</u>
1	226 - 363	4.1	0.49
2	363 - 383	4.2	0.52
3	383 - 426	4.9	0.52

Removal of Tritium from Shale

Although the mechanism by which tritium is held in contaminated shale is not known at this time, it appears likely that it is present as tritiated water and that tritiation of the shale hydrocarbons occurs during retorting. We have been able to remove most of the tritium from contaminated shale by contacting it with a gas phase containing water vapor for prolonged periods. About 95% of the tritium was removed from a sample of contaminated shale ($0.3 \mu\text{c/g}$) by treating it for 15 days at a temperature of 200°C with a gas stream that had been saturated with water at 38°C (Fig. 6). About 40% of the tritium was removed from the shale in the 4-hr period required to heat the shale from room temperature to 200°C , whereas a total of 70% was removed in the first day of treatment at 200°C . The oil that was retorted from the shale after 15 days of treatment contained $0.12 \mu\text{c}$ of tritium per gram, which is equivalent to slightly more than 1% of the tritium that was added to the reaction flask at the beginning of the test. Originally, the shale was contaminated with tritium by heating it at 85°C for 25 days with tritiated water. In the tritium removal test, a 100-g sample of the contaminated shale was heated at 200°C in the retort, and the gas stream (24 ml/min of N_2 plus 24 ml/min of CO_2) was saturated with water at 38°C and passed through the shale. In a similar test with a shale sample that had been exposed to tritiated water vapor for 108 days, about 90% of the tritium was removed from the shale in 15 days of treatment at 200°C , and the oil that was retorted from the shale after the treatment contained $0.20 \mu\text{c}$ of tritium per gram.

The removal of tritium from contaminated shale by intermittent treatment with moist air at lower temperatures was less efficient. In these tests, the contaminated shale ($0.3 \mu\text{c/g}$) was treated with preheated water-saturated air for 2 hr each day at the rate of 20 ml/min . The shale was held at temperature between the treatments. Slightly more than 80% of the tritium was removed from the shale in 6 treatments at 95°C , and about 50% was removed in 8 treatments at 85°C . In other tests, more than 80% of the tritium was removed from contaminated shale in two 1-week submersions in hot water (95°C) and about 50% was removed by heating a shale sample for 24 hr at 110°C under reduced pressure (1 mm Hg) while passing air through the shale.

The removal of tritium from a shale cube that measured 28 mm on a side was somewhat less efficient than removal from the 4.8- to 8.0-mm shale used in the tests described above. The shale cube, contaminated with tritium by exposure to tritiated water vapor for 25 days at 85°C , was heated for 10 days in a sealed flask at 95°C . For 2 hr each day, air saturated with water at 85°C was passed through the flask at the rate of 20 ml/min . This treatment removed only 20% of the tritium from the shale and forced a portion of the remaining tritium deeper into the cube. The outer 4-mm layer contained $0.39 \mu\text{c}$ of tritium per gram, the 5- to 8-mm-deep layer contained $0.48 \mu\text{c/g}$, and the center 10-mm cube contained $0.43 \mu\text{c/g}$.

These tests indicate that a significant fraction of the tritium could probably be removed from the shale by passing moist air through the chimney prior to retorting. Appreciable removal may also occur as a natural result of the retorting operation since the shale over most of the length of the chimney will be exposed to a flow of hot moist gases for a prolonged period prior to attainment of the retorting temperature. Some provision for removing the tritiated water from the effluent gases would probably be needed before the gases are recycled to the chimney. The efficiency of tritium removal may be limited by deep penetration into large shale chunks since the removal of tritium from this material will be much less efficient than from smaller shale pieces.

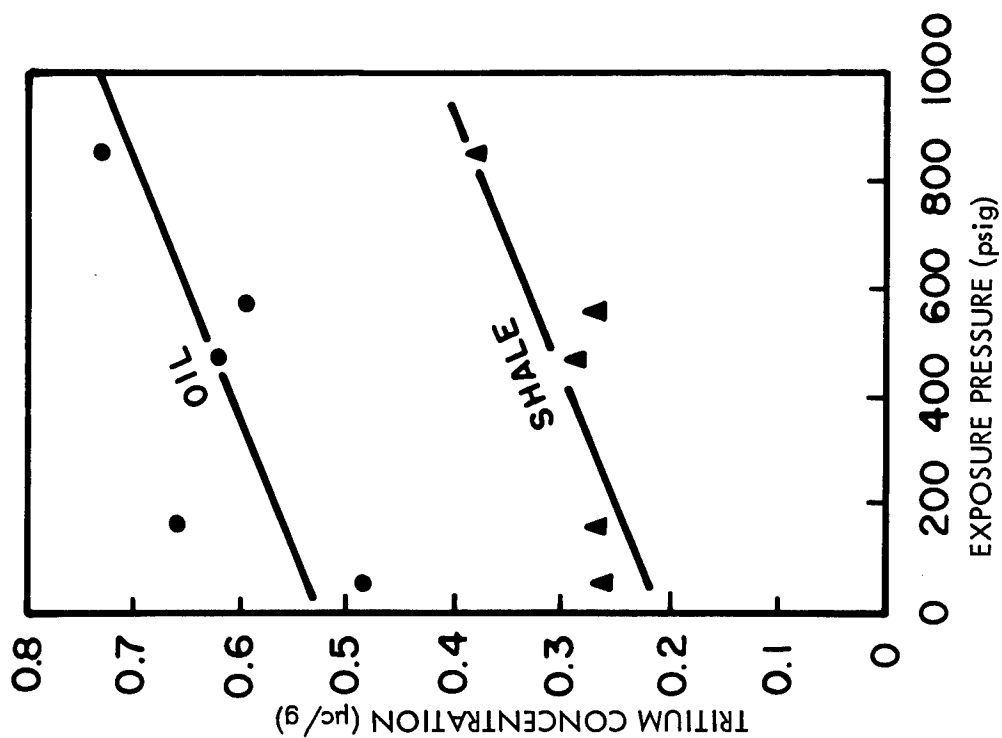


Fig. 5. Effect of Exposure Pressure on Tritium Concentration of Shale and Oil. Procedure: 120g of shale and 1.2 ml of water containing about 120 μ c of tritiated water were heated for 25 days at 85°C and at the indicated pressures. After the shale was washed with water and dried with air at 65°C, oil was re-torted from a 100-g sample.

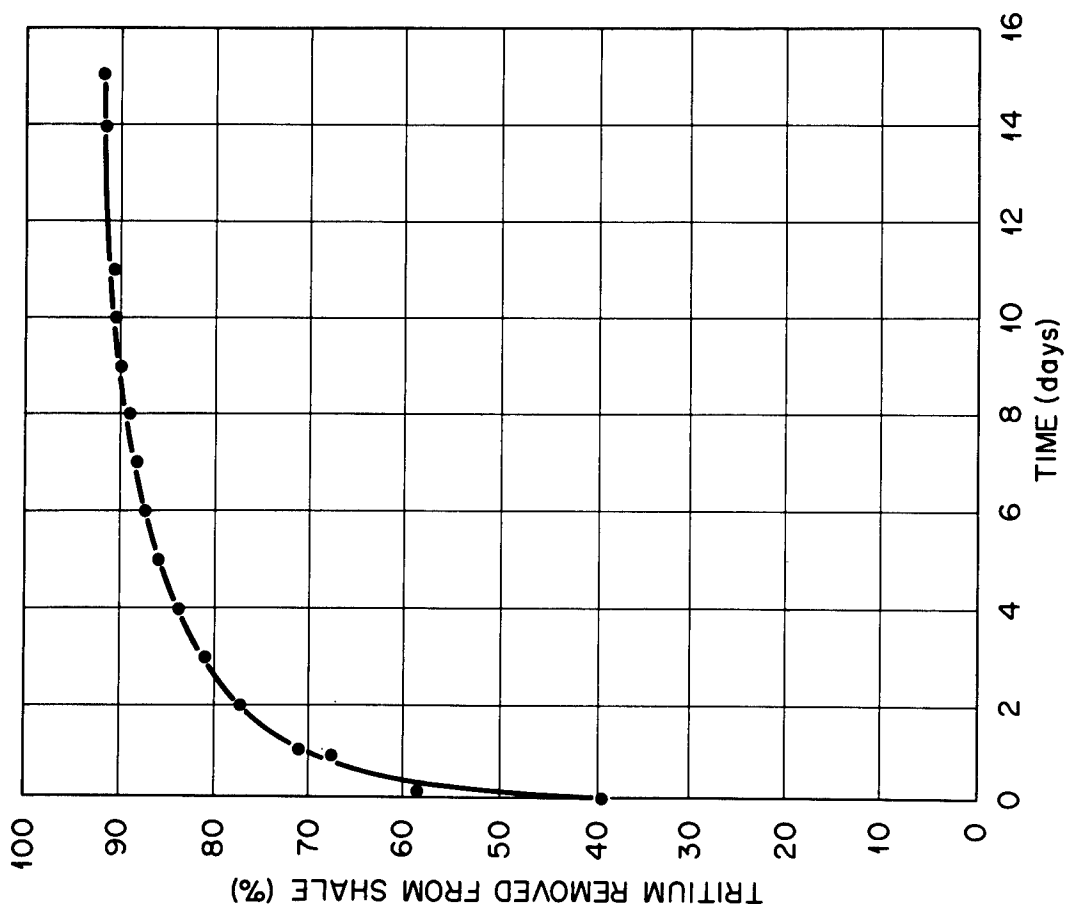


Fig. 6. Removal of Tritium from Shale at 200°C. Procedure: 100 g of tritiated shale (0.3 μ c/g) was heated at 200°C in a gas stream that had been saturated with water at 38°C.

Removal of Tritium from Shale Oil

Tritium is not easily removed from contaminated oil. Tests showed that prolonged refluxing of tritiated oil with water removed only a few percent, while none was removed by equilibrating the oil with solid drying agents.

Failure to remove more of the tritium from the oil under these conditions indicates that the tritium is probably present in the oil as part of the hydrocarbon structure rather than as tightly bound water. Further evidence lending credence to this hypothesis was obtained by distilling a tritiated oil sample. Each of the oil fractions, the residuum, and the small amount of recovered water were found to have about the same tritium content; the tritium concentration in these fractions was also about the same as that in the original crude oil (Table III). Further fractionation, by gas-liquid chromatography, of the naphtha showed that it contained at least 20 components. Tritium could not be detected in the minor peaks, but was definitely present in the three major peak groups.

Fission Products

Most of the fission products from the nuclear detonation will be trapped in the fused rock (puddle glass) that accumulates at the bottom of the chimney. However, the crushed shale will be contaminated to some extent with fission products that have gaseous precursors (e.g., ^{90}Sr and ^{137}Cs) and those that form volatile compounds (e.g., ^{106}Ru and ^{125}Sb). These fission products will be deposited on the surfaces of the broken shale and could contaminate the oil as it flows down the chimney. The potential contamination of oil with fission products was studied by heating crude shale oil samples with underground test-shot debris and measuring the radioactivity of the oil. Tests were made both with aged debris (several years old) and with debris only a few months old.

The aged debris consisted of chimney rubble and puddle glass from the bottom of the chimney. At $68,000 \text{ counts min}^{-1} \text{ g}^{-1}$, the gross gamma activity of the puddle glass was an order of magnitude greater than that of the rubble (Table IV). The dominant radionuclides were ^{144}Ce , ^{90}Sr , and ^{60}Co in the glass and ^{137}Cs , ^{90}Sr , and ^{106}Ru in the rubble. Barely measurable oil contamination occurred when 10-ml samples of shale oil were heated under reflux with 10-g samples of the debris fractions. After 4 hr at an oil temperature of 220°C , the gamma activity of the oil samples was only about 130 counts/min (40% of background count):

<u>Debris Fraction</u>	<u>Total Activity of Oil (counts/min)</u>
Rubble	129
Glass	138

The major radionuclides in the newer debris sample, a mixture of rubble and puddle glass, were ^{95}Zr - ^{95}Nb , ^{103}Ru , and ^{141}Ce , which are all relatively short-lived isotopes. This debris was much more radioactive than the older sample; the gross gamma activity was about $3.5 \times 10^7 \text{ counts min}^{-1} \text{ g}^{-1}$. Longer-lived radionuclides, such as ^{106}Ru , ^{137}Cs , and ^{144}Ce that would be of greater importance at the time of oil recovery were not detected in the initial radiometric analysis due to interference from the short-lived radionuclides; however, they were detected in a later analysis of the debris. Shale

Table III. Distillation of Tritiated Shale Oil

Procedure: 100 ml of tritiated shale oil (prepared by contacting Green River oil shale with water vapor containing tritiated water for 25 days at 85°C in a sealed flask and retorting; to increase the volume of oil for the distribution test, the oil was diluted with uncontaminated shale oil to give oil with 0.056 μc of tritium per ml).

Fraction	Temp. Range (°C)	Pressure	Distillate Volume (ml)	Tritium Concentration ($\mu\text{c}/\text{ml}$)
Naphtha	To 200	Atmospheric	10	0.051
Light oil	To 225	40 mm Hg	26	0.037
Heavy oil	225-300	40 mm Hg	29	0.047
Residuum		40 mm Hg	33	0.055
Water ^a			1	0.048

^aWater taken from cold trap. None of the oil fractions contained any visible water.

oil that had been heated in contact with the debris became contaminated with the fission products present in the debris (Table V). The gross gamma activity of a 25-ml oil sample that had been heated for 4 hr with 5.2 g of the debris under reflux conditions at 220°C was found to be about 1×10^5 counts $\text{min}^{-1} \text{ml}^{-1}$. Releaching the debris with two additional portions of fresh oil yielded oil that was contaminated to the same level as the first oil sample. The activity of the oil obtained from two final leaches, each with 50 ml of fresh oil, was 5×10^4 counts $\text{min}^{-1} \text{ml}^{-1}$. Based on the measurements of the gross gamma activity, the combined oil samples contained 7.5% of the radioactive material initially present in the debris. Most of the radioactivity of the oil was due to ^{95}Zr - ^{95}Nb and ^{103}Ru . The combined oil samples contained about 2% of the ^{95}Zr - ^{95}Nb and 5% of the ^{103}Ru along with 2% of the ^{141}Ce and 1% of the ^{140}Ba - ^{140}La initially present in the debris. As was true for the debris sample, the longer-lived radionuclides were not detected in the contaminated oil samples.

Much of the radioactive contamination of the oil was due to the entrainment of finely dispersed solids rather than to dissolved radionuclides. When the oil from the leaching tests was diluted with crude shale oil and subsequently distilled, more than 99% of the radioactive material remained in the pot residue (Table VI). The heavy oil fraction contained only about 0.3% of the radioactive material initially present in the crude oil, and the amounts detected in the naphtha and light oil fractions were barely detectable. When 3-g samples of the crude oil and residuum from the distillation were treated at 60°C with 4 successive 5-ml portions of hexane, the insoluble residue accounted for 35 to 40% of the gross gamma activity but only 0.2% and 0.5%, respectively, of the initial sample weights. Filtration of the hexane solutions through a Millipore filter containing stacked papers of 8- μ , 0.8- μ , and 0.1- μ pore size removed an additional 45% of the radioactive material (0.9% and 2.5% of initial sample weight, respectively). Most of the solids that

Table IV. Radiochemical Analysis of Underground
Test-Shot Debris

Radionuclide	Concentration (dis min ⁻¹ g ⁻¹)		
	Sample A ^a		Sample B ^b
	Rubble	Glass	
⁶⁰ Co	0.081 x 10 ³	3.0 x 10 ⁴	c
⁸⁹ Sr	c	c	0.28 x 10 ⁷
⁹⁰ Sr	0.86 x 10 ³	3.9 x 10 ⁴	c
⁹⁵ Zr- ⁹⁵ Nb	c	c	9.3 x 10 ⁷
¹⁰³ Ru	c	c	1.9 x 10 ⁷
¹⁰⁶ Ru	0.39 x 10 ³	0.65 x 10 ⁴	0.7 x 10 ⁷ (ref. e)
¹³⁷ Cs	21.0 x 10 ³	1.3 x 10 ⁴	0.04 x 10 ⁷ (ref. e)
¹⁴⁰ Ba- ¹⁴⁰ La	c	c	0.28 x 10 ⁷
¹⁴¹ Ce	c	c	1.4 x 10 ⁷
¹⁴⁴ Ce	0.094 x 10 ³	5.2 x 10 ⁴	0.5 x 10 ⁷ (ref. e)
Gross gamma ^d	6.8 x 10 ³	6.8 x 10 ⁴	3.5 x 10 ⁷

^aSeveral years old.

^bSeveral months old.

^cNot detected.

^dGross gamma activity is given in counts min⁻¹ g⁻¹.

^eNot detected in initial analysis; measured after short-lived radionuclides had decayed; concentration calculated to date of initial analysis.

were filtered out of the hexane solutions were found on the 8-μ paper. The dried solids were gray-black in color and flocculent.

Discussion

Our investigation thus far indicates that oil recovered from nuclear-broken shale is more likely to be contaminated with tritium than with fission products if a fusion device is used. The extent of the tritium contamination of the shale and oil will depend on the form in which the tritium exists in the chimney. Appreciable contamination will occur from tritiated water or tritiated hydrogen, but much less is expected from tritiated hydrocarbons. Tritium contamination will possibly be reduced by the removal of a significant fraction of the tritiated compounds from the shale by the front of hot moist gases that precedes the retorting front down the chimney. This will be limited to some extent, however, by the relatively inefficient removal of the tritiated compounds that penetrate deeply into large chunks of shale. The removal of tritium from the retorted oil does not appear practical at this point since it evidently is present in the oil as part of the hydrocarbon structure.

Table V. Results Obtained by Leaching Test-Shot
Debris with Shale Oil

Procedure: 5.2 g of test-shot debris (see Table IV for analysis) was heated successively with three 25-ml portions and two 50-ml portions of shale oil at 220°C under reflux conditions. The contact time for each leach was 4 hr. The oil was centrifuged before analysis.

Radionuclide	Radioactivity of Combined Oil Samples	
	dis min ⁻¹ ml ⁻¹	% of Initial
⁹⁵ Zr- ⁹⁵ Nb	5.6 x 10 ⁴	2.0
¹⁰³ Ru	2.9 x 10 ⁴	5.2
¹⁴¹ Ce	8.6 x 10 ³	2.1
¹⁴⁰ Ba- ¹⁴⁰ La	8.7 x 10 ²	1.0
Gross gamma ^a	7.8 x 10 ⁴	7.5

^aGross gamma activity is measured in counts min⁻¹ ml⁻¹.

The amount of tritium in the chimney could be drastically reduced by using an all-fission device to break the shale. This would increase the relative importance of the fission products with respect to radioactive contamination of the oil product. Although fission product behavior has not been studied as extensively as tritium behavior, our test results indicate that the fission products will not significantly contaminate the overhead distillate fractions, which are the most valuable shale oil products. Subsequent use and processing of the residuum to recover by-products, however, could be complicated by the presence of fission products.

Acknowledgment

We are indebted to W. B. Howerton, D. R. Shaw, and D. E. Spangler for technical assistance in these studies. J. W. Landry designed the retort and made some of the initial retorting runs. Measurements of the physical properties of the shale samples and many of the radiochemical analyses were made in the ORNL Analytical Chemistry Division.

Table VI. Distillation of Contaminated Shale Oil

Procedure: 100 ml of oil contaminated with fission products was distilled. The gross gamma activity of the crude oil was $3930 \text{ counts min}^{-1} \text{ ml}^{-1}$.

Fraction	Temp Range (°C)	Pressure	Volume (ml)	Gross Gamma Activity	
				counts $\text{min}^{-1} \text{ ml}^{-1}$	% of Total
Naphtha	To 200	Atmospheric	7	10	< 0.05
Light oil	To 225	40 mm Hg	25	< 10	< 0.05
Heavy oil	225 to 300	40 mm Hg	34	30	0.3
Residuum			35	11,640	99.7
Water ^a			0.6	190	< 0.05

^aRecovered from cold trap.

References

1. P. R. Tiscot and W. I. R. Murphy, Physical Structure of Green River Oil Shale from Colorado, USBM-R1-6184 (1963).
2. Mineral Facts and Problems, U. S. Bureau of Mines Bulletin 585 (1960).
3. D. C. Duncan and V. E. Swanson, Organic-Rich Shale of the United States and World Land Areas, U. S. Department of the Interior GSC 523 (1965).
4. J. A. Miskel, Characteristics of Radioactivity Produced by Nuclear Explosives, Third Plowshare Symposium, TID-7695 (April 1964).
5. Project Bronco, PNE-1400 (Oct. 13, 1967).

NUCLEAR EXCAVATION II

EJECTA FROM SINGLE-CHARGE CRATERING EXPLOSIONS

By R. H. Carlson

ABSTRACT

The objective was to obtain experimental data tracing the location of ejecta to its origin within the crater region. The experiment included ten high-explosive spherical charges weighing from 8 to 1000 pounds and detonated in a playa dry lake soil on the Tonopah Test Range. Each event included from 24 to 40 locations of distinctly different tracer material embedded in a plane in the expected crater region. Tracers consisted of glass, ceramic and bugle beads, chopped metal, and plastic wire. Results of this experiment yielded data on tracer dispersion as a function of charge weight, charge burial depth and tracer emplacement position. Tracer pattern parameters such as center-of-tracer mass, range to center-of-tracer mass, and angle to center-of-tracer mass were determined. There is a clear tendency for range (to center-of-tracer mass) and the size of the dispersion pattern to decrease as tracer emplacement depth increases. Increasing tracer emplacement depth and range tends to decrease the area over which tracers are dispersed on the ground surface. Tracers at the same scaled position relative to the charge were deposited closer to the crater (on a scaled basis) as charge weight was increased.

INTRODUCTION

When excavation involves simultaneous explosive detonations such as for a harbor or a canal, ejecta is generally of no concern. Directed blasting, that is, blasting beneath a surface which is shaped such that ejecta is directed in an asymmetrical pattern, results in some portion of the ejecta being directed toward the pre-existing excavation causing it to be partially backfilled. Examples of directed blasting are "nibbling" techniques, joining of rows, detonation of short rows (less than 5 to 7 charges), two stage excavation, and non-simultaneous detonation of charges in a row or rows of charges. It is for the application of these sophisticated charge arrays that an understanding of ejecta mechanisms is required. Because theory is lacking, these data must be obtained experimentally.

Cost prohibits extensive ejecta tracer experimentation on large explosions. Thus, results from small scale experiments must be used to predict full scale applications, even though it is clear that such data cannot be easily scaled. The experiment described here illustrates the complex nature of the mechanisms by which material is ejected from single charge explosive craters. These data permit us to begin to acquire an understanding for the origin of the material which becomes fallback and that which becomes ejecta. These data also permit some understanding of the temporal and spatial sequence of ejecta and fallback deposition, the location of ejecta as a function of its origin, and the characteristics of dispersion patterns exhibited by surface ejecta.

This paper is a brief summary of an experimental report (Ejecta from Single-Charge Cratering Explosions, SC-RR-69-1, by Roland H. Carlson and Robert T. Newell) which will be released by Sandia Laboratory in the near future. In this paper examples of ejecta tracer behavior for various combinations of tracer emplacement position, charge weight and charge burial depth are presented. Although in most cases these examples seem typical, the reader is encouraged to review the detailed data in the experimental report cited above and then make his own judgment regarding typical ejecta tracer behavior.

The objective of this experimental program was to study the relationship between soil crater ejecta distribution and its origin within the crater region for single explosive charges of varying weights detonated at varying burst depths. A further purpose was to develop information on which a calculational model of ejecta mechanics could be constructed and against which it could be checked, however, the development of such a model was not a part of this program.

This research was funded under the U. S. Atomic Energy Plowshare Program. Field work was conducted by the Sandia Corporation Field Test Organization at the Tonopah Test Range in Nevada. Tracer recovery was by Alpha Testing Laboratories, Inc. in Albuquerque, New Mexico. Analysis, data reduction and reporting was done under Contract 59-1240 between The Boeing Company and Sandia Laboratory.

SCOPE OF EXPERIMENTAL PROGRAM

This program consisted of ten, single charge cratering events. A series of four 64-pound charges detonated at depths of 4, 5, 6, and 7 feet were used to study depth effects, and to determine an optimum crater burst depth which could be scaled to study yield effects. Two charges weighing 8 and 256 pounds were fired at the optimum scaled depth determined from the 64-pound charge series. Four surface charges were also fired; two weighed 64 pounds and two weighed 1000 pounds. This selection of events was made to permit the study of tracer dispersion both as a function of charge weight and burst depth. All charges were cast TNT spheres, centrally detonated. Table 1 indicates the scope of the program and the measurements which were made on each event.

All shots were fired in the playa soil of Antelope Dry Lake on the Tonopah Test Range in Nevada. This soil is described as a tan, clayey silt at the surface to brown silt with traces of fine to medium sand at depths of 5 or more feet. The water content varies from about 12 percent at the surface to approximately 21 percent at a depth of 15 feet. The wet bulk density varies between 84 pounds per cubic foot and 117 pounds per cubic foot. A weighted value for in situ density of the playa in the region of the crater for events in this experiment is about 100 pounds per cubic foot.

EXPERIMENTAL PROCEDURE

On each shot, tracer beads were placed at varying ranges and depths in a single, vertical plane along the 0 degree or magnetic north azimuth. Figure 1 indicates the plane of tracer emplacement for the 1000-pound surface event. The shaded regions indicate placement of cement coloring agents in the lower portion of the tracer emplacement holes to aid in post-shot identification of the true crater boundary. Tracers were emplaced to a depth which was expected to exceed the true crater boundary.

Ejecta tracers were multicolored beads, plastic pellets, and aluminum pellets. Each tracer was approximately 0.1 inch in diameter or about 50 times as large as the mean particle size of the playa soil. The bulk density of the tracers approximated the playa in situ density. On all shots, in an attempt to assure tracer survival, care was taken to emplace metal tracers in positions near the charge. Exact quantities of tracers were determined prior to tracer emplacement. Tracer locations included from 3750 tracers for the 8-pound event to 25,000 tracers for the 1000-pound event.

Ejecta and fallback were recovered in accordance with the station layout illustrated in Figure 2. The recovery surface was a 90-degree quadrant which extended from 315 degrees to 45 degrees in azimuth. The recovery surface was bisected by the plane of tracer emplacement oriented along the 0 degree azimuth. Recovery from this quadrant was complete--it extended from a predetermined outer range inward to the edge of the true crater. For each event it was predicted that this outer recovery range would exceed the maximum range to which ejecta would be deposited. A second surface recovery plan involved a series of annular ring segments of varying widths and ranges through the 270 degrees of surface not included in the surface quadrant of complete recovery. Each ring segment in this

Table 1 Scope of Program

Shot	Charge Weight (lbs)	Burst Depth		Measurements			
		Actual (ft)	Scaled (ft/lb ^{1/3})	Apparent Crater	True Crater	Ejecta Mass	Tracers
211-54	8	3	1.50	x	x	x	x
211-51	64	0	0	x	x	x	
211-53	64	0	0	x	x	x	x
211-40	64	4	1.00	x	x	x	x
211-47	64	5	1.25	x	x	x	x
211-48	64	6	1.50	x	x	x	x
211-49	64	7	1.75	x	x	x	x
211-55	256	9.5	1.50	x	x	x	x
211-52	1000	0	0	x	x		
211-56	1000	0	0	x	x	x	x

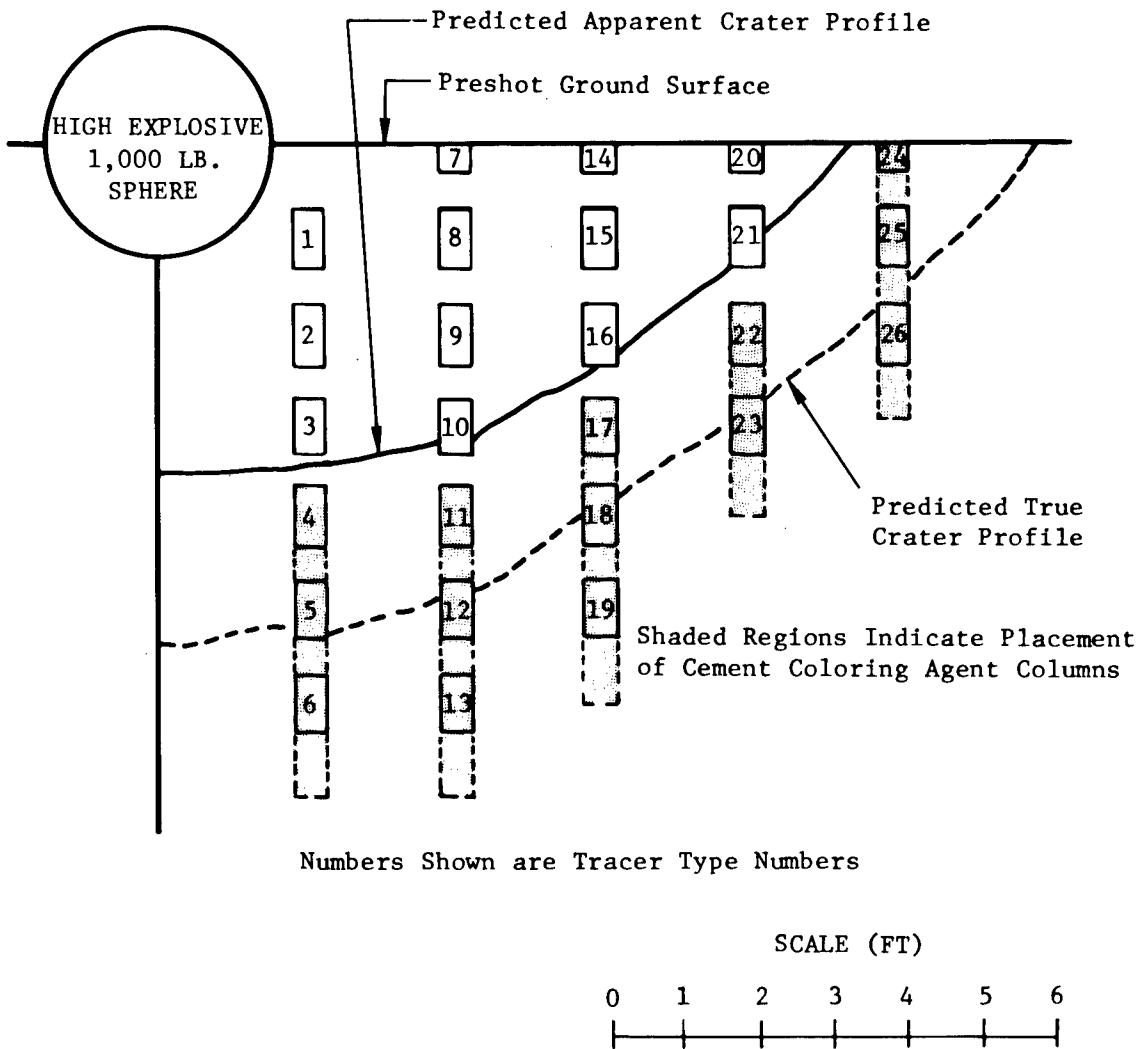
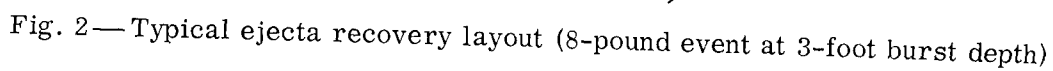


Fig. 1—Tracer emplacement positions for the 1000-pound surface shot



270-degree region was connected to a ring segment in the quadrant of complete recovery of the same width to form a series of continuous 360-degree annular ring recovery regions. The 270-degree segments of these ring recovery regions were divided into nine 30-degree sectors for sampling purposes. The quadrant was divided into 5-degree sectors. A number and letter system was used to identify sampling areas and recovered samples.

Also shown in Figure 2 is the recovery plan for fallback in the crater region. Fallback samples approximately one square foot in area were collected in 4-inch lifts normal to the apparent crater surface. Fallback samples were recovered in a quadrant of the apparent crater defined by the 315-degree and 45-degree azimuth.

Ejecta samples removed from the surface and crater were placed in plastic bags, sealed, tagged and shipped to Alpha Testing Laboratories in Albuquerque, New Mexico. Here, samples were weighed and analyzed to determine number and type of tracers which it contained. Data were then submitted to The Boeing Company in Albuquerque for analysis and reporting.

American Aerial Surveys, Inc., Covina, California, made conventional aerial stereophotographs of the craters and compiled crater contour maps. These contour maps were used to determine apparent crater dimensions and mass parameters.

RESULTS

Craters

Apparent crater radius and depth as a function of actual charge burst depth for the 64-pound events are shown in Figure 3. The 6-foot burst depth produced an optimum crater. The depth-of-burst curves shown in Figure 3 are typical and as expected from prior explosive cratering studies.

An 8-pound and 256-pound charge were detonated at the same scaled charge burst depth ($1.5 \text{ ft/lb}^{1/3}$) as the 64-pound optimum event following the assumption that optimum craters would result. For these three charge weights the apparent crater radius scaled as charge weight to about 0.35 power, apparent crater depth scaled as charge weight to about the 0.48 power and apparent crater volume scaled as charge weight to about the 1.2 power.

The 64-pound data obtained in this study were scaled and compared with depth-of-burst data from a series of 256-pound charges in Nevada Test Site playa resulting from the AIR VENT study (Reference 1). These data are also shown in Figure 3. Although both the 64- and 256-pound charges produced essentially the same scaled apparent crater radius and depth at the surface, they deviate significantly at depths approaching optimum. This difference could probably be reduced by searching for a better scaling exponent, however, this experiment was directed primarily at the study of ejecta tracer dispersion and cratering scaling was not studied.

It appears that 8-pound and 256-pound charges in this test series probably did not produce an optimum crater when detonated at the same scaled depth which resulted in an optimum crater for the 64-pound charge. Both the

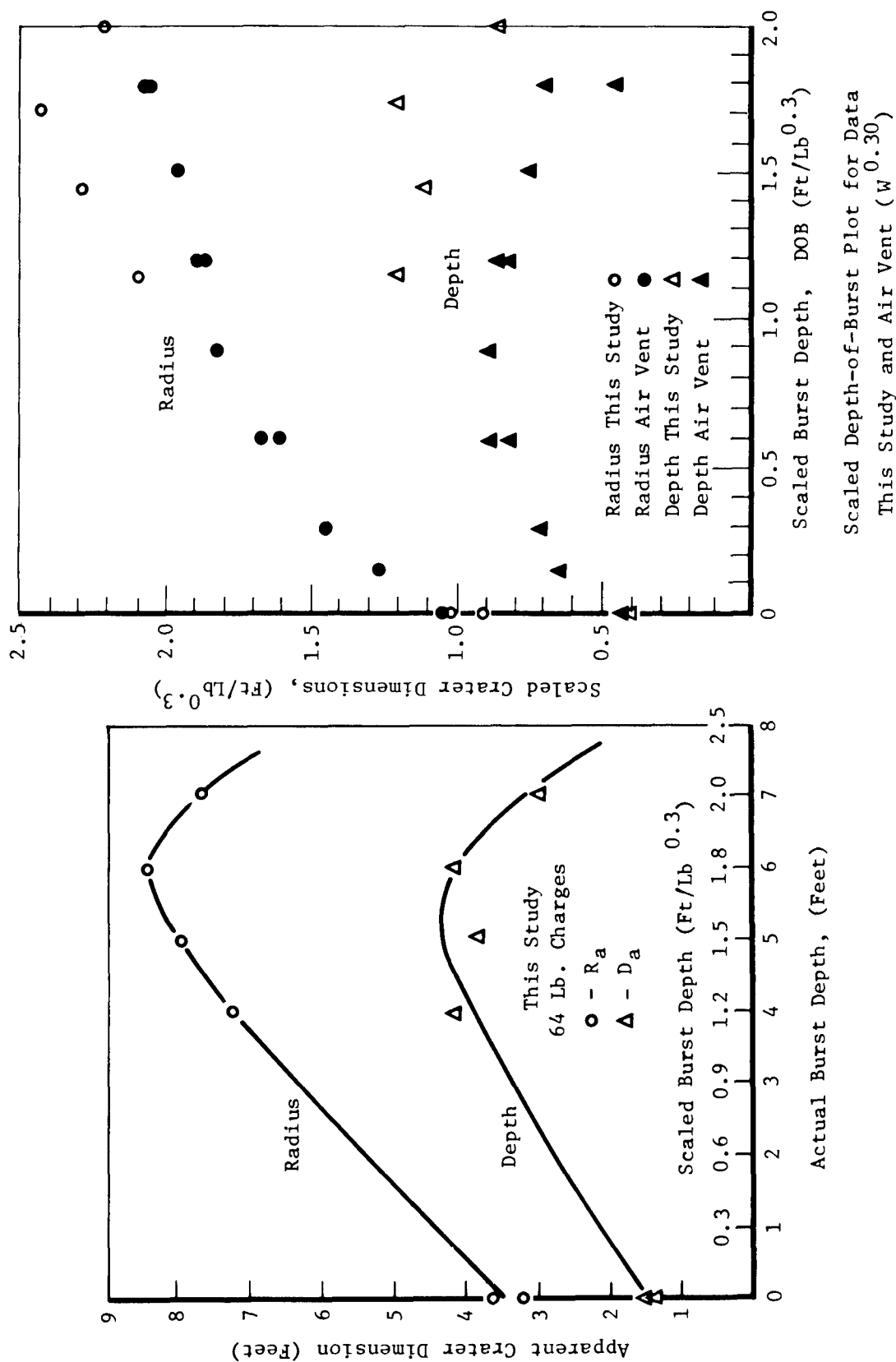


Fig. 3—Apparent crater radius and depth as a function of charge burst depth

8-pound and the 256-pound charges were probably below the optimum apparent crater burst depth. This should be considered when attempting to correlate tracer dispersions observed for the three charge weights detonated at the same scaled burst depth in this experiment.

Ejecta Areal Density

Figure 4 shows ejecta areal density data as a function of radial distance for two events in this experiment. The data point represents the mean of all measurements made at a fixed radial distance. Maximum and minimum observations at any fixed distance are indicated by the vertical bar. A straight line relationship determined mathematically by the Method of Least Squares is shown for each event. As indicated by the correlation coefficient, the 8-pound event at 3-foot burst depth yielded the poorest fit and the 64-pound event at 4-foot burst depth yielded the best fit.

Plots such as shown in Figure 4 are used to determine total ejecta mass for crater mass balance studies. The empirical model for ejecta areal density based on tracer data and discussed in a later section of this paper is checked against the actual areal density versus range observations shown in Figure 4.

Tracer Patterns

Considering the tremendous effort involved in recovering the several hundred thousand tracers involved in this experiment, tracer recovery percentages are quite satisfactory. Generally, recovery percentages were better than 80 or 90 percent for tracers which were emplaced in soil completely ejected from the crater. Certain low recoveries occurred near the charge because of tracer destruction. There are of course a number of anomalous low tracer recoveries which cannot be explained.

A rather exhaustive dispersion analysis was done for every tracer included in the experiment. An illustrative dot pattern was developed for tracers deposited on the surface and in the crater fallback. For surface tracer dispersion patterns the location of the center-of-tracer-mass was determined. The radius of the circle which included 50 percent of the recovered tracers was calculated. The percentage of each tracer recovered in the various reaction regions (ejecta, fallback, undisturbed playa) was tabulated. Plots of percentage of total tracers recovered as a function of radial distance were made for the surface quadrant of complete recovery. Similar plots were made for percentage of surface tracers recovered as a function of azimuth. Tracer recovery percentage in the crater was plotted as a function of recovery depth in the fallback.

Figure 5 illustrates the effect of near-surface tracer horizontal emplacement range on the surface tracer dispersion pattern for the 8-pound event at 3-foot burst depth. Tracers were emplaced at a depth of 3 inches below the ground surface. All of emplaced tracer types 1, 5, 10, 15, and 20 were recovered on the surface. Tracers 25 and 29 are transitional tracers, the larger portion of tracer 25 being recovered on the surface and the larger portion of tracer 29 being recovered in the crater. All of tracers 33 and 36 were recovered in the crater fallback. Figure 5 shows the location of the center-of-tracer-mass, the circle containing 50 percent of the recovered

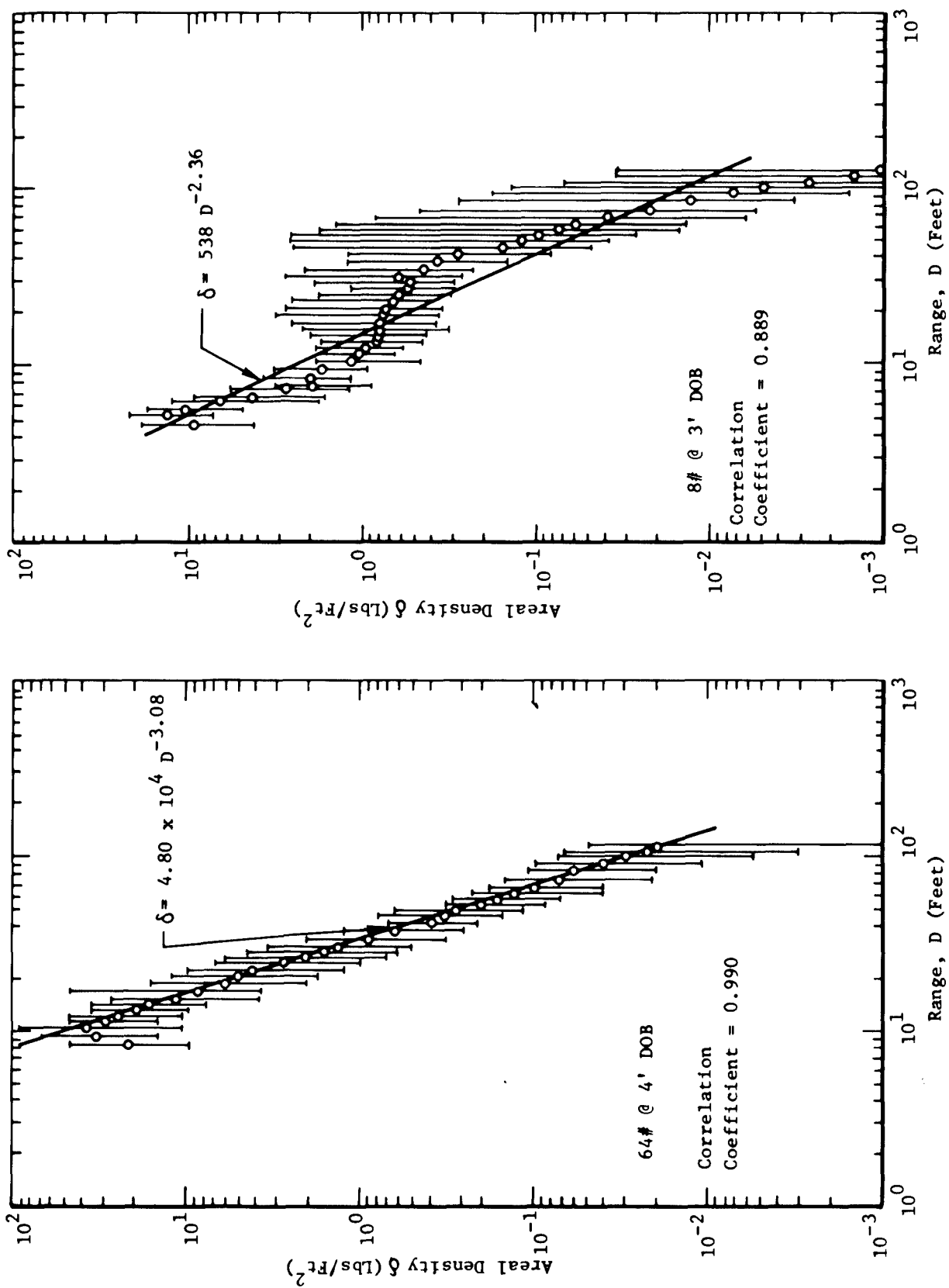


Fig. 4—Ejecta areal density as a function of radial range

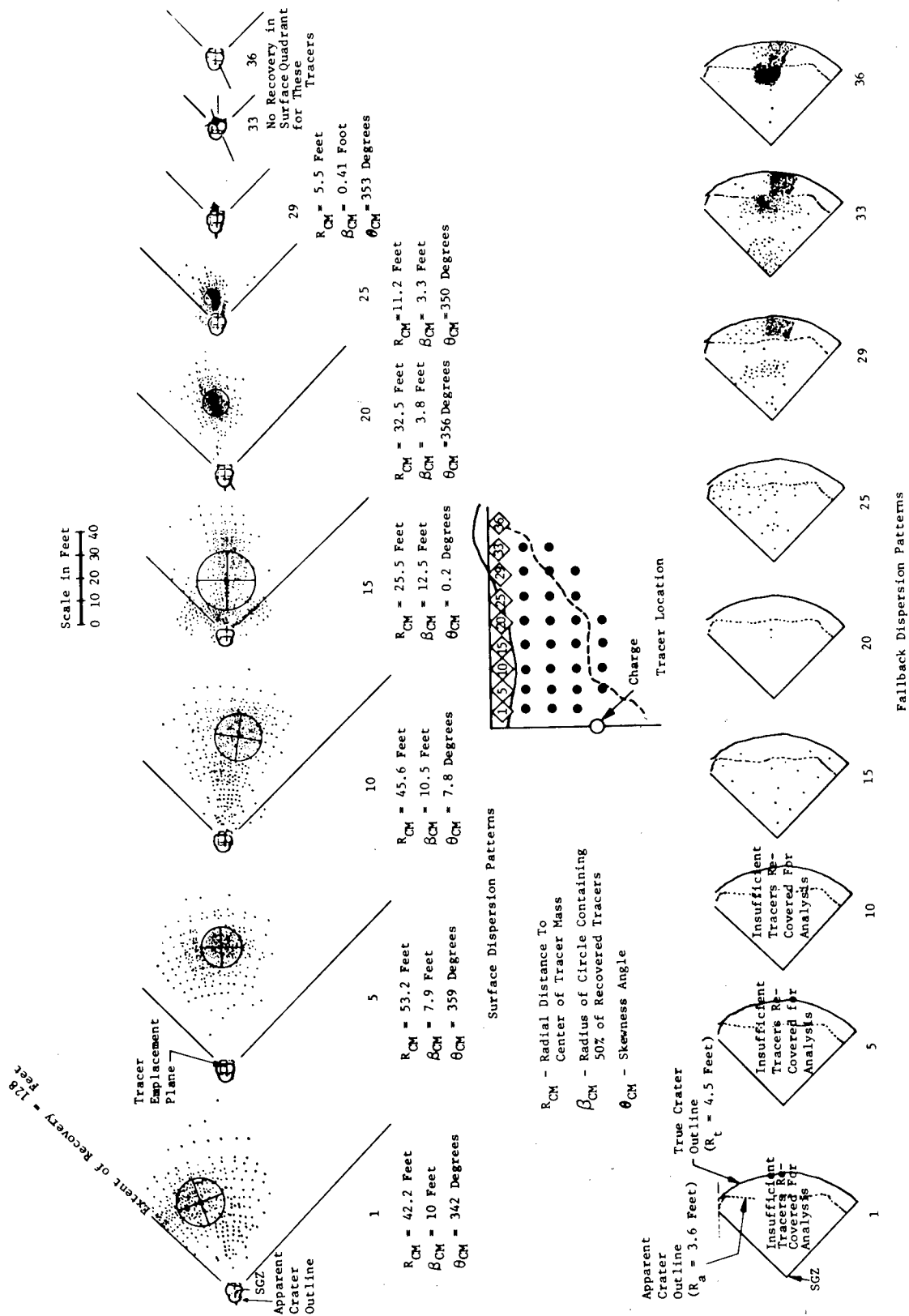


Fig. 5—Effect of tracer emplacement range on surface dispersion patterns
(8-pound charge at 3-foot burst depth)

tracers, and the skewness angle for the center-of-tracer mass. The relationship of these parameters to emplacement range is shown in Figure 6.

Figure 6 illustrates the relationship between tracer dispersion and horizontal distance from the explosive epicenter for the 8-pound charge detonated at a 3-foot depth. Range to center-of-tracer mass seems to increase to a maximum at a tracer emplacement range close to the epicentral axis and then it decreases with greater emplacement range. This trend is generally observed for buried events. The same relationship is observed for the radius of the circle containing 50 percent of the tracers recovered on the surface. The center-of-tracer mass is skewed counter-clockwise at near emplacement range, clockwise at intermediate emplacement range and counter-clockwise again at the greater ranges.

Figure 7 shows recovery percentage as a function of radial range for the tracers emplaced horizontally at the same depth. These data are for the same tracers on the same event as discussed for Figures 5 and 6. Data points represent the total percentage of tracers recovered from rings in the quadrant of complete recovery. The continuous function is for a normal or gaussian distribution having mean range and standard deviation determined from the data. The form of this function is:

$$P_k(D) = \frac{1}{\sigma_{Dk} \sqrt{2\pi}} \exp - \left[\frac{(D - \bar{D}_k)^2}{2(\sigma_{Dk})^2} \right]$$

where \bar{D}_k is the mean range of the distribution which is given by:

$$\bar{D}_k = \sum_{\text{all } i} \left(\frac{D_i + D_{i+1}}{2} \right) P_{ki}$$

D_i and D_{i+1} are consecutive range values and P_{ki} is the percentage of the total amount of tracers recovered from the ejecta which were between D_i and D_{i+1} . The standard deviation of the distribution, σ_{Dk} , is given by:

$$\sigma_{Dk}^2 = \sum_{\text{all } i} \left[\left(\frac{D_i + D_{i+1}}{2} \right) - \bar{D}_k \right]^2 P_{ki}$$

All i applies to the total range of ejecta containing tracer type k . One can find many examples of radial tracer distributions for which a gaussian distribution appears to be a good assumption. There are other examples where skewness of the distribution is apparent.

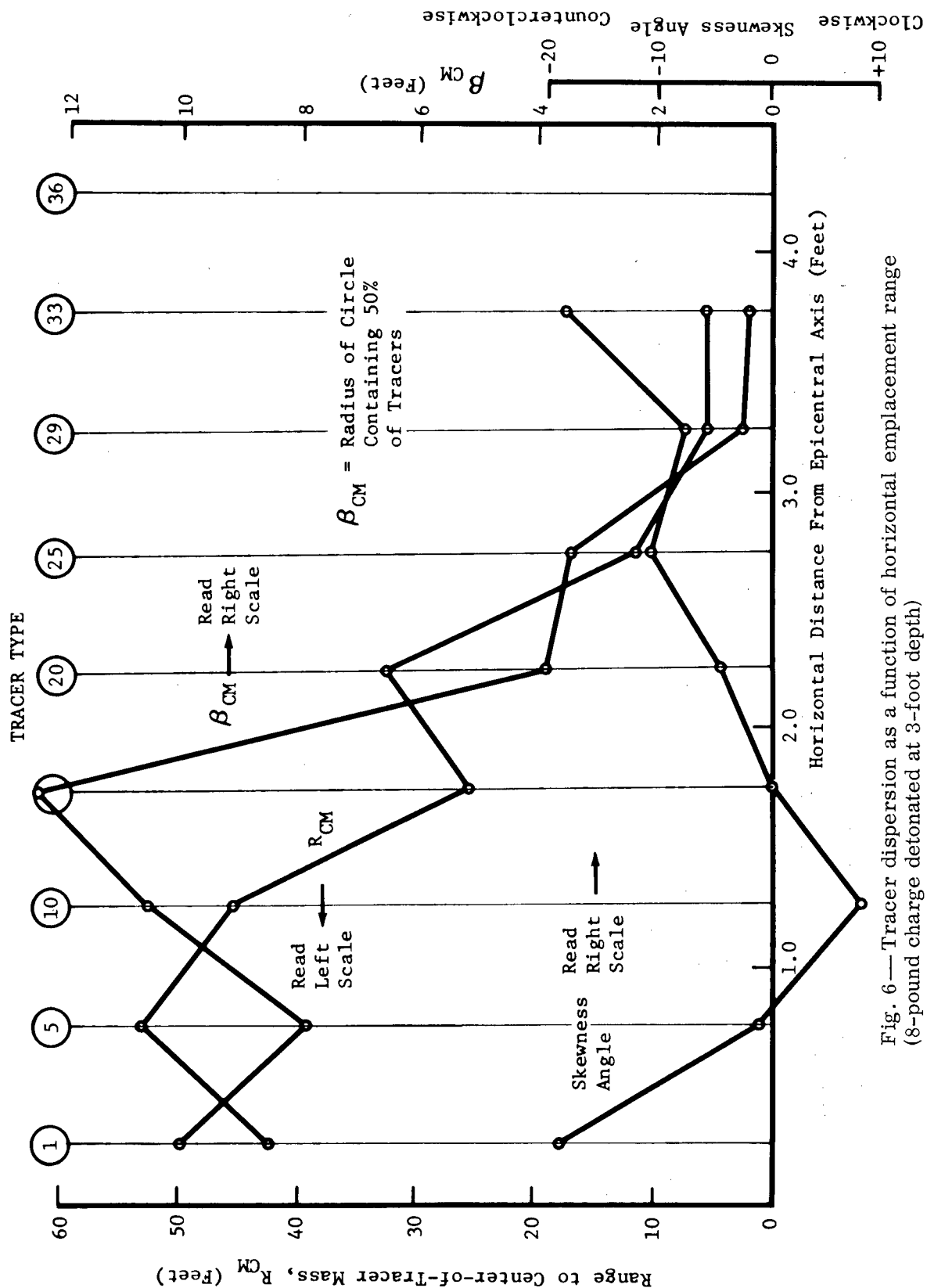


Fig. 6—Tracer dispersion as a function of horizontal emplacement range (8-pound charge detonated at 3-foot depth)

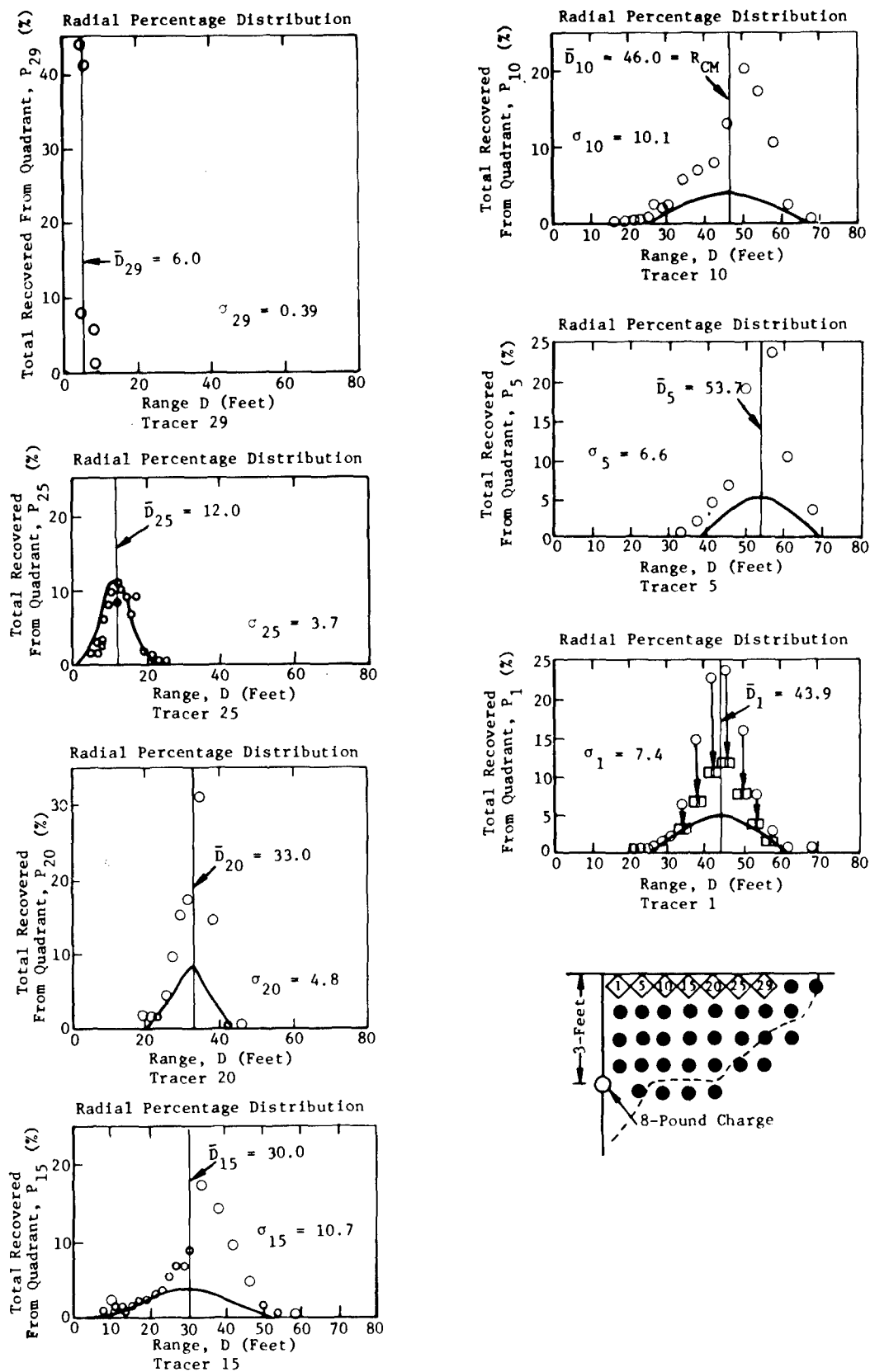


Fig. 7—Recovery percentage as a function of radial range for tracers emplaced horizontally at same depth (8-pound event at 3-foot burst depth)

Data points shown in Figure 7 are somewhat misleading because they represent recovery rings of differing widths. In the illustration shown for tracer 1 data points have been adjusted such that each represents a ring of the same width. These data compare favorably with the gaussian distribution. A good fit could be made by adjusting or normalizing the gaussian distribution in some way. An in-depth analysis of statistical tracer distributions will be the subject of another study.

Figure 8 shows near-surface tracer emplacement horizontal range effects on circumferential distribution for the 8-pound event at 3-foot burst depth. Again, the same tracers discussed for the three previous figures are included here. Azimuthal percentages are based on tracers recovered in the 5-degree sectors. Note the increase in circumferential distribution for the shorter emplacement ranges. Generally tracers emplaced closer to the epicentral axis are spread over a larger area and would thus show the larger percentages over the greater azimuthal spread as in Figure 8. Note that over 80 percent of emplaced tracers were recovered on the surface for all tracers except number 29. For this tracer only 12 percent of the emplaced tracer was recovered on the ground surface. The trimodal distribution for tracer 15 is unique, however, there are numerous cases of bimodal circumferential distribution.

Figure 9 illustrates emplacement horizontal range effects on tracer deposition in the fallback within the crater. Tracers were at a constant emplacement depth of 1.75 feet for the 8-pound charge detonated at a 3-foot burial depth. (Note that tracers in the four prior illustrations were at a constant emplacement depth of 0.5 feet.) Over 98 percent of tracer 35 was recovered in its original emplacement position. All of tracers 22, 27 and 31 were recovered and all were found in the crater fallback. Tracers 27 and 31 were recovered at a depth of about 16 inches. Fifty percent of tracer 22 was recovered in the first 4-inch shell of fallback material--the remaining 50 percent was recovered in decreasing percent increments to a depth of 30 inches. Only about 10 percent of tracer 17 was recovered in the fallback. Negligible amounts of tracers 3, 7 and 12 were recovered in the fallback. Generally when a significant amount of tracer was found in the crater, it was well distributed vertically in the fallback profile.

Figure 10 illustrates the effect of surface tracer emplacement range on dispersion patterns for the 64-pound surface event. Note the large dispersion associated with tracers emplaced near the charge. Skewness of the center of the tracer pattern is clockwise except for tracer 20 which is slightly clockwise. Range to center-of-tracer mass and dispersion decrease as tracer emplacement range increases. For this surface event we do not see an increase to a maximum range followed by a decrease as generally observed for buried events. Only for location 24 was there significant tracer recovery (54 percent) in the crater fallback.

The effect of tracer emplacement depth on dispersion patterns is shown for the 8-pound event at 3-foot depth in Figure 11. Note that range to center-of-tracer mass decreases as tracer emplacement depth increases. Dispersion as evidenced by the radius of the circle containing 50 percent of the recovered tracers also decreases as tracer emplacement depth increases. There is consistent counter-clockwise skewness for this particular column of tracers. All of tracers 5, 6, 7 and 8 were recovered in the surface quadrant. All of

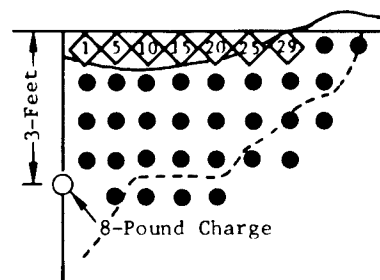
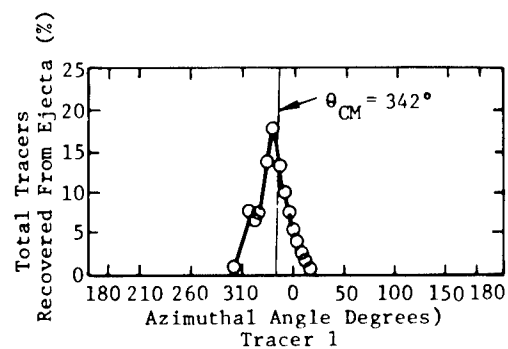
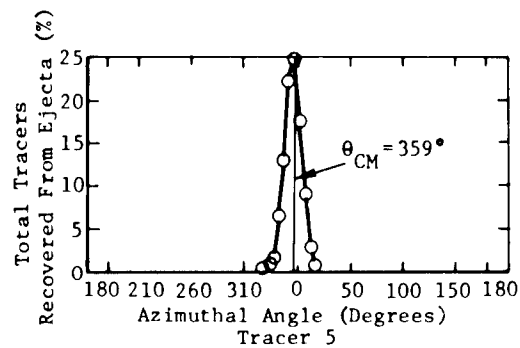
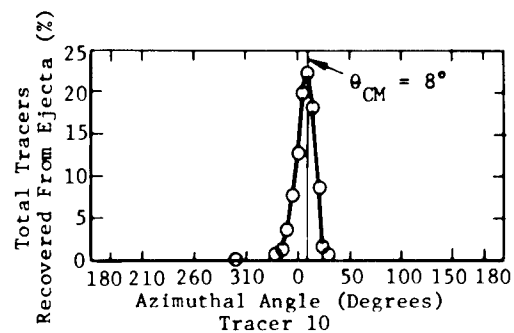
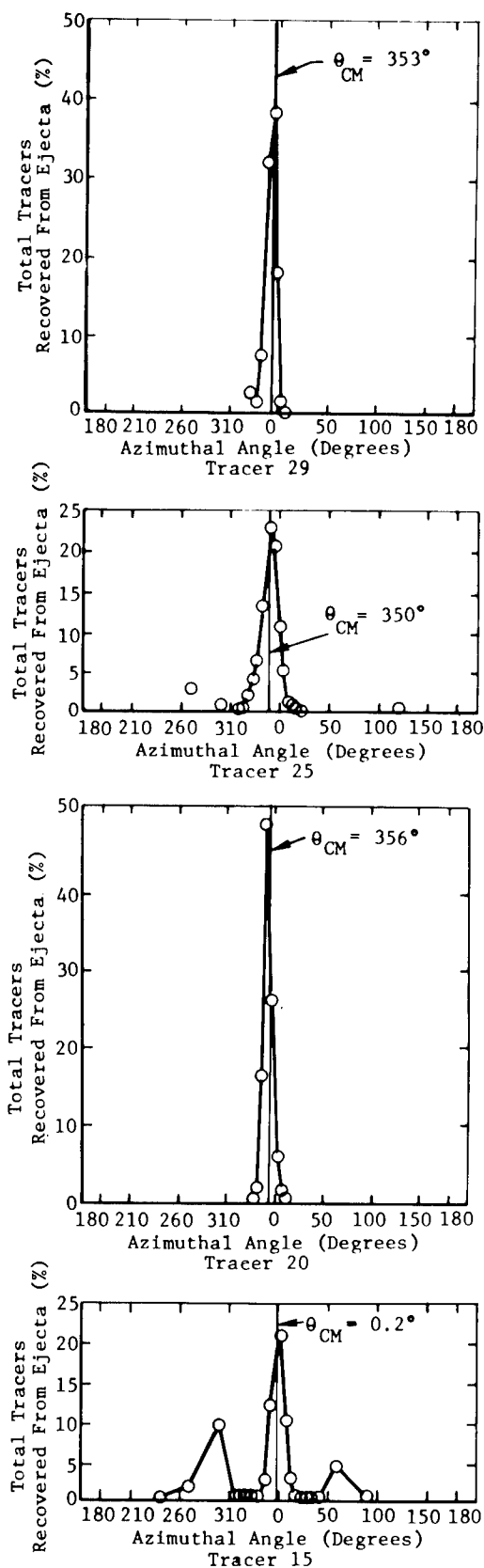


Fig. 8—Percentage of tracers recovered as a function of azimuth for tracers emplaced horizontally at the same depth (8-pound event at 3-foot burst depth)

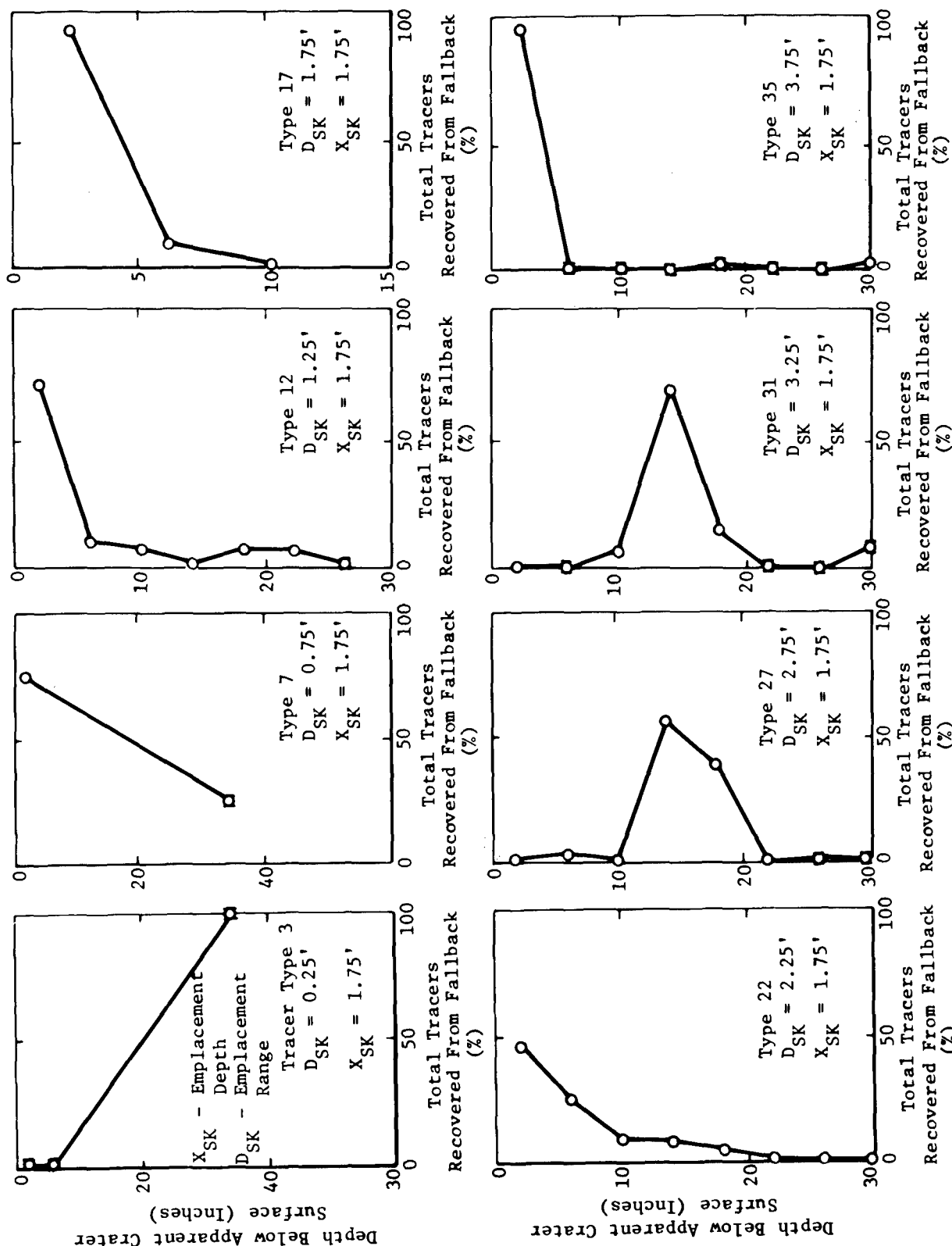


Fig. 9—Percentage of tracers recovered as a function of depth in crater fallback for emplacement locations horizontally at the same depth (8-pound event at 3-foot burst depth)

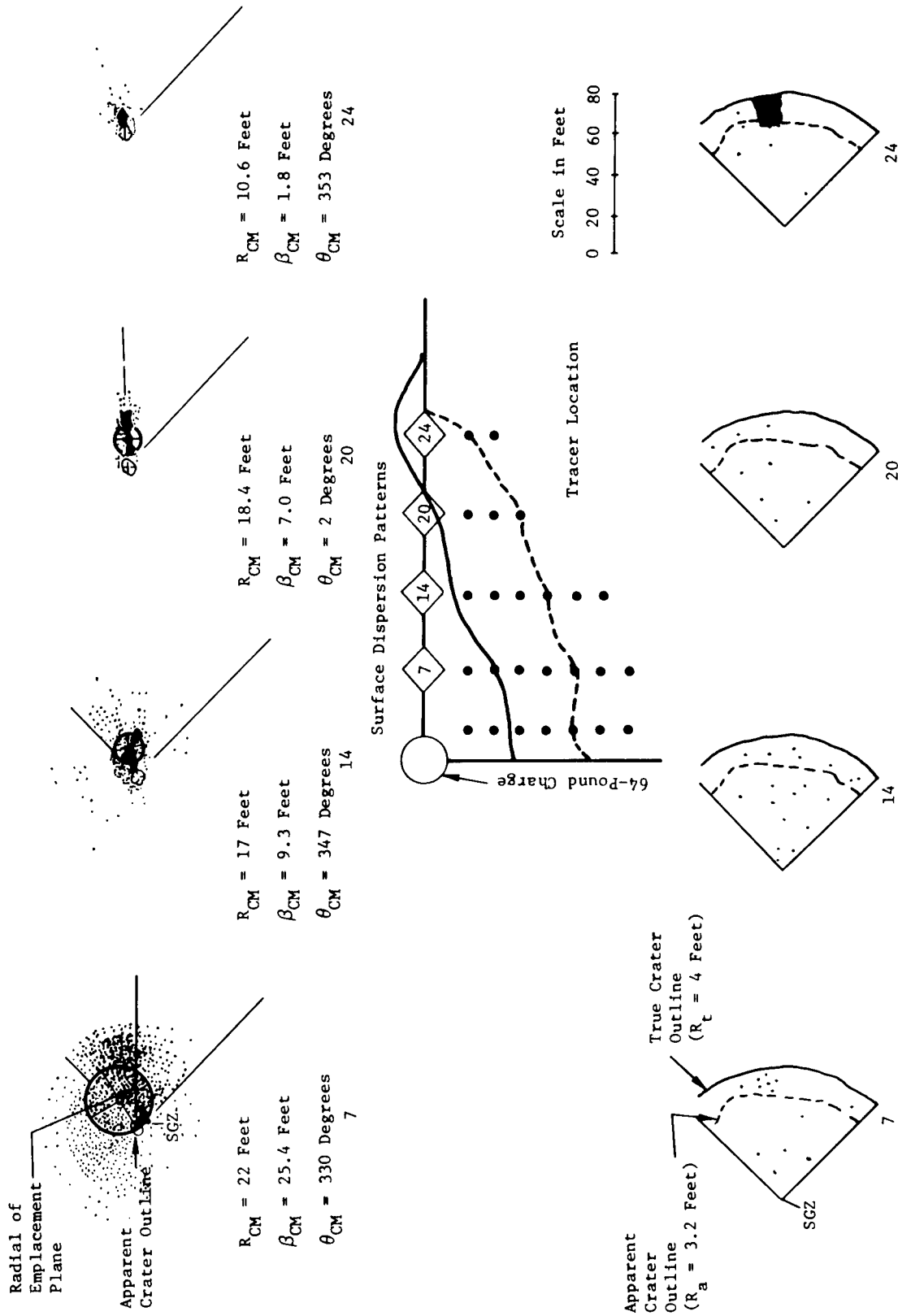


Fig. 10—The effect of tracer emplacement range on surface dispersion patterns for a 64-pound surface charge

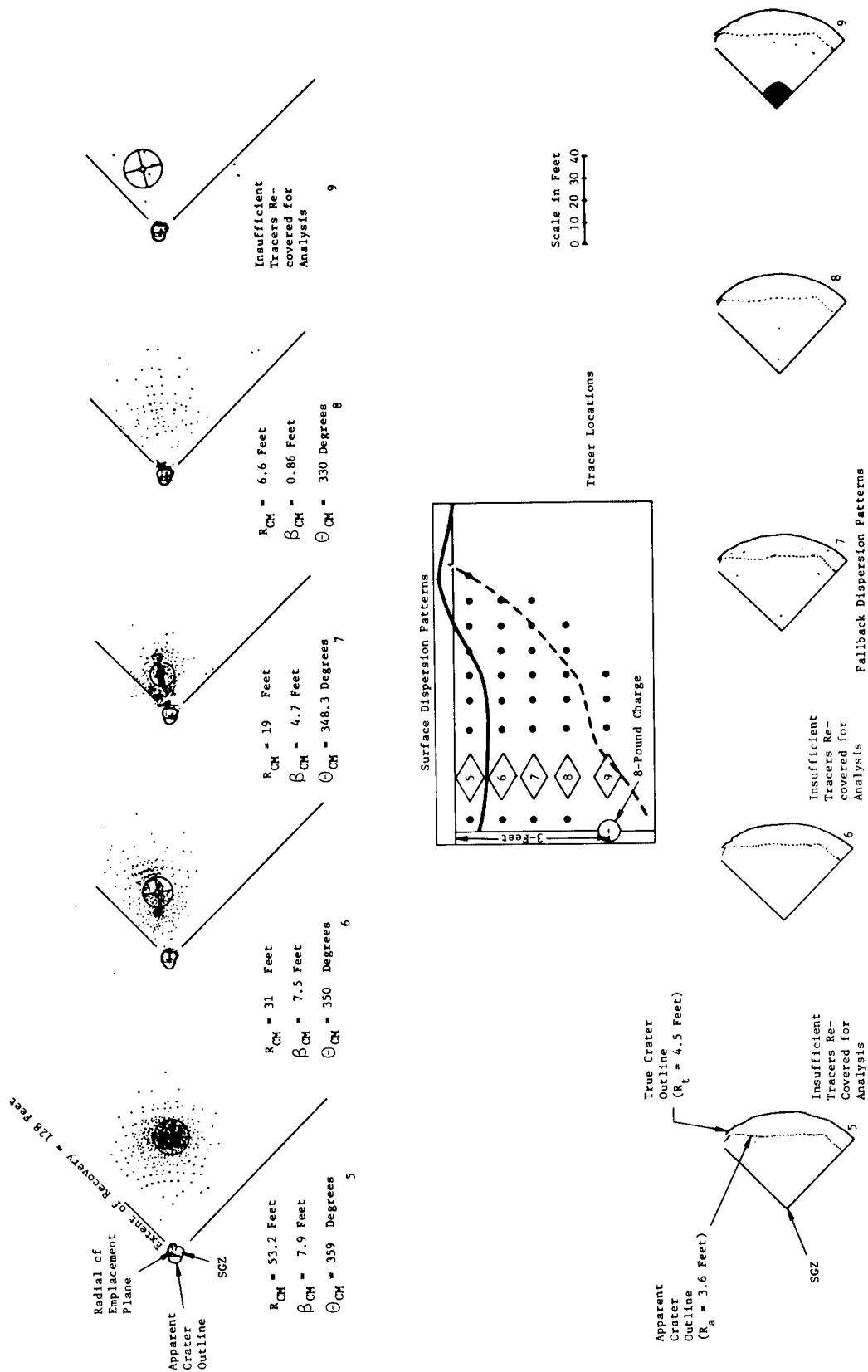


Fig. 11—The effect of tracer emplacement depth on dispersion patterns for an 8-pound charge buried at 3 feet

tracer 9 was recovered in the crater fallback close to its original emplacement position.

The effect of tracer emplacement depth on dispersion patterns for the 1000-pound surface charge is illustrated in Figure 12. Note the large difference between dispersion patterns for surface tracer location 7 and tracer location 8 (15 inches below the surface). Tracer 9 was totally recovered in the crater fallback. Apparently tracer location 10 spanned the true crater boundary because a portion (60 percent) was found in the original emplacement hole. Total tracers were found in original emplacement positions for locations 11, 12 and 13.

Figure 13 illustrates dispersion for a tracer location at 1.5 foot range from surface zero and 0.5 foot depth from ground surface for varying charge burst depth. Charges were 64 pounds and burst depths were 0, 4, 5, 6 and 7 feet. The charge detonated at the 6-foot depth produced the optimum crater. For the optimum cratering situation the center-of-tracer mass was at the greatest range, skewness was at the greatest counter-clockwise angle and dispersion (as indicated by the radius of the 50 percent circle) was least when compared to shots at lesser burst depths. For the event at a burst depth greater than optimum, the range to center-of-tracer mass and the size of the areal tracer pattern were significantly reduced. Figure 14 is an additional illustration showing the effect of charge burst depth on tracer dispersion patterns. For this illustration the tracer was emplaced at a range of 2.5 feet from surface zero and a depth from the surface of 2.0 feet. Again, the charge which produced the optimum crater (64-pound charge at 6-foot burst depth) exhibited a range to center-of-tracer mass which was greatest, tracer dispersion which was smallest and a counter-clockwise skewness angle which was greatest when compared to similar parameters for events at lesser burst depths. As observed in the previous illustration, for the charge at a depth greater than that which created an optimum crater, range to center-of-tracer mass and the size of the areal tracer pattern were significantly reduced. There seems to be a maximum range to center-of-tracer mass and a minimum tracer areal dispersion for the optimum crater when comparing these parameters for tracers at the same emplacement range and depth for the same charge weight at lesser burial depths.

The effect of charge weight on tracer dispersion is illustrated in Figure 15. Compared here is the 8-, the 64-, and the 256-pound events, each detonated at a scaled depth of $1.5 \text{ ft}/\text{lb}^{1/3}$. For these events tracer 6 is always at the same scaled emplacement location (range of 0.375 and depth of $0.50 \text{ ft}/\text{lb}^{1/3}$.) Note that the larger the charge, the closer the tracer is deposited to the crater on a scaled basis. It is also interesting to note that the percentage of tracers recovered in the fallback increased as charge weight was increased. This is true regardless of the scaling technique used for range, that is, whether distance to center-of-tracer mass is divided by cube root of charge weight or by apparent crater radius. Again, this is typical for comparisons of any set of tracers at the same scaled emplacement locations for the three charge weights included at a common scaled burst depth in this experiment.

Figure 16 shows dispersion patterns for tracers at close emplacement range and shallow emplacement depth for a 1000-pound surface and a 256-pound buried explosive charge. Tracers were emplaced at the surface for the surface charge and at a depth of 0.8 feet for the buried charge. Large tracer

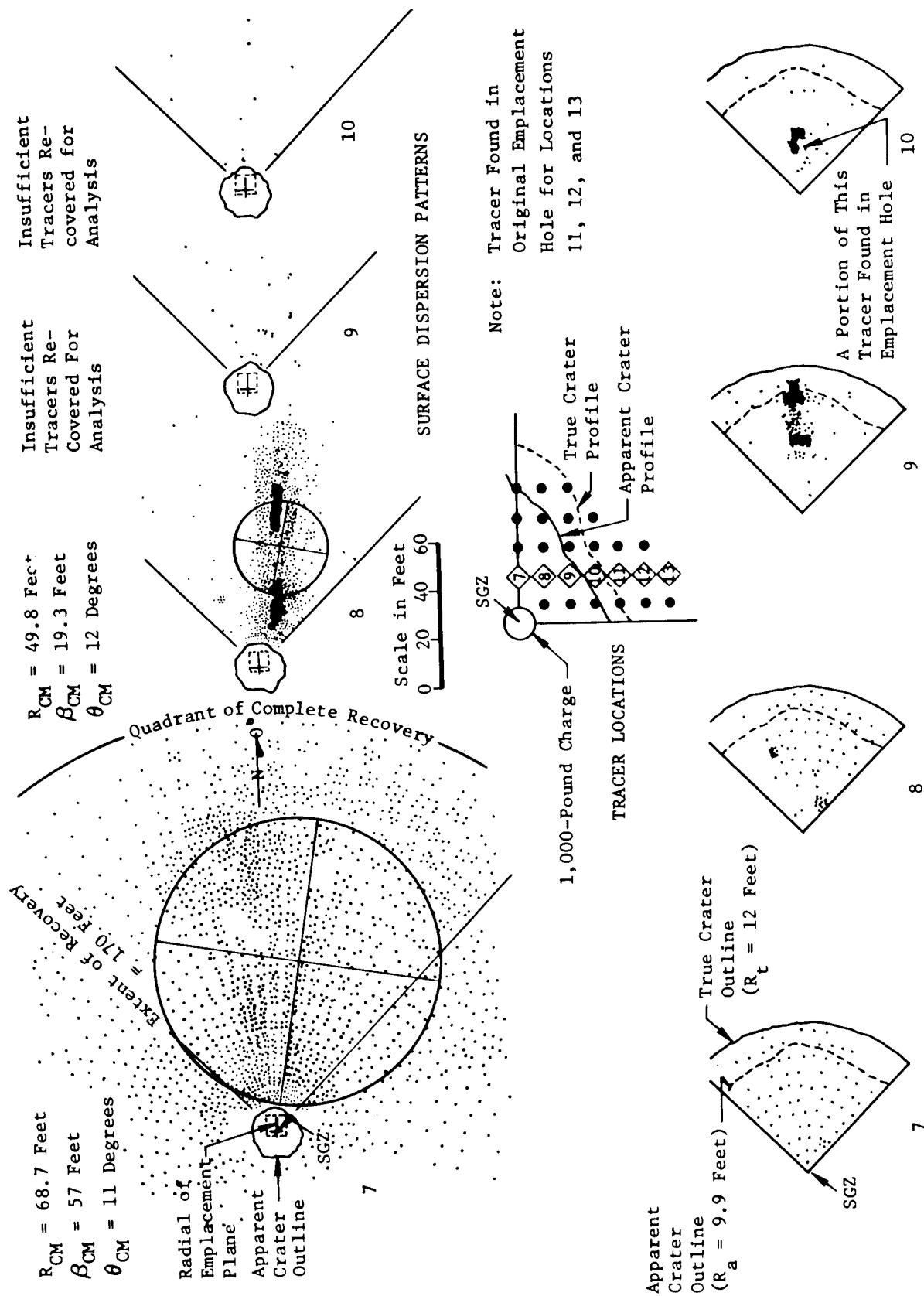


Fig. 12—The effect of tracer emplacement depth on dispersion patterns for a 1000-pound surface charge

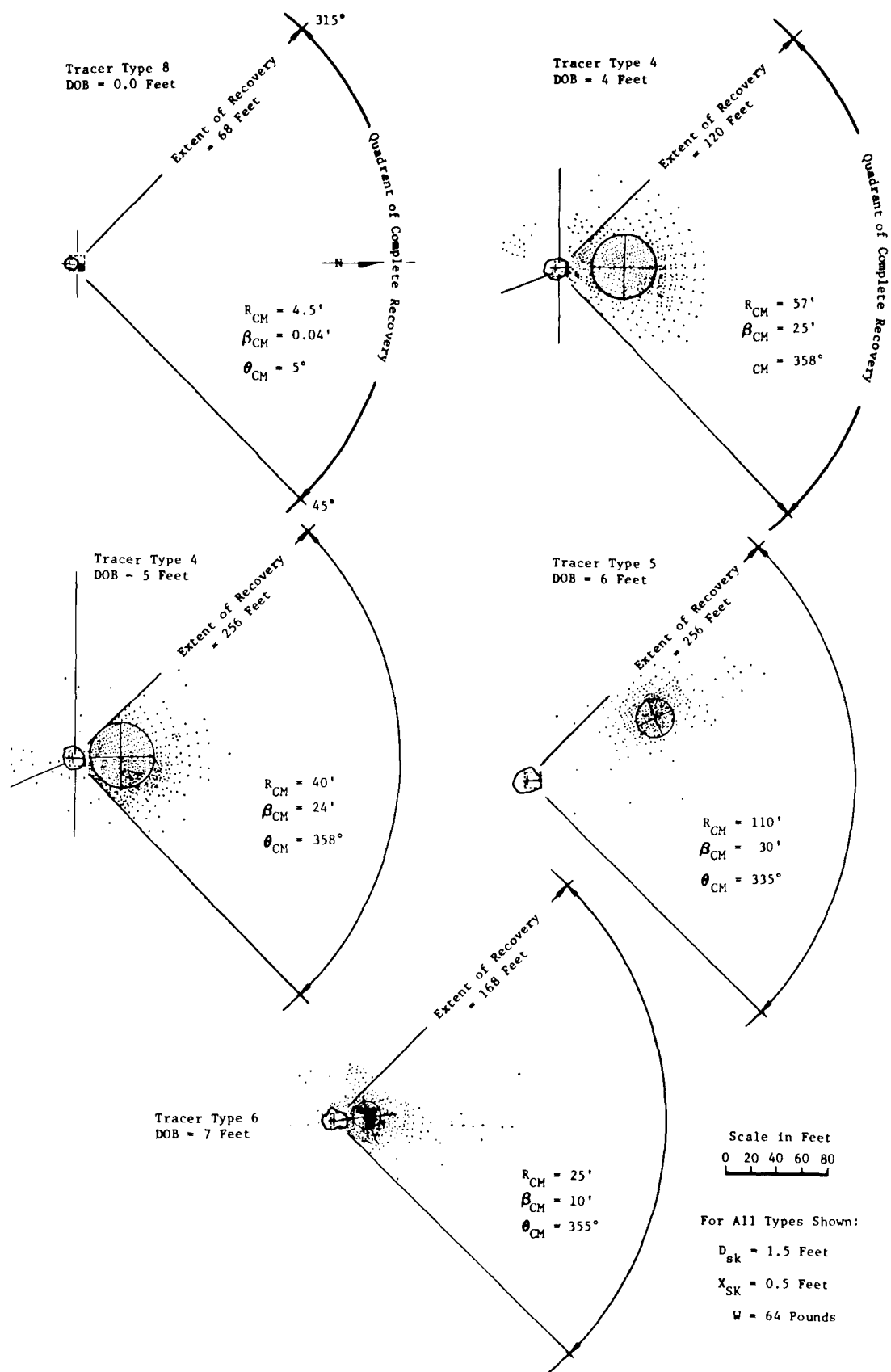
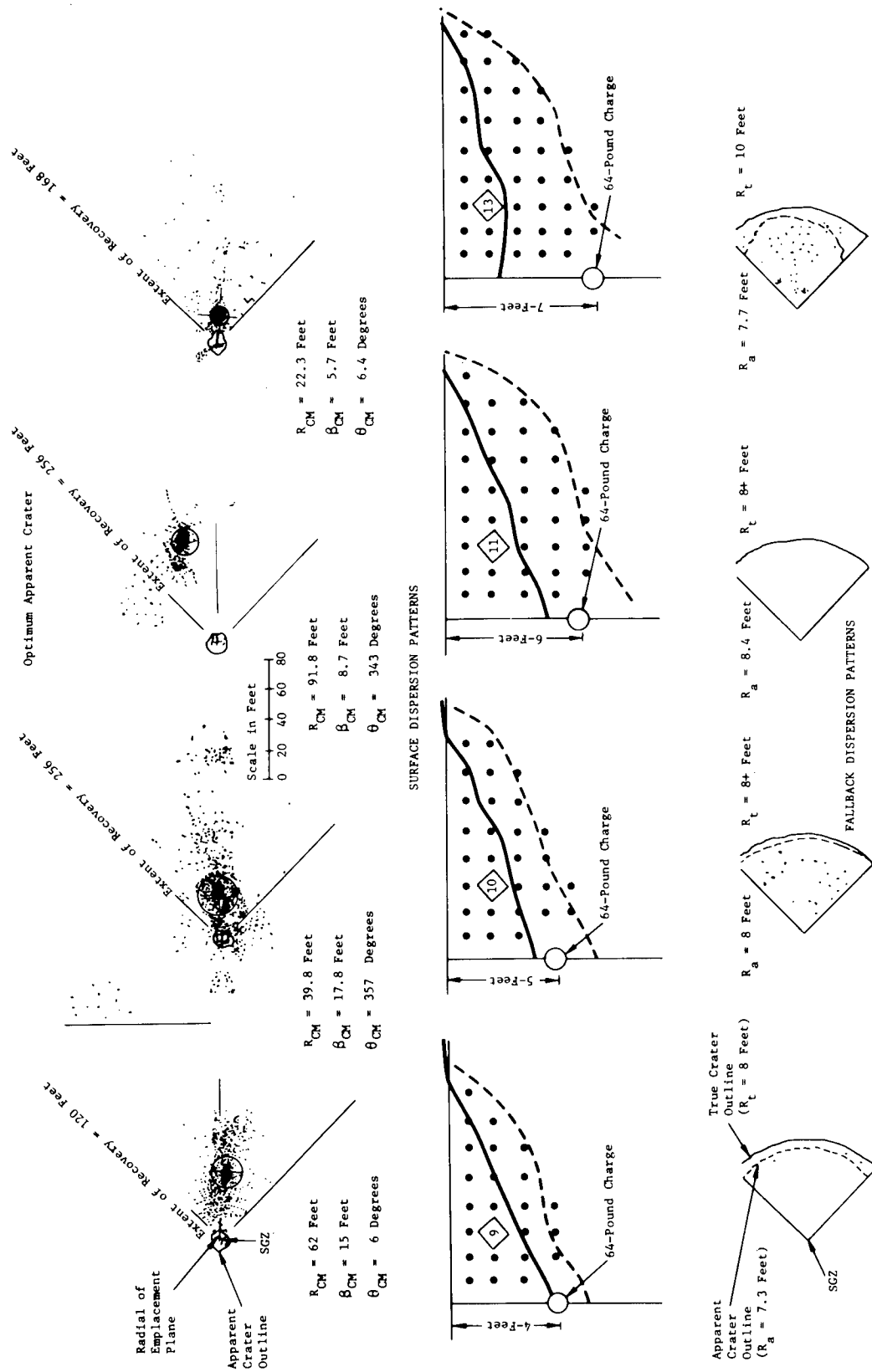
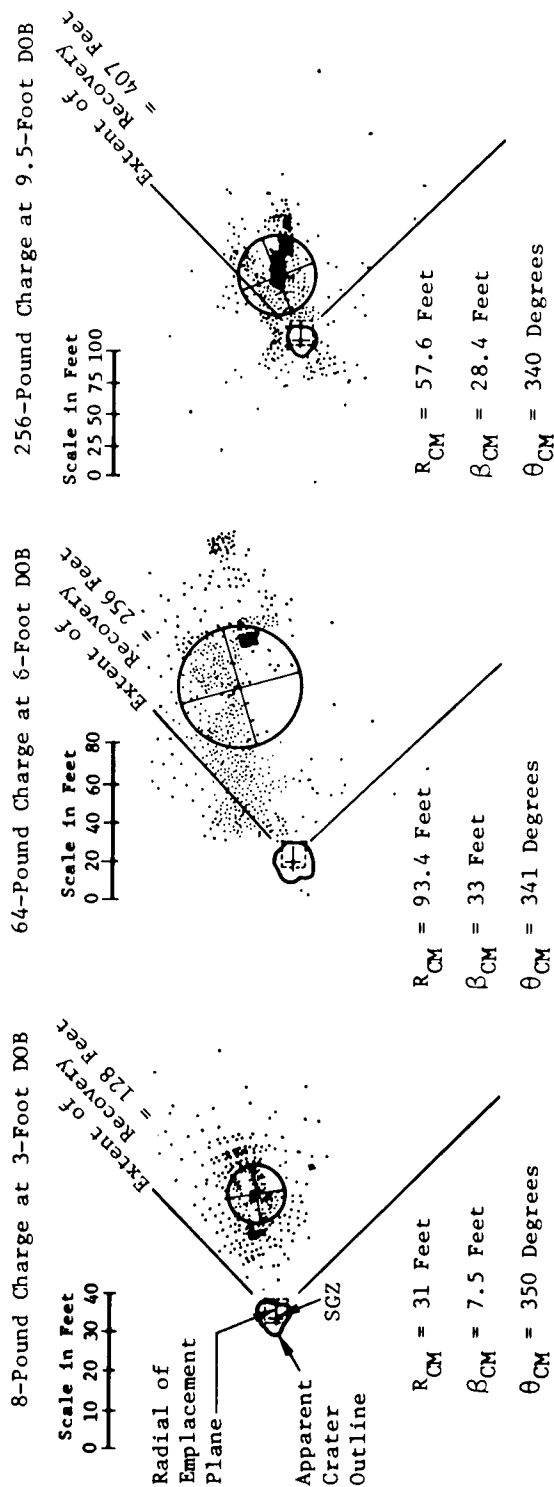


Fig. 13—The effect of charge burst depth on dispersion patterns for tracers at same actual near-surface location relative to Ground Zero (64-pound charges)

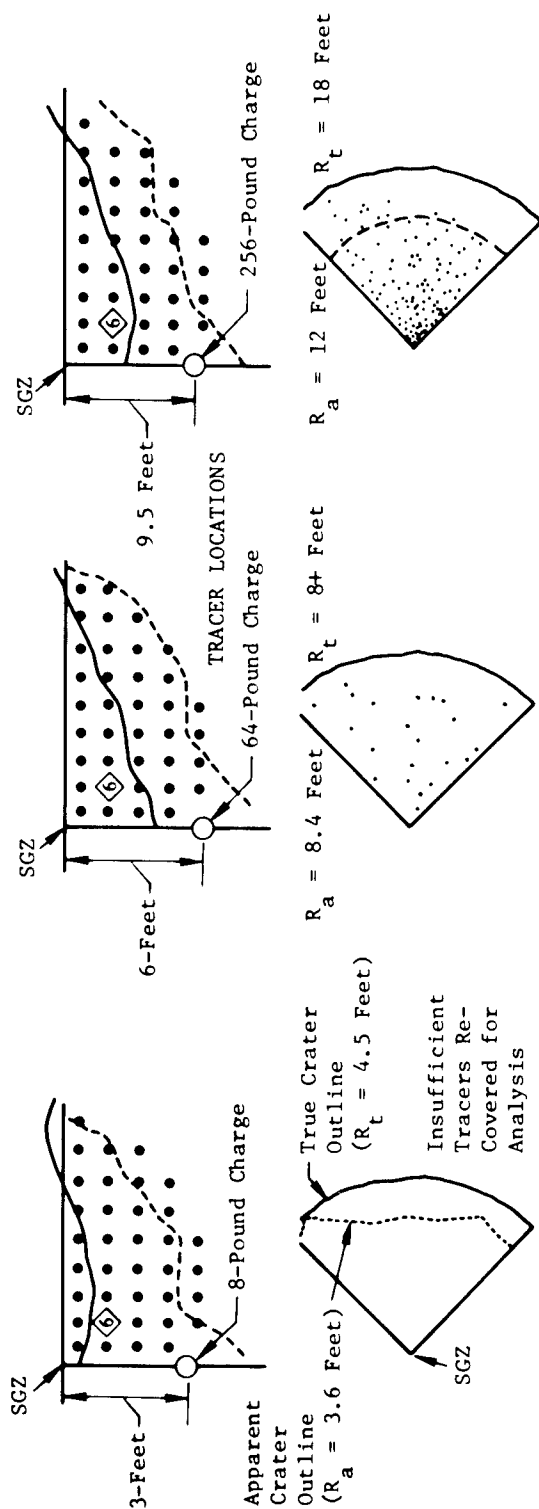


Note: All Tracers at Same Actual Emplacement Range and Depth.

Fig. 14—The effect of charge burst depth on dispersion patterns for tracers at the same actual buried emplacement location relative to Ground Zero (64-pound charges)



SURFACE DISPERSION PATTERNS



FALLBACK DISPERSION PATTERNS

Note: Tracer 6 For These Events at a Scaled Emplacement Range of $0.375 (Ft/Lb^{1/3})$ and Depth of $0.50 (Ft/Lb^{1/3})$ - All events at a Scaled Burst Depth of $1.5 (Ft/Lb^{1/3})$

Fig. 15—The effect of charge weight on tracer dispersion for charges detonated at same scaled burst depth ($1.5 \text{ FT/LBS}^{1/3}$)

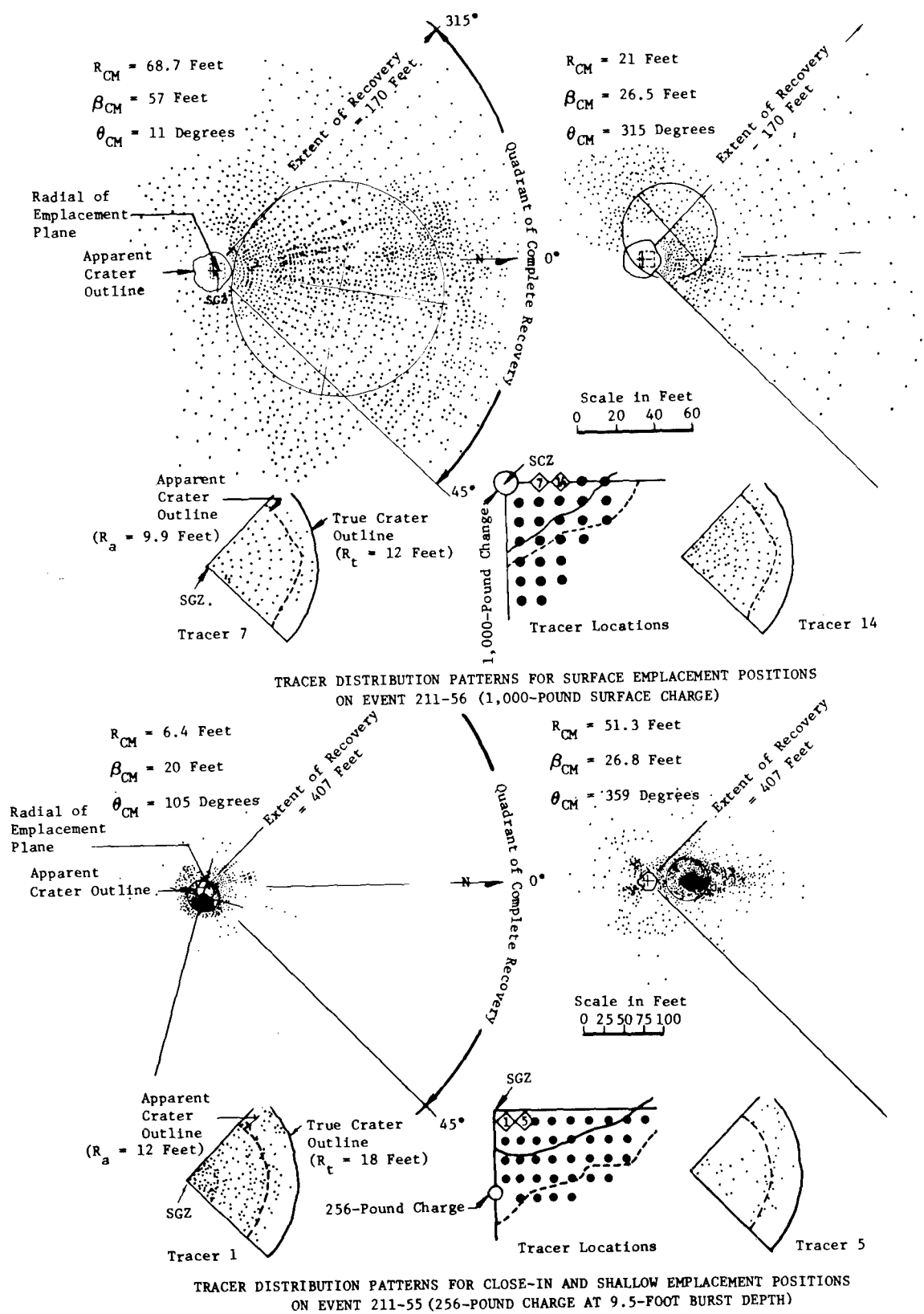


Fig. 16—Tracer dispersion patterns for close-in and shallow emplacement positions for a surface and buried charge

areal dispersions were observed for the surface event when compared to the buried charge. It should also be noted when making this comparison that tracers were closer to surface zero (on a scaled basis) for the buried charge. This greater areal dispersion is probably due to a higher range of divergence in initial particle exit angles and to particle interaction with greater gas turbulence when compared to similar parameters for the buried charge.

EMPIRICAL MODEL

It is possible to make an empirical prediction of ejecta areal density as a function of radial range using only tracer data. Inasmuch as direct measurements of ejecta areal density were made over a rather large surface area for each event in this experiment, such an empirical model can be checked for accuracy.

Referring to Figure 17, consider a ring-shaped mass element (rectangular or square cross-sectional) with its centroid at a radius D_{sk} and depth X_{sk} (oriented in a plane parallel to the ground surface.) Consider further that the center of this ring is at the vertical epicentral axis through the charge and Ground Zero. Such a ring element may be constructed as a solid of revolution by rotating one of the cross-sections shown in Figure 17 through 2π about the vertical axis. We can assign a mass M_k (k is an index of tracer position) to each ring mass element by multiplying the volume of each ring by the in situ soil density. Although our single point tracers exhibit a radial and azimuthal dispersion, one can speculate that a ring tracer source would exhibit radial dispersion only. In other words, azimuthal variations would average out if there were no rays produced. If this is the case, after detonation ejecta from the ring mass element would be distributed uniformly at any radial distance for all azimuths, that is, the same radial dispersion will be observed for all azimuths. By making this assumption the dispersion of the ring mass element can be expressed wholly in terms of radial dispersion. Furthermore, radial dispersion of a single point of this mass element (such as that represented by a zone of particulate coded tracers) should approximate the radial dispersion of the ring mass element for any azimuth. When radial percentage data such as obtained in this experiment are used, one is actually using data for all azimuths.

In this study we obtain ejecta radial percentage distribution for each tracer and the fraction of the total recovered amount of each tracer which is found in the ejecta. We can enforce the assumption that each M_k (ring mass element) be distributed radially for any azimuth according to the radial distribution of tracer type k . We first obtain the fraction m_k of M_k which becomes ejecta by simply multiplying M_k by the portion of tracer k which is recovered from the ejecta. We then assume each m_k is distributed radially along all azimuths as observed radially for tracer type k . In an approximation this observed radial dispersion is in the form of tracer recovery data, that is, percent of total tracers in ejecta between two ranges (D_i to D_{i+1}) at all angles, versus the mean of these ranges,

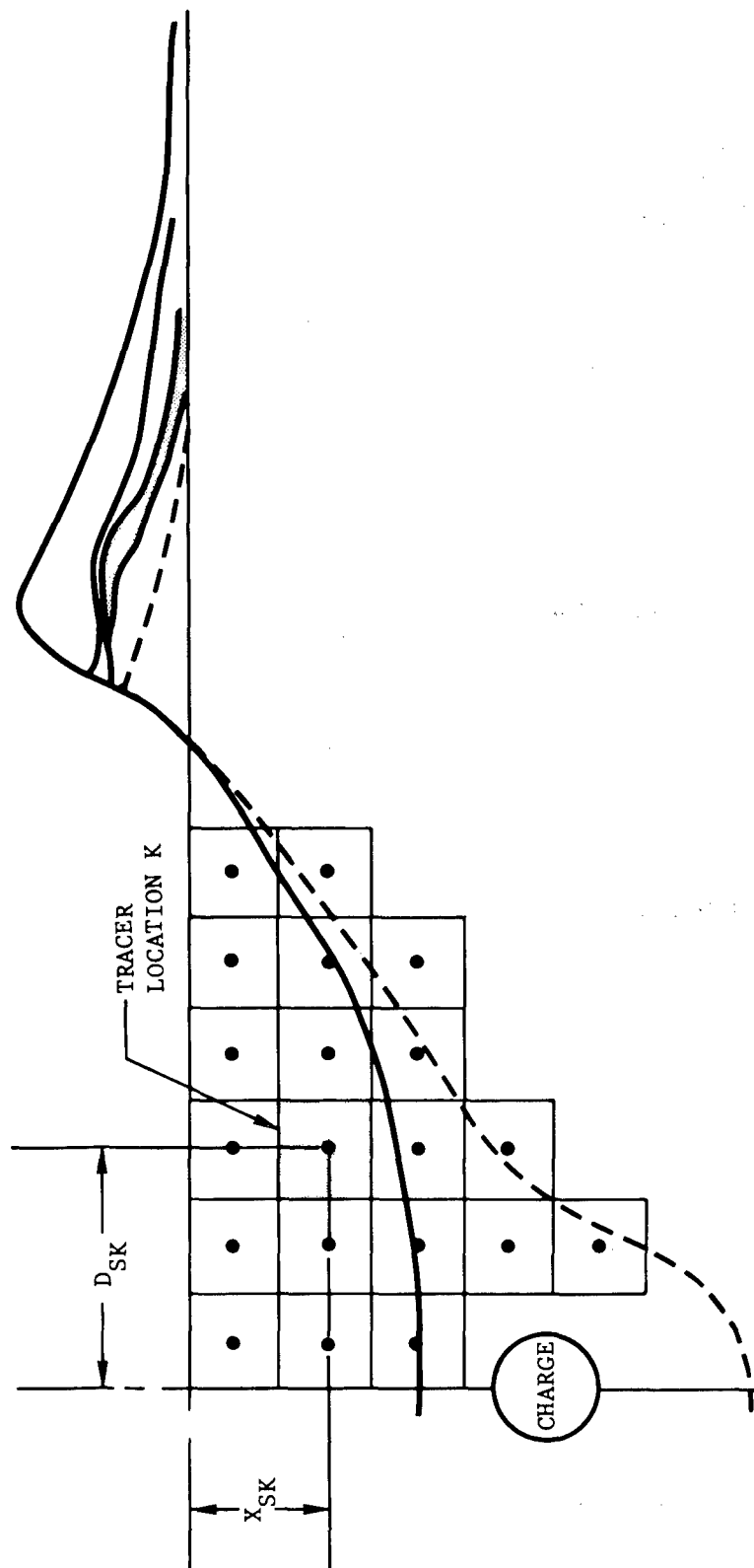


Fig. 17—Illustration of method for determining ejecta areal density using coded tracers

$$\left(\frac{D_i + D_{i+1}}{2} \right)$$

Next, we need a function $P_k(D)$ where P_k is percent of tracers on surface at range D . To a simple approximation, a logical and rather simple function is the normal or gaussian distribution function described in a prior section of this report and illustrated in Figure 8.

Accepting this normal distribution function we can now assume that for tracer position k we have a ring mass element M_k of which a fraction becomes ejecta, m_k . This ejecta mass, m_k , is distributed radially according to the gaussian relationship. We can define a new value, m_{ki} , by the following relation:

$$m_{ki} = m_k P_{ki}$$

where

$$P_{ki} = \int_{D_i}^{D_{i+1}} P_k(D) dD$$

and m_{ki} is the portion of m_k of ejecta between the ranges D_i and D_{i+1} . The total amount of ejecta between D_i and D_{i+1} , (m_i), is then given by:

$$m_i = \sum_{\text{all } k} m_{ki}$$

An areal density value (δ_i) may now be obtained by the relation

$$\delta_i = m_i / \pi (D_{i+1}^2 - D_i^2)$$

A log-log least squares fit may be made to the areal density versus range data

$$\delta_i \text{ versus } \frac{D_i + D_{i+1}}{2}$$

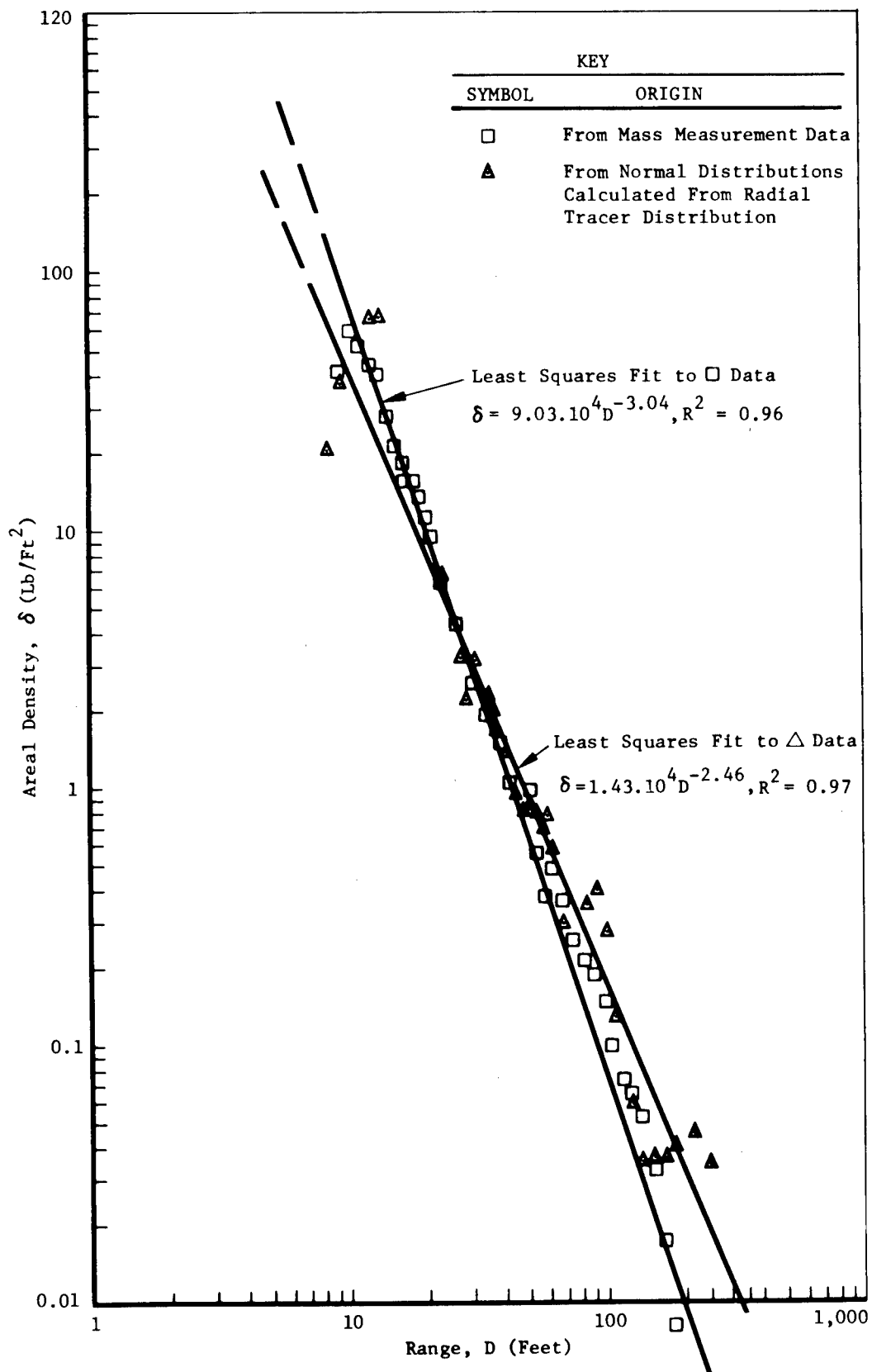


Fig. 18—Comparison of measured to calculated areal density ejecta data for the 64-pound charge detonated at 6-foot depth

to obtain a relation of the form

$$\delta = KD^{-b}$$

which may be compared with a similar relation determined from experimentally obtained ejecta data.

An illustration of areal density data determined from this model is shown in Figure 18. The event was 64 pounds detonated at a depth of 6 feet. For the measured data a least squares straight line fit yields a correlation coefficient of 0.97. For the calculated or model data a least squares straight line fit also yields a correlation coefficient of 0.97. The relationship between these areal density relationships is also illustrated in Figure 18.

CONCLUSIONS

The following conclusions regarding tracer dispersion are drawn from this experiment:

1. As a first approximation, many tracer dispersion patterns appear to be gaussian.
2. There is a tendency for range (to center-of-tracer mass) and dispersion to initially increase and then decrease as tracer emplacement horizontal range from the epicentral explosion axis is increased.
3. There is a clear tendency for range (to center-of-tracer mass) and dispersion to decrease as tracers are emplaced deeper.
4. Range (to center-of-tracer mass) tends to increase with increasing charge burst depth until optimum is reached after which this range decreases.
5. When dispersion parameters were compared for charges of differing weights detonated at the same scaled burst depth, similar tracers were deposited closer to the crater and exhibited lesser areal dispersion (on a scaled basis) for the larger charge.
6. Over 60 percent of the tracers included in this experiment exhibited a counter-clockwise skewness of their centers-of-tracer mass.
7. Increasing tracer emplacement range and depth results in increasingly deeper deposition of the tracer in the fallback.

REFERENCES

1. Flanagan, T. J., Crater Studies, SC-RR-64-1704, Sandia Laboratories, Albuquerque, New Mexico, April 1966 (U).

AN INTERIOR SEAWAY FOR NORTHERN AFRICA

J. B. F. Champlin*
Westinghouse Electric Corporation
Environmental Systems
J. W. Poston, J. A. Lake
Georgia Institute of Technology

FOREWORD

One of the difficulties confronted in advancing explosives-engineering is that experimentation is both hazardous and expensive. This is particularly true of engineering experiments employing nuclear explosives, because there is a possibility that personnel located many miles from the center of the atomic blast may suffer from fallout or the migration of radioactivity through ground-water to public sources of drinking water. As a consequence, in order to establish courses of instruction in nuclear explosives engineering, it is necessary to use the special technique of deep consideration of a problem as a substitute for a laboratory exercise. This paper represents a summary of one such exercise in which students were assigned the task of performing the preliminary engineering on a project which could, if implemented, have considerable beneficial effect on a rather large area of the world. The possibilities of this project coming into being are quite remote in our time, largely due to the political ramifications and the current tendency to overemphasize the hazards of anything pertaining to nuclear explosions. But, as a classroom device, the use of the Project Analysis as a teaching tool has proved invaluable in training the students to think of the whole system involved rather than a part of it. This paper, primarily a summary of a report submitted by a student team in the course of Engineering with Nuclear Explosives at Georgia Tech in the summer of 1968, speaks for itself in its inventiveness and its expression of deliberate concern for the betterment of mankind. A minimal amount of additional material was added by the senior author to draw attention to recent related events and publications.

The students named the study "Project Pecos Bill" after an American folklore character, a mythical super cowboy who invented roping and other cowboy skills. During a very dry spell, Pecos Bill is said to have used a pointed stick to dig the Rio Grande River and bring water from the Gulf of Mexico. The poignant results of his work can be seen in the agricultural splendor that is the Rio Grande Valley. The parallel to this present study is obvious.

* Formerly at Georgia Institute of Technology.

INTRODUCTION

After the U. S. Atomic Energy Commission established the Plowshare Program in 1957 to investigate and develop peaceful uses for nuclear explosives, several possible applications were considered that were primarily large scale excavations of a magnitude greater than was economically feasible with conventional explosives. To date, these peaceful applications of atomic energy have been restricted to experimental blasts in several different media and depths, two of the more recent being the gas-sands shot at Rulison, Colorado and the deep blast in the igneous rock of the Aleutian Islands. Until early in 1969 it was hoped that it might be possible to make a real excavation for a harbor on the west coast of Australia to aid in the shipping of newly proven deposits of iron ore. Unfortunately, that development was postponed rather indefinitely.

Nonetheless, many regions of the world could greatly benefit from applications of nuclear explosives. In spite of the emotional and political deterrents involved in the use of nuclear explosives, the prime reason for their use is economy. This is true even in this day of rapidly developing social conscience about contamination of the atmosphere and hydrosphere. There is no less expensive source of large quantities of energy and no less expensive way to move large quantities of earth than with nuclear explosives. Man now possesses the ability to control this explosive energy and from it derive enormous benefit. Through such studies as this, it may be shown that nuclear explosive engineering can be far less contaminating to the environment than the conventional alternative methods for doing the same job. To determine and examine the criteria for such a task can be sufficient justification in itself. This report is such a study.

The area chosen for this study was the chott region in central Tunisia and Algeria, North Africa, Figure 1. This region is characterized by the series of so-called dry lakes or "chotts" which stretch across a considerable section of the northern Sahara desert region from the Gulf of Gabes in Tunisia on the east to the eastern borderlands of Morocco on the West. The sections in Tunisia and Algeria appear on the geographic maps to have been parts of a bay-like extension or arm of the Mediterranean Sea which recently (geologically speaking) have been cut off by the intrusion of sand bars and sand dunes. Construction of a canal by nuclear excavation would open this area to the sea.

The immediate benefits of such an excavation are several:

- 1) A plentiful water supply could turn this arid land into a more useful agricultural area. New developments in arid-agriculture in Israel have shown that the problematic sand dunes can be a blessing in disguise when combined with irrigation from salt water sources such as seawater.
- 2) Tunisia has about one-third of the world's phosphate deposits. The proposed canal would provide a sea route to within 25 miles of those deposits and could conceivably make them more economical to mine and market.

- 3) Such a canal would provide ready access to vast petroleum deposits in east-central Algeria. At present the petroleum produced in this area must be moved via pipeline over the Atlas mountains to the coastal cities of northern Algeria.

The impact of such a project on the entire economic structure of both Tunisia and Algeria is difficult to evaluate at this point. The very presence of the waterway and relatively large lagoons would provide excellent opportunities for recreational development. While considered fairly remote at present this area is much closer to large population centers than many of the coastal African cities now used by Europeans for recreational spots, such as Dakar, Agadir, etc. Potential changes in humidity could enhance rainfall probabilities not only in Tunisia and Algeria but possibly in other countries such as Libya and Egypt. Salt farming, for centuries the prerogative of legendary Timbuctu, could take place in various locations across north Africa with better production methods and products. Indeed, cave paintings found in the southern Sahara suggest that well established agriculture and much game (now restricted to savannah country far to the south) once existed here. Obviously, the economic potentials could be as great as there are imaginative minds and ambitious capital to bring them about.

Project Pecos Bill, as it was originally conceived, would link several of the larger chotts and would terminate at the Chott Chergui. The lack of concrete geologic and physiographic detail on the area and deeper consideration of the proposed route to Morocco made it advisable to terminate it in the Chott Djerid. While the possibility of extension of the project to full length is good, engineering planning for that extension must wait until more adequate information on the area becomes available.

The Physiography of North Africa

The north coast of Africa west of Libya features a rather continuous chain of mountains of moderate height. These mountains have their easternmost expression in the highlands of northern Tunisia. South of this relatively narrow mountain chain that characterizes northern Algeria and Tunisia is a series of wide basins, the centers of which are commonly below sea level. The climate in the area of the basins is predominately arid with an annual rainfall of a few hundred millimeters. Even in the highlands the rainfall passes through a "ten" year cycle and the monthly discharge of the Wadi Nabhanah varies through the year from about 0.05 cubic meters per second to as much as 25 M³/s. The level of the fresh groundwater in the countryside surrounding the basins is strongly influenced by the degree of accumulation of runoff in the so-called dry lakes or "chotts" that occupy the central or deepest portion of the basins.^{1*}

Despite the physiographic appearance of the chotts that suggests a geologic history as an arm of the Mediterranean Sea, paleontologic evidence does not seem to justify this assumption. The Chott Djerid is a basin caused by tectonic movement during Cretaceous and Tertiary times and much of its present depth is attributed to the scouring effect of the desert winds. Chott Fedjadj is located between two prominent anticlines. The Tebaga Dome extends for approximately 100 kilometers (62 miles) along the entire southern boundary of the basin from Chott Djerid to the easternmost point of Chott Fedjadj where another anticline begins that extends roughly 20 kilometers (13 miles) to the Gulf of Gabes. Along the northern reaches of the chott area a system of anticlines extends approximately 250 miles from west of the Chott Djerid eastward to the Gulf of Gabes. The Djerid Range of mountains formed by these anticlines reach elevations greater than 600 meters, dropping off rapidly to the south to elevations below sea level in the chotts.²

Terraces which rise a few meters above the saline flats of the sebkhas** or more generally the haliferous steppes that surround the sebkhas, are vestiges of a series of geologic events that date from the early Quaternary geomorphic processes. These are best seen in the Cardium lagoon sequence which dates from the Villafranchian. Many of the terraces are structural and contain intercalations of massive beds of gypsum in the Villafranchian lagoonal facies which locally includes a gypsiferous Cardium coquina. Gypsiferous surface deposits on the terrace surfaces serve to protect them from erosion by the wind. No doubt the fact that the evaporation rate is on the order of 5 to 10 times the precipitation rate in this area helps to maintain these vestiges of earlier times through the continual redeposition of dissolved salts in the surface soils.^{3,4}

The soils in the Chotts and directly east toward the Gulf of Gabes is an alluvium of clay-marl with some sand and salt encrustation. The southeastern shoreline of Djerid appears to contain a large proportion of sand with many irregular dunes. Along the Fedjadj shoreline, clays that originated from weathered limestone predominate. Further from the basin center, alternating layers of clay and calcareous material appear on both sides of Fedjadj.

* Superscript numeral refer to the Reference list at the end of the paper.

** The term sebkha refers to the general flat plain area in which the dry lakes occupy the most depressed position.

Two fault zones extend perpendicular to the anticlines mentioned above in the eastern section of the Chott Fedjadj. This region appears to be severely faulted. One of these faults, crossing the Fedjadj at the mouth of the Nakrla River (wet weather flow only), is located at the narrowest point of the chott.^{2,4} This fault could pose a problem since large nuclear devices would be required to excavate the channel here. The eastern fault line should present no problems since it is not in an area where extensive excavation would be required.

The primary area of excavation obviously must be in the thirteen mile area between the eastern points of the Chott Fedjadj and the Gulf of Gabes. One obvious route extends along the Telman and Akarit Rivers, the former flowing into Chott Fedjadj and the latter flowing into the Gulf of Gabes. This route is primarily composed of undulating alluvium and sand with dune heights up to about 75 meters. The drainage divide for the two streams is estimated at 30 to 40 meters above sea level. While there is a possibility that this height may be primarily the result of centuries of worked and reworked sand dunes that are salt-cemented in part, there is an equal chance that they are underlain by a rock level that is higher than in the chotts because of the intersection of the anticline systems. Only geophysical and coring studies can determine this point. The determination of paleoecological conditions in the general basin area may give substance to one or the other possibility. However, geomorphic tilting of the basin bottom may have favored fresh-water outflow to the east from the chotts at one time while permitting marine flooding or seepage through the sand dune "plug" at another.

Along this route 300-foot borings at one kilometer spacing would be desirable. In the chott itself (Fedjadj) the same approximate depth of bore hole could be maintained at a 3 kilometer spacing. Assuming uniformity of the profile, this program could be extended into the Chott Djerid. Extra boring or coring in the faulted areas should be used to define conditions better in those regions. The alluvial soil along the route and the frequent fault zones and anticline structures will serve to restrict shock wave propagation from the nuclear blasting. At least one cratering experiment should be included in the Chott Fedjadj to provide local material constants for the cratering equations.

Environmental Survey

In such a project, it is desirable to conduct pre-shot and post-shot environmental surveys. Of the two, the pre-shot survey is more likely to be time consuming and expensive, for it must set the stage for the post-shot survey. Such an environmental study must include such topics as a qualitative and quantitative radioactive analysis of typical surface soils, plants and animals to determine the various routes taken by radionuclides into the food chains. This should include all elements possible that might be produced in the nuclear reaction (at least as groups) even though they have not been established as necessary constituents of the nutritional (micro- or macro-) requirements of living things.

The proposed canal would form an inland embayment from the Mediterranean Sea from what is now the Chott Djerid and possibly sections of Chott Djerid. The aquatic life of the chotts is probably similar (if it exists at all) to that of the playa lakes of Nevada, consisting of some forms of algae, bacteria, brine shrimp, etc., that are capable of enduring dessication during part of the year. The water that occasionally fills the chotts is probably never in a state that could be called "fresh" because of the ready availability of soluble salts in the chott sediments and in the subsoils of the terraces and hills surrounding the area. Consequently, the aquatic life of concern would be that introduced by the opening of the chott area to the sea and it would primarily be derived from the Gulf of Gabes.

A preliminary survey of the marine life in the Gulf of Gabes indicates that those which would quickly migrate into the seaway and inner salt water lakes would be the sardines, pilchards, tunny, whitefish and sponges.⁵ Some ecologic consideration also should be made of the possible local damage to aquatic life in the Gulf by the outflow of the more saline and relatively warmer waters from the flooded chotts.

The micro-organisms most likely to be involved in concentration of radioactive traces of various nutritional elements are the phytoplankton. These simple plants, characteristic of all aquatic environments, serve as food to almost all levels of fish and other aquatic life. After they have died or been killed by some environmental change, their organic and inorganic remains serve as nutrients for other sea plants and bottom feeders. Lowman^{6,7} found these phytoplankton to concentrate such induced activities as ⁶⁵Zn, ⁵⁷Co, ⁶⁰Co, ⁵⁴Mn, ⁵⁵Fe, ⁴⁵Ca, ⁴¹Ca to a greater extent than fission products. Since these isotopes represent typical minor to major constituent ions in the salts or residual clays described for the chott areas, they are certainly of concern. In addition, ⁹⁰Sr and ¹³⁷Cs also may be concentrated by the phytoplankton in relatively large quantities.

The radioactive materials produced by the nuclear explosions probably will not present any hazard to the workmen concerned with construction of the canal. However, once the seaway has water in it, the radioactive nuclides will have the opportunity to diffuse into the aquatic environment. Since fish tend to concentrate the ferrous metals, zinc and manganese, it would be advantageous to minimize the content of these materials in the explosive devices. Use of borated materials in the explosive devices might also help reduce the development of induced activity in soil minerals. A continuous survey on the economically important fish species for about one year after introduction of water into the area would be imperative. It is doubtful, however, that an effective ban on fishing in the Gulf could be enforced for this period even if it were desirable. Control of the chott area would provide sufficient data on radionuclide retention by induced species of fish and plant life. Finishing the seaway after the use of explosives will take at least a year so fishing restrictions in the chotts could be maintained during this period.

The domestic animal life in the southern region consists of camels, cattle, broad-tailed sheep and goats. The wildlife consists of gazelle, antelope, fennec and small rodents. Bird life in this portion of Tunisia is not rich but includes such species as grouse and bustards. Reptiles such as monitors, horned vipers, and oil palm lizards are also found in the area but in general do not constitute a common segment of the food chain.^{5,8}

The land plant life in the area consists of shrubs, wild grasses and bushy-joint fir. There are minor opportunities for small scale irrigation of vegetables, forage crops, and dates in the area but the severe variation in rainfall restricts the number of farms possible under such a system at present. Most important economically are the olive and citrus groves, the former being most prevalent along the more humid coastal areas between Gabes and Cekhira.⁸

Probability of migration of radioactivity buried in the debris of a crater to plant roots in an irrigated farm under the hydrographic conditions of the area is quite small within the lifetime of the radioisotopes produced. However, foliar deposition from fallout would be a distinct possibility within these lifetimes. The relative uptake of various radionuclides from soils is approximately the following:

Sr >> I > Ba > Cs, Ru > Ce > Y Pm, Zr, Nb > Pu.

While it is unlikely that foliar adsorption to the exterior of the plant would occur in that order, one might have to be concerned about the same group. Actually, the heavy oil coating on the surface of the leaves of olive and citrus trees would favor the penetration of those elemental, oxide, or ionic forms that are most soluble in organic solvents. The fraction of radionuclides formed that would escape from the crater would be small; nonetheless surveillance of the plant consumption in the area should be maintained to minimize the possibility of radionuclides reaching the food chain of man. Complete quarantine for human and animal consumption of any vegetation until the completion of the project (2-5 years) would be an expensive and probably unnecessary restriction to avoid contamination. More to the point would be the removal and burial of all plant life near the excavation found to be significantly contaminated and the establishment of a commission that would actively monitor plant and animal life in the area to determine if any significant levels of radioactivity develop.

The route chosen would enter the Tunisian Coast from the Gulf of Gabes approximately 20 miles north of Gabes. Continuing on a west-south westerly direction until it reaches the Chott Fedjadj, it then would run generally westward until reaching the Chott Djerid. Table 1 lists the major population centers that might see or experience some effects from the explosions and their distances from the proposed route. Mass evacuation from these populated areas probably is not needed nor advisable. For those closest to the seaway development, careful preparation to prevent collapse of man-made structures as a result of seismic waves generated by the blasts might be more important than protection of the populace against radiation or fallout. Hopefully, the excavation would be so adequately engineered that there would be neither radiation nor fallout of any significance.

The economy of Gabes and the immediate vicinity depends on factors such as the fisheries (largest and most important in Tunisia), small scale vegetable crops, olive, almond, citrus trees and date palms, and moderate development of grazing animals.⁵ The most important economic feature of this region, as in most parts of Tunisia, is unemployment. Mobilization of the populace by the government for road, dam, well digging and general construction helps to some extent. The employment offerings of a major construction job such as this seaway would help to provide political impetus to the project.

If found to be necessary, quarantine on the fisheries and fruit tree crops could prove a temporary disadvantage to the area. If imposed, it would last only until the completion of the canal. A nominal cost of relocation of the populace to areas beyond a nominal 25-mile limit, if shown to be desirable, was taken to be about \$1500 per person. This cost would include transportation, construction of temporary housing facilities, meals, and medical attention. Minimization of factor is, of course, an advantage both financially and in the development of public (local) support for the project.

On a long term basis, the advantages definitely outweigh the disadvantages. With the seaway would come shipping, development of industries along the waterway and general development of harbor areas. Resort areas could be made widely available and a great expansion of the olive and citrus groves that thrive on the near-shore night humidity could be undertaken. Fishing in the relatively shallow basins that were the chotts could become as rich an industry as that in the Caspian, Black, or Tiberian Seas. Salt cropping and possible industrial development of the sea water trace elements or the salts leachable or mineable from the soil deposits could become economic with the relatively cheap shipping that could become a reality with such a seaway.

Table 1—Population Centers Near Evacuation Route
(in kilometers)

Category I 15,000 - 30,000	
Gabes	20
Gafsa	30
Kabih	17
Tozeur	15

Category II 5,000 - 15,000	
Katena	30
Mahares	40
Graiba	23
Maknassy	23
Matmata	35
Douz	36
Kriz	15

Category III < 5000	
El Guettar	28
Oum Sema	10
Sabria	30
Jarsine	23
Rhidma	30
Djerbs	44
Oudref	15
El Hama	14
Cekhira	6
Meheri Zebbeus	46
Meich	18
Sened	20
Isles of Kneiss	7
Chenva	23
Toujane	40
Arram	42
Tamerred	35

Emplacement and Firing Sequence

The optimum yield for the devices, optimum depth of burial, and row spacing were calculated according to these requirements. The proposed canal route covers about 107.5 miles in Tunisia from north of Gabes to the Chott Djerid and consists of five straight-line segments. A canal suitable for large ships should have minimum dimensions 60 feet in depth and 1000 feet in width at sea level. Segment A of the route begins some 18 miles north of Gabes and runs southwest for 15 miles to Skret el Hamma. Segment B is 17 miles long, Segment C is 16 miles long, and each of these two segments follow a west by northwest direction terminating in the mid portion of Chott el Fedjadj. Segment D, the longest, is 37 miles long, heads generally westward, and ends in the northeast portion of Chott el Djerid. The last segment considered in this study is 23 miles long and terminates near the center of the Chott el Djerid which is approximately 10 meters below sea level. The emplacement of the thermonuclear fusion devices will be on the lines connecting the termini of the various segments shown in Figure 2.

The route described above was chosen to provide maximum utilization of the depressions which form the lake beds of Skret el Hamma, Chott el Fedjadj and Chott el Djerid thus minimizing the amount of earth that must be moved. Safety of the nearby populated areas from radiation and shock also entered into the choice of some of the route segments. For example, Segment A could have been shorter, but that would have endangered the cities of Metouia and Rhennouch. Consequently, Segment A follows the ravine formed by the El Telmam River northeast from Skret el Hamma, then across a watershed and into the El Akarit river basin to the coast. An intervening mountainous area makes this route even more acceptable because the range provides protection to the cities mentioned above from shock and radiation.

With the exception of the village of El Hamma, Segments B-E are well removed from population centers. El Hamma, at a distance of six miles from the proposed route might have to be evacuated for a few weeks.

Cratering calculations of minimum device yields necessary to obtain a 1,000-foot wide channel, 60 feet deep gave values which varied from a minimum of 100 kilotons to 300 kilotons along the proposed route according to the topography. The following equation⁹ was used:

$$E + D_o = d_1 \left(Y^{1/3.4} - \frac{L_o^2}{W_1^2 Y^{1/3.4}} \right)$$

where E = ground surface elevation above mean sea level, meters

D_o = depth of canal below mean sea level at width L_o

d_1 = depth of crater

W = width of crater at original ground-surface elevation

L_o = width of canal at depth D_o below mean sea level

Y = yield of device in kilotons

Typical data from this calculation are shown in Figure 3.

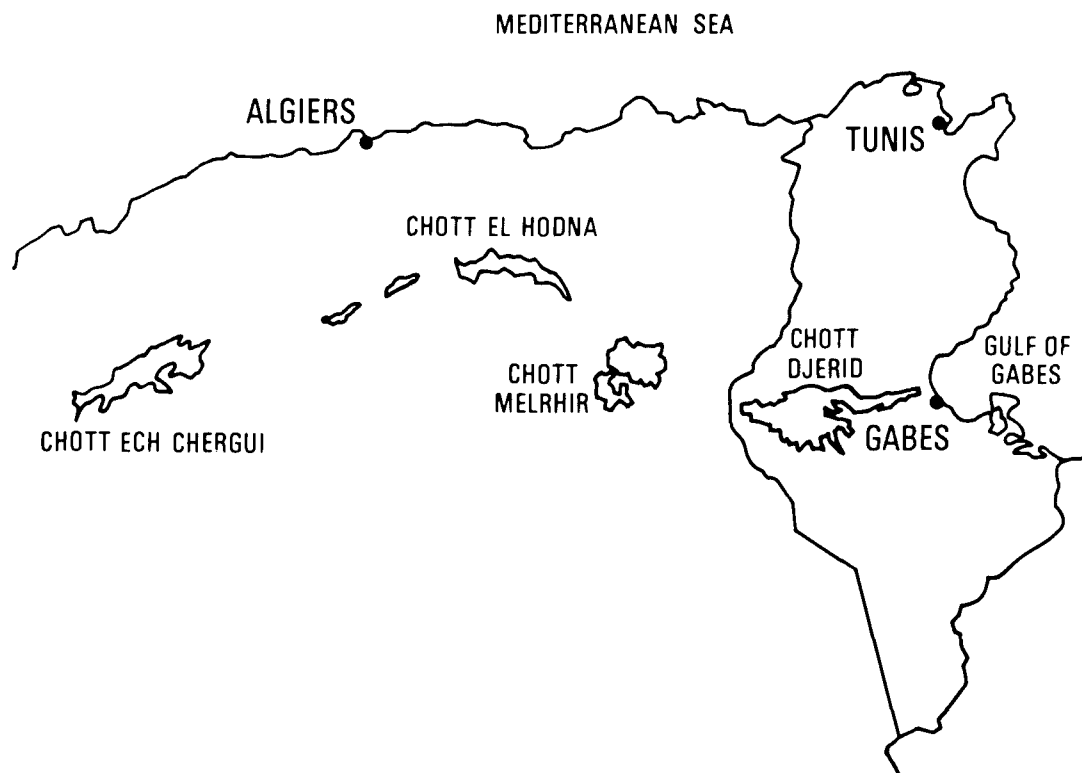


Figure 1. The Chotts of Northern Africa

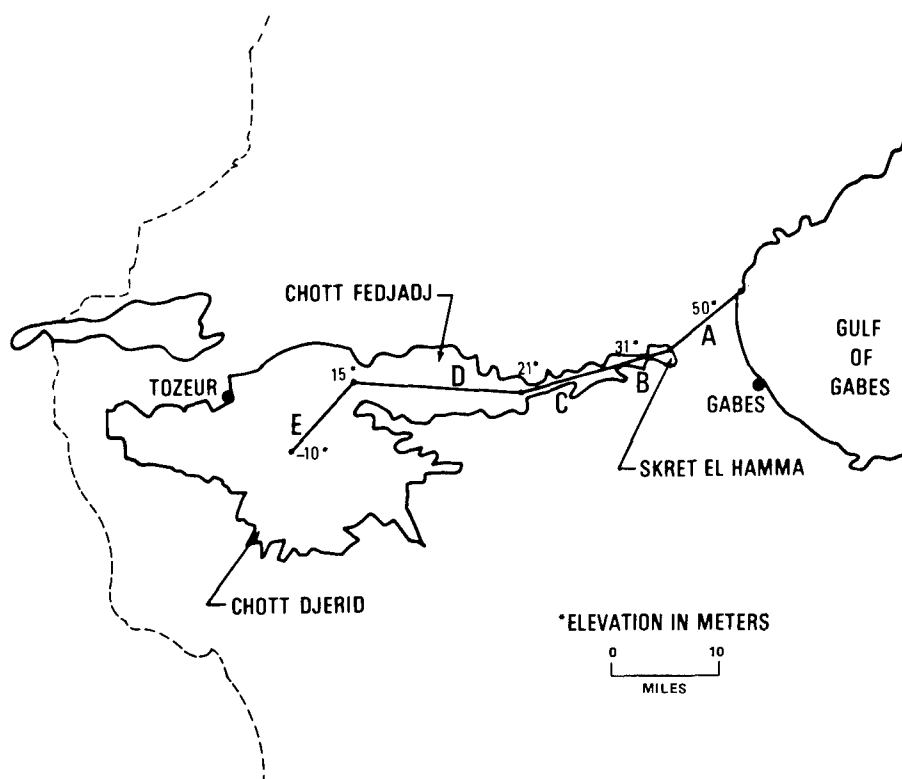


Figure 2. The Proposed Route Through the Tunisian Chotts

For the most of the proposed route, the minimum device yield required would be on the order of 150 kilotons. Therefore, the required spacing of several 150 kiloton devices in a row charge such that a smooth channel will be formed is approximately 715 feet. Under such presumptions, a minimum of 790 devices with a total yield of 119 megatons would be required to cut the desired 107-mile long channel. Spacing relative to device size is illustrated in Figure 4.

While the use of such small devices would be effective, it does not take several factors into consideration. First, for device sizes from 100 kilotons to two megatons, the rate of change of crater dimensions versus device size is greater than the rate of change of device cost versus device size. In fact, device costs versus yields from published AEC figures show a linear rate increase which is not quite double for a 200-fold increase in yield of the device. Hence, the device cost appears to be almost constant and relatively independent of other considerations. It is evident therefore, that although larger devices do cost more, a considerably smaller number of them would be required to do the job with the result that the overall project device-costs drop. Second, radiation levels resulting from the larger devices are not substantially greater than that from the 150 kiloton devices, since activity release is produced primarily from the fission "trigger" and not from the energy-producing portion of the nuclear interaction. The fission trigger is relatively constant in size and relatively similar amounts of activity are released for dissimilar yields.

Based on these and other considerations, a device yield of two megatons was chosen for the canal construction. This decision was made primarily because a two megaton device is not so unduly large as to complicate handling and (according to published AEC specifications) is capable of being emplaced in a 30 inch diameter hole. In addition, the depth of burial for cratering applications of a device of this size is approximately 1500 feet ... a reasonable depth for drilling at a remote location, and certainly for one which is near well developed oil fields.

Using two megaton devices to produce a navigational channel of 60 foot depth, the width will vary from 1310 to 1400 feet depending on the surface elevation. A calculation with the devices placed uniformly at 1530 feet below the surface at a spacing of 1450 feet for the row charges gives a requirement of 390 devices with a total yield of 780 megatons. This scheme would provide a savings of \$140 million over the minimum megatonnage program.

The number of devices to be combined in a single detonation would be limited to five. This number was obtained from calculations of probable surface particle velocity induced by the nuclear explosions. The particle velocity, v , was obtained from the equation⁹

$$v = 0.422 \left(\frac{R}{Y^{1/3}} \right)^{-1.65}$$

where R = radial distance from blast, $18 \leq R \leq 350$ kilometers and Y = yield in tons. A row charge of five devices or 10 megatons total yield would induce a particle velocity of 3.0 cm/sec at 20 miles which is the average approximate distance to the closest populated areas from the proposed construction route. The plaster cracking limit of the particle velocity is 10 cm/sec. Greater charges would crowd this arbitrary limit and cause difficulties because of the large distance involved between the ends of the row.

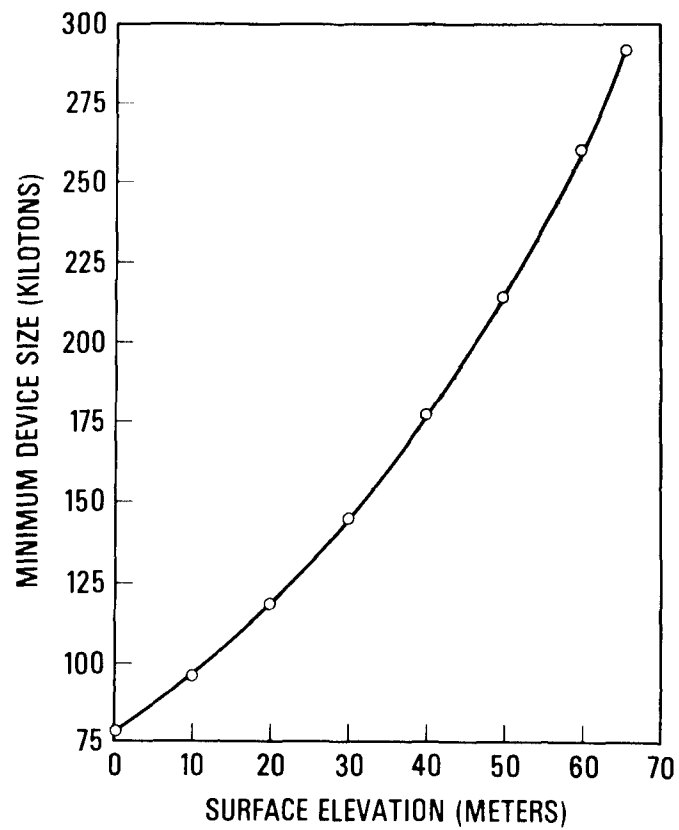


Figure 3. Minimum Device Yield as a Function of Surface Elevation

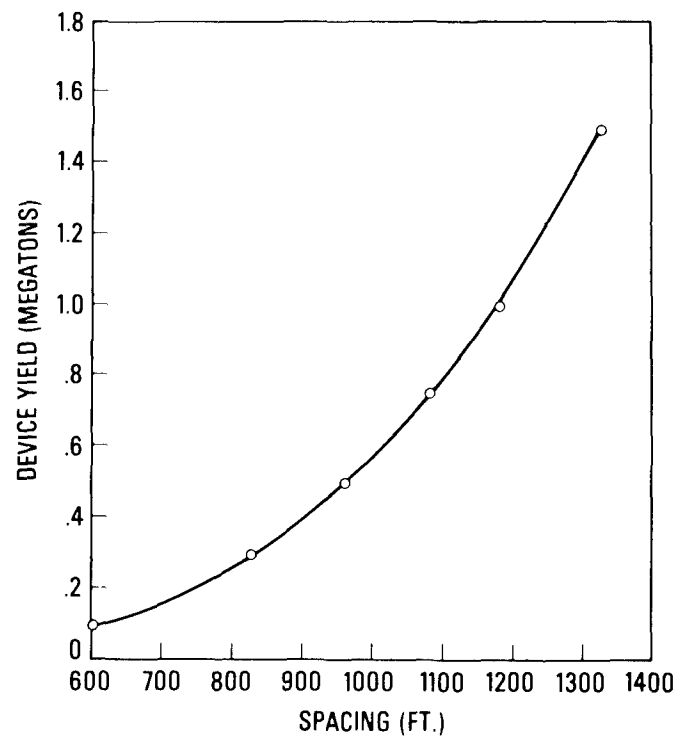


Figure 4. Device Yield versus Spacing Requirements

Each row of five devices will excavate 1.4 miles of canal. The detonation order would be in alternate blocks of five devices returning to detonate the remaining blocks after a short period allowed for activity decay. This technique would be especially useful to prevent long distance on rushes of water from the Gulf of Gabes that might result in severe erosion and deposition of large quantities of loose sediment in the chott and canal bottoms, rendering the seaway useless.

Post-Shot Civil Engineering

Once the craters are formed, the problem of completing the project is mainly in the province of the Civil Engineer. He must analyze the final soil and foundation conditions in the area, determine the best fallback slope and slope stability, and determine the amount of clean-up excavation required and the optimum means of accomplishing that.

Since the type of material being considered is alluvium with a small amount of limestone, the most conservative design¹⁰ would be to assume the alluvium to be non-cohesive and to require a small angle of repose. The angle chosen for this work would be about 28°. In the days or weeks allowed for conditions in the excavation area to reach a state of safe working conditions, both wind and occasional rain will act to stabilize the surface through erosion of the fine loose material and cementation by haliferous and gypsiferous deposits. The least expensive procedure would be to use sufficient explosive to produce a channel that would stabilize to the depth (and effective width) desired. The alternate would be to use less explosives and operate with conventional means (drag lines, dredges, trucks, power shovels etc.) to refine the canal to the desired depth and width. Considering the remoteness of the area, the "prefinished" job requiring minimum labor and machinery to complete would be much more desirable. Figure 5 shows the proposed crater cross-section for such a procedure with the effective navigational prism superimposed on it. The large crater size would have the added advantage of eliminating the need for operational maintenance such as periodic dredging of the channel to remove alluvium accumulated from erosion and silting. In addition, the shallow side slopes would easily allow for recreational beach development all along the channel length. Since this is designed as a sea-level canal, no primary civil engineering structures such as locks, dams or other hydraulic forms would be required. Secondary development may lead to many structures and harbor support facilities that are impossible to estimate in a primary analysis such as this. In essence, the only earthwork required would be the final grading of the area near the channel. The debris cast out from the crater is most likely to be small or pulverizable by relatively simple machinery such as bull-dozers, ditch diggers etc. and should provide no untoward difficulty in the finishing work.

Reconnaissance

Should evacuation of the populace along the route of the seaway be necessary, temporary evacuation centers could be built south of Arram. In addition to the principal population centers around Gabes, Kebih, Kriz, Oum Sema, El Hamma, and Oudref, there are nomadic people who do not congregate in any one center. On the assumption that 100,000 people might have to be moved at a cost of \$1500 per person, the outlay for evacuation would be about 150 million dollars. The facilities at the relocation centers may need to sustain the population for a probable maximum of two years. In most cases the residence time should be only a few weeks, but some of the villages along the route may suffer sufficient damage that reconstruction or major repair of structures would be necessary before replacing the population in the area. In any event, special sociological teams should go into the area early in the

pre-shot survey periods to explain the reasons for the move, the local and national advantages of the project, to help prepare people for the move should it prove necessary and to instigate such repair and strengthening of existing structures as necessary to prevent housing and superstructure (chimneys, overhangs etc.) collapse during the passage of the seismic wave.

Meteorologically, common winds are from the west or southwest with so-called "hot winds" blowing off the desert whenever low pressure systems enter the area. Figure 6 shows two areas for which the dose-rate was calculated for one hour after the nuclear detonation. The isodose curves were developed from the empirical equation

$$D_1 = D_2 \left(\frac{V_2}{V_1} \right)^2 \cdot \left(\frac{S_1}{S_2} \right) \left(\frac{F_2}{F_1} \right) \left(\frac{W_2}{W_1} \right) \left(\frac{h_2}{h_1} \right)^2$$

for which the variables are

V = mean wind speed

S = wind shear

F = fraction of radioactivity escaping

W = fission yield

h = main cloud height

X = distance from ground zero and

$$X_2 \approx X_1 (V_2/V_1) (h_2/h_1)$$

The subscripts refer to two explosive events, (1) being some previous Plowshare shot used as a standard. In the case here, the SEDAN shot was used as a standard⁹ and the wind conditions considered as double those observed in that shot. The data shown in the illustration was programmed on a PDP-8 computer using series of 5 two megaton devices at a 2000 foot spacing. Conclusions drawn from this and other parameters were that each series of five devices detonated should be followed by a week of cooling time before the next series is shot. By following these measures, the radiation level at 25 miles should be less than 15 mR/hr. at H + 1.

Both geophysical and radiological surveying should be made of the area before, during, and after the blasts. This information can be used to guide the decisions regarding re-entry of both the working crew and general populace back into the area. Even use of seismic recorders at some distance from the blast center could provide additional badly needed information about the subsurface nature of the chotts and the barriers that separate them.

Economic Aspects

The cost of such a project is, of course, enormous from the layman's point of view, but an overall project cost of the order of one billion dollars does not seem so great when measured against the financial gain this will represent as an investment. It is proposed that the financial load be split four ways with the United States and other interested countries 25 percent, the World Bank 25 percent, the governments of Tunisia and Algeria 25 percent; and the balance be provided by bond issues sold by an operating company for whom operation of the canal is guaranteed for 50 years. At the end of that

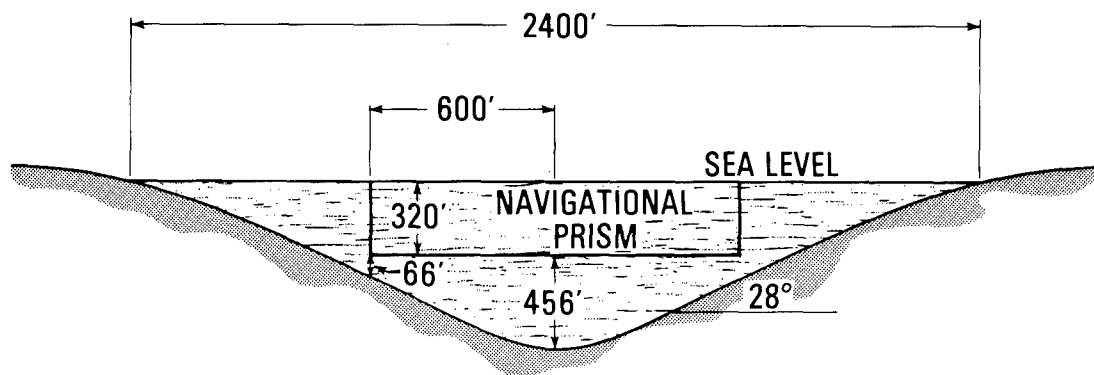


Figure 5. Crater Cross Section and Navigational Prism

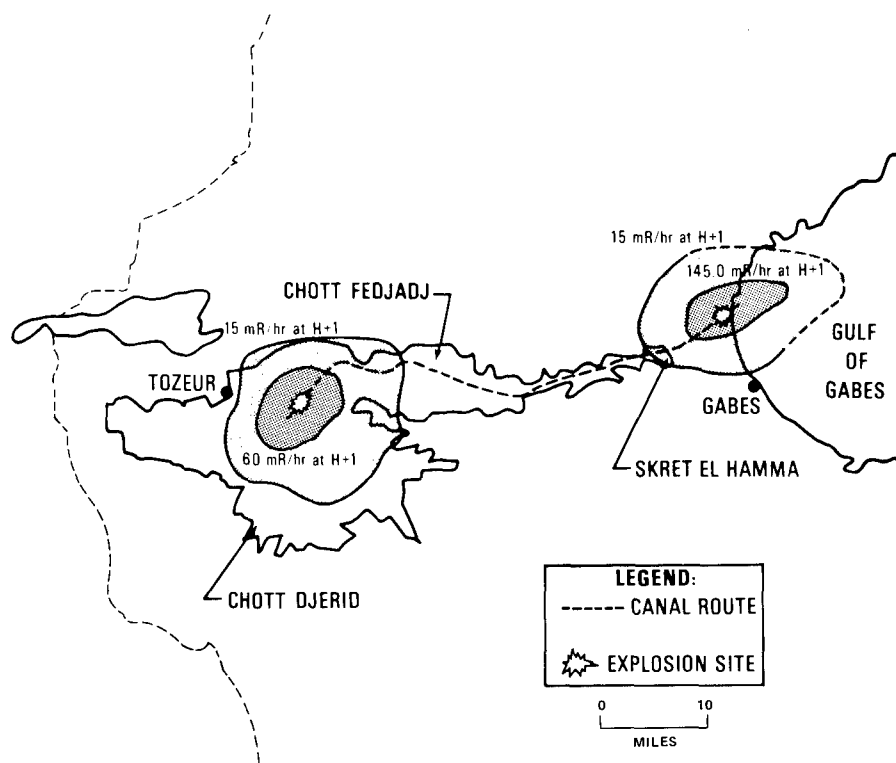


Figure 6. Isodose Curves at H + 1

period renegotiation of the contract would be undertaken by the company and the two participating countries, Algeria and Tunisia.

The loans from the principals would be secured at 3 percent (per 1968 money costs) because of the political advantages offered. The World Bank loan would be at 5 percent and the commercial loan at 6* percent. The company would contract through the USAEC for the devices desired and the latter will assume the responsibility of construction, testing, transporting, and detonating the devices. Other work would be contracted through the IAEC and interested companies.

Not including the possible 150 million dollars required for populace relocation, the total estimated costs (as of 1968) are shown in Table 2. Note that the largest item is the cost for the nuclear explosives, calculated at \$600,000⁹ per 2-megaton device. The harbor and port facilities are minimal in this initial development. Additional harbor facilities will not be provided by the company unless requested to do so by the governments of the individual countries in which the harbor facilities are to be located. Even then the company would undertake management services and the entire cost would be underwritten by the government of the host country in whatever way would be most profitable or expedient to do so.

Using a capital recovery factor of 6 percent¹¹ to cover interest and owner's return on investment for 50 years, the annual cost would be 51.1 million dollars. With bonds being paid off in semi-annual installments the annual costs are 48.3 million dollars in addition to the 16.1 million dollars required to pay off the 807.5 million dollars in fifty years. These payments require that the excess of revenues over expenses annually should average 64.4 million dollars. In the currency of Tunisia, the total cost (not including relocation expenses) would be 942.7 million dinar. At approximately 6 percent average interest on that money, the annual return necessary would be about 60 million dinar. By comparison, the 1963 budget of the Tunisian government was 59.95 million dinar.¹²

Summary

It appears that the construction of a canal linking the chott region with the Mediterranean Sea can be accomplished in a relatively short time with nuclear excavation. With the limited overview afforded by this study, the project appears technically and economically feasible. Extensive gathering of additional detail must be required, however, in almost every area of the program. Field surveys will be required to satisfy geologic, environmental, and radiologic safety requirements, and every economic factor must be closely scrutinized and developed so that the greatest possible reward be derived from such a gigantic undertaking. The advances in current technology may help to counter the effects of inflation, but for those involved in preparing the final evaluation of such a project, the latest and most detailed data involving device design, emplacement and cratering factors must be made available.

In any regard, the construction of such a canal should be considered in the list of feasible peaceful uses of nuclear explosives in the Plowshare program.

* Although this is low according to current bank interest rates, it is a conceivable value in non-inflationary "equilibrium" financial condition.

Table 2—Estimated Cost of Project (1968 Financial Rates)

Nuclear explosives	\$234.0 million
Emplacement	105.8
Port construction, harbors, and clean up	108.5
Construction camps, access roads, etc.	115.3
Miscellaneous	27.0
Interest during construction	<u>97.0</u>
	\$687.4 million

REFERENCES

1. "Surface Water and Related Climate Features of the Sahil Susah Area Tunisia" USGS Water Supply Paper 1757F
2. Shea, John C., Guidebook to the Geology and History of Tunisia, Petroleum Exploration Society of Libya, Ninth Annual Field Conference, 1967.
3. Coque, Roger, La Tunisia Presahariene, Armand Colin, Paris, 1962.
4. Marliare, E. C., "Engineering-Geology Problems in Tunisia," Geologic Society of America, Special Paper No. 68, p. 47, 1962.
5. Benton, Wm., Publ. Encyclopedia Britannica, V. 22, Chicago, Ill., 1967.
6. Lowman, F. G., R. F. Palumbo and D. L. South, "Occurrence and Distribution of Radioactive Non-Fission Products in Plants and Animals of the Pacific Proving Grounds." USAEC, UWFL-51, 1957.
7. Lowman, F. G. "Radionuclides in Plankton near the Marshall Islands, 1956." USAEC, UWFL-54, 1958.
8. Encyclopedia Americana, 1969.
9. Teller, E., W. K. Talley, G. H. Higgins, G. W. Johnson. The Constructive Uses of Nuclear Explosives, McGraw-Hill Book Co., New York, (1968).
10. Sowers, George B. and George F. Sowers. Introductory Soil Mechanics and Foundations. The Macmillan Company. 1961, pp 386.
11. Samuelson, Paul A., Economics, 6th Edition, McGraw-Hill, New York, 1964.
12. Steinberg, S. H., Editor, Statesman's Year Book, p. 1490, St. Martins Press New York, 1968-1969.

STABILITY OF NUCLEAR CRATER SLOPES IN ROCK

Robert W. Fleming
Alton D. Frandsen
LTC Robert L. LaFrenz

U. S. Army Engineer Nuclear Cratering Group
Lawrence Radiation Laboratory
Livermore, California

INTRODUCTION

The United States Army Engineer Nuclear Cratering Group was established in 1962 to participate with the Atomic Energy Commission in a joint research and development program to develop nuclear engineering and construction technology. A major part of this research effort has been devoted to studies of the engineering properties of craters. The program to date has included field investigations of crater properties in various media over a broad range of chemical and nuclear explosive yields, studies of man-made and natural slopes, and studies directed toward the development of analytical and empirical methods of crater stability analysis. From this background, a general understanding has been developed of the effects of a cratering explosion on the surrounding medium and of physical nature of the various crater zones which are produced. The stability of nuclear crater slopes has been a subject of prime interest in the feasibility study being conducted for an Atlantic-Pacific sea-level canal.

Based on experimental evidence assembled to date, nuclear crater slopes in dry dock and dry alluvium have an initially stable configuration. There have been five nuclear craters produced to date with yields of 0.4 kt or more on which observations are based and the initial configurations of these craters have remained stable for over seven years. The medium, yield, crater dimensions, and date of event for these craters are summarized in Table I. It is interesting to note that the Sedan Crater has been subjected to strong seismic motions from nearby detonations without adverse effects.

TABLE I

APPROXIMATE DIMENSIONAL DATA FOR NUCLEAR CRATERS IN ROCK

<u>Event</u>	<u>Rock Type</u>	<u>Yield (kt)</u>	<u>Height of Crater Slope (ft.)</u>	<u>Average Slope Inclination (degrees)</u>	<u>Date</u>
SEDAN	Alluvium	100	390	31	6 July 1962
SCHOONER	Tuff	35 (\pm 5)	250	37	8 Dec. 1968
BUGGY	Basalt	1.2 (\pm 0.2)*	100	38	12 Mar. 1968
CABRIOLET	Porphyritic Rhyolite	2.3 (\pm 0.5)	140	38	26 Mar. 1968
DANNY BOY	Basalt	.42(\pm .08)	80	35	5 Mar. 1962

* Row charge, 5 devices of yield 1.2 kt.

Numerous chemical explosives cratering experiments have been conducted in materials similar to those shown in Table I, as well as in wet clay shale. Several of these are listed in Table II.

Table II

MAJOR CHEMICAL EXPLOSIVE CRATERING EXPERIMENTS

<u>EVEN (SHOTS)</u>	<u>EXPLOSIVE CHARGE PER SHOT</u>	<u>MATERIAL</u>
<u>Single Charge Experiments</u>		
STAGECOACH (Three)	20 tons TNT	Alluvium
BUCKBOARD (Three)	20 tons TNT	Basalt
SCOOTER (One)	500 tons TNT	Alluvium
Pre-SCHOONER I (Four)	20 tons NM*	Basalt
Pre-SCHOONER II (One)	85 tons NM	Rhyolite
Pre-GONDOLA I (Four)	20 tons NM	Wet Clay Shale
Project TUGBOAT, Phase I	1 and 10 tons AL-NH ₄ NO ₃ **	Saturated Coral
<u>Multiple Charge Experiments</u>		
Pre-BUGGY I Rows (Four)	5 at 1/2 ton NM	Alluvium
Pre-BUGGY II Rows (Eight)	5 at 1/2 ton NM	Alluvium
DUGOUT Row (One)	5 at 20 tons NM	Basalt
Pre-GONDOLA II Row (One)	2 at 40, 3 at 20 tons NM	Wet Clay Shale
Pre-GONDOLA III, Phase I, 3-Row Array (Two)	14 at 1 then 7 at 1 ton NM***	Wet Clay Shale
Pre-GONDOLA III, Phase II, Row (One)	7 at 30 tons NM	Wet Clay Shale
Pre-GONDOLA III, Phase III, Row (One)	1 at 35, 1 at 15, 1 at 10, 2 at 5 tons AL-NH ₄ NO ₃	Wet Clay Shale

Due to the limited experience in wet media, other than the relatively low-yield clay shale craters, this paper will be concerned mainly with dry materials, although some qualitative discussion of seepage effects is included. Crater geometry, the factors affecting slope stability and the methods of analysis are discussed in general. This is followed by a discussion of those aspects of a crater slope which seem to bear directly on its potential stability. For convenience, the potential stability of fallback materials and rupture zone materials are discussed separately followed by a discussion of seepage characteristics. Finally, an example of stability analysis is presented.

Crater Geometry. A nuclear cratering detonation produces a crater with relatively predictable characteristics. A typical cross-section of a crater which illustrates crater nomenclature is shown in Figure 1.

*Liquid explosive nitromethane.

**Aluminized ammonium nitrate slurry blasting agent.

***Two outside rows fired simultaneously; center row then fired to produce a crater with flat side slopes.

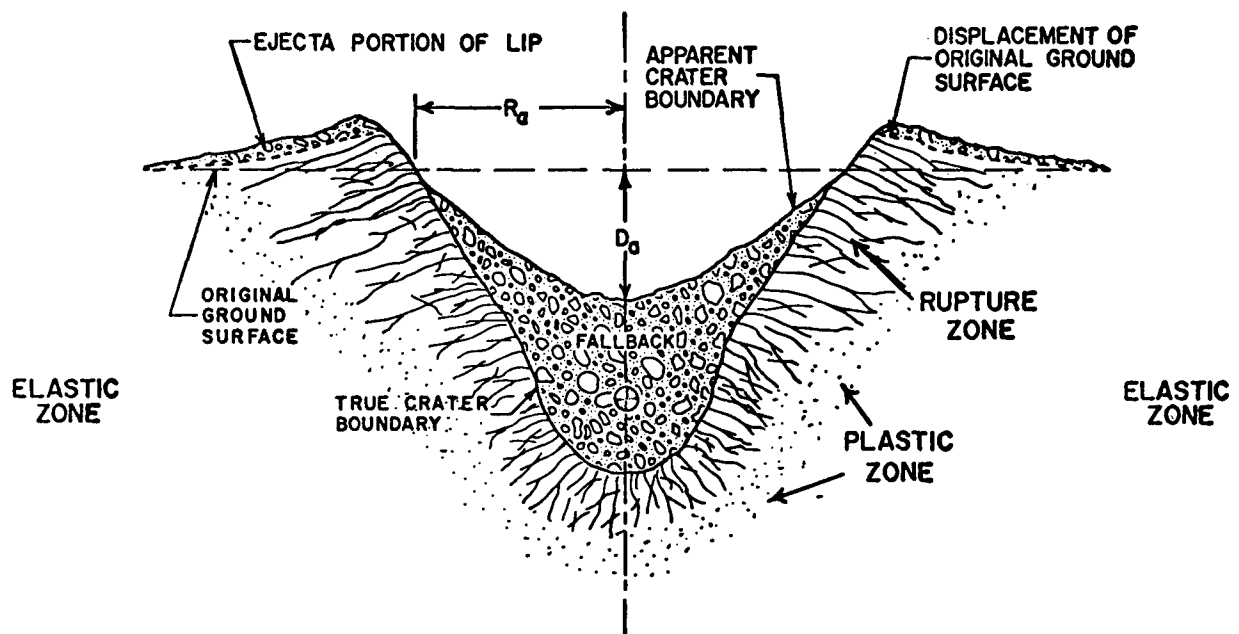


Figure 1. Cross Section of typical crater in hard rock showing zones of disturbance.

Empirical scaling laws have been developed that correlate crater dimensions with explosive yield. The apparent, or visible, crater is bounded by material which may be classified into three categories: the fallback and ejecta zone, the rupture zone and the intact material zone. The geometry of each zone is approximately as shown in Figure 1.

Factors Affecting Crater Stability. In addition to crater geometry, an analysis of crater stability requires a knowledge of the post-detonation physical and structural properties of the medium and the impact of such external factors as seepage, weathering and seismic loading. The post-detonation properties are predicted from pre-detonation investigations of the undisturbed medium. The state-of-the-art at the present time is such that external affects can only be discussed qualitatively.

METHODS OF ANALYSIS

Two basic methods of evaluating crater stability are normally cited: (1) the analytical approach and (2) the empirical approach. However, the technique presently used to assess slope stability involves a semi-empirical evaluation based primarily on a knowledge of crater phenomenology, various empirical studies and engineering judgment. This approach is dictated due to the general lack of detailed reliable prediction capabilities with respect to both crater geometry and physical properties in the range of yields significantly higher than those already tested.

The analytical approach involves the application of computational methods of slope analysis to crater geometry. This method as well as the empirical approach requires detailed information on slope configuration and material properties including susceptibility to weathering. The analytical approach is commonly used in soils engineering and rock mechanics studies but its applicability to explosive excavation is limited and principally of theoretical interest. This is because there is not yet a sufficient body of knowledge of relationships between preshot conditions and postshot materials properties and behavior to allow for rigorous analytical solutions. The empirical approach compares the anticipated crater geometry and material properties with observed behavior of natural or man-made cuts in similar materials and environment. This approach must be used with caution since crater formation processes result in slopes that are uniquely dissimilar to those produced by any other means, either natural or man-made.

Analytical approach. The analytical or direct approach to crater stability would involve limiting equilibrium or stress-strain analyses. The limiting equilibrium method compares the forces or strength supporting the slope with the forces tending to cause the slope to fail along assumed failure surfaces. The method results in a calculated factor of safety which is the ratio of resisting to driving forces. Several different limiting equilibrium techniques are applicable depending on the nature of slope materials and the assumed failure geometry. For those materials which derive their strength primarily from cohesion, a slip circle or composite curved failure surface is applied. If the strength of the material is largely due to frictional resistance between fragments or along discontinuities, a planar or wedge-shaped surface is assumed. In both of these techniques, several trial failure surfaces are employed to obtain the location with a minimum factor of safety for the strength conditions assumed. The stress-strain method of analysis predicts the distribution of magnitude of stresses in the slope. Stress-strain characteristics of the cratered materials are compared with the calculated stress distribution to determine if there are zones of overstressed material. other techniques, including the finite element method, may be used depending on the complexity of the problem. Stress-strain methods do not develop a factor of safety as defined previously. However, they do

delineate the zones of high stress concentration within a slope and may be useful in predicting the location of potential failure surfaces.

Reliable estimates of the predetonation medium properties are required to perform a stability analysis of a crater slope. For a homogenous, relatively soft medium, such as a soil or weak rock, the pertinent properties are density, strength, and seepage characteristics. In a fractured hard rock medium, the strength along structural discontinuities must also be estimated. A stress-strain analysis requires deformation characteristics including the Modulus of Elasticity and Poisson's Ratio for all of the materials. Analysis of the stability of slopes in a planned nuclear crater requires an accurate prediction of the above postshot parameters based on preshot measurements. To date, this has only been accomplished for the smallest scale craters.

To conduct an analytical study of crater stability, a numerical stability analysis would first be made based on the site data and a prediction of crater geometry and crater zone properties. From this numerical analysis, engineering judgment and technical experience, an assessment of stability would be developed.

Empirical approach. In the empirical or indirect approach, some of the properties necessary for an analytical analysis are used as indices to assess the overall characteristics of the materials. On the basis of the performance of natural and man-made slopes in similar materials and environment, a judgment is made of the stability of the predicted crater. The procedure for developing an empirical analysis includes an estimate of the crater zone properties based on site data and predicted crater geometry followed by a comparison of this information with appropriate empirical criteria developed from observations from man-made and natural slopes in various geographical locations. Utilizing this information, technological experience, and engineering judgment a prediction is made of the potential stability of the planned crater.

STABILITY CHARACTERISTICS OF CRATERS IN ROCK

As mentioned previously, site data are usually insufficient to predict crater zone properties in the detail necessary for a rigorous analysis*. (Satisfactory site documentation is especially difficult for crater slopes in hard rock when the mass strength is governed by the spacing, orientation and surface characteristics of discontinuities.) However, there are a number of general characteristics of crater slopes in rock that make them inherently stable and it can be shown that, except in unusual cases, they are initially stable. This can best be illustrated by a discussion of the stability characteristics of the individual crater zones.

Fallback and Ejecta. The formation of a crater in hard dry rock or dry alluvium results in cohesionless fallback and ejecta which have come to rest after violent impact. The density, size distribution and particle shape of the material comprising the fallback and ejecta are dependent on both the preshot media and the detonation. In hard rock the particle shape will generally be angular. The angle at which the fallback and ejecta come to rest is termed the angle of deposition. This angle corresponds to the cessation of particle movement and is generally several degrees flatter than the angle of repose which represents the angle at which particle movement resumes. The angle of repose is the maximum stable slope angle for a given cohesionless material. Table III contains typical angles of repose for various materials (MacIver, 1967). In general, the angle of repose for angular materials varies between 37 and 45 degrees. For nuclear craters in rock, slope angles generally range between 30 and 38 degrees.

*Equally true for conventional cuts.

Table III

TYPICAL ANGLES OF REPOSE FOR VARIOUS MATERIALS

<u>Material</u>	<u>Angle of Repose (Degree)</u>
Shingle Stone	39
Ore, broken	45
Shale, broken	30-35
Shale, fragments	34-38
Marl, fragments	33-36
Metamorphic Rock, fragments	34-38
Stone, crushed	37
Limestone, fragments	38-42
Sandstone, soft	33-37
Sandstone, fragments	45
Igneous Rock	37-42
Rubble	45

after MacIver, 1967

The factor of safety of a cohesionless slope is usually expressed as

$$F.S. = \frac{\tan \phi}{\tan B}$$

where B is the angle of slope inclination and ϕ is the angle of internal friction. If it is assumed that the angle of internal friction equals the angle of repose,¹ the factor of safety against surficial sliding can be calculated. MacIver (1967) found that for common methods of deposition such as dumping from trucks or conveyors, the factor of safety varied between 1.1 and 1.5.

Fallback stability was examined at the Pre-SCHOONER II crater in southwestern Idaho. This crater was produced by an 85.5-ton single charge of nitromethane. The total slope height was about 70-feet and inclination about 37 degrees. The fallback material consisted of sub-round to angular particles of vitrophyre and felsite having an average particle size of 0.63-inches and a maximum size of 75-inches. The slopes were undercut by removing fallback materials from the bottom of the crater which steepened the slope from the initial angle of about 37 degrees to 42 degrees. By surficial readjustment, the slopes degraded to 38 degrees. The initial factor of safety against surficial adjustment was over 1.1. Thus it appears that the fallback materials are not only in themselves stable but they also provide a buttressing effect for the rupture zone and enhance the overall crater slope stability.

Rupture Zone. The materials in the rupture zone are similar to intact materials except they are more highly fractured. For other than very weak rocks, the strength of the rock mass against sliding is governed by the spacing and orientation of the natural and blast induced fractures and the frictional resistances of these fractures. The cratering phenomenon tends

¹The angle of internal friction actually is often greater than the angle of repose. This introduces a conservative element into the calculated factor of safety.

to disrupt natural discontinuities in the rupture zone. Figure 2 shows sub-surface displacements produced by the Pre-GONDOLA I Bravo high-explosive detonation. This experiment was a 20-ton single charge of nitromethane in clay shale at Fort Peck, Montana. Crater dimensions are also shown on Figure 2. Witness pellets were placed in the ground prior to the detonation and were recovered following the event. Large sub-surface displacements did occur in this relatively small cratering experiment. Disruption appeared to increase toward the surface such that the throughgoing fractures near the top of the slope may well have been offset. Although dependent on initial orientation of faults, fractures, and planes of weakness, deep-seated displacements resulting from an explosion are generally radial, hence a major throughgoing discontinuity such as a gouge zone associated with a fault might not be completely offset depending on its orientation, of course. This could result in a serious crater slope weakness depending on orientation and properties and illustrates the necessity for careful site documentation. Also, it has not been verified that the displacements measured in the Pre-GONDOLA I test can be extrapolated to detonations of larger yield.

In general, induced fractures in rock will be clean. That is, the fracture will not initially be filled with clay or other weak material and the potential stability along the fracture can be compared to the frictional resistance of sliding rock against rock. If the fracture is continuous and impinges on both the ground surface and the fallback materials, a block of rupture zone material will be in a state of incipient failure for those cases when the inclination of the fracture equals the friction angle (see Figure 3). Examples of measured frictional resistance on dry natural and sawed joints for quartz monzonite, granite and dolomite are presented in Figure 4 together with results of testing on intact specimens. (Lane, 1967). The frictional resistance along clean natural joints varied from 31 to 34 degrees and along a surface prepared by sawing the quartz monzonite, it was 28 degrees.

These data suggest that for dry materials, a throughgoing clean discontinuity dipping toward the crater would have to be inclined steeper than about 30 degrees to develop an unstable block. The combination of approximately 30 degree frictional resistance for the extreme assumption of a throughgoing fracture, the apparent increase in disruption of material toward the surface (Figure 2) and the relatively flat crater slope suggests that failures of this type are unlikely without outside loading.

Seepage Characteristics. The seepage of ground water through a crater slope could affect stability through the development of seepage forces or by erosive action. None of the large craters produced to date have been in saturated materials so that seepage effects must be inferred from direct data.

Seepage pressures are a function of the permeability of the medium and the amount of water available (storage and infiltration) which may flow through the slope. Although specific values of permeability are not required for a stability analysis, knowledge of relative permeabilities between zones is required to assess seepage pressures. The effective porosity is determined by the extent and magnitude of interconnected voids and fractures. Figure 5 is a plot showing both the effective porosity and percent increase in fractures surrounding a crater in rock. There is more than 20 percent increase in effective porosity and a 400 percent increase in fractures. The increase in permeability associated with the increase in effective porosity cannot be quantitatively determined, but is estimated to be substantially increased over the intact material probably by more than an order of magnitude. The porosity of the fallback has been calculated from bulk densities to be on the order of 29 to 37 percent for basalt and rhyolite at the Nevada Test Site (Hughes, 1968). Although this porosity is generally higher than that in the rupture zone, there are presently no other data available to evaluate

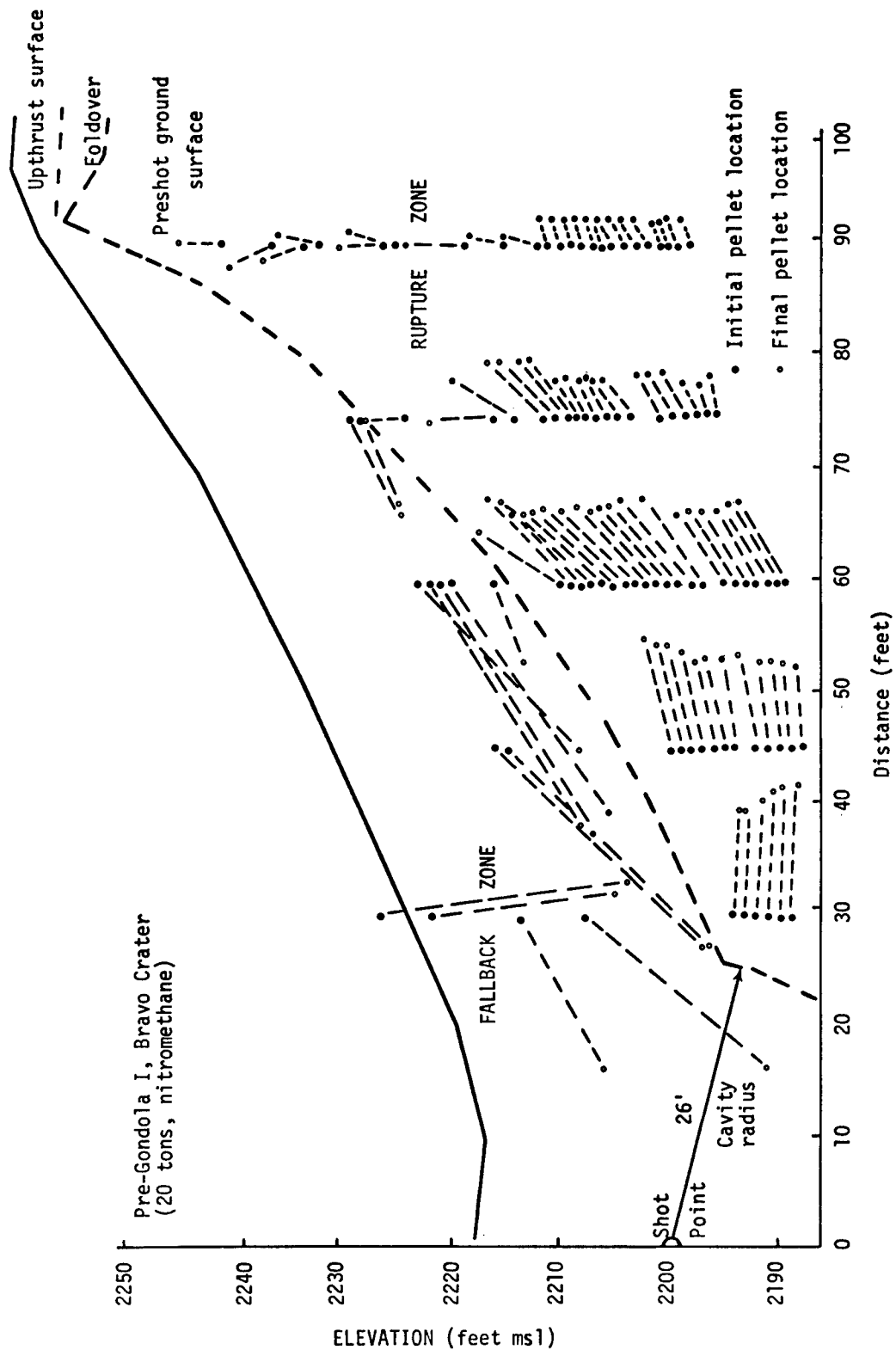


Figure 2. Subsurface displacements in close-in portion of Pre-GONDOLA I, BRAVO, rupture zone (displacement along radial line).

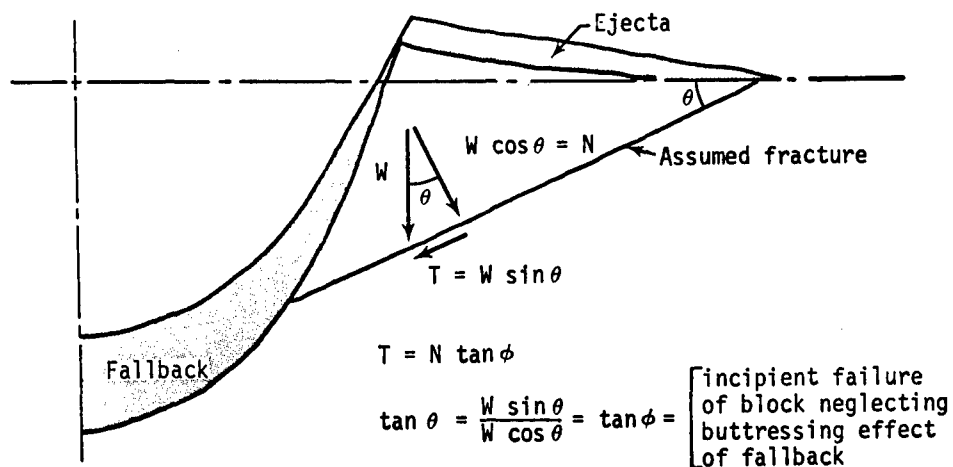


Figure 3. Fracture in the rupture zone showing relationship between inclination of fracture and friction angles.

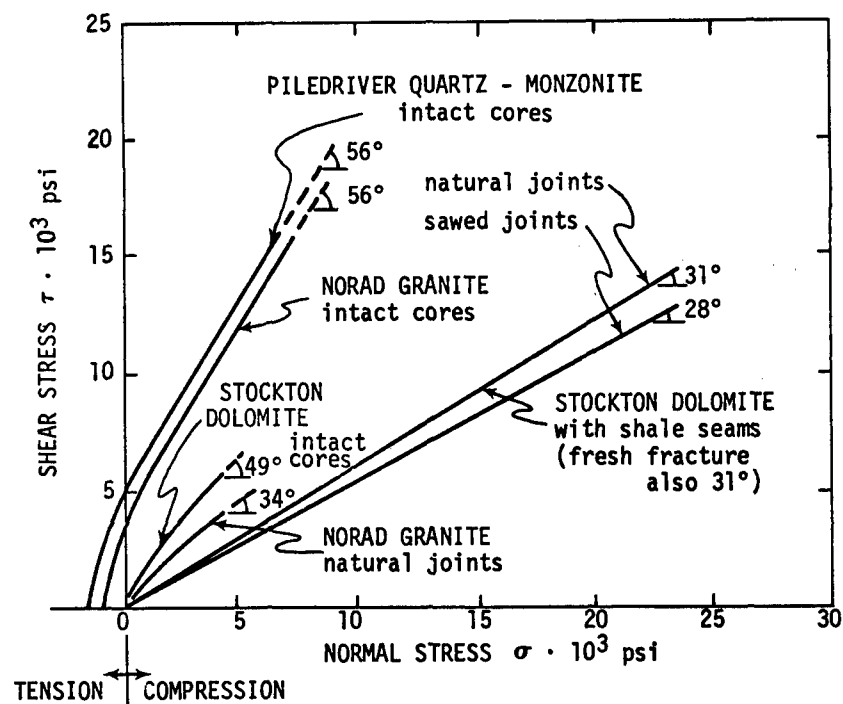


Figure 4. Intact strength versus frictional strength along fractures for selected competent rocks (after Lane, 1967).

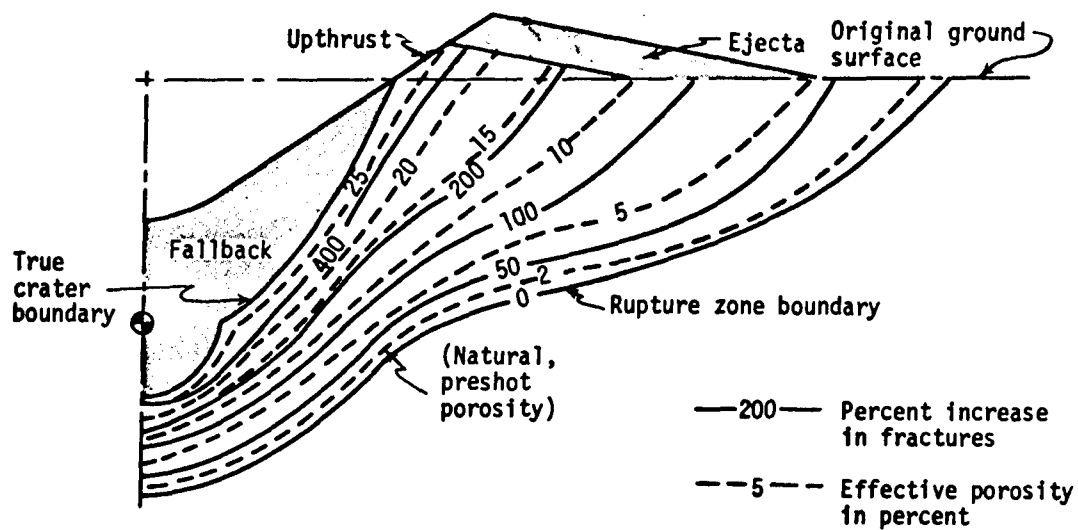


Figure 5.

Representation of decrease in intensity of blast-induced fracturing and effective porosity with distance from true crater.

differences in the permeability between the two zones. If the permeability of the fallback is less than the rupture zone, adverse seepage conditions may occur when infiltration or the amount of water in storage is very large. More likely the reverse case should occur and seepage will be vertical and enhance stability.

SAMPLE STABILITY APPRAISAL

A number of alinements have been investigated as potential routes for a sea-level canal. The following is an example of a stability appraisal performed on the materials along Route 25 in northwest Colombia to help assess project feasibility. Two of the alignments are shown on Figure 6. Predicted crater slope heights for the alinement 25E ranged from 550-feet in the shallower cuts to 1950-feet in the Continental Divide area.

Summary of Route Geology and Physical Properties. The principal rocks along the nuclear portion of the Route 25 alinement are the Choco volcanics. Outcrops of younger sedimentary rocks are faulted into the volcanic rocks in the vicinity of the Nercua-Upper Truando Valley area and along the east flank of the Saltos Highlands.

The Choco volcanics consist of a number of related rock types, all of which are "basic igneous" or closely related pyroclastics. The distinction between these rock types is commonly obscure. The dominant type is basalt, which grades to diabase and gabbro, or to agglomerate and flow breccia due to local changes in grain size or structure. The Choco volcanics are described as "massive" showing no discernible attitudes.

The sedimentary rocks along the alinement belong to the Sautata, Nercua and Truando groups. The Sautata group is primarily tuffaceous calcareous siltstone and sandstone, grading in places into tuffaceous limestone and calcareous tuff. The rocks are thin to medium bedded.

The rocks of the Nercua group are mainly conglomerates, composed of basalt fragments in a sandy calcareous matrix. Some pebbly siltstones and sandstones are also present. The rocks are thin to medium bedded, and generally hard and dense. Neither of these groups has been penetrated by borings.

The Truando group consists of various sedimentary rock types. The most common is tuffaceous siltstone, moderately soft to moderately hard, thin to medium bedded but occasionally massive. Interbedded with this rock type are tuffaceous sandstones; some of which are soft and friable, and some of which are calcareous and moderately hard. The Truando group also includes interbedded tuffaceous limestones, thin beds of conglomerate, and thin beds of claystones.

The physical properties of the rocks along the alinement were determined from geophysical logging, borehole photography and laboratory testing. Test results are summarized on Table IV.

Average unconfined compressive strengths for the Choco volcanics is about 6500 psi. The average seismic velocity is about 14,000 ft/sec with an in situ density of about 2.7 gm/cm³. The physical properties of the sedimentary rocks are variable, but generally less competent than the Choco volcanics with the exception of the calcareous sandstone of the Truando group. Rocks of the Nercua and Sautata groups were not tested but are generally considered somewhat similar to the Truando group based on the visual description and type of topography in the outcrop areas.

Natural Slope Data - Route 25 Area. The alinement for Route 25 was

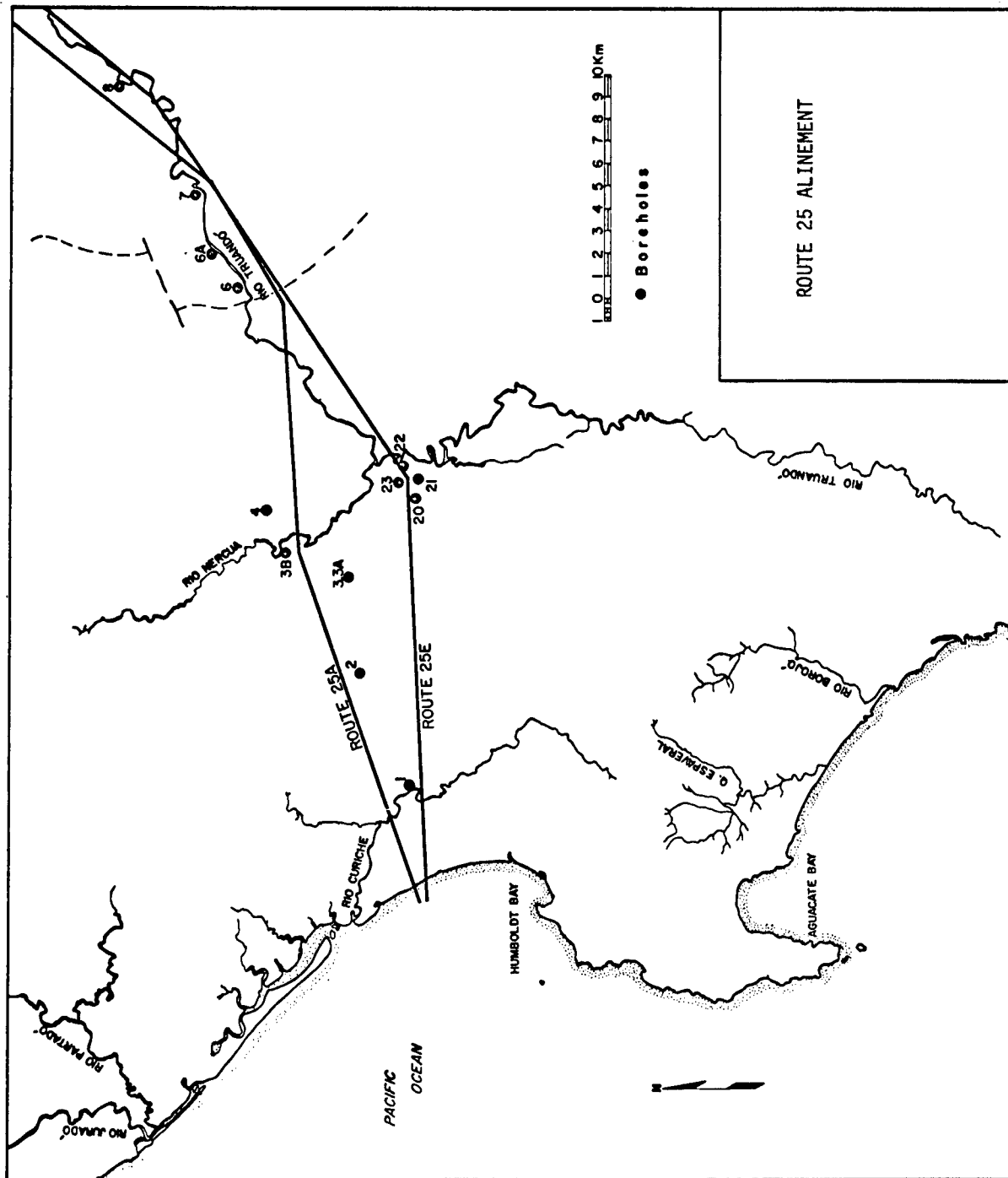


Figure 6. Route 25 alinement.

Table IV

AVERAGE VALUES OF SELECTED PHYSICAL PROPERTIES, ROUTE 25

ROCK TYPES Description	Water		Porosity %	Saturation %	Laboratory		Unconfined Compressive Strength (psi)	Average P-Wave Seismic Velocity (ft/sec)	In Situ Density (g/cm ³)
	Content %				Wet Bulk Density (g/cm ³)				
CHOCO VOLCANICS "igneous"	3		10	86	2.67		6500	13,400	2.7
CHOCO VOLCANICS "pyroclastic"	4		12	83	2.62		6400	14,300	2.6
SANDSTONE, CALCAREOUS, TRUANDO GROUP	6		16	84	2.41		6200	---	2.3
CONGLOMERATE, TRUANDO GROUP	13		29	86	2.14		2200	---	2.4
SILTSTONE, TRUANDO GROUP	41		54	93	1.74		1000	7,000	1.7
SANDSTONE, POROUS	17		36	80	2.08		690	---	2.3

selected in part on the basis of its relatively low topographic expression across the Continental Divide. Greater relief is present both north and south of the planned route. The highest and steepest slopes in highland and coastal areas up to 15 km south of Route 25E were measured from aerial photographs and topographic maps. The highest slope, measured along the coast where wave action is impinging on the toe, is 1300-feet at an inclination of 35 degrees. Slopes about a thousand feet high exist at inclinations of about 29 degrees. No significant slope failures were observed on the aerial photographs indicating that the slopes have been formed by erosional processes rather than through mass wasting.

Slope Data - Other Geographic Areas. Slope information for areas other than along Route 25 were investigated for high steep slopes underlain by materials with properties similar to the Choco volcanics. The general conclusion reached from these studies was that, for hard rock with unconfined compressive strengths of two thousand psi or greater, stability of slopes to a height of 2000-feet is largely independent of the intact rock strength.

One of the areas studied was Waimea Canyon and the leeward side of the island of Kauai, Hawaii. The rocks consist of thin to massive flows of sub-aerial picrite and olivine basalts (Tertiary-Pliocene age) with scattered pyroclastic rocks including volcanic ash and cinders present locally. Mean annual rainfall varies greatly up to a maximum on Mt. Waiaheale of 466-inches. Weathering extends to depths of 200-feet near the headwaters of Waimea Canyon. No strength data are available on these rocks but P-wave seismic velocities are about the same as the Choco volcanics (U. S. Corps of Engineers, Hawaii). The U. S. Bureau of Reclamation investigated a dam site (Kokee Water Project) a few miles east of Waimea Canyon. The deepest borings (150-feet) did not entirely penetrate through the weathered zone. Table V summarizes some index properties of weathered to fresh basalt obtained from the borings.

Table V
SUMMARY INDEX PROPERTIES

	Highly Weathered	Transition Zone	Moderately Weathered	Fresh
Apparent Sp G	3.61 to 3.65	3.43 to 3.41	3.10 to 3.23	3.17 --
Bulk Sp G	1.17 to 1.45	1.78 to 1.89	2.63 to 2.75	2.84 to 2.74
Estimated Bulk Sp G	1.27	1.78	2.75	3.07
Percent Porosity	68	48	19	11
Unit Weight, lbs/cu. ft.	73-90	109-118	164-173	177-191
Data courtesy of USBR				

Highest, steepest slopes were measured from topographic maps. (See Figures 7 and 8 for location and results). Slopes range from about 1/2 horizontal to 1 vertical for slopes 900-feet high to 1 1/2 horizontal to 1 vertical for slopes 3600-feet high. Admittedly, the comparison of slopes in Hawaii to Colombia is very tenuous and dependent on assumed physical and environmental similarity.

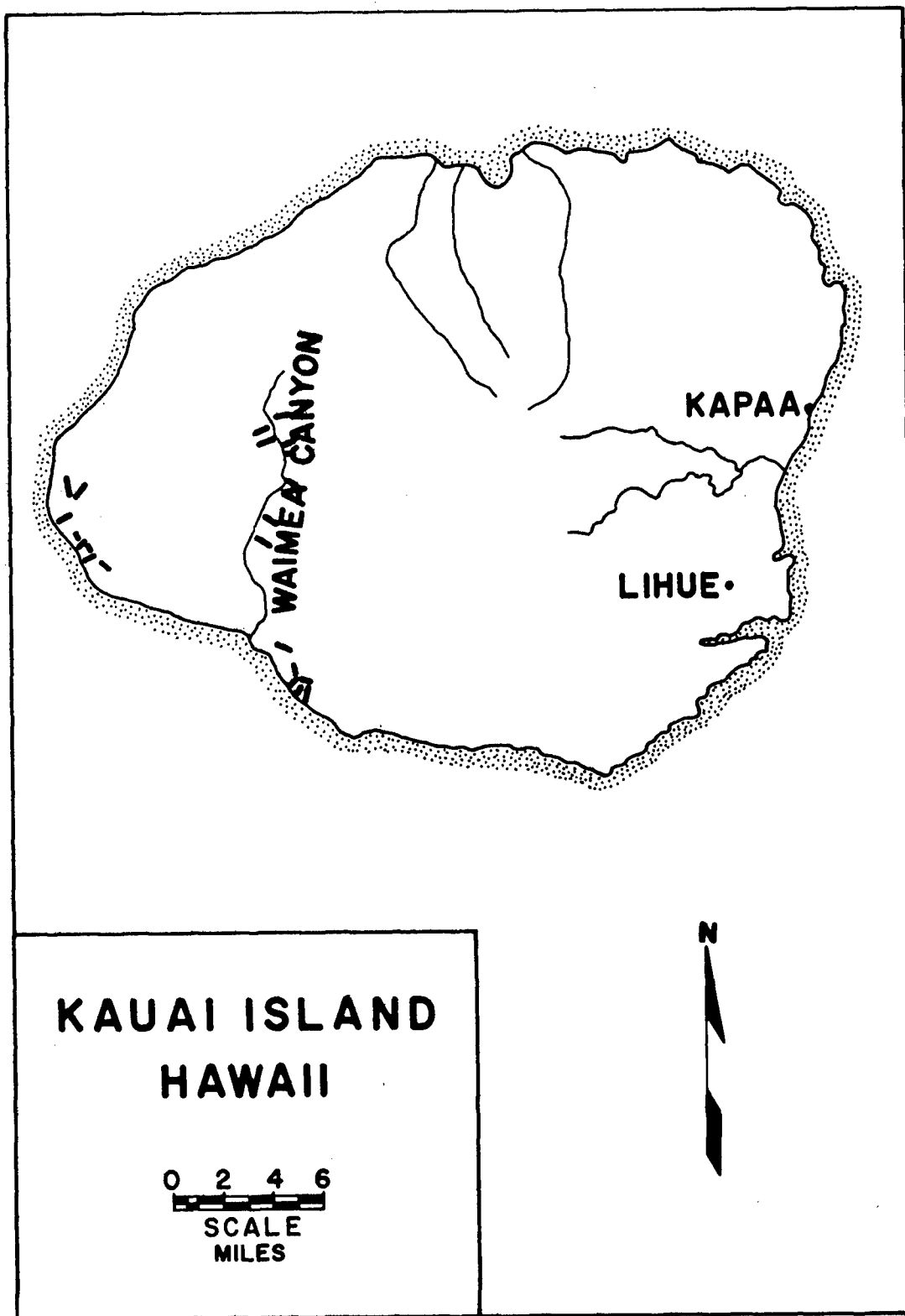


Figure 7. Scaled slope location.

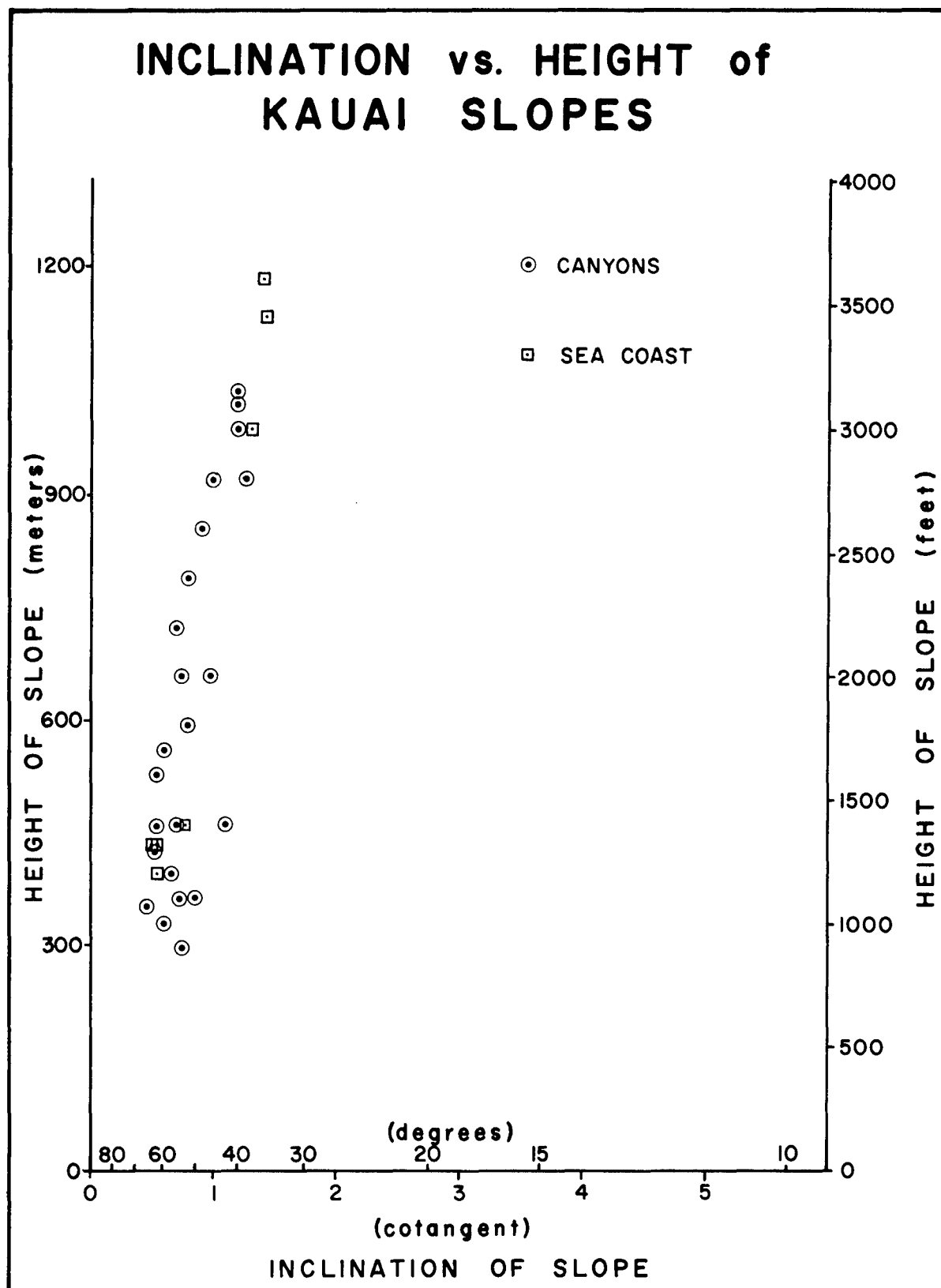


Figure 8.

Slope Stability. The rock types to be encountered along Route 25 will produce a fallback zone exhibiting characteristics of angular, cohesionless materials. In the Choco volcanics the particle sizes are expected to be relatively coarse with only moderate amounts of fine material. In the sedimentary units relative particle size is uncertain, but due to the weak nature of some of the beds a considerably larger volume of fines is expected. These materials will come to rest at their angle of deposition, resulting in an initially stable configuration.

In the areas where the alinement crosses the Choco volcanics, slope heights range from 550 to 1950 feet. Most of the rock is highly and irregularly fractured. The fractures are commonly healed. Laboratory slaking tests indicate that where volcanic breccia occurs, with high percentages of montmorillonite, the materials are susceptible to rapid weathering. The rest of the Choco volcanics are not expected to weather rapidly. Because of the general lack of any well developed or consistent structure dipping towards the alinement, and since the major part of these rocks probably weather slowly, no large sections of instability are expected. Local failures could occur where the alinement intersects faults, although only a few such faults have been mapped.

The alinement crosses beds of the Nercua and Sautata groups where slope heights will range from 875 to 1350 feet. Very little information is available for these rocks. However, descriptions of the rocks indicate they are generally thin-bedded, hard, and highly fractured. Some less competent beds can be expected in the Sautata group which generally overlies the Nercua. Bedding in the Sautata and Nercua groups apparently strikes about normal to the alinement and dips about 30 degrees SW. Weathering characteristics are unknown. Based on lithologic descriptions in the data collection reports and the fact that topography in this area is relatively rugged and steep, crater slopes are generally expected to remain stable.

Where the alinement crossed the Truando group slope heights range from 900 to 1350 feet. Limited laboratory tests show that at least part of these sediments are very weak and may even be partially unconsolidated. The extent of failures which may occur will be dependent on the distribution and orientation of the weak beds in the section. The general dip of the beds is towards the Atrato Lowlands at a low angle. Since the strike is generally perpendicular to the crater centerline, it is the least critical. However, since the median grain size of the fallback and ejecta is expected to be relatively small, sheet erosion and associated weathering could cause some modification of the crater slopes over the life of the project.

Appraisal Summary. In summary, because of the extreme paucity of detailed information along Route 25E, predictions concerning stability are somewhat tenuous. However, based on the information that is available and considering the nature of cratering explosions, it appears reasonable to believe that instability would be restricted to areas underlain by the weaker rock types of the sedimentary units and local areas of adverse geologic structures. These areas have to be identified during the design stages.

Summary. The assessment of crater slope stability in rock requires specific information on crater geometry, geologic conditions and rock properties at the site and seepage and weathering characteristics of the materials. Normally,

documentation of site characteristics and prediction of crater characteristics are not sufficiently refined to permit rigorous analysis and a more generalized approach incorporating empirical data and engineering judgment must be applied. Craters are not strictly analogous to other slopes so that a straight empirical evaluation has limited uses.

Fortunately there are certain general characteristics of craters and crater slopes that make them inherently stable. Fallback from hard dry rock media will behave as cohesionless material and may be studied using methods developed for stability of rubble, talus and rockfill. Factors of safety for the fallback portion of a crater slope should range between 1.1 and 1.5. One experiment which consisted of increasing the steepness of fallback to the point of failure revealed an initial factor of safety of over 1.1 against surficial sliding. Rupture zone materials would most likely fail along surfaces of natural or blast-induced fractures if the strength of the intact rock is significantly larger than the frictional resistance to sliding. Tests of frictional resistance on material and sawed discontinuities in an igneous rock and dolomite measured strengths of 28 to 34 degrees compared to an intact strength of 49 to 56 degrees. The combined observations of near 30 degree frictional resistance along a throughgoing fracture, disarrangement of fractures in the rupture zone making throughgoing fractures unlikely and the relatively flat overall crater slope (30 to 38 degrees) suggest the rupture zone will be stable.

Likewise, seepage problems in rock slopes are unlikely unless the crater intercepts a major surface drainage or the rock contains an unusually large amount of water in storage. As part of the cratering mechanism, excellent drainage characteristics are provided through the development of a system of fractures that progressively increase in number from intact rock to the fallback. Hydraulic conductivity of the fallback has been calculated empirically for two materials at the Nevada Test Site and could vary from 1 to 1000 cm per second. Materials of this type are for all practical purposes free draining.

A sample empirical stability analysis for planned slopes along an inter-oceanic canal route is provided to illustrate the types of information assembled and the way it is used. A major uncertainty in sample analysis in the assessment of crater stability in general is the possibility of long-term changes in strength and seepage characteristics in response to weathering agents.

REFERENCES CITED

1. Davis, S. N. and De Wiest, R. J. M. (1966), Hydrogeology: J. Wiley & Sons, N. Y.
2. Fisher, P. R. (1968) Engineering Properties of Craters, Description of Crater Zones and Site Investigation Methods, Report 1; PNE Report 5012-I.
3. Hughes, B. C. (1968) Nuclear Construction Engineering Technology; Nuclear Cratering Group Technical Report No. 2.
4. Lane, K. S. (1967) Stability of Reservoir Slopes; in Proc. 8th Rock Mech. Symp., Univ. Minnesota; Publ. by AIME, N. Y.
5. Mac Iver, N. N. (1967) The Formation and Initial Stability of Slopes on Cohesionless Materials; PNE Report 5009.

A CONCEPT OF ROW CRATER ENHANCEMENT

B. B. Redpath
U. S. Army Engineer Nuclear Cratering Group
Lawrence Radiation Laboratory
Livermore, California

INTRODUCTION

Linear craters formed by the simultaneous detonation of a row of buried explosives will probably have a wider application than single charges in the explosive excavation of engineering structures. Most cratering experience to date has been with single charges, and an analytical procedure for the design of a row of charges to excavate a crater with a specified configuration has been lacking. There are no digital computer codes having direct application to a row of charges as there are for single charges. This paper derives a simple relationship which can be used to design row charges with some assurance of achieving the desired result and with considerable flexibility in the choice of explosive yield of the individual charges.

BACKGROUND

A characteristic of row craters is that their width $[W_a]$ and depth $[D_a]$ are generally larger than the diameter $[2R_a]$ and depth $[D_a]$ of a single crater excavated by a charge equal in yield to one of the charges in the row. This characteristic is called enhancement, and the size of a row crater can be expressed in terms of enhanced single crater dimensions. Because enhancement increases as the charge spacing is decreased, the size of a row crater can be altered by changing the layout of the charges rather than their yield. This concept found particular application in the design of detonation programs for the Interoceanic Canal Studies [IOCS] where, in response to potentially severe ground shock hazards, the total yield of a number of critical detonations was reduced by employing relatively closely spaced charges.

It became apparent in developing the nuclear excavation technology for the IOCS that the results of existing row crater experience were too inconsistent for direct quantitative application to the design of detonation programs. Fig. 1 shows the dimensions of several of these experimental row craters as a function of charge spacing and relative to single crater dimensions. It was primarily in response to the need of the IOCS program that an attempt was made to arrive at a quantitative rule relating enhancement and spacing.

The successful development of a relationship between enhancement and spacing would mean that a row charge design could be based on single crater dimensions, and these dimensions can be acquired either from calibration shots or from the computational techniques currently in use at institutions such as the Lawrence Radiation Laboratory.

This paper also presents the preliminary results of an experimental program of row cratering designed to test the dependence of enhancement on charge spacing.

CONCEPT

The following assumptions were made in deriving a plausible connection between row crater size and charge spacing:

- [1] A decrease in the spacing of the explosives in a row is equivalent to increasing the apparent yield of each explosive.
- [2] The cross sectional geometry of a row crater is a hyperbola, is not dependent on charge spacing over the range of interest (spacing = $0.5 R_a$ to $1.2 R_a$), and is the same as the optimum (largest) single crater in the same medium.
- [3] The volume of apparent crater excavated by each charge in a row is independent of charge spacing and is greater, by some factor 'k', than the volume of the largest crater excavated by a single charge of the same yield.

The second assumption implies that the width and depth of a row crater will be enhanced equally at any given spacing, and that the depth of burst [DOB] of the charges should be the optimum single charge depth increased by the amount of enhancement. The assumption of an hyperbolic cross section is, in fact, an experimental observation.

The third assumption can be stated:

$$A_r e^2 S = k V_s$$

where A_r = cross section area of optimum single crater or unenhanced row crater

e = enhancement

S = charge spacing

k = volume excavated by a charge in a row relative to a single charge

V_s = volume of optimum single charge crater so that:

$$e = \left[\frac{k V_s}{A_r S} \right]^{1/2}$$

i.e. the enhancement of row crater dimensions is inversely proportional to the square root of the charge spacing.

Fig. 2 is a schematic cross section of a crater illustrating the elements of hyperbolic geometry. The area A_r and the volume V_s are easily evaluated for any crater.

The equation above can also be written:

$$e = \left[\frac{k V_s}{A_r R_a [S/R_a]} \right]^{1/2}$$

and it is interesting to note that the quantity:

$$\frac{V_s}{A_r R_a}$$

varies only over the range of 1.05 to 1.15 for an extremely wide range of crater

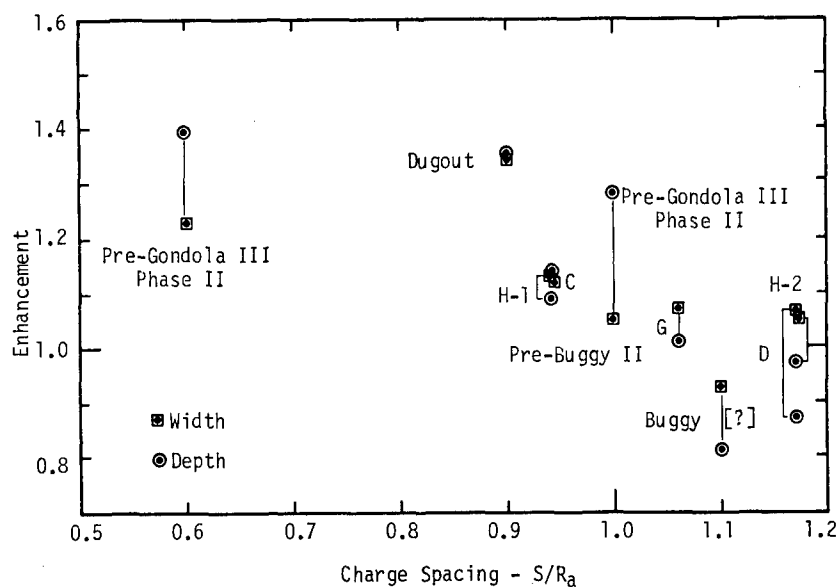
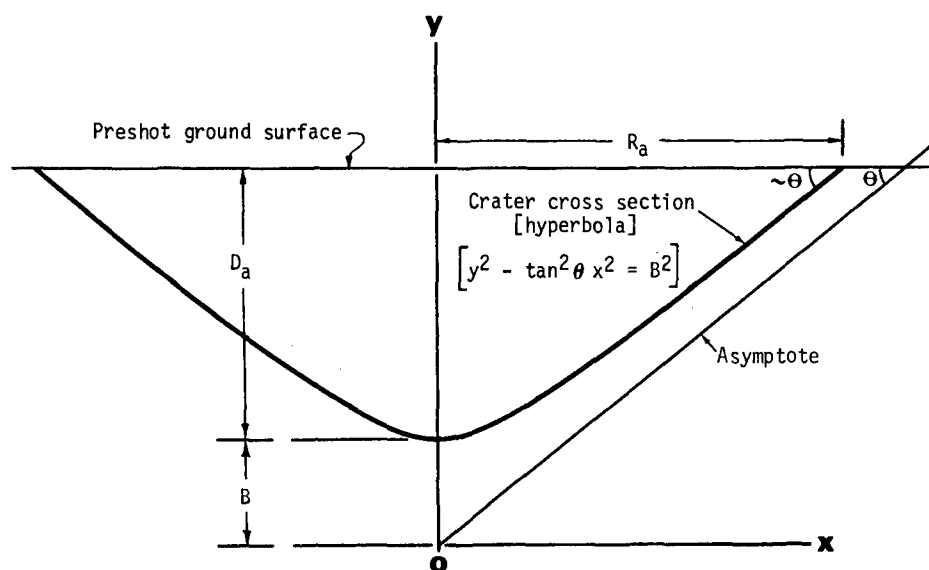


Fig. 1 Enhancement of row crater dimensions as a function of charge spacing.



Volume of crater:
$$V_s = \frac{\pi}{3 \tan^2 \theta} [1 + 3b] D_a^3$$

Cross sectional area:
$$A_r = \frac{1}{\tan \theta} \left[(1 + b) \sqrt{1 + 2b} + b^2 \ln \left(\frac{b}{1 + b + \sqrt{1 + 2b}} \right) \right] D_a^2$$

$$b = \frac{r^2 \tan^2 \theta - 1}{2} \quad B = b D_a$$

$$r = \frac{R_a}{D_a}$$

Fig. 2 Schematic cross section of a crater illustrating hyperbolic geometry.

geometries, and has a value of approximately 1.1 for most craters. As a consequence, the enhancement equation can be simplified to:

$$e = \left[\frac{1.1 k}{[S/R_a]} \right]^{1/2}$$

It is evident that the volume factor k is now the most important unknown.

The volume factor k has been determined in a number of experiments and some of these values are listed in Table I.

TABLE I
Volume Efficiency of Row Charges

<u>Experiment</u>	<u>Medium</u>	$k = \left[\frac{\text{Volume per row charge}}{\text{Single crater volume}} \right]$
Pre-GONDOLA II	Shale	0.82 (entire crater)
Pre-GONDOLA III Phase II [S=0.6 R _a]	Shale	0.78
Pre-GONDOLA III Phase II [S=1.0 R _a]	Shale	1.05
Pre-BUGGY II [C]	Alluvium	1.12
Pre-BUGGY II [D]	Alluvium	1.18
DUGOUT	Basalt	1.70**

It is believed that the large variations in the value of k have been caused by the lack of a consistent design procedure and less than optimum placement of charges in some experiments. The next section discusses further work on the experimental determination of k.

EXPERIMENT

The enhancement concept was the basis for a series of row cratering experiments using 1-ton charges of nitromethane. The objectives were to verify the inverse square root relation between enhancement and charge spacing and to determine the relative efficiency of row charges. The experiment was conducted as part of Phase III of Project Pre-GONDOLA III in October 1969 by the U. S. Army Engineer Nuclear Cratering Group in a shale medium adjacent to the Fort Peck Reservoir in Montana.

The single crater dimensions shown in Fig. 3 had been obtained previously by detonating 1-ton charges in an adjacent area. The following parameters are applicable to the optimum 1-ton single crater:

$$R_a = 27 \text{ ft}$$

$$D_a = 13 \text{ ft}$$

$$\theta = 33^\circ$$

The value of k was judged to be approximately 1.1 on the basis of information

** The value of k = 1.70 for DUGOUT is suspect because more than 40 tons of the explosive nitromethane leaked from the cavities during filling operations.

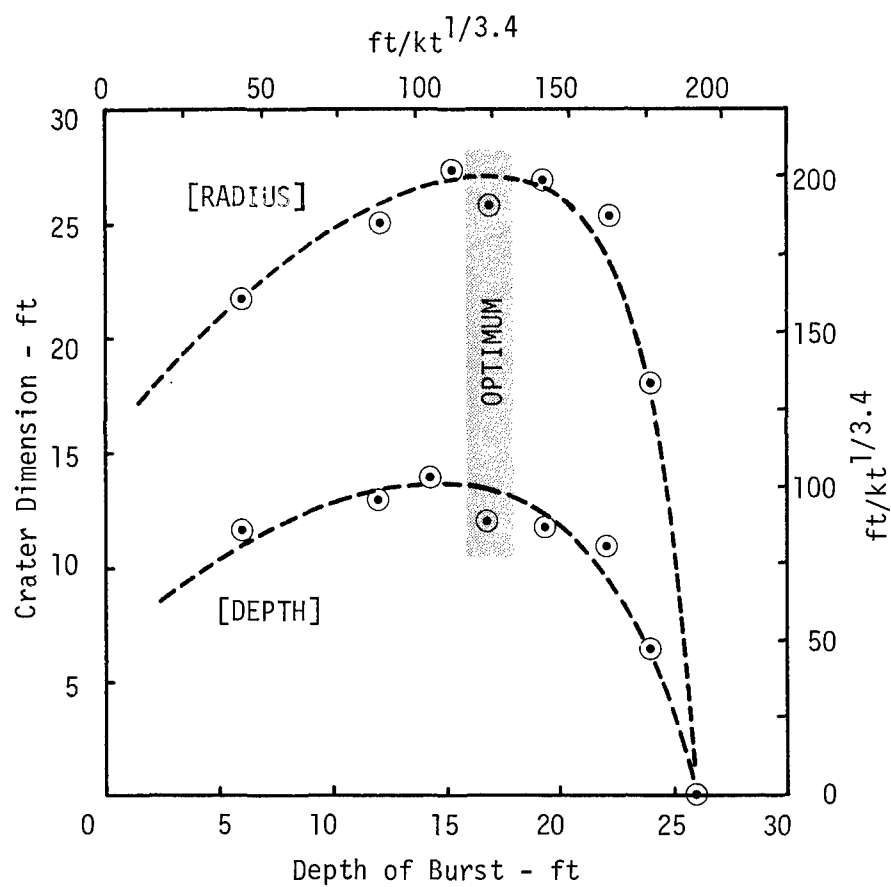


Fig. 3 Crater dimensions vs depth of burst for 1-ton charges in shale.

available from previous experiments [Table I]. The value of $[V_s/(A_r R_a)]$ is 1.1 so that the equation for enhancement was assumed to be:

$$e = \left[\frac{1.21}{S/R_a} \right]^{1/2}$$

A total of six row charges with five combinations of DOB and spacing and one duplication were detonated. Table II summarizes the shot layouts. An additional objective of this series was to test several schemes for smoothly connecting one row crater to another, however, this aspect of the experiment will not be discussed here. Also, in some rows the placement of the end charges differed from the remainder of the row.

Longitudinal profiles and typical cross sections of the craters are shown in Fig. 4 and aerial views are shown in Fig. 5. It should be noted that the center rows [A1 and B1] were detonated and surveyed before the end rows. When the end rows were fired they deposited some material in the center craters as shown on the longitudinal profiles and in the photographs.

The preliminary dimensions were averaged over the linear section** of each crater and are shown in Fig. 6 together with the 1-ton single crater dimensions. Despite the scatter, it is evident that the row crater dimensions plot along lines which pass through zero and the peaks of the single charge curves. This indicates that the cross sections of the rows are very similar to that of the optimum single charge crater.

The preliminary dimensions are shown in Fig. 7 in the format of enhancement vs. charge spacing. A curve which varies as the inverse square root of the charge spacing has been drawn through the data points in Fig. 7. The widths show less scatter about this curve than the depths, and the two rows with a spacing of $0.85 R_a$ demonstrate the scatter inherent in the data. The predicted enhancement is also shown in Fig. 7 and it is evident that the craters were larger than anticipated. There are two primary factors which may account for this. First, there is no single charge 1-ton crater immediately adjacent to the rows; previous experience in this region has demonstrated that the surface geology and its effect on crater dimensions are variable. Consequently, the size of the single crater to which the enhancements are referenced may be incorrect. An increase of 10% in the reference crater dimensions would shift the observed values of enhancement onto the predicted curve. Second, it is very probable that the factor k , assumed to be 1.1, is actually higher. If the reference crater were correct, then the observed row crater dimensions indicate that k is approximately 1.3.

Crater volume excavated per ton of explosive is plotted against charge spacing in Fig. 8 together with a volume computed for the reference crater on the basis of its geometry. The row craters averaged approximately 16,000 cu. ft. per ton of explosive compared with about 12,000 cu. ft. for the optimum one-ton single crater.

The row charge detonations were photographed with high speed motion picture cameras and mound surface velocities were obtained from analysis of the films. The peak mound surface velocities are plotted as a function of scaled depth of burst in Fig. 9 together with maximum single charge mound surface velocities observed in previous Pre-GONDOLA experiments. Although the row

** The linear section of a row crater is generally the portion bounded by points midway between the two charges at each end. In some of the rows the position of the end charges was varied for other reasons. Dimensions were measured only over the portion of the rows where the charge layout was uniform.

TABLE II
Pre-Gondola III Phase III Row Charges

<u>Row</u>	<u>Charge Spacing</u> <u>S/Ra</u>	<u>Absolute</u>	<u>Depth of Burst</u> <u>Scaled</u>	<u>Absolute</u>	<u>Number</u> <u>of Charges</u>	<u>Predicted</u> <u>Enhancement</u>	<u>Predicted Dimensions</u> <u>Wa/2</u>	<u>Da/2</u>
A1	1.0	27 ft	143	19.3 ft	6	1.10	29.7 ft	14.3 ft
A2	0.85	23	155	21.0	7	1.20	32.4	15.6
A3	1.15	31	133	17.9	5	1.03	27.8	13.4
B1	0.7	19	170	23.0	7	1.32	35.6	17.2
B2	0.85	23	155	21.0	6	1.20	32.4	15.6
B3	0.55	15	192	26.0	9	1.49	40.4	19.4

$$[= ft/kt^{1/3.4}]$$

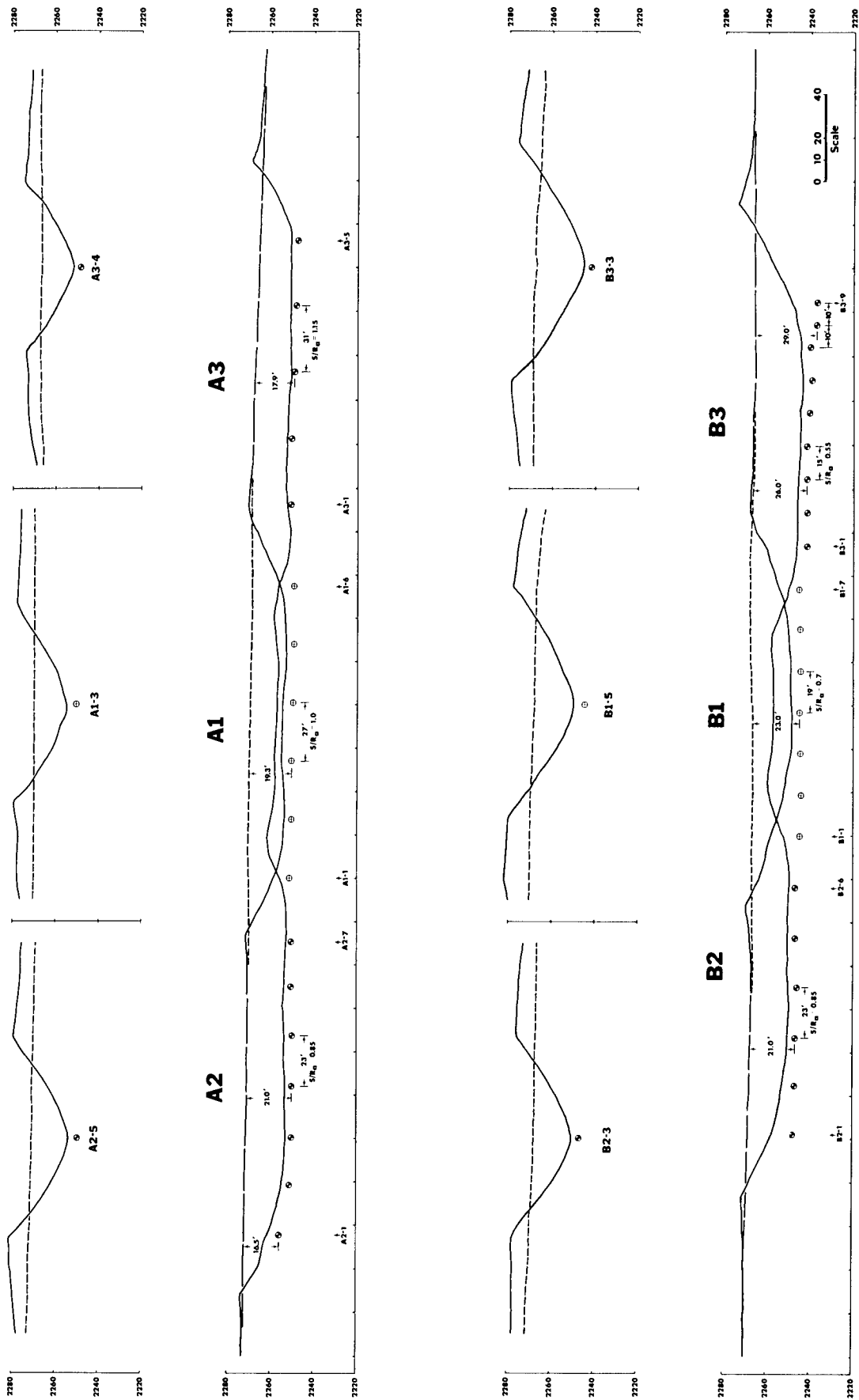


Fig. 4 Longitudinal profiles and typical cross sections for Pre-GONDOLA III Phase III row craters.



(a)



(b)

Fig. 5 Pre-GONDOLA III Phase III row crater experiment in shale at Fort Peck, Montana. [a] Aerial view of craters A1, A2, A3, and B1. [b] Aerial view of row craters after detonation of rows B2 and B3.

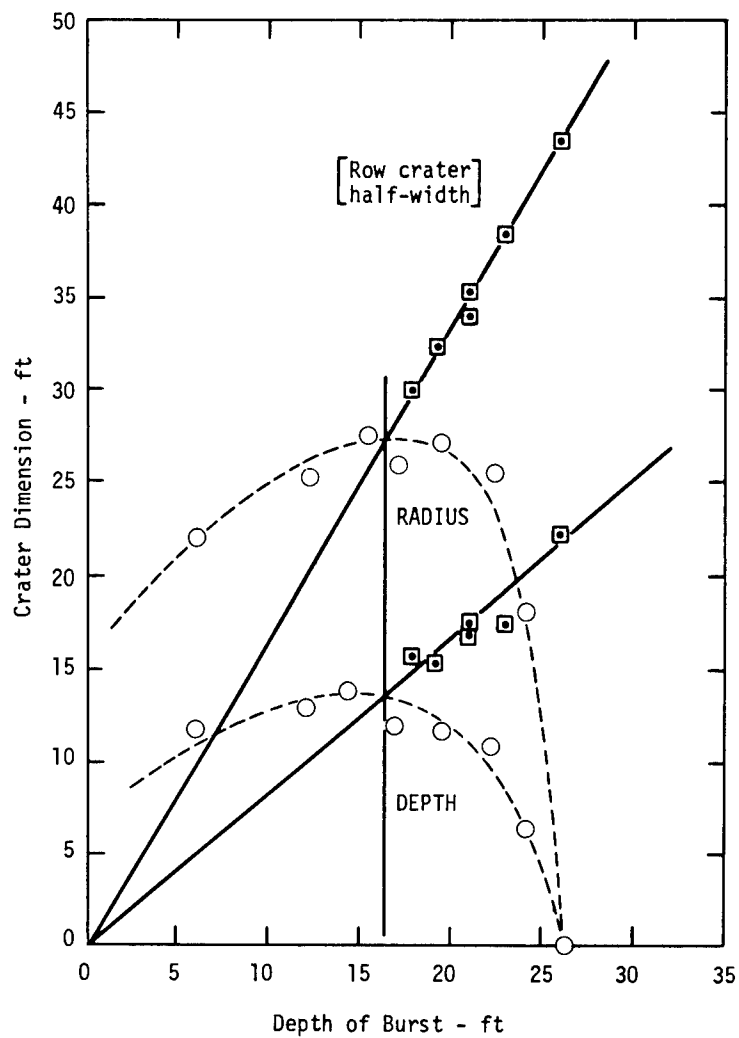


Fig. 6 Dimensions of single and row craters vs depth of burst.

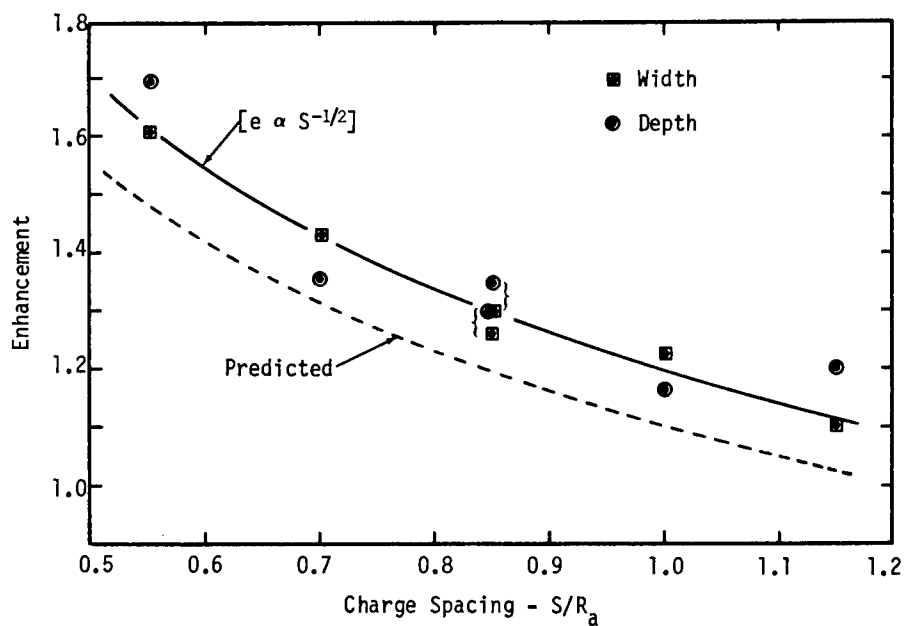


Fig. 7 Enhancement of Pre-GONDOLA III Phase III row crater dimensions as a function of charge spacing.

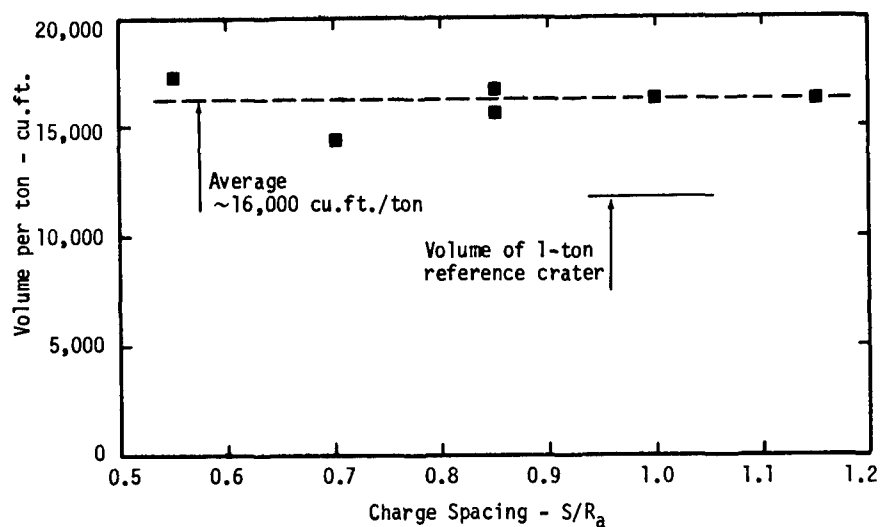


Fig. 8 Volume of apparent crater per ton of explosive as a function of charge spacing.

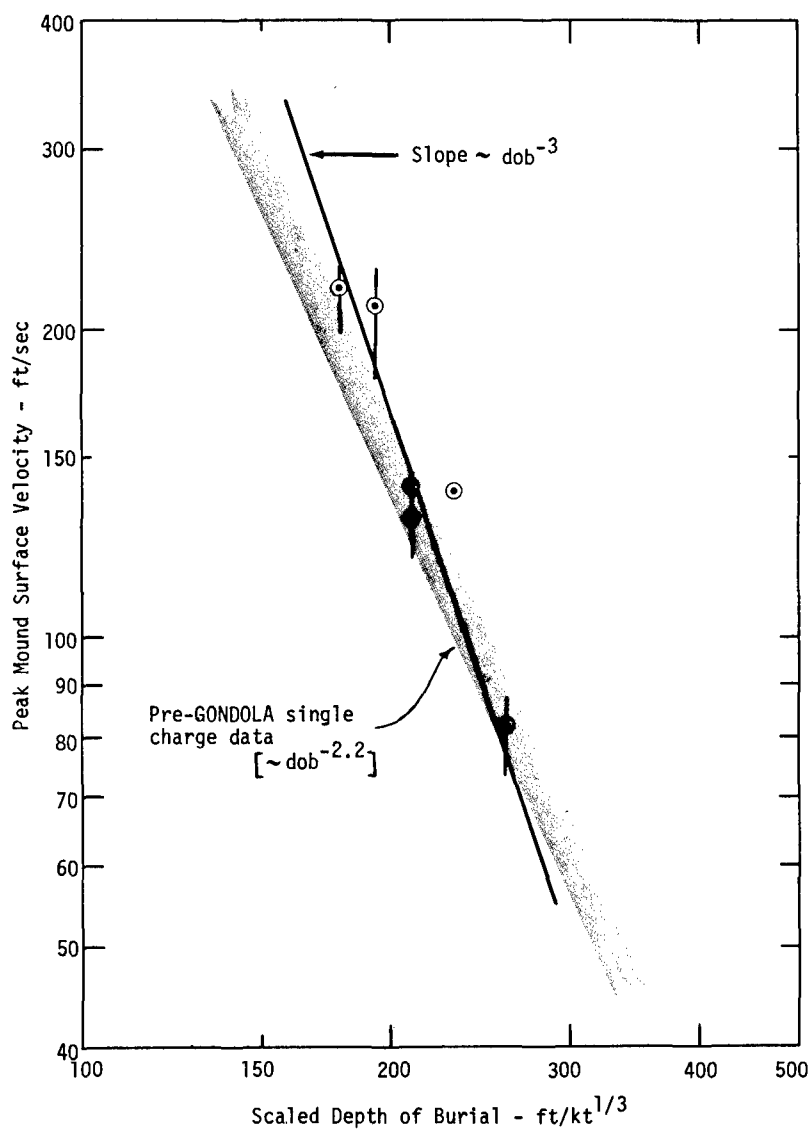


Fig. 9 Variation of maximum surface velocity with depth of burst

charge velocities appear to be more dependent on depth of burst than the single charge mound surface velocities, they are approximately the same as the single charge velocities. It is interesting to note that row crater dimensions increased as the peak mound surface velocity decreased, and that the largest of the six row craters had depth of burst and a peak mound surface velocity which would be characteristic of a retarc in the case of a single charge in the same material. Previously, craters have not been produced in either shale or dry hard rock when peak mound surface velocities were observed to be less than about 100 ft/sec.

It will be noted that more charges were used in the rows with the closer charge spacings. This was done to insure that the craters would have a reasonable ratio of length to width and not be elliptical in plan.

APPLICATION

In order to illustrate application of the concept, assume that we wish to excavate a 15 ft. deep channel in rock and that 1-ton charges are desirable from a construction standpoint. What is the appropriate charge spacing and DOB assuming that the optimum single crater has the following properties:

$$\begin{aligned}r_a &= 150 \text{ ft/kt}^{1/3.4} \\d_a &= 90 \text{ ft/kt}^{1/3.4} \\ \text{optimum dob} &= 140 \text{ ft/kt}^{1/3.4} \\ \theta &= 37^\circ\end{aligned}$$

and assuming, for the present, that $k = 1.2$.

The required scaled crater depth is

$$\frac{15}{.001^{1/3.4}} = 114 \text{ ft/kt}^{1/3.4}$$

so that the necessary enhancement of single crater depth is

$$e = \frac{114}{90} = 1.27$$

the appropriate charge spacing will be given by

$$\begin{aligned}\frac{S}{R_a} &= \frac{1.1 k}{e^2} \\ &= 0.82, \text{ say } 0.8,\end{aligned}$$

therefore,

$$\begin{aligned}S &= 0.8 R_a \\ &= 0.8 \times 150 \times .001^{1/3.4} \\ &= 15.7 \text{ ft.}\end{aligned}$$

and the DOB will be

$$\begin{aligned}&= 140 \times 1.27 \times .001^{1/3.4} \\ &= 23.3 \text{ ft.}\end{aligned}$$

It is interesting to note that if enhancement were not used, then each charge would require a yield of

$$\left[\frac{15 \text{ ft.}}{90 \text{ ft/kt}^{1/3.4}} \right]^{3.4} = 2.3 \text{ tons}$$

in order to excavate the same channel.

CONCLUSIONS

It appears that the concept relating enhancement and charge spacing is essentially correct. The experiment based on this concept indicates that enhancement does vary inversely as the square root of the charge spacing provided that the depth of burst is increased correspondingly. The efficiency of a row charge in excavating shale appears to be about 30 percent greater than a series of single charges. The relative efficiencies of row charges and single charges in other media should be determined empirically.

The observation that mound surface velocity decreased with increasing crater size and the association of the largest row crater with a velocity characteristic of a single charge retarc would suggest that peak mound surface velocity should be used cautiously as a row charge design tool.

A departure from a row charge design consisting of charges spaced one radius apart and buried at optimum DOB for a single charge has been, in the past, an uncertain procedure. It is believed that there is now a flexible and reliable basis for row charge design.

This concept has already found application to the feasibility studies of an interoceanic canal, however, it is anticipated that it will find the widest application to excavation projects with chemical explosives where emplacement costs can be reduced by employing smaller charges.

TORRES STRAIT: A Channel Clearing Project
Stanley Bankert
Department of Applied Science
University of California - Davis

The Torres Strait is a reef-laden stretch of water lying south of New Guinea and north of the tip of the Cape York Peninsula of northeastern Australia (See Figure 1). Because of its location and geologic structure it is particularly hazardous to shipping, and limits passage through the area. It was suggested [8] that nuclear explosives might be used to create a safe shipping channel through the strait, and in this paper that possibility will be explored.

The Cape York peninsula of Australia projects some 150-200 miles into the Pacific Ocean, separating the Arafura Sea to the west from the Coral Sea to the east. The population density of the peninsula is quite low on the northern tip (~ 0.1 inhabitants/sq mi) and increases slightly (to 25 inhabitants/sq mi) further south. The peninsula is covered with monsoon forest (moist deciduous forest) and some tropical rain forest. The inhabitants are for the most part primitive people engaged in hunting, fishing, gathering, and primitive agriculture. Southern New Guinea is of a similar nature in that it is covered by scrub, grass, monsoon forest and mangrove swamps. There are less than 25 inhabitants per square mile, and the inhabitants are on the same primitive level as the inhabitants of the Cape York peninsula [1].

Starting near the eastern tip of New Guinea and running south parallel to the eastern Australian coast is the Great Barrier Reef which varies in width from 2 to 45 miles. The Reef is perilous to navigate and about 10 fair weather passages lead through it. Just east of the reef the water depth is 250 to 300 feet (see Figure 2). However, just west of the reef at the "Yule Entrance", which is the entrance nearest the Torres Strait, the depth is only 60 to 100 feet. Travelling further west the water depth decreases to about 50 feet in 70 miles. In the next 50 miles the water depth decreases to 20 to 30 feet between the exposed reefs, and having passed the most treacherous area one must still travel another 40 miles west to again reach waters whose depths are 120 to 150 feet. The depth of the water somewhat limits the size of the vessels which can pass through the Strait and generally they are in the 25,000 ton (dead weight) class [2]. The navigational difficulties in the area are further increased by extremely complicated tides. The Torres Strait separates two tidal systems, and high and low tides may occur simultaneously on both sides of the strait. This leads to high velocity currents (6 knots) and shifting sand banks and ridges which limit passage to fair weather and skilled pilots [4,10]. In toto, there are about 120 to 180 miles of treacherous waters through which a safe channel might be opened. To do so by conventional explosives would be impossible because of the amount of material to be moved and the cost of the explosive. It would, however, be feasible using nuclear explosives.

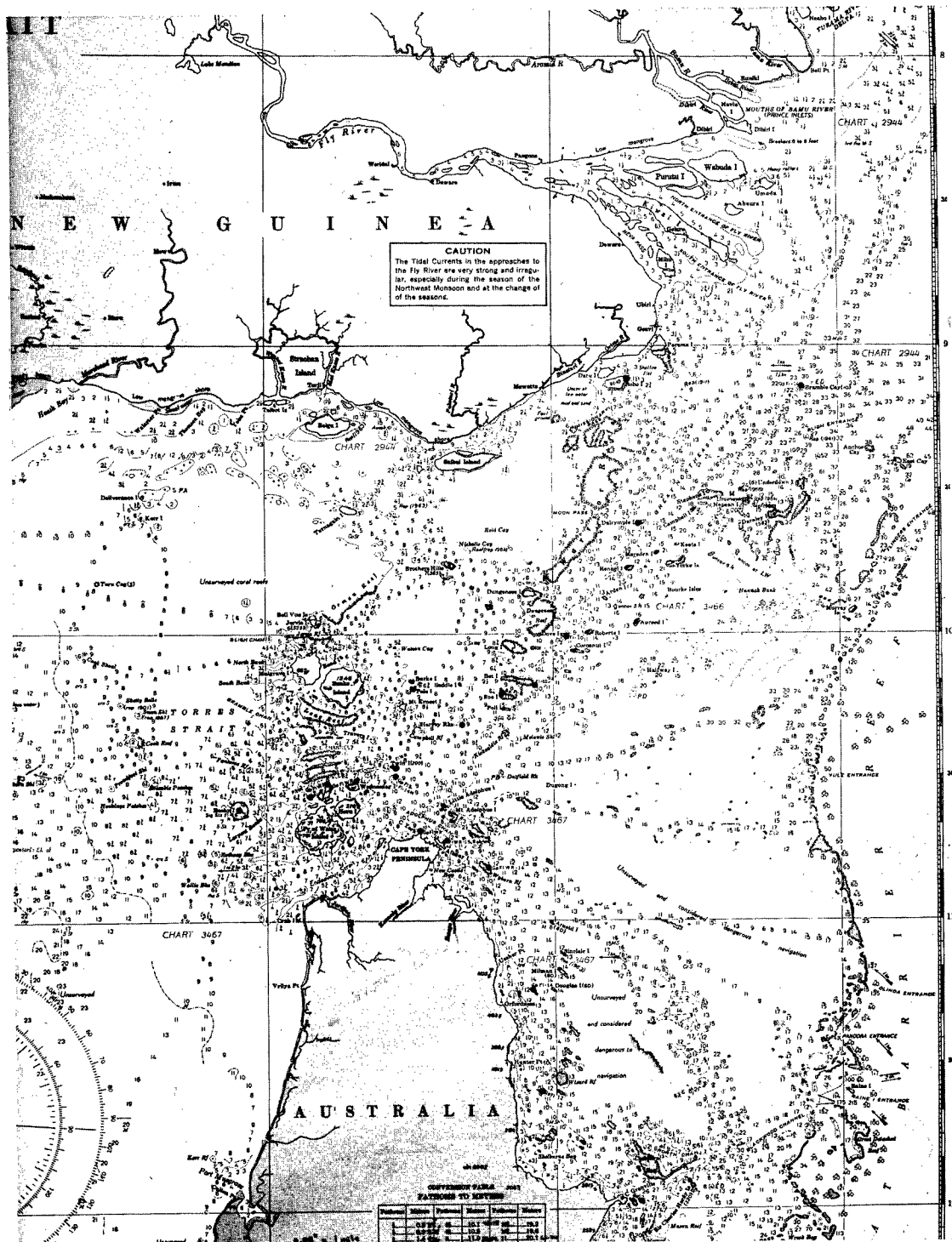
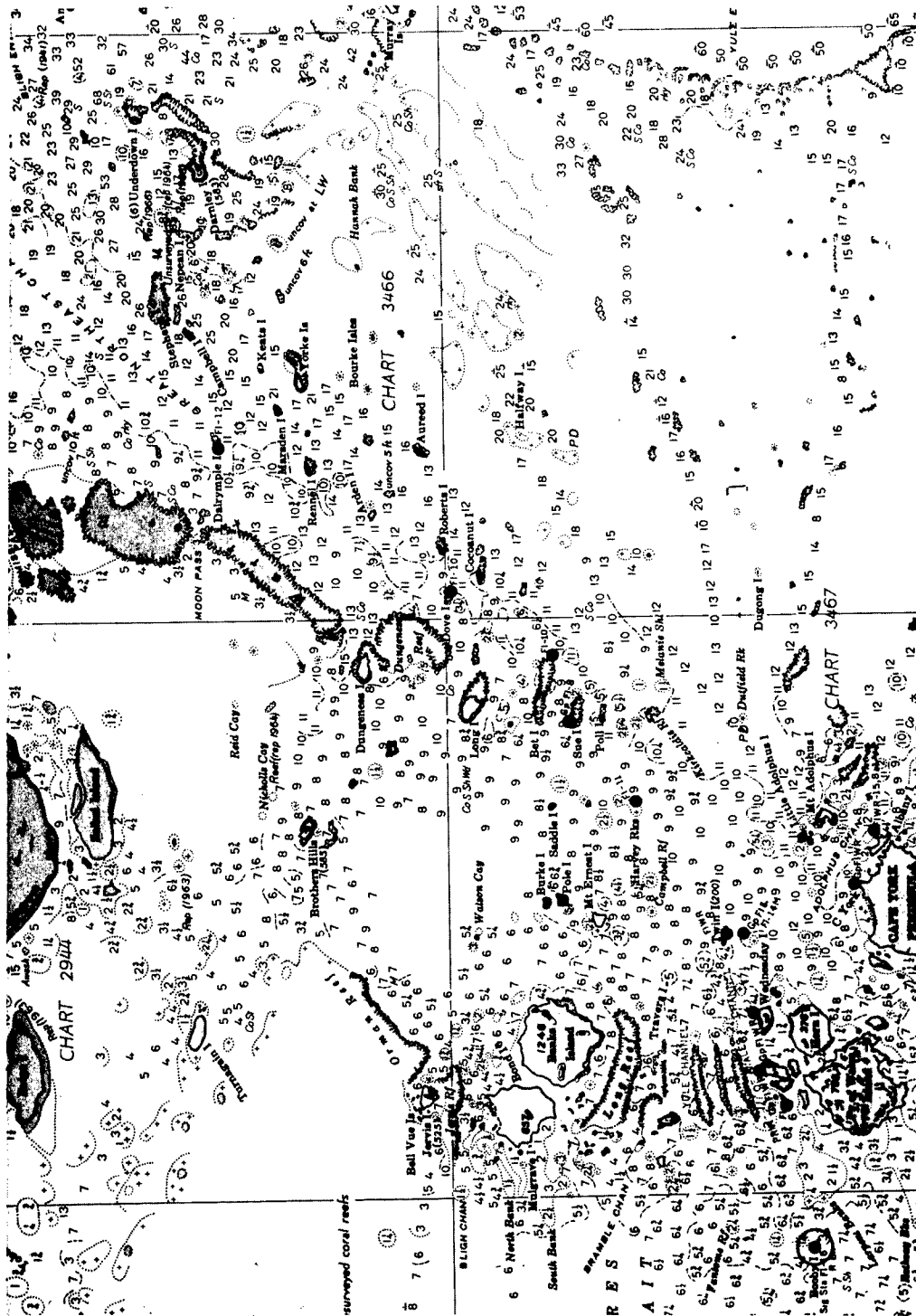


Figure 1 - Torres Strait Area approximately 185 by 250 miles.
Depth in fathoms



Determining what would constitute a safe channel would require extensive studies of the sand motion and currents. As a first estimate, a channel of the size of the proposed Transisthmian Canal can be used. This would be about 1000 feet wide and 225 to 250 feet deep. The length of the channel would be 180 miles. A shallower channel, say 150 to 200 feet need not be quite as long and would significantly reduce the amount of explosive required (due to the decrease in apparent crater size). The media across the strait vary from mud, coral, and other sediments to shales, sandstones, and some volcanics with no regularity [4].

The Transisthmian Canal study serves as an excellent guide to the construction of a long channel. Like the canal the Torres Strait Channel will best be constructed in a series of dashes about 10 miles long, and this will mean up to 100 charges per dash. Each single charge will produce a crater with a diameter of 1000 to 2000 feet at the ocean surface, and the net result of the row charge will be a 10-20% increase in ditch dimensions [7]. Using these assumptions to calculate the charge size should yield a conservative estimate of the total row shot charge. Further assumptions must be made about what scaling laws can be used and what type of material to scale.

The coral, sand, sedimentary material, and rock have no analogies in past experiments with nuclear explosives because of the water involved. The water not only changes the properties of the medium, but may be considered as either part of the medium to be moved (with different properties) or as an increased resistance to the moving of the medium. In this paper the coral-mud-sediment media was assumed to be an average of alluvium and tuff. This assumption was also made when the water was considered as part of the media to be moved. Alluvium was chosen because of its "sandiness" and the tuff because of its porous structure. The simple scaling law:

$$x_2 = x_1 \left(\frac{Y_2}{Y_1} \right)^{1/3.4}$$

was assumed to hold. Here the Y_i are the yields and the x_i may be the depth of burst, apparent crater radius or apparent crater depth. The data used in scaling is indicated in Table I.

TABLE I
Data Scaled [5]

Shot name	Medium	Yield(kt)	DOB(ft)	apparent radius(ft)	depth(ft)
Jangle U	alluvium	1.2	17	130	53
Neptune	tuff	0.115	100	100	35

The question of when the overlying water behaves as part of the medium and when it acts as a resistance to moving the medium is not easy to answer. In 1958, 2 kt of conventional explosives were used to remove a shipping hazard called "Ripple Rock" about 120 miles north of Vancouver, B.C. [6]. The hazard consisted of two underwater pinnacles, extending to within 9 and 20 feet of the surface at low tide, joined by a saddle 70 feet below the surface. The two pinnacles were removed, and in the research to determine the amount of explosive to be used it was found that the same particle acceleration could be obtained in water as in air if

twice the amount of explosive were used. This worked as predicted in the removal of Ripple Rock.

Taking Ripple Rock as an example, it was assumed that if the water depth were greater than 25 feet, the amount of explosive would be doubled. The water was then a resistance to the moving of the medium while if the water depth were less than 25 feet, the water would be considered as part of the medium to be moved. This meant that for a water depth of 100 feet for a 250 foot channel, the necessary apparent crater depth was assumed to be 150 feet and the yield was doubled. For 10 feet of water, however, the necessary apparent crater depth was assumed to be the channel depth, 250 feet.

In order to carry out the computations, a simple computer program was written, into which the depth of water was inputted at 5000 foot intervals from the Great Barrier Reef to 180 miles west. At each point, yield, depth of burst, crater radius and other data were calculated from the necessary apparent crater depth required by the water depth. Explosives cost was evaluated at each point [7] and multiplied by a factor of 5 to cover the 5000 foot stretch. Drilling costs were assumed to be \$300/foot based on the Transisthmian Canal study. The sum of explosives cost and the drilling made up approximately 1/3 of the Transisthmian Canal estimate, and the total cost of the Torres Strait Channel was estimated on this basis.

Some typical values from this program are given in Table II. Table III gives an idea of the total costs of the Torres Strait project as well as the total amount of explosive required. From Table II we see that the maximum explosive required per 10 mile dash would be 11 Mt. This is considerably less than the 12 Mt per 6 mile dash required by the Transisthmian Canal. The maximum aggregate yield of 157 Mt is also considerably lower than the Canal's 170-300 Mt and is spread over 180 miles rather than 43-48 miles. It would appear that none of the devices need be larger than 165 kt as compared to a 35-40 Mt maximum for the Canal. The Torres Strait Channel would have less radioactivity and blast effects per shot, per dash, per maximum shot, and in total than the proposed Transisthmian Canal. The total costs of the channel would be higher because of the increased number of shots and the associated drilling, dredging, and study costs. The relative isolation and low population density of the area reduces many of the problems associated with radioactivity and blast.

Consider the maximum explosive, 11 Mt, spread evenly over 10 miles; first for radioactivity problems, and then for blast effects. In neither case are there equivalent experiments which can be scaled. Glasstone indicates that the fallout from the shallow underwater Bikini BAKER test was very much like that from an underground shot [3]. Since the explosions will always be underground and also underwater, a first guess estimate of the released radioactivity pattern can be obtained from scaling the pattern from a previous underground shot in alluvium. The 0.1R integrated dose contour from the SEDAN (100 Kt) event extended approximately 100 miles downwind [7]. Use of the 1/3.4 scaling law (Glasstone uses 1/3 for surface bursts) puts the 0.1R integrated dose contour some 400 miles downwind of the dash. A westerly wind would carry any fallout pattern out over the Arafura Sea. A southeasterly would carry it out over the Coral Sea. In either case there is nothing for at least six hundred miles. The cross wind width of the SEDAN 0.1R contour was about 5 miles. This scales to about 20 miles and will cover no major land bodies in the Torres Strait itself. It may be possible with the proper choice of wind direction and duration to keep the integrated dose in all

TABLE II

Typical Values for a 250' Channel

Distance from Great Barrier Reef	16.1 mi	40.7 mi	94.7 mi
Water depth, feet	150.0	54.0	0.0
Yield, kt	14.5	142.6	163.1
Depth of burst, feet	375.	495.	459.
Hole depth, feet	225.	441.	459.
Surface width, feet	685.	1342.	1396.
Hole cost, \$ x 10 ⁻⁴ /shot	\$ 6.75	13.23	13.76
Explosive cost, \$ x 10 ⁻⁴ /shot	\$ 3.91	48.79	49.36

TABLE III

Yield and Cost Data for
Torres Strait Channel

180 mile channel

	225 Ft. depth	250 Ft. depth
Total yield	102 Mt	157 Mt
Explosives cost	\$ 395 million	\$ 414 million
Drilling cost	88 million	102 million
Est. total cost	1600 million	1750 million

120 mile channel

	225 Ft. depth	250 Ft. depth
Total yield	58 Mt	85 Mt
Explosives cost	\$ 280 million	\$ 290 million
Drilling cost	66 million	75 million
Est. total cost	1235 million	1310 million

inhabited areas well below 0.1R per dash. The predominant winds in the area are from the southeast to the northwest and the surface water currents are from the Coral Sea to the Arafura Sea [1,4]. Summer (January) is monsoon season so the channel will have to be constructed during Winter (July). Construction should be from west to east to minimize delays. It appears then that the radioactive fallout over populated areas can be kept to a minimum and evacuation may not be necessary. This is facilitated by the fact that there are no large cities within 100 miles and only 4 or 5 within 300 miles of the Torres Strait.

Blast may be more of a problem than radioactive fallout because it has three forms:

- a) Air blast - air motion
- b) Seismic effects - ground motion
- c) Tsunami - water motion

Air blast would not be a problem beyond 600 miles downwind and like radioactive fallout should pose no difficulties provided the shots take place during winds from the east or the northwest. Seismic effects cannot be directed by the wind and therefore may be important. Using an equation given by Teller et al [7] for ground motion:

$$v = k Y^{0.67} R^{-1.5}$$

for an 11 Mt shot in alluvium, $v = 8$ cm/sec at 20 km and 0.75 cm/sec at 100 km. For granite these values must be multiplied by about a factor of 8. Hence close to the shots (say 10 miles) some ground motion damage might be expected (window breakage, plaster cracking) although none of the larger communities should be affected. The problem of tsunami production is not soluble until tests in similar media are carried out. However, waves could be very large, on the order of hundreds of feet trough to crest [3], and something would have to be known about the normal wave patterns and heights in the area to assess possible damage. Blast effects are something which must be considered further when better geological data is available and in particular close attention will have to be paid to tsunami production.

It would appear that the construction of a Torres Strait Channel is technically feasible, but economic feasibility and environmental effects need also be considered. The economic gains from the construction of such a channel stem from two sources: reduced shipping costs and economic development of new areas. Australian shipping is about 35 million tons per year of which the majority is coastal shipping between different sections of the country [9]. Half of this coastal shipping passes through the Torres Strait along with any shipping from southeastern Australia and eastern New Guinea to Indonesia, Indochina, and Japan [1]. These vessels are small (in the 25,000 ton class), and the construction of the Torres Strait Channel would allow the use of much larger vessels with lower shipping costs as a direct result. Northwestern Australia is an important contributor of raw materials to the Australian economy, and these pass through the Torres Strait. Construction of a safe channel would add incentive to the development of northwestern Australia because of the greater ease and lower cost of shipping. This is particularly true in light of the proposed nuclear excavated harbor in northwestern Australia. Taken in the perspective of lower shipping costs and the development of northwestern Australia, the \$2-3 billion construction cost is quite reasonable and the project appears economically feasible.

Environmental effects appear in the interaction of the channel and its construction with the people and the ecology of the region, and in depth consideration of them is beyond the scope of this paper. One of the questions which arises is: What will be the effect of the channel on the Great Barrier Reef? The Reef is protected by Australian law and is considered to be the "world's largest wildlife sanctuary" [4]. While the salinity (34-35%), chlorinity (19%), and water temperature (29°C) are nearly the same throughout the region and do not present a problem, the effect of the channel on the ecology of the Reef is a complete unknown and will require very thorough study. The oceanic transport of the radioactivity deposited in the ocean presents still another problem. Where will it go?; What species will take it in?, and How much will it be concentrated? are all questions which need as yet unavailable answers. The population of the region while sparse also presents some interesting questions. Since they are extremely primitive and live by hunting, fishing, gathering and primitive agriculture, it is important that it be known how the sudden contact with civilization that the channel construction will bring will affect them. Their roaming and gathering existence will put them in greater contact with even small amounts of radioactivity, but it is not known how much of an effect this will be. There are many other questions like these which need to have answers before the channel can be constructed.

While the construction of the Torres Strait Channel appears feasible from both a technical and an economic point of view, a great deal of further research will have to be done in a number of areas. The Channel would be a great economic boost to northwestern Australia and to trade between southeast Asia and Australia, but its effect on the Great Barrier Reef and the people of the region will require serious consideration.

Bibliography

1. The Times Atlas of the World, John Bartholomew, ed., Vol. 1, Houghton Mifflin Company, 1958.
2. Bird, J., Seaport Gateways of Australia, Oxford University Press, 1968.
3. The Effects of Nuclear Weapons, Samuel Glasstone, ed., USAEC 1957.
4. Maxwell, W.G.H., Atlas of the Great Barrier Reef, Elsevier Publishing Company, 1968.
5. Nordyke, Progress in Nuclear Excavation Technology, UCRL-12248, 1964.
6. Ripple Rock, Hazard to Navigation Destroyed, "Civil Engineering", Vol. 28, May 1958.
7. Teller, E., et al, Constructive Uses of Nuclear Explosives, McGraw-Hill, 1968.
8. Teller, Edward, article that I have not been able to relocate.
9. Theel, Gustav, The World Shipping Scene, Westadt-Verlag, 1963.
10. Worrell, Eric, The Great Barrier Reef, Angus and Robertson, Ltd., 1966.

A STUDY OF UNDERGROUND EXPLOSION CRATERING PHENOMENA
IN
DESERT ALLUVIUM

By

H. C. Saxe* and D. D. DelManzo, Jr.**

INTRODUCTION

With the advent of the nuclear age, man now has within his grasp the ability to liberate vast quantities of energy for the performance of constructive work for our mutual welfare. The feasibility of using nuclear energy for earth excavation on an unprecedented scale is one such peacetime application which appears to have particular merit.

In order to optimize the efficient engineering application of any large-scale detonation, however, whether of the nuclear or conventional high explosive type, some means of accurate prediction of its effects must be available to the scientific community. Considerable progress toward this goal has been made under the sponsorship of the Division of Peaceful Nuclear Explosives of the Atomic Energy Commission through their "Plowshare" Program, as well as by investigators, primarily of other governmental agencies. In view of the restrictions which have been placed upon nuclear testing in the atmosphere of recent years, the nuclear field testing program has been curtailed to the point where nuclear cratering data in the regime of interest from the nuclear excavation viewpoint has been minimal.

In view of this impasse, an alternative and logical approach is to make further use of such cratering data from conventional high explosives as are available, and to use these results to predict what ostensibly might result from nuclear events occurring in the same media.

Consequently, the purpose of this paper is to provide an in-depth study of the feasibility of conventional high explosive to nuclear scaling as applied to explosion cratering in the underground regime of interest from the point of view of earth and rock excavation. Toward the accomplishment of this objective, the authors have chosen to concentrate their efforts upon available high explosive and nuclear crater data resulting from the extensive series of tests performed in Desert Alluvium of the A.E.C.'s Nevada Test Site during roughly the past two decades.

* Dean, University of Louisville, Speed Scientific School

** Lieutenant, Civil Engineering Corps, U.S. Navy

It is precisely this medium for which the largest number of carefully controlled, well documented cratering test data are available for both conventional high explosive and nuclear cratering events, a factor of prime concern if one is to attempt conventional HE-Nuclear scaling within reasonable limits of confidence. Exact details and excellent bibliographies relative to these and other cratering results are contained in papers by VAILE (1), CHABAI (2), NORDYKE (3, 4), and TOMAN (5).

CRATER SCALING

General Considerations

A vital aspect of any attempt to develop a conventional HE-nuclear explosive scaling capability is a critical analysis of the applicable scaling laws for crater dimensions and associated phenomena utilizing the principles of dimensional analysis. Excellent studies of the principles of dimensional analysis relevant to the cratering problem have been performed by LAMPSON (6), VAILE (1), CHABAI (2), and others in the United States, and by POKROVSKII and FEDOROV (7), and SEDOV (8) in the USSR.

Let us assume that the following j physical variables expressible in terms of the four fundamental physical dimensions M , L , T , and θ are deemed applicable to cratering, and formulate a dimensional matrix D of order $j \times 4$, the elements of the matrix indicating the respective exponents of the physical variables in terms of the fundamental physical dimensions. According to the principles of dimensional analysis, we may develop a set of $(j-4)$ linearly independent solutions in the form of non-dimensional parameters referred to as P_i terms which are expressible as arguments of some operation f , such that

$$f(P_{i1}; P_{i2}; P_{i3} \dots P_{i(j-4)}) = 0 \quad \text{-----} \quad \underline{1}$$

We may arbitrarily rearrange the rows and subdivide the dimensional matrix D into the submatrices D_1 and D_2 of orders $(j-4) \times 4$, and 4×4 respectively, with the stipulation that D_2 be a nonsingular matrix of rank four. Following this procedure, the matrix of solutions for the $(j-4)$ P_i terms of equation 1 may be obtained from the expression:

$$P_i' = \begin{bmatrix} I & -D_1 & D_2^{-1} \end{bmatrix} V' \quad \text{-----} \quad \underline{2}$$

where

P_i' = The logarithm of the matrix of solutions for the $(j-4)$ P_i terms of equation 1

I = An identity matrix of order $(j-4) \times (j-4)$

V' = The logarithm of the j physical variables deemed applicable to the problem

A solution of a dimensional analysis problem by equation 2 has the characteristic that resulting P_i terms will contain the physical variables contained in the D_2 submatrix as repeating variables, i.e. they will appear in one or more of the P_i terms, but those variables isolated into the D_1 matrix will appear in one and only one P_i term.

This is particularly important in those cases where lack of complete dimensional homogeneity in a physical problem is anticipated due to the presence of a particular physical variable or dimensional constant, allowing us to isolate this variable by confirming it to only one Pi term. An example of such a dimensional constant in the case at hand is the effect of gravity upon the scaling of underground explosion craters.

CRATER SCALING WITHOUT GRAVITY EFFECTS

First let us apply the foregoing method of analysis to the cratering problem specifically to the case where the effects of the acceleration of gravity are to be ignored. Assuming that we arbitrarily select a group of 19 physical variables as having relevance to the cratering problem, we form the dimensional matrix D of Table I.

TABLE I
Typical Physical Variables of Cratering Problem

<u>No.</u>	<u>Physical Variables</u>	<u>Symbols</u>	<u>Dimensional Matrix D</u>			
			<u>M</u>	<u>L</u>	<u>T</u>	<u>θ</u>
1.	Length (Rad, Dob, etc.)	R	0	1	0	0
2.	Volume	V	0	3	0	0
3.	Velocity; Brisance; Acceleration Impulse	B	0	1	-1	0
4.	Momentum	Mv	1	1	-1	0
5.	Acceleration (inc. gravity)	g	0	1	-2	0
6.	Weight of TNT	W	1	1	-2	0
7.	Power of Explosive	P	1	2	-3	0
8.	Duration of Pulse	t	0	0	1	0
9.	Medium Viscosity	μ	1	-1	-1	0
10.	Medium Heat Transfer Coefficient	h	1	0	-3	1
11.	Heat of Change of State	Hvf	0	2	-2	0
12.	Explosive Heat Yield Per Unit Weight	Hy	-1	1	0	0
13.	Specific Heat of Medium	C	0	2	-2	-1
14.	Medium Thermal Conductivity	k	1	1	-3	-1

No.	Physical Variables	Symbols	Dimensional Matrix D			
			M	L	T	Θ
15.	Acoustical Impedance	Ia	1	-2	-1	0
16.	Medium Mass Density	ρ	1	-3	0	0
17.	Energy Release or Yield	E	1	2	-2	0
18.	Energy Density of Explosive; Medium Strain Energy per Unit Volume; Pressure	Q	1	-1	-2	0
19.	Medium Coef. of Thermal Expansion	β	0	0	0	-1

Note that the dimensional matrix D of Table I has been partitioned into the aforementioned submatrices D₁ and D₂, the variables ρ , E, Q and β thus being selected as the repeating variables, all others being of the non-repeating type. This is particularly important for g the acceleration of gravity, as we desire to isolate its effects upon the other variables.

Utilizing Equation 2 we now develop the complete set of 15 Pi terms of Table II

TABLE II

Pi Term	Dimensionless Product	Pi Term	Dimensionless Product
1.	$RQ^{1/3}/E^{1/3}$	9.	$\mu/\rho^{1/2} E^{1/3} Q^{1/6}$
2.	VQ/E	10.	$h \rho^{1/2} \beta/Q^{3/2}$
3.	$B \rho^{1/2}/Q^{1/2}$	11.	$(Hvf)\rho/Q$
4.	$(Mv) \rho^{1/2}/Q^{1/2}$	12.	$(Hy) \rho E^{2/3}/Q^{2/3}$
5.	$g \rho E^{1/3}/Q^{4/3}$	13.	$C \rho/Q \beta$
6.	$W/E^{2/3} Q^{1/3}$	14.	$k \rho^{1/2}/E^{1/3} Q^{7/6} \beta$
7.	$P \rho^{1/2}/E^{2/3} Q^{5/6}$	15.	$(Ia)/\rho^{1/2} Q^{1/2}$
8.	$tQ^{5/6}/\rho^{1/2} E^{1/3}$		

Note that the first Pi term suggests that cube root scaling of the charge energy E is applicable for linear dimensions R for charges of a specified energy density Q. Or, more generally we may write

$K_R = K_E^{1/3}/K_Q^{1/3}$, the K's representing the scaling factors from model to prototype event, e.g. $K_R = R_M/R_P$, the subscripts M and P

denoting the model and prototype respectively. In the case of purely HE to HE scaling utilizing a specified high explosive such as TNT, $K_Q = 1$ and hence $K_R = K_E^{1/3}$.

Continuing with this reasoning, and having established $K_Q = 1$, from the 2nd Pi term we note that for volume $K_V = K_E$. Additionally the 3rd Pi term yields K_B (the scale factor for wave velocity in the medium, or detonation velocity - "brisance" of the charge) = $K_Q^{1/2} K_\rho^{-1/2}$, with K_ρ equalling the scaling factor for mass density. For model and prototype of similar charges in the same medium, we would expect $K_B = K_Q = K_\rho = 1$, and hence dimensional homogeneity has, as yet, not been violated. Continuing to the 5th Pi term containing g , the acceleration of gravity, we find $K_g K_\rho K_E^{1/3} = K_Q^{4/3}$, or since the unit weight $\gamma = \rho g$ we may say that $K_\gamma K_E^{1/3} = K_Q^{4/3}$. For model and prototype events in the same medium $K_\gamma = 1$, and since for similar explosive types we have already established $K_Q = 1$, we find that $K_E = 1$. In other words, complete dimensional homogeneity is violated unless $K_E = 1$, i.e. the model and prototype events are of the same yield. Similar deviations from complete similitude can be detected in terms containing the mass density ρ , since $\rho = \gamma/g$, hence exhibiting gravity effects and thus distortional effects.

Earlier experience with field cratering experiments is in-parallel with the foregoing discussion, in that the distortional scale effects resulting from cube root scaling, assuming gravity effects to be minimal, were tolerable as long as the scaling ratios from model to prototype were not large. Later high explosive field tests of larger yields and those with extremely large nuclear explosions indicated that gravity effects associated with cube root scaling could no longer be ignored, and that proper scaling was more nearly proportional to the 3/10th rather than the 1/3rd power of the released energy.

The works of VAILE (1), NORDYKE (3, 4), and CHABAI (2) clearly pointed in this direction.

Crater Scaling - Gravity Included

Since we are concerned with cratering in the range where gravity effects can no longer be ignored, let us now develop a new series of Pi terms in the manner outlined for cases where gravity effects may be considered negligible. Reordering the dimensional matrix D of Table I, so that the physical variables g , γ , E , and β are placed in the submatrix D_2 , and thus selected as repeating variables in the revised complete set of Pi terms, we develop the new set of dimensionless products listed in Table III. Since terms for the unit weight γ , and the medium acceleration \underline{a} have been added, there is now a total of 17 dimensionless products in this new set.

TABLE III

<u>Pi Term</u>	<u>Dimensionless Product</u>	<u>Pi Term</u>	<u>Dimensionless Product</u>
I	$R\gamma^{1/4}/E^{1/4}$	IX	$Q/\gamma^{3/4}E^{1/4}$
II	$V\gamma^{3/4}/E^{3/4}$	X	$\mu g^{1/2}/\gamma^{5/8}E^{5/8}$
III	$B\gamma^{1/8}/g^{1/2}E^{1/8}$	XI	$\rho g/\gamma$
IV	$(Mv) g^{1/2}/\gamma^{1/8}E^{7/8}$	XII	$h\beta/g^{1/2}\gamma^{5/8}E^{3/8}$
V	\underline{a}/g (where \underline{a} = Acceleration)	XIII	$(Hvf) g\gamma^{1/4}/E^{1/4}$
VI	$W/\gamma^{1/4}E^{3/4}$	XIV	$(Hy) \gamma^{1/2}E^{1/2}/g$
VII	$P/g^{1/2}\gamma^{1/8}E^{7/8}$	XV	$Cg\gamma^{1/4}/E^{1/4}\beta$
VIII	$t\gamma^{1/8}g^{1/2}/E^{1/8}$	XVI	$k/g^{1/2}\gamma^{3/8}E^{5/8}$
		XVII	$(Ia) g^{1/2}/\gamma^{7/8}E^{1/8}$

As in the previous section, we will now examine sequentially some of the scaling factors associated with the respective Pi terms to detect deviations from complete similitude.

From Pi term I, we find $K_R = K_E^{1/4} K_\gamma^{-1/4}$. If the unit weights γ of the model and prototype media are equal, $K_\gamma = 1$ and hence $K_R = K_E^{1/4}$. In other words, 1/4th root scaling is now in order. From Pi II, with $K_\gamma = 1$, $K_V = K^{3/4}$, and from Pi III with $K_\gamma = 1$, and since

in the presence of a constant gravity field $K_g = 1$, we find $K_B = K_E^{1/8}$. Recognizing that the term B has dimensions of LT^{-1} , and could represent either wave velocity in the medium or the brisance of the explosive, K_B is usually $= 1$, thus Pi III yields $K_E = 1$, i.e. yield of model and prototype events should be the same if complete similitude is to be preserved. Continuing to Pi IX, we find for $K_\gamma = 1$, that $K_Q = K_E^{1/4}$ which for $K_Q = 1$ requires that the scale factor for yield equal unity.

In summary, we note that as in the case of cube root scaling, complete dimensional homogeneity in the cratering problem is not maintained in the presence of a constant gravity field if 1/4th root scaling is used for prediction purposes. In concluding an excellent discussion of this fact, SEDOV (8) in essence states:

"Therefore the actual relative deformation at full scale is larger than on small models for constant mass density, pressure and acceleration of gravity if E is proportional to length dimensions to the fourth power; the actual relative deformation at full scale is less than on small models if E is proportional to length dimensions cubed."

Crater Scaling in Absence of Complete Similitude

Recognizing that complete similitude is not possible in cratering field tests due to the presence of a constant gravity field, and that quarter root and cube root scaling will yield results on both the low and high sides, an expedient approach is to strike for an empirical scaling exponent somewhere between the two limits. A good approximation, to a more correct scaling exponent is to work from the sets of Pi terms obtained by cube root and quarter root scaling enumerated in Tables II and III respectively.

Since the lack of complete similitude inherent in each of these scaling techniques results in prediction errors which bracket actual experimental results, there is no reason to prefer one method to the other. A middle ground is to ascribe to them equality of status using the Pi transformation

$$(Pi)' = \left[(Pi)_{1/3} \times (Pi)_{1/4} \right]^{1/2} \text{ ----- } \underline{3}$$

where $(Pi)'$ = The resulting compromise Pi term

$(Pi)_{1/3}$ = The respective Pi terms using cube root scaling

$(Pi)_{1/4}$ = The corresponding Pi term obtained by quarter root scaling

Applying Equation 3 to a selected few of the Pi terms of Tables II and III we obtain a revised set of approximate Pi terms listed in Table IV.

TABLE IV
Crater Scaling - Approximate Pi Terms

<u>No.</u>	<u>Term No. From</u> <u>Table II</u>	<u>Term No. From</u> <u>Table III</u>	<u>Approximate</u> <u>Pi Term</u>
1a	1.	I	$RQ^{1/6} \gamma^{1/8} / E^{7/24}$
2a	2.	II	$VQ^{1/2} \gamma^{3/8} / E^{7/8}$
3a	3.	III	$B \rho^{5/16} / Q^{1/4} g^{3/16} / E^{1/16}$
6a	6.	VI	$W / \gamma^{1/8} E^{17/24} Q^{1/6}$
8a	8.	VIII	$t g^{1/2} Q^{5/12} / \gamma^{3/16} E^{11/48}$

Observing the first of these approximate Pi terms No. 1a, and assuming that for a given high explosive and medium $K_Q = K_\gamma = 1$, then we obtain $K_R = K_E^{7/24}$. We immediately note that the exponent $7/24 = .29167 = 1/3.429$, which is essentially in agreement with the $1/3.4$ scaling attributed to VAILE (1) and currently in use by many investigators.

Although the set of approximate Pi terms of Table IV again does not provide complete similitude in the presence of a constant gravity field, it is felt that they will provide as good an approximation as can be derived from purely dimensional analysis alone. Further improvements beyond this for a particular medium may only be obtained by statistical means based upon an extensive test program in that medium.

ANALYSIS OF TESTS IN DESERT ALLUVIUM

General Comments

At the onset of this study of conventional high explosive and nuclear explosion tests in the Desert Alluvium of the A.E.C. Nevada Test Site, the decision was made to use the scaling factor obtained from statistical analysis of all cratering tests which provided the best fit to the experimental data rather than to adhere to the 7/24th scaling of Pi term 1a of Table IV. It was felt that this was the only way in which the effects of the $Q^{1/6}$ and $\gamma^{1/8}$ could be evaluated since strict adherence of the scaling factors $K_Q^{1/6} = K_\gamma^{1/8} = 1$ could hardly be expected.

In addition, it was decided to make minimal use of the traditional plots of scaled apparent crater radius vs. scaled depth of burial, and scaled apparent crater depth vs. scaled depth of burial, since the usual curvilinear form of these relationships was not considered amenable to the development of simple scaling relationships for cratering effects.

As an alternative working parameter, the following dimensionless expressions were deemed to be worthy of investigation:

$$\theta = \text{Dob/Ra} \text{ ----- } \underline{4}$$

$$\text{and } \Phi = \text{Dob/Da} \text{ ----- } \underline{5}$$

where

θ = "Throwout" Ratio, so called because
of its relation to ejecta studies

Φ = "Depth" Ratio

Dob = Depth of charge burial

Ra = Radius of apparent crater

Da = Depth of apparent crater

It was reasoned that both the Throwout Ratio θ and the Depth Ratio ϕ would have the added advantage of being relatively free of the effects of energy density Q and unit weight γ which are present in the dimensionless products for scaled linear dimensions such as P_i term 1a of Table IV.

HE Test Results - Radius

For purposes of statistical analysis, a total of 49 high explosion tests in the underground regime of NTS Desert Alluvium were assembled having yields ranging from 216 lbs. to 1,000,000 lbs. of high explosive. In recognition of the rapid decoupling of explosive energy which takes place at depths of burial close to the Air-Medium Interface (AMI), as defined by SAXE (9), tests which exhibited a Throwout Ratio θ of less than approximately 0.09 were excluded from consideration. None of the indicated 49 tests were eliminated by this criteria, although several surface events had been removed from consideration earlier.

Figure 1 shows a plot of the scaled radius of apparent crater, R_a' as a function of the Throwout Ratio θ with high explosive test events in the approximate range $0.09 < \theta < 1.2$. Notice the pronounced peak experienced at the optimal Throwout Ratio $\theta^* = 0.797$, and the close adherence to linearity of the test data in the "frontslope" range. In this region the results of a best-fit linear regression analysis based on equal weighting of test points are as follows:

Best Scaling Exponent	n	0.2993	(0.30)
Optimal Throwout Ratio	θ_R^*	0.797	(0.80)
Standard Deviation	σ	11.688	$(ft/KT^{0.3})$
Slope of Mean Frontslope	m_r	130.260	" "
Upper Bound for R_a' at $\theta = 0$	$(R_a')_0$	114.650	" "

From the foregoing, the general expression for scaled radius of apparent crater in terms of θ in the frontslope region is

$$R_a' = (R_a')_0 + m_r \theta \text{ ----- } \underline{6}$$

with $R_a' =$ Scaled radius of apparent crater
 $= (ft/KT^{0.3})$
 $(R_a')_0 =$ Scaled radius at $\theta = 0$ $(ft/KT^{0.3})$
 $m_r =$ Mean frontslope

For the case at hand

$$R_a' = 114.65 + 130.26 \theta \text{ ----- } \underline{6a}$$

At the optimal Throwout Ratio $\theta_R^* = .796$, the optimal scaled radius value $(Ra)^* = 218.3$, and the corresponding optimal depth of burial $(Dob)_R^*$ equals 173.8.

Since $\theta = Dob/Ra = Dob/Ra$, we may write Equation 6 in terms of scaled depth of burial Dob as

$$Ra = (Ra)_o/2 + \sqrt{\left[(Ra)_o/2\right]^2 + m_r Dob} \quad \text{----- } 7$$

and for HE events in Desert Alluvium

$$Ra = 57.325 + \sqrt{3286.2 + 130.26 Dob} \quad \text{----- } 7a$$

Figure 2 shows the characteristic shape of the Ra vs. θ plot at Throwout Ratios in excess of the optimal Throwout Ratio for radius θ_R^* . Recognizing the hyperbolic form of the curve in the larger Throwout Ratio region, it is advantageous to replot these data in the form of Figure 3, the ordinate being the inverse of the scaled radius. The statistical analysis of this region greater than θ_R^* yielded:

Best Scaling Exponent	n	0.2993	(0.30)
Standard Deviation	σ	0.000676	$(KT^{0.3}/ft)$
Slope of Mean Backslope	m_r	0.002471	" "
The $1/(Ra)$ Intercept	$1/(Ra)_o$	0.002614	" "

In the region between θ_R^* and containment θ_{RC}^* , we may thus say for HE events

$$1/Ra = 1/(Ra)_o + m_r \theta \quad \text{----- } 8$$

and specifically for Desert Alluvium

$$1/Ra = 0.002614 + 0.002471 \theta \quad \text{----- } 8a$$

SYMBOLS FOR HE EVENTS

<u>SERIES</u>	<u>DESIGNATION</u>	<u>SYMBOL</u>
Jangle	HE-1	□
Jangle	HE-7	□
Jangle	HE-6	□
Jangle	HE-5	□
Jangle	HE-3	□
Jangle	HE-2	●
Mole	205	+
Mole	204	+
Mole	203	+
Mole	202	+
Mole	212	+
Mole	403	+
Mole	405	+
Mole	401	+
Mole	406	+
Mole	402	+
Mole	404	+
Sandia I	8	°
Sandia I	2	°
Sandia I	9	°
Sandia I	10	°
Sandia I	16	°
Sandia I	4	°
Sandia I	11	°
Sandia I	12	°
Sandia I	17	°
Sandia I	15	°
Sandia II	11	°
Sandia II	10	°
Sandia II	9	°
Sandia II	8	°
Sandia II	7	°
Sandia II	6	°
Sandia II	5	°
Sandia II	4	°
Stagecoach	II	■
Stagecoach	III	■
Stagecoach	I	■
Scooter	I	✦
	None	X
Jangle	HE-9	+
Jangle	HE-10	+
Pre-Buggy	None	

Fig. 1a

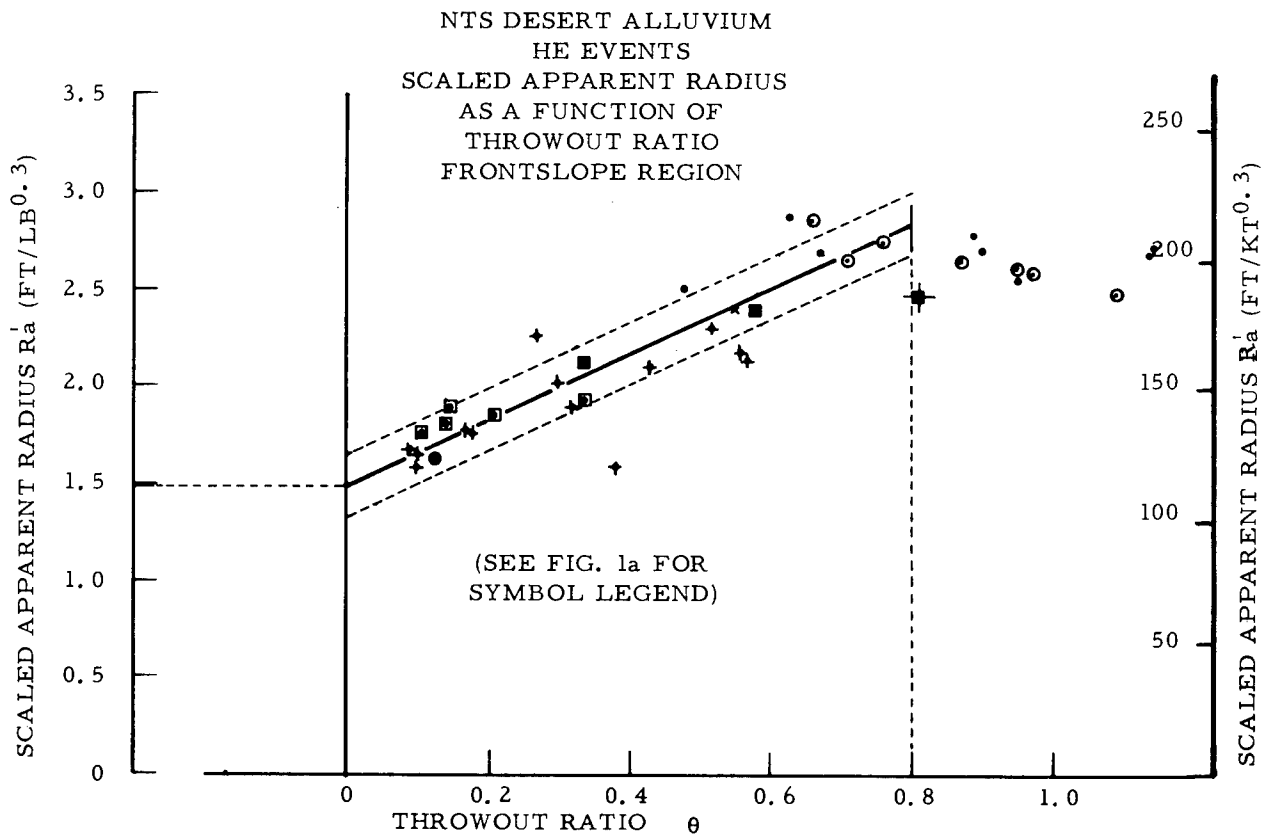


FIG. 1

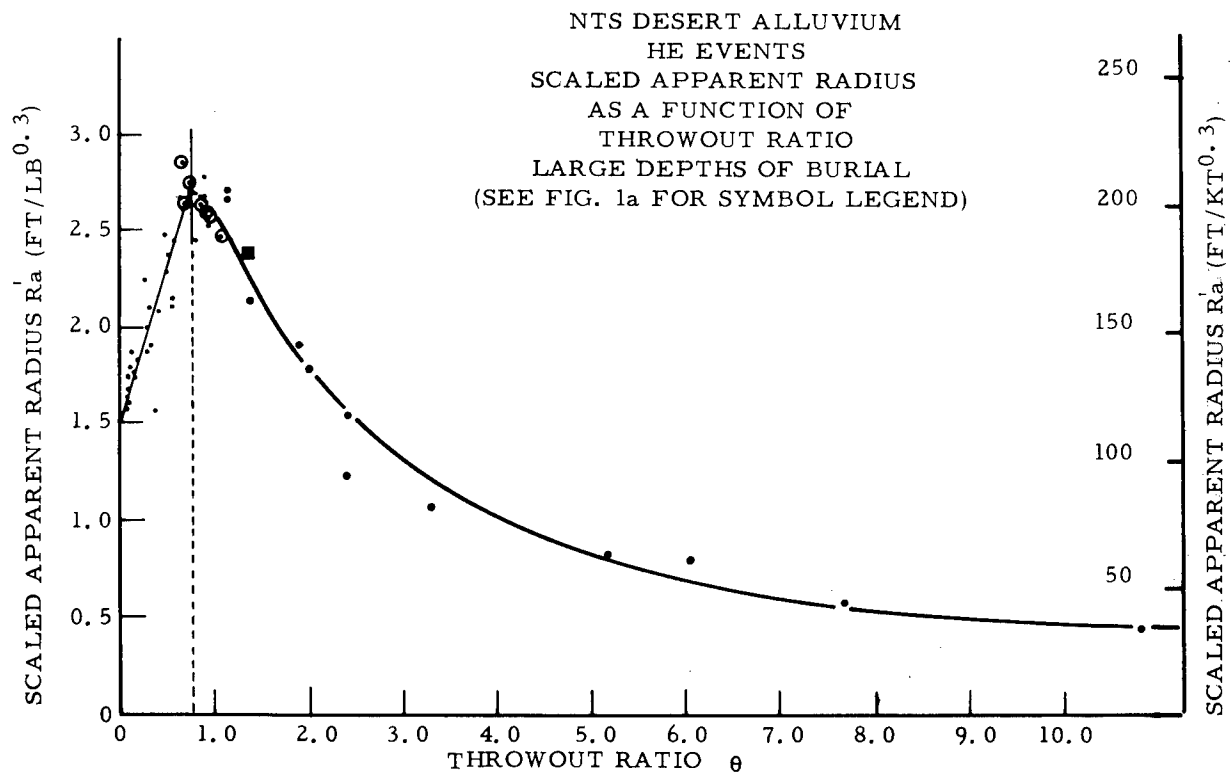


FIG. 2

Again, since $\theta = \dot{Dob}/\dot{Ra}$, we may express \dot{Ra} in terms of \dot{Dob} by

$$\dot{Ra} = (\dot{Ra})_0 \left[1 - m_r \dot{Dob} \right] \text{-----} \underline{9}$$

specifically

$$\dot{Ra} = 382.56 - 0.9453 \dot{Dob} \text{-----} \underline{9a}$$

Thus a linear relationship of negative slope on a conventional \dot{Ra} vs. \dot{Dob} plot, with containment depth $(\dot{Dob})_{RC}$, corresponding to $\dot{Ra} = 0$, at a value of 404.7 (ft/KT^{0.3}). This value of the containment depth may also be obtained from the inverse slope of Equation 8, i.e. $1/m_r$.

HE Test Results - Depth

By a line of reasoning similar to that used for prediction of radius, the depth of apparent crater was now investigated as a function of the Throwout Ratio θ . Figures 4 and 5 demonstrate the variation in scaled depth of apparent crater both in the shallower θ range and over the θ range from 0 to approximately 10 respectively. From Figure 4, we again observe the linear frontslope region as experienced in the case of scaled apparent radius. Statistical analysis of the test data yielded for the frontslope

Best Scaling Exponent	n	0.2993	(0.30)
Optimal Throwout Ratio	θ_D^*	0.654	(0.65)
Standard Deviation	σ	10.381	(ft/KT ^{0.3})
Slope of Mean Frontslope	m_d	109.883	" "
Depth at $\theta = 0$	$(\dot{Da})_0$	35.295	" "

Yielding the general relationship for scaled depth of apparent crater

$$\dot{Da} = (\dot{Da})_0 + m_d \theta \text{-----} \underline{10}$$

and specifically for Desert Alluvium,

$$\dot{Da} = 35.295 + 109.883 \theta \text{-----} \underline{10a}$$

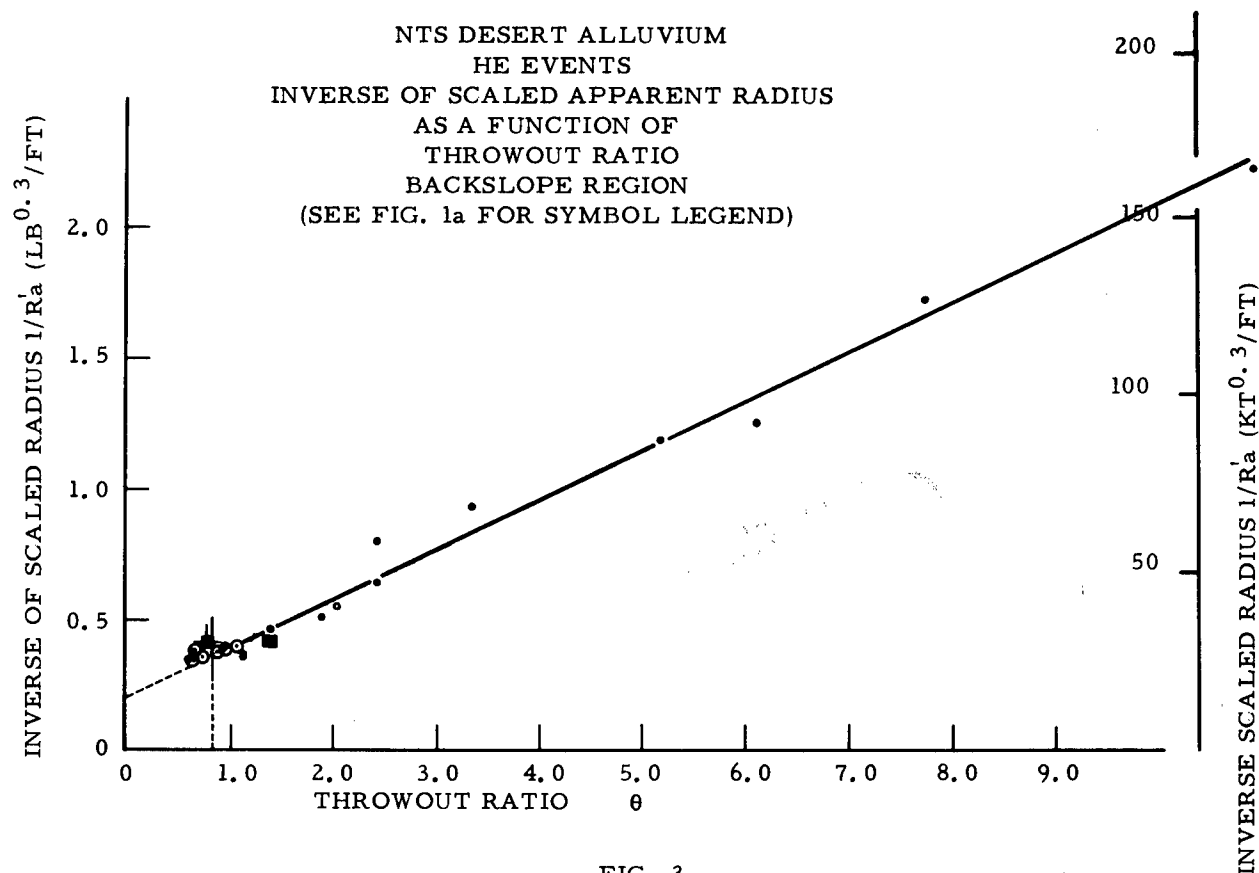


FIG. 3

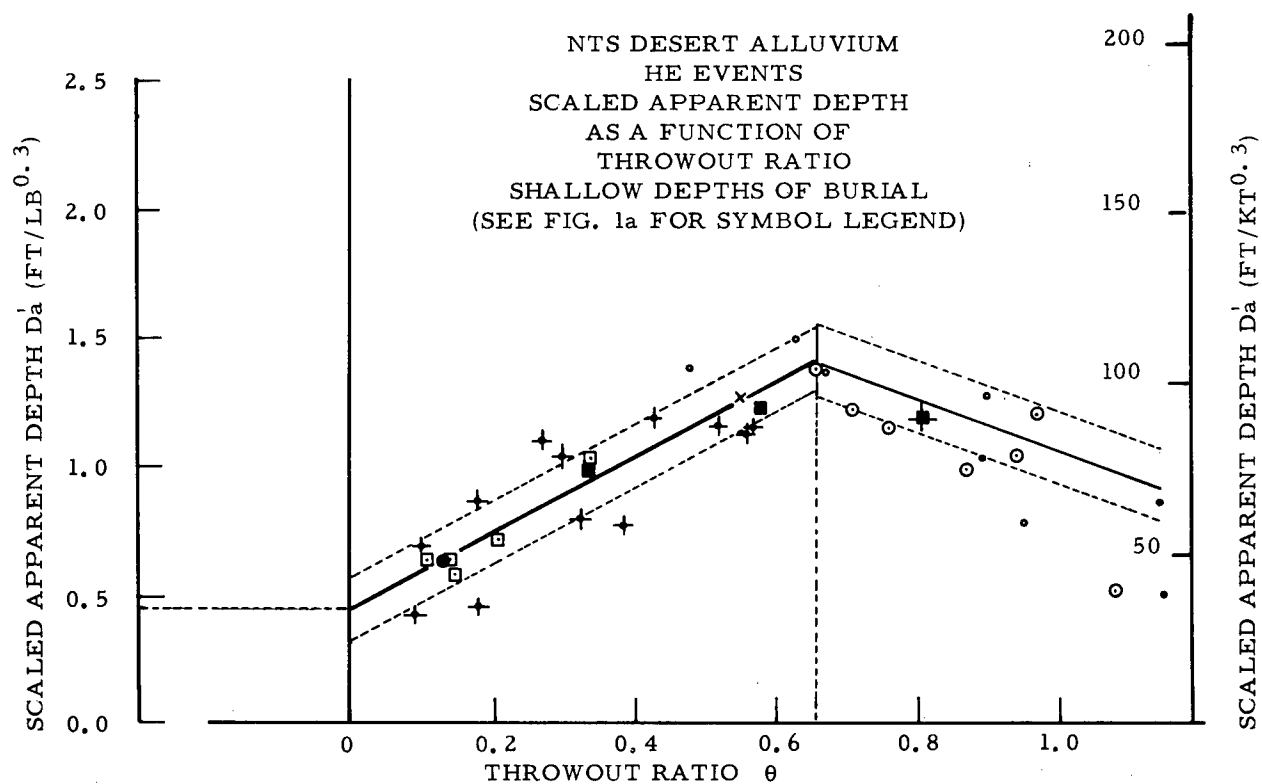


FIG. 4

Observing Figure 5, we note that, unlike the experience encountered when dealing with apparent radius in the region beyond optimum, the apparent depth can best be approximated by two backslope regions, one in the approximate region $\theta = 0.65$ to 1.45 , and the second of very flat slope beyond 1.45 , a phenomenon in all probability associated with the gas acceleration phase of the cratering mechanism. The statistical data for the first backslope region are:

Best Scaling Exponent	n	0.2993	(0.30)
Throwout Range	θ	0.654 - 1.452	(0.65 - 1.45)
Standard Deviation	σ	10.919	(ft/KT ^{0.3})
Slope of 1st Backslope	m_d'	-113.805	" "
Intercept at $\theta = 0$	$(Da')_0'$	181.549	" "

yielding

$$Da' = 181.549 - 113.805 \theta \text{ ----- } \underline{11}$$

with a value at optimal, $\theta_D^* = 0.654$, of $Da' = 107.12$ (ft/KT^{0.3}). Since from Equation 6a the corresponding apparent radius $Ra' = 199.84$, (note that this value is not optimal for radius) the corresponding $Dob = 130.70$ (ft/KT^{0.3}).

The statistical data for the second backslope region are:

Best Scaling Exponent	n	0.2993	(0.30)
Throwout Range	θ	1.452	-containment
Standard Deviation	σ	6.613	(ft/KT ^{0.3})
Slope of 2nd Backslope	m_d''	-0.6075	" "
Intercept at $\theta = 0$	$(Da'')_0''$	17.224	" "

producing

$$Da' = 17.224 - 0.6075 \theta \text{ ----- } \underline{12}$$

Although the expressions shown in plots of Da' vs. θ appear to have some measure of validity, particularly in the frontslope region, the authors were not too satisfied with the agreement obtained in the first backslope region, especially from the pre-buggy events. Consequently, it was decided to investigate the validity of using ϕ in lieu of θ in dealing with depth. Figures 6 and 7 show the resulting Da' vs. ϕ plots with statistical results as follows:

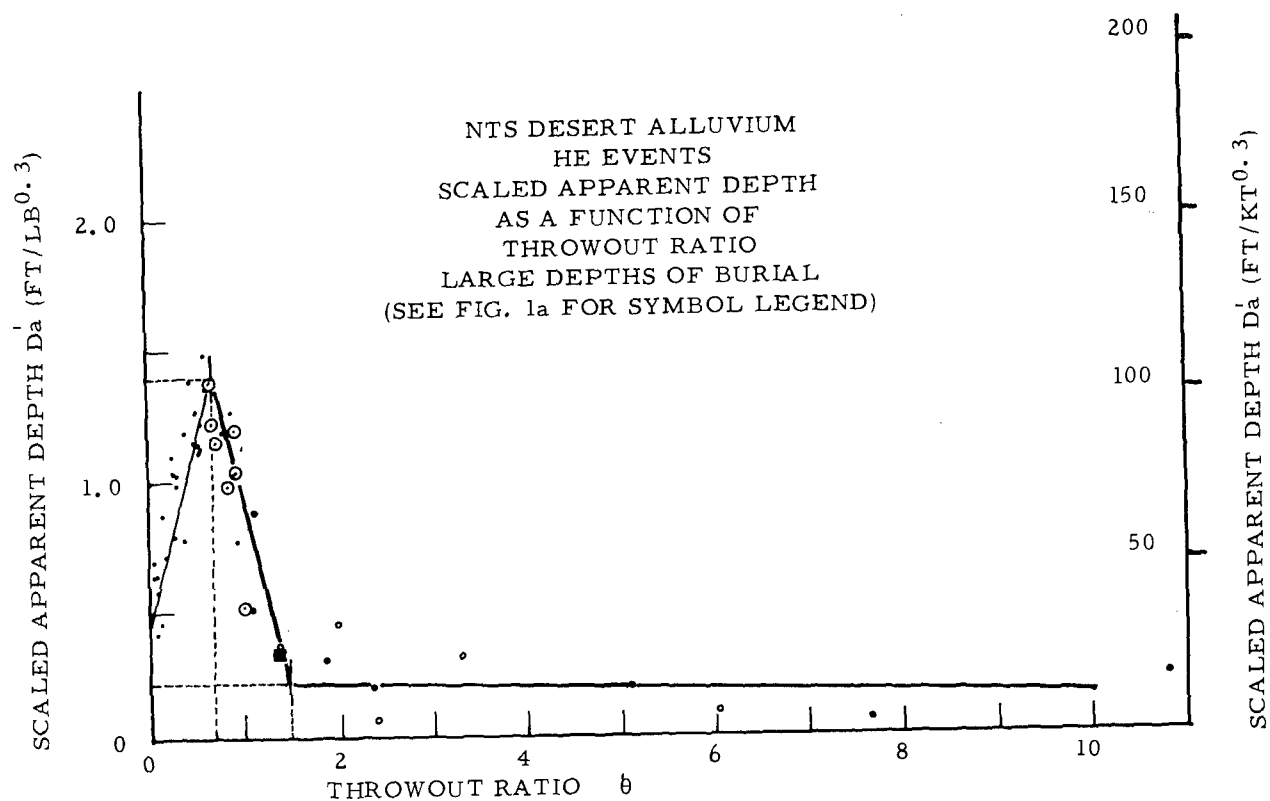


FIG. 5

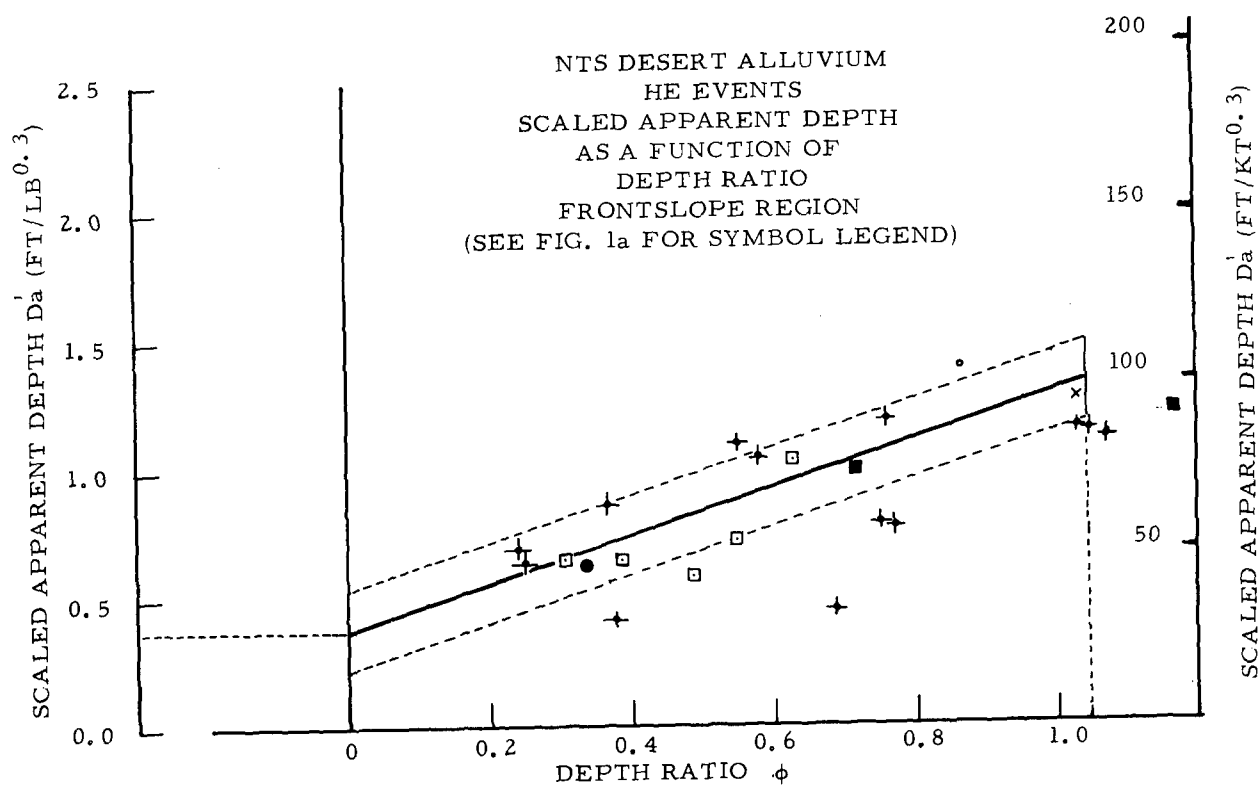


FIG. 6

For Frontslope

Optimal Throwout Ratio	Φ^*	1.040	(1.04)
Standard Deviation	σ	12.611	(ft/KT ^{0.3})
Fronslope	p_d	69.282	" "
Depth at $\Phi = 0$	$(D_a)_0$	28.913	" "

resulting in

$$D_a' = 28.913 + 69.282 \Phi \text{ ----- } \underline{13}$$

which for optimal depth ratio yields $D_a' = 101.0$ at a D_{ob}' of 105.0 as compared to the values of 107.1 and 130.7, respectively, previously obtained from Equation 10. For the frontslope region, it is probably better to use Equation 10, in lieu of Equation 13 in view of the lower standard deviation obtained in the D_a' vs. Φ relationship in this region.

For the 1st Backslope

Throwout Range	Φ	1.040 - 6.112	(1.0 - 6.1)
Standard Deviation	σ	6.459	(ft/KT ^{0.3})
Slope of 1st Backslope	p_d'	-15.225	" "
Intercept at $\Phi = 0$	$(D_a)_0$	116.496	" "

yielding

$$D_a' = 116.496 - 15.225 \Phi \text{ ----- } \underline{14}$$

For the 2nd Backslope

Throwout Range	Φ	6.11	-containment
Standard Deviation	σ	4.460	(ft/KT ^{0.3})
Slope of 2nd Backslope	p_d''	-0.3614	" "
Intercept at $\Phi = 0$	$(D_a)_0$	27.528	" "

from whence

$$D_a' = 27.528 - 0.3614 \Phi \text{ ----- } \underline{15}$$

In summary, it is probably better to use Equations 14 and 15 for depth of apparent crater in lieu of Equations 11 and 12 because of the lower standard deviations associated with the former group, although the differences are not dramatic. It is significant that, in spite of the fact that equal weighting of all test charges was used in the statistical analysis regardless of the charge size, practically all of the experimental data lying beyond the standard deviation lines were the smaller charge sizes. Figure 4 for the frontslope and Figure 7 for the 1st backslope clearly demonstrate this effect.

Nuclear Test Results - Radius

One would reasonably expect that direct scaling of explosion crater results from smaller yield high explosive tests to much larger scale nuclear events would not be possible due to the entirely different mechanisms involved in the two types of explosives. Experience to date has certainly demonstrated the plausibility of this assumption at least for crater radius, although reasonably good agreement has been obtained in most instances when dealing with apparent depth.

Extending the Throwout Ratio concept to the case of scaled radii resulting from reported nuclear events, the R_a versus θ plot of Figure 8 results (the double primes referring to nuclear events). Shown on the graph are the mean lines for all experimental HE data as expressed by Equations 6a and 8a respectively. Also shown are all reported nuclear cratering results having exhibiting a θ value of less than approximately 1.2, including not only tests in NTS Desert Alluvium, but others carried out in hard rock media. The nuclear data also include the results of the above ground event, Jangle "S", although this test is not part of the underground regime.

The nuclear results clearly point out the direct scaling of radius from HE to Nuclear events in Desert Alluvium is not possible.

The R_a'' vs. θ plot, however, does provide a means of developing relatively simple relationships between the radius and Throwout Ratio in much the same manner as in the case of HE events. The relationships are: 1) A close fit to a straight line between the Jangle "S" and Jangle "U" events; 2) A linear relationship from the "U" event to an increased value of optimal Throwout Ratio for radius θ_R^* experienced in the HE events. Note that the theoretical upper bound value of this straight line at $\theta = 0$ is essentially the same as the one obtained from the HE test results, and; 3) A backslope from optimum, similar in shape to the flat hyperbolic curve obtained for HE explosives, but at a slightly attenuating percentage of the HE results expected at a homologous θ value.

In the first and second regions, we may say

$$R_a'' = (R_a'')_0 + M_r \theta \text{ ----- } \underline{16}$$

or,

$$R_a'' = (R_a'')_0/2 + \sqrt{(R_a'')_0/2^2 + M_r^2 \theta^2} \text{ -- } \underline{17}$$

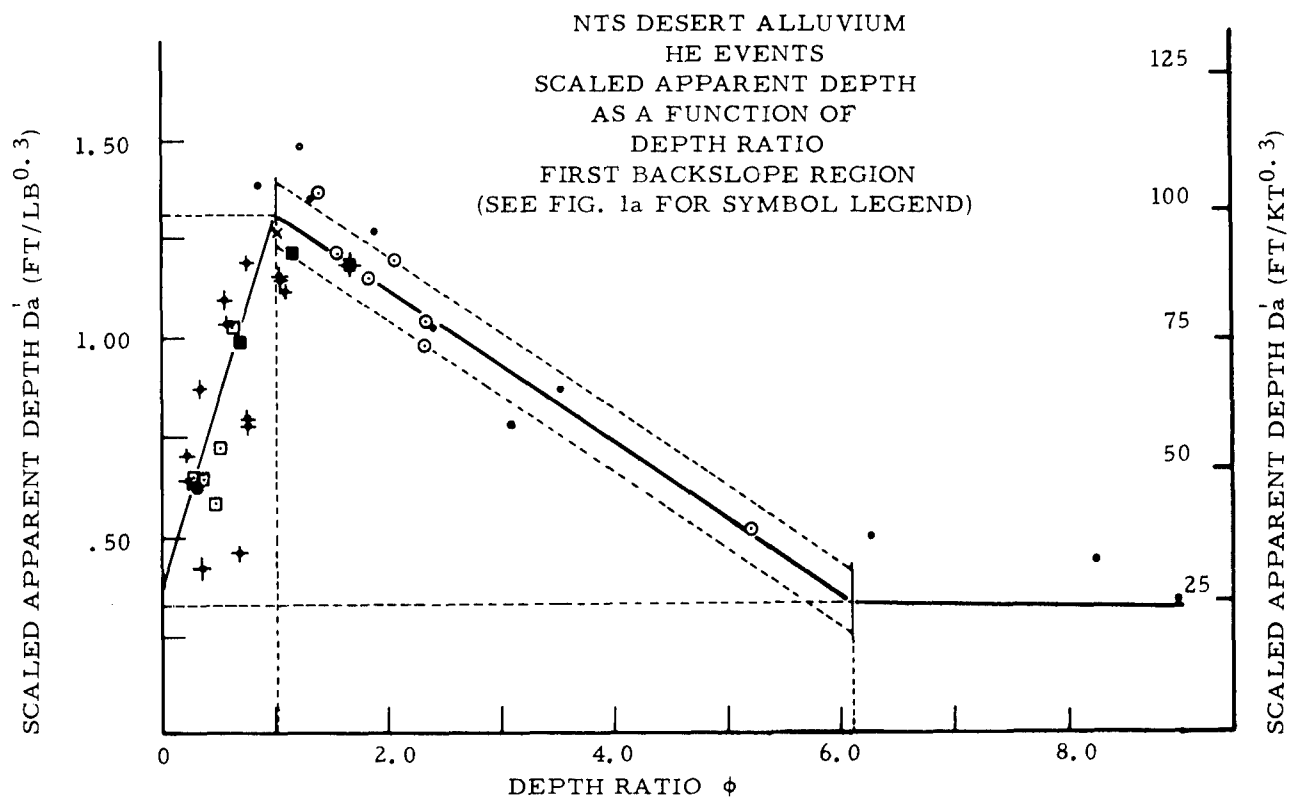


FIG. 7

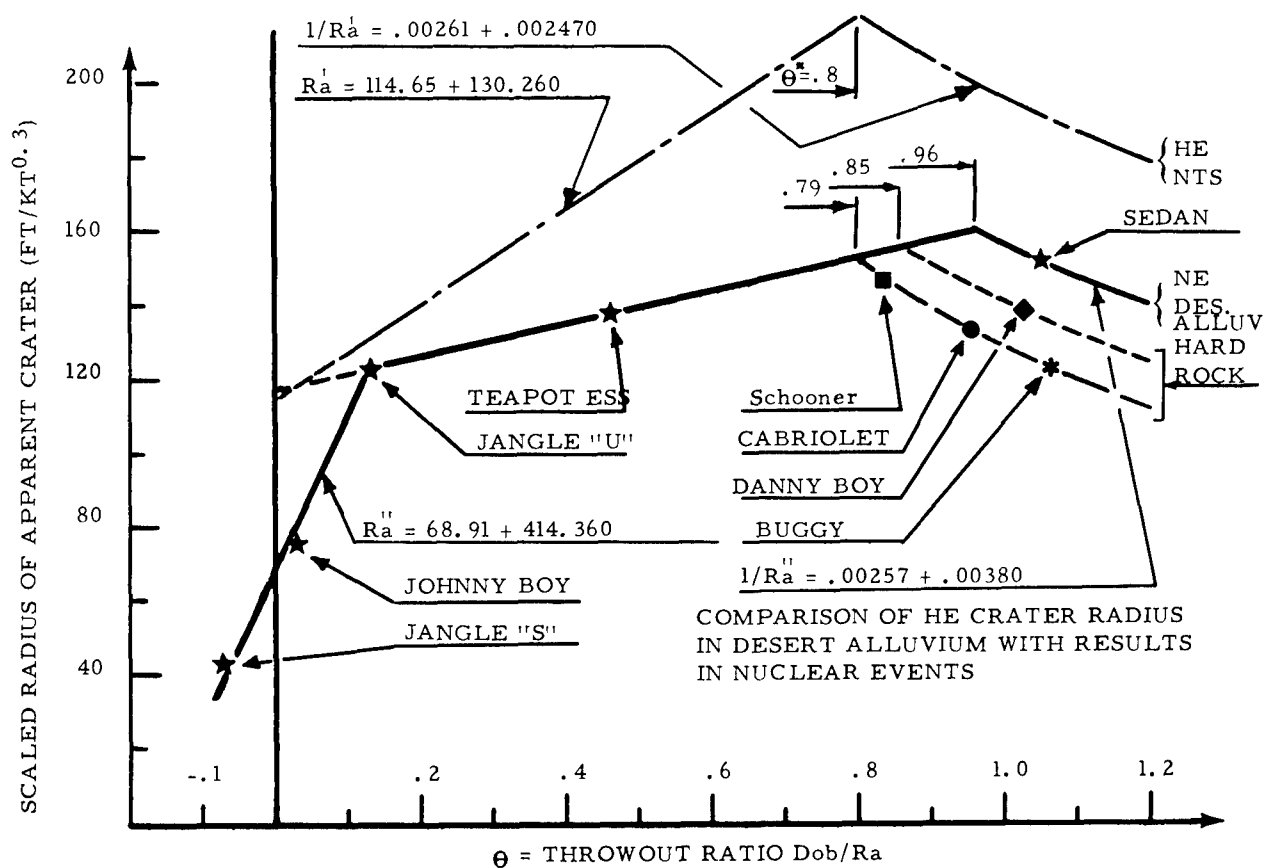


FIG. 8

which for nuclear events in Desert Alluvium become

a For the first region $\{-0.08 \leq \theta \leq .13\}$:

$$R_a'' = 68.91 + 414.36 \theta \text{ ----- } \underline{16a}$$

$$R_a'' = 34.46 + \sqrt{1187.25 + 414.36 \text{ Dob}''} \text{ ---- } \underline{17a}$$

b For the second region $\{.13 \leq \theta \leq .8\}$

$$R_a'' = 117.06 + 46.17 \theta \text{ ----- } \underline{16b}$$

$$R_a'' = 58.53 + \sqrt{342.57 + 46.17 \text{ Dob}''} \text{ ----- } \underline{17b}$$

For nuclear results in NTS Desert Alluvium, it appears that the optimal Throwout Ratio for radius O_R^* has increased slightly to a value in the vicinity of 0.96. For the Sedan event at a Throwout Ratio of 1.051, the actual scaled crater radius obtained was 152.2 using 3/10th scaling. At this same value of the Throwout Ratio, a scaled crater radius of 191.9 would be possible with conventional HE scaling according to Equation 8a, thus the nuclear result was roughly 79.3% of the homologous HE result.

Since Sedan is the only nuclear cratering result in the backslope region for Desert Alluvium, we had no way of ascertaining the shape of the curve in this region. Fortunately, however, the Schooner, Cabriolet, and Buggy results in hard rock media were available to provide an insight as to the shape of the curve for Desert Alluvium in the Throwout Range of interest.

A significant fact about these three hard rock events is that they exhibit an essentially constant difference from the HE scaled radius that would be obtained in Desert Alluvium according to Equation 8a, at the specified Throwout Ratios. For example Schooner, Cabriolet and Buggy. Each exhibit differences of 67.0, 66.9, and 67.4 (ft/KT^{0.3}) on the low side of the corresponding HE value for Desert Alluvium, with slightly attenuating values on a percentage scale of 68.7%, 66.7%, 64.7%. Postulating that a similar constant difference is likely to occur in Desert Alluvium, the actual difference between Sedan and its HE counterpart, 39.7 (ft/KT^{0.3}) was assumed to occur in the same region spanned by the three hard rock nuclear events, yielding

$$1/R_a'' = .002573 + .003802 \theta \text{ ----- } \underline{18}$$

and

$$R_a'' = 388.66 - 1.478 \text{ Dob}'' \text{ ----- } \underline{19}$$

producing a containment depth of 263.0 (ft/KT^{0.3}) for nuclear events in Desert Alluvium, as compared to the containment depth in this medium of 404.7 previously obtained for HE, i.e. a Dob for nuclear equal to approximately 65% of the HE value for containment.

For the Buckboard Basalt of the Danny Boy event, utilizing its difference of 55.30 (ft/KT^{0.3}) from its corresponding value in alluvium, and assuming this to be constant over the Schooner-Buggy region, we obtain

$$1/R_a'' = .002422 + .004656 \Phi \text{ ----- } \underline{20}$$

and

$$R_a'' = 412.90 - 1.923 \text{ Dob}'' \text{ ----- } \underline{21}$$

having a containment depth of 214.8 (ft/KT^{0.3})

Similarly for the hard rock media of the Schooner and Cabriolet types we find

$$1/R_a'' = .002092 + .005654 \Phi \text{ ----- } \underline{22}$$

or

$$R_a'' = 477.97 - 2.702 \text{ Dob}'' \text{ ----- } \underline{23}$$

with a containment depth of 176.9 (ft/KT^{0.3})

Nuclear Test Results - Depth

Let us now turn our attention to the apparent depth of craters associated with nuclear events. Figure 9 shows the scaled depth of apparent crater D_a'' for all reported nuclear cratering tests as a function of the Depth Ratio Φ over the range of roughly -0.25 to 3.5. Examining the frontslope region we observe that the nuclear tests provide remarkable agreement with the mean line for HE events previously obtained from Equation 13, and hence will be used for nuclear events as well.

In the backslope region we find that, with the exception of the Schooner and Buggy tests, all other tests conform closely to a straight line, although the attenuation rate of apparent depth as a function of Depth Ratio is greater than for the HE tests in the backslope region.

An expression for depth of apparent crater due to nuclear events on the backslope in terms of depth ratio is

$$D_a'' = 118.22 - 18.94 \Phi \text{ ----- } \underline{24}$$

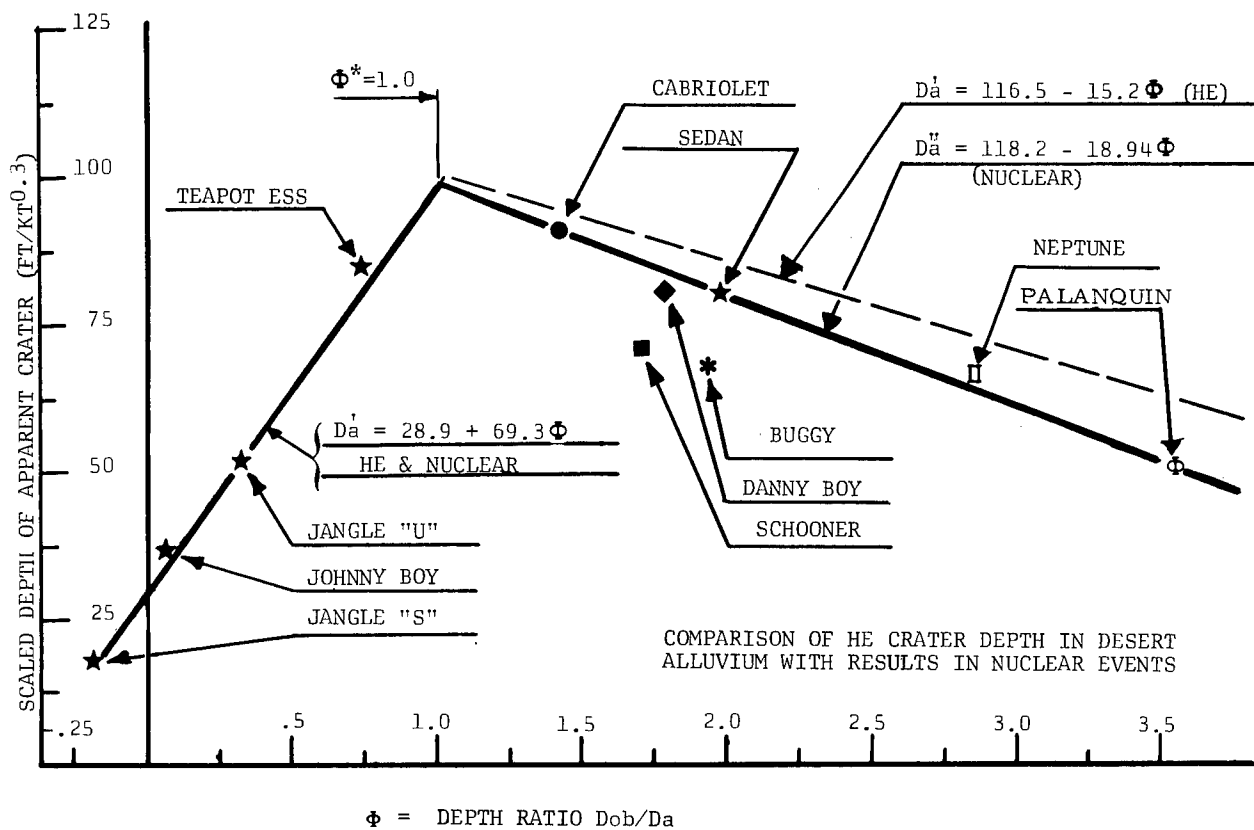


FIG. 9

and in terms of depth of burial

$$D_a'' = 59.11 + \sqrt{3257.7 - 18.94 D_b''} \text{ ---- } \underline{25}$$

Through the simultaneous solution of Equations 24 and 13, we find that the optimal depth ratio for depth of apparent crater $\overline{O_p}$ is equal 1.001 (1.0), as compared to 1.04 for HE tests. In other words, optimal depth of crater will occur when the charge is placed at a depth of burial numerically equal to the optimal depth sought.

SUMMARY AND CONCLUSIONS

The authors have presented an analysis of the complete series of high explosive and nuclear cratering tests performed primarily in Desert Alluvium located at the Nevada Test Site. It is felt that the dimensionless parameter referred to as the Throwout Ratio and Depth Ratio provide investigators with a very simple method of crater prediction. The linear relationships developed can furnish further insight into the mechanism of cratering, and provide us with a capability of scaling from HE to Nuclear Events not only for a particular radius or depth, but for shape as well, i.e. maintenance of a specified radius to depth ratio.

REFERENCES

1. Vaile, R. B.
"Pacific Craters and Scaling Laws"
J. Geo. Res. Vol. 66, No. 10 (1961)
2. Chabai, A. J.
Project Stagecoach: 20-Ton HE Cratering Experiments in Desert Alluvium
Final Report, Sandia Corporation
Rept. SC-4596 (RR), TID-4500 (16th Ed.) (1962)
3. Nordyke, M.D.
"Nuclear Craters and a Preliminary Theory of the Mechanics of Explosive Crater Formation"
J. Geo. Res. Vol. 66, No. 10 (1961)
4. Nordyke, M.D.
"Cratering Experiences with Chemical and Nuclear Explosives"
Proc. 3rd Plowshare Symposium-Engineering with Nuclear Explosives, U.S. Atomic Energy Commission, TID-7695 (1964)
5. Toman, J.
Summary of Results of Cratering Experiments
Lawrence Radiation Laboratory, Livermore
Rept. No. UCRL-71456 (1969)
6. Lampson, C. W.
"Explosions in Earth"
Effects of Impact and Explosion, Vol. I, Part II, Chapter 3
Office of Scientific Research and Development
Washington, D. C. (1946)
7. Pokrovskii, G.I. and Fedorov, I.S.
"Effect of Shock and Explosion on Deformable Media"
Gos. Izd. (1957)
8. Sedov, L.I.
"Similarity and Dimensional Methods in Mechanics"
Academic Press, New York (1959)
9. Saxe, H. C.
"Explosion Crater Prediction Utilizing Characteristic Parameters"
Rock Mechanics, Proc. 5th Symposium on Rock Mechanics
C. Fairhurst, Ed., Pergamon Press, New York (1963)

A SIMPLE TECHNIQUE TO DETERMINE THE SIZE DISTRIBUTION OF NUCLEAR CRATER FALLBACK AND EJECTA

CPT Brooks D. Anderson, II
U. S. Army Engineer Nuclear Cratering Group
Lawrence Radiation Laboratory
Livermore, California

INTRODUCTION

This report describes the results of an investigation to find an economic method for determining the block size distribution of nuclear crater fallback and ejecta.

It is shown that the modal analysis method of determining relative proportions can be applied with the use of a special sampling technique, to provide a size distribution curve for clastic materials similar to one obtainable by sieving and weighing the same materials.

BACKGROUND

The size distribution of nuclear crater fallback and ejecta is a necessary parameter for input into the analysis of crater slope stability, fallback and rupture zone permeability and the production of aggregate and riprap by nuclear means. Methods presently in use by the Corps of Engineers to determine size distributions of fallback and ejecta have the drawbacks of being either very expensive, in the case of sieving and weighing, or not accurate enough, as in the case of a newly developed grid photography technique. The reason for the lack of reliability in data obtained by grid photography was shown by Anderson (1969) to be due to the low scale level of information obtained by measuring particle size in two dimensions on a photograph and the failure to differentiate between particle size distributions by number and by weight. Because of the expense of sieving and weighing and the lack of accuracy of grid photography, it became imperative to find an alternative to these techniques. This report presents the results of an investigation to find such an alternative.

THEORY

The theoretical concepts which form the basis of a new technique for the modal analysis of fragmental material are developed in this section. A brief review of common geologic sampling techniques is first presented to emphasize the difference between size distribution by number and by weight. Because the measure of "size" obtained by the new modal analysis technique is somewhat different than that obtained by sieving, and the size distribution obtained by application of the two techniques to the same material are to be compared, a justification for using that measure is presented. Sampling requirements of the new technique are stated and the effects of porosity, density, and layering on the sampling technique are discussed.

COMMON GEOLOGIC SAMPLING TECHNIQUES

SIEVING

The size measurement obtained in sieving is very dependent upon the shape of the particle. It is primarily a function of the least cross-sectional area of the particle which is most influenced by the particle's intermediate and short axis. There are other factors which affect the passage of a particle of a given "size" through a sieve. They are; (1) the sphericity and roundness of the particle, (2) the length of time of sieving, which affects the probability of a particle achieving the proper orientation for passage, (3) the type of motion the sieves are subjected to and (4) variation in the individual sieve openings. In summary, any measure of size is merely a function of sample-technique. Different techniques give different measures of size.

MODAL ANALYSIS

Modal analysis is the term given to a method of determining the volume percentage of the mineral constituents of a rock by means of point counts on its surface. It is based upon the discovery by Delesse in 1848 of the equivalence of areal and volumetric proportions. However, it was not until 1956 that Chayes was able to give a mathematical proof to the relationship. Until this time, its application to the study of the mineral content of rocks was seriously hindered. Because Chayes' (1956) mathematical proof of the Delesse relation is germane to the argument for the application of areal modal analysis to clastic rocks it is presented here.

POINT SUMS AS ESTIMATORS OF AREAL PROPORTIONS

To paraphrase Chayes: a small irregular area (B) is enclosed in a large irregular area (B+W). The probability that a point located simply at random in (B+W)¹ will also lie in B is, by definition, the ratio of the areas,

$$p = \left(\frac{A_B}{A_{(B+W)}} \right)$$

Where A_B = area designated B

$A_{(B+W)}$ = area designated (B + W)

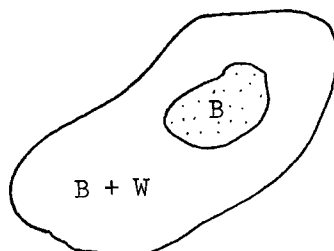


Figure 1: Small area (B) enclosed in large area (B + W), the ratio of the areas to be estimated by the sums of points chosen simply at random in the region (B + W).

The expected number of points E which fall in B in a particular sample containing n points is

$$E = np = n \left(\frac{A_B}{A_{(B+W)}} \right)$$

the fraction μ of the total number of points in the sample that fall in the area

¹The total area.

B is

$$\mu = \frac{E}{n} = p = \frac{A_B}{A_{(B+W)}}$$

Therefore, the fraction of the total number of points that fall in the smaller area is an unbiased estimate of the ratio of the smaller to larger area.²

DELESSE RELATION

The area-volume relation,³ which determines whether estimates of relative area may also be regarded as consistent estimates of relative volume is both simpler and more widely misunderstood than any other part of the theory of modal analysis.

If the area of a section of a solid parallel to the xy plane is a function of z, $A = f(z)$, and sections through the solid can be chosen simply at random normal to OZ in the region $c \leq z \leq d$, the element of frequency is dz, and the total frequency is (Figure 2)

$$F = \frac{1}{d - c} \int_c^d dz = 1$$

and the expected value $E(A)$ of the area A is

$$E(A) = \frac{1}{d - c} \int_c^d A dz = \frac{V}{d - c}$$

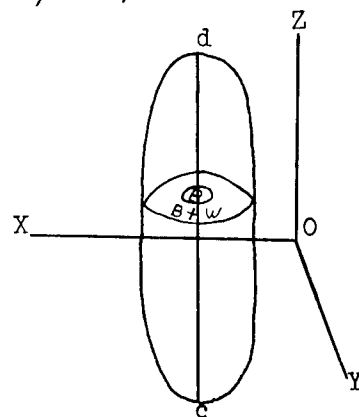


Figure 2: Solid in XYZ Space, c - d Perpendicular to Area B + W.

where A and V represent area and volume respectively. We have at once that

$$\frac{E(A_B)}{E(A_{(B+W)})} = \frac{V_B}{V_{(B+W)}}$$

where the ratio of an unbiased estimate of the area A_B to an unbiased estimate of the total area $A_{(B+W)}$, obtained by point counting, is also the ratio of the volume V_B to the total volume $V_{(B+W)}$. It is apparent then that as long as we have an unbiased estimate of the relative areal proportions, taken from a surface of a representative sample of rock, then we also have an unbiased estimate of the volumetric proportions of the constituents of that rock.

The preceding proof says nothing about how the estimates of the relative areas are to be obtained. But if we can accept this proof then the determination of relative proportions of minerals in a rock becomes relatively simple.

GRAIN COUNTS

A number of techniques have been developed for grain size analysis of

²i.e., in such fashion that each point in the area (B + W) has the same probability of being selected as any other point.

³Delesse relation.

loose grains, mainly dependent upon the average size of the material. Sands are generally analyzed by making grain counts using sized material obtained by sieving. A precise subdivision of the sample is required so that the several hundred grains in the count are representative of the sample. The grains are counted either by using a grid micrometer or with a mechanical stage and a mechanical counting device. The number of grains in a given grid square, or successively encountered along a line, is counted.

For analysis of gravel deposits, Griffiths and Kahn (1967) have recommended that, depending upon the detail of information required, pebbles can be selected along a line or a number of lines placed at random on the deposit surface. The data obtained by this technique are analyzed in a manner similar to that obtained by grain counting under a microscope. Some work has concentrated on the conversion of number frequency data to size or weight frequency. However, most geologists do not consider the results of these conversions to be sufficiently reliable to permit their general adoption, hence the basic discrimination between number frequency and weight frequency has been maintained.

In summary, the development of techniques designed to acquire data from mixtures of geologic materials has taken two parallel but distinct paths of development. One path has been toward continuing refinement of estimates of the volumes or weights of rocks or minerals in a sample and the other directed toward determining the size distribution by number. There is one exception to this trend: a paper published by M. Gordon Wolman titled, "A Method of Sampling Coarse River-Bed Material."

WOLMAN TECHNIQUE

According to Wolman (1954) it is possible to determine a size-frequency distribution of the clastic material on the bed of a stream based upon an analysis of the area covered by particles of given sizes. Wolman collected his sample of 100 pebbles from the bottom of the stream from the points of intersection of a grid system. He applied the technique to a number of river bottoms, and reproduced his work several times by having his students collect on different days and by having different students make the collection. The results of his studies are plotted in Figure 3.

Wolman found that when he compared samples determined from pebble counts with samples of the same material analyzed by sieving and weighing that the median diameter of the sample determined by the point sampling methods was considerably larger, (twice as large), than the median diameter of the sieved sample (see Figure 3).

It is not immediately clear why Wolman got the results he did, although, what is thought to be a reasonable explanation will be offered as we further develop the new technique of modal analysis of clastic materials, so called because of its similarity to the modal analysis technique of sampling minerals in rocks.

MODAL ANALYSIS OF CLASTIC ROCKS

According to Wolman (1954) it is possible to determine a size-frequency distribution of the clastic material on the bed of a stream based upon an analysis of the relative area covered by particles of a given size. This statement is the key to the unification of modal analysis and particle counting. It is a statement of the Delesse relation which relates areal proportions to volumetric proportions.

The question remains, does the Delesse relation actually hold for clastic rocks? If so, can a technique be developed to yield results comparable to those

Cumulative percent of sample finer than a given size

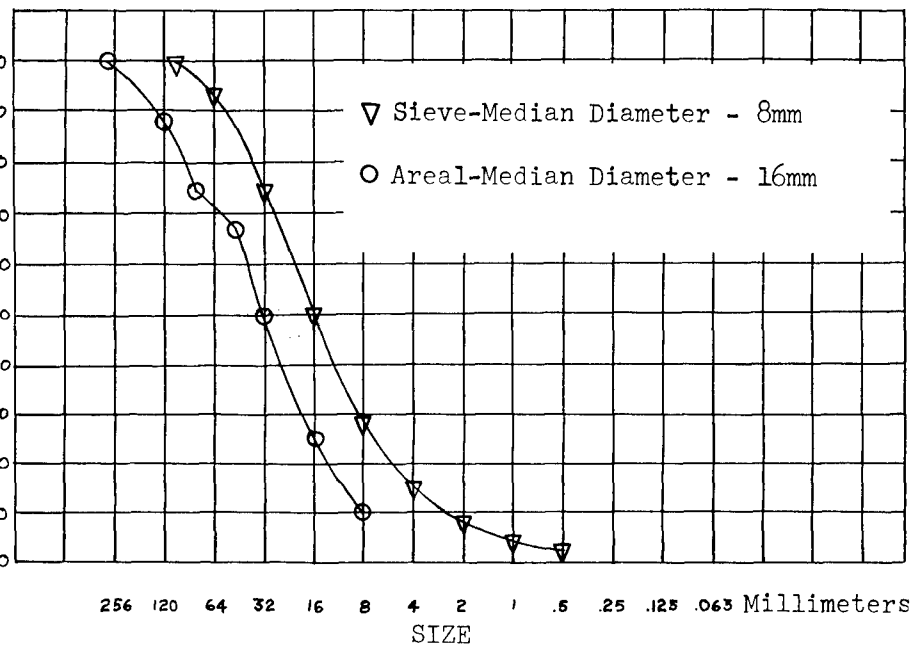


Figure 3. Comparison of samples obtained from sieve and areal analysis (from Wolman, 1954).

obtained by sieving and weighing the same material?

Size is determined directly by measuring in the application of the point sampling technique, however, the weight distribution must be inferred by an inductive argument. Therefore, we are concerned with size and weight, and how to obtain these parameters (sampling).

SIZE

Many techniques, to include sieving, produce measures of "size" which are not "clean," that is, they confound variation from a number of sources. The "size" distribution curves produced by sieving and weighing are a function of the size, shape and composition of the sieved material. Because the measure of size obtained by sieving is to be compared with one based upon a single measurement it is necessary to choose a measure of size that would closely approximate that obtained by sieving. In this study the "b" intermediate axis (see Figure 4) was selected. This is defined as the axis most closely approximating the nominal diameter of the least cross-sectional area which determines whether or not a particle of a given "size" will pass through a sieve opening.

WEIGHT

In modal analysis the volume of minerals in a rock is inferred by the analysis of an area. The relative weights of the minerals are not directly inferred but must be calculated by considering their relative densities. It is immediately apparent that we are faced with a similar situation in the determination of the size-weight distribution of rocks by this method. The calculation of weight from relative volumes has two pitfalls; one has to do with possible differences in porosity within the sampled material and the other has to do with possible differences in density between individual clasts sampled.

POROSITY

Porosity, as such, presents no obstacle to the application of the Delesse relation except for certain cases which are amenable to rational analysis. For example (see Figure 5), consider a sandstone in which the grains are of a uniform size-sand size. This sandstone has a porosity of 25%.

Now, if we scatter 100 points over the surface of the sandstone and select 100 grains lying beneath these points, we will always encounter a grain and never a pore space, because in practice we are sampling the projections of the grains to a plain surface. This characteristic of the sampling technique has important implications in practice. These 100 grains of sand-size represent 100% of the sampled surface. There should be little difficulty, in concept, to extend this proportion (100% sand-size grains) to volume and weight and saying that 100% of the particles by volume and by weight are sand-size.

However, differential porosity could have a deleterious effect on the estimate. The diagram in Figure 6 shows a "horrible example" in which 50% of the mass is solid and 50% of the mass contains 25% pore space. Calculations pertaining to the example in Figure 6 give an indication of the size of the error of the estimate.

If the solid is considered to be a block of a given "size" and the porous material to be composed of fragments of a smaller "size" then it is apparent that although both occupy the same volume (and from the idealized case for the Delesse relation, the same surface area) but, the solid material of the two "sizes" would not weigh the same. In fact, only 37.5 units of the total weight is concentrated in the porous material (considering that 25% of the 50 estimated (units) is 12.5 (pores) and $50 - 12.5 = 37.5$). Now, if all the grains in

VARIATE: SIZE AS DEFINED BY "b" AXIS, "b" DEFINED
AS THE MAXIMUM INTERMEDIATE DIAMETER THAT WOULD
"PASS" A GIVEN SIEVE (\perp TO GRID DIAGONAL NOT CONSIDERED)
MEASUREMENT WITH CALIPERS (ACCURATE TO .001")

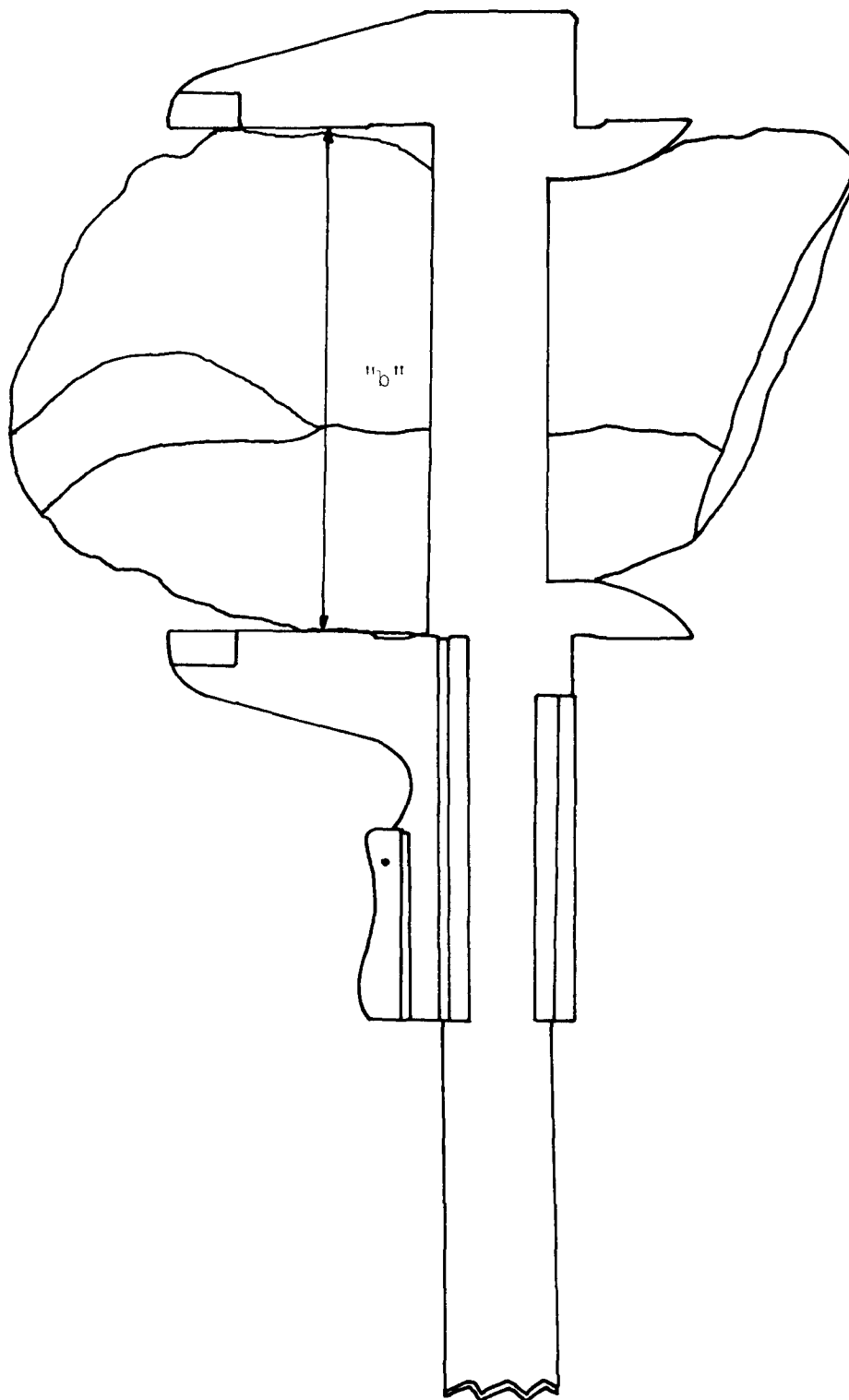


Fig. 4 Measurement of "b" Intermediate Axis of Rock with Calipers

the porous material were packed into a solid, but with the individual grain boundaries still defined, the top surface of the compacted material would be representative of the 37.5 (units) of granular material. Reestimating the relative volumes from the relative surface area (Delesse relation) it is found that the true relative proportions are 57.1% and 42.9% (where 50 units are 57.1% of 87.5 and 37.5 units are 42.9% of 87.5). As a point of interest, it should be noted that this is probably the worst case we are likely to encounter under natural conditions. The absolute error of the estimate of relative proportions drops off rapidly away from 50%. The Delesse relation is based upon relative rather than absolute proportions. It can be seen that the error of the estimate ranges from about 14% in our "horrible example," to zero in the sandstone with 25% porosity. In the example in Figure 6 we would have estimated relative proportions of clasts of different sizes at 50% each instead of their true proportions of 57.1% and 42.9%. However, all that is required to correct this error is an estimate of the porosity of the porous material and the correction can be done in the same way as was done in the preceding example.

DENSITY

At first, differing densities between rocks would seem to be a troublesome point. However, if we are dealing with rocks of essentially the same composition then their density, and hence weight, become a constant and can be ignored. In practice, the range in density of most rocks is not significantly different, and in fact, differences in density of fragments would only become serious, for practical purposes, if there was a significant grouping of fragments of different densities in different size classes. The only suggestion that can be made at this point is that the operator make a preliminary investigation to determine if the aforementioned situation has indeed occurred. If it has, it is a simple matter to note the compositions of the rocks when they are measured and prior to generating a cumulative size-weight distribution curve compensate for their different densities.

SAMPLING

In the practical case, application of this technique becomes a sampling problem. When we sample, we are in effect measuring or counting some fraction of elements of a larger or more numerous entity in order to draw some inference about that entity. Assuming that we have taken precautions to insure that our sampling procedure is unbiased and consistent, it is of considerable interest to know how many samples to take in order to accurately characterize the parent population. Chang (1967) has addressed the problem of determining how many individuals, assigned to a given class, should be used in order to get an accurate percentage representation of that class. The result of Chang's work is presented in Figure 7. He assumed that the variability of the percentage estimation, which causes the error of the population estimate, to be due to the probability associated with random sampling. He then demonstrated that the maximum error of the estimate is likely to occur when two classes are present in the relative proportions of 50% each. Interestingly enough, a similar phenomenon is found to cause the maximum error of the estimate of relative proportions in the case of differential porosity. This maximized standard deviation, d (two classes present in proportions of 50% each, and $1d = 68.27\%$, $2d = 95.45\%$ and $3d = 99.73\%$ confidence levels), is plotted as a function of the number of samples taken, n . For example, if an investigator samples 500 clasts from a large group of clasts, by referring to Figure 7, he finds that the error of the estimate at the 95.4% confidence level is 4%. Therefore, if the clasts are present in only 2 sizes in the relative proportions of 50% each, 95.4% of the time the percentage of the size clast estimated will be less than or equal to $\pm 4\%$. Because this is the maximum error expectable, clasts with sizes present in other proportions will give a smaller error of the estimate. Knowing the maximum error of the estimate likely to occur it is now possible to determine the number

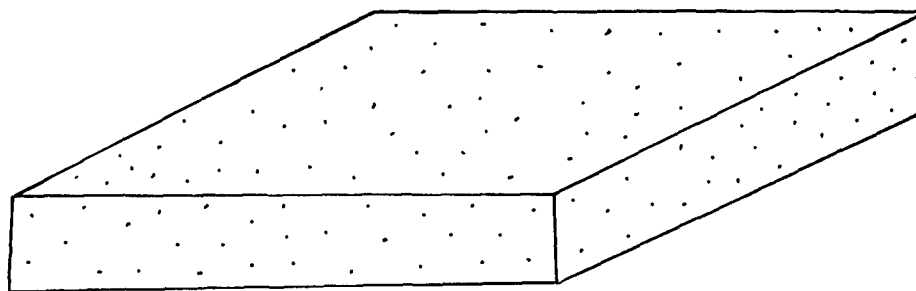
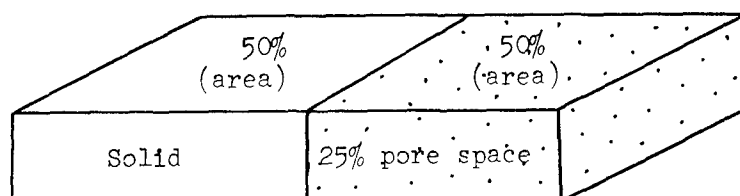


Figure 5. Sandstone, 25% Pore Space.



50.00 units Volume (solid)
 + 37.50 units Volume occupied
 by solids in porous
 material
 ———
 87.50 Total Volume of Solids

Figure 6. Differential Porosity.

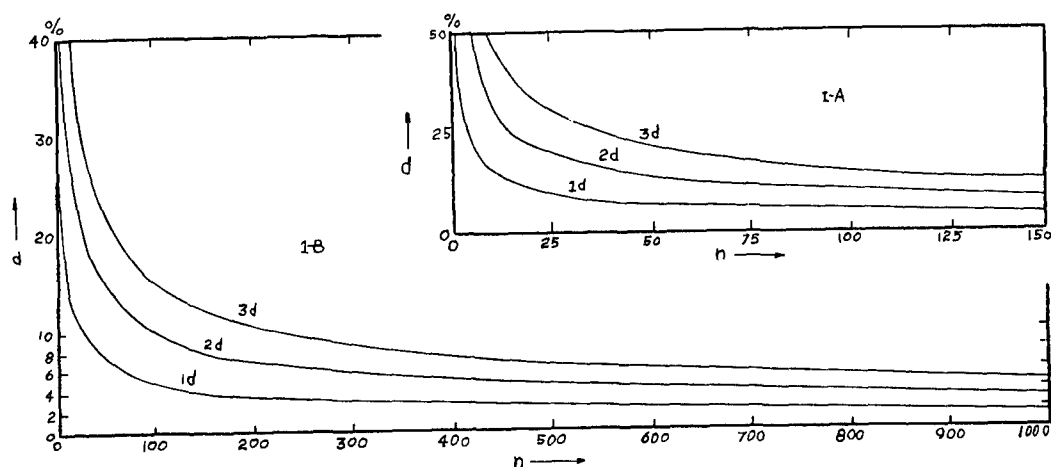


Figure 7. From Chang (1967). Relationship of the maximized standard deviation (d) to the studied population number (n). (1-A). Both d and n are in the same scale (1-B). d and n are in different scales; the n scale is reduced so that it is 10 times smaller than the d scale.

of samples to take, at a given confidence level, to obtain an estimate with minimum statistical error consistent with the objective of the study.

Since the technique proposed herein is not simple random sampling (like drawing colored balls out of a bag) but is a systematic sampling of an area, it is of interest to know the size of the area to sample. Although there are several sophisticated methods to determine the area necessary to examine in order to obtain a representative sample, the formula presented below is both simple and readily applicable in the field. The formula is:

$$\text{Total Sample Area} = n (\text{Grid Spacing})^2$$

Where n = number of samples to be taken at a predetermined confidence level
(obtained from graph by Chang, 1967, Figure 7)

And Grid spacing is determined by the size of the largest block likely to be encountered (determined by a preliminary reconnaissance of the sample area).

THE EFFECTS OF LAYERING

The example in Figure 8 demonstrates a case in which a sample of the available population, the surface of a gravel deposit, although an unbiased sample of the available population would provide a very poor estimate of the parameters of the whole deposit.

However, it can also be seen that if the samples are taken at any angle to the layering, other than parallel to it, the sampling surface will consist of a series of parallel bands containing rocks of different sizes (see Figure 9).

It can readily be seen that a sample taken in the preceding manner would provide statistical estimators that would slowly converge on their corresponding population parameters. Further, it is apparent that the most efficient sampling program would be one in which the samples were taken perpendicular to the layering. In the absence of layering, or only weakly developed layering, as might occur in crater fallback and ejecta, this sampling problem does not appear to be serious.

APPLICATION OF THE METHOD

SAMPLING PROCEDURES

Comparative Test on a Small Scale

A comparative test between sieving and weighing and the newly developed modal analysis technique for clastic material was conducted using approximately five tons of homogenized gravel. As specified, the gravel ranged in size from about 5 inches down to 1/2 inch. Although the specification of a well-graded mixture was not met, it is believed that this characteristic of the material had little effect on the test results. The gravel was spread out to a uniform depth of approximately 1 foot. The experimental program included sieving and weighing of five samples of 100 pounds of the 5 tons of gravel and conducting 5 separate modal analyses on the gravel using a sample size of $n = 100$ clasts for each analysis.

Five samples of gravel, each weighing 100 pounds, were removed by shovel from the parent population of five tons of gravel. Three different operators took a total of five different samples on different days. The same three operators sampled the gravel using the modal analysis technique taking five samples of $n = 100$. Each of the 100 clasts in the five samples was selected from the deposit on the basis of a grid system established by using a 1/4-inch rope

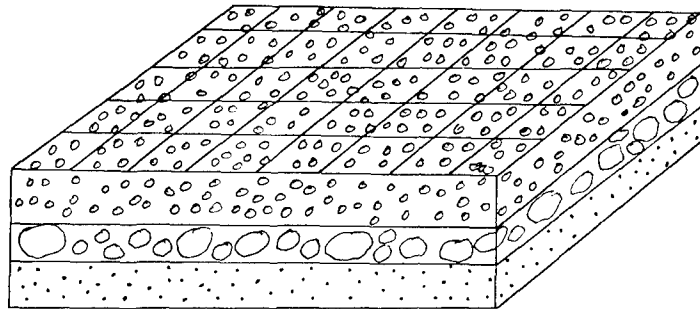


Figure 8. Error of Estimate of Relative Proportions due to Layering.

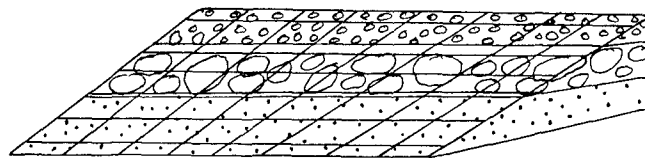


Figure 9. Sampling of Layered deposit to obtain a Representative sample.

marked at 1-foot intervals. The "b" intermediate axis was measured by means of a caliper (see Figure 4). As a further check on the sampling technique the 500 pounds of previously sieved and weighed material was spread out on the ground and a sample of $n = 100$ was taken in the same manner as the other samples. The results were tallied and plotted. Points were connected by straight lines and curves were not "smoothed" in order to emphasize differences in results.

Application to Craters

Several craters were investigated at the Nevada Test Site. These included both chemical and nuclear explosive craters (Table 1). A systematic grid was laid out on the surface of the ejecta, using a tape and compass for orientation, and samples (measurements) were taken at an interval larger than the largest particle likely to be encountered - ten- to twenty feet. These samples were taken in groups of 100 each over different parts of the fallback and ejecta. Samples totaling 300 to 600 clasts were taken, depending upon the variability in the distributions obtained in the samples. These measurements were grouped into geometric size classes, each class being twice as large as the preceding one, and the numbers of measurements in all classes were summed. These measurements were plotted as cumulative percent using the midpoint of each class size as the data point for that size class.

RESULTS

The results of Site 300 investigations are shown in Figures 10 and 11. These figures are composite plots showing the results of both the point sampling technique and sieving and weighing of material taken from the same parent population. The results of the studies of craters at the Nevada Test Site are presented in Figures 12 through 14. Figures 12 and 13 are composite plots showing the results of the point sampling technique and sieving and weighing material from the same crater. Figure 14 shows the results of applying the point sampling technique to several craters - sieving and weighing data from the DANNY BOY crater only is plotted for comparison.

DISCUSSION

SMALL-SCALE COMPARATIVE TESTS

It is apparent that, within the limits of error of the techniques used, the curves obtained by sieving and weighing and that obtained by modal analysis rather consistently lie on top of each other for the small-scale comparative tests (Figures 10 and 11). Therefore, it is postulated that the ratio of the area occupied by particles of a given size to the area occupied by all other sizes, in the area under investigation, is a consistent estimate of the volume percentage of that size!

These results suggest that Wolman did not sample the same population when he sampled the surface of the stream bottom by his grid point count technique and when he dug into the stream bottom for samples to sieve.

The "fit" of the curves obtained by the two techniques used in the small-scale tests is not perfect. However, what are considered to be reasonable explanations for the observed discrepancies are presented. The variability in the upper end of the sieving size-distribution curves is attributed to two sources. First, it was necessary to use hand sieves. It is a difficult task to obtain reproducible results by hand shaking 100 pounds of gravel through a 40-pound set of sieves. Also, individual fragments weighing as much as 15 pounds were encountered in some of the samples and, therefore, a 100-pound sample is too small. The modal analysis results were considerably more internally consistent than the sieving results. The modal analysis technique forces an operator to take a

TABLE 1

DESCRIPTION OF CRATERS, NEVADA TEST SITE

<u>CRATER</u>	<u>CHARGES</u>	<u>DOB</u>	<u>MEDIUM</u>	<u>CHARGE SIZE</u>	<u>RADIUS</u>
1. DANNY BOY	Single	110	Basalt	0.42 kt*	107'
2. CABRIOLET	Single	171	Rhyolite	2.3 kt	179'
3. Pre-SCHOONER ALPHA	Single	58	Basalt	20 tons**	50'
4. Pre-SCHOONER BRAVO	Single	50	Basalt	20 tons	49'
5. Pre-SCHOONER CHARLIE	Single	66	Basalt	20 tons	Mound
6. BUGGY	Row	135	Basalt	5 Devices 1.1 kt	Row
7. SULKY	Single	90	Basalt	.085 kt	Mound
8. DUGOUT	Row	58	Basalt	5 charges 20 tons each	Row

* kt = nuclear

** tons = high explosive

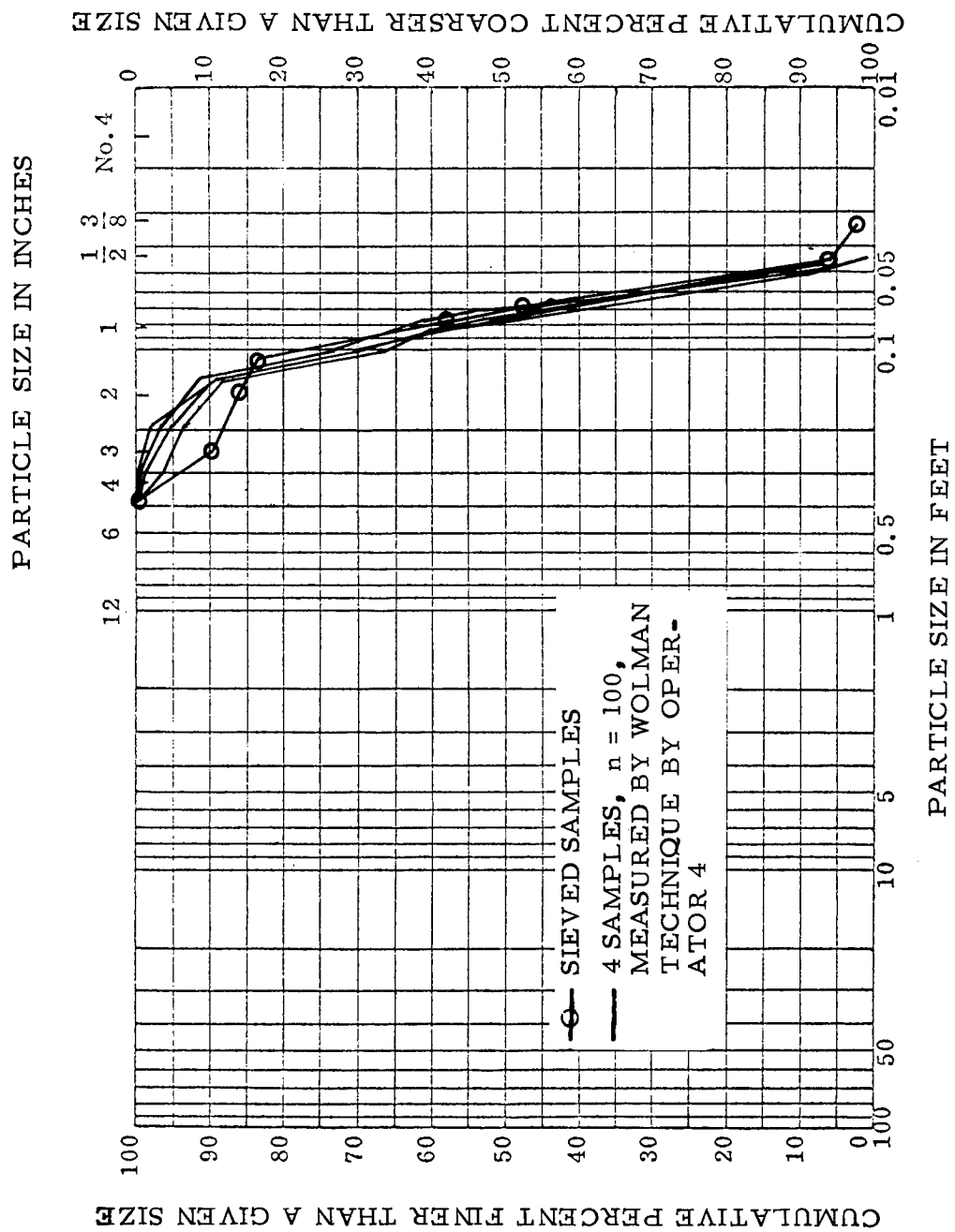


Figure 10. Particle size distribution, Site 300 Test, Operator 4.

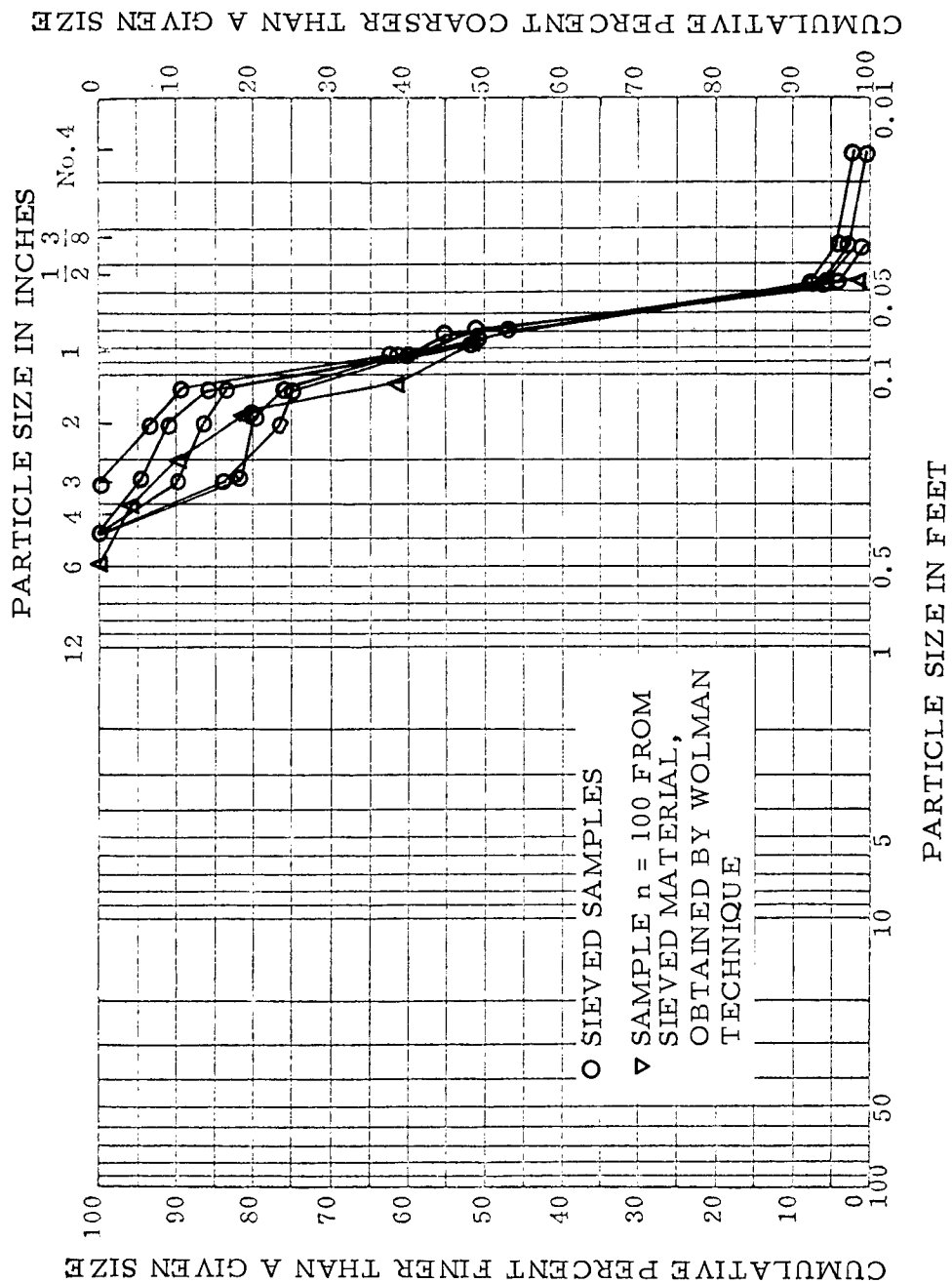


Figure 11. Particle size distribution, Site 300 Test, Sample n = 100 of sieved material obtained by Wolman Technique.

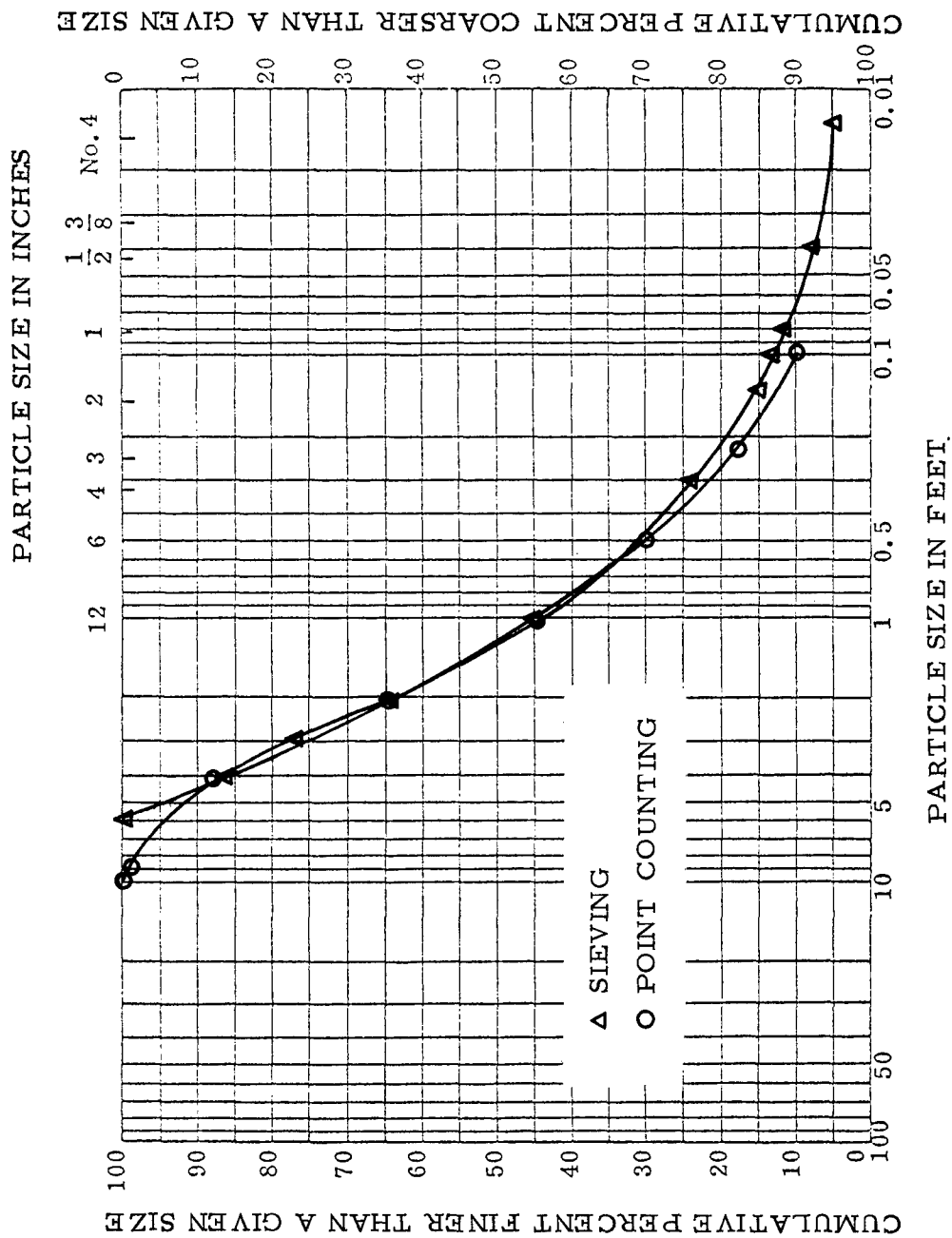


Figure 12. Particle size distribution, DANNY BOY Crater.

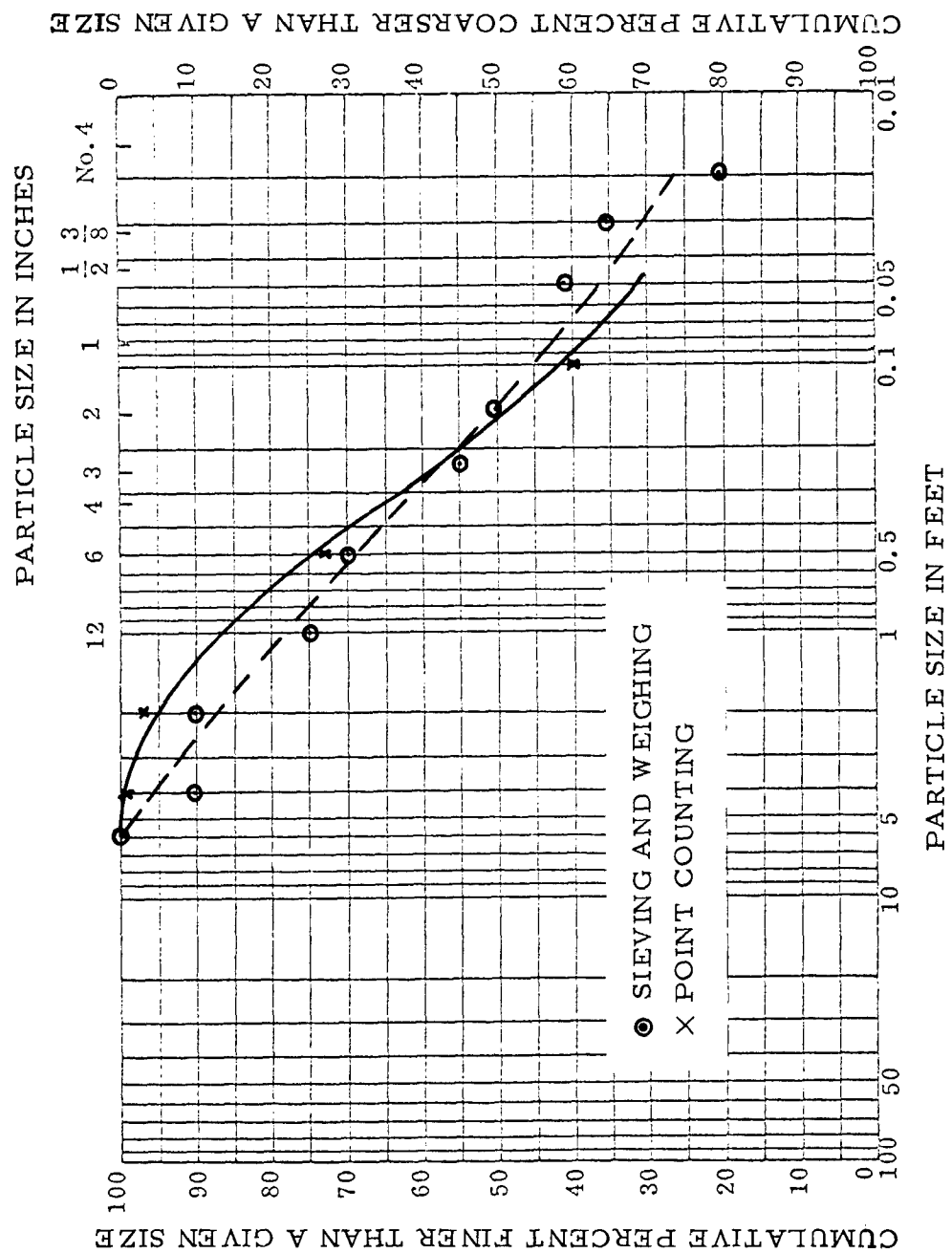


Figure 13. Particle size distribution, CABRIOLET Crater.

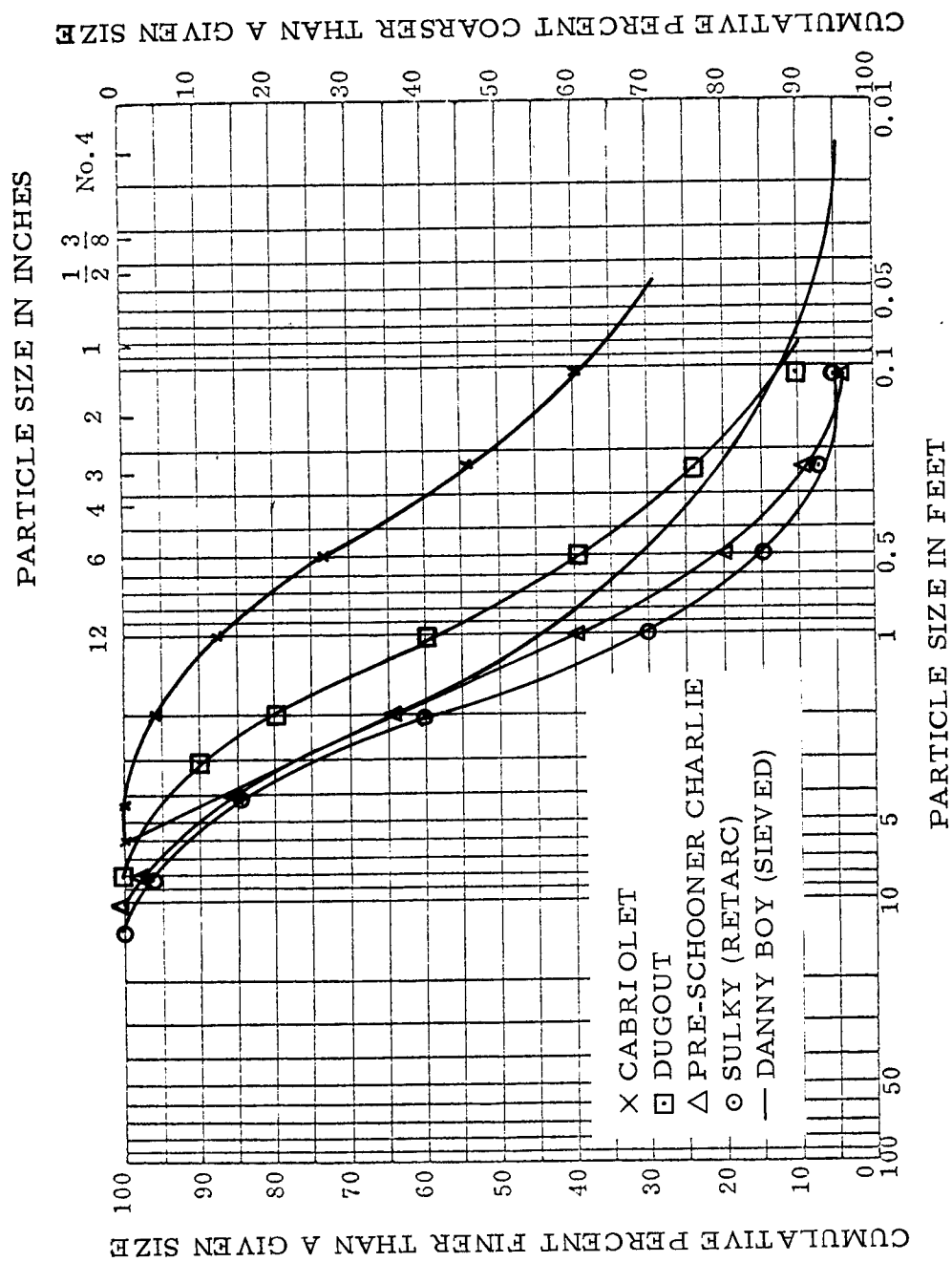


Figure 14. Particle size distribution of five N.T.S. Craters.

sample at a given point in order to avoid allowing personal prejudices to dictate where a "representative" sample should be taken.

Sources of "error" include: the predilection of different operators for selecting pebbles of different sizes thus contributing to differences between sample means; different operators choice of the "b" intermediate axis leading to variation in estimates between samples, and variation between sieving and "b" axis measurements as estimators of the population values.

APPLICATION TO CRATERS

It is apparent that the fit between the size distribution curves obtained at the DANNY BOY Crater (Figure 12) by sieving and weighing, and by modal analysis is quite good. The same comparison of CABRIOLET, Figure 13, is less satisfactory, although the maximum absolute deviation is less than 7%. There is, however, considerable scatter in the sieve data points and the curve, almost a straight line, is not the normal "S" shaped curve one might expect.

Because there is no sieving data to compare with from the other craters, the particle size distributions of the other NTS craters obtained by modal analysis have been plotted on a graph along with a size distribution obtained by sieving ejecta from the DANNY BOY Crater. The data from the other basalt craters seem reasonable in light of the data from the DANNY BOY Crater. As is apparent from visual inspection, the SULKY mound has considerably larger blocks than the craters in the same material.

ACCURACY AND APPLICABILITY

Because samples (measurements) are obtained in different ways by sieving and by the modal analysis, the size distributions obtained by these two techniques will not be exactly the same. However, the real question is, are the observed differences significant? To answer that question we must have an idea of what a "significant" difference should amount to and we probably would like the answer in quantitative terms.

Rogers (1956) has done considerable work investigating the question of how much variation in size distribution can be expected from common geologic sampling techniques. Techniques he investigated were: sieving, size measurement in thin-section, grain mounts and pipette analysis. Rogers concluded that different operators using the different techniques mentioned above should yield means reproducible to within 25% for each of the geometric size classes, i.e., 2", 4", 8", etc., commonly used to designate a set of U. S. Standard Sieves, and standard deviations to within 20%.

The reproducibility of the point sampling technique is certainly within these limits. And, the size distributions obtained by sieving and weighing and by point sampling also lie within the limits expectable for two different techniques. The question whether this stated accuracy is acceptable is a much more subjective question. The answer to this question depends upon the objective of the observations.

The sample size and area determination techniques presented herein are meant to provide the investigator a method by which he can get a preliminary estimate of these parameters. In reality, it is not possible to determine "a priori" how many samples to take to obtain an unbiased and consistent estimate of the size distribution of the clastic material. Generally, it is necessary to take a preliminary sample and test it against some constant probability model like the normal, log-normal or Poisson distribution. If the size distribution does not approximate this model then it is necessary to take more samples or change the sampling technique or the model against which it is being tested. In

the case of particle size distributions this approximation can often be accomplished by some suitable transformation of the variate.

CONCLUSIONS

The sampling technique presented herein permits the modal analysis of clastic materials yielding results comparable with those obtained by sieving and weighing of the same materials. It appears that this technique has application to any clastic material from which a representative sample can be obtained. In conclusion it is necessary to point out that the Delesse relation and the point sampling technique provide a very powerful tool for the size analysis of clastic materials and the effects of porosity and layering.

SUMMARY

A sampling technique was developed by Wolman (1954). A small-scale comparative test of this technique was carried out using presized gravel. The sampling technique was reevaluated in light of the results obtained during these tests. The Delesse relation was used to develop a model that theoretically justifies the results achieved. Criteria were established for the number of samples to be taken and the area to cover in sampling. In light of the results achieved, the use of the "b" intermediate axis as a measure of size for clasts seems justified. A test of the new method was accomplished at the AEC Nevada Test Site on several craters. The results achieved during these tests are considered "satisfactory".

REFERENCES

1. Anderson, II, B. D., 1969, An Analysis of the Grid Photography Technique as a Means of Determining the Size Distribution of Crater Fallback and Ejecta, NCG Technical Memorandum 68-15, U. S. Army Corps of Engineers, Nuclear Cratering Group, Lawrence Radiation Laboratory, Livermore, California, p. 24.
2. Chang, Yi-Maw, 1967, "Accuracy of Fossil Percentage Estimation," Jour. Paleo. v. 41, n. 2, p. 500-502.
3. Chayes, F., 1956, Petrographic Modal Analysis, an Elementary Statistical Appraisal, John Wiley & Sons, Inc., New York, 113 p.
4. Griffiths and Kahn, 1967, "Sampling a Geological Population," a pre-meeting short course, American Geological Institute, Washington, D. C.
5. Rogers, J. J. W., 1965, "Reproducibility and Significance of Measurements of Sedimentary Size Distributions," Jour. Sed. Petrol., v. 35, n. 3, p. 722-732.
6. Wolman, M. G., 1954, "A Method of Sampling Coarse River-Bed Materials," Transactions, American Geophysical Union, v. 35, n. 6, 951-956.

SCHOONER EJECTA STUDIES

Robert W. Henny
University of New Mexico*

Introduction

This paper presents a preliminary analysis of the Schooner ejecta and missile population. Our work on the Schooner event results from a continuing interest in cratering phenomenology with emphasis directed towards development of photographic techniques for the documentation of static and dynamic aspects of large ejecta and missile populations.

Project Schooner was a nuclear experiment in a layered tuffaceous medium executed as part of the Plowshare program for development of nuclear excavation. Schooner was detonated on December 8, 1968 at approximately 0800:00.149.6 (PST), 1600:00.149.6 (GMT), in area 20, Nevada Test Site (NTS). The resultant yield was 31 ± 4 KT. The emplacement hole was U20u at geodetic coordinates:

Longitude: W 116° 33' 57.1419"
Latitude: N 37° 20' 36.3187"

Surface ground zero (GZ) was 5,562.4 feet mean sea level (MSL); emplacement depth (to the working point) was 108.2 meters (355 feet). Listed below are basic crater and ejecta data:

	<u>Average</u>	<u>Range</u>
(1) Depth of Burst	(DOB): 355 ft	
(2) Yield	(W): 31 KT	27-35 KT
(3) Apparent Crater Radius	(R _a): 426 ft	366-484 ft
(4) Apparent Crater Depth	(D _a): 208 ft	
(5) Apparent Lip Height	(H _{al}): 44 ft	33-57 ft
(6) Apparent Lip Crest Radius	(R _{al}): 483 ft	440-570 ft
(7) Continuous Ejecta Limit	(R _{eb}):	1,700-2,700 ft
(8) Maximum Missile Range	(R _m):	7,000-10,000 ft
(9) Maximum Missile Size	(M _m): 30x20x20 ft	
(10) Apparent Crater Volume	(V _a): 2,282,870 yd ³	
(11) Apparent Lip Volume	(V _{al}): 2,745,330 yd ³	

*Now at Air Force Weapons Laboratory.

Reference 1 should be consulted for preshot information including geology, material properties, device design, radiation and crater predictions. Reference 2, a paper presented at this symposium, should be referred to for general post-shot results. Reference 3 documents the University of New Mexico's participation in the Schooner event and presents early observations and results concerning the crater and ejecta.

The Schooner test site is located in the middle of a relatively flat portion of Pahute Mesa, having a relief of less than 40 feet within 1,500 feet of ground zero. Figures 1 and 2 give the location and topography of the site. Figure 3 provides two views of the site.

The stratigraphy consists of a layered sequence of welded and bedded tuffs and ash flows in nearly horizontal position overlaid by 1 to 4 feet of soil cover. The lithology, as interpreted from the AFWL drilling program (ref. 4), consists of three major units with the following average properties:

- (1) Welded Tuff, 0-124 ft, $\rho = 2.4$ g/cc, $c = 7,000$ fps.
- (2) Bedded Tuff, 125-339 ft, $\rho = 1.5$ g/cc, $c = 4,000$ fps.
- (3) Welded Tuff, 340-368+ ft, $\rho = 2.3$ g/cc, $c = 7,000$ fps.

Examples of typical core from the welded and bedded units are shown in figure 4. Note the near vertical jointing in the welded tuff and apparent lack of jointing in the bedded tuff (horizontal fractures are drilling breaks).

Measurements of joints in outcrops from stream cuts in the vicinity of U20u revealed two prominent, near vertically dipping joint sets orientated approximately N-S and E-W. The water table in the GZ area exceeds 800 feet.

Crater

Figure 5 is an eastward facing view of the Schooner crater showing the slumped sides and flat bottom. Preshot and post-shot topographical maps of the area were prepared from aerial stereo-photographs by American Aerial Surveys for the US Army Nuclear Cratering Group. An isopach map obtained by subtracting the pre-shot map from the post-shot map is reproduced in figure 6.

Three profiles across the crater constructed from the isopach map are presented in figure 7. The crater is characterized by a prominent flat bottom with radius between 110 and 140 feet. The crater walls consist of two distinct zones. The upper zone consisting of intact "bare" rock maintains a constant slope of 60-65 degrees. The lower zone, consisting of fallback and slumped ejecta, continues downward to the crater bottom with a slope of 30-35 degrees. The contact between zones varies from 20 to 125 feet below original ground surface, depending upon the azimuth.

Significant slumping on the crater walls was observed immediately following the event (up to 1/2 hour). This short-term slumping had greatly subsided after 1-1/2 hours and effectively terminated after 6 hours. Observations of the crater on several occasions during the past year reveal continued long-term slumping,

LEGEND

AREA BOUNDARY	PRIMARY	SECONDARY
PAVED ROAD	PRIMARY	SECONDARY
DIRT ROAD	PRIMARY	SECONDARY
WATER	PRIMARY	SECONDARY
LOCKED BARRICADES	PRIMARY	SECONDARY
BUFFER ZONE BOUNDARY	PRIMARY	SECONDARY

GRAPHIC SCALE

10,000 0 10,000 20,000 30,000 FT

UNITED STATES ATOMIC ENERGY COMMISSION

NEVADA TEST SITE

ROAD & FACILITY MAP

NEVADA
N.M.S.
UTAH

5

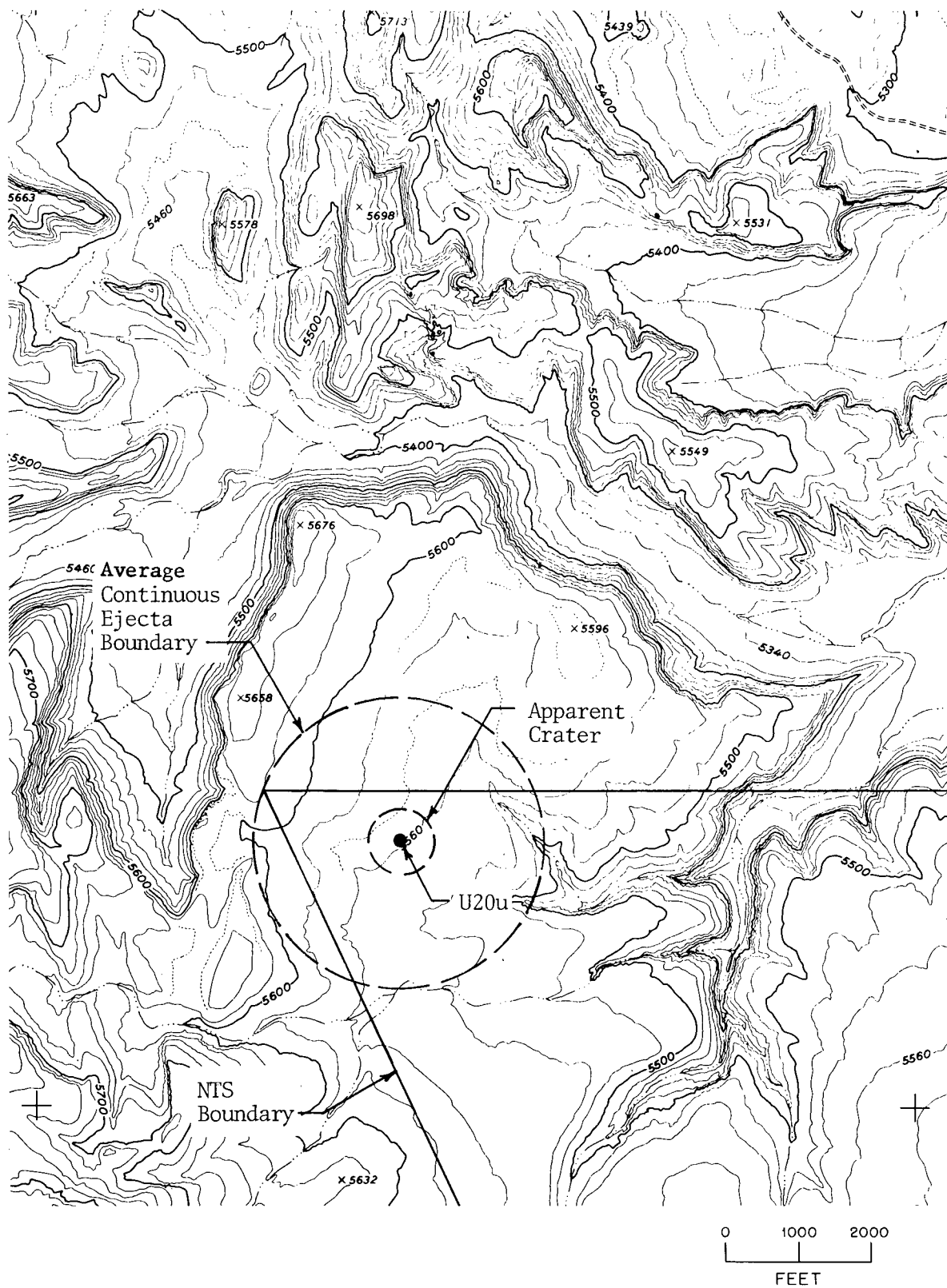
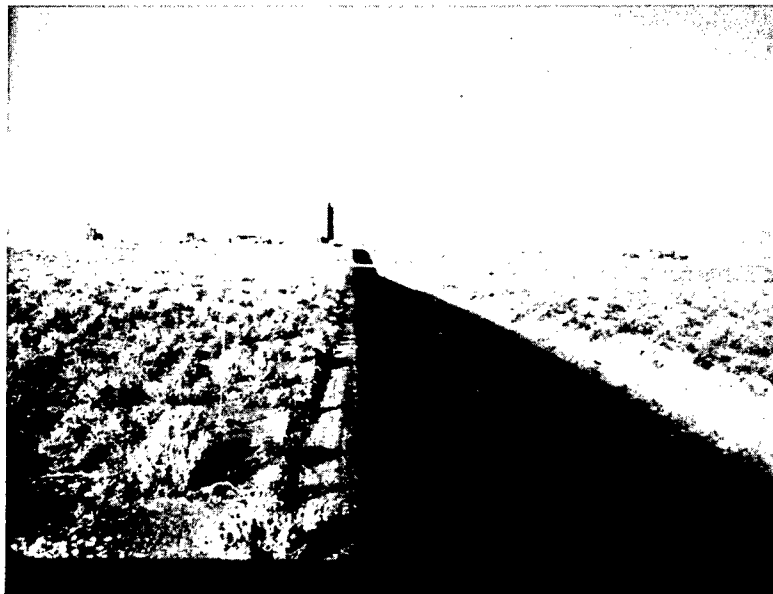


Fig. 2 —Topographic Map of SCHOONER Test Site

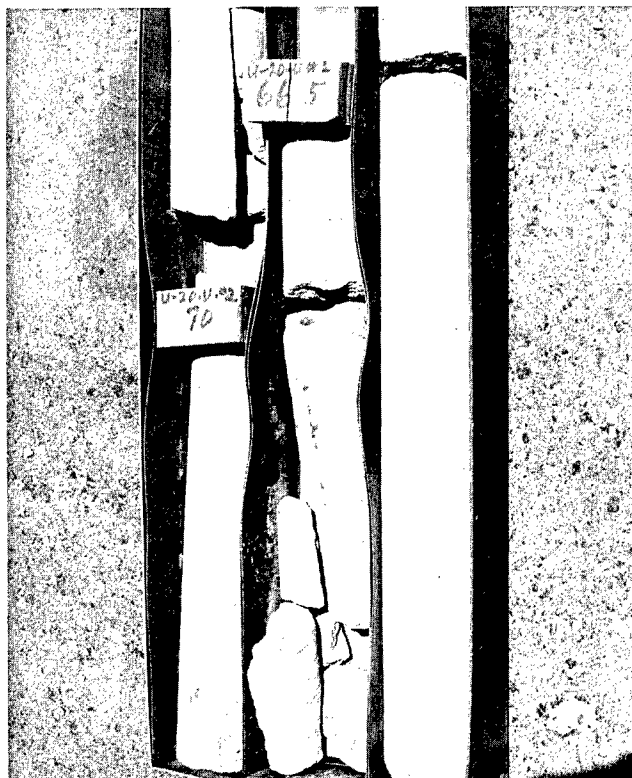


Several Miles South of GZ

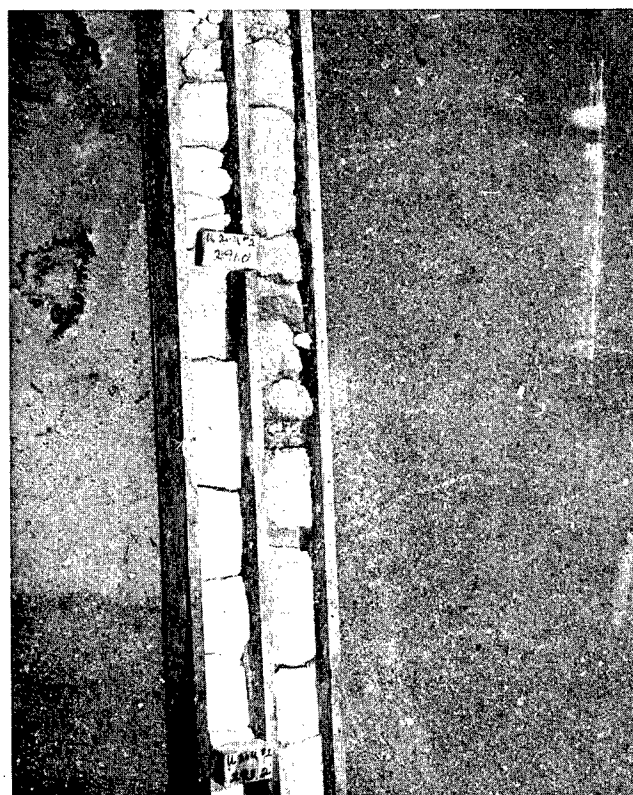


Along S35°W Radial at 1000 Feet

Fig. 3—SCHOONER Test Site, View of Ground Zero Area



Welded Tuff



Bedded Tuff

Fig. 4



Fig. 5—Oblique View of SCHOONER toward East

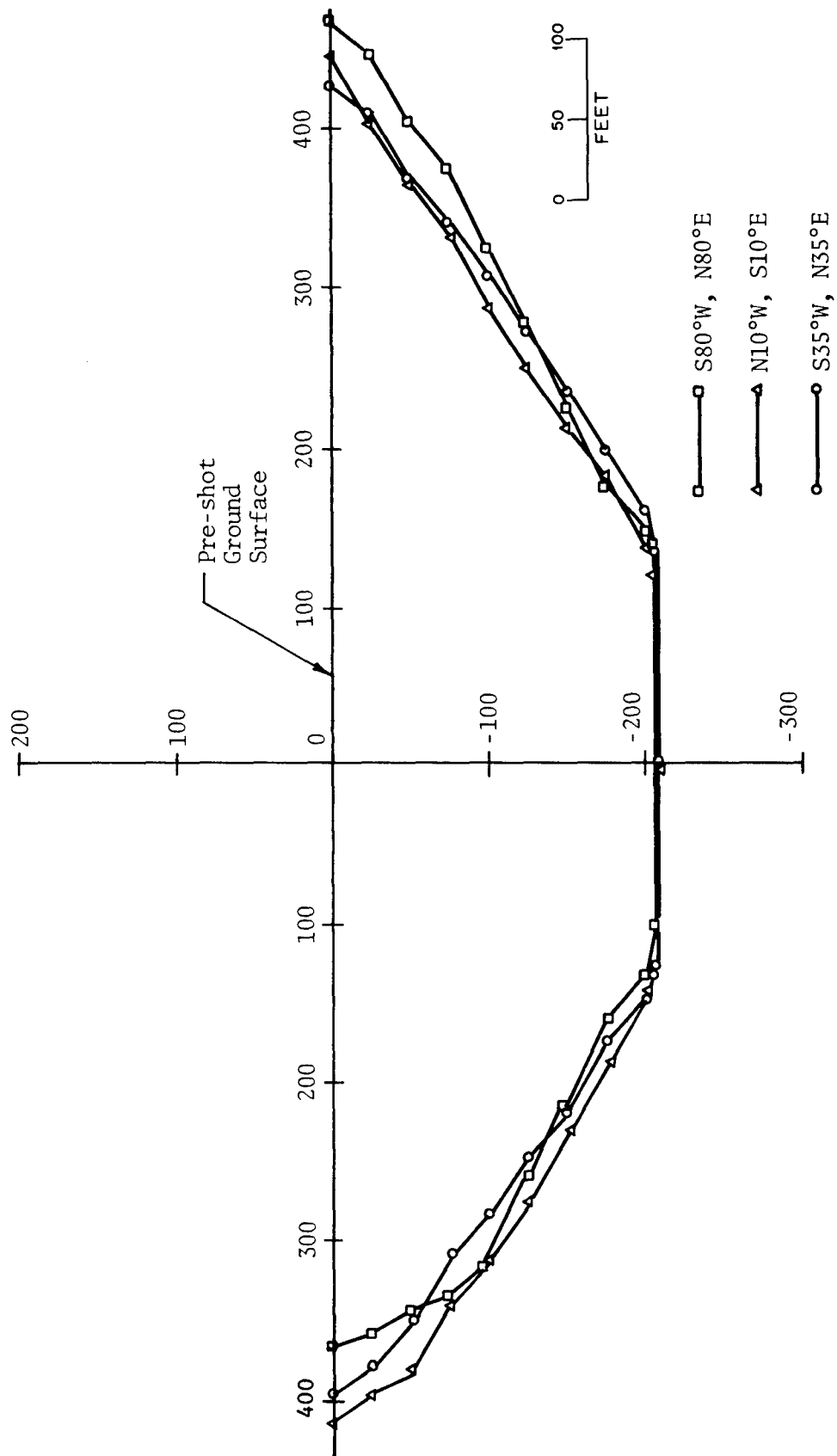


Fig. 7—SCHOONER Apparent Crater Cross Sections

with a number of large missiles (one measuring over 20x20x20 feet) having moved down the walls onto the crater bottom.

Ejecta - Static Aspects

The Schooner ejecta population is distributed in a highly asymmetrical manner. The thickness, size distribution and other related characteristics vary significantly with respect to both radial distance and azimuth. The ejecta population, exclusive of base surge deposit, can be divided into a close-in continuous region bounded by the continuous ejecta limit followed by a far-out discontinuous region bounded by the maximum missile range. Figure 8 is an overhead view of the crater and ejecta with north at the top of the page. A number of normal and skewed ejecta rays are discernible emanating from the crater rim area and terminating beyond the continuous ejecta limit. In addition there are several large, isolated masses of ejecta beyond the continuous ejecta limit not connected to the crater by rays. Relatively close agreement is obtained in shape between figure 8 and the 5-foot contour on the isopach map.

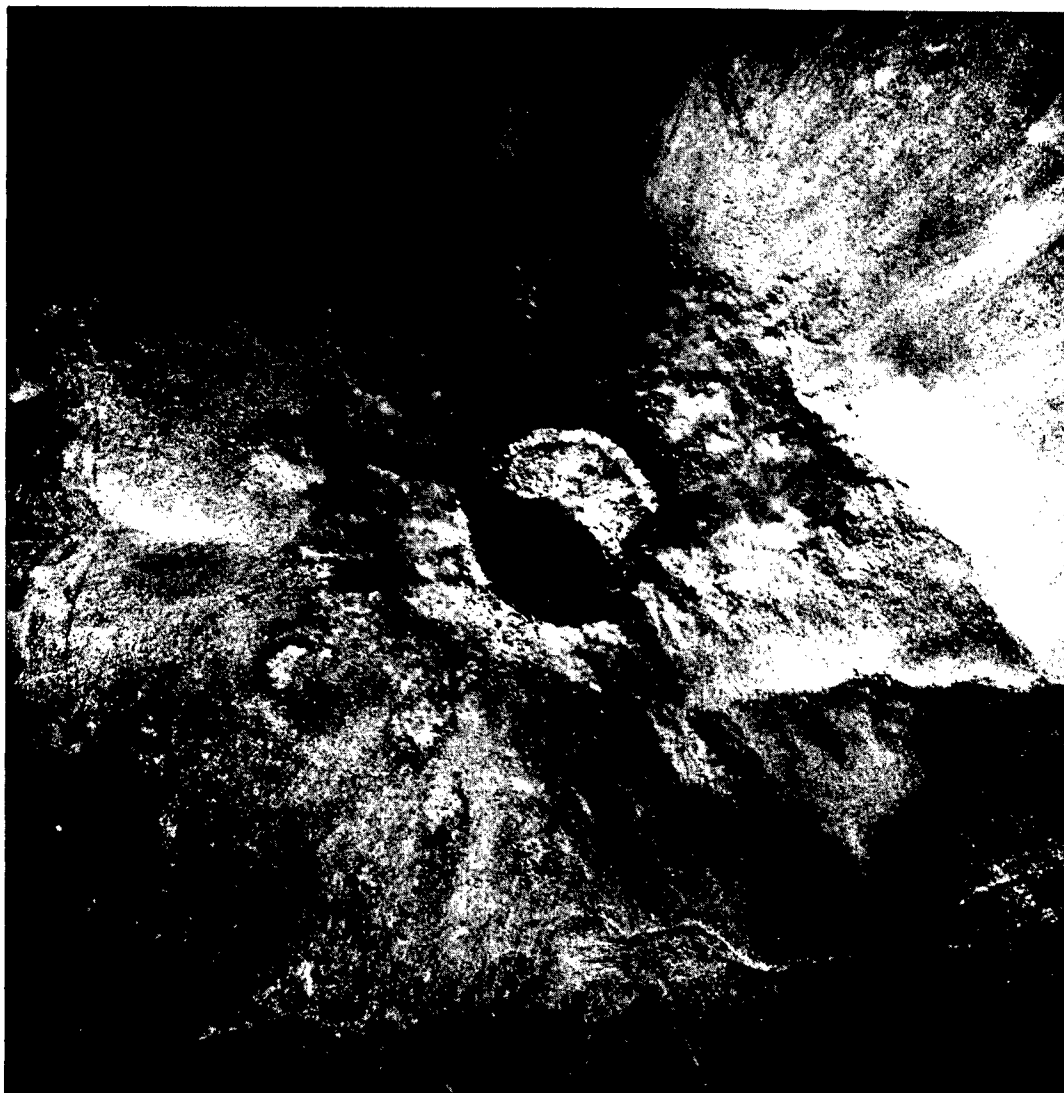
By considering the 5-foot contour pattern on the isopach map, together with observations of the crater area from overhead, the spatial distribution of the ejecta population can be grossly related to the inferred surface joint pattern; i.e., roughly directed N-S and E-W. A more definitive agreement perhaps should not be expected in lieu of at least two factors: (1) only the welded tuff in the upper 125 feet of the ejected mass contained well defined joints and (2) the welded tuff unit contained several distinct flows each of which may have exhibited a slightly different joint pattern.

The ejecta population is bi-modal consisting of fines (sand size and smaller) derived primarily from the bedded tuff unit and discrete blocks and fragments of competent rock derived primarily from the welded tuff units. Ejecta, as used in this paper, include all soil and rock ejected from the crater. The term missile is used to describe the discrete blocks of rock.

The continuous ejecta limit for Schooner, while difficult to precisely pinpoint, is estimated to fall within a narrow zone ranging from 1,700 to 2,700 feet with azimuth. Within the confines of the continuous ejecta region the visible surface consists predominantly of fines partially covering numerous isolated and a few prominent zones of competent missile blocks and superimposed with scattered but locally concentrated quantities of fused glass. Figure 9 shows selected photographs of the Schooner ejecta population.

To date one trench has been cut from the south crater edge radially outward for 1,500 feet. Along this trench the ejecta with depth is exposed as readily defined zones or beds differentiated by color and texture, each representing a different lithologic entity. Missiles of all sizes are visible, but appear to be concentrated at depth. Maximum ejecta thickness is 15 feet.

Using the isopach map in figure 6, ejecta-uplift profiles were constructed along each 10 degrees and circumferentially along each 1/2 crater radii. The maximum and minimum profiles vary from the mean profile by factors up to 3 and 5 respectively. The mean radial profile decreases smoothly outward from the crater lip. Specific radial profiles, however, often contain significant



0 500 1000
FEET

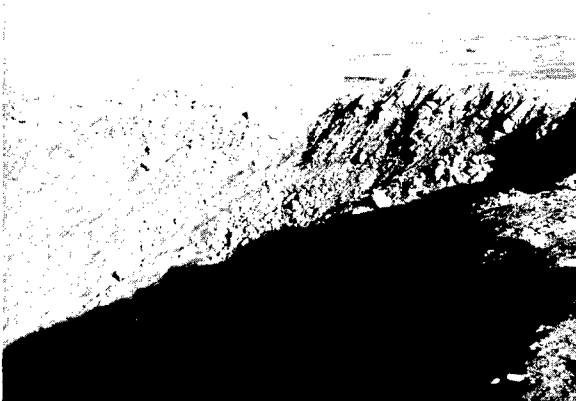
Fig. 8—Overhead Closeup of SCHOONER



Toward GZ (2000 ft, S10E)



Away from GZ (2000 ft, S10E)



Crater (S35W)



From Crater Edge along S10E Radial



Facing NW (700 ft, N45E)



Joint Controlled Blocks
(600 ft, N45E)

Fig. 9—Selected Photographs of SCHOONER Ejecta Population

increases in thickness due to large masses of ejecta forming local topographic "highs" at distances from the crater. Figure 10 presents the computed maximum, mean and minimum profiles.

Along a given circumferential profile the ejecta-uplift thickness often varies considerably; i.e., at 1.5 crater radii the thickness varies by a factor of four within 20 degrees. Figure 11 presents three partial circumferential profiles.

The discontinuous ejecta region extends from the continuous ejecta limit out to the maximum missile range. Maximum missile range, while difficult to determine because of topographic relief, is estimated between 7,000 to 10,000 feet. One unverified missile three feet long was observed on aerial photographs at 9,000 feet. The ejecta in the discontinuous region consist primarily of discrete missile blocks with minor quantities of fines and some fused glass, all superimposed by numerous secondary craters.

Field observations indicate that missile shapes and sizes are controlled by preexisting joints and fractures to a degree increasing with missile size. The largest missile observed to date measures approximately 30x20x20 feet; lying on the crater edge, it is a well-shaped hexagonal block. Figure 12 presents selected photographs of the missile population.

For the preliminary aerial photographic data analysis, missiles were counted in a number of 100x100 foot areas located on a polar grid centered on ground zero and extending out to 5,000 feet. In addition, the five largest missiles and all resolvable secondary craters were measured in 500 foot by 10 degree sections out to 4,000 feet from ground zero. Figure 13 depicts the sampling pattern. Measurements of missiles and secondary craters were made from aerial photographs at a scale of 1 in. = 560 ft using a millimeter optical comparator in conjunction with a 10-power binocular microscope. Only the longest visible dimension was recorded.

There are at least three basic problem areas associated with this aerial photographic method of data acquisition.

(1) Missile Identification

Within the continuous ejecta limit it is relatively easy from photos to identify a missile down to the resolution size (≈ 1.5 feet). Beyond the continuous ejecta limit identification of the larger missiles (greater than 5 feet) is likewise relatively easy. For smaller missiles, however, the vegetation and the shadows and washouts caused by the vegetation provide serious problems. Even within the continuous ejecta limit, shadows from the larger missiles can effectively block out smaller missiles. Beyond the base surge deposit it is difficult to identify even larger missiles due to a lack of color contrast.

(2) Missile Position

Within the continuous ejecta limit only surface missiles are visible which are themselves in various stages of burial. Only with trenching can the size distribution of missiles with depth be determined. The orientation of the missile with respect to the ground surface is important. Field observations indicate a

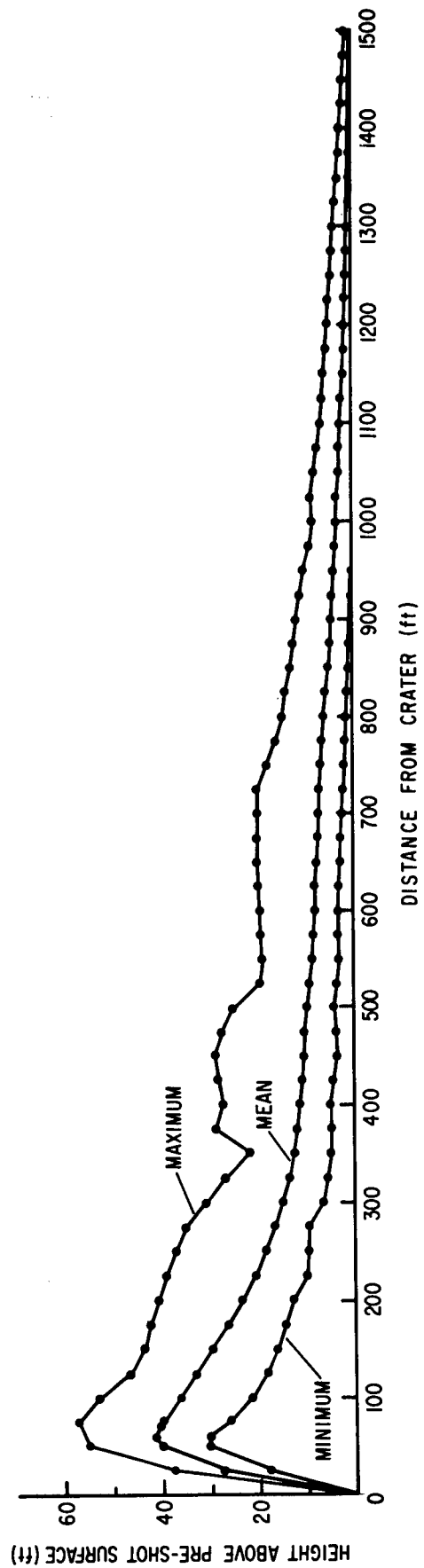


Fig. 10—Ejecta-Uplift Radial Profiles

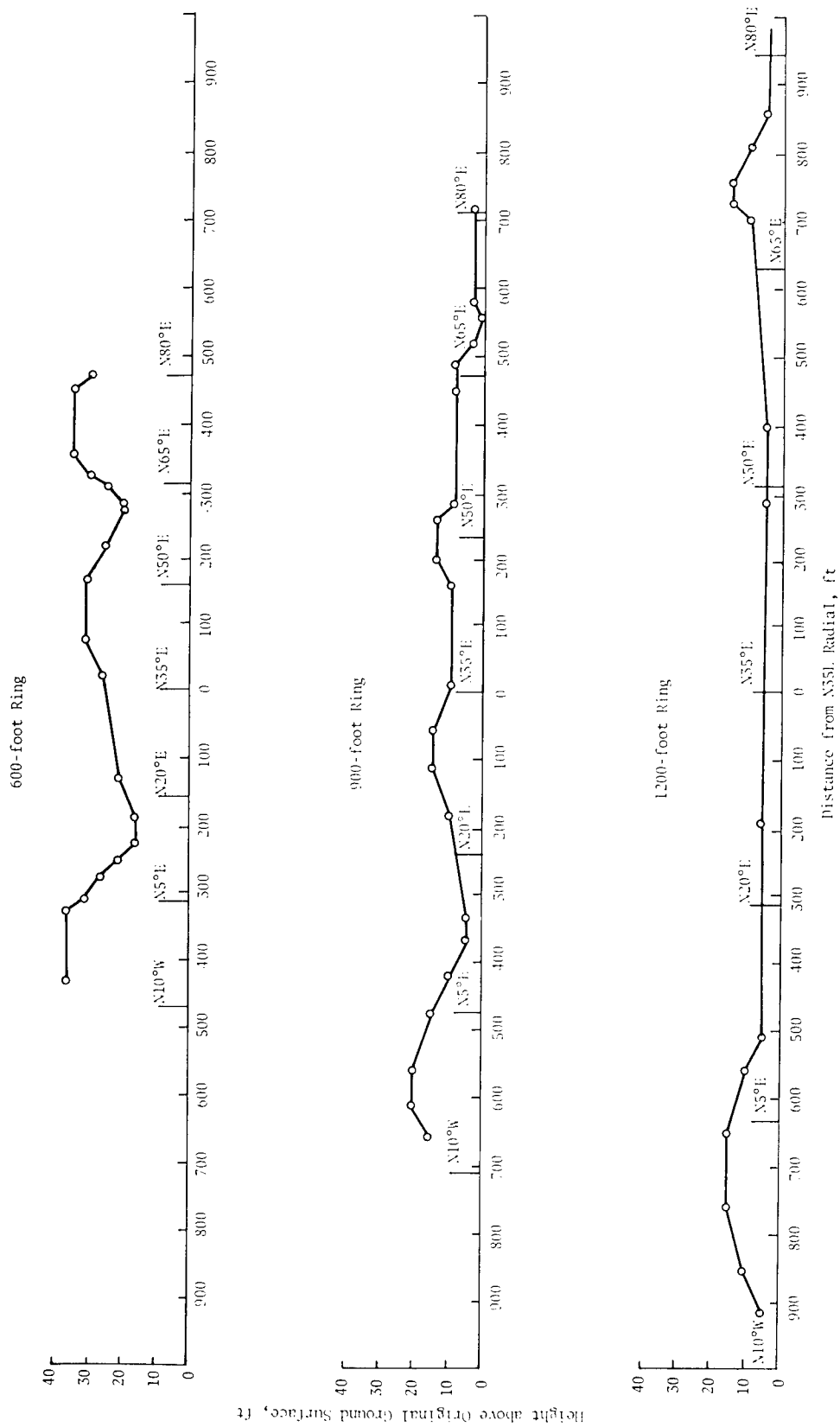
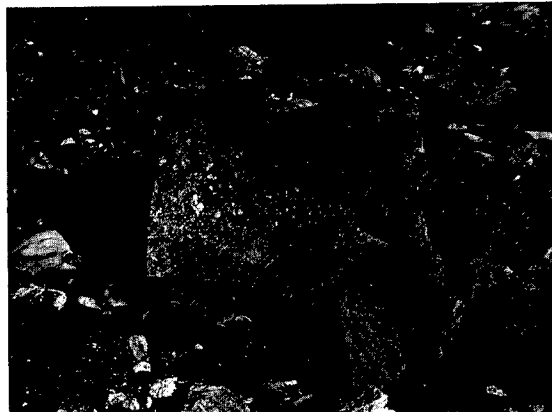


Fig. 11 — Uplift-Ejecta Profiles Along Three Circumferential Rings



Ejecta Distribution @ 180°, 2000 ft



Missile Encased in Fused Glass



Ejecta Tray @ 215°, 2800 ft



Ejecta Tray @ 215°, 2500 ft



Ejecta Tarp @ 215°, 2400 ft



Ejecta Tarp @ 80°, 2100 ft

Fig. 12—Selected Photographs of SCHOONER Missile Population

significant number of missiles with their longest dimensions not exposed to an overhead view. And finally, in order to convert the measured dimension (longest dimension) to some equivalent set of dimensions (i.e., sieve size dimension), data relating missile shape to missile size are required.

(3) Missile Measurement

The accuracy with which a missile can be measured depends primarily upon the photo scale and its uniformity throughout. Using the measurement techniques described above, the measurement accuracy is estimated to be ± 1.5 feet.

For secondary craters, in addition to the preceding problems, it is difficult to resolve the exact boundaries due to the shallow dip of the crater walls. The measurement accuracy from photos for secondary craters is estimated to be ± 3 feet.

For the above reasons, the missile and secondary crater data presented in this paper should be treated as preliminary. It is believed, however, that while the absolute dimensions are subject to the above limitations, the relationships and trends established are real and valid.

Figure 14 presents data on the maximum, mean, median and standard deviation of missile size as a function of distance from ground zero. The bars surrounding each datum represent the azimuthal variation. This variation, which is a factor of four or more within two crater radii, decreases to a factor of two or less beyond six crater radii. Figure 15 presents cumulative missile curves for each of several distances from ground zero. The apparently misplaced position of the 1000-foot curve and the depression in the plots at 1000 feet in figure 14 result from a sparsity of missiles at this range. This sparsity may be real, but more likely is a result of burial by the continuous ejecta blanket.

Figure 16 presents a plot of specific area (square feet per missile) as a function of distance from ground zero. The curve must be corrected downward for distances closer than 2000 feet because of the continuous ejecta blanket. The upward extension of this curve should approach an asymptote at maximum missile range.

Missile length as a function of distance from the crater and azimuth for the maximum, mean and minimum size of the five largest missiles measured in the 500-foot by 10-degree sampling areas is given in figure 17. A similar plot for all measured secondary craters is given in figure 18. It is interesting to note that while there is a slight correlation between maximum missile size and maximum crater size with azimuth, there is no correlation with distance. The mean crater size remains constant from 1,500 to 4,000 feet. Figures 19 and 20 plot crater frequency by size group as a function of distance and azimuth respectively. With respect to distance, the crater frequency up to a 20-foot diameter peaks between 2,000 and 2,500 feet; larger craters peak slightly closer to GZ. With respect to azimuth, the total crater frequency varies by more than a factor of six.

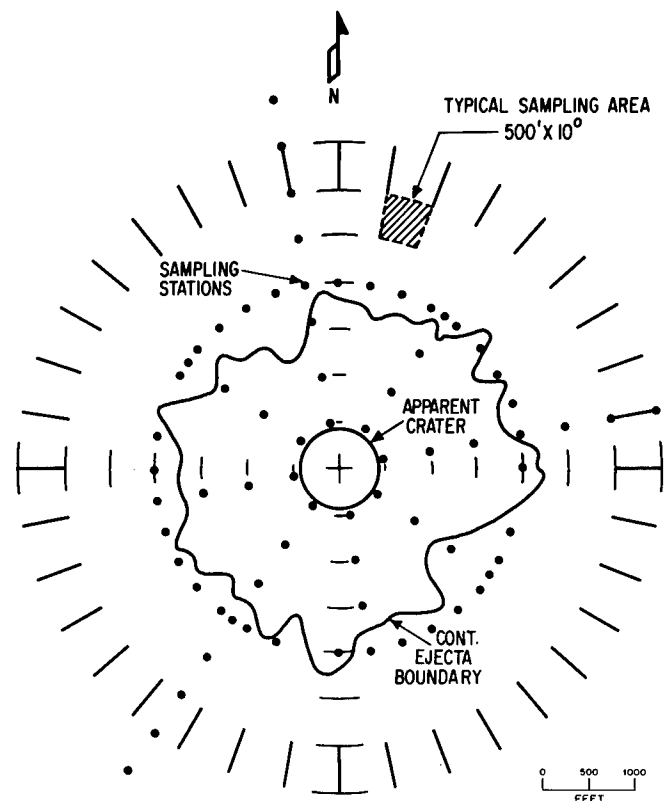


Fig. 13—Photographic Sampling Grid

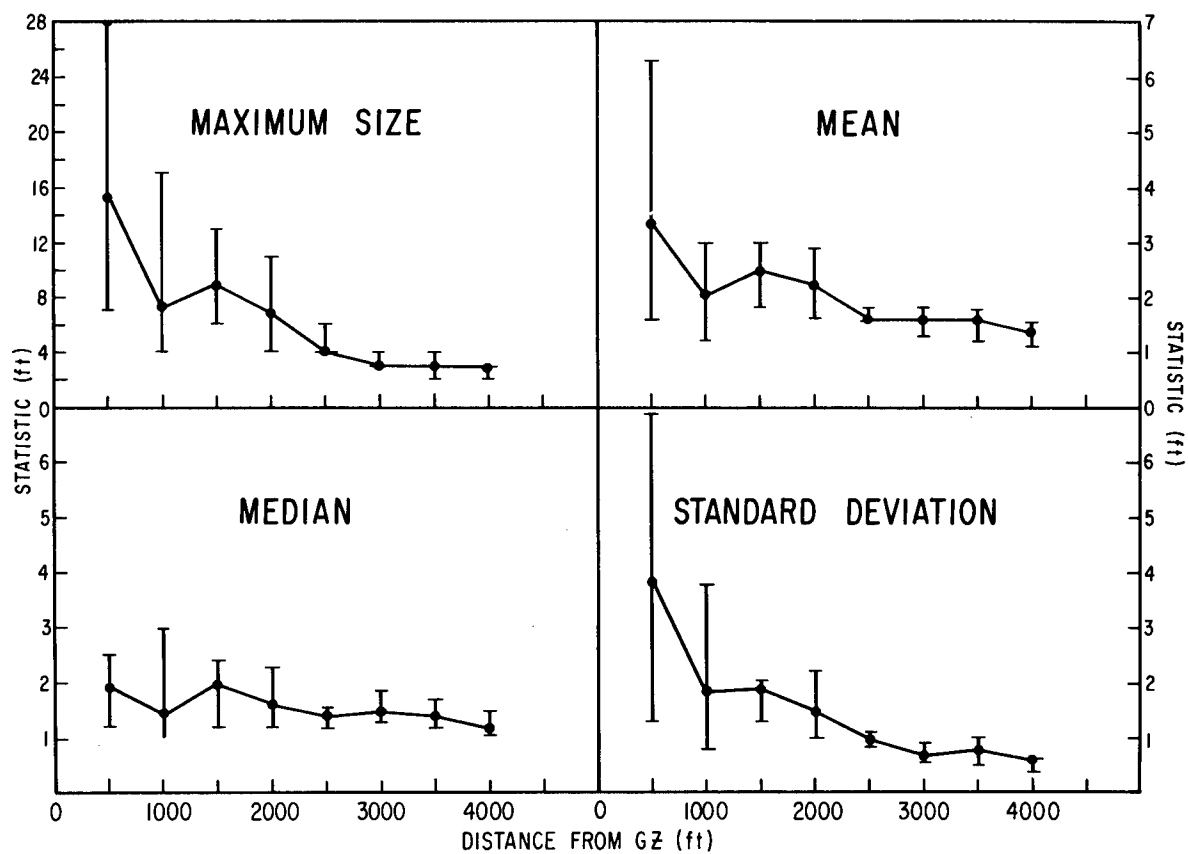


Fig. 14—Missile Size Statistics as a Function of Distance from GZ

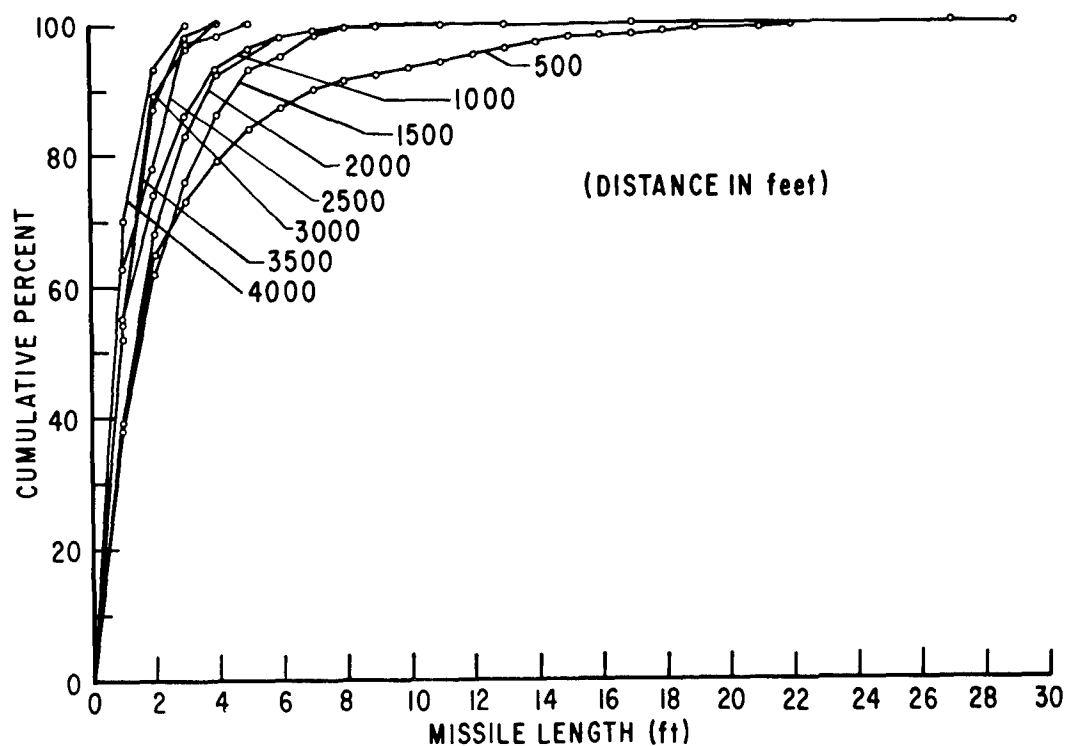


Fig. 15—Cumulative Missile Size Distributions at Discrete Distances from GZ

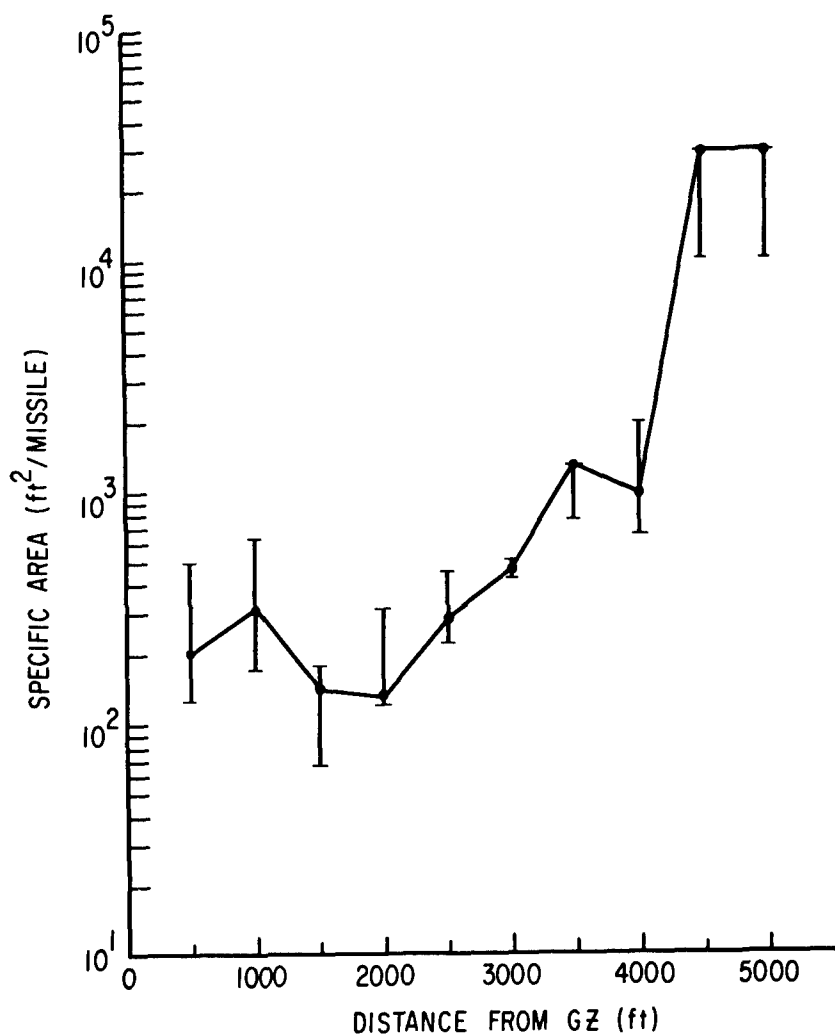


Fig. 16—Missile Specific Area as a Function of Distance from GZ

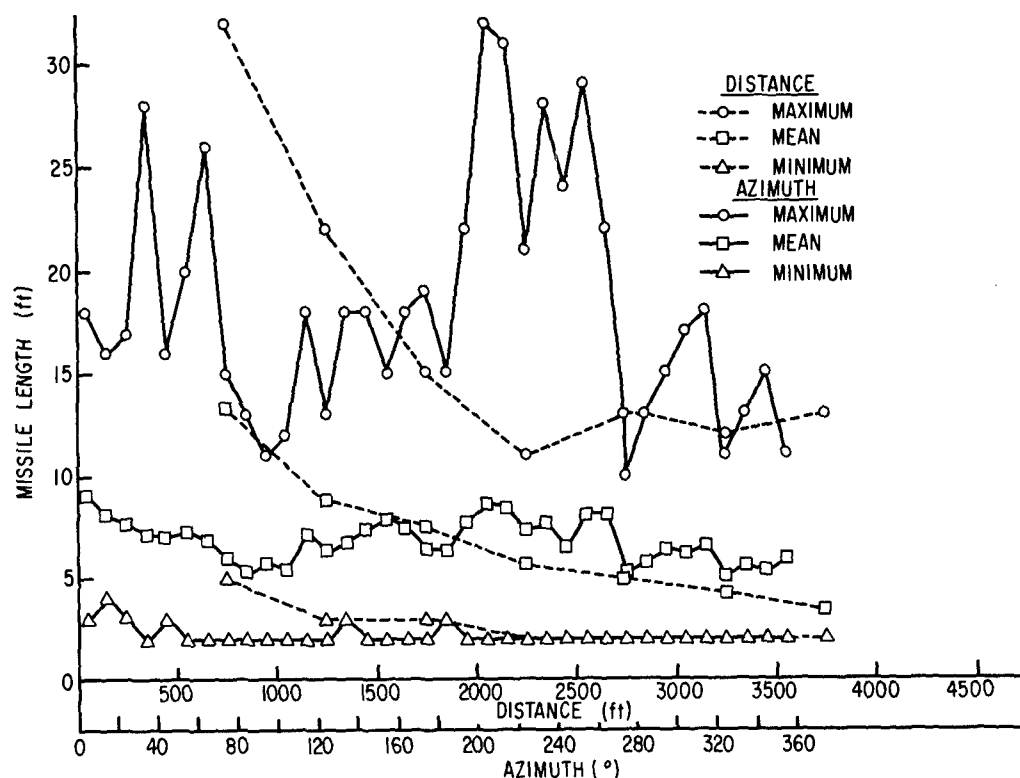


Fig. 17—Length of Large Missiles as a Function of Distance from GZ and Azimuth

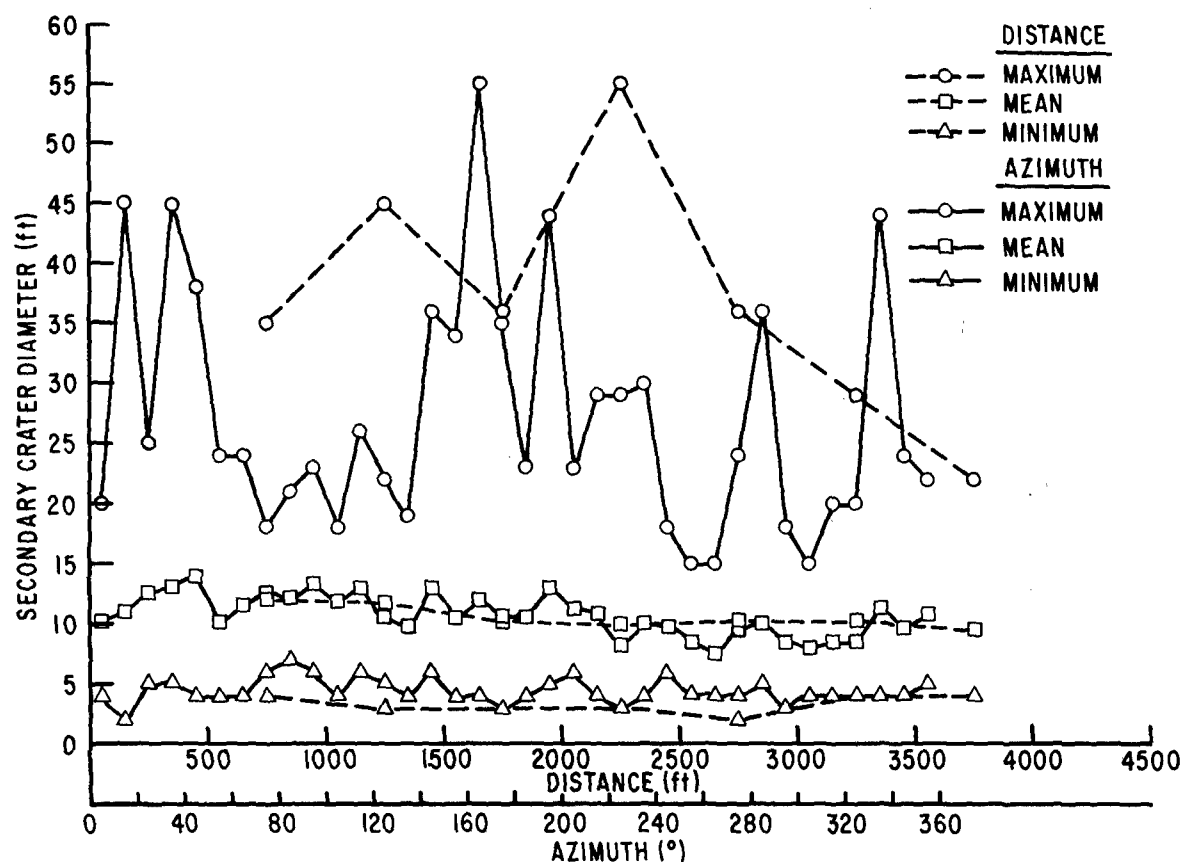


Fig. 18—Secondary Crater Diameter as a Function of Distance from GZ and Azimuth

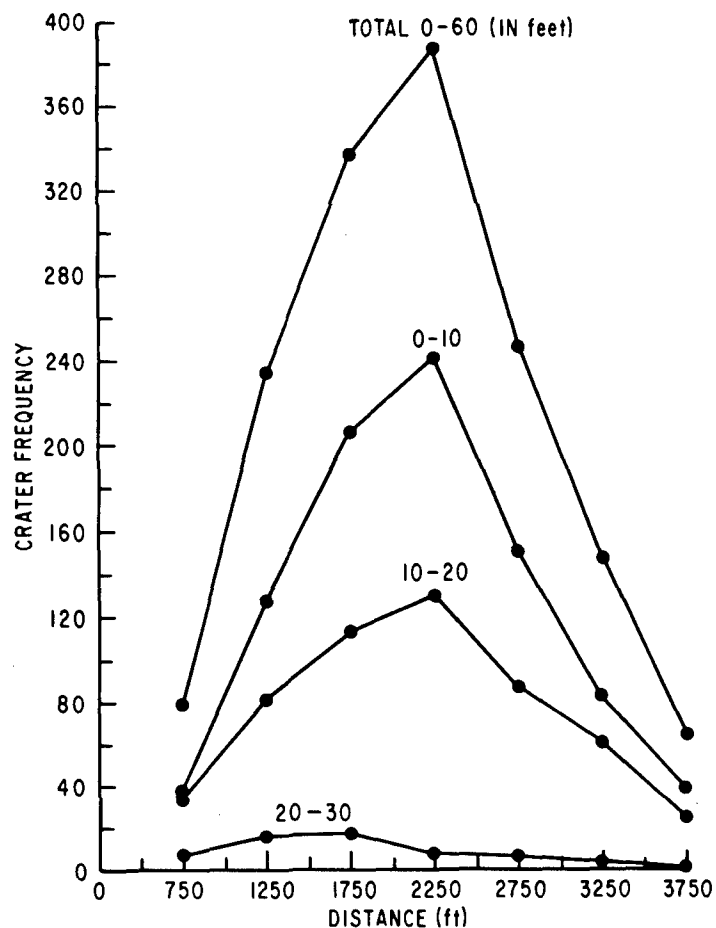


Fig. 19—Secondary Crater Frequency by Size as a Function of Distance from GZ

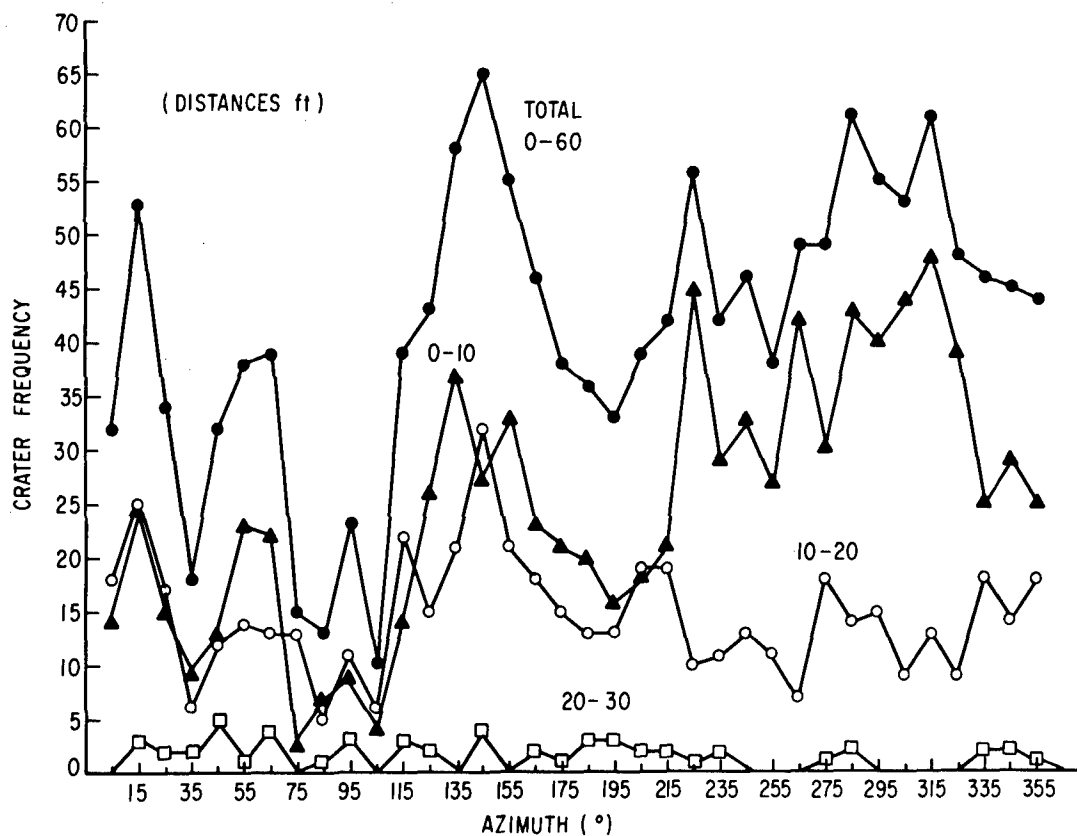


Fig. 20—Secondary Crater Frequency by Size as a Function of Azimuth

Ejecta - Dynamic Aspects

Figure 21 presents selected views of the Schooner detonation with approximate times indicated. Individual missiles and trains of missiles can be observed in various portions of their trajectories. An effort is currently underway to obtain missile velocity and impact angle data as a function of exit angle and time. Preliminary data for "typical" missiles give terminal velocities and impact angles ranging from 150 to 350 feet per second and 40 to 60 degrees respectively.

Impacting missiles have been counted in eight 10-degree sectors from a series of time-sequence aerial photographs taken from vertically above GZ. Missiles are observed to impact up to 60 seconds after flare initiation and out to a maximum range of 6,500 feet. Along any given azimuth, and particularly along an ejecta ray, impacts progressed steadily outward from the crater with time. The rate at which missiles were observed to impact is a function of both distance from ground zero and azimuth. Figure 22 is the combined cumulative time history plot. Time history plots at incremental distances and frequency of impacts as a function of distance are presented in figure 23. In both figures time is with respect to flare initiation which is approximately three to four seconds prior to zero time. Contrary to expectations the peak impact distance does not correspond to the peak secondary crater distance.

As stated previously, the data presented in this paper are preliminary, conclusions drawn from which are tentative and subject to revision. The status of each class of data presented is outlined below:

(1) Profile Data

Crater and ejecta-uplift data as presented are final; however, it is anticipated that additional data will be acquired, analysis of which may slightly extend the range of values reported.

(2) Missile and Secondary Crater Data

These data are subject to the limitations discussed previously. It is intended to establish a grid of sampling stations in the field, data from which will be used to verify and calibrate the photo data. A new and more thorough missile count is scheduled, using either new photographs or enlargements of present photographs. While absolute data values are expected to be refined, the relationships and trends presented here are expected to remain essentially unchanged.

(3) Velocity Data

Movies of the Schooner event are currently being analyzed; data presented in this report are preliminary.

(4) Time History Data

Data acquisition is complete for 360 degrees; data presented here is limited to only eight 10-degree sectors.



.8 sec



1.9 sec



2.6 sec



4.0 sec



6.0 sec



13.0 sec

Fig. 21—SCHOONER Time Sequence

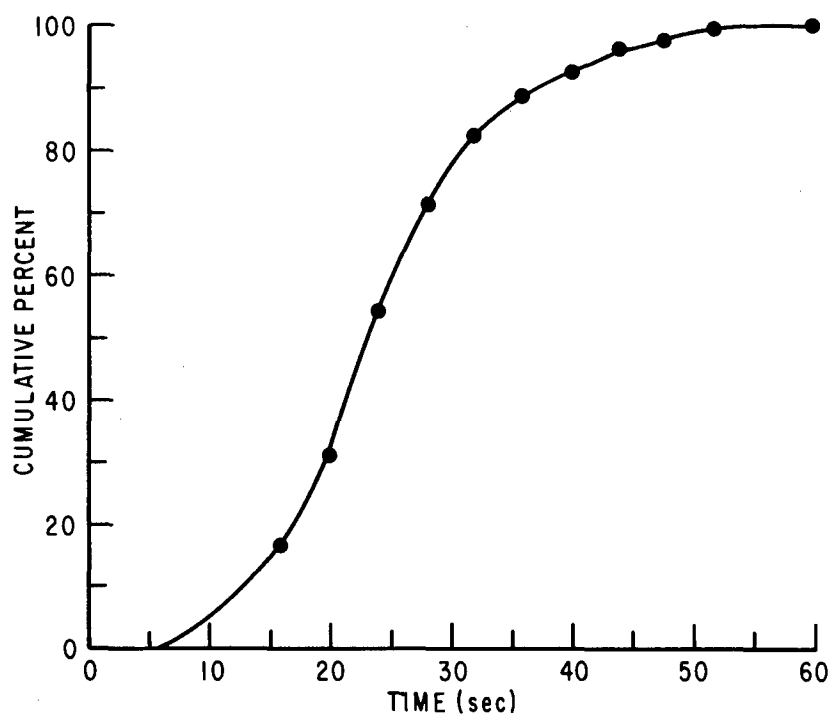


Fig. 22—Cumulative Time History Plot for Impacting Missiles

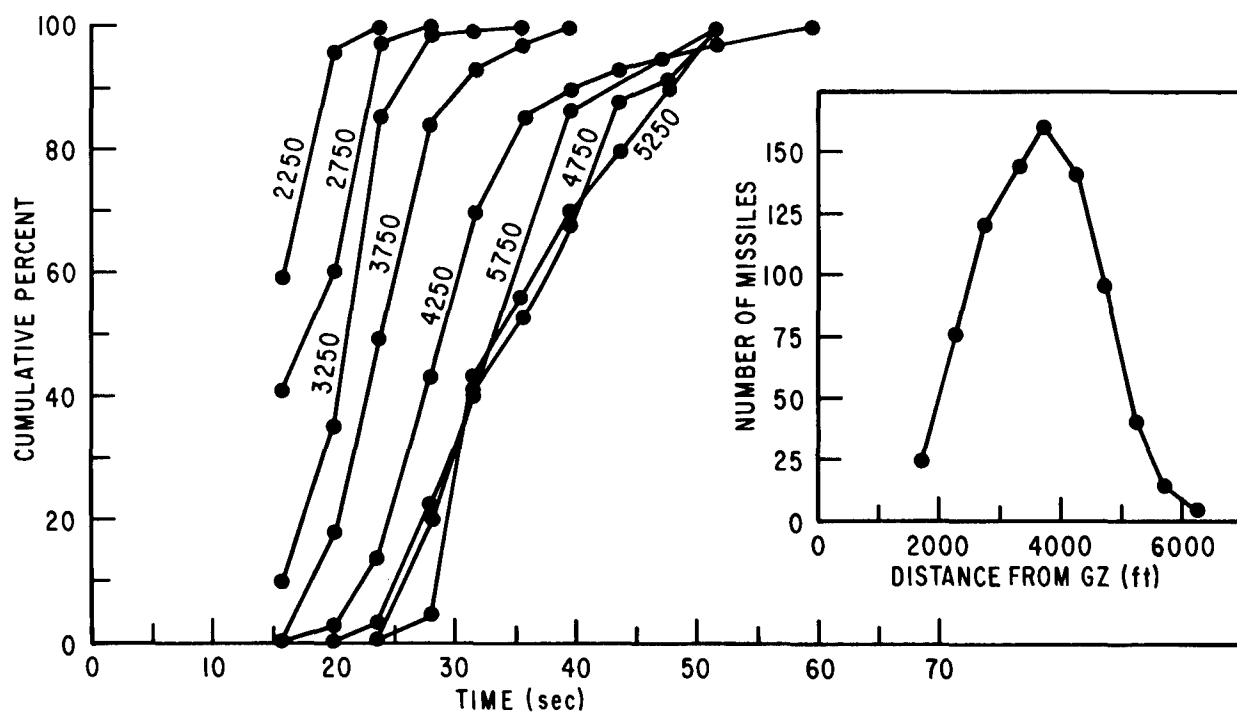


Fig. 23—Cumulative Time History Plots for Impacting Missiles at Discrete Distances from GZ

In addition to the work presented in this paper, other studies of the Schooner ejecta and missile population are either currently underway or scheduled for the near future. Projects include size analysis of the ejecta collected from preplaced trays and tarps, collection and analysis of preplaced color-coded grout columns, comminution studies of ejected rock, material property evaluation of pre- and post-shot rock, and analysis of secondary craters.

References

1. Lessler, R. M., "Schooner Pre-shot Analysis (U)," UCRL-50530, Lawrence Radiation Laboratory, Livermore, California, November, 1968, (S-RD).
2. Tewes, H., "Results of Schooner Excavation Experiment," Symposium on Engineering with Nuclear Explosives, January, 1970.
3. Henny, R. W., "Schooner Observations and Early Results - Interim Report," AFWL-TR-69-133, September, 1969.
4. Purtymun, W. D., Harrill, J., and Rush, F. E., "Geologic Data for U20u Satellite Holes #1, #2, #3, #4, and Studies of the Orientation of Joints in the Thirsty Canyon Tuff, Area 20, Pahute Mesa, Nevada Test Site," U.S. Geol. Survey, Open-File Report, 1969.

CLOSING REMARKS* BY DOCTOR GLENN C. WERTH
ASSOCIATE DIRECTOR FOR PLOWSHARE
LAWRENCE RADIATION LABORATORY
AT THE
AMERICAN NUCLEAR SOCIETY-ATOMIC ENERGY COMMISSION
SPONSORED SYMPOSIUM
ON
"ENGINEERING WITH NUCLEAR EXPLOSIVES"
DUNES HOTEL
LAS VEGAS, NEVADA
JANUARY 16, 1970

All 112 papers have been presented, and the 17 technical sessions are over. If single sessions had been scheduled instead of parallel sessions, we would have been here for two weeks. The Organizing Committee is to be congratulated for a job well done. But in all due respect, it really hasn't been the ideal technical meeting I'd like to go to someday. That would be the meeting where you could somehow absorb all the papers that were presented, yet you could also spend all your time out in the corridor talking with the individual scientists and finding out what the real problems are.

Obviously I didn't hear all of the papers, so I make no claims that the following technical highlights are the optimum set. I have divided my comments into three parts: the highlights of the data from nuclear events, highlights from the broader research papers, and a discussion of some of the application papers.

PART I: NUCLEAR EVENT DATA

The final set of Gasbuggy papers has been presented. The formation was thoroughly fractured beyond the chimney, and gas production is up. But, on

*Work performed under the auspices of the U.S. Atomic Energy Commission

careful examination, we find that the production should have been up even more if these fractures had really played the role that was anticipated. Why wasn't it? Was it because Gasbuggy was in a predominantly fracture-controlled reservoir and we failed to tap into a new fracture system? Or was it because the fractures have partially healed? We don't know the answer, but it does point up that in Plowshare, as in any new scientific area, while the first pioneering experiment answers a great many questions, new problems are opened up as well.

We are anticipating with considerable technical excitement the production tests on Rulison. A better explosive was used in regard to its diameter, handling in the field, and a simpler firing system. Rulison will clearly take its place among the significant events of the Plowshare Program.

We have heard the final summary report of the 31-kt Schooner cratering event. It is unfortunate that there isn't time on the Nevada Test Site tour to see this crater, for it is an impressive sight. A most remarkable explosive with very special minimum radioactive characteristics was used. Some day we hope to be able to give complete information on radioactivity from cratering events. Should this happen, I think you will be duly impressed.

Perhaps not many of you attended the Scientific Applications section in which the Hutch experiment was described. A very specially designed nuclear explosive was used to produce a concentrated neutron flux that impinged on a target with the objective of making heavy isotopes. The neutron flux achieved was 35 moles/cm². No fermium-259 or heavier isotopes were made, and the reason remains a mystery. It could possibly be that the half-lives are too short or too long to be observed in the recovery and data analysis. On the other hand, there may be some very fundamental physics that nature is trying to tell us about that we are not quite sharp enough to understand. Our physicists and chemists are anxious to repeat the experiment with larger recovery operations so that targets can be made for use in accelerators and Van de Graaff machines. Fundamental physics experiments could be done to learn more about heavy elements and perhaps make new isotopes of element 104. Another interesting result of that session on Scientific Applications was the report on the use of nuclear explosives to produce spin-polarized neutrons.

We are very pleased that the French scientists were able to be here to present data on their nuclear events. This French data is technically exciting. Being based on thirteen events in granite, it is far more complete than the U.S. data, which is based on three events. A very careful job has been done in preshot geologic work, postshot drilling, mineralization studies, chemistry studies, and so on, and it is very refreshing to see something besides the Hardhat chimney used in application concepts. A most significant apparent contradiction is the fact that the cavity radii from the Sahara events are only about half as long as those of the Nevada test events. We don't know the answer to this problem, but perhaps we have some clues. It may have to do with the Hoggar Massif being very dry, very hard, and unfractured. The differences between the nuclear effects are quite substantial, and it's going to take considerably more interaction between scientists of the two countries to unravel this technical problem.

We have heard data presented on two Soviet experiments, and we are sorry that the Soviet scientists couldn't be here to present their own data -- I refer, of course, to the 1.1-kt contained event in salt that produced the

elliptical cavity, and the 1-kt cratering experiment in sandstone. The data and analysis of the radioactivity from the cratering event are quite extensive; they are very well done technically. While discussing this with the radiochemists at LRL, I was told, "You won't even let us propose such extensive work, let alone actually get them funded and carried out."

Now we have three of the five nuclear countries presenting data relevant to the question of peaceful uses of nuclear explosives. I think this is a most significant result of this particular technical meeting.

PART II: BROADER RESEARCH PAPERS

There were quite a few broader research papers on the question of a theoretical understanding of the outgoing shock wave, cavity growth, and fracturing. We heard papers on the finite difference method of making calculations and were pleased that the United Kingdom has mounted an effort. One of the symposium papers will have the listing of the LRL one-dimensional program. Let me caution you that it takes a great deal of effort, both in the field and in the laboratory, to measure the rock properties to obtain a proper description of the material to make these calculations useful. When Plowshare moves into new situations, such theoretical calculations with their accompanying equation-of-state and logging data can help us avoid multi-million dollar mistakes. Therefore, the effort is clearly going to pay for itself many times over in a very practical sense. Now, that's not to say that there isn't room for the analytical approach. That is the simpler approach of interpreting data and scaling. That's the first approach of project design, and if we are operating within the realm of past experience, that's the way it should be done. It is gratifying to see a number of papers to improve those techniques and make them more generally available, more useful, and more accurate.

In the chemistry area, the French data on the analysis of the residual gases that they have observed (hydrogen, methane, etc.), and the fact that perhaps 50 percent of the tritium is trapped in the melt is new information and a significant contribution. To interpret this data, more work will be needed on the silicon hydroxides that are thought to play a dominant role in the cooling of the cavity gas.

Turning now to the seismic area, one of the biggest technical setbacks that the Plowshare Program has ever had was the firing of the Salmon Event, with the totally unexpected number of plaster crackings and other architectural-type complaints. It was "back to the drawing boards, the high explosive criteria for quarry blasting won't work." Over the years, through the contributions of many organizations, we have developed an understanding of the problem and now have methods to predict the damage and to assess the cost. The work that was done on Rulison in ground motion, building surveys, and analysis of damage has demonstrated these methods. On future projects, I think there will be less expense; the technical methods appear quite adequate. Both Gasbuggy and Rulison have taught us that with these high overburdens, at least in those kinds of rock, there is more energy, proportionately, in the higher frequency band. So those shots have taught us that, because of attenuation there are higher amplitudes close in and lower amplitudes farther out than were previously anticipated.

A session was devoted to engineering developments for the first time. Curves relating cost of explosives and cost of drilling were presented. Projections of costs as a function of diameter and depth are beginning to appear. Unfortunately, the costs are relative, but some day soon we hope that actual cost data can be presented. We have had some descriptions of radio fire links that can cut costs, as well as methods for emplacement, stemming, reentry, and shock mounting of equipment. All these areas are unclassified, and we hope that industry can make major contributions to them in the future. We would certainly encourage you to do so, to reduce costs and make these field operations more efficient.

PART III: APPLICATIONS

Many applications were discussed in the meeting. I have just sorted out in my own mind some of those that I would like to comment on, and by no means do I feel the list is complete. The granddaddy of all of the applications that have been studied, of course, is the interoceanic canal. Field data have come from Panama and Colombia. There were surprises -- the clay shales on Route 17 were unexpected, and the solution seems to be to excavate through the clay shale portion conventionally, at a higher cost. When the plans were laid to consider the feasibility of an interoceanic canal, it was presumed that as the field data came in, the nuclear technology data, including high yield explosions and rows of high yield explosions, would be available. Well, it didn't work out that way. What can be said at this point is that if our projections are correct about nuclear excavation, if the megaton craters are as calculated and presented at this symposium, if the enhancement is as hypothesized based on Buggy and Dugout experiments and on the various HE experiments, then it is indeed feasible to build the canal. However, there needs to be experimental verification of these concepts. The potential saving of over one billion dollars is still there, and I, for one, hope that we'll be able to prove those concepts before the final canal decision is made.

In the gas stimulation field, there is a great deal of momentum that you are all aware of. I'll not stand here and discuss the plans of various companies; it would be inappropriate. But, I think the progress that has been made in analyzing the Gasbuggy gas, its chemistry, and its radiochemistry, and the work on how that gas would be diluted in pipelines and distribution systems (not that this has been done or is planned) is a most interesting and significant development in the gas stimulation field.

An oil stimulation project was proposed in the soviet paper. We also heard a French paper on the subject. The U.S. papers on the subject -- well the silence is deafening. I suppose there are good economic reasons for that.

Regarding storage concepts, we evidently have reached the era of careful design and cost analysis and it indeed looks favorable. Again we find soviet projects proposed. We find extensive discussion in the United Kingdom paper, and I would hope that we will be moving forward very quickly in the storage area.

Progress in oil shale is, frankly, disappointing. Although we are, of course, pleased that the Bureau of Mines, 150-ton retort is on stream and giving data, we'll be looking forward to a complete report.

In the mining session, a number of very fine review papers were presented. The interesting new development is the leaching of deep sulfide copper ores. Leach rates of sulfide ores at normal pressure are very slow, but the concept put forward was to use a high pressure system where the oxygen is put into solution. It is projected that the leaching rate can be speeded up by a factor of 300. If this technique can be proven out economically, we may indeed have a new, unique approach to the recovery of copper ores.

In the area of waste disposal we have one interesting paper, but I was frankly a little surprised that we didn't have more. Of course, we at LRL have been looking at waste disposal over the years and had become a bit discouraged because no one, until recently, wanted to pay to clean up the environment. Times are changing, and I would hope some industrial company would perform a very thorough and very careful analysis of the waste disposal problem using a nuclear solution.

Lastly, I wish to mention geothermal heat. Plowshare could be opening up a new industry. It could be a very important industry in the control of smog and air pollutants, because geothermal heat requires no release of burned hydrocarbons to the atmosphere.

Now, a few concluding statements. Commissioner Thompson described the National Environment Policy Act, which became the law of the land January 1. This country is dedicated to a positive program for improving the quality of our air and water. These are right and proper goals and should be carefully analyzed and systematically approached, but I think we need a yardstick, a measure of pollution. Why not use the ratio of the pollutant to natural background? The pre-man level? By that yardstick, the nuclear energy industry has a very proud record indeed. Improving the quality of our air and water will be very costly, as Commissioner Thompson has said, but the way for that improvement is through technology. If we have the foresight to set aside emotional irrationalities, we can move forward using nuclear energy and nuclear explosions to improve our environment. The papers presented at this symposium have recognized the importance of the environment. If smog can be reduced, if mining dumps can be avoided, if waste can be disposed, and if nonfossil fuel energy can be tapped, indeed, Plowshare will have made a most important positive contribution to cleaning up the environment.

LIST OF ATTENDEES

Mr. G. W. Adair Reynolds Electrical & Engineering Co., Inc.	Mr. R. C. Ayres The Bendix Corporation, Kansas City Division	Mr. H. M. Boeker Bureau of Sports Fisheries & Wildlife
Mr. Robert Adamson Nucleonics Week	Mr. R. E. Bachman Holmes & Narver, Inc.	Mr. T. S. Bohn Lawrence Radiation Laboratory
Mr. C. R. Adelman, Jr. Lawrence Radiation Laboratory	Mr. K. F. Bailey EG&G, Inc.	Mr. H. G. Booth U. S. Department of Commerce, ESSA-ARL
Dr. T. J. Ahrens Lawrence Radiation Laboratory	Mr. F. E. Baker Federal Power Commission	Mr. Myran Borders United Press International
Mr. Rafi Al-Hussainy Mobil Research & Development Corporation	Mr. John Balagna Los Alamos Scientific Laboratory	Mr. C. R. Bowman El Paso Natural Gas Company
Dr. R. T. Allen Applied Nuclear	Mr. O. C. Baldonado Holmes & Narver, Inc.	Miss Antoinette Boyle United Mine Workers of America
Mr. R. E. Allen U. S. Atomic Energy Commission	Mr. L. B. Ballou Lawrence Radiation Laboratory	Mr. D. N. Brady Reynolds Electrical & Engineering Co., Inc.
Mr. Lee Allison University of California, Riverside	Dr. J. R. Banister Sandia Corporation	Mr. W. J. Brady Reynolds Electrical & Engineering Co., Inc.
Mr. V. D. Allred Marathon Oil Company	Mr. Stanley Bankert University of California, Davis	Mr. C. W. Brandt Agbabian-Jacobsen Associates
Mr. B. D. Anderson, II U. S. Army Engineering Nuclear Cratering Group	Mr. J. P. Baptist U. S. Fish & Wildlife Service	Mr. J. F. Brennan Westinghouse Electrical Corporation
Mr. D. C. Anderson IIT Research Institute	Mr. C. H. Barnes, Jr. The Dow Chemical Company	Mr. J. P. Brennan United Mine Workers of America
Mr. E. V. Anderson Johnson & Higgins	Mr. Harley Barnes U. S. Geological Survey	Mr. G. E. Brethauer U. S. Geological Survey
Mr. J. T. Anderson University of Nevada, Reno	Mr. James Barrows Las Vegas Sun	Mr. C. D. Broadbent Kennecott Copper Corporation
Mr. A. B. Andrews E. I. du Pont de Nemours & Co.	Mr. A. J. Barthoux French Commissariat a l'Energie Atomique	Mr. G. A. Broadman Lawrence Radiation Laboratory
Mr. R. T. Andrews Lawrence Radiation Laboratory	Mr. R. E. Batzel Lawrence Radiation Laboratory	Mr. Sylvain Brouard Geonuclear Nobel Paso
Mr. S. J. Andrews, Jr. Argonne National Laboratory	Mr. G. V. Beard Associated Western Universities	Mr. G. E. Brown, Jr. Consultant on Industrial Applications
Mr. G. O. Argall World Mining	Professor Tom Beasley University of Washington	Lt. Col. L. F. Brown U. S. Arms Control and Disarmament Agency
Mr. A. B. Arnett, Jr. U. S. Department of Commerce, ESSA-ARL	Mr. F. A. Belle Holmes & Narver, Inc.	Mr. L. T. Brown Union Oil Company, California
Mr. J. T. Arnett El Paso Natural Gas Company	Mr. D. L. Bernreuter Lawrence Radiation Laboratory	Professor W. S. Brown University of Utah
Mr. W. D. Arnold Oak Ridge National Laboratory	Mr. K. L. Berry Pan American Petroleum Corporation	Mr. C. D. Broyles Sandia Corporation
Mr. H. H. Aronson CER Geonuclear Corporation	Mr. F. W. Bingham Sandia Corporation	Mr. T. D. Brumleve Sandia Corporation
Mr. R. H. Ashlock Fenix & Scisson, Inc.	Mr. T. H. Blankenship U. S. Atomic Energy Commission	Mr. R. S. Brundage CER Geonuclear Corporation
Mr. Leon Atek University of Arizona	Mr. J. A. Blasy U. S. Atomic Energy Commission	Mr. F. A. Bryan Research Triangle Institute
Mr. K. O. Austin Rocky Mountain Natural Gas Co.	Mr. W. A. Bliss U. S. Public Health Service	Mr. David Buchla Lawrence Radiation Laboratory
Mr. R. D. Austin Bureau of Reclamation	Mr. Oliver U. J. Block Kansas State University	Mr. R. C. Bucknam U. S. Geological Survey
Mr. J. W. Ayres Reynolds Electrical & Engineering Co., Inc.	Dr. J. A. Blume John A. Blume & Associates	Mr. J. B. Burnham, Jr. Battelle-Northwest
	Mr. C. R. Boardman CER Geonuclear Corporation	

Mr. R. S. Burton Reynolds Electrical & Engineering Co., Inc.	Mr. P. J. Closmann Shell Development Company	Mr. M. E. Day Bureau of Reclamation
Mr. H. M. Byars H. M. Byars Construction Co.	Dr. D. F. Coates Department of Energy & Mines, Canada	Mr. S. S. Day University of California, Riverside
Mr. Humberto Calderon Ministry of Mines and Hydrocarbons, Venezuela	Mr. O. R. Coats CER Geonuclear Corporation	Mr. T. P. Day The Boeing Company
Mr. B. W. Calston U. S. Atomic Energy Commission	Dr. H. F. Coffey CER Geonuclear Corporation	Mr. W. C. Day U. S. Army Engineering Nuclear Cratering Group
Dr. I. G. Cameron United Kingdom Atomic Energy Authority	Mr. Pierre Cohen French Commissariat a l'Energie Atomique	Mr. E. P. Delany L. T. A. Limited
Mr. R. H. Campbell Los Alamos Scientific Laboratory	Dr. V. S. Colter The Gas Council	Mr. Francis Delort French Commissariat a l'Energie Atomique
Mr. B. J. Candela Hudson Institute	Mr. H. F. Cooper, Jr. Air Force Weapons Laboratory	Mr. F. C. Dennis Caterpillar Tractor Company
Mr. J. H. Carlson U. S. Atomic Energy Commission	Mr. M. J. Cortez University of Arizona	Mr. H. S. Derlich French Commissariat a l'Energie Atomique
Mr. R. H. Carlson The Boeing Company	Mr. G. A. Cowan Los Alamos Scientific Laboratory	Mr. K. D. DeVine U. S. Atomic Energy Commission
Mr. H. C. Carpenter U. S. Bureau of Mines	Mr. G. R. Cowan E. I. du Pont de Nemours & Co.	Mr. D. D. Dickey U. S. Geological Survey
Mr. A. J. Carrea Comision Nacional de Energia Atomica, Argentina	Mr. V. R. Cowart Geonuclear Nobel Paso	Mr. P. W. Dickson Westinghouse Astronuclear
Dr. Edward Catalano Lawrence Radiation Laboratory	Mr. J. L. Cramer Lawrence Radiation Laboratory	Mr. Alexander Dingee EG&G, Inc.
Mr. Ricardo Cesped Kaiser Engineering	Mr. T. V. Crawford Lawrence Radiation Laboratory	Major L. A. Dillon Texas A&M University
Mr. J. B. F. Champlin Westinghouse Astronuclear	Mr. P. V. Crooks Australian Atomic Energy Commission	Mr. G. U. Dinneen U. S. Bureau of Mines
Mr. Clair Chapin Lawrence Radiation Laboratory	Mr. D. J. Crouse Oak Ridge National Laboratory	Mr. B. C. Diven Los Alamos Scientific Laboratory
Mr. P. F. Chapski EG&G, Inc.	Mrs. B. K. Crowley Lawrence Radiation Laboratory	Mr. R. P. Dixon American Oil Shale Corporation
Professor J. A. Cheney University of California, Davis	Mr. D. P. Cullen CER Geonuclear Corporation	Mr. W. L. Dixon United States Air Force
Dr. J. T. Cherry Lawrence Radiation Laboratory	Mr. R. E. Cunningham U. S. Atomic Energy Commission	Mr. Max R. Dolenc ATCOR, Inc.
Mr. E. W. Chew El Paso Natural Gas Company	Mr. C. J. Dahn IIT Research Institute	Dr. Matteo Donato Commission of European Community
Dr. Frank Chilton Stanford Research Institute	Captain E. B. Danber U. S. Air Force Academy	Dr. B. J. Donham Los Alamos Scientific Laboratory
Mr. James Chimbidis Argonne National Laboratory	Mr. D. V. D'Andrea U. S. Bureau of Mines	Mr. C. T. Donnenworth Lockheed Missiles & Space Company
Mr. W. D. Churchill U. S. Army Corps of Engineers	Mr. Walter Danilchik U. S. Geological Survey	Dr. H. J. Donnert Kansas State University
Major L. J. Circeo Defense Atomic Support Agency	Mr. Denys D'Anselme Geonuclear Nobel Paso	Mr. Jaime Donoso Chilean Development Corporation
Mr. R. D. Clarke Birdwell Division of S. S. C.	Mr. Harold Davis Engineering & Mining Journal	Mr. L. P. Donovan CER Geonuclear Corporation
Mr. R. B. Clay IRECO Chemicals	Professor R. R. Davison Texas A&M University	Mr. P. M. Dougan Equity Oil Company
Dr. G. W. Clevon Federal Highway Administration	Mr. J. K. Davy U. S. Atomic Energy Commission	Lt. Gen. J. H. Doolittle Plowshare Advisory Committee

Dr. Todd Doscher Shell Oil Company	Dr. A. G. Everett U. S. Department of the Interior	Mr. Andre Gauvenet French Commissariat a l'Energie Atomique
Mr. E. B. Douglas American Metals Climax, Inc	Mr. G. C. Facer U. S. Atomic Energy Commission	Mr. H. B. Gayle Holmes & Narver, Inc.
Mrs. G. S. Douglas U. S. Public Health Service	Mr. J. R. Faure French Commissariat a l'Energie Atomique	Mr. J. R. Gayle Stanford Research Institute
Mr. R. L. Douglas U. S. Public Health Service	Mr. G. F. Ferber U. S. Department of Commerce, ESSA	Mr. E. L. Geiger Eberline Instrument Corporation
Dr. E. M. Douthett U. S. Atomic Energy Commission	Mr. H. A. Ferrieux French Commissariat a l'Energie Atomique	Mr. C. R. Gerber U. S. Atomic Energy Commission
Mr. C. E. Downs Teledyne-Isotopes	Mr. P. V. Fillo U. S. Bureau of Mines	Mr. L. S. Germain Lawrence Radiation Laboratory
Mr. F. M. Drake Holmes & Narver, Inc.	Mr. S. J. Fisher Mountain Fuel Supply Company	Mr. David Gerry University of California, Riverside
Mr. J. L. Drake U. S. Army Eng. Waterways Experiment Station	Mr. W. G. Flangas Reynolds Electrical & Engineering Co., Inc.	Mr. George Getze Los Angeles Times
Ing. Hans-L. H. Dreissigacker Federal Ministry of Science, Germany	Mr. M. G. Fletcher U. S. Department of Defense	Mr. Harry Gevertz El Paso Natural Gas Company
Mr. F. E. Driggers E. I. du Pont de Nemours & Co.	Mr. D. E. Fogelson U. S. Bureau of Mines	Mr. G. H. Gibson The Gas Council
Mr. R. E. Duff Applied Nuclear	Mr. R. M. Forrest Columbia Gas System Service	Mr. T. A. Gibson, Jr. Lawrence Radiation Laboratory
Mr. J. E. Duncan Lawrence Radiation Laboratory	Professor R. R. Fox George Washington University	Mr. R. H. Gifford Southern Interstate Nuclear Board
Mr. H. F. Dunlap Atlantic Richfield Company	Mr. A. D. Frandsen U. S. Army Engineering Nuclear Cratering Group	Mr. E. R. Giusti Lawrence Radiation Laboratory
Mr. L. M. Dunn U. S. Public Health Service	Miss Karen Frandsen Reynolds Electrical & Engineering Co., Inc.	Mr. Mateo L. P. Go University of Hawaii
Mr. J. J. Durek Kaiser Exploration & Mining Co.	Colonel J. F. Fraser U. S. Army Combat Developments Command-INS	Mr. C. S. Godfrey Physics International Company
Mr. O. J. DuTemple American Nuclear Society	Mr. G. A. Frazier California Institute of Technology	Mr. H. J. Gomberg Puerto Rico Nuclear Center
Mr. S. F. Eccles Lawrence Radiation Laboratory	Mr. H. R. Fredrickson Colorado Interstate Gas Company	Captain A. H. Graubart Wasag-Chemie A.G.
Mr. T. O. Edwards EG&G, Inc.	Mr. A. E. Fritzsche EG&G, Inc.	Mr. W. C. Grayson, Jr. Lawrence Radiation Laboratory
Dr. D. M. Ellett Sandia Corporation	Mr. J. J. Fuquay Battelle-Northwest	Mr. R. F. Griffin Bechtel Corporation
Mr. H. H. Elliott Institute of Gas Technology	Mr. J. W. Gabelman U. S. Atomic Energy Commission	Mr. G. B. Griswold New Mexico Institute of Mining & Technology
Mr. P. A. Ellis Kaman Nuclear	Mr. G. D. Gallup A. I. M. E.	Dr. Ernest Grosch Dynamit-Nobel
Mr. D. O. Emerson Lawrence Radiation Laboratory	Mr. Luis Galvez University of Mexico	Mr. B. C. Groseclose Lawrence Radiation Laboratory
Mr. D. E. Engstrom Reynolds Electrical & Engineering Co., Inc.	Mr. P. L. Gant Continental Oil Company	Mr. Edward Gross Science News Magazine
Mr. E. H. Essington Teledyne-Isotopes	Mr. L. M. Gard U. S. Geological Survey	Mr. Frank Grossman U. S. Public Health Service
Mr. Bryant Evans The San Diego Union	Dr. Heinrich Gattineau Wasag-Chemie A. G.	Colonel Benjamin Grote Defense Atomic Support Agency
Mr. R. B. Evans U. S. Public Health Service		Brigadier General R. H. Groves U. S. Army Corps of Engineers

Mr. P. H. Gudiksen
Lawrence Radiation Laboratory

Mr. C. W. Gulick
Sandia Corporation

Mr. R. R. Gunny
Holmes & Narver, Inc.

Mr. K. W. Gustafson
Eberline Instrument Corporation

Mr. W. H. Guthrie
Reynolds Electrical &
Engineering Co., Inc.

Mr. L. G. Guymon
Lawrence Radiation Laboratory

Lt. Col. Zach Hagedorn
U. S. Atomic Energy Commission

Mr. W. W. Kakala
Environmental Research Corp.

Mr. E. C. Hale
Mineral Properties

Mr. L. A. Hale
Mountain Fuel Supply Company

Mr. Richard Hamburger
U. S. Atomic Energy Commission

Mr. J. H. Hancock
Holmes & Narver, Inc.

Mr. J. E. Hardaway
Federal Water Pollution Control
Administration

Mr. Victor Hardy C.
Solum Sociedad Anonima

Professor G. C. Hart
University of California,
Los Angeles

Mr. H. L. Hartman
Sacramento State College

Mr. J. M. Hassoldt
Public Service Company of
Colorado

Mr. Ronald Hauber
U. S. Atomic Energy Commission

Dr. H. C. Heard
Lawrence Radiation Laboratory

Mr. R. A. Heckman
Lawrence Radiation Laboratory

Mr. Warren Heckrotte
Lawrence Radiation Laboratory

Mr. Milton Heinberg
Lawrence Radiation Laboratory

Mr. L. F. Heising
U. S. Bureau of Mines

Professor Edward Held
University of Washington

Mr. E. J. Hennelly
E. I. du Pont de Nemours & Co.

Mr. R. W. Henny
Air Force Weapons Laboratory

Mr. Michael Herry
French Embassy

Mr. Clark Hickman
Orange County Health Department

Dr. G. H. Higgins
Lawrence Radiation Laboratory

Mr. Norman Hilberry
University of Arizona

Mr. E. E. Hill
Lawrence Radiation Laboratory

Mr. J. H. Hill
Lawrence Radiation Laboratory

Dr. L. R. Hill
Sandia Corporation

Mr. O. F. Hill
Atlantic Richfield Hanford Company

Mr. R. E. Hill
Geonuclear Nobel Paso

Mr. Vern Hillyard
Christensen Diamond Production Co.

Mr. L. D. Hobbs
Department of Water Affairs

Mr. R. W. Hoff
Lawrence Radiation Laboratory

Mr. Marvin Hoffman
Los Alamos Scientific Laboratory

Mr. Gale Holladay
Lawrence Radiation Laboratory

Mr. W. L. Holley
Sandia Corporation

Mr. William Holt
Marsh & McLennan, Incorporated

Mr. Alfred Holzer
Lawrence Radiation Laboratory

Mr. Robert Hooper
Las Vegas News Bureau

Mr. D. L. Hoover
U. S. Geological Survey

Mr. R. B. Hopler
Hercules Incorporated

Mr. T. R. Horton
U. S. Public Health Service

Mr. F. N. Houser
U. S. Geological Survey

Mr. W. A. Hoyer
ESSO Production Research Company

Mr. E. W. Hribar
Aerojet General Corporation

Mr. N. M. Hulings, Jr.
Oklahoma Natural Gas Company

Mr. A. I. Ingham
Consolidated Natural Gas Company

Mr. Harry Isakari
Kaiser Engineers

Mr. Santo Italia
The Aerospace Corporation

Mr. E. P. Ix, Jr.
Lehman Brothers

Mr. D. G. Jackson
U. S. Atomic Energy Commission

Mr. E. C. Jackson
Lawrence Radiation Laboratory

Mr. C. M. Jaco, Jr.
DRAVO Corporation

Mr. D. G. Jacobs
Oak Ridge National Laboratory

Mr. Robert Jacobs
U. S. Public Health Service

Mr. E. E. Jaramillo
EG&G, Inc.

Mr. G. W. Johnson
Gulf General Atomic

Mr. W. C. Johnson
University of Chicago

Mr. G. D. Jones
The Boeing Company

Mr. M. O. Jones
Sandia Corporation

Mr. S. C. Jones
XANCO a Division of Kelco Company

Antionette Joseph
U. S. Atomic Energy Commission

Mr. W. J. Karwoski
The Boeing Company

Mrs. G. Y. Kauffman
Nevada Open Spaces Council
News Bulletin

Dr. S. Kaufman
Shell Development Company

Mr. B. L. Kelchner
The Dow Chemical Company

Mrs. I. D. Keller
U. S. Atomic Energy Commission

Dr. Keaton Keller
Consulting Physicist

Mr. G. A. Keyworth
Los Alamos Scientific Laboratory

Mr. J. E. King
Self Employed

Mr. J. F. Kmetz
United Mine Workers of America

Mr. G. W. Knobloch
Los Alamos Scientific Laboratory

Dr. J. B. Knox
Lawrence Radiation Laboratory

Dr. C. F. Knutson
CER Geonuclear Corporation

Dr. E. Kober
Wasag-Chemie A. G.

Mr. J. J. Koranda Lawrence Radiation Laboratory	Mr. R. F. Lemon El Paso Natural Gas Company	Mr. M. G. McKinnon Pan American World Airways, Inc.
Mr. J. A. Korver Lawrence Radiation Laboratory	Mr. Richard Lessler Lawrence Radiation Laboratory	Mr. R. R. McLellan U. S. Bureau of Mines
Mr. F. J. Kouba Bureau of Reclamation	Mr. A. E. Lewis Lawrence Radiation Laboratory	Mr. D. A. McNaughton Consultant
Mr. Walt Kozlowski Nevada Environmental Foundation	Mr. W. F. Lindsay EG&G, Inc.	Mr. T. C. Mehas Reynolds Electrical & Engineering Co., Inc.
Mr. Otto Krause Lawrence Radiation Laboratory	Mr. L. J. Little Lawrence Radiation Laboratory	Mr. Tsvi Meidav University of California, Riverside
Mr. O. H. Krikorian Lawrence Radiation Laboratory	Mr. J. R. Loftfield Holmes & Narver, Inc.	Mr. T. F. Meinhold Nuclear News
Mr. D. B. Krinsley U. S. Geological Survey	Dr. D. B. Lombard Lawrence Radiation Laboratory	Mr. R. G. Menzel U. S. Department of Agriculture
Mr. R. F. Krueger Union Oil Company	Mr. T. H. W. Loomis Bureau of Land Management	Mr. R. W. Merrian The Boeing Company
Professor Paul Kruger Stanford University	Mr. Raul Lopez Solum Sociedad Anonima	Mr. J. H. Meyer International Atomic Energy Agency
Mr. M. Kutyn Canadian Industries Limited	Mr. P. C. Loux Environmental Research Corp.	Mr. L. R. Michaud French Commissariat a l'Energie Atomique
Mr. T. B. Lacaff Western Oil Shale Company	Mr. G. R. Luetkehans CER Geonuclear Corporation	Mr. A. B. Miller Lawrence Radiation Laboratory
Mr. R. L. LaFrenz U. S. Army Engineering Nuclear Cratering Group	Mr. A. W. Lundberg Lawrence Radiation Laboratory	Mr. E. L. Miller Ed Miller & Sons, Inc.
Mr. J. A. Lahoud Environmental Research Corp.	Mr. C. M. MacDonald Holmes & Narver, Inc.	Mr. R. E. Miller U. S. Atomic Energy Commission
Mr. H. A. Lamonds EG&G, Inc.	Mr. C. R. MacFadyen Converse, Davis and Associates	Mr. R. L. Miller Ken O'Brien & Associates
Dr. Phil LaMori Battelle Memorial Institute	Dr. J. S. Malik Los Alamos Scientific Laboratory	Mr. R. L. Miller Ed Miller & Sons, Inc.
Mr. C. A. Lane Halliburton Services	Mr. R. L. Mann CER Geonuclear Corporation	Mr. F. A. Minton U. S. Atomic Energy Commission
Dr. Michael Langer Bundesanstalt fur Bodenforschung	Mr. R. E. Marks Lawrence Radiation Laboratory	Mr. E. L. Moffatt CER Geonuclear Corporation
Mr. Gaetano Lanzano Comitato Nazionale per l'Energia Nucleare	Mr. D. A. Marostica Pacific Lighting Service Company	Mr. D. T. Moore Colorado Interstate Gas Company
Mr. J. A. Larned U. S. Atomic Energy Commission	Mr. R. L. Marovelli U. S. Bureau of Mines	Mr. F. J. Morales, Jr. Framorco, S. A.
Mr. K. H. Larson Battelle-Northwest	Mr. C. L. Marshall U. S. Atomic Energy Commission	Mr. G. B. Morgan National Air Pollution Control-ADM
Mr. H. A. Larson Reynolds Electrical & Engineering Co., Inc.	Mr. J. R. Martin Lawrence Radiation Laboratory	Mr. M. Morgan Stanford Research Institute
Mr. David Layton Natural Gas Pipeline Company	Mr. W. B. Mathis Westinghouse Electric Corporation	Colonel MacPherson Morgan Stanford Research Institute
Mr. E. J. Leahy U. S. Army Engineering Nuclear Cratering Group	Dr. J. R. Maxfield, Jr. Maxfield Radiological Center	Mr. P. J. Morris URS Research Company
Mr. L. A. Lee John A. Blume & Associates	Mr. Neil Mazurek Review-Journal	Mr. R. H. Morris U. S. Geological Survey
Mr. Mike Lekas Geckinetics, Incorporated	Mr. C. E. McColley U. S. Atomic Energy Commission	Mr. J. M. Morrison AECOP-Du Pont
Mr. P. N. Lem U. S. Public Health Service	Mr. James McKewon, Jr. U. S. Atomic Energy Commission	Mr. Georges Mouglin Sodeteg Incorporated
	Mr. W. B. McKinnis Lawrence Radiation Laboratory	

Mr. P. H. Moulthrop Lawrence Radiation Laboratory	Mr. J. Y. Paulding Consultant	Mr. R. J. Prestwood Los Alamos Scientific Laboratory
Mr. R. A. Mueller Environmental Research Corp.	Mr. Fernando Paz-Castillo Stanford University	Mr. C. L. Pringle ATCOR, Inc.
Mr. Pablo Mulas Instituto Politecnico Nacional	Mr. C. R. Penwell Reynolds Electrical & Engineering Co., Inc.	Mr. R. F. Pritchett Reynolds Electrical & Engineering Co., Inc.
Mr. J. W. Mullins U. S. Public Health Service	Mr. F. R. Perchalski Environmental Research Corp.	Mr. Dick Prouty The Denver Post
Mr. R. J. Mulvihill Holmes & Narver, Inc.	Mr. M. C. Perkins Skelly Oil Company	Commander E. A. Quarterman (Ret.) U. S. Naval Reserve
Dr. W. J. Murri Stanford Research Institute	Mr. E. N. Perry Lockheed Missiles & Space Company	Mr. S. Quiros-Guardia Government of Panama
Mr. D. S. Myers Lawrence Radiation Laboratory	Mr. K. R. Peterson Lawrence Radiation Laboratory	Mr. D. D. Rabb Lawrence Radiation Laboratory
Mr. M. W. Nathans Trapelo-Division of LFE Corp.	Mr. R. J. Peterson Richard Peterson & Son	Mr. W. F. Ragsdale Lawrence Radiation Laboratory
Mr. Richard Navarro U. S. Coast & Geodetic Survey	Captain B. R. Petrie, Jr. U. S. Navy	Mr. L. D. Ramspott Lawrence Radiation Laboratory
Mr. J. J. Neuer Lockheed Missiles & Space Company	Mr. M. J. Pettid General Adjustment Bureau, Inc.	Mr. C. S. Randall Oak Ridge Associated Universities
Mr. R. W. Newlin U. S. Atomic Energy Commission	Mr. F. M. Pfeffer U. S. Department of the Interior	Dr. P. L. Randolph El Paso Natural Gas Company
Mr. K. E. Niermeyer The Anaconda Company	Mr. J. F. Philip U. S. Atomic Energy Commission	Mr. J. A. Raulston U. S. Air Force
Mr. W. J. Niles Applied Theory, Inc.	Mr. J. P. Phillippe Panhandle Eastern Pipe Line Company	Mr. D. E. Rawson Gulf General Atomic
Mr. M. D. Nordyke Lawrence Radiation Laboratory	Mr. J. M. Picq French Commissariat a l'Energie Atomique	Mr. W. A. Reardon Battelle-Northwest
Mr. C. H. Noren E. I. du Pont de Nemours & Co.	Mr. E. J. Pierczynski Los Alamos Scientific Laboratory	Mr. B. B. Redpath U. S. Army Engineering Nuclear Cratering Group
Major L. R. Nunn U. S. Air Force Academy	Mr. A. M. Piper U. S. Geological Survey	Mr. J. W. Reed Sandia Corporation
Mr. B. J. O'Keefe EG&G, Inc.	Mr. John Pirro ATCOR, Inc.	Mr. L. D. Reed University of California, Riverside
Mr. B. P. O'Neill United States Steel Corporation	Dr. Hal Plank Bechtel Corporation	Dr. J. E. Regnier U. S. Public Health Service
Mr. P. O. Orkild U. S. Geological Survey	Mr. Paul Poinssot Geonuclear Nobel Paso	Mr. Roy Reider Los Alamos Scientific Laboratory
Mr. Ernest J. Orozco Seismograph Service Corporation of Mexico	Mr. L. O. Pope Sperry-Sun Well Survey Company	Mr. V. M. Reinecke Anglo American
Mr. D. L. Orphal Environmental Research Corp.	Mr. L. D. Porter Lawrence Radiation Laboratory	Mr. H. B. Renfro H. B. Renfro & Company
Mr. Harry Otway Los Alamos Scientific Laboratory	Mr. M. A. Porter E. I. du Pont de Nemours & Co.	Mr. J. V. Retief Stanford University
Dr. Kenneth Parker Atomic Weapons Research Establishment	Professor R. G. Post University of Arizona	Mr. G. H. Reynolds Goodyear Atomic Corporation
Mr. F. J. Parsons Pacific Gas & Electric Company	Miss L. L. Poulsen U. S. Air Force	Mr. M. A. Rex Fenix & Scisson, Inc.
Mr. T. O. Passell Physics International Company	Mr. D. V. Power El Paso Natural Gas Company	Mr. Miles Reynolds, Jr. Austral Oil Company Incorporated
Mr. R. M. Patterson The Dow Chemical Company	Mr. Howard Pratt Terra Tek, Inc.	Mr. D. L. Rigotti U. S. Army Ballistics Research Laboratory

Mr. J. S. Rinehart ESSA Research Laboratories	Mr. J. B. Savy Stanford University	Mr. J. L. Smith Converse, Davis and Associates
Mr. Anthony Ripley New York Times	Dr. H. C. Saxe University of Louisville, Speed School	Mr. R. M. Smith EG&G, Inc.
Mr. G. C. Rizer Lawrence Radiation Laboratory	Mr. R. D. Scarrow Scarrow & Walker, Inc.	Mr. Sam Smith El Paso Natural Gas Company
Mr. C. H. Roach U. S. Bureau of Mines	Mr. Joseph Schneider Lawrence Radiation Laboratory	Mr. J. E. Sohngen Atomic Industrial Forum, Inc.
Mr. L. M. Roberts U. S. Air Force	Mr. Robert Schneider U. S. Geological Survey	Mr. H. W. Sohns U. S. Bureau of Mines
Mr. T. C. Roberts Terradynamics, Inc.	Dr. R. N. Schock Lawrence Radiation Laboratory	Mr. E. L. Sorom Reynolds Electrical & Engineering Co., Inc.
Dr. C. P. Robinson Los Alamos Scientific Laboratory	Mr. D. F. Schutz Teledyne-Isotopes, Inc.	Mr. Gilles Soviche ELF-ERAP
Dr. Morris Rockstein University of Miami, School of Medicine	Mr. K. R. Schwenn Lockheed Missiles & Space Company	Mr. Karl Spalvins Air Force Weapons Laboratory
Mr. H. C. Rodean Lawrence Radiation Laboratory	Mr. Frederic Scofield University of Arizona	Mr. U. M. Staebler U. S. Atomic Energy Commission
Dr. D. J. Roddy U. S. Geological Survey	Mr. Jimm Seaney KWSR Radio	Mr. D. B. Starkey Sandia Corporation
Mr. A. J. Rodriguez-Diaz Instituto Nacional de Canalizaciones	Mr. R. A. Selby Battelle-Northwest	Dr. F. W. Stead U. S. Geological Survey
Mr. L. A. Rogers El Paso Natural Gas Company	Mr. A. H. Seymour University of Washington	Mr. C. R. Steadman U. S. Department of Commerce ESSA-ARL
Mr. J. W. Rold U. S. Geological Survey	Mr. Harlan Shaw Trapelo/West	Mr. R. H. Steed Marathon Oil Company
Professor R. R. Rollins University of Missouri	Mr. H. E. Shaw AECOP	Mr. J. F. Steelman Department of the Army
Mr. J. B. Rosenbaum U. S. Bureau of Mines	Mr. Philip Sherlock Harza Engineering Company	Mr. Jerry Steltenpohl TRW Systems Group
Mr. C. E. Rosenberry Reynolds Electrical & Engineering Co., Inc.	Mr. W. C. Sherman Waterways Experiment Station	Mr. D. R. Stephens Lawrence Radiation Laboratory
Mr. R. P. Rossman Lawrence Radiation Laboratory	Mr. R. A. Siddons Atomic Weapons Research Establishment	Mr. T. S. Sterrett U. S. Atomic Energy Commission
Mr. G. K. Roth General Research Consultants	Mr. Wyatt Silker Battelle-Northwest	Mr. N. B. Steuer PARCO, Inc.
Mr. Leonard Rudlin U. S. Naval Ordnance Laboratory	Mr. W. E. Siri University of California, Berkeley	Mr. C. D. Stewart U. S. Atomic Energy Commission
Mr. P. L. Russell U. S. Bureau of Mines	Professor R. L. Skaggs University of Nevada, Las Vegas	Mr. D. H. Stewart Battelle-Northwest
Dr. C. L. Sandler Battelle Seattle Research Center	Mr. J. T. Skeith Oklahoma Natural Gas Company	Major K. V. Stewart Atomic Weapons Research Establishment
Colonel R. R. Sandoval U. S. Army Combat Developments Command-INS	Mr. R. E. Skjei John A. Blume & Associates	Mr. R. M. Stewart The Anaconda Company
Professor L. W. Saperstein Pennsylvania State University	Major D. J. Slezak U. S. Atomic Energy Commission	Mr. Daniel Stiles Bureau of Sports, Fisheries & Wildlife
Mr. L. A. Sarkes American Gas Association, Inc.	Mr. A. E. Smith Atlantic Richfield Hanford Company	Mr. R. P. Stock Lawrence Radiation Laboratory
Mr. F. M. Sauer Physics International Company	Mr. B. A. Smith Reynolds Electrical & Engineering Co., Inc.	Mr. G. W. Stockton Associated Press
Mr. L. E. Savory Pennzoil United, Inc.	Mr. C. F. Smith, Jr. Lawrence Radiation Laboratory	Mr. R. E. Stone Lawrence Radiation Laboratory
	Mr. D. S. Smith U. S. Atomic Energy Commission	
	Mr. F. L. Smith Consulting Engineer	

Mr. E. J. Story EG&G, Inc.	Mr. R. L. Tremain, Jr. Pan American World Airways, Inc.	Mr. J. W. Watkins U. S. Bureau of Mines
Mr. George Stosur Gulf Research & Development Co.	Mr. J. C. Trippe Attorney	Mr. Mason Watson Aerospace Corporation
Mr. J. N. Strange Waterways Experiment Station	Mr. R. T. Trolan Eberline Instrument Corporation	Mr. W. D. Weart Sandia Corporation
Mr. T. F. Stubbs Lawrence Radiation Laboratory	Mr. G. E. Tucker, Jr. Sandia Corporation	Mr. J. E. Weir, Jr. U. S. Geological Survey
Mr. W. M. Sturdevant Birdwell Division of S.S.C.	Professor P. T. Tueller University of Nevada, Reno	Mr. H. C. Wells University of Nevada, Las Vegas
Mr. C. L. Sturtz Reynolds Electrical & Engineering Co., Inc.	Mr. P. M. Turkheimer Wyle Laboratories	Mr. I. J. Wells Reynolds Electrical & Engineering Co., Inc.
Mr. J. D. Sudbury Continental Oil Company	Mr. W. S. Twenhofel U. S. Geological Survey	Dr. G. C. Werth Lawrence Radiation Laboratory
Mr. R. J. Sullivan Caterpillar Tractor Company	Mr. R. E. Uhrig University of Florida	Mr. A. W. Western Reynolds Electrical & Engineering Co., Inc.
Mr. G. E. Summers Fenix & Scisson, Inc.	Lt. G. W. Ullrich U. S. Air Force-SAMSO	Dr. J. A. Wethington, Jr. University of Florida
Mr. H. W. Swainston EG&G, Inc.	Mr. V. D. Urban U. S. Department of Commerce, ESSA-ARL	Professor G. A. Whan University of New Mexico
Mr. L. S. Sygitowicz Reynolds Electrical & Engineering Co., Inc.	Mr. Roland A. J. Valentin French Commissariat a l'Energie Atomique	Mr. James Wharton Lawrence Radiation Laboratory
Mr. H. C. Talley, Jr. United States Government	Mr. W. E. Vandenberg U. S. Army Engineering Nuclear Cratering Group	Dr. A. T. Whatley Western Interstate Nuclear Board
Dr. W. K. Talley Department of Health, Education and Welfare	Mr. Leo van der Harst CER Geonuclear Corporation	Mr. J. E. Wilkins, Jr. Gulf General Atomic
Mr. T. M. Tami U. S. Army Engineering Nuclear Cratering Group	Mr. J. A. Van Prooyen University of Arizona	Mr. D. W. Wilson U. S. Atomic Energy Commission
Mr. R. W. Taylor Lawrence Radiation Laboratory	Mr. L. A. Velez United States Government-SAFSEA	Mr. H. D. Wilson Lawrence Radiation Laboratory
Professor E. L. Teller Lawrence Radiation Laboratory	Mr. H. G. Vermillion U. S. Atomic Energy Commission	Mr. K. L. Wilson University of California, Riverside
Mr. R. W. Terhune Lawrence Radiation Laboratory	Mr. G. V. Vieira Lawrence Radiation Laboratory	Professor P. A. Witherspoon University of California, Berkeley
Mr. P. M. Terlecky, Jr. Air Force Weapons Laboratory	Mr. Pierre Villaros French Embassy	Mr. N. A. Wogman Battelle-Northwest
Mr. H. A. Tewes Lawrence Radiation Laboratory	Mr. P. T. Voegeli U. S. Geological Survey	Mr. J. R. Wojcik ASARCO
Commissioner T. J. Thompson U. S. Atomic Energy Commission	Mr. H. L. Volchok U. S. Atomic Energy Commission	Dr. J. N. Wolfe U. S. Atomic Energy Commission
Dr. A. D. Thornbrough U. S. Atomic Energy Commission	Mr. W. C. Vollendorf Sandia Corporation	Dr. B. C. Woodfine Associated Nuclear Services
Mr. T. H. Timmins Mobil Research & Development Corporation	Mr. L. J. Vortman Sandia Corporation	Professor G. L. Woodruff University of Washington
Dr. E. A. Tkachenko McDonnell Douglas Company- Western Division, Astronautics	Mr. Henry Wachter Sperry-Sun Well Surveying Company	Mr. L. A. Woodruff U. S. Atomic Energy Commission
Mr. John Toman Lawrence Radiation Laboratory	Mr. H. A. Wahl Continental Oil Company	Mr. W. R. Woodruff Lawrence Radiation Laboratory
Mr. Bud Tourtelotte Las Vegas News Bureau	Mr. F. D. Waltman Fenix & Scisson, Inc.	Mr. L. T. Wright American Oil Company
	Mr. D. C. Ward U. S. Bureau of Mines	Mr. D. T. Wruble U. S. Public Health Service

Mr. C. T. Yates, Jr.
Arizona Public Service Company

Mr. W-F. Yau
E. I. du Pont de Nemours & Co.

Mr. F. W. Young
CER Geonuclear Corporation

Mr. G. A. Young
Agbabian-Jacobsen Associates

Mr. P. F. Zimmer
Kennecott Copper Corporation

Professor L. R. Zumwalt
North Carolina State University

AUTHOR INDEX

- Ahrens, Thomas J., 1150
 Anderson, Brooks D. II, 1726
 Arnold, W. D., 1569, 1597
 Atkinson, C. H., 722
 Baldonado, Orlino C., 994
 Bankert, Stanley, 1692
 Bayhurst, B. P., 1306
 Bernreuter, D. L., 979
 Block, Oliver, U. J., 1456
 Blume, John A., 1103
 Boardman, Charles R., 43
 Bowman, Charles R., 732, 831
 Bray, Bruce G., 597, 1343
 Broadman, Gene A., 931
 Brumleve, T. D., 1014
 Burnham, J. B., 1376
 Cameron, I. G., 221
 Campbell, R. H., 752
 Carlson, R. H., 1613
 Carpenter, H. C., 1364
 Catalano, Edward, 493
 Champlin, J. B. F., 1643
 Chapin, C. E., 463
 Cheney, James A., 1474
 Cherry, J. T., 142, 334
 Chilton, Frank, 1474
 Coffey, H. F., 577
 Cowan, G. A., 1246, 1306
 Cramer, J. L., 974
 Crawford, Todd V., 381
 Crouse, D. J., 1569, 1597
 Crowley, Barbara K., 545
 Day, Walter C., 360, 1544
 DelManzo, D. D. Jr., 1701
 Delort, Francis, 649, 1386
 Derlich, S., 505
 Dinneen, G. U., 1364
 Diven, B. C., 1246, 1253
 Duff, Russell E., 815
 Eccles, Samuel F., 1269
 Ehrlich, Thomas, 294
 Evans, Roy B., 1222
 Faure, Jean, 1406
 Ferrieux, Henri, 1136
 Fleming, Robert W., 1661
 Frandsen, Alton D., 1661
 Frank, G. W., 577
 Ganus, William J., 1174
 Gauvenet, André, 240
 Gilmore, J. S., 1306
 Griffen, Roger F., 1184
 Groseclose, B. Clark, 24
 Groves, R. H., 280
 Hakala, W. W., 1428
 Heard, Hugh C., 127
 Heckman, Richard A., 1295
 Henny, Robert W., 1746
 Higgins, Gary H., 29
 Hill, Ernest E., 68
 Hill, J. H., 794
 Hoff, R. W., 1283
 Hoffman, Marvin M., 1257
 Holzer, Alfred, 662
 Hulet, E. K., 1283
 Hurst, F. J., 1569
 Jackson, E. C., 979
 Jacobs, D. G., 831
 Jordan, C. F., 422
 Kelly, John S., 5
 Kline, J. R., 422
 Knobeloch, G. W., 1306
 Knutson, C. F., 1322
 Koranda, John J., 400, 422
 Krikorian, Oscar H., 481
 Kruger, Paul, 439, 1222
 LaFrenz, Robert L., 1661
 Lake, J. A., 1643
 Lee, E. L., 794
 Lee, Lloyd A., 1083
 Lessler, Richard M., 1563
 Lewis, A. E., 909
 Lilley, E. M., 89
 Lombard, David B., 1343
 Loux, P. C., 1069
 Luetkehans, G. R., 577
 Lundberg, A. W., 938
 McKinney, W. A., 877
 Mann, Robert L., 597
 Martin, John R., 400, 422
 Maw, J. R., 230
 Meyer, Walter, 1456
 Michaelson, S. D., 859
 Miller, A. B., 979
 Mishra, R., 918
 Mueller, R. A., 1051
 Niermeyer, Karl E., 864
 Nordyke, Milo D., 1384
 Parker, K., 629
 Petersen, F. L., 142
 Picq, Jean Maurice, 850
 Piper, Arthur M., 1164
 Porter, Lawrence D., 1118
 Post, Roy G., 1169
 Poston, J. W., 1643
 Power, Dean V., 732
 Prestwood, R. J., 1306
 Rabb, David D., 888
 Ragsdale, William F., 964
 Rawson, Donald E., 75
 Redpath, B. B., 1679
 Reed, Jack W., 1485
 Reynolds, Miles Jr., 597
 Rinehart, John S., 1095
 Rodean, Howard C., 1024
 Rogers, Leo A., 519, 698
 Rosenbaum, Joe B., 877
 Saperstein, L. W., 918
 Saxe, H. C., 1701
 Schock, R. N., 110
 Scorgie, G. C., 221
 Siddons, R. A., 753
 Skjei, Roger E., 1083
 Smith, C. F., 775, 818
 Smith, Sam, 13
 Sohns, Harold W., 1343, 1364
 Stephens, D. R., 89
 Stewart, D. H., 1376
 Stewart, Richard M., 864
 Struxness, E. G., 831
 Stuart, Marshall, 400
 Stubbs, T. F., 334
 Supiot, F., 649
 Tami, Thomas M., 1544
 Taylor, R. W., 794
 Teller, Edward, 560
 Terhune, R. W., 334
 Tewes, Howard A., 306, 375
 Thompson, Theos J., 1
 Todd, David K., 1160
 Toman, John, 245
 Vandenberg, William E., 360
 van der Harst, L., 1322
 Vortman, L. J., 1508
 Ward, Don C., 722
 Watkins, J. Wade, 567
 Wells, W. H., 938
 Werth, Glenn C., 1771
 Wethington, John A. Jr., 1589
 Wikkerink, Robert, 400
 Witherspoon, Paul A., 1315
 Young, G. A., 1198